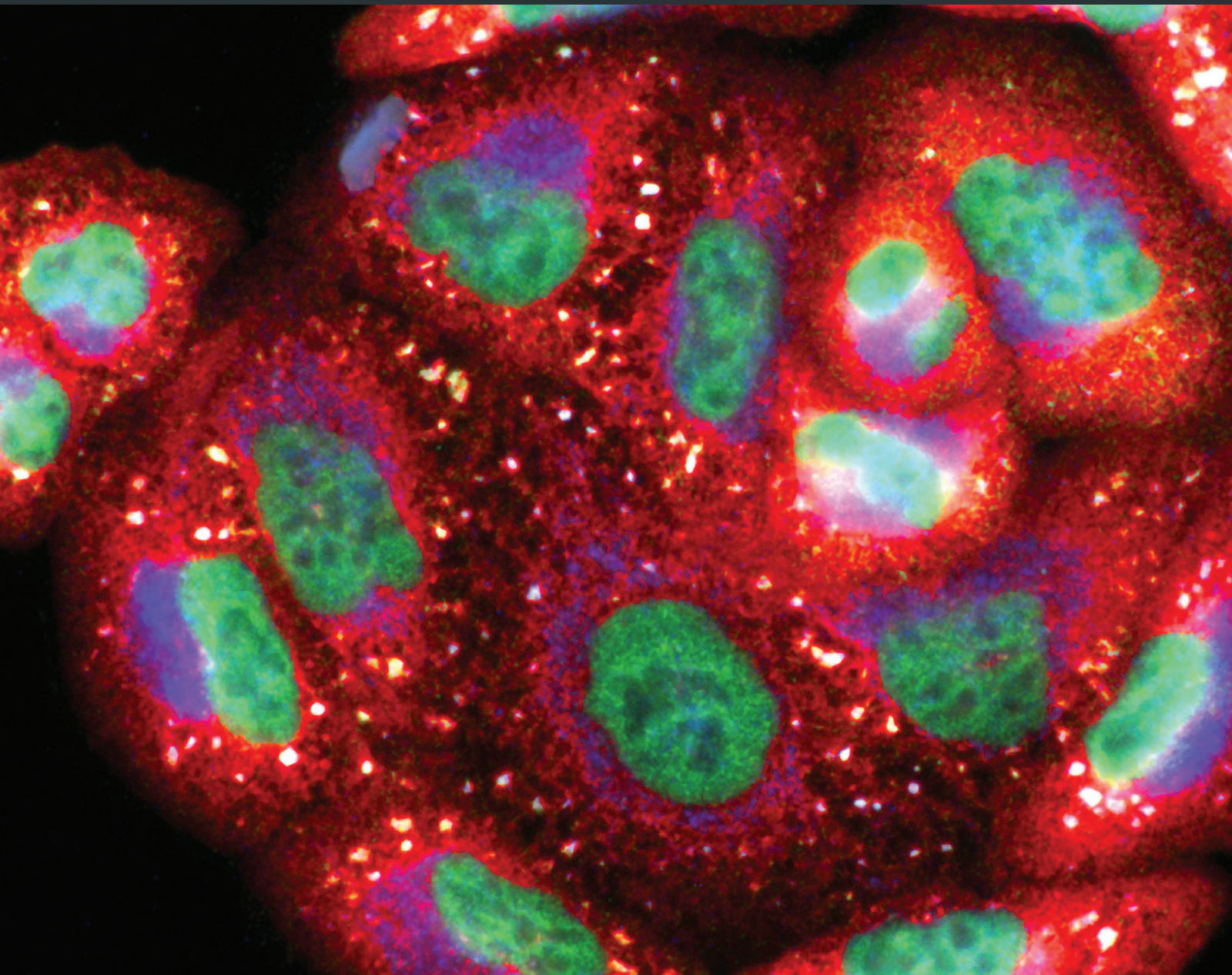


Oxidative Medicine and Cellular Longevity

Mitochondrial Structure, Function, and Dynamics: The Common Thread across Organs, Disease, and Aging

Lead Guest Editor: Moh H. Malek

Guest Editors: Maik Hüttemann and Icksoo Lee





**Mitochondrial Structure, Function,
and Dynamics: The Common Thread
across Organs, Disease, and Aging**

Oxidative Medicine and Cellular Longevity

**Mitochondrial Structure, Function,
and Dynamics: The Common Thread
across Organs, Disease, and Aging**

Lead Guest Editor: Moh H. Malek

Guest Editors: Maik Hüttemann and Icksoo Lee



Copyright © 2018 Hindawi. All rights reserved.

This is a special issue published in "Oxidative Medicine and Cellular Longevity." All articles are open access articles distributed under the Creative Commons Attribution License, which permits unrestricted use, distribution, and reproduction in any medium, provided the original work is properly cited.

Editorial Board

Antonio Ayala, Spain
Peter Backx, Canada
Damian Bailey, UK
Consuelo Borrás, Spain
Vittorio Calabrese, Italy
Angel Catalá, Argentina
Shao-Yu Chen, USA
Ferdinando Chiaradonna, Italy
Zhao Zhong Chong, USA
Giuseppe Cirillo, Italy
Massimo Collino, Italy
Mark Crabtree, UK
Manuela Curcio, Italy
Andreas Daiber, Germany
Felipe Dal Pizzol, Brazil
Francesca Danesi, Italy
Domenico D'Arca, Italy
Claudio De Lucia, Italy
Yolanda de Pablo, Sweden
Grégory Durand, France
Javier Egea, Spain
Ersin Fadillioglu, Turkey
Qingping Feng, Canada
Giuseppe Filomeni, Italy
Swaran J. S. Flora, India
Rodrigo Franco, USA
José Luís García-Giménez, Spain
Janusz Gebicki, Australia
Husam Ghanim, USA
Daniela Giustarini, Italy
Saeid Golbidi, Canada
Aldrin V. Gomes, USA
Tilman Grune, Germany
Tim Hofer, Norway
Silvana Hrelia, Italy
Maria G. Isagulians, Sweden
Vladimir Jakovljevic, Serbia
Peeter Karihtala, Finland
Eric E. Kelley, USA
Kum Kum Khanna, Australia
Neelam Khaper, Canada
Thomas Kietzmann, Finland
Jean-Claude Lavoie, Canada
Christopher Horst Lillig, Germany
Paloma B. Liton, USA
Nageswara Madamanchi, USA
Kenneth Maiese, USA
Tullia Maraldi, Italy
Reiko Matsui, USA
Steven McAnulty, USA
Bruno Meloni, Australia
Trevor A. Mori, Australia
Ryuichi Morishita, Japan
Ange Mouithys-Mickalad, Belgium
Hassan Obied, Australia
Pál Pacher, USA
Valentina Pallottini, Italy
Daniela Pellegrino, Italy
Serafina Perrone, Italy
Tiziana Persichini, Italy
Vincent Pialoux, France
Ada Popolo, Italy
José L. Quiles, Spain
Walid Rachidi, France
Kota V. Ramana, USA
Sid D. Ray, USA
Alessandra Ricelli, Italy
Francisco J. Romero, Spain
H. P. Vasantha Rupasinghe, Canada
Gabriele Saretzki, UK
Honglian Shi, USA
Cinzia Signorini, Italy
Shane Thomas, Australia
Rosa Tundis, Italy
Giuseppe Valacchi, Italy
Jeannette Vasquez-Vivar, USA
Victor M. Victor, Spain
Michal Wozniak, Poland
Sho-ichi Yamagishi, Japan
Liang-Jun Yan, USA
Guillermo Zalba, Spain
Jacek Zielonka, USA

Contents

Mitochondrial Structure, Function, and Dynamics: The Common Thread across Organs, Disease, and Aging

Moh H. Malek , Maik Hüttemann , and Icksoo Lee

Volume 2018, Article ID 1863414, 2 pages

ZP2495 Protects against Myocardial Ischemia/Reperfusion Injury in Diabetic Mice through Improvement of Cardiac Metabolism and Mitochondrial Function: The Possible Involvement of AMPK-FoxO3a Signal Pathway

Shuang Li, Hao Wu , Dong Han , Mingming Zhang, Na Li, Weihua Yu, Dongdong Sun, Zhongchan Sun, Sai Ma , Erhe Gao, Congye Li, Min Shen, and Feng Cao 

Volume 2018, Article ID 6451902, 15 pages

Slower Dynamics and Aged Mitochondria in Sporadic Alzheimer's Disease

Patricia Martín-Maestro, Ricardo Gargini, Esther García, George Perry, Jesús Avila, and Vega García-Escudero

Volume 2017, Article ID 9302761, 14 pages

Blood-Based Bioenergetic Profiling Reflects Differences in Brain Bioenergetics and Metabolism

Daniel J. Tyrrell, Manish S. Bharadwaj, Matthew J. Jorgensen, Thomas C. Register, Carol Shively, Rachel N. Andrews, Bryan Neth, C. Dirk Keene, Akiva Mintz, Suzanne Craft, and Anthony J. A. Molina

Volume 2017, Article ID 7317251, 9 pages

Generation and Bioenergetic Profiles of Cybrids with East Asian mtDNA Haplogroups

Huaibin Zhou, Ke Nie, Ruyi Qiu, Jingting Xiong, Xiaoli Shao, Bingqian Wang, Lijun Shen, Jianxin Lyu, and Hezhi Fang

Volume 2017, Article ID 1062314, 12 pages

Mitochondria-Targeted Antioxidants SkQ1 and MitoTEMPO Failed to Exert a Long-Term Beneficial Effect in Murine Polymicrobial Sepsis

Pia Rademann, Adelheid Weidinger, Susanne Drechsler, Andras Meszaros, Johannes Zipperle, Mohammad Jafarmadar, Sergiu Dumitrescu, Ara Hacobian, Luisa Ungelenk, Franziska Röstel, Jozsef Kaszaki, Andrea Szabo, Vladimir P. Skulachev, Michael Bauer, Soheyl Bahrami, Sebastian Weis, Andrey V. Kozlov, and Marcin F. Osuchowski

Volume 2017, Article ID 6412682, 14 pages

β -Naphthoflavone-Induced Mitochondrial Respiratory Damage in Cyp1 Knockout Mouse and in Cell Culture Systems: Attenuation by Resveratrol Treatment

Suresh Kumar Anandasadagopan, Naveen M. Singh, Haider Raza, Seema Bansal, Venkatesh Selvaraj, Shilpee Singh, Anindya Roy Chowdhury, Nicolae Adrian Leu, and Narayan G. Avadhani

Volume 2017, Article ID 5213186, 13 pages

Testosterone Upregulates the Expression of Mitochondrial ND1 and ND4 and Alleviates the Oxidative Damage to the Nigrostriatal Dopaminergic System in Orchiectomized Rats

Wensheng Yan, Yunxiao Kang, Xiaoming Ji, Shuangcheng Li, Yingkun Li, Guoliang Zhang, Huixian Cui, and Geming Shi

Volume 2017, Article ID 1202459, 13 pages

Caffeic Acid Phenethyl Ester Reduces Ischemia-Induced Kidney Mitochondrial Injury in Rats

Sonata Trumbeckaite, Neringa Pauziene, Darius Trumbeckas, Mindaugas Jievaltas, and Rasa Baniene
Volume 2017, Article ID 1697018, 11 pages

Increased Mitochondrial Mass and Cytosolic Redox Imbalance in Hippocampal Astrocytes of a Mouse Model of Rett Syndrome: Subcellular Changes Revealed by Ratiometric Imaging of JC-1 and roGFP1 Fluorescence

Dörthe F. Bebensee, Karolina Can, and Michael Müller
Volume 2017, Article ID 3064016, 15 pages

Pleiotropic Effects of Biguanides on Mitochondrial Reactive Oxygen Species Production

Alena Pecinova, Zdenek Drahota, Jana Kovalcikova, Nikola Kovarova, Petr Pecina, Lukas Alan, Michal Zima, Josef Houstek, and Tomas Mracek
Volume 2017, Article ID 7038603, 11 pages

Elucidation of Molecular Mechanisms of Streptozotocin-Induced Oxidative Stress, Apoptosis, and Mitochondrial Dysfunction in Rin-5F Pancreatic β -Cells

Arwa M. T. Al Nahdi, Annie John, and Haider Raza
Volume 2017, Article ID 7054272, 15 pages

Combined Respiratory Chain Deficiency and UQCC2 Mutations in Neonatal Encephalomyopathy: Defective Supercomplex Assembly in Complex III Deficiencies

René G. Feichtinger, Michaela Brunner-Krainz, Bader Alhaddad, Saskia B. Wortmann, Reka Kovacs-Nagy, Tatjana Stojakovic, Wolfgang Erwa, Bernhard Resch, Werner Windischhofer, Sarah Verheyen, Sabine Uhrig, Christian Windpassinger, Felix Locker, Christine Makowski, Tim M. Strom, Thomas Meitinger, Holger Prokisch, Wolfgang Sperl, Tobias B. Haack, and Johannes A. Mayr
Volume 2017, Article ID 7202589, 11 pages

Disrupted Skeletal Muscle Mitochondrial Dynamics, Mitophagy, and Biogenesis during Cancer Cachexia: A Role for Inflammation

Brandon N. VanderVeen, Dennis K. Fix, and James A. Carson
Volume 2017, Article ID 3292087, 13 pages

Mitochondrial Respiration in Human Colorectal and Breast Cancer Clinical Material Is Regulated Differently

Andre Koit, Igor Shevchuk, Lyudmila Ounpuu, Aleksandr Klepinin, Vladimir Chekulayev, Natalja Timohhina, Kersti Tepp, Marju Puurand, Laura Truu, Karoliina Heck, Vahur Valvere, Rita Guzun, and Tuuli Kaambre
Volume 2017, Article ID 1372640, 16 pages

Mitochondria-Targeted Antioxidant SkQ1 Improves Dermal Wound Healing in Genetically Diabetic Mice

Ilya A. Demyanenko, Vlada V. Zakharova, Olga P. Ilyinskaya, Tamara V. Vasilieva, Artem V. Fedorov, Vasily N. Manskikh, Roman A. Zinovkin, Olga Yu Pletjushkina, Boris V. Chernyak, Vladimir P. Skulachev, and Ekaterina N. Popova
Volume 2017, Article ID 6408278, 10 pages

Oxidative Phosphorylation System in Gastric Carcinomas and Gastritis

René G. Feichtinger, Daniel Neureiter, Tom Skaria, Silja Wessler, Timothy L. Cover, Johannes A. Mayr, Franz A. Zimmermann, Gernot Posselt, Wolfgang Sperl, and Barbara Kofler

Volume 2017, Article ID 1320241, 14 pages

MNRR1, a Biorganellar Regulator of Mitochondria

Lawrence I. Grossman, Neeraja Purandare, Rooshan Arshad, Stephanie Gladysck, Mallika Somayajulu, Maik Hüttemann, and Siddhesh Aras

Volume 2017, Article ID 6739236, 12 pages

Mitochondrial Nucleoid: Shield and Switch of the Mitochondrial Genome

Sung Ryul Lee and Jin Han

Volume 2017, Article ID 8060949, 15 pages

Mitochondrial Uncoupler Prodrug of 2,4-Dinitrophenol, MP201, Prevents Neuronal Damage and Preserves Vision in Experimental Optic Neuritis

Reas S. Khan, Kimberly Dine, John G. Geisler, and Kenneth S. Shindler

Volume 2017, Article ID 7180632, 10 pages

Impact of Aging and Exercise on Mitochondrial Quality Control in Skeletal Muscle

Yuho Kim, Matthew Triolo, and David A. Hood

Volume 2017, Article ID 3165396, 16 pages

Evidence of Mitochondrial Dysfunction in Autism: Biochemical Links, Genetic-Based Associations, and Non-Energy-Related Mechanisms

Keren K. Griffiths and Richard J. Levy

Volume 2017, Article ID 4314025, 12 pages

Mitophagy Transcriptome: Mechanistic Insights into Polyphenol-Mediated Mitophagy

Sijie Tan and Esther Wong

Volume 2017, Article ID 9028435, 13 pages

Tissue- and Condition-Specific Isoforms of Mammalian Cytochrome *c* Oxidase Subunits: From Function to Human Disease

Christopher A. Sinkler, Hasini Kalpage, Joseph Shay, Icksoo Lee, Moh H. Malek, Lawrence I. Grossman, and Maik Hüttemann

Volume 2017, Article ID 1534056, 19 pages

The Stimulated Glycolytic Pathway Is Able to Maintain ATP Levels and Kinetic Patterns of Bovine Epididymal Sperm Subjected to Mitochondrial Uncoupling

João D. A. Losano, Juan Fernando Padín, Iago Méndez-López, Daniel S. R. Angrimani, Antonio G. García, Valquiria H. Barnabe, and Marcilio Nichi

Volume 2017, Article ID 1682393, 8 pages

Editorial

Mitochondrial Structure, Function, and Dynamics: The Common Thread across Organs, Disease, and Aging

Moh H. Malek ^{1,2,3} **Maik Hüttemann** ^{3,4} and **Icksoo Lee**⁵

¹Physical Therapy Program, Department of Health Care Sciences, Eugene Applebaum College of Pharmacy & Health Sciences, Wayne State University, Detroit, MI 48201, USA

²Integrative Physiology of Exercise Laboratory, Department of Health Care Sciences, Eugene Applebaum College of Pharmacy & Health Sciences, Wayne State University, Detroit, MI 48201, USA

³Cardiovascular Research Institute, Wayne State University School of Medicine, Detroit, MI 48201, USA

⁴Center for Molecular Medicine and Genetics, Wayne State University School of Medicine, Detroit, MI 48201, USA

⁵College of Medicine, Dankook University, Cheonan-si, Chungcheongnam-do 31116, Republic of Korea

Correspondence should be addressed to Moh H. Malek; en7488@wayne.edu

Received 16 November 2017; Accepted 16 November 2017; Published 8 February 2018

Copyright © 2018 Moh H. Malek et al. This is an open access article distributed under the Creative Commons Attribution License, which permits unrestricted use, distribution, and reproduction in any medium, provided the original work is properly cited.

Mitochondria are central to all basic and advanced cellular and organismal functions. In addition to the vast majority of cellular energy generated by these unique organelles, they are also essential signaling hubs and communicate with the rest of the cell through various means including reactive oxygen species. Their dysfunction is implicated in nearly all common diseases ranging from neuromuscular to diabetes to cancer. In this special issue, “Mitochondrial Structure, Function, and Dynamics: The Common Thread across Organs, Disease, and Aging”, we wanted to provide the readership of *Oxidative Medicine and Cellular Longevity* with a variety of examples of how mitochondria function and how different adverse conditions result in their dysfunction. The articles in this special issue can be categorized into examining mitochondria related to topics such as Alzheimer’s, cancer cachexia, diabetes and wound healing, and sepsis.

In the current issue, several articles focus on the role of mitochondria in the brain. For example, P. Martín-Maestro and colleagues report a downregulation of genes involved in mitochondrial dynamics in patients diagnosed with Alzheimer’s, whereas D. J. Tyrrell et al. examined blood-based bioenergetic profiles as potential biomarkers for changes in brain metabolism. D. F. Bebensee and colleagues used a transgenic murine model (*Mecp2* null) to examine oxidative stress in the hippocampus region, and

the potential clinical application of their findings resides in understanding a neurodevelopmental disorder called Rett syndrome. In addition, the article by K. K. Griffiths and R. J. Levy provides an excellent review on the role of mitochondrial dysfunction in autism. Taken together, these studies provide valuable insight into the role of mitochondria function in the brain.

Another tissue in which mitochondria play a critical role in bioenergetics is skeletal muscle, which comprises 50% of an individual’s total body mass. Skeletal muscle is dynamic and, therefore, responds to positive stimuli such as exercise as well as negative stimuli such as aging. In this special issue, three articles are presented that provide further insight into the role of mitochondria in skeletal muscle. R. G. Feichtinger and colleagues present a case study of a child who suffered from respiratory distress syndrome soon after birth and needed to be placed on mechanical ventilation. In addition, this patient required surfactant replacement therapy. This report discusses UQCC2 mutation in neonatal encephalomyopathy with particular focus on complex III. In addition to this case report, two review articles are presented from the Hood and Carson laboratories on the “Impact of Aging and Exercise on Mitochondrial Quality Control in Skeletal Muscle” and “Disrupted Skeletal Muscle Mitochondrial Dynamics, Mitophagy, and Biogenesis during Cancer Cachexia: A

Role for Inflammation”, respectively. These articles present two different scenarios (aging/exercise and cancer cachexia) and how skeletal muscle responds to these stimuli and the potential impact on mitochondrial structure and function.

Another area of research that is presented is the effect of cancer on various tissues and its role on mitochondrial function. The report by A. Koit and colleagues shows that there are differences between mitochondrial respiration as well as membrane permeability in breast cancer patients relative to patients diagnosed with colorectal cancer. The investigators use a combination of human tissue samples as well as cell culture models to distinguish differences in mitochondrial responses. In another article by R. G. Feichtinger and colleagues, the investigators explore OXPHOS complexes in two main types of gastric cancer.

Mitochondrial-targeted ROS scavengers have gained major interest in the scientific community as they go, that is, localize, to the heart of the problem, the mitochondria. Compounds, such as MitoQ, MitoTEMPO, and SKQ1, combine the ROS scavenger with the positively charged triphenylphosphonium moiety, which targets the compounds to the negatively charged inside of the mitochondria resulting in several orders of magnitude of enrichment. As such, P. Rademann and colleagues used a rodent model of sepsis to determine the effect of SkQ1 and MitoTEMPO on attenuating inflammatory responses, which did not improve animal survival and even decreased survival rates for SKQ1. Ilya and colleagues, however, used SkQ1 in a murine model of diabetes, to determine whether or not it would improve dermal wound healing. The authors reported several beneficial effects including reduced lipid peroxidation, increased α -smooth muscle actin-positive cells and wound closure. In conclusion, although the therapeutic benefit of mitochondrial-targeted ROS scavengers has been convincingly demonstrated for a range of acute and chronic disease conditions involving mitochondrial ROS, they may not be considered a universal treatment modality with certain exceptions such as acute inflammatory signaling as seen in sepsis.

To provide more insight into the role of mitochondrial function, we provide an extensive review of cytochrome *c* oxidase subunits from function to human disease. S. Tan and E. Wong also present a review on the role and efficiency of polyphenols on mitochondrial quality control. In addition, J. D. A. Losano et al. examined the metabolic pathways in epididymal bovine sperm, whereas W. Yan and colleagues examine the interaction between testosterone and oxidative damage in orchietomized rats.

In conclusion, all the articles presented in this special issue highlight the importance of proper mitochondrial function for healthy organ and organism performance, whereas mitochondrial dysfunction, triggered by a variety of causes ranging from specific mutations to aging as the arguably ultimate mitochondrial disease, takes center stage in an ever-increasing number of pathologies including all common diseases.

*Moh H. Malek
Maik Hüttemann
Icksoo Lee*

Research Article

ZP2495 Protects against Myocardial Ischemia/Reperfusion Injury in Diabetic Mice through Improvement of Cardiac Metabolism and Mitochondrial Function: The Possible Involvement of AMPK-FoxO3a Signal Pathway

Shuang Li,^{1,2} Hao Wu ,³ Dong Han ,⁴ Mingming Zhang,⁵ Na Li,⁴ Weihua Yu,³ Dongdong Sun,⁴ Zhongchan Sun,⁴ Sai Ma ,⁴ Erhe Gao,⁶ Congye Li,⁴ Min Shen,⁴ and Feng Cao ¹

¹Department of Cardiology & National Clinical Research Center of Geriatrics Disease, Chinese PLA General Hospital, Beijing 100853, China

²Department of Cardiology, Chengdu Military General Hospital, Chengdu 610083, China

³Department of Toxicology, School of Public Health, Fourth Military Medical University, Xi'an, Shaanxi 710032, China

⁴Department of Cardiology, Xijing Hospital, Fourth Military Medical University, Xi'an, Shaanxi 710032, China

⁵Department of Cardiology, Tangdu Hospital, Fourth Military Medical University, Xi'an, Shaanxi 710032, China

⁶Center of Translational Medicine, Temple University School of Medicine, Philadelphia, PA 19107, USA

Correspondence should be addressed to Feng Cao; fengcao8828@163.com

Shuang Li, Hao Wu, and Dong Han contributed equally to this work.

Received 23 April 2017; Revised 23 August 2017; Accepted 14 September 2017; Published 17 January 2018

Academic Editor: Jacek Zielonka

Copyright © 2018 Shuang Li et al. This is an open access article distributed under the Creative Commons Attribution License, which permits unrestricted use, distribution, and reproduction in any medium, provided the original work is properly cited.

Coronary heart disease patients with type 2 diabetes were subject to higher vulnerability for cardiac ischemia-reperfusion (I/R) injury. This study was designed to evaluate the impact of ZP2495 (a glucagon-GLP-1 dual-agonist) on cardiac function and energy metabolism after myocardial I/R injury in db/db mice with a focus on mitochondrial function. C57BLKS/J-*lepr*⁺/*lepr*⁺ (BKS) and db/db mice received 4-week treatment of glucagon, ZP131 (GLP-1 receptor agonist), or ZP2495, followed by cardiac I/R injury. The results showed that cardiac function, cardiac glucose metabolism, cardiomyocyte apoptosis, cardiac mitochondrial morphology, and energetic transition were improved or ameliorated by ZP2495 to a greater extent than that of glucagon and ZP131. *In vitro* study showed that ZP2495, rather than glucagon, alleviated mitochondrial depolarization, cytochrome C release, and mitochondria ROS generation in neonatal rat ventricular myocytes subjected to high-glucose and simulated I/R injury conditions, the effects of which were weaker in the ZP131 group. Furthermore, the expressions of Akt, FoxO3a, and AMPK phosphorylation were elevated by ZP2495 to a greater extent than that of ZP131. In conclusion, ZP2495 may contribute to the improvement of cardiac function and energy metabolism in db/db mice after myocardial I/R injury by improving mitochondrial function possibly through Akt/FoxO3a and AMPK/FoxO3a signal pathways.

1. Introduction

Type 2 diabetes is one of the strong independent risk factors for cardiovascular disease and death [1, 2]. Lots of studies including our previous studies have demonstrated that

patients with type 2 diabetes have higher vulnerability of cardiac ischemia/reperfusion (I/R) injury as a result of the exposure to abnormal substrate and cytokines [3, 4]. However, effective strategies which can reduce cardiac I/R injury under diabetic conditions are not well developed in a clinic setting.

Glucagon-like peptide-1 (GLP-1) is derived from a proglucagon precursor and secreted by intestinal L-cells in response to oral nutrient ingestion, which acts through G protein-coupled receptor (GLP-1R) on pancreatic beta-cells to exert glucoregulatory and insulinotropic actions [5, 6]. GLP-1R agonists have been reported to have cardiac and vascular actions in rodents and humans, including effects on myocardial contractility, blood pressure, cardiac output, and cardioprotection [7–9]. Glucagon exerts biochemical and physiological effects on heart muscle partly by stimulating Ca^{2+} currents via cAMP production and inhibition of phosphodiesterases [9–11], leading to increased contractility. Although cardiac contractility can be enhanced by glucagon administration, it will increase cardiac mortality since glucagon increases cardiomyocyte consumption of energy after myocardial infarction [12]. Therefore, it will be ideal to find a medicine with both inotropic and metabolic effects that could potentially have beneficial effects on the prevention of the heart injury induced by ischemia.

Earlier reports suggested the combination of GLP-1 and glucagon makes an attractive proposition for obesity therapy [13, 14]. However, the protective role of glucagon and GLP-1 dual-agonist against I/R injury has not previously been demonstrated. Even in the absence of diabetes, a switch from glucose to fatty acid metabolism contributes to the severity of an ischemic injury and can impair functional recovery during and following ischemia. This is particularly evident during the reperfusion phase of the ischemic myocardium [15–17]. As a result, diabetes-induced changes in energy metabolism have the potential to significantly impact on the ability of the heart to withstand an I/R injury [18]. This study was designed to evaluate the impact of a glucagon-GLP-1 dual-agonist ZP2495 on cardiac function and energy metabolism after myocardial I/R injury in db/db mice and to investigate the underlying mechanisms involved.

2. Materials and Methods

2.1. Animal Modeling and Grouping. Male C57BLKS/J-lepr^{db}/lepr^{db} diabetic (db/db; stock number 000642) and nondiabetic C57BLKS/J-lepr⁺/lepr⁺ (BKS; stock number 000662) mice (8–10 weeks) were obtained from Jackson Laboratory (Bar Harbor, Maine, USA) and housed on a 12:12 h light-dark cycle at 22°C with free access to food and water. db/db mice at the age of 12–16 weeks (50–60 g) when they had developed overt diabetes were used. All experiments were performed in adherence with the National Institutes of Health Guidelines on the Use of Laboratory Animals and were approved by the Fourth Military Medical University Committee on Animal Care (ID 2013052).

db/db mice were randomly allocated into the following groups with $n = 20$ each: (1) BKS + sham (sham); (2) db/db + sham (db/db); (3) db/db + I/R (I/R); (4) db/db + ZP2495 + I/R (ZP2495); (5) db/db + glucagon + I/R (glucagon); and (6) db/db + ZP131 + I/R (ZP131). The ZP2495 group was subcutaneously injected daily with ZP2495 at 70 nmol/kg of body weight for 4 weeks. The glucagon group received subcutaneous injections of glucagon at 70 nmol/kg of body weight daily for 4 weeks. The ZP131 group received daily

subcutaneous injections of ZP131 at 70 nmol/kg of body weight for 4 weeks. The mice in the sham group were injected with saline at the same volume instead.

Mice were anesthetized with 2% isoflurane in 1.5 L/min O_2 . After exteriorizing the heart via a left thoracic incision, myocardial ischemia/reperfusion was induced by ligation of the left descending coronary artery for 30 minutes as previously described [19]. After 30 minutes of ischemia, hearts were harvested 3 hours (for TUNEL, caspase activity, and Western blot assay) or 24 hours (for echocardiographic, hemodynamic, and metabolic assessments and infarct size measurement) after the myocardium reperfusion.

2.2. Echocardiographic and Hemodynamic Measurements. Cardiac function was determined by echocardiography (VisualSonics, Canada) and invasive hemodynamic evaluation by a 1.4 French micromanometer (Millar Instruments, USA) at different time points after ischemia/reperfusion. Echocardiography was performed under anesthesia using a 30 MHz transducer on a Vevo 2100 ultrasound system (VisualSonics, Canada) as previously described [20].

2.3. ^{18}F -Fluorodeoxyglucose Positron Emission Tomography/Computed Tomography to Assess Cardiac Glucose Metabolism. Positron emission tomography/computed tomography (PET/CT) scanning was performed using a Nano PET/CT (Mediso, Hungary) as described previously. Before imaging study, mice were maintained under fasting condition for 12–14 h, and fasting blood glucose levels were maintained between 6.0 and 7.5 mmol/L. Every animal was injected with 3.7 MBq (100 μCi) of ^{18}F -FDG via tail vein injection. To obtain the best signal-to-background ratio, the animals were anesthetized under 2% isoflurane in 1.5 L/min O_2 and acquired for whole body static PET/CT imaging at 30 min postadministration with 10 min acquisition time, energy window at 400–600 keV, and coincidence relation with 1:3. CT scan was subsequently obtained with 45 kV and 179 mA for 10 min. The PET images were reconstructed using ordered subset expectation maximization reconstruction (OSEM) with the SSRB 2D LOR algorithm with decay correction, CT imaging-based attenuation correction, and random corrections from raw framed sinograms. The voxel size of the PET image was $0.796 \times 0.861 \times 0.861$ mm, for a total of $128 \times 128 \times 159$ voxels. After PET-CT registration, 3-dimensional regions of interest (3D-ROI) were drawn over the heart region on whole body axial PET/CT fusion images. Relative accumulation of the radioactivity in particular regions of interest was expressed as standardized uptake value (SUV). Nano PET/CT images were analyzed using InterView™ Fusion software (Mediso, Hungary).

2.4. Myocardial Infarct Size Measurement. Myocardial infarct size was evaluated by Evans Blue/TTC staining as previously described [21].

2.5. Detection of Cardiomyocyte Apoptosis in Hearts. TUNEL staining and caspase-3 activity assay were used to determine cardiomyocyte apoptosis as previously described [22].

2.6. Transmission Electron Microscopy (TEM). Ultrathin sections were observed under a TEM (JEM-2100, JEOL, Tokyo, Japan) at 60 kV. Mitochondria were imaged at $\times 10,000$ (10 K) and $\times 40,000$ (40 K) magnifications.

2.7. Measurement of Neonatal Rat Ventricular Myocyte (NRVM) Apoptosis Induced by Simulated Ischemial Reperfusion (S/IR) Injury. Primary cultures of NRVMs were obtained from 1- or 2-day-old SD rats as described previously [23]. Media were replaced to different conditions after confluence: normal glucose medium (5.5 mmol/L), high-glucose medium (25 mmol/L), and high-glucose plus ZP2495 (10^{-7} mol/L), glucagon (10^{-7} mol/L), or ZP131 (10^{-7} mol/L). Simulated I/R (S/IR) was performed by transferring cardiomyocytes into an ischemic buffer adapted from Esumi et al. [24] containing (in mmol/L) NaCl 137, KCl 3.8, MgCl₂ 0.49, CaCl₂·2H₂O 0.9, and HEPES 4 supplemented with deoxyglucose 10, sodium dithionite 0.75, KCl 12 and lactate 20, and pH 6.5, for 3 h in a humidified cell culture incubator (21% O₂, 5% CO₂, and 94% N₂, 37°C). After simulated ischemia, cells were transferred to DMEM for 3 h in a humidified cell culture incubator (21% O₂, 5% CO₂, and 74% N₂, 37°C) to simulate reperfusion.

NRVM apoptosis was determined using an Annexin V-FITC/PI Kit (Merck, USA) as previously described [25].

2.8. Measurement of Mitochondrial Membrane Potential ($\Delta\Psi_m$) (MMP). The impact of ZP2495, glucagon, or ZP131 on mitochondrial $\Delta\Psi_m$ in cardiomyocytes was determined by sensitive and relatively mitochondrion-specific lipophilic cationic probe fluorochrome JC-1 as previously described [26]. Cardiomyocytes were incubated with JC-1 Mitochondrial Potential Sensors (Invitrogen, USA), and images were visualized and photographed with confocal microscopy (Olympus, Japan). In order to measure the internalization of JC-1, cardiomyocytes were stained with the JC-1 Assay Kit for flow cytometry (Mitoprobe, Invitrogen, USA) according to the manufacturer's protocol and analyzed by subsequent flow cytometry (BD Bioscience, USA). To exclude cell debris and doublets, cells were gated the same number in each group, 1×10^4 gated events per sample were collected from three to four independent samples per treatment condition, and the experiments were repeated at least three times. The presented data are normalized to the control group for the treated group (100%).

2.9. Measurement of Respiration of Mouse Cardiomyocyte. Respiration was assayed in freshly isolated mitochondria with a high-throughput-automated 96-well extracellular flux analyzer (XF96; Seahorse Bioscience, USA) as previously described [26].

2.10. Assessment of Mitochondrial Cytochrome c Release and ATP Content. To evaluate the subcellular localization of cytochrome c, we used confocal imaging of cells double labeled with Mitotraker Red CMX Ros (Molecular Probes, USA) and cytochrome c antibody (Cell Signaling Technology, USA). The ATP content of the myocardium was measured using an ATP bioluminescent assay kit (Beyotime, China).

2.11. Detection of Reactive Oxygen Species (ROS) by Mitochondria. ROS production by the mitochondria was assessed by using Mito SOX Red (Invitrogen, USA) according to product protocol. Briefly, slides were labeled with Mito SOX Red (300 nM) and Mito Tracker green (100 nM) for 20 min at 37°C, then observed by confocal microscopy (FV1000, Olympus) with the excitation wavelength at 488 and 543 nm.

2.12. Western Blot Assay. Cardiac tissues from the area at risk (AAR) were lysed, sonicated, and centrifuged. Western blotting was performed following standard protocol. The following primary antibodies were used: anti-phospho-FoxO3a (Thr32) (rabbit polyclonal IgG, Abcam, 1:100); anti-phospho-FoxO3a (Ser413) (rabbit polyclonal IgG, Cell Signaling Technology, 1:1000); anti-FoxO3a (rabbit polyclonal IgG, Cell Signaling Technology, 1:1000); anti-phospho-Akt (Ser473) (rabbit polyclonal IgG, Cell Signaling Technology, 1:1000); anti-phospho-Akt (Thr308) (rabbit polyclonal IgG, Cell Signaling Technology, 1:1000); anti-Akt (rabbit polyclonal IgG, Cell Signaling Technology, 1:1000); anti-AMPK (rabbit polyclonal IgG, Cell Signaling Technology, 1:1000); anti-phospho-AMPK (Thr172) (rabbit polyclonal IgG, Cell Signaling Technology, 1:1000); anti-caspase-3 (rabbit polyclonal IgG, Merck Millipore, 1:200); anti-cleaved caspase-3 (rabbit polyclonal IgG, Merck Millipore, 1:200); anti-Bim (rabbit polyclonal IgG, Abcam, 1:1000); anti-Bax (rabbit polyclonal IgG, Abcam, 1:1000); anti-Bcl-2 (rabbit monoclonal IgG, Abcam, 1:500); anti-Bad (rabbit polyclonal IgG, Cell Signaling Technology, 1:1000); anti-phospho-Bad (rabbit polyclonal IgG, Cell Signaling Technology, 1:1000); anti-MnSOD (rabbit polyclonal IgG, Abcam, 1:5000); anti-Catalase (rabbit polyclonal IgG, Abcam, 1:2000); anti-Sirt1 (rabbit polyclonal IgG, Abcam, 1:1000); anti-PGC-1 α (rabbit polyclonal IgG, Abcam, 1:1000); acetylated-lysine (rabbit polyclonal IgG, Cell Signaling Technology, 1:1000); anti-Nrf-1 (rabbit monoclonal IgG, Abcam, 1:5000); anti-Tfam (rabbit polyclonal IgG, Abcam, 1:2000); and β -actin (rabbit polyclonal IgG, Santa Cruz Biotechnology, 1:1000). The details are described previously [25].

2.13. Statistics Analysis. All data were expressed as mean \pm SD and were analyzed using ANOVA, followed by a Bonferroni correction for post hoc *t*-test (with exception of Western blot). Western blot densities were analyzed with the Kruskal-Wallis test, followed by Dunn's post hoc test. A value of $P < 0.05$ was considered to be statistically significant. All statistical tests were performed using SPSS software package version 14.0 (SPSS, Chicago, IL, USA).

3. Results

3.1. Coagonist Treatment Improved Cardiac Function of db/db Mice after Myocardial I/R Injury. LVEF and LVFS were enhanced significantly in the glucagon or ZP131 group compared with the db/db + I/R group. ZP2495 enhanced LVEF and LVFS more significantly as compared with that of the glucagon or ZP131 group (Figures 1(a)–1(c)). Maximal

velocity of pressure development and decline (\pm LV dP/dt max) also revealed a significant improvement in response to glucagon or ZP131 pretreatment in diabetic mice which underwent cardiac I/R injury. The \pm LV dP/dt max was significantly higher in the ZP2495 group compared with the glucagon or ZP131 group (Figures 1(d) and 1(e)). Moreover, administration of glucagon or ZP131 reduced infarct size after cardiac I/R injury in db/db mice. The mice treated with ZP2495 exhibited much greater decline of infarct size as compared with the glucagon or ZP131 group. There was no significant difference in the area at risk (AAR) between groups (Figures 1(h)–1(j)).

3.2. Regulation of Cardiac Glucose Metabolism Prevented from Cardiac I/R Injury in db/db Mice. To examine the role of cardiac glucose metabolism after ZP2495, glucagon, or ZP131 treatment in db/db mice subjected to I/R, 18 F-FDG was used to analyze the level of myocardial glucose uptake. Our data revealed that diabetic mice which underwent cardiac I/R injury had defective 18 F-FDG uptake in the heart, which was significantly improved by glucagon or ZP131 treatment. Moreover, 18 F-FDG uptake was significantly higher in the ZP2495 group as compared with the glucagon or ZP131 group (Figures 1(f) and 1(g)).

3.3. Coagonist Exerted Antiapoptotic Effect on Cardiomyocyte in db/db Mice after Cardiac I/R Injury. Apoptotic cardiomyocytes labeled by TUNEL positivity were more frequently observed in the db/db + I/R group, glucagon group, and ZP131 group compared with the ZP2495 group (Figure 2(a)). Quantitative analyses demonstrated that the percentage of TUNEL-positive cardiomyocytes was significantly less in the ZP2495 group compared with the db/db + I/R group or the glucagon group. However, there was no significant difference between the percentages of TUNEL-positive cardiomyocytes in the ZP2495 group and ZP131 group (Figure 2(b)). Consistent with its antiapoptotic effect, ZP2495 attenuated the expression of the cleaved, activated forms of caspase-3 (Figures 2(c) and 2(d)).

3.4. Antiapoptotic Effect of ZP2495 on High-Glucose-Induced NRVMs under SI/R Injury. To analyze the antiapoptotic effect of ZP2495 on high-glucose-induced NRVMs after SI/R injury, we performed flow cytometry, TUNEL, and caspase-3 activity assays. Representative flow cytometry results (Figure 3(a)) indicated that high-glucose and SI/R injury significantly increased the percentage of apoptotic NRVMs. ZP2495 treatment decreased high-glucose and SI/R-induced apoptosis of NRVMs. As shown in Figures 3(b)–3(e), the antiapoptotic effect of ZP2495 on NRVMs was also evidenced by increased TUNEL (green) staining of cells (Figures 3(b)–3(d)) and upregulation of caspase-3 enzymatic activities (Figure 3(e)).

3.5. Antioxidation Effect of ZP2495 on Cardiomyocyte in db/db Mice under Cardiac I/R Injury via a Akt/FoxO3a-Dependent Mechanism. To further understand the mechanism of the protective effect of ZP2495, we examined the expressions of Akt, FoxO3a, and apoptosis-related proteins using Western blot (Figure 4). ZP2495 administration

increased the levels of phospho-Akt in myocardial tissue of db/db mice after cardiac I/R injury (Figures 4(a) and 4(b)). Consistently, our data further revealed reduction of the Akt-engaged phosphorylation of FoxO3 at Thr32 following ZP2495 treatment. Diabetes with cardiac I/R injury decreased FoxO3a phosphorylation at Thr32 (Figures 4(a) and 4(d)). To further examine FoxO3a activation, we measured the expression levels of its apoptosis-related downstream targets, including proapoptotic proteins BimEL and Bax, as well as antiapoptotic protein Bcl-2. The representative Western blot results demonstrated that diabetes with cardiac I/R injury increased the expressions of BimEL (Figure 4(e)) and Bax and decreased the levels of Bcl-2. ZP2495 treatment balanced the expression between pro- and antiapoptotic proteins (Figures 4(a) and 4(g)). As demonstrated in Figures 4(a) and 4(f), diabetes and I/R injury could moderately induce myocardial mitochondrial antioxidative enzyme expressions including MnSOD and catalase. ZP2495 upregulated the expression of these enzymes.

3.6. Coagonist Treatment Improved Mitochondrial Ultrastructural Morphology in Myocardium of db/db Mice Subjected to Cardiac I/R Injury. Alterations in mitochondrial ultrastructure were observed by TEM. As shown in Figure 5(a), in the db/db + I/R group, most of the mitochondria from the peri-infarct zone presented significant disorders, including abnormal cristae or areas of the matrix. In some mitochondria, the cristae and matrix were cleared out, resulting in vacuoles; some mitochondria were swelling and presented with crista disorientation and breakage. The derangement in the ultrastructural morphology of mitochondria was improved in the ZP2495 treatment group, as evidenced by normalized crista density and architecture. Most of the mitochondria in this group presented sharply defined cristae. The number of swelling mitochondria was less, and no obvious vacuoles could be found in the ZP2495 treatment group.

3.7. Coagonist Treatment Improved Mitochondrial Energetic Transition in Myocardium of db/db Mice Subjected to Cardiac I/R Injury. We measured mitochondrial respiration, coupling of oxidative phosphorylation (OxPhos), and the relative ATP level in isolated mitochondria from hearts of all groups. Mitochondrial respiration was first quantified in the presence of substrates of complex I, II, and IV and the coupling of OxPhos under each condition (Figures 5(b)–5(d)). The basic bioenergetic behavior of mitochondria from hearts of the ZP2495 treatment group was noticeably improved. The RCR (state 3/4), a measure of the degree of coupling of OxPhos, was markedly decreased at the level of the three main respiratory complexes in mitochondria of the db/db and db/db + I/R groups (Figure 5(e)). In these two groups of mitochondria, a trend to higher values of state 4 respiration was evident in complex I, II, and IV (Figures 5(b)–5(d)). Likewise, the relative ATP levels in the db/db and db/db + I/R groups, the myocardia were also significantly decreased, and ZP2495 treatment preserved the reduction (Figure 5(f)).

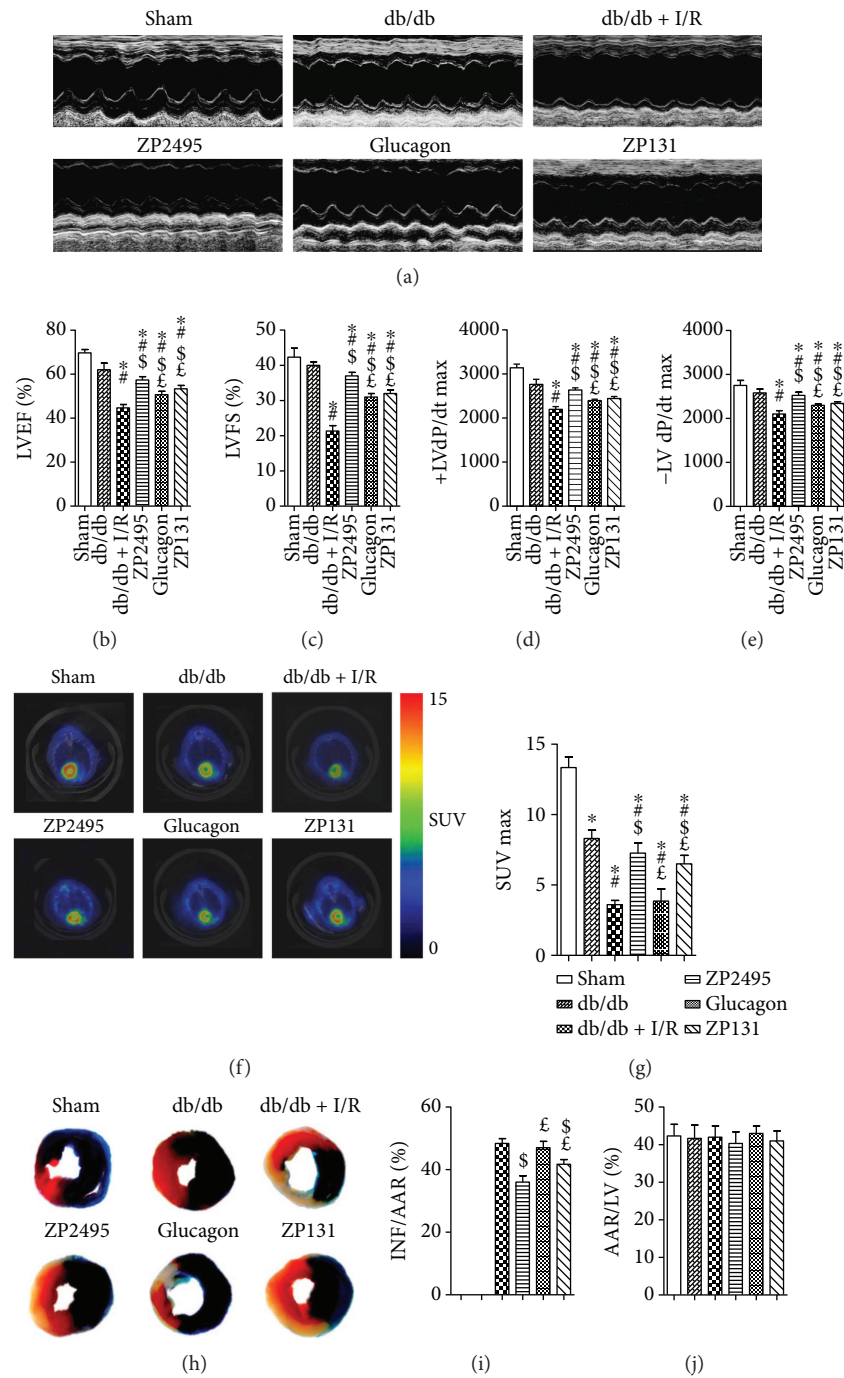


FIGURE 1: Effects of ZP2495, glucagon, and ZP131 on cardiac function and hemodynamic and cardiac glucose metabolism in db/db mice after I/R injury. (a) Representative M-mode echocardiography images. (b) Measurement of left ventricular ejection fraction (LVEF). (c) Measurement of left ventricular fractional shortening (LVFS). (d, e) Measurement of maximal velocity of pressure development and decline (\pm dP/dt). (f) Representative PET/CT scan images from each group. Higher glucose uptake level is evidenced by an increase in the intensity of red color. (g) Quantification of accumulated 18 F-fluorodeoxyglucose (18 F-FDG) in the heart. Relative accumulation of the radioactivity in particular regions of interest was expressed as standardized uptake value (SUV). (h) Myocardial infarct size was assessed by Evans blue/2,3,5-triphenyl-2H-tetrazolium chloride (TTC) double staining. Evans blue stained areas (black) indicated nonischemic/reperfused area. TTC-stained areas (red staining) indicated ischemic but viable tissue. Evans blue/TTC staining negative areas indicated infarcted myocardium. (i) Summary of infarct area (INF) per area at risk (AAR). (j) Summary of AAR per left ventricle (LV). Sham: BKS + sham group; db/db: db/db + sham group; I/R: db/db + I/R group; ZP2495: db/db + I/R + ZP2495 group; glucagon: db/db + I/R + glucagon group; and ZP131: db/db + I/R + ZP131 group. Presented values are mean \pm SEM. * P < 0.05 versus the sham group; # P < 0.05 versus the db/db group; § P < 0.05 versus the db/db + I/R group; and $^{\text{E}}$ P < 0.05 versus the db/db + I/R + ZP2495 group.

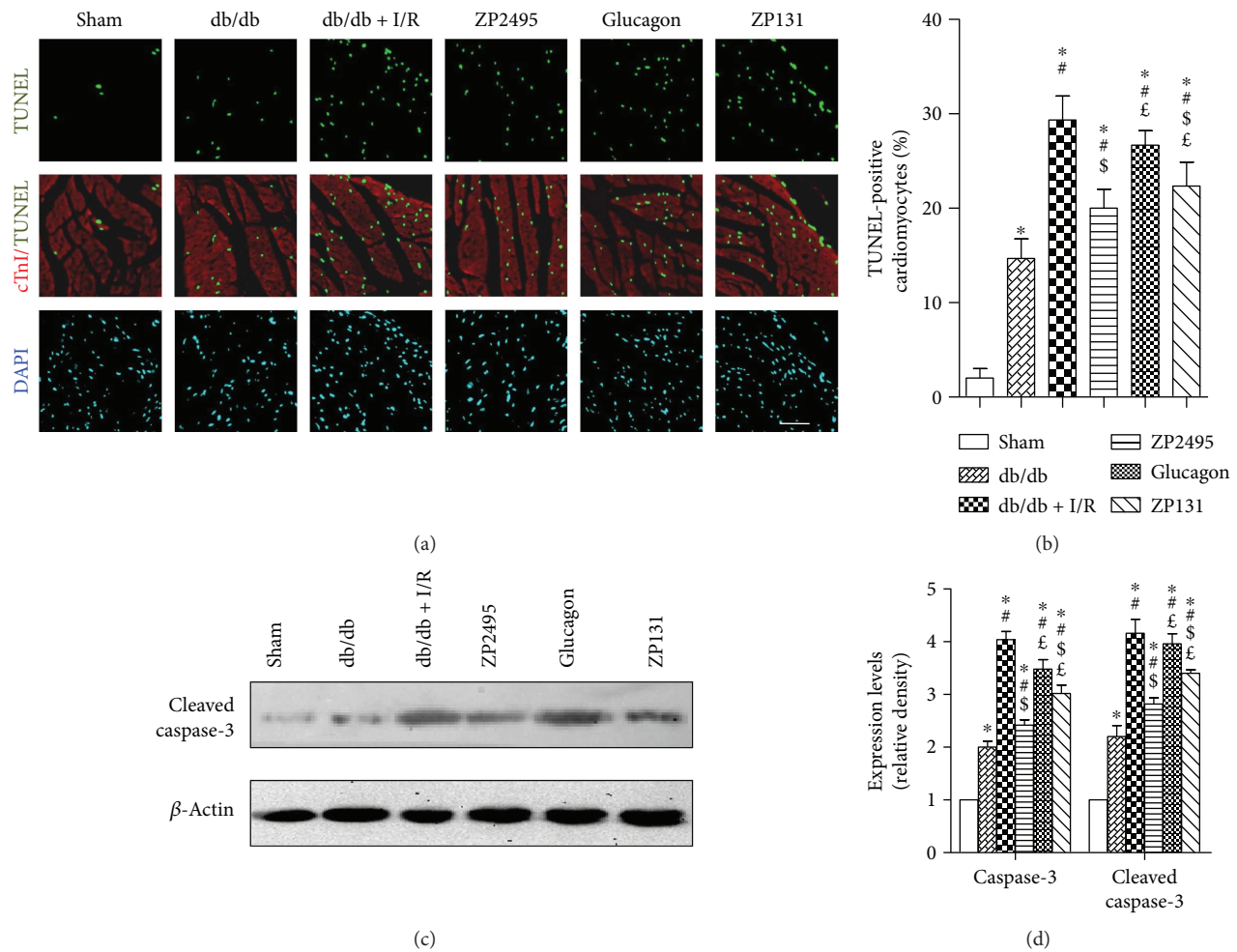


FIGURE 2: ZP2495 exerted antiapoptotic effect on cardiomyocyte of db/db mice. (a) Representative photomicrograph shows TUNEL-positive cardiomyocyte ratio, which was significantly decreased in the ZP2495 group. Apoptotic nuclei were identified as TUNEL positive (green). Myocardium was stained using a monoclonal antibody against troponin I (cTnI) (red) and total nuclei by DAPI counterstaining (blue) (scale bar = 100 μ m). (b) Quantitative analysis of apoptotic nuclei. Apoptotic index was termed as the percentage of apoptotic cells. (c) Representative blots of caspase-3 and cleaved caspase-3 in cardiomyocyte of db/db mice subjected to I/R. (d) Semi-quantitative analysis of the Western blots. Sham: BKS + sham group; db/db: db/db + sham group; I/R: db/db + I/R group; ZP2495: db/db + I/R + ZP2495 group; glucagon: db/db + I/R + glucagon group; and ZP131: db/db + I/R + ZP131 group. Presented values are mean \pm SEM. * P < 0.05 versus the sham group; # P < 0.05 versus the db/db group; $^{\$}$ P < 0.05 versus the db/db + I/R group; and $^{\text{E}}$ P < 0.05 versus the db/db + I/R + ZP2495 group.

3.8. Coagonist Treatment Prevented Mitochondrial Depolarization and Reduced Cytochrome *c* Release and Mitochondria ROS Generation in High-Glucose-Induced NRVMs after SI/R Injury. As is shown in Figure 6(a), there were stronger red fluorescent signals and weaker green fluorescent signals in the control group, indicating intact high mitochondria membrane potential. However, red fluorescent signals had almost disappeared and green fluorescent signals were greatly enhanced in the HG (high-glucose) and HG + SI/R group, suggesting typical mitochondrial membrane potential collapse. While in the ZP2495 treated group, there were more red fluorescent signals remaining, along with fewer green fluorescent signals, which indicated that ZP2495 treatment prevented mitochondrial depolarization (Figure 6(b)). In the control group, cytochrome *c* immunoreactivity was colocalized with mitotracker red fluorescence, indicating that the cytochrome *c* was confined to the

mitochondria. After high-glucose and SI/R injury, cytochrome *c* immunoreactivity was diffusely distributed throughout the cytoplasm and an increase in mitochondria-associated cytochrome *c*, indicating that cytochrome *c* was released from mitochondria to the cytoplasm. On the contrary, fewer cells exhibited such cytochrome *c* release pattern in the ZP2495 treatment group (Figure 6(c)). High glucose with SI/R injury-induced mitochondrial ROS generation was assessed by MitoSox fluorescence (Figure 6(d)). Mitochondria were visualized with Mitotracker. Image merging of MitoSox with Mitotracker showed that the diminished ROS was generated from mitochondria in the ZP2495 treatment group.

3.9. Coagonist Increased Mitochondrial Biogenesis in Hearts of db/db Mice Subjected to I/R Injury through AMPK/FoxO3a and AMPK-SIRT1-PGC-1 α Pathway. To investigate

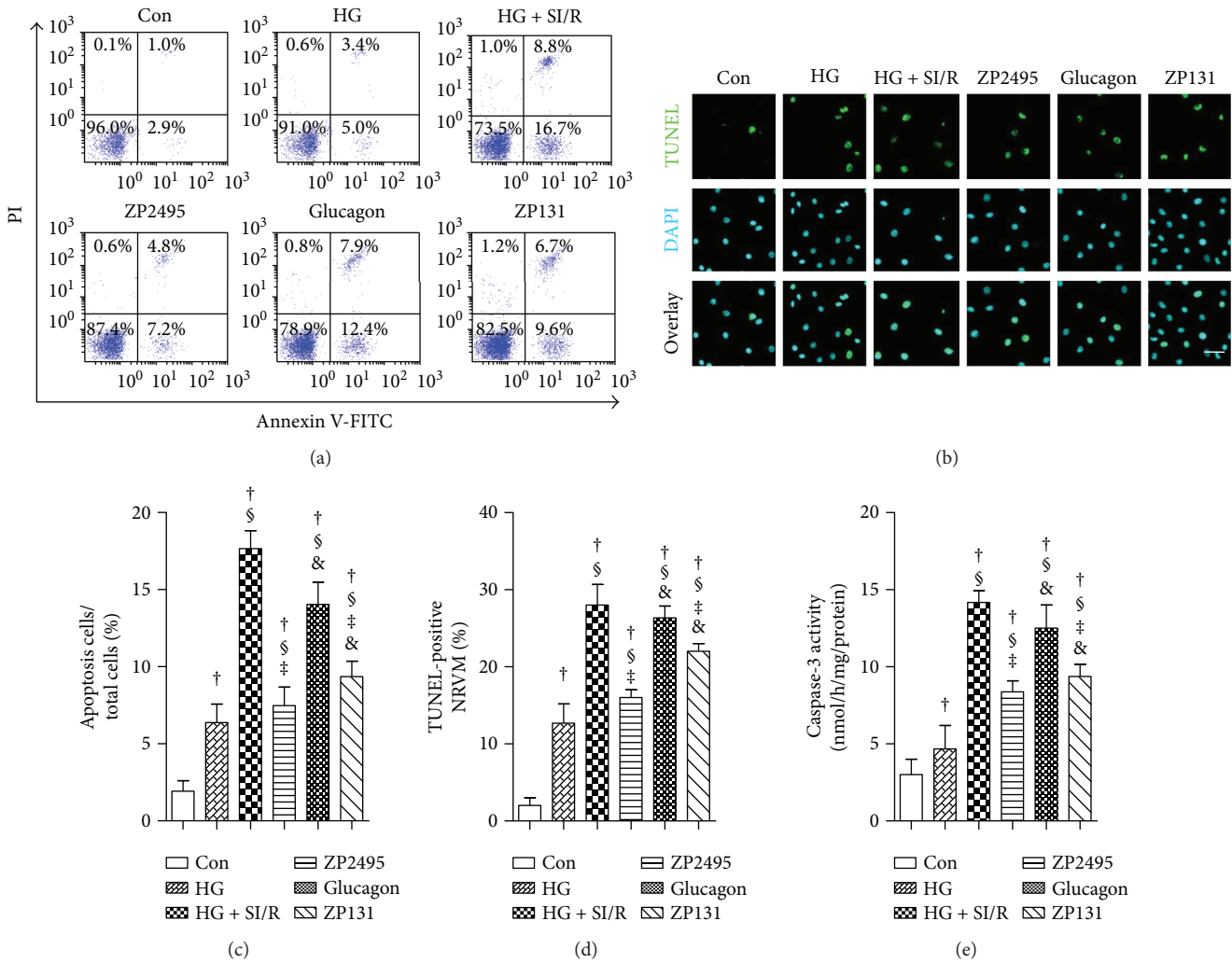


FIGURE 3: ZP2495 exerted antiapoptotic effect on high-glucose-induced NRVMs after SI/R injury. (a) Apoptosis of the NRVMs determined by annexin V/propidium iodide (PI) double staining and flow cytometry. Region Q2 late apoptotic cells, region Q3 vital cells, and region Q4 early apoptotic cells. (b) Representative images of immunostaining for apoptotic (TUNEL) cells (scale bar = 100 μ m). (c) Quantification of apoptosis cell by flow cytometry and TUNEL staining. (d) Quantification of apoptosis cell by TUNEL staining. (e) Activities of caspase-3. Con: normal glucose medium group; HG: high-glucose medium group; HG + SI/R: HG + SI/R group; ZP2495: HG + SI/R + ZP2495 group; glucagon: HG + SI/R + glucagon group; and ZP131: HG + SI/R + ZP131 group. Presented values are mean \pm SEM. † P < 0.05 versus the control group; § P < 0.05 versus the HG group; ‡ P < 0.05 versus the HG + SI/R group; and & P < 0.05 versus the HG + SI/R + ZP2495 group.

the potential signaling pathways involved in which ZP2495 improved cardiomyocyte energy metabolism after diabetes with myocardial I/R injury, we examined the level of AMPK. Our results indicated that I/R injury markedly decreased phosphorylation of AMPK in db/db mice, which was abrogated by ZP2495 (Figures 7(a) and 7(b)). Furthermore, we found reduction of AMPK-activated Foxo3 phosphorylation at the Ser413 site following ZP2495 treatment (Figures 7(a) and 7(c)). As shown in Figures 7(a)–7(e), AMPK α phosphorylation and SIRT1 expression level was dramatically lower and PGC-1 α acetylation was increased in the db/db and the db/db + I/R groups. However, AMPK α and PGC-1 α protein levels of cardiac tissue did not display a measurable difference between groups. ZP2495 treatment stimulated AMPK α phosphorylation and PGC-1 α deacetylation without altering PGC-1 α protein expression (Figures 7(a) and 7(e)). In the

meanwhile, ZP2495 treatment significantly increased SIRT1 expression (Figures 7(a) and 7(d)). We next determined whether administration of ZP2495 could increase mitochondrial biogenesis in hearts of db/db mice subjected to I/R. ZP2495 treatment also significantly restored the protein levels of Nrf-1 and Tfam (Figures 7(a) and 7(f)). The effects of ZP2495 on mitochondrial biogenesis in db/db mice subjected to cardiac I/R injury were related to the AMPK-SIRT1-PGC-1 α pathway (Figure 8).

4. Discussion

It is increasingly recognized that the occurrence of coronary artery disease contributes to an increased risk for the development of heart failure in diabetic patients. Although the pathophysiological mechanisms are certainly multifactorial,

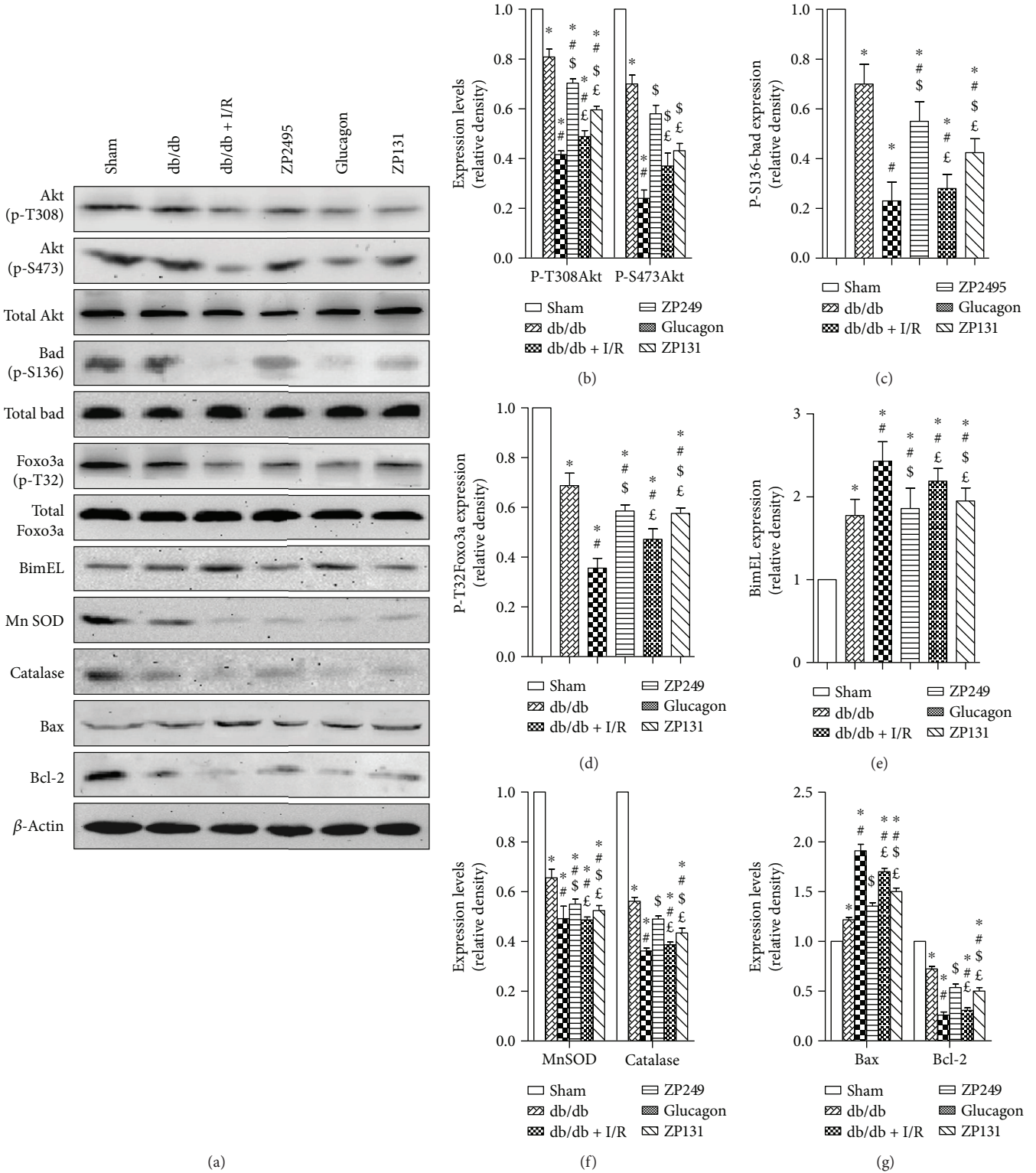


FIGURE 4: ZP2495 regulated Akt, FoxO3a, and apoptosis-related protein expression. (a) Representative blots of p-Akt, Akt, p-Bad, Bad, p-FoxO3a, FoxO3a, BimEL, MnSOD, catalase, Bax, and Bcl-2 in cardiomyocyte of db/db mice subjected to I/R. (b–g) Semiquantitative analysis of the Western blots. Sham: BKS + sham group; db/db: db/db + sham group; I/R: db/db + I/R group; ZP2495: db/db + I/R + ZP2495 group; glucagon: db/db + I/R + glucagon group; and ZP131: db/db + I/R + ZP131 group. Presented values are mean \pm SEM. * P < 0.05 versus the sham group; # P < 0.05 versus the db/db group; ϵ P < 0.05 versus the db/db + I/R group; and ϵ P < 0.05 versus the db/db + I/R + ZP2495 group.

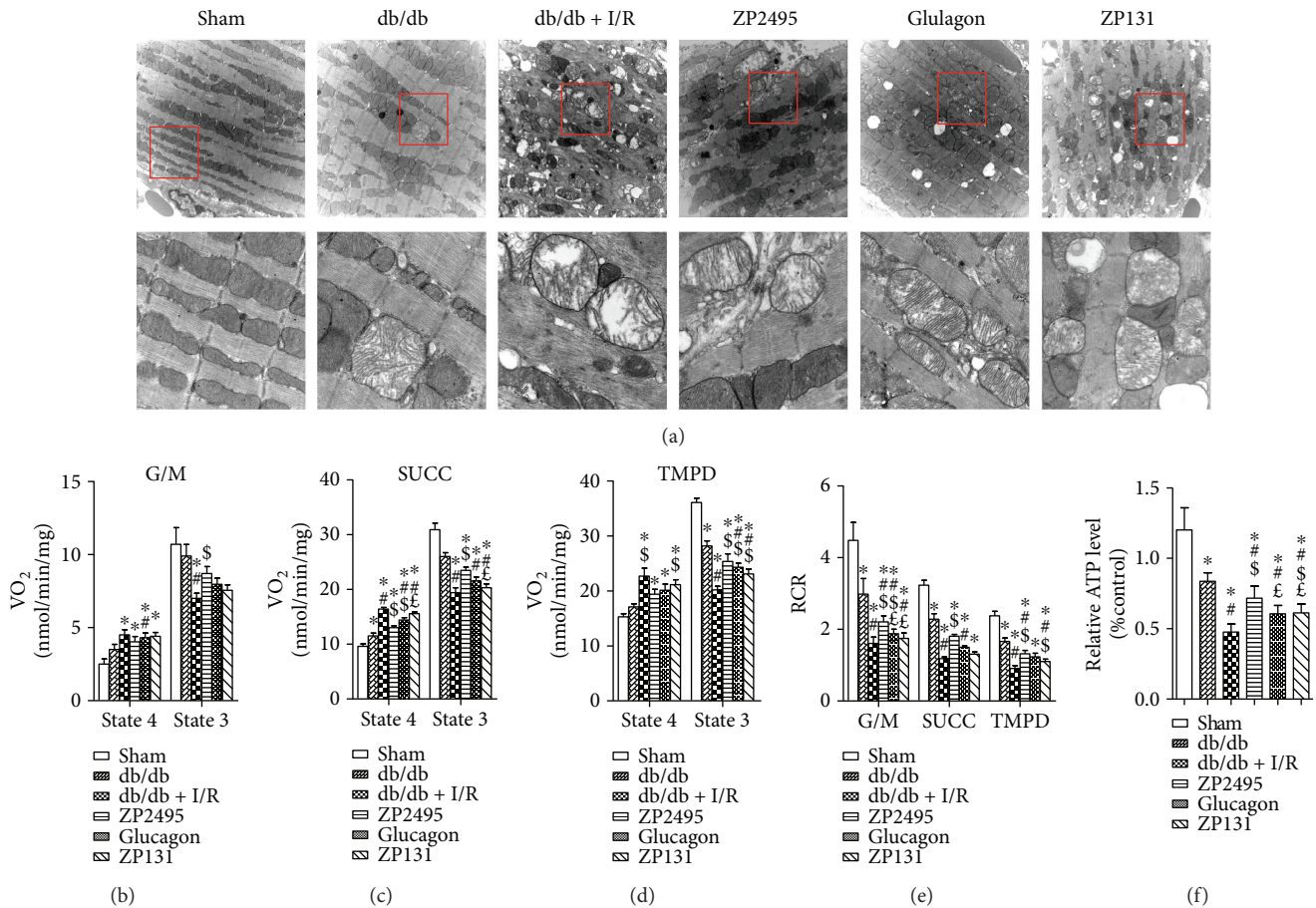


FIGURE 5: ZP2495 improved mitochondrial function and biogenesis in the myocardium of db/db mice subjected to I/R. (a) Representative transmission electron micrographs of mitochondria in the LV myocardium. Original magnification $\times 10,000$ (scale bar = $1 \mu\text{m}$) (A1) and $\times 40,000$ (scale bar = 250 nm) (A2). (b–d) Respiration in freshly isolated heart mitochondria from each group mice was analyzed with a SeaHorse XF96 analyzer. Mitochondria were assayed under state 4, that is, substrate but no ADP (sometimes also referred to as state 2), and state 3, that is, substrate and ADP present respiration (VO_2) with substrates from complex I (5 mmol/L G/M) (b), complex II (5 mmol/L Succ and $1 \text{ mmol/L rotenone}$) (c), and complex IV ($0.5 \text{ mmol/L N,N,N}_9\text{-tetramethyl-p-phenylenediamine (TMPD)}$ and $3 \text{ mmol/L sodium ascorbate}$) (d). State 3 was induced with 1 mmol/L ADP in all cases. (e) The RCR was determined as the ratio of state 3 to state 4. The bars plotted correspond to $n = 8$ replicates from two experiments. (f) Relative ATP level change in different treatments. Sham: BKS + sham group; db/db: db/db + sham group; I/R: db/db + I/R group; ZP2495: db/db + I/R + ZP2495 group; glucagon: db/db + I/R + glucagon group; and ZP131: db/db + I/R + ZP131 group. Presented values are mean \pm SEM. * $P < 0.05$ versus the sham group; # $P < 0.05$ versus the db/db group; \$ $P < 0.05$ versus the db/db + I/R group; and $\epsilon P < 0.05$ versus the db/db + I/R + ZP2495 group.

emerging evidence suggests that derangements in cardiac energy metabolism play a fundamental role in the pathogenesis of diabetic cardiomyopathy. Recent studies focusing on the mitochondria show an important role of abnormal mitochondrial function [27]. Previous studies revealed that glucagon-GLP-1 dual-agonist ZP2495 was superior compared with glucagon alone in the improvement of cardiac function in subjects with insulin resistance (IR) [28]. The data by Axelsen et al. have presented that perfusion buffer containing ZP131 failed to change cardiac function in hearts from either control or IR rats compared with vehicle-perfused hearts. In contrast, glucagon and ZP2495 perfusion improved cardiac function in control hearts. By comparison, in hearts from IR rats, however, only ZP2495 significantly increased cardiac power. Although their findings did not elucidate the protective effect of ZP2495 in the presence of diabetes, these evidences might indicate the protective

role of ZP2495 in the diabetic heart because insulin resistance was usually conceived as the earlier stage of diabetes. Furthermore, ZP2495 increased glucose oxidation and glycolytic rates in IR hearts as glucagon did avoid the concomitant accumulation of AMP or ADP [28]. In line with these findings, in our current study, dual-agonist ZP2495 induced superior cardioprotection (decreased infarct size, enhanced cardiac function, and ameliorated cardiac apoptosis) in diabetic hearts subjected to myocardial I/R compared with that of ZP131 or glucagon, which might be ascribed to its stronger capacity to upregulate cardiac glucose metabolism and mitochondrial function as compared to ZP131 or glucagon. Taken together, both our studies depicted the superiority of dual-agonist ZP2495 compared with ZP131 or glucagon in the treatment of cardiometabolic diseases with cardiac glucose metabolism defects.

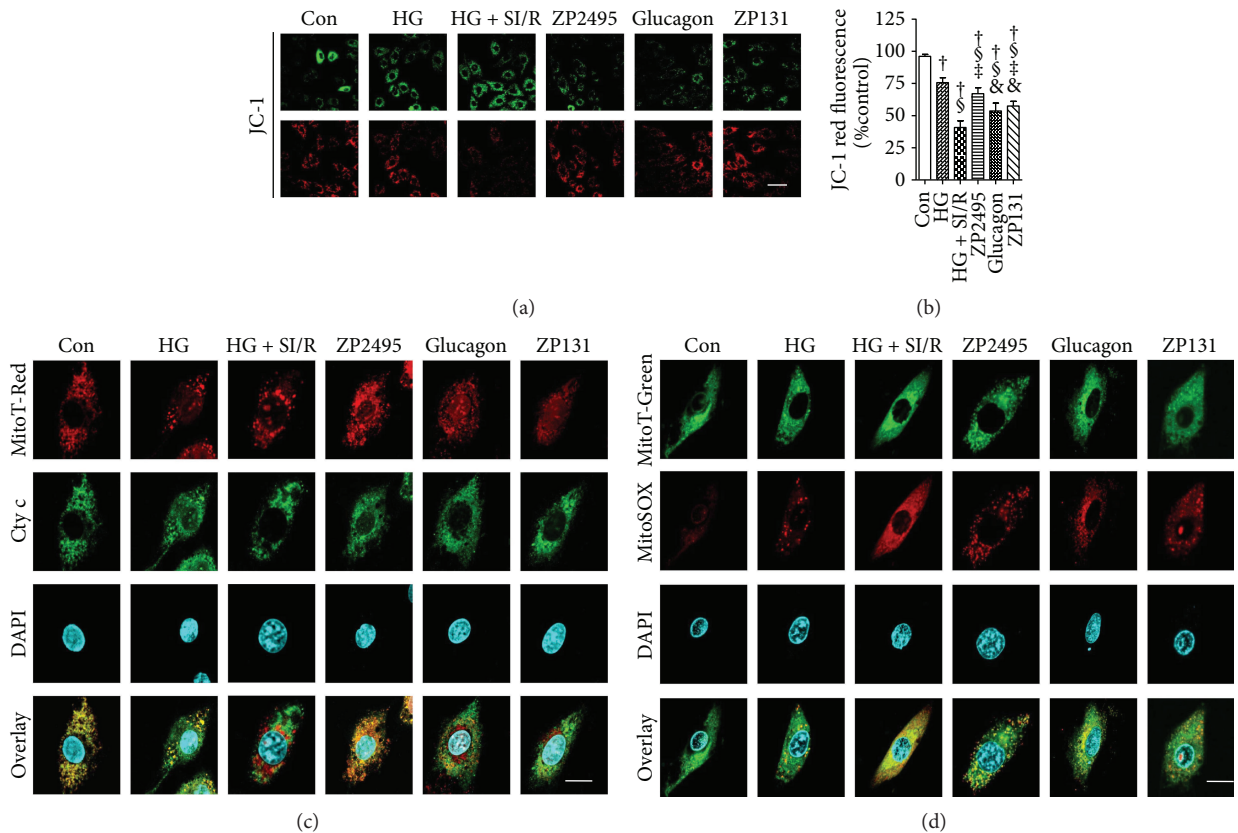


FIGURE 6: ZP2495 prevented high-glucose and SI/R-induced mitochondrial depolarization and decreased cytochrome c release and reactive oxygen species (ROS) generation from mitochondria in NRVMs. (a) Mitochondrial membrane potential (MMP) was analyzed by JC-1 fluorescence. Upper panels of green fluorescence indicated cellular uptake of JC-1, while lower panels of red fluorescence suggested intact mitochondria. HG and SI/R-treated NRVMs showed significantly reduced red fluorescence as compared with the control group, whereas ZP2495 treatment prevented the breakdown of the MMP as indicated by preservation of the red JC-1 fluorescence (scale bar = 100 μm). (b) FACS analyses of three independent experiments with 10,000 cells per treatment condition reveal a decrease of the red JC-1 fluorescence to 41% of control levels after HG and SI/R treatment, which was prevented by ZP2495. (c) Mitotracker red fluorescence (red), cytochrome c immunoreactivity (green), DAPI staining (blue), and merged images (yellow indicates sites of colocalization) in NRVMs. Note the localization of cytochrome c in mitochondria in the NRVM control cells and ZP2495-treated cells and the diffused localization of cytochrome c in the cytoplasmic compartment of NRVM cells in HG- and SI/R-treated cultures. Representative of 25–30 cells each in 3 separate experiments (scale bar = 20 μm). (d) ROS stained with MitoSOX (red) were colocalized with MitoTracker (green). Representative of 25–30 cells each in 3 separate experiments (scale bar = 20 μm). Con: normal glucose medium group; HG: high-glucose medium group; HG + SI/R: HG + SI/R group; ZP2495: HG + SI/R + ZP2495 group; glucagon: HG + SI/R + glucagon group; and ZP131: HG + SI/R + ZP131 group. Presented values are mean \pm SEM. $^{\dagger}P < 0.05$ versus the control group; $^{\ddagger}P < 0.05$ versus the HG group; $^{\S}P < 0.05$ versus the HG + SI/R group; $^{\&}P < 0.05$ versus the HG + SI/R + ZP2495 group.

The present study demonstrates that the metabolic effects observed in different regions of the ischemia-injured heart may in large part contribute to the cardioprotection observed with GLP-1 treatment [29]. However, our current study failed to analyze metabolic changes triggered by treatments in terms of ischemic versus remote regions. These changes could provide more information about a metabolic shift in viable regions of the hearts subjected to I/R injury, and we will explore this operation in our future experiments.

Myocardial I/R injury can induce additional injury to the myocardium, due to excessive oxygen free radicals, calcium overload, neutrophil infiltration, depletion of energy stores, and changes in subcellular activities including the opening of the mitochondrial permeability transition pore (MPTP) [30]. All of these changes are detrimental to ischemic cardiomyocyte and may reduce the beneficial effects of reperfusion

[31]. Notably, the mechanisms activating during ischemia may lead to necrotic cell death in cardiomyocytes, while hallmarks of apoptosis mainly occur after reperfusion [32]. Accordingly, both necrotic and apoptotic cardiomyocyte cell deaths contribute to the final myocardial infarction (MI) size. Enormous preclinical and clinical studies have demonstrated that diabetes will increase the vulnerability of diabetic hearts subjected to ischemic injury and result in higher mortality [33]. Our results from the present study exhibited that ZP2495 significantly reduced infarct size after cardiac I/R injury in db/db mice, mainly by exerting an antiapoptotic effect on cardiomyocyte both *in vivo* and *in vitro*.

Cardiac mitochondria are vital organelles that supply energy to support the high ATP consumption of a beating heart [34]. The irreversible mitochondrial dysfunction is a crucial event in cardiomyocyte death during myocardial I/R

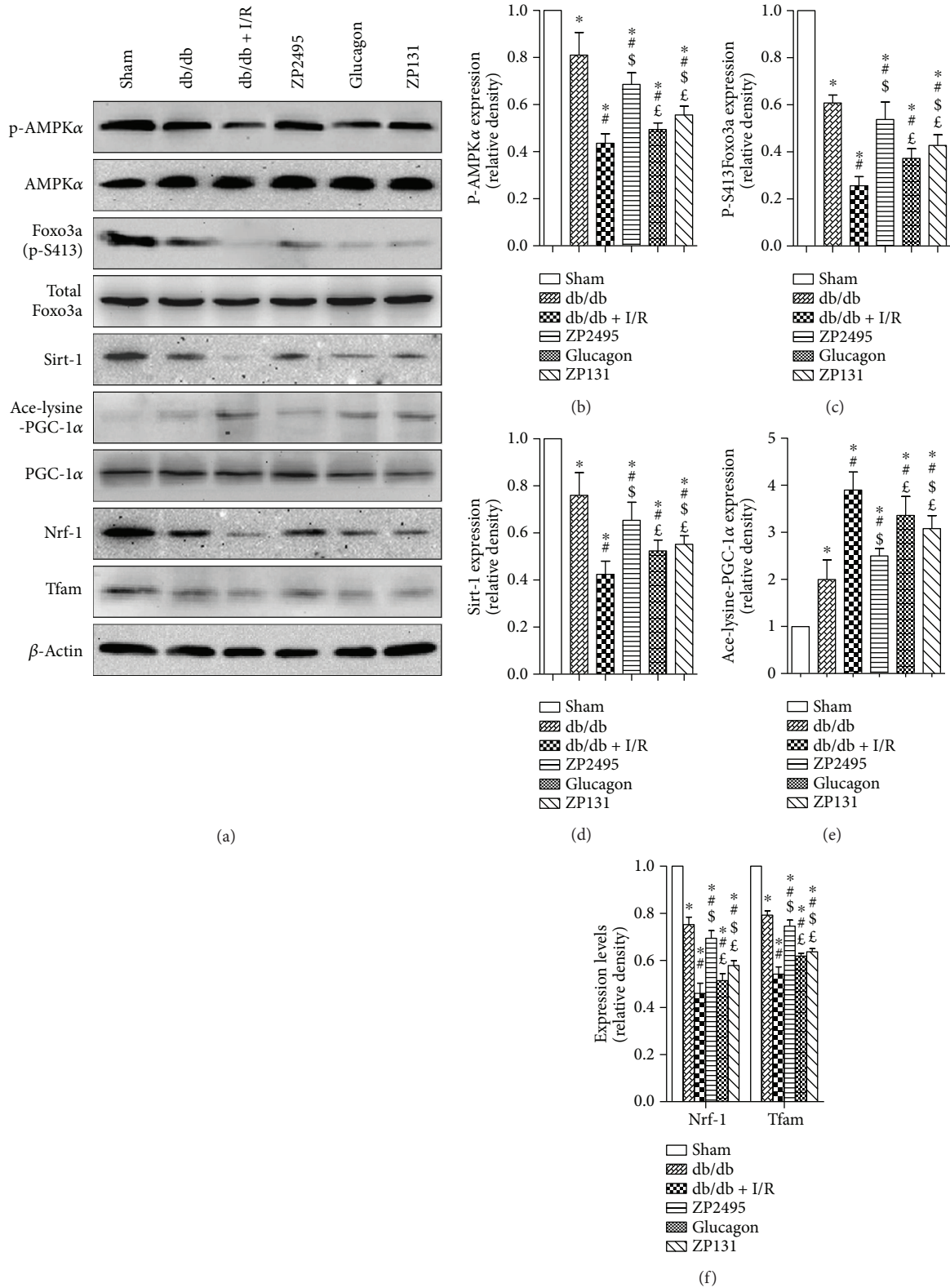


FIGURE 7: ZP2495 increased mitochondrial biogenesis in hearts of db/db mice subjected to I/R. (a) Representative blots of p-AMPK, AMPK, p-FoxO3a, FoxO3a, Sirt1, Ace-lysine-PGC-1 α , PGC-1 α , Nrf-1, and Tfam in cardiomyocyte of db/db mice subjected to I/R. (b-e) Semiquantitative analysis of the Western blots. Sham: BKS+sham group; db/db: db/db+sham group; I/R: db/db+I/R group; ZP2495: db/db+I/R+ZP2495 group; glucagon: db/db+I/R+glucagon group; ZP131: db/db+I/R+ZP131 group. Presented values are mean \pm SEM. * $P < 0.05$ versus the sham group; # $P < 0.05$ versus the db/db group; \$ $P < 0.05$ versus the db/db+I/R group; and £ $P < 0.05$ versus the db/db+I/R+ZP2495 group. Data shown are representative of six independent experiments.

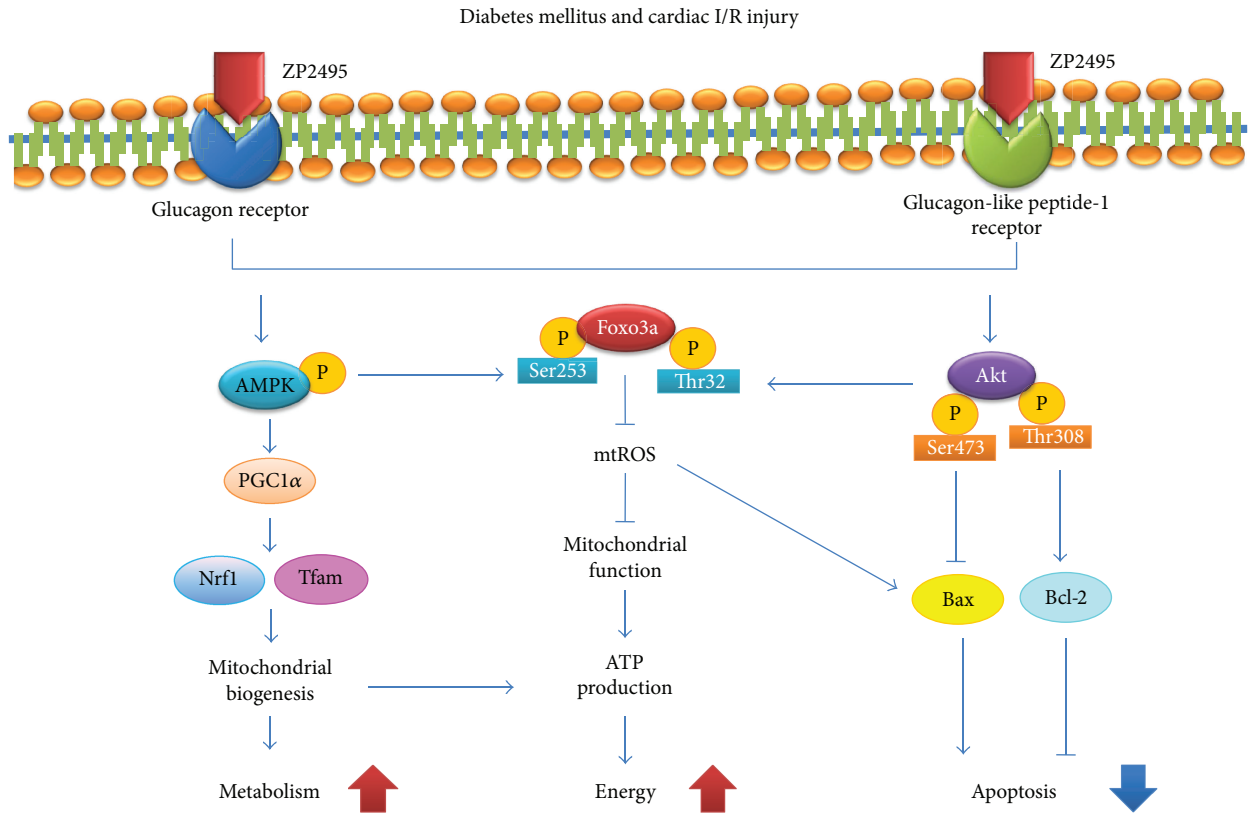


FIGURE 8: Proposed scheme for the protective effect of ZP2495 on cardiomyocyte. A summary of our current hypothesis about the mechanisms that the glucagon and GLP-1 dual-agonist (ZP2495) protects against myocardial I/R injury in db/db diabetic mice. The protective effects of ZP2495 may be associated with the activation of Akt/FoxO3 and AMPK/FoxO3a signaling pathways.

injury. After reperfusion, intracellular Ca^{2+} elevation triggers mPTP opening, leading to the depletion of ATP and loss of mitochondrial integrity [35, 36]. Therefore, alleviating mitochondrial dysfunction may decrease cardiac I/R injury. Meanwhile, modulating mitochondrial function may improve insulin resistance and reduce subsequent cardiac mortality. In addition, many studies have documented signs of mitochondrial dysfunction, including impaired respiration, damaged oxidative phosphorylation, altered substrate utilization, decreased ATP production, and impaired ATP transfer [37]. In the present study, we observed both structural and functional mitochondrial impairment in the myocardium of db/db mice subjected to cardiac I/R injury. ZP2495 treatment improved mitochondrial ultrastructural morphology. These findings were in line with the alleviated functional damage observed in the mitochondria in ZP2495-treated mice.

A large accumulation of myocardial mitochondrial ROS was observed in both permanently occluded and reperfused myocardia, especially in diabetic animals, suggesting that oxidative stress in mitochondrial may contribute to cardiac dysfunction [4]. It would result in electron transport chain deterioration, mitochondrial membrane depolarization, apoptotic pathway activation, and cardiomyocyte death [4, 38]. In this study, administration of ZP2495 reduced high-glucose and SI/R injury-induced mitochondrial ROS generation, which may be responsible for preventing mitochondrial

depolarization and attenuating the release of cytochrome c. These observations provide strong evidence for the notion that reduction in cardiac mitochondrial injury may represent a critical event in the cardioprotective effect of ZP2495.

Several studies have found that PGC-1 α is important for controlling metabolic pathways in the heart during development as well as in response to physiological stressors and pathological stimuli [39, 40]. PGC-1 α is a positive regulator of mitochondrial biogenesis and respiration and plays roles in neurodegenerative disorders and heart failure and pathological conditions that are strongly associated with mitochondrial defects [39]. Recent studies have shown that PGC-1 α acetylation was a kind of protein modification with inactivation effects [41]. PGC-1 α activity has also been reported to be modulated by several modifications, such as phosphorylation by AMPK or deacetylation by AMPK and sirtuin 1 (SIRT1). In the current study, we observed that ZP2495 upregulated PGC-1 α and its downstream Nrf-1 and Tfam expressions, which was associated with an increase in mitochondrial DNA copies in db/db mouse hearts. These results indicated that ZP2495 may exhibit its effect of cardioprotection through improving mitochondrial biogenesis by activating the AMPK/PGC-1 α pathway.

Another important observation of our study is that FoxO3a may play an important role in protecting the myocardium from injury. The FoxO transcription factors, including FoxO1, FoxO3a, FoxO4, and FoxO6, belong to the

forkhead family of transcriptional regulators. FoxO transcription factors have been implicated in regulating diverse cellular functions such as differentiation, metabolism, proliferation, and apoptosis [42, 43], especially for Akt-mediated antiapoptotic properties [23]. Furthermore, FoxO3a has been considered a converging point for Akt and AMPK signaling pathways [44, 45]. AMPK phosphorylation of FoxO3a at the site of Ser413 enhances the stress resistance and longevity [46–50]. On the other hand, Akt phosphorylation of FoxO3a at Thr32 site inhibits FoxO3a transcriptional activity, promoting antiapoptosis and insulin sensitivity [51]. Therefore, Akt and AMPK signaling may elicit transcriptional regulation via FoxO3a to allow organismal adaptation for physiological or pathophysiological changes. The convergence of the two pathways at the level of FoxO3a may play a critical role in the crosstalk between Akt and AMPK. Our data revealed that the protective effect of ZP2495 was related to FoxO3a activation mediated by the PI3K/Akt and AMPK pathways. We found that ZP2495 phosphorylated FoxO3a to inhibit the transcription of proapoptotic gene Bim, which resulted in decreased expression of proapoptotic proteins such as Bim and Bax. Consequently, cytochrome c was released into the cytosol and the caspase cascade was activated. In parallel, ZP2495 increased levels of the antiapoptotic proteins Bad and Bcl-2, which alleviated the apoptosis induced by diabetes and cardiac I/R injury. Collectively, we demonstrated that ZP2495 exerted an antiapoptotic effect by inhibiting ROS production, cytochrome c release, and caspase-3 activation through Akt/FoxO3a and AMPK/FoxO3a pathways. In the present study, myocardial I/R injury induced loss of phosphorylation of Akt and AMPK in db/db mice. These data suggested a potential role of Akt-FoxO3a and AMPK-FoxO3a in cardiac I/R injury and diabetes-induced mitochondrial dysfunction and apoptosis. Our data revealed a novel mechanism whereby ZP2495 exerted its protective effect by activating FoxO3a through the Akt and AMPK signaling pathways.

4.1. Limitations. Other members of the RISK pathway may also participate in the link between ZP2495 and its cardiac protection effects. In order to further demonstrate the efficacy of ZP2495 administration on cardiomyocyte mitochondrial biogenesis and function, AMPK-related pathways should be investigated in future studies. More studies should be performed to figure out whether ZP2495 activates Akt/FoxO3a and AMPK/FoxO3a pathways by different mechanisms in diabetic mice or nondiabetic mice which underwent cardiac I/R injury.

5. Conclusion

In conclusion, we provided evidences that glucagon and GLP-1 dual-agonist ZP2495 protected against myocardial I/R injury in db/db mice, which may be attributed to the improvement of cardiac mitochondrial function and energy metabolism. These protective effects of ZP2495 might be associated with Akt/FoxO3a and AMPK/FoxO3a signaling pathways.

Disclosure

This work was presented at The 25th Great Wall International Congress of Cardiology 2014. The corresponding meeting abstract (GW25-e4495) was also presented in Supplement of *Journal of the American College of Cardiology* (JACC, 21; 64(16):C44. DOI:10.1016/j.jacc.2014.06.213).

Conflicts of Interest

The authors have declared that no competing interest exists.

Acknowledgments

This work was supported by the National Key Research Project (2016YFA0100903), China National Funds for Distinguished Young Scientists (81325009), National Nature Science Foundation of China (nos. 81270168, 81300149, 81530058, and 81570272), Innovation Team Grant of Shanxi Province (no. 2014KCT-20) to Feng Cao (BWS12J037), and Beijing Natural Science Foundation (7152131).

References

- [1] ACCORD Study Group, H. C. Gerstein, M. E. Miller et al., “Long-term effects of intensive glucose lowering on cardiovascular outcomes,” *The New England Journal of Medicine*, vol. 364, no. 9, pp. 818–828, 2011.
- [2] R. W. Coch and J. B. Green, “Current cardiovascular outcomes trials in type 2 diabetes: perspectives and insight,” *Nutrition, Metabolism & Cardiovascular Diseases*, vol. 26, no. 9, pp. 767–772, 2016.
- [3] D. Sun, K. Narsinh, H. Wang et al., “Effect of autologous bone marrow mononuclear cells transplantation in diabetic patients with ST-segment elevation myocardial infarction,” *International Journal of Cardiology*, vol. 167, no. 2, pp. 537–547, 2013.
- [4] S. Koka, A. Das, F. N. Salloum, and R. C. Kukreja, “Phosphodiesterase-5 inhibitor tadalafil attenuates oxidative stress and protects against myocardial ischemia/reperfusion injury in type 2 diabetic mice,” *Free Radical Biology & Medicine*, vol. 60, pp. 80–88, 2013.
- [5] D. J. Drucker, S. I. Sherman, F. S. Gorelick, R. M. Bergenstal, R. S. Sherwin, and J. B. Buse, “Incretin-based therapies for the treatment of type 2 diabetes: evaluation of the risks and benefits,” *Diabetes Care*, vol. 33, no. 2, pp. 428–433, 2010.
- [6] D. J. Drucker, “The cardiovascular biology of glucagon-like peptide-1,” *Cell Metabolism*, vol. 24, no. 1, pp. 15–30, 2016.
- [7] M. Wallner, E. Kolesnik, K. Ablasser et al., “Exenatide exerts a PKA-dependent positive inotropic effect in human atrial myocardium: GLP-1R mediated effects in human myocardium,” *Journal of Molecular and Cellular Cardiology*, vol. 89, Part B, pp. 365–375, 2015.
- [8] Z. Sun, G. Tong, T. H. Kim et al., “PEGylated exendin-4, a modified GLP-1 analog exhibits more potent cardioprotection than its unmodified parent molecule on a dose to dose basis in a murine model of myocardial infarction,” *Theranostics*, vol. 5, no. 3, pp. 240–250, 2015.
- [9] S. P. Marso, G. H. Daniels, K. Brown-Frandsen et al., “Liraglutide and cardiovascular outcomes in type 2 diabetes,” *The New England Journal of Medicine*, vol. 375, no. 4, pp. 311–322, 2016.

- [10] A. Farah and R. Tuttle, "Studies on the pharmacology of glucagon," *The Journal of Pharmacology and Experimental Therapeutics*, vol. 129, pp. 49–55, 1960.
- [11] P. F. Mery, V. Brechler, C. Pavoine, F. Pecker, and R. Fischmeister, "Glucagon stimulates the cardiac Ca^{2+} current by activation of adenylyl cyclase and inhibition of phosphodiesterase," *Nature*, vol. 345, no. 6271, pp. 158–161, 1990.
- [12] S. E. Mayer, D. H. Namm, and L. Rice, "Effect of glucagon on cyclic 3',5'-AMP, phosphorylase activity and contractility of heart muscle of the rat," *Circulation Research*, vol. 26, no. 2, pp. 225–233, 1970.
- [13] W. C. Stanley, G. D. Lopaschuk, and J. G. McCormack, "Regulation of energy substrate metabolism in the diabetic heart," *Cardiovascular Research*, vol. 34, no. 1, pp. 25–33, 1997.
- [14] S. J. Henderson, A. Konkar, D. C. Hornigold et al., "Robust anti-obesity and metabolic effects of a dual GLP-1/glucagon receptor peptide agonist in rodents and non-human primates," *Diabetes, Obesity and Metabolism*, vol. 18, no. 12, pp. 1176–1190, 2016.
- [15] G. D. Lopaschuk, S. R. Wall, P. M. Olley, and N. J. Davies, "Etomoxir, a carnitine palmitoyltransferase I inhibitor, protects hearts from fatty acid-induced ischemic injury independent of changes in long chain acylcarnitine," *Circulation Research*, vol. 63, no. 6, pp. 1036–1043, 1988.
- [16] L. C. Heather, K. M. Pates, H. J. Atherton et al., "Differential translocation of the fatty acid transporter, FAT/CD36, and the glucose transporter, GLUT4, coordinates changes in cardiac substrate metabolism during ischemia and reperfusion," *Circulation: Heart Failure*, vol. 6, no. 5, pp. 1058–1066, 2013.
- [17] G. D. Lopaschuk, R. B. Wambolt, and R. L. Barr, "An imbalance between glycolysis and glucose oxidation is a possible explanation for the detrimental effects of high levels of fatty acids during aerobic reperfusion of ischemic hearts," *The Journal of Pharmacology and Experimental Therapeutics*, vol. 264, no. 1, pp. 135–144, 1993.
- [18] B. Liu, A. S. Clanachan, R. Schulz, and G. D. Lopaschuk, "Cardiac efficiency is improved after ischemia by altering both the source and fate of protons," *Circulation Research*, vol. 79, no. 5, pp. 940–948, 1996.
- [19] E. Gao, Y. H. Lei, X. Shang et al., "A novel and efficient model of coronary artery ligation and myocardial infarction in the mouse," *Circulation Research*, vol. 107, no. 12, pp. 1445–1453, 2010.
- [20] M. Zhang, D. Sun, S. Li et al., "Lin28a protects against cardiac ischaemia/reperfusion injury in diabetic mice through the insulin-PI3K-mTOR pathway," *Journal of Cellular and Molecular Medicine*, vol. 19, no. 6, pp. 1174–1182, 2015.
- [21] D. Sun, J. Huang, Z. Zhang et al., "Luteolin limits infarct size and improves cardiac function after myocardium ischemia/reperfusion injury in diabetic rats," *PLoS One*, vol. 7, no. 3, article e33491, 2012.
- [22] H. K. Gao, Z. Yin, N. Zhou, X. Y. Feng, F. Gao, and H. C. Wang, "Glycogen synthase kinase 3 inhibition protects the heart from acute ischemia-reperfusion injury via inhibition of inflammation and apoptosis," *Journal of Cardiovascular Pharmacology*, vol. 52, no. 3, pp. 286–292, 2008.
- [23] W. Yan, H. Zhang, P. Liu et al., "Impaired mitochondrial biogenesis due to dysfunctional adiponectin-AMPK-PGC-1 α signaling contributing to increased vulnerability in diabetic heart," *Basic Research in Cardiology*, vol. 108, no. 3, p. 329, 2013.
- [24] K. Esumi, M. Nishida, D. Shaw, T. W. Smith, and J. D. Marsh, "NADH measurements in adult rat myocytes during simulated ischemia," *The American Journal of Physiology*, vol. 260, 6, Part 2, pp. H1743–H1752, 1991.
- [25] Z. Zhang, S. Li, M. Cui et al., "Rosuvastatin enhances the therapeutic efficacy of adipose-derived mesenchymal stem cells for myocardial infarction via PI3K/Akt and MEK/ERK pathways," *Basic Research in Cardiology*, vol. 108, no. 2, p. 333, 2013.
- [26] N. Li, Y. Yuan, S. Li et al., "PDE5 inhibitors protect against post-infarction heart failure," *Frontiers in Bioscience*, vol. 21, pp. 1194–1210, 2016.
- [27] S. Boudina, S. Sena, H. Theobald et al., "Mitochondrial energetics in the heart in obesity-related diabetes: direct evidence for increased uncoupled respiration and activation of uncoupling proteins," *Diabetes*, vol. 56, no. 10, pp. 2457–2466, 2007.
- [28] L. N. Axelsen, W. Keung, H. D. Pedersen et al., "Glucagon and a glucagon-GLP-1 dual-agonist increases cardiac performance with different metabolic effects in insulin-resistant hearts," *British Journal of Pharmacology*, vol. 165, no. 8, pp. 2736–2748, 2012.
- [29] K. Aravindhan, W. Bao, M. R. Harpel, R. N. Willette, J. J. Lepore, and B. M. Jucker, "Cardioprotection resulting from glucagon-like peptide-1 administration involves shifting metabolic substrate utilization to increase energy efficiency in the rat heart," *PLoS One*, vol. 10, no. 6, article e0130894, 2015.
- [30] G. Rosano, M. Fini, G. Caminiti, and G. Barbaro, "Cardiac metabolism in myocardial ischemia," *Current Pharmaceutical Design*, vol. 14, no. 25, pp. 2551–2562, 2008.
- [31] B. Ibanez, V. Fuster, J. Jimenez-Borreguero, and J. J. Badimon, "Lethal myocardial reperfusion injury: a necessary evil?," *International Journal of Cardiology*, vol. 151, no. 1, pp. 3–11, 2011.
- [32] R. A. Gottlieb, K. O. Bureson, R. A. Kloner, B. M. Babior, and R. L. Engler, "Reperfusion injury induces apoptosis in rabbit cardiomyocytes," *The Journal of Clinical Investigation*, vol. 94, no. 4, pp. 1621–1628, 1994.
- [33] L. Tao, E. Gao, X. Jiao et al., "Adiponectin cardioprotection after myocardial ischemia/reperfusion involves the reduction of oxidative/nitrosative stress," *Circulation*, vol. 115, no. 11, pp. 1408–1416, 2007.
- [34] H. Lemieux, S. Semsroth, H. Antretter, D. Hofer, and E. Gnaiger, "Mitochondrial respiratory control and early defects of oxidative phosphorylation in the failing human heart," *The International Journal of Biochemistry & Cell Biology*, vol. 43, no. 12, pp. 1729–1738, 2011.
- [35] B. A. Miller, N. E. Hoffman, S. Merali et al., "TRPM2 channels protect against cardiac ischemia-reperfusion injury: role of mitochondria," *The Journal of Biological Chemistry*, vol. 289, no. 11, pp. 7615–7629, 2014.
- [36] O. L. Woodman, R. Long, S. Pons, N. Eychenne, A. Berdeux, and D. Morin, "The cardioprotectant 3',4'-dihydroxyflavonol inhibits opening of the mitochondrial permeability transition pore after myocardial ischemia and reperfusion in rats," *Pharmacological Research*, vol. 81, pp. 26–33, 2014.
- [37] S. Arkat, P. Umbarkar, S. Singh, and S. L. Sitasawad, "Mitochondrial Peroxiredoxin-3 protects against hyperglycemia induced myocardial damage in diabetic cardiomyopathy," *Free Radical Biology & Medicine*, vol. 97, pp. 489–500, 2016.
- [38] G. Loor, J. Kondapalli, H. Iwase et al., "Mitochondrial oxidant stress triggers cell death in simulated ischemia-reperfusion,"

- Biochimica et Biophysica Acta (BBA) - Molecular Cell Research*, vol. 1813, no. 7, pp. 1382–1394, 2011.
- [39] B. N. Finck and D. P. Kelly, “Peroxisome proliferator-activated receptor γ coactivator-1 (PGC-1) regulatory cascade in cardiac physiology and disease,” *Circulation*, vol. 115, no. 19, pp. 2540–2548, 2007.
- [40] C. C. Huang, T. Wang, Y. T. Tung, and W. T. Lin, “Effect of exercise training on skeletal muscle SIRT1 and PGC-1 α expression levels in rats of different age,” *International Journal of Medical Sciences*, vol. 13, no. 4, pp. 260–270, 2016.
- [41] E. H. Jenninga, K. Schoonjans, and J. Auwerx, “Reversible acetylation of PGC-1: connecting energy sensors and effectors to guarantee metabolic flexibility,” *Oncogene*, vol. 29, no. 33, pp. 4617–4624, 2010.
- [42] A. van der Horst and B. M. T. Burgering, “Stressing the role of FoxO proteins in lifespan and disease,” *Nature Reviews Molecular Cell Biology*, vol. 8, no. 6, pp. 440–450, 2007.
- [43] Y. Wang, Y. Zhou, and D. T. Graves, “FOXO transcription factors: their clinical significance and regulation,” *BioMed Research International*, vol. 2014, Article ID 925350, 13 pages, 2014.
- [44] E. L. Greer, P. R. Oskoui, M. R. Banko et al., “The energy sensor AMP-activated protein kinase directly regulates the mammalian FOXO3 transcription factor,” *The Journal of Biological Chemistry*, vol. 282, no. 41, pp. 30107–30119, 2007.
- [45] S. Paula-Gomes, D. Gonçalves, A. Baviera, N. Zanon, L. Navegantes, and I. Kettelhut, “Insulin suppresses atrophy- and autophagy-related genes in heart tissue and cardiomyocytes through AKT/FOXO signaling,” *Hormone and Metabolic Research*, vol. 45, no. 12, pp. 849–855, 2013.
- [46] E. L. Greer, D. Dowlatshahi, M. R. Banko et al., “An AMPK-FOXO pathway mediates longevity induced by a novel method of dietary restriction in *C. elegans*,” *Current Biology*, vol. 17, no. 19, pp. 1646–1656, 2007.
- [47] C. Bodur, B. Karakas, A. C. Timucin, T. Tezil, and H. Basaga, “AMP-activated protein kinase couples 3-bromopyruvate-induced energy depletion to apoptosis via activation of FoxO3a and upregulation of proapoptotic Bcl-2 proteins,” *Molecular Carcinogenesis*, vol. 55, no. 11, pp. 1584–1597, 2016.
- [48] E. A. I. F. Queiroz, Z. B. Fortes, M. A. A. da Cunha, A. M. Barbosa, N. Khaper, and R. F. H. Dekker, “Antiproliferative and pro-apoptotic effects of three fungal exocellular β -glucans in MCF-7 breast cancer cells is mediated by oxidative stress, AMP-activated protein kinase (AMPK) and the forkhead transcription factor, FOXO3a,” *The International Journal of Biochemistry & Cell Biology*, vol. 67, pp. 14–24, 2015.
- [49] A. Shrestha, S. Nepal, M. J. Kim et al., “Critical role of AMPK/FoxO3A Axis in globular adiponectin-induced cell cycle arrest and apoptosis in cancer cells,” *Journal of Cellular Physiology*, vol. 231, no. 2, pp. 357–369, 2016.
- [50] W. Xia, F. Zhang, C. Xie, M. Jiang, and M. Hou, “Macrophage migration inhibitory factor confers resistance to senescence through CD74-dependent AMPK-FOXO3a signaling in mesenchymal stem cells,” *Stem Cell Research & Therapy*, vol. 6, no. 1, p. 82, 2015.
- [51] Y. G. Ni, N. Wang, D. J. Cao et al., “FoxO transcription factors activate Akt and attenuate insulin signaling in heart by inhibiting protein phosphatases,” *Proceedings of the National Academy of Sciences of the United States of America*, vol. 104, no. 51, pp. 20517–20522, 2007.

Research Article

Slower Dynamics and Aged Mitochondria in Sporadic Alzheimer's Disease

Patricia Martín-Maestro,^{1,2,3} Ricardo Gargini,¹ Esther García,^{1,2} George Perry,⁴ Jesús Avila,^{1,2} and Vega García-Escudero^{1,2,5}

¹Centro de Biología Molecular "Severo Ochoa" (UAM-CSIC), Nicolás Cabrera, 1. Cantoblanco 28049 Madrid, Spain

²Centro de Investigación Biomédica en Red de Enfermedades Neurodegenerativas (CIBERNED), Valderrebollo, 5, 28031 Madrid, Spain

³Brain and Mind Research Institute, Weill Cornell Medical College, Cornell University, 407 E 61st St. 1300 York Avenue, New York, NY 10065, USA

⁴University of Texas at San Antonio, One UTSA Circle, San Antonio, TX 78249-0667, USA

⁵Departamento de Anatomía, Histología y Neurociencia, Facultad de Medicina, UAM, Arzobispo Morcillo, 4, 28029 Madrid, Spain

Correspondence should be addressed to Jesús Avila; javila@cbm.csic.es and Vega García-Escudero; v.garcia-escudero@uam.es

Received 31 March 2017; Revised 25 July 2017; Accepted 17 August 2017; Published 19 October 2017

Academic Editor: Icksoo Lee

Copyright © 2017 Patricia Martín-Maestro et al. This is an open access article distributed under the Creative Commons Attribution License, which permits unrestricted use, distribution, and reproduction in any medium, provided the original work is properly cited.

Sporadic Alzheimer's disease corresponds to 95% of cases whose origin is multifactorial and elusive. Mitochondrial dysfunction is a major feature of Alzheimer's pathology, which might be one of the early events that trigger downstream principal events. Here, we show that multiple genes that control mitochondrial homeostasis, including fission and fusion, are downregulated in Alzheimer's patients. Additionally, we demonstrate that some of these dysregulations, such as diminished DLP1 levels and its mitochondrial localization, as well as reduced STOML2 and MFN2 fusion protein levels, take place in fibroblasts from sporadic Alzheimer's disease patients. The analysis of mitochondrial network disruption using CCCP indicates that the patients' fibroblasts exhibit slower dynamics and mitochondrial membrane potential recovery. These defects lead to strong accumulation of aged mitochondria in Alzheimer's fibroblasts. Accordingly, the analysis of autophagy and mitophagy involved genes in the patients demonstrates a downregulation indicating that the recycling mechanism of these aged mitochondria might be impaired. Our data reinforce the idea that mitochondrial dysfunction is one of the key early events of the disease intimately related with aging.

1. Introduction

Alzheimer's disease (AD) is a common and devastating dementia that is pathologically defined by the accumulation of extracellular amyloid beta- ($A\beta$ -) containing plaques and intraneuronal hyperphosphorylated Tau protein aggregates associated with neuronal loss in the cerebral cortex. Studies of whole-genome gene expression profiling have identified that AD patients exhibit mitochondrial impairment together with altered calcium signaling and inflammation [1]. Defects in mitochondrial function generate oxidative stress increase due to mitochondrial electron transport chain leakage. The generated reactive oxygen species (ROS) oxidize multiple cell components, being an important issue to trigger protein

misfolding [2]. It has been proposed that oxidative stress could be one of the primary events in the development of AD and plays a pivotal role in its pathogenesis [3, 4]. At the same time, mitochondria are targets of ROS causing the oxidation of their components increasing mitochondrial deterioration. This mitochondrial dysfunction may be one of the earliest and most prominent features of AD [5, 6]. Several works that show downregulation of mitochondrial genes in Alzheimer's have also demonstrated a reduced metabolic rate in the brain of these patients measured by fluorodeoxyglucose PET [7]. Metabolic abnormalities besides the damage of both components and the structure of mitochondria are well described in AD [8–10]. Moreover, several models have revealed that mitochondrial dysfunction triggers the aberrant

processing of APP and tau [11–15]. Another deregulated aspect in AD is calcium signaling, which is closely related to functional the status of mitochondria. Experimental models have demonstrated that mitochondrial dysfunction favors tau phosphorylation, microtubule depolymerization, and neurofibrillary tangle-like pathology [11]. Hippocampal neurons exhibited AD-like tau phosphorylation and high calcium levels due to glutamate exposition impairing mitochondrial function [16].

Mitochondria are dynamic organelles that continuously undergo fission and fusion events which are necessary for cell survival as well as adaptation to changing conditions needed for cell growth, division and morphology, and distribution of mitochondria [17]. Mitochondrial dynamics is regulated by a machinery involving large dynamin-related GTPases where mitofusin 1 (MFN1), mitofusin 2 (MFN2), and optic atrophy 1 (OPA1) are involved in mitochondrial fusion [18], whereas mitochondrial fission is mediated by dynamin-like protein 1 (DLP1) through the interaction with four mitochondrial receptor proteins [18–20]. Dynamic fusion and fission processes allow damaged mitochondria to be recycled by a degradation mechanism termed mitophagy [21]. This pathway is partially driven by PINK1 and PARK2. When mitochondria are damaged and membrane potential is lost, there is a rapid recruitment of PARK2 to the mitochondria mediated by PINK1 that promotes K63-linked ubiquitin chain signaling [22]. Adaptor proteins of the autophagic system that recognize the ubiquitinated cargo through ubiquitin-binding domains (UBDs) and microtubule-associated proteins 1A/1B light chain 3 (LC3)/GABAA receptor-associated protein (GABARAP) attach to autophagosomal membranes via an LC3-interacting region (LIR) [22]. The autophagy machinery promotes the ubiquitinated cargo engulfment by autophagosomes and its final degradation [23].

In AD, mitochondrial failure might arise from a deficient dynamic balance of mitochondrial fission and fusion that is greatly shifted toward fission, and it may result in the presence of dysfunctional mitochondria in damaged neurons as well as fibroblasts from AD patients characterized by their accumulation into the perinuclear areas [24, 25]. In addition, autophagy dysfunction in brain and peripheral tissues of AD patients is widely documented [26]. This has been mainly associated to reduce degradative function, insufficient lysosomal pH acidification, and low hydrolases activity [27, 28] impairing the recycling of damaged mitochondria and generating a mitophagy failure [26].

In the present work, we have demonstrated a downregulation of genes involved in mitochondrial dynamics as well as in autophagy and mitophagy in Alzheimer’s patients. Consequently, we have found slower mitochondrial dynamics correlating with diminished STOML2, MFN2, and DLP1 levels, showing the last one reduced mitochondrial localization, and therefore causing the accumulation of aged mitochondria in fibroblasts from AD patients.

2. Materials and Methods

2.1. Primary Cells and Culture Conditions. Primary skin fibroblasts were obtained from Coriell Institute for Medical

TABLE 1: Core set of fibroblast cell lines.

Line	Age/sex	Clinical diagnosis
AG11362	63/F	Nonaffected
AG05813	67/F	Nonaffected
AG07803	66/M	Nonaffected
AG07310	60/F	Nonaffected
AG11020	79/F	Nonaffected
AG05809	63/F	Moderate dementia
AG06263	67/F	Moderate dementia
AG06262	66/M	Moderate dementia
AG06869	60/F	Moderate dementia
AG05810	79/F	Severe dementia

Coriell Institute for Medical Research.

Research (NJ, USA). Five fibroblast cell lines from SAD patients and five correspondent apparently healthy sex- and age-matched samples have been used (see Table 1 for details about age, sex, and stage of the disease). Human fibroblasts were cultured in Dulbecco’s modified Eagle’s medium (DMEM) supplemented with 10% (*v/v*) heat-inactivated fetal bovine serum (FBS), 2 mM glutamine, 10 U/ml penicillin, and 10 μ g/ml streptomycin, in 5% CO₂ in a humid incubator at 37°C. The use of fibroblasts has been restricted to a maximum of 10 cell passages to avoid replicative senescence, and cultures were always kept below confluence.

2.2. Microarray Analysis. The analysis of specific gene expression profiling by array (Affymetrix Human Gene 1.0 ST Array) of DLP1, GDAP1, MIEF1, MFN2, OPA1, STOML2, Optineurin, ATG5, ATG12, Beclin1, PI3K class III, ULK1, AMBRA1, BNIP3, BNIP3L, FUNDC1, VDAC1, and VPC/p97 of human brain samples was retrieved from Berchtold data set [29]. This study contains 253 samples from 84 patients, of which 173 are samples of different brain zones of 56 healthy subjects (aged 20–99 years) and 80 are samples of different brain zones of 28 AD patients (aged 28–99 years). Microarray data were obtained from 4 brain regions: the hippocampus, entorhinal cortex, superior frontal cortex, and postcentral gyrus. A similar analysis was performed in an additional data set of human brain samples classified into healthy ($n = 47$) versus AD ($n = 32$) patients obtained from the Hisayama study [30]. Differences in gene expression between healthy and AD patients were calculated using Student’s *t*-test.

2.3. Antibodies. The primary antibodies used were TOMM20 (sc-11415), MFN2 (sc-515647), and STOML2 (sc-376165) and were purchased from Santa Cruz Biotechnology, Santa Cruz, CA, USA; DLP1 (611112, BD Biosciences); GAPDH (ab8245, Abcam, Cambridge, UK); and β -tubulin (T4026, Sigma-Aldrich). The secondary antibodies for Western blot studies were horseradish peroxidase-conjugated antimouse IgGs (P0161, DAKO) and for immunofluorescence were antirabbit IgGs alexa-488 or antimouse alexa-555 labelled (Molecular Probes, Millipore, Waltham, MA).

2.4. Western Blot Analysis. The cells and tissue samples were homogenized in lysis buffer (50 mM pH 7.5 HCl-Tris, 300 mM NaCl, 0.5% SDS, and 1% Triton X-100) and incubated 15 min at 95°C. Protein concentration of the extracts was measured using the DC protein assay kit (500–0111, Bio-Rad). Equal amounts of total protein extract from healthy and SAD cells were resolved by SDS-PAGE and then transferred to nitrocellulose (G9917809, Amersham, Germany) or PVDF (IPVH00010, Merck Millipore, Cork, Ireland) membranes. Western blot and immunoreactive proteins were developed using an enhanced chemiluminescence detection kit (NEL105001EA, Perkin Elmer) following instructions of the supplier. Quantification was performed by densitometry of the obtained bands in each lane with respect to the correspondent housekeeping protein such as GAPDH or β -tubulin band in each experiment (Quantity One software, Bio-Rad).

2.5. Lentivirus Production. Pseudotyped lentivectors were produced using reagents and protocols from Prof. Didier Trono. Briefly, viral stocks were produced by transient cotransfection of 293 T cells with 5 μ g of the corresponding lentivector plasmid, 5 μ g of the packaging plasmid pCMVdr8.74 (Addgene plasmid 22036) and 2 μ g of the VSV-G envelope protein plasmid pMD2G (Addgene plasmid 12259) using Lipofectamine and Plus reagents following instructions of the supplier (18324 and 11514, resp., Life Technologies). Lentiviral titer was calculated by infecting cells with increasing amounts of lentiviral supernatant, and the percentage of infected cells was detected by flow cytometry (FACSCalibur, BD Biosciences, San Jose, CA).

2.6. Mitochondrial Dynamics Study. Cells were infected at an approximate multiplicity of infection (MOI) of 5–10 with a lentivector encoding DsRed2-Mito construct obtained from Clontech (632421) that was kindly provided by Dr. Ismael Santa-María (Columbia University, NY). Cells were treated with 20 μ M carbonyl cyanide *m*-chlorophenylhydrazone (CCCP, Sigma, St. Louis Missouri) for 6 h and, in the reversible condition, CCCP was removed after 1 h and the medium was replaced for DMEM 10% FCS. After the treatments cells were fixed with 4% paraformaldehyde (PFA) and the mitochondrial pattern was observed with an Axioskop2 plus microscope coupled to a CCD color camera (Zeiss). For analysis, we used the Mitochondrial Network Analysis (MiNa) toolset, a combination of different ImageJ macros that allows the semiautomated analysis of mitochondrial networks in cultured mammalian cells [31]. Briefly, the image was converted to binary by thresholding following the conversion to a skeleton that represents the features in the original image using a wireframe of lines of one pixel wide. All pixels within a skeleton were then grouped into three categories: end point pixels, slab pixels, and junction pixels. The plugin analyzes how the pixels are spatially related and defined to measure the length of each branch and the number of branches in each skeletonized feature as well as the mitochondrial network morphology. The parameters used in the study were (1) individuals, punctate, rods, and large/round mitochondrial structures; (2) networks, mitochondrial structures with

at least a single node and three branches; (3) the mean number of branches per network; and (4) the average of length of rods/branches. Ten randomly chosen fields containing between 10 and 15 cells were used to quantify the pattern of mitochondria. We classify the mitochondrial morphology into three different subtypes according to the length of the branches: filamentous (long and spaghetti-like shape; branch $> 2.3 \mu\text{m}$), fragmented (completely dotted; branch $< 1.8 \mu\text{m}$), and intermediate pattern (when both filamentous and fragmented mitochondria were found; $1.8 \mu\text{m} \leq \text{branch} \leq 2.3 \mu\text{m}$).

2.7. Immunocytochemistry. Fibroblasts were grown on sterile glass coverslips, treated as described for each experiment, followed by washing with PBS and fixing with 4% PFA in PBS for 30 min at room temperature. After blocking with PBS containing 1% BSA and permeabilizing with 0.1% Triton X-100 and 1 M glycine for 30 minutes, cells were then stained with DLP1 and TOMM20 antibody diluted according to the manufacturer's recommendation in blocking buffer overnight at 4°C. Cells were washed with PBS and stained with secondary antibody (1:500 in blocking buffer) for 2 h at room temperature. Samples were mounted with ProLongGold Antifade (P-36930, Life Technologies) and randomly chosen field images were obtained in an Invert Confocal LSM510 (Zeiss, Oberkochen, Germany) fluorescence microscope.

2.8. Colocalization Study. Colocalization analysis was performed with ImageJ software (Bethesda, MD). The background of different channels was edited with the subtract background tool with a rolling ball radius of 30 pixels, and binary images were obtained by a threshold intensity. The logical operation AND of the Image Calculator tool was used to generate an image harboring only overlapping structures of both channels. Colocalization measurement was obtained by quantifying the area occupied by the overlapping elements per cell. At least 200 cells were measured for each cell line.

2.9. Mitochondrial Potential Measurement. After treatment, fibroblasts were incubated with 200 nM TMRM (T668, Molecular Probes, Waltham, MA, USA) for 30 min at 37°C and analyzed by flow cytometry (FACSCalibur, BD Biosciences). Mitochondrial membrane potential for each condition was represented as the percentage of the fluorescence intensity mean with respect to the fluorescence intensity mean exhibited when these cells remained untreated.

2.10. Study of Mitochondrial Age. MitoTimer transgene was amplified by PCR from the plasmid pTRE-Tight-MitoTimer (Plasmid number 50547, Addgene, MA, USA) using the oligos: CCTGGAGAATTCAGATCTCCAC and GATCCTGATCACTACAGGAACAGGTGGTGGC, and amplicon was cloned into lentiviral construct pLVX-TetOne-Puro (631849, Clontech, CA, USA) by restriction sites EcoRI and BclI. Fibroblasts were infected by packaged lentiviral particles at an approximated MOI of 5–10. Forty-eight hours postinfection, the expression of the transgene was induced with 2 $\mu\text{g}/\text{ml}$ of doxycycline during 24 h and then removed from the media to analyze it at different times.

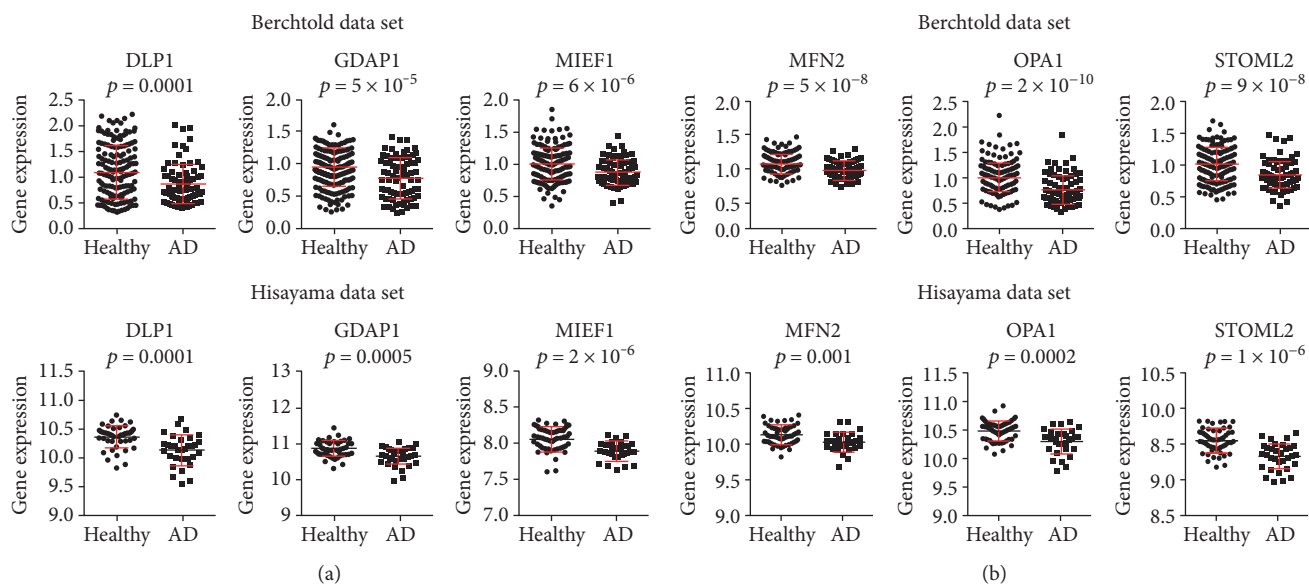


FIGURE 1: Downregulation of dynamics genes in AD brains. (a)-(b) Analysis of microarray expression in two independent data sets of genes involved in mitochondrial fission (a) and fusion (b). Graphs show dot plots of the expression of the indicated genes using in upper row $n = 253$ samples from 84 patients, of which $n = 56$ are healthy subjects and $n = 28$ are AD patients retrieved from Berchtold data set [29] and in lower row $n = 47$ controls and $n = 32$ AD brain samples from the Hisayama study data set [30]. Correspondent p value was determined by Student's t -test and is showed for each graph.

On the other hand, after 24 h of doxycycline, cells were treated with CCCP (20 μ M) for 24 h and then removed from media to be analyzed. Red and green fluorescence intensity was followed over time by flow cytometry (FACSCalibur, BD Biosciences). Aged mitochondrial quantification was calculated as the percentage of red fluorescence intensity mean at each point with respect to the one of the untreated cells at the beginning of the study (doxycycline removal, 0 h).

2.11. Statistical Analysis. Graphs represent means and standard deviations of the values obtained from experimental triplicates. When necessary, values represented in the graphs were obtained by normalizing every SAD sample data with its correspondent age-matched healthy sample. Statistical comparison of the data sets was performed by the Student's t -test. Two-way analysis of variance test was performed to examine the differences between experimental factors and their interaction. A post hoc Bonferroni test was used when more than two experimental groups were compared.

3. Results

3.1. Gene Expression Alteration of Mitochondrial Dynamics Proteins in AD Brains. Mitochondrial function disruption has been proposed long time ago as an early alteration in Alzheimer's pathology [32]. Mitochondria are a dynamic tubular network that undergo fission and fusion as a fundamental process for mitochondrial renewal and elimination of damaged ones [21]. Here, we observed that several fission proteins such as DLP1, GADP1, and MIEF1 appeared diminished in AD brain samples in Berchtold et al. [29] and Hokama et al. [30] data sets (Figure 1(a)). Multiple works

have shown DLP1 is recruited to mitochondria to constrict the membranes upon assembly into spirals and to induce the scission of mitochondria upon GTP hydrolysis [33]. Membrane stabilization of DLP1 is regulated by GADP1 and MIEF1 [33]. On the other hand, fusion proteins such as MFN2, OPA1, and STOML2 have been shown diminished in Alzheimer's brain in both data sets (Figure 1(b)). Fusion is coordinated by MFN1/2 and OPA1, where the first one catalyzes the fusion of external membrane and the second one is associated to the internal membrane [34, 35]. An additional system named hyperfusion is controlled by STOML2/OPA1, which is stimulated under stress conditions favoring cell survival [36]. In summary, we could observe that both fission and fusion processes were reduced in AD brain accordingly with the mitochondrial dysfunction that takes place in this pathology.

3.2. Downregulation of Mitochondrial Dynamics Proteins in SAD Fibroblasts. Taking into account the previous results, we next examined whether proteins that control mitochondrial dynamics could be altered in patient-derived peripheral cells such as fibroblasts. As several works have shown reduced levels of DLP1 in neurons as well as in fibroblasts from sporadic AD patients [37, 38], we focused our attention in this protein. We could observe a decrease in DLP1 fission protein level, in SAD cells as it was previously described by Zhu and coworkers [38] (Figure 2(a)). DLP1 function depends on its subcellular localization [39]; therefore, we studied its distribution by immunofluorescence analysis of mitochondria labeled with TOMM20 (Figure 2(b)). Quantitative analysis revealed a decrease of DLP1 on mitochondria in SAD fibroblasts compared to healthy ones (Figure 2(c)). Additionally, the mitochondrial surface was

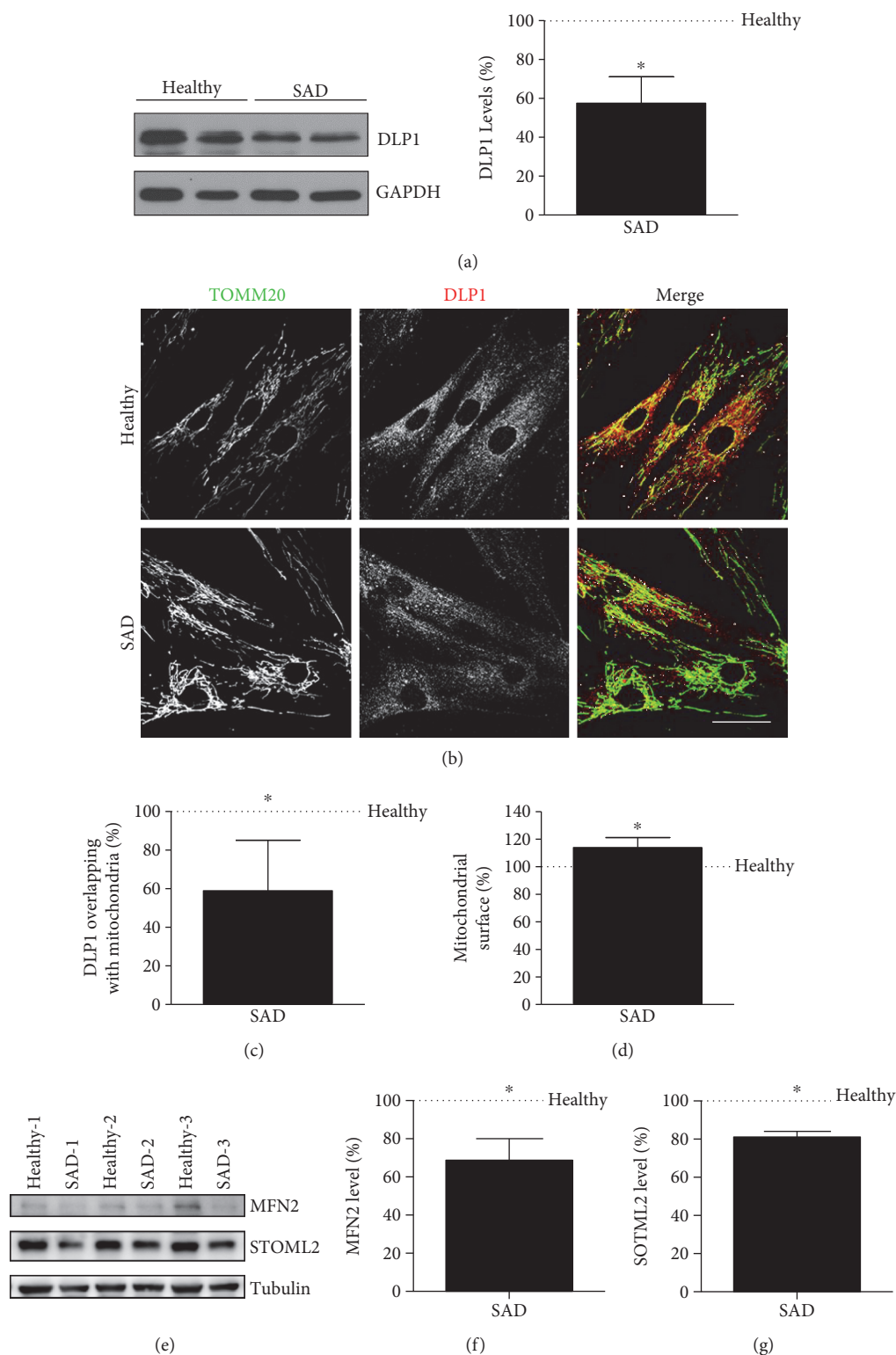


FIGURE 2: Decreased fission and fusion protein levels in SAD cells. (a) Representative Western blot analysis and quantification of DLP1 in healthy and SAD fibroblasts under basal conditions. (b) Representative confocal microscopy images showing TOMM20 in green and DLP1 in red in basal conditions. (c) Quantification of the amount of DLP1 in mitochondria per cell in the images represented in (b). (d) Quantification of mitochondrial surface measured by TOMM20 label per cell in the images represented in (b). (e)–(g) Representative Western blot analysis and quantification of MFN2/mitofusin 2 (f) and STOML2 (g) in healthy and SAD fibroblasts under basal conditions. Graphs show means and standard deviations of the healthy/AD age- and sex-matched couple samples: AG11020/AG05810 and AG11362/AG05809; AG07310/AG06869; AG05813/AG06263; AG07803/AG06262 (a)–(e) and AG11020/AG05810; AG11362/AG05809; and AG07310/AG06869 (g). Scale bar: 40 μ m. * p < 0.05.

increased in SAD fibroblasts with respect to the healthy ones (Figure 2(d)), as we have previously reported [26]. Finally, as it has been described for patients' brain [40], we have also observed diminished fusion protein levels such as MFN2/mitofusin2 and STOML2 in SAD fibroblasts (Figures 2(e), 2(f), and 2(g)). These data indicate that the putative mitochondrial defect associated to AD may be also found in fibroblasts.

3.3. Mitochondrial Dynamics Alteration in SAD Fibroblasts. Abnormal mitochondrial distribution and morphology have been described in SAD fibroblasts [38]. These data together with the downregulation of mitochondrial dynamics proteins previously described led us to conclude that mitochondrial dynamics may be altered in SAD fibroblasts. To seek for a possible functional defect in mitochondrial dynamics, we studied a reversible process of mitochondrial fragmentation. Healthy and SAD cells, which had similar growth rates, were plated and infected with a lentivector encoding Mito-DsRed2 for better mitochondria visualization and treated with carbonyl cyanide *m*-chlorophenylhydrazone (CCCP). These conditions induce a reversible depolarization of mitochondria without causing any toxic effect, and the viability of fibroblasts was not compromised (data not shown). The analysis of the images was done by the Mitochondrial Network Analysis (MiNa) toolset [31]. The patterns of mitochondria were classified into three categories according to the length of the branches: filamentous, fragmented, and intermediate (Figure 3(a); see Materials and Methods). Analysis was carried out by the quantification of mitochondrial shape in all the different experimental conditions. SAD and healthy cells exhibited similar mitochondrial pattern under resting conditions (Figure 3(b)) where most cells showed a filamentous and intermediate morphology. Conversely, the mitochondrial morphology was mainly fragmented when we treated the cells with CCCP for 7 h (Figure 3(c)).

Although there were no substantial differences in the static pictures before and after CCCP treatment between healthy and SAD fibroblasts, we sought for a possible alteration during the process of fragmentation or fusion as a consequence of the dynamic proteins' downregulation as described. With this aim, we carried out a time course analysis of the mitochondrial morphology recovery over the time. Thus, fibroblasts were treated with CCCP for 6 h ($t = 0$ h); afterwards, they were allowed to recover during different time points (Figure 3(d)). We saw that after CCCP removal, there was a rapid initial recovery of filamentous morphology of both healthy and SAD cells within the first 30 min. However, after this time point, there was no recovery of filamentous morphology in SAD cells in the following 30 min, contrary to healthy fibroblasts that exhibited a quicker increase of filamentous mitochondria. Moreover, we observed that both healthy and SAD fibroblasts recovered the filamentous morphology over the time up to the percentages of untreated cells (Figure 3(d), -360 min). Thus, we chose 1 h of recovery after CCCP treatment to analyze the mitochondrial morphology recovery in all the control/SAD fibroblasts couples used in this work (Figures 4(a), 4(b),

4(c), and 4(d)). As before, healthy and SAD cells exhibited similar mitochondrial pattern under resting conditions (Figures 4(a) and 4(b)) or after 7 h of CCCP treatment (Figures 4(a) and 4(c)). However, after the reversible challenge with CCCP, SAD fibroblasts exhibited significantly increased percentage of cells with fragmented mitochondria with respect to their correspondent healthy fibroblasts, which showed a significantly higher proportion of cells that had recovered filamentous morphology (Figures 4(a) and 4(d)). Additionally, we could observe that CCCP treatment induced similar mitochondrial potential membrane ($\Delta\Psi_m$) loss in healthy and SAD fibroblasts (Figure 4(e)). However, when these cells were allowed to recover, only healthy fibroblasts recovered $\Delta\Psi_m$ up to the levels of untreated cells (Figure 4(e)). On the contrary, SAD fibroblasts although some increase of $\Delta\Psi_m$ was observed indicating that cells tend to recover, there were no significant differences with respect to total CCCP condition and still maintaining significant differences with respect to untreated condition (Figure 4(e)). These results suggest a delayed recovery of mitochondrial filamentous morphology and membrane potential in SAD fibroblasts after a reversible insult.

Then, we moved further into the morphological features of mitochondria to study in detail the mitochondrial network. We examined the mitochondrial network skeleton in representative images of the three experimental conditions (control, reversion and total CCCP) in both healthy and SAD fibroblasts, and the network parameter values were then calculated (Figure 5(a)). Although, there were no differences in the number of individuals (puncta and rods mitochondrial structures, Figure 5(b)) as well as networks (mitochondrial structures with at least a single node and three branches, Figure 5(c)) between healthy and SAD cells, we observed that the treatment with CCCP increased the number of individuals and networks in both cases (Figures 5(b) and 5(c)). The augmented number of networks was related to the fragmentation of larger networks with more branches into many smaller networks as it was reflected by the decreased number of branches per network after the treatment with CCCP (Figure 5(d)). Additionally, we analyzed the length of the branches in each condition (Figure 5(e)). As expected, we saw that the branch length was remarkably diminished after the CCCP treatment in both cells lines (Figure 5(e)). Surprisingly, we noticed that after 1 h of recovery without CCCP, the length of the branches in SAD cells was the same than after 7 h of CCCP. In contrast, healthy fibroblasts exhibited a recovery of the branch length up to the values of the untreated condition, suggesting once again a delayed recovery of the mitochondrial network in SAD cells (Figure 5(e)).

3.4. Increased Mitochondrial Aging in SAD Fibroblasts due to Recycling Impairment. To investigate whether the mitochondrial dynamics failure could affect the quality of the mitochondria, we analyzed the mitochondrial turnover in healthy and SAD fibroblasts by using the MitoTimer tool. With this aim, we cloned the MitoTimer gene [41] into a lentiviral vector that encodes all the regulatory elements to allow transgene expression activation in response to doxycycline, pLVX-TetOne-Puro (631849, Clontech, CA, USA).

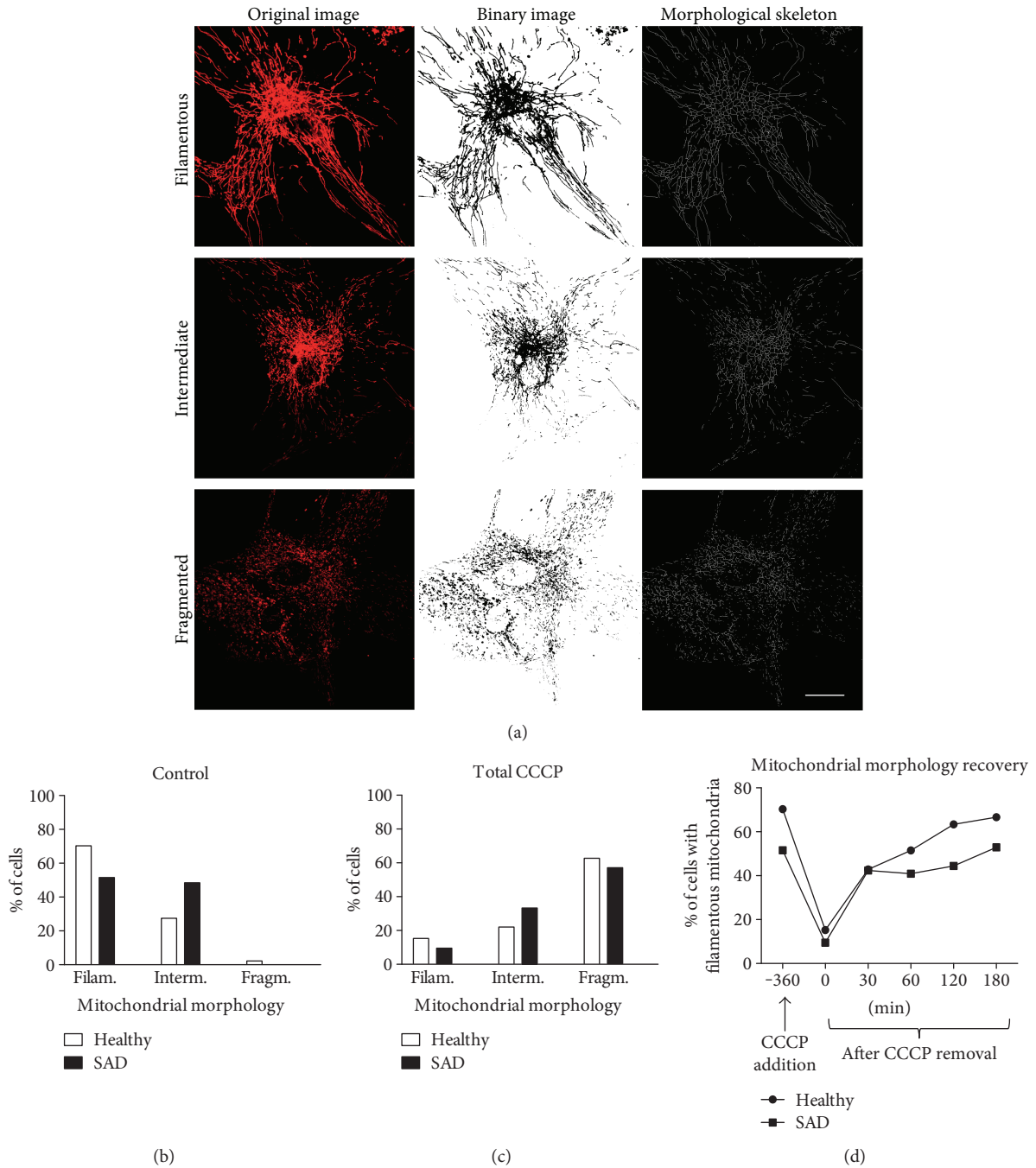


FIGURE 3: Mitochondrial dynamics alterations in SAD fibroblasts. (a) Representative confocal microscopy images showing the three different mitochondrial morphologies in which they will be classified followed by binary image and the subsequently morphological skeleton generated by Mitochondrial Network Analysis (MiNa) toolset [31]. (b)–(c) Quantification of mitochondrial morphology of healthy and SAD couple under basal conditions (b) and treated with 20 μ M CCCP for 7 h (c). (d) Time course of the mitochondrial morphology recovery in healthy and AD fibroblasts reversibly treated with CCCP. Mitochondrial morphology classification according to the length of the branches in filamentous (branch $> 2.3 \mu$ m), fragmented (branch $< 1.8 \mu$ m), and intermediate ($1.8 \geq$ branch $\geq 2.3 \mu$ m) patterns. Graphs represent the data of AG11362/AG05809 healthy/AD age- and sex-matched couple. Scale bar: 40 μ m.

MitoTimer provides a fluorescent readout which directly relates to the mitochondrial turnover and quality control described in several studies based on a time-sensitive fluorescent protein fused to the mitochondrial targeting sequence of COX8A subunit, which targets MitoTimer to the

mitochondrial matrix. Timer, initially fluorescence green, changes over time so the emission shifts from green to red. Healthy and SAD fibroblasts were infected with the lentivirus encoding MitoTimer and, after 48 h, transgene expression was induced by doxycycline treatment for 24 h, after what CCCP was added during 24 h (Figure 6(a)). We

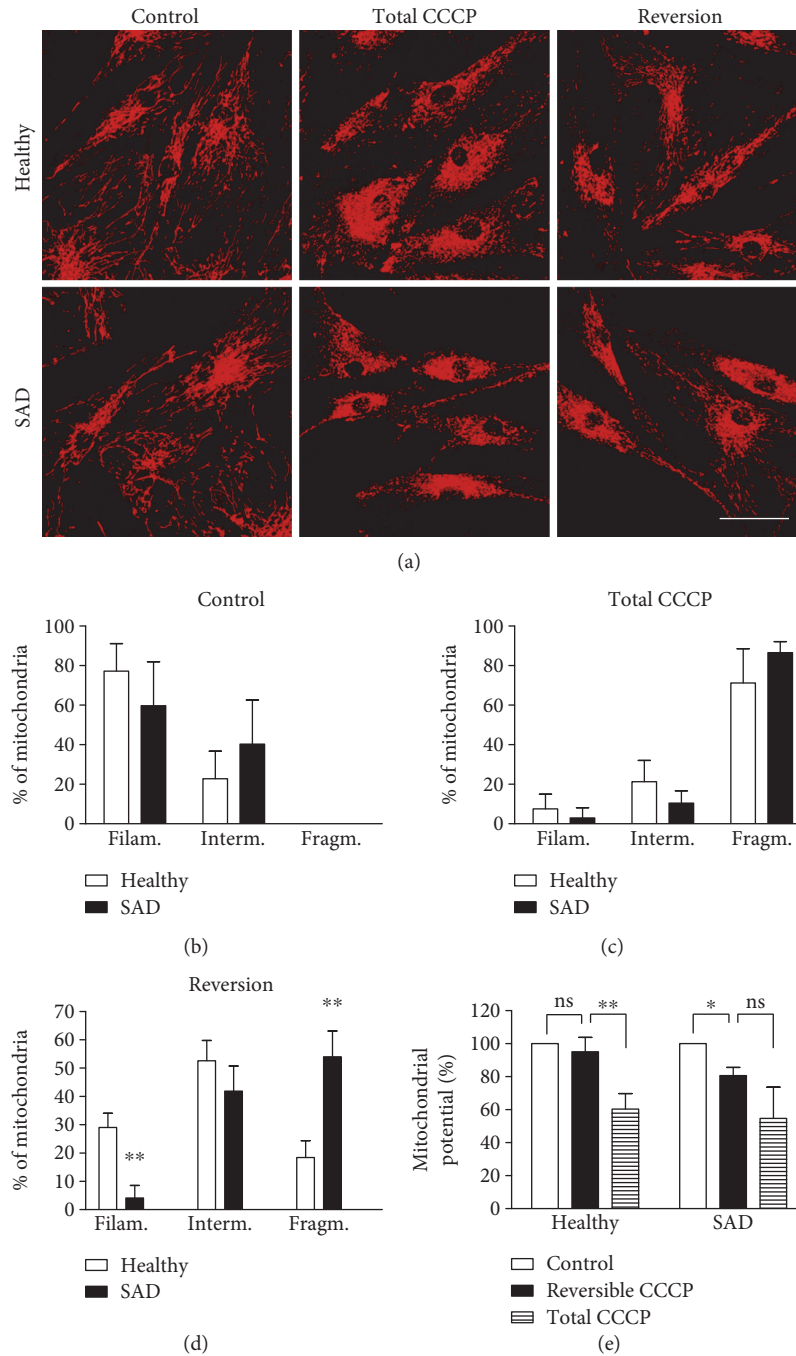


FIGURE 4: Delayed recovery of mitochondrial filamentous morphology in SAD fibroblasts. (a) Representative confocal microscopy images showing the mitochondrial morphology of healthy and SAD fibroblasts untreated (control), after 7 h with 20 μM CCCP (total CCCP) or after 6 h of CCCP treatment followed by 1 h without it (reversion). (b)–(d) Quantification of mitochondrial morphology of healthy-SAD couples when the cells remain untreated (b), treated with CCCP for 7 h (c), or reversibly treated with CCCP (d). (e) Mitochondrial membrane potential measured by TMRM of fibroblasts treated as in (a). Mitochondrial morphology classification according the length of the branches in filamentous (branch $> 2.3 \mu\text{m}$), fragmented (branch $< 1.8 \mu\text{m}$), and intermediate ($1.8 \geq \text{branch} \geq 2.3 \mu\text{m}$) patterns. $n = 3$ different healthy/AD sex- and age-matched couple samples: AG11362/AG05809, AG07310/AG06869, and AG11362/AG05809. Scale bar: 40 μm . * $p < 0.05$ and ** $p < 0.01$; ns: not significant.

monitored by flow cytometry the amount of aged mitochondria measured by red fluorescence. After doxycycline removal, aged mitochondria were increased similarly in both healthy and SAD fibroblasts during the first 24 h (Figure 6(b), 24 h). However, the recycling of these aged mitochondria

was slightly faster in healthy cells with respect to SAD ones (Figure 6(b), 48 h). When we boosted mitochondrial recycling process by the addition of CCCP, we could observe that aged mitochondria were diminished in healthy fibroblasts due to an efficient degradation of dysfunctional

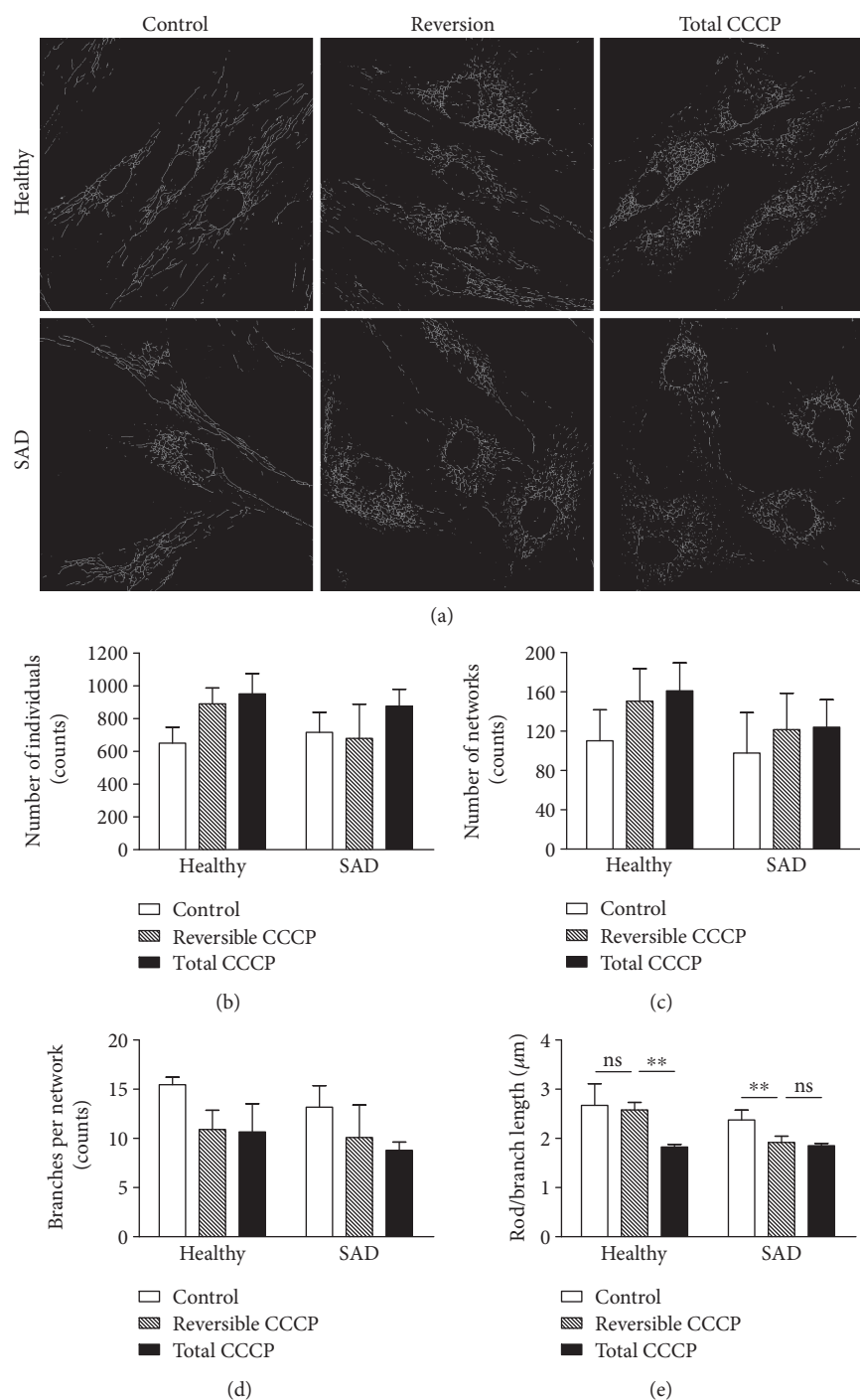


FIGURE 5: Analysis of mitochondria network. (a) Representative images showing mitochondrial morphological skeleton obtained with MiNa toolset [31] of healthy and SAD fibroblasts untreated (control), after 6 h of CCCP treatment followed by 1 h without it (reversion) or after 7 h with 20 μM CCCP (total CCCP). (b)–(e) Quantification of number of individuals (b), networks (c), branches per network (d), or length of the branches (e) of $n = 3$ different healthy/AD sex- and age-matched couple samples: AG11362/AG05809, AG07310/AG06869, and AG11362/AG05809. ** $p < 0.01$; ns: not significant.

mitochondria (Figure 6(c), 24 h healthy). Meanwhile, in SAD fibroblasts, there was no degradation of aged mitochondria during the treatment with CCCP (Figure 6(c), 24 h SAD). After removal of CCCP, there were still significant differences in the amount of aged mitochondria

between healthy and SAD fibroblasts (Figure 6(c), 48 h), correlating with our previous results of a slower mitochondrial dynamics and membrane potential recovery. Our results indicate that SAD fibroblasts exhibited aged mitochondria compared to healthy cells and the recycling

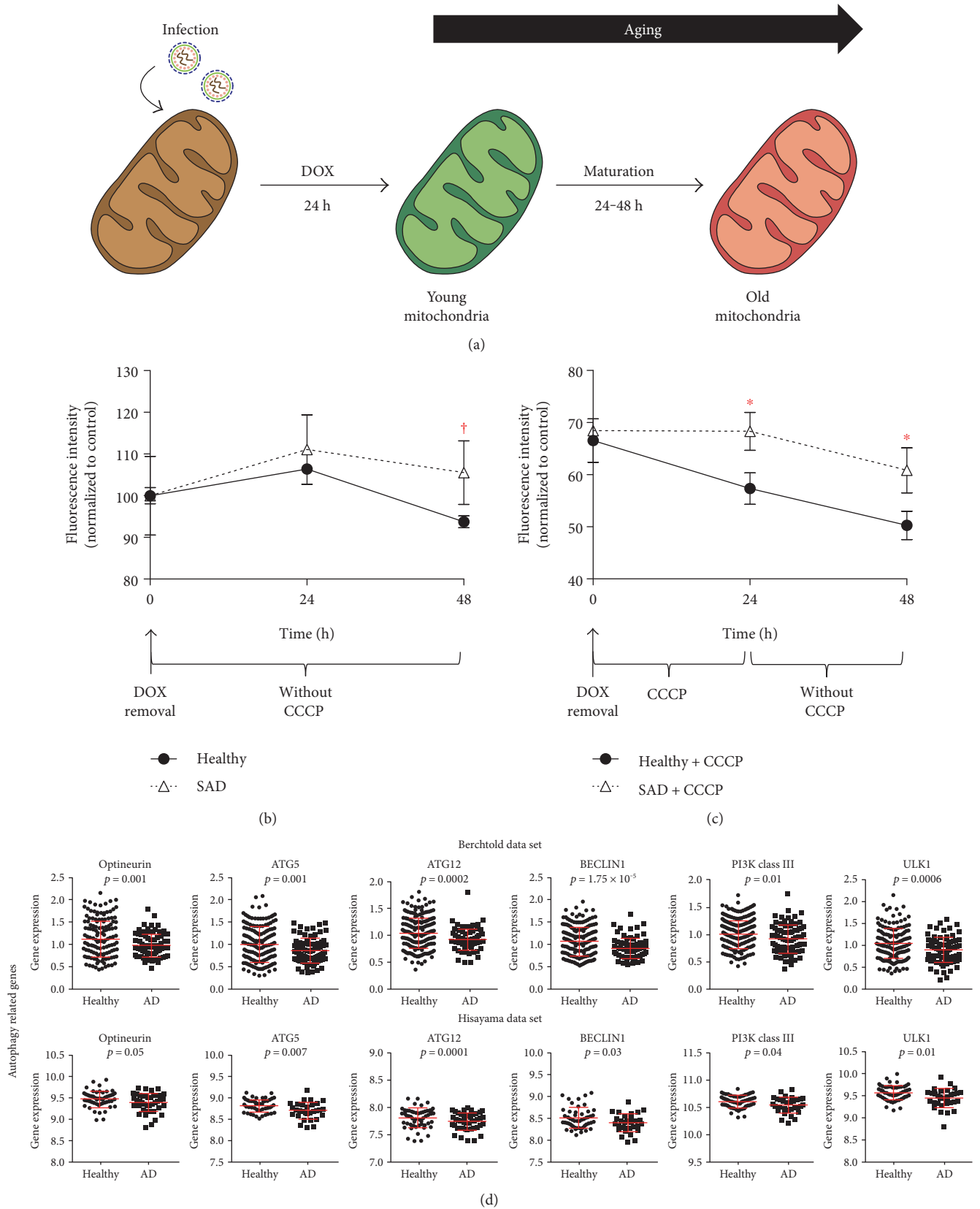


FIGURE 6: Continued.

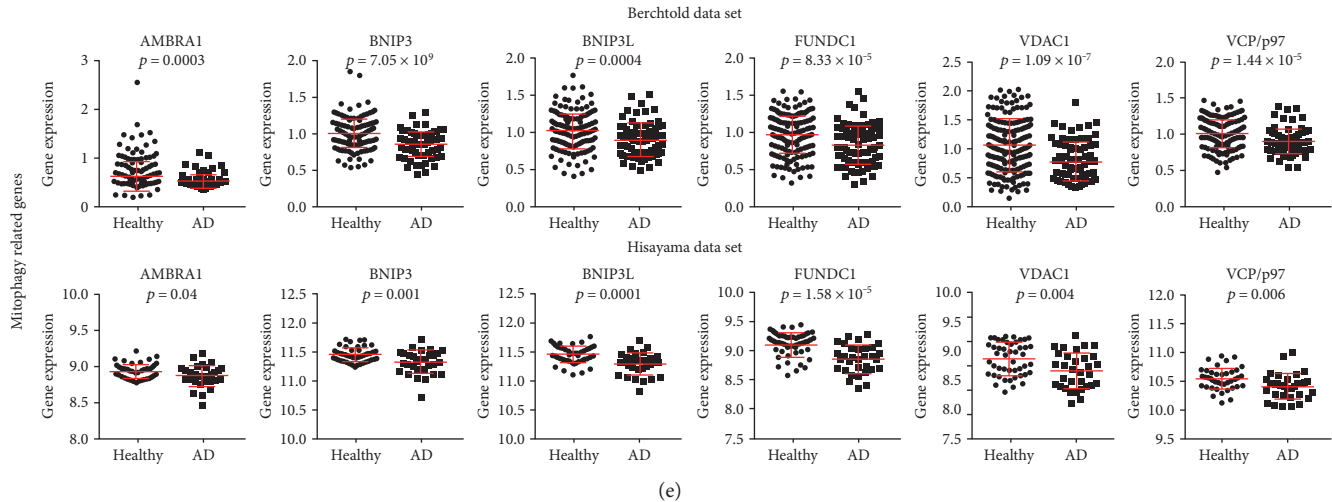


FIGURE 6: Aged mitochondria due to defective mitochondrial recycling in AD. (a) Scheme of the function of lentiviral MitoTimer tool. (b) Graph showing intensity of red fluorescence per cell measured by flow cytometry over timer in healthy and SAD fibroblasts previously infected by a lentivirus encoding MitoTimer and treated for 24h with doxycycline. (c) Graph representing a similar study but in the presence of CCCP (20 μ M) for 24h after doxycycline removal. (b)–(c) Values represent means and standard deviations of the percentage of red fluorescence intensity mean per cell (aged mitochondria) with respect to control condition that is the average of red fluorescence intensity mean after doxycycline removal without CCCP (0h time point) ($n = 3$ independent experiments using the healthy/SAD couple AG01362/AG05859, $\dagger p < 0.08$, and $* p < 0.05$). (d)–(e). Analysis of microarray expression of genes involved in autophagy (d) and mitophagy (e). Graphs show dot plots of the expression of the indicated genes using in upper rows $n = 253$ samples from 84 patients, of which $n = 56$ are healthy subjects and $n = 28$ are AD patients retrieved from Berchtold data set [29], and in lower rows $n = 47$ controls and $n = 32$ AD brain samples retrieved from the Hisayama study [13]. Correspondent p value was determined by Student's t -test and is showed for each graph.

process was impaired. This result correlates with our previous work in which we have demonstrated a functional impairment of autophagy and, more specifically, of mitophagy in this set of SAD fibroblasts [26].

3.5. Alzheimer's Disease Patients Exhibit Reduced Expression of Autophagy and Mitophagy-Associated Genes. Numerous works have focused their efforts in the study of mitochondrial recycling mechanisms due to their relevance in aging [44]. Mitochondrial fusion and fission processes are closely related with the removal of damaged mitochondria executed by mitophagy. Due to the fact that we have observed the accumulation of aged mitochondria in SAD fibroblasts, we wondered whether autophagy and mitophagy genes may be altered in the two sets of samples where we previously observed a downregulation of mitochondrial dynamics genes. We observed that a high number of autophagy associated genes such as Optineurin, ATG5, ATG12, Beclin1, PI3K class III, and ULK1 (Figure 6(d)) and mitophagy such as AMBRA1, BNIP3, BNIP3L, FUNDC1, VDAC1, and VCP/P97 (Figure 6(e)) were downregulated in AD brain with respect to healthy controls.

4. Discussion

4.1. Alteration of the Expression of Fission and Fusion-Related Genes. Alzheimer's is the most prevalent neurodegenerative disease and is characterized by progressive dementia that initiates as short-term memory impairment. In the past decade,

a wide number of gene profiling analysis have been performed in patient-derived postmortem brains as well as peripheral tissues. These studies have revealed a narrow relationship of mitochondrial dysfunction, calcium signaling, and neuroinflammation with AD pathology [1]. Particularly interesting is the involvement of mitochondria in AD, in fact, several lines of evidence propose mitochondrial anomalies as one of the primary factors that lead to late-onset SAD pathology [9, 45]. Here, we analyzed gene profiling data of genes involved in mitochondrial dynamics and we could observe a pleiotropic downregulation of gene expression of both fission and fusion processes, correlative to other studies in which diminished levels of these proteins have been demonstrated in patients' brain [40]. Accordingly, we have shown that SAD fibroblasts exhibited lower levels of proteins involved in fission-like DLP1 and fusion such as MFN2 and STOML2. Other authors have shown that mitochondrial failure may arise from a deficient dynamic balance of mitochondrial fission and fusion that, in AD, is greatly shifted toward fission, due to a defect in fusion. This may result in the presence of dysfunctional mitochondria in damaged neurons as well as fibroblasts from AD patients characterized by their accumulation into perinuclear areas [24, 25]. We confirmed the downregulation of several fission genes, but also important fusion genes such as MFN2 and OPA1 appeared downregulated, what had been demonstrated to inhibit this process [46, 47]. Furthermore, fusion and fission proteins have been found diminished in fibroblasts suggesting that both processes are affected.

4.2. Downregulation of Fusion and Fission Genes Lead to Slower Dynamics. Vulnerable neurons in AD's brain exhibit significant reduction in mitochondrial length and increased width with a significant augmented overall size consistent with unopposed fission suggesting alterations of mitochondrial dynamics [38, 48]. In agreement with these findings, abnormal distribution of mitochondria was found in pyramidal neurons of AD-affected individuals where mitochondria were redistributed away from axons [40]. Accordingly, levels of fusion proteins OPA1, MFN1, and MFN2 were significantly reduced, whereas levels of Fis1 were significantly increased in AD [40]. Primary hippocampal neurons treated with A β -derived diffusible ligands (ADDLs) demonstrated shortened mitochondria in neurons and alteration of fission and fusion proteins [40]. Moreover, time-lapse recordings in these neurons showed impairment of both fission and fusion processes, with fusion being more severely affected [40]. These authors discuss that the observed imbalance of fusion and fission proteins does not explain the observed time-lapse recordings where both processes are affected. This last result correlates with our observations of slower mitochondrial dynamics after the addition and removal of CCCP.

Abnormal mitochondrial morphology had been previously found in fibroblasts from sporadic AD patients, where they become significantly elongated and form a highly connected network [38]. However, in our hands, we could not detect significant differences in the number of individuals, networks, branches per network, or length of the branches of mitochondria between healthy and SAD fibroblasts. Only increased mitochondrial surface was detected in SAD fibroblasts. This discrepancy in mitochondrial morphology with the data reported in neurons may be due to variations in the expression pattern of proteins involved in dynamics as well as different mitochondrial function requirements between both cell types. As we have seen a pleiotropic downregulation of fusion and fission genes in brains, our functional study in fibroblasts was focused in both processes. Accordingly, we could observe that the whole dynamics system was affected.

The alteration in mitochondrial dynamics leads to severe consequences in the cell such as structural changes in the cristae formation and assembly of electron transport complex compromising bioenergetics and causing calcium dys-homeostasis, increased oxidative stress, mtDNA damage, and synaptic dysfunction [25].

In addition to the defect observed in fusion/fission, defects in mitochondrial mobility have also been observed in AD causing a mitochondrial reduction in neurites [25]. A β induces a reduction in motile mitochondria [49], and ADDLs impair anterograde and retrograde axonal transport of mitochondria in hippocampal neurons [50]. We have also observed the downregulation of many genes involved in mitochondrial transport such as the family of dynactins (DCTN1, 2, 3, 5, and 6), dyneins (DYNC1H1, DYNC111, and DYNC1LI1), kinesins (KIF1B and KIF5C), and Miro (data not shown). It has been described that PINK1 and PARK2 target Miro for phosphorylation and degradation to arrest mitochondrial motility keeping in quarantine damaged mitochondria prior to their clearance by mitophagy [51].

Therefore, Miro downregulation may affect to the correct segregation of dysfunctional mitochondria and its subsequently recycling.

4.3. Autophagy/Mitophagy Defect and the Resulting Accumulation of Damaged Mitochondria. Numerous works have demonstrated that autophagy is dysregulated in AD pathology, even when autophagy induction has been considered a therapeutic target [52]. More recently, we have reported mitophagy impairment in these patients' brain and peripheral tissue due to insufficient generation of autophagic vesicles together with deficient PARK2 signaling, leading to the accumulation of damaged mitochondria, strong oxidative damage, and accumulation of polyubiquitinated proteins [26]. Accordingly, we now report the downregulation of multiple genes involved in autophagy and mitophagy that was accompanied by the accumulation of aged mitochondria. For this study, we have developed a new lentiviral vector that allows the induction of MitoTimer tool [41, 53] under the control of doxycycline. Our vector has the ability to infect any kind of cell independently of its proliferative state and through a single virus infection achieves the complete regulation of the transgene. This tool will allow the study of mitochondrial aging as well as recycling in vitro and in vivo in any cell or animal model.

5. Conclusions

Here, we report numerous data that reveal a deep deregulation of mitochondrial homeostasis in Alzheimer's disease. We have observed a downregulation of mitochondrial fusion and fission in the disease. Accordingly, mitochondrial dynamics is slowed down in these patients' fibroblasts after an insult. This is accompanied by a downregulation of autophagy and mitophagy genes together with the accumulation of aged mitochondria which may be a cornerstone of Alzheimer's pathology due to their involvement in ROS production, elevated calcium levels, and neuroinflammation observed in these patients. Our data continue in fueling the hypothesis that AD is an acceleration of aging caused by malfunction of recycling.

Conflicts of Interest

The authors declare that there are no competing interests regarding the publication of this paper.

Acknowledgments

The authors would like to acknowledge Dr. Ismael Santa-María (Columbia University, NY) for providing us the lentivector encoding DsRed2-Mito. This work was supported by the Ministerio de Economía y Competitividad (SAF 2011 program, Project 24841 and Grant BES-2012-055068) from Spain and the Centro de Investigación en Red de Enfermedades Neurodegenerativas (CIBERNED, ISCIII, JA) as well as by a grant from the National Institute on Minority Health and Health Disparities (G12-MD007591) from the National Institute of Health.

References

- [1] J. Cooper-Knock, J. Kirby, L. Ferraiuolo, P. R. Heath, M. Rattray, and P. J. Shaw, "Gene expression profiling in human neurodegenerative disease," *Nature Reviews Neurology*, vol. 8, no. 9, pp. 518–530, 2012.
- [2] R. X. Santos, S. C. Correia, X. Wang et al., "A synergistic dysfunction of mitochondrial fission/fusion dynamics and mitophagy in Alzheimer's disease," *Journal of Alzheimer's Disease*, vol. 20, Supplement 2, pp. S401–S412, 2010.
- [3] D. J. Bonda, X. Wang, G. Perry et al., "Oxidative stress in Alzheimer disease: a possibility for prevention," *Neuropharmacology*, vol. 59, no. 4-5, pp. 290–294, 2010.
- [4] A. Nunomura, G. Perry, G. Aliev et al., "Oxidative damage is the earliest event in Alzheimer disease," *Journal of Neuro-pathology & Experimental Neurology*, vol. 60, no. 8, pp. 759–767, 2001.
- [5] K. Schmitt, A. Grimm, A. Kazmierczak, J. B. Strosznajder, J. Götz, and A. Eckert, "Insights into mitochondrial dysfunction: aging, amyloid- β , and tau-A deleterious trio," *Antioxidants & Redox Signaling*, vol. 16, no. 12, pp. 1456–1466, 2012.
- [6] S. Hauptmann, I. Scherping, S. Dröse et al., "Mitochondrial dysfunction: an early event in Alzheimer pathology accumulates with age in AD transgenic mice," *Neurobiology of Aging*, vol. 30, no. 10, pp. 1574–1586, 2009.
- [7] G. E. Alexander, K. Chen, P. Pietrini, S. I. Rapoport, and E. M. Reiman, "Longitudinal PET evaluation of cerebral metabolic decline in dementia: a potential outcome measure in Alzheimer's disease treatment studies," *The American Journal of Psychiatry*, vol. 159, no. 5, pp. 738–745, 2002.
- [8] J. P. Blass, R. K. Sheu, and G. E. Gibson, "Inherent abnormalities in energy metabolism in Alzheimer disease. Interaction with cerebrovascular compromise," *Annals of the New York Academy of Sciences*, vol. 903, pp. 204–221, 2000.
- [9] R. H. Swerdlow and S. M. Khan, "A "mitochondrial cascade hypothesis" for sporadic Alzheimer's disease," *Medical Hypotheses*, vol. 63, no. 1, pp. 8–20, 2004.
- [10] R. H. Swerdlow and S. J. Kish, "Mitochondria in Alzheimer's disease," *International Review of Neurobiology*, vol. 53, pp. 341–385, 2002.
- [11] M. P. Mattson, M. Gleichmann, and A. Cheng, "Mitochondria in neuroplasticity and neurological disorders," *Neuron*, vol. 60, no. 5, pp. 748–766, 2008.
- [12] J. Yao, R. W. Irwin, L. Zhao, J. Nilsen, R. T. Hamilton, and R. D. Brinton, "Mitochondrial bioenergetic deficit precedes Alzheimer's pathology in female mouse model of Alzheimer's disease," *Proceedings of the National Academy of Sciences of the United States of America*, vol. 106, no. 34, pp. 14670–14675, 2009.
- [13] P. Mao, M. Manczak, M. J. Calkins et al., "Mitochondria-targeted catalase reduces abnormal APP processing, amyloid β production and BACE1 in a mouse model of Alzheimer's disease: implications for neuroprotection and lifespan extension," *Human Molecular Genetics*, vol. 21, no. 13, pp. 2973–2990, 2012.
- [14] G. U. Hoglinger, A. Lannuzel, M. E. Khondiker et al., "The mitochondrial complex I inhibitor rotenone triggers a cerebral tauopathy," *Journal of Neurochemistry*, vol. 95, no. 4, pp. 930–939, 2005.
- [15] A. K. Kondadi, S. Wang, S. Montagner et al., "Loss of the m-AAA protease subunit AFG(3)L(2) causes mitochondrial transport defects and tau hyperphosphorylation," *The EMBO Journal*, vol. 33, no. 9, pp. 1011–1026, 2014.
- [16] M. P. Mattson, W. Fu, G. Waeg, and K. Uchida, "4-Hydroxynonenal, a product of lipid peroxidation, inhibits dephosphorylation of the microtubule-associated protein tau," *Neuroreport*, vol. 8, no. 9-10, pp. 2275–2281, 1997.
- [17] A. M. van der Bliek, Q. Shen, and S. Kawajiri, "Mechanisms of mitochondrial fission and fusion," *Cold Spring Harbor Perspectives in Biology*, vol. 5, no. 6, 2013.
- [18] H. M. Ni, J. A. Williams, and W. X. Ding, "Mitochondrial dynamics and mitochondrial quality control," *Redox Biology*, vol. 4, pp. 6–13, 2015.
- [19] O. C. Loson, Z. Song, H. Chen, and D. C. Chan, "Fis1, Mff, MiD49, and MiD51 mediate Drp1 recruitment in mitochondrial fission," *Molecular Biology of the Cell*, vol. 24, no. 5, pp. 659–667, 2013.
- [20] C. S. Palmer, L. D. Osellame, D. Laine, O. S. Koutsopoulos, A. E. Frazier, and M. T. Ryan, "MiD49 and MiD51, new components of the mitochondrial fission machinery," *EMBO Reports*, vol. 12, no. 6, pp. 565–573, 2011.
- [21] V. Garcia-Escudero, P. Martin-Maestro, G. Perry, and J. Avila, "Deconstructing mitochondrial dysfunction in Alzheimer disease," *Oxidative Medicine and Cellular Longevity*, vol. 2013, Article ID 162152, 13 pages, 2013.
- [22] T. N. Nguyen, B. S. Padman, and M. Lazarou, "Deciphering the molecular signals of PINK1/Parkin mitophagy," *Trends in Cell Biology*, vol. 26, no. 10, pp. 733–744, 2016.
- [23] Y. Wang, M. Serricchio, M. Jauregui et al., "Deubiquitinating enzymes regulate PARK2-mediated mitophagy," *Autophagy*, vol. 11, no. 4, pp. 595–606, 2015.
- [24] D. J. Bonda, X. Wang, G. Perry, M. A. Smith, and X. Zhu, "Mitochondrial dynamics in Alzheimer's disease: opportunities for future treatment strategies," *Drugs & Aging*, vol. 27, no. 3, pp. 181–192, 2010.
- [25] X. Zhu, G. Perry, M. A. Smith, and X. Wang, "Abnormal mitochondrial dynamics in the pathogenesis of Alzheimer's disease," *Journal of Alzheimer's Disease*, vol. 33, Supplement 1, pp. S253–S262, 2013.
- [26] P. Martin-Maestro, R. Gargini, G. Perry, J. Avila, and V. Garcia-Escudero, "PARK2 enhancement is able to compensate mitophagy alterations found in sporadic Alzheimer's disease," *Human Molecular Genetics*, vol. 25, no. 4, pp. 792–806, 2016.
- [27] J. H. Lee, W. H. Yu, A. Kumar et al., "Lysosomal proteolysis and autophagy require presenilin 1 and are disrupted by Alzheimer-related PS1 mutations," *Cell*, vol. 141, no. 7, pp. 1146–1158, 2010.
- [28] D. S. Yang, P. Stavrides, P. S. Mohan et al., "Therapeutic effects of remediating autophagy failure in a mouse model of Alzheimer disease by enhancing lysosomal proteolysis," *Autophagy*, vol. 7, no. 7, pp. 788–789, 2011.
- [29] N. C. Berchtold, D. H. Cribbs, P. D. Coleman et al., "Gene expression changes in the course of normal brain aging are sexually dimorphic," *Proceedings of the National Academy of Sciences of the United States of America*, vol. 105, no. 40, pp. 15605–15610, 2008.
- [30] M. Hokama, S. Oka, J. Leon et al., "Altered expression of diabetes-related genes in Alzheimer's disease brains: the Hisayama study," *Cerebral Cortex*, vol. 24, no. 9, pp. 2476–2488, 2014.
- [31] A. J. Valente, L. A. Maddalena, E. L. Robb, F. Moradi, and J. A. Stuart, "A simple ImageJ macro tool for analyzing

- mitochondrial network morphology in mammalian cell culture," *Acta Histochemica*, vol. 119, no. 3, pp. 315–326, 2017.
- [32] J. P. Blass and G. E. Gibson, "The role of oxidative abnormalities in the pathophysiology of Alzheimer's disease," *Revue Neurologique (Paris)*, vol. 147, no. 6-7, pp. 513–525, 1991.
- [33] A. M. Bertholet, T. Delerue, A. M. Millet et al., "Mitochondrial fusion/fission dynamics in neurodegeneration and neuronal plasticity," *Neurobiology of Disease*, vol. 90, pp. 3–19, 2016.
- [34] Z. Song, M. Ghochani, J. M. McCaffery, T. G. Frey, and D. C. Chan, "Mitofusins and OPA1 mediate sequential steps in mitochondrial membrane fusion," *Molecular Biology of the Cell*, vol. 20, no. 15, pp. 3525–3532, 2009.
- [35] S. Meeusen, R. DeVay, J. Block et al., "Mitochondrial inner-membrane fusion and crista maintenance requires the dynamin-related GTPase Mgm1," *Cell*, vol. 127, no. 2, pp. 383–395, 2006.
- [36] D. Tondera, S. Grandemange, A. Jourdain et al., "SLP-2 is required for stress-induced mitochondrial hyperfusion," *The EMBO Journal*, vol. 28, no. 11, pp. 1589–1600, 2009.
- [37] B. Bossy, A. Petrilli, E. Klinglmayr et al., "S-Nitrosylation of DRP1 does not affect enzymatic activity and is not specific to Alzheimer's disease," *Journal of Alzheimer's Disease*, vol. 20, Supplement 2, pp. S513–S526, 2010.
- [38] X. Wang, B. Su, H. Fujioka, and X. Zhu, "Dynamin-like protein 1 reduction underlies mitochondrial morphology and distribution abnormalities in fibroblasts from sporadic Alzheimer's disease patients," *The American Journal of Pathology*, vol. 173, no. 2, pp. 470–482, 2008.
- [39] E. Smirnova, L. Griparic, D. L. Shurland, and A. M. van der Bliek, "Dynamin-related protein Drp1 is required for mitochondrial division in mammalian cells," *Molecular Biology of the Cell*, vol. 12, no. 8, pp. 2245–2256, 2001.
- [40] X. Wang, B. Su, H. G. Lee et al., "Impaired balance of mitochondrial fission and fusion in Alzheimer's disease," *The Journal of Neuroscience*, vol. 29, no. 28, pp. 9090–9103, 2009.
- [41] G. Hernandez, C. Thornton, A. Stotland et al., "MitoTimer: a novel tool for monitoring mitochondrial turnover," *Autophagy*, vol. 9, no. 11, pp. 1852–1861, 2013.
- [42] A. W. Ferree, K. Trudeau, E. Zik et al., "MitoTimer probe reveals the impact of autophagy, fusion, and motility on sub-cellular distribution of young and old mitochondrial protein and on relative mitochondrial protein age," *Autophagy*, vol. 9, no. 11, pp. 1887–1896, 2013.
- [43] J. A. Williams, K. Zhao, S. Jin, and W. X. Ding, "New methods for monitoring mitochondrial biogenesis and mitophagy in vitro and in vivo," *Experimental Biology and Medicine*, vol. 242, no. 8, pp. 781–787, 2017.
- [44] E. M. Fivenson, S. Lautrup, N. Sun et al., "Mitophagy in neurodegeneration and aging," *Neurochemistry International*, 2017, In press.
- [45] R. H. Swerdlow, J. M. Burns, and S. M. Khan, "The Alzheimer's disease mitochondrial cascade hypothesis: progress and perspectives," *Biochimica et Biophysica Acta (BBA) - Molecular Basis of Disease*, vol. 1842, no. 8, pp. 1219–1231, 2014.
- [46] H. Chen, J. M. McCaffery, and D. C. Chan, "Mitochondrial fusion protects against neurodegeneration in the cerebellum," *Cell*, vol. 130, no. 3, pp. 548–562, 2007.
- [47] A. M. Bertholet, A. M. Millet, O. Guillermin et al., "OPA1 loss of function affects in vitro neuronal maturation," *Brain*, vol. 136, Part 5, pp. 1518–1533, 2013.
- [48] X. Wang, B. Su, S. L. Siedlak et al., "Amyloid-beta overproduction causes abnormal mitochondrial dynamics via differential modulation of mitochondrial fission/fusion proteins," *Proceedings of the National Academy of Sciences of the United States of America*, vol. 105, no. 49, pp. 19318–19323, 2008.
- [49] Y. Rui, P. Tiwari, Z. Xie, and J. Q. Zheng, "Acute impairment of mitochondrial trafficking by β -amyloid peptides in hippocampal neurons," *The Journal of Neuroscience*, vol. 26, no. 41, pp. 10480–10487, 2006.
- [50] X. Wang, G. Perry, M. A. Smith, and X. Zhu, "Amyloid- β -derived diffusible ligands cause impaired axonal transport of mitochondria in neurons," *Neurodegenerative Diseases*, vol. 7, no. 1–3, pp. 56–59, 2010.
- [51] X. Wang, D. Winter, G. Ashrafi et al., "PINK1 and Parkin target Miro for phosphorylation and degradation to arrest mitochondrial motility," *Cell*, vol. 147, no. 4, pp. 893–906, 2011.
- [52] H. Harris and D. C. Rubinsztein, "Control of autophagy as a therapy for neurodegenerative disease," *Nature Reviews. Neurology*, vol. 8, no. 2, pp. 108–117, 2011.
- [53] K. M. Trudeau, R. A. Gottlieb, and O. S. Shirihai, "Measurement of mitochondrial turnover and life cycle using MitoTimer," *Methods in Enzymology*, vol. 547, pp. 21–38, 2014.

Research Article

Blood-Based Bioenergetic Profiling Reflects Differences in Brain Bioenergetics and Metabolism

Daniel J. Tyrrell,¹ Manish S. Bharadwaj,² Matthew J. Jorgensen,² Thomas C. Register,² Carol Shively,² Rachel N. Andrews,² Bryan Neth,³ C. Dirk Keene,⁴ Akiva Mintz,⁵ Suzanne Craft,³ and Anthony J. A. Molina³

¹Frankel Cardiovascular Center, Department of Internal Medicine, University of Michigan Medical School, Ann Arbor, MI 48109, USA

²Section on Comparative Medicine, Department of Pathology, Wake Forest School of Medicine, Winston-Salem, NC 27157, USA

³Section on Gerontology and Geriatrics, Sticht Center for Healthy Aging and Alzheimer's Prevention & Department of Internal Medicine, Wake Forest School of Medicine, Winston-Salem, NC 27157, USA

⁴Department of Pathology, University of Washington, Seattle, WA, USA

⁵Department of Radiology, Wake Forest School of Medicine, Winston-Salem, NC 27157, USA

Correspondence should be addressed to Anthony J. A. Molina; amolina@wakehealth.edu

Received 30 March 2017; Revised 9 June 2017; Accepted 20 July 2017; Published 2 October 2017

Academic Editor: Maik Hüttemann

Copyright © 2017 Daniel J. Tyrrell et al. This is an open access article distributed under the Creative Commons Attribution License, which permits unrestricted use, distribution, and reproduction in any medium, provided the original work is properly cited.

Blood-based bioenergetic profiling provides a minimally invasive assessment of mitochondrial health shown to be related to key features of aging. Previous studies show that blood cells recapitulate mitochondrial alterations in the central nervous system under pathological conditions, including the development of Alzheimer's disease. In this study of nonhuman primates, we focus on mitochondrial function and bioenergetic capacity assessed by the respirometric profiling of monocytes, platelets, and frontal cortex mitochondria. Our data indicate that differences in the maximal respiratory capacity of brain mitochondria are reflected by CD14+ monocyte maximal respiratory capacity and platelet and monocyte bioenergetic health index. A subset of nonhuman primates also underwent [¹⁸F] fluorodeoxyglucose positron emission tomography (FDG-PET) imaging to assess brain glucose metabolism. Our results indicate that platelet respiratory capacity positively correlates to measures of glucose metabolism in multiple brain regions. Altogether, the results of this study provide early evidence that blood-based bioenergetic profiling is related to brain mitochondrial metabolism. While these measures cannot substitute for direct measures of brain metabolism, provided by measures such as FDG-PET, they may have utility as a metabolic biomarker and screening tool to identify individuals exhibiting systemic bioenergetic decline who may therefore be at risk for the development of neurodegenerative diseases.

1. Introduction

There is mounting evidence that blood-based respirometric profiling can report on systemic bioenergetic capacity. Previous studies link mitochondrial parameters measured in peripheral blood mononuclear cells (PBMCs), made up of monocytes and lymphocytes, and platelets to various age-related diseases and disorders such as AD, diabetes, and frailty [1–6]. Our previous studies have shown that the respirometric profiles of blood cells are related to features of aging that are associated with morbidity and mortality, including

reduced physical ability and inflammation [7, 8]. More recently, we reported that blood cell respirometry reflects the bioenergetic capacity of highly metabolically active tissues such as skeletal and cardiac muscles [9]. These studies support potential diagnostic applications of minimally invasive, blood-based measures of mitochondrial function [10]. The goal of this study was to expand on this body of knowledge by investigating the relationships of blood cell respirometry to measures of brain bioenergetics and metabolism.

Highly metabolically active tissues are particularly susceptible to bioenergetic decline. The adult brain, which accounts

for just ~2% of total body weight, utilizes ~20% of total body O_2 consumption and ~60% of total body glucose and requires a daily energy input of ~420 kcal [11, 12]. This exceptionally high metabolic demand makes the brain remarkably sensitive to the deleterious effects of mitochondrial dysfunction. In 2004, Swerdlow and Khan proposed the “mitochondrial cascade hypothesis” for the development of sporadic late-onset AD, stating that mitochondrial dysfunction is the primary event leading to the deposition of senile plaques and neurofibrillary tangles that are hallmarks of this disease [13]. Over the past decade, it has been increasingly recognized that changes in mitochondrial function are apparent at the earliest presymptomatic stages of AD and related to the progression of disease [14]. Multiple studies link the deposition of amyloid- β ($A\beta$) to alterations in mitochondrial bioenergetics, for example, depolarization, uncoupling of the electron transport chain (ETC), reduced ATP production, and increased reactive oxygen species generation [15–18]. Studies of patients and animal models indicate that AD is associated with the accumulation of amyloid precursor protein (APP) and $A\beta$ on brain mitochondria, leading to bioenergetic changes [19–24]. Greater AD risk is associated with reduced cerebral glucose metabolic rate, measured by [^{18}F] fluorodeoxyglucose positron emission tomography (FDG-PET), which can appear years before dementia onset [25, 26]. Thus, FDG-PET has emerged as a powerful method for the early detection of AD and may help differentiate mild AD from other forms of dementia [27, 28]. A subset of primates utilized in this project underwent brain FDG-PET imaging, providing us with a unique opportunity to obtain preliminary data on the relationships between blood cell respirometry and brain glucose metabolism.

Multiple lines of evidence indicate that peripheral mitochondrial dysfunction accompanies changes in brain mitochondria in AD. Analysis of white blood cells from patients with early AD shows that the expression of mitochondrial respiratory complex I–V genes and subunits of the core mitochondrial ribosome complex are decreased compared to controls [29]. The authors report that these differences mirror changes observed in AD brains. Circulating lymphocytes from patients with AD also exhibit a pathological pattern of mitochondrial dysfunction and increased oxidative damage [30–32]. Platelet mitochondrial function has been shown to be impaired in patients with mild cognitive impairment (MCI) and AD compared to healthy age-matched controls [1, 33, 34]. Several groups are now exploring the use of blood cells for early diagnosis of AD [35–37]. The goal of this project is to expand on this growing body of knowledge by examining the relationships between brain bioenergetics and metabolism with CD14+ monocyte and platelet mitochondrial function.

First described in 1955, respirometry remains the gold standard assessment of mitochondrial function and is able to capture the cumulative effects of intrinsic and extrinsic factors on bioenergetic capacity [29–31]. In this study, we utilized mitochondrial respirometry to assess mitochondrial function in circulating cells and isolated brain (frontal cortex) mitochondria. The assessments were performed on nonhuman primates, representing various levels of cardiometabolic

health across young and old age groups. This broad selection criterion was utilized in order to maximize potential differences in systemic bioenergetic capacity between animals. We tested the hypothesis that the respirometric profile of circulating cells reflects differences in systemic bioenergetic capacity, including differences in brain bioenergetics and metabolism. This hypothesis is based on the recognition that blood cells are continuously exposed to circulating factors such as inflammatory cytokines, redox stress [36], and recently described mitokines [37], which can affect mitochondrial function across different tissues and organ systems. Our goal is to examine blood-based bioenergetic profiling as a potential biomarker for changes in brain metabolism that has been linked to the development of neurodegenerative diseases such as AD.

2. Materials and Methods

2.1. Animals. Female vervet/African green monkeys (*Chlorocebus aethiops sabaenus*) ranging in age from 8.2 to 23.4 years were utilized for this study. Animals were socially housed in stable groups of 11–49 in housing units with indoor and outdoor access of approximately 28 m² indoors and 111 m² outdoors which contained perches, platforms, elevated climbing structures, and a base composed of smooth stones. Prior to the study, 7 of the 18 animals were moved to indoor housing (pair- or individually housed). All animals were fed with a standard monkey chow diet (Lab Diet 1538) that was supplemented with fruits and vegetables 5 times per week. Water was available ad libitum. Immediately prior to necropsy, blood samples were collected from anesthetized animals. Frontal cortex tissues were taken during necropsy.

2.2. Body Mass and Blood Glucose. Body weight was measured at the time of necropsy. Fasting glucose was determined via an autoanalyzer (ACE Alera) from Alfa Wassermann Diagnostic Technologies (West Caldwell, NJ). These analyses were performed in the Wake Forest Comparative Medicine Clinical Chemistry and Endocrinology Laboratory 4–12 months prior to necropsy.

2.3. Isolation of Blood Cells. Acid citrate dextrose (ACD) tubes (Vacutainer; Becton Dickinson, Franklin Lakes, NJ) were used to collect 8 ml of blood from fasted monkeys. Samples were maintained at room temperature and processed immediately to obtain platelet and CD14+ monocyte populations. The method for isolating platelets and CD14+ monocytes has been described [38]. Whole blood was centrifuged at 500 \times g for 15 minutes in ACD tubes with no brake at room temperature. Platelet rich plasma was removed and centrifuged at 1500 \times g for 10 minutes to isolate platelets which were washed in phosphate-buffered saline (PBS) with prostaglandin E₁ (PGE₁; Cayman Chemical, Ann Arbor, MI) and resuspended in extracellular flux (XF) assay buffer (Seahorse Biosciences, North Billerica, MA) containing 1 mM Na⁺ pyruvate, 1 mM GlutaMAX (Gibco, Grand Island, NY), 11 mM D-glucose, and PGE₁ (pH 7.4). At the same time, the peripheral blood mononuclear cell (PBMC) layer was extracted, diluted in RPMI 1640 (Gibco), and layered

onto 3 mL of polysucrose solution at a density of 1.077 g/mL (Sigma Histopaque®-1077, St. Louis, MO) in 15 mL centrifuge tubes. This was centrifuged at 700 ×g for 30 minutes with no brake to purify the PBMCs and remove red blood cells. The purified PBMC layer was obtained and washed in PBS. Finally, CD14+ monocytes were isolated using CD14-labeled magnetic microbeads (Miltenyi Biotec, San Diego, CA) according to the manufacturer's instructions using modified RPMI 1640 + fatty acid free bovine serum albumin (BSA) media. Platelets and monocytes were counted via a hemacytometer. Monocytes were washed again, using the same buffer, and resuspended in XF assay buffer without PGE1.

2.4. *Respirometry of Blood Cells.* Respirometry of blood cells was carried out using the Seahorse XF24-3 extracellular flux analyzer (Seahorse Bioscience, Agilent) with 250,000 monocytes and ~25,000,000 platelets in quadruplicate [39]. The methods of bioenergetic profiling have been described before [40]. Basal oxygen consumption rate (OCR) measures were monitored prior to any chemical additions. Then, sequential additions of oligomycin (750 nM), carbonyl cyanide-4-(trifluoromethoxy) phenylhydrazone (FCCP; 1 μM), and antimycin A + rotenone (A/R; both 1 μM) (all from Sigma-Aldrich) were added with measurements taken after each. FCCP stimulates the maximal OCR. The difference between the maximal OCR and basal OCR is termed the reserve capacity which has been reported on previously [41, 42]. The difference between basal and oligo is the ATP-linked OCR [43]. The difference between the oligomycin-induced respiration (oligo) and A/R is reported as leak respiration. The bioenergetic health index (BHI) was calculated according to the equation from Chacko et al. [38]. Monocyte respiration is reported as pmol/min/250,000 cells and platelet respiration was normalized to total protein content (mg), determined by Pierce BCA assay (Thermo Fisher Scientific, Grand Island, NY), and reported as pmol/min/mg protein.

2.5. *FDG-PET Imaging.* Animals were anesthetized with ketamine for transfer to the imaging suite. Animals were then intubated and maintained on isoflurane for the duration of the imaging. An indwelling venous catheter was introduced into the saphenous vein for continuous blood sampling during scan acquisition and a second catheter placed in the contralateral saphenous vein for the injection of 5 mCi of tracer. Blood samples were obtained at 3, 8, 16, 24, 35, and 55 min after FDG infusion.

¹⁸F-FDG-PET imaging used the time frames 12 × 10 sec, 8 × 30 sec, 6 × 4 min, and 3 × 10 min, for a total length of 60 min. PET images were preprocessed and coregistered to T1-weighted anatomical magnetic resonance (MR) images using a cross-modality 3D image fusion tool in PMOD 3.5. MR images were acquired on a 3 T Siemens Skyra MRI scanner using a 3D volumetric MPRAGE sequence (TR = 2700 msec; TE = 3.39 msec; TI = 880 msec; FA = 8 degrees; and 160 slices, voxel dimension = 0.5 × 0.5 × 0.5 mm). Coregistered PET images were corrected for partial-volume effect with the modified Müller-Gartner method. Using the PMOD 3.5 pixel-wise kinetic modeling tool, parametric images of cerebral metabolic

rate of glucose (CMRg) were produced. CMR quantification included an arterial input function, determined by tracing regions of interest on the internal carotid arteries with the aid of coregistered MR images. The lumped constant used for the CMRg calculation was set to 0.344.

The CMR data for this study were processed with two atlases. Data for components of the vervet anterior cingulate cortex (Brodmann areas 24, 25, and 32), amygdala, and the anterior/posterior hippocampus were defined with methods described in [44]. Data for the frontal cortex were defined from a well-established nonhuman primate atlas, UNCParcellation [45]. Complete methods for regional CMR generation with the two atlases can be found at Maldjian et al. 2015 [46].

2.6. *Euthanasia.* Ketamine (10–15 mg/kg, IM) followed by sodium pentobarbital (60–100 mg/kg, IV) was the method of euthanasia used to attain deep surgical anesthesia followed by exsanguination in accordance with guidelines established by the Panel on Euthanasia of the American Veterinary Medical Association. All procedures were approved and performed according to the guidelines of state and federal laws, the US Department of Health and Human Services, and the Animal Care and Use Committee of Wake Forest School of Medicine.

2.7. *Isolation of Mitochondria from the Frontal Cortex.* Methods of isolating mitochondria have been described previously and were modified slightly for frontal cortex samples [47]. For each animal, ~50 mg of tissue was minced into small pieces and resuspended in Chappell-Perry buffer I (CP I) containing ~1 mg/ml Nagarse (Sigma-Aldrich) for 5 minutes at room temperature. Frontal cortex samples were homogenized by 6 strokes using a glass-on-glass dounce homogenizer. The homogenate was washed with an equal volume of CP I and 2x volume of CP II buffer by centrifuging at 600 ×g at 4°C for 10 minutes (Eppendorf Centrifuge 5804R, Eppendorf AG, Hamburg, Germany). The supernatant was then filtered through cheese cloth and subsequently centrifuged at 10,000 ×g at 4°C for 10 minutes using a Beckman centrifuge, model J2-21 M Induction drive centrifuge (Beckman-Coulter, Inc., Brea, CA). The mitochondrial pellet was washed twice more with the same conditions then resuspended in mitochondrial assay solution (mannitol and sucrose buffer: MAS; sucrose 35 mM, mannitol 110 mM, KH₂PO₄ 2.5 mM, MgCl₂ 2.5 mM, HEPES 1.0 mM, EGTA 0.5 mM, fatty acid free BSA 0.10%, and pH 7.4) prior to respirometry. The protein content of the purified frontal cortex mitochondria was determined by Pierce BCA assay (Thermo Fisher Scientific, Grand Island, NY). From 50 mg of tissue, ~500 μg of purified mitochondria was obtained.

2.8. *Respirometry of Isolated Mitochondria.* Respirometry of frontal cortex-isolated mitochondria was performed using the XF24-3 as previously described in other tissues [47, 48]. This protocol was optimized for respiration driven by complex 2, which provides consistently higher values in accordance with previous reports [48]. Chemical additions were prepared in 1x MAS at 10x the final concentration

TABLE 1: Demographics: *Chlorocebus aethiops sabaesus*.

<i>N</i> = 15	Mean	Range	SD
Age (yrs)	15.2	8.2–23.4	6.20
Weight (kg)	4.8	3.3–6.9	0.88
Fasting glucose (mg/dL)	128.6	61–319	70.31

required (2 mM ADP, 2 μ M oligomycin, 6 μ M FCCP, and 2 μ M antimycin A). Isolated mitochondria (5 μ g) were plated in quadruplicate in 50 μ l and attached via centrifugation at 2000 \times g at 4°C for 20 minutes. After centrifugation, 450 μ l of 1x MAS containing succinate (10 mM) and rotenone (2 μ M) was gently added to each well to a total volume of 500 μ l. The respirometric profiling procedure first stimulates maximal State 3 respiration with ADP, followed by inhibition of ATP synthase with oligo, providing the State 4o. Then, FCCP is injected which uncouples the electron transport chain to induce another measure of maximal respiration. Finally, antimycin A is titrated to block the flow of electrons at complex III and halt respiration. The respiration of isolated mitochondria is reported as pmol/min/5 μ g mitochondrial protein.

2.9. Statistical Analyses. Shapiro-Wilk tests ensured that all variables were normally distributed. Pearson correlation coefficients were assessed between all variables, and partial correlations for age, weight, and glucose level were also assessed. Analyses of monocyte and platelet respirometry were focused on maximal uncoupled respiration induced by FCCP, reserve capacity (calculated by subtracting basal from maximal respiration), and BHI. In order to provide a corresponding measure from contemporaneous respirometric profiling of brain mitochondria, analyses of frontal cortex mitochondrial respiration were focused on maximal uncoupled respiration induced by FCCP. Analyses of brain metabolism by FDG-PET focused on multiple brain regions in order to account for potential regional differences. Significance was set at an α -level of 0.05. The analyses were performed (SPSS v22; Armonk, NY).

3. Results

3.1. Characterization of Primates. Female vervets were selected to represent a wide range of metabolic health status as evidenced by insulin resistance as well as body mass indices from lean to obese across young and old age groups. Age, body weight, and fasting glucose are summarized in Table 1. A total of 15 vervets were studied with a mean age of 15.2 years. Ages ranged from 8.2 to 23.4 years. The mean weight of the animals was 4.8 kg, ranging from 3.3–6.9 kg. Fasting plasma glucose level averaged 128.6 mg/dL, ranging from 61–319 mg/dL. Bioenergetic characteristics of monocytes, platelets, and isolated brain mitochondria are tabulated in Table 2. Large standard deviations reflect the intended diversity of our cohort.

3.2. Pearson and Partial Correlations between Monocyte/Platelet Respiration and the Bioenergetic Capacity of Mitochondria

TABLE 2: Respiratory parameters for monocytes, platelets, and isolated brain mitochondria.

	Mean	SD
<i>Monocyte respiration</i> (pmol/min/250,000 cells)		
Basal	50.64	20.82
Maximal	98.65	42.80
Leak	6.25	9.30
Nonmitochondrial	22.08	14.02
Reserve	48.02	27.56
Bioenergetic health index	1.58	1.50
<i>Platelet respiration</i> (pmol/min/mg protein)		
Basal	210.04	87.71
Maximal	419.93	161.31
Leak	17.95	28.38
Nonmitochondrial	85.92	20.76
Reserve	209.88	88.46
Bioenergetic health index	2.40	0.85
<i>Brain-isolated mitochondria</i> (pmol/min/5 μ g mitochondrial protein)		
State 3	250.31	112.86
State 4o	66.01	46.83
Maximal FCCP-linked	268.42	102.87
Nonmitochondrial	22.58	42.50

Monocyte: *N* = 13; platelet: *N* = 15; isolated brain mitochondria: *N* = 15.

TABLE 3: Pearson and partial correlations between CD14+ monocyte and isolated brain mitochondrial respiration.

Frontal cortex mitochondria: maximal respiration	Maximal		Reserve		BHI	
	<i>R</i>	<i>p</i>	<i>R</i>	<i>p</i>	<i>R</i>	<i>p</i>
Pearson:	0.59	0.04	0.49	0.09	0.59	0.03
<i>Partial correlations</i>						
Age	0.62	0.03	0.56	0.06	0.43	0.16
Body weight	0.62	0.03	0.56	0.06	0.42	0.17
Plasma glucose	0.65	0.02	0.65	0.02	0.58	0.05

Isolated from the Frontal Cortex Tissue. Pearson correlation coefficients were used to compare blood cell bioenergetic parameters with brain-isolated mitochondrial respiration. The relationships between monocyte respiratory parameters (maximal OCR, reserve capacity, and OCR) and the maximal respiration of mitochondria isolated from the frontal cortex tissue are summarized in Table 3. Representative regression plots are shown in Figure 1. Maximal FCCP-linked respiration in monocytes was significantly positively correlated with maximal FCCP-linked respiration measured from brain mitochondria ($R = 0.59$, $p = 0.04$). This relationship remained significant even when controlling for age, body weight, and plasma glucose concentration. Similar results are observed when comparing monocyte reserve capacity to brain mitochondria; however, statistical significance was only evident when controlling for glucose ($R = 0.65$, $p = 0.02$). BHI was significantly positively correlated with brain mitochondrial respiration

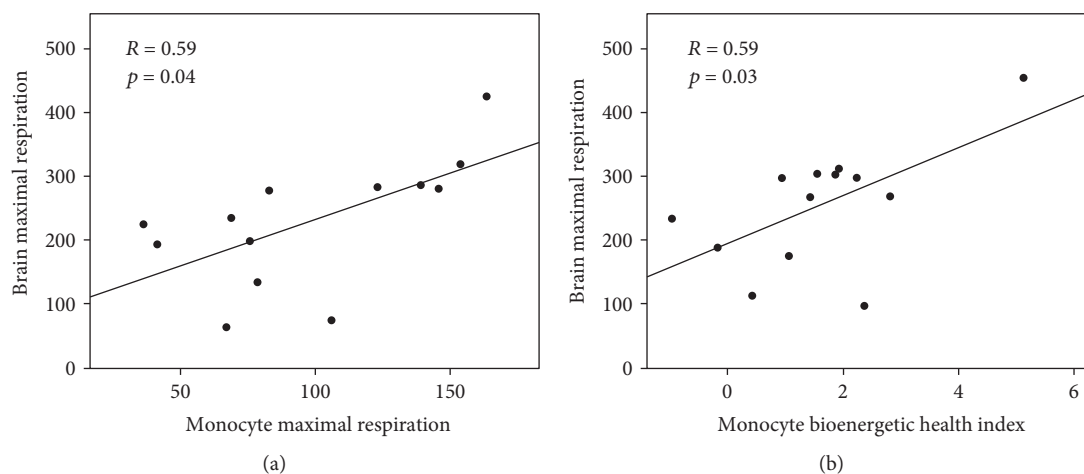


FIGURE 1: Associations of CD14⁺ monocyte (a) maximal respiration (pmol/min/250,000 cells) and (b) BHI with the maximal respiratory capacity of frontal cortex mitochondria (pmol/min/5 μ g mitochondrial protein). Pearson's correlations and p values for each association are shown.

TABLE 4: Pearson and partial correlations between platelet and isolated brain mitochondrial respiration.

Frontal cortex mitochondria: maximal respiration	Maximal		Reserve		BHI	
	R	p	R	p	R	p
Pearson	-0.34	0.21	-0.05	0.86	0.63	0.01
<i>Partial Correlations</i>						
Age	-0.28	0.33	-0.01	0.98	0.67	0.01
Body weight	-0.33	0.25	-0.10	0.73	0.58	0.03
Plasma glucose	-0.31	0.28	-0.00	0.99	0.65	0.01

($R = 0.59$, $p = 0.03$). This relationship was maintained when controlling for glucose; however, only trends are maintained when controlling for age and body weight.

Relationships between platelet respiratory parameters and the maximal respiration of mitochondria isolated from the frontal cortex tissue are summarized in Table 4. A representative regression plot is shown in Figure 2. For platelets, BHI was significantly positively correlated with brain mitochondrial maximal respiration ($R = 0.63$, $p = 0.01$), even when controlling for age, body weight, and plasma glucose concentration. Interestingly, maximal OCR and reserve capacity were not associated.

3.3. Pearson and Partial Correlations between Monocyte/Platelet Respiration and Brain Glucose Metabolism. A subset of 5 animals was analyzed for both CD14⁺ respiration and brain metabolism by FDG-PET (summarized in Table 5). A subset of 7 animals was analyzed for both platelet respiration and brain metabolism (summarized in Table 6). Strong trends for positive correlations between monocyte BHI and FDG-PET were observed when controlling for age; statistical significance was reached for the amygdala and frontal cortex regions ($R = 0.96$, $p = 0.04$; $R = 0.96$, $p = 0.04$; resp.). For platelets, reserve respiratory capacity and BHI were positively correlated with FDG-PET measures in all brain areas

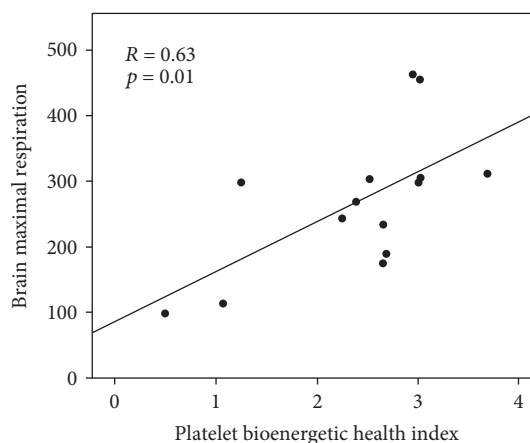


FIGURE 2: Association of platelet BHI with the maximal respiratory capacity of frontal cortex mitochondria (pmol/min/5 μ g mitochondrial protein). Pearson's correlation and p value are shown.

examined. Strong trends are apparent throughout, and statistically significant relationships were observed between reserve capacity with the anterior cingulate cortex (Brodmann area 32), amygdala, and anterior hippocampus ($R = 0.80$, $p = 0.03$; $R = 0.79$, $p = 0.04$; $R = 0.78$, $p = 0.04$; resp.). These relationships remained statistically significant when controlling for body weight.

4. Discussion

Blood-based bioenergetic profiling has been proposed to be a minimally invasive indicator of mitochondrial health [9, 38]. While respirometric profiling of circulating cells is now being utilized in various human studies, little is known about how these measures relate to the bioenergetic capacity of various tissues of interest. Using a nonhuman primate model, we recently reported that the bioenergetic capacity of circulating

TABLE 5: Pearson and partial correlations between monocyte respiration and brain glucose metabolism (FDG-PET).

FDG-PET: brain region	Maximal		Reserve		BHI	
	<i>R</i>	<i>p</i>	<i>R</i>	<i>p</i>	<i>R</i>	<i>p</i>
<i>Pearson</i>						
Area 24	0.46	0.44	0.26	0.67	0.40	0.50
Area 25	0.39	0.51	0.19	0.75	0.41	0.50
Area 32	0.50	0.39	0.28	0.64	0.43	0.46
Amygdala	0.42	0.48	0.23	0.71	0.28	0.65
Ant. hippocampus	0.46	0.44	0.31	0.61	0.26	0.68
Post. hippocampus	0.39	0.52	0.27	0.66	0.18	0.77
Frontal cortex	0.32	0.59	0.06	0.93	0.37	0.55
<i>Partial for age</i>						
Area 24	0.46	0.54	0.16	0.84	0.92	0.08
Area 25	0.38	0.62	0.08	0.92	0.89	0.11
Area 32	0.50	0.50	0.19	0.81	0.93	0.07
Amygdala	0.45	0.55	0.08	0.92	0.96	0.04
Ant. hippocampus	0.49	0.51	0.20	0.80	0.91	0.09
Post. hippocampus	0.42	0.58	0.13	0.87	0.89	0.11
Frontal cortex	0.31	0.69	-0.12	0.88	0.96	0.04
<i>Partial for weight</i>						
Area 24	0.11	0.89	0.04	0.96	0.36	0.64
Area 25	0.05	0.95	-0.02	0.98	0.36	0.64
Area 32	0.16	0.84	0.06	0.94	0.40	0.60
Amygdala	-0.07	0.93	-0.07	0.93	0.20	0.80
Ant. hippocampus	0.07	0.93	0.10	0.90	0.17	0.83
Post. hippocampus	-0.03	0.97	0.04	0.96	0.07	0.93
Frontal cortex	-0.26	0.74	-0.35	0.65	0.32	0.68
<i>Partial for plasma glucose</i>						
Area 24	0.46	0.54	0.28	0.72	0.41	0.59
Area 25	0.40	0.61	0.21	0.79	0.41	0.59
Area 32	0.51	0.50	0.31	0.69	0.45	0.56
Amygdala	0.46	0.55	0.32	0.68	0.33	0.68
Ant. hippocampus	0.47	0.53	0.36	0.64	0.27	0.73
Post. hippocampus	0.41	0.59	0.33	0.67	0.20	0.80
Frontal cortex	0.39	0.61	0.18	0.82	0.45	0.55

Areas 24, 25, and 32 = Brodmann areas (anterior cingulate cortex); Ant. = anterior; Post. = posterior; *N* = 5.

cells is significantly positively related to skeletal and cardiac muscle bioenergetics. In this report, we focus on the brain, the organ with the highest metabolic demand. We show for the first time significant positive correlations between contemporaneous blood cell and brain mitochondrial respirometry. Furthermore, brain glucose metabolism assessed by FDG-PET imaging was similarly positively associated with the bioenergetic profile of circulating blood cells.

Mitochondrial dysfunction is apparent in the pathophysiology of various diseases and is widely recognized to be a potential target for intervention. Bioenergetic deficits may be the result of genetic abnormalities, acute disruptions, or accumulated damage as is the case with chronic diseases, including those associated with aging. Neuronal

TABLE 6: Pearson and partial correlations between platelet respiration and brain glucose metabolism (FDG-PET).

FDG-PET: brain region	Maximal		Reserve		BHI	
	<i>R</i>	<i>p</i>	<i>R</i>	<i>p</i>	<i>R</i>	<i>p</i>
<i>Pearson</i>						
Area 24	0.55	0.20	0.72	0.07	0.74	0.06
Area 25	0.50	0.25	0.67	0.10	0.73	0.06
Area 32	0.65	0.11	0.80	0.03	0.75	0.05
Amygdala	0.67	0.10	0.79	0.04	0.70	0.08
Ant. hippocampus	0.64	0.12	0.78	0.04	0.74	0.06
Post. hippocampus	0.59	0.16	0.73	0.06	0.72	0.07
Frontal cortex	0.56	0.19	0.68	0.09	0.58	0.17
<i>Partial for age</i>						
Area 24	0.47	0.35	0.67	0.14	0.70	0.12
Area 25	0.41	0.42	0.62	0.19	0.69	0.13
Area 32	0.57	0.24	0.76	0.08	0.70	0.12
Amygdala	0.54	0.27	0.71	0.11	0.58	0.22
Ant. hippocampus	0.51	0.30	0.71	0.12	0.65	0.17
Post. hippocampus	0.43	0.39	0.64	0.17	0.60	0.21
Frontal cortex	0.45	0.38	0.60	0.21	0.47	0.35
<i>Partial for weight</i>						
Area 24	0.66	0.15	0.79	0.06	0.76	0.08
Area 25	0.60	0.21	0.74	0.10	0.74	0.09
Area 32	0.72	0.11	0.83	0.04	0.75	0.09
Amygdala	0.72	0.10	0.81	0.05	0.70	0.12
Ant. hippocampus	0.70	0.12	0.81	0.05	0.74	0.09
Post. hippocampus	0.66	0.16	0.77	0.08	0.72	0.11
Frontal cortex	0.66	0.15	0.74	0.09	0.58	0.23
<i>Partial for plasma glucose</i>						
Area 24	0.57	0.25	0.73	0.10	0.74	0.09
Area 25	0.50	0.31	0.68	0.14	0.73	0.10
Area 32	0.65	0.16	0.80	0.06	0.75	0.09
Amygdala	0.68	0.14	0.80	0.06	0.71	0.12
Ant. hippocampus	0.64	0.17	0.78	0.07	0.74	0.09
Post. hippocampus	0.60	0.21	0.74	0.09	0.72	0.11
Frontal cortex	0.58	0.22	0.72	0.11	0.60	0.21

Areas 24, 25, and 32 = Brodmann areas (anterior cingulate cortex); Ant. = anterior; post. = posterior; *N* = 7.

mitochondrial dysfunction is particularly damaging, likely due to the high metabolic demands of the brain. Numerous studies have linked mitochondrial alterations to the development of AD. Neuronal $A\beta$ has been shown to directly interact with mitochondria to inhibit complex IV of the ETC [49]. Alterations in mitochondrial quality control processes, such as mitochondrial fusion, fission, and autophagy, are also associated with neurodegeneration and specifically to AD [50–57]. Specific mitochondrial DNA (mtDNA) mutations are related to cognitive function, AD status, and risk [58–62]. These alterations can all contribute to bioenergetic decline and alterations in brain metabolism associated with AD. As a result, measures of brain metabolism are currently being utilized to study the pathophysiology of AD and are

widely recognized to have important diagnostic implications. The study reported here provides the first evidence suggesting that brain mitochondrial metabolism may be related to the bioenergetic profiles of blood cells.

Previous studies employing blood cell respirometry have focused on heterogeneous cell populations such as mixed peripheral blood mononuclear cells (PBMCs). In order to avoid the potential confounding effects of changes in PBMC cellular composition, this study focused on purified CD14+ monocytes. It is notable that a recent large-scale study of CD14+ monocytes from 1264 individuals reported that networks of genes related to oxidative phosphorylation and mitochondrial protein synthesis were differentially expressed based on chronological age [63]. We also performed respiratory analyses on platelets which are readily available and easy to isolate. Several groups are already exploring the potential utility of platelets in the diagnosis of diseases such as AD. Moreover, a recent study has reported that platelet bioenergetic capacity is related to AD status [34].

Blood-based bioenergetic profiling is not a surrogate for direct measures of brain metabolism. Rather, it may serve as a cost-effective screening tool to identify patients who may be more likely to exhibit neuronal bioenergetic deficits, based on systemic changes in mitochondria function. Our results indicating that blood-based bioenergetic profiling is related to FDG-PET measures of brain glucose metabolism were obtained from a small subset of primates and should be considered preliminary. A large-scale study is underway to confirm these findings in human subjects.

Our predetermined selection criteria were focused on maximizing differences in age and cardiometabolic health between animals. Hence, we include analyses controlling for age, body weight, and blood glucose in this report. Our sample size is not adequate to study the individual or interactive effects of each of these parameters. As designed, differences in cardiometabolic health were apparent across our younger as well as older animals. Indeed, comparing body weight and blood glucose between younger and older animals showed no statistical significance and a high level of variability. Larger scale future studies are required in order to determine how age, obesity, and insulin sensitivity/resistance are individually related to blood and brain bioenergetics.

5. Conclusions

Our data provide evidence that blood-based bioenergetic profiling can serve as a minimally invasive measure of systemic bioenergetic capacity that is positively related to measures of brain mitochondrial function and metabolism.

Conflicts of Interest

The authors declare that they have no conflicts of interest.

Acknowledgments

This work was financially supported by the Wake Forest Alzheimer's Disease Core Center (P30AG049638), the Wake Forest Claude D. Pepper Older Americans Independence

Center (P30-AG21332), the Translational Imaging Program of the Wake Forest CTSA (UL1TR001420), the Wake Forest Vervet Research Colony (OD010965), the University of Washington Alzheimer's Disease Research Center (P50AG005136), and Wake Forest Innovations.

References

- [1] C. Shi, K. Guo, D. T. Yew et al., "Effects of ageing and Alzheimer's disease on mitochondrial function of human platelets," *Experimental Gerontology*, vol. 43, no. 6, pp. 589–594, 2008.
- [2] C. Avila, R. J. Huang, M. V. Stevens et al., "Platelet mitochondrial dysfunction is evident in type 2 diabetes in association with modifications of mitochondrial anti-oxidant stress proteins," *Experimental and Clinical Endocrinology & Diabetes*, vol. 120, no. 4, pp. 248–251, 2012.
- [3] A. M. Japiassu, A. P. Santiago, J. C. d'Avila et al., "Bioenergetic failure of human peripheral blood monocytes in patients with septic shock is mediated by reduced F1Fo adenosine-5'-triphosphate synthase activity," *Critical Care Medicine*, vol. 39, no. 5, pp. 1056–1063, 2011.
- [4] M. L. Hartman, O. S. Shirihai, M. Holbrook et al., "Relation of mitochondrial oxygen consumption in peripheral blood mononuclear cells to vascular function in type 2 diabetes mellitus," *Vascular Medicine*, vol. 19, no. 1, pp. 67–74, 2014.
- [5] M. E. Widlansky, J. Wang, S. M. Shenouda et al., "Altered mitochondrial membrane potential, mass, and morphology in the mononuclear cells of humans with type 2 diabetes," *Translational Research*, vol. 156, no. 1, pp. 15–25, 2010.
- [6] M. D. Cordero, M. F. A. M. de MM, I. M. Carmona Lopez et al., "Mitochondrial dysfunction and mitophagy activation in blood mononuclear cells of fibromyalgia patients: implications in the pathogenesis of the disease," *Arthritis Research & Therapy*, vol. 12, no. 1, article R17, 2010.
- [7] D. J. Tyrrell, M. S. Bharadwaj, C. G. Van Horn, S. B. Kritchevsky, B. J. Nicklas, and A. J. Molina, "Respirometric profiling of muscle mitochondria and blood cells are associated with differences in gait speed among community-dwelling older adults," *The Journals of Gerontology Series A, Biological Sciences and Medical Sciences*, vol. 70, no. 11, pp. 1394–1399, 2014.
- [8] D. J. Tyrrell, M. S. Bharadwaj, C. G. Van Horn, A. P. Marsh, B. J. Nicklas, and A. J. Molina, "Blood-cell bioenergetics are associated with physical function and inflammation in overweight/obese older adults," *Experimental Gerontology*, vol. 70, pp. 84–91, 2015.
- [9] D. J. Tyrrell, M. S. Bharadwaj, M. J. Jorgensen, T. C. Register, and A. J. Molina, "Blood cell respirometry is associated with skeletal and cardiac muscle bioenergetics: implications for a minimally invasive biomarker of mitochondrial health," *Redox Biology*, vol. 10, pp. 65–77, 2016.
- [10] B. K. Chacko, P. A. Kramer, S. Ravi et al., "The bioenergetic health index: a new concept in mitochondrial translational research," *Clinical Science*, vol. 127, no. 6, pp. 367–373, 2014.
- [11] D. D. Clarke and L. Sokoloff, "Circulation and energy metabolism of the brain," *Basic neurochemistry: molecular, cellular and medical aspects*, vol. 6, pp. 637–669, 1999.
- [12] J. M. Berg, J. L. Tymoczko, and L. Stryer, *Each Organ has a Unique Metabolic Profile*, W H Freeman, New York, NY, USA, 2002.

- [13] R. H. Swerdlow and S. M. Khan, "A "mitochondrial cascade hypothesis" for sporadic Alzheimer's disease," *Medical Hypotheses*, vol. 63, no. 1, pp. 8–20, 2004.
- [14] G. E. Gibson and Q. Shi, "A mitocentric view of Alzheimer's disease suggests multi-faceted treatments," *Journal of Alzheimer's Disease*, vol. 20, Supplement 2, pp. S591–S607, 2010.
- [15] S. M. Cardoso, I. Santana, R. H. Swerdlow, and C. R. Oliveira, "Mitochondria dysfunction of Alzheimer's disease cybrids enhances A β toxicity," *Journal of Neurochemistry*, vol. 89, no. 6, pp. 1417–1426, 2004.
- [16] M. F. Galindo, I. Ikuta, X. Zhu, G. Casadesus, and J. Jordán, "Mitochondrial biology in Alzheimer's disease pathogenesis," *Journal of Neurochemistry*, vol. 114, no. 4, 2010.
- [17] P. H. Reddy and M. F. Beal, "Amyloid beta, mitochondrial dysfunction and synaptic damage: implications for cognitive decline in aging and Alzheimer's disease," *Trends in Molecular Medicine*, vol. 14, no. 2, pp. 45–53, 2008.
- [18] H. M. Wilkins and R. H. Swerdlow, "Amyloid precursor protein processing and bioenergetics," *Brain Research Bulletin*, vol. 133, pp. 71–79, 2016.
- [19] L. Devi, B. M. Prabhu, D. F. Galati, N. G. Avadhani, and H. K. Anandatheerthavarada, "Accumulation of amyloid precursor protein in the mitochondrial import channels of human Alzheimer's disease brain is associated with mitochondrial dysfunction," *The Journal of Neuroscience*, vol. 26, no. 35, pp. 9057–9068, 2006.
- [20] N. Dragicevic, M. Mamcarz, Y. Zhu et al., "Mitochondrial amyloid-beta levels are associated with the extent of mitochondrial dysfunction in different brain regions and the degree of cognitive impairment in Alzheimer's transgenic mice," *Journal of Alzheimer's Disease*, vol. 20, Supplement 2, pp. S535–S550, 2010.
- [21] H. Du, L. Guo, S. Yan, A. A. Sosunov, G. M. McKhann, and Y. S. ShiDu, "Early deficits in synaptic mitochondria in an Alzheimer's disease mouse model," *Proceedings of the National Academy of Sciences*, vol. 107, no. 43, pp. 18670–18675, 2010.
- [22] C. Caspersen, N. Wang, J. Yao et al., "Mitochondrial Abeta: a potential focal point for neuronal metabolic dysfunction in Alzheimer's disease," *The FASEB Journal*, vol. 19, no. 14, pp. 2040–2041, 2005.
- [23] C. A. Hansson Petersen, N. Alikhani, H. Behbahani et al., "The amyloid beta-peptide is imported into mitochondria via the TOM import machinery and localized to mitochondrial cristae," *Proceedings of the National Academy of Sciences of the United States of America*, vol. 105, no. 35, pp. 13145–13150, 2008.
- [24] M. Manczak, T. S. Anekonda, E. Henson, B. S. Park, J. Quinn, and P. H. Reddy, "Mitochondria are a direct site of a beta accumulation in Alzheimer's disease neurons: implications for free radical generation and oxidative damage in disease progression," *Human Molecular Genetics*, vol. 15, no. 9, pp. 1437–1449, 2006.
- [25] L. Mosconi, R. Mistur, R. Switalski et al., "FDG-PET changes in brain glucose metabolism from normal cognition to pathologically verified Alzheimer's disease," *European Journal of Nuclear Medicine and Molecular Imaging*, vol. 36, no. 5, pp. 811–822, 2009.
- [26] S. Minoshima, B. Giordani, S. Berent, K. A. Frey, N. L. Foster, and D. E. Kuhl, "Metabolic reduction in the posterior cingulate cortex in very early Alzheimer's disease," *Annals of Neurology*, vol. 42, no. 1, pp. 85–94, 1997.
- [27] C. Marcus, E. Mena, and R. M. Subramaniam, "Brain PET in the diagnosis of Alzheimer's disease," *Clinical Nuclear Medicine*, vol. 39, no. 10, pp. e413–e422, 2014.
- [28] L. M. Bloudek, D. E. Spackman, M. Blankenburg, and S. D. Sullivan, "Review and meta-analysis of biomarkers and diagnostic imaging in Alzheimer's disease," *Journal of Alzheimer's Disease*, vol. 26, no. 4, pp. 627–645, 2011.
- [29] K. Lunnon, Z. Ibrahim, P. Proitsi et al., "Mitochondrial dysfunction and immune activation are detectable in early Alzheimer's disease blood," *Journal of Alzheimer's Disease*, vol. 30, no. 3, pp. 685–710, 2012.
- [30] K. Leuner, J. Pantel, C. Frey et al., "Enhanced apoptosis, oxidative stress and mitochondrial dysfunction in lymphocytes as potential biomarkers for Alzheimer's disease," *Journal of Neural Transmission. Supplementa*, vol. 72, pp. 207–215, 2007.
- [31] E. Kadioglu, S. Sardas, S. Aslan, E. Isik, and K. A. Esat, "Detection of oxidative DNA damage in lymphocytes of patients with Alzheimer's disease," *Biomarkers*, vol. 9, no. 2, pp. 203–209, 2004.
- [32] P. Mecocci, M. C. Polidori, T. Ingegni et al., "Oxidative damage to DNA in lymphocytes from AD patients," *Neurology*, vol. 51, no. 4, pp. 1014–1017, 1998.
- [33] J. Valla, L. Schneider, T. Niedzielko et al., "Impaired platelet mitochondrial activity in Alzheimer's disease and mild cognitive impairment," *Mitochondrion*, vol. 6, no. 6, pp. 323–330, 2006.
- [34] Z. Fišar, J. Hroudová, H. Hansíková et al., "Mitochondrial respiration in the platelets of patients with Alzheimer's disease," *Current Alzheimer research*, vol. 13, no. 8, pp. 930–941, 2016.
- [35] B. Borroni, D. Perani, M. Broli et al., "Pre-clinical diagnosis of Alzheimer disease combining platelet amyloid precursor protein ratio and rCBF spect analysis," *Journal of Neurology*, vol. 252, no. 11, pp. 1359–1362, 2005.
- [36] F. Colciaghi, B. Borroni, L. Pastorino et al., "[alpha]-secretase ADAM10 as well as [alpha]APPs is reduced in platelets and CSF of Alzheimer disease patients," *Molecular medicine (Cambridge, Mass)*, vol. 8, no. 2, pp. 67–74, 2002.
- [37] P. E. Coskun, J. Wyrembak, O. Derbereva et al., "Systemic mitochondrial dysfunction and the etiology of Alzheimer's disease and Down syndrome dementia," *Journal of Alzheimer's Disease*, vol. 20, Supplement 2, pp. S293–S310, 2010.
- [38] B. K. Chacko, P. A. Kramer, S. Ravi et al., "The bioenergetic health index: a new concept in mitochondrial translational research," *Clinical Science (London, England)*, vol. 127, no. 6, pp. 367–373, 2014.
- [39] D. J. Tyrrell, M. S. Bharadwaj, M. J. Jorgensen, T. C. Register, and A. J. Molina, "Blood cell respirometry is associated with skeletal and cardiac muscle bioenergetics: implications for a minimally invasive biomarker of mitochondrial health," *Redox Biology*, vol. 10, pp. 65–77, 2016.
- [40] B. P. Dranka, G. A. Benavides, A. R. Diers et al., "Assessing bioenergetic function in response to oxidative stress by metabolic profiling," *Free Radical Biology & Medicine*, vol. 51, no. 9, pp. 1621–1635, 2011.
- [41] C. Desler, T. L. Hansen, J. B. Frederiksen, M. L. Marcker, K. K. Singh, and R. L. Juel, "Is there a link between mitochondrial reserve respiratory capacity and aging?," *Journal of Aging Research*, vol. 2012, Article ID 192503, 9 pages, 2012.

- [42] D. A. Ferrick, A. Neilson, and C. Beeson, "Advances in measuring cellular bioenergetics using extracellular flux," *Drug Discovery Today*, vol. 13, no. 5-6, pp. 268–274, 2008.
- [43] M. B. Jekabsons and D. G. Nicholls, "In situ respiration and bioenergetic status of mitochondria in primary cerebellar granule neuronal cultures exposed continuously to glutamate," *The Journal of Biological Chemistry*, vol. 279, no. 31, pp. 32989–33000, 2004.
- [44] S. L. Willard, B. Uberseder, A. Clark et al., "Long term sertraline effects on neural structures in depressed and nondepressed adult female nonhuman primates," *Neuropharmacology*, vol. 99, pp. 369–378, 2015.
- [45] M. Styner, R. Knickmeyer, S. Joshi, C. Coe, S. J. Short, and J. Gilmore, Eds., *Automatic Brain Segmentation in Rhesus Monkeys. Medical Imaging*, International Society for Optics and Photonics, San Diego, CA, USA, 2007.
- [46] J. A. Maldjian, C. A. Shively, M. A. Nader, D. P. Friedman, and C. T. Whitlow, "Multi-atlas library for eliminating normalization failures in non-human primatesNeuroinformatics," vol. 14, no. 2, pp. 183–190, 2015.
- [47] M. S. Bharadwaj, D. J. Tyrrell, M. F. Lyles, J. L. Demons, G. W. Rogers, and A. J. Molina, "Preparation and respirometric assessment of mitochondria isolated from skeletal muscle tissue obtained by percutaneous needle biopsy," *Journal of Visualized Experiments*, no. 96, 2015.
- [48] G. W. Rogers, M. D. Brand, S. Petrosyan et al., "High throughput microplate respiratory measurements using minimal quantities of isolated mitochondria," *PLoS One*, vol. 6, no. 7, article e21746, 2011.
- [49] P. J. Crouch, R. Blake, J. A. Duce et al., "Copper-dependent inhibition of human cytochrome c oxidase by a dimeric conformer of amyloid- β_{1-42} ," *The Journal of Neuroscience*, vol. 25, no. 3, pp. 672–679, 2005.
- [50] X. Wang, B. Su, H.-G. Lee et al., "Impaired balance of mitochondrial fission and fusion in Alzheimer's disease," *The Journal of Neuroscience*, vol. 29, no. 28, pp. 9090–9103, 2009.
- [51] X. Wang, B. Su, L. Zheng, G. Perry, M. A. Smith, and X. Zhu, "The role of abnormal mitochondrial dynamics in the pathogenesis of Alzheimer's disease," *Journal of Neurochemistry*, vol. 109, pp. 153–159, 2009.
- [52] X. Wang, B. Su, S. L. Siedlak et al., "Amyloid-beta overproduction causes abnormal mitochondrial dynamics via differential modulation of mitochondrial fission/fusion proteins," *Proceedings of the National Academy of Sciences of the United States of America*, vol. 105, no. 49, pp. 19318–19323, 2008.
- [53] X. Wang, B. Su, H. Fujioka, and X. Zhu, "Dynamin-like protein 1 reduction underlies mitochondrial morphology and distribution abnormalities in fibroblasts from sporadic Alzheimer's disease patients," *The American Journal of Pathology*, vol. 173, no. 2, pp. 470–482, 2008.
- [54] H. Chen and D. C. Chan, "Mitochondrial dynamics – fusion, fission, movement, and mitophagy – in neurodegenerative diseases," *Human Molecular Genetics*, vol. 18, no. R2, pp. R169–R176, 2009.
- [55] H. Chen, J. M. McCaffery, and D. C. Chan, "Mitochondrial fusion protects against neurodegeneration in the cerebellum," *Cell*, vol. 130, no. 3, pp. 548–562, 2007.
- [56] D. Narendra, A. Tanaka, D.-F. Suen, and R. J. Youle, "Parkin-induced mitophagy in the pathogenesis of Parkinson disease," *Autophagy*, vol. 5, no. 5, pp. 706–708, 2009.
- [57] M. T. Lin and M. F. Beal, "Mitochondrial dysfunction and oxidative stress in neurodegenerative diseases," *Nature*, vol. 443, no. 7113, pp. 787–795, 2006.
- [58] G. J. Tranah, J. S. Yokoyama, S. M. Katzman et al., "Mitochondrial DNA sequence associations with dementia and amyloid- β in elderly African Americans," *Neurobiology of Aging*, vol. 35, no. 2, pp. 442.e1–442.e8, 2014.
- [59] P. G. Ridge, T. J. Maxwell, C. D. Corcoran et al., "Mitochondrial genomic analysis of late onset Alzheimer's disease reveals protective haplogroups H6A1A/H6A1B: the Cache County Study on Memory in Aging," *PLoS One*, vol. 7, no. 9, article e45134-e, 2012.
- [60] P. G. Ridge, A. Koop, T. J. Maxwell et al., "Mitochondrial haplotypes associated with biomarkers for Alzheimer's disease," *PLoS One*, vol. 8, no. 9, article e74158-e, 2013.
- [61] A. Santoro, V. Balbi, E. Balducci et al., "Evidence for sub-haplogroup h5 of mitochondrial DNA as a risk factor for late onset Alzheimer's disease," *PLoS One*, vol. 5, no. 8, article e12037-e, 2010.
- [62] M. J. Keogh and P. F. Chinnery, "Mitochondrial DNA mutations in neurodegeneration," *Biochimica et Biophysica Acta (BBA) - Bioenergetics*, vol. 1847, no. 11, pp. 1401–1411, 2015.
- [63] L. M. Reynolds, J. Ding, J. R. Taylor et al., "Transcriptomic profiles of aging in purified human immune cells," *BMC Genomics*, vol. 16, p. 333, 2015.

Research Article

Generation and Bioenergetic Profiles of Cybrids with East Asian mtDNA Haplogroups

Huaibin Zhou,¹ Ke Nie,¹ Ruyi Qiu,^{1,2} Jingting Xiong,¹ Xiaoli Shao,¹ Bingqian Wang,¹ Lijun Shen,¹ Jianxin Lyu,^{1,3} and Hezhi Fang¹

¹Key Laboratory of Laboratory Medicine, Ministry of Education, Zhejiang Provincial Key Laboratory of Medical Genetics, College of Laboratory Medicine and Life Sciences, Wenzhou Medical University, Wenzhou, Zhejiang 325035, China

²Zhejiang Provincial Hospital of TCM, Hangzhou, Zhejiang 310000, China

³Hangzhou Medical College, Hangzhou, Zhejiang, China

Correspondence should be addressed to Jianxin Lyu; jxlu313@163.com and Hezhi Fang; fangh@wmu.edu.cn

Received 30 March 2017; Revised 6 July 2017; Accepted 14 August 2017; Published 28 September 2017

Academic Editor: Icksoo Lee

Copyright © 2017 Huaibin Zhou et al. This is an open access article distributed under the Creative Commons Attribution License, which permits unrestricted use, distribution, and reproduction in any medium, provided the original work is properly cited.

Human mitochondrial DNA (mtDNA) variants and haplogroups may contribute to susceptibility to various diseases and pathological conditions, but the underlying mechanisms are not well understood. To address this issue, we established a cytoplasmic hybrid (cybrid) system to investigate the role of mtDNA haplogroups in human disease; specifically, we examined the effects of East Asian mtDNA genetic backgrounds on oxidative phosphorylation (OxPhos). We found that mtDNA single nucleotide polymorphisms such as m.489T>C, m.10398A>G, m.10400C>T, m.C16223T, and m.T16362C affected mitochondrial function at the level of mtDNA, mtRNA, or the OxPhos complex. Macrohaplogroup M exhibited higher respiratory activity than haplogroup N owing to its higher mtDNA content, mtRNA transcript levels, and complex III abundance. Additionally, haplogroup M had higher reactive oxygen species levels and NAD⁺/NADH ratios than haplogroup N, suggesting difference in mitonuclear interactions. Notably, subhaplogroups G2, B4, and F1 appeared to contribute significantly to the differences between haplogroups M and N. Thus, our cybrid-based system can provide insight into the mechanistic basis for the role of mtDNA haplogroups in human diseases and the effect of mtDNA variants on mitochondrial OxPhos function. In addition, studies of mitonuclear interaction using this system can reveal predisposition to certain diseases conferred by variations in mtDNA.

1. Introduction

Mitochondria are cytoplasmic organelles of eukaryotic cells with a double membrane and tortuous cristae structure that generate the bulk of ATP for cellular process including DNA decoding, kinase activation, and nutrient transport. ATP is produced in mitochondria via the oxidative phosphorylation (OxPhos) system, a functional unit located in the inner mitochondrial membrane. In mammals, the OxPhos machinery consists of five protein complexes—complex I (NADH:quinone oxidoreductase), complex II (succinate dehydrogenase), complex III (ubiquinol-cytochrome c reductase), complex IV (cytochrome c oxidase), and complex V (ATP synthase)—and two small molecules (coenzyme Q10 and cytochrome c). Components of all OxPhos complexes, with the exception of complex II, are mitochondrially encoded. Therefore, genetic

variations in the mitochondrial genome can impact human health and disease.

Human mtDNA is double-stranded and circular with a length of 16,569 bp; it contains 37 genes, encoding 13 proteins of the OxPhos machinery and 22 tRNAs and two rRNAs for mitochondrial translation. mtDNA mutations cause changes in OxPhos system function, which have been implicated in various neuromuscular disorders such as Leigh syndrome and myoclonic epilepsy with ragged red fibers (MERRF) [1]. On the other hand, hundreds of mtDNA single nucleotide polymorphisms (SNPs) that can lead to nondeleterious alterations in OxPhos function have survived selective forces exerted by environmental factors and random drift during evolution [1].

A haplogroup is defined by variations in human mitochondrial DNA (i.e., SNPs) that are fixed and share a

common ancestry. mtDNA haplogroups and their characteristic SNPs—for example, m.10398A/G [2], m.5178C/A [3], and m.152T/C [4]—can be advantageous or detrimental and have been implicated in a number of diseases and pathological conditions, including cancer [5], aging [6], diabetes [7], osteoarthritis [8], schizophrenia [9], and Leber's hereditary optic neuropathy [10]. A phylogenetic tree of L3 subhaplogroups that migrated from Africa to East Asia [11, 12] revealed that many of the subclades were associated with metabolic and degenerative diseases [13, 14]. The link between mtDNA haplogroup/SNPs and disease has been attributed to possible changes in mitochondrial reactive oxygen species (ROS) levels, respiration capacity, and ATP production [15, 16]. Functional analysis of mtDNA SNPs identified a common mtDNA variation, m.9821insA/AA, that affected mitochondrial ROS generation and OxPhos in mouse cells [17], while another showed that mtDNA haplogroups influence phenotypic variability in mice [18]. We and others have used transmitochondrial cytoplasmic hybrids (cybrids) to investigate the effects of mtDNA haplogroups/SNPs on disease conditions in human cells. Haplogroups related or unrelated to disease were fused with human 143B osteosarcoma cells lacking mtDNA rho zero ($\rho 0$) cells [19], respectively. The effects of East Asian haplogroups/SNPs G versus B4 on osteoarthritis [15] and m.8584A/10398G versus m.8584G/10398A on Parkinson's disease [20] and of haplogroup B4 versus D4 on diabetes [14] and haplogroup B4 and E on biliary atresia [21] have been analyzed. However, mitochondrial function profile of the entire mtDNA phylogenetic tree was not reported.

To this end, in the present study, we used transmitochondrial technology to construct 21 cybrid cells representing different haplogroups to cover the entire Han Chinese mtDNA phylogenetic tree. The mtDNA phylogeny of the Han population, the largest ethnic group in China, is representative of that of all East Asian mtDNA phylogeny. We analyzed respiratory activity, mtDNA copy number, and retrograde signaling molecules in cybrid cells to define the spectrum of mitochondrial OxPhos in East Asian mtDNA haplogroups and to provide a foundation for mitochondria-based evolutionary medicine.

2. Materials and Methods

2.1. Generation of Cell Lines and Culture Conditions. 143B $\rho 0$ human osteosarcoma cells lacking mtDNA were cultured in high-glucose Dulbecco's modified Eagle's medium (DMEM, Thermo Fisher Scientific, Waltham, MA, USA) containing 10% fetal bovine serum (Thermo Fisher Scientific), 100 $\mu\text{g}/\text{ml}$ pyruvate, and 50 $\mu\text{g}/\text{ml}$ uridine. Cybrids were formed by fusing 143B $\rho 0$ cells and platelets from healthy individuals with different haplotypes [15]. Cybrid clones were cultured in high-glucose DMEM containing 10% fetal bovine serum at 37°C in an atmosphere with 5% carbon dioxide.

2.2. mtDNA Sequencing, Genotyping, and Rebuilding the mtDNA Phylogenetic Tree. A total of 21 volunteers (mean \pm SD: age 22 \pm 0 years; 14 women and eight men) with different mtDNA haplotypes were recruited from the medical

examination center of the First Affiliated Hospital of Wenzhou Medical University. Written informed consent was obtained from each participant. The study protocol was approved by the Ethics Committee of Wenzhou Medical University. Genomic DNA from the volunteers was extracted using sodium dodecyl sulfate (SDS) lysis buffer as described previously [8]. Sanger sequencing was performed for the entire mtDNA of each individual on an ABI 3730XL system (Thermo Fisher Scientific) with 24 primer pairs [15]. Detailed mtDNA haplotypes were annotated for each subject based on an established mtDNA tree [11, 12]. A phylogenetic mtDNA tree was reconstructed from the data derived from the 21 subjects according to an established East Asian mtDNA tree [11].

2.3. Quantification of mtDNA Copy Number. To determine mtDNA copy number, cells were incubated in SDS lysis buffer for more than 12 hours prior to genomic DNA extraction [22]. The $\Delta\Delta\text{CT}$ was used to determine the relative values of mtDNA copy number [23]. Briefly, Ct values generated from mtDNA were normalized to the housekeeping gene 18sDNA (2 [Ct mtDNA–Ct 18sDNA]). Relative mtDNA copy number for each cybrid was obtained by comparing to the average Ct value of mtDNA from 21 cybrids (2 [average Ct mtDNA–[Ct mtDNA–Ct 18sDNA]]). Real-time PCR was performed on an ABI Step-One Plus Real-Time PCR System (Thermo Fisher Scientific) using SYBR Green qPCR Mastermix (Takara Bio, Dalian, China) and the following primers were used: human mtDNA (human-tRNA leucine 1+transcription terminator+5S-like sequence), forward, 5'-CACCCAAGAACAGGGTTTGT-3' and reverse, 5'-TGGCCATGGGTATGTTGTTAA-3' and human nuclear DNA (18s ribosomal DNA), forward, 5'-TAGAGGGACAAGTGGCGTTC-3' and reverse, 5'-CGCTGAGCCAGTCA GTGT-3'. The efficiency of the primers was 90%–110%.

2.4. Quantitative Reverse Transcriptase PCR Analysis. RNA was extracted from cybrids with Trizol reagent [24]. Total RNA (5 μg) was reverse-transcribed into cDNA using an RNA reverse transcription kit (Takara Bio). Briefly, Ct values generated from mtRNA were normalized to that of the housekeeping gene 18S rRNA (2 [Ct mtRNA–Ct18srRNA]). The relative mtRNA level was obtained for each cybrid by comparing to the average Ct value of mtRNA from 21 cybrids (2 [average Ct mtRNA–[Ct mtRNA–Ct 18S RNA]]). Three sets of primers were used to determine the level of mtDNA transcripts started at the L, H1, and H2 promoters. The primer sets were as follows: (1) L strand: forward, 5'-GGTAGAGGCGACAAACCTACCG-3' and reverse, 5'-TTTAGGCCTACTATGGGTGT-3' [25]; (2) H1 strand: forward, 5'-GGCCAACCTCCTACTCC-3' and reverse, 5'-GATGGTAGATGTGGCGGGTT-3' [26]; and (3) H2 strand: forward, 5'-AGCCACTTCCACACAGACAT C-3' and reverse, 5'-GTTAGGCTGGTGTAGGGTTCT-3' [26]. Target mRNA levels were normalized against that of 18S rRNA. The 18S rRNA primers used were as follows: forward, 5'-GACGATCAGATACCGTCGTA-3' and reverse,

5'-TGAGGTTTCCCGTGTGAGT-3'. Data obtained from qRT-PCR were analyzed with the $\Delta\Delta\text{CT}$ method.

2.5. Mitochondrial Protein Preparation, Blue Native PAGE, and Immunoblotting. Mitochondrial proteins were isolated from cultured cells using 2% Triton-20 (Sigma-Aldrich, St. Louis, MO, USA) [27]. Proteins (30–60 μg) mixed with 0.5% Blue G-250 (Sigma-Aldrich) and 5% glycerol were run on 3%–11% gradient blue native gels [27]. Antibodies against gene associated with retinoic-interferon-induced mortality 19, succinate dehydrogenase complex, subunit A, ubiquinol-cytochrome C reductase core protein 2, cyclooxygenase IV, and ATP synthase subunit 5 α (all from MitoSciences, Eugene, OR, USA) were used to detect mitochondrial OxPhos complexes. Antibodies against voltage-dependent anion channel (Cell Signaling Technology, Danvers, MA, USA) and actin (Santa Cruz Biotechnology, Dallas, TX, USA) were used for loading controls. All primary antibodies were used at dilutions of 1:1000. Alkaline phosphatase- or horseradish peroxidase-conjugated anti-mouse IgG (both from Cell Signaling Technology) and anti-rabbit IgG (Thermo Fisher Scientific) secondary antibodies were used at 1:2000 dilution. Immunoreactivity was detected with the Super Signal West Pico chemiluminescence reagent (Thermo Fisher Scientific) or 5-bromo-4-chloro-3-indolyl phosphate/nitro blue tetrazolium substrates (Sigma-Aldrich). Signal of luminol-based enhanced chemiluminescence was detected using ChemiDoc imaging system (Bio-Rad, Hercules, CA, USA). Integrated optical density (IOD) quantification of immunoblots was performed using a Gel-Pro Analyzer 4.0 (Media Cybernetics, Warrendale, PA, USA).

2.6. Measurement of Endogenous Oxygen Consumption. Endogenous oxygen consumption of intact cells was determined using a Clark-type oxygen electrode (OROBOROS, Innsbruck, Austria) as described previously [28]. After recording basal respiration, oligomycin (0.1 mg/mL) (Thermo Scientific, Waltham, MA, USA) was added to detect uncoupling respiration. The standard protein content was measured using a BCA kit (Thermo Scientific, Waltham, MA, USA) to adjust experimental results.

2.7. Measurement of NAD⁺/NADH and Mitochondrial ROS. The NAD⁺/NADH ratio was detected in cultured cells with an NAD⁺/NADH ratio assay kit (Abcam, Cambridge, MA, USA) [15]. Briefly, cells were washed with phosphate-buffered saline (PBS) buffer and lysed with lysis buffer for 15 minutes at room temperature. Then, the NAD and NADH extraction reagents were added and the reaction was proceeded at room temperature for 15 minutes. PBS was used as blank control, and the fluorescence signal was measured after 30 minutes in conditions of excitation (540 nm) and emission (590 nm) with a Varioskan™ Flash Multimode Reader (Thermo Scientific, Waltham, MA, USA). Mitochondrial ROS were measured according to a previously published protocol [15]. Briefly, cells were washed with Hank's buffered salt solution (HBSS) and incubated with HBSS containing 5 μM Mito SOX (Thermo Scientific, Waltham, MA, USA) at 37°C for 20 minutes. Cells were

washed three times with HBSS, and fluorescence signal was detected using a Varioskan Flash Multimode Reader (Thermo Scientific, Waltham, MA, USA) under the conditions of excitation (488 nm) and emission (530 nm).

2.8. Fluorescence Microscopy of Mitochondrial Morphology. Cells were incubated with 500 nM MitoTracker Red (Thermo Scientific, Waltham, MA, USA) for 30 minutes and fixed for 15 minutes with 4% paraformaldehyde at room temperature. The cells were then permeabilized with 0.2% Triton X-100 (Sigma, St. Louis, MO, USA), stained with DAPI (Thermo Scientific, Waltham, MA, USA), and observed using an Olympus imaging system (Olympus FV1000, Melville, NY, USA). The length and complexity of the mitochondria were determined by measuring the form factor (FF) and aspect ratio (AR), respectively [29].

2.9. MMP Measurements. MMP was determined using the cationic fluorescent redistribution dye TMRM (Thermo Scientific, Waltham, MA, USA) as described previously [30]. Briefly, in the nonquenching mode, cells were incubated with 30 nM TMRM in a 37°C CO₂ incubator for 30 min. Cells were washed three times with HBSS, and fluorescence signal was detected using a Varioskan Flash Multimode Reader (Thermo Scientific) under the conditions of excitation (350 nm) and emission (461 nm).

2.10. Statistical Analysis. Results are expressed as mean \pm SEM and were analyzed with the Mann-Whitney *U* test using SPSS v.17.0 software (IBM, Armonk, NY, USA). Statistical analysis was performed only when specific SNPs were identified in three or more cybrids. For relative comparisons, results obtained from one cybrid were compared to the average value of all 21 cybrids. *P* < 0.05 was considered statistically significant.

3. Results

3.1. Generation of Cybrid Cell Lines Covering the Major East Asian mtDNA Haplogroups. To investigate the effects of East Asian mtDNA haplogroups on OxPhos, we generated cybrid cell lines containing different mtDNA haplogroups in the same osteosarcoma 143B nuclear background from Han Chinese, a population that comprises most East Asian haplogroup. Based on the mtDNA haplogroup classification tree [31, 32], 21 cybrid cell lines with D, G, M8, M7, A, N9, B, and R9 basal mtDNA haplogroups were generated to cover the common mtDNA macrohaplogroups of China, excluding two small clades [33], M9 and M10, enriched in Tibet (Figure 1). Four of the cybrid cell lines with haplogroups B4 and G were previously generated in our laboratory [15]. Entire mtDNA from cybrid cell lines was subject to Sanger sequencing and aligned to the mtDNA revised Cambridge Reference Sequence (rCRS, GenBank accession number NC_012920). An mtDNA phylogenetic tree was then reconstructed based on these sequencing results and the existing phylogenetic tree [12, 31, 32]. We detected 79, 160, and 31 variants in the D-loop, coding region, and tRNA/rRNAs, respectively, in the 21 cybrid cell lines (Figure 2 and Table S1 available online at <https://doi.org/10.1155/2017/1062314>).

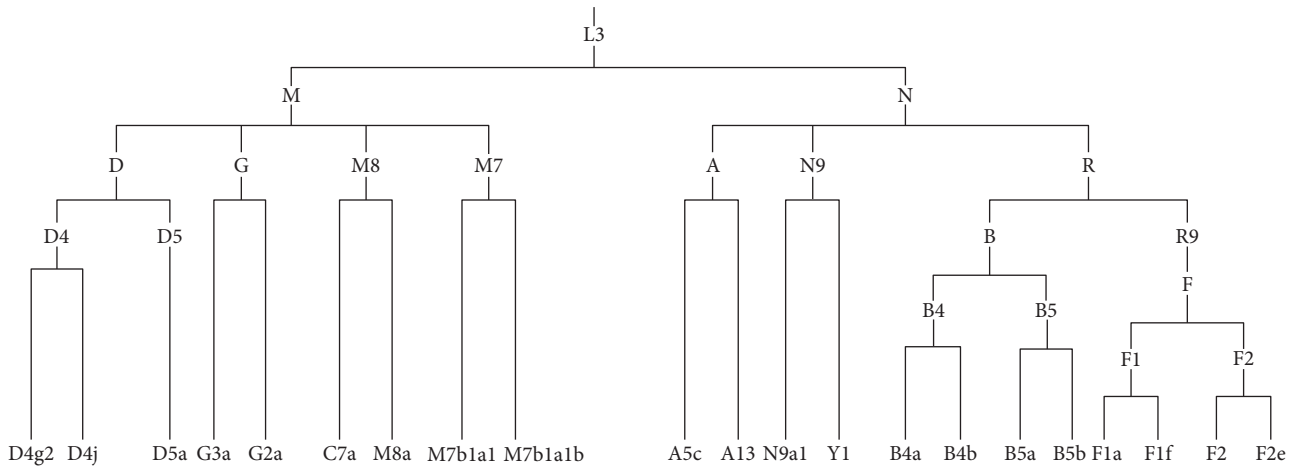


FIGURE 1: mtDNA tree of the 21 cybrids in China.

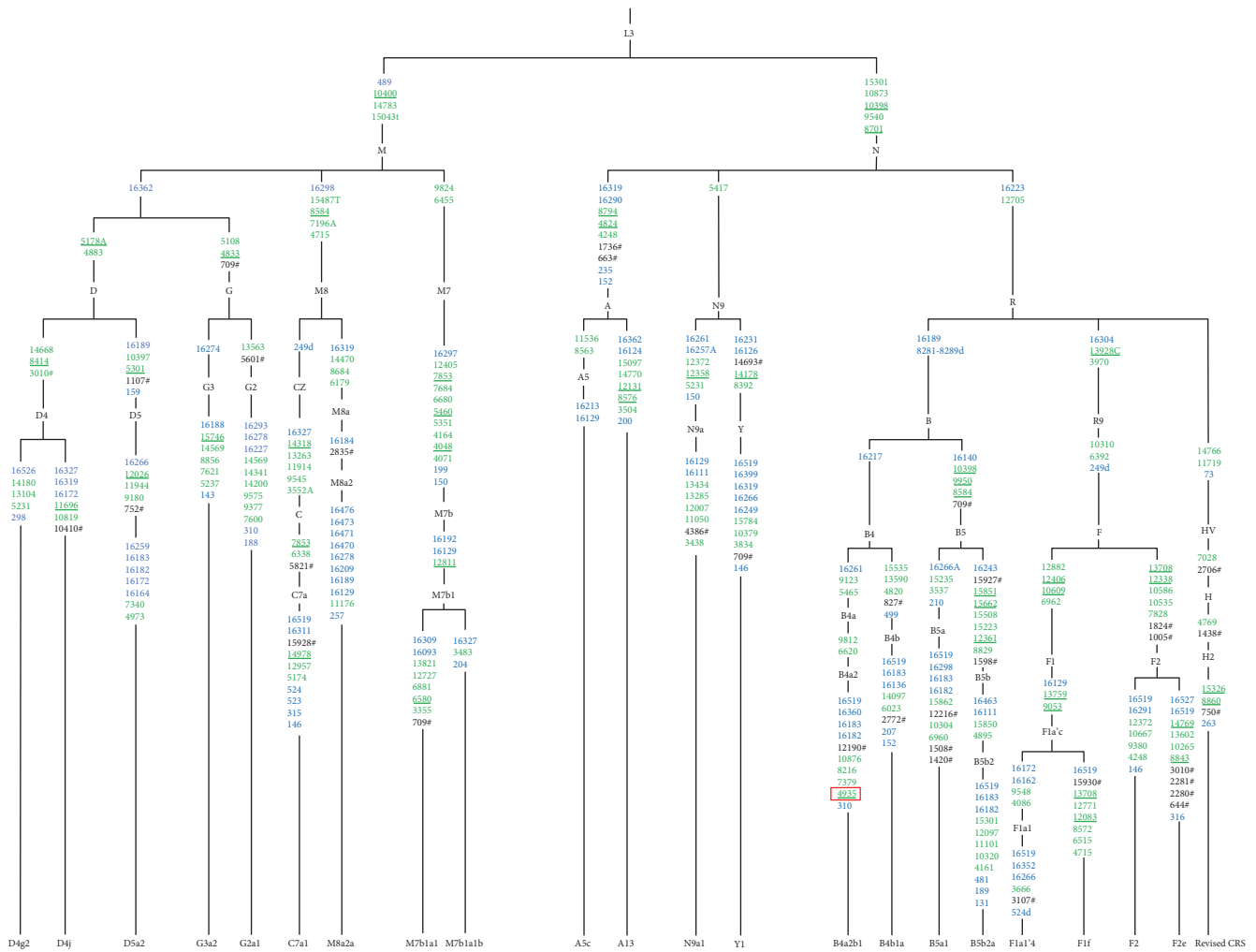


FIGURE 2: Relocation of mtDNA variants of 21 cybrids in the mtDNA tree. Blue and green colors represent control and coding regions, respectively. Nonsynonymous variants are shown in green and are underlined. The hatch marks indicate RNA variations, and the red box denotes novel mutations not reported in published databases. rCRS: revised Cambridge Reference Sequence.

Most variants detected in this study can be retrieved as SNPs in published databases (e.g., mitomap, mtddb, and mtSNP) except m.4935G>A (Thr-Ala, ND2), a novel mutation of the B4a2b1 haplogroup identified in this study. However, this variant does not affect OxPhos function [15].

3.2. mtDNA Copy Number Variation in Different mtDNA Haplogroups. To analyze the effects of mtDNA haplogroups and their expression on the regulation of OxPhos complexes, we determined mtDNA copy number and transcriptional profiles by quantitative real-time PCR in the 21 cybrid cell lines. Nonsynonymous mutations were identified in 146 of the 270 identified SNPs. mtDNA copy number was lower in cybrids containing 4 SNPs (m.249del, m.13708A, m.13928C, and m.16304C) and higher in those containing the SNPs m.489C, m.8701G, m.10398G, and m.10400T as compared to than in cybrids containing rCRS bases (Table S2). It is worth noting that six of these eight SNPs (m.489C, m.8701G, m.13708A, m.13928C, m.16304C, and m.10400T) are unique diagnostic SNPs of a specific mtDNA haplogroup in East Asia, whereas 10398G and m.249del are representative SNPs of two more haplogroups, suggesting that a different mtDNA haplogroup contributed to the difference in mtDNA copy number. Additionally, m.16223T and m.16266A showed slightly higher and lower mtDNA copy number, respectively, as compared to cybrids containing rCRS bases. To be noted, most mtDNA copy number variations were minor (<30%).

We analyzed macrohaplogroups M and N using marker SNPs unique to East Asian haplogroups. mtDNA copy numbers were 25% higher in cybrid cell lines with haplogroup M than in those with haplogroup N (Figure 3). The higher mtDNA copy number in haplogroup M was largely due to subhaplogroups M7b1a1 and M7b1a1b (both contributing a 1.51-fold difference) (Figure 3). Conversely, cybrids with subhaplogroup F1a containing m.16162G exhibited lowest mtDNA copy number and contributed to the greatest degree to the lower mtDNA copy number of haplogroup N (Figure 3). In addition, diagnostic SNPs of haplogroup M (m.489C, m.10398G, and m.10400T) showed a significantly higher mtDNA copy number than cybrids containing rCRS bases (Table S2).

3.3. Profiles of mtRNA and OxPhos Complex Levels in Cells with Different mtDNA Haplogroups. Next, we evaluated the expression of mtRNA in cybrid cells with different haplogroups. By measuring the mRNA levels of 16S rRNA, ND1, and 7S RNA from the primary transcripts of H1, H2, and L strands, respectively. The L strand encodes ND6 and eight tRNAs; its relative mRNA levels varied from 0.28 to 4.36, which were higher for m.16362C than for m.16362T (Table S3). H1 encodes 12S rRNA, 16S rRNA, and two tRNAs; relative H1 strand transcript levels varied from 0.47 to 2.17, which were lower for m.3010A than for m.3010G, while higher H1 transcript levels were observed for m.709A than for m.709G (Table S3). Relative transcript levels of the H2 strand, which encodes 12 tRNAs and 12 OxPhos subunits, varied from 0.56 to 1.74. Although H2 transcript

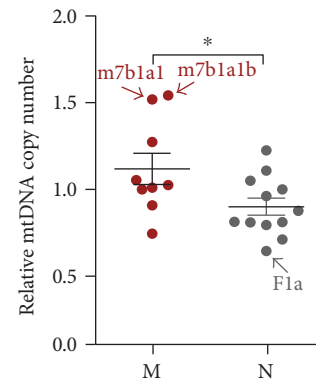


FIGURE 3: mtDNA copy number is higher in haplogroup M than in haplogroup N. Scatter plots represent mtDNA level relative to the average value for 21 cybrids. Data represents mean \pm SEM of at least two independent experiments with 3 replicates each per cybrid. * $P \leq 0.05$.

levels were higher in cybrids containing the five SNPs m.489C, m.8701G, m.10398G, m.10400T, and m.16223T and lower in those containing m.16519C versus their rCRS bases (Table S3), H2 strand transcripts showed fewer variations than L and H1 strands. These results suggest that mtDNA transcription did not change significantly during mtDNA evolution. Additionally, most mtRNA transcription-related SNPs were diagnostic SNPs of mtDNA haplogroups.

For haplogroups, we found that both L strand and H1 strand transcripts did not differ significantly between macrohaplogroups M and N (Figures 4(a) and 4(b)). However, L strand in haplogroup G2a is extremely higher than other haplogroups (Figure 4(a)). Transcriptional levels of the H2 strand in cybrid cell lines with haplogroup M increased significantly compared with those of haplogroup N (Figure 4(c)). Furthermore, M7b1a1b had the highest H2 transcripts in macrohaplogroup M, whereas the H2 transcripts in B4a and F1a were lowest in macrohaplogroup N (Figure 4(c)). However, the average increase of H2 transcripts in haplogroup M could be less than 20% compared with that of haplogroup N. Taken together, these results show that mtDNA genetic background does affect mtRNA transcription, but that the effect is limited.

Next, we examined individual OxPhos complexes I, III, IV, and V components using blue native PAGE in Triton X-100 solubilized whole cells and Western blot analysis. Both mtDNA copy number and mtRNA transcription were significantly affected in cybrid cells with haplogroups M and N. Moreover, our analysis showed that the level of complex III was significantly higher in haplogroup M than in haplogroup N, while complexes I, IV, and V were similar between these two haplogroups (Figure 5).

3.4. Mitochondrial Function in Cells Harboring Different mtDNA Haplogroups. To determine whether mitochondrial function in cybrid cells was affected by difference in mtDNA, mtRNA, and OxPhos complex profiles, we measured endogenous oxygen consumption in cells harboring different mtDNA haplogroups. The respiration assays revealed that

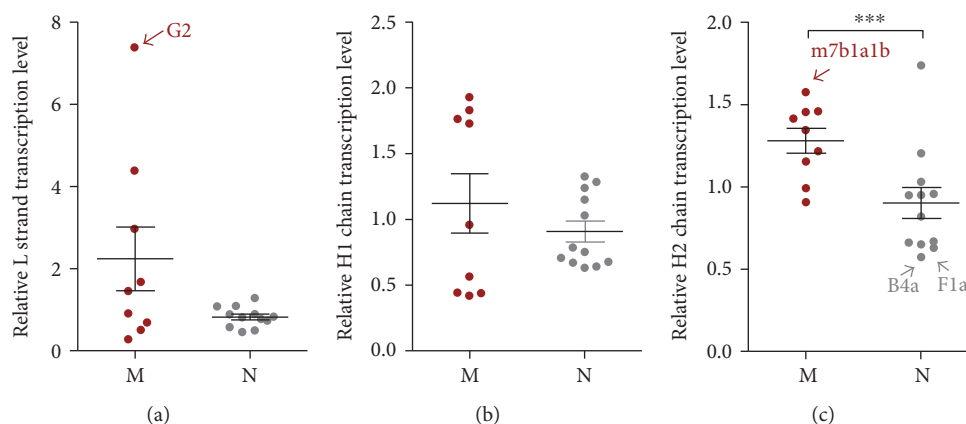


FIGURE 4: mtDNA transcript levels are higher in haplogroup M than in haplogroup N. Relative mtRNA expression was quantified by quantitative real-time PCR. The mRNA levels of 16S rRNA, ND1, and 7S RNA from the primary transcript represent H1, H2, and L strands of mtDNA, respectively. (a) Increased relative transcript level of mitochondrial L strand in haplogroup M. (b) Relative level of mitochondrial H1 strand transcript. (c) Higher relative transcript level of mitochondrial H2 strand in haplogroup M than in haplogroup N. Data represent mean \pm SEM of two independent experiments with 3 replicates each per cybrid. *** $P < 0.001$.

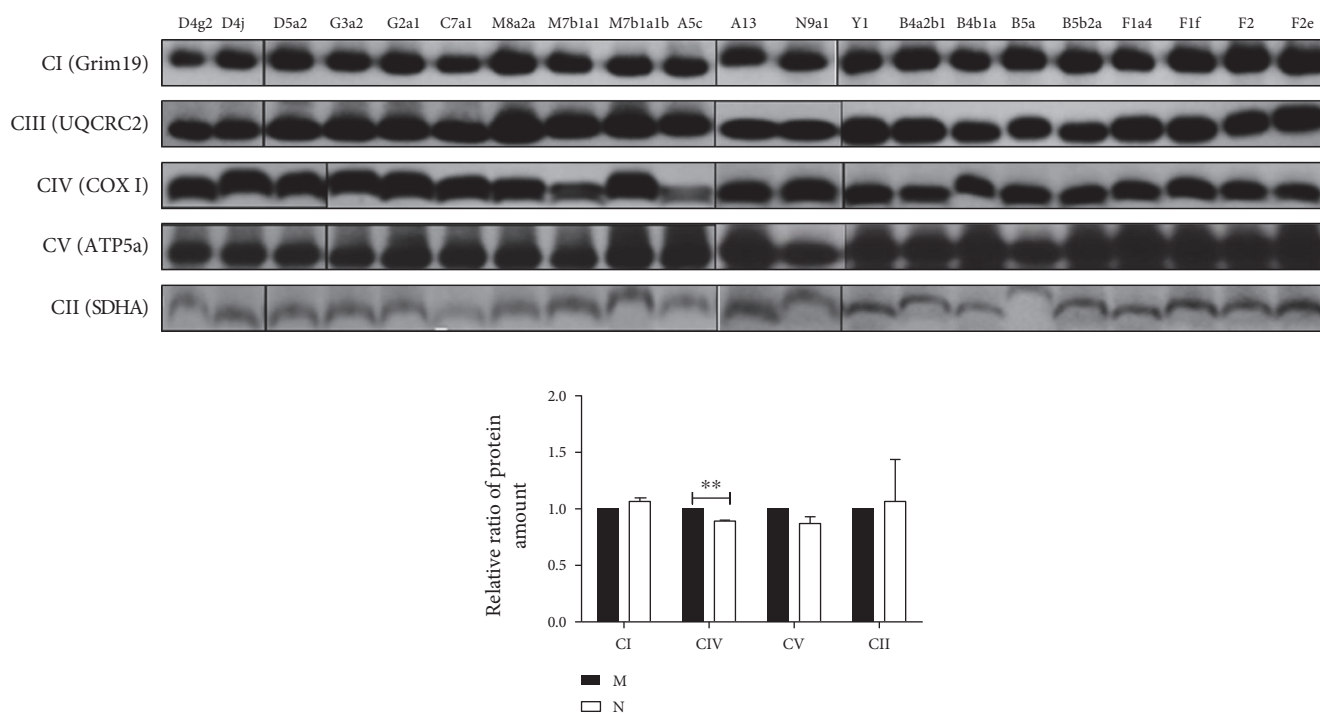


FIGURE 5: Respiratory chain complex III protein expression is higher in haplogroup M than in haplogroup N. Whole cell extracts of mitochondrial respiratory complex from 21 cybrid cell lines were solubilized in Triton-100 at a final concentration of 2% and subjected to blue native PAGE/immunoblot analysis. Complex I, complex II, complex III, complex IV, and complex V proteins were detected with antibodies against gene associated with retinoic-interferon-induced mortality (Grim19), succinate dehydrogenase complex, subunit (SDHA), ubiquinol-cytochrome C reductase core protein (UQCRC2), cyclooxygenase (COXIV), and ATP synthase subunit (ATP5 α), respectively. Data represent mean \pm SEM ($n = 3$). ** $P < 0.01$.

seven SNPs significantly affected basal mitochondrial respiration. Of these, six and one SNPs were associated with lower and higher respiration activity, respectively, as compared with cybrids containing rCRS bases (Table S4). It is worth noting that three SNPs related to high basal respiration were diagnostic SNPs of haplogroup M (m.489C, m.8701G, and

m.10400T). Basal respiration rates in cybrids harboring these seven SNPs ranged from 8.36 to 20.62 nmol/min/mg protein. Furthermore, oxygen consumption in the presence of oligomycin, an ATPase proton channel blocker, showed that four (m.489C, m.8701G, m.10400T, and m.16223T) and one (m.16519C) SNPs associated with higher and lower

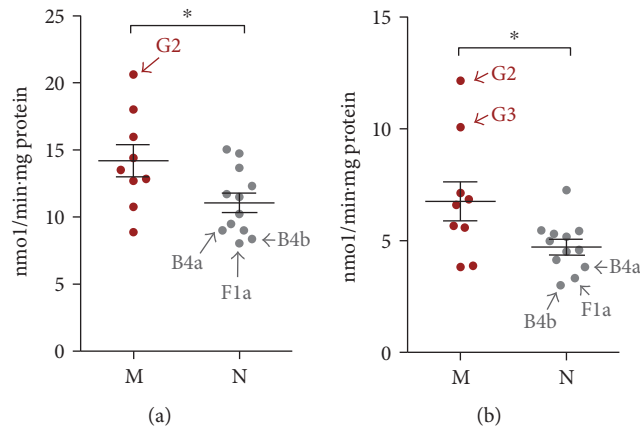


FIGURE 6: Oxygen consumption rate (OCR) is higher in haplogroup M than in haplogroup N. OCR values were measured in 21 cybrid cell lines after sequential treatments with oligomycin (0.1 mg/ml) and the OxPhos uncoupling agent trifluoromethoxy carbonyl cyanide phenylhydrazone (FCCP; 0.1 μ M). (a, b) Comparison of basal (a) and uncoupled (b) mitochondrial respiratory activity. Values represent mean \pm SEM of at least two independent replicates. * $P \leq 0.05$.

respiration, respectively, as compared with cybrids containing rCRS bases (Table S4).

Basal mitochondrial respiration in cybrid cell lines with haplogroup M (m.489C, m.8701G, m.10400T, and most of m.10398G) was higher than that in cybrid cells with haplogroup N (Figure 6(a)). Furthermore, haplogroup G2 had the highest whereas B4b, B4a, and F1a had the lowest basal mitochondrial respiration rates in macrohaplogroups M and N, respectively. In addition, the degree of OxPhos uncoupling was higher in haplogroup M than in haplogroup N (Figure 6(b)). In haplogroup M, this was most apparent in sub-haplogroup G2/3, which explains why “uncoupling mtDNA haplogroup” G was enriched in Siberia (Figure 6(b)). Accordingly, uncoupling respiration in B4b, B4a, and F1a was lowest in haplogroup N, contributing significantly to the respiration in macrohaplogroup N.

To determine whether OxPhos function was altered, we measured mitochondrial inner membrane potential (MMP) in cybrid cell lines. The MMP of haplogroup M was slightly higher than that of haplogroup N (Figure 7), but this difference was not statistically significant ($P = 0.11$).

3.5. Mitochondrial Fragmentation in Cybrid Cells with Different mtDNA Genetic Background. To investigate differences in mitochondrial morphology, mitochondria were stained with MitoTracker and visualized by confocal microscopy. Mitochondria fragmentation was determined by measuring the AR and FF of each mitochondrion, with high AR and FF reflecting increased mitochondrial length/width and branching, respectively. We found that AR was unaffected by mtDNA SNPs (Figure 8(a) and Table S5) and that most variations in these SNPs were limited ($\sim 10\%$). However, we identified two SNPs that slightly affected mitochondrial fragmentation ($P < 0.01$) (Figure 8(a) and Table S6). Thus, the percentage of mitochondrial fragmentation did not differ between mtDNA macrohaplogroups M and N (Figures 8(a), 8(b), and 8(c)).

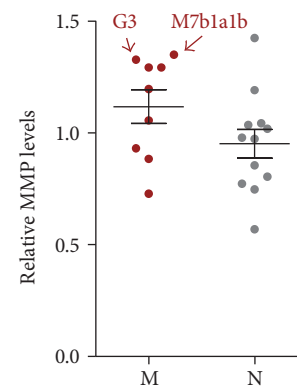


FIGURE 7: MMP is higher in haplogroup M than in haplogroup N. MMP levels were measured in cells treated with 30 nM tetramethylrhodamine (TMRM) for 30 min. Relative MMP levels were calculated by comparing reads obtained from the plate reader to the average value for all 21 cybrids. Data represent mean \pm SEM of two independent experiments with 3 replicates each per cybrid.

3.6. Measurement of Intracellular Mitochondrial Signals in Cybrid Cell Lines. We and others previously reported that mitochondrial haplogroups play an important role in mitonuclear interaction [15, 18, 34], in which, signals such as ROS, NAD^+/NADH , and adenosine monophosphate activate or suppress retrograde signaling pathways in the nucleus. We found here that ROS levels did not differ significantly between macrohaplogroups M and N in the 21 cybrid cell lines (Figure 9(a)). Overall mitochondrial function and NAD^+/NADH ratio were higher in cybrid cells with haplogroup M than haplogroup N (Figure 9(b)). However, there were no differences in ROS levels and NAD^+/NADH ratio in haplogroups G2, B4, and F1a corresponding to the changes in mitochondrial function shown in Figure 6.

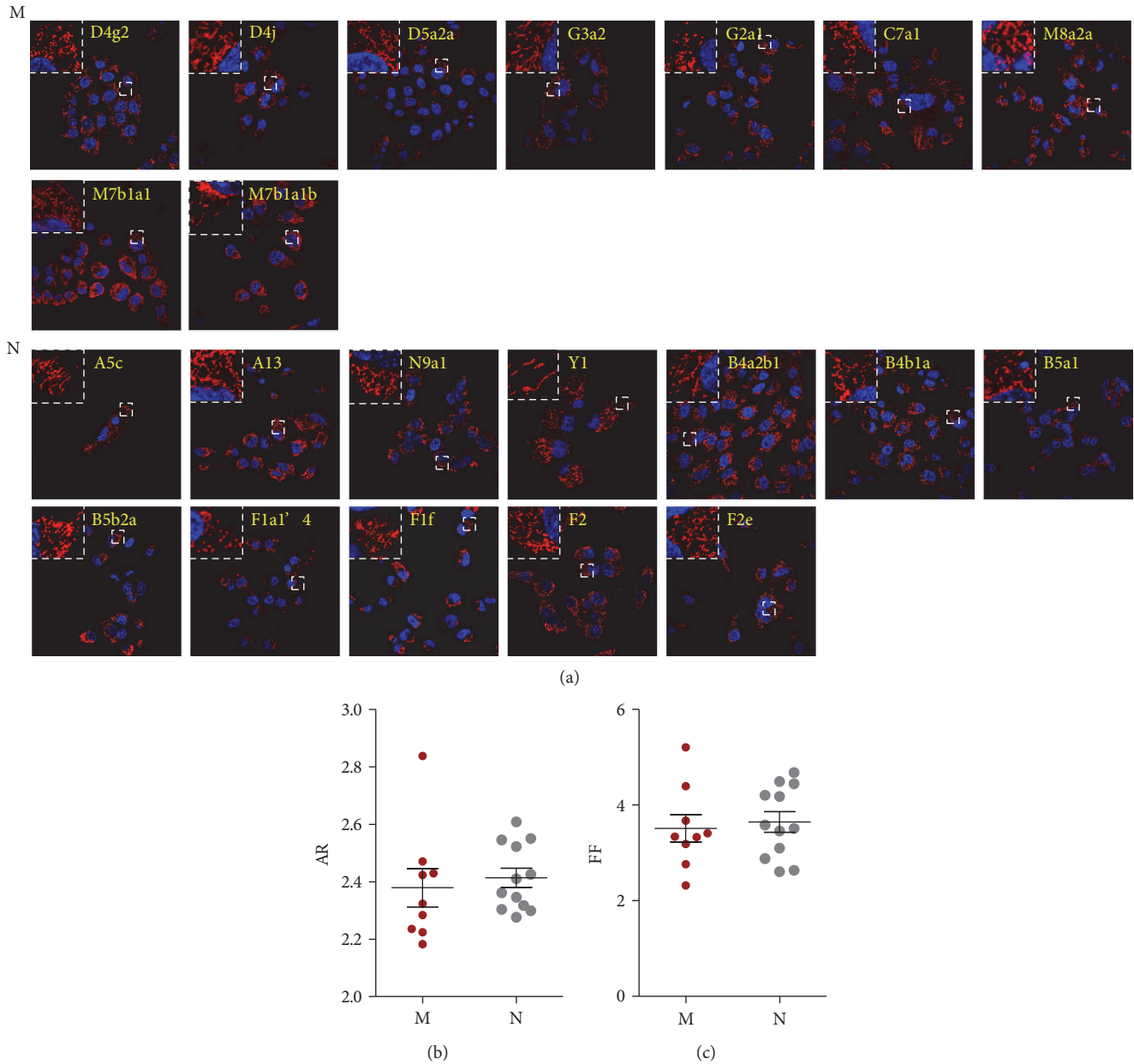


FIGURE 8: Morphometric analysis of mitochondria in cybrid cells. (a) Confocal micrographs of 21 cybrid cells in which the mitochondria were stained with MitoTracker Red ($n=3$). Images are shown at 600x magnification. The upper and lower two rows show cybrid cells with macrohaplogroups M and N, respectively. mtDNA haplogroups are shown in yellow color. (b, c) Mitochondrial fragmentation was determined by AR (b) and FF (c), with higher values representing increased mitochondrial length/width and branching, respectively.

4. Discussion

Molecular epidemiology studies of mtDNA SNPs/haplogroups have revealed the contribution of mtDNA genetic background to human degenerative disease. The underlying etiological causes and mechanisms by which mtDNA haplogroups influence degenerative diseases are frequently investigated using cybrid technology. This approach allows us to establish multiple stable cell lines containing different mtDNA haplogroups in the same nuclear background [15, 35, 36]. Generally, cybrid-based studies examine all or some of mtDNA copy number, mtRNA expression level,

OxPhos enzyme abundance and activity, and mitochondrial bioenergetics including respiration capacity, ATP generation, and MMP [15, 37–40]. In this study, we successfully generated 21 cybrid cell lines covering most East Asian haplogroup branches of the mtDNA phylogenetic tree. Previous cybrid analyses of mtDNA haplogroups in Taiwanese populations have been undertaken to examine the effect of mtDNA haplogroups B4/B5 in Parkinson's disease [41, 42] and B4/D4/N9 in diabetes [14, 38]. However, analyses of East Asian haplogroups and how they influence mitochondrial function have been limited. Thus, our system provides the first description of

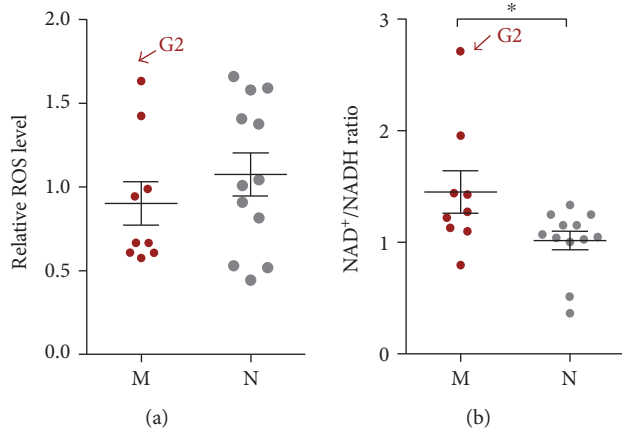


FIGURE 9: Measurement of intracellular mitochondrial signals in cybrid cell lines. (a) Comparison of intracellular ROS levels in cybrid cells. ROS levels were determined by staining cells with dichlorofluorescein diacetate. (b) NAD^+/NADH ratio was higher in cybrid cells with haplogroup M than in those with haplogroup N. NAD^+ and NADH levels in cell extracts were quantified based on fluorescence. Relative ROS levels were calculated by comparing reads obtained from the plate reader to the average value for all 21 cybrids. Data represent mean \pm SEM of three independent experiments with 3 replicates each per cybrid. * $P < 0.05$.

the spectrum of mitochondrial alterations that occur with different mtDNA haplogroups in East Asia. Secondly, our results provide a guideline to pinpoint specific disease-related risk/protective mtDNA haplogroups in molecular epidemiology studies. Lastly, we have established a comprehensive platform to further investigate the effect of mtDNA haplogroups on retrograde signaling at transcriptional, proteomic, and metabolomic levels [18].

Here, we first described the differences in OxPhos function observed in different mtDNA genetic backgrounds from East Asia at the DNA, RNA, and protein level. Copy number analysis showed that 8 SNPs, m.249del, m.13708A, m.13928C, m.489C, m.8701G, m.10398G, m.10400T and m.16304C, might influence mtDNA replication, while others such as m.16362C may bear minor influence. Of which, m.489C, m.10398G, and m.10400T are genetically associated characteristic SNPs of macrohaplogroup M. These results are consistent with the observations that particular mtDNA haplogroups, with characteristic control region mutations, contribute to mtDNA replication [43, 44]. m.13708A and m.13928C, which exhibited lower mtDNA copy numbers than other SNPs, were found to be associated with increased risk of various diseases and pathological conditions [45, 46], whereas m.489C, m.10398G, and m.10400T with higher mtDNA copy numbers than rCRS bases had protective effects against disease [47, 48]. In addition, the disease-related SNPs m.489C, m.8701G, m.10398G, and m.10400T, as well as m.16362C/m.709A/m.16223T and m.3010A/m.16519C were associated with higher and lower mtRNA expression levels, respectively, than their rCRS bases. This suggests that these SNPs play a role in degenerative disease and should be included in molecular epidemiology studies.

Functional analysis of respiratory activity in cybrid cells confirmed that SNPs such as m.709A/m.16223C and m.13708A/m.16519C were associated with higher and lower endogenous mitochondrial respiratory activity, respectively, than their rCRS bases. Other SNPs, such as m.16362T>C, m.150C>T, and a 9 bp deletion, were shown to affect uncoupled mitochondrial respiration in the present study. However, no epidemiological studies have established a link between these SNPs and human degenerative disease. One limitation of our study is that nonhaplogroup defining SNPs were not examined, although the effects of SNPs from other sites cannot be ruled out by logistic regression with limited sample size. Additionally, an induced point mutation target to the candidate SNP may help to elucidate the function implication of specific SNP [49].

We also examined the effect of East Asian mtDNA haplogroups on mitochondrial function. Here, we focused on two macrohaplogroups M and N, while haplogroups M and N are the only two subhaplogroups of L3 immigrated from Africa into Eurasia during evolution. In Han Chinese, haplogroups M and N settled down and gave birth to their sublineages with the frequencies of 40–50% and 50–60%, respectively [11]. It is important to note that m.10398G represents haplogroup M and haplogroup B5, a subhaplogroup of N bearing a back mutation at m.10398. Cells with haplogroup M and m.10398G showed increased mtDNA copy number, L and H2 strand transcription, and respiratory chain complex III expression. Furthermore, cells bearing haplogroup M and m.10398G exhibited higher mitochondrial respiration (both coupled and uncoupled) than cells with haplogroup N and m.10398A, respectively. However, mitochondrial morphology did not differ between haplogroups M and N, nor between m.10398G and m.10398A. Although it has been suggested in previous reports, ours is the first study to analyze the specific mitochondrial biogenetic profiles between haplogroups M and N [50]. mtDNA haplogroups M/N and related SNPs such as m.489T/C, m.8701A/G, m.10398A/G, and m.10400C/T, have been implicated in various pathological conditions. For example, mtDNA haplogroup M, m.10398G, and m.10400T were found to protect against aging [51], Alzheimer's disease [52], and Parkinson's disease [20], whereas mtDNA haplogroup N, m.10398A, and m.10400C are considered as risk factors. Whether haplogroups M and N are protective or risk-associated depends on the condition [2]. In fact, both mitonuclear interactions (retrograde signaling) and mitochondrial OxPhos function contribute to the development of disease [15, 18, 34], while variations in mitonuclear interactions have been reported in the two mtDNA haplogroups [15, 53]. Our data showed that the ratio of NAD^+/NADH , a redox and energy stress marker, differed significantly between haplogroups M and N (Figure 9(b)), supporting the notion that haplogroups M and N exhibit distinct mitonuclear interaction patterns. However, mitochondrial ROS level did not differ between the two haplogroups (Figure 9(a)). Notably, subhaplogroup G of haplogroup M and subhaplogroups F1a and B4 of haplogroup N frequently reflected the functional differences

between M and N in our analyses, suggesting that they play critical roles in degenerative disease. In addition, cell metabolism may be similarly affected by the same mtDNA with nuclear backgrounds from different races [18, 54]. Although our results indicate that haplogroups M and N differentially affect disease development, the use of Caucasian nuclear background-based cybrid system in the current work may limit the significance of this study, and further studies using $\rho 0$ cells with Asian background are required to clarify this relationship.

5. Conclusions

In summary, we generated a cybrid-based system to investigate the mechanisms underlying the functional significance of mtDNA haplogroups that can provide molecular level insight into the role of mtDNA variants in human disease at the molecular level.

Conflicts of Interest

The authors declare that there is no conflict of interests regarding the publication of this article.

Authors' Contributions

Huaibin Zhou, Ke Nie, and Ruyi Qiu contributed equally to this work.

Acknowledgments

The authors thank the members in Jianxin Lyu's laboratory for valuable discussions on this work and Dr. Yidong Bai for providing $\rho 0$ human osteosarcoma 143B cells. This work was supported by the National Natural Science Foundation of China (31671486, 31501156, and 31670784) and Zhejiang Provincial Natural Science Foundation of China (LY15H060007).

References

- [1] D. C. Wallace, "Genetics: mitochondrial DNA in evolution and disease," *Nature*, vol. 535, no. 7613, pp. 498–500, 2016.
- [2] G. Hudson, A. Gomez-Duran, I. J. Wilson, and P. F. Chinnery, "Recent mitochondrial DNA mutations increase the risk of developing common late-onset human diseases," *PLoS Genetics*, vol. 10, no. 5, article e1004369, 2014.
- [3] A. M. Gusdon, F. Fang, J. Chen et al., "Association of the mtND2 5178A/C polymorphism with Parkinson's disease," *Neuroscience Letters*, vol. 587, pp. 98–101, 2015.
- [4] C. W. Liou, J. B. Chen, M. M. Tiao et al., "Mitochondrial DNA coding and control region variants as genetic risk factors for type 2 diabetes," *Diabetes*, vol. 61, no. 10, pp. 2642–2651, 2012.
- [5] L. Shen, H. Fang, T. Chen et al., "Evaluating mitochondrial DNA in cancer occurrence and development," *Annals of the New York Academy of Sciences*, vol. 1201, pp. 26–33, 2010.
- [6] W. H. Ren, X. H. Li, H. G. Zhang et al., "Mitochondrial DNA haplogroups in a Chinese Uygur population and their potential association with longevity," *Clinical and Experimental Pharmacology & Physiology*, vol. 35, no. 12, pp. 1477–1481, 2008.
- [7] H. Lu, V. Koshkin, E. M. Allister, A. V. Gyulkhandanyan, and M. B. Wheeler, "Molecular and metabolic evidence for mitochondrial defects associated with beta-cell dysfunction in a mouse model of type 2 diabetes," *Diabetes*, vol. 59, no. 2, pp. 448–459, 2010.
- [8] H. Fang, X. Liu, L. Shen et al., "Role of mtDNA haplogroups in the prevalence of knee osteoarthritis in a southern Chinese population," *International Journal of Molecular Sciences*, vol. 15, no. 2, pp. 2646–2659, 2014.
- [9] R. Bi, J. Tang, W. Zhang et al., "Mitochondrial genome variations and functional characterization in Han Chinese families with schizophrenia," *Schizophrenia Research*, vol. 171, no. 1–3, pp. 200–206, 2016.
- [10] H. Sudoyo, H. Suryadi, P. Lertrit, P. Pramoonjago, D. Lyrawati, and S. Marzuki, "Asian-specific mtDNA backgrounds associated with the primary G11778A mutation of Leber's hereditary optic neuropathy," *Journal of Human Genetics*, vol. 47, no. 11, pp. 594–604, 2002.
- [11] Q. P. Kong, H. J. Bandelt, C. Sun et al., "Updating the east Asian mtDNA phylogeny: a prerequisite for the identification of pathogenic mutations," *Human Molecular Genetics*, vol. 15, no. 13, pp. 2076–2086, 2006.
- [12] M. van Oven and M. Kayser, "Updated comprehensive phylogenetic tree of global human mitochondrial DNA variation," *Human Mutation*, vol. 30, no. 2, pp. E386–E394, 2009.
- [13] Q. Niu, W. Zhang, H. Wang, X. Guan, J. Lu, and W. Li, "Effects of mitochondrial haplogroup N9a on type 2 diabetes mellitus and its associated complications," *Experimental and Therapeutic Medicine*, vol. 10, no. 5, pp. 1918–1924, 2015.
- [14] H. M. Kuo, S. W. Weng, A. Y. Chang et al., "Altered mitochondrial dynamics and response to insulin in cybrid cells harboring a diabetes-susceptible mitochondrial DNA haplogroup," *Free Radical Biology and Medicine*, vol. 96, pp. 116–129, 2016.
- [15] H. Fang, F. Zhang, F. Li et al., "Mitochondrial DNA haplogroups modify the risk of osteoarthritis by altering mitochondrial function and intracellular mitochondrial signals," *Biochimica et Biophysica Acta (BBA) - Molecular Basis of Disease*, vol. 1862, no. 4, pp. 829–836, 2016.
- [16] A. Gomez-Duran, D. Pacheu-Grau, E. López-Gallardo et al., "Unmasking the causes of multifactorial disorders: OXPHOS differences between mitochondrial haplogroups," *Human Molecular Genetics*, vol. 19, no. 17, pp. 3343–3353, 2010.
- [17] R. Moreno-Loshuertos, R. Acín-Pérez, P. Fernández-Silva et al., "Differences in reactive oxygen species production explain the phenotypes associated with common mouse mitochondrial DNA variants," *Nature Genetics*, vol. 38, no. 11, pp. 1261–1268, 2006.
- [18] A. Latorre-Pellicer, R. Moreno-Loshuertos, A. V. Lechuga-Vieco et al., "Mitochondrial and nuclear DNA matching shapes metabolism and healthy ageing," *Nature*, vol. 535, no. 7613, pp. 561–565, 2016.
- [19] M. P. King and G. Attardi, "Human cells lacking mtDNA: repopulation with exogenous mitochondria by complementation," *Science*, vol. 246, no. 4929, pp. 500–503, 1989.
- [20] J. M. van der Walt, K. K. Nicodemus, E. R. Martin et al., "Mitochondrial polymorphisms significantly reduce the risk of Parkinson disease," *American Journal of Human Genetics*, vol. 72, no. 4, pp. 804–811, 2003.

- [21] M. M. Tiao, C. W. Liou, L. T. Huang et al., "Associations of mitochondrial haplogroups b4 and e with biliary atresia and differential susceptibility to hydrophobic bile acid," *PLoS Genetics*, vol. 9, no. 8, article e1003696, 2013.
- [22] J. Sambrook and D. W. Russell, *Molecular Cloning: A Laboratory Manual*, Cold Spring Harbor Laboratory Press, New York, 2001.
- [23] X. Zhang, X. Zuo, B. Yang et al., "MicroRNA directly enhances mitochondrial translation during muscle differentiation," *Cell*, vol. 158, no. 3, pp. 607–619, 2014.
- [24] D. C. Rio, M. Ares Jr, G. J. Hannon, and T. W. Nilsen, "Purification of RNA using TRIzol (TRI reagent)," *Cold Spring Harbor Protocols*, vol. 2010, no. 6, article pdb.prot5439, 2010.
- [25] H. Hao, G. Manfredi, and C. T. Moraes, "Functional and structural features of a tandem duplication of the human mtDNA promoter region," *American Journal of Human Genetics*, vol. 60, no. 6, pp. 1363–1372, 1997.
- [26] A. K. Hyvarinen, M. K. Kumanto, S. K. Marjavaara, and H. T. Jacobs, "Effects on mitochondrial transcription of manipulating mTERF protein levels in cultured human HEK293 cells," *BMC Molecular Biology*, vol. 11, p. 72, 2010.
- [27] I. Wittig, H. P. Braun, and H. Schagger, "Blue native PAGE," *Nature Protocols*, vol. 1, no. 1, pp. 418–428, 2006.
- [28] D. Sun, B. Li, R. Qiu, H. Fang, and J. Lyu, "Cell type-specific modulation of respiratory chain supercomplex organization," *International Journal of Molecular Sciences*, vol. 17, no. 6, 2016.
- [29] B. Aravamudan, A. Kiel, M. Freeman et al., "Cigarette smoke-induced mitochondrial fragmentation and dysfunction in human airway smooth muscle," *American Journal of Physiology. Lung Cellular and Molecular Physiology*, vol. 306, no. 9, pp. L840–L854, 2014.
- [30] L. K. Sharma, H. Fang, J. Liu, R. Vartak, J. Deng, and Y. Bai, "Mitochondrial respiratory complex I dysfunction promotes tumorigenesis through ROS alteration and AKT activation," *Human Molecular Genetics*, vol. 20, no. 23, pp. 4605–4616, 2011.
- [31] Q. P. Kong, Y. G. Yao, C. Sun, H. J. Bandelt, C. L. Zhu, and Y. P. Zhang, "Phylogeny of East Asian mitochondrial DNA lineages inferred from complete sequences," *American Journal of Human Genetics*, vol. 73, no. 3, pp. 671–676, 2003.
- [32] Y. G. Yao, Q. P. Kong, H. J. Bandelt, T. Kivisild, and Y. P. Zhang, "Phylogeographic differentiation of mitochondrial DNA in Han Chinese," *American Journal of Human Genetics*, vol. 70, no. 3, pp. 635–651, 2002.
- [33] M. Tanaka, V. M. Cabrera, A. M. González et al., "Mitochondrial genome variation in eastern Asia and the peopling of Japan," *Genome Research*, vol. 14, no. 10A, pp. 1832–1850, 2004.
- [34] S. R. Atilano, D. Malik, M. Chwa et al., "Mitochondrial DNA variants can mediate methylation status of inflammation, angiogenesis and signaling genes," *Human Molecular Genetics*, vol. 24, no. 16, pp. 4491–4503, 2015.
- [35] S. Chae, B. Y. Ahn, K. Byun et al., "A systems approach for decoding mitochondrial retrograde signaling pathways," *Science Signaling*, vol. 6, no. 264, article rs4, 2013.
- [36] M. Picard, J. Zhang, S. Hancock et al., "Progressive increase in mtDNA 3243A>G heteroplasmy causes abrupt transcriptional reprogramming," *Proceedings of the National Academy of Sciences of the United States of America*, vol. 111, no. 38, pp. E4033–E4042, 2014.
- [37] R. Pello, M. A. Martín, V. Carelli et al., "Mitochondrial DNA background modulates the assembly kinetics of OXPHOS complexes in a cellular model of mitochondrial disease," *Human Molecular Genetics*, vol. 17, no. 24, pp. 4001–4011, 2008.
- [38] S. W. Weng, H. M. Kuo, J. H. Chuang et al., "Study of insulin resistance in cybrid cells harboring diabetes-susceptible and diabetes-protective mitochondrial haplogroups," *Mitochondrion*, vol. 13, no. 6, pp. 888–897, 2013.
- [39] M. C. Kenney, M. Chwa, S. R. Atilano et al., "Inherited mitochondrial DNA variants can affect complement, inflammation and apoptosis pathways: insights into mitochondrial-nuclear interactions," *Human Molecular Genetics*, vol. 23, no. 13, pp. 3537–3551, 2014.
- [40] A. Gomez-Duran, D. Pacheu-Grau, I. Martínez-Romero et al., "Oxidative phosphorylation differences between mitochondrial DNA haplogroups modify the risk of Leber's hereditary optic neuropathy," *Biochimica et Biophysica Acta (BBA) - Molecular Basis of Disease*, vol. 1822, no. 8, pp. 1216–1222, 2012.
- [41] T. K. Lin, H. Y. Lin, S. D. Chen et al., "The creation of cybrids harboring mitochondrial haplogroups in the Taiwanese population of ethnic Chinese background: an extensive in vitro tool for the study of mitochondrial genomic variations," *Oxidative Medicine and Cellular Longevity*, vol. 2012, Article ID 824275, 13 pages, 2012.
- [42] C. W. Liou, J. H. Chuang, J. B. Chen et al., "Mitochondrial DNA variants as genetic risk factors for Parkinson disease," *European Journal of Neurology*, vol. 23, no. 8, pp. 1289–1300, 2016.
- [43] S. Suissa, Z. Wang, J. Poole et al., "Ancient mtDNA genetic variants modulate mtDNA transcription and replication," *PLoS Genetics*, vol. 5, no. 5, article e1000474, 2009.
- [44] E. Jemt, Ö. Persson, Y. Shi et al., "Regulation of DNA replication at the end of the mitochondrial D-loop involves the helicase TWINKLE and a conserved sequence element," *Nucleic Acids Research*, vol. 43, no. 19, pp. 9262–9275, 2015.
- [45] X. Yu, D. Koczan, A. M. Sulonen et al., "mtDNA nt13708A variant increases the risk of multiple sclerosis," *PLoS One*, vol. 3, no. 2, article e1530, 2008.
- [46] P. Korkiamaki, M. Kervinen, K. Karjalainen, K. Majamaa, J. Uusimaa, and A. M. Remes, "Prevalence of the primary LHON mutations in Northern Finland associated with bilateral optic atrophy and tobacco-alcohol amblyopia," *Acta Ophthalmologica*, vol. 91, no. 7, pp. 630–634, 2013.
- [47] K. Darvishi, S. Sharma, A. K. Bhat, E. Rai, and R. N. Bamezai, "Mitochondrial DNA G10398A polymorphism imparts maternal haplogroup N a risk for breast and esophageal cancer," *Cancer Letters*, vol. 249, no. 2, pp. 249–255, 2007.
- [48] J. A. Canter, T. G. Hayes, S. Zheng et al., "Mitochondrial DNA G10398A polymorphism and invasive breast cancer in African-American women," *Cancer Research*, vol. 65, no. 17, pp. 8028–8033, 2005.
- [49] M. Hashimoto, S. R. Bacman, S. Peralta et al., "MitoTALEN: a general approach to reduce mutant mtDNA loads and restore oxidative phosphorylation function in mitochondrial diseases," *Molecular Therapy*, vol. 23, no. 10, pp. 1592–1599, 2015.
- [50] A. A. Kazuno, K. Munakata, T. Nagai et al., "Identification of mitochondrial DNA polymorphisms that alter mitochondrial matrix pH and intracellular calcium dynamics," *PLoS Genetics*, vol. 2, no. 8, article e128, 2006.

- [51] A. K. Niemi, J. S. Moilanen, M. Tanaka et al., “A combination of three common inherited mitochondrial DNA polymorphisms promotes longevity in Finnish and Japanese subjects,” *European Journal of Human Genetics*, vol. 13, no. 2, pp. 166–170, 2005.
- [52] J. M. van der Walt, Y. A. Dementieva, E. R. Martin et al., “Analysis of European mitochondrial haplogroups with Alzheimer disease risk,” *Neuroscience Letters*, vol. 365, no. 1, pp. 28–32, 2004.
- [53] S. Hwang, S. H. Kwak, J. Bhak et al., “Gene expression pattern in transmitochondrial cytoplasmic hybrid cells harboring type 2 diabetes-associated mitochondrial DNA haplogroups,” *PLoS One*, vol. 6, no. 7, article e22116, 2011.
- [54] L. Levin, A. Blumberg, G. Barshad, and D. Mishmar, “Mitonuclear co-evolution: the positive and negative sides of functional ancient mutations,” *Frontiers in Genetics*, vol. 5, p. 448, 2014.

Research Article

Mitochondria-Targeted Antioxidants SkQ1 and MitoTEMPO Failed to Exert a Long-Term Beneficial Effect in Murine Polymicrobial Sepsis

Pia Rademann,¹ Adelheid Weidinger,¹ Susanne Drechsler,¹ Andras Meszaros,² Johannes Zipperle,¹ Mohammad Jafarmadar,¹ Sergiu Dumitrescu,¹ Ara Hacobian,¹ Luisa Ungelenk,³ Franziska Röstel,³ Jozsef Kaszaki,² Andrea Szabo,² Vladimir P. Skulachev,⁴ Michael Bauer,^{3,5} Soheyl Bahrami,¹ Sebastian Weis,^{3,5} Andrey V. Kozlov,¹ and Marcin F. Osuchowski¹

¹Ludwig Boltzmann Institute for Experimental and Clinical Traumatology in the Trauma Research Center of AUVA, Vienna, Austria

²Institute of Surgical Research, Faculty of Medicine, University of Szeged, Szeged, Hungary

³Department of Anesthesiology and Intensive Care Medicine, Jena University Hospital, Jena, Germany

⁴A.N. Belozersky Institute of Physico-Chemical Biology, M.V. Lomonosov Moscow State University, Leninskie Gory Moscow 119992, Russia

⁵Center for Sepsis Control and Care, Jena University Hospital, Jena, Germany

Correspondence should be addressed to Marcin F. Osuchowski; marcin.osuchowski@trauma.lbg.ac.at

Received 30 March 2017; Revised 22 June 2017; Accepted 2 August 2017; Published 19 September 2017

Academic Editor: Moh H. Malek

Copyright © 2017 Pia Rademann et al. This is an open access article distributed under the Creative Commons Attribution License, which permits unrestricted use, distribution, and reproduction in any medium, provided the original work is properly cited.

Mitochondrial-derived reactive oxygen species have been deemed an important contributor in sepsis pathogenesis. We investigated whether two mitochondria-targeted antioxidants (mtAOX; SkQ1 and MitoTEMPO) improved long-term outcome, lessened inflammation, and improved organ homeostasis in polymicrobial murine sepsis. 3-month-old female CD-1 mice ($n = 90$) underwent cecal ligation and puncture (CLP) and received SkQ1 (5 nmol/kg), MitoTEMPO (50 nmol/kg), or vehicle 5 times post-CLP. Separately, 52 SkQ1-treated CLP mice were sacrificed at 24 h and 48 h for additional endpoints. Neither MitoTEMPO nor SkQ1 exerted any protracted survival benefit. Conversely, SkQ1 exacerbated 28-day mortality by 29%. CLP induced release of 10 circulating cytokines, increased urea, ALT, and LDH, and decreased glucose but irrespectively of treatment. Similar occurred for CLP-induced lymphopenia/neutrophilia and the NO blood release. At 48 h post-CLP, dying mice had approximately 100-fold more CFUs in the spleen than survivors, but this was not SkQ1 related. At 48 h, macrophage and granulocyte counts increased in the peritoneal lavage but irrespectively of SkQ1. Similarly, hepatic mitophagy was not altered by SkQ1 at 24 h. The absence of survival benefit of mtAOX may be due to the extended treatment and/or a relatively moderate-risk-of-death CLP cohort. Long-term effect of mtAOX in abdominal sepsis appears different to sepsis/inflammation models arising from other body compartments.

1. Introduction

Sepsis is a deleterious clinical condition caused by a deregulated host response to infection associated with organ damage [1]. In immunocompetent individuals, sepsis provokes a robust systemic inflammatory response (which can coexist with concurrently developing immunosuppression). Various

microbial, fungal, or viral components in the invaded host lead to a rapid, simultaneous release of pro- and anti-inflammatory mediators [2] and general activation of the innate/adaptive immunity. The acute phase of humoral and cellular response is accompanied by a rapid production of reactive oxygen species (ROS) [3]. Under physiological conditions, ROS are produced by different intra-/extracellular

sources [4] with mitochondria as one of the main sites [5, 6]. Tightly regulated by cellular antioxidant mechanisms, at low-to-moderate concentrations, ROS have potent beneficial effects as an intrinsic part of various intracellular signaling pathways [5, 7, 8]. In contrast, increased ROS concentration (e.g., caused by depletion of regulatory antioxidants, inadequate antioxidative response [9], and/or altered ROS release) can elicit a chain reaction cascade that can damage the cells and tissues of the host [4]. This oxidative stress has been considered as one of the key contributors to the development of organ failure in sepsis and linked to a deregulation of mitochondrial function [10–12].

Numerous preclinical studies demonstrated clear benefits of an antioxidant-dependent inhibition of ROS production/release in different pathophysiological conditions [13, 14] including sepsis [15–19]. In contrast, clinical trials either failed to show any survival benefit in septic patients or were inconclusive [20–22]. In general, the incompatibility between preclinical and clinical studies (and among the clinical studies themselves) is due to numerous reasons including nonmatching models, erroneous study design, and/or non-specific therapeutics. First, endotoxemia/LPS models are now considered inappropriate in recapitulating human sepsis syndromes [23]. Furthermore, due to a lack of clear dose-limiting toxicities, the dosages used in clinical trials are typically selected based on an “appeared feasible” subjective approach rather than preverified dose response studies [22]. For example, failure of a nonselective nitric oxide synthase inhibitor (46C88; L-NMMA acronym) phase 3 trial (versus phase 2) was partly attributed to the excessive L-NMMA dose and suboptimal selection of septic patients [24, 25]. Equally important is the element of therapeutic specificity: majority of studies applied nonselective antioxidants such as selenium, melatonin, ascorbic acid, n-acetylcystein, and α -tocopherol whose actions may be simultaneously too wide ranging and/or mistargeted.

Regarding the latter shortcoming, various conjugation protocols were developed (e.g., with lipophilic cations) to target the exogenous antioxidants directly to mitochondria. The best characterized to date is triphenylphosphonium (TPP) formulation [26]: it enables precise and uncorrupted cross-membrane delivery of antioxidants [27, 28] and has led to development of two very promising substances. SkQ1 is a novel, rechargeable plastoquinone derivative, which accumulates in the inner mitochondrial membrane due to its molecular charge and lipophilic properties [29, 30]. It shows antioxidant effects at much lower concentrations than other TPP conjugates, thus the “window” between anti- and prooxidant effects is larger [30]. MitoTEMPO is a piperidine-based nitroxide that works as a hydrophilic superoxide dismutase mimetic in the mitochondrial matrix. Positive preclinical results of SkQ1 and MitoTEMPO in various diseases including CLP [13, 31–35] and their strong immunomodulatory properties [36, 37] have been largely attributed to their high-target specificity.

Until now, MitoTEMPO (as mitochondria-specific ROS scavenger) was studied in the mouse CLP model for only a short term [35]. However, sepsis causes severe protracted sequelae and neither of those compounds has

ever been tested in a clinically relevant sepsis model for their long-term effects. Hence, in this study, we investigated the influence of these two specific TPP-conjugated ROS scavengers, SkQ1 and MitoTEMPO, upon inflammatory response, organ function, and long-term outcome in a mouse model of polymicrobial acute sepsis originating from the abdominal compartment.

2. Materials and Methods

2.1. Animals. Female, 3-month-old, outbred CD-1 mice (Charles River Laboratories; $n = 142$) were used for all experiments (the exact n /group is specified in the legend to each figure). The genetic diversity of the CD-1 outbred strain (e.g., compared to BALB/c) is closer to patient diversity and therefore clinically more relevant. We chose sexually mature, healthy females to exclude confounding tangibles such as comorbidities and young/old age and to follow on the NIH recommendation to study females given their underrepresentation in preclinical intensive care research. Experiments 1 and 2 were performed in Ludwig Boltzmann Institute for Experimental and Clinical Traumatology (LBI), Vienna, Austria, and experiment 3 was performed in Institute of Surgical Research (ISR), University of Szeged, Faculty of Medicine, Szeged, Hungary. All mice were allowed to acclimatize to their new environment for at least one week after arrival. Mice were housed on a 12 h light-dark cycle with controlled temperature (21–23°C) and provided with standard rodent diet and water *ad libitum*.

2.2. Ethics Statement. All animal procedures were approved by the Viennese (Austria) Legislative Committee (Animal Use Proposal Permission number: 006596/2011/11) and the Hungarian Scientific Ethical Committee on Animal Experimentation (Animal Use Proposal Permission number: V./148/2013) All experiments were conducted according to the National Institutes of Health guidelines.

All mice were monitored by trained professionals at least three times per day and more whenever an animal's condition deteriorated [38, 39]. In order to avoid unnecessary suffering of CLP mice facing imminent death, we use in our laboratory a custom-developed scoring approach that combines the mouse clinical assessment scoring system (M-CASS) and sequential body temperature (BT) measurements. In brief, well-being and general condition of mice (i.e., fur, posture, mobility, alertness, weight, and startle reflex) were assessed every 12 hours (starting 12 h post-CLP), by assigning mice to one out of maximum three severity grades (i.e., 0, 1, or 2 points). Additionally, we measured inner BT. Mice were euthanized once the score indicated imminent death, that is, a score ≥ 8 and/or inability to trigger the startle reflex and/or BT $< 28^\circ\text{C}$ (recorded in at least two sequential measurements; the score sheet in Supplementary Figure 1 available online at <https://doi.org/10.1155/2017/6412682>). This approach is generally in line with the recent mouse M-CASS philosophy proposed by Lilley et al. [40]. The BT-based prediction of outcome we have developed in our laboratory is very precise (AUC = 0.94; [41]). Combination of the BT-based prediction with our custom-developed

(M-CASS-like) scoring system prevents overliberal euthanasia decision-making, that is, allocation of potential survivors to the P-DIE group in survival studies.

2.3. Sepsis Model. Mice were subjected to cecal ligation and puncture (CLP) surgery according to the protocol by Wichterman et al. [42] with modifications described elsewhere [43]. We performed a medium severe CLP (18G needle) to reach an approximately 40% mortality (i.e., by day 28 post-CLP) that corresponds to mortality of human patients suffering from abdominal sepsis [44, 45]. Briefly, after opening the abdominal cavity via midline laparotomy, the cecum was exposed, ligated, and punctured twice (small amount of feces was extruded to ensure patency of the punctures). After repositioning of the cecum, the abdomen was closed with two single button sutures and Histoacryl® skin adhesive. Starting 2 hours post-CLP, all mice received subcutaneous broad-spectrum antibiotic therapy (25 mg/kg imipenem/cilastatin, Zienam®) and fluid resuscitation (1 ml Ringer's solution) with analgesia (0.05 mg/kg buprenorphine, Bupaq®) twice daily (in approx. 12 h intervals) for five consecutive days (experiment 1) or until the time point of euthanasia (in experiments 2 and 3). Five-day course of antibiotic coverage is routinely employed in CLP studies [46].

2.4. Study Design

2.4.1. CLP Experiments. The entire study was performed in three separate experimental blocks: experiment 1 as the main survival part (SkQ1 and MitoTEMPO; Figures 1, 2, 3, 4, and 5) and follow-up experiment 2 (SkQ1 only; Figures 6 and 7; both in LBI) and experiment 3 (SkQ1 only; Figure 8; in ISR). To maximize reliability and minimize random effects in experiment 1, we conducted CLP in small groups of 15 mice per repetition (6 repetitions in total). Moreover, irrespective of location, all CLP surgeries were performed by the same operator (P.R.).

The follow-up experiments 2 and 3 had different sacrifice time points: at 48 h in experiment 2 and at 24 h post-CLP in experiment 3 (Figure 9 scheme). The time points were chosen based on the investigated endpoints: 48 h time point for bacterial load at the time of the maximal post-CLP mortality (experiment 2) and 24 h time point for potential mitophagy; the period closely preceding the most robust post-CLP deaths (experiment 3).

To ensure similar CLP severity between LBI (experiments 1 and 2) and ISR (experiment 3), we used BT profiling, that is, three (separate) pilot CLP runs were performed in ISR and the BT profiles of CLP mice (Supplementary Figure 1) were compared to the main CLP survival study (experiment 1). The third CLP run (i.e., experiment 3) showed nearly an identical BT profile to experiment 1 and was extended to reach the total $n = 28$.

2.4.2. Treatment. All animals (total of $n = 90$ in experiment 1; $n = 24$ in experiment 2; and $n = 28$ in experiment 3; detailed n /group distribution in legends to figures) were randomly assigned to receive (in a blinded manner) either SkQ1 (5 nmol/kg), MitoTEMPO (50 nmol/kg), or placebo treatment (saline) via intraperitoneal injection at maximally

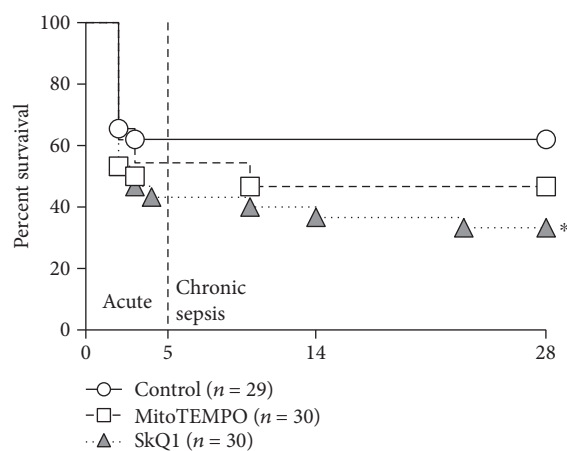


FIGURE 1: 28-day survival of SkQ1-, MitoTEMPO-, and placebo-treated control mice. Mortality of treated and placebo mice subjected to CLP sepsis. Number of mice in each group listed in the legend (in brackets). SkQ1 versus control: * $p = 0.03$; MitoTEMPO versus control: $p = 0.24$.

five subsequent time points (i.e., 1, 12, 24, 36, and 48 h) post-CLP (see Figure 9 scheme for detailed description of experimental groups). For SkQ1, this amounts to 0.0062 mg/kg/d for the first two days and 0.0031 mg/kg/d for the third day. For MitoTEMPO, this amounts to 0.051 mg/kg/d for the first two days and 0.0255 mg/kg/d for the third day.

For all experiments, SkQ1/MitoTEMPO was dissolved in ethanol (96%) and diluted in saline in further steps. Freshly prepared dilutions were divided into aliquots (one for each treatment time point separately) and stored frozen at -80°C protected from light until use. The presence of SkQ1/MitoTEMPO molecules was verified on the first and the last days of experiments. The concentration of SkQ1 was tested spectrophotometrically as described in Antonenko et al. 2008 [30]. MitoTEMPO was measured with electron spin resonance spectroscopy as previously described [47].

We elected to administer the first antioxidant dose 1 h post-CLP to approach clinical relevance. We treated mice over the period of 48 h post-CLP given that it directly precedes/overlaps with the period of the most robust mortality in the acute CLP phase [48, 49]. Our treatment scheme is consistent with the one employed by Plotnikov et al. [13]. The selected antioxidant concentrations were adopted from Weidinger et al. [50]. Given that the effects of SkQ1 were predominantly examined in rats, we have compared the effects of increasing SkQ1 concentrations on the respiratory activity of mitochondria in liver homogenates from rats and mice. This was done to ensure that we remain within the nontoxic range of SkQ1 concentrations (Supplementary Figure 2).

In the follow-up experiments 2 and 3, SkQ1 (or placebo) was tested given that only SkQ1 treatment significantly exacerbated mortality in experiment 1. In experiment 2, mice received four injections (the last at 36 h post-CLP) and were sacrificed for peritoneal lavage and spleen collection. In experiment 3, mice received three injections (the last at

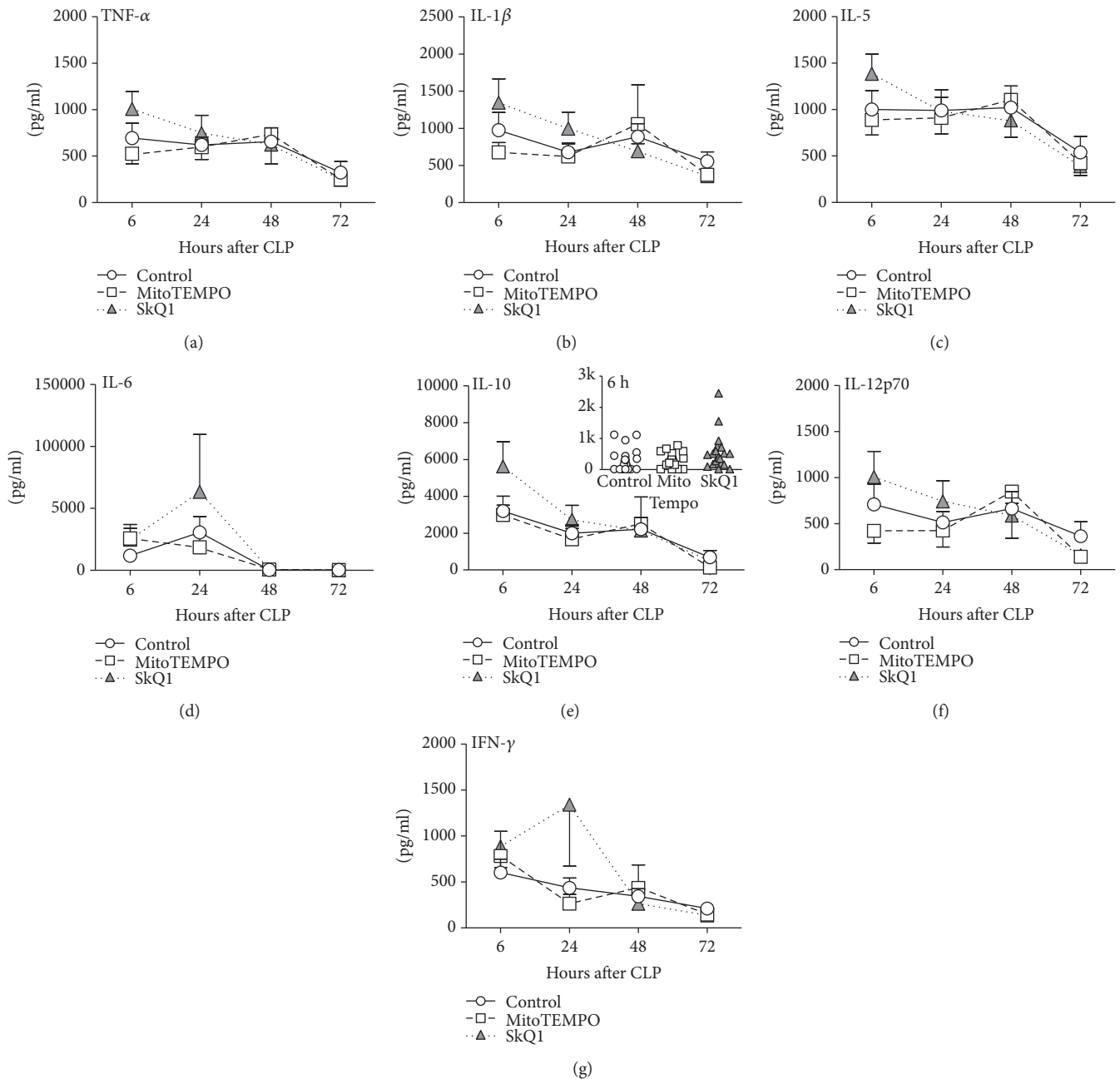


FIGURE 2: Comparison of circulating cytokines between SkQ1-, MitoTEMPO-, and placebo-treated control mice. (a–g) Plasma levels of TNF- α , IL-1 β , IL-5, IL-6, IL-10, IL-12p70, and IFN- γ in treated mice (SkQ1 or MitoTEMPO) at 6, 24, 48, and 72 h post-CLP were compared to the placebo group (CLP + NaCl). For (a–g): at 6 h: control $n \geq 19$, SkQ1 $n = 19$, MitoTEMPO $n = 19$; at 24 h: control $n = 19$, SkQ1 $n = 17$, MitoTEMPO $n = 15$; at 48 h: control $n = 13$, SkQ1 $n = 12$, MitoTEMPO $n = 10$; at 72 h: control $n = 13$, SkQ1 $n = 11$, MitoTEMPO $n = 9$. Data points shown as mean \pm SEM. The exemplary IL-10 inset depicts scatter plot of all groups at 6 h post-CLP time point. 2k (for brevity) corresponds to 2000 pg/ml.

24 h post-CLP) and were sacrificed to collect the liver for mitophagy assessment (Figure 9 scheme). Irrespective of sacrifice, the identical protocol for treatment and sampling procedures was used in experiment 1 and both follow-up experiments 2 and 3.

Of note, in experiment 2, to generate Figure 6(a), septic mice were compared using the above-described M-CASS-like criteria, that is, using our custom-developed scoring system and BT monitoring; we retrospectively assigned mice

into either predicted-to-die (P-DIE; inner BT $\leq 28^\circ\text{C}$) or predicted-to-survive (P-SUR; inner BT $\geq 35^\circ\text{C}$) group. For maximally conservative approach, all mice featured in Figure 6(a) met the objective [41] BT cut-off criteria (i.e., mice meeting the euthanasia threshold based solely on the clinical assessment ≥ 8 points were not included).

2.5. Blood Sampling. Repeated low-volume blood sampling was used in all groups reducing the total number of mice

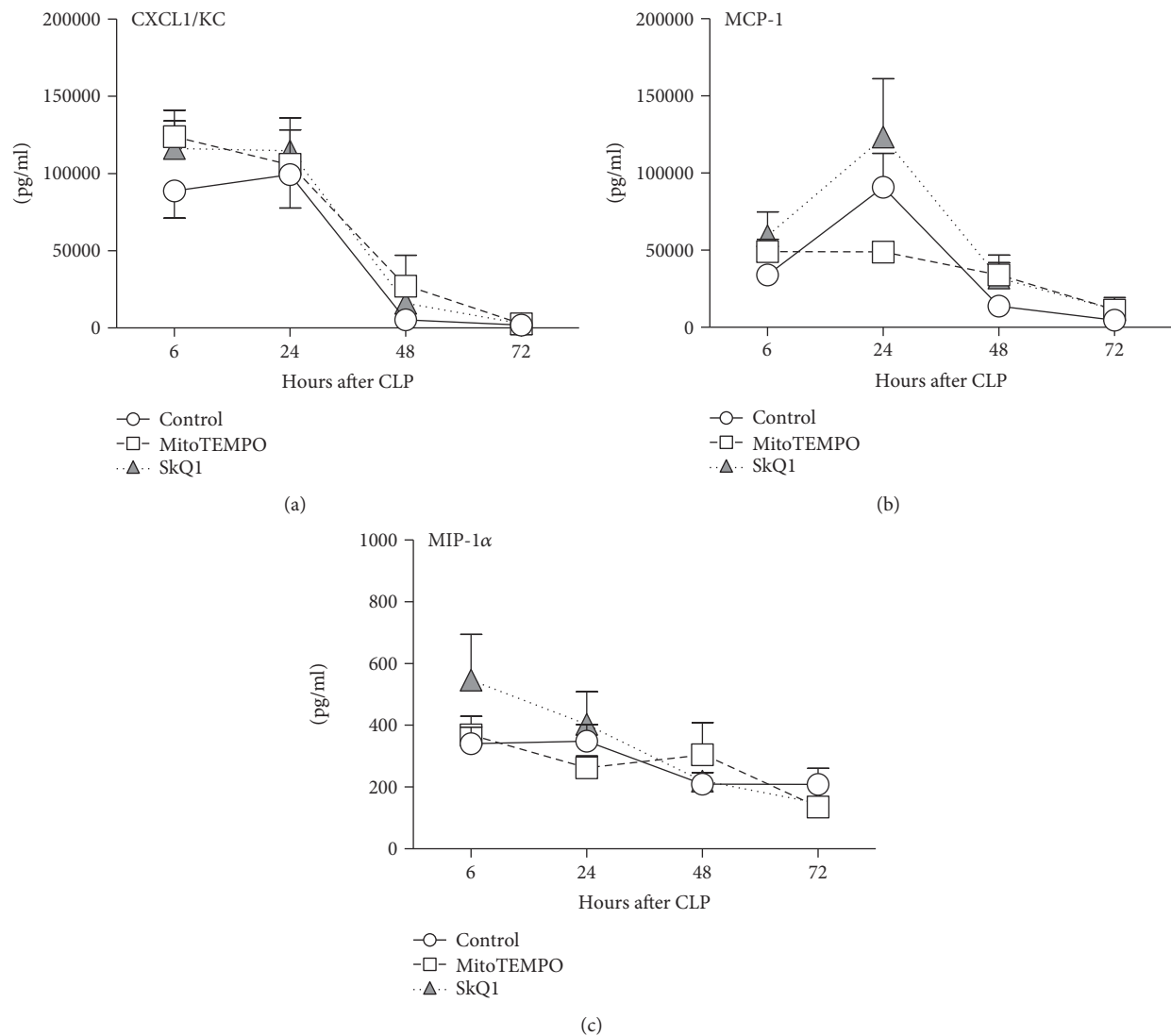


FIGURE 3: Comparison of circulating chemokines between SkQ1-, MitoTEMPO-, and placebo-treated control mice. (a–c) Plasma levels of CXCL1, MCP-1, and MIP-1 α in treated mice (SkQ1 or MitoTEMPO) at 6, 24, 48, and 72 h post-CLP were compared to the placebo group (CLP + NaCl). For (a–c): at 6 h: control $n = 19$, SkQ1 $n = 19$, MitoTEMPO $n = 19$; at 24 h: control $n = 19$, SkQ1 $n = 17$, MitoTEMPO $n = 15$; at 48 h: control $n = 13$, SkQ1 $n = 12$, MitoTEMPO $n = 10$; at 72 h: control $n = 13$, SkQ1 $n = 11$, MitoTEMPO $n = 9$. Data points shown as mean \pm SEM.

needed for the study [51]. Blood was collected immediately before CLP (baseline) and at 6, 24, 48, and 72 h thereafter in experiment 1 and for shorter periods (depending on the sacrifice time point) in experiments 2 and 3 (Figure 9 scheme).

Specifically, 30 μ l of blood was drawn by puncturing the facial vein (*vena submandibularis*) with a 23 gauge needle. Samples were then collected with a pipette rinsed with ethylenediaminetetraacetic acid (K_3 -EDTA) (diluted 1:50) and immediately diluted 1:10 in PBS. After centrifugation (1000 \times g, 5 min, 22°C), 270 μ l of plasma was removed and stored at -80°C until further analysis.

2.6. Abdominal Lavage. In experiment 2, after sacrifice (isoflurane anesthesia followed by cervical dislocation), we performed abdominal lavages with 5 ml cold PBS/3% fetal

calf serum, using an adapted protocol from Ray and Dittel [52]. The collected cell suspension was deposited in tubes and kept on ice until further FACS analysis.

2.7. Complete Blood Count. After plasma was removed, we resuspended the remaining blood pellet with 180 μ l Cell-Dyn buffer with EDTA and a complete blood count with differential (erythrocytes, hemoglobin, platelets, white blood cells, neutrophil granulocytes, and lymphocytes) was performed with a Cell-Dyn 3700 counter (Abbott Laboratories, Illinois, USA) as previously described [51].

2.8. Cytokine and Chemokine Measurement. Interleukin (IL)-1 β , IL-5, IL-6, IL-10, and IL-12p70, interferon (IFN)- γ , tumor necrosis factor (TNF)- α , macrophage inflammatory protein (MIP)-1 α , chemokine ligand (KC; CXCL-1), and

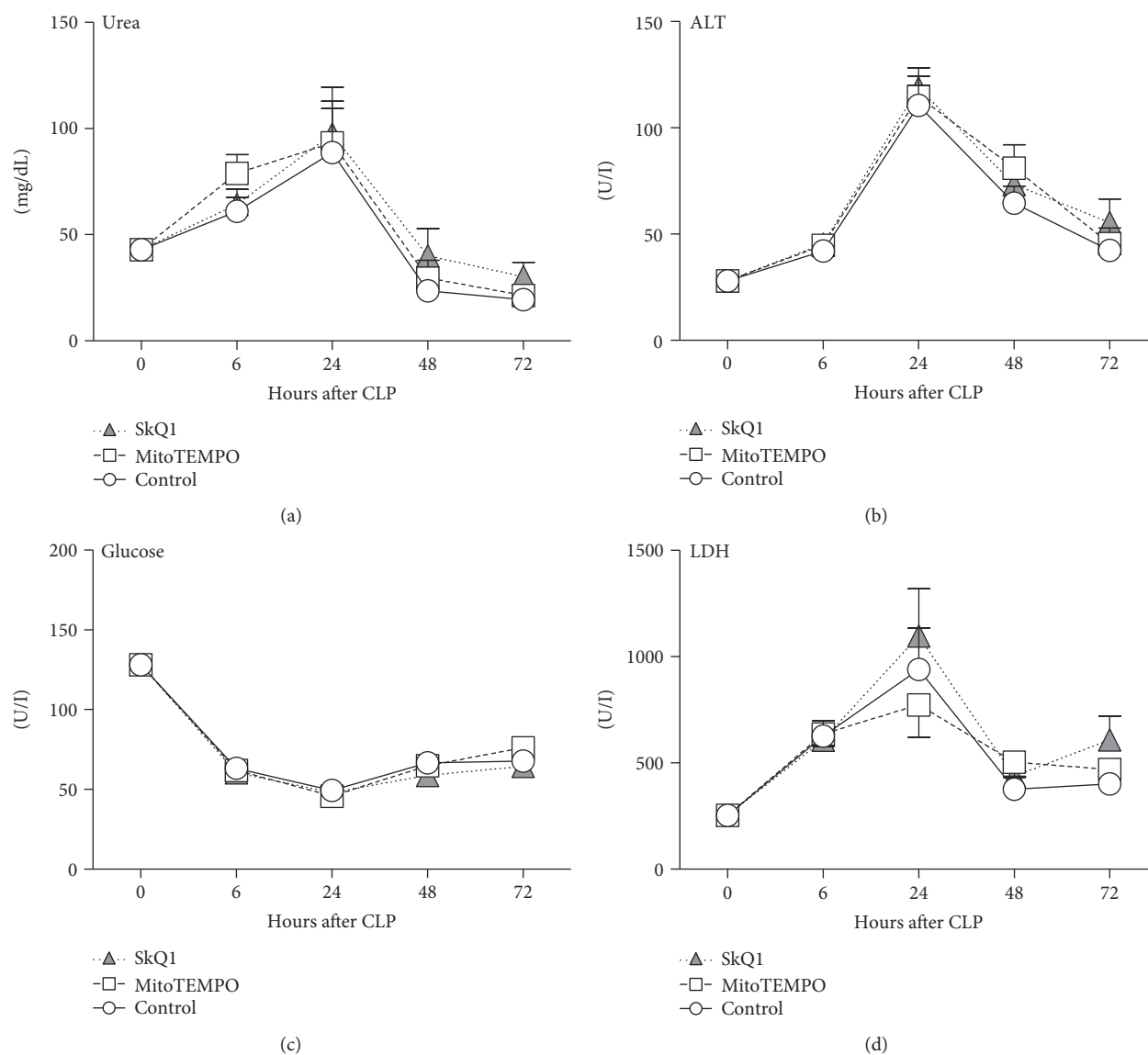


FIGURE 4: Comparison of organ function parameters between SkQ1-, MitoTEMPO-, and placebo-treated control mice. Plasma levels of treated mice (SkQ1 or MitoTEMPO) of (a) urea, (b) ALT, (c) glucose, and (d) LDH in mice at baseline and post-CLP were compared to the control group (CLP + placebo). For (a–d): at BL $n = 20$; at 6 h control $n = 20$, SkQ1 $n = 19$, MitoTEMPO $n = 19$; at 24 h control $n = 19$, SkQ1 $n = 17$, MitoTEMPO $n = 17$; at 48 h control $n = 13$, SkQ1 $n = 12$, MitoTEMPO $n = 10$; at 72 h control $n = 13$, SkQ1 $n = 11$, MitoTEMPO $n = 9$. Data points shown as mean \pm SEM.

monocyte chemoattractant protein-1 (MCP-1) were analyzed from plasma samples according to the manufacturer's protocol using FlowCytomix™ Multiplex Kits (eBioscience, USA).

2.9. Metabolic and Organ Function/Cell Injury. Plasma levels of urea, glucose, lactate dehydrogenase (LDH), and alanine transaminase (ALT) were analyzed with Cobas c111 analyzer (Roche, Switzerland). The lower detection limit for urea was 3 mg/dL, for glucose 1.98 mg/dL, for LDH 10 U/L, and for ALT 2 U/L. The inner body temperature was measured (at least twice per 24 h) using a Fluke 52 Series II thermometer (Fluke, USA) with a rectal probe.

2.10. Nitrate/Nitrite (NO_x) Measurement. The Nitric Oxide Analyzer (NOA) (Nitric Oxide Analyzer Sievers 280i, GE

Analytical Instruments, USA) consisted of a glassware system and an electronic detection unit. Plasma samples were injected through a septum into the glass vessel, where NO species were converted selectively to NO_(g) by a redox active reagent (VCl₃ for total NO). Following the reduction step, NO molecules are carried to the reaction chamber of the detection unit by N₂, an inert gas which was constantly purged through the mixture during measurements. Inside the reaction chamber, NO from the gas phase reacted rapidly with O₃ to form NO₂^{*} in an excited state (NO + O₃ → NO₂^{*} + O₂). As the excited e⁻ returned to its ground state, a photon was emitted and detected as chemiluminescence ($h\nu$) (NO₂^{*} → NO₂ + $h\nu$). Emitted light was detected and amplified by a photo multiplier tube (PMT) to generate an electric signal. The detection limit for NO and related species in liquid samples was ~1 pmol.

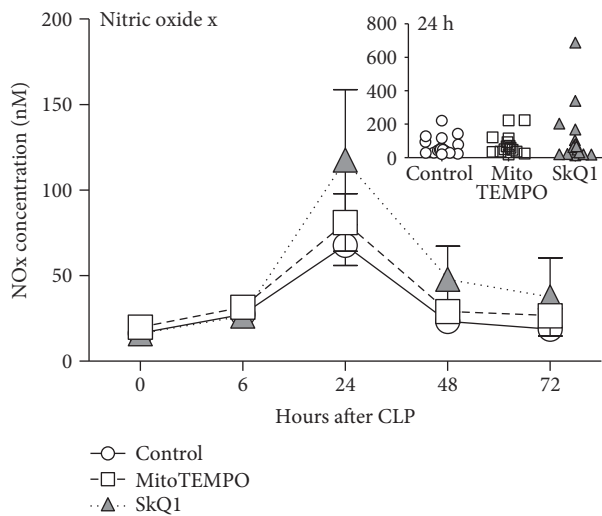


FIGURE 5: NOx concentration in the blood plasma. All forms of NO (NOx) in plasma were measured at BL (0 h), 6, 24, 48, and 72 h post-CLP. At BL: control $n = 20$, SkQ1 $n = 20$, MitoTEMPO $n = 20$; at 6 h: control $n = 20$, SkQ1 $n = 19$, MitoTEMPO $n = 19$; at 24 h: control $n = 19$, SkQ1 $n = 17$, MitoTEMPO $n = 15$; at 48 h: control $n = 13$, SkQ1 $n = 12$, MitoTEMPO $n = 10$; at 72 h: control $n = 13$, SkQ1 $n = 11$, MitoTEMPO $n = 9$. Data points shown as mean \pm SEM. The inset depicts scatter plot of all groups at 24 h post-CLP time point.

2.11. Flow Cytometry. Peritoneal lavage fluid samples were kept in 50 ml Falcon tubes on ice and were processed within 1 hour of collection. After red blood cell lysis, the cell suspension was filtered through a 70 μ m cell strainer (BD, Bedford, MA, USA) to singularize the cells, washed with PBS, and adjusted to the recommended cell count for staining. A total of 100 μ L of the suspension was then transferred to FACS tubes (Beckman Coulter, Brea, CA, USA) and incubated with fluorophore-conjugated antibodies on ice for 30 min. If not indicated otherwise, all antibodies were purchased from eBioscience (Vienna, Austria). Leukocyte subsets in the lavage fluid were identified by morphology and the positivity/negativity for the following antigens: presence of the integrin subunit CD11b (-FITC conjugate) and the granulocyte cell surface determinant Ly6-G (Gr-1, APC-conjugate) as well as the absence of the macrophage adhesion receptor F4-80 (PE-conjugate) was used to determine neutrophil populations. CD11b/F4-80-positive and Ly6-G-negative subsets were identified as macrophages. Cell suspensions were washed with PBS and were measured on a FC-500 flow cytometer (Beckman Coulter, Brea, CA, USA). A minimum of 1×10^4 intact cells were recorded and analyzed in FlowJo software (FlowJo LLC., Ashland, Oregon); Leukocyte subsets were displayed as % of intact cells.

2.12. Bacterial Growth Assessment. The spleens were obtained immediately after sacrifice under sterile conditions following the protocol of Barquero-Calvo et al. [53] allowing small modifications. We used nine parts of PBS containing 0.1% Tween 20 per g of spleen (dilution 1 : 10), assuming that the volume of 1 g of spleen corresponds to 1 ml of PBS (e.g., 0.5 g of spleen and 4.5 ml of PBS 0.1% Tween 20). Isolated

spleens were homogenized using pellet pestles (Dstroy-S-15, Biozym, Oldendorf). After centrifugation at 13000 rpm for 10 minutes, supernatant was removed and serially diluted with PBS for subsequent plating on lysogeny broth (LB) agar plates (Miller, USA) and incubation overnight at 37°C. Colony-forming units were counted after 24 h.

2.13. Western Blotting. Mice were euthanized at 24 h post-CLP, and liver samples were immediately snap-frozen in liquid nitrogen and stored at -80°C for further analysis. All analyses were performed in Jena University Hospital (Germany). Total protein content was isolated from the frozen tissue samples by a protein isolation buffer pH 7.5 (10 mM Tris, 250 mM saccharose, 1 mM EDTA, 1% phosphatase-inhibitor cocktail, and 1% protease inhibitor 2) using a dounce homogenizer (Kimble Chase, Mexico). Homogenates were centrifuged at 900g for 10 min at 4°C to obtain the post nucleus fraction, followed by 100,000g for 1 h at 4°C to separate the cytosolic and microsomal fractions. Protein content in the post nucleus supernatant was determined using the bicinchoninic acid (BCA) assay (Sigma Aldrich, Hamburg, Germany). Fractions were used as indicated. 20 μ g protein was loaded on a sodium dodecyl sulfate (SDS) gel and transferred to a polyvinylidene difluoride (PVDF)-membrane (Roth, Karlsruhe, Germany). Membranes were incubated with 5% N,O-bis(trimethylsilyl)acetamid (BSA) or skim milk (Sigma-Aldrich, Hamburg, Germany) in tris-buffered saline with Tween20 (TBST) for 1 h at room temperature. Primary antibodies in 5% BSA or skim milk were incubated on a shaker overnight at 4°C. Horseradish peroxidase (HRP)-conjugated secondary antibodies (1 : 5000) were incubated for 1 hour at room temperature. The following primary antibodies were used: anti-LC3B, TOM20, cytochrome C (Cell Signaling Technology®, Danvers, USA), and p62 or anti- β -actin (Abcam®, Cambridge, UK). Detection of the secondary antibody by chemiluminescence was performed using HRP substrate (Immobilon Western HRP Substrat, Merck Millipore, Darmstadt, Germany) by the LAS3000 (GE Healthcare, Frankfurt, Germany). Protein content was quantified using software *ImageJ* (National Institutes of Health, Bethesda, MD, USA). β -Actin or Coomassie-stained gel served as loading control to calculate the differences in the protein expression between the groups. To quantify the level of autophagy, the LC3B-II : LC3B-I ratio was calculated based on a densitometric analysis and normalized to β -actin.

2.14. Statistical Analysis. The Kaplan-Meier method was used to plot and compare the 28-day survival in experiment 1. All other data sets were tested for normality before further analysis. Abnormally distributed data sets were log-transformed to achieve normal distribution. Comparisons among the three groups were made using one-way ANOVA and Bonferroni's Multiple Comparison Test for the parametric data and Kruskal-Wallis Test and Dunn's Multiple Comparison Test for the nonparametric data. To compare the SkQ1 with the placebo group, we used the unpaired Student *t*-test for parameters with parametric distribution or the Mann-Whitney Test for parameters with nonparametric distribution. The level of significance

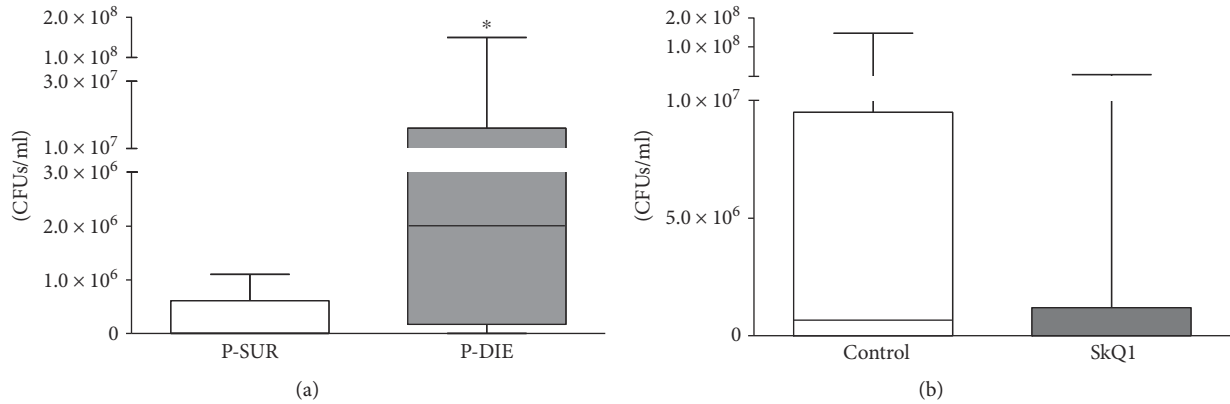


FIGURE 6: Bacterial load in the spleen. Number of colony-forming units (CFUs) per ml spleen homogenate. (a) Mice that were predicted-to-die (P-DIE; $n = 7$) versus predicted-to-live (P-SUR; $n = 11$). Prediction of outcome was performed retrospectively based on the body temperature recordings taken before sacrifice time point at 48 h post-CLP. (b) Placebo-treated ($n = 7$) versus SkQ1-groups ($n = 10$). Data as (min–max) box-and-whiskers plots * $p < 0.05$.

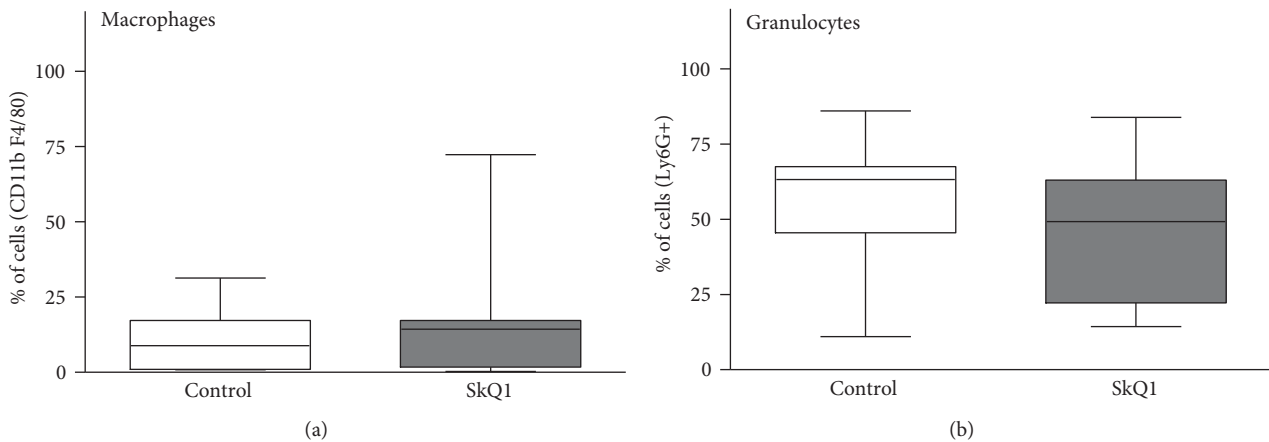


FIGURE 7: Distribution of macrophages and neutrophils in peritoneal lavages of the placebo-treated control group versus SkQ1-treated group. Flow cytometry determination of macrophages and neutrophils, displayed as percent of intact measured cells. Placebo $n = 7$, SkQ1 $n = 9$. Data as (min–max) box-and-whiskers plots.

was set at $p < 0.05$. All statistical analyses and graphs were made with GraphPad (San Diego, USA).

3. Results

3.1. Application of Mitochondrial ROS Scavengers Exacerbated Mortality. Survival was monitored for 28 days post-CLP. To be consistent with clinical severity of abdominal sepsis, mice were subjected to a medium-severe CLP with 38% mortality (average of six CLP repetitions). Neither MitoTEMPO nor SkQ1 exerted a protracted survival benefit. Conversely, SkQ1 treatment exacerbated mortality to 67% ($p = 0.03$) by day 28 (Figure 1). This negative effect was consistent in all six CLP repetitions (Supplementary Figure 3); it was apparent immediately in the acute phase (i.e., within 1–5 days post-CLP; in four CLP repetitions) and continued into the chronic phase until the end of the observation period. MitoTEMPO effect was inconsistent among individual repetitions (not shown) and did not reach statistical significance ($p = 0.24$; Figure 1).

3.2. Application of Mitochondrial ROS Scavengers Did Not Modulate the Inflammatory Response to Polymicrobial Sepsis. We examined a comprehensive set of circulating cytokines that are typically upregulated in both human and mouse sepsis [54, 55]. In general, CLP induced an increase of all cytokines measured; the strongest concentration was recorded for IL-6, MCP-1, CXCL-1, and MIP-1 α at 24 h (Figures 2 and 3). None of those post-CLP increases was further significantly modified by either SkQ1 or MitoTEMPO.

Following acute sepsis, a strong rearrangement of cell populations occurs. We found out that neither SkQ1 nor MitoTEMPO affected the CLP-induced lymphopenia (at 24 h: placebo 1.2 pg/ml versus SkQ1 1.1 pg/ml versus MitoTEMPO 0.9 pg/ml) and neutrophilia (at 24 h: placebo 0.4 pg/ml versus SkQ1 0.4 pg/ml versus MitoTEMPO 0.3 pg/ml) when compared to the placebo group (Supplementary Figure 5).

3.3. Application of Mitochondrial ROS Scavengers Did Not Change Organ Function/Injury and Metabolic Parameters. Functional tissue damages are hallmarks of sepsis

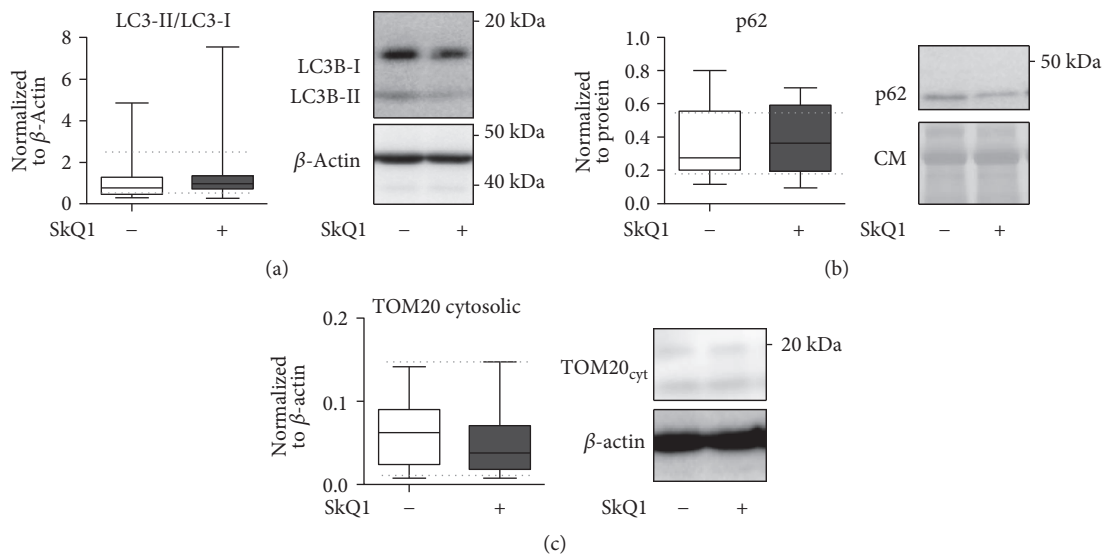


FIGURE 8: Comparison of mitophagy and mitochondrial integrity in the liver of placebo-treated control versus SkQ1-treated groups at 24 h post-CLP. CLP mice received a total of three SkQ1/placebo injections before sacrifice at 24 h. All panels display densitometric analysis of the Western blot assay as well as representative Western blots. (a) LC3-II-to-LC3-I ratio (normalized to total actin), (b) p62 (normalized to total protein), and (c) cytosolic TOM-20 release (normalized to actin). Total number of CLP mice loaded on three different gels: SkQ1 $n=16$; control (placebo) $n=12$. Data as (min-max) box-and-whiskers plots. Dotted lines indicate upper/lower standard deviation calculated based on eight healthy control mice (no CLP, no treatment) that were analyzed together with the CLP mice. CM: Coumassie stained gel.

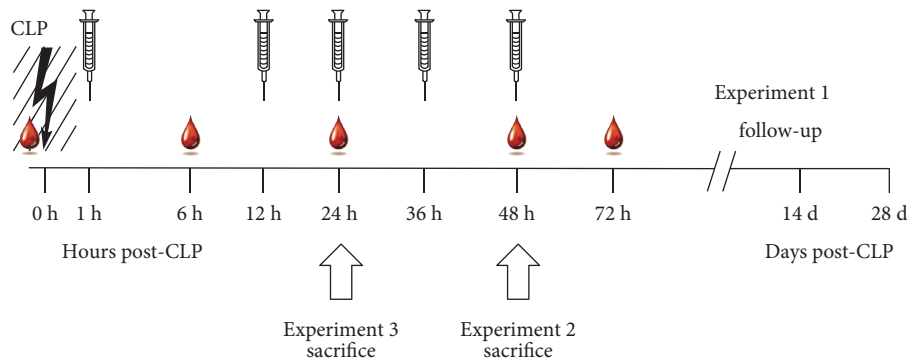


FIGURE 9: Schematic illustration of treatment, blood/tissue sampling, and monitoring. The entire study was divided into three experimental parts that followed the same treatment protocol with specific modifications described below and depicted graphically in the figure. 3-month-old female mice were subjected to polymicrobial CLP sepsis. Mice were subjected to low-volume repetitive blood sampling ($30\ \mu\text{l}$ blood volume/sampling; time points indicated by a single blood drop) maximally five times: At baseline (BL, immediately before CLP) 6 h, 24 h, 48 h, and 72 h post-CLP. Maximally, five intraperitoneal injections with either SkQ1, MitoTEMPO, or placebo treatment were conducted at 1 h, 12 h, 24 h, 36 h, and 48 h post-CLP (indicated by syringes). In experiment 1: mice ($n=90$) were monitored for 28 days (all five blood collections and treatment injections performed). In experiment 2: mice ($n=24$) were sacrificed at 48 h post-CLP (four blood collections and treatment injections performed). In experiment 3: mice ($n=28$) were sacrificed at 24 h post-CLP (three blood collections and treatment injections performed). White block arrows indicate sacrifice time point for experiments 2 and 3.

pathogenesis [9]. We followed temporal fluctuations of glucose (GLU), alanine aminotransferase (ALT), lactate dehydrogenase (LDH), and urea in septic mice after CLP. In general, all groups displayed similar trajectories at all time points (Figure 4). Specifically, ALT, LDH, and urea peaked in all treatment groups at 24 h (ALT: placebo 111 U/l versus SkQ1 119 U/l versus MitoTEMPO 115 U/l; LDH: placebo 940 U/l versus SkQ1 1097 U/l versus MitoTEMPO 773 U/l; urea: placebo 89 mg/dl versus SkQ1 97 mg/dl versus MitoTEMPO 93 mg/dl), while blood glucose decreased by

approx. 63% (BL: 128 mg/dl versus 24 h: 49 mg/dl) in the placebo group. Hypoglycemia persisted until 72 h post-CLP (placebo 68 mg/dl versus SkQ1 64 mg/dl versus MitoTEMPO 76 mg/dl), while the other parameters recovered.

3.4. Application of Mitochondrial ROS Scavengers Did Not Affect NO_x Concentration in Plasma. Nitric oxide (NO) and its metabolized forms nitrite (NO₂⁻) and nitrate (NO₃⁻; both referred to as NO_x) play a central role in inflammation and correlate with severity of sepsis. We

measured NO_x concentration in plasma at BL, 6, 24, 48, and 72 h post-CLP (Figure 5); there were no significant intergroup NO_x changes. Similar to the organ function parameters, NO_x peaked at 24 h post-CLP (approx. 4-fold higher than baseline).

3.5. SkQ1 Treatment Did Not Impair the Bacterial Clearance in the Spleen. Because of the consistent survival deterioration after SkQ1 (but not MitoTEMPO), we only compared the SkQ1 and placebo groups in experiment 2. First, to verify the bacterial clearance, we determined colony-forming units (CFUs) in the spleen homogenates. Mice that were predicted to die post-CLP had approximately 100-fold more CFUs in the spleen than mice that were predicted to survive CLP (Figure 6(a); $p = 0.03$). However, this effect was not related to antioxidant treatment (Figure 6(b)).

3.6. SkQ1 Treatment Did Not Change Macrophage or Granulocyte Counts from Peritoneal Lavages. In experiment 2, to identify potential treatment-related differences in the abdominal leukocyte populations, we performed peritoneal lavages at 48 h post-CLP and analyzed cells by FACS. In general, the cell counts were similar between both groups (Figures 7(a) and 7(b)): macrophages (CD11b+/F4/80+) reached 11% in placebo and 16% in SkQ1, while granulocytes (Ly6G+) reached 56% in placebo and 45% in SkQ1.

3.7. SkQ1 Treatment Did Not Modify the Mitochondrial Autophagy. Finally, we investigated mitophagy and integrity of mitochondria in the liver (as a relatively sensitive organ) to establish whether SkQ1 exerted a direct detrimental effect upon this organelle. Western blot analysis of key proteins involved in autophagy (i.e., LC3B, p62) [56], mitochondrial membrane integrity (i.e., TOM20; Figures 8(a), 8(b), and 8(c)), and apoptosis (i.e., cytochrome C; Supplementary Figure 5) was performed. Compared to CLP mice treated with placebo, SkQ1 failed to reveal any modulation in the expression of those markers in the liver at 24 h post-CLP. This implies that the SkQ1-induced exacerbation of CLP mortality was not caused by direct mitochondrial damage.

4. Discussion

Recently, Sepsis-3 guidelines redefined sepsis as a “life-threatening organ dysfunction caused by a dysregulated host response to infection” [1]. ROS production/release is thought to play a major part in the progression of organ failure and mitochondrial dysfunction [12, 57]. Therefore, we aimed to improve the outcome of mice with polymicrobial sepsis by selectively inhibiting ROS at one of its key formation sites, the mitochondrion. Surprisingly, none of the tested antioxidants demonstrated any benefits, while SkQ1 markedly increased CLP mortality.

Best to our knowledge, this is the only study demonstrating a negative long-term impact of targeted mitochondrial antioxidant scavenging (i.e., by SkQ1) upon abdominal sepsis survival. The majority of rodent studies showed benefits of SkQ1 and/or MitoTEMPO in acute inflammatory conditions including pyelonephritis [13], gastritis [58], cardiomyopathy [31], SIRS [59], and sepsis [35]. Similar was true in a rat

model of pneumosepsis [60] and endotoxemia [14]. Antioxidant (not mitochondria targeted) treatment did not improve survival only in three mouse studies, acute pancreatitis [61], pancreatic cancer [62], and CLP [63] models. While surprising, our protracted study design (Supplementary Figure 3) allows postulating that the reduction of survival due to SkQ1 was not a coincidental observation.

First, we examined two main elements of the systemic CLP response, inflammation, and organ function, to discern the deleterious mechanism(s). We repeatedly measured over twenty relevant parameters in mice enrolled in the survival study. This ensured maximal synchrony between the end-outcome effect and detection of a potential mechanism-of-action. CLP-induced dysregulation of the inflammatory and organ function system was consistent with data reported by us [64, 65] and others [66]. Surprisingly, we failed to observe any additional consistent changes caused by the SkQ1 and/or MitoTEMPO. This is suggestive of two things. First, the increased mortality in the SkQ1 mice did not appear to be caused by an evidently exacerbated early systemic inflammatory response, especially given that the four-day cytokine trajectories preceded/overlaid with the period of the highest acute mortality (days 1–3 post-CLP). Second, hepatocyte damage and/or impaired kidney function as well as dysregulation of carbohydrate metabolism was not a culprit either. The latter, however, does not exclude potential late derangements occurring in those and other organs (e.g., heart, lungs, and intestines) and/or systems (e.g., microcirculation, coagulation) that we did not examine. The protracted readout of the CLP-induced NO_x fluctuations in the blood was consistent with the above changes. Similar to other works [67], the post-CLP peak of circulating nitrate/nitrite occurred in our study at 24 h time point but it was not further modified by antioxidants.

Next, we tested whether SkQ1 modulated the abdominal cellular characteristics and/or impeded bacterial clearance. We performed two-tier retrospective comparison: (1) treatment versus control as well as (2) predicted-to-die versus predicted-to-live using the body temperature-based prediction of outcome [41]. Such an approach allows more precise verification of the potential treatment effect upon the lethal phenotype. Our data show that compared to (predicted-to-be) survivors, predicted-to-die mice had much more pronounced bacterial load in the spleen. Yet again, the placebo treatment comparison revealed that SkQ1 neither altered the abdominal recruitment of phagocytes nor interfered with the bacterial clearance.

Impaired mitochondrial function was not always detected in CLP models, particularly in rodents [68]. Yet, the absence of a visible mitochondrial dysfunction in such cases was explained by activation of the effective autophagy process and removal of nonfunctional mitochondria. Thus, the autophagy appeared to us as a very sensitive sensor of the potential impairment of mitochondrial function. The final experiment 3 showed, however, that SkQ1 treatment was not by itself harmful to mitochondria (in the liver) given that neither autophagy (i.e., mitophagy) nor mitochondrial membrane integrity was altered by SkQ1 at the administered dose. This is in line with the nontoxicity

assessment of SkQ1 in liver homogenates of healthy mice and rats (Supplementary Figure 2).

This leaves us with a negative effect of SkQ1 upon sepsis survival and insufficient understanding what this effect can be attributed to. There are several ways to explain the absence of the expected antioxidant benefits as well as the uncertain mechanism-of-action behind the worsened mortality. First, a proper dose fine tuning of the antioxidants appears important. For example, at micromolar concentrations, cationic quinone derivatives have a strong pro- not antioxidant effect [29]. Thus, it is unlikely that a higher dose would have lessened (reversed) the observed adverse SkQ1 effect. We rather consider inapt treatment timing and/or relatively low-risk-of-death sepsis CLP cohort as culprits. Specifically, we used a repeated treatment to cover the first two post-CLP days, the phase with the most frequent acute sepsis mortality. It seems now that such a blanket coverage might have been too aggressive and/or wide ranging, especially in a nonoverly lethal sepsis environment of our study. A minimal threshold of mitochondrial ROS (mtROS) is key for maintaining intracellular defense signaling pathways [69, 70] to enable, for example, a proper response to bacterial invasion [71]. Although we did not see a post-SkQ1 exacerbation of microbial load in the spleen, a complete blockage of mtROS (not detrimental to mitochondria themselves) could have impeded bacterial clearance at other sites. Likewise, blanket mtROS scavenging could have deregulated transcription of protective hypoxia inducible factors [72, 73] that we did not examine. Of note, there is an emerging role of cell-free hemoglobin in sepsis-induced organ failure [74]. For example, the recent clinical trial showed that blocking ferryl hemoglobin with acetaminophen improved sepsis outcome [75]. Thus, in addition to mtROS, rich amounts of ROS are generated by different intra/extracellular sources such as NADPH-oxidase, myeloperoxidase, and ferryl hemoglobin. Future studies need to explain precise site- and cell-specific roles of oxidative stress in sepsis. Of note, recent antioxidant treatment using N-acetylcystein and butylated hydroxyanisole (unspecific ROS scavengers) improved survival of mice with specific deletion of the iron sequestering protein ferritin heavy chain (FTH); restoration of hepatic glucose production was identified as the key mechanism of this benefit [76]. Given that our CLP mice did not enter a prolonged (potentially deadly) hypoglycemia, this beneficial effect would not have applied.

The two recent sepsis studies offer some relevant clues regarding the antioxidant treatment timing/dosage and model severity [13, 63]. At first, CLP mice were given a single-bolus coenzyme Q10 (strong mitochondria-targeted antioxidant) at 5 h and 20 h post-CLP. Only the latter attenuated organ injury and (insignificantly) improved survival [58]. The authors also noted that when sham (also control) mice were treated with coenzyme Q10, their injury score doubled (versus untreated sham/control) and a (statistically insignificant) decline in survival occurred in sham + coenzyme Q10 mice. This indicates a predilection for detrimental effects of coenzyme Q10 in a nonlethal milieu. The second study was performed in rats with acute pyelonephritis (APN) who benefited from SkQR1 (we reproduced their treatment protocol) [13]. There are four major

differences between that study and ours: cumulative dosage (500 versus 25 nmol/kg), species (rat versus mouse), origin of sepsis (urosepsis versus abdominal), and the infection severity. We consider the latter two elements as essential. First, the rat APN model displayed approx. 70% while our model reached a total 40% mortality by day 28. We believe that treatment benefits are much more likely to occur in a lethal versus moderate severity. For example, inhibition of murine leukotriene B4 synthesis improved CLP survival in severe sepsis [77], while the same agent worsened survival by 50% in a sublethal CLP [78]. We recently showed that only CLP mice predicted-to-die benefited from dexamethasone [49], whereas PAI-1 inhibition exacerbated CLP mortality in mice that were predicted to survive [79]. A similar response scenario cannot be ruled out in our study given that on average surviving mice outweighed those with the lethal CLP phenotype as opposed to the (beneficial) coenzyme Q10 treatment (65% mortality) [63], Mito-TEMPO mouse experiment (60% mortality), and SkQR1 APN rat study [13]. Likewise, in the recent SIRS study, 48 h pretreatment with SkQ1 improved mouse survival in a lethal but not in 50% mortality setup [59].

The negative effect of SkQ1 can be also attributed to the specificity of CLP; SkQ1 at the identical (pretreatment) dose was protective in the LPS rat model [50]. CLP only reproduces polymicrobial human sepsis of abdominal origin, and it cannot be reflexively extended to other sepsis types [2]. SkQ1 was never tested in CLP, and it is plausible that its negative effects may arise only in sepsis originating from this particular body compartment. Of note, our study monitored survival for 28 days. Although advised in preclinical sepsis [2], a protracted followup has never been tested before for targeted antioxidant treatment in sepsis. Had we used a 7-day observation, the SkQ1-induced effect would have been statistically insignificant.

There are several limitations in our study. First, only placebo versus verum CLP mice were compared and sham controls were not employed. Second, we did not assess the mitochondria-and/or cell-derived ROS. Third, mitophagy assessment was limited to a single (i.e., 24 h post-CLP) time point. Finally, CLP experiments were performed at two different locations (i.e., LBI and ISR) and the potential influence of microbiome fluctuations was not verified.

It is also possible that the rodent CLP model is not an appropriate testing model for antioxidant therapies given the overall higher resistance of rodents to trauma/infection [2] and the qualitative difference in ROS release [80] under infectious and/or endotoxic stimuli (rodents versus humans). Thus, the sudden ROS release might not be as damaging in septic rodents as it is in patients. Long-term mouse studies using pneumosepsis, CASP, and candidiasis models as well as testing the mitochondria-specific antioxidants in various sepsis severity protocols will verify whether the negative effect observed here can be attributed to the CLP model itself, species used, the magnitude of the sepsis insult, or combination thereof. Finally, our study can be also considered as cautionary; it suggests that in certain severe inflammatory states, mtROS scavenging can be therapeutically inefficient and/or deleterious.

Disclosure

Pia Rademann's current address is Center for Experimental Medicine, Medical Faculty, University of Cologne, Cologne, Germany.

Conflicts of Interest

Vladimir P. Skulachev is a board member of Mitotech LLC (Russia), a company developing SkQ1-based pharmaceuticals. The other authors declare that there is no conflict of interests regarding the publication of this paper.

Acknowledgments

The authors gratefully acknowledge the expert technical help of Anton Klotz and Anna Khadem. Additionally, the first author expresses her sincere gratefulness to the entire team for the selfless and continuous support during the project. Susanne Drechsler is supported by FWF, Austria, Hertha-Firnberg (Project no. T707 B13). Sebastian Weis is supported by the Integrated Research and Treatment Center—Center for Sepsis Control and Care (CSCC) at the Jena University Hospital. The CSCC is funded by the German Ministry of Education and Research (BMBF no. 01 EO 1002, 01EO1502). Andrea Szabo and Jozsef Kaszaki are supported by the National Research, Development and Innovation Office (NKFIH K116689).

References

- [1] M. Singer, C. S. Deutschman, C. W. Seymour et al., "The third international consensus definitions for sepsis and septic shock (sepsis-3)," *The Journal of the American Medical Association*, vol. 315, no. 8, pp. 801–810, 2016.
- [2] K. N. Iskander, M. F. Osuchowski, D. J. Stearns-Kurosawa et al., "Sepsis: multiple abnormalities, heterogeneous responses, and evolving understanding," *Physiological Reviews*, vol. 93, pp. 1247–1288, 2013.
- [3] M. Rocha, R. Herance, S. Rovira, A. Hernández-Mijares, and V. M. Victor, "Mitochondrial dysfunction and antioxidant therapy in sepsis," *Infectious Disorders Drug Targets*, vol. 12, pp. 161–178, 2012.
- [4] A. Phaniendra, D. B. Jestadi, and L. Periyasamy, "Free radicals: properties, sources, targets, and their implication in various diseases," *Indian Journal of Clinical Biochemistry*, vol. 30, pp. 11–26, 2015.
- [5] J. F. Turrens, "Mitochondrial formation of reactive oxygen species," *The Journal of Physiology*, vol. 552, pp. 335–344, 2003.
- [6] M. P. Murphy, "How mitochondria produce reactive oxygen species," *The Biochemical Journal*, vol. 417, pp. 1–13, 2009.
- [7] M. Valko, D. Leibfritz, J. Moncol, M. T. D. Cronin, M. Mazur, and J. Telser, "Free radicals and antioxidants in normal physiological functions and human disease," *The International Journal of Biochemistry & Cell Biology*, vol. 39, pp. 44–84, 2007.
- [8] J. Nordberg and E. S. Arnér, "Reactive oxygen species, antioxidants, and the mammalian thioredoxin system," *Free Radical Biology and Medicine*, vol. 31, pp. 1287–1312, 2001.
- [9] M. P. Soares, R. Gozzelino, and S. Weis, "Tissue damage control in disease tolerance," *Trends in Immunology*, vol. 35, pp. 483–494, 2014.
- [10] I. B. Slimen, T. Najar, A. Ghram, H. Dabbebi, M. Ben Mrad, and M. Abdrabbah, "Reactive oxygen species, heat stress and oxidative-induced mitochondrial damage. A review," *International Journal of Hyperthermia*, vol. 30, pp. 513–523, 2014.
- [11] E. R. Stadtman and R. L. Levine, "Protein oxidation," *Annals of the New York Academy of Sciences*, vol. 899, pp. 191–208, 2000.
- [12] E. D. Crouser, "Mitochondrial dysfunction in septic shock and multiple organ dysfunction syndrome," *Mitochondrion*, vol. 4, pp. 729–741, 2004.
- [13] E. Y. Plotnikov, M. A. Morosanova, I. B. Pevzner et al., "Protective effect of mitochondria-targeted antioxidants in an acute bacterial infection," *Proceedings of the National Academy of Sciences of the United States of America*, vol. 110, pp. E3100–E3108, 2013.
- [14] I. I. Galkin, O. Y. Pletjushkina, R. A. Zinovkin et al., "Mitochondria-targeted antioxidants prevent TNF α -induced endothelial cell damage," *Biochemistry (Moscow)*, vol. 79, pp. 124–130, 2014.
- [15] D. A. Lowes, N. R. Webster, M. P. Murphy, and H. F. Galley, "Antioxidants that protect mitochondria reduce interleukin-6 and oxidative stress, improve mitochondrial function, and reduce biochemical markers of organ dysfunction in a rat model of acute sepsis," *British Journal of Anaesthesia*, vol. 110, pp. 472–480, 2013.
- [16] D. A. Lowes, B. M. V. Thottakam, N. R. Webster, M. P. Murphy, and H. F. Galley, "The mitochondria-targeted antioxidant MitoQ protects against organ damage in a lipopolysaccharide-peptidoglycan model of sepsis," *Free Radical Biology & Medicine*, vol. 45, pp. 1559–1565, 2008.
- [17] G. Sener, H. Toklu, C. Kapucu et al., "Melatonin protects against oxidative organ injury in a rat model of sepsis," *Surgery Today*, vol. 35, pp. 52–59, 2005.
- [18] H. Macarthur, D. M. Couri, G. H. Wilken et al., "Modulation of serum cytokine levels by a novel superoxide dismutase mimetic, M40401, in an Escherichia coli model of septic shock: correlation with preserved circulating catecholamines," *Critical Care Medicine*, vol. 31, pp. 237–245, 2003.
- [19] G. S. Supinski, M. P. Murphy, and L. A. Callahan, "MitoQ administration prevents endotoxin-induced cardiac dysfunction," *American Journal of Physiology Regulatory, Integrative and Comparative Physiology*, vol. 297, pp. R1095–R1102, 2009.
- [20] D. Heyland, J. Muscedere, P. E. Wischmeyer et al., "A randomized trial of glutamine and antioxidants in critically ill patients," *The New England Journal of Medicine*, vol. 368, pp. 1489–1497, 2013.
- [21] B. J. Snow, F. L. Rolfe, M. M. Lockhart et al., "A double-blind, placebo-controlled study to assess the mitochondria-targeted antioxidant MitoQ as a disease-modifying therapy in Parkinson's disease," *Movement Disorders*, vol. 25, pp. 1670–1674, 2010.
- [22] P. Kaufmann, J. L. P. Thompson, G. Levy et al., "Phase II trial of CoQ10 for ALS finds insufficient evidence to justify phase III," *Annals of Neurology*, vol. 66, pp. 235–244, 2009.
- [23] M. F. Osuchowski, D. G. Remick, J. A. Lederer et al., "Abandon the mouse research ship? Not just yet!," *Shock*, vol. 41, pp. 463–475, 2014.

- [24] R. Phillip Dellinger and J. E. Parrillo, "Mediator modulation therapy of severe sepsis and septic shock: does it work?," *Critical Care Medicine*, vol. 32, pp. 282–286, 2004.
- [25] W. Stahl, M. Matejovic, and P. Radermacher, "Inhibition of nitric oxide synthase during sepsis: revival because of isoform selectivity?," *Shock*, vol. 34, pp. 321–322, 2010.
- [26] M. P. Murphy and R. A. J. Smith, "Targeting antioxidants to mitochondria by conjugation to lipophilic cations," *Annual Review of Pharmacology and Toxicology*, vol. 47, pp. 629–656, 2007.
- [27] M. F. Ross, G. F. Kelso, F. H. Blaikie et al., "Lipophilic triphenylphosphonium cations as tools in mitochondrial bioenergetics and free radical biology," *Biochemistry (Moscow)*, vol. 70, pp. 222–230, 2005.
- [28] H. F. Galley, "Bench-to bedside review: targeting antioxidants to mitochondria in sepsis," *Critical Care*, vol. 14, p. 230, 2010.
- [29] V. P. Skulachev, "A biochemical approach to the problem of aging: "megaproject" on membrane-penetrating ions. The first results and prospects," *Biochemistry (Moscow)*, vol. 72, pp. 1385–1396, 2007.
- [30] Y. N. Antonenko, A. V. Avetisyan, L. E. Bakeeva et al., "Mitochondria-targeted plastoquinone derivatives as tools to interrupt execution of the aging program. 1. Cationic plastoquinone derivatives: synthesis and *in vitro* studies," *Biochemistry (Moscow)*, vol. 73, pp. 1273–1287, 2008.
- [31] V. N. Manskikh, O. S. Gancharova, A. I. Nikiforova et al., "Age-associated murine cardiac lesions are attenuated by the mitochondria-targeted antioxidant SkQ1," *Histology and Histopathology*, vol. 30, pp. 353–360, 2015.
- [32] V. N. Anisimov, M. V. Egorov, M. S. Krasilshchikova et al., "Effects of the mitochondria-targeted antioxidant SkQ1 on lifespan of rodents," *Aging (Albany, New York)*, vol. 3, pp. 1110–1119, 2011.
- [33] A. E. Dikalova, A. T. Bikineyeva, K. Budzyn et al., "Therapeutic targeting of mitochondrial superoxide in hypertension," *Circulation Research*, vol. 107, pp. 106–116, 2010.
- [34] Z. Wang, F. Cai, X. Chen, M. Luo, L. Hu, and Y. Lu, "The role of mitochondria-derived reactive oxygen species in hyperthermia-induced platelet apoptosis," *PLoS One*, vol. 8, article e75044, 2013.
- [35] N. K. Patil, N. Parajuli, L. A. MacMillan-Crow, and P. R. Mayeux, "Inactivation of renal mitochondrial respiratory complexes and manganese superoxide dismutase during sepsis: mitochondria-targeted antioxidant mitigates injury," *American Journal of Physiology Renal Physiology*, vol. 306, pp. F734–F743, 2014.
- [36] Y. Yang, S. Karakhanova, S. Soltek, J. Werner, P. P. Philippov, and A. V. Bazhin, "In vivo immunoregulatory properties of the novel mitochondria-targeted antioxidant SkQ1," *Molecular Immunology*, vol. 52, pp. 19–29, 2012.
- [37] Q. Ma, S. Chen, Q. Hu, H. Feng, J. H. Zhang, and J. Tang, "NLRP3 inflammasome contributes to inflammation after intracerebral hemorrhage," *Annals of Neurology*, vol. 75, pp. 209–219, 2014.
- [38] J. A. Nemzek, K. M. S. Hugunin, and M. R. Opp, "Modeling sepsis in the laboratory: merging sound science with animal well-being," *Comparative Medicine*, vol. 58, pp. 120–128, 2008, <http://www.Ncbi.Nlm.Nih.Gov/pubmed/18524169>.
- [39] J. A. Nemzek, H.-Y. Xiao, A. E. Minard, G. L. Bolgos, and D. G. Remick, "Humane endpoints in shock research," *Shock*, vol. 21, pp. 17–25, 2004.
- [40] E. Lilley, R. Armstrong, N. Clark et al., "Refinement of animal models of sepsis and septic shock," *Shock*, vol. 43, pp. 304–316, 2015.
- [41] S. Drechsler, K. M. Weixelbaumer, A. Weidinger et al., "Why do they die? Comparison of selected aspects of organ injury and dysfunction in mice surviving and dying in acute abdominal sepsis," *Intensive Care Medicine Experimental*, vol. 3, p. 48, 2015.
- [42] K. A. Wichterman, A. E. Baue, and I. H. Chaudry, "Sepsis and septic shock—a review of laboratory models and a proposal," *The Journal of Surgical Research*, vol. 29, pp. 189–201, 1980.
- [43] P. Raeven, G. A. Feichtinger, K. M. Weixelbaumer et al., "Compartment-specific expression of plasminogen activator inhibitor-1 correlates with severity/outcome of murine polymicrobial sepsis," *Thrombosis Research*, vol. 129, pp. e238–e245, 2012.
- [44] T. M. Osborn, J. K. Tracy, J. R. Dunne, M. Pasquale, and L. M. Napolitano, "Epidemiology of sepsis in patients with traumatic injury," *Critical Care Medicine*, vol. 32, pp. 2234–2240, 2004.
- [45] J.-L. Vincent, Y. Sakr, C. L. Sprung et al., "Sepsis in European intensive care units: results of the SOAP study," *Critical Care Medicine*, vol. 34, pp. 344–353, 2006.
- [46] K. N. Iskander, M. Vaickus, E. R. Duffy, and D. G. Remick, "Shorter duration of post-operative antibiotics for cecal ligation and puncture does not increase inflammation or mortality," *PLoS One*, vol. 11, article e0163005, 2016.
- [47] C. Piskernik, S. Haindl, T. Behling et al., "Antimycin A and lipopolysaccharide cause the leakage of superoxide radicals from rat liver mitochondria," *Biochimica et Biophysica Acta (BBA) - Molecular Basis of Disease*, vol. 1782, pp. 280–285, 2008.
- [48] M. F. Osuchowski, K. Welch, J. Siddiqui, and D. G. Remick, "Circulating cytokine/inhibitor profiles reshape the understanding of the SIRS/CARS continuum in sepsis and predict mortality," *Journal of Immunology*, vol. 177, pp. 1967–1974, 2006.
- [49] M. F. Osuchowski, J. Connett, K. Welch, J. Granger, and D. G. Remick, "Stratification is the key: inflammatory biomarkers accurately direct immunomodulatory therapy in experimental sepsis," *Critical Care Medicine*, vol. 37, pp. 1567–1573, 2009.
- [50] A. Weidinger, A. Müllebnner, J. Paier-Pourani et al., "Vicious inducible nitric oxide synthase-mitochondrial reactive oxygen species cycle accelerates inflammatory response and causes liver injury in rats," *Antioxidants & Redox Signaling*, vol. 22, pp. 572–586, 2015.
- [51] K. M. Weixelbaumer, P. Raeven, H. Redl, M. v. Griensven, S. Bahrami, and M. F. Osuchowski, "Repetitive low-volume blood sampling method as a feasible monitoring tool in a mouse model of sepsis," *Shock*, vol. 34, pp. 420–426, 2010.
- [52] A. Ray and B. N. Dittel, "Isolation of mouse peritoneal cavity cells," *Journal of Visualized Experiments*, vol. 35, 2010.
- [53] E. Barquero-Calvo, C. Chacon-Diaz, E. Chaves-Olarte, and E. Moreno, "Bacterial counts in spleen," *BIO-PROTOCOL*, vol. 3, 2013.
- [54] H. Chaudhry, J. Zhou, Y. Zhong et al., "Role of cytokines as a double-edged sword in sepsis," *In Vivo*, vol. 27, pp. 669–684, 2013, <http://www.Ncbi.Nlm.Nih.Gov/pubmed/24292568>.

- [55] J.-M. Cavaillon, M. Adib-Conquy, C. Fitting, C. Adrie, and D. Payen, "Cytokine cascade in sepsis," *Scandinavian Journal of Infectious Diseases*, vol. 35, pp. 535–544, 2003.
- [56] S. Wang, C. Wang, F. Yan et al., "N-Acetylcysteine attenuates diabetic myocardial ischemia reperfusion injury through inhibiting excessive autophagy," *Mediators of Inflammation*, vol. 2017, Article ID 9257291, 10 pages, 2017.
- [57] H. F. Galley, "Oxidative stress and mitochondrial dysfunction in sepsis," *British Journal of Anaesthesia*, vol. 107, pp. 57–64, 2011.
- [58] S. Mazumder, R. De, S. Sarkar et al., "Selective scavenging of intra-mitochondrial superoxide corrects diclofenac-induced mitochondrial dysfunction and gastric injury: a novel gastroprotective mechanism independent of gastric acid suppression," *Biochemical Pharmacology*, vol. 121, pp. 33–51, 2016.
- [59] V. V. Zakharova, O. Y. Pletjushkina, I. I. Galkin et al., "Low concentration of uncouplers of oxidative phosphorylation decreases the TNF-induced endothelial permeability and lethality in mice," *Biochimica et Biophysica Acta (BBA)-Molecular Basis of Disease*, vol. 1863, pp. 968–977, 2017.
- [60] Q. S. Zang, H. Sadek, D. L. Maass et al., "Specific inhibition of mitochondrial oxidative stress suppresses inflammation and improves cardiac function in a rat pneumonia-related sepsis model," *American Journal of Physiology Heart and Circulatory Physiology*, vol. 302, pp. H1847–H1859, 2012.
- [61] W. Huang, N. Cash, L. Wen et al., "Effects of the mitochondria-targeted antioxidant mitoquinone in murine acute pancreatitis," *Mediators of Inflammation*, vol. 2015, Article ID 901780, 13 pages, 2015.
- [62] A. V. Bazhin, Y. Yang, J. G. D'Haese, J. Werner, P. P. Philipov, and S. Karakhanova, "The novel mitochondria-targeted antioxidant SkQ1 modulates angiogenesis and inflammatory micromilieu in a murine orthotopic model of pancreatic cancer," *International Journal of Cancer*, vol. 139, pp. 130–139, 2016.
- [63] S. Abitagaoglu, S. B. Akinci, F. Saricaoglu et al., "Effect of coenzyme Q10 on organ damage in sepsis," *Bratislava Medical Journal*, vol. 116, pp. 433–439, 2015.
- [64] S. Drechsler, K. M. Weixelbaumer, H. Redl, M. van Griensven, S. Bahrami, and M. F. Osuchowski, "Experimentally approaching the ICU: monitoring outcome-based responses in the two-hit mouse model of posttraumatic sepsis," *Journal of Biomedicine and Biotechnology*, vol. 2011, Article ID 357926, 12 pages, 2011.
- [65] M. F. Osuchowski, F. L. Craciun, E. Schuller, C. Sima, R. Gyurko, and D. G. Remick, "Untreated type 1 diabetes increases sepsis-induced mortality without inducing a pre-lethal cytokine response," *Shock*, vol. 34, pp. 369–376, 2010.
- [66] M.-H. Liao, S.-J. Chen, C.-M. Tsao, C.-C. Shih, and C.-C. Wu, "Possible biomarkers of early mortality in peritonitis-induced sepsis rats," *The Journal of Surgical Research*, vol. 183, pp. 362–370, 2013.
- [67] Y.-J. Zhang, M. Li, M. Meng, M. Feng, and C.-Y. Qin, "The effect of ulinastatin on the small intestine injury and mast cell degranulation in a rat model of sepsis induced by CLP," *Experimental and Toxicologic Pathology*, vol. 61, pp. 481–490, 2009.
- [68] A. V. Kozlov, J. R. Lancaster, A. T. Meszaros, and A. Weidinger, "Mitochondria-mediated pathways of organ failure upon inflammation," *Redox Biology*, vol. 13, pp. 170–181, 2017.
- [69] A. C. Bulua, A. Simon, R. Maddipati et al., "Mitochondrial reactive oxygen species promote production of proinflammatory cytokines and are elevated in TNFR1-associated periodic syndrome (TRAPS)," *The Journal of Experimental Medicine*, vol. 208, pp. 519–533, 2011.
- [70] R. Zhou, A. S. Yazdi, P. Menu, and J. Tschopp, "A role for mitochondria in NLRP3 inflammasome activation," *Nature*, vol. 469, pp. 221–225, 2011.
- [71] E. Naik and V. M. Dixit, "Mitochondrial reactive oxygen species drive proinflammatory cytokine production," *The Journal of Experimental Medicine*, vol. 208, pp. 417–420, 2011.
- [72] A. Weidinger and A. V. Kozlov, "Biological activities of reactive oxygen and nitrogen species: oxidative stress versus signal transduction," *Biomolecules*, vol. 5, pp. 472–484, 2015.
- [73] T. Klimova and N. S. Chandel, "Mitochondrial complex III regulates hypoxic activation of HIF," *Cell Death and Differentiation*, vol. 15, pp. 660–666, 2008.
- [74] D. R. Janz and L. B. Ware, "The role of red blood cells and cell-free hemoglobin in the pathogenesis of ARDS," *Journal of Intensive Care*, vol. 3, p. 20, 2015.
- [75] D. R. Janz, J. A. Bastarache, T. W. Rice et al., "Acetaminophen for the reduction of oxidative injury in severe sepsis study group, randomized, placebo-controlled trial of acetaminophen for the reduction of oxidative injury in severe sepsis: the acetaminophen for the reduction of oxidative injury in severe sepsis trial," *Critical Care Medicine*, vol. 43, pp. 534–541, 2015.
- [76] S. Weis, A. R. Carlos, M. R. Moita et al., "Metabolic adaptation establishes disease tolerance to sepsis," *Cell*, vol. 169, article e14, pp. 1263–1275, 2017.
- [77] C. F. Benjamim, C. Canetti, F. Q. Cunha, S. L. Kunkel, and M. Peters-Golden, "Opposing and hierarchical roles of leukotrienes in local innate immune versus vascular responses in a model of sepsis," *Journal of Immunology*, vol. 174, pp. 1616–1620, 2005.
- [78] F. Rios-Santos, C. F. Benjamim, D. Zavery, S. H. Ferreira, and F. de Queiroz Cunha, "A critical role of leukotriene B4 in neutrophil migration to infectious focus in cecal ligation and puncture sepsis," *Shock*, vol. 19, pp. 61–65, 2003.
- [79] P. Raeven, S. Drechsler, K. M. Weixelbaumer et al., "Systemic inhibition and liver-specific over-expression of PAI-1 failed to improve survival in all-inclusive populations or homogeneous cohorts of CLP mice," *Journal of Thrombosis and Haemostasis*, vol. 12, pp. 958–969, 2014.
- [80] J. Bylund, M. Samuelsson, L. V. Collins, and A. Karlsson, "NADPH-oxidase activation in murine neutrophils via formyl peptide receptors," *Experimental Cell Research*, vol. 282, pp. 70–77, 2003.

Research Article

β -Naphthoflavone-Induced Mitochondrial Respiratory Damage in Cyp1 Knockout Mouse and in Cell Culture Systems: Attenuation by Resveratrol Treatment

Suresh Kumar Anandasadagopan,¹ Naveen M. Singh,¹ Haider Raza,² Seema Bansal,¹ Venkatesh Selvaraj,¹ Shilpee Singh,¹ Anindya Roy Chowdhury,¹ Nicolae Adrian Leu,¹ and Narayan G. Avadhani¹

¹Department of Biomedical Sciences, School of Veterinary Medicine, University of Pennsylvania, Philadelphia, PA 19104-6009, USA

²Department of Biochemistry, College of Medicine and Health Sciences, United Arab Emirates University, Al-Ain, UAE

Correspondence should be addressed to Narayan G. Avadhani; narayan@vet.upenn.edu

Received 4 April 2017; Accepted 15 August 2017; Published 14 September 2017

Academic Editor: Icksoo Lee

Copyright © 2017 Suresh Kumar Anandasadagopan et al. This is an open access article distributed under the Creative Commons Attribution License, which permits unrestricted use, distribution, and reproduction in any medium, provided the original work is properly cited.

A number of xenobiotic-inducible cytochrome P450s (CYPs) are now known to be localized in the mitochondrial compartment, though their pharmacological or toxicological roles remain unclear. Here, we show that BNF treatment markedly inhibits liver mitochondrial O₂ consumption rate (OCR), ADP-dependent OCR, and also reserve OCR, in wild-type mice but not in *Cyp1a1/1a2(-/-)* double knockout mice. BNF treatment markedly affected mitochondrial complex I and complex IV activities and also attenuated mitochondrial gene expression. Furthermore, under in vitro conditions, BNF treatment induced cellular ROS production, which was inhibited by mitochondria-targeted antioxidant Mito-CP and CYP inhibitor proadefin, suggesting that most of the ROS production was intramitochondrial and probably involved the catalytic activity of mitochondrial CYP1 enzymes. Interestingly, our results also show that the AHR antagonist resveratrol, markedly attenuated BNF-induced liver mitochondrial defects in wild-type mice, confirming the role of AHR and AHR-regulated CYP1 genes in eliciting mitochondrial dysfunction. These results are consistent with reduced BNF-induced mitochondrial toxicity in *Cyp1a1/1a2(-/-)* mice and elevated ROS production in COS cells stably expressing CYP1A1. We propose that increased mitochondrial ROS production and respiratory dysfunction are part of xenobiotic toxicity. Resveratrol, a chemopreventive agent, renders protection against BNF-induced toxicity.

1. Introduction

Studies from our laboratory as well as from others have shown that xenobiotic-inducible CYPs (CYP1A1, 1A2, 1B1, 2E1, 2B1, 2C8, and 3A4/5), as well as the constitutively expressed CYP2D6, are also targeted to mitochondria where they actively catalyze substrate oxidation in association with adrenodoxin (ADX) and adrenodoxin reductase (ADR). In several cases, these mitochondria-localized CYPs exhibit altered substrate specificity [1–6]. Recent studies also suggest that aryl hydrocarbon receptor (AHR), a ligand-activated basic helix-loop-helix (bHLH) transcription factor [7] is also

localized in the mitochondrial intermembrane space [8], although its role in mitochondrial gene expression or biogenesis remains unclear. AHR ligands in the cytoplasmic compartment include polycyclic aromatic hydrocarbons (PAHs) and halogenated aromatic hydrocarbons (including 2,3,7,8-tetrachloro-dibenzo-p-dioxin, TCDD). In addition, a large number of as-yet-unidentified endogenous compounds also activate AHR [7, 9, 10].

PAHs induce transcriptional activation of the *Cyp1* (*CYP1a1*, *1a2*, and *1b1*) gene family in addition to induction of an array of phase II drug-detoxifying enzymes such as glutathione transferases and glucuronyl transferases [11–14].

CYP1A1, 1A2, and 1B1 are also major enzymes which metabolize and eliminate PAHs [15–17] that are components of cigarette smoke, cooked food, and industrial pollution. All three CYP1 family members are induced abundantly in the lung, skin, brain, intestine, and bone marrow cells in response to exposure to AHR agonists, whereas in the mammalian liver only 1A1 and 1A2 are induced [9, 16, 18, 19]. In a recent study, we showed that BaP treatment induced lung mitochondrial dysfunction including reduced respiratory capacity, altered cytochrome c oxidase (CcO) activity, and decreased mtDNA levels. Transgenic *Cyp1a1/1a2* (–/–) double knockout and *Cyp1b1*–/– mice were relatively resistant to BaP-induced mitochondrial toxicity [20]. Furthermore, shRNA-mediated knockdown of NADPH-cytochrome P450 oxidoreductase (NPOR) and ADX mRNA suggested that mitochondrial CYP1A1 and 1B1-dependent metabolism play a role in BaP-induced lung mitochondrial dysfunction [20].

Previous studies by Senft et al. [21, 22] showed that TCDD induces ROS production and mitochondrial respiratory defects possibly through AHR activation mechanism. A recent study showed that TCDD induces degradation of mitochondrial AHR in a manner similar to the nuclear/cytoplasmic AHR [8]. Studies in our laboratory showed that TCDD imparts both AHR-dependent and independent effects on mitochondrial function and nuclear gene expression [23]. Specifically, we showed that TCDD induces mitochondrial dysfunction and retrograde signaling which is likely due to the direct action of xenobiotic on mitochondrial inner membrane rather than through AHR activation [23].

We therefore hypothesized that BaP-mediated mitochondrial dysfunction could be attributed to two possible mechanisms: (a) CYP1 monooxygenase activity might directly or indirectly contribute to oxidative stress affecting mitochondrial function, or (b) resulting reactive oxygen species (ROS) and metabolites could damage mtDNA or mitochondrial integrity leading to mitochondrial dysfunction. In this study, therefore, using transgenic *Cyp* double (*Cyp1a1/1a2*) or triple (*Cyp1a1/1a2/1b1*) KO mice, *in vivo* and C6 glioma cell culture *in vitro*, we investigated the effects of β -naphthoflavone (BNF), a known inducer of CYP1A1/1A2 and an AHR agonist, whose metabolic products, unlike other PAHs like BaP, are neither reactive nor toxic. Our results show that BNF induces oxidative stress and mitochondrial dysfunction similar to that observed in BaP-treated lung mitochondria [3, 24]. Furthermore, the BNF-induced toxicity is probably due to CYP1 enzyme-mediated ROS production which is attenuated by resveratrol, a naturally occurring polyphenolic compound, using both *in vivo* and *in vitro* model systems. In addition, we have also demonstrated that mitochondria-targeted antioxidant, Mito-CP, and CYP inhibitor proadifen also inhibit BNF-induced mitochondrial dysfunction suggesting the role of oxidative stress and CYP catalytic activity in BNF-induced toxicity.

2. Materials and Methods

2.1. Experimental Models. We used Wt and *Cyp1a1/1a2* (–/–) and *Cyp1a1/1a2/1b1* (–/–) mice to evaluate the roles of these CYPs in BNF-induced effects on liver mitochondrial

respiration and electron transport chain complex activities. To evaluate the generality of BNF-mediated effects on mitochondrial function and ROS production, we used C6 glioma, a neuroglial cell line. COS-7 cell lines stably expressing full-length CYP1A1 and N-terminal truncated +331A1, which is preferentially targeted to the mitochondria ([1]; Dasari et al. 2006), were used to evaluate the role of CYP1A1 catalytic activity in ROS production. Also, use of these cell lines allowed the facile evaluation of different pharmacological agents on BNF-mediated effects.

2.2. Reagents and Cell Cultures. β -Naphthoflavone (BNF), DMSO, catalase, ubiquinol, ADP, sodium succinate, NADH, cytochrome C, lauryl maltoside, oligomycin, 2,4-dinitrophenol (DNP), rotenone, antimycin, CH223191, proadifen, and resveratrol were obtained from Sigma Chemical Co. (St Louis, MO). ROS probes 2',7'-dichlorofluorescein diacetate (DCFDA) and Amplex Red reagents were purchased from Abcam (Cambridge, MA) and Invitrogen, (Carlsbad, CA), respectively. Rat C6 glioma and COS cells were purchased from American Type Culture Collection (ATCC) (Manassas, VA) and grown in DMEM/F12 or MDM2 media obtained from Invitrogen, (Carlsbad, CA). In all cases, cells were grown in culture medium supplemented with 10% fetal bovine serum, 1% penicillin-streptomycin at 5% CO₂, and 95% air (v/v), at 37°C in the incubator. In some cases, cells were also treated for 24–48 hrs with BNF dissolved in dimethylsulfoxide (DMSO; 25–50 μ M) in the presence or absence of resveratrol (10 μ M), Mito-CP (2 μ M), AHR inhibitor CH223191 (25 μ M), and CYP inhibitor proadifen (5 μ M), whereas the control cells were treated with vehicle alone.

2.3. Animal Studies. Wild type (Wt), *Cyp1a1/1a2* (–/–) double KO, and *Cyp1a1/1a2/1b1* (–/–) triple KO mice were obtained from the Daniel Nebert's mouse colony (University of Cincinnati Medical Center). Male mice aged (6–8 weeks) were divided into three different groups ($n = 4 - 5$ each). Group I (controls) received intraperitoneal (i.p.) corn oil as vehicle control. Group II animals were treated intraperitoneal (IP) with BNF alone (50 mg/kg body weight) in corn oil for 7 consecutive days. Group III mice were treated IP with BNF (50 mg/kg body weight) plus resveratrol (20 mg/kg body weight). The dosage and time points for BNF treatment *in vivo* were based on previous literature and our own published studies [25, 26], and the resveratrol dose was based on [27, 28]. Mice were euthanized by CO₂ asphyxiation protocol using a Crainey Tech asphyxiation chamber in accordance with the American Veterinary Medical Association (AVMA) and National Institutes of Health (NIH) approved guidelines. The livers from control and treated mice were collected and used for preparing subcellular fractions for further studies and extraction of total RNA or total DNA.

2.4. Preparation of Mitochondrial Extracts. The livers were perfused and rinsed with phosphate-buffered saline and homogenized in a motor-driven glass-Teflon homogenizer in H-medium (70 mM sucrose, 220 mM mannitol, 2.5 mM Hepes, pH 7.4, 2 mM EDTA, and complete protease inhibitor

mixture). Mitochondria and microsomes from freshly extracted mouse liver were prepared by differential centrifugation and suspended in 20 mM K_2HPO_4 buffer containing 20% glycerol with added leupeptin, pepstatin, antipain, and PMSF as described previously [29, 30]. Treatment with protease inhibitor was excluded when mitochondria or microsomes were used for enzyme assays or respiratory measurements. Protein concentration of cell fractions was determined by the method of Lowry et al. [31].

2.5. Measurement of Mitochondrial Electron Transport Enzyme Activity. Complex I (NADH: ubiquinone oxidoreductase) and complex IV (cytochrome c oxidase (CcO)) activities were measured according to the method of Birch-Machin and Turnbull [32]. Briefly, complex I assay was carried out, by incubating 15 μ g of freeze-thawed mitochondrial extract in 1 mL of assay medium (25 mM potassium phosphate, pH 7.4, 5 mM $MgCl_2$, 2 mM NaCN, 2.5 mg/ml bovine serum albumin, 13 mM NADH, 65 μ M ubiquinone, and 2 μ g/ml antimycin A), and then measuring the decrease in absorbance at 340 nm due to NADH oxidation using a Cary 1E UV-visible spectrophotometer. Rotenone-sensitive complex I activity was measured by addition of 40 μ M rotenone. Complex IV (CcO) activity was measured by incubating 2–10 μ g of freeze-thawed mitochondrial extract in 1 mL of assay medium (25 mM potassium phosphate, pH 7.4, and 0.45 mM dodecylmaltoside). Ferrocytochrome c (15 μ M) was added, and reaction rates were measured using a Cary 1E spectrophotometer. First-order rate constants were calculated based on regression analysis, using the Cary-Win kinetics software. The molar extinction coefficient (ϵ) of 21.1 was used for the conversion of OD units to molar amounts of reduced cytochrome c oxidized as described before [20, 33].

2.6. Measurement of Mitochondrial Respiration. Seahorse XF24 Extracellular Flux Analyzer (Seahorse Biosciences, North Billerica, MA, USA) was used to assess mitochondrial respiratory function. Freshly isolated mitochondria (10 μ g/well) from control and treated mouse livers were plated onto Seahorse poly-L-lysine plates. Mitochondria were energized by adding 8 mM succinate. Respiration was sequentially measured in energized mitochondria (basal respiration), followed by state 3 (phosphorylating respiration, in the presence of 5 mM ADP), and state 4o (resting respiration) with the addition of 3 μ g/mL oligomycin, an inhibitor of mitochondrial ATPase. Uncoupled maximal respiration (state 3u) was determined by the administration of 150 μ M DNP. Finally, for complete inhibition of mitochondrial respiration, complex III inhibitor antimycin A (4 μ g/ml) was added. Results were plotted as percentage value of state 3 respiration of respective control, set as 100%.

2.7. Measurement of ROS Formation. ROS formation was measured, using DCFDA or Amplex Red as probes, according to manufacturer suggested protocols described before [20, 34]. Briefly, 10–20 μ g of mouse liver mitochondria from control and BNF-treated mice were incubated in mitochondrial buffer (H-medium) pH 7.4 in the presence of 1 μ g of sodium dodecylmaltoside and 20 μ M NADH with or without

2 μ g/mL catalase followed by 10 min incubation at 37°C. For measuring cellular ROS in untreated and treated MCF-7 and A549 cells, the DCFDA method was used as described above. ROS formation was measured using the LPS-220B Photon Technology International Fluorescence Instrument (Birmingham, NJ). For DCFDA assay, we measured ROS formation at excitation wavelength 485 nm and emission wavelength 535 nm or for the Amplex Red assay at excitation wavelength 530 nm and emission 590 nm, and probes using MicroWin chameleon multilabel detection platform were used. Membrane permeable SOD was used as a control to confirm H_2O_2 production.

2.8. Quantification of mRNA. Total RNA was isolated from fresh liver slices or cell pellets using TRIzol reagent (Invitrogen) using the manufacturer's recommended protocol. For real-time PCR analysis, RNA was digested with turbo DNase I (Ambion, Inc.), and cDNA was synthesized using 1 μ g total RNA as template by using the High-Capacity cDNA Archive kit (Applied Biosystems, Inc.). Relative mRNA levels of CYP1A1, CYP1A2, and CYP1B1 were measured by standard SYBR Green real-time PCRs on an ABI 7300 real-time PCR machine as described before [29]. Transcript levels were normalized to the housekeeping gene β -actin (ACTB) as an internal control and expressed as % change relative to ACTB mRNA.

2.9. Preparation of COS Cells Stably Expressing CYP1A1 Protein. Full-length and N-terminal truncated +331A1 cDNAs were cloned in BamHI and XBA-1 sites of pGP Lenti (Addgene, Cambridge, MA) vector, and fully assembled viral particles were generated by transfection in 293T cells. To generate stable lines, COS-7 cells were transduced with Lenti viral constructs as per the vendor's protocol. Transduced cells were selected based on resistance to 2 μ g/mL puromycin (Invitrogen, Carlsbad, CA). Fresh puromycin-containing media was exchanged every other day for ~2 weeks. After 8–10 days, individual colonies were selected and trypsinized using 0.05% Trypsin EDTA (Thermo Fisher, Waltham, MA) and transferred to a new six-well plate for another 2–4 days or until the cell density reached 50–70% confluence. Monoclonal selection was achieved by means of serial dilution to 2 cells/mL and plated at 100 μ L DMEM F12 puromycin-containing media per well in a 96-well plate. Wells contained colonies derived from a single cell were selected and expanded into a 24-well plate. Protein levels were measured by immunoblotting with an anti-CYP1A1 antibody (in house generated [2]).

2.10. SDS-PAGE and Immunoblot Analysis. For SDS-PAGE analysis, mitochondrial protein (50 μ g) was separated on 12% SDS-polyacrylamide gels. Proteins were then transferred to nitrocellulose membranes (Bio-Rad) and probed with the appropriate antibodies. Antibodies specific to CcO I (cat. number ab14705), CcO IVi1 (cat. number ab110272), CcO Vb (cat. number ab110263), succinate dehydrogenase complex flavoprotein subunit A (SDHA) (cat. number ab14715), and voltage-dependent anion channel (VDAC) (cat. number ab61273) were obtained from Abcam (Cambridge, MA).

Antibodies for CYP1A2 (cat. number sc-30,085), NADPH-P450 oxidoreductase (NPOR) (cat. number sc-25,270), and β -actin (cat. number sc-1616) were purchased from Santa Cruz Biotechnology, Inc. (Dallas, TX). Blots were probed with appropriate dilution of primary (concentration $\sim 1 \mu\text{g/ml}$) followed by corresponding secondary antibodies (manufacturer recommended concentration). The blots were developed using the SuperSignal West Femto System (Pierce) and imaged on a Bio-Rad VersaDoc Imaging System or an Odyssey Licor (Licor Biotechnology, Lincoln, NE). Digital image analysis was performed using Quantity One Version 4.5 software from Bio-Rad.

The blue native gel electrophoresis protocol (BNGE) for the separation respiratory complexes was as described before [35]. Mitochondrial membrane complexes solubilized in 1% laurylmaltoside were clarified at $100,000 \times g$ for 30 min and mixed with 5% Serva blue dye. BNGE was performed on a native 6–13% polyacrylamide gradient gel starting with a current of 100 V and increasing to a constant current of 250 V. Individual complexes were identified based on the size and reactivity to antibodies [35].

2.11. Statistical Analysis. The means \pm SEM were calculated from three to five independent experimental values. Statistical significance (p values) between control and experimental or paired experiments were calculated using Student's t -test. A p value of ≤ 0.05 was considered significant.

3. Results

3.1. BNF-Induced Mitochondrial Respiratory Defects and the Effects of Resveratrol Treatment. We compared the effects of BNF and resveratrol treatment on respiration profiles of wild-type mice as well as the double (*Cyp1a1/1a2*^{-/-}) and triple knockout (*Cyp1a1/1a2/1b1*^{-/-}) groups of mice. The rationale was to see if BNF, a relatively nontoxic AHR agonist, induced respiratory dysfunction in the liver and if the toxicity was associated with the expression of CYP1A1/1A2/1B1 proteins. We measured the respiratory parameters including the baseline OCR, OCR linked to ATP synthesis, maximal respiration, and the state 3 respiration. Results show that BNF treatment markedly reduced the maximal respiration (after addition of DNP) as well as the reserve respiration in Wt mice but had no significant effect in *Cyp1a1/1a2*^{-/-} and *Cyp1a1/1a2/1b1*^{-/-} triple knockout mice (Figures 1(a), 1(b), and 1(c)). These results suggest that BNF induced respiratory impairment in Wt mice that was likely associated with the expression of CYP1 and/or CYP1A2 proteins.

As shown in Figure 1, the average baseline OCR for wild-type liver mitochondria seeded at $10 \mu\text{g/well}$ was 230 pmol O₂/min, including nonmitochondrial oxygen consumption, which was determined after the addition of antimycin, a potent inhibitor of complex III which channels electrons from both NADH (complex I) and FADH₂ (succinate) (complex II). The portion of mitochondrial oxygen consumption devoted to ATP synthesis (which is blocked by oligomycin) was $\sim 70\%$, while the remaining $\sim 30\%$ fed into proton leak. Maximal respiratory rate was determined after addition of DNP, an ionophore which transfers protons

across the membrane independently of ATP synthesis and reveals the full potential for O₂ consumption. The difference between maximal and baseline OCR is defined as reserve respiratory capacity. Our results show that the hepatic mitochondrial oxygen consumption is markedly inhibited by BNF in wild-type mice (Figure 1(a)); however, no significant inhibition was observed in double (*Cyp1a1/1a2*^{-/-}) (Figure 1(a)) and triple knockout (*Cyp1a1/1a2/1b1*^{-/-}) (Figure 1(c)) groups of mice.

Mitochondria from Wt mice treated with BNF showed 45% reduction in state 3 respiration as compared with 100% for mitochondria from untreated mice. As seen from Figure 2(a), administration of resveratrol alleviated BNF-induced reduction in state 3 OCR. The state 3 respiration was minimally affected in the double (Figure 2(b)) and triple knockout mice (Figure 2(c)) by BNF treatment, and as expected, resveratrol had no significant effect on the respiration. Consistent with this, BNF treatment in wild-type mice resulted in $\sim 50\%$ decrease in ATP-linked OCR which was restored to 70% after resveratrol treatment (Figure 2(d)). These results show that BNF treatment affected mitochondrial respiratory controls in a CYP1 gene dependent manner, and the AHR antagonist resveratrol had a protective effect on BNF-induced respiratory defects.

3.2. Effects of BNF and Resveratrol on Liver Mitochondrial Electron Transport Complex Activities. We investigated the effects of BNF on complex I activity, which is a major contributor of ROS production in the mitochondrial compartment, and complex IV activity, which is the terminal oxidase of the mitochondrial electron transport chain. The results show that complex I activity was significantly inhibited ($\sim 45\%$) in the BNF-treated liver mitochondria as compared with control livers and resveratrol treatment restored the activity close to the untreated control level (Figure 3(a)). We also observed steady decrease ($\sim 40\%$) in CcO activity in the livers of mice treated with BNF as compared with control (Figure 3(b)). Resveratrol treatment brought both complex I and IV activities close to controls (Figures 3(a) and 3(b)). Figure 3(c) shows that mitochondrial ROS production in mouse liver mitochondria, as measured by Amplex Red increased (~ 1.7 fold of control) after BNF treatment. Catalase treatment in both BNF-treated and untreated liver mitochondria attenuated the ROS production suggesting that the increased fluorescence signal observed with BNF treatment was indeed due to increased H₂O₂ production. The BNGE pattern of mitochondrial complexes in Figure 3(d) shows that the relative band intensities for complex I, III, and IV were significantly lower in mitochondria from BNF-treated mice (48 h) that was attenuated by coadministration of resveratrol. These results are consistent with the enzyme activity data presented in Figures 3(a) and 3(b).

3.3. Effects of BNF and Resveratrol on the Steady State Levels of CcO Subunits. In previous studies, we found that CcO complex is an important biomarker for mitochondrial stress, since the levels of several subunits (I, IVi1, and Vb) were reduced under various stress conditions [34–36]. To assess

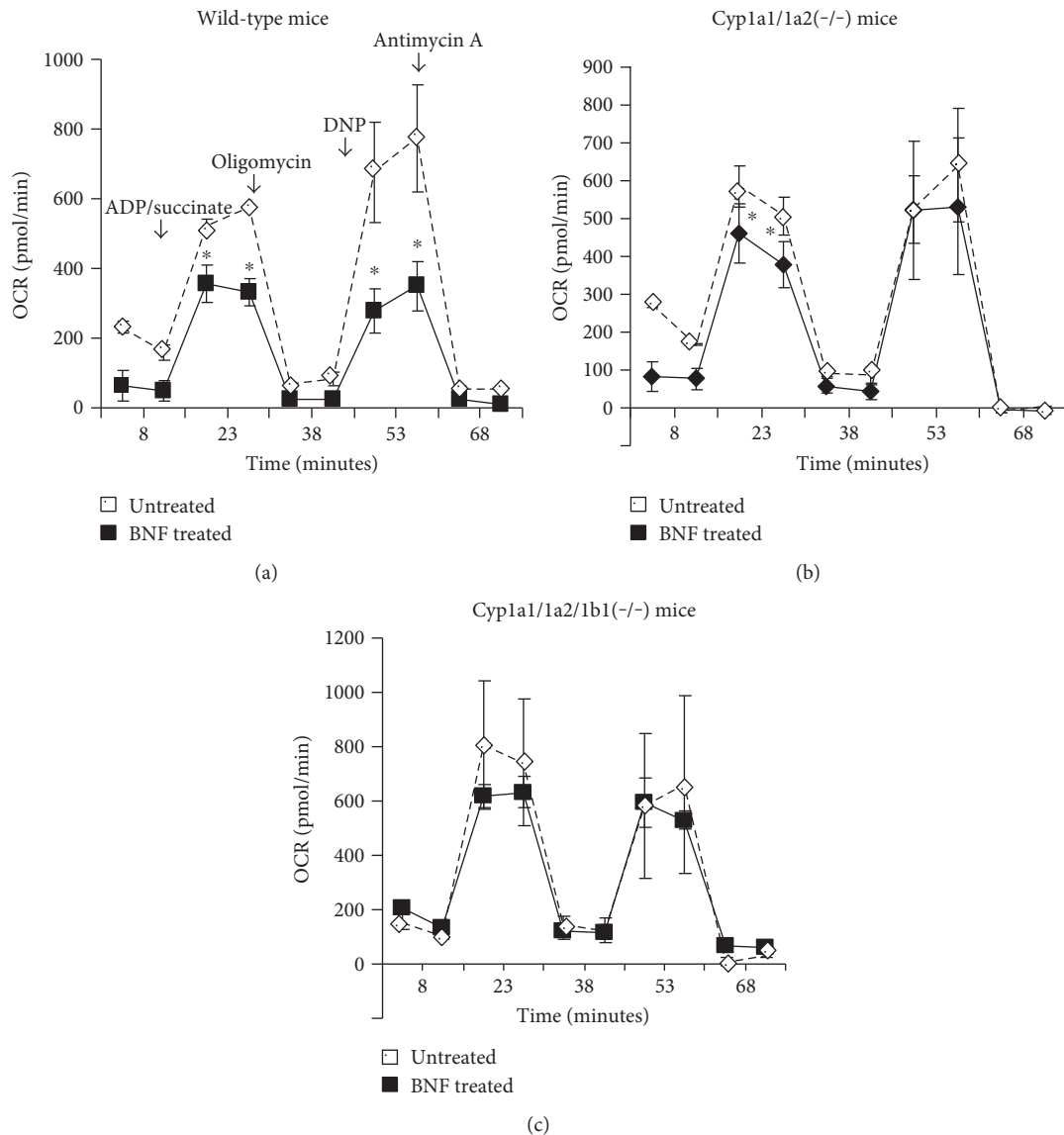


FIGURE 1: Effect of BNF and resveratrol treatment on mitochondrial respiration in wild-type, double *Cyp1a1/1a2(-/-)*, and triple *Cyp1a1/1a2/1b1(-/-)* knockout mice. Oxygen consumption rate (OCR) in mouse ($n = 4$) liver mitochondria isolated from wild-type (a), double knockout *Cyp1a1/1a2(-/-)* (b), and triple knockout *Cyp1a1/1a2/1b1(-/-)* mice (c) treated with BNF was monitored through Seahorse XF-24 Extracellular Flux Analyzer as described in Materials and Methods. Baseline, ATP synthesis, proton leak, and spare respiratory capacity are presented as means \pm SEM for at least 4 independent experiments. * $p < 0.05$ versus respective untreated and BNF-treated groups of mice.

the nature of BNF-induced changes in CcO complex, we assessed the levels of CcO subunits from control and *Cyp1a1/1a2(-/-)* mice. As shown in Figure 4, regions of the same blot corresponding to the indicated proteins were excised and probed with appropriate antibodies including CcO subunits Vb, IV-i1 and I, and also with antibody against SDHA. It is seen that subunits Vb (Figure 4(a)), IVi1 (Figure 4(b)), and CcOI (Figure 4(c)) levels were significantly reduced in Wt mice treated with BNF. Notably, resveratrol treatment in Wt mice restored the subunit level to near control level confirming the role of AHR-induced CYP1 genes in this loss. In contrast, BNF failed to affect the CcO subunit levels in *Cyp1a1/1a2(-/-)* mice and also resveratrol had no effect on these CcO subunits, confirming that BNF-induced

CcO subunit loss requires the expression of CYP1A1 and 1A2 proteins. These results along with the results of Figures 3(a) and 3(b) suggest that the BNF toxicity targets complex I and IV of the mitochondrial electron transport chain. Results also show that resveratrol prevents the loss of enzyme activity as well as subunits of the CcO complex.

3.4. Effects of BNF and Resveratrol on *Cyp1a1/1a2* Gene and Protein Expression. We tested the ability of resveratrol to inhibit BNF-mediated induction of CYP1A1 and 1A2 proteins in the liver mitochondria and microsomes by Western blot analysis. As seen from Figure 5(a), BNF induced high levels of hepatic mitochondrial CYP1A1/1A2 expression in Wt mice and more robust induction in the

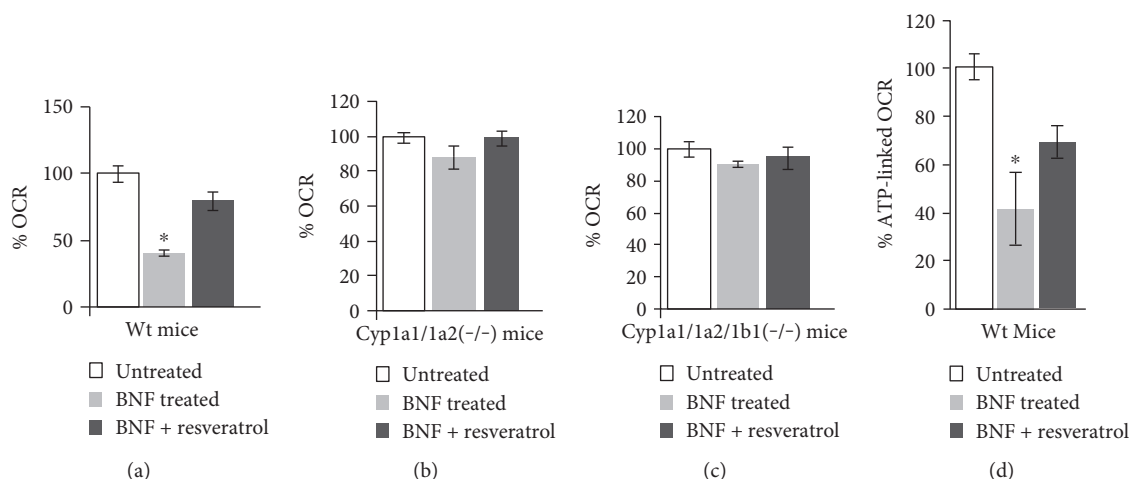


FIGURE 2: Quantitation of state 3 mitochondrial respiration in BNF-treated wild-type and knockout mice. State 3 respiration capacity was measured in mouse liver mitochondria isolated from BNF- and resveratrol-treated wild-type (a), *Cyp1a1/1a2(-/-)* (b), and triple *Cyp1a1/1a2/1b1(-/-)* (c) knockout mice ($n = 4$ each) along with nontreated control mice as in Figure 1. Changes in % ATP-linked OCR (d) were measured using XF24 metabolic analyzer. Values are presented as means \pm SEM of at least 4 independent measurements for each mouse. * $p < 0.05$ versus respective wild-type control, BNF, and resveratrol treatment.

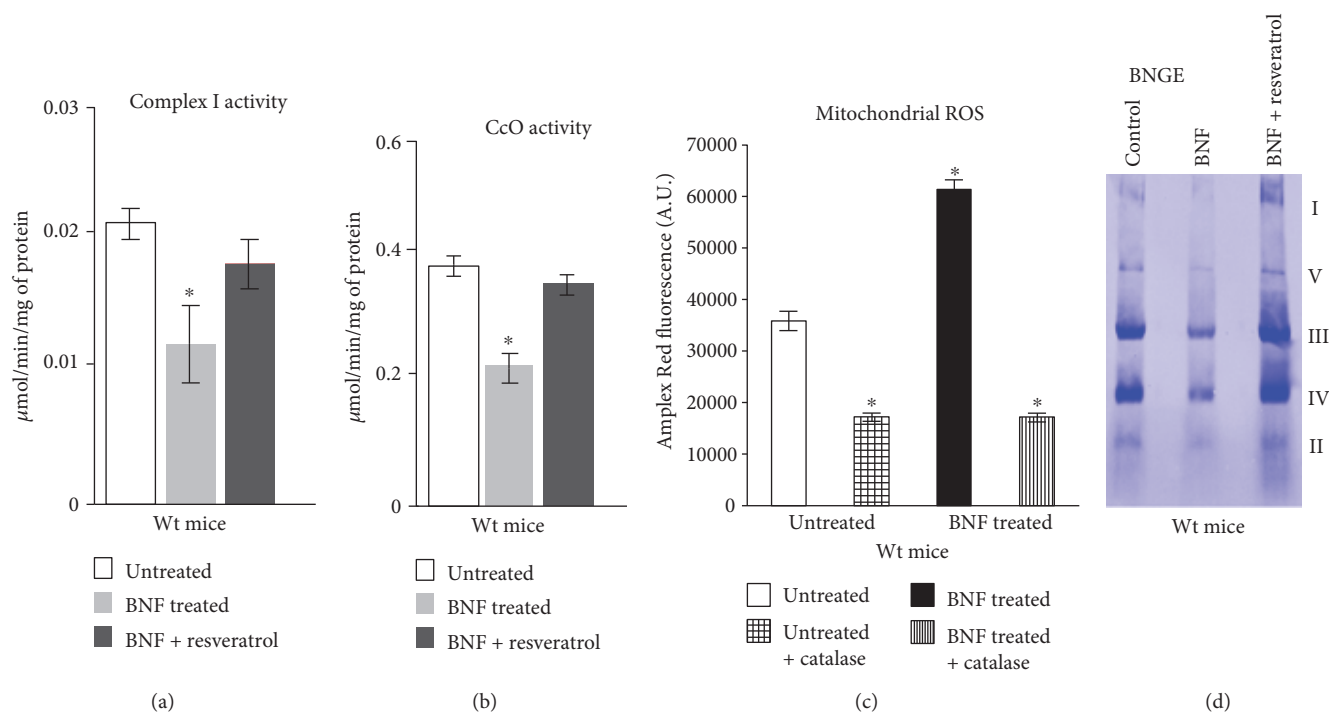


FIGURE 3: Effects of BNF and resveratrol on mitochondrial function and ROS production in wild-type mouse liver. Complex I activity (a) and CCo activity (b) were measured in mitochondria isolated from control, BNF-, and resveratrol-treated groups ($n = 4$ each). ROS formation was measured in control and BNF-treated mouse liver mitochondria by Amplex Red assay system (c) using MicroWin chameleon multilabel detection platform at excitation wavelength 530 nm and emission 590 nm as described in materials and methods. (d) Blue Native Gel resolution of mitochondrial complexes from livers of control (untreated), BNF-treated and BNF plus resveratrol-treated mice. The pattern was repeated three times using extracts ($80 \mu\text{g}$ each) from three separate mice for each group. Details were as described in Materials and Methods. Results represent mean \pm SEM from 4 independent assays. * denotes $p < 0.05$.

microsome. In both cases, resveratrol treatment attenuated BNF-mediated induction of CYP1A1/1A2. The level of NADPH-P450 oxidoreductase (NPOR) and mitochondria-

specific marker voltage-dependent anion channel (VDAC) were used as markers for microsome and mitochondria, respectively. The levels of these markers show that the

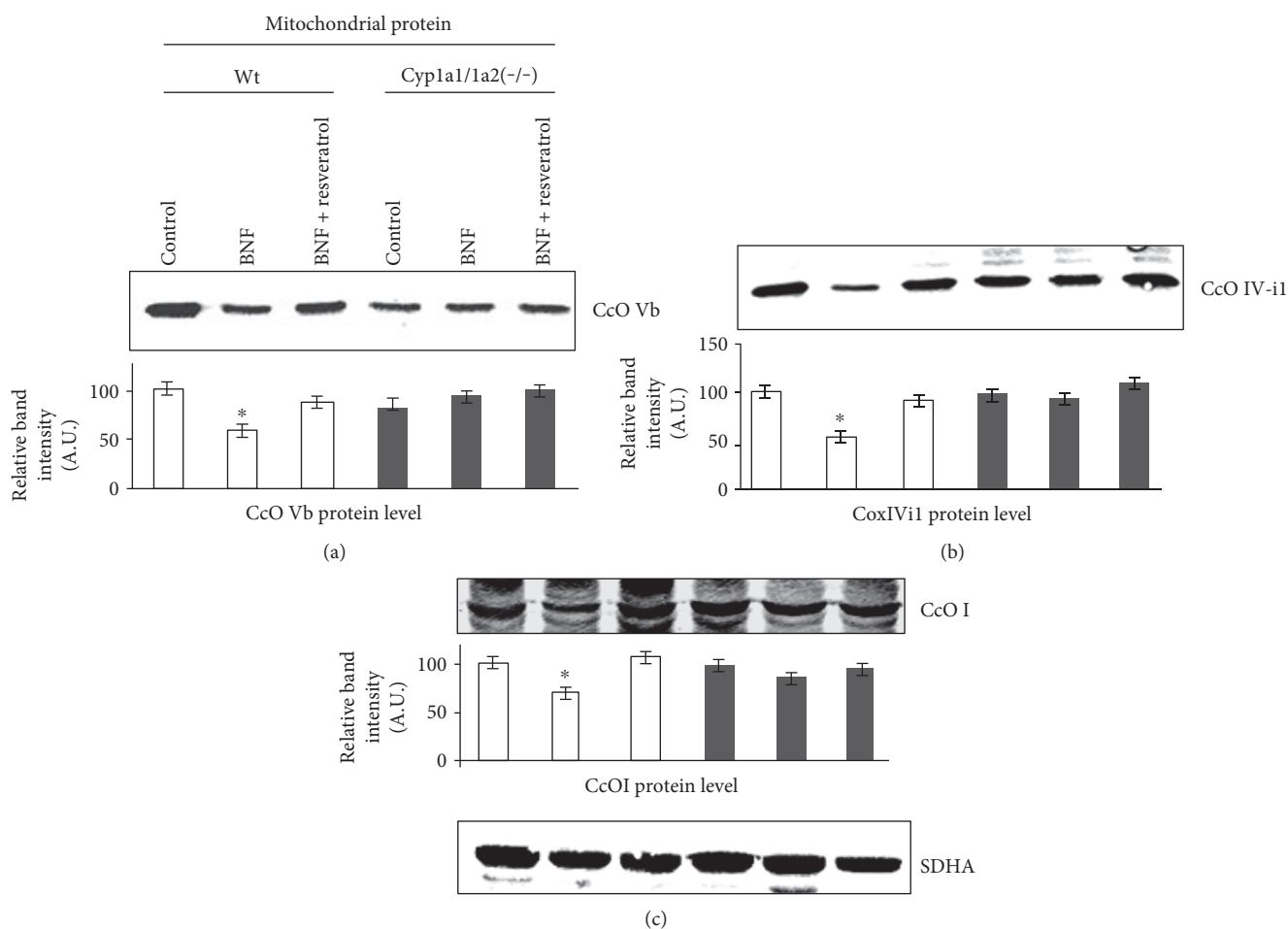


FIGURE 4: Effects of BNF and resveratrol on CcO subunit levels by immunoblot analysis. Immunoblot analysis of mitochondrial proteins from wild-type and double *Cyp1a1/1a2(-/-)* knockout, BNF-, and resveratrol-treated groups ($n = 4$ each). Mitochondrial proteins ($50 \mu\text{g}$ each) were resolved by SDS-PAGE on a 12% gel and the regions of blots corresponding to CcOVb, CcOIVi1, CcOI, and SDHA were excised based on apparent molecular masses and corresponding membrane strips were subjected to immunoblot analysis with anti-CcOVb (a), anti-CcO IVi1(b), and anti-CcOI (c) antibodies. Membrane strip corresponding to ~ 78 kDa was probed with antibody to the mitochondrion-specific marker succinate dehydrogenase (SDHA) as loading controls. The blots were imaged through a Li-Cor Odyssey Infrared Imaging System, and the band densities were quantified using the Volume analysis software. The values in the bar diagrams represent mean \pm SEM of 4 independent experiment from different mice.

subcellular fractions used were devoid of significant cross-contamination. In agreement with results of the Western blot (Figure 5(a)), real-time PCR analysis of total liver RNA also showed that *CYP1A1* mRNA was induced by >100 fold by BNF treatment, which was reduced to near control level in mice coadministered with resveratrol (Figure 5(b)). Similarly, *CYP 1A2* mRNA was also induced by about 10-fold by BNF (Figure 5(c)). Coadministration with resveratrol effectively inhibited ($<80\%$) BNF-mediated induction of both *CYP1A1* and *CYP1A2* mRNAs in mouse liver. As previously reported, resveratrol treatment on its own did not affect the expression of the *CYP1A1* and *CYP1A2* mRNAs [37].

3.5. Effect of BNF on ROS Production and Mitochondrial Respiratory Complexes in C6 Glioma Cells. To further investigate the effects of BNF on ROS formation, we used C6 glioma cells expressing AHR-inducible *CYP450s*. As

shown in Figures 6(a) and 6(b), ROS formation was significantly induced by BNF treatment, while resveratrol, and CH223191, both AHR antagonists *CYP450* inhibitor proadifen, and Mito-CP treatment markedly inhibited BNF-induced ROS production, confirming the involvement of AHR-dependent *CYP450* catalysis in ROS production. Mitochondrial respiratory enzyme activities were also measured in C6 glioma cells. Results show that the complex I enzyme activity was inhibited by about 60% (Figure 6(b)) while the complex IV (CcO) activity was inhibited by about 30% in BNF-treated cells (Figure 6(c)) when compared to untreated control.

To elucidate the possible mechanism by which BNF affects mitochondrial respiratory controls, we measured the level of mitochondrial gene expression at different times of BNF treatment from 24 to 72 h in C6 glioma cells. The relative mRNA levels for mitochondrial genome-coded ATP6, CcOI, cytochrome b, ND1, and ND6 were

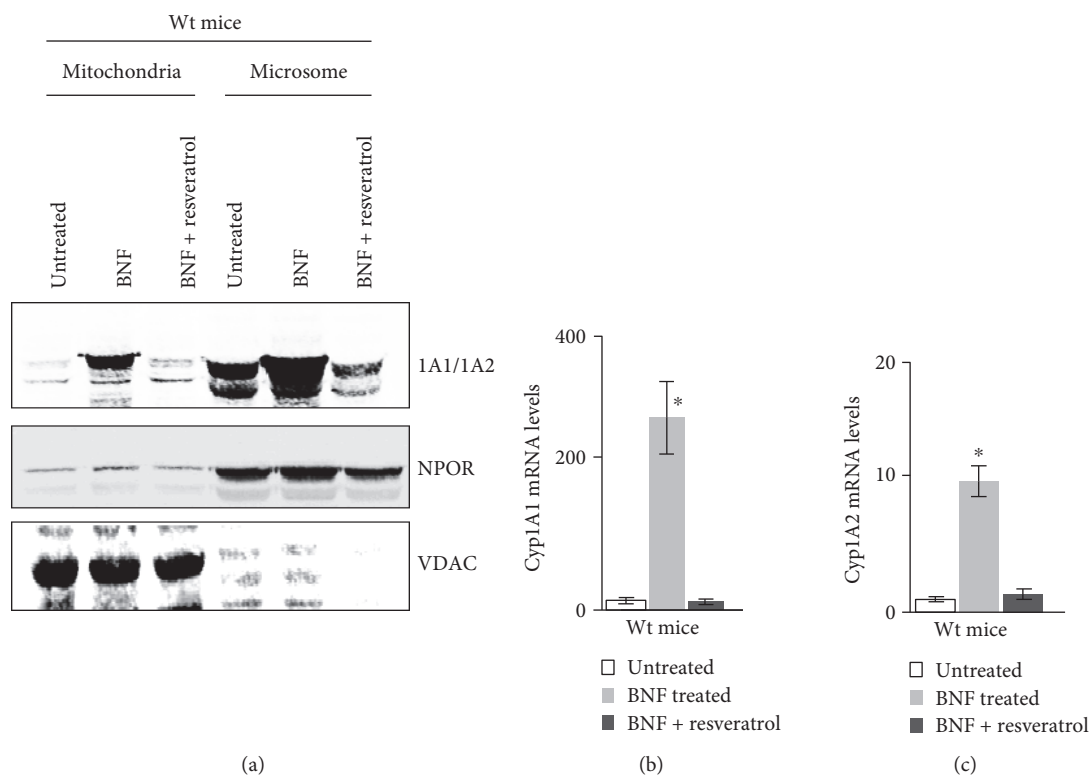


FIGURE 5: Effects of BNF and resveratrol treatment on CYP1A1/1A2 mRNA and protein expression levels. Immunoblot analysis of hepatic mitochondrial and microsomal proteins from wild-type control, BNF-, and resveratrol-treated mice ($n = 4$ each) following seven days of treatment. Proteins ($50 \mu\text{g}$ each) were resolved by SDS-PAGE on a 12% gel and subjected to immunoblot analysis with anti-CYP1A1/1A2 antibodies. Representative blot from one treated and untreated liver each has been presented. As described in Figure 4, all the three blocks of membranes were derived from the same blot. The blots were also probed with an antibody to the mitochondrion-specific marker voltage-dependent anion channel (VDAC) as loading controls (a). CYP1A1 (b) and CYP1A2 (c) mRNA levels were measured by real-time PCR in Wt control, BNF-, and resveratrol-treated mice as described in Materials and Methods. Results represent mean \pm SEM from 4 independent experiments. * denotes $p < 0.05$.

significantly increased (about 2-fold) by 24 h of treatment (Figure 7(a)), modestly reduced by 48 h of treatment (Figure 7(b)) and markedly reduced by 72 h of treatment (Figure 7(c)). The increase in transcription at early time period of 24 h probably represents a compensatory response to drug-induced mitochondrial toxicity representing extensive fission and fusion for repairing mitochondria. Continued exposure to the drug, however, induces time-dependent inhibition. These results show that BNF elicits marked inhibition of mitochondrial DNA transcription past the 48 h treatment time. Taken together, our results show that increased ROS production and mitochondrial dysfunction may be associated with induced expression of the AHR-regulated *CYP1A1* and *CYP1A2* genes.

3.6. Effects of BNF and CYP450 Inhibitor on ROS Production in Mitochondria from Treated Livers. Since studies with hepatic tissue from BNF-treated mice and C6 glioma cell point to the catalytic activity of CYP1A1 and 1A2 as possible sources of ROS, we used COS cells stably expressing CYP1A1 to further ascertain this possibility. Immunoblot in Figure 8(a) shows the level of expression of full-length (microsomal) and N-terminal truncated (+33) (mitochondrial) CYP1A1 in COS-7 cells. Several previous studies

([1, 2]; Dasari et al. (2010); [38]) showed that N-terminal truncated CYP1A1 is more predominantly targeted to the mitochondria. The results of ROS measurements in Figure 8(b) show that BNF treatment induced ROS production in both Wt CYP1A1 expressing and +33-1A1 expressing cells. Proadifen, an inhibitor of CYP, and also Mito-CP markedly inhibited ROS production. These results confirm that the catalytic cycle of CYPs induce ROS production and much of the ROS produced is of mitochondrial origin.

4. Discussion

The toxic effects of TCDD and PAHs are thought to be mediated via AHR signaling [39]. Structural similarity of BNF, a flavonoid compound present in edible plants and fruits, with many PAHs and their respective amines make it a powerful activator of AHR, which in turn induces CYP1 genes along with an array of genes involved in inflammatory response ([14, 25, 39–41]). However, the mechanism involved in PAH toxicity is far from clear, and pharmacological tools have been routinely utilized to establish a cause-effect relationship between AHR activation and toxicities. Unlike the large number of PAHs from industrial sources whose metabolic products form adducts with DNA and induce

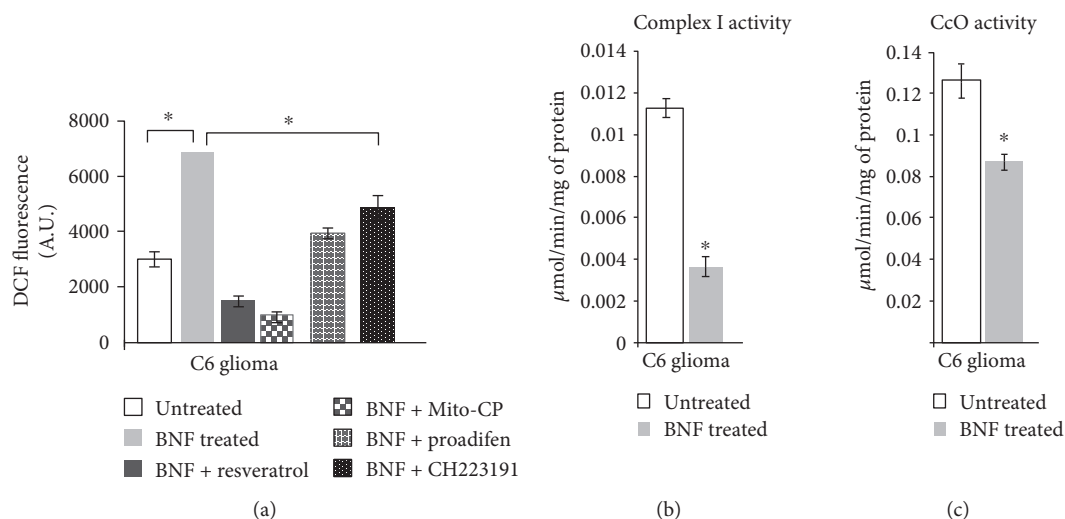


FIGURE 6: Effects of BNF on ROS production and mitochondrial respiratory complexes. ROS formation in C6 glioma cells treated with BNF, resveratrol, proadifen, or CG223191 was measured as described in Materials and Methods (a). Complex I assay was carried out using Cary 1E UV-visible spectrophotometer by incubating $10 \mu\text{g}$ of freeze-thawed mitochondrial extract in 1 ml of assay medium. The assay medium consisted of 25 mM potassium phosphate, pH 7.4, 5 mM MgCl_2 , 2 mM NaCN, 2.5 mg/ml bovine serum albumin, 13 mM NADH, $65 \mu\text{M}$ ubiquinone, and $2 \mu\text{g}/\text{ml}$ antimycin A. The decrease in absorbance at 340 nm because of NADH oxidation was measured (b). CcO activity was measured by incubating $10 \mu\text{g}$ of freeze-thawed mitochondrial extract from control and BNF-treated cells in 1 ml of assay medium (25 mM potassium phosphate, pH 7.4, 0.45 mM dodecylmaltoide, and $15 \mu\text{M}$ reduced cytochrome c) (c). Results represent mean \pm SEM of at least 4 independent experiments. * denotes $p < 0.05$.

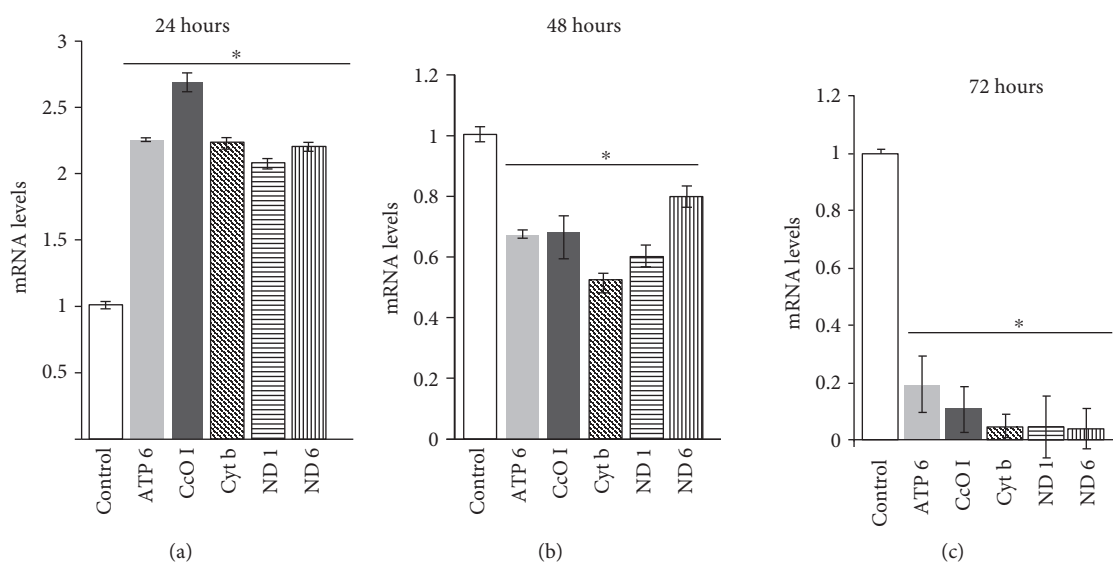


FIGURE 7: Effects of BNF on the expression of mitochondrial and nuclear genome-coded respiratory genes in C6 glioma cells. Mitochondrial genome-coded mRNA levels for ATP 6, CcO I, Cyt b, ND1, and ND6 from BNF-treated C6 glioma cells treated for 24 hours (a), 48 hours (b), and 72 hours (c) were quantified by real-time PCR with β -actin gene as internal control as described in Materials and Methods. Results represent mean \pm SEM of 3 independent experiments. * denotes $p < 0.05$.

mutations, BNF is not a mutagen because its metabolites are not highly reactive. Despite its suspected nonmutagenic and noncarcinogenic properties, reports suggest that BNF may affect some aspects of early development and cell differentiation [42]. In this study using *CYP1a1/1a2*^{-/-} (double knockout) and *CYP1a1/1a2/1b1*^{-/-} (triple knockout) mice as well as cell culture models, we show that BNF induces liver

mitochondrial respiratory defect which is mediated through activated AHR and metabolic activities of AHR-induced CYP1A1 and 1A2 enzymes. Our results show that BNF treatment inhibits hepatic mitochondrial OCR by about 30–50% in wild-type mice. In contrast, in both double KO and triple KO mice, the BNF-induced inhibition of OCR was only marginal. Furthermore, the difference between the double

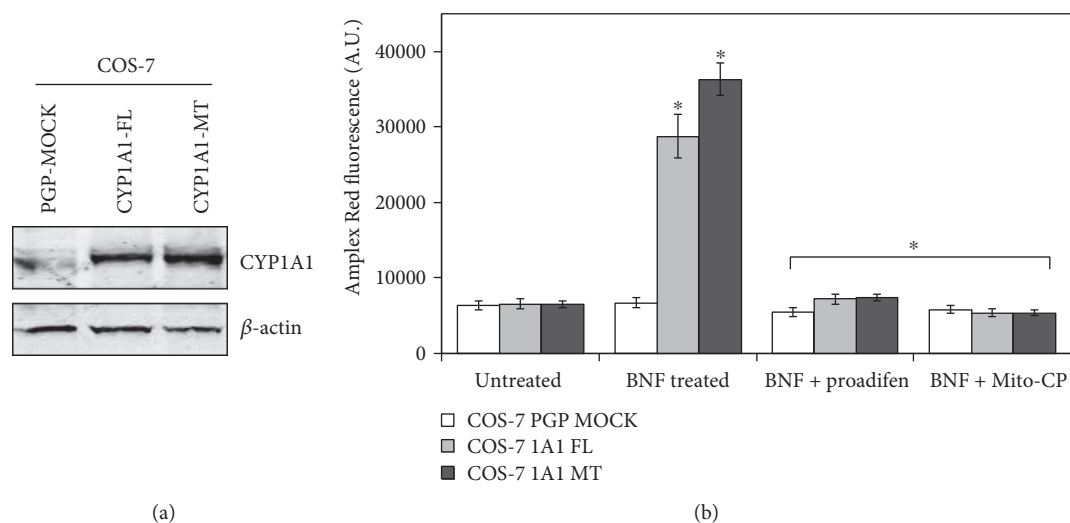


FIGURE 8: BNF-induced ROS production in COS-7 cells stably expressing CYP1A1 protein. COS-7 cells stably expressing full-length and N-terminal truncated (+33) CYP1A1 was generated as described in Materials and Methods. (a) Immunoblot shows the level of CYP1A1 expression in the two cell lines expressing full-length and +331A1 proteins. Total cell extracts (50 μ g protein each) were resolved on 12% polyacrylamide SDS gel, and the proteins were transferred to membranes as described in Materials and Methods. The blot was probed with antibody to rat CYP1A1 (1:1000 dilution) and β -actin. (b) ROS production as measured by Amplex Red method. Proadifen and Mito-CP were added as described in Figure 7. The immunoblot pattern in A is reproducible in multiple runs. The values in (Figure 8(b)) represent mean \pm SEM of 3 independent experiments. * denotes $p < 0.05$.

KO and triple KO was not significant. This is consistent with several reports showing very low or no detectable CYP1B1 expression in rodent livers. Results also show that state 3 respiration, ATP-coupled respiration, as well as maximum uncoupled respiration was affected by BNF treatment. The reduced respiratory capacity is most likely associated with the inhibition of the activities of respiratory complexes, complex I and complex IV (CcO) (Figure 3). Similar results were also obtained when C6 glioma cells were tested under *in vitro* conditions. Results therefore suggest that inhibition of mitochondrial respiratory complexes by BNF may be mainly responsible for the observed mitochondrial dysfunction.

The induction of CYP1A1 mRNA and resulting enzyme activity has long been used as a sensitive indicator of AHR activation in numerous *in vitro* and *in vivo* models for screening a variety of compounds and environmental toxicants [43]. A strong correlation between AHR-binding affinity of the promoter sites, CYP1A1 induction, and dioxin-like toxicity of structurally related PAHs has been used as a biomarker for hazard identification and risk assessment of environmental pollutants, industrial chemicals, and therapeutic compounds [43, 44]. The present study also points to novel aspects of mitochondrial respiratory controls and electron transfer complexes as possible targets of AHR. In this study, we show that BNF treatment not only inhibits respiratory controls but also mitochondrial transcription in a time-dependent manner. The immediate effects of BNF at early time point (24 h) is increased transcription which is probably a compensatory effect of reduced electron transport chain activity. At 48 and 72 h of treatment, there is a time-dependent inhibition of mtDNA transcription. With a view to understand the molecular basis of this inhibition, we also measured ROS production and mitochondrial function in C6 glioma cell culture system which expresses CYP 1 genes.

Our results show high level of ROS production accompanied by reduced mitochondrial complex activities in C6 glioma cells treated with BNF confirming the *in vivo* animal study on KO mice. Using Ahr and CYP specific inhibitors CH223191 and proadifen, respectively, we also demonstrated that ROS production was markedly inhibited suggesting the role of Ahr-dependent CYP activities in BNF-induced ROS production in the cell system. Some studies suggest that CH223191 is a more potent Ahr receptor antagonist against dioxin treatment in comparison to BNF [45]. In our cell systems, however, we found that resveratrol is equally or more potent antagonist of AHR based on CYP1A1 gene expression and ROS production.

We suggest that mitochondrial ROS production is most likely the cause of reduced respiratory enzyme activities and inhibition of mtDNA transcription. In this study, our results imply that CYP1A1 and 1A2 together induce mitochondrial dysfunction which might be critically important for reported toxic effects of BNF. A previous study from Nebert's group showed that microsomal CYP1A1 plays an important role in the elimination of BaP from the hepatic tissue for reducing xenotoxicity [21, 22, 38, 46]. Similarly, a previous study from our laboratory showed that TCDD induces mitochondrial dysfunction and retrograde signaling by directly acting on mitochondrial membrane complexes rather than through AHR activation [23]. In this respect, the two xenobiotics elicit mitochondrial toxicity through different mechanisms.

Resveratrol is a naturally occurring polyphenolic compound that occurs in grapes, peanuts, berries, and a number of plants used in traditional Asian medicine [47, 48]. This compound displays chemopreventive and several other properties useful for human health, including cardioprotective activity and inhibitory activity toward the ageing process. Several studies have reported that resveratrol inhibits the

expression of a number of cytochrome P450 genes, including CYP1A1, CYP1B1, CYP1A2, CYP2E1, CYP2C8, CYP3A, and aromatase (CYP19) in cancer cell lines of different tissue origin in humans and other mammals, and also inhibits the catalytic activities of several of these CYPs, and it has been suggested that these inhibitions may underlie some of the cancer chemopreventive activity of this compound [49–53]. Several studies [27] suggest that low doses of resveratrol may help alleviate oxidative stress though its precise mechanism of action remains unclear. Using *in vitro* cell culture and *in vivo* mouse KO models, our results showed marked reversibility of mitochondrial toxicity by resveratrol. Our results with *CYP1a1/1a2*^{-/-} double KO mice also show that the metabolic activities of mitochondrial CYP1A1/1A2 may be critical factors in inducing mitochondrial ROS production and associated mitochondrial dysfunction. Results with stable cells expressing Wt and N-terminal truncated CYP1A1 further support this possibility.

Abbreviations

ADX:	Adrenodoxin
ADR:	Adrenodoxin reductase
AHR:	Aryl hydrocarbon receptor
BNF:	β -naphthoflavone
BaP:	Benzo[<i>a</i>]pyrene
CcO:	Cytochrome c oxidase
CYP:	cytochrome P450
NPOR:	NADPH-cytochrome P450 oxidoreductase
DCFDA:	2',7'-dichlorofluorescein diacetate
mtDNA:	Mitochondrial DNA
OCR:	Oxygen consumption rate
ROS:	Reactive oxygen species.

Conflicts of Interest

The authors declare that they have no conflicts of interest.

Acknowledgments

The authors acknowledge the comments and suggestion of the Avadhani lab members. The authors also thank Dr. B. Kalyanaraman for generously providing the Mito-CP used in this work and Dr. Daniel W. Nebert for providing the transgenic mouse strains. The authors gratefully acknowledge the research support from NIH Grants R01 GM-034883 and R01-AA022986 and an endowment from the Harriet Ellison Woodward Trust to Narayan G. Avadhani.

References

- [1] S. Addya, H. K. Anandatheerthavarada, G. Biswas, S. V. Bhagwat, J. Mullick, and N. G. Avadhani, "Targeting of NH₂-terminal-processed microsomal protein to mitochondria: a novel pathway for the biogenesis of hepatic mitochondrial P450MT₂," *The Journal of Cell Biology*, vol. 139, pp. 589–599, 1997.
- [2] H. K. Anandatheerthavarada, C. Vijayarathy, S. V. Bhagwat, G. Biswas, J. Mullick, and N. G. Avadhani, "Physiological role of N-terminal processed CYP1A1 targeted to mitochondria in erythromycin metabolism and reversal of erythromycin-mediated inhibition of mitochondrial protein synthesis," *The Journal of Biological Chemistry*, vol. 274, pp. 6617–6625, 1999.
- [3] N. G. Avadhani, M. C. Sanger, S. Bansal, and P. Bajpai, "Bimodal targeting of cytochrome P450s to endoplasmic reticulum and mitochondria: the concept of chimeric signals," *The FEBS Journal*, vol. 278, pp. 4218–4229, 2011.
- [4] M. A. Robin, H. K. Anandatheerthavarada, G. Biswas et al., "Bimodal targeting of microsomal CYP2E1 to mitochondria through activation of an N-terminal chimeric signal by cAMP-mediated phosphorylation," *The Journal of Biological Chemistry*, vol. 277, pp. 40583–40593, 2002.
- [5] M. A. Robin, H. K. Anandatheerthavarada, J. K. Fang, M. Cudic, L. Otvos, and N. G. Avadhani, "Mitochondrial targeted cytochrome P450 2E1 (P450 MT₅) contains an intact N terminus and requires mitochondrial specific electron transfer proteins for activity," *The Journal of Biological Chemistry*, vol. 276, pp. 24680–24689, 2001.
- [6] M. C. Sanger, S. Bansal, and N. G. Avadhani, "Bimodal targeting of microsomal cytochrome P450s to mitochondria: implications in drug metabolism and toxicity," *Expert Opinion on Drug Metabolism & Toxicology*, vol. 6, no. 10, pp. 1231–1251, 2010.
- [7] D. W. Nebert and C. L. Karp, "Endogenous functions of the aryl hydrocarbon receptor (AHR): intersection of cytochrome P450 1 (CYP1)-metabolized eicosanoids and AHR biology," *The Journal of Biological Chemistry*, vol. 283, no. 52, pp. 36061–36065, 2008.
- [8] H. J. Hwang, P. Dornbos, M. Steidemann, T. K. Dunivine, M. Rizzoc, and J. J. LaPres, "Mitochondrial-targeted aryl hydrocarbon receptor and the impact of 2,3,7,8-tetrachlorodibenzo-p-dioxin on cellular respiration and the mitochondrial proteome," *Toxicology and Applied Pharmacology*, vol. 304, pp. 121–132, 2016.
- [9] M. S. Denison and S. R. Nagy, "Activation of the aryl hydrocarbon receptor by structurally diverse exogenous and endogenous chemicals," *Annual Review of Pharmacology and Toxicology*, vol. 43, pp. 309–334, 2003.
- [10] T. Shimada, K. Inoue, Y. Suzuki et al., "Arylhydrocarbon receptor-dependent induction of liver and lung cytochromes P450 1A1, 1A2, and 1B1 by polycyclic aromatic hydrocarbons and polychlorinated biphenyls in genetically engineered C57BL/6J mice," *Carcinogenesis*, vol. 23, pp. 1199–1207, 2002.
- [11] O. Hankinson, "The aryl hydrocarbon receptor complex," *Annual Review of Pharmacology and Toxicology*, vol. 35, pp. 307–340, 1995.
- [12] D. W. Nebert, A. L. Roe, M. Z. Dieter, W. A. Solis, Y. Yang, and T. P. Dalton, "Role of the aromatic hydrocarbon receptor and [Ah] gene battery in the oxidative stress response, cell cycle control, and apoptosis," *Biochemical Pharmacology*, vol. 59, pp. 65–85, 2000.
- [13] S. Uno, K. Sakurai, D. W. Nebert, and M. Makishima, "Protective role of cytochrome P450 1A1 (CYP1A1) against benzo[*a*]pyrene-induced toxicity in mouse aorta," *Toxicology*, vol. 316, pp. 34–42, 2014.
- [14] C. L. Wilson and S. Safe, "Mechanisms of ligand-induced aryl hydrocarbon receptor-mediated biochemical and toxic responses," *Toxicologic Pathology*, vol. 26, pp. 657–671, 1998.
- [15] R. Mikstacka, D. Przybylska, A. M. Rimando, and W. Baer-Dubowska, "Inhibition of human recombinant cytochromes P450 CYP1A1 and CYP1B1 by trans-resveratrol methyl

- ethers," *Molecular Nutrition & Food Research*, vol. 51, pp. 517–524, 2007.
- [16] D. W. Nebert, T. P. Dalton, A. B. Okey, and F. J. Gonzalez, "Role of aryl hydrocarbon receptor-mediated induction of the CYP1 enzymes in environmental toxicity and cancer," *The Journal of Biological Chemistry*, vol. 279, pp. 23847–23850, 2004.
- [17] S. Rendic, "Summary of information on human CYP enzymes: human P450 metabolism data," *Drug Metabolism Reviews*, vol. 34, no. 1-2, pp. 83–448, 2002.
- [18] F. P. Guengerich and T. Shimada, "Activation of procarcinogens by human cytochrome P450 enzymes," *Mutation Research*, vol. 400, no. 1-2, pp. 201–213, 1998.
- [19] J. P. Whitlock Jr, C. H. Chichester, R. M. Bedgood et al., "Induction of drug-metabolizing enzymes by dioxin," *Drug Metabolism Reviews*, vol. 29, no. 4, pp. 1107–1127, 1997.
- [20] S. Bansal, A. N. Leu, F. J. Gonzalez et al., "Mitochondrial targeting of cytochrome P450 (CYP) 1B1 and its role in polycyclic aromatic hydrocarbon-induced mitochondrial dysfunction," *The Journal of Biological Chemistry*, vol. 289, no. 14, pp. 9936–9951, 2014.
- [21] A. P. Senft, T. P. Dalton, D. W. Nebert, M. B. Genter, R. J. Hutchinson, and H. G. Shertzer, "Dioxin increases reactive oxygen production in mouse liver mitochondria," *Toxicology and Applied Pharmacology*, vol. 178, pp. 15–21, 2002.
- [22] A. P. Senft, T. P. Dalton, D. W. Nebert et al., "Mitochondrial reactive oxygen production is dependent on the aromatic hydrocarbon receptor," *Free Radical Biology and Medicine*, vol. 33, pp. 1268–1278, 2002.
- [23] G. Biswas, S. Srinivasan, H. K. Anandatheerthavarada, and N. G. Avadhani, "Dioxin-mediated tumor progression through activation of mitochondria-to-nucleus stress signaling," *Proceedings of the National Academy of Sciences of the United States of America*, vol. 105, no. 1, pp. 186–191, 2008.
- [24] S. V. Bhagwat, G. Biswas, H. K. Anandatheerthavarada, S. Addya, W. Pandak, and N. G. Avadhani, "Dual targeting property of the N-terminal signal sequence of P4501A1, targeting of heterologous proteins to endoplasmic reticulum and mitochondria," *The Journal of Biological Chemistry*, vol. 274, pp. 24014–24022, 1999.
- [25] E. Boopathi, H. K. Anandatheerthavarada, S. V. Bhagwat, G. Biswas, J. K. Fang, and N. G. Avadhani, "Accumulation of mitochondrial P450MT2, NH₂-terminal truncated cytochrome P4501A1 in rat brain during chronic treatment with beta-naphthoflavone. A role in the metabolism of neuroactive drugs," *The Journal of Biological Chemistry*, vol. 275, pp. 34415–34423, 2000.
- [26] J. Iqbal, L. Sun, J. Cao et al., "Smoke carcinogens cause bone loss through the aryl hydrocarbon receptor and induction of Cyp1 enzymes," *Proceedings of the National Academy of Sciences of the United States of America*, vol. 110, no. 27, pp. 11115–11120, 2013.
- [27] J. A. Baur, K. J. Pearson, N. L. Price et al., "Resveratrol improves health and survival of mice on a high-calorie diet," *Nature*, vol. 444, no. 7117, pp. 337–342, 2006.
- [28] M. Jang, L. Cai, G. O. Udeani et al., "Cancer chemopreventive activity of resveratrol, a natural product derived from grapes," *Science*, vol. 275, no. 5297, pp. 218–220, 1997.
- [29] S. Bansal, C. P. Liu, N. B. Sepuri et al., "Mitochondria targeted P450 2E1 induces oxidative damage and augments alcohol mediated oxidative stress," *The Journal of Biological Chemistry*, vol. 285, pp. 24609–24619, 2010.
- [30] B. G. Niranjana, N. M. Wilson, C. R. Jefcoate, and N. G. Avadhani, "Hepatic mitochondrial cytochrome P-450 system. Distinctive features of cytochrome P-450 involved in the activation of aflatoxin B1 and benzo(a)pyrene," *The Journal of Biological Chemistry*, vol. 259, pp. 12495–12501, 1984.
- [31] O. H. Lowry, N. J. Rosebrough, A. L. Farr, and R. J. Randall, "Protein measurement with the Folin phenol reagent," *The Journal of Biological Chemistry*, vol. 193, pp. 265–275, 1951.
- [32] M. A. Birch-Machin and D. M. Turnbull, "Assaying mitochondrial respiratory complex activity in mitochondria isolated from human cells and tissues," *Methods in Cell Biology*, vol. 65, pp. 97–117, 2001.
- [33] H. Raza, S. K. Prabu, A. John, and N. G. Avadhani, "Impaired mitochondrial respiratory functions and oxidative stress in streptozotocin-induced diabetic rats," *International Journal of Molecular Sciences*, vol. 12, no. 5, pp. 3133–3147, 2011.
- [34] S. Bansal, S. Srinivasan, S. Anandasadagopan et al., "Additive effects of mitochondrion-targeted cytochrome CYP2E1 and alcohol toxicity on cytochrome c oxidase function and stability of respirasome complexes," *The Journal of Biological Chemistry*, vol. 287, pp. 15284–15297, 2012.
- [35] S. K. Prabu, H. K. Anandatheerthavarada, H. Raza, S. Srinivasan, J. F. Spear, and N. G. Avadhani, "Protein kinase A-mediated phosphorylation modulates cytochrome c oxidase function and augments hypoxia and myocardial ischemia-related injury," *The Journal of Biological Chemistry*, vol. 281, pp. 2061–2070, 2006.
- [36] S. Srinivasan and N. G. Avadhani, "Cytochrome c oxidase dysfunction in oxidative stress," *Free Radical Biology and Medicine*, vol. 53, pp. 1252–1263, 2012.
- [37] S. R. Beedanagari, I. Bebenek, P. Bui, and O. Hankinson, "Resveratrol inhibits dioxin-induced expression of human CYP1A1 and CYP1B1 by inhibiting recruitment of the aryl hydrocarbon receptor complex and RNA polymerase II to the regulatory regions of the corresponding genes," *Toxicological Sciences*, vol. 110, no. 1, pp. 61–67, 2009.
- [38] H. Dong, T. P. Dalton, M. L. Miller et al., "Knock-in mouse lines expressing either mitochondrial or microsomal CYP1A1: differing responses to dietary benzo[a]pyrene as proof-of-principle," *Molecular Pharmacology*, vol. 75, pp. 555–567, 2009.
- [39] S. Safe, F. Wang, W. Porter, R. Duan, and A. McDougal, "Ah receptor agonists as endocrine disruptors: anti-estrogenic activity and mechanisms," *Toxicology Letters*, vol. 102–103, pp. 343–347, 1998.
- [40] S. V. Bhagwat, J. Mullick, H. Raza, and N. G. Avadhani, "Constitutive and inducible cytochromes P450 in rat lung mitochondria: xenobiotic induction, relative abundance, and catalytic properties," *Toxicology and Applied Pharmacology*, vol. 56, pp. 231–240, 1999.
- [41] B. Burchell and M. W. H. Coughtrie, "UDP-Glucuronosyltransferases," *Pharmacology & Therapeutics*, vol. 43, pp. 261–289, 1989.
- [42] D. McKillop and D. E. Case, "Mutagenicity, carcinogenicity, and toxicity of β -naphthoflavone, a potent inducer of P448," *Biochemical Pharmacology*, vol. 41, no. 1, pp. 1–7, 1991.
- [43] P. A. Behnisch, K. Hosoe, and S. Sakai, "Bioanalytical screening methods for dioxins and dioxin-like compounds a review of bioassay/biomarker technology," *Environment International*, vol. 27, pp. 413–439, 2001.

- [44] P. A. Behnisch, K. Hosoe, A. Brouwer, and S. Sakai, "Screening of dioxin-like toxicity equivalents for various matrices with wildtype and recombinant rat hepatoma H4IIE cells," *Toxicological Sciences*, vol. 69, pp. 125–130, 2002.
- [45] B. Zhao, D. E. DeGroot, A. Hayashi, G. He, and M. S. Denison, "CH223191 is a ligand-selective antagonist of the ah (dioxin) receptor," *Toxicological Sciences*, vol. 117, no. 2, pp. 393–403, 2010.
- [46] H. Dong, H. G. Shertzer, M. B. Genter et al., "Mitochondrial targeting of mouse NQO1 and CYP1B1 proteins," *Biochemical and Biophysical Research Communications*, vol. 435, no. 4, pp. 727–732, 2013.
- [47] M. H. Aziz, R. Kumar, and N. Ahmad, "Cancer chemoprevention by resveratrol: in vitro and in vivo studies and the underlying mechanisms (review)," *International Journal of Oncology*, vol. 23, pp. 17–28, 2003.
- [48] G. S. Jayatilake, H. Jayasuriya, E. S. Lee et al., "Kinase inhibitors from *Polygonum cuspidatum*," *Journal of Natural Products*, vol. 56, pp. 1805–1810, 1993.
- [49] N. Aluru and M. M. Vijayan, "Resveratrol affects CYP1A expression in rainbow trout hepatocytes," *Aquatic Toxicology*, vol. 77, pp. 291–297, 2006.
- [50] R. F. Casper, M. Quesne, I. M. Rogers et al., "Resveratrol has antagonist activity on the aryl hydrocarbon receptor: implications for prevention of dioxin toxicity," *Molecular Pharmacology*, vol. 56, pp. 784–790, 1999.
- [51] T. K. Chang, J. Chen, and W. B. Lee, "Differential inhibition and inactivation of human CYP1 enzymes by trans-resveratrol: evidence for mechanism-based inactivation of CYP1A2," *The Journal of Pharmacology and Experimental Therapeutics*, vol. 299, pp. 874–882, 2001.
- [52] Z. H. Chen, Y. J. Hurh, H. K. Na et al., "Resveratrol inhibits TCDD induced expression of CYP1A1 and CYP1B1 and catechol estrogen mediated oxidative DNA damage in cultured human mammary epithelial cells," *Carcinogenesis*, vol. 25, pp. 2005–2013, 2004.
- [53] B. Piver, F. Berthou, Y. Dreano, and D. Lucas, "Inhibition of CYP3A, CYP1A and CYP2E1 activities by resveratrol and other non volatile red wine components," *Toxicology Letters*, vol. 125, pp. 83–91, 2001.

Research Article

Testosterone Upregulates the Expression of Mitochondrial ND1 and ND4 and Alleviates the Oxidative Damage to the Nigrostriatal Dopaminergic System in Orchiectomized Rats

Wensheng Yan,^{1,2} Yunxiao Kang,¹ Xiaoming Ji,¹ Shuangcheng Li,³ Yingkun Li,³ Guoliang Zhang,^{1,3} Huixian Cui,³ and Geming Shi¹

¹Department of Neurobiology, Hebei Medical University, Shijiazhuang, Hebei 050017, China

²Department of Human Anatomy, Shijiazhuang Medical College, Shijiazhuang, Hebei 050599, China

³Department of Human Anatomy, Hebei Medical University, Shijiazhuang, Hebei 050017, China

Correspondence should be addressed to Geming Shi; shigeming@163.com

Received 29 March 2017; Revised 1 August 2017; Accepted 7 August 2017; Published 24 August 2017

Academic Editor: Icksoo Lee

Copyright © 2017 Wensheng Yan et al. This is an open access article distributed under the Creative Commons Attribution License, which permits unrestricted use, distribution, and reproduction in any medium, provided the original work is properly cited.

Testosterone deficiency, as a potential risk factor for aging and aging-related neurodegenerative disorders, might induce mitochondrial dysfunction and facilitate the declines of the nigrostriatal dopaminergic system by exacerbating the mitochondrial defects and increasing the oxidative damage. Thus, how testosterone levels influence the mitochondrial function in the substantia nigra was investigated in the study. The present studies showed that testosterone deficiency impaired the mitochondrial function in the substantia nigra and induced the oxidative damage to the substantia nigra as well as the deficits in the nigrostriatal dopaminergic system. Of four mitochondrial respiratory chain complexes, castration of male rats reduced the activity of mitochondrial complex I and downregulated the expression of ND1 and ND4 of 7 mitochondrial DNA- (mtDNA-) encoded subunits of complex I in the substantia nigra. Supplements of testosterone propionate to castrated male rats ameliorated the activity of mitochondrial complex I and upregulated the expression of mitochondrial ND1 and ND4. These results suggest an important role of testosterone in maintaining the mitochondrial function in the substantia nigra and the vulnerability of mitochondrial complex I to testosterone deficiency. Mitochondrial ND1 and ND4, as potential testosterone targets, were implicated in the oxidative damage to the nigrostriatal dopaminergic system.

1. Introduction

Oxidative stress plays a key role in aging and aging-related neurodegenerative disorders [1–3], such as Parkinson's disease (PD). Testosterone deficiency, as a potential risk factor for neurodegenerative disorders [4], is implicated in oxidative stress [5–8]. Orchiectomy elevates the susceptibility of brain tissue to oxidative stress [6, 7]. Oxidative stress-mediated damage to neurons can be manipulated by testosterone administration [5–8]. Testosterone supplements reduce the oxidative damage by increasing antioxidant enzyme levels [6] and ameliorating the oxidative stress parameters [8, 9] in brain tissues. In vitro studies reveal that the cerebellar

granule cells from neonatal rats treated with testosterone are selectively protected against oxidative stress-induced cell death [5]. Testosterone is involved in the protection of neurons via suppressing oxidative stress.

Normal neuronal activities are critically dependent on mitochondrial function [10]. Mitochondria, as primary sources of reactive oxygen species (ROS) and primary targets of ROS damage [1, 2, 11–13], have been proposed to play an important role in the pathogenesis of neurodegenerative disorders [1, 2, 14, 15]. The defects of mitochondria, such as the reduced activity of the mitochondrial respiratory chain and the overproduced ROS, are detected in the brains of subjects with aging-related neurodegenerative disorders [16–21].

Mitochondrial dysfunction induces a progressive disruption of the redox balance and is implicated in aging or aging-related neurodegeneration.

In normal aging, the nigrostriatal dopaminergic system progressively declines [22–25], with a decrease in the number of dopaminergic neurons [22, 23] and dopamine (DA) content [24, 25]. Although several factors have been proposed for the declined dopaminergic system in the aging process, one of the major contributors is oxidative stress [26–28]. PD, as a common neurodegenerative movement disorder, pathologically undergoes neurodegenerative loss of dopamine neurons in the substantia nigra [29]. Age-related mitochondrial alterations are demonstrated in the human skeletal muscle beginning at 40 ~ 50 years of age [30, 31]. Coincidentally, changes in the sexual hormonal state of individuals also start at this age interval [32], which suggests a relationship between hormonal levels and mitochondrial status [33]. With advancing age, the reduced levels of testosterone in aged males [34–37] might facilitate the declines of the nigrostriatal dopaminergic system by exacerbating the mitochondrial defects [15, 38] and increasing the oxidative damage in the substantia nigra.

Based on the effects of testosterone on oxidative stress-mediated damage to neurons [5–9], the association of mitochondria with oxidative stress [11, 12], and the amelioratory effects of testosterone on the deficits in the nigrostriatal dopaminergic system of aged male rats [9, 39, 40], we presumed that the amelioratory effects of testosterone on the impaired nigrostriatal dopaminergic system might be realized by regulating the function of mitochondria in a way. Testosterone deficiency might intervene the mitochondrial function in the substantia nigra. Therefore, in the present study, the dopaminergic markers in the nigrostriatal dopaminergic system and the parameters related to mitochondria were analyzed in male rats by manipulating serum testosterone levels to testify which of mitochondrial DNA- (mtDNA-) encoded subunits, as potential testosterone targets, was implicated in the substantia nigra.

2. Materials and Methods

2.1. Animals. Adult male Sprague–Dawley rats (280–300 g) were supplied by the Experimental Animal Center of Hebei Medical University. All of the rats were kept in groups of four per cage and housed under controlled temperature ($22 \pm 1^\circ\text{C}$) and humidity conditions with a 12 h light-dark cycle (lights on 06:00 h). Food and water were available ad libitum. The experimental procedures followed the rules in the “Guidelines for the Care and Use of Mammals in Neuroscience and Behavioral Research” and were approved by the Committee of Institutional Animal Care and Use of Hebei Medical University.

2.2. Treatments. For testosterone deficiency, the rats anesthetized with chloral-hydrate (300 mg/kg) were gonadectomized (GDX) by the removal of the testes, epididymis, and epididymal fat under aseptic conditions, and the incisions were closed using surgical staples. The sham-operated rats experienced the same surgical treatment except for the bilateral

orchietomies (sham) [41]. For testosterone replacement, testosterone propionate (TP) was injected subcutaneously to GDX rats based on the following experimental schemes. The GDX rats receiving sesame oil treatment were used as a control.

2.3. Designs

2.3.1. Experiment 1. Eighty rats were used to determine the optimal dose of testosterone replacement by detecting the levels of malondialdehyde (MDA), hydrogen peroxide (H_2O_2), reduced glutathione (GSH), and oxidized glutathione (GSSG) in the substantia nigra (SN). They were included in the following groups: sham ($n = 8$), GDX ($n = 8$), or GDX-TP ($n = 64$). Eight rats in GDX-TP received 28-day treatment of TP at 0.5, 0.75, 1.0, 1.25, 1.5, 2.0, 2.5, or 3.0 mg/kg.

2.3.2. Experiment 2. Sixty-four rats were used to investigate the effect of testosterone deficiency and testosterone replacement on the nigrostriatal dopaminergic system. They were included in the following four groups: sham ($n = 16$), GDX ($n = 16$), GDX-0.5TP ($n = 16$), or GDX-1.0TP ($n = 16$). Eight rats in each group were used for real-time quantitative PCR (qPCR) and liquid chromatography coupled with tandem mass spectrometry (LC-MS/MS) assay or for Western blot detection. The rats in GDX-0.5TP and GDX-1.0TP experienced 28-day treatment of TP at 0.5 mg/kg and 1.0 mg/kg, respectively. Two TP doses were chosen based on the results in the experiment 1.

2.3.3. Experiment 3. One hundred and twenty-eight rats were used to investigate the effect of testosterone deficiency and testosterone replacement on mitochondrial function. They were included in the following four groups: sham ($n = 32$), GDX ($n = 32$), GDX-0.5TP ($n = 32$), or GDX-1.0TP ($n = 32$). Eight rats in each group were used for detection of the mitochondrial membrane potential and the activity of mitochondrial complexes, qPCR, or Western blot detection. The rats in GDX-0.5TP and GDX-1.0TP experienced 28-day treatment of TP at 0.5 mg/kg and 1.0 mg/kg, respectively. TP dose was chosen based on the results in experiment 1.

2.4. Sample Preparation. The rats were sacrificed by decapitation. The tissue block containing the SN (between 3.00 mm and 4.08 mm rostral to the interaural axis) or the caudate-putamen (CPU; between 10.08 mm and 8.64 mm rostral to the interaural axis) [42] was dissected on an ice-cold plate, using a scalpel for ophthalmic surgery and stereomicroscopy. It was immediately processed for assays of MDA, H_2O_2 , GSH/GSSG, and mitochondrial membrane potential as well as the activity of mitochondrial complexes or stored at -80°C after being frozen in liquid nitrogen until further qPCR, Western blot, or LC-MS/MS assay based on the experiment purposes.

2.5. Mitochondrial Membrane Potential. The mitochondrial membrane potential in the SN was detected using the rhodamine 123 (Rh123) fluorescence method [10]. The pieces containing the SN were grinded with a balanced salt solution and filtered through a nylon mesh screen. The cells were collected

TABLE 1: Validation parameters of the LC-MS/MS method.

Analyte	<i>r</i>	LLOQ (ng/g)	Recovery (%)	Intraprecision (RSD %)	Interprecision (RSD %)
DA	0.9969	2.0	94.6 ± 8.7	10.3	12.4
DOPAC	0.9982	72.0	93.4 ± 6.6	8.9	7.5
HVA	0.9977	50.0	95.3 ± 7.4	7.7	11.3

DA: dopamine; DOPAC: 3,4-dihydroxyphenylacetic acid; HVA: homovanillic acid.

and incubated in Rh123 solution (10 μ g/mL, Sigma, USA) at 37°C for 30 min. After being washed and resuspended in 1 mL PBS, the cells were immediately analyzed by flow cytometry (excitation/emission wavelengths, 488/534 nm). The mitochondrial membrane potential was assessed by the change in the intensity of Rh123 fluorescence. Weak fluorescent intensity of Rh123 reflects the decreased mitochondrial membrane potential.

2.6. Biochemical Analysis. For MDA assay, SN tissue block was homogenized with 10 times (*w/v*) ice-cold 0.1 M phosphate buffer (PB) at pH 7.4. The homogenate was then centrifuged at 14,000*g* for 15 min at 4°C followed by recovery of the supernatant. The supernatant of SN homogenates was used to detect MDA. The levels of MDA were measured spectrophotometrically according to the protocol of the detection kits. The detection kit (Code A003-1) was obtained from the Jiancheng Institute of Biotechnology of China.

For the detection of H₂O₂ and GSH/GSSG in mitochondria of the SN, the mitochondria were isolated using the Tissue Mitochondria Isolation Kit (Code C3606, Beyotime Institute of Biotechnology, China). In brief, SN tissue was homogenized in ice-cold buffer (10 mM HEPES, pH 7.5, including 200 mM mannitol, 70 mM sucrose, 1.0 mM EGTA, and 2.0 mg/mL serum albumin) and centrifuged at 1000*g* at 4°C for 10 min. The supernatant was centrifuged again at 3500*g* at 4°C for 10 min to collect a mitochondrial pellet. The levels of H₂O₂, GSH, and GSSG in the mitochondria were measured spectrophotometrically according to the protocol of the detection kits (H₂O₂: Code A064-1, GSH: Code A006-1, and GSSG: Code A061-2; Jiancheng Institute of Biotechnology, China).

For the activity of mitochondrial complexes, isolated mitochondria were detected by spectrophotometric assays to reveal the complex activity of the mitochondrial electron transfer chain. The activity of complexes I, II, III, and IV was measured according to the protocol of the detection kits. The detection kits for complex I (Code S50007), complex II (Code S50008), complex III (Code S50009), and complex IV (Code S50010) were obtained from the Nanjing Jiancheng Institute of Biotechnology of China.

2.7. LC-MS/MS Assay. CPU tissue block in experiment 2 was weighed and homogenized in 80% acetonitrile containing 0.1% formic acid (5 μ L). The homogenates were centrifuged at 14,000*g* for 10 min at 4°C. The supernatants were collected and stored at -80°C. DA, 3,4-dihydroxyphenylacetic acid (DOPAC), and homovanillic acid (HVA) were determined by the use of LC-MS/MS. LC separation was performed on the Agilent 1200 LC system (Agilent, Santa Clara, USA)

using a Synergi Fusion-RP C18 column (50 mm × 3.0 mm, 4 μ m) provided by Phenomenex. MS/MS detection was carried out using the 3200 QTRAP LC-MS/MS System (Applied Biosystems, Foster City, CA, USA). The multiple-reaction monitoring mode was used for the quantification. The principal validation parameters of the LC-MS/MS were set up as showed in Table 1.

2.8. qPCR Analysis. 2 μ g of total RNA from SN tissue block was subjected to reverse transcription using random primers to obtain the first-strand cDNA template. qPCR was performed with 0.8 μ L cDNA (diluted 1:10), 2 μ L specific primers, and 2× GoTaq® Green Master Mix (Promega, USA) with a final volume of 20 μ L. PCR was performed as follows: an initial cycle at 95°C for 10 min, followed by 40 cycles at 95°C for 15 s, 58°C for 20 s, and 60°C for 15 s. Then, PCR products were analyzed by the melting curve to confirm the specificity of amplification. Expression of tyrosine hydroxylase (TH) and dopamine transporter (DAT) genes as well as mtDNA-encoded complex I genes was analyzed using GAPDH or β -actin as an internal control. The relative quantification was calculated using the 2^{- $\Delta\Delta$ ct} method. The sets of primers were as follows—TH: (forward) 5'-GCTTC TCTGACCAGGTGTATCG-3' and (reverse) 5'-GCAATC TCTTCCGCTGTGTAT-3', DAT: (forward) 5'-ACTCTGTG AGGCATCTGTGTG-3' and (reverse) 5'-TGTAAGTGA GAAGGCAATCAG-3', GAPDH: (forward) 5'-TGAACG GGAAGCTCACTG-3' and (reverse) 5'-GCTTCAACCACC TTCTTGATG-3', ND1: (forward) 5'-CCTATGAATCCGA GCATCC-3' and (reverse) 5'-ATTGCAGGGAAATGTAT CA-3', ND2: (forward) 5'-CAACCAACAACAACCTCCAAA-3' and (reverse) 5'-AAAGCGGTAGGGTAAGGGTA-3', ND3: (forward) 5'-AGTTCTGCACGCCTTCCTT-3' and (reverse) 5'-ATCCACACAGATGCCTCACA-3', ND4: (forward) 5'-CCCTACCCTCAACATGATCC-3' and (reverse) 5'-GGAGCTTCTACGTGGCTTT-3', ND4L: (forward) 5'-TCCACATTAACCTCCAACCTCCA-3' and (reverse) 5'-CG TAGTCTGTTCCGTAAGTATTTGA-3', ND5: (forward) 5'-CCAACCCTACCTTGCTTTCC-3' and (reverse) 5'-GGC TCCCATAATGAGACAA-3', ND6: (forward) 5'-GTCTC CGGGTACTCCTCAGT-3' and (reverse) 5'-GTGGGCTTG GATTGATTGTT-3', and β -actin: (forward) 5'-TCATGA AGTGTGACGTTGACATCCGT-3' and (reverse) 5'-CCTA GAAGCATTTGCGGTGCACGATG-3'.

2.9. Western Blot Analysis. The tissue block for Western blot was homogenized in radioimmunoprecipitation assay (RIPA) buffer containing 1% Triton X-100, 0.1% SDS, 0.5% sodium deoxycholate, and protease inhibitors (100 μ g/mL phenylmethanesulfonyl fluoride, 30 μ g/mL aprotinin, and

1 mM sodium orthovanadate) and then sonicated for 4×10 s. After centrifugation at $12,000g$ for 20 min at 4°C , the supernatant was collected and centrifuged again as above. The final resulting supernatant was stored at -80°C until use. Samples from the SN or CPU were diluted in $2\times$ sample buffer (50 mM Tris (pH 6.8), 2% SDS, 10% glycerol, 0.1% bromophenol blue, and 5% β -mercaptoethanol), heated for 5 min at 95°C before SDS-PAGE on a 10% gel, and subsequently transferred to a PVDF membrane (Millipore). The membrane was incubated for 2 h with 5% nonfat dry milk in Tris-buffered saline (TBS) containing 0.05% Tween-20 (TBST). The membrane was rinsed in three changes of TBST and then incubated overnight with mouse anti-TH monoclonal antibody (1:10,000; T2928, Sigma), rabbit anti-DAT polyclonal antibody (1:4000; AB2231, Millipore), rabbit anti-ND1 monoclonal antibody (1:2000; ab181848, Abcam), or rabbit anti-ND4 monoclonal antibody (1:200; HPA053928, Sigma) at 4°C according to the experiment purposes. After three washes, the membrane was incubated for 1 h with IRDye[®] 800-conjugated goat anti-mouse second antibody (1:3000; Rockland) or goat anti-rabbit second antibody (1:5000; Rockland). The bands were scanned by an Odyssey infrared scanner (LI-COR Biosciences). Following stripping, each PVDF membrane was subsequently immunoblotted with mouse anti- β -actin monoclonal antibody (Santa Cruz Biotechnology). The labeling densities for TH, DAT, ND1, or ND4 were compared with those for β -actin, which were the endogenous control.

2.10. Testosterone Measurement. Trunk blood was collected from the rats after decapitation in experiment 1. Serum samples were prepared by centrifugation at $3000g$ for 15 min at 4°C and stored at -80°C until assay. Testosterone levels in the serum and in the SN supernatant of experiment 1 were measured by radioimmunoassay using the testosterone radioimmunoassay kit (Tianjin Nine Tripods Medical and Bioengineering Co. Ltd., China) in accordance with the manufacturer's protocol.

2.11. Statistical Analysis. All of the data are presented as the mean \pm SD. We applied tests of normality (Kolmogorov-Smirnov test) and homogeneity variance (Levene's test). If both normal distribution ($P > 0.1$) and homogeneity of variance ($P > 0.1$) were found, then, parametric testing was performed by one-way analysis of variance (one-way ANOVA) followed by a Student-Newman-Keuls post hoc test for multiple comparisons. Otherwise, nonparametric statistics were done by the Kruskal-Wallis test followed by the Mann-Whitney U test for post hoc analysis between groups. The level of significance was taken as $P < 0.05$.

3. Results

3.1. Experiment 1. To choose the optimal doses of TP supplements in ameliorating the oxidative damage to the SN of GDX rats, MDA, mitochondrial H_2O_2 , and mitochondrial GSH/GSSG were tested in rats by manipulating testosterone levels. Furthermore, the testosterone levels in serum and the SN were measured in experimental rats.

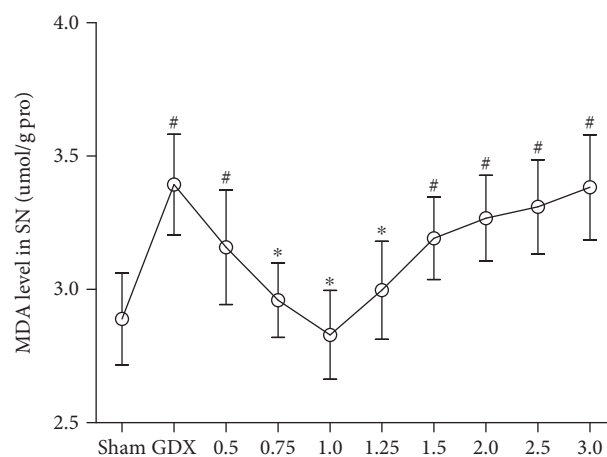


FIGURE 1: The level of MDA in the SN was dependent on the doses of TP supplements to GDX rats. $n = 8$ per group, expressed as mean \pm SD. # $P < 0.01$ versus sham rats, * $P < 0.01$ versus GDX rats.

3.1.1. MDA. Group differences were found in the level of MDA (Figure 1; one-way ANOVA, $F(9,70) = 10.250$, $P < 0.01$) among all groups. The post hoc test revealed that the level of MDA in the SN was significantly higher in GDX rats than in sham rats ($P < 0.01$). Supplements of TP at the dose of 0.75, 1.0, or 1.25 mg/kg reduced MDA in GDX rats to the level of the sham rats. TP supplements at a dose of over 1.5 mg/kg to GDX rats increased the level of MDA compared with the level of MDA of sham rats ($P < 0.01$).

3.1.2. H_2O_2 and GSH/GSSG. There were group differences in mitochondrial H_2O_2 (Figure 2(a); Kruskal-Wallis test, $\chi^2 = 59.609$, $P < 0.01$) and in mitochondrial GSH/GSSG (Figure 2(b); one-way ANOVA, $F(9,70) = 11.340$, $P < 0.01$) among all groups. The post hoc test showed the increased mitochondrial H_2O_2 production as well as the decreased mitochondrial GSH/GSSG in the SN of GDX rats compared with sham rats ($P < 0.01$). Increased mitochondrial H_2O_2 in GDX rats was restored to the levels in sham rats via TP supplement to GDX rats at the dose of 0.75, 1.0, or 1.25 mg/kg. The supplements of TP to GDX rats at the dose of 0.75, 1.0, 1.25, or 1.5 mg/kg brought the decreased GSH/GSSG to sham level.

3.1.3. Testosterone Levels. Group differences among sham, GDX, and GDX-TP rats were found in the testosterone levels of serum (Figure 3(a); Kruskal-Wallis test, $\chi^2 = 73.342$, $P < 0.01$) and the SN (Figure 3(b); Kruskal-Wallis test, $\chi^2 = 74.194$, $P < 0.01$). GDX rats had the lowest serum and SN testosterone levels, which were hardly detected. Serum and SN testosterone levels in GDX rats that received the supplements of TP at 0.75, 1.0, or 1.25 mg/kg were in the same levels as those in sham rats. Supplements of TP at a dose of over 1.5 mg/kg to GDX rats resulted in supraphysiological levels of serum and SN testosterone ($P < 0.01$).

3.2. Experiment 2. The markers of the nigrostriatal dopaminergic system were analyzed to investigate the deficits in

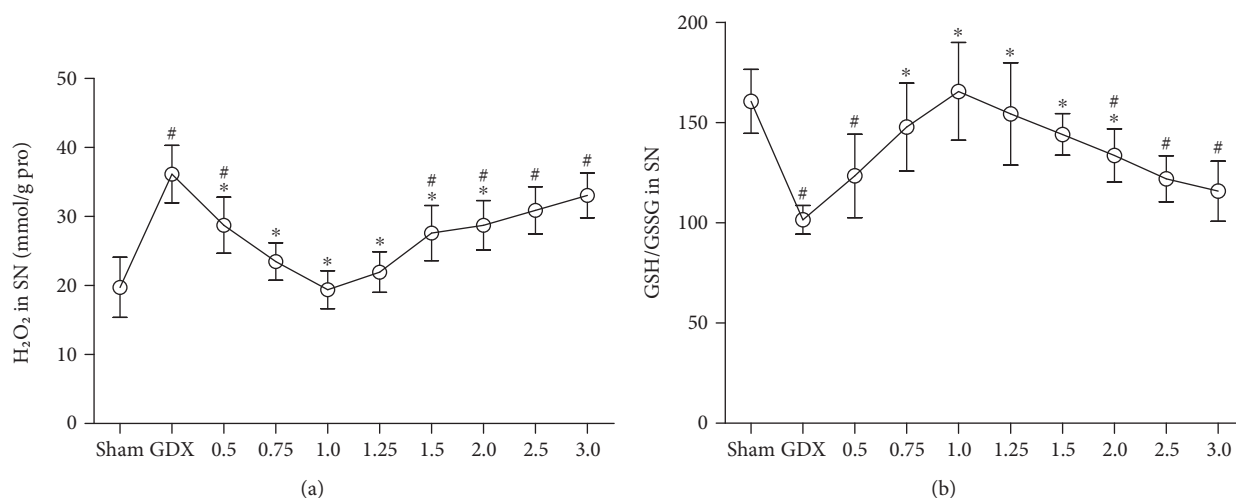


FIGURE 2: The mitochondrial H₂O₂ and GSH/GSSG in the SN were dependent on the doses of TP supplements to GDX rats. (a) Mitochondrial H₂O₂, (b) Mitochondrial GSH/GSSG. $n = 8$ per group, expressed as mean \pm SD. [#] $P < 0.01$ versus sham rats, ^{*} $P < 0.01$ versus GDX rats.

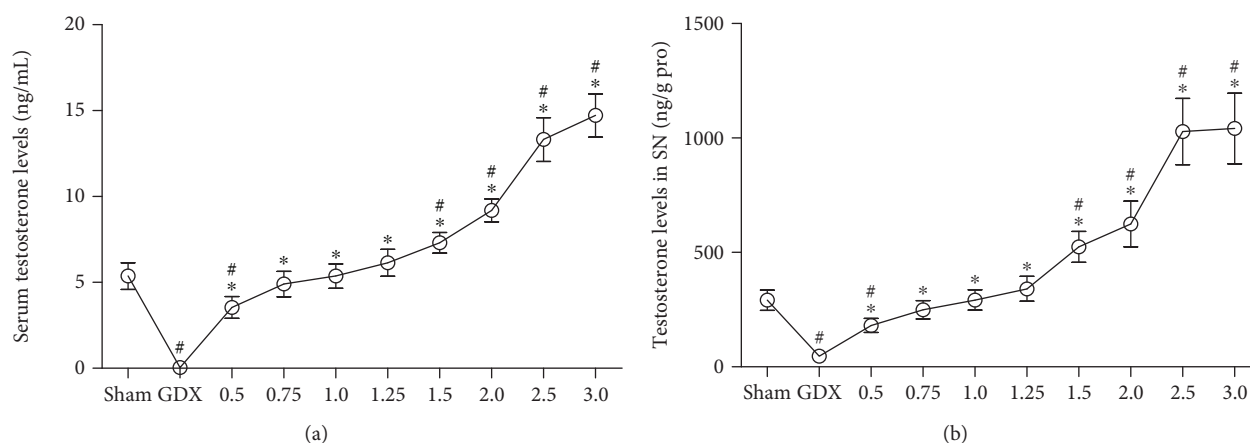


FIGURE 3: The testosterone levels in serum and in the SN were dependent on the doses of TP supplements to GDX rats. (a) Serum. (b) SN. $n = 8$ per group, expressed as mean \pm SD. [#] $P < 0.01$ versus sham rats, ^{*} $P < 0.01$ versus GDX rats.

the nigrostriatal dopaminergic system and the effects of TP supplements on the impaired nigrostriatal dopaminergic system in GDX rats.

3.2.1. DA and Its Metabolites. There were group differences in the levels of DA (Figure 4(a); one-way ANOVA, $F(3, 28) = 29.021$, $P < 0.01$), DOPAC (Figure 4(b); one-way ANOVA, $F(3, 28) = 18.676$, $P < 0.01$), and HVA (Figure 4(c), one-way ANOVA, $F(3, 28) = 18.004$, $P < 0.01$) in the CPu among sham, GDX, GDX-0.5TP, and GDX-1.0TP rats. The levels of DA, DOPAC, and HVA were decreased in GDX rats over sham rats by 36.68%, 26.63%, and 22.62% ($P < 0.01$), respectively. TP supplements to GDX rats at 1.0 mg/kg reversed them to the levels in sham rats. Supplements of TP at 0.5 mg/kg did not restore them to sham levels.

3.2.2. TH and DAT. Group differences were found in TH and DAT at the level of mRNA in the SN (Figure 5(a); TH:

Kruskal-Wallis test, $\chi^2 = 26.208$, $P < 0.01$; Figure 5(b); DAT: one-way ANOVA, $F(3, 28) = 61.358$, $P < 0.01$) and at the level of protein both in the SN (Figures 5(c) and 5(e); TH: Kruskal-Wallis test, $\chi^2 = 18.872$, $P < 0.01$; Figures 5(d) and 5(f); DAT: Kruskal-Wallis test, $\chi^2 = 26.189$, $P < 0.01$) and in the CPu (Figures 5(c) and 5(e); TH: Kruskal-Wallis test, $\chi^2 = 26.253$, $P < 0.01$; Figures 5(d) and 5(f); DAT: one-way ANOVA, $F(3, 28) = 174.783$, $P < 0.01$) among sham, GDX, GDX-0.5TP, and GDX-1.0TP rats. The post hoc test showed that the TH and DAT mRNAs in the SN were, respectively, decreased by 39.68% and 36.31% in GDX rats over sham rats ($P < 0.01$). A 40.92% and 44.04% reduction in TH proteins, respectively, in the SN and in the CPu and a 66.41% and 49.78% decrease in DAT proteins were found in GDX rats compared with sham rats ($P < 0.01$). The significantly reduced TH and DAT at mRNA and protein levels in GDX rats were restored to the level in sham rats by the supplements of TP at 1.0 mg/kg, not at 0.5 mg/kg except for the protein level of TH in the SN.

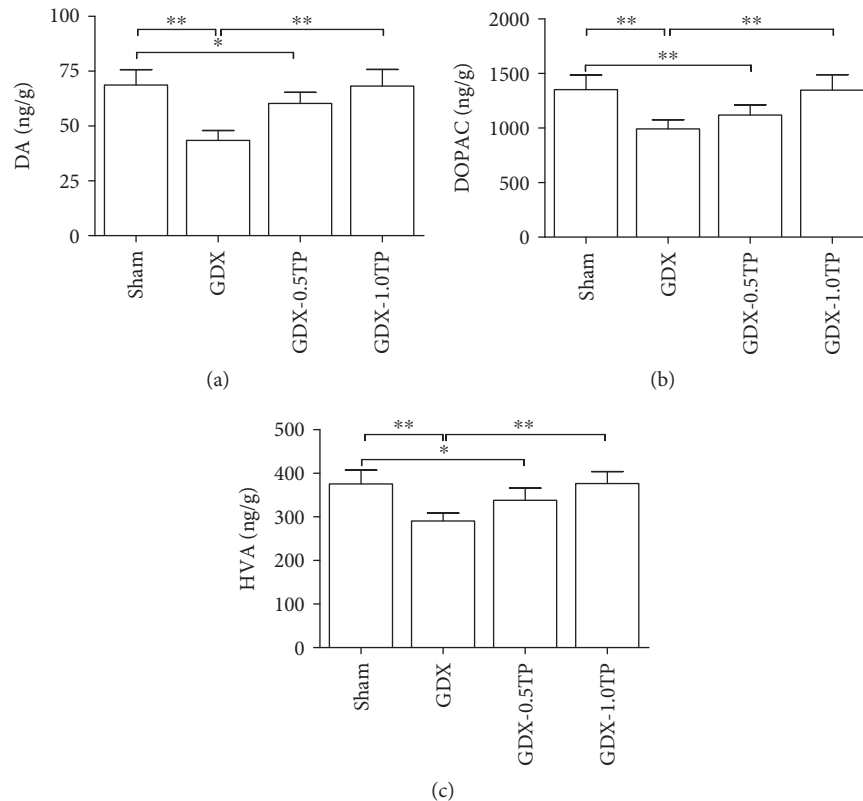


FIGURE 4: The effects of TP supplements on DA and its metabolites in the CPu of GDX rats. (a) DA. (b) DOPAC. (c) HVA. $n = 8$ per group, expressed as mean \pm SD. * $P < 0.05$; ** $P < 0.01$.

3.3. Experiment 3. To determine the effects of testosterone on mitochondria in the SN, the parameters related to mitochondria were analyzed in male rats by manipulating serum testosterone levels and the implicated mtDNA-encoded subunits were identified in the substantia nigra of GDX rats.

3.3.1. Mitochondrial Membrane Potential. Group differences of the Rh123 fluorescence intensity in the SN were found among sham, GDX, GDX-0.5TP, and GDX-1.0TP rats (Figure 6; one-way ANOVA, $F(3,28) = 12.497$, $P < 0.01$). The value of Rh123 fluorescence intensity was significantly lower in GDX rats than in sham rats by 19.12% ($P < 0.01$). Supplements of TP at 1.0 mg/kg, not at 0.5 mg/kg, restored the value of Rh123 fluorescence intensity in the SN of GDX rats to the level in sham rats.

3.3.2. Mitochondrial Complex Activities. Of the four complexes of the mitochondrial respiratory chain, complex I in the SN showed a significant group difference among sham, GDX, GDX-0.5TP, and GDX-1.0TP rats (Figure 7; one-way ANOVA, $F(3, 28) = 16.602$, $P < 0.01$). The activity of complex I in the SN was significantly reduced by 26.77% in GDX rats compared to sham rats ($P < 0.01$). Supplements of TP at 1.0 mg/kg, not at 0.5 mg/kg, restored the activity of complex I in the SN of GDX rats to the level in sham rats. No significant differences were detected in the activity of complex II, III, or IV among sham, GDX, GDX-0.5TP, and GDX-1.0TP rats (Table 2).

3.3.3. mtDNA-Encoded Subunits of Complex I. Of the 7 mtDNA-encoded subunits in complex I, both ND1 and ND4 showed a significant group differences at the level of mRNA among sham, GDX, GDX-0.5TP, and GDX-1.0TP rats (Figure 8(a); ND1: one-way ANOVA, $F(3,28) = 14.530$, $P < 0.01$; Figure 8(b); ND4: one-way ANOVA, $F(3,28) = 16.536$, $P < 0.01$). The post hoc test found a 10.23% and 15.24% reduction, respectively, in ND1 mRNA and in ND4 mRNA of GDX rats over sham rats ($P < 0.01$). Supplements of TP to GDX rats at 1.0 mg/kg, not at 0.5 mg/kg, increased ND1 and ND4 mRNAs to the level in sham rats. No significant differences were detected at the mRNA level of ND2, ND3, ND4L, ND5, or ND6 among sham, GDX, and GDX-TP rats (Table 3).

3.3.4. ND1 and ND4. ND1 and ND4 were analyzed at the protein level based on the findings of mtDNA-encoded subunit mRNAs of complex I. Group differences of ND1 and ND4 at the protein level were disclosed in the SN among sham, GDX, GDX-0.5TP, and GDX-1.0TP rats (Figures 8(c) and 8(e); ND1: one-way ANOVA, $F(3,28) = 149.744$, $P < 0.01$; Figures 8(d) and 8(f); ND4: one-way ANOVA, $F(3,28) = 175.603$, $P < 0.01$). A 69.85% and 61.44% reduction, respectively, in ND1 protein and in ND4 protein was found in GDX rats over sham rats ($P < 0.01$). The supplements of TP to GDX rats at 1.0 mg/kg, not at 0.5 mg/kg, upregulated ND1 and ND4 to the level in sham rats.

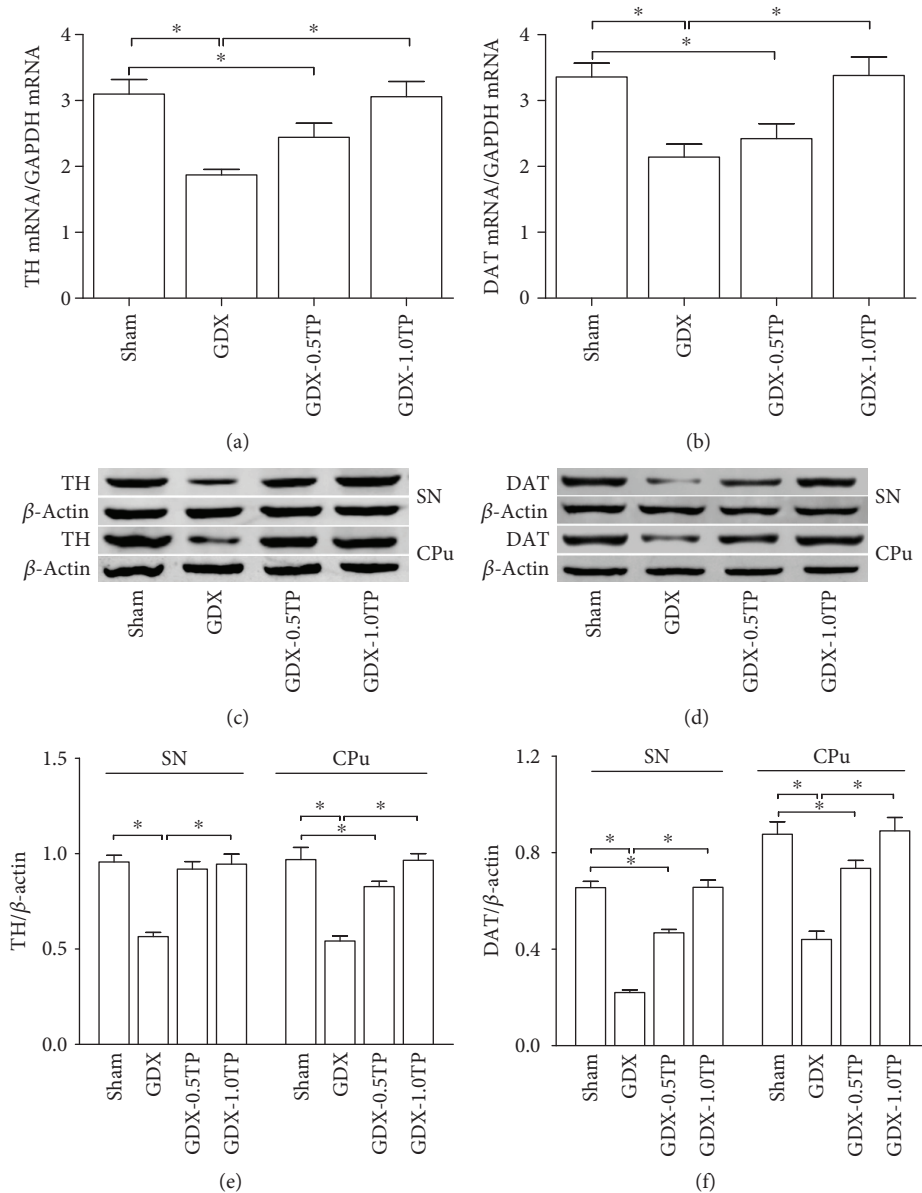


FIGURE 5: The effects of TP supplements on TH and DAT in GDX rats. (a–b) TH or DAT mRNA in the SN was detected by qPCR. (c–f) TH or DAT protein in the SN and CPu was measured by Western blot. $n = 8$ per group, expressed as mean \pm SD. * $P < 0.01$.

4. Discussion

The present study revealed that the testosterone deficiency impaired the mitochondrial function of the substantia nigra and induced the deficits in the nigrostriatal dopaminergic system. The decreased mitochondrial membrane potential, the increased oxidative stress in the SN, and the reduced expression of DA, its metabolites, TH, and DAT in the nigrostriatal dopaminergic system were found in GDX rats. Of the four mitochondrial respiratory chain complexes, castration reduced the activity of mitochondrial complex I in the SN and induced the declined expression of mitochondrial ND1 and ND4 of 7 mtDNA-encoded subunits of complex I. Supplements of TP to GDX rats ameliorated the mitochondrial defects, increased the activity of mitochondrial

complex I, and upregulated the expression of mitochondrial ND1 and ND4. The reduced activity of mitochondrial complex I and the downregulated expression of mitochondrial ND1 and ND4 in the SN of 28-day testosterone-deprived rats suggested an important role of testosterone in maintaining the mitochondrial function of the nigrostriatal dopaminergic system and the vulnerability of mitochondrial complex I to testosterone deficiency. Mitochondrial ND1 and ND4, as potential testosterone targets, were implicated in the oxidative damage to the nigrostriatal dopaminergic system.

There is a controversy about androgens and neuroprotection in the central nervous system [6, 43–45]. Dosing of testosterone seems very important in evaluating the results [44]. In the present study, TP supplements to GDX rats at the doses of 0.75, 1.0, and 1.25 mg/kg restored MDA, mitochondrial H_2O_2 ,

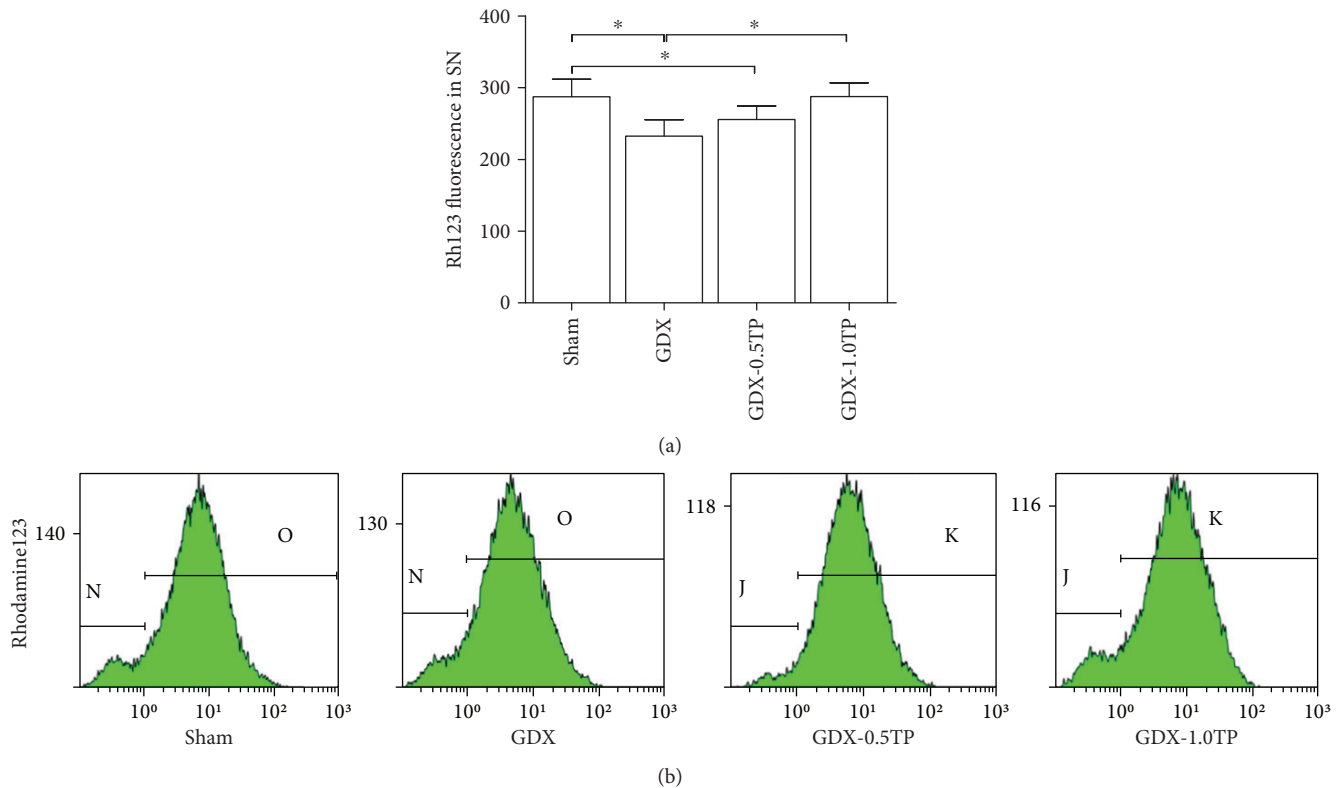


FIGURE 6: The effects of TP supplements on the mitochondrial membrane potential in the SN of GDX rats. $n = 8$ per group, expressed as mean \pm SD. * $P < 0.01$.

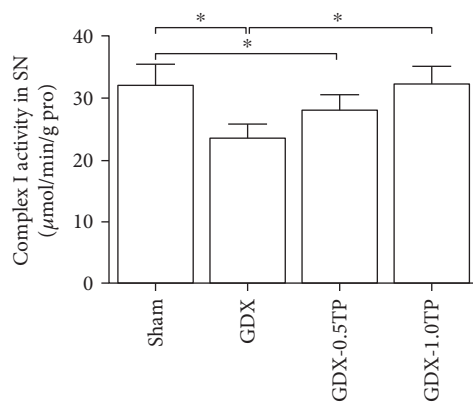


FIGURE 7: The effects of TP supplements on the activity of mitochondrial complex I in the SN of GDX rats. $n = 8$ per group, expressed as mean \pm SD. * $P < 0.01$.

and mitochondrial GSH/GSSG in the SN to sham levels. However, TP supplements at the dose of 0.5, 1.5, 2.0, 2.5, or 3 mg/kg to GDX rats resulted in infraphysiological or supraphysiological levels of the serum and SN testosterone and induced the increased MDA and mitochondrial H_2O_2 in the SN. The results were consistent with the experiments in which moderate, but not very low or very high, doses of testosterone had beneficial effects on behavioral measures such as memory [44], and testosterone at high concentrations induced harmful activity and initiated the apoptosis process [46]. The detected

testosterone levels in the serum and SN of GDX rats after TP supplementation at the doses of 0.75, 1.0, and 1.25 mg/kg were in the same levels as those in sham rats, which indicated that the administration of TP at doses of 0.75–1.25 mg to GDX rats reached physiological levels of testosterone.

MDA, an important end product of lipid peroxidation, reflect free radical-mediated cell membrane damage [3, 47]. A marked increase in MDA in the present study suggested the overproduced free radicals and the occurred oxidative stress in the SN of GDX rats. One of the main factors involved in oxidative stress is superoxide anion (O_2^-) [48]. Superoxide anion production occurs mainly inside the mitochondrion. It can be converted to O_2 and H_2O_2 . GSH and GSSG are redox couples. Glutathione peroxidase catalyzes the reduction of H_2O_2 using GSH to produce GSSG and water [49]. The increased H_2O_2 and decreased GSH/GSSG in SN mitochondria further revealed the existed oxidative stress in GDX rats. The oxidative stress is closely related to mitochondrial dysfunction [11, 50]. Mitochondrial dysfunction induces free radical overproduction and increases lipid peroxidation [38, 51, 52]. Mitochondria are responsible for generating cellular energy, altering the reduction-oxidation potential of cells, and regulating cell viability [53, 54]. Their function can be evaluated by analyzing the parameters of mitochondria, such as mitochondrial membrane potential [10, 50]. A decrease in the mitochondrial membrane potential can compromise cell viability. The increased lipid peroxidation and mitochondrial H_2O_2 , as well as the decreased mitochondrial GSH/GSSG and mitochondrial membrane

TABLE 2: Effects of TP on the activity of mitochondrial complexes ($\mu\text{mol}/\text{min}/\text{g}$ pro).

Enzyme	Sham	GDX	GDX-0.5TP	GDX-1.0TP
Complex I	32.12 \pm 3.46	23.52 \pm 2.32*	27.96 \pm 2.64* [#]	32.21 \pm 2.91* [#] [△]
Complex II	21.96 \pm 3.08	21.45 \pm 2.86	21.69 \pm 2.58	22.87 \pm 3.41
Complex III	32.72 \pm 3.37	31.77 \pm 3.78	31.91 \pm 3.48	33.06 \pm 2.75
Complex IV	15.65 \pm 2.02	14.49 \pm 2.26	14.55 \pm 2.12	16.19 \pm 2.22

* $P < 0.01$ versus sham; [#] $P < 0.01$ versus GDX group; [△] $P < 0.01$ versus GDX-0.5TP group.

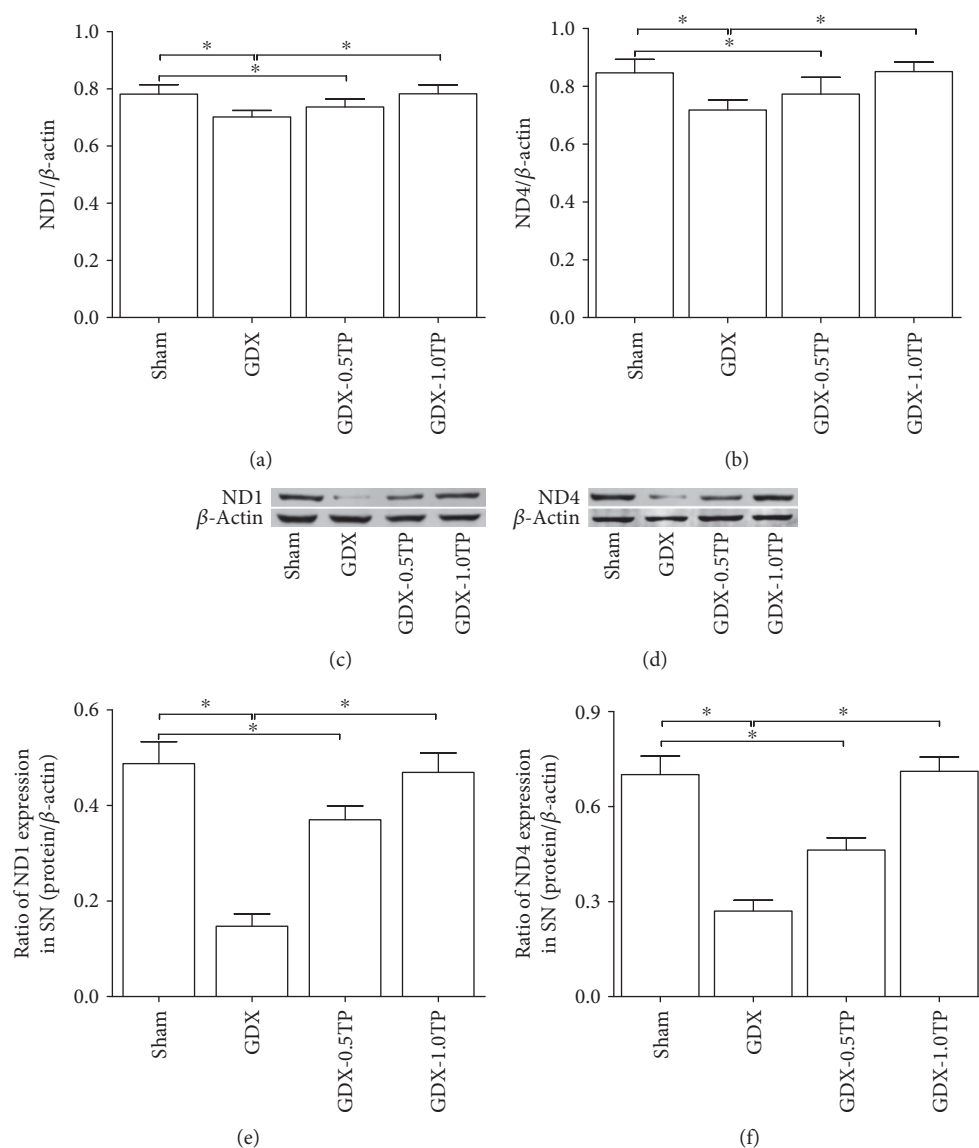


FIGURE 8: The effects of TP supplements on ND1 and ND4 in the SN of GDX rats. (a-b) ND1 or ND4 mRNA was detected by qPCR. (c-f) ND1 or ND4 protein was measured by Western blot. $n = 8$ per group, expressed as mean \pm SD. * $P < 0.01$.

potential in the SN of GDX rats, suggested that testosterone deficiency disturbed the mitochondrial function. Supplements of TP at 1.0 mg/kg to GDX rats restored the mitochondrial membrane potential as well as the status of oxidative stress in the SN. However, TP supplements at 0.5 mg/kg could not restore them in the SN of GDX rats. The present

results indicated that the antioxidant role of testosterone [6, 55] might be realized via testosterone-regulating mitochondrial function in some extent. Mitochondrial dysfunction might underlie the defects of the nigrostriatal dopaminergic system of GDX rats. Orchiectomy reduced the expression of DA and its metabolites, as well as that of TH and DAT

TABLE 3: Effects of TP on the mRNA levels of mtDNA-encoded subunits of complex I.

Subunits	Sham	GDX	GDX-0.5TP	GDX-1.0TP
ND1	0.78 ± 0.03	0.71 ± 0.04*	0.74 ± 0.03** [#]	0.78 ± 0.04** [#] △
ND2	0.85 ± 0.04	0.84 ± 0.03	0.82 ± 0.04	0.86 ± 0.04
ND3	0.93 ± 0.04	0.91 ± 0.03	0.91 ± 0.05	0.92 ± 0.03
ND4	0.85 ± 0.05	0.72 ± 0.03*	0.77 ± 0.06** [#]	0.85 ± 0.03** [#] △
ND4L	0.90 ± 0.04	0.89 ± 0.06	0.86 ± 0.06	0.91 ± 0.05
ND5	0.90 ± 0.05	0.88 ± 0.05	0.89 ± 0.05	0.91 ± 0.05
ND6	0.92 ± 0.05	0.90 ± 0.04	0.90 ± 0.05	0.92 ± 0.04

* $P < 0.01$ versus sham; ** $P < 0.05$ versus GDX; ** $P < 0.01$ versus GDX; △ $P < 0.01$ versus GDX-0.5TP group.

in the nigrostriatal dopaminergic system. Supplements of TP at physiological levels restored the impaired nigrostriatal dopaminergic system. The restoration by TP supplements of nigrostriatal dopaminergic activity might be involved in the amelioration of behavioral deficits in open-field activity of TP-treated GDX rats. Gonadectomy in male rats decreases the behavioral parameters of open-field activity, such as walking, climbing, and total path length [41]. Supplement of TP improves the decreased behavioral parameters of open-field activity in GDX rats [41].

As an important indicator of mitochondrial function [10, 56], mitochondrial membrane potential is created by the proton gradient across the inner mitochondrial membrane through the proton-extruding system including complexes I, III, and IV of the respiratory chain [10]. Testosterone deficiency might interfere with the mitochondrial function by affecting the proton-extruding system of the mitochondrial respiratory chain. So the influence of TP on complexes I, III, and IV of the respiratory chain in the SN became our main concern in the studies. Of the three mitochondrial respiratory chain complexes in the proton-extruding system, the activity of complex I was altered due to testosterone deficiency. The reduced activity of complex I was found in the SN of GDX rats. The following reasons might explain the reduced activity of complex I in the SN of GDX rats. One is nonspecific oxidative damage. The SN is rich in dopamine. Dopamine itself can be a source of oxidative stress [26], and dopaminergic neurons experience the detriments in auto-oxidation of dopamine [57, 58]. The increased oxidative stress induced by testosterone deficiency might aggravate the oxidative damage of auto-oxidation of dopamine to mitochondrial complexes in the nigrostriatal dopaminergic system of GDX rats. Complex I seem more vulnerable than complexes II, III, and IV to oxidative damage caused by testosterone deficiency. Another reason might be that testosterone specifically regulates the subunits of complex I either via androgen receptor [59, 60] or via estrogen receptor [61, 62] when testosterone is aromatized to estrogen. Whether estrogen was involved in the regulation of complex I subunits is necessary to be investigated in following studies by ovariectomy in female rats. Immunocytochemical [59, 62] and in situ hybridization [60, 61] studies identify the subpopulations of intracellular gonadal hormone receptor-bearing

neurons in the SN, which suggested that specific subsets of midbrain dopaminergic neurons might be direct targets of gonadal hormones. Testosterone deficiency specifically caused the decreased activity of complex I and resulted in oxidative stress. The duration after orchietomy in rats was 28 days. 28-day oxidative stress induced by the reduced activity of complex I in GDX rats might not be enough to affect complexes II, III, and IV. If the duration extended longer, the activities of complexes II, III, and IV would be affected as the ROS was accumulated in GDX rats.

Complex I is a major entry point of the mitochondrial respiratory chain, and its deficiencies constitute an important step in the cascade of events leading to the death of the dopaminergic cells [63]. In 44 subunits of complex I, 7 subunits (ND1, ND2, ND3, ND4, ND4L, ND5, and ND6) are encoded by the mtDNA [64]. In the present study, we found that gonadectomy in male rats resulted in the reduction in ND1 and ND4 of 7 mtDNA-encoded subunits in complex I. Supplements of TP upregulated or restored the expression of ND1 and ND4 in GDX rats, which was dependent on the physiological levels of testosterone in serum and the SN following TP supplementation. Considering the deficits in the nigrostriatal dopaminergic system in GDX rats in the present study and lower testosterone levels in some PD [65, 66] as well as the complex I deficiency in the pathogenesis of PD [16, 18–21], testosterone regulation of both ND1 and ND4 seemed related to the pathogenesis of PD with testosterone deficiency. Manipulating ND1 and ND4 expressions by TP would be a potential approach to prevent mesodopaminergic neurons from further degeneration in testosterone-deficient PD patients in a way. Aging, as an important risk factor for neurodegenerative disorders, is associated with a decrease in protein and mRNA levels of the respiratory chain in mitochondria [15, 38]. Whether testosterone supplements might ameliorate the deficits in mitochondrial protein expression of the mitochondrial respiratory chain in aging should be testified in future studies.

There are some problems unresolved in the present study. We only analyzed MDA, mitochondrial H_2O_2 , and mitochondrial GSH/GSSG in GDX rats. However, in addition to ROS, oxidative stress has been shown to be associated with reactive nitrogen species (RNS). Thus, the parameters associated with RNS should be measured in GDX rats. Moreover, mitochondrial bioenergetics and ATP production should be detected to confirm the mitochondrial dysfunction. Although 7 mtDNA-encoded transcripts in complex I were mainly analyzed, whether nuclear DNA-encoded complex I mRNAs are also affected in testosterone deficiency is worthwhile further investigation.

In conclusion, testosterone at the physiological levels is necessary for the mitochondrial functions in the substantia nigra. Testosterone deficiency induced the mitochondrial dysfunction and reduced the activity of complex I of the four mitochondrial respiratory chain complexes in the substantia nigra. The reduced activity of complex I was related to the downregulated expression of mitochondrial ND1 and ND4 due to testosterone deficiency. Mitochondrial ND1 and ND4, as potential testosterone targets, were implicated in the oxidative damage to the nigrostriatal dopaminergic system.

Conflicts of Interest

The authors have no competing interests in the manuscript.

Authors' Contributions

Wensheng Yan and Yunxiao Kang contributed equally to this work.

Acknowledgments

This project was financially supported by the Natural Science Foundation of China (no. 81200252), the Natural Science Foundation of Hebei Province of China (no. C2017206072), and the Research Development Fund of Hebei Medical University (no. kyfz023).

References

- [1] S. Gandhi and A. Y. Abramov, "Mechanism of oxidative stress in neurodegeneration," *Oxidative Medicine and Cellular Longevity*, vol. 2012, Article ID 428010, 11 pages, 2012.
- [2] S. Manoharan, G. J. Guillemin, R. S. Abiramasundari, M. M. Essa, M. Akbar, and M. D. Akbar, "The role of reactive oxygen species in the pathogenesis of Alzheimer's disease, Parkinson's disease, and Huntington's disease: a mini review," *Oxidative Medicine and Cellular Longevity*, vol. 2016, Article ID 8590578, 15 pages, 2016.
- [3] E. Niedzielska, I. Smaga, M. Gawlik et al., "Oxidative stress in neurodegenerative diseases," *Molecular Neurobiology*, vol. 53, no. 6, pp. 4094–4125, 2016.
- [4] W. Lv, N. Du, Y. Liu et al., "Low testosterone level and risk of Alzheimer's disease in the elderly men: a systematic review and meta-analysis," *Molecular Neurobiology*, vol. 53, no. 4, pp. 2679–2684, 2016.
- [5] E. Ahlbom, G. S. Prins, and S. Ceccatelli, "Testosterone protects cerebellar granule cells from oxidative stress-induced cell death through a receptor mediated mechanism," *Brain Research*, vol. 892, no. 2, pp. 255–262, 2001.
- [6] S. Meydan, I. Kus, U. Tas et al., "Effects of testosterone on orchietomy-induced oxidative damage in the rat hippocampus," *Journal of Chemical Neuroanatomy*, vol. 40, no. 4, pp. 281–285, 2010.
- [7] S. W. Son, J. S. Lee, H. G. Kim, D. W. Kim, Y. C. Ahn, and C. G. Son, "Testosterone depletion increases the susceptibility of brain tissue to oxidative damage in a restraint stress mouse model," *Journal of Neurochemistry*, vol. 136, no. 1, pp. 106–117, 2016.
- [8] G. L. Zhang, W. Wang, Y. X. Kang et al., "Chronic testosterone propionate supplement could activated the Nrf2-ARE pathway in the brain and ameliorated the behaviors of aged rats," *Behavioural Brain Research*, vol. 252, pp. 388–395, 2013.
- [9] G. Zhang, S. Li, Y. Kang et al., "Enhancement of dopaminergic activity and region-specific activation of Nrf2-ARE pathway by intranasal supplements of testosterone propionate in aged male rats," *Hormones and Behavior*, vol. 80, pp. 103–116, 2016.
- [10] K. A. Foster, F. Galeffi, F. J. Gerich, D. A. Turner, and M. Müller, "Optical and pharmacological tools to investigate the role of mitochondria during oxidative stress and neurodegeneration," *Progress in Neurobiology*, vol. 79, no. 3, pp. 136–171, 2006.
- [11] T. R. Figueira, M. H. Barros, A. A. Camargo et al., "Mitochondria as a source of reactive oxygen and nitrogen species: from molecular mechanisms to human health," *Antioxidants & Redox Signaling*, vol. 18, no. 16, pp. 2029–2074, 2013.
- [12] I. E. Scheffler, "A century of mitochondrial research: achievements and perspectives," *Mitochondrion*, vol. 1, no. 1, pp. 3–31, 2001.
- [13] A. A. Starkov, "The role of mitochondria in reactive oxygen species metabolism and signaling," *Annals of the New York Academy of Sciences*, vol. 1147, pp. 37–52, 2008.
- [14] D. J. Bonda, X. Wang, G. Perry, M. A. Smith, and X. Zhu, "Mitochondrial dynamics in Alzheimer's disease: opportunities for future treatment strategies," *Drugs & Aging*, vol. 27, no. 3, pp. 181–192, 2010.
- [15] P. H. Reddy, "Mitochondrial medicine for aging and neurodegenerative diseases," *Neuromolecular Medicine*, vol. 10, no. 4, pp. 291–315, 2008.
- [16] N. Hattori, M. Tanaka, T. Ozawa, and Y. Mizuno, "Immunohistochemical studies on complexes I, II, III, and IV of mitochondria in Parkinson's disease," *Annals of Neurology*, vol. 30, no. 4, pp. 563–571, 1991.
- [17] P. Mao and P. H. Reddy, "Aging and amyloid beta-induced oxidative DNA damage and mitochondrial dysfunction in Alzheimer's disease: implications for early intervention and therapeutics," *Biochimica et Biophysica Acta*, vol. 1812, no. 11, pp. 1359–1370, 2011.
- [18] A. H. Schapira, J. M. Cooper, D. Dexter, J. B. Clark, P. Jenner, and C. D. Marsden, "Mitochondrial complex I deficiency in Parkinson's disease," *Journal of Neurochemistry*, vol. 54, no. 3, pp. 823–827, 1990.
- [19] A. H. Schapira, V. M. Mann, J. M. Cooper et al., "Anatomic and disease specificity of NADH CoQ1 reductase (complex I) deficiency in Parkinson's disease," *Journal of Neurochemistry*, vol. 55, no. 6, pp. 2142–2145, 1990.
- [20] L. K. Sharma, J. Lu, and Y. Bai, "Mitochondrial respiratory complex I: structure, function and implication in human diseases," *Current Medicinal Chemistry*, vol. 16, no. 10, pp. 1266–1277, 2009.
- [21] K. F. Winklhofer and C. Haass, "Mitochondrial dysfunction in Parkinson's disease," *Biochimica et Biophysica Acta*, vol. 1802, no. 1, pp. 29–44, 2010.
- [22] C. R. Cabello, J. J. Thune, H. Pakkenberg, and B. Pakkenberg, "Ageing of substantia nigra in humans: cell loss may be compensated by hypertrophy," *Neuropathology and Applied Neurobiology*, vol. 28, no. 4, pp. 283–291, 2002.
- [23] G. A. Gerhardt, W. A. Cass, A. Yi, Z. Zhang, and D. M. Gash, "Changes in somatodendritic but not terminal dopamine regulation in aged rhesus monkeys," *Journal of Neurochemistry*, vol. 80, no. 1, pp. 168–177, 2002.
- [24] J. W. Haycock, L. Becker, L. Ang, Y. Furukawa, O. Hornykiewicz, and S. J. Kish, "Marked disparity between age-related changes in dopamine and other presynaptic dopaminergic markers in human striatum," *Journal of Neurochemistry*, vol. 87, no. 3, pp. 574–585, 2003.
- [25] J. F. Marshall and A. J. Rosenstein, "Age-related decline in rat striatal dopamine metabolism is regionally homogeneous," *Neurobiology of Aging*, vol. 11, no. 2, pp. 13–17, 1990.
- [26] L. Chen, Y. Ding, B. Cagniard et al., "Unregulated cytosolic dopamine causes neurodegeneration associated with oxidative stress in mice," *The Journal of Neuroscience*, vol. 28, no. 2, pp. 425–433, 2008.

- [27] V. Dias, E. Junn, and M. M. Mouradian, "The role of oxidative stress in Parkinson's disease," *Journal of Parkinson's Disease*, vol. 3, no. 4, pp. 461–491, 2013.
- [28] O. Hwang, "Role of oxidative stress in Parkinson's disease," *Experimental Neurobiology*, vol. 22, no. 1, pp. 11–17, 2013.
- [29] L. S. Forno, "Neuropathology of Parkinson's disease," *Journal of Neuropathology and Experimental Neurology*, vol. 55, no. 3, pp. 259–272, 1996.
- [30] J. D. Crane, M. C. Devries, A. Safdar, M. J. Hamadeh, and M. A. Tarnopolsky, "The effect of aging on human skeletal muscle mitochondrial and intramyocellular lipid ultrastructure," *The Journals of Gerontology. Series A, Biological Sciences and Medical Sciences*, vol. 65, no. 2, pp. 119–128, 2010.
- [31] V. Pesce, A. Cormio, F. Fracasso et al., "Age-related mitochondrial genotypic and phenotypic alterations in human skeletal muscle," *Free Radical Biology & Medicine*, vol. 30, no. 11, pp. 1223–1233, 2001.
- [32] S. W. Lamberts, A. W. van den Beld, and A. J. van der Lely, "The endocrinology of aging," *Science*, vol. 278, no. 5337, pp. 419–424, 1997.
- [33] A. Vasconsuelo, L. Milanese, and R. Boland, "Actions of 17 β -estradiol and testosterone in the mitochondria and their implications in aging," *Ageing Research Reviews*, vol. 12, no. 4, pp. 907–917, 2013.
- [34] R. L. Cunningham, T. Macheda, L. T. Watts et al., "Androgens exacerbate motor asymmetry in male rats with unilateral 6-hydroxydopamine lesion," *Hormones and Behavior*, vol. 60, no. 5, pp. 617–624, 2011.
- [35] R. Ghanadian, J. G. Lewis, and G. D. Chisholm, "Serum testosterone and dihydrotestosterone changes with age in rat," *Steroids*, vol. 25, no. 6, pp. 753–762, 1975.
- [36] S. M. Harman, E. J. Metter, J. D. Tobin, J. Pearson, and M. R. Blackman, "Longitudinal effects of aging on serum total and free testosterone levels in healthy men, Baltimore Longitudinal Study of Aging," *The Journal of Clinical Endocrinology and Metabolism*, vol. 86, no. 2, pp. 724–731, 2001.
- [37] E. R. Rosario, L. Chang, E. H. Head, F. Z. Stanczyk, and C. J. Pike, "Brain levels of sex steroid hormones in men and women during normal aging and in Alzheimer's disease," *Neurobiology of Aging*, vol. 32, no. 4, pp. 604–613, 2011.
- [38] M. T. Lin and M. F. Beal, "Mitochondrial dysfunction and oxidative stress in neurodegenerative diseases," *Nature*, vol. 443, no. 7113, pp. 787–795, 2006.
- [39] R. Cui, G. Zhang, Y. Kang et al., "Amelioratory effects of testosterone propionate supplement on behavioral, biochemical and morphological parameters in aged rats," *Experimental Gerontology*, vol. 47, no. 1, pp. 67–76, 2012.
- [40] L. Wang, Y. Kang, G. Zhang et al., "Deficits in coordinated motor behavior and in nigrostriatal dopaminergic system ameliorated and VMAT2 expression up-regulated in aged male rats by administration of testosterone propionate," *Experimental Gerontology*, vol. 78, pp. 1–11, 2016.
- [41] G. Zhang, G. Shi, H. Tan, Y. Kang, and H. Cui, "Intranasal administration of testosterone increased immobile-sniffing, exploratory behavior, motor behavior and grooming behavior in rats," *Hormones and Behavior*, vol. 59, no. 4, pp. 477–483, 2011.
- [42] G. Paxinos and C. Watson, "The rat brain in stereotaxic coordinates," Academic Press, Orlando, FL, sixth edition, 2007.
- [43] V. Chisu, P. Manca, G. Lepore, S. Gadau, M. Zedda, and V. Farina, "Testosterone induces neuroprotection from oxidative stress. Effects on catalase activity and 3-nitro-L-tyrosine incorporation into alpha-tubulin in a mouse neuroblastoma cell line," *Archives Italiennes de Biologie*, vol. 144, no. 2, pp. 63–73, 2006.
- [44] M. D. Spritzer, E. D. Daviau, M. K. Coneeny, S. M. Engelman, W. T. Prince, and K. N. Rodriguez-Wisdom, "Effects of testosterone on spatial learning and memory in adult male rats," *Hormones and Behavior*, vol. 59, no. 4, pp. 484–496, 2011.
- [45] B. B. Yeap, Z. Hyde, O. P. Almeida et al., "Lower testosterone levels predict incident stroke and transient ischemic attack in older men," *The Journal of Clinical Endocrinology and Metabolism*, vol. 94, no. 7, pp. 2353–2359, 2009.
- [46] M. Estrada, A. Varshney, and B. E. Ehrlich, "Elevated testosterone induces apoptosis in neuronal cells," *The Journal of Biological Chemistry*, vol. 281, no. 35, pp. 25492–25501, 2006.
- [47] A. A. Kamal, A. Goma, M. e. Khafif, and A. S. Hammad, "Plasma lipid peroxides among workers exposed to silica or asbestos dust," *Environmental Research*, vol. 49, no. 2, pp. 173–180, 1989.
- [48] A. Melo, L. Monteiro, R. M. Lima, D. M. Oliveira, M. D. Cerqueira, and R. S. El-Bachá, "Oxidative stress in neurodegenerative diseases: mechanisms and therapeutic perspectives," *Oxidative Medicine and Cellular Longevity*, vol. 2011, Article ID 467180, 14 pages, 2011.
- [49] N. Cardenas-Rodriguez, B. Huerta-Gertrudis, L. Rivera-Espinosa et al., "Role of oxidative stress in refractory epilepsy: evidence in patients and experimental models," *International Journal of Molecular Sciences*, vol. 14, no. 1, pp. 1455–1476, 2013.
- [50] J. Ruzkiewicz and J. Albrecht, "Changes in the mitochondrial antioxidant systems in neurodegenerative diseases and acute brain disorders," *Neurochemistry International*, vol. 88, pp. 66–72, 2015.
- [51] D. J. Bonda, X. Wang, G. Perry et al., "Oxidative stress in Alzheimer disease: a possibility for prevention," *Neuropharmacology*, vol. 59, no. 4-5, pp. 290–294, 2010.
- [52] H. A. Funes, N. Apostolova, F. Alegre et al., "Neuronal bioenergetics and acute mitochondrial dysfunction: a clue to understanding the central nervous system side effects of efavirenz," *The Journal of Infectious Diseases*, vol. 210, no. 9, pp. 1385–1395, 2014.
- [53] B. Poljsak, "Strategies for reducing or preventing the generation of oxidative stress," *Oxidative Medicine and Cellular Longevity*, vol. 2011, Article ID 194586, 15 pages, 2011.
- [54] T. Ozawa, "Genetic and functional changes in mitochondria associated with aging," *Physiological Reviews*, vol. 77, no. 2, pp. 425–464, 1997.
- [55] D. C. Guzmán, G. B. Mejía, I. E. Vázquez, E. H. García, D. S. del Angel, and H. J. Olguín, "Effect of testosterone and steroids homologues on indolamines and lipid peroxidation in rat brain," *The Journal of Steroid Biochemistry and Molecular Biology*, vol. 94, no. 4, pp. 369–373, 2005.
- [56] A. Schloesser, T. Esatbeyoglu, S. Piegholdt et al., "Dietary tocotrienol/ γ -cyclodextrin complex increases mitochondrial membrane potential and ATP concentrations in the brains of aged mice," *Oxidative Medicine and Cellular Longevity*, vol. 2015, Article ID 789710, 8 pages, 2015.
- [57] B. Fornstedt, E. Pileblad, and A. Carlsson, "In vivo autoxidation of dopamine in guinea pig striatum increases with age," *Journal of Neurochemistry*, vol. 55, no. 2, pp. 655–659, 1990.

- [58] A. Slivka and G. Cohen, "Hydroxyl radical attack on dopamine," *The Journal of Biological Chemistry*, vol. 260, no. 29, pp. 15466–15472, 1985.
- [59] M. F. Kritzer, "Selective colocalization of immunoreactivity for intracellular gonadal hormone receptors and tyrosine hydroxylase in the ventral tegmental area, substantia nigra, and retrochubral fields in the rat," *The Journal of Comparative Neurology*, vol. 379, no. 2, pp. 247–260, 1997.
- [60] R. B. Simerly, C. Chang, M. Muramatsu, and L. W. Swanson, "Distribution of androgen and estrogen receptor mRNA-containing cells in the rat brain: an in situ hybridization study," *The Journal of Comparative Neurology*, vol. 294, no. 1, pp. 76–95, 1990.
- [61] P. J. Shughrue, M. V. Lane, and I. Merchenthaler, "Comparative distribution of estrogen receptor-alpha and -beta mRNA in the rat central nervous system," *The Journal of Comparative Neurology*, vol. 388, no. 4, pp. 507–525, 1997.
- [62] P. J. Shughrue and I. Merchenthaler, "Distribution of estrogen receptor beta immunoreactivity in the rat central nervous system," *The Journal of Comparative Neurology*, vol. 436, no. 1, pp. 64–81, 2001.
- [63] M. Marella, B. B. Seo, T. Yagi, and A. Matsuno-Yagi, "Parkinson's disease and mitochondrial complex I: a perspective on the Ndi1 therapy," *Journal of Bioenergetics and Biomembranes*, vol. 41, no. 6, pp. 493–497, 2009.
- [64] R. Vartak, J. Deng, H. Fang, and Y. Bai, "Redefining the roles of mitochondrial DNA-encoded subunits in respiratory complex I assembly," *Biochimica et Biophysica Acta*, vol. 1852, no. 7, pp. 1531–1539, 2015.
- [65] M. S. Okun, B. L. Walter, W. M. McDonald et al., "Beneficial effects of testosterone replacement for the nonmotor symptoms of Parkinson disease," *Archives of Neurology*, vol. 59, no. 11, pp. 1750–1753, 2002.
- [66] R. E. Ready, J. Friedman, J. Grace, and H. Fernandez, "Testosterone deficiency and apathy in Parkinson's disease: a pilot study," *Journal of Neurology, Neurosurgery, and Psychiatry*, vol. 75, no. 9, pp. 1323–1326, 2004.

Research Article

Caffeic Acid Phenethyl Ester Reduces Ischemia-Induced Kidney Mitochondrial Injury in Rats

Sonata Trumbeckaite,^{1,2} Neringa Pauziene,³ Darius Trumbeckas,⁴ Mindaugas Jievaltas,⁴ and Rasa Baniene^{1,5}

¹Neuroscience Institute, Lithuanian University of Health Sciences, Eiveniu Str. 4, LT-50161 Kaunas, Lithuania

²Department of Pharmacognosy, Medical Academy, Lithuanian University of Health Sciences, Eiveniu Str. 13, LT-50166 Kaunas, Lithuania

³Institute of Anatomy, Lithuanian University of Health Sciences, Mickeviciaus Str. 9, LT-44307 Kaunas, Lithuania

⁴Department of Urology, Medical Academy, Lithuanian University of Health Sciences, Eiveniu g. 2, LT-50161 Kaunas, Lithuania

⁵Department of Biochemistry, Medical Academy, Lithuanian University of Health Sciences, Eiveniu Str. 4, LT-50161 Kaunas, Lithuania

Correspondence should be addressed to Sonata Trumbeckaite; trumbeckaite@gmail.com

Received 31 March 2017; Accepted 19 June 2017; Published 13 August 2017

Academic Editor: Moh H. Malek

Copyright © 2017 Sonata Trumbeckaite et al. This is an open access article distributed under the Creative Commons Attribution License, which permits unrestricted use, distribution, and reproduction in any medium, provided the original work is properly cited.

During partial nephrectomy, the avoidance of ischemic renal damage is extremely important as duration of renal artery clamping (i.e., ischemia) influences postoperative kidney function. Mitochondria (main producer of ATP in the cell) are very sensitive to ischemia and undergo damage during oxidative stress. Finding of a compound which diminishes ischemic injury to kidney is of great importance. Caffeic acid phenethyl ester (CAPE), biologically active compound of propolis, might be one of the promising therapeutic agents against ischemia-caused damage. Despite wide range of biological activities of CAPE, detailed biochemical mechanisms of its action at the level of mitochondria during ischemia are poorly described and need to be investigated. We investigated if CAPE (22 mg/kg and 34 mg/kg, injected intraperitoneally) has protective effects against short (20 min) and longer time (40 min) rat kidney ischemia in an *in vitro* ischemia model. CAPE ameliorates in part ischemia-induced renal mitochondrial injury, improves oxidative phosphorylation with complex I-dependent substrate glutamate/malate, increases Ca²⁺ uptake by mitochondria, blocks ischemia-induced caspase-3 activation, and protects kidney cells from ischemia-induced necrosis. The protective effects on mitochondrial respiration rates were seen after shorter (20 min) time of ischemia whereas reduction of apoptosis and necrosis and increase in Ca²⁺ uptake were revealed after both, shorter and longer time of ischemia.

1. Introduction

Kidney ischemia-reperfusion (I/R) injury is characterized by restriction of blood supply to an organ followed by restoration of blood flow and reoxygenation. Kidney injury may occur after infarction and sepsis, during partial nephrectomy and a surgical procedure, and when kidney tumor is removed after clamping renal artery [1]. Clamping time (i.e., duration of ischemia) is thought to be a major factor in determining postoperative kidney dysfunction. During partial nephrectomy, the avoidance of ischemic renal damage is extremely important as duration of renal artery clamping influences

postoperative kidney function. It is well described that mitochondria are very sensitive to ischemia-induced injury and undergo damage during oxidative stress [2]. Impairment in Ca²⁺ homeostasis, formation of reactive oxygen species (ROS), release of proapoptotic proteins, and loss of ATP synthesis occur during ischemia [3], and all these processes might lead to cell death in the form of apoptosis or necrosis. Recently, when more and more partial kidney resections are performed for bigger kidney tumors, the time of ischemia is extremely important for postoperative kidney function. Completion of open partial nephrectomy with 30 minutes renal artery clamping is generally easily achieved in standard

T1 stage renal tumor, but longer ischemia time is necessary in bigger tumors or in tumors of unfavorable localization [4]. This can be achieved using cold ischemia when kidney can tolerate ischemia up to two hours [5]. However, cooling of kidney during laparoscopic procedure is technically complicated and so rarely used. Therefore, there is a need of anti-ischemic agents in situations when longer time of kidney clamping is necessary. For improving ischemia tolerance, much attention has focused on new antioxidants or free radical scavengers with high potency, easy permeability to cellular compartments, and low toxicity. Caffeic acid phenethyl ester (CAPE) due to high lipophilicity might be one of the promising therapeutic agents against I/R-caused damage. Finding of a biologically active compound which diminishes negative ischemia impact to kidney function would be a solution in situations when longer time of kidney clamping is necessary.

CAPE is one of the most active compounds of propolis, exhibiting wide range of biological properties. CAPE possesses antioxidant, anti-inflammatory, and anticancer activity and regulates apoptosis [6, 7]. It has been demonstrated that CAPE (10 $\mu\text{mol/kg/day}$ for 11 days) prevents cyclosporine A and lipid peroxidation-mediated nephrotoxicity via inhibition of oxidative process [8]. Another study showed that pretreatment with intraperitoneal CAPE (10 $\mu\text{mol/kg/day}$) protects kidney from ischemia/reperfusion injury [9] by partial inhibition of neutrophil sequestration into the kidney. In contrast, Roso et al. state [10] that CAPE (10 $\mu\text{mol/kg/day}$) demonstrated greater functional and anatomic renal injury during ischemia and reperfusion in rats anesthetized with isoflurane [10] and no beneficial CAPE effect in the glycerol-induced acute renal failure model [11]. Wei et al. showed that intraperitoneal injections of CAPE (40 mg/kg/day) protected hypoxic ischemia-induced neonatal rat brain damage by inhibiting caspase-3 activation, expression of inducible nitric oxide synthase, and Ca^{2+} -induced cytochrome *c* release [12]. Khan et al. observed that CAPE (1–10 mg/kg) protected the brain from ischemia-reperfusion-induced injury, increased nitric oxide and glutathione levels, and decreased lipid peroxidation [13]. Parlakpınar et al. indicated that CAPE (50 $\mu\text{mol/kg}$) had protective effect against cardiac ischemia-reperfusion-induced apoptosis and acts in the heart as scavenger of free radicals [14]. Despite all these controversial data, detailed biochemical mechanisms at the level of mitochondria during ischemia/reperfusion are poorly described and need to be investigated.

Thus, the aim of this study was to test our hypothesis if caffeic acid phenethyl ester (CAPE) may protect kidney mitochondria from ischemic injury.

2. Materials and Methods

2.1. Animals and Experimental Model. The experimental procedures used in the present study were performed according to the permission of the Lithuanian Committee of Good Laboratory Animal Use Practice (number 0228/2012). Adult male Wistar rats weighing 200–250 g were housed under standard laboratory conditions and maintained on natural

light and dark cycle and had free access to food and water. Animals were acclimatized to laboratory conditions before the experiment. Animals were pretreated with two doses (22 mg/kg and 34 mg/kg) of intraperitoneal injections of CAPE 1.5 h prior induction of ischemia. Then, animals were sacrificed and the kidneys were removed, washed free of blood in warm (37°C) 0.9% KCl solution, placed in a humidified chamber maintained at 37°C, and were exposed for 20 min, 40 min of total (*in vitro*) ischemia. After that time, kidney tissue was used for isolation of mitochondria.

2.2. Chemicals. Succinic acid, glutamic acid, cytochrome *c* from bovine heart, adenosine-5'-diphosphate sodium salt (ADP), CAPE, malic acid, KH_2PO_4 , ethylene glycol-bis-(*b*-aminoethylether)-*N,N,N',N'*-tetraacetic acid (EGTA), ethylenediamine tetraacetic acid (EDTA), Tris, amytal, and atractyloside were obtained from "Sigma." Mannitol, sucrose, KCl, HEPES, and MgCl_2 were obtained from "Roth."

2.3. Preparation of Renal Mitochondria. Kidney tissue was cut into small pieces and homogenized in the medium containing 250 mM sucrose, 10 mM Tris-HCl, and 1 mM EDTA (pH 7.3). Cytosolic and mitochondrial fractions were separated by differential centrifugation (5 min at 750 $\times g$ and 10 min at 10,000 $\times g$, two times), and pellet was suspended in an isolation medium.

2.4. Measurement of Mitochondrial Respiration. Mitochondrial respiration (oxygen consumption) rate was measured at 37°C using Clark-type electrode in 1.5 ml incubation medium containing 150 mM KCl, 10 mM Tris-HCl, 5 mM KH_2PO_4 , and 1 mM $\text{MgCl}_2 \times 6\text{H}_2\text{O}$, pH 7.2. The mitochondrial leak respiration (V_0) was recorded in the medium supplemented with mitochondria and respiratory substrates: complex I dependent (5 mM glutamate + 5 mM malate) or complex II dependent (15 mM succinate + 2 mM amytal) but without ADP. Glutamate dehydrogenase oxidizes glutamate to α -ketoglutarate, and in this reaction, NAD^+ is reduced to NADH (NADH is a substrate for complex I of mitochondrial respiratory chain). Oxidation of succinate is coupled with reduction of FAD to FADH_2 (FADH_2 is a substrate for complex II of mitochondrial respiratory chain). Then, excess of ADP (1 mM) was added in order to measure the state 3 respiration rate (V_3). After addition of cytochrome *c*, respiration rate $V_3 + \text{cyt } c$ was registered. The increase in $V_3 + \text{cyt } c$ represents the damage of mitochondrial outer membrane and release of cytochrome *c*. Nonphosphorylating respiration rate (V_{ATR}) was measured in the presence of excess of atractyloside (0.12 mM) in order to inhibit ATP/ADP translocator and to block ATP synthesis.

2.5. Measurement of Complex I Activity. Mitochondria immediately after isolation were freeze-thawed four times. Complex I activity was determined spectrophotometrically by following the kinetics of NADH oxidation at 340 nm, in the medium containing 10 mM KH_2PO_4 (pH 8.0), 1 mg/ml Antimycin A, 0.1 mM NADH, 100 mM coenzyme Q_1 , and 0.05 mg/ml fractured mitochondria. Rotenone-sensitive NADH oxidation rate was recorded in the presence of 10 μmol of rotenone. Complex I activity was calculated

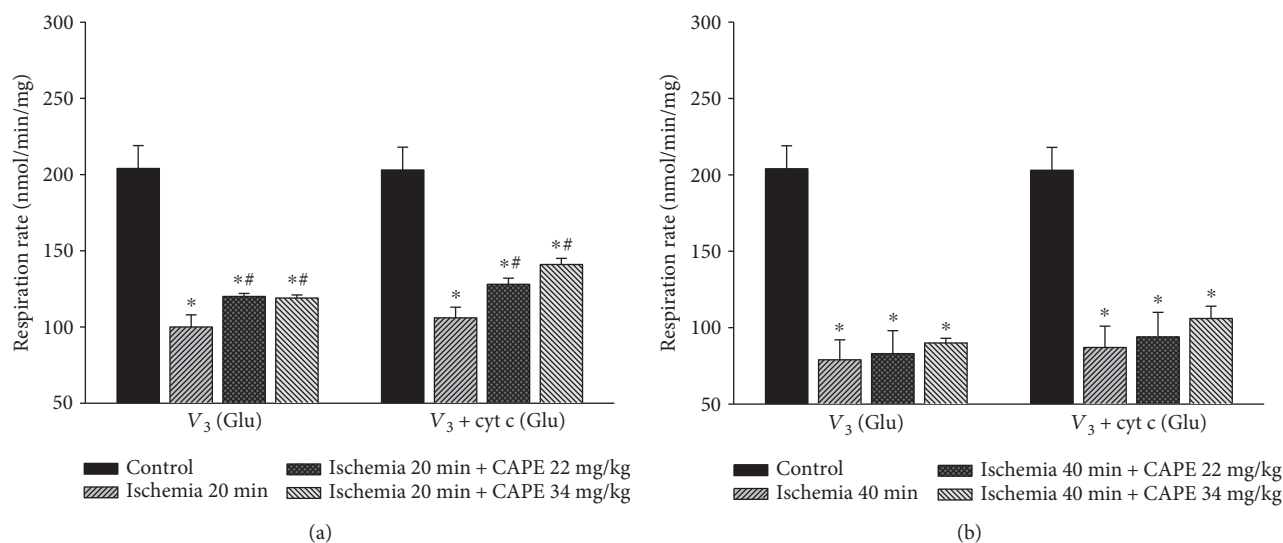


FIGURE 1: Effects of ischemia on renal mitochondrial state 3 respiration rate with glutamate/malate as substrates. Mitochondrial respiration rate was measured as described in Materials and Methods using 6 mM glutamate plus 6 mM malate as substrates; V_3 : state 3 respiration rate in the presence of 1 mM ADP; $V_3 + \text{cyt c}$: state 3 respiration rate in the presence of 32 μM cytochrome c. Each column represents the mean \pm SEM of 4 independent experiments; * $p < 0.05$ versus control; # $p < 0.05$ versus ischemia alone.

as the difference between NADH oxidation rate without/with rotenone using the NADH extinction coefficient $6.22 \text{ M}^{-1} \text{ cm}^{-1}$.

2.6. Measurement of Mitochondrial Calcium Uptake Capacity. Mitochondrial calcium uptake capacity was measured fluorimetrically (at 37°C) with Calcium Green-5N (excitation at 506 nm, emission at 535 nm) in medium containing 200 mM sucrose, 1 mM KH_2PO_4 , 10 mM Tris-HCl, 10 μM EGTA, 0.3 mM pyruvate plus 0.3 mM malate, pH 7.4, and 0.05 mg/ml of mitochondrial protein as described previously [15]. For calibration of the signal, known amounts of CaCl_2 (100 μM) were added. Then, CaCl_2 (100 μM) was added in two-minute intervals until opening of permeability transition pore occurred.

2.7. Measurement of Caspase Activity. Postmitochondrial supernatant was additionally centrifuged for 30 min at $10000\times g$, and the resulting supernatant was used for determination of caspase activity. For measurement of caspase-3-like activity, 1 mg/ml of total cytosolic protein was incubated for 60 min in buffer containing 250 mM sucrose, 5 mM HEPES, 2 mM EGTA (pH 7.3 at 37°C), and 0.1 mM acetyl-Asp-Glu-Val-Asp-7-amido-4-methylcoumarin (DEVD). The hydrolysis of caspase substrate was followed fluorimetrically, excitation was set at 380 nm, and emission at 460 nm. Substrate cleaving activity was completely suppressed by 0.02 mM N-acetyl-Asp-Glu-Val-Asp-aldehyde, a reversible inhibitor of caspase-3.

2.8. Electron Microscopy. The control and ischemic samples of 1.2×2.3 mm from the kidneys were transferred to the fixative buffer containing 2.5% glutaraldehyde in 0.1 M phosphate buffer (pH 7.4). The taken samples were stored in

fixative for at least 4 h at room temperature or overnight at 4°C and analyzed as described in [15].

2.9. Statistical Analysis. Data are presented as mean \pm SEM of 4 separate experiments. The mean for individual experiment was obtained from at least three repetitive measurements. Statistical analysis was performed using the software package SPSS version 16.0 for Windows.

3. Results

3.1. Effect of CAPE on Ischemia-Induced Mitochondrial Injury. To investigate if CAPE protects mitochondria from ischemia-induced mitochondrial damage, short time (20 min) and longer time periods (40 min) of ischemia were chosen. As shown in Figure 1(a), ADP-dependent (state 3) respiration (V_3) after 20 min of ischemia was decreased by 52% with glutamate/malate and by 44% with succinate, $p < 0.05$ (Figure 2(a)). Longer duration (40 min) of ischemia caused even greater (by 62%, Figure 1(b)) decrease of the state 3 respiration rate with glutamate/malate and succinate (decreased by 56%, Figure 2(b)). Respiratory control index (RCI) decreased by 58% and 70% with glutamate/malate as substrate and by 41% and 54% ($p < 0.05$) with succinate as substrate (Figures 3(a) and 3(b)) after 20 min and 40 min of ischemia, respectively, in accordance with the decrease in state 3 respiration rate. Leak respiration rate (i.e., without addition of ADP) remained unchanged (not shown). After addition of exogenous cytochrome c during state 3 respiration, respiratory rate ($V_3 + \text{cyt c}$) with glutamate + malate increased by 9% and 12% and with succinate by 32% and 93% ($p < 0.05$) after 20 min and 40 min of ischemia, respectively, as compared to the control group (Figures 2(a) and 2(b)), indicating that ischemia induced damage of mitochondrial outer membrane, which increased with the duration of

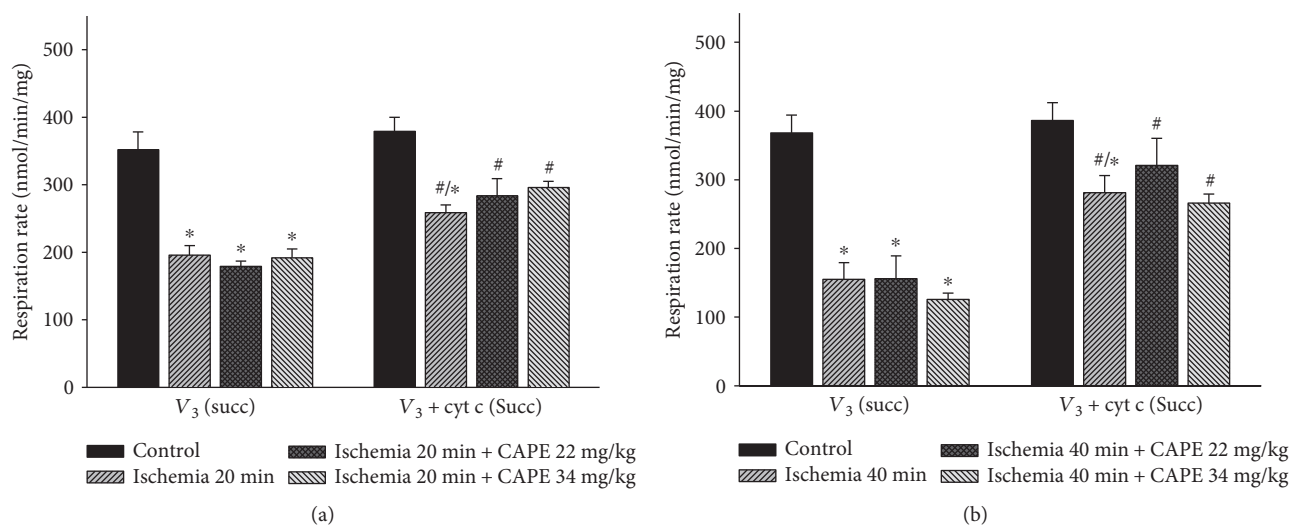


FIGURE 2: Effects of ischemia on renal mitochondrial state 3 respiration rate with succinate as substrate. Mitochondrial respiration rate was measured as described in Materials and Methods using 15 mM succinate (+2 mM amytal) as substrates. V_3 : state 3 respiration rate in the presence of 1 mM ADP; $V_3 + \text{cyt c}$: state 3 respiration rate in the presence of 32 μM cytochrome c. Each column represents the mean \pm SEM of 4 independent experiments; * $p < 0.05$ versus control; # $p < 0.05$ versus V_3 of respective group.

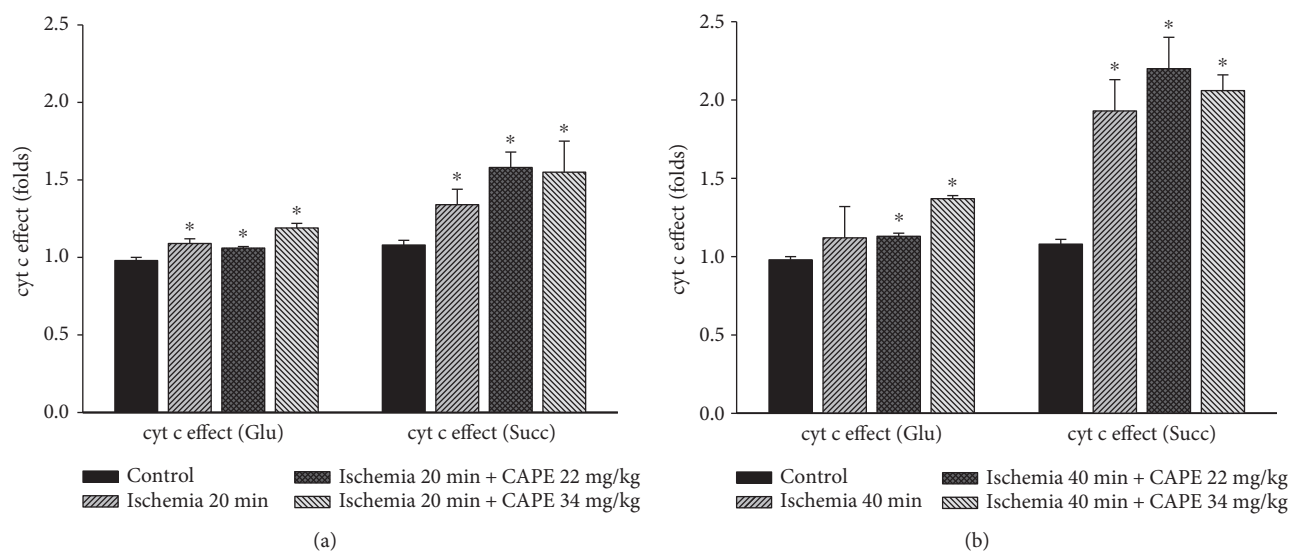


FIGURE 3: Influence of ischemia on cytochrome c effect. Cytochrome c effect was calculated as the $V_3 + \text{cyt c}/V_3$ ratio. $V_3 + \text{cyt c}$ respiration rate was measured in the presence of 1 mM ADP and 32 μM cytochrome c. Each column represents the mean \pm SEM of 4 independent experiments; * $p < 0.05$ versus control.

ischemia. The effect of cytochrome c ($V_3 + \text{cyt c}/V_3$ ratio), showing the stimulation of state 3 respiration rate after addition of cytochrome c after 20 min and 40 min of ischemia for both substrates glutamate/malate (1.09 and 1.12, resp.) and succinate (1.34 and 1.93, resp.) is shown in Figure 3. It clearly indicates the ischemia-caused damage of mitochondrial outer membrane, which was the most evidently observed in mitochondria respiring on succinate. After pretreatment of rats with two different doses (22 mg/kg and 34 mg/kg) of CAPE before 20 min of ischemia, the mitochondrial state 3 respiration (V_3) increased by 20% and 19% ($p < 0.05$), respectively (Figure 1(a)), and respiratory control index

(RCI) by 33% and 21% (Figure 4(a)) $p < 0.05$ with glutamate/malate as substrates. However, pretreatment of rats with the same doses of CAPE before longer time, 40 min of ischemia, had no protective effects on mitochondrial respiration rates. Moreover, CAPE had no protective effects on succinate oxidation neither after 20 min nor 40 min of ischemia (Figures 2 and 4). There was no protective effect on the mitochondrial outer membrane after pretreatment with CAPE, as the state 3 respiration rate in the presence of cytochrome c ($V_3 + \text{cyt c}$), Figures 1 and 2, and cytochrome c effect ($V_3 + \text{cyt c}/V_3$ ratio, Figure 3) remained similar with both substrates as compared to ischemia group.

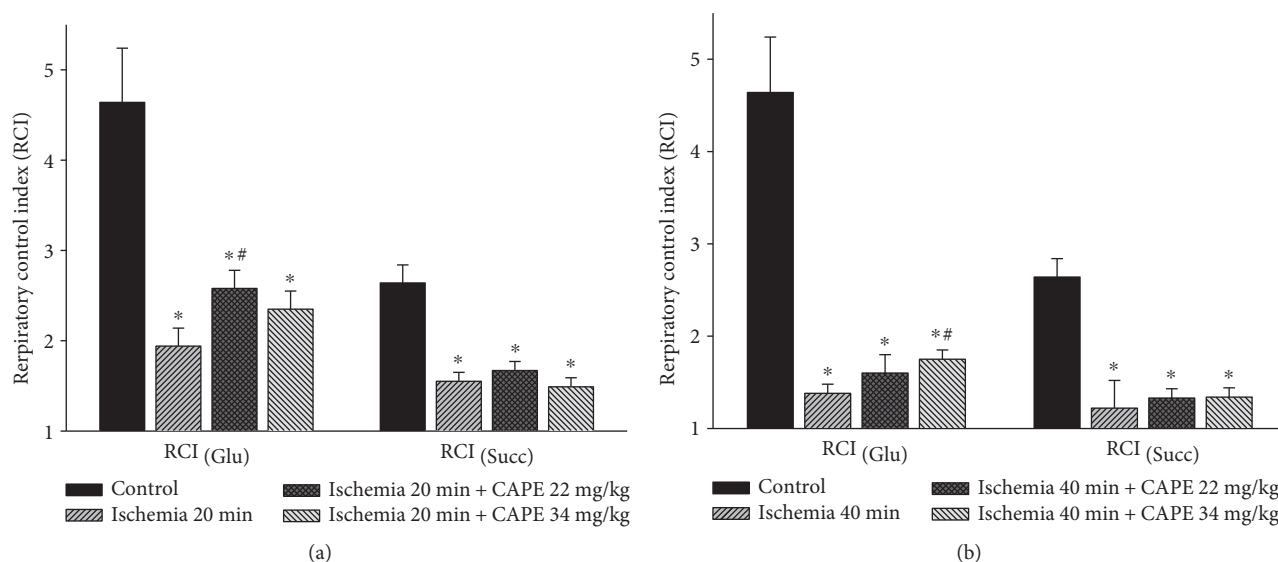


FIGURE 4: Effect of ischemia on mitochondrial respiratory control index (RCI). Measurements were performed in the presence of 5 mM glutamate + 5 mM malate or 15 mM succinate (+2 mM amytal) as substrates. Mitochondrial respiratory control index (RCI), that is, the ratio between oxygen uptake rates in state 3 and routine respiration rate ($RCI = V_3/V_0$). Each column represents the mean \pm SEM of 4 independent experiments; * $p < 0.05$ versus control; # $p < 0.05$ versus ischemia alone.

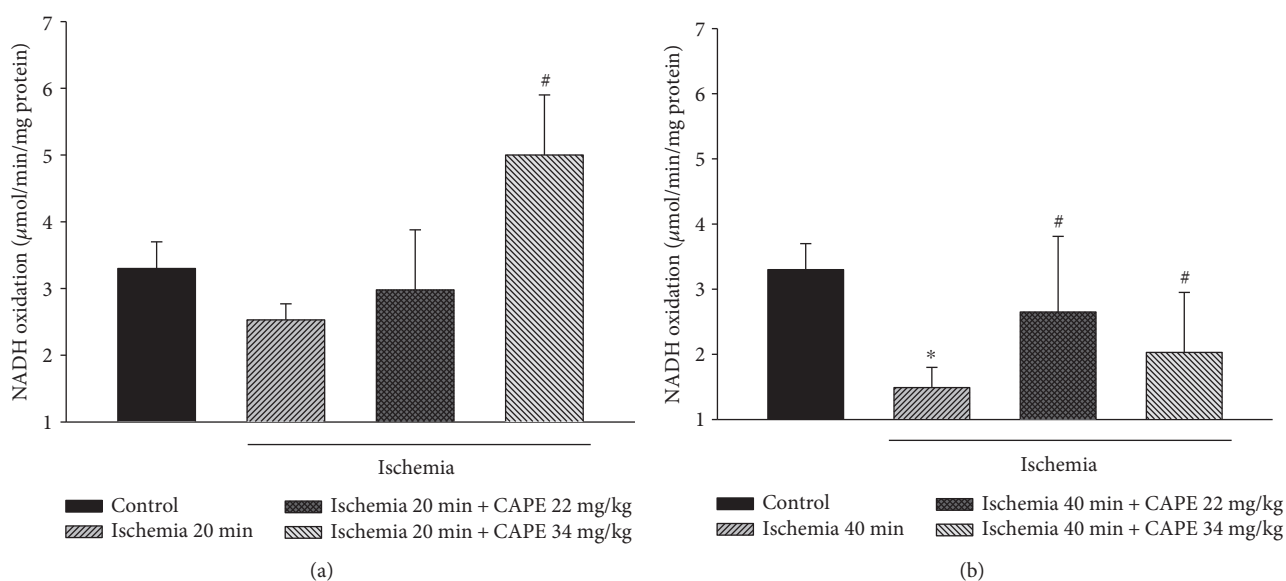


FIGURE 5: Effect of ischemia on complex I activity in kidney mitochondria. The complex I activity was measured spectrophotometrically at 340 nm as described in Materials and Methods. Each column represents the mean \pm SEM of 4 independent experiments; * $p < 0.05$ versus control; # $p < 0.05$ versus ischemia alone.

3.2. Effect of CAPE on Complex I Activity. As our results showed that mitochondrial respiration rate with glutamate/malate (complex I-linked substrates) was clearly reduced after ischemia, in addition, we measured the effects of ischemia on mitochondrial complex I activity. Our data revealed that the reduction of state 3 respiration rate after 20 min of ischemia was associated with the decrease in complex I activity by 23% (Figure 5(a)). After 40 min of ischemia, mitochondrial complex I activity was diminished by 54% ($p < 0.05$, Figure 5(b)). Pretreatment of animals with two different

doses of CAPE (22 mg/kg and 34 mg/kg) had protective effect on mitochondrial respiratory chain. After pretreatment with CAPE, complex I activity after 20 min of ischemia increased by 18% (22 mg/kg CAPE) and by 98%, $p < 0.05$ (34 mg/kg CAPE, Figure 5(a)). After 40 min of ischemia, complex I activity increased by 77%, $p < 0.05$ (22 mg/kg CAPE), and by 36%, $p < 0.05$ (34 mg/kg CAPE, Figure 5(b)).

3.3. CAPE Increases Mitochondrial Ca^{2+} Uptake. It is well known that mitochondria play a crucial role in intracellular

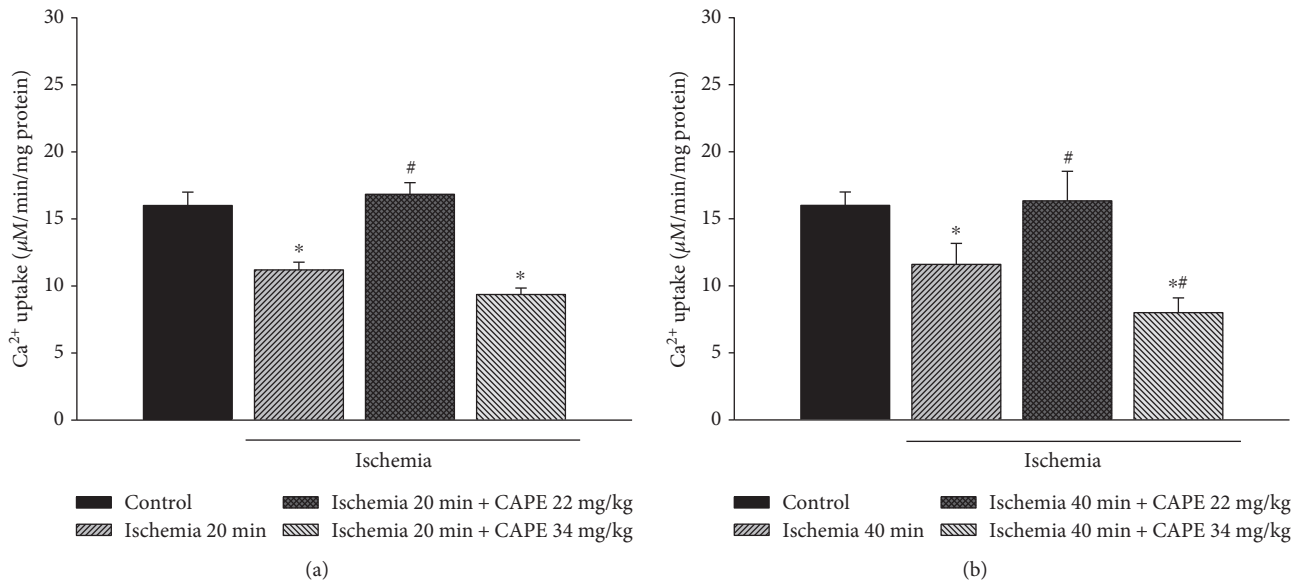


FIGURE 6: Mitochondrial Ca²⁺ uptake: effect of ischemia. Ca²⁺ uptake was measured fluorimetrically (excitation at 506 nm, emission at 535 nm) as described in Materials and Methods. Each column represents the mean \pm SEM of 4 independent experiments; * $p < 0.05$ versus control; # $p < 0.05$ versus ischemia alone.

Ca²⁺ signaling, taking up and releasing calcium upon different cellular conditions such as ischemia, oxidative stress, etc. Elevation of intramitochondrial calcium concentration after ischemia can trigger opening of mitochondrial permeability transition pore and cell death.

Fluorimetric Ca²⁺ measurements were performed in order to measure Ca²⁺ uptake by mitochondria after 20 and 40 min of ischemia alone or after pretreatment with CAPE. Our results indicated that in control mitochondria, Ca²⁺ uptake was 15.99 $\mu\text{mol}/\text{min mg protein}$. Ischemia 20 and 40 min reduced accumulation of calcium in mitochondria by 30% (Figures 6(a) and 6(b)). Pretreatment of rats with CAPE (22 mg/kg) significantly increased the mitochondrial Ca²⁺ uptake by 50% after 20 min of ischemia and by 41% after 40 min of ischemia (Figures 6(a) and 6(b)) as compared to ischemia alone. Pretreatment of animals with higher concentration of CAPE (34 mg/kg) had no protective effect on calcium accumulation in kidney mitochondria after ischemia.

3.4. CAPE Reduces Caspase Activation. As an indicator for apoptosis, we measured DEVD-cleaving caspase-3-like protease activity. After 20 min of ischemia, caspase-3-like activity in cytosolic fraction was increased by 1.15-fold as compared to control, whereas after pretreatment with CAPE (22 mg/kg and 34 mg/kg), caspase-3-like activity was diminished by 1.52 fold, $p < 0.05$, and returned to control level (Figure 7(a)). After 40 min of ischemia, caspase-3-like activity in cytosolic fraction was increased by 1.86-fold as compared to control. CAPE (22 mg/kg and 34 mg/kg) diminished caspase-3-like activity to control level (Figure 7(b)).

3.5. CAPE Reduced Lactate Dehydrogenase (LDH) Activity in Cytosolic Fraction. As an indicator for necrosis, lactate dehydrogenase (LDH) activity was measured in cytosolic fractions

in the control group and after ischemia (with and without pretreatment with CAPE). LDH activity in cytosolic fraction of control mitochondria was 27.8 ± 5.1 IU/mg protein and decreased by 35% and 56% after 20 min and 40 min of ischemia, respectively (Figures 8(a) and 8(b)). Pretreatment with CAPE (22 mg/kg) had no protective effect after 20 min of ischemia, but improved it after 40 min of ischemia (Figures 8(a) and 8(b)), that is, LDH activity in cytosolic fraction increased by 74% (to 21.1 IU/mg protein). After pretreatment with higher dose (34 mg/kg) of CAPE, activity of LDH was restored nearly to control level after both times of ischemia (Figures 8(a) and 8(b)).

3.6. Kidney Electron Microscopy. Electron microscopical findings revealed that CAPE (22 mg/kg and 34 mg/kg) did not affect the ultrastructure of control mitochondria—they showed normal mitochondrial ultrastructure—parallel cristae, uniform matrix, and uninterrupted outer membrane. Both parts of intermembrane space—intracristal and peripheral—are narrow and even (Figures 9(a) and 9(b)). CAPE pretreatment before 20 min of ischemia affected mainly mitochondrial matrix making it slightly swollen and perforated by empty patches in some cells. Mitochondria after pretreatment with CAPE (22 mg/kg) showed less swollen matrix (Figure 9(c)) comparing with the higher CAPE concentration (34 mg/kg) (Figure 9(d)). Following enlarged matrix cristae lose their parallel arrangement and rearrange to radial location filling almost all volume of mitochondria (Figure 9(d)). After 40 min of ischemia, mitochondria increased in size due to enlarged amount of matrix; their cristae lost parallel arrangement. Seldom, mitochondria were seen broken (Figures 9(e) and 9(f)). However, CAPE (22 mg/kg) preserved continuous matrix with sporadically seen small patches and only partly lost cristae parallelism (Figure 9(e)). Higher dose of CAPE (34 mg/kg) preserved

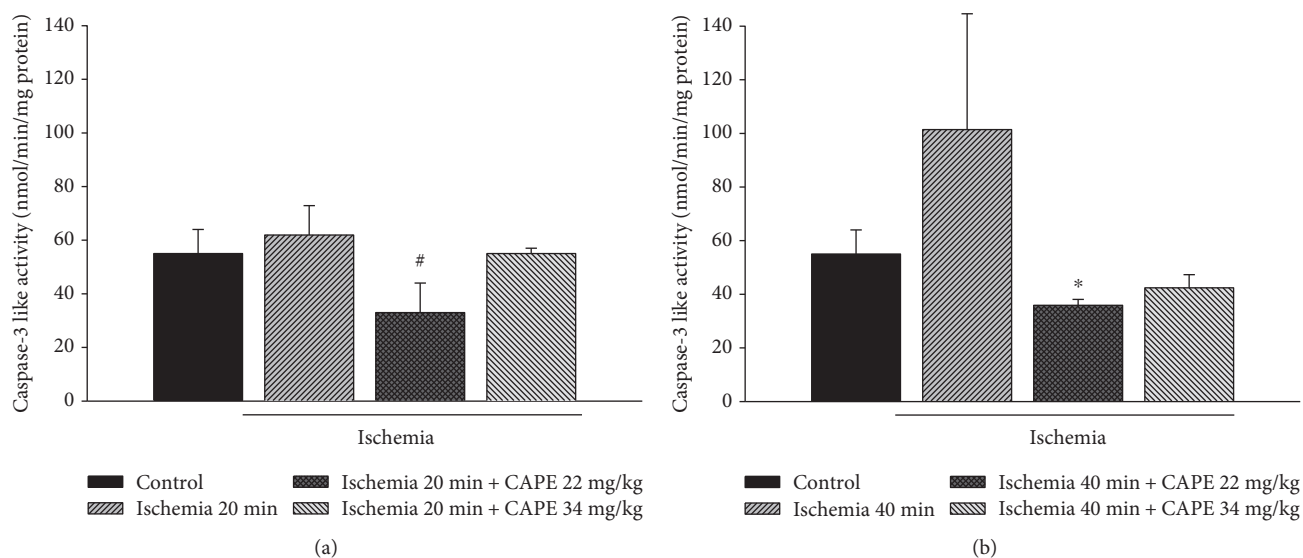


FIGURE 7: Effect of ischemia on caspase-3 activity. The caspase-3 activity was measured as described in Materials and Methods. Each column represents the mean \pm SEM of 4 independent experiments; * $p < 0.05$ versus control; # $p < 0.05$ versus ischemia alone.

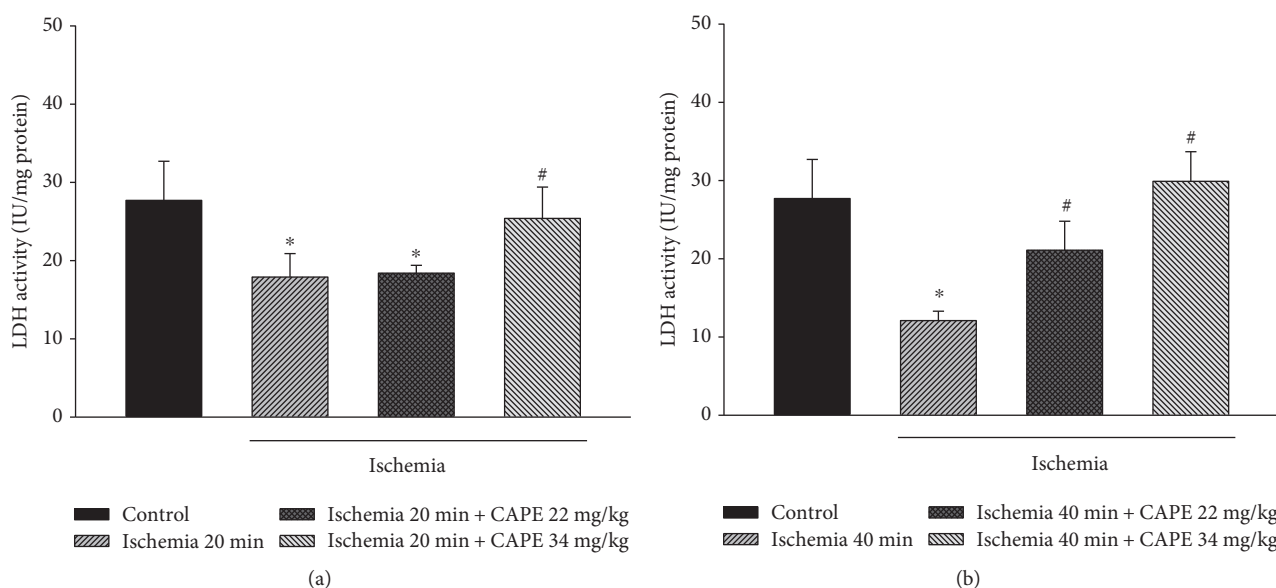


FIGURE 8: LDH activity in cytosolic fraction after ischemia. LDH activity was measured as described in Materials and Methods. Each column represents the mean \pm SEM of 4 independent experiments; * $p < 0.05$ versus control; # $p < 0.05$ versus ischemia alone.

ultrastructure of mitochondria; less and swollen matrix with disintegrated cristae and ruptured outer membrane were usually observed (Figure 9(f)). Intermembrane space in all experimental groups was narrow and even.

4. Discussion

Mitochondria play an important role in the pathogenesis of ischemic kidney injury as they are responsible for more than 90 percent energy production by oxidative phosphorylation [16]. Therefore, the decrease in mitochondrial function may lead to renal dysfunction and cell death. The protective

substances against ischemic kidney injury especially when prolonged time of ischemia during kidney surgery is necessary are of great importance.

In this study, we investigated if CAPE has potential protective effects against short (20 min) and longer time (40 min) ischemia-induced kidney damage in an *in vitro* rat model of warm kidney ischemia. We measured mitochondrial functions, mitochondrial calcium uptake, caspase-3 activation, and lactate dehydrogenase amount. Our novel finding is that CAPE ameliorates in part ischemia (20 min)-induced renal mitochondrial injury in rats, improves oxidative phosphorylation with complex I-dependent substrate glutamate/malate,

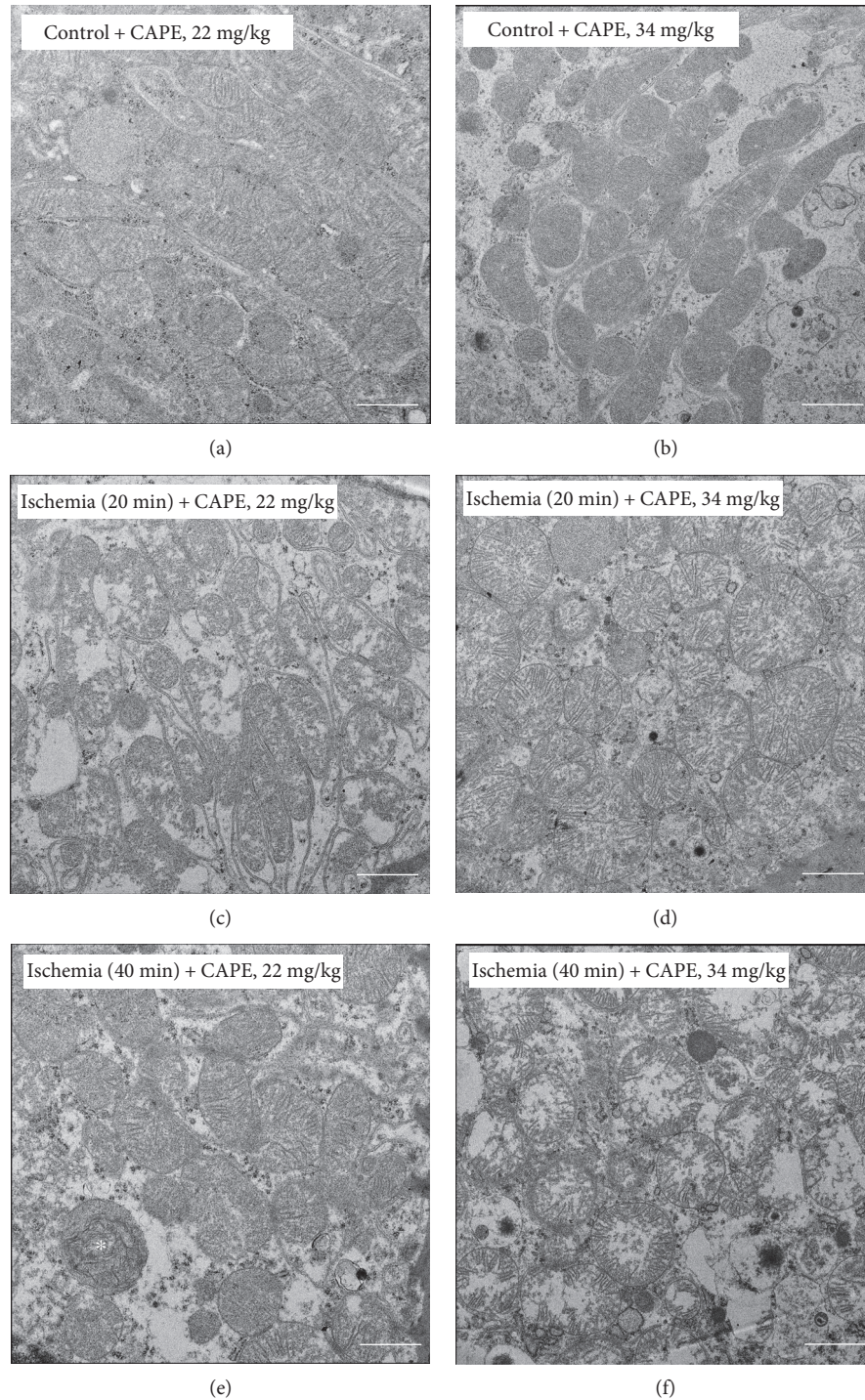


FIGURE 9: Ultrastructural changes to mitochondria. (a, b) Control. Mitochondria display normal morphology—shape is from round to elongate depending on the section, cristae are arranged in parallel rows at regular intervals, and the matrix is evenly dense. Note that normal morphology is characteristic to all mitochondria despite their irregular distribution in renal cells. (c, d) 20 min ischemia affected mitochondria: matrix is enlarged, uneven, and partly interrupted by empty patches; the outer and inner mitochondrial membranes are close and parallel. In 22 mg/kg CAPE group (c), cristae are parallel ranged; however, in CAPE 34 mg/kg group (d), irregular orientation of cristae can be seen. (e, f) 40 min ischemia affected mitochondria. (e) Cell with moderately preserved mitochondria in CAPE 22 mg/kg group: matrix is slightly enlarged with seldom empty patches, cristae are irregularly oriented, and the outer membrane is discontinuous. Note a mitochondrion with fully lost inner structure (*). (f) Mitochondria in CAPE 34 mg/kg group possess noticeably swollen matrix and exclusively peripheral cristae, while the outer membrane is ruptured in many places. N: nucleus; RER: rough endoplasmic reticulum; Ex: extracellular space. Scale bar: 1 μm .

increases Ca^{2+} uptake by mitochondria, partially blocks ischemia-induced caspase-3 activation, and protects kidney cells from ischemia-induced necrosis. Thus, a single intraperitoneal injection of CAPE (22 mg/kg and 34 mg/kg) 1.5 hour before ischemia partially protects mitochondria from injury caused by ischemia. The protective effects on mitochondrial respiration rates were seen after shorter (20 min) time of ischemia whereas reduction of apoptosis and necrosis and increase in Ca^{2+} uptake were revealed after both, shorter (20 min) and longer (40 min) time of ischemia.

The model of 20 and 40 min kidney ischemia *in vitro* was chosen because, according to our results [15], 20 min was the shortest period of ischemia that induced statistically significant changes in renal mitochondrial respiratory functions. Moreover, our results showed that 40 min of kidney ischemia induced much more severe mitochondria structural and metabolic changes. The dose of CAPE (22 mg/kg or 34 mg/kg) was chosen based on the reported doses (intraperitoneal or intravenous) in the literature, ranging between from 1 mg/kg to 40 mg/kg [12, 13, 17]. They showed that CAPE at abovementioned doses ameliorates oxidative damage caused by ischemia/reperfusion in brain, or intestine tissue [12, 13, 17]. According to literature data, CAPE distributes into tissues extensively [18] and the elimination half-life is ranging between 21.2–26.7 min [18] after intravenous administration.

Ince et al. described cardioprotective effects of CAPE in short time ischemia (8 min)-reperfusion (8 min) model of rats. The protective effects are explained by decreased activity of xanthine oxidase and direct antioxidant effects [19]. Other authors [20–24] showed the protective effects of CAPE against oxidative stress-induced kidney injury. CAPE exerts antioxidant activity by suppressing lipid peroxidation, scavenging ROS, and inhibiting activity of nitric oxide synthase and xanthine oxidase [25]. It has been shown [26] that CAPE at concentration of 10 μM inhibited the xanthine/xanthine oxidase system in human neutrophils and decreased production of reactive oxygen species. It is known that CAPE is a lipophilic compound and may interact with phospholipid bilayers of membranes, including mitochondria, and in this way might protect cell organelles from ROS-induced damage. Phenethyl group enhanced the radical scavenging capacity of CAPE as esterification of phenolic acids increases lipophilicity, and they can better incorporate into membranes. The antiradical activities of CAPE are explained by orthodihydroxyl functionality in the catechol ring [27]. So, we hypothesize that at least a partial protective effects against oxidative stress-induced tissue damage may be related to CAPE action at the mitochondrial level. However, most of the studies were done by investigating the markers of oxidative stress, and there is a lack of data on mitochondrial status. There are only a few studies regarding CAPE effects on mitochondria. Recently, Kobroob et al. [23] showed that CAPE restored the decline in mitochondrial membrane potential in renal mitochondria during oxidative stress caused by cadmium and attenuated cadmium-induced swelling of mitochondria. Moreover, another study [28] revealed that CAPE and its related compounds protect mouse brain and liver mitochondria from damage during *in vitro* anoxia-

reoxygenation. Thus, our study revealed a partial increase in mitochondrial oxidative phosphorylation capacity with NAD-linked substrate glutamate/malate after administration of CAPE prior induction of short (20 min) ischemia. We also showed that the ischemia-diminished activity of complex I was also protected after CAPE injection. As complex II—dependent substrate—succinate oxidation was not improved by CAPE, we conclude that CAPE has specific action on complex I.

Feng et al. revealed that the protective effects of CAPE are due to limiting of mitochondrial membrane lipoperoxidation, membrane fluidity, and protein carbonylation in anoxia-reoxygenation, which resulted in the maintenance of mitochondrial function [28]. Our results also revealed the restoration of mitochondrial functions (a partial increase in the state 3 respiration rate and in a respiratory control index) after CAPE pretreatment before 20 min of ischemia. However, pretreatments of rats with CAPE before induction of severe 40 min ischemia had no protective effects on mitochondrial respiration rates, but it had positive effects on reduction of apoptosis, necrosis, and Ca^{2+} uptake by mitochondria.

It is well known that mitochondria play a crucial role in intracellular Ca^{2+} signaling. Mitochondria can transiently accumulate large amounts of Ca^{2+} if cytosolic Ca^{2+} concentration increases as response to ischemia, stress, or other pathological conditions. They can locally buffer Ca^{2+} modulating the activity of Ca^{2+} channels if there is Ca^{2+} influx through the plasma membrane. In mitochondria, Ca^{2+} at physiological concentrations can regulate mitochondrial energy metabolism whereas calcium overload can induce the release of cytochrome c and activation of apoptotic cell death [29]. Our results indicated that in kidney mitochondria, ischemia (20 and 40 min) induced decreases in oxidative phosphorylation and subsequent Ca^{2+} uptake. It is important to note that mitochondrial Ca^{2+} uptake after ischemia (20 min and 40 min) was clearly improved after administration of CAPE (22 mg/kg). The increased capacity of mitochondria to uptake calcium may be due to increase in oxidative phosphorylation capacity caused by CAPE.

Moreover, we also revealed that increase in caspase-3 activation during ischemia was blocked by CAPE (22 mg/kg). These results are in line with the observation of Tan et al. who showed that in heart mitochondria, CAPE (3 mg/kg), injected 60 min before ischemia, protects from calcium-induced caspase-3 activation [30]. Thus, CAPE, depending on concentration, has a protective effect from caspase activation. Moreover, our results showed that not only apoptosis but also necrosis occurs after ischemia: as LDH changes in cytosolic fraction after both time of ischemia as compared to control, it shows the signs of necrosis as well. It is possible that both, apoptosis and necrosis, occur in ischemic kidney. Our results revealed that both used concentrations of CAPE-reduced LDH release and diminished necrosis.

Ultrastructural investigation revealed that CAPE had protected from ischemia (20 min)-induced mitochondrial damage. Previously, we have demonstrated that ischemia mainly affects the mitochondrial intermembrane space,

where intracristal space was found enlarged resulting in ballooned cristae as well as enlarged peripheral space followed by detachment of outer and inner membranes [15]. Application of CAPE preserved intermembrane space from edema after 20 min of ischemia, as it was found narrow and uniform in all experimental groups. No ballooned cristae, with enlarged intracristal space or detachment of outer and inner membranes resulting in enlarged peripheral space, were observed in this study. Though pretreatment with the higher dose (34 mg/kg) of CAPE protected slightly mitochondrial functions (oxidative phosphorylation, activity of mitochondrial complex I, LDH), whereas ultrastructure of mitochondria in some kidney tissue slices showed swollen matrix with disintegrated cristae and ruptured outer mitochondrial membrane, thus it seems that higher dose of CAPE did not protect ultrastructure of mitochondria. The obtained effects may be associated with the heterogeneity of mitochondria. Our observations suggest that different renal cell types are affected by ischemia to a different extent. Thus, it would be feasible to investigate the protective properties of CAPE in different renal cell types.

In conclusion, our study revealed partial protection of mitochondrial function after pretreatment of rats with intraperitoneal injection of CAPE. Since CAPE has beneficial, including antioxidant and anti-inflammatory, effects as well as partially preserves mitochondrial function, we think that this compound may have a potential to protect the kidney from ischemia-induced damage. The mechanisms of protection are not fully understood yet, but at least, partially, it is associated with the improvement of mitochondrial status in the cells. Further studies will be required for the better characterization of the mechanism of CAPE action.

Disclosure

The manuscript is based on the paper published as an abstract in *European Urology Supplements Journal* 2014 and available at the following link: <http://www.eusupplements.europeanurology.com/article/S1569-9056>.

Conflicts of Interest

The authors confirm that this article content has no conflict of interests.

References

- [1] M. Malek and M. Nematbakhsh, "Renal ischemia/reperfusion injury; from pathophysiology to treatment," *Journal of Renal Injury Prevention*, vol. 4, no. 2, pp. 20–27, 2015.
- [2] F. Becker, H. Van Poppel, O. W. Hakenberg et al., "Assessing the impact of ischaemia time during partial nephrectomy," *European Urology*, vol. 56, pp. 625–634, 2009.
- [3] G. Kroemer and J. C. Reed, "Mitochondrial control of cell death," *Nature Medicine*, vol. 6, pp. 513–519, 2000.
- [4] R. H. Thompson, B. R. Lane, C. M. Lohse et al., "Every minute counts when the renal hilum is clamped during partial nephrectomy," *European Urology*, vol. 58, pp. 340–345, 2010.
- [5] D. J. Parekh, J. M. Weinberg, B. Ercole et al., "Tolerance of the human kidney to isolated controlled ischemia," *Journal of the American Society of Nephrology*, vol. 24, pp. 506–517, 2013.
- [6] Y. J. Chen, A. C. Huang, H. H. Chang et al., "Caffeic acid phenethyl ester, an antioxidant from propolis, protects peripheral blood mononuclear cells of competitive cyclists against hyperthermal stress," *Journal of Food Science*, vol. 74, pp. H162–H167, 2009.
- [7] L. M. LeBlanc, A. F. Pare, J. Jean-Francois, M. J. Hebert, M. E. Surette, and M. Touaibia, "Synthesis and antiradical/antioxidant activities of caffeic acid phenethyl ester and its related propionic, acetic, and benzoic acid analogues," *Molecules*, vol. 17, pp. 14637–14650, 2012.
- [8] A. Gokce, S. Oktar, Z. Yonden et al., "Protective effect of caffeic acid phenethyl ester on cyclosporine A-induced nephrotoxicity in rats," *Renal Failure*, vol. 31, pp. 843–847, 2009.
- [9] A. Gurel, F. Armutcu, S. Sahin et al., "Protective role of alpha-tocopherol and caffeic acid phenethyl ester on ischemia-reperfusion injury via nitric oxide and myeloperoxidase in rat kidneys," *Clinica Chimica Acta*, vol. 339, pp. 33–41, 2004.
- [10] N. C. Roso, R. R. Correa, Y. M. Castiglia et al., "Caffeic acid phenethyl ester effects in the kidney during ischemia and reperfusion in rats anesthetized with isoflurane," *Transplantation Proceedings*, vol. 44, pp. 1211–1213, 2012.
- [11] N. Aydogdu, G. Atmaca, O. Yalcin, K. Batcioglu, and K. Kaymak, "Effects of caffeic acid phenethyl ester on glycerol-induced acute renal failure in rats," *Clinical and Experimental Pharmacology & Physiology*, vol. 31, pp. 575–579, 2004.
- [12] X. Wei, L. Zhao, Z. Ma et al., "Caffeic acid phenethyl ester prevents neonatal hypoxic-ischaemic brain injury," *Brain*, vol. 127, pp. 2629–2635, 2004.
- [13] M. Khan, C. Elango, M. A. Ansari, I. Singh, and A. K. Singh, "Caffeic acid phenethyl ester reduces neurovascular inflammation and protects rat brain following transient focal cerebral ischemia," *Journal of Neurochemistry*, vol. 102, pp. 365–377, 2007.
- [14] H. Parlakpinar, E. Sahna, A. Acet, B. Mizrak, and A. Polat, "Protective effect of caffeic acid phenethyl ester (CAPE) on myocardial ischemia-reperfusion-induced apoptotic cell death," *Toxicology*, vol. 209, pp. 1–14, 2005.
- [15] R. Baniene, D. Trumbeckas, M. Kincius et al., "Short ischemia induces rat kidney mitochondria dysfunction," *Journal of Bioenergetics and Biomembranes*, vol. 48, no. 1, pp. 77–85, 2016.
- [16] R. Che, Y. Yuan, S. Huang, and A. Zhang, "Mitochondrial dysfunction in the pathophysiology of renal diseases," *American Journal of Physiology-Renal Physiology*, vol. 306, pp. F367–F378, 2014.
- [17] Y. Yildiz, M. Serter, R. O. Ek et al., "Protective effects of caffeic acid phenethyl ester on intestinal ischemia-reperfusion injury," *Digestive Diseases and Sciences*, vol. 54, pp. 738–744, 2009.
- [18] S. Akyol, Z. Ginis, F. Armutcu, G. Ozturk, M. R. Yigitoglu, and O. Akyol, "The potential usage of caffeic acid phenethyl ester (CAPE) against chemotherapy-induced and radiotherapy-induced toxicity," *Cell Biochemistry and Function*, vol. 30, pp. 438–443, 2012.
- [19] H. Ince, E. Kandemir, C. Bagci, M. Gulec, and O. Akyol, "The effect of caffeic acid phenethyl ester on short-term acute myocardial ischemia," *Medical Science Monitor*, vol. 12, pp. BR187–BR193, 2006.

- [20] M. Ogeturk, I. Kus, N. Colakoglu, I. Zararsiz, N. Ilhan, and M. Sarsilmaz, "Caffeic acid phenethyl ester protects kidneys against carbon tetrachloride toxicity in rats," *Journal of Ethnopharmacology*, vol. 97, pp. 273–280, 2005.
- [21] S. Ozen, O. Akyol, M. Iraz et al., "Role of caffeic acid phenethyl ester, an active component of propolis, against cisplatin-induced nephrotoxicity in rats," *Journal of Applied Toxicology*, vol. 24, pp. 27–35, 2004.
- [22] O. Wongmekiat, S. Gomonchareonsiri, and K. Thamprasert, "Caffeic acid phenethyl ester protects against oxidative stress-related renal dysfunction in rats treated with cyclosporin A," *Fundamental & Clinical Pharmacology*, vol. 25, pp. 619–626, 2011.
- [23] A. Kobroob, N. Chattipakorn, and O. Wongmekiat, "Caffeic acid phenethyl ester ameliorates cadmium-induced kidney mitochondrial injury," *Chemico-Biological Interactions*, vol. 200, pp. 21–27, 2012.
- [24] P. Gong, F. Chen, X. Liu, X. Gong, J. Wang, and Y. Ma, "Protective effect of caffeic acid phenethyl ester against cadmium-induced renal damage in mice," *The Journal of Toxicological Sciences*, vol. 37, pp. 415–425, 2012.
- [25] M. Hosnuter, A. Gurel, O. Babuccu, F. Armutcu, E. Kargi, and A. Isikdemir, "The effect of CAPE on lipid peroxidation and nitric oxide levels in the plasma of rats following thermal injury," *Burns*, vol. 30, pp. 121–125, 2004.
- [26] G. F. Sudina, O. K. Mirzoeva, M. A. Pushkareva, G. A. Korshunova, N. V. Sumbatyan, and S. D. Varfolomeev, "Caffeic acid phenethyl ester as a lipoxygenase inhibitor with antioxidant properties," *FEBS Letters*, vol. 329, pp. 21–24, 1993.
- [27] W. M. Wu, L. Lu, Y. Long et al., "Free radical scavenging and antioxidative activities of caffeic acid phenethyl ester (CAPE) and its related compounds in solution and membranes: a structure–activity insight," *Food Chemistry*, vol. 105, no. 1, pp. 107–115, 2007.
- [28] Y. Feng, Y. W. Lu, P. H. Xu et al., "Caffeic acid phenethyl ester and its related compounds limit the functional alterations of the isolated mouse brain and liver mitochondria submitted to in vitro anoxia-reoxygenation: relationship to their antioxidant activities," *Biochimica et Biophysica Acta (BBA) - General Subjects*, vol. 1780, pp. 659–672, 2008.
- [29] K. S. Kumaran and P. S. Prince, "Caffeic acid protects rat heart mitochondria against isoproterenol-induced oxidative damage," *Cell Stress & Chaperones*, vol. 15, pp. 791–806, 2010.
- [30] K. Nomura, H. Imai, T. Koumura, T. Kobayashi, and Y. Nakagawa, "Mitochondrial phospholipid hydroperoxide glutathione peroxidase inhibits the release of cytochrome c from mitochondria by suppressing the peroxidation of cardiolipin in hypoglycaemia-induced apoptosis," *The Biochemical Journal*, vol. 351, pp. 183–193, 2000.

Research Article

Increased Mitochondrial Mass and Cytosolic Redox Imbalance in Hippocampal Astrocytes of a Mouse Model of Rett Syndrome: Subcellular Changes Revealed by Ratiometric Imaging of JC-1 and roGFP1 Fluorescence

Dörthe F. Bebensee,^{1,2} Karolina Can,^{1,2} and Michael Müller^{1,2}

¹Center for Nanoscale Microscopy and Molecular Physiology of the Brain (CNMPB), Georg-August-Universität Göttingen, Universitätsmedizin Göttingen, Göttingen, Germany

²Zentrum Physiologie und Pathophysiologie, Institut für Neuro- und Sinnesphysiologie, Humboldtallee, 23 Göttingen, Germany

Correspondence should be addressed to Michael Müller; mmuelle7@gwdg.de

Received 15 March 2017; Revised 16 June 2017; Accepted 27 June 2017; Published 13 August 2017

Academic Editor: Icksoo Lee

Copyright © 2017 Dörthe F. Bebensee et al. This is an open access article distributed under the Creative Commons Attribution License, which permits unrestricted use, distribution, and reproduction in any medium, provided the original work is properly cited.

Rett syndrome (RTT) is a neurodevelopmental disorder with mutations in the *MECP2* gene. Mostly girls are affected, and an apparently normal development is followed by cognitive impairment, motor dysfunction, epilepsy, and irregular breathing. Various indications suggest mitochondrial dysfunction. In Rett mice, brain ATP levels are reduced, mitochondria are leaking protons, and respiratory complexes are dysregulated. Furthermore, we found in *MeCP2*-deficient mouse (*Mecp2*^{-/-}) hippocampus an intensified mitochondrial metabolism and ROS generation. We now used emission ratiometric 2-photon imaging to assess mitochondrial morphology, mass, and membrane potential ($\Delta\Psi_m$) in *Mecp2*^{-/-} hippocampal astrocytes. Cultured astrocytes were labeled with the $\Delta\Psi_m$ marker JC-1, and semiautomated analyses yielded the number of mitochondria per cell, their morphology, and $\Delta\Psi_m$. *Mecp2*^{-/-} astrocytes contained more mitochondria than wild-type (WT) cells and were more oxidized. Mitochondrial size, $\Delta\Psi_m$, and vulnerability to pharmacological challenge did not differ. The antioxidant Trolox opposed the oxidative burden and decreased the mitochondrial mass, thereby dampening the differences among WT and *Mecp2*^{-/-} astrocytes; mitochondrial size and $\Delta\Psi_m$ were not markedly affected. In conclusion, mitochondrial alterations and redox imbalance in RTT also involve astrocytes. Mitochondria are more numerous in *Mecp2*^{-/-} than in WT astrocytes. As this genotypic difference is abolished by Trolox, it seems linked to the oxidative stress in RTT.

1. Introduction

Rett syndrome (RTT) is a postnatal, X-chromosome linked, progressive neurodevelopmental disorder. The first RTT cases were reported in 1966 by the Austrian pediatrician Andreas Rett [1]; the characteristic symptoms include autistic features, dementia, motor dysfunction, loss of facial expressions, stereotypical hand movements, severe respiratory disturbances, and epilepsy [1–3]. RTT almost exclusively affects girls, typically at an incidence of 1:10,000–15,000 [4]. In boys, it is either lethal or due to severe neonatal encephalopathy death occurs during the first year [5]. Despite

being a rare disease, RTT—next to Down syndrome—is the second most common genetic cause of severe cognitive disabilities in girls [4].

The main causes of classical RTT are de novo mutations of the *MECP2* (methyl-CpG-binding protein 2) gene. It is located on the long arm of the X chromosome (Xq28) [6] and functions as a transcriptional modulator by either mediating gene silencing [7] or acting as transcriptional activator [8]. The spontaneous *MECP2* mutations underlying RTT mostly occur in the paternal X chromosome [9, 10]. In the affected girls, the disease manifests in early childhood and progresses in four stages: An initial and apparently normal

development (stage 1) is followed by a fast regression (stage 2), and then, a plateau or pseudostationary phase manifests (phase 3), which is concluded by a late motor deterioration (phase 4) [3, 11]. The life expectancy varies with clinical severity, and some Rett patients may reach the age of 70 years [12]. Often, death arises from cardiac/respiratory insufficiency, acute infections, or sudden incidents at night [12, 13]. A causal therapy for RTT is currently not available. Yet, some symptoms can be partly ameliorated by pharmacotherapy [14, 15], occupational therapy, and/or physical therapy [16, 17].

The past years revealed that RTT is closely associated with mitochondrial alterations, and in view of the multitude of mitochondrial functions, these defects were proposed to contribute to disease progression [18, 19]. It was even speculated whether RTT may represent a mitochondrial disease [20]. Morphological alterations of mitochondria were first detected in muscle biopsy samples of Rett patients, whose mitochondria appeared swollen or dumbbell-shaped [21] and exhibited granular inclusions, vacuolizations, and membranous changes [22, 23]. Post mortem studies on frontal lobe confirmed structural changes of mitochondria also for the brain [22].

Detailed follow-up biochemical analyses revealed a reduced expression of a subunit of cytochrome c oxidase (complex IV of the respiratory chain) in post mortem frontal cortex [24], which could impair ATP synthesis. Furthermore, comparative gene-array analyses on patient lymphomonocytes indicated a differential expression of various genes pivotal to mitochondrial function and/or organization [25]. In mouse models of RTT, symptomatic animals also showed reduced enzyme activities of respiratory chain complexes II, III, IV, and ANT1, as well as reduced glutathione levels in the brain and/or skeletal muscle [26–29]. Furthermore, the *ANT1* gene encoding the mitochondrial adenine nucleotide translocase is highly upregulated in the *Mecp2*^{-/-} mouse brain and Rett patient fibroblasts [30], the latter of which also show clear signs of metabolic mitochondrial dysregulation, oxidative stress, and diminished redox-balancing capabilities [31]. Also, the elevated blood lactate and pyruvate levels suggest defects in the mitochondrial respiratory chain and the urea cycle [32]. Obvious consequence of these mitochondrial changes is a less efficient respiratory chain and thus limited ATP synthesis. Indeed, magnetic resonance tomography and biochemical assays confirmed reduced brain ATP levels in male and female *Mecp2*-mutant mice [26, 33]. In view of the severe respiratory disturbances and frequent apneas in Rett patients [34–36], systemic hypoxia may occur and challenge mitochondrial function further. This led to the assumption that the various mitochondrial abnormalities are causal events in RTT. They may contribute to the complex symptoms of RTT and promote disease progression either directly or indirectly by generating free radicals and provoking redox imbalance [18, 19, 28, 29, 37–40].

The mostly neuronal alterations in RTT [41–43] originally suggested a purely neuronal disorder. Only later glial cells were confirmed to contain MeCP2 and to be affected by *Mecp2* mutations as well [44]. Meanwhile, it is clear that

also glial cells contribute to disease progression by exerting negative effects on neurons [45, 46]. In MeCP2-deficient mice, re-expression of MeCP2 specifically in astrocytes improved motor function, respiratory regularity, and anxiety, and the life-expectancy increased significantly as compared to mice lacking MeCP2 [45]. Restoring MeCP2 in oligodendrocytes was also beneficial, ameliorating motor symptoms and normalizing body weights [46]. Also, MeCP2-deficient microglia contribute to disease progression, as its intensified glutamate release provokes dendritic malformations, microtubule derangement, and damage of postsynaptic glutamatergic components [47]. Therefore, we here assessed to what degree also astrocytes show mitochondrial alterations. Using advanced optical tools, we took a closer look at the function and morphology of these organelles in cultured astrocytes of neonatal *Mecp2*^{-/-} and WT mice and also quantified cellular redox conditions. Our particular focus was on the hippocampus, as this brain area is metabolically demanding and vulnerable to oxidative stress.

2. Materials and Methods

This study was performed on *Mecp2* knockout mice [B6.129P2(C)-*Mecp2*^{tm.1.1Bird}, [48]]. To ensure uniform conditions, that is, total MeCP2 deficiency, only male wild-type (WT) and male Rett mice (*Mecp2*^{-/-}) were used. *Mecp2*^{-/-} mice show a more severe disease progression and develop earlier symptoms as compared to heterozygous female Rett mice [48]. All procedures met the German regulations and were authorized by the Office of Animal Welfare of the University Medical Center Göttingen.

2.1. Solutions. If not mentioned differently, all compounds were purchased from Sigma-Aldrich. The artificial cerebrospinal fluid (ACSF) contained 130 mM NaCl, 3.5 mM KCl, 1.25 mM NaH₂PO₄, 24 mM NaHCO₃, 1.2 mM CaCl₂, 1.2 mM MgSO₄, and 10 mM dextrose. It was aerated continuously with carbogen gas mixture (95% O₂, 5% CO₂) to maintain a stable pH of 7.4 and a proper O₂ supply of the cells during the imaging experiments.

Minimum essential cell culture medium (MEM, Invitrogen) was supplemented with 0.2 mg/ml NaHCO₃, 0.1 mg/ml transferrin (Calbiochem/Merck), and 5 mg/ml glucose. For the initial plating of the cells, it furthermore contained 10% FCS (fetal calf serum, Biochrom), 25 μg/ml insulin, and 2 mM L-glutamine. After the first day in culture, a slightly different medium was used (growth medium), which contained 5% FCS, 0.5 mM L-glutamine, 20 μl/ml B27 50x supplement (Invitrogen), and 100 μg/ml penicillin-streptomycin (Biochrom).

For most drugs, we first prepared stock solutions. Sodium cyanide (CN⁻) was dissolved as 1 M aqueous stock and stored at -20°C; other experimental solutions containing CN⁻ were prepared from this stock right before use. FCCP (carbonylcyanide-4-(trifluoromethoxy) phenylhydrazone, Tocris Bioscience) was dissolved as 10 mM stock in dimethyl sulfoxide (DMSO) and stored at 4°C. The mitochondrial markers JC-1 (5,5',6,6'-tetrachloro-1,1',3,3'-tetraethylbenzimidazolylcarbocyanine iodide, Thermo Fisher Scientific)

and MitoTracker Red FM (Thermo Fisher Scientific) were dissolved in DMSO as 2 mg/ml and 1 μ M stocks, respectively, and kept frozen. The free-radical scavenger Trolox ((\pm)-6-hydroxy-2,5,7,8-tetramethylchromane-2-carboxylic acid) was first dissolved in DMSO and then added to cell culture medium for overnight treatment.

2.2. Preparation of Dissociated Hippocampal Cell Cultures. Cell cultures of hippocampal neurons and glial cells were prepared from 2- to 4-day-old mice as described earlier [49]. In brief, mice were decapitated, the brain was gently but quickly removed and immersed in ice-cold HBSS (Hank's balanced salt solution) containing 20% FCS. Both hippocampi were then isolated, cut with a scalpel into smaller pieces, and trypsinated (5 mg/ml, 10 min, 37°C). The cells were then dissociated by trituration and centrifuged (1500 rpm, 10 min, 4°C), and the pellet obtained was resuspended. Next, this cell suspension was plated on Matrigel (BD Biosciences)-coated glass cover slips, which were placed in 4-well culture plates (Nunc). Dissociated cell cultures were incubated at 37°C (5% CO₂ atmosphere). After 24 h, the medium was replaced with growth medium, and after another 3 days, growth factors as well as half of the medium were refreshed again. Experiments were performed between 3 and 10 days in vitro.

2.3. Multiphoton Imaging of Mitochondrial JC-1 Fluorescence. To visualize mitochondria and monitor their membrane potentials ($\Delta\Psi$ m), the membrane potential probe JC-1 was chosen. JC-1 accumulates in mitochondria depending on their $\Delta\Psi$ m, and it is ratiometric by emission [50–55]. Cells were bulk loaded with JC-1 (1 μ g/ml, 15 min) immediately before the experiments.

Our 2-photon laser-scanning microscope (TPLSM, Figure 1) is composed of a Ti:Sa laser system (Mai Tai eHP DS, Newport-Spectra Physics) and an upright microscope (BX51WI, Olympus) equipped with a TriM Scope II scan-head and ImSpector Control Software (LaVision BioTec). To separate the emitted fluorescence and the laser excitation, a 670 nm beam splitter (670DCXXR) was combined with an IR-block filter (HC 680/SP). Fluorescence was detected in nondescanned mode by highly sensitive photomultiplier tubes (PMTs; H7421/H7422, Hamamatsu). For emission ratiometric analyses, JC-1 was excited at 925 nm, and the emission was divided further in its green and red spectral components by using a 570 nm beam splitter (570DCXR) as well as 525/50 nm (green) and 617/73 nm (red) bandpass filters [54]. All optical filters were obtained from AHF Analysentechnik AG (Tübingen, Germany). For optimized optical resolution and detection efficiency, we chose a 63x 1.0 NA water immersion objective (Plan Achromat VIS-IR, Zeiss).

For the experiments, cell culture cover slips were placed in a submersion-style recording chamber, which was perfused continuously with warm (37°) ACSF at 4 ml/min flow rate. JC-1-labeled cells were allowed to adjust for 15–20 min, and then experiments were started. Imaging of individual cells was performed using a scanfield size of 80 \times 80 μ m (resolution 80 nm/pixel) and 1200 Hz line-scanning

frequency. To reduce pixel noise, 5-fold line averaging was applied. All 3-dimensional (3-d) image stacks were recorded with axial (Z)-increments of 0.25 μ m.

Before the analysis, each 3-d stack underwent blind deconvolution (Autodeblur 9.3, AutoQuant Imaging), based on the objective used (1.0 NA) and the center wavelengths of the two different emission channels (525 nm and 617 nm). For all further image analyses, Metamorph Offline 7.5 (Molecular Devices) was used. Background subtraction was not performed during the ratiometric calculations, as in the case of 2-photon excitation, out-of-focus light is virtually nonexistent. However, to ensure a sufficient coverage of the 8-bit pseudocolor palette, a scaling factor of 200 was introduced, and the JC-1 ratio was calculated as

$$R_{\text{JC-1}} = \left(\frac{F_{\text{green (530 nm)}} * 200}{F_{\text{red (590 nm)}}} \right). \quad (1)$$

2.4. Excitation Ratiometric Redox Imaging. Cytosolic redox balance was determined with the excitation ratiometric optical redox indicator roGFP1 (oxidation-reduction sensitive green fluorescent protein 1) [56]. Within 2-3 days upon transfection (lipofection) with roGFP1 expressing plasmids (see [57]), cultured astrocytes sufficiently expressed roGFP1. For excitation-ratiometric analyses, roGFP1 was excited alternately at 395 nm (100 ms exposure) and 470 nm (150 ms exposure) with frame rates of 0.1 Hz. The emission was recorded by a fully computerized CCD-camera imaging system (Polychrome II, TILL Photonics) at 525 nm, using a 63x 1.0 NA objective (Zeiss W-Plan Achromat VIS-IR) and applying 4 \times 4 pixel binning. The roGFP1 fluorescence ratio F_{395}/F_{470} was calculated in real time, as described earlier [40, 57–59]. For true quantitation, roGFP1 responses were calibrated to saturating doses of H₂O₂ (5 mM, 5 min) and DTT (10 mM, 5 min), to obtain those ratiometric values representing complete sensor oxidation/reduction. Based on these calibrations, the relative degree of roGFP1 oxidation (OxD_{roGFP1}) and the reduction potential (E_{roGFP1}) was calculated [57, 58, 60, 61] for WT and *Mecp2*^{-/-} astrocytes.

2.5. MitoTracker-Based Visualization of Mitochondria. Occasionally, we used MitoTracker Red to visualize mitochondria. Bulk-loaded cell cultures (1 μ g/mg, 20 min, 37°C) were excited at 550 nm, using the abovementioned CCD-camera imaging system and a 40x 0.8 NA water immersion objective (Zeiss Achroplan). MitoTracker emission was separated by a 570 nm dichroic mirror and a 590 nm longpass emitter, and single images were taken at an exposure time of 300 ms. Pixel binning was not applied.

2.6. Statistics. The analyzed neuron/glial cultures were obtained from 14 male WT and 15 male *Mecp2*^{-/-} mice. During experiments and data analyses, the genotype was still blinded; genotyping was performed at a later time-point from tail biopsies collected during dissection. Data are shown as mean \pm standard deviation, *n* reports the number of astrocytes studied. Depending on the type of experiment, significance of the differences and drug effects observed were determined using either paired or unpaired two-tailed

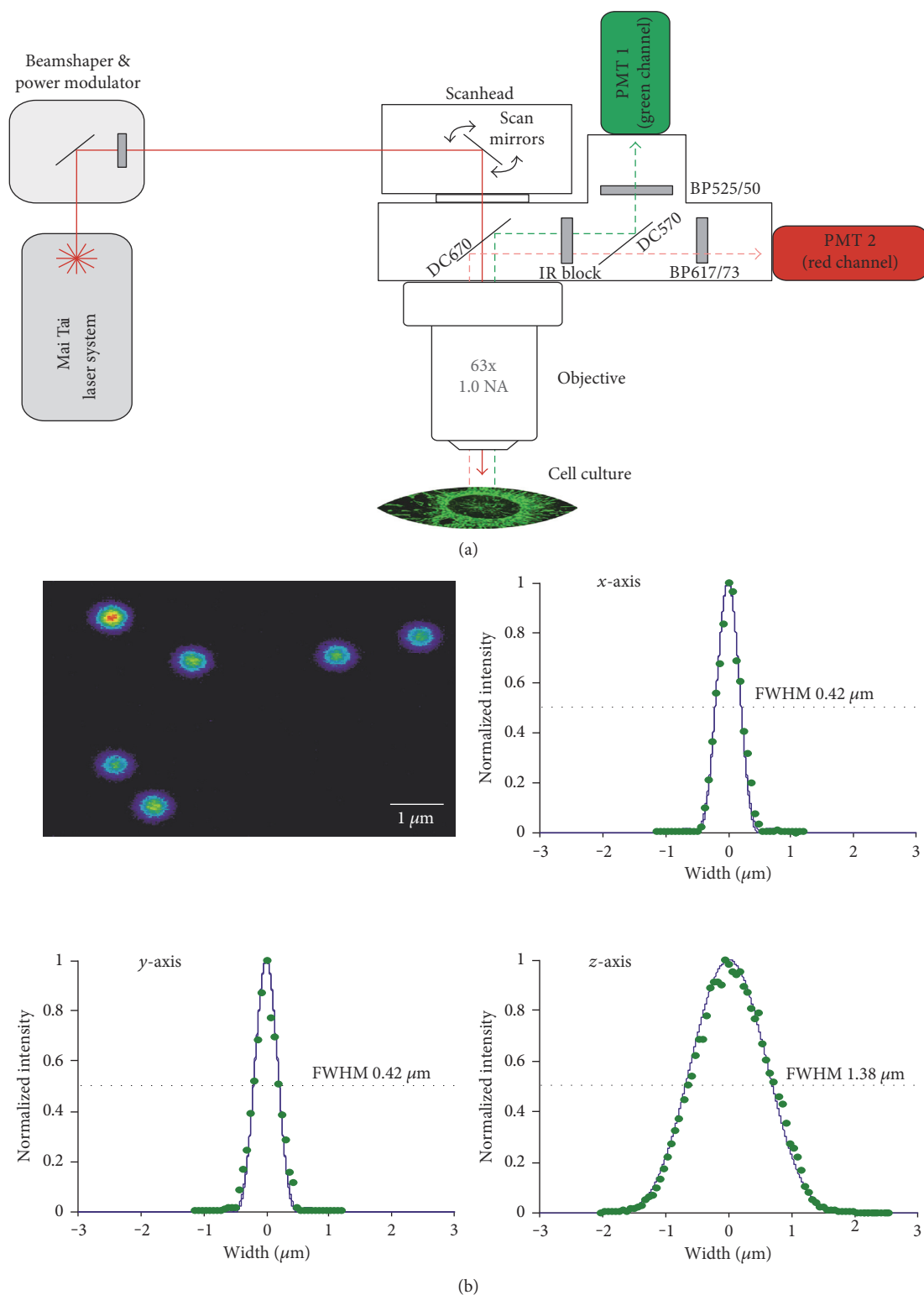


FIGURE 1: Two-photon laser-scanning microscope (TPLSM) and its point spread functions. (a) General layout of our TPLSM. Fluorescence emission was detected in nondescanned mode by photomultiplier tubes (PMTs). For ratiometric JC-1 imaging, green and red components of JC-1 emission were separated spectrally and detected by the two detection channels. (b) To estimate the spatial resolution, the point spread function of our TPLSM was determined from the intensity profiles of subresolution (100 nm) beads. Displayed intensity profiles are the averages of 24 beads, and excitation wavelength was 800 nm. Their full width at half maximum (FWHM) yields a lateral (X,Y) resolution of 0.4 μm and an axial (Z) resolution of 1.4 μm .

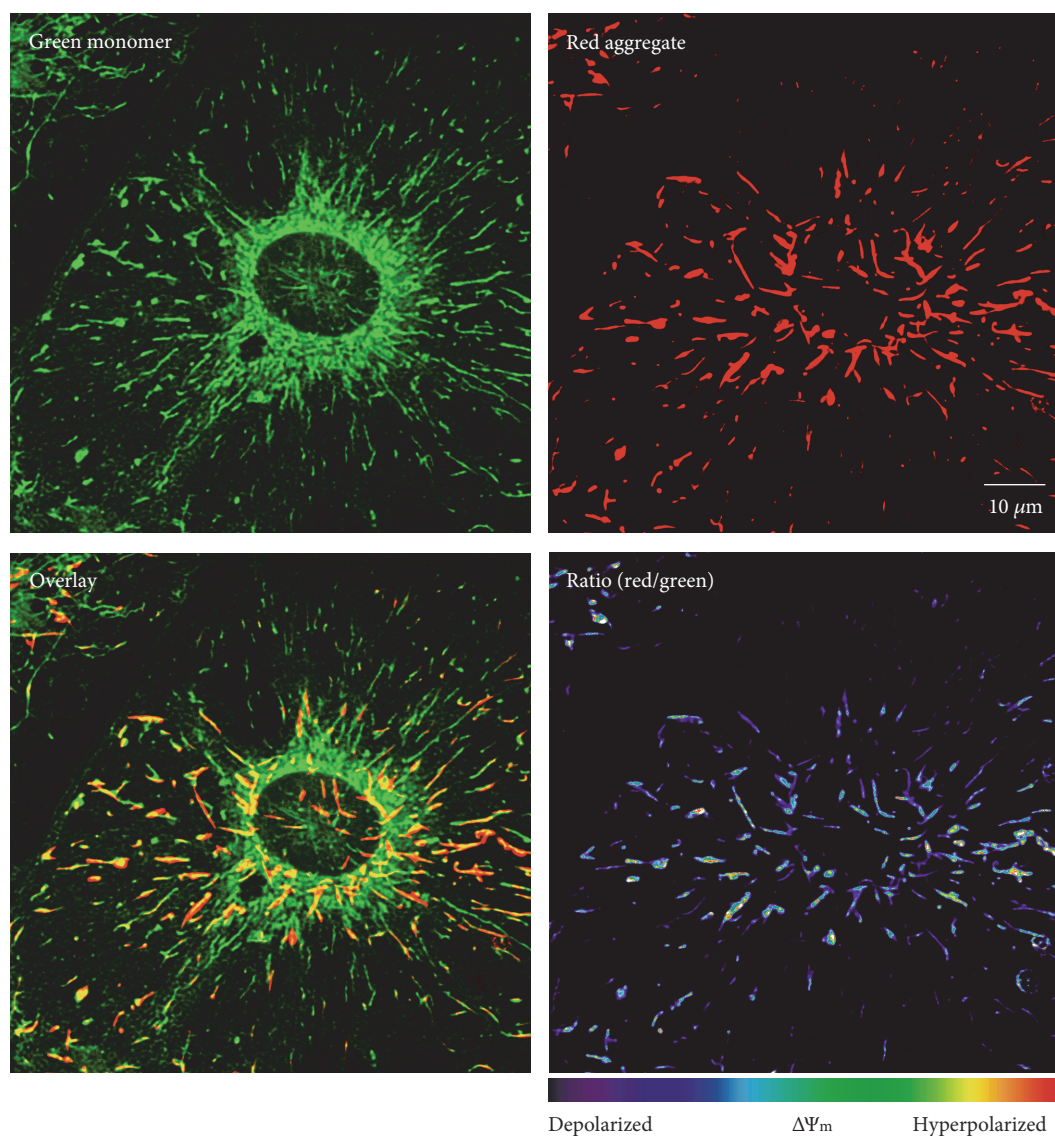


FIGURE 2: Sample images of a JC-1-labeled hippocampal astrocyte. Displayed are the individual raw images acquired by the two detection channels, representing JC-1 monomers and J-aggregates, respectively. The offline computed overlay image confirms the perfect alignment of the spectrally differing images. The calculated JC-1 ratio (red/green) represents the $\Delta\Psi_m$ range of individual mitochondria and their morphological/functional heterogeneity.

Student's *t*-tests. In the diagrams, genotype-related differences are indicated by asterisks ($***p < 0.001$, $**p < 0.01$, and $*p < 0.05$), and genotype-matched differences among recording conditions (drug-induced effects) are marked by crosshatches ($###p < 0.001$, $##p < 0.01$, and $\#p < 0.05$).

3. Results

JC-1 is present as either monomer or J-aggregate. The monomers predominate in depolarized mitochondria and emit green fluorescence (~ 530 nm). Oligomers (J-aggregates) only form in mitochondria with a $\Delta\Psi_m < -140$ mV and emit red fluorescence (~ 590 nm) [50–53]. Accordingly, JC-1 is ratiometric by emission, and—as we have shown earlier [54]—the relative green and red components of JC-1 fluorescence allow to distinguish mitochondria

with high and low $\Delta\Psi_m$ and to detect spontaneous and evoked $\Delta\Psi_m$ changes. For the current analyses, an updated and further improved version of our TPLSM [54, 62] was used (Figure 1(a)). Therefore, we first ran initial tests with standardized fluorescent beads, to determine the lateral and axial resolution of the upgraded system (Figure 1(b)).

To analyze mitochondrial structure and function, cell cultures were bulk loaded with JC-1. Once labeled, astrocytes could be identified clearly by their large cell size and flatly grown shape (Figure 2). Individual astrocytes were then imaged as 3-d image stacks, selecting those cells whose boundaries could be identified clearly and which were not overlapping with other cells. Based on the acquired green and red channels, overlay and ratiometric images were then calculated offline (Figure 2).

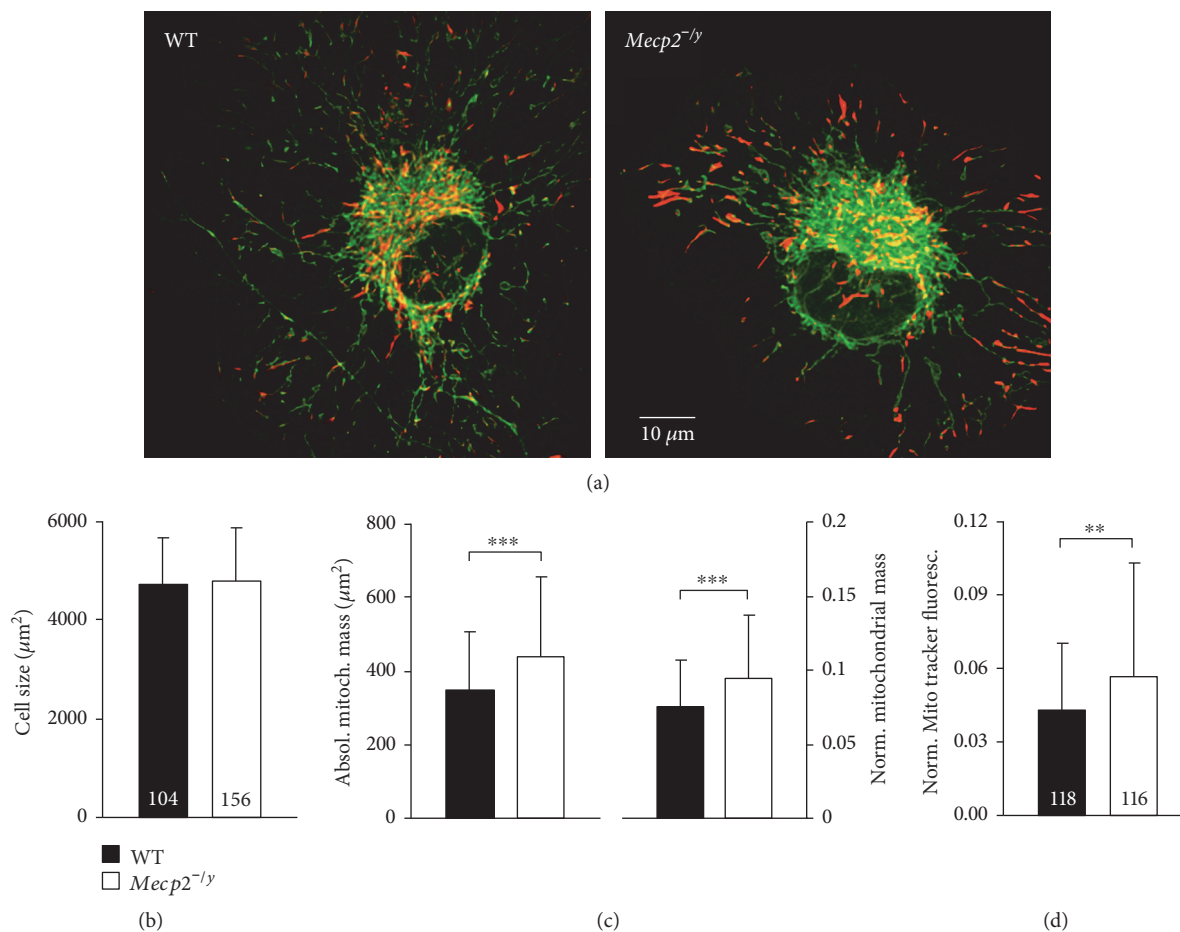


FIGURE 3: Increased mitochondrial mass in *Mecp2*^{-/-} astrocytes. (a) In general appearance, WT and *Mecp2*^{-/-} astrocytes did not differ noticeably. Displayed images are overlays of the green and red JC-1 emissions. (b) Astrocytic cell size, determined by circling the outer cell boundaries, was also indistinguishable. Plotted data are mean \pm standard deviations, and the number of cells analyzed is included into each bar. Bar shading is identical for the following panels. (c) The absolute mitochondrial mass was higher in *Mecp2*^{-/-} astrocytes than in WT cells (left side), and this difference was still present, when the mitochondrial mass was normalized to cell size (right side). Cell numbers analyzed are identical to panel B. Genotypic differences are indicated by asterisks (***) $p < 0.001$. (d) Using the mitochondria-specific marker, MitoTracker Red confirmed the increased mitochondrial mass in *Mecp2*^{-/-} astrocytes. Displayed is the normalized intensity of astrocytic MitoTracker Red fluorescence as referred to individual cell size (** $p < 0.01$).

To identify potential differences in mitochondrial structure and/or function among WT and *Mecp2*^{-/-} astrocytes, these parameters had to be determined for individual mitochondria. Therefore, we developed a semiautomated routine to detect and analyze single particles. First, by blind deconvolution, pixel noise and out-of-focus light were removed, resulting in an improved contrast. Then, the best focal plane of the deconvolved stack was identified by visual inspection and collapsed with its adjacent two upper and two lower planes into a single plane, before thresholding was performed to obtain a binary mask discriminating among mitochondria and background. Spatial filtering then excluded all particles overlapping with others (ramified particles), lying at the margin of the image (truncated particles), or lying outside the size expected for mitochondria (individual bright pixels, or large aggregates in which individual organelles could not be discriminated). The resulting particle mask then included only those mitochondria, which would also be identified

visually as individual particles. For each of these particles, the morphological characteristics (particle length) and the functional information (JC-1 ratio) were then extracted from the ratiometric source image.

In total, 104 WT and 156 *Mecp2*^{-/-} astrocytes were imaged and underwent the abovementioned analysis routines. Furthermore, we determined the size of each cell—by circling the outer cell boundaries—as well as the total volume of all JC-1-labeled structures. As total brain size and neuronal complexity differ among WT and Rett mice [42, 63], we first assessed potential genotypic differences in the size of the hippocampal astrocytes. With average cell areas of $4702 \pm 950 \mu\text{m}^2$ ($n = 104$) and $4774 \pm 1097 \mu\text{m}^2$ ($n = 156$), respectively, cultured WT and *Mecp2*^{-/-} astrocytes did not differ at all (Figures 3(a) and 3(b)). Yet, total mitochondrial mass was higher in *Mecp2*^{-/-} ($440 \pm 214 \mu\text{m}^2$) than in WT astrocytes ($348 \pm 160 \mu\text{m}^2$) (Figure 3(c)). This still was the case, when mitochondrial content was normalized to cell size,

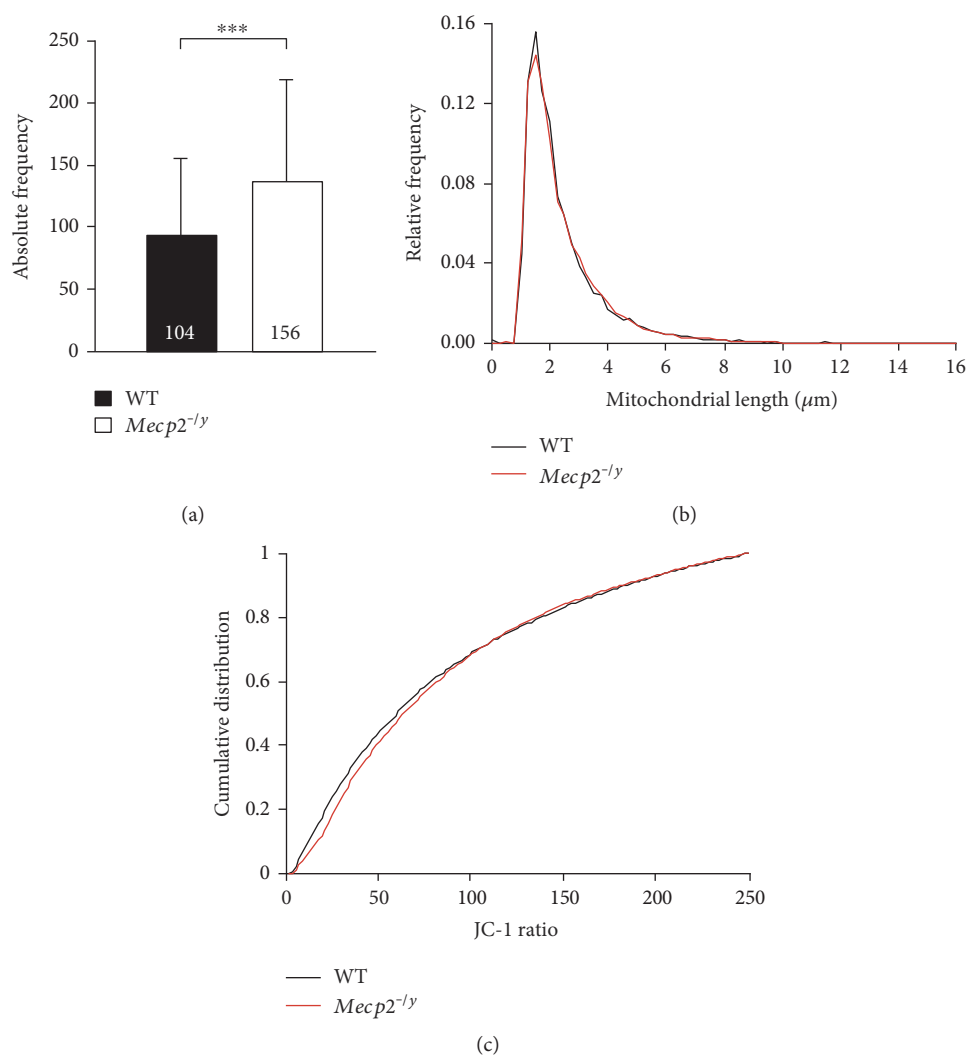


FIGURE 4: Functional parameters of individual mitochondria. (a) In line with the increased total mitochondrial mass in *Mecp2*^{-/-} astrocytes, also more individual organelles could be detected in these cells as compared to WT (***) $p < 0.001$. (b) Genotypic differences in the length of the individual mitochondria were not found. The histogram-type distribution represents the entirety of all individual mitochondrial particles detected by the automated analyses in WT (9769 mitochondria) and *Mecp2*^{-/-} astrocytes (21,424 mitochondria). (c) The degree of polarization did not differ either among the genotypes. Plotted is the cumulative distribution function of the $\Delta\Psi_m$ of individual mitochondria of WT and *Mecp2*^{-/-} astrocytes. It is based on the distribution of all recorded JC-1 ratios and indicates on the ordinate the probability that a WT or *Mecp2*^{-/-} mitochondrion has a given $\Delta\Psi_m$ (or less).

yielding an average mitochondrial density of $0.094 \pm 0.044/\mu\text{m}^2$ for *Mecp2*^{-/-} astrocytes ($n = 156$) and $0.076 \pm 0.032/\mu\text{m}^2$ for WT astrocytes ($n = 104$, Figure 3(c)).

To validate this finding, we ran control experiments with the established mitochondrial marker MitoTracker Red [53, 64]. Images of individual astrocytes were acquired with a CCD-camera system, and the cellular intensity of MitoTracker Red fluorescence was normalized to the size of the respective cell. Again, the more intense fluorescence detected in *Mecp2*^{-/-} (0.057 ± 0.046 ; $n = 116$) than in WT astrocytes (0.043 ± 0.028 ; $n = 118$) indicated a higher mitochondrial content for *Mecp2*^{-/-} astrocytes (Figure 3(d)).

To take a closer look at the genotypic difference in mitochondrial mass, we performed single particle analyses on JC-1-labeled mitochondria. A total of 9769 mitochondria in WT

and 21,424 mitochondria in *Mecp2*^{-/-} astrocytes were classified, and more individual mitochondria could be detected in *Mecp2*^{-/-} ($136.5 \pm 81.5/\text{cell}$, $n = 156$) than in WT astrocytes ($93.1 \pm 6.0/\text{cell}$, $n = 104$) (Figure 4(a)). Comparing the morphological characteristics, that is, the length of individual mitochondria, did however not reveal any genotypic differences. On average, mitochondria measured $2.34 \mu\text{m}$ in WT and $3.32 \mu\text{m}$ in *Mecp2*^{-/-} astrocytes (Figure 4(b)). Analyzing the average degree of polarization, assessed as JC-1 ratio, did not reveal any differences either, as indicated by the cumulative distribution function of their $\Delta\Psi_m$ (Figure 4(c)). In addition, correlation analysis confirmed that the size of a given mitochondrion does not correlate with its $\Delta\Psi_m$ (WT correlation coefficient 0.0895; *Mecp2*^{-/-} correlation coefficient 0.103).

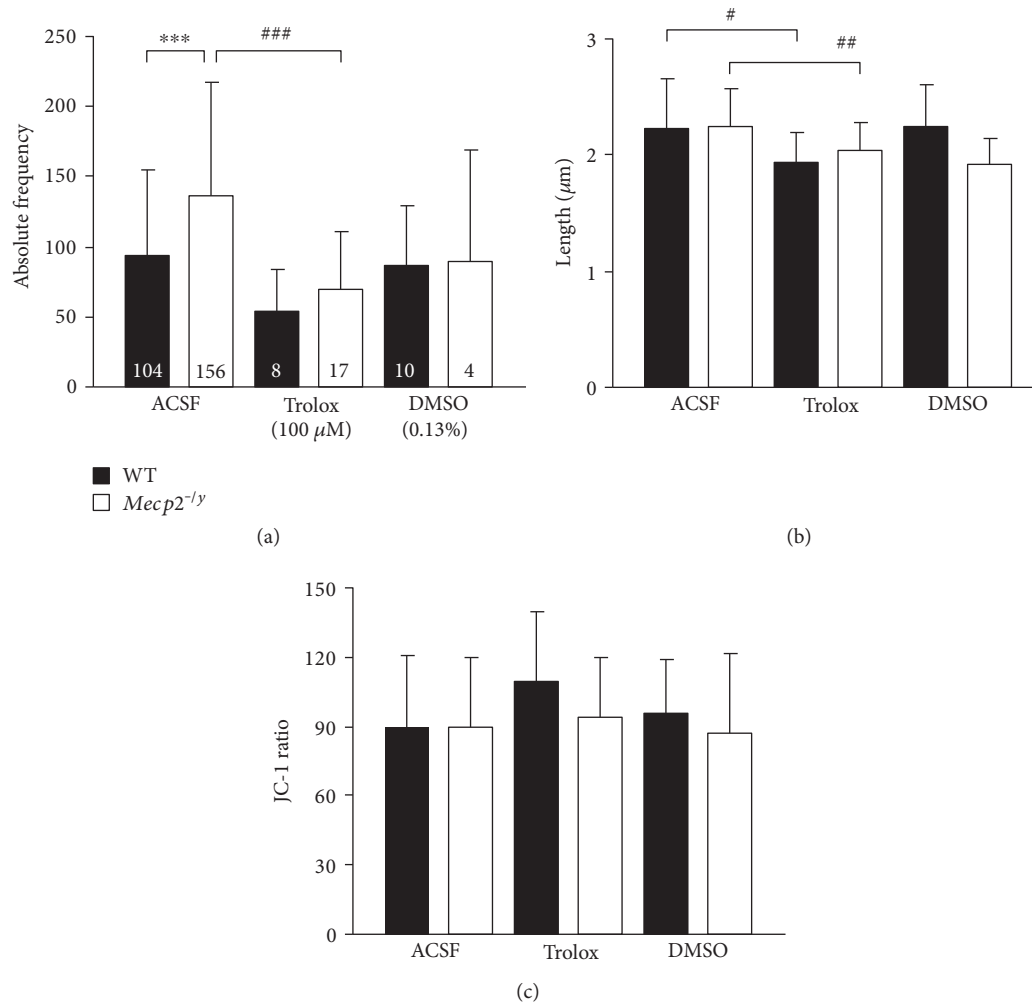


FIGURE 5: Free-radical scavenger treatment abolishes the differences in mitochondrial mass between WT and *Mecp2*^{-/-} astrocytes. (a) Overnight Trolox treatment decreased (or tended to decrease) mitochondrial mass. As a result, the genotypic difference seen under control conditions among WT and *Mecp2*^{-/-} astrocytes was no longer detectable. The solvent DMSO itself also tended to decrease the mitochondrial content of *Mecp2*^{-/-} astrocytes, but not to the degree seen with Trolox. Bar shading and the number of cells analyzed apply also to the following two panels. Genotype-related differences are indicated by asterisks (***) and drug-induced genotype-matched differences by crosshatches (###). (b) Trolox slightly but significantly decreased the length of individual mitochondria to an equal degree in WT and *Mecp2*^{-/-} astrocytes. (c) Significant changes in $\Delta\Psi_m$ could not be observed in response to Trolox treatment. In WT astrocytes, a trend towards increased $\Delta\Psi_m$ became obvious though.

3.1. Modulation of Mitochondrial Parameters by Radical Scavenger Treatment. Lowered vitamin E levels were found in the blood plasma of Rett patients [65]. Also, we previously confirmed that the vitamin E derivative Trolox improves cellular redox balance as well as synaptic function of the *Mecp2*^{-/-} hippocampus in vitro [40, 66], and it ameliorates some RTT symptoms when applied systemically to *Mecp2*^{-/-} mice [67]. Therefore, we assessed potential Trolox-mediated effects on mitochondrial function by incubating cell cultures overnight with this free-radical scavenger (100 μM, 12–14 h).

Interestingly, Trolox significantly decreased the number of mitochondrial particles in *Mecp2*^{-/-} astrocytes and showed a corresponding trend ($p = 0.076$) in WT astrocytes (Figure 5(a)). As a result, the genotypic differences in mitochondrial density among WT and *Mecp2*^{-/-} astrocytes were

abolished (Figure 5(a)). Part of this effect can also be achieved by the solvent DMSO itself, which also mediates antioxidant capacity by scavenging hydroxyl radicals [68]. Furthermore, in both genotypes, the size of individual mitochondria was slightly smaller in Trolox-incubated than in untreated control cells (Figure 5(b)). Significant effects of Trolox on the $\Delta\Psi_m$ of WT or *Mecp2*^{-/-} astrocytes were not found, but in WT astrocytes, a trend ($p = 0.093$) towards increased (more negative) $\Delta\Psi_m$ became apparent (Figure 5(c)).

3.2. Cytosolic Redox Balance. To confirm the assumption that the differences in mitochondrial mass are closely associated with differences in redox balance among WT and *Mecp2*^{-/-} astrocytes, we quantified cellular redox conditions by using the genetically encoded redox sensor roGFP1 (Figure 6(a)). Expressing roGFP1 in the cytosol reported for steady-state

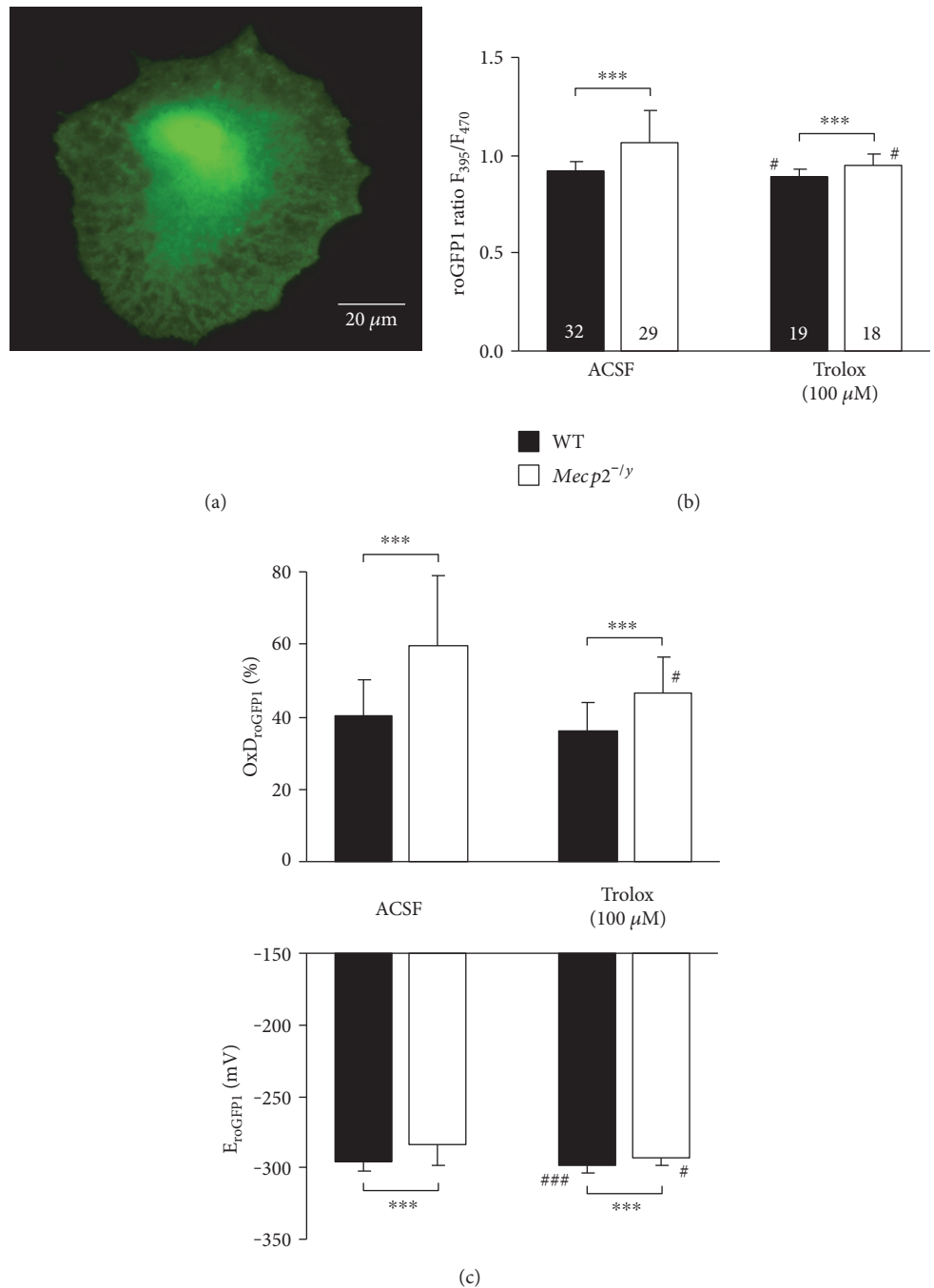


FIGURE 6: Optical redox imaging with the genetically encoded roGFP1 sensor confirms more oxidized conditions in *Mecp2*^{-/-} astrocytes. (a) CCD camera image of a *Mecp2*^{-/-} astrocyte expressing cytosolic roGFP1. (b) Under control conditions, fluorescence ratios were higher (more oxidized) in the cytosol of *Mecp2*^{-/-} than of WT astrocytes. Trolox induced a shift towards more reducing conditions especially in *Mecp2*^{-/-} astrocytes (** $p < 0.001$, # $p < 0.05$). (c) Calculating the relative degree of roGFP1 oxidation (OxD_{roGFP1}) and the corresponding reduction potentials (E_{roGFP1}) confirms the more oxidized conditions in *Mecp2*^{-/-} astrocytes as well as the antioxidant effect mediated by Trolox (### $p < 0.001$).

resting conditions a fluorescence ratio of 0.92 ± 0.05 ($n = 32$) in WT astrocytes, whereas the fluorescence ratio in *Mecp2*^{-/-} astrocytes was slightly higher, that is, more oxidized (1.06 ± 0.17 , $n = 29$; Figure 6(b)). This also is evident from the relative degrees of roGFP1 oxidation (WT $40.4 \pm 9.8\%$; *Mecp2*^{-/-} $59.7 \pm 19.5\%$) as well as the corresponding reduction potentials (Figure 6(c)). To verify that Trolox (100 μM) improved cellular redox balance, we also quantified cytosolic redox

conditions after overnight treatment with this free-radical scavenger. Indeed in WT cells, the relative degree of roGFP1 oxidation slightly decreased to $36.0 \pm 7.7\%$ ($n = 19$), whereas it decreased more intensely in *Mecp2*^{-/-} astrocytes to $46.7 \pm 9.9\%$ ($n = 18$). As a result of this treatment, the genotypic differences in roGFP1 ratio, relative roGFP1 oxidation level, and reduction potential became less pronounced as compared to the untreated astrocytes (Figures 6(b) and 6(c)).

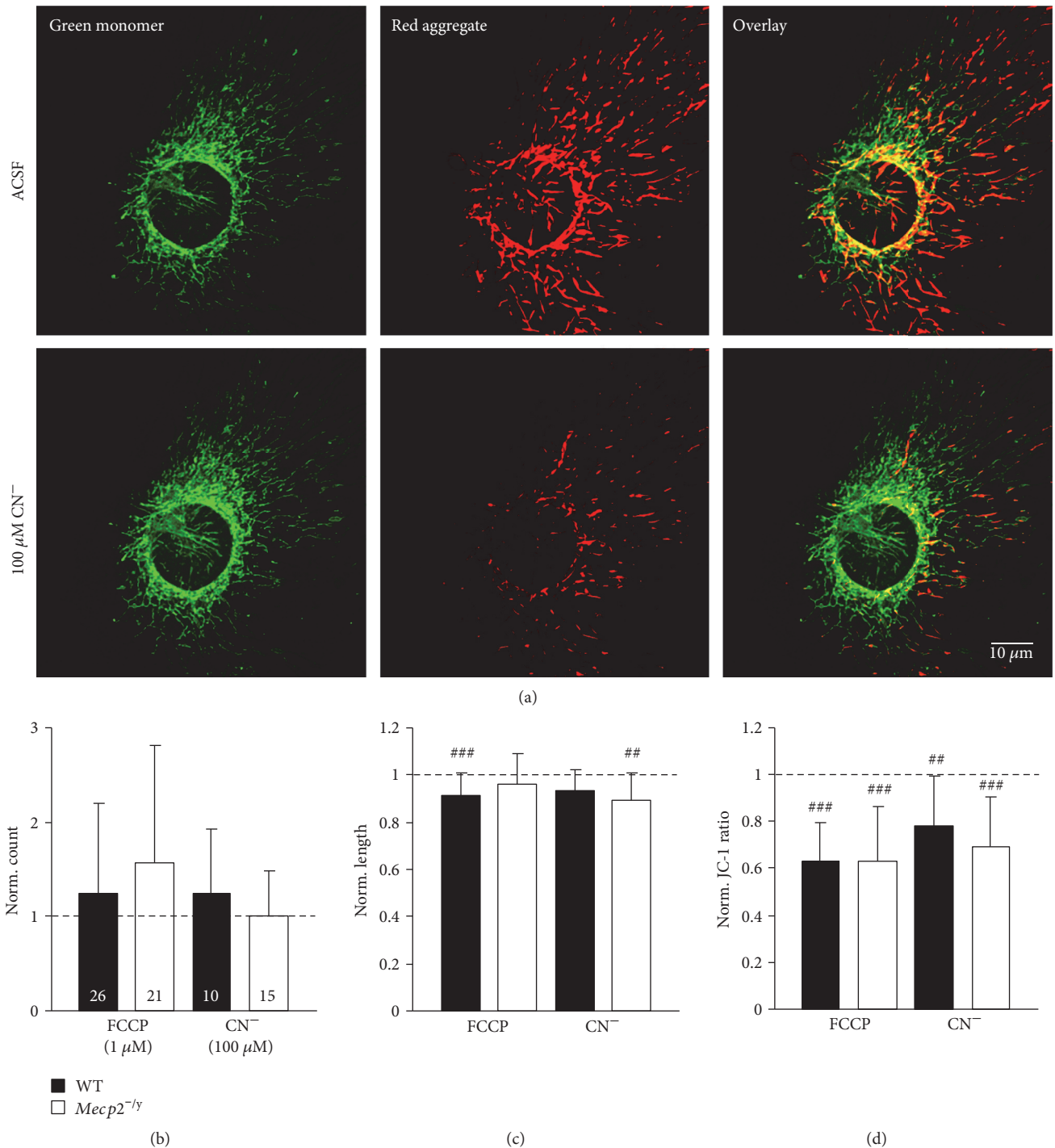


FIGURE 7: WT and $\text{Mecp2}^{-/-}$ astrocytes show similar vulnerabilities to mitochondrial compromise. (a) CN^- treatment (100 μm , 5 min) evoked a clear decrease in JC-1 ratio, which is evident as the green shift of the dual color emission and indicates a marked mitochondrial depolarization; displayed is a WT astrocyte. (b) Significant changes in mitochondrial content (mitochondria/cell) were not evoked by FCCP or CN^- treatment. (c) The length of individual mitochondria was affected only very moderately ($^{\#}p < 0.01$, $^{\#\#\#}p < 0.001$). (d) As expected, both treatments evoked a clear mitochondrial depolarization. Significant genotypic differences were not observed in response to chemically induced hypoxia (CN^-) or mitochondrial uncoupling (FCCP).

3.3. Effects of Mitochondrial Stressors. Previously, we found that the hippocampus of adult $\text{Mecp2}^{-/-}$ mice shows an exaggerated hypoxia susceptibility [69] and also in neonatal hippocampal organotypic slice cultures, we detected exaggerated redox responses to O_2 shortage [40]. Therefore, we also

assessed the effects of mitochondrial stress, by exposing cultured astrocytes to the mitochondrial uncoupler FCCP or by blocking mitochondrial respiration by CN^- (Figure 7). To assess the effects of these compounds, each astrocyte was recorded before and after drug treatment, and all drug-

induced changes were referred (normalized) to pretreatment control conditions.

Treatment with either FCCP (1 μ M, 5 min) or CN⁻ (100 μ M, 5 min) markedly decreased the JC-1 fluorescence ratio, indicating a pronounced mitochondrial depolarization (Figures 7(a) and 7(d)). A typical response of mitochondria exposed to such stress is the so-called thread-grain transition, that is, a disruption of longer mitochondrial filaments and a rounding of the individual particles [70–72]. Also here, this was elicited by FCCP in some astrocytes, and it resulted in a markedly increased variability of mitochondrial counts (Figure 7(b)) as well as in a moderately reduced length of the individual mitochondria (Figure 7(c)). As expected, the extent of the FCCP-induced mitochondrial depolarization was identical in WT and *Mecp2*^{-/-} cells (Figure 7(d)); this compound acts as protonophore and completely collapses $\Delta\Psi_m$. Also CN⁻ treatment elicited a pronounced mitochondrial depolarization in both genotypes, which tended to be slightly more intense in *Mecp2*^{-/-} than in WT astrocytes (Figure 7(d)). Nevertheless, obvious genotypic differences in mitochondrial vulnerability to these pharmacological insults were not detected.

4. Discussion

Due to the various alterations of mitochondrial structure and function, which are associated with RTT, mitochondrial dysfunction has been proposed to contribute to disease progression (see [18–20, 28, 29]). Earlier, we found in the hippocampal slices of neonatal *Mecp2*^{-/-} mice an increased ratio of FAD/NADH autofluorescence, which indicates an intensified mitochondrial metabolism [40]. This difference was present in *st. pyramidale*, which is largely dominated by pyramidal cell somata, but also in *st. radiatum*, a mixed layer containing neurons and glia. Hence, glial cells may show mitochondrial alterations as well. Therefore, we now conducted optical analyses in WT and *Mecp2*^{-/-} glia to characterize further the spectrum of mitochondrial alterations in RTT. Due to their pivotal roles in extracellular ion homeostasis [73], transmitter uptake [74], and blood-brain barrier formation [75], we focused on astrocytes.

The earliest analyses of mitochondria in RTT took advantage of electron microscopy to assess changes in the mitochondrial ultrastructure [20, 22, 76], but this approach lacks functional information. Later, biochemical and molecular biological assays were performed to identify altered enzyme activities and protein levels [23, 25, 29, 77]. Such assays are usually based on full brain or large tissue samples and yield valuable functional insights, but they do not provide single cell resolution. Our 2-photon microscopy study ensured both, functional information as well as sub-cellular resolution.

Using this technological advantage in combination with the developed semiautomated analysis-routines, we confirmed that mitochondria are more numerous in *Mecp2*^{-/-} hippocampal astrocytes. Since the individual mitochondria did not differ in their size and since genotypic differences in cell dimensions were not found, this points out to an increased total mitochondrial mass in *Mecp2*^{-/-} astrocytes.

One may argue now that the higher number of individual mitochondria identified in cultured *Mecp2*^{-/-} astrocytes could arise from a less dense mitochondrial packaging, which facilitated a successful single-particle detection in these cells. Yet, the total mitochondrial content determined in parallel and labeling with the mitochondria-specific marker MitoTracker Red also confirm an increased mitochondrial mass in *Mecp2*^{-/-} astrocytes. It therefore seems that the increased mitochondrial content constitutes a cell-endogenous response to compensate for the mitochondria-related deficits and their limited metabolic/respiratory capacity in RTT [26, 27, 31, 40]. Interestingly, an increased mitochondrial mass was also reported for *Mecp2*^{-/-} microglia of the juvenile mouse brain [78]. In contrast, *Mecp2*-null mouse skin fibroblasts (cultured in regular medium) and stem-cell derived *Mecp2*-mutant neurons do not differ in their mitochondrial contents [79, 80].

Obvious differences in the size or $\Delta\Psi_m$ of individual mitochondria could not be detected among WT and *Mecp2*^{-/-} astrocytes. This suggests that the immediate functional impact of the mitochondrial alterations in RTT is rather subtle, which is also indicated by the fact that—in contrast to other mitochondrialopathies—a marked degree of neurodegeneration is not evident in RTT [41].

Earlier studies have convincingly linked RTT to cellular redox changes and oxidative stress [37, 40, 81]. The conducted redox analyses now confirm for the first time that the oxidative burden in RTT also applies to astrocytes. As we verified earlier, the free-radical scavenger Trolox improved the cellular redox balance in organotypic hippocampal slices [40], dampened neuronal hyperexcitability in adult hippocampal slices of symptomatic *Mecp2*^{-/-} mice, and also improved the hypoxia tolerance as well as certain types of synaptic plasticity [66, 67]. In these studies, any adverse impact of Trolox on mitochondrial function could be ruled out, and also here, an overnight incubation of astrocytes with Trolox did not affect mitochondrial shape or $\Delta\Psi_m$. However, Trolox incubation clearly improved cytosolic redox balance in WT and even more so in *Mecp2*^{-/-} astrocytes, thereby dampening the genotypic differences and opposing the oxidative stress in *Mecp2*^{-/-} cells. As Trolox also slightly reduced the number of mitochondria per cell and thereby eliminated the genotypic differences seen in untreated astrocytes, it can therefore be concluded that the redox imbalance in RTT is one of the factors that underlies the increased mitochondrial mass in *Mecp2*^{-/-} astrocytes.

Furthermore, we assessed potentially different responses of WT and *Mecp2*^{-/-} astrocytes to different mitochondria-directed drugs. FCCP evoked marked mitochondrial depolarizations in both genotypes by abolishing the proton gradient across the inner mitochondrial membrane. In addition, it slightly reduced the size of mitochondria in WT astrocytes. As structural changes, or even mitochondrial fragmentation, are quite commonly induced by FCCP [70, 82]; this explains the decreased mitochondrial length and increased number of individual mitochondria detected in some of the WT and *Mecp2*^{-/-} astrocytes upon mitochondrial uncoupling. The inhibition of respiratory complex IV by CN⁻ also markedly depolarized mitochondria; the trend towards a more

intense depolarization of *Mecp2*^{-/-} astrocytes may reflect the increased hypoxia susceptibility we found earlier in the hippocampal and brainstem slices of *Mecp2*^{-/-} mice [69, 83–85]. Furthermore, mitochondria of *Mecp2*^{-/-} astrocytes became slightly smaller upon CN⁻ treatment. Changes in mitochondrial content were, however, not detectable in any genotype. Therefore, as pronounced genotype-related changes were not detected for mitochondrial size, mitochondrial content, and $\Delta\Psi_m$, it has to be assumed that mitochondria in WT and *Mecp2*^{-/-} astrocytes do not noticeably differ in their vulnerabilities to uncoupling and chemical hypoxia. In view of the earlier detected increased hypoxia susceptibility of hippocampal and brainstem networks of MeCP2-deficient mice [69, 85], this is an important finding. Yet, it also has to be considered that the pharmacological challenges applied in the present study were quite intense.

Our 2-photon analyses were based on the emission ratiometric $\Delta\Psi_m$ indicator JC-1. We developed and thoroughly tested this JC-1-based emission ratiometric 2-photon imaging approach earlier [54], and it allows not only to visualize individual mitochondria but also to compare their $\Delta\Psi_m$ and quantify any $\Delta\Psi_m$ changes. JC-1 clearly differs from other dyes, as it is the only emission ratiometric indicator detecting $\Delta\Psi_m$ changes with sufficient sensitivity. Often criticized is that JC-1 reacts more slowly than other mitochondrial markers, which do not form aggregates. Hence, the true kinetics of fast $\Delta\Psi_m$ changes might be underestimated [54, 86]. However, as we did not aim to resolve temporally any $\Delta\Psi_m$ changes, but rather compared steady-state conditions or drug treatment endpoints, this should be of no concern. A true drawback of JC-1 is, however, that comparative $\Delta\Psi_m$ analyses in more intact preparations are hardly possible, as the excessive background fluorescence of interstitial JC-1 monomers prevents a meaningful JC-1 staining in, for example, acute or organotypic tissue slices.

Nevertheless, JC-1 and its derivatives are the only ratiometric mitochondrial $\Delta\Psi_m$ indicators, and as such, their fluorescence response is not affected by the extent of dye uptake and/or differences in cellular mitochondrial content. All of these apply, however, to other nonratiometric $\Delta\Psi_m$ indicators (e.g., rhodamine 123 or TMRM), and it may markedly complicate data analyses, especially when these compounds are used in low-resolution approaches, such as flow-cytometry and cuvette-based spectrophotometric assays. Only recently, an improved variant of JC-1, termed JC-10, became available. It functions just as JC-1 but offers higher water solubility and an improved dynamic response range (see <http://www.enzolifesciences.com/fileadmin/reports/Datasheet-ENZ-52305.pdf>). Thus, it may prove more advantageous also for future emission-ratiometric 2-photon imaging applications of $\Delta\Psi_m$ alterations in individual mitochondria or $\Delta\Psi_m$ differences among various cell types and/or genotypes.

5. Conclusions

Focusing on astrocytes, we performed functional optical analyses on the subcellular level, to extend earlier findings

on mitochondrial alterations and redox imbalance in RTT. As the entire study is based on dissociated cell cultures, it can only reflect the neonatal developmental stage. Nevertheless, an increased mitochondrial mass and more oxidized cytosolic redox conditions were already detectable in *Mecp2*^{-/-} hippocampal astrocytes of presymptomatic mice. This genotypic difference in mitochondrial mass was obvious for absolute mitochondrial content, its normalization to cell size, and MitoTracker labeling. This confirms that also astrocytes undergo clear alterations already during the neonatal and presymptomatic stages of RTT, which further supports the hypothesis that mitochondrial alterations and the associated oxidative burden drive the progression of this neurodevelopmental disorder. Trolox did not mediate any adverse effects on mitochondria, which is certainly of interest for free-radical scavenger- and antioxidant-based pharmacotreatment concepts in RTT. More importantly, this free-radical scavenger successfully abolished the genotypic differences in mitochondrial content among WT and *Mecp2*^{-/-} astrocytes and improved cytosolic redox balance especially in *Mecp2*^{-/-} astrocytes. This identifies cellular redox imbalance as one of the mechanisms underlying the increased mitochondrial mass in *Mecp2*^{-/-} astrocytes.

Conflicts of Interest

The authors declare that there is no conflict of interest regarding the publication of this paper.

Acknowledgments

The authors are grateful to Belinda Kempkes for her excellent technical assistance and to Professor S. James Remington (Institute of Molecular Biology, University of Oregon, Eugene, OR) for making the plasmids expressing roGFP1 available to them. This study was supported by the Cluster of Excellence and DFG Research Center Nanoscale Microscopy and Molecular Physiology of the Brain (CNMPB) as well as by the University Medical Center Göttingen and the State of Lower Saxony (Large-Scale Equipment Grant INST 1525/14-1 FUGG).

References

- [1] A. Rett, "Über ein eigenartiges hirnatrophisches Syndrom bei Hyperammonämie im Kindesalter," *Wiener Medizinische Wochenschrift* (1946), vol. 116, pp. 723–726, 1966.
- [2] B. Hagberg, J. Aicardi, K. Dias, and O. Ramos, "A progressive syndrome of autism, dementia, ataxia, and loss of purposeful hand use in girls: Rett's syndrome: report of 35 cases," *Annals of Neurology*, vol. 14, pp. 471–479, 1983.
- [3] M. Chahrouh and H. Y. Zoghbi, "The story of Rett syndrome: from clinic to neurobiology," *Neuron*, vol. 56, pp. 422–437, 2007.
- [4] B. Hagberg, "Rett's syndrome: prevalence and impact on progressive severe mental retardation in girls," *Acta Paediatrica Scandinavica*, vol. 74, pp. 405–408, 1985.
- [5] L. Villard, "MECP2 mutations in males," *Journal of Medical Genetics*, vol. 44, pp. 417–423, 2007.

- [6] R. E. Amir, I. B. VeyverVan den, M. Wan, C. Q. Tran, U. Francke, and H. Y. Zoghbi, "Rett syndrome is caused by mutations in X-linked *MECP2*, encoding methyl-CpG-binding protein 2," *Nature Genetics*, vol. 23, pp. 185–188, 1999.
- [7] X. Nan, S. Cross, and A. Bird, "Gene silencing by methyl-CpG-binding proteins," *Novartis Foundation Symposium*, vol. 214, pp. 6–16, 1998, discussion 16–21, 46–50.
- [8] M. Chahrouh, S. Y. Jung, C. Shaw et al., "MeCP2, a key contributor to neurological disease, activates and represses transcription," *Science*, vol. 320, pp. 1224–1229, 2008.
- [9] R. Trappe, F. Laccone, J. Cobilanschi et al., "*MECP2* mutations in sporadic cases of Rett syndrome are almost exclusively of paternal origin," *American Journal of Human Genetics*, vol. 68, pp. 1093–1101, 2001.
- [10] J. Dragich, I. Houwink-Manville, and C. Schanen, "Rett syndrome: a surprising result of mutation in *MECP2*," *Human Molecular Genetics*, vol. 9, pp. 2365–2375, 2000.
- [11] B. Hagberg and I. Witt-Engerström, "Rett syndrome: a suggested staging system for describing impairment profile with increasing age towards adolescence," *American Journal of Medical Genetics Supplement*, vol. 1, pp. 47–59, 1986.
- [12] B. Hagberg, M. Berg, and U. Steffenburg, "Three decades of sociomedical experiences from West Swedish Rett females 4–60 years of age," *Brain dev*, vol. 23, Supplement 1, pp. S28–S31, 2001.
- [13] A. M. Kerr, D. D. Armstrong, R. J. Prescott, D. Doyle, and D. L. Kearney, "Rett syndrome: analysis of deaths in the British survey," *European Child & Adolescent Psychiatry*, vol. 6, Supplement 1, pp. 71–74, 1997.
- [14] C. A. Chappleau, J. Lane, L. Pozzo-Miller, and A. K. Percy, "Evaluation of current pharmacological treatment options in the management of Rett syndrome: from the present to future therapeutic alternatives," *Current Clinical Pharmacology*, vol. 8, pp. 358–369, 2013.
- [15] D. M. Katz, A. Bird, M. Coenraads et al., "Rett syndrome: crossing the threshold to clinical translation," *Trends in Neurosciences*, vol. 39, pp. 100–113, 2016.
- [16] M. Lotan and S. Hanks, "Physical therapy intervention for individuals with Rett syndrome," *TheScientificWorldJOURNAL*, vol. 6, pp. 1314–1338, 2006.
- [17] S. B. Hanks, "The role of therapy in Rett syndrome," *American Journal of Medical Genetics Supplement*, vol. 1, pp. 247–252, 1986.
- [18] M. Müller and K. Can, "Aberrant redox homeostasis and mitochondrial dysfunction in Rett syndrome," *Biochemical Society Transactions*, vol. 42, pp. 959–964, 2014.
- [19] N. Shulyakova, A. C. Andrezza, L. R. Mills, and J. H. Eubanks, "Mitochondrial dysfunction in the pathogenesis of Rett syndrome: implications for mitochondria-targeted therapies," *Frontiers in Cellular Neuroscience*, vol. 11, p. 58, 2017.
- [20] O. Eeg-Olofsson, A. G. al-Zuhair, A. S. Teebi et al., "Rett syndrome: a mitochondrial disease?," *Journal of Child Neurology*, vol. 5, pp. 210–214, 1990.
- [21] O. Eeg-Olofsson, A. G. Al-Zuhair, A. S. Teebi, and M. M. Al-Essa, "Abnormal mitochondria in the Rett syndrome," *Brain and Development*, vol. 10, pp. 260–262, 1988.
- [22] M. E. Cornford, M. Philippart, B. Jacobs, A. B. Scheibel, and H. V. Vinters, "Neuropathology of Rett syndrome: case report with neuronal and mitochondrial abnormalities in the brain," *Journal of Child Neurology*, vol. 9, pp. 424–431, 1994.
- [23] M. T. Dotti, L. Manneschi, A. Malandrini, N. StefanoDe, F. Caznerale, and A. Federico, "Mitochondrial dysfunction in Rett syndrome. An ultrastructural and biochemical study," *Brain and Development*, vol. 15, pp. 103–106, 1993.
- [24] J. H. Gibson, B. Slobedman, K. N. Harikrishnan et al., "Downstream targets of methyl CpG binding protein 2 and their abnormal expression in the frontal cortex of the human Rett syndrome brain," *BMC Neuroscience*, vol. 11, no. 1, p. 53, 2010.
- [25] A. Pecorelli, G. Leoni, F. Cervellati et al., "Genes related to mitochondrial functions, protein degradation, and chromatin folding are differentially expressed in lymphomonocytes of Rett syndrome patients," *Mediators of Inflammation*, vol. 2013, Article ID 137629, 18 pages, 2013.
- [26] B. FilippisDe, D. Valenti, L. Baride et al., "Mitochondrial free radical overproduction due to respiratory chain impairment in the brain of a mouse model of Rett syndrome: protective effect of CNF1," *Free Radical Biology and Medicine*, vol. 83, pp. 167–177, 2015.
- [27] S. Kriaucionis, A. Paterson, J. Curtis, J. Guy, N. Macleod, and A. Bird, "Gene expression analysis exposes mitochondrial abnormalities in a mouse model of Rett syndrome," *Molecular and Cellular Biology*, vol. 26, pp. 5033–5042, 2006.
- [28] D. Valenti, L. Baride, B. FilippisDe, A. Henrion-Caude, and R. A. Vacca, "Mitochondrial dysfunction as a central actor in intellectual disability-related diseases: an overview of Down syndrome, autism, Fragile X and Rett syndrome," *Neuroscience and Biobehavioral Reviews*, vol. 46, Part 2, pp. 202–217, 2014.
- [29] W. A. Gold, S. L. Williamson, S. Kaur et al., "Mitochondrial dysfunction in the skeletal muscle of a mouse model of Rett syndrome (RTT): implications for the disease phenotype," *Mitochondrion*, vol. 15, pp. 10–17, 2014.
- [30] G. Forlani, E. Giarda, U. Ala et al., "The MeCP2/YY1 interaction regulates ANT1 expression at 4q35: novel hints for Rett syndrome pathogenesis," *Human Molecular Genetics*, vol. 19, pp. 3114–3123, 2010.
- [31] C. Cervellati, C. Sticozzi, A. Romani et al., "Impaired enzymatic defensive activity, mitochondrial dysfunction and proteasome activation are involved in RTT cell oxidative damage," *Biochimica et Biophysica Acta*, vol. 1852, pp. 2066–2074, 2015.
- [32] T. Matsuishi, F. Urabe, A. K. Percy et al., "Abnormal carbohydrate metabolism in cerebrospinal fluid in Rett syndrome," *Journal of Child Neurology*, vol. 9, pp. 26–30, 1994.
- [33] V. Saywell, A. Viola, S. Confort-Gouny, Y. FurLe, L. Villard, and P. J. Cozzone, "Brain magnetic resonance study of *Mecp2* deletion effects on anatomy and metabolism," *Biochemical and Biophysical Research Communications*, vol. 340, pp. 776–783, 2006.
- [34] P. O. Julu, A. M. Kerr, F. Apartopoulos et al., "Characterisation of breathing and associated central autonomic dysfunction in the Rett disorder," *Archives of Disease in Childhood*, vol. 85, pp. 29–37, 2001.
- [35] G. M. Stettner, S. Zanella, P. Huppke, J. Gärtner, G. Hilaire, and M. Dutschmann, "Spontaneous central apneas occur in the C57BL/6J mouse strain," *Respiratory Physiology & Neurobiology*, vol. 160, pp. 21–27, 2008.
- [36] D. M. Katz, M. Dutschmann, J. M. Ramirez, and G. Hilaire, "Breathing disorders in Rett syndrome: progressive neurochemical dysfunction in the respiratory network after

- birth," *Respiratory Physiology & Neurobiology*, vol. 168, pp. 101–108, 2009.
- [37] C. Sierra, M. A. Vilaseca, N. Brandi et al., "Oxidative stress in Rett syndrome," *Brain and Development*, vol. 23, Supplement 1, pp. S236–S239, 2001.
- [38] C. FeliceDe, L. Ciccoli, S. Leoncini et al., "Systemic oxidative stress in classic Rett syndrome," *Free Radical Biology and Medicine*, vol. 47, pp. 440–448, 2009.
- [39] C. FeliceDe, F. Della Ragione, C. Signorini et al., "Oxidative brain damage in *Mecp2*-mutant murine models of Rett syndrome," *Neurobiology of Disease*, vol. 68, pp. 66–77, 2014.
- [40] E. Großer, U. Hirt, O. A. Janc et al., "Oxidative burden and mitochondrial dysfunction in a mouse model of Rett syndrome," *Neurobiology of Disease*, vol. 48, pp. 102–114, 2012.
- [41] D. D. Armstrong, "Neuropathology of Rett syndrome," *Journal of Child Neurology*, vol. 20, pp. 747–753, 2005.
- [42] P. V. Belichenko, E. E. Wright, N. P. Belichenko et al., "Widespread changes in dendritic and axonal morphology in *Mecp2*-mutant mouse models of Rett syndrome: evidence for disruption of neuronal networks," *The Journal of Comparative Neurology*, vol. 514, pp. 240–258, 2009.
- [43] P. Moretti, J. M. Levenson, F. Battaglia et al., "Learning and memory and synaptic plasticity are impaired in a mouse model of Rett syndrome," *The Journal of Neuroscience*, vol. 26, pp. 319–327, 2006.
- [44] N. Ballas, D. T. Lioy, C. Grunseich, and G. Mandel, "Non-cell autonomous influence of MeCP2-deficient glia on neuronal dendritic morphology," *Nature Neuroscience*, vol. 12, pp. 311–317, 2009.
- [45] D. T. Lioy, S. K. Garg, C. E. Monaghan et al., "A role for glia in the progression of Rett's syndrome," *Nature*, vol. 475, pp. 497–500, 2011.
- [46] M. V. Nguyen, C. A. Felice, F. Du et al., "Oligodendrocyte lineage cells contribute unique features to Rett syndrome neuropathology," *The Journal of Neuroscience*, vol. 33, pp. 18764–18774, 2013.
- [47] I. Maezawa and L. W. Jin, "Rett syndrome microglia damage dendrites and synapses by the elevated release of glutamate," *The Journal of Neuroscience*, vol. 30, pp. 5346–5356, 2010.
- [48] J. Guy, B. Hendrich, M. Holmes, J. E. Martin, and A. Bird, "A mouse *Mecp2*-null mutation causes neurological symptoms that mimic Rett syndrome," *Nature Genetics*, vol. 27, pp. 322–326, 2001.
- [49] J. Weller, K. M. Kizina, K. Can, G. Bao, and M. Müller, "Response properties of the genetically encoded optical H₂O₂ sensor HyPer," *Free Radical Biology and Medicine*, vol. 76, pp. 227–241, 2014.
- [50] T. J. Sick and M. A. Perez-Pinon, "Optical methods for probing mitochondrial function in brain slices," *Methods*, vol. 18, pp. 104–108, 1999.
- [51] S. T. Smiley, M. Reers, C. Mottola-Hartshorn et al., "Intracellular heterogeneity in mitochondrial membrane potentials revealed by a J-aggregate-forming lipophilic cation JC-1," *Proceedings of the National Academy of Sciences of the United States of America*, vol. 88, pp. 3671–3675, 1991.
- [52] M. R. Duchen, A. Surin, and J. Jacobson, "Imaging mitochondrial function in intact cells," *Methods in Enzymology*, vol. 361, pp. 353–389, 2003.
- [53] K. A. Foster, F. Galeffi, F. J. Gerich, D. A. Turner, and M. Müller, "Optical and pharmacological tools to investigate the role of mitochondria during oxidative stress and neurodegeneration," *Progress in Neurobiology*, vol. 79, pp. 136–171, 2006.
- [54] V. C. Keil, F. Funke, A. Zeug, D. Schild, and M. Müller, "Ratiometric high-resolution imaging of JC-1 fluorescence reveals the subcellular heterogeneity of astrocytic mitochondria," *Pflügers Archiv*, vol. 462, pp. 693–708, 2011.
- [55] M. Reers, S. T. Smiley, C. Mottola-Hartshorn, A. Chen, M. Lin, and L. B. Chen, "Mitochondrial membrane potential monitored by JC-1 dye," *Methods in Enzymology*, vol. 260, pp. 406–417, 1995.
- [56] G. T. Hanson, R. Aggeler, D. Oglesbee et al., "Investigating mitochondrial redox potential with redox-sensitive green fluorescent protein indicators," *The Journal of Biological Chemistry*, vol. 279, pp. 13044–13053, 2004.
- [57] F. Funke, F. J. Gerich, and M. Müller, "Dynamic, semi-quantitative imaging of intracellular ROS levels and redox status in rat hippocampal neurons," *NeuroImage*, vol. 54, pp. 2590–2602, 2011.
- [58] K. C. Wagener, B. Kolbrink, K. Dietrich et al., "Redox-indicator mice stably expressing genetically-encoded neuronal roGFP: versatile tools to decipher subcellular redox dynamics in neuropathophysiology," *Antioxidants & Redox Signaling*, vol. 25, pp. 41–58, 2016.
- [59] K. Can, S. Kügler, and M. Müller, "Live imaging of mitochondrial ROS production and dynamic redox balance in neurons," in *Techniques to Investigate Mitochondrial Function in Neurons*, S. Strack and Y. M. Usachev, Eds., pp. 179–197, Springer Science+Business Media, 2017.
- [60] C. T. Dooley, T. M. Dore, G. T. Hanson, W. C. Jackson, S. J. Remington, and R. Y. Tsien, "Imaging dynamic redox changes in mammalian cells with green fluorescent protein indicators," *The Journal of Biological Chemistry*, vol. 279, pp. 22284–22293, 2004.
- [61] A. J. Meyer and T. P. Dick, "Fluorescent protein-based redox probes," *Antioxidants & Redox Signaling*, vol. 13, pp. 621–650, 2010.
- [62] M. Müller, J. Schmidt, S. L. Mironov, and D. W. Richter, "Construction and performance of a custom-built two-photon laser scanning system," *Journal of Physics D: Applied Physics*, vol. 36, pp. 1747–1757, 2003.
- [63] N. P. Belichenko, P. V. Belichenko, H. H. Li, W. C. Mobley, and U. Francke, "Comparative study of brain morphology in *Mecp2* mutant mouse models of Rett syndrome," *The Journal of Comparative Neurology*, vol. 508, pp. 184–195, 2008.
- [64] M. Poot, Y. Z. Zhang, J. A. Kramer et al., "Analysis of mitochondrial morphology and function with novel fixable fluorescent stains," *The Journal of Histochemistry and Cytochemistry*, vol. 44, pp. 1363–1372, 1996.
- [65] P. Formichi, C. Battisti, M. T. Dotti, G. Hayek, M. Zappella, and A. Federico, "Vitamin E serum levels in Rett syndrome," *Journal of the Neurological Sciences*, vol. 156, pp. 227–230, 1998.
- [66] O. A. Janc and M. Müller, "The free radical scavenger Trolox dampens neuronal hyperexcitability, reinstates synaptic plasticity, and improves hypoxia tolerance in a mouse model of Rett syndrome," *Frontiers in Cellular Neuroscience*, vol. 8, p. 56, 2014.
- [67] O. A. Janc, M. A. Hüser, K. Dietrich et al., "Systemic radical scavenger treatment of a mouse model of Rett syndrome: merits and limitations of the vitamin E derivative Trolox," *Frontiers in Cellular Neuroscience*, vol. 10, p. 266, 2016.

- [68] J. W. Phillis, A. Y. Estevez, and M. H. O'Regan, "Protective effects of the free radical scavengers, dimethyl sulfoxide and ethanol, in cerebral ischemia in gerbils," *Neuroscience Letters*, vol. 244, pp. 109–111, 1998.
- [69] M. Fischer, J. Reuter, F. J. Gerich et al., "Enhanced hypoxia susceptibility in hippocampal slices from a mouse model of Rett syndrome," *Journal of Neurophysiology*, vol. 101, pp. 1016–1032, 2009.
- [70] M. Müller, S. L. Mironov, M. V. Ivannikov, J. Schmidt, and D. W. Richter, "Mitochondrial organization and motility probed by two-photon microscopy in cultured mouse brainstem neurons," *Experimental Cell Research*, vol. 303, pp. 114–127, 2005.
- [71] G. L. Rintoul, A. J. Filiano, J. B. Brocard, G. J. Kress, and I. J. Reynolds, "Glutamate decreases mitochondrial size and movement in primary forebrain neurons," *The Journal of Neuroscience*, vol. 23, pp. 7881–7888, 2003.
- [72] V. P. Skulachev, "Mitochondrial filaments and clusters as intracellular power-transmitting cables," *Trends in Biochemical Sciences*, vol. 26, pp. 23–29, 2001.
- [73] E. A. Newman, D. A. Frambach, and L. L. Odette, "Control of extracellular potassium levels by retinal glial cell K^+ siphoning," *Science*, vol. 225, pp. 1174–1175, 1984.
- [74] L. K. Bak, A. Schousboe, and H. S. Waagepetersen, "The glutamate/GABA-glutamine cycle: aspects of transport, neurotransmitter homeostasis and ammonia transfer," *Journal of Neurochemistry*, vol. 98, pp. 641–653, 2006.
- [75] R. C. Janzer and M. C. Raff, "Astrocytes induce blood-brain barrier properties in endothelial cells," *Nature*, vol. 325, pp. 253–257, 1987.
- [76] A. Ruch, T. W. Kurczynski, and M. E. Velasco, "Mitochondrial alterations in Rett syndrome," *Pediatric Neurology*, vol. 5, pp. 320–323, 1989.
- [77] S. B. Coker and A. R. Melnyk, "Rett syndrome and mitochondrial enzyme deficiencies," *Journal of Child Neurology*, vol. 6, pp. 164–166, 1991.
- [78] L. W. Jin, M. Horiuchi, H. Wulff et al., "Dysregulation of glutamine transporter SNAT1 in Rett syndrome microglia: a mechanism for mitochondrial dysfunction and neurotoxicity," *The Journal of Neuroscience*, vol. 35, pp. 2516–2529, 2015.
- [79] Y. Li, H. Wang, J. Muffat et al., "Global transcriptional and translational repression in human-embryonic-stem-cell-derived Rett syndrome neurons," *Cell Stem Cell*, vol. 13, pp. 446–458, 2013.
- [80] N. O. Shulyakova, "Studies of mitochondrial dysfunction in models of Rett syndrome. Thesis," Department of Physiology, University of Toronto, Toronto, Canada, 2016.
- [81] C. FeliceDe, C. Signorini, S. Leoncini et al., "The role of oxidative stress in Rett syndrome: an overview," *Annals of the New York Academy of Sciences*, vol. 1259, pp. 121–135, 2012.
- [82] D. F. Suen, K. L. Norris, and R. J. Youle, "Mitochondrial dynamics and apoptosis," *Genes & Development*, vol. 22, pp. 1577–1590, 2008.
- [83] M. Kron and M. Müller, "Enhanced anoxia susceptibility of MeCP2-deficient CA1 neurons involves altered K^+ conductances," *Society for Neuroscience, Abstract Viewer/Itinerary Planner*, p. 732.736, 2009.
- [84] M. Kron and M. Müller, "Impaired hippocampal Ca^{2+} homeostasis and concomitant K^+ channel dysfunction in a mouse model of Rett syndrome during anoxia," *Neuroscience*, vol. 171, pp. 300–315, 2010.
- [85] M. Kron, J. L. Zimmermann, M. Dutschmann, F. Funke, and M. Müller, "Altered responses of MeCP2-deficient mouse brain stem to severe hypoxia," *Journal of Neurophysiology*, vol. 105, pp. 3067–3079, 2011.
- [86] A. Mathur, Y. Hong, B. K. Kemp, A. A. Barrientos, and J. D. Erusalimsky, "Evaluation of fluorescent dyes for the detection of mitochondrial membrane potential changes in cultured cardiomyocytes," *Cardiovascular Research*, vol. 46, pp. 126–138, 2000.

Research Article

Pleiotropic Effects of Biguanides on Mitochondrial Reactive Oxygen Species Production

Alena Pecinova, Zdenek Drahota, Jana Kovalcikova, Nikola Kovarova, Petr Pecina, Lukas Alan, Michal Zima, Josef Houstek, and Tomas Mracek

Institute of Physiology of the Czech Academy of Sciences, Vídeňská, 1083 Prague, Czech Republic

Correspondence should be addressed to Tomas Mracek; tomas.mracek@fgu.cas.cz

Received 29 March 2017; Accepted 13 June 2017; Published 9 August 2017

Academic Editor: Jacek Zielonka

Copyright © 2017 Alena Pecinova et al. This is an open access article distributed under the Creative Commons Attribution License, which permits unrestricted use, distribution, and reproduction in any medium, provided the original work is properly cited.

Metformin is widely prescribed as a first-choice antihyperglycemic drug for treatment of type 2 diabetes mellitus, and recent epidemiological studies showed its utility also in cancer therapy. Although it is in use since the 1970s, its molecular target, either for antihyperglycemic or antineoplastic action, remains elusive. However, the body of the research on metformin effect oscillates around mitochondrial metabolism, including the function of oxidative phosphorylation (OXPHOS) apparatus. In this study, we focused on direct inhibitory mechanism of biguanides (metformin and phenformin) on OXPHOS complexes and its functional impact, using the model of isolated brown adipose tissue mitochondria. We demonstrate that biguanides nonspecifically target the activities of all respiratory chain dehydrogenases (mitochondrial NADH, succinate, and glycerophosphate dehydrogenases), but only at very high concentrations (10^{-2} – 10^{-1} M) that highly exceed cellular concentrations observed during the treatment. In addition, these concentrations of biguanides also trigger burst of reactive oxygen species production which, in combination with pleiotropic OXPHOS inhibition, can be toxic for the organism. We conclude that the beneficial effect of biguanides should probably be associated with subtler mechanism, different from the generalized inhibition of the respiratory chain.

1. Introduction

Metformin (dimethyl biguanide) is the most widely used frontline drug for treatment of type II diabetes mellitus [1, 2]. At the whole-body level, it effectively decreases blood glucose and insulin levels during hyperglycemia [3]. Several possible mechanisms of its action have been suggested, including inhibition of adenylate cyclase [4], interference with mitochondrial dynamics [5], alterations in gut microbiota composition [6], or inhibition of mitochondrial respiratory chain [7, 8]. Some of the proposed mechanisms oscillate around AMP-activated protein kinase (AMPK) activation, which in itself was also suggested as a direct target for biguanides [5, 9]. However, precise molecular mechanism of its action remains questionable [10, 11].

Metformin utility was also explored in the model of heart failure where epidemiologic evidence suggests its protective effect [12, 13]. Nevertheless, at the molecular level, a direct

effect on mitochondria is observed in some cases [14], but not in others [15].

In addition to its antihyperglycemic effect, a broad range of epidemiologic studies showed that chronic metformin treatment is associated with a reduced risk of cancer [16–18]. As well as in the case of diabetes, the explicit mechanism of its antineoplastic action is not yet clear [11]. Metformin was proposed to act either indirectly by decreasing levels of insulin [19] or directly by suppression of mitochondrial-dependent biosynthetic pathways [20, 21]. One of the most studied possible molecular targets for biguanides action is their inhibitory action on respiratory chain complex I (NADH dehydrogenase, NDH), first described in liver tissue [8, 22]. Since then, it was confirmed for various tissues and cellular models and crucially also for cancer cells [11, 23, 24]. Hypothetical model proposes that NDH inhibition leads to decreased respiration and consequently to activation of AMPK, the key player in cellular

energy homeostasis [25]. The exact site of biguanide binding to NDH is ambiguous; it was found to influence reactivity of its flavin cofactor, but it also inhibits ubiquinone reduction in a noncompetitive manner [23]. In addition to NDH, metformin was shown to inhibit other enzymes of the mitochondrial oxidative phosphorylation apparatus, including mitochondrial glycerophosphate dehydrogenase (mGPDH) and ATP synthase [7, 10, 23]. Interestingly, the viability of cancer cells lacking mitochondrial DNA (rho0 cells) is also affected by the drug, making its putative action on respiratory chain complexes rather questionable [26].

Respiratory chain is also a predominant source of reactive oxygen species (ROS), and targeting individual complexes may modulate ROS production and thus influence various pathological processes and/or signaling in different metabolic pathways [27]. Using specific substrates and inhibitors of respiratory chain enzymes, it is possible to localize the site of ROS generation or conversely the binding site of the inhibitor. In isolated mitochondria, the electron leak occurs mainly under the conditions of high NAD(P)H pool reduction [28, 29] or high ubiquinone pool reduction (high proton motive force) [29–31]. Essentially, all of the dehydrogenases in the respiratory chain were under certain conditions demonstrated to allow electron leak and ROS production. Flavin site of complex I (I_F) was identified as a site of superoxide production using NADH-linked substrates [32, 33]. Under the conditions of high flux from succinate oxidation and high proton motive force, the electrons can backflow to NDH and escape at the level of Q site (I_Q) towards the molecular oxygen [30, 31]. SDH itself was shown to produce significant amounts of ROS, especially when succinate levels are low (submillimolar). Under these conditions, flavin site (II_F) is not fully occupied by the substrate and is more accessible to oxygen allowing superoxide generation [34]. Mitochondrial mGPDH was also shown to act as a potent ROS producer [35] even in mitochondria from tissues with low amount of the enzyme [36]. ROS production from mGPDH can reach the levels of ROS from complex III when inhibited with antimycin A (the most potent source of ROS in mitochondria) [37]. Since mGPDH-dependent ROS production increases linearly with increasing GP concentration, the most plausible site of electron leak is the Q site or the semiquinone formed here [27].

Given the conflicting reports regarding the molecular target of biguanides in mitochondria, in this study, we addressed the direct impact of biguanides metformin and phenformin on NDH, SDH, and mGPDH, mitochondrial glycerophosphate dehydrogenases, which feed electrons into respiratory chain and were proposed to be a target of these drugs. We used mitochondria isolated from brown adipose tissue (BAT), which are advantageous for such study as they contain comparable amounts of these dehydrogenases. Furthermore, uncoupling protein 1 (UCP1) dissipates mitochondrial membrane potential ($\Delta\psi_m$) in the isolated BAT mitochondria so that the cationic biguanides are much less concentrated in mitochondrial matrix, and therefore, the determined concentrations of these drugs are very close to the actual ones required for inhibition. We compared the effects of biguanides on dehydrogenases with their

typical inhibitors (rotenone, atpenin A5, and iGP-1) using activity assays, mitochondrial oxygen consumption, and ROS production.

2. Materials and Methods

2.1. Isolation of Mitochondria from Brown Adipose Tissue. We used interscapular brown adipose tissue (BAT) of four-week-old Wistar rats kept at 22°C under 12 h/12 h light/dark cycle on a standard diet and water supply ad libitum. All animal works were approved by the institutional ethics committee and were in accordance with the EU Directive 2010/63/EU for animal experiments. Mitochondria were isolated in STE medium (250 mM sucrose, 10 mM Tris-HCl, 1 mM EDTA, pH 7.4) and supplemented with BSA (10 mg/mL) by differential centrifugation [38]. Quality of isolation was routinely checked by oxygraph, and fresh mitochondria were used for measurements of oxygen consumption and hydrogen peroxide production. Subsequently, frozen-thawed mitochondria were used for determination of enzymatic activities; as in such preparations, the integrity of mitochondrial membrane is disrupted and NADH has therefore access to the oxidation site of NDH. Also, freezing/thawing ensures that the membrane potential is not maintained.

2.2. Enzyme Activity Assays. Activities of mitochondrial dehydrogenases were determined spectrophotometrically as NADH oxidoreductases (NDH, monitored at 340 nm, $\epsilon_{340} = 6.22 \text{ mM}^{-1}\cdot\text{cm}^{-1}$) or CoQ₁ oxidoreductases (SDH and mGPDH, monitored at 275 nm, $\epsilon_{275} = 13.6 \text{ mM}^{-1}\cdot\text{cm}^{-1}$). The assay medium contained 50 mM KCl, 20 mM Tris-HCl, 1 mM EDTA, 1 mg/mL BSA, 2 mM KCN, pH 7.4, and 50 μM CoQ₁. The reaction was started by adding 100 μM NADH, 25 mM glycerophosphate (GP), or 25 mM succinate, respectively, and after 5–10 minutes, changes of absorbance were monitored at 30°C. Enzyme activities were expressed as pmol/s/mg protein.

2.3. Determination of Mitochondrial Membrane Potential. The changes in mitochondrial membrane potential ($\Delta\psi_m$) were measured with TPP⁺-selective electrode as described in [39, 40]. Isolated BAT mitochondria (0.4 mg/mL) were resuspended in KCl medium and subsequently supplemented with 10 mM GP, 0.3% BSA, 1 mM GDP, and 1 μM carbonyl cyanide-p-trifluoromethoxyphenylhydrazone (FCCP). The electrode was calibrated by stepwise addition of TPP⁺ (1–6 μM) before each measurement, and $\Delta\psi_m$ changes were plotted as pTPP, that is, the negative common logarithm of TPP⁺ concentration.

2.4. Fluorometric Detection of Hydrogen Peroxide Production. Hydrogen peroxide production was determined fluorometrically by measuring oxidation of Amplex UltraRed (Thermo Fisher) essentially as before [27]. Fluorescence of the Amplex UltraRed oxidation product was measured at 37°C using Tecan Infinite M200 multiwell fluorometer. Excitation/emission wavelengths were 544 nm (bandwidth 15 nm)/590 nm (bandwidth 30 nm). The assay was performed with 10 μg of mitochondrial protein in KCl-based medium

(120 mM KCl, 3 mM HEPES, 5 mM KH_2PO_4 , 3 mM MgSO_4 , 1 mM EGTA, 3 mg/mL BSA, pH 7.2) supplemented either with 10 mM pyruvate plus 2 mM malate, 10 mM succinate, or 10 mM GP. Amplex UltraRed was used at the final concentration of 50 μM with horseradish peroxidase (HRP) at 1 U/mL. Fluorescence signal from the well containing all substrates and inhibitors, but not mitochondria, was subtracted as a background for every experimental condition used. Background, caused mostly by autoxidation of the dye or nonenzymatic effect of inhibitors on apparent ROS production, varied between conditions from 0 to 1 pmol/s/mg and was uniform across respective titration points. Signal was calibrated using H_2O_2 at the final concentration of 0–5 μM , and H_2O_2 stock concentration was routinely checked by measuring its absorption at 240 nm.

2.5. Western Blotting. BAT and liver homogenates were denatured at 65°C for 15 min in a sample lysis buffer (2% (v/v) 2-mercaptoethanol, 4% (w/v) SDS, 50 mM Tris-HCl, pH 7.0, 10% (v/v) glycerol, and 0.017% (w/v) Coomassie Brilliant Blue R-250), and Tricine SDS-PAGE [41] was performed on 10% (w/v) polyacrylamide slab gels at room temperature. The gels were blotted onto a PVDF membrane (Immobilon P, Merck Millipore) by semidry electrotransfer at 0.8 mA/cm² for 1 h. Membranes were blocked in 5% nonfat dried milk dissolved in TBS (150 mM NaCl, 10 mM Tris-HCl, pH 7.5) for 1 h at room temperature and incubated for 2 h with the following primary antibodies: antibody to NADH dehydrogenase (NDUFA9 subunit of complex I)—Abcam ab14713, succinate dehydrogenase complex (subunit A (SDHA) of complex II)—Abcam ab14715, Core2 subunit of complex III—Abcam ab14745, actin—Millipore MAB1501, rabbit polyclonal antibody to porin (1:1000) was a kind gift from Professor Vito de Pinto (Dipartimento di Scienze Chimiche, Catania, Italy), and rabbit polyclonal antibody to mGPDH was custom prepared [42]. Membranes were then incubated for 1 h with corresponding secondary fluorescent antibodies, IRDye 680- or 800-conjugated donkey anti-mouse IgG (Thermo Fischer) or donkey anti-rabbit IgG (LI-COR Biosciences), respectively. The fluorescence was detected using ODYSSEY infra-red imaging system (LI-COR Biosciences), and the signal was quantified using Aida 3.21 Image Analyzer software (RayTest).

2.6. Polarographic Detection of Oxygen Consumption. Oxygen consumption was measured at 30°C as described before [35] using Oxygraph-2k (Oroboros, Austria). Measurements were performed in 2 mL of KCl medium (80 mM KCl, 10 mM Tris-HCl, 3 mM MgCl_2 , 1 mM EDTA, 5 mM K-Pi, pH 7.4) using 15–60 μg protein/mL of freshly isolated mitochondria. For measurements, 10 mM pyruvate plus 2 mM malate, 10 mM succinate, or 10 mM GP, respectively, were used. The oxygen consumption was expressed in pmol oxygen/s/mg protein.

3. Results and Discussion

The direct mechanistic knowledge on how biguanides (metformin, phenformin) influence mitochondrial function

is not yet clear. While their inhibitory effect on NADH dehydrogenase (complex I, NDH) received most attention [8, 23, 24], it was also reported that biguanides can inhibit other dehydrogenases in the mitochondrial respiratory chain, namely, succinate dehydrogenase (SDH) [10] and mitochondrial glycerophosphate dehydrogenase (mGPDH) [7]. As those dehydrogenases substantially differ in their architecture of substrate sites, coenzyme Q (CoQ), binding sites and pathways of the electron transfer from substrate to CoQ, such as lack of selectivity, is rather surprising. Therefore, we focused on the action of biguanides on NDH, SDH, and mGPDH and compared it with canonical specific inhibitors of ubiquinone binding site of complex I (rotenone) [31], ubiquinone site of SDH (atpenin A5) [43], and the novel specific inhibitor of mGPDH (iGP-1) [44].

As a model, we chose isolated mitochondria from brown adipose tissue (BAT), as they have several advantages for such study. First, compared to the liver, where the inhibitory action of biguanides on mGPDH was originally described [7], they contain near equimolar levels of all three dehydrogenases studied. This can be documented both at the level of protein quantity (Figure 1(a)) and enzyme activity (NDH, SDH, and mGPDH, Figure 1(b)). The differences in response between dehydrogenases in BAT cannot therefore be ascribed to the varying content of enzymes studied. It is well established [36] and also obvious from Figure 1(b) that mGPDH activity in the liver is particularly low, and this can render the accurate measurement of inhibitory effects on GQR quite difficult. Another advantage of BAT mitochondria is the presence of UCP1 protein [45] which under native conditions allows the flow of protons back to the matrix (Figure 1(c)) and thus effectively discharges the mitochondrial membrane potential to the same level as prototypic uncoupler FCCP as can be seen by direct $\Delta\psi_m$ determination on TPP⁺-selective electrode (Figure 1(d)). This means that studied ROS production is independent of OXPHOS coupling. On the other hand, mitochondria can easily be coupled by the inhibitory action of guanosine diphosphate (GDP) on the UCP1 and contribution of electron backflow can then be established. Finally, lack of coupling together with physiologically low levels of mitochondrial F_0F_1 ATP synthase makes the action of biguanides on mitochondrial dehydrogenases rather independent of ATP synthase activity. This is quite important as F_0F_1 ATP synthase was also shown to be inhibited by biguanides [23] and thus may blur the picture in other model systems.

3.1. Effect of Biguanides on Enzymatic Activities. As a first step, we estimated direct impact of metformin on activity of each complex measured as individual dehydrogenase activity (substrate:coenzyme Q) in frozen-thawed mitochondria or in the context of electron transport chain in intact mitochondria measured as oxygen consumption using respective substrates (Figure 2). Metformin inhibited all enzymes studied, but only at very high concentrations (IC_{50} varied from 80 to 180 mM, Figures 2(a), 2(b), and 2(c)). Out of those activities, NDH was the most sensitive to the inhibitory action of metformin (Figure 2(a)). Similarly, at the same concentrations, metformin also inhibited respiration with pyruvate

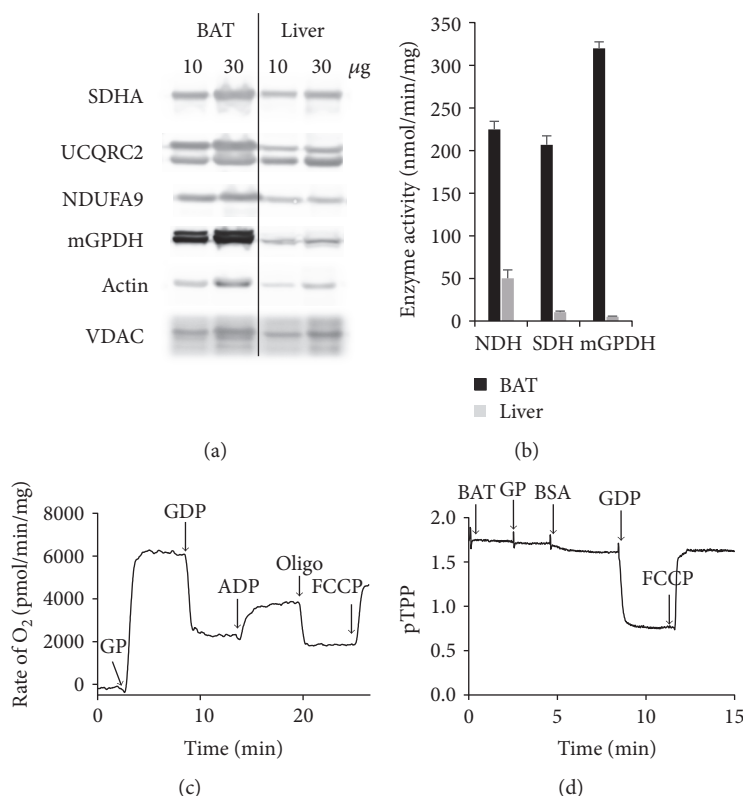


FIGURE 1: Characterization of brown adipose tissue (BAT) mitochondria. (a) SDS-PAGE and Western blot analysis of mitochondrial respiratory chain complexes in BAT and liver homogenates by polyclonal antibodies against mGPDH and VDAC and monoclonal antibodies against representative subunits of NDH (subunit NDUFA9), SDH (subunit SDHA), complex III (subunit UCQRC2), and actin. Two protein concentrations were loaded as indicated, representative image of three biological replicates. (b) Enzyme activities of mitochondrial dehydrogenases in mitochondria isolated from the BAT and liver. Activities were determined as rates of CoQ₁ reduction using respective substrates. Results are means \pm SEM from three independent measurements. (c) Representative quality control curve of O₂ consumption and (d) representative trace of $\Delta\psi_m$ measurement in isolated BAT mitochondria. The following compounds were added: 10 mM glycerophosphate (GP), 0.3% BSA, 1 mM GDP, 1 mM ADP, 1 μ M oligomycin (oligo), and 1 μ M carbonyl cyanide-p-trifluoromethoxyphenylhydrazone (FCCP).

and malate used as substrates for NDH (Figure 2(d)), succinate for SDH (Figure 2(e)), and glycerophosphate (GP) for mGPDH (Figure 2(f)). Another biguanide, phenformin, behaved analogously to metformin, but its inhibitory effect was more efficient; the IC₅₀ varied between 10 and 25 mM for both isolated enzyme activities and respiration of all three dehydrogenases (Figure 3). Because of the limited permeability of the biguanides, we waited to reach plateau (approximately 5 min) before proceeding to the next addition. It is to be stressed that IC₅₀ values of observed inhibitory effects in uncoupled mitochondria (oxygraphy) were the same or slightly higher than corresponding IC₅₀ values in frozen-thawed mitochondria (spectrophotometry), thus conferring comparable concentration of biguanides on both sides of the inner mitochondrial membrane. Determined IC₅₀ in our case is rather high in comparison with that previously reported [7, 33]. This can be most likely attributed to the uncoupled state of BAT mitochondria which prevents accumulation of biguanides in mitochondria (see below).

Subsequently, we focused on the action of canonical inhibitors on individual complexes. As expected, rotenone completely inhibited complex I enzyme activity as well as

pyruvate plus malate-supported oxygen consumption at 500 nM. Similarly, complete inhibition of SDH by atpenin A5 using succinate as a substrate was achieved at even lower concentrations (20 nM) and activity of mGPDH was abolished at 50 μ M of iGP-1. Interestingly, we also observed some nonspecific actions of iGP-1 on SDH (Figures 4(b) and 4(d)), but the IC₅₀ was significantly higher (\sim 80 μ M) than that in the case of mGPDH (Figures 4(a) and 4(c)).

Given the extremely high IC₅₀ we identified for phenformin and metformin, it is to be questioned whether their effects on respiratory chain enzymes are pharmacologically relevant and can affect mitochondrial function in tumors. As already mentioned, isolated BAT mitochondria with inherently low levels of mitochondrial membrane potential represent a model free of the effect of metformin partitioning due to its charge. Biguanides carry a positive charge, which means that they do accumulate in cells and mitochondria in dependence on membrane potential across both cellular and mitochondrial membranes. Thus, the concentration could be 100 to 300 times higher inside energized mitochondria (compared to concentration in cytosol) with the difference in mitochondrial membrane potential between

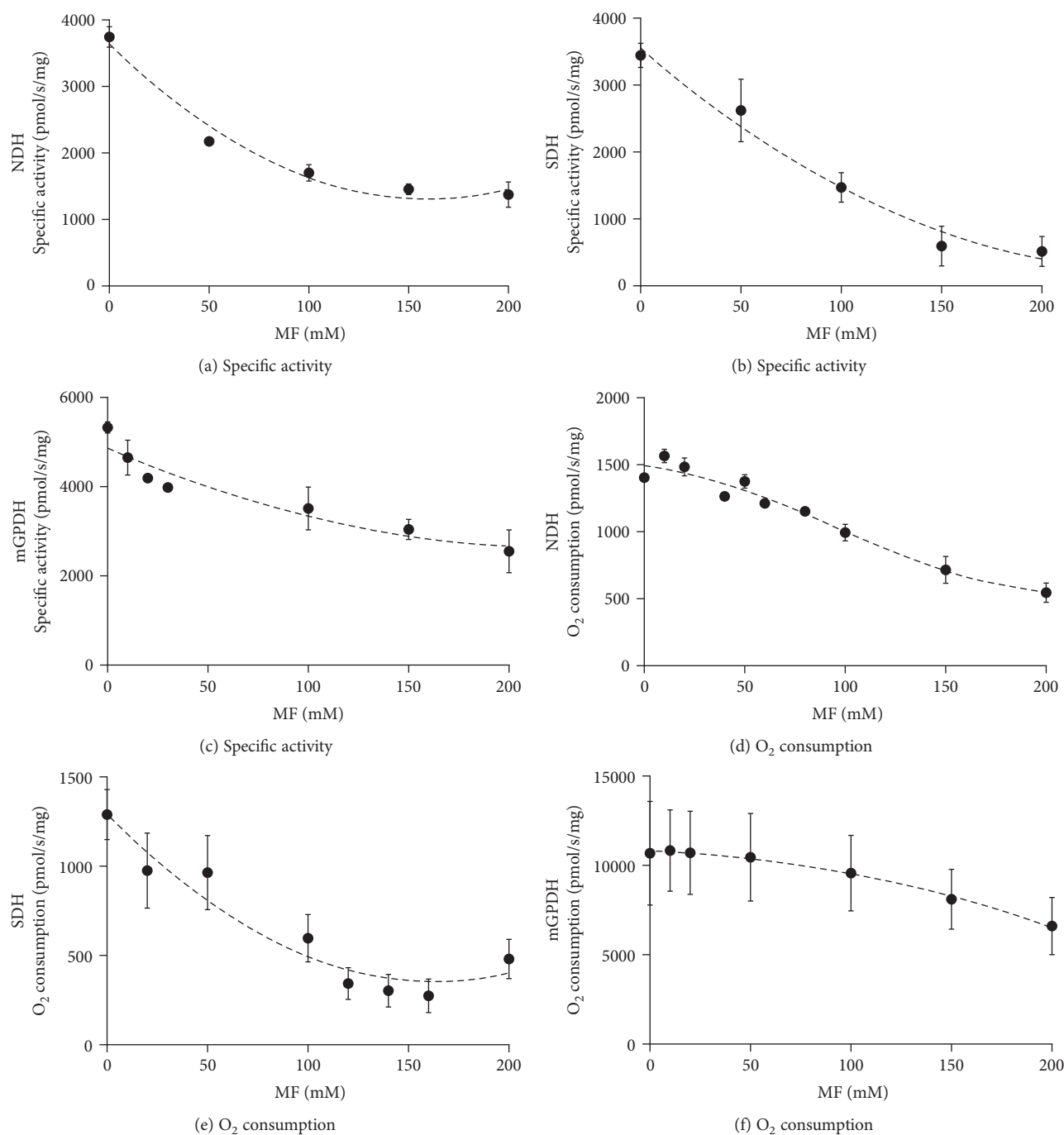


FIGURE 2: Respiratory chain dehydrogenase sensitivity to metformin titration. Specific enzyme activities (a, b, c) or oxygen consumption (d, e, f) of BAT mitochondria was titrated with 0–200 mM metformin using 100 μ M NADH (a) or 10 mM pyruvate plus 2 mM malate (d), 10 mM succinate (b, e), and 25 mM (c) or 10 mM glycerophosphate (f). Individual points represent means \pm SEM of at least three independent measurements.

120 and 150 mV [23]. Since the reported values for metformin concentration inside tumors are in 1–10 μ M range [21], the actual concentration in respiring mitochondria could reach mM values, which is likely not sufficient for the inhibitory action on mitochondrial oxidative phosphorylation. Indeed, in this regard, it is important to note that two recent reports demonstrated higher tumor antiproliferative efficiency for mitochondrially targeted (through positive

charge of conjugated TPP moiety) analogs of metformin [46, 47]. However, metformin and its conjugated analogs accumulate in the mitochondrial matrix, where they can act on enzyme complexes facing this compartment, namely, NDH and SDH. The effect on mGPDH is more questionable, since this enzyme is located on the outer face of the inner membrane, facing the mitochondrial intermembrane space and does not span to the matrix [48]. One of the reports

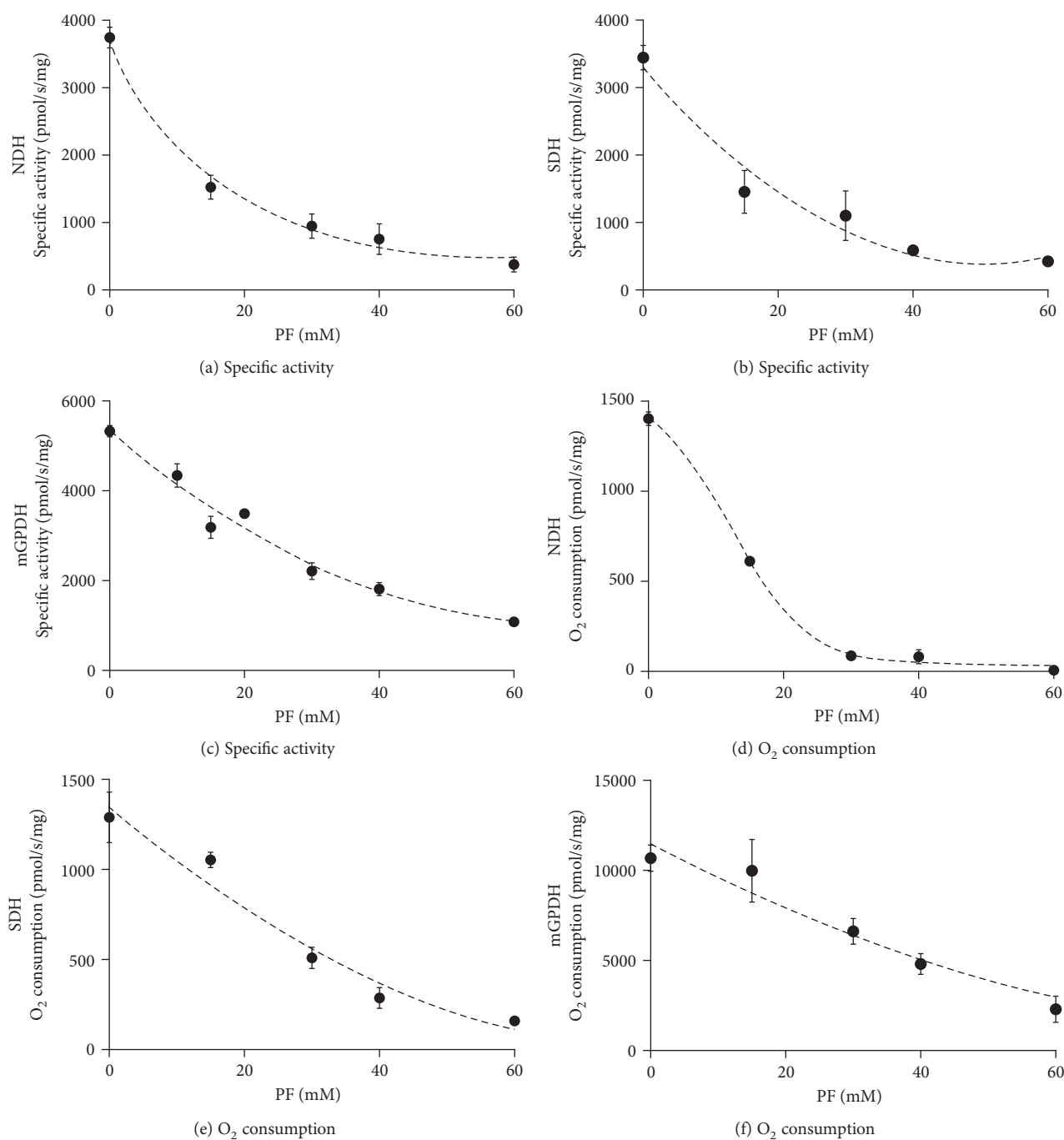


FIGURE 3: Respiratory chain dehydrogenases sensitivity to phenformin titration. Specific enzyme activities (a, b, c) or oxygen consumption (d, e, f) of BAT mitochondria was titrated with 0–60 mM phenformin using 100 μ M NADH (a) or 10 mM pyruvate plus 2 mM malate (d), 10 mM succinate (b, e), and 25 mM (c) or 10 mM glycerophosphate (f). Individual points represent means \pm SEM of at least three independent measurements.

using mitochondrially targeted metformin analogs [46] reported also higher potency of that compound on GP-dependent respiration, which would be in line with rather generalized nonspecific mode of action for example through the influencing of mitochondrial membrane properties.

3.2. Reactive Oxygen Species Production. Action of pharmacologically active compounds on suppression of cancer cell

proliferation may not only be achieved by decreased flow of electrons through respiratory chain and associated impairment of aerobic ATP production. Another successful antiproliferative strategy may be to increase in reactive oxygen species (ROS) production and subsequent induction of apoptosis [49, 50]. It was also proposed for biguanides that their primary antiproliferative effect is manifested through increase in ROS production [21, 23], which also holds true

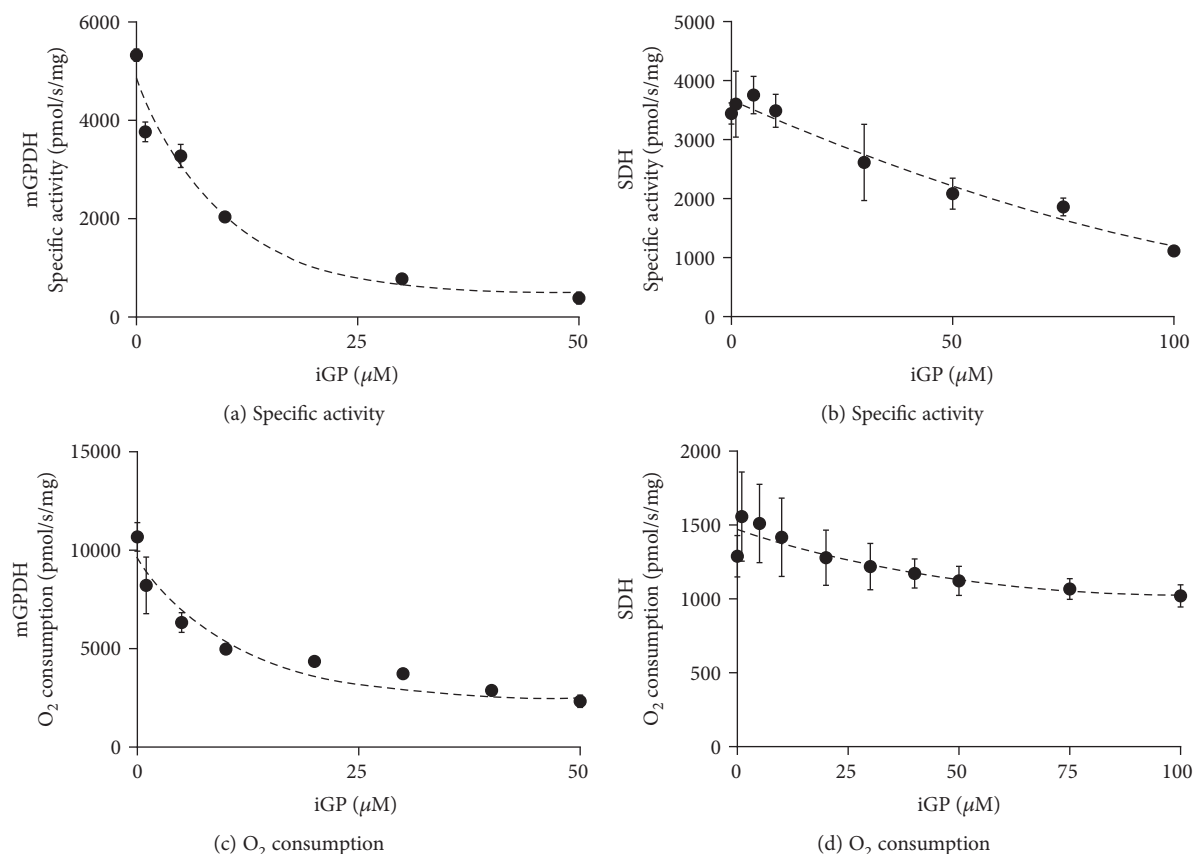


FIGURE 4: Comparison of iGP-1 effect on respiratory chain dehydrogenases mGPDH and SDH. Specific enzyme activities (a, b) or oxygen consumption (c, d) of BAT mitochondria was titrated with 0–100 μM iGP-1 using 25 mM (a) or 10 mM glycerophosphate (c) and 10 mM succinate (b, d). Individual points represent means \pm SEM of at least three independent measurements.

for the mitochondria-targeted analogs [51]. In this case, the mitochondrial ROS also interfered with redox signaling events. Mitochondrial respiratory chain contains numerous sites which may leak electrons to molecular oxygen and produce superoxide [27, 34, 35, 52–55]. The major superoxide-producing sites in mitochondrial respiratory chain were proposed to be NDH [53, 56], complex III [53, 57], mGPDH [27, 35], and, under certain circumstances, also SDH [34].

To distinguish sites in mitochondrial respiratory chain, where biguanides may induce electron leak, we followed the rates of ROS production (detected as H_2O_2 upon conversion by superoxide dismutase) in fresh mitochondria from BAT, where the respiratory chain is not reduced due to uncoupling by UCP1. First, using the established inhibitors of individual dehydrogenases and their respective substrates, we established ROS production pattern characteristic for each site in BAT mitochondria (Figure 5). As expected, also in BAT mitochondria, rotenone increased the rate of H_2O_2 production with NADH-linked substrates (pyruvate and malate), indicative of ROS production from I_F site (Figure 5(a)).

Using high concentrations of succinate (10 mM), very low levels of ROS were produced in uncoupled state, which is in agreement with the previously published data [29] and this leak occurs at the Q site of SDH (Figure 5(b)). After GDP coupling, ROS were produced by the electron backflow at the I_Q site of NDH (Figure 5(b)). Low levels of succinate

led to pronounced increase in ROS production from flavin of SDH (inhibition of the Q site by atpenin A5, Figure 5(c)).

GP-dependent ROS production was quite high even when respiratory chain was not reduced and did not increase further after GDP addition, again in agreement with previously reported data [37, 58], and it was inhibited by mGPDH inhibitor iGP-1 (Figure 5(d)).

Compared to typical inhibitors, both metformin and phenformin induced dose-dependent increase in ROS production, but it seemed rather indiscriminate, as its pattern was highly similar for all substrates tested (Figures 5(e) and 5(f)). It suggests that these compounds do not bind directly to either flavin or ubiquinone-binding site of either of the dehydrogenases studied and that biguanides can affect mitochondria by different mechanisms, for example, they can influence membrane phospholipid environment.

4. Conclusions

Our data demonstrate that the inhibitory effect of biguanides on OXPHOS enzymes is rather pleiotropic including the previously reported inhibition of NADH and mGPDH dehydrogenases. Drug sensitivity of respiratory chain complexes in brown adipose tissue was comparable, with IC_{50} higher than 80 mM in case of metformin or ranging from 20 to 30 mM in case of the more potent phenformin.

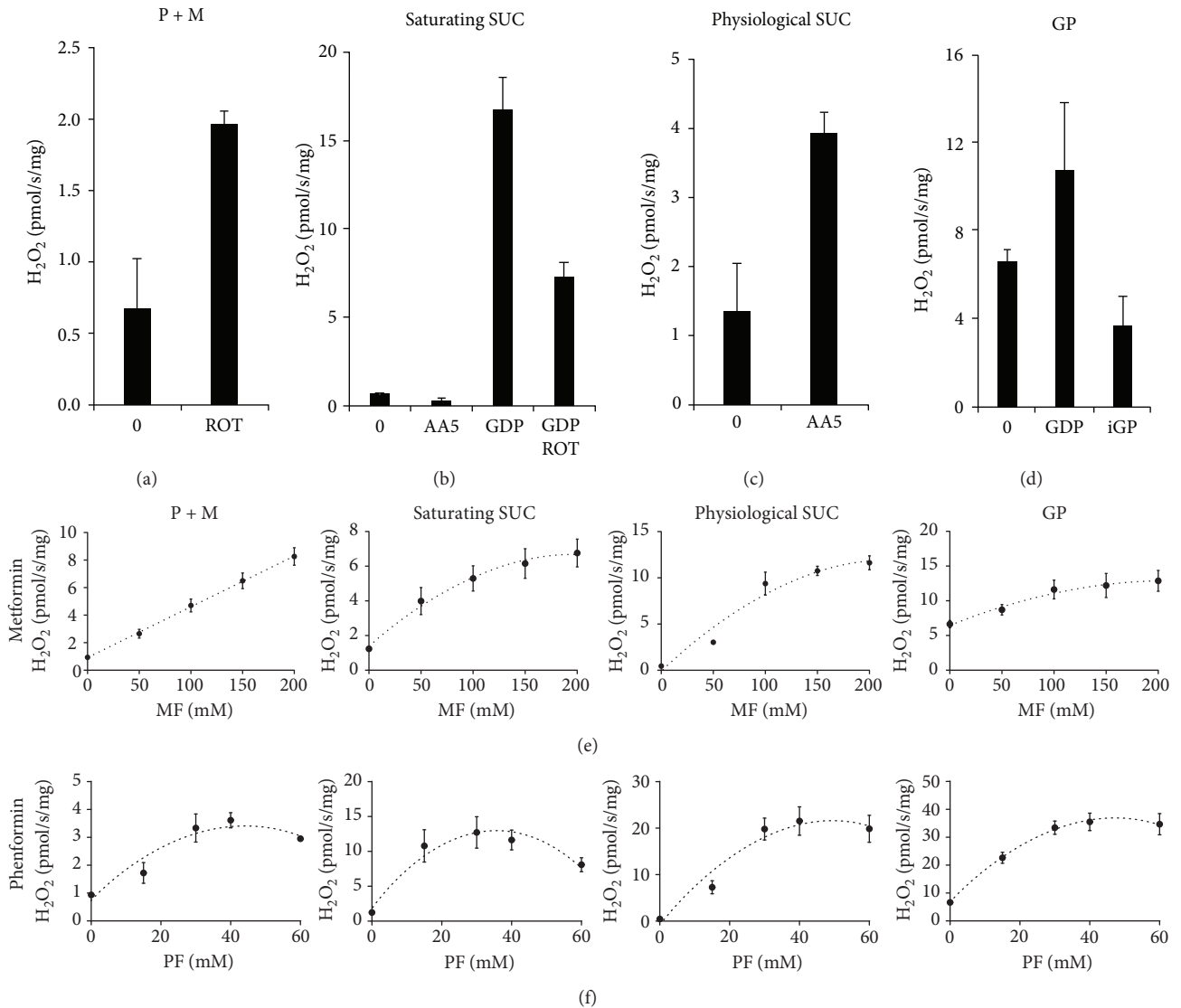


FIGURE 5: Effect of biguanides on reactive oxygen species (ROS) production compared to typical inhibitors. The rate of H₂O₂ generation was estimated by Amplex red assay. H₂O₂ production with (a) 10 mM pyruvate and 2 mM malate (P + M) with or without 1 μ M rotenone (ROT), (b) 10 mM succinate (saturating SUC) with or without 0.5 μ M atpenin A5 (AA5) or 1 μ M rotenone, (c) 0.4 mM succinate (physiological SUC) with or without 0.5 μ M atpenin A5, and (d) 10 mM glycerophosphate (GP) with or without 100 μ M iGP-1 (iGP) were indicated; BAT mitochondria were coupled with 1 mM guanosine diphosphate (GDP). (e) Titration of H₂O₂ production by biguanides metformin (MF, 0–200 mM) or (f) phenformin (PF, 0–60 mM) using the same substrate concentrations as in respective experiments in (a–d). Each point is the mean \pm SEM of at least three independent measurements.

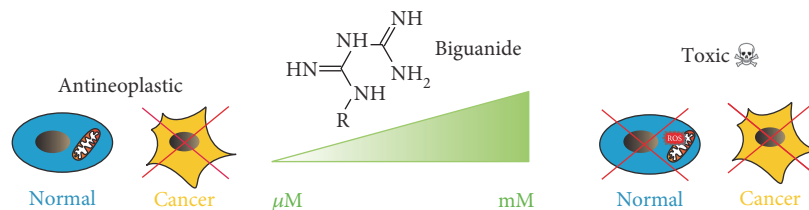


FIGURE 6: Proposed scheme of biguanide action. While at micromolar concentrations, biguanides confer antineoplastic action; at millimolar ones, they inhibit mitochondrial respiratory chain complexes and are toxic for all the cells.

Moreover, these biguanide concentrations induce nonspecific increase of mitochondrial reactive oxygen species production. Our data suggest that biguanides do not bind to any specific sites on respiratory chain dehydrogenases and require high concentrations to be effective. Under these conditions, their effect on dehydrogenases remains therapeutically questionable. Indeed, phenformin use had to be discontinued due to induction of lactic acidosis in treated patients. As summarized in Figure 6, we propose that pharmacologically relevant concentrations of biguanides confer their antineoplastic effect through yet unidentified target in mitochondrial metabolism, different from the inhibition of individual dehydrogenases.

Abbreviations

BAT:	Brown adipose tissue
NDH:	NADH dehydrogenase
SDH:	Succinate dehydrogenase
mGPDH:	Mitochondrial glycerophosphate dehydrogenase
OXPPOS:	Oxidative phosphorylation
GDP:	Guanosine diphosphate
ROS:	Reactive oxygen species
MF:	Metformin
PF:	Phenformin
UCP1:	Uncoupling protein 1
I _Q :	Coenzyme Q binding site of respiratory chain complex I
I _F :	Flavin site of respiratory chain complex I
I _{II} :	Flavin site of respiratory chain complex II.

Conflicts of Interest

All authors declare that there is no conflict of interests.

Acknowledgments

This work was supported by the Grant Agency of the Czech Republic (16-12726S) and the Ministry of Education, Youth and Sports of the Czech Republic (ERC CZ: LL1204). Institutional support was provided through the Project RVO:67985823.

References

- [1] E. Bosi, "Metformin—the gold standard in type 2 diabetes: what does the evidence tell us?," *Diabetes, Obesity & Metabolism*, vol. 11, Supplement 2, pp. 3–8, 2009.
- [2] R. K. Campbell, J. R. White Jr., and B. A. Saulie, "Metformin: a new oral biguanide," *Clinical Therapeutics*, vol. 18, no. 3, pp. 360–371, 1996.
- [3] W. C. Knowler, E. Barrett-Connor, S. E. Fowler et al., "Reduction in the incidence of type 2 diabetes with lifestyle intervention or metformin," *The New England Journal of Medicine*, vol. 346, no. 6, pp. 393–403, 2002.
- [4] R. A. Miller, Q. Chu, J. Xie, M. Foretz, B. Viollet, and M. J. Birnbaum, "Biguanides suppress hepatic glucagon signalling by decreasing production of cyclic AMP," *Nature*, vol. 494, no. 7436, pp. 256–260, 2013.
- [5] Q. Wang, M. Zhang, G. Torres et al., "Metformin suppresses diabetes-accelerated atherosclerosis via the inhibition of Drp1-mediated mitochondrial fission," *Diabetes*, vol. 66, no. 1, pp. 193–205, 2017.
- [6] K. Forslund, F. Hildebrand, T. Nielsen et al., "Disentangling type 2 diabetes and metformin treatment signatures in the human gut microbiota," *Nature*, vol. 528, no. 7581, pp. 262–266, 2015.
- [7] A. K. Madiraju, D. M. Erion, Y. Rahimi et al., "Metformin suppresses gluconeogenesis by inhibiting mitochondrial glycerophosphate dehydrogenase," *Nature*, vol. 510, no. 7506, pp. 542–546, 2014.
- [8] M. R. Owen, E. Doran, and A. P. Halestrap, "Evidence that metformin exerts its anti-diabetic effects through inhibition of complex I of the mitochondrial respiratory chain," *The Biochemical Journal*, vol. 348, no. 3, pp. 607–614, 2000.
- [9] G. Zhou, R. Myers, Y. Li et al., "Role of AMP-activated protein kinase in mechanism of metformin action," *The Journal of Clinical Investigation*, vol. 108, no. 8, pp. 1167–1174, 2001.
- [10] Z. Drahota, E. Palenickova, R. Endlicher et al., "Biguanides inhibit complex I, II and IV of rat liver mitochondria and modify their functional properties," *Physiological Research*, vol. 63, no. 1, pp. 1–11, 2014.
- [11] M. Foretz, B. Guigas, L. Bertrand, M. Pollak, and B. Viollet, "Metformin: from mechanisms of action to therapies," *Cell Metabolism*, vol. 20, no. 6, pp. 953–966, 2014.
- [12] D. T. Eurich, S. R. Majumdar, F. A. McAlister, R. T. Tsuyuki, and J. A. Johnson, "Improved clinical outcomes associated with metformin in patients with diabetes and heart failure," *Diabetes Care*, vol. 28, no. 10, pp. 2345–2351, 2005.
- [13] F. A. Masoudi, S. E. Inzucchi, Y. Wang, E. P. Havranek, J. M. Foody, and H. M. Krumholz, "Thiazolidinediones, metformin, and outcomes in older patients with diabetes and heart failure: an observational study," *Circulation*, vol. 111, no. 5, pp. 583–590, 2005.
- [14] D. Sun and F. Yang, "Metformin improves cardiac function in mice with heart failure after myocardial infarction by regulating mitochondrial energy metabolism," *Biochemical and Biophysical Research Communications*, vol. 486, no. 2, pp. 329–335, 2017.
- [15] J. Benes, L. Kazdova, Z. Drahota et al., "Effect of metformin therapy on cardiac function and survival in a volume-overload model of heart failure in rats," *Clinical Science*, vol. 121, no. 1, pp. 29–41, 2011.
- [16] A. Decensi, M. Puntoni, P. Goodwin et al., "Metformin and cancer risk in diabetic patients: a systematic review and meta-analysis," *Cancer Prevention Research*, vol. 3, no. 11, pp. 1451–1461, 2010.
- [17] G. Libby, L. A. Donnelly, P. T. Donnan, D. R. Alessi, A. D. Morris, and J. M. Evans, "New users of metformin are at low risk of incident cancer: a cohort study among people with type 2 diabetes," *Diabetes Care*, vol. 32, no. 9, pp. 1620–1625, 2009.
- [18] M. Pollak, "Potential applications for biguanides in oncology," *The Journal of Clinical Investigation*, vol. 123, no. 9, pp. 3693–3700, 2013.
- [19] M. Pollak, "The insulin and insulin-like growth factor receptor family in neoplasia: an update," *Nature Reviews Cancer*, vol. 12, no. 3, pp. 159–169, 2012.
- [20] T. Griss, E. E. Vincent, R. Egnatchik et al., "Metformin antagonizes cancer cell proliferation by suppressing mitochondrial

- dependent biosynthesis," *PLoS Biology*, vol. 13, no. 12, article e1002309, 2015.
- [21] X. Liu, I. L. Romero, L. M. Litchfield, E. Lengyel, and J. W. Locasale, "Metformin targets central carbon metabolism and reveals mitochondrial requirements in human cancers," *Cell Metabolism*, vol. 24, no. 5, pp. 728–739, 2016.
- [22] M. Y. El-Mir, V. Nogueira, E. Fontaine, N. Averet, M. Rigoulet, and X. Leverve, "Dimethylbiguanide inhibits cell respiration via an indirect effect targeted on the respiratory chain complex I," *The Journal of Biological Chemistry*, vol. 275, no. 1, pp. 223–228, 2000.
- [23] H. R. Bridges, A. J. Jones, M. N. Pollak, and J. Hirst, "Effects of metformin and other biguanides on oxidative phosphorylation in mitochondria," *The Biochemical Journal*, vol. 462, no. 3, pp. 475–487, 2014.
- [24] W. W. Wheaton, S. E. Weinberg, R. B. Hamanaka et al., "Metformin inhibits mitochondrial complex I of cancer cells to reduce tumorigenesis," *eLife*, vol. 3, article e02242, 2014.
- [25] B. Viollet, B. Guigas, N. Sanz Garcia, J. Leclerc, M. Foretz, and F. Andreelli, "Cellular and molecular mechanisms of metformin: an overview," *Clinical Science*, vol. 122, no. 6, pp. 253–270, 2012.
- [26] X. Liu, R. R. Chhipa, S. Pooya et al., "Discrete mechanisms of mTOR and cell cycle regulation by AMPK agonists independent of AMPK," *Proceedings of the National Academy of Sciences of the United States of America*, vol. 111, no. 4, pp. E435–E444, 2014.
- [27] T. Mracek, E. Holzerova, Z. Drahota et al., "ROS generation and multiple forms of mammalian mitochondrial glycerol-3-phosphate dehydrogenase," *Biochimica et Biophysica Acta (BBA) - Bioenergetics*, vol. 1837, no. 1, pp. 98–111, 2014.
- [28] A. P. Kudin, N. Y. Bimpong-Buta, S. Vielhaber, C. E. Elger, and W. S. Kunz, "Characterization of superoxide-producing sites in isolated brain mitochondria," *The Journal of Biological Chemistry*, vol. 279, no. 6, pp. 4127–4135, 2004.
- [29] C. L. Quinlan, J. R. Treberg, I. V. Perevoshchikova, A. L. Orr, and M. D. Brand, "Native rates of superoxide production from multiple sites in isolated mitochondria measured using endogenous reporters," *Free Radical Biology and Medicine*, vol. 53, no. 9, pp. 1807–1817, 2012.
- [30] S. S. Korshunov, V. P. Skulachev, and A. A. Starkov, "High protonic potential actuates a mechanism of production of reactive oxygen species in mitochondria," *FEBS Letters*, vol. 416, no. 1, pp. 15–18, 1997.
- [31] A. J. Lambert and M. D. Brand, "Superoxide production by NADH: ubiquinone oxidoreductase (complex I) depends on the pH gradient across the mitochondrial inner membrane," *The Biochemical Journal*, vol. 382, Part 2, pp. 511–517, 2004.
- [32] A. Herrero and G. Barja, "Sites and mechanisms responsible for the low rate of free radical production of heart mitochondria in the long-lived pigeon," *Mechanisms of Ageing and Development*, vol. 98, no. 2, pp. 95–111, 1997.
- [33] J. Hirst, M. S. King, and K. R. Pryde, "The production of reactive oxygen species by complex I," *Biochemical Society Transactions*, vol. 36, Part 5, pp. 976–980, 2008.
- [34] C. L. Quinlan, A. L. Orr, I. V. Perevoshchikova, J. R. Treberg, B. A. Ackrell, and M. D. Brand, "Mitochondrial complex II can generate reactive oxygen species at high rates in both the forward and reverse reactions," *The Journal of Biological Chemistry*, vol. 287, no. 32, pp. 27255–27264, 2012.
- [35] Z. Drahota, S. K. Chowdhury, D. Floryk et al., "Glycerophosphate-dependent hydrogen peroxide production by brown adipose tissue mitochondria and its activation by ferricyanide," *Journal of Bioenergetics and Biomembranes*, vol. 34, no. 2, pp. 105–113, 2002.
- [36] T. Mracek, A. Pecinova, M. Vrbacky, Z. Drahota, and J. Houstek, "High efficiency of ROS production by glycerophosphate dehydrogenase in mammalian mitochondria," *Archives of Biochemistry and Biophysics*, vol. 481, no. 1, pp. 30–36, 2009.
- [37] M. Vrbacky, Z. Drahota, T. Mracek et al., "Respiratory chain components involved in the glycerophosphate dehydrogenase-dependent ROS production by brown adipose tissue mitochondria," *Biochimica et Biophysica Acta (BBA) - Bioenergetics*, vol. 1767, no. 7, pp. 989–997, 2007.
- [38] B. Cannon and O. Lindberg, "Mitochondria from brown adipose tissue: isolation and properties," *Methods in Enzymology*, vol. 55, pp. 65–78, 1979.
- [39] A. Labajova, A. Vojtiskova, P. Krivakova, J. Kofranek, Z. Drahota, and J. Houstek, "Evaluation of mitochondrial membrane potential using a computerized device with a tetraphenylphosphonium-selective electrode," *Analytical Biochemistry*, vol. 353, no. 1, pp. 37–42, 2006.
- [40] A. Pecinova, Z. Drahota, H. Nuskova, P. Pecina, and J. Houstek, "Evaluation of basic mitochondrial functions using rat tissue homogenates," *Mitochondrion*, vol. 11, no. 5, pp. 722–728, 2011.
- [41] H. Schagger and G. von Jagow, "Tricine-sodium dodecyl sulfate-polyacrylamide gel electrophoresis for the separation of proteins in the range from 1 to 100 kDa," *Analytical Biochemistry*, vol. 166, no. 2, pp. 368–379, 1987.
- [42] T. Mracek, P. Jesina, P. Krivakova et al., "Time-course of hormonal induction of mitochondrial glycerophosphate dehydrogenase biogenesis in rat liver," *Biochimica et Biophysica Acta (BBA) - General Subjects*, vol. 1726, no. 2, pp. 217–223, 2005.
- [43] H. Miyadera, K. Shiomi, H. Ui et al., "Atpenins, potent and specific inhibitors of mitochondrial complex II (succinate-ubiquinone oxidoreductase)," *Proceedings of the National Academy of Sciences of the United States of America*, vol. 100, no. 2, pp. 473–477, 2003.
- [44] A. L. Orr, D. Ashok, M. R. Sarantos et al., "Novel inhibitors of mitochondrial sn-glycerol 3-phosphate dehydrogenase," *PLoS One*, vol. 9, no. 2, article e89938, 2014.
- [45] J. Houstek, B. Cannon, and O. Lindberg, "Glycerol-3-phosphate shuttle and its function in intermediary metabolism of hamster brown-adipose tissue," *European Journal of Biochemistry*, vol. 54, no. 1, pp. 11–18, 1975.
- [46] S. Boukalova, J. Stursa, L. Werner et al., "Mitochondrial targeting of metformin enhances its activity against pancreatic cancer," *Molecular Cancer Therapeutics*, vol. 15, no. 12, pp. 2875–2886, 2016.
- [47] G. Cheng, J. Zielonka, O. Ouari et al., "Mitochondria-targeted analogues of metformin exhibit enhanced antiproliferative and radiosensitizing effects in pancreatic cancer cells," *Cancer Research*, vol. 76, no. 13, pp. 3904–3915, 2016.
- [48] T. Mracek, Z. Drahota, and J. Houstek, "The function and the role of the mitochondrial glycerol-3-phosphate dehydrogenase in mammalian tissues," *Biochimica et Biophysica Acta (BBA) - Bioenergetics*, vol. 1827, no. 3, pp. 401–410, 2013.

- [49] K. Kluckova, M. Sticha, J. Cerny et al., "Ubiquinone-binding site mutagenesis reveals the role of mitochondrial complex II in cell death initiation," *Cell Death & Disease*, vol. 6, article e1749, 2015.
- [50] J. Rohlena, L. F. Dong, K. Kluckova et al., "Mitochondrially targeted alpha-tocopheryl succinate is antiangiogenic: potential benefit against tumor angiogenesis but caution against wound healing," *Antioxidants & Redox Signaling*, vol. 15, no. 12, pp. 2923–2935, 2011.
- [51] B. Kalyanaraman, G. Cheng, M. Hardy et al., "Modified metformin as a more potent anticancer drug: mitochondrial inhibition, redox signaling, antiproliferative effects and future EPR studies," *Cell Biochemistry and Biophysics*, 2017.
- [52] E. Cadenas and K. J. Davies, "Mitochondrial free radical generation, oxidative stress, and aging," *Free Radical Biology and Medicine*, vol. 29, no. 3-4, pp. 222–230, 2000.
- [53] Q. Chen, E. J. Vazquez, S. Moghaddas, C. L. Hoppel, and E. J. Lesnefsky, "Production of reactive oxygen species by mitochondria: central role of complex III," *The Journal of Biological Chemistry*, vol. 278, no. 38, pp. 36027–36031, 2003.
- [54] P. Schonfeld and L. Wojtczak, "Brown adipose tissue mitochondria oxidizing fatty acids generate high levels of reactive oxygen species irrespective of the uncoupling protein-1 activity state," *Biochimica et Biophysica Acta (BBA) - Bioenergetics*, vol. 1817, no. 3, pp. 410–418, 2012.
- [55] L. Tretter and V. Adam-Vizi, "Generation of reactive oxygen species in the reaction catalyzed by alpha-ketoglutarate dehydrogenase," *The Journal of Neuroscience*, vol. 24, no. 36, pp. 7771–7778, 2004.
- [56] L. Kussmaul and J. Hirst, "The mechanism of superoxide production by NADH:ubiquinone oxidoreductase (complex I) from bovine heart mitochondria," *Proceedings of the National Academy of Sciences of the United States of America*, vol. 103, no. 20, pp. 7607–7612, 2006.
- [57] C. L. Quinlan, A. A. Gerencser, J. R. Treberg, and M. D. Brand, "The mechanism of superoxide production by the antimycin-inhibited mitochondrial Q-cycle," *The Journal of Biological Chemistry*, vol. 286, no. 36, pp. 31361–31372, 2011.
- [58] I. G. Shabalina, M. Vrbacky, A. Pecinova et al., "ROS production in brown adipose tissue mitochondria: the question of UCP1-dependence," *Biochimica et Biophysica Acta (BBA) - Bioenergetics*, vol. 1837, no. 12, pp. 2017–2030, 2014.

Research Article

Elucidation of Molecular Mechanisms of Streptozotocin-Induced Oxidative Stress, Apoptosis, and Mitochondrial Dysfunction in Rin-5F Pancreatic β -Cells

Arwa M. T. Al Nahdi, Annie John, and Haider Raza

Department of Biochemistry, College of Medicine and Health Sciences (CMHS), UAE University, Al Ain, UAE

Correspondence should be addressed to Haider Raza; h.raza@uaeu.ac.ae

Received 26 April 2017; Revised 12 June 2017; Accepted 2 July 2017; Published 6 August 2017

Academic Editor: Maik Hüttemann

Copyright © 2017 Arwa M. T. Al Nahdi et al. This is an open access article distributed under the Creative Commons Attribution License, which permits unrestricted use, distribution, and reproduction in any medium, provided the original work is properly cited.

Streptozotocin is a pancreatic beta-cell-specific cytotoxin and is widely used to induce experimental type 1 diabetes in rodent models. The precise molecular mechanism of STZ cytotoxicity is however not clear. Studies have suggested that STZ is preferably absorbed by insulin-secreting β -cells and induces cytotoxicity by producing reactive oxygen species/reactive nitrogen species (ROS/RNS). In the present study, we have investigated the mechanism of cytotoxicity of STZ in insulin-secreting pancreatic cancer cells (Rin-5F) at different doses and time intervals. Cell viability, apoptosis, oxidative stress, and mitochondrial bioenergetics were studied. Our results showed that STZ induces alterations in glutathione homeostasis and inhibited the activities of the respiratory enzymes, resulting in inhibition of ATP synthesis. Apoptosis was observed in a dose- and time-dependent manner. Western blot analysis has also confirmed altered expression of oxidative stress markers (e.g., NOS and Nrf2), cell signaling kinases, apoptotic protein-like caspase-3, PARP, and mitochondrial specific proteins. These results suggest that STZ-induced cytotoxicity in pancreatic cells is mediated by an increase in oxidative stress, alterations in cellular metabolism, and mitochondrial dysfunction. This study may be significant in better understanding the mechanism of STZ-induced β -cell toxicity/resistance and the etiology of type 1 diabetes induction.

1. Introduction

Streptozotocin (STZ), [N-(methylnitrosocarbamoyl)- α -D-glucosamine], is a broad spectrum antibiotic derived from the bacterium *Streptomyces achromogenes* [1]. It is a DNA alkylating agent and is often used as an antibacterial as well as anticancer agent [2, 3]. However, it is not a preferred drug for the treatment of cancers. This is due to genotoxic effects which lead to drug resistance [4]. STZ is known to be a pancreatic beta-cell-specific cytotoxin and is therefore being widely used to induce experimental type 1 diabetes in rodent models [5, 6].

STZ is a glucose analogue that is selectively accumulated in pancreatic beta-cells via a GLUT 2 glucose transporter in the plasma membrane [7, 8]. STZ toxicity in beta-cells is dependent on GLUT 2 expression. Hosokawa and his colleagues revealed that in transgenic mice, GLUT 2-expressing

beta-cells are sensitive to the toxic effects of STZ whereas GLUT 1-expressing islets are completely resistant [9]. After entering the beta-cells via the GLUT 2 transporter, it causes DNA damage due to the DNA alkylating activity of its methyl nitrosourea moiety [10, 11], which, in turn, results in DNA fragmentation [12]. Subsequently, the fragmented DNA activates poly (ADP-ribose) synthetase to repair DNA. Poly ADP-ribosylation leads to the depletion of cellular NAD⁺ and ATP [12, 13]. The decreased ATP synthesis is demonstrated by dephosphorylation which provides more substrates for xanthine oxidase, resulting in the formation of hydrogen peroxide and hydroxyl radicals [14, 15] causing oxidative stress. Furthermore, the presence of N-methyl-N-nitrosourea side chain has the ability to release nitric oxide [16, 17] that inhibits aconitase activity, resulting in mitochondrial dysfunction. STZ is diabetogenic due to its targeted GLUT 2-dependent action in the pancreatic β -cells. The

exact mechanism of cytotoxicity is still not clear. However, both apoptotic and necrotic cell deaths of β -cells have been reported. The cytotoxicity of STZ is presumed to be mediated by reactive oxygen species (ROS), reactive nitric oxide species (NO/RNS), and induction of inflammatory responses [16, 17]. Using both in vitro cell culture and in vivo diabetic rodent models for STZ-induced toxicity, we have demonstrated that STZ induces cellular oxidative stress and mitochondrial respiratory dysfunction [18–20].

In the present study, we have further investigated the mechanism of STZ cytotoxicity on insulin-secreting Rin-5F cells. Our results demonstrate that the effects of STZ are dose and time dependent, causing oxidative stress-associated alterations in GSH redox metabolism and mitochondrial respiratory dysfunction leading to increased apoptosis in Rin-5F cells. We have also identified some of the key apoptotic and oxidative stress molecular markers which exhibit altered expression in STZ-treated Rin-5F cells. In addition, we have also demonstrated that STZ treatment has induced the activities of CYP1A2 and CYP1A1 suggesting their potential role in STZ metabolism. These results may be significant in understanding the mechanism of STZ-induced β -cell cytotoxicity/apoptosis and the ability of pancreatic cells to metabolize other xenobiotics in oxidative stress conditions.

2. Materials and Methods

2.1. Materials. Streptozotocin (STZ), reduced and oxidized glutathione (GSH/GSSG), 1-chloro 2,4-dinitrobenzene (CDNB), cumene hydroperoxide, glutathione reductase, 3-(4,5-dimethylthiazol-2-yl)-2,5-diphenyltetrazolium bromide (MTT), NADH, NADPH, cytochrome c, coenzyme Q2, sodium succinate, antimycin A, dodecyl maltoside, resorufin, 7-ethoxyresorufin, methoxyresorufin, Hoechst 33342, and ATP bioluminescent somatic cell assay kits were purchased from Sigma-Aldrich (St. Louis, MO, USA). 2',7'-Dichlorofluorescein diacetate (DCFDA) was procured from molecular probes (Eugene, OR, USA). Kits for nitric oxide and caspase-3 and caspase-9 assays were purchased from R&D Systems Inc., MN, USA, and that for lipid peroxidation (LPO) from Oxis International Inc. (CA, USA). Kits for GSH/GSSG assay were procured from Promega Corp. (Madison, WI, USA). Apoptosis detection kits for flow cytometry were purchased from BD Pharmingen (BD Biosciences, San Jose, USA). Rin-5F cells were obtained from American Type Culture Collection (Manassas, VA, USA). Polyclonal antibodies against beta-actin, caspase-3, PARP, NOS-2, Nrf2, GLUT 2, Bax, Bcl-2, Akt, and p-Akt were purchased from Santa Cruz Biotechnology Inc. (Santa Cruz, CA, USA). Reagents for cell culture, SDS-PAGE, and Western blot analyses were purchased from Gibco BRL (Grand Island, NY, USA) and Bio-Rad Laboratories (Richmond, CA, USA).

2.2. Cell Culture and Treatment. Rin-5F cells were grown in poly-L-lysine-coated 75 cm² flasks (~ 2.0 – 2.5×10^6 cells/mL) in RPMI1640 medium supplemented with 1% nonessential amino acids, 2 mM glutamine, and 10% heat-inactivated fetal bovine serum in a humidified incubator in the presence of

5%–95% CO₂ air at 37°C. Cells were treated with different concentrations of STZ (0–10 mM) dissolved in citrate buffer, pH 4.4, and diluted in RPMI1640 to appropriate concentrations just before use for different time intervals (24 h–48 h). Control cells were treated with vehicle alone. Concentrations and time points for STZ treatment in this study were based on MTT cytotoxicity tests and previously published reports [18, 21]. After the desired time of treatment, cells were harvested, washed with PBS (pH 7.4), and homogenized in H-medium buffer (70 mM sucrose, 220 mM mannitol, 2.5 mM HEPES, 2 mM EDTA, and 0.1 mM phenylmethylsulfonylfluoride, pH 7.4) at 4°C. Mitochondrial and post-mitochondrial fractions were then isolated by differential centrifugation. Cellular fractionation to prepare mitochondria fractions was performed by centrifugation, and the purity of the isolated fractions for cross contaminations was checked as described previously [20]. Protein concentration was determined by the Bradford method [22].

2.3. MTT Cell Viability Test. Mitochondrial dehydrogenase-based cell viability test in 96-well plates ($\sim 2 \times 10^4$ cells/well) was assayed by MTT conversion to formazan after treatment with different concentrations (0–10 mM) of STZ for different time intervals (24 h–48 h). The viable cells were quantitated using an ELISA reader (Anthos Laboratories, Salzburg, Germany) at 550 nm after subtracting the appropriate control value.

2.4. Measurement of Reactive Oxygen Species (ROS), NO, and LPO. Intracellular production of reactive oxygen species was measured using the cell permeable probe, DCFDA. Briefly, STZ-treated and control cells ($\sim 1 \times 10^5$ cells/mL) were grown on cover slips and incubated with 5 μ M DCFDA for 30 min at 37°C. Cells were washed twice with PBS, and fluorescence was immediately visualized using the Olympus fluorescence microscope. DCFDA-based ROS assay was also performed and measured fluorimetrically as described before [18].

For NO assay, Rin-5F cells (2×10^5 cells/well) were cultured in petri plates for 24 h prior to STZ treatments. NO production was determined by measuring the concentration of total nitrite in the culture supernatants using Griess reagent (R&D Systems Inc.).

LPO in the cell extracts of STZ-treated and control Rin-5F cells was measured using the LPO-586 kit according to the manufacturer's recommended protocol and the concentration of MDA calculated from the standard curve.

2.5. Apoptosis Measurement after STZ Treatments

2.5.1. Nuclear Staining with Hoechst33342. Apoptosis measurement was performed by Hoechst dye staining of fragmented nuclei. Cover slips with adherent cells were treated with STZ, and cells were fixed with 3.7% formaldehyde and stained with Hoechst33342 (10 μ g/mL) for 20 min at room temperature. The cover slips were washed, mounted on glass slides, and analyzed by fluorescence microscopy. Cells with signs of apoptosis showed fragmented nuclei.

2.5.2. Flow Cytometry. The apoptosis assay using flow cytometry was performed according to the vendor's protocol (BD

Pharmingen, BD Biosciences, San Jose, USA) as described before [23]. Briefly, treated and control untreated cells were trypsinized, washed in PBS, and resuspended (1×10^6 cells/mL) in binding buffer (10 mM HEPES, pH 7.4, 140 mM NaCl, 2.5 mM CaCl_2). A fraction ($100 \mu\text{L}/1 \times 10^5$ cells) of the cell suspension was incubated with $5 \mu\text{L}$ annexin V conjugated to FITC and $5 \mu\text{L}$ propidium iodide (PI) for 15 min at 25°C in the dark. $400 \mu\text{L}$ of binding buffer was added to the suspension, and apoptosis was measured immediately using a Becton Dickinson FACScan analyzer. The apoptotic cells were estimated by the percentage of cells that were stained positive for annexin V-FITC while remaining impermeable to PI (AV+/PI-). This method was also able to distinguish viable cells (AV-/PI-) and cells undergoing necrosis (AV+/PI+).

2.5.3. Assay of Caspase Activities. Caspase-3 and caspase-9 activities were measured in the cell lysate using detection kits as per the vendor's protocol. The assay is based on spectrophotometric detection of the chromophore p-nitroanilide (pNA) after cleavage from the labeled substrates, DEVD-pNA, and LEHD-pNA to measure the activities of caspase-3 and caspase-9, respectively. The pNA light emission was then quantified using a microtiter plate reader at 405 nm.

2.6. SDS-PAGE and Western Blot Analysis. Proteins from cell extracts ($30 \mu\text{g}$) from control and STZ-treated cells were separated electrophoretically on 12% SDS-PAGE [24] and transferred on to nitrocellulose paper by Western blotting [25]. Transferred proteins were probed with primary antibodies against caspase-3, PARP, Akt, p-Akt, NOS-2, Nrf2, Bax, Bcl-2, and GLUT 2. Immunoreactive bands were visualized using the appropriate conjugated secondary antibodies. Equal loading of protein was confirmed using beta-actin as the loading control. After the development of the blots, the bands were visualized and further densitometric analysis was performed using the Typhoon FLA 9500 system (GE Healthcare, Uppsala, Sweden) and expressed as relative ratios normalized against actin or other proteins as appropriate.

2.7. Measurement of CYP 450-Dependent Enzyme Activities. CYP1A1 and CYP1A2 activities in the microsomal fraction from treated and untreated control cells were measured spectrofluorometrically using 7-ethoxyresorufin and methoxyresorufin, respectively, as substrates [26, 27] by standard methods as described before [28–30].

2.8. Measurement of GSH Metabolism. Rin-5F cells were treated with different doses of STZ for different time intervals as mentioned above. GSH/GSSG ratios and activities of GSH-Px and glutathione S-transferase (GST) were measured in the STZ-treated and STZ-untreated control cell extracts. GSH/GSSG ratios were measured using the GSH/GSSG-Glo kit as per the vendor's protocol. Briefly, STZ-treated and STZ-untreated control cells were lysed with either total or oxidized glutathione reagent. For the oxidized glutathione measurement, the total GSH was blocked using NEM reagent and the oxidized glutathione was reduced. The total reduced glutathione then converts a specific probe, luciferin-NT to luciferin in the presence of a GST enzyme coupled to firefly

luciferase. The luciferin formed gives a luminescent signal, which is proportional to the amount of GSH. The total glutathione and oxidized glutathione are then measured from the standard curve, and the GSH/GSSG ratios calculated. GST activity using CDNB [31] and GSH-Px activity using cumene hydroperoxide [32] as substrates were measured by standard protocols as described before [33–36].

2.9. Measurement of Activities of Mitochondrial Respiratory Enzyme Complexes and ATP Content. Cell extracts ($5 \mu\text{g}$ protein) from STZ-treated and STZ-untreated control Rin-5F cells were suspended in 1.0 mL of 20 mM KPi buffer, pH 7.4, in the presence of the detergent, lauryl maltoside (0.2%). NADH ubiquinone oxidoreductase (complex I), succinate-cytochrome c reductase (complex II/III), and cytochrome c oxidase (complex IV) were measured using the substrates coenzyme Q2, succinate-cytochrome c, and reduced cytochrome c, respectively, by the methods of Birch-Machin and Turnbull [37] as described before [35, 36]. The ATP content in control and STZ-treated cells was determined using the ATP bioluminescent cell assay kit according to the manufacturer's suggestion (Sigma-Aldrich, St Louis, MO), and samples were read using the TD-20/20 luminometer (Turner Designs, Sunnyvale, CA).

2.10. Statistical Analysis. Values shown are expressed as mean \pm SEM of three individual experiments. Statistical significance of the data was assessed using SPSS software (version 23) by analysis of variance followed by Dunnett's post hoc analysis. *P* values ≤ 0.05 were considered statistically significant.

3. Results

3.1. Effect of STZ on Rin-5F Cell Morphology and Viability. A decrease in mitochondrial dehydrogenase-based cell survival was observed only with higher concentrations of STZ after 2–12 h (Figure 1(a)). Significant alterations in cell viability were observed even at low concentration after 24–48 h treatments. The maximum inhibition (60–70%) was observed in cells treated with 10 mM STZ for 24 h and 48 h. Since significant alterations in cell viability were observed at 24 h and 48 h, with minimal toxicity using 1 mM STZ and maximal toxicity using 10 mM STZ, these two time points and concentrations were used in our further studies to elucidate the mechanism of STZ toxicity.

Figure 1(b) shows the morphology of control untreated Rin-5F cells as well as cells treated with different doses of STZ at different time intervals. As seen in the figure, after STZ treatment, the normal flattened cells tend to round off, losing their normal morphology. When the cells were treated with 10 mM STZ for 48 h, the rounded cells started detaching from the plate, indicating increased cell death.

3.2. Effect of STZ on Oxidative Stress. Increased ROS production in Rin-5F cells treated with different doses of STZ at different time intervals was captured microscopically using the probe, DCFDA, which measures the overall ROS production. Maximum fluorescence was observed with 10 mM STZ at 24 h and 48 h (Figure 2(a)). A time- and dose-dependent

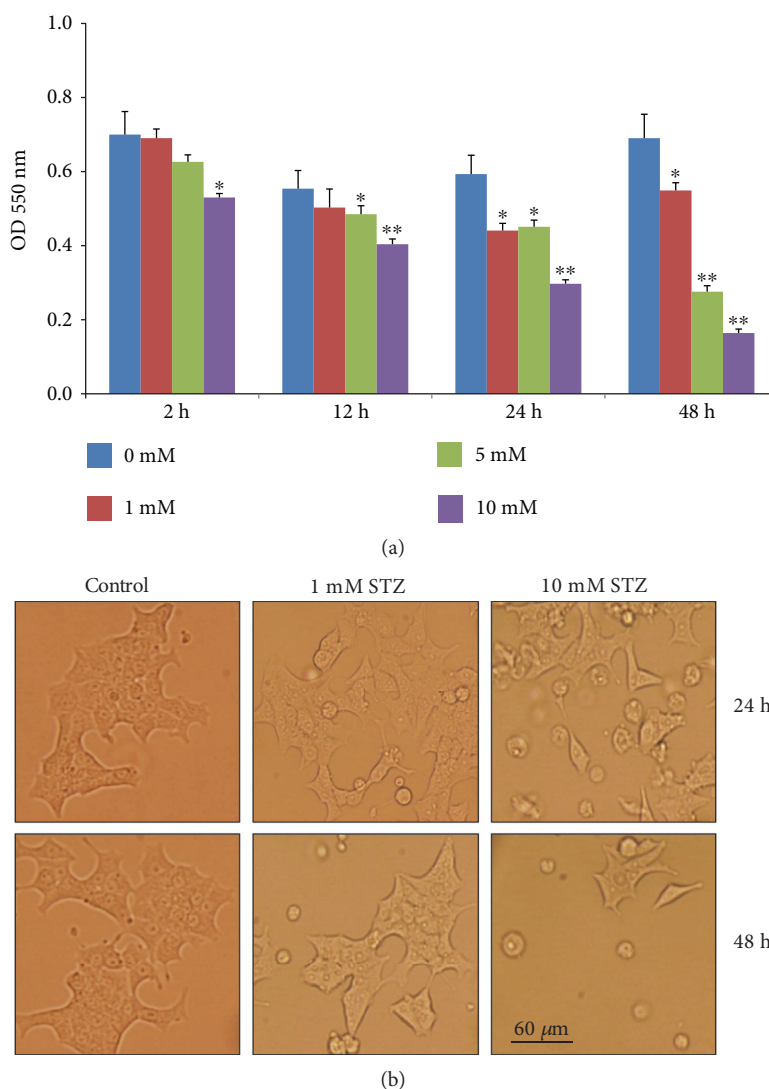


FIGURE 1: MTT cell viability assay and morphology of cells after STZ treatment. Rin-5F cells ($\sim 2 \times 10^4$) were grown in 96-well plates for 24 h and treated with different concentrations (0–10 mM) of STZ for different time intervals. The formazan crystals formed, following the reduction of MTT by metabolically active (viable) cells, were solubilized in acidified isopropanol and quantitated using the ELISA reader at 550 nm (a). Results are expressed as mean \pm SEM for three experiments. Asterisks indicate significant difference ($*p \leq 0.05$, $**p \leq 0.005$) relative to the untreated control cells. The morphological integrity of the STZ-treated and STZ-untreated control cells was also checked and photographed (20x) under a light microscope (b).

increase in intracellular ROS production was also measured fluorometrically as shown in Figure 2(b). Significant increases in ROS production were observed, with a marked increase (2-fold and 3-fold) observed with 10 mM STZ at 24 h and 48 h, respectively.

NO production was significantly increased (25–40%) in Rin-5F cells treated with 10 mM STZ for 24 or 48 h (Figure 3(a)) whereas a marginal increase was observed with 1 mM STZ treatment after 48 h.

In parallel to ROS production, LPO was significantly increased in a dose- and time-dependent manner after treatment with STZ (Figure 3(b)). Treatment with 10 mM STZ for 48 h had markedly increased the production of malondialdehyde (MDA). These results clearly indicate the increased oxidative stress in Rin-5F cells treated with STZ.

3.3. Effects of STZ on Cell Survival and Apoptosis. STZ induced time- and dose-dependent apoptosis in Rin-5F cells as detected by an increase in nuclear condensation as observed by Hoechst staining (Figure 4).

Figure 5(a) shows a significant increase in the percentage of cells undergoing early/late apoptosis by increasing the time and dose of STZ treatment. Treatment of Rin-5F cells with 1 mM STZ for 24 h caused 12% of cells to go into late apoptosis, which further increased to 22% at 10 mM STZ. Moreover, increasing the time of STZ treatment caused a further increase in the late apoptotic cells (almost 20% to 36% at 1 mM and 10 mM, respectively). The histogram in Figure 5(a) represents the percentage of total apoptotic cells after treatment with STZ at different concentrations and time intervals. This increase in apoptosis was also confirmed by

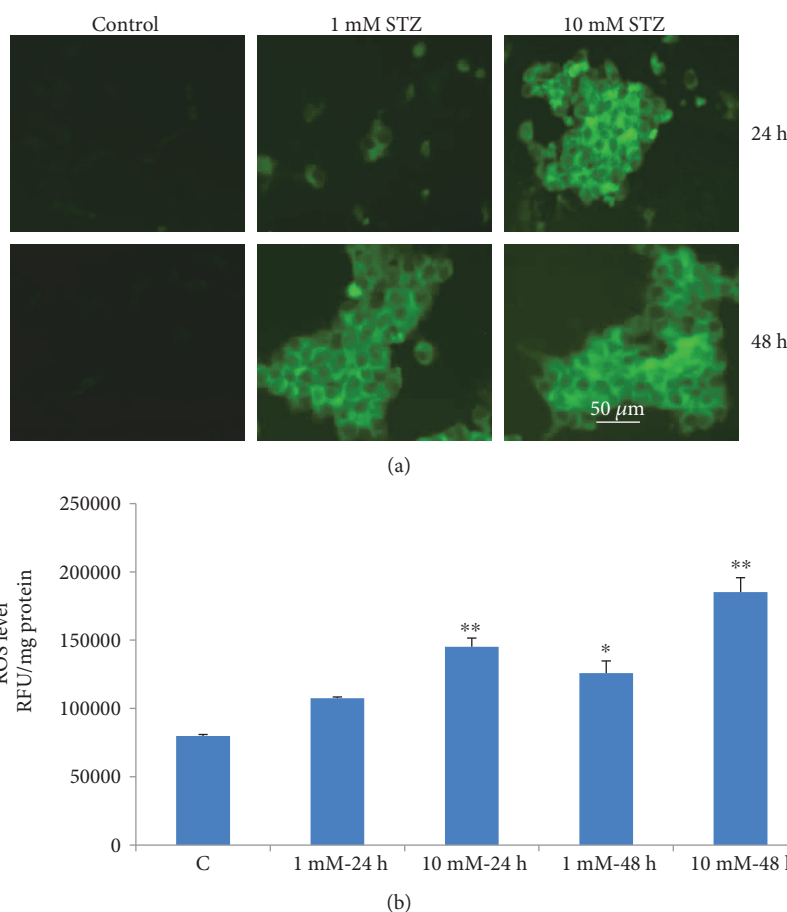


FIGURE 2: ROS production in STZ-induced cells. Intracellular production of reactive oxygen species was measured in control untreated and STZ-treated Rin-5F cells with different concentrations (0–10 mM) for different time intervals, using the cell permeable probe, DCFDA. Cells ($\sim 1 \times 10^5$ cells/mL) were grown on cover slips and incubated with $5 \mu\text{M}$ DCFDA for 30 min at 37°C . Cells were washed twice with PBS, and fluorescence was immediately visualized using an Olympus fluorescence microscope. Representative slides from untreated control and STZ-treated cells from three experiments are shown (a). Original magnification $\times 200$. Production of reactive oxygen species was also measured fluorimetrically in control untreated and STZ-treated cells (b). Results are expressed as mean \pm SEM of three experiments. Asterisks indicate significant difference ($*p \leq 0.05$, $**p \leq 0.005$) relative to the untreated control cells.

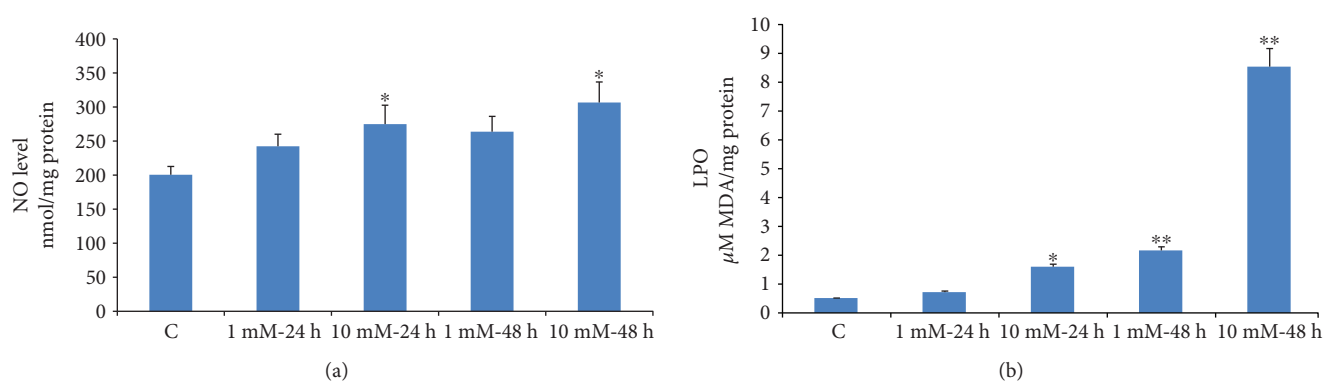


FIGURE 3: NO production and lipid peroxidation in STZ-induced cells. NO production was determined by measuring the concentration of total nitrite in the culture supernatants (a) with Griess reagent (R&D Systems Inc.). Lipid peroxidation (LPO) in the control and STZ-treated cells was measured as total amount of malondialdehyde (b) as per the vendor's protocol (Oxis Research Inc.). Results are expressed as mean \pm SEM of three experiments. Asterisks indicate significant difference ($*p \leq 0.05$, $**p \leq 0.005$) relative to the untreated control cells.

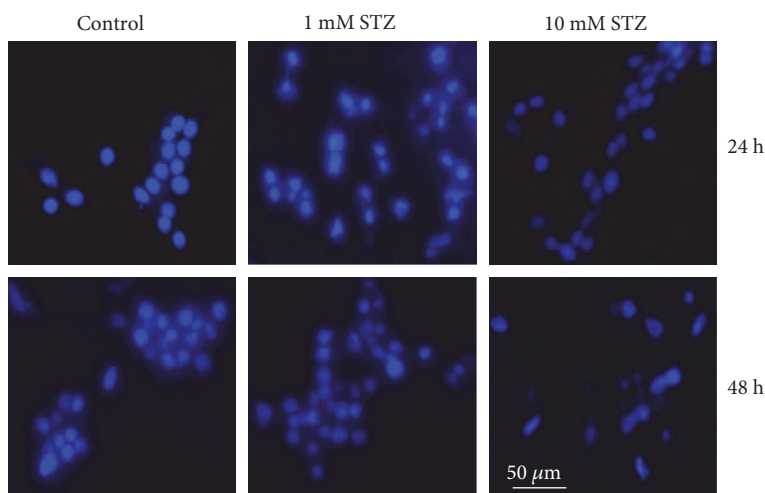


FIGURE 4: STZ-induced DNA fragmentation. Staining of fragmented nuclei of STZ-treated and STZ-untreated cells was performed by using Hoechst33342 dye. Cover slips with adherent cells were treated with STZ, fixed with 3.7% formaldehyde, and stained with Hoechst33342 (10 $\mu\text{g}/\text{mL}$) for 20 min at room temperature. The cover slips were washed, mounted on glass slides, and analyzed by fluorescence microscopy. Cells with signs of apoptosis showed fragmented nuclei. Representative slides from three experiments are shown. Original magnification $\times 200$.

increased activities of caspase isoenzymes (3 and 9) (Figure 5(b)). The activity of intrinsic apoptotic enzyme caspase-9 significantly increased with increasing time and dose of STZ treatment. However, the activities of terminal apoptotic enzyme caspase-3 showed significant increase after treatment with 10 mM STZ at 24 h and 48 h.

3.4. Effect of STZ on the Expression of Apoptotic Marker Proteins. Figure 6(a) shows alterations in the expression of oxidative stress marker proteins, NOS-2 and Nrf2. In increased phosphorylation of the cell signaling kinase, Akt was observed at high doses of STZ. A mild increase in GLUT 2 expression was observed suggesting increased STZ/glucose uptake through this mechanism. Figure 6(b) shows a marked cleavage of apoptotic marker protein, caspase-3, as well as PARP and alterations in the expression of intrinsic mitochondrial-specific proteins like Bcl-2 and Bax which were also observed at high doses. All of these results confirm the increased oxidative stress observed in these cells after STZ treatment.

3.5. Effects of STZ on CYP 450 Activities. Isoenzyme-specific substrates were used to measure the microsomal activities of CYP1A1 and CYP1A2 in Rin-5F cells treated with STZ at different doses and time intervals. CYP1A1 activity showed significant increase with 10 mM STZ at 24 h and 48 h (Figure 7(a)) while no significant increase of enzyme activity was observed with 1 mM STZ. CYP1A2 activity, on the other hand, increased significantly (2-3 fold) at all doses and time points (Figure 7(b)). These results may suggest the involvement of CYP1A family of isoenzymes in STZ metabolism.

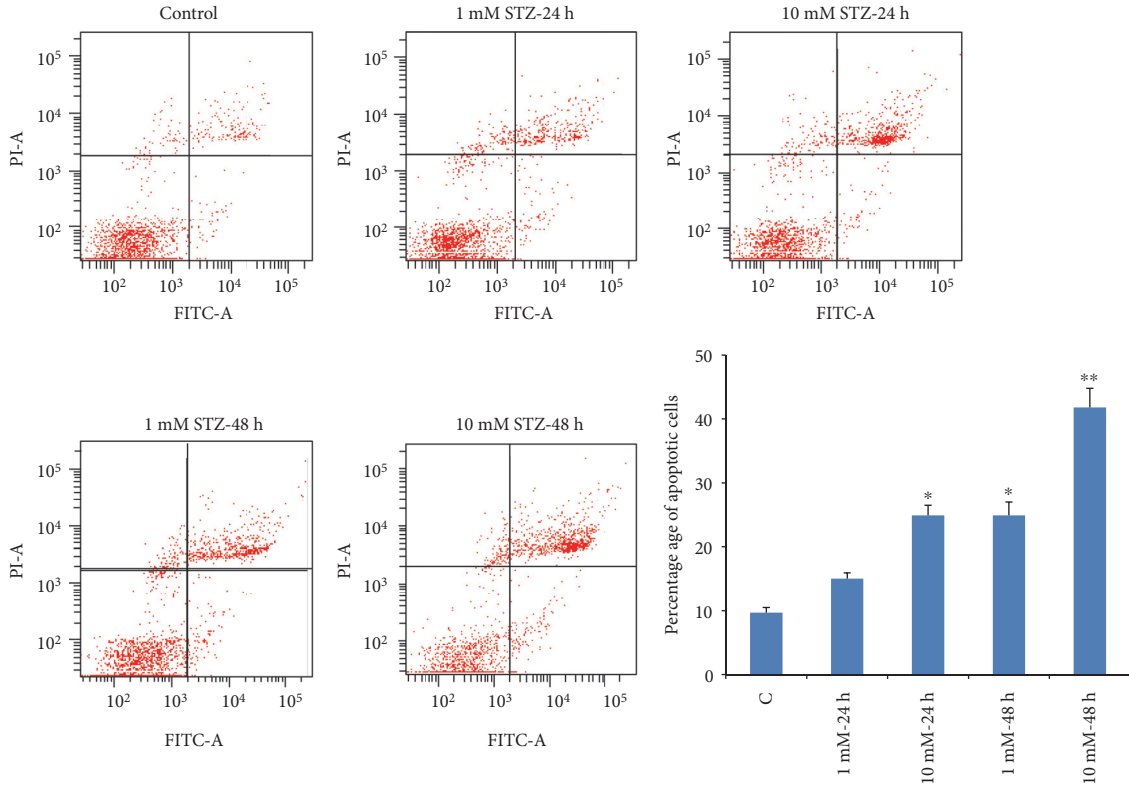
3.6. Effects of STZ on the GSH/GSSG Ratio and GSH Metabolism. Dose- and time-dependent decrease (60–70%) in the ratio of cellularly reduced GSH and oxidized GSSG

was observed after STZ treatment (Figure 8(a)). However, a slight recovery in the GSH/GSSG ratio after 48 h of treatment with lower dose of STZ suggests some delay in recycling of oxidized GSSG.

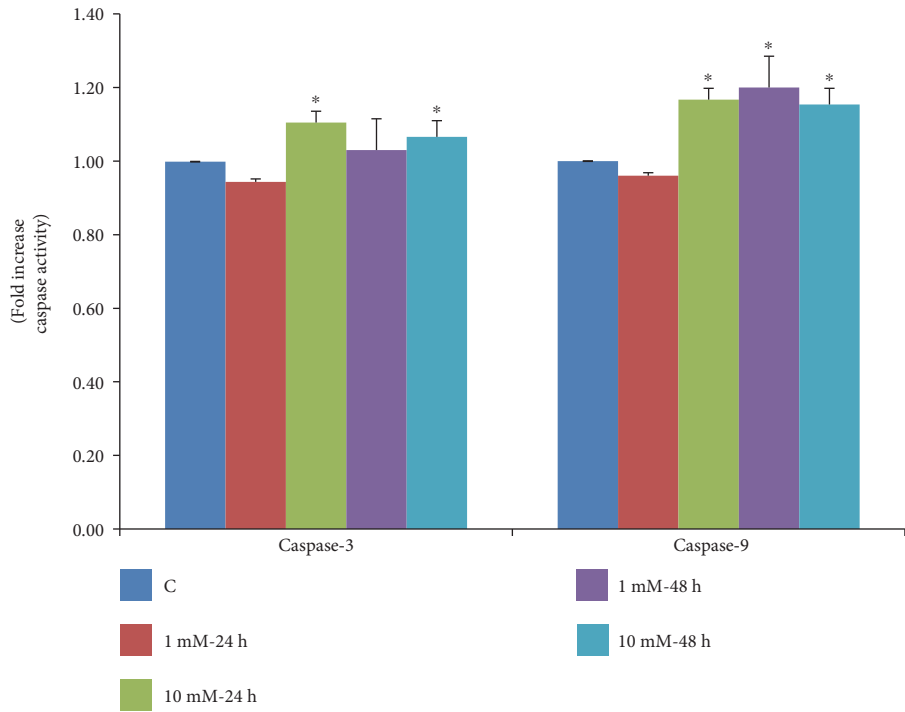
GSH-conjugating enzyme, GST, was however significantly increased (almost 2 fold) at high doses of STZ (Figure 8(b)). On the other hand, a marginal increase was observed with 1 mM STZ at 48 h. A marked increase (about 6–8 fold) in GSH-Px activity was also observed when cells were treated with 10 mM STZ both at 24 h and 48 h (Figure 8(c)). Though statistically not significant, a marginal increase in enzyme activity was also observed in cells treated with 1 mM STZ for 24 h. These results may suggest an increased cellular GSH conjugation and detoxification mechanism as an adaptation towards STZ metabolism and toxicity.

3.7. Effects of STZ on Mitochondrial Respiratory Function and ATP Production. Figure 9 shows the effects of STZ treatment on mitochondrial respiratory enzymes and bioenergetics. Both 1 mM and 10 mM STZ caused a significant inhibition (40–50%) in NADH ubiquinone oxidoreductase (complex I) enzyme activity after 24 h and 48 h (Figure 9(a)). The activity of succinate-cytochrome c reductase (complex II/III) was also significantly inhibited (40–65%) after 24 h and 48 h, with both 1 mM and 10 mM STZ (Figure 9(b)). On the other hand, the activity of the terminal respiratory enzyme complex IV was markedly inhibited (6–8 fold) by increasing the dose and time of STZ treatment (Figure 9(c)). Consistent to the reduction in mitochondrial respiratory activity, ATP levels were also markedly decreased by increasing the dose and the time of STZ treatment (Figure 9(d)).

3.8. The Mechanism of STZ-Induced Cytotoxicity in Rin-5F Cells. Figure 10 shows a schematic model depicting the mechanisms of STZ-induced cytotoxicity in Rin-5F cells.



(a)



(b)

FIGURE 5: STZ-induced apoptosis. Apoptosis was measured in Rin-5F cells treated with different doses of STZ at different time intervals by flow cytometry using FACSDiva software. Representative dot plots are shown, and percentage of apoptotic cells is represented as a histogram (a). Activity of caspases was measured in cells (b) treated with different doses of STZ at different time intervals colorimetrically using the respective substrates as described in the vendor's protocol (R&D Systems Inc.). Results are expressed as mean \pm SEM of three experiments. Asterisks indicate significant difference (* $p < 0.05$, ** $p < 0.001$) relative to the untreated control cells.

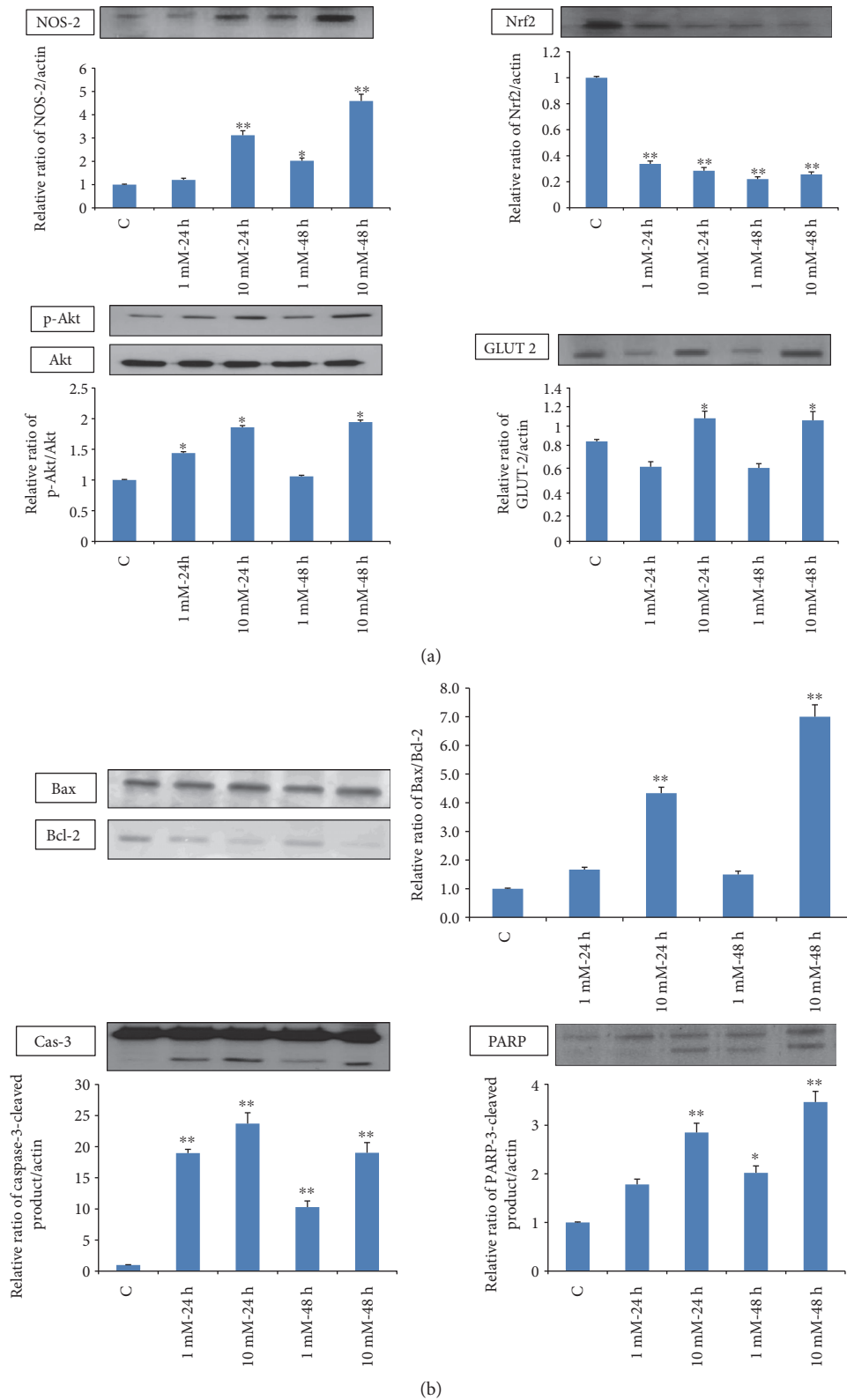


FIGURE 6: Expression of apoptotic protein markers. Total extracts (30 μ g protein) from control and Rin-5F cells treated with different doses of STZ at different time intervals were separated on 12% SDS-PAGE and transferred on to nitrocellulose paper by Western blotting. NOS-2, Nrf2, Akt, p-Akt, and GLUT 2 (a) and caspase-3, PARP, Bax, and Bcl-2 proteins (b) were detected using specific antibodies against these proteins. Beta-actin was used as a loading control. The quantitation of proteins bands is expressed as relative ratios normalized against actin or other proteins as appropriate. The figures are representative of three experiments. Asterisks indicate significant difference (* $p < 0.05$, ** $p < 0.005$) relative to the untreated control cells.

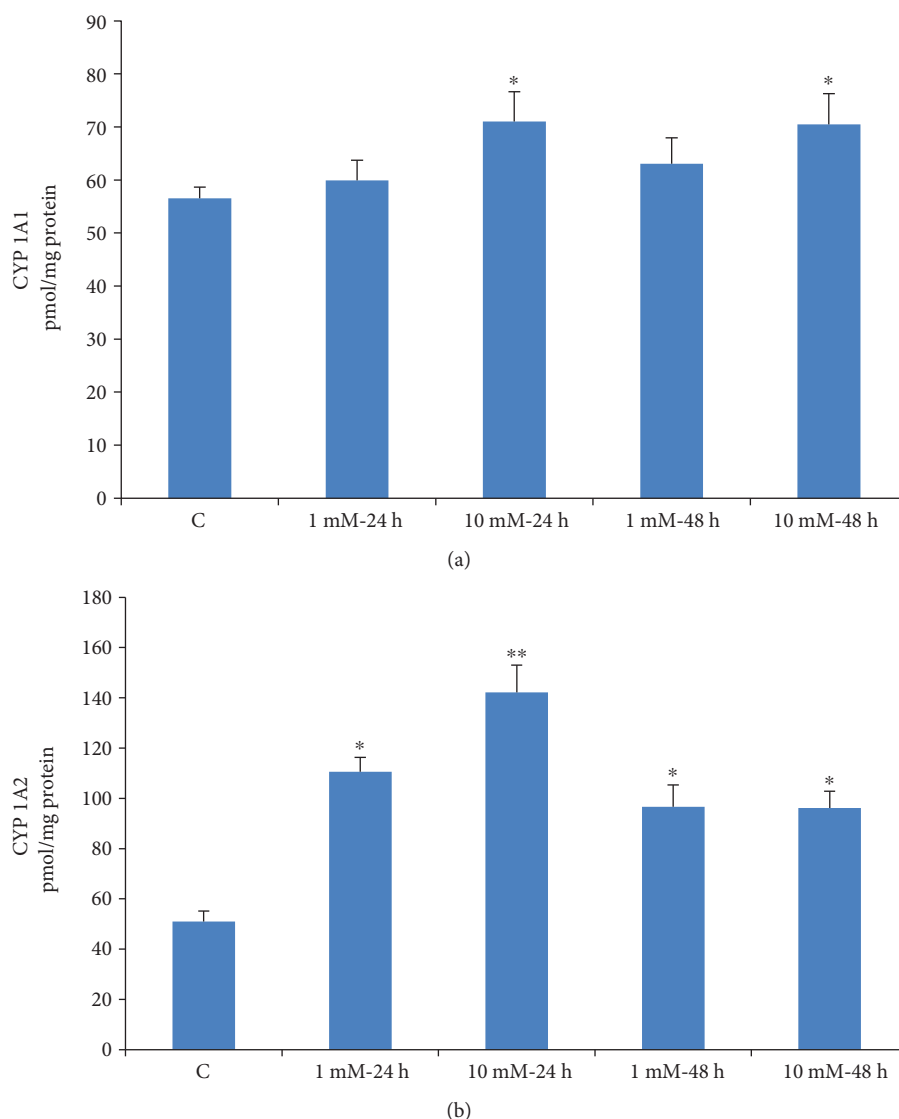


FIGURE 7: STZ-induced alterations in CYP activities. CYP 1A1 and CYP 1A2 activities were measured in Rin-5F cells treated with different doses of STZ at different time intervals using the respective substrates as described in the Materials and Methods. Results are expressed as mean \pm SEM of three experiments. Asterisks indicate significant difference (* $p \leq 0.05$, ** $p \leq 0.001$) relative to the untreated control cells.

STZ competes with glucose to enter the cells via GLUT 2 receptors, causing Akt phosphorylation, which in turn, causes further translocation of the GLUT 2 receptors. STZ-induced cytotoxicity increased ROS/NOS production, LPO, and DNA damage and decreased the GSH/GSSG ratio. Moreover, STZ induced mitochondrial dysfunction through inhibition of the activities of the mitochondrial respiratory enzymes, complex I, complex II/III, and complex IV, and decreased ATP production. STZ treatment induced apoptosis by both caspase-dependent pathway through the activation of caspase-3 and caspase-9 and caspase-independent pathway by DNA fragmentation and PARP activation.

4. Discussion

Pancreatic β -cell cytotoxicity has been observed even at therapeutic doses (up to 15 mM) of STZ when used as an

antineoplastic drug for different types of cancer, and this level of STZ induces apoptosis in pancreatic β -cells [10, 15, 38, 39]. Recent studies have shown that STZ is also toxic to neuroendocrine cells of the gut [40] as well as other GLUT 2-expressing organs such as the kidneys, liver, and brain [41]. It has been reported that single intracerebroventricular STZ injection chronically decreases glucose uptake and produces effects that resemble features of Alzheimer's disease [41]. Since the cellular uptake of STZ competes with glucose uptake and is considered to be dependent upon the specific expression of selective Glut transporters [9, 42], the differential cytotoxicity by STZ in different cellular systems may be associated with the selective uptake of STZ, its metabolic activation, and detoxification in specific cell types as well as on the redox homeostasis and mitochondrial bioenergetics in these cells [14, 43]. We have previously demonstrated that STZ induces oxidative stress and mitochondrial respiratory

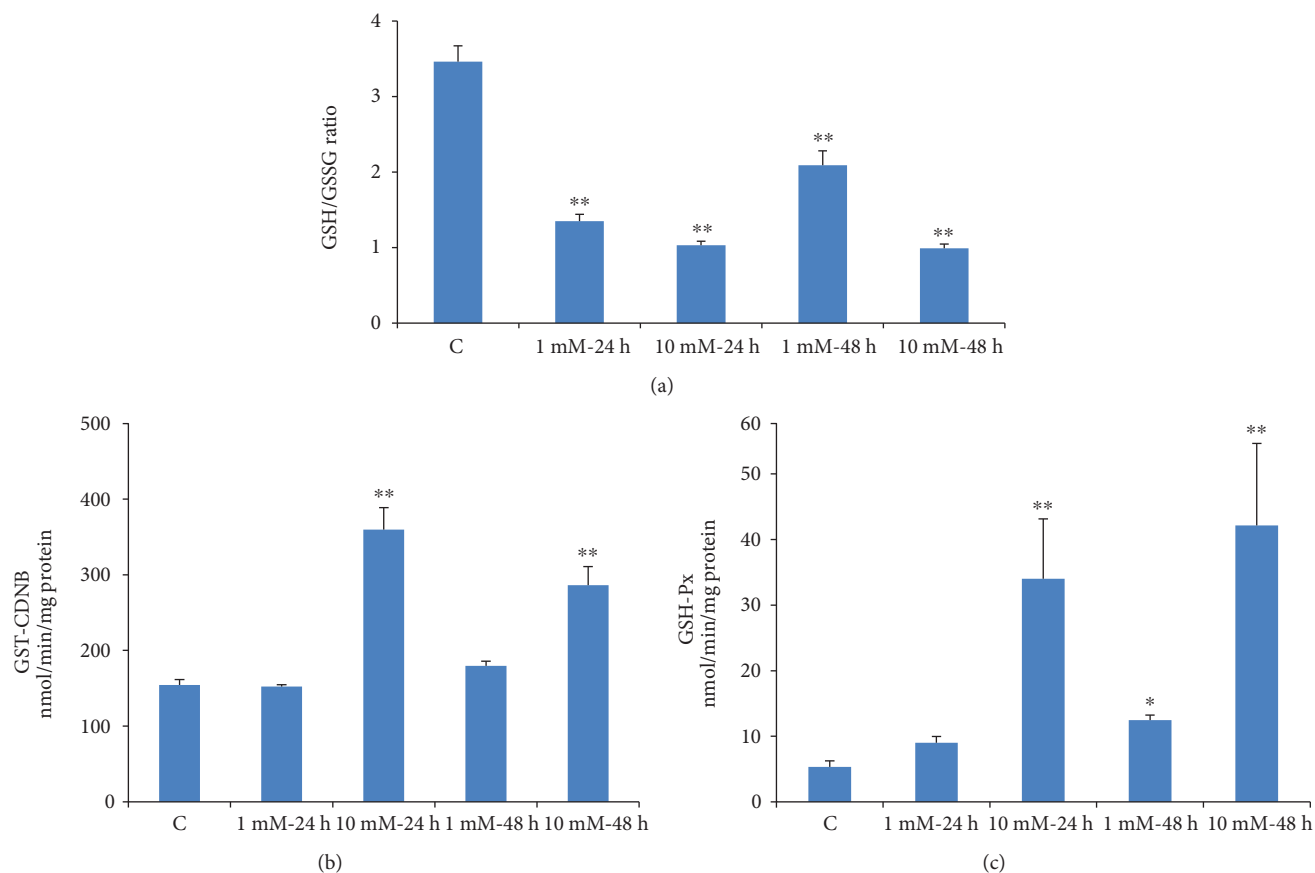


FIGURE 8: STZ-induced alterations in GSH metabolism. Rin-5F cells were treated with different doses of STZ for different time intervals. GSH/GSSG ratio (a), GST (b), and GSH-Px (c) were measured. Results are expressed as mean \pm SEM of three experiments. Asterisks indicate significant difference (* $p \leq 0.05$, ** $p \leq 0.005$) relative to the untreated control cells.

dysfunction not only in the pancreas but also in the liver, kidney, and other organs [20, 44]. We have also shown that offspring born to STZ-treated diabetic mother rats also exhibited oxidative stress-associated complications in different organs [19]. We have previously reported STZ-induced apoptotic cell death, oxidative stress, and mitochondrial dysfunction in HepG2 cells [18]. Oxidative/nitrosative stress and alterations in mitochondrial function and NF- κ B-dependent apoptosis were also reported when HepG2 cells were treated with STZ [18]. Our present study has been further extended to elucidate the mechanism of STZ-induced oxidative stress, alterations in respiratory function, and identification of apoptotic markers in Rin-5F cells treated at different doses and time points. The selection of time points and doses of STZ was based on the alterations in cell viability and morphology (as shown in Figures 1(a) and 1(b)) and also based on our previous studies on HepG2 cells where treatment at lower doses for short time periods had minimum effects on cell viability [18]. Our present results on STZ-treated Rin-5F cells have clearly indicated the increase in ROS/RNS production, increased lipid peroxidation, increased expression of oxidative stress marker protein NOS-2, inhibition in GSH synthesis, and alteration in GSH metabolism by GST and GSH-Px. Increased activities of GST and GSH-Px suggest that STZ-induced oxidative stress triggers the activation of

antioxidant defensive mechanism to protect the beta-cell death. We also observed marked activation of CYP1A2 activity and moderate activation of CYP1A1 activity in STZ-treated Rin-5F cells, probably suggesting the metabolism of STZ by the arylhydrocarbon receptor- (Ahr-) activated CYP1 enzymes. We have previously reported increased expression of CYP isoenzymes in STZ-treated type 1 and type 2 diabetic models [19, 36, 45, 46]. However, decreased expression of the antioxidant responsive protein, Nrf2, was observed after STZ treatment, which decreased drastically after 48 h. Pancreatic cells contain very low levels of antioxidant enzymes; thus, these cells are particularly sensitive to oxidative stress [47]. Nrf2 is considered a master regulator of the antioxidant response, and decreased expression of Nrf2 by STZ has been shown by various researchers [48, 49]. The reason for this loss of Nrf2 expression in pancreatic cells could be due to the STZ-induced increased intracellular ROS and oxidized-to-reduced GSH ratio which has been reported in this study as well as by other researchers. Glutathione transferase (GST) is a detoxifying enzyme that plays a protective role against oxidative stress. The induction of this family of enzymes is thought to be an adaptive response to chemical toxicity and oxidative stress within cells. In addition to Nrf2, GST induction is under the regulation of the "Ahr gene battery" as well as other transcription

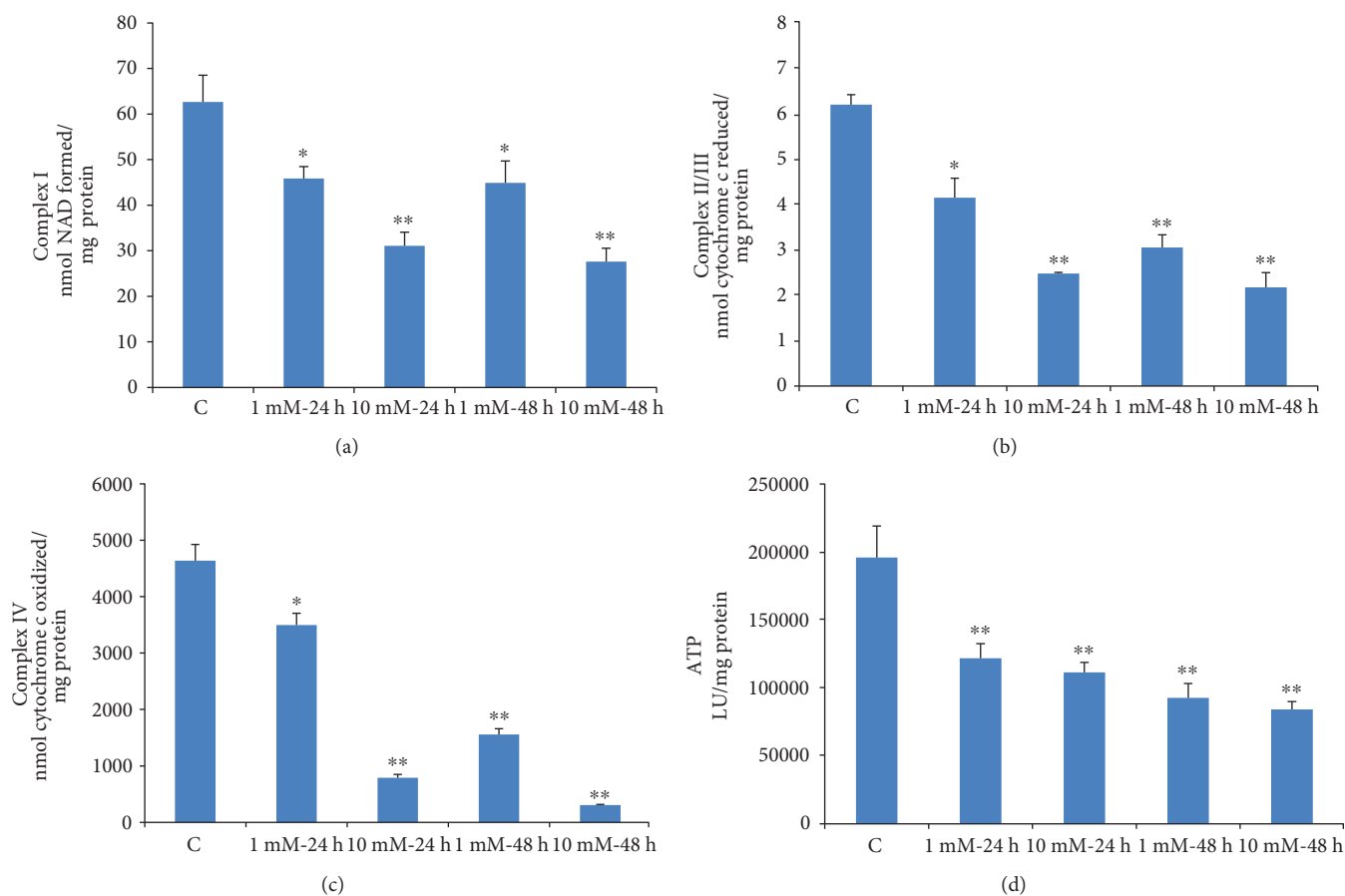


FIGURE 9: STZ-induced alterations in mitochondrial enzyme activity. Rin-5F cells were treated with different doses of STZ for different time intervals. Respiratory complex I (a) complex II/II (b), and complex IV (c) were measured using their respective substrates as described in the Materials and Methods. ATP content (d) was measured using the ATP bioluminescent somatic cell assay kit. Results are expressed as mean \pm SEM of three experiments. Asterisks indicate significant difference (* $p \leq 0.05$, ** $p \leq 0.001$) relative to the untreated control cells.

factors which are activated during chemical detoxification and oxidative stress with increased ROS production. Reports also suggest that the induction of AhR-regulated enzymes, CYP1A1 and 1A2, by xenobiotics also induces various forms of GSTs for their metabolic detoxifications [50–52]. Our present study also demonstrates that the activities of both CYP1A1/1A2 and GST enzymes have been activated after STZ treatment in Rin-5F cells, suggesting the involvement of AhR-dependent activation of CYP1A1/1A2 and GSTs. It has been shown that Nrf2 protein upregulates the antiapoptotic protein, Bcl-2, along with a battery of other cytoprotective proteins and enzymes and prevents cellular apoptosis [53]. In our study, we observed a dose-dependent decrease in Bcl-2 expression with a concomitant increase in proapoptotic protein, Bax, and increased cleavage of caspase-3. This could be due to the reduced expression of Nrf2 protein. A dose-dependent increase in PARP cleavage was also observed, which supported our observation on fragmentation of DNA at high doses.

Like HepG2 cells [18], the STZ-treated Rin-5F cells also exhibited mitochondrial dysfunction followed by apoptosis. Activities of mitochondrial respiratory enzymes complex I, complex II/III, and complex IV were significantly inhibited, though the inhibition of complex IV was more pronounced

than those of the other complexes, as some recovery in the enzyme activity was seen when cells were treated with 1 mM STZ for 48 h. As expected under these conditions, ATP level was also reduced in STZ-treated cells in a dose- and time-dependent manner. Increased oxidative stress and mitochondrial dysfunction resulted in increased apoptosis in STZ-treated Rin-5F cells. More apoptotic cell death was observed with high concentration of STZ (10 mM) for longer duration (48 h) compared to 1 mM STZ for 24 h (Figures 4 and 5). DNA fragmentation and activation of caspase-3 and caspase-9 confirmed the increased apoptosis after STZ treatment. Thus, the decrease in mitochondrial ATP synthesis and inhibition of respiratory enzymes, increased ROS/RNS production, lipid peroxidation and DNA fragmentation, and increased apoptosis have further confirmed and supported our previous studies as well as numerous other reports on the mechanism of STZ-induced cytotoxicity, in various in vivo and in vitro models, particularly in insulin-secreting pancreatic Rin-5F cells [14, 18, 19, 54–56]. Furthermore, our present study has also identified the increased expression of molecular oxidative stress and apoptotic marker such as NOS-2, as well as cleavage of caspase-3 and PARP in STZ-treated Rin-5F cells. In addition, our study also showed that STZ increases the phosphorylation of prosurvival protein,

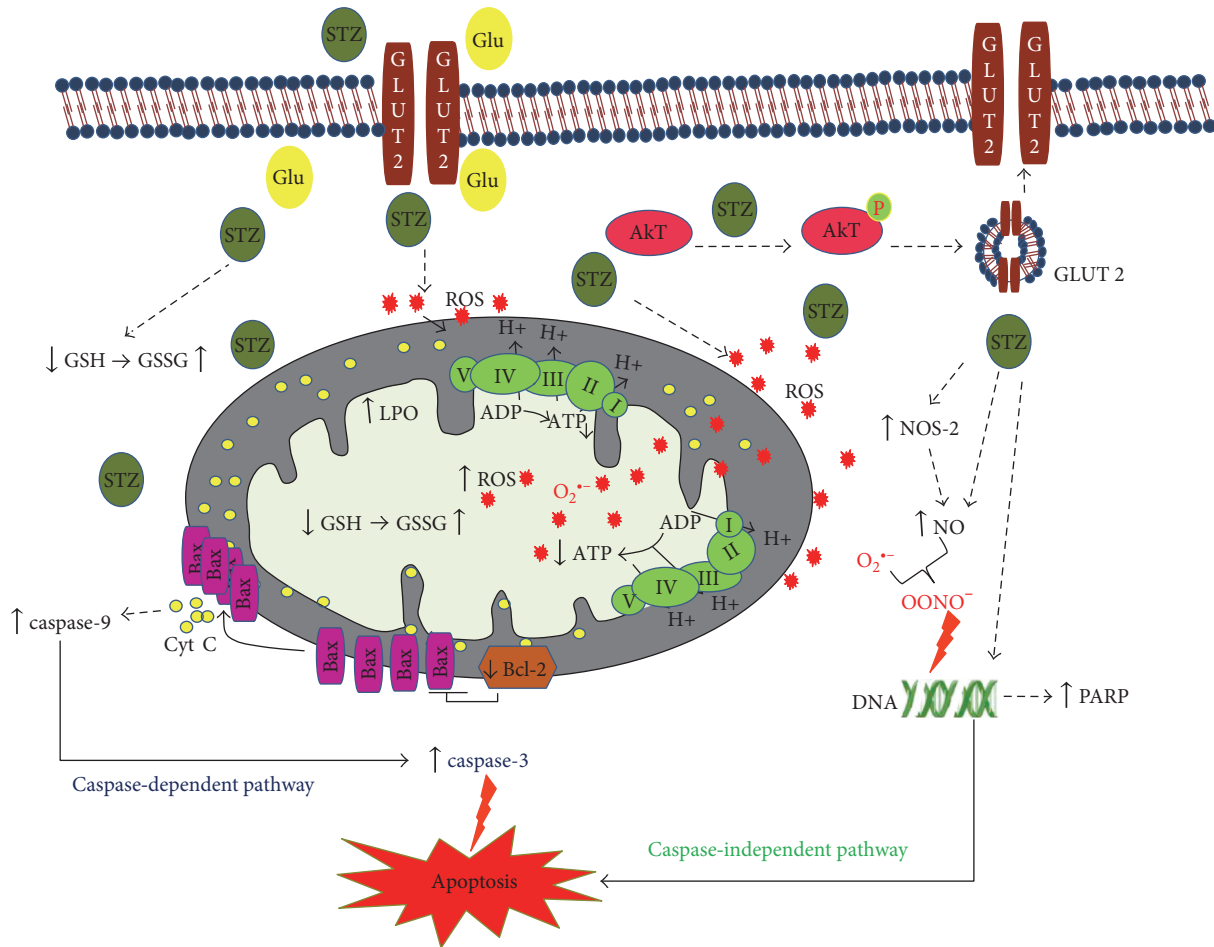


FIGURE 10: Schematic model depicting the mechanism of STZ-induced cytotoxicity in Rin-5F cells. STZ competes with glucose (Glu) to enter the cells via GLUT 2 receptors, causing Akt phosphorylation, which, in turn, causes further translocation of the GLUT 2 receptors. The model also shows that STZ induces cytotoxicity and apoptosis by increased ROS/NOS production, oxidative/nitrosative stress, increased LPO, DNA damage, a decreased GSH/GSSG ratio, and mitochondrial dysfunction. Upward arrows (\uparrow) indicate increase and downward arrows (\downarrow) indicate decrease.

Akt, suggesting a role in altering insulin signaling and GLUT expression. It is possible that STZ stimulates Akt phosphorylation in Rin-5F cells to increase GLUT 2 transport to the membrane for the transport of STZ itself and to protect the cells from further oxidative/metabolic insult. Some studies have reported a correlation between Akt phosphorylation and GLUT 2 expression and translocation. Their reports suggest that expression and membrane translocation of GLUT 2 are substantially reduced in Akt knockout mice [57]. Our study has also confirmed increased GLUT 2 expression with increased Akt phosphorylation at high doses of STZ treatment.

Our results also support the observation reported that STZ induces cell resistance in β -cells towards its own toxicity. One explanation for this could be that, in addition to the other mechanisms as reported, the STZ-treated cell might be activating the prosurvival signals (e.g., Akt, as observed in this study) and increasing GLUT 2 levels, thus modulating glucose metabolism and uptake. Another reason could be the increased GST/GSH-Px-dependent detoxification processes in β -cells in order to defend cells from the deleterious effects

of STZ and ROS [58, 59]. The altered expression of redox-sensitive protein, Nrf2, could also be a line of defense to protect the cells from the cytotoxic effects of STZ. A recent study has shown that cellular GST acts as a reservoir for NO and thus scavenges NO and detoxifies ROS [60] via GSH conjugation. This along with the increased GST/GSH-Px-dependent efflux/detoxification of STZ could render increased resistance to the cells against ROS/NO cytotoxicity.

5. Conclusion

In summary, here we provide additional evidence and have confirmed that the mechanism of STZ-induced cytotoxicity and apoptosis in Rin-5F cells is mediated by increased oxidative/nitrosative stress, mitochondrial dysfunction, and alterations in cell signaling. In addition, our results also suggest that STZ-treated Rin-5F cells also induces some cellular protection pathways as indicated by altered cell signaling and detoxification mechanisms which might be associated with the development of cellular resistance towards STZ. These results may be

significant in better understanding the etiological mechanisms involved in STZ-induced toxicity/resistance in pancreatic as well as in other cellular systems.

Abbreviations

STZ:	Streptozotocin
MTT:	3-(4,5-Dimethylthiazol-2-yl)-2,5-diphenyltetrazolium bromide
ROS:	Reactive oxygen species
NO:	Nitric oxide
LPO:	Lipid peroxidation
GSH:	Glutathione
GST:	Glutathione S-transferase
GSH-Px:	Glutathione peroxidase
Nrf2:	Nuclear factor erythroid 2-related factor 2
CDNB:	1-Chloro 2,4-dinitrobenzene
DCFDA:	2',7'-Dichlorofluorescein diacetate
SDS-PAGE:	Sodium dodecyl sulfate polyacrylamide gel electrophoresis.

Disclosure

Part of this research may also be used for the fulfillment of Ph.D. thesis requirement for Ms. Arwa M. T. Al Nahdi.

Conflicts of Interest

There is no conflict of interest to disclose for any of the authors and funding sources regarding the publication of this manuscript.

Acknowledgments

The authors wish to thank Sheikh Hamdan Bin Rashed Al Maktoum Award for Medical Research (Haider Raza) for their generous support. Thanks are also due to the support from Research Committee, College of Medicine and Health Sciences, UAE University.

References

- [1] C. Lewis and A. R. Barbiers, "Streptozotocin, a new antibiotic. In vitro and in vivo evaluation," *Antibiotics Annual*, vol. 7, pp. 247–254, 1959.
- [2] R. B. Weiss, "Streptozocin: a review of its pharmacology, efficacy, and toxicity," *Cancer Treatment Reports*, vol. 66, pp. 427–438, 1982.
- [3] M. Eileen Dolan, "Inhibition of DNA repair as a means of increasing the antitumor activity of DNA reactive agents," *Advanced Drug Delivery Reviews*, vol. 26, pp. 105–118, 1997.
- [4] M. S. Capucci, M. E. Hoffmann, and A. T. Natarajan, "Streptozotocin-induced genotoxic effects in Chinese hamster cells: the resistant phenotype of V79 cells," *Mutation Research*, vol. 347, pp. 79–85, 1995.
- [5] M. S. Islam and D. T. Loots, "Experimental rodent models of type 2 diabetes: a review," *Methods and Findings in Experimental and Clinical Pharmacology*, vol. 31, pp. 249–261, 2009.
- [6] L. Wei, Y. Lu, S. He et al., "Induction of diabetes with signs of autoimmunity in primates by the injection of multiple-low-dose streptozotocin," *Biochemical and Biophysical Research Communications*, vol. 412, pp. 373–378, 2011.
- [7] H. Tjälve, E. Wilander, and E. B. Johansson, "Distribution of labelled streptozotocin in mice: uptake and retention in pancreatic islets," *The Journal of Endocrinology*, vol. 69, pp. 455–456, 1976.
- [8] E. H. Karunanayake, J. R. Baker, R. A. Christian, D. J. Hearse, and G. Mellows, "Autoradiographic study of the distribution and cellular uptake of (¹⁴C) - streptozotocin in the rat," *Diabetologia*, vol. 12, pp. 123–128, 1976.
- [9] M. Hosokawa, W. Dolci, and B. Thorens, "Differential sensitivity of GLUT1- and GLUT2-expressing beta cells to streptozotocin," *Biochemical and Biophysical Research Communications*, vol. 289, pp. 1114–1117, 2001.
- [10] S. P. LeDoux, S. E. Woodley, N. J. Patton, and G. L. Wilson, "Mechanisms of nitrosourea-induced beta-cell damage. Alterations in DNA," *Diabetes*, vol. 35, pp. 866–872, 1986.
- [11] M. Murata, A. Takahashi, I. Saito, and S. Kawanishi, "Site-specific DNA methylation and apoptosis: induction by diabetogenic streptozotocin," *Biochemical Pharmacology*, vol. 57, pp. 881–887, 1999.
- [12] H. Yamamoto, Y. Uchigata, and H. Okamoto, "Streptozotocin and alloxan induce DNA strand breaks and poly(ADP-ribose) synthetase in pancreatic islets," *Nature*, vol. 294, pp. 284–286, 1981.
- [13] S. Sandler and I. Swenne, "Streptozotocin, but not alloxan, induces DNA repair synthesis in mouse pancreatic islets in vitro," *Diabetologia*, vol. 25, pp. 444–447, 1983.
- [14] M. Nukatsuka, Y. Yoshimura, M. Nishida, and J. Kawada, "Importance of the concentration of ATP in rat pancreatic beta cells in the mechanism of streptozotocin-induced cytotoxicity," *The Journal of Endocrinology*, vol. 127, pp. 161–165, 1990.
- [15] T. Szkudelski, "The mechanism of alloxan and streptozotocin action in B cells of the rat pancreas," *Physiological Research*, vol. 50, pp. 537–546, 2001.
- [16] M. Friederich, P. Hansell, and F. Palm, "Diabetes, oxidative stress, nitric oxide and mitochondria function," *Current Diabetes Reviews*, vol. 5, pp. 120–144, 2009.
- [17] K. Van Dyke, E. Ghareeb, M. Van Dyke, A. Sosa, R. D. Hoeldtke, and D. H. Van Thiel, "Luminescence experiments involved in the mechanism of streptozotocin diabetes and cataract formation," *Luminescence*, vol. 23, pp. 386–391, 2008.
- [18] H. Raza and A. John, "Streptozotocin-induced cytotoxicity, oxidative stress and mitochondrial dysfunction in human hepatoma HepG2 cells," *International Journal of Molecular Sciences*, vol. 13, pp. 5751–5767, 2012.
- [19] H. Raza and A. John, "Glutathione metabolism and oxidative stress in neonatal rat tissues from streptozotocin-induced diabetic mothers," *Diabetes/Metabolism Research and Reviews*, vol. 20, pp. 72–78, 2004.
- [20] H. Raza, S. K. Prabu, A. John, and N. G. Avadhani, "Impaired mitochondrial respiratory functions and oxidative stress in streptozotocin-induced diabetic rats," *International Journal of Molecular Sciences*, vol. 12, pp. 3133–3147, 2011.
- [21] S. Bathina, N. Srinivas, and U. N. Das, "BDNF protects pancreatic β cells (RIN5F) against cytotoxic action of alloxan, streptozotocin, doxorubicin and benzo(a)pyrene in vitro," *Metabolism*, vol. 65, pp. 667–684, 2016.
- [22] M. M. Bradford, "A rapid and sensitive method for the quantitation of microgram quantities of protein utilizing the

- principle of protein-dye binding," *Analytical Biochemistry*, vol. 72, pp. 248–254, 1976.
- [23] H. Raza and A. John, "Implications of altered glutathione metabolism in aspirin-induced oxidative stress and mitochondrial dysfunction in HepG2 cells," *PLoS One*, vol. 7, article e36325, 2012.
- [24] U. K. Laemmli, "Cleavage of structural proteins during the assembly of the head of bacteriophage T4," *Nature*, vol. 227, pp. 680–685, 1970.
- [25] H. Towbin, T. Staehelin, and J. Gordon, "Electrophoretic transfer of proteins from polyacrylamide gels to nitrocellulose sheets: procedure and some applications. 1979," *Biotechnology (Reading, Mass)*, vol. 24, pp. 145–149, 1992.
- [26] R. J. Pohl and J. R. Fouts, "A rapid method for assaying the metabolism of 7-ethoxyresorufin by microsomal subcellular fractions," *Analytical Biochemistry*, vol. 107, pp. 150–155, 1980.
- [27] P. V. Nerurkar, S. S. Park, P. E. Thomas, R. W. Nims, and R. A. Lubet, "Methoxyresorufin and benzyloxyresorufin: substrates preferentially metabolized by cytochromes P4501A2 and 2B, respectively, in the rat and mouse," *Biochemical Pharmacology*, vol. 46, pp. 933–943, 1993.
- [28] H. Raza, A. John, and J. Shafarin, "NAC attenuates LPS-induced toxicity in aspirin-sensitized mouse macrophages via suppression of oxidative stress and mitochondrial dysfunction," *PLoS One*, vol. 9, article e103379, 2014.
- [29] H. Raza, A. John, and A. Nemmar, "Short-term effects of nose-only cigarette smoke exposure on glutathione redox homeostasis, cytochrome P450 1A1/2 and respiratory enzyme activities in mice tissues," *Cellular Physiology and Biochemistry*, vol. 31, pp. 683–692, 2013.
- [30] H. Raza, A. John, and F. C. Howarth, "Increased metabolic stress in Zucker diabetic fatty rat kidney and pancreas," *Cellular Physiology and Biochemistry*, vol. 32, pp. 1610–1620, 2013.
- [31] W. H. Habig, M. J. Pabst, and W. B. Jakoby, "Glutathione S-transferases. The first enzymatic step in mercapturic acid formation," *The Journal of Biological Chemistry*, vol. 249, pp. 7130–7139, 1974.
- [32] D. E. Paglia and W. N. Valentine, "Studies on the quantitative and qualitative characterization of erythrocyte glutathione peroxidase," *The Journal of Laboratory and Clinical Medicine*, vol. 70, pp. 158–169, 1967.
- [33] H. Raza and A. John, "4-hydroxynonenal induces mitochondrial oxidative stress, apoptosis and expression of glutathione S-transferase A4-4 and cytochrome P450 2E1 in PC12 cells," *Toxicology and Applied Pharmacology*, vol. 216, pp. 309–318, 2006.
- [34] H. Raza, M.-A. Robin, J. K. Fang, and N. G. Avadhani, "Multiple isoforms of mitochondrial glutathione S-transferases and their differential induction under oxidative stress," *The Biochemical Journal*, vol. 366, pp. 45–55, 2002.
- [35] H. Raza, A. John, and J. Shafarin, "Potentiation of LPS-induced apoptotic cell death in human hepatoma HepG2 cells by aspirin via ROS and mitochondrial dysfunction: protection by N-acetyl cysteine," *PLoS One*, vol. 11, article e0159750, 2016.
- [36] H. Raza, A. John, and F. C. Howarth, "Increased oxidative stress and mitochondrial dysfunction in Zucker diabetic rat liver and brain," *Cellular Physiology and Biochemistry*, vol. 35, pp. 1241–1251, 2015.
- [37] M. A. Birch-Machin and D. M. Turnbull, "Assaying mitochondrial respiratory complex activity in mitochondria isolated from human cells and tissues," *Methods in Cell Biology*, vol. 65, pp. 97–117, 2001.
- [38] J. Wu and L.-J. Yan, "Streptozotocin-induced type 1 diabetes in rodents as a model for studying mitochondrial mechanisms of diabetic β cell glucotoxicity," *Diabetes, Metabolic Syndrome and Obesity: Targets and Therapy*, vol. 8, pp. 181–188, 2015.
- [39] K. S. Saini, C. Thompson, C. M. Winterford, N. I. Walker, and D. P. Cameron, "Streptozotocin at low doses induces apoptosis and at high doses causes necrosis in a murine pancreatic beta cell line, INS-1," *Biochemistry and Molecular Biology International*, vol. 39, pp. 1229–1236, 1996.
- [40] O. Brenna, G. Qvigstad, E. Brenna, and H. L. Waldum, "Cytotoxicity of streptozotocin on neuroendocrine cells of the pancreas and the gut," *Digestive Diseases and Sciences*, vol. 48, pp. 906–910, 2003.
- [41] P. Grieb, "Intracerebroventricular Streptozotocin injections as a model of Alzheimer's disease: in search of a relevant mechanism," *Molecular Neurobiology*, vol. 53, pp. 1741–1752, 2016.
- [42] W. J. Schnedl, S. Ferber, J. H. Johnson, and C. B. Newgard, "STZ transport and cytotoxicity. Specific enhancement in GLUT2-expressing cells," *Diabetes*, vol. 43, pp. 1326–1333, 1994.
- [43] S. Zheng, M. Zhao, Y. Ren, Y. Wu, and J. Yang, "Sesamin suppresses STZ induced INS-1 cell apoptosis through inhibition of NF- κ B activation and regulation of Bcl-2 family protein expression," *European Journal of Pharmacology*, vol. 750, pp. 52–58, 2015.
- [44] H. Raza, I. Ahmed, and A. John, "Tissue specific expression and immunohistochemical localization of glutathione S-transferase in streptozotocin induced diabetic rats: modulation by *Momordica charantia* (karela) extract," *Life Sciences*, vol. 74, pp. 1503–1511, 2004.
- [45] H. Raza, A. John, J. Shafarin, and F. C. Howarth, "Exercise-induced alterations in pancreatic oxidative stress and mitochondrial function in type 2 diabetic Goto-Kakizaki rats," *Physiological Reports*, vol. 4, 2016.
- [46] H. Raza, I. Ahmed, A. John, and A. K. Sharma, "Modulation of xenobiotic metabolism and oxidative stress in chronic streptozotocin-induced diabetic rats fed with *Momordica charantia* fruit extract," *Journal of Biochemical and Molecular Toxicology*, vol. 14, pp. 131–139, 2000.
- [47] Y. Y. Jang, J. H. Song, Y. K. Shin, E. S. Han, and C. S. Lee, "Protective effect of boldine on oxidative mitochondrial damage in streptozotocin-induced diabetic rats," *Pharmacological Research*, vol. 42, pp. 361–371, 2000.
- [48] B. Elango, S. Dornadula, R. Paulmurugan, and K. M. Ramkumar, "Pterostilbene ameliorates Streptozotocin-induced diabetes through enhancing antioxidant signaling pathways mediated by Nrf2," *Chemical Research in Toxicology*, vol. 29, pp. 47–57, 2016.
- [49] K. A. Kang, J. S. Kim, R. Zhang et al., "KIOM-4 protects against oxidative stress-induced mitochondrial damage in pancreatic β -cells via its antioxidant effects," *Evidence-Based Complementary and Alternative Medicine: ECAM*, vol. 2011, Article ID 978682, 11 pages, 2011.
- [50] H. M. Korashy and A. O. S. El-Kadi, "The role of aryl hydrocarbon receptor and the reactive oxygen species in the modulation of glutathione transferase by heavy metals in

- murine hepatoma cell lines,” *Chemico-Biological Interactions*, vol. 162, pp. 237–248, 2006.
- [51] T. R. Knight, S. Choudhuri, and C. D. Klaassen, “Induction of hepatic glutathione S-transferases in male mice by prototypes of various classes of microsomal enzyme inducers,” *Toxicological Sciences*, vol. 106, pp. 329–338, 2008.
- [52] M. Connolly, M. L. Fernández-Cruz, and J. M. Navas, “Recovery of redox homeostasis altered by CuNPs in H4IIE liver cells does not reduce the cytotoxic effects of these NPs: an investigation using aryl hydrocarbon receptor (AhR) dependent antioxidant activity,” *Chemico-Biological Interactions*, vol. 228, pp. 57–68, 2015.
- [53] S. K. Niture and A. K. Jaiswal, “Nrf2 protein up-regulates anti-apoptotic protein Bcl-2 and prevents cellular apoptosis,” *The Journal of Biological Chemistry*, vol. 287, pp. 9873–9886, 2012.
- [54] L. Boquist, S. Boquist, and U. Alehagen, “Mitochondrial changes and associated alterations induced in mice by streptozotocin administered in vivo and in vitro,” *Diabetes Research and Clinical Practice*, vol. 3, pp. 179–190, 1987.
- [55] N. G. Morgan, H. C. Cable, N. R. Newcombe, and G. T. Williams, “Treatment of cultured pancreatic B-cells with streptozotocin induces cell death by apoptosis,” *Bioscience Reports*, vol. 14, pp. 243–250, 1994.
- [56] K. B. Koo, H. J. Suh, K. S. Ra, and J. W. Choi, “Protective effect of cyclo(his-pro) on streptozotocin-induced cytotoxicity and apoptosis in vitro,” *Journal of Microbiology and Biotechnology*, vol. 21, pp. 218–227, 2011.
- [57] W. S. Chen, X.-D. Peng, Y. Wang et al., “Leptin deficiency and beta-cell dysfunction underlie type 2 diabetes in compound Akt knockout mice,” *Molecular and Cellular Biology*, vol. 29, p. 3151, 2009.
- [58] H. K. Liu, J. T. McCluskey, N. H. McClellan, and P. R. Flatt, “Streptozotocin-resistant BRIN-BD11 cells possess wide spectrum of toxin tolerance and enhanced insulin-secretory capacity,” *Endocrine*, vol. 32, pp. 20–29, 2007.
- [59] D. L. Eizirik and M. I. Darville, “Beta-cell apoptosis and defense mechanisms: lessons from type 1 diabetes,” *Diabetes*, vol. 50, Supplement 1, pp. S64–S69, 2001.
- [60] H. C. Lok, S. Sahni, P. J. Jansson, Z. Kovacevic, C. L. Hawkins, and D. R. Richardson, “A nitric oxide storage and transport system that protects activated macrophages from endogenous nitric oxide cytotoxicity,” *The Journal of Biological Chemistry*, vol. 291, pp. 27042–27061, 2016.

Research Article

Combined Respiratory Chain Deficiency and UQCC2 Mutations in Neonatal Encephalomyopathy: Defective Supercomplex Assembly in Complex III Deficiencies

René G. Feichtinger,¹ Michaela Brunner-Krainz,² Bader Alhaddad,³ Saskia B. Wortmann,^{1,3,4} Reka Kovacs-Nagy,³ Tatjana Stojakovic,⁵ Wolfgang Erwa,⁵ Bernhard Resch,⁶ Werner Windischhofer,² Sarah Verheyen,⁷ Sabine Uhrig,⁷ Christian Windpassinger,⁷ Felix Locker,⁸ Christine Makowski,⁹ Tim M. Strom,^{3,4} Thomas Meitinger,^{3,4} Holger Prokisch,^{3,4} Wolfgang Sperl,¹ Tobias B. Haack,^{3,4} and Johannes A. Mayr¹

¹Department of Pediatrics, Salzburger Landeskliniken (SALK) and Paracelsus Medical University (PMU), 5020 Salzburg, Austria

²Division of General Pediatrics, Department of Pediatrics and Adolescent Medicine, Medical University of Graz, 8010 Graz, Austria

³Institute of Human Genetics, Technische Universität München, 81675 Munich, Germany

⁴Institute of Human Genetics, Helmholtz Zentrum München, 85764 Neuherberg, Germany

⁵Clinical Institute of Medical and Chemical Laboratory Diagnostics, Medical University of Graz, 8010 Graz, Austria

⁶Division of Neonatology, Department of Pediatrics and Adolescent Medicine, Medical University of Graz, 8010 Graz, Austria

⁷Department of Human Genetics, Medical University of Graz, 8010 Graz, Austria

⁸Laura Bassi Centre of Expertise-THERAPEP, Research Program for Receptor Biochemistry and Tumor Metabolism, Department of Pediatrics, Paracelsus Medical University, 5020 Salzburg, Austria

⁹Department for Paediatric and Adolescent Medicine, Schwabing Hospital, Technische Universität München, 80804 Munich, Germany

Correspondence should be addressed to René G. Feichtinger; r.feichtinger@salk.at

Received 26 January 2017; Revised 22 March 2017; Accepted 4 June 2017; Published 19 July 2017

Academic Editor: Maik Hüttemann

Copyright © 2017 René G. Feichtinger et al. This is an open access article distributed under the Creative Commons Attribution License, which permits unrestricted use, distribution, and reproduction in any medium, provided the original work is properly cited.

Vertebrate respiratory chain complex III consists of eleven subunits. Mutations in five subunits either mitochondrial (MT-CYB) or nuclear (CYC1, UQCRC2, UQCRB, and UQCRQ) encoded have been reported. Defects in five further factors for assembly (TTC19, UQCC2, and UQCC3) or iron-sulphur cluster loading (BCS1L and LYRM7) cause complex III deficiency. Here, we report a second patient with UQCC2 deficiency. This girl was born prematurely; pregnancy was complicated by intrauterine growth retardation and oligohydramnios. She presented with respiratory distress syndrome, developed epileptic seizures progressing to status epilepticus, and died at day 33. She had profound lactic acidosis and elevated urinary pyruvate. Exome sequencing revealed two homozygous missense variants in *UQCC2*, leading to a severe reduction of UQCC2 protein. Deficiency of complexes I and III was found enzymatically and on the protein level. A review of the literature on genetically distinct complex III defects revealed that, except TTC19 deficiency, the biochemical pattern was very often a combined respiratory chain deficiency. Besides complex III, typically, complex I was decreased, in some cases complex IV. In accordance with previous observations, the presence of assembled complex III is required for the stability or assembly of complexes I and IV, which might be related to respirasome/supercomplex formation.

1. Introduction

Vertebrate complex III (coenzyme Q:cytochrome *c* oxidoreductase) consists of 11 subunits. Mutations in five subunits (MT-CYB, CYC1, UQCRC2, UQCRB, and UQCRQ), three factors for protein complex assembly (TTC19, UQCC2, and UQCC3), and two factors (BCS1L and LYRM7) involved in loading of the [2Fe-2S] iron sulphur cofactor on the Rieske protein of complex III were described [1–10]. *MT-CYB* is a mitochondrial gene-encoding cytochrome *b*. Complex III transports electrons from ubiquinol to cytochrome *c*. Cytochrome *c*1, cytochrome *b*, and the Rieske protein represent the redox center. The heme group from cytochrome *c*1 is located in the intermembrane space, where it accepts electrons from the Rieske protein. Complex III is associated with complexes I and IV to form the respirasome. UQCC2 is required for complex III assembly. The protein can affect insulin secretion, mitochondrial ATP production, and myogenesis via modulation of the respiratory chain activity [11]. UQCC2 interacts with UQCC1 to mediate cytochrome *b* expression and subsequent complex III assembly [7]. UQCC1 and 2 might specifically bind to newly synthesized cytochrome *b* at the nucleotide where they are stabilized [7, 12]. UQCC2 is mainly expressed in the brain, kidney, heart, and skeletal muscle [12].

The majority of complex I is found bound with a complex III dimer and complex IV (CI, CIII₂, and CIV) termed respirasome or with a complex III dimer alone (CI, CIII₂). In addition, CIII dimers can form a complex with CIV (CIII₂-CIV) independent of complex I. Very recently, the structure of respiratory chain supercomplexes revealed several interaction sites between complexes III, I, and IV. In total, nine interaction sites between supercomplexes were described [13].

All complex III deficiencies show an autosomal recessive mode of inheritance with the exception of cytochrome *b* defects that either show maternal inheritance or occur spontaneously, since this subunit is encoded by the mitochondrial genome (mtDNA). Heterogeneous clinical phenotypes have been described in relation to respiratory chain complex III deficiency.

Here, we report on a second patient with mutations in the complex III assembly factor *UQCC2* who showed pronounced deficiency of complexes I and III. Furthermore, we give an overview on the biochemical findings in patients with mutations in distinct complex III subunits or assembly factors.

2. Material and Methods

2.1. Ethics. The study was performed according to the Austrian Gene Technology Act. Experiments were conducted in accordance with the Helsinki Declaration of 1975 (revised 1983) and the guidelines of the Salzburg State Ethics Research Committee (ethical agreement: AZ 209-11-E1/823-2006), being no clinical drug trial or epidemiological investigation. All clinical data and samples were obtained with written informed consent of the patients' parents. The ethical committee of the Technische Universität München approved the exome sequencing studies.

2.2. Exome Sequencing. Exome sequencing was performed from peripheral-blood DNA samples as reported previously [14]. In brief, coding regions were enriched using a SureSelect Human All Exon V5 kit (Agilent) followed by sequencing as 100 base-pairs paired-end runs on an Illumina HiSeq2500. Reads were aligned to the human reference genome (UCSC Genome Browser build hg19) using Burrows-Wheeler Aligner (v.0.7.5a) [15]. Single-nucleotide variants and small insertions and deletions (indels) were detected with SAMtools (version 0.1.19) [16].

Confirmation was performed by Sanger sequencing using the following forward 5'-CTCCCGCTCCACTCCTAAG-3' and reverse 5'-GTCCTTTCCTCCCCTCGTC-3' primers.

2.3. Enzyme Activity of the OXPHOS Complexes. Spectrophotometric measurement of OXPHOS enzyme and citrate synthase activity was performed as previously described [17, 18]. Muscle tissue (20–100 mg) was homogenized in extraction buffer (250 mM sucrose, 40 mM KCl, 2 mM EGTA, 20 mM Tris-HCl, pH 7.6). The postnuclear supernatant (600 ×g homogenate) containing the mitochondrial fraction was used for measurement of enzyme activities and Western blot analysis.

2.4. Western Blot Analysis on SDS-PAGE. 600g homogenates were separated on acrylamide/bisacrylamide gels and transferred to nitrocellulose membranes. Immunological detection of proteins was carried out as described previously [17]. The following primary antibodies were used: polyclonal rabbit anti-UQCC2 (Proteintech, 1:1000, overnight 4°C), monoclonal mouse anti-NDUFS4 (Abcam, 1:1000, 1 h RT), monoclonal mouse anti-UQCRC2 (Abcam, 1:1500, 1 h RT), polyclonal rabbit anti-COX2 (Abcam, 1:1000, overnight 4°C), monoclonal mouse anti-porin 31HL (Abcam, 1:1000, 1 h RT), and polyclonal rabbit anti-GAPDH (Trevigen, 1:5000, 1 h RT). GAPDH was used as a loading control.

2.5. Blue Native-PAGE (Lauryl Maltoside Solubilization). For blue-native gel electrophoresis, 600 ×g supernatants of muscle tissue or isolated mitochondria from fibroblasts were used. Solubilized mitochondrial membranes were prepared from isolated fibroblast mitochondria as described previously [19]. Briefly, fibroblast mitochondria or 600g supernatants were sedimented by centrifugation at 13,000g for 15 min. Samples were solubilized with 1.5% lauryl maltoside for 15 min and centrifuged for 20 min at 13,000g. Samples were loaded on a 5% to 13% polyacrylamide gradient gel and separated electrophoretically. For immunoblot analysis, preparations were separated by BN-PAGE (5–13%) and blotted onto polyvinylidene difluoride membrane (Hybond-P, GE Healthcare) using a CAPS buffer (10 mmol/l 3-cyclohexylamino-1-propane sulfonic acid pH 11, 10% methanol). The membrane was washed in 100% methanol for 2 min and blocked for 30 min at room temperature in 1% blocking solution (Roche) dissolved in TBS-T. The primary antibodies, diluted in 1% blocking solution-TBS-T, were added 1 h at room temperature. The following primary antibody dilutions were used: complex I subunit NDUFS4 monoclonal antibody (1:1000; Abcam), complex III subunit core 2 monoclonal

antibody (1:1500; Abcam), and complex V subunit α monoclonal antibody (1:1000; Abcam). After extensive washing, blots were incubated for 1 h at RT with secondary mouse antibody (1:100; DAKO polymer Envision Staining Kit). Detection was carried out with Lumi-LightPLUS POD substrate (Roche).

2.6. Blue Native-PAGE (Digitonin Solubilization). Gel electrophoresis was performed as previously described [20]. The blotting procedure is described in Section 2.5. The following primary antibody dilutions were used: complex I subunit NDUFS4 monoclonal antibody (1:1000; Abcam), complex V subunit α monoclonal antibody (1:1000; Abcam), complex III subunit Core 2 monoclonal antibody (1:1500; Abcam), complex IV subunit 2 polyclonal antibody (1:1000; Abcam), and complex II subunit SDHA monoclonal antibody (1:30,000; Abcam). The PVDF membrane was incubated with COX2 and NDUFS4 antibodies overnight at 4°C. Incubation with all other primary antibodies was performed for 1 h at RT.

2.7. Immunofluorescence Staining. Fibroblasts were grown on chamber slides. Cells were allowed to attach for 24 hours. At the next day, the medium was removed, and chamber slides were twice washed with PBS pH 7.4 and fixed in formalin overnight at 4°C. After washing cells three times 3 min with PBS-T (pH 7.5; 0.05% Tween-20), heat-induced epitope retrieval was done in 1 mM EDTA, 0.01% Tween-20, pH 8 at 95°C for 45 min. The solution was allowed to cool down to room temperature and chamber slides were washed with PBS-T. The chamber slides were incubated 1 h at RT with primary antibodies against rabbit-polyclonal porin 31HL (1:400), mouse-monoclonal NDUFS4 (1:100), and mouse-monoclonal UQCRC2 (1:400). 1st antibodies were diluted in DAKO antibody diluent with background-reducing components. After washing with PBS-T, cells were incubated 1 h at RT in dark with secondary antibodies (Alexa Fluor 594 donkey anti-rabbit antibody, 1:500 and Alexa Fluor 488 donkey anti-mouse IgG (H + L), 1:1000). After washing the chamber slides with PBS-T, they were incubated with DAPI diluted 1:2000 in PBS-T for 10 min. Chamber slides were mounted in fluorescence mounting media from DAKO.

3. Results

3.1. Clinical Report. The girl is the first child of healthy consanguineous Turkish parents (first-degree cousins). Pregnancy was complicated by intrauterine growth restriction (IUGR), oligohydramnios, and breech presentation. She was born at 32 weeks of gestation by Caesarean section, body weight: 1430 g (<25th centile), body length: 42 cm (3rd centile), and head circumference: 30.7 cm (10th centile). APGAR scores were 8/9/9 after 1/5/10 minutes, and umbilical artery pH was 7.34.

She suffered from respiratory distress syndrome (IRDS) grades III-IV and required CPAP-ventilation followed by endotracheal intubation and mechanical ventilation at the age of three hours. Within the first 4 days of life, she required 4 times surfactant (Curosurf©) replacement therapy. At day

14, she presented with pulmonary haemorrhage and the first epileptic seizures which progressed into a status epilepticus. Despite total parenteral nutrition (oral feedings caused recurrent vomiting), weight gain remained poor. She had no obvious dysmorphic features, physical examination was unremarkable, and neurological examination was influenced by sedation and analgesia during continuous mechanical ventilation, but showed a generally low muscle tone. Ophthalmological investigation was normal, a hearing test was not performed, and echocardiography and ECG revealed normal results. The EEG showed low-voltage activity. Repetitive cranial ultrasound examinations showed periventricular echodensities, a noncalcifying vasculopathy in the basal ganglia region, and signs of general hypoxemic encephalopathy. She died due to respiratory failure on day 33.

3.2. Laboratory Findings. A profound and recurrent lactic acidosis (max. 20 mmol/l, ref. <2.4 mmol/l) was evident starting at the age of 4 hours and lasting until her death. Extended newborn screening was unremarkable. Blood counts, C-reactive protein, interleukin-6, procalcitonin, and liver enzymes were repetitively within normal limits, creatinine (1.49 mg/dl) was slightly elevated (ref. 0.90–1.40 mg/dl), urea was normal (39 mg/dl), and coagulation analysis was within normal limits. High pyruvate excretion was noted. The karyotyping (46 XX) was unremarkable. SNP analysis confirmed consanguinity of the patients' parents and revealed a large homozygosity-by-descent (HBD) region of about 54 Mb including almost the entire p-arm of chromosome 6; this area contains 690 genes, including *UQCC2* as potential disease-causing gene.

3.3. Exome Sequencing. Sequencing revealed two homozygous missense mutations c.[23G>C;28C>T];[23G>C;28C>T] and p.[Arg8Pro;Leu10Phe];[Arg8Pro;Leu10Phe] in the ubiquinol-cytochrome c reductase complex assembly factor 2, encoded by *UQCC2*, GenBank accession NM_032340.3 (Figure 1). Both mutations affect phylogenetically conserved amino acids and were predicted to be of pathogenic relevance by all used prediction programs (Polyphen-2, SIFT, Provean, MutationTaster, CADD; Supplemental Table 1 available online at <https://doi.org/10.1155/2017/7202589>). Both variants seem to be very rare since they are neither found in 1000 Genome nor in the ExAC databases. These variants were confirmed by the Sanger sequencing; the mother is a heterozygous carrier (Figure 1(b)).

3.4. Enzymatic Measurements. Spectrophotometric measurement revealed a combined reduction of complex III (111 mUnits/mg protein; normal range: 230–486) and complex I (9 mUnits/mg protein; normal range: 30–84) in the muscle (Table 1). No reduction of respiratory chain enzymes was obvious in patient fibroblasts (Table 1) suggesting some tissue specificity of the *UQCC2* defect.

3.5. Western Blot Analysis. Almost complete loss of *UQCC2* protein was present in the muscle and fibroblasts of the affected individual (Figure 2(a)). A severe reduction of complex III and complex I in the muscle and fibroblasts was also

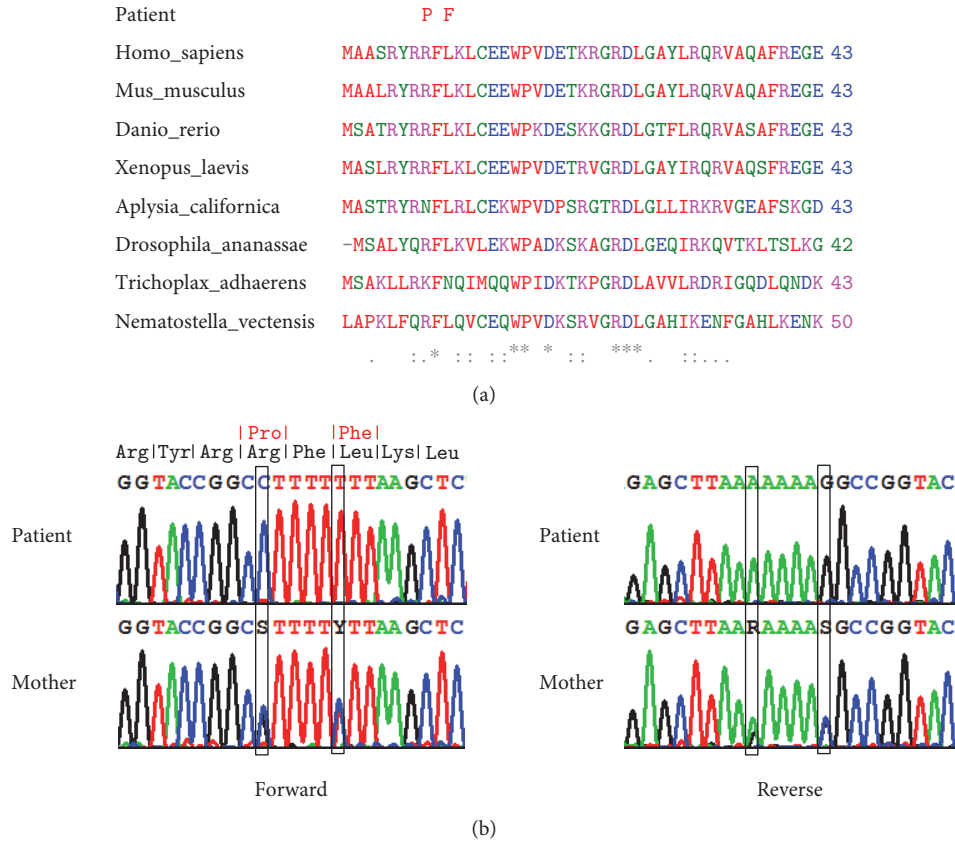


FIGURE 1: Conservation of affected amino acid residues and enzymatic activities of respiratory chain complexes in the muscle and fibroblasts. (a) Phylogenetic conservation of UQCC2. The two homozygous missense mutation affect highly conserved amino acid residues: c.[23G>C; 28C>T]; [23G>C; 28C>T], (p.[Arg8Pro; Leu10Phe]; [Arg8Pro; Leu10Phe]), and reference sequence GenBank NM_032340.3. (b) UQCC2-sequencing chromatograms of the patient and mother.

TABLE 1: Enzymatic activity of the OXPHOS complexes in muscle and fibroblasts.

	Mean	Muscle		Control range	Fibroblasts	
		M1	M2		Patient	Control range
Citrate synthase	140	140	139	(166–311)	210	(225–459)
Complex I	9	10	8	(30–84)	20	(18–53)
Complex I + III	30	30	30	(27–58)	152	(73–220)
Complex II	38	40	36	(53–102)	74	(64–124)
Complex II + III	34	31	36	(41–84)	125	(79–219)
Complex III	111	108	115	(230–486)	555	(208–648)
Complex IV	233	229	237	(205–739)	380	(175–403)
Complex V	79	72	85	(78–178)	92	(43–190)

Values are given in mUnits/mg protein. M1 and M2: values of two measurements.

confirmed by the immunoblot analyzed (Figures 2(a) and 2(b)). Complex IV was not affected (Figure 2(b)).

3.6. Immunofluorescence Staining. A reduction of protein amount of both complex III and complex I was present in patient fibroblasts as found by immunohistochemical staining (Figure 2(c)).

3.7. Blue-Native Gel Electrophoresis. A decreased amount of assembled complexes III and I was present in the muscle

(Figure 3(a)). In fibroblasts, complex III was decreased as well, whereas normal amounts of complex I were detected (Figure 3(d)). Loss of complex III and supercomplexes containing complex III was observed in digitonin solubilized muscle of the UQCC2 patient as shown by Western blot analysis with an AB raised against the core 2 subunit of complex III and staining with Serva Blue G (Figure 3(g)). A reduction was also present in a patient with a pathogenic NDUFS4 mutation. No significant reduction was present in the muscle of a patient carrying a pathogenic SURF1

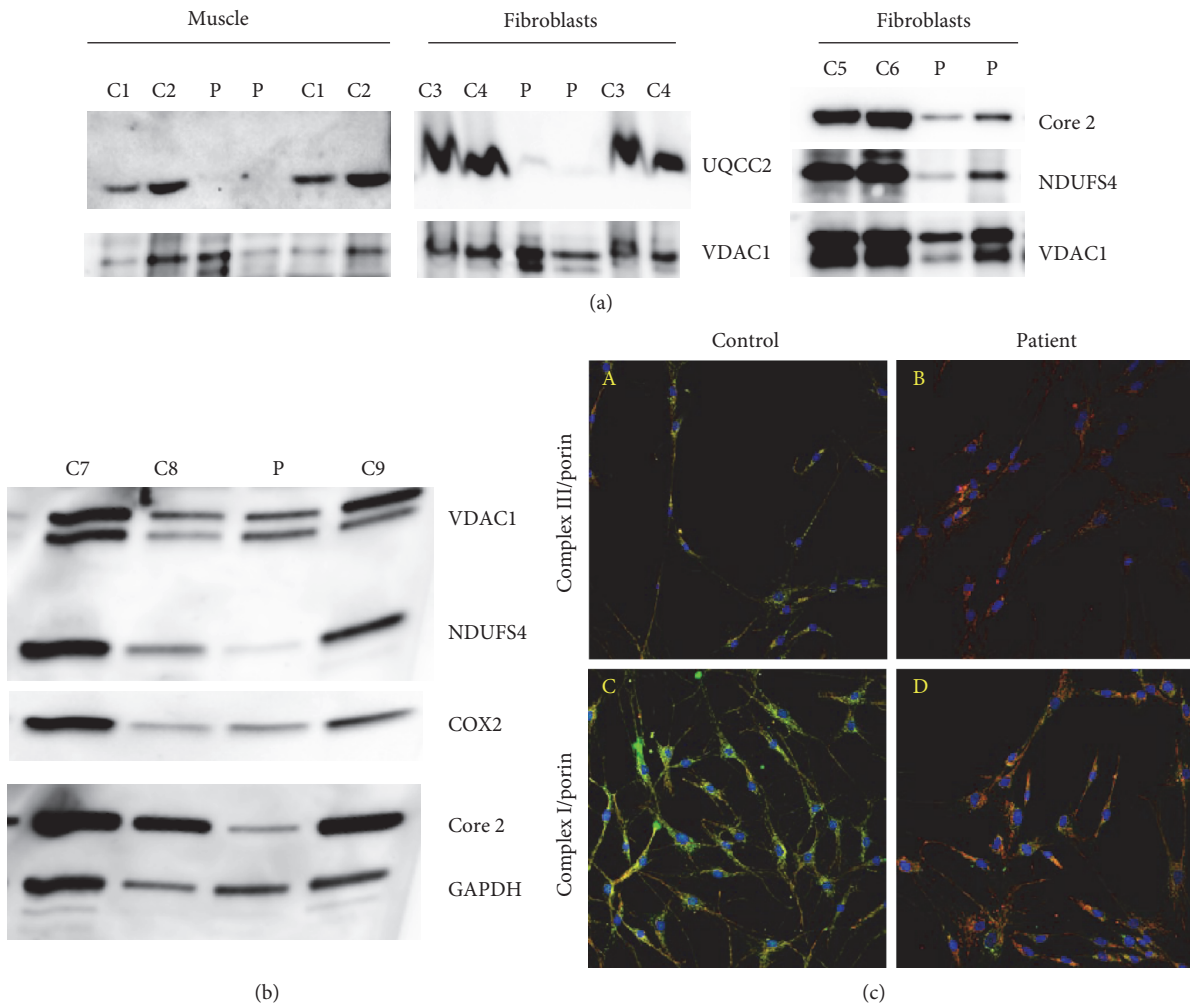


FIGURE 2: SDS Western blot analysis of muscle and immunofluorescence staining of the OXPHOS complexes of fibroblasts. (a) SDS Western blot analysis of UQCC2, Core 2, NDUFS4, and VDAC1 of muscle 600 g supernatant and isolated fibroblast mitochondria. Two different amounts of mitochondrial proteins were loaded of controls and patient muscle/fibroblasts. (b) SDS Western blot analysis of the OXPHOS complexes of muscle 600 g supernatant of the OXPHOS complexes. (c) Immunofluorescence staining of complexes III and I in fibroblasts. (A, B) Staining of complex III and porin. (C, D) Staining of complex I and porin. (A, C) Control. (B, D) Patient. Magnification 20x.

mutation. To further underline the findings, the Western blot was also analyzed with antibodies against NDUFS4 and COX2. A reduction of complex I containing supercomplexes was observed in muscle homogenates of the UQCC2-deficient patient and also in patients with loss of function mutations in either NDUFS4 or SURF1 (Figure 3(g)) shown with an antibody against NDUFS4. No signal was present at the size of the supercomplexes for COX2 in the muscle of all patients compared to healthy controls. Normal amounts of monomeric complex IV were present in UQCC2 and NDUFS4 muscle, whereas a severe reduction was found in the SURF1 patient. No differences were present regarding complexes V and II between patients and controls.

4. Discussion

Here, we report on a second patient with mutations in UQCC2, an assembly factor of complex III. The clinical phenotype in our patient is difficult to interpret as many findings

seem to be related to the prematurity (IRDS with respiratory problems and periventricular echodensities on brain ultrasound). However, as she was born at a gestational age of 32 weeks, the clinical course was clearly more severe than expected usually for preterm infants at this week of gestation: key features represented the recurrent neonatal seizures and severe lactic acidosis. These findings might indicate that the severe course of the disease was due to the underlying mitochondrial disorder. Further speculation about a distinctive clinical pattern is impossible due to mechanical ventilation throughout her life and the influence of sedation and analgesia. Interestingly, clinical information on the first reported patient was also limited [7]. It might be worth mentioning that IUGR was found in our patient and also in the other UQCC2 patient, while this has not been reported for other complex III-related genetic disorders.

In general, the clinical course in relation with respiratory chain complex III deficiency is heterogenous [21]. Given the small number of patients reported, it might be even broader

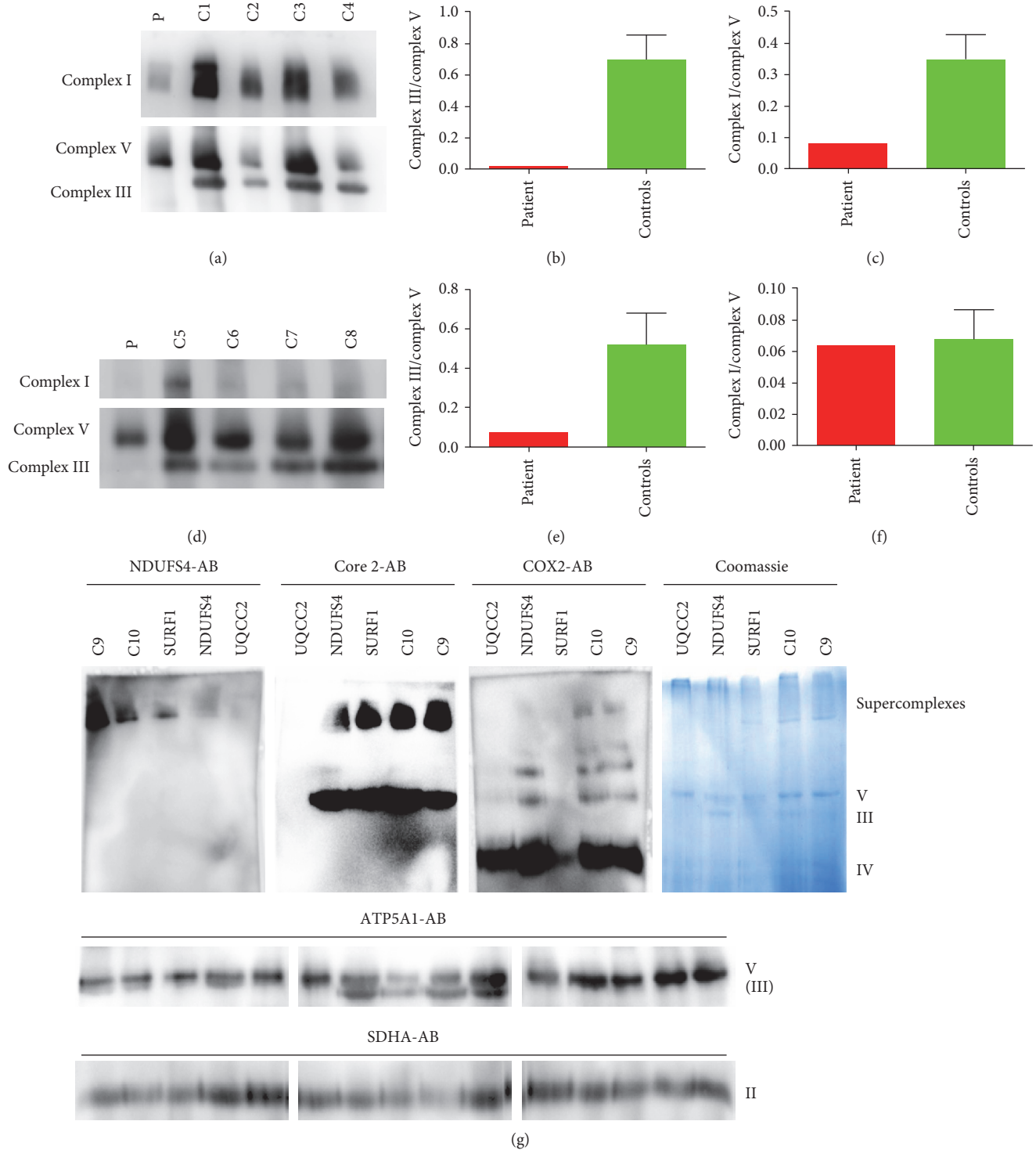


FIGURE 3: Blue native (BN) gel electrophoresis of muscle and fibroblasts. (a) BN-PAGE of the muscle with lauryl maltoside solubilization. (b, c) Densitometric analysis of BN-PAGE from the muscle. (d) BN-PAGE of fibroblasts. (e, f) Densitometric analysis of BN-PAGE from fibroblasts. (g) BN-PAGE of the muscle with a digitonin solubilization. The membrane was incubated with antibodies targeted against NDUFS4, Core 2, COX2, ATP5A1, and SDHA. C1–C10 are normal controls. In addition, muscle homogenates from patients with loss of function mutations in either *SURF1* (NM_003172.3) c.11_30del20 (p.Val4Alafs*49) or *NDUFS4* (NM_002495.2) c.466_469dupAAGT (p.Ser157*) were used as disease controls.

(Table 2). Based on clinical presentation, it is impossible to distinguish between subunits or assembly factor defects.

A distinctive and comparable clinical pattern was reported in six patients from five families. These individuals with mutations in UQCRB, UQCRC2, and CYC1 presented with neonatal or early infancy onset, recurrent metabolic crises with elevated lactate and hypoglycaemia, from which they completely and quickly recovered with intravenous glucose. All but one showed a normal development and intellect [2, 6, 22]. A more variable clinical picture is seen with *BCSIL* mutations including lactic acidosis, renal and liver involvement, encephalopathy, hearing loss, and seizures [23]. A cohort of seven patients with *LYRM7* mutations were found to have a consistent magnetic resonance imaging pattern of progressive signal abnormalities with multifocal small cavitations in the periventricular and deep cerebral white matter [24] while another *LYRM7* patient was reported with liver involvement [10]. Patients with *TTC19* mutations are described as having an already delayed development which progresses via extrapyramidal movement disorder to a minimal residual state. One big Bedouin kindred with 25 affected individuals carrying homozygous mutations in UQCRQ has been described with a developmental delay progressing toward an extrapyramidal movement disorder, the oldest affected patients of this kindred were in their thirties [1].

Genetically, these two UQCC2 patients are distinct in terms of homozygous missense mutation in our case, while the other patient had a splice-site mutation affecting position -3 of the splice acceptor (c.214-3C>G), which might allow the formation of a small amount of wild-type protein and possibly explain the milder clinical outcome.

Biochemically, our patient presented with a severe reduction of complexes I and III of the respiratory chain in the muscle tissue. In fibroblasts, the activity of complex III was normal. This might be due to higher reserve capacity in less energy-dependent fibroblast or may be due to differences in posttranscriptional regulation as observed for complexes I and IV [25–28]. Combined deficiency of complex I and III deficiency is consistent with the previous reported patient with UQCC2 mutations who also showed reduced complex I on the level of enzymatic activity and BN-PAGE in addition to complex III deficiency. Furthermore, lack of complex III dimer and minimal complex III bound in supercomplexes in digitonin-solubilized fibroblasts of the UQCC2-deficient patient was described [7]. In agreement, we also show that in the muscle tissue of our UQCC2 patient, the formation of respiratory chain supercomplexes is diminished. Wanschers et al. reported a case with *UQCC3* mutations. Also, in this protein assembly factor disorder, combined reduction of the activity of complexes III and I was found in the muscle. In addition, diminished levels of assembled complexes III and I were present in patient fibroblasts [8]. No mutations in UQCC1 have been described so far. Both patients showed reduction of complex I and in one case complex IV activity.

In 2004, Acín-Pérez et al. observed that complex III is required to maintain complex I in mitochondria in a study with rodent cells and mutations of the cytochrome b gene,

which is encoded on the mitochondrial DNA [29]. Combined deficiency of complex I and complex III was reported for some patients with *MT-CYB* mutations. In line with these findings, we and others identified homoplasmic loss of function mutations in *MT-CYB* with severe complex I and complex III deficiency in renal oncocyoma, a human tumor characterised by loss of complex I or combined deficiency of complex I and other respiratory chain enzymes [3, 30, 31]. Simultaneously, Schägger et al. also reported that primary complex III assembly deficiencies present as combined complex III/I defects also shown for cytochrome b gene mutations [32].

In *Caenorhabditis elegans*, it was shown that complex III is important for supercomplex assembly. Furthermore, it was proven that complex III uniquely affects complex I, either by decreasing the amount of complex I or the I-III-IV supercomplex. A mutation in *isp-1* (ortholog of the Rieske protein) can reduce the amount of fully assembled complex I. Mutations in *ctb-1* (cytochrome b ortholog) can cause a reduction in complex I activity without affecting the complex I assembly [33].

Most of the nine so far described defects of nuclear-encoded complex III subunits or assembly factors have been published after the initial and important observation in 2004. Remarkably, in most of these papers, reduction of complex I and in some cases complex IV was found in addition to complex III deficiency (Table 3):

- (1) Haut et al. described a boy with isolated complex III deficiency caused by a mutation in UQCRB. However, a moderate reduction of complex I activity was present in the patients' liver [22].
- (2) Barel et al. described a patient with UQCRQ mutation with complex III deficiency, a variable decrease of complex I activity in skeletal muscle biopsies [1].
- (3) Miyake et al. described a patient with a mutation in UQCRC2. The activity of complex I was increased threefold in the skeletal muscle. However, the authors showed impaired supercomplex formation in patient fibroblasts affecting complexes I and IV [6]. Very recently, Gaignard et al. also reported a patient with a reduced complex III and I activity in fibroblasts. In addition, the native complexes I and III were both reduced. Neither complex IV activity nor complex IV assembly was diminished [34].
- (4) Gaignard et al. reported that loss of cytochrome *c1* encoded by *CYC1* causes an isolated complex III deficiency in two children. However, a reduced complex I activity was shown for the liver. In addition, the authors described secondary reduction of assembly-dependent subunits of complexes I and IV [2]. A reduction of supercomplexes was present as shown by BN-PAGE. Taken together, these results indicate that *CYC1* mutations might cause a defect in respirasome assembly and a combined OXPHOS deficiency.

TABLE 2: Clinical features of complex III deficiencies.

Gene	Complex III subunits				Complex III assembly factors						
	MT-CYB	CYCI	UQCRB	UQCR2	UQCRQ	UQCC2	UQCC2	UQCC3	TTC19	LYRM7	BCSIL
MIM accession	516020	615453	615158	615160	615159	615824	615824	616097	615157	615838	124000
Number of patients	>50	1	1	4	25, 1 kindred	1	1, this study	1	Ca. 15	9	>30
Onset	Childhood, adulthood	Infancy, early childhood	Late infancy	Neonatal	First months of life	Intrauterine	Intrauterine	Birth	Late infancy, adulthood	Infancy, 14 years	First years, infancy
Intrauterine growth retardation						Yes	Yes				
Hearing impairment						Yes	n.a.	No			Yes
Hypotonia	Yes					Yes	Yes	Yes		Yes	Yes
Seizures						Yes	Yes	No			Yes
Abnormal EEG							Yes	Yes			Yes
Metabolic crisis			Yes				Yes	Yes		Yes	
Lactic acidosis	Yes	Yes	Yes	Yes	Yes	Yes	Yes	Yes		Yes	Yes
Increased CSF lactate	Yes		Yes			Yes					
Hypoglycaemia		Yes	Yes	Yes				Yes			
Developmental disability		No	No	No		No	n.a.	Yes	Yes	Yes	Yes
Intellectual disability		No	No	Yes (1)/no (1)	Yes		n.a.	Yes		Yes	Yes
Other features		In one hyperammonemic liver failure			Extrapyramidal movement disorder, survival into thirties	Renal tubular acidosis, no information after 9 years of age	Status epilepticus, died at 33 days of life	Muscular weakness	Later regression with spasticity and movement disorder leading to minimal residual state	Deterioration after metabolic crises, specific MRI pattern (multifocal cavitating leukoencephalopathy)	Hepatopathy, renal involvement, often early death

TABLE 3: Results of enzymatic investigations and BN-PAGE electrophoresis of patients with complex III deficiencies.

Reduction of enzymes [tissue]	MT-CYB	CYC1	UQCRB	UQCRC2	UQCRCQ	UQCC2	UQCC3	TTC19	LYRM7	BCS1L
Complex III [muscle]	Yes	3\$/3	n.a.	1\$/1	3/3 (22 = n.a.)	1/1	1/1	Most	6/9 (3 = n.a.)	Reduced
Complex III [fibroblasts]	Yes	2/2	1/1	2/2 (2 = n.a.)	n.a.	1/1	1/1	Some	1/9 (8 = n.a.)	Reduced
Complex III [liver]		1/1 (1 = n.a.)	1/1	n.a.	n.a.	n.a.	n.a.	n.a.	1/9 (8 = n.a.)	Variable
Complex I [muscle]	Yes	1\$/2 (1 = n.a.)	n.a.	1\$/1	3/3 (22 = n.a.)	1/1	1/1	Normal	1/9 (8 = n.a.)	Variabe
Complex I [fibroblasts]		n.a.	n.a.	1/2 (2 = n.a.)	n.a.	1/1	0/1	Normal	n.a.	Variable
Complex I [liver]		1/1 (1 = n.a.)	1/1	n.a.	n.a.	n.a.	n.a.	n.a.	n.a.	Variable
Complex I [BN-PAGE] fibroblasts	Muscle	1/2	n.a.	2/2 (2 = n.a.)	n.a.	1/1	1/1	Normal	0/1 (8 = n.a.)	Variable
Complex IV [muscle]		1\$/3	n.a.	1\$/1	2/3 (22 = n.a.)	1/1	0/1	Normal	n.a.	Variable
Complex IV [fibroblasts]		0/1 (1 = n.a.)	1/1	0/2 (2 = n.a.)	n.a.	1/1	0/1	Normal	n.a.	Variable
Complex IV [liver]		0/1 (1 = n.a.)	0/1	n.a.	n.a.	n.a.	n.a.	n.a.	n.a.	
Complex IV [BN-PAGE] fibroblasts		0/2	n.a.	1/2 (2 = n.a.)	n.a.	Normal	0/1	Normal	0/1 (8 = n.a.)	Variable
Literature	Gasparre et al. [3] Zimmermann et al. [9] Blakely et al. [39]	Gaignard et al. [34], Some patient from Tucker et al. [7], no values provided	Haut et al. [22]	Gaignard et al. [34], Gasparre et al. [3], Some patient from Tucker et al. [7], no values provided	Barel et al. [1]	Tucker et al. [7]	This study	Wanschers et al. [8]	Koch et al. [5], Ardissonne et al.	Invernizzi et al. [4] Dallabona et al. [24] Kremer et al. [10] Moran et al. [23]

- (5) As reported here and in the paper of Tucker et al. [7], UQCC2 deficiency causes combined complex I and complex III deficiency. A reduction of supercomplexes was present in both cases.
- (6) As already mentioned above, UQCC3 deficiency causes combined complex III and complex I deficiency [8].
- (7) Combined deficiencies of complex III, complex I, and/or complex IV were also reported for patients with mutations in *BCS1L*, especially in patients with severe clinical symptoms [23]. In addition, *BCS1L* defects manifest in a highly tissue-specific pattern.
- (8) Two other complex III assembly factors are known *LYRM7* and *TTC19* although they seem to be involved in different aspects of assembly. *LYRM7* plays a role in iron sulphur cluster biogenesis. However, besides severe complex III deficiency, minor reduction of complex I or complex IV in patient muscle was reported [4, 10]. The function of *TTC19* is still a matter of debate although most patients show an isolated complex III deficiency. However, we reported on a *TTC19* patient even without any signs of complex III changes [5].

Indeed, isolated complex III deficiency might be the exception rather than the rule. Since the presence of assembled complex III seems to be crucial for respirasome assembly and maybe for the stability or assembly of complexes I and IV. Complex III dimers are mainly found in three different complexes, one supercomplex termed respirasome (CI, CIII₂, and CIV), one with complex I (CI, CIII₂), or one with complex IV (CIII₂, CIV). The supercomplexes interact at nine sites [13]. *COX7a2L* was the first factor designated as a supercomplex assembly factor. However, it is still debated if *COX7a2L* also influences respirasome assembly [35, 36]. In addition, *HIGD1a* was reported to promote supercomplex formation [37].

Therefore, UQCC2 deficiency, like most other disorders of complex III subunits and most assembly factors, has to be considered as disorders of respirasome assembly rather than isolated complex III defects. This finding is of diagnostic relevance since a combined reduction of complexes III and I is likely an indication for mutations in complex III-related genes. Since isolated complex III is not determined in all laboratories [38], those defects might be misdiagnosed as either complex I or complex IV deficiency. This wrong categorisation might result in selection of inappropriate panels for genetic workup.

Disclosure

Sabine Uhrig present address: Praxis für Humangenetik, Paul-Ehrlich-Str. 23, 72076 Tübingen, Germany.

Conflicts of Interest

The authors declare that there are no conflicts of interest regarding the publication of this paper.

Acknowledgments

The study was supported by the E-Rare project GENOMIT (01GM1603, Austrian Science Funds (FWF): I 2741-B26) and the Vereinigung zur Förderung Pädiatrischer Forschung und Fortbildung Salzburg.

References

- [1] O. Barel, Z. Shorer, H. Flusser et al., "Mitochondrial complex III deficiency associated with a homozygous mutation in *UQCRQ*," *American Journal of Human Genetics*, vol. 82, no. 5, pp. 1211–1216, 2008.
- [2] P. Gaignard, M. Menezes, M. Schiff et al., "Mutations in *CYC1*, encoding cytochrome c1 subunit of respiratory chain complex III, cause insulin-responsive hyperglycemia," *American Journal of Human Genetics*, vol. 93, no. 2, pp. 384–389, 2013.
- [3] G. Gasparre, E. Hervouet, E. de Laplanche et al., "Clonal expansion of mutated mitochondrial DNA is associated with tumor formation and complex I deficiency in the benign renal oncocytoma," *Human Molecular Genetics*, vol. 17, no. 7, pp. 986–995, 2008.
- [4] F. Invernizzi, M. Tigano, C. Dallabona et al., "A homozygous mutation in *LYRM7/MZM1L* associated with early onset encephalopathy, lactic acidosis, and severe reduction of mitochondrial complex III activity," *Human Mutation*, vol. 34, no. 12, pp. 1619–1622, 2013.
- [5] J. Koch, P. Freisinger, R. G. Feichtinger et al., "Mutations in *TTC19*: expanding the molecular, clinical and biochemical phenotype," *Orphanet Journal of Rare Diseases*, vol. 10, no. 1, p. 40, 2015.
- [6] N. Miyake, S. Yano, C. Sakai et al., "Mitochondrial complex III deficiency caused by a homozygous UQCRC2 mutation presenting with neonatal-onset recurrent metabolic decompensation," *Human Mutation*, vol. 34, no. 3, pp. 446–452, 2013.
- [7] E. J. Tucker, B. F. Wanschers, R. Szklarczyk et al., "Mutations in the UQCC1-interacting protein, UQCC2, cause human complex III deficiency associated with perturbed cytochrome b protein expression," *PLoS Genetics*, vol. 9, no. 12, article e1004034, 2013.
- [8] B. F. Wanschers, R. Szklarczyk, M. A. van den Brand et al., "A mutation in the human *CBP4* ortholog UQCC3 impairs complex III assembly, activity and cytochrome b stability," *Human Molecular Genetics*, vol. 23, no. 23, pp. 6356–6365, 2014.
- [9] F. A. Zimmermann, J. A. Mayr, D. Neureiter et al., "Lack of complex I is associated with oncocytic thyroid tumours," *British Journal of Cancer*, vol. 100, no. 9, pp. 1434–1437, 2009.
- [10] L. S. Kremer, C. L'Hermitte-Stead, P. Lesimple et al., "Severe respiratory complex III defect prevents liver adaptation to prolonged fasting," *Journal of Hepatology*, vol. 65, no. 2, pp. 377–385, 2016.
- [11] L. Cambier, P. Rassam, B. Chabi et al., "M19 modulates skeletal muscle differentiation and insulin secretion in pancreatic beta-cells through modulation of respiratory chain activity," *PLoS One*, vol. 7, no. 2, article e31815, 2012.
- [12] M. Sumitani, K. Kasashima, E. Ohta, D. Kang, and H. Endo, "Association of a novel mitochondrial protein M19 with mitochondrial nucleoids," *Journal of Biochemistry*, vol. 146, no. 5, pp. 725–732, 2009.
- [13] J. A. Letts, K. Fiedorczuk, and L. A. Sazanov, "The architecture of respiratory supercomplexes," *Nature*, vol. 537, no. 7622, pp. 644–648, 2016.

- [14] L. S. Kremer, K. Danhauser, D. Herebian et al., "NAXE mutations disrupt the cellular NAD(P)HX repair system and cause a lethal neurometabolic disorder of early childhood," *American Journal of Human Genetics*, vol. 99, no. 4, pp. 894–902, 2016.
- [15] H. Li and R. Durbin, "Fast and accurate short read alignment with burrows-wheeler transform," *Bioinformatics*, vol. 25, no. 14, pp. 1754–1760, 2009.
- [16] H. Li, B. Handsaker, A. Wysoker et al., "The sequence alignment/map format and SAMtools," *Bioinformatics*, vol. 25, no. 16, pp. 2078–2079, 2009.
- [17] R. G. Feichtinger, S. Weis, J. A. Mayr et al., "Alterations of oxidative phosphorylation complexes in astrocytomas," *Glia*, vol. 62, no. 4, pp. 514–525, 2014.
- [18] R. G. Feichtinger, F. Zimmermann, J. A. Mayr et al., "Low aerobic mitochondrial energy metabolism in poorly- or undifferentiated neuroblastoma," *BMC Cancer*, vol. 10, p. 149, 2010.
- [19] J. A. Mayr, J. Paul, P. Pecina et al., "Reduced respiratory control with ADP and changed pattern of respiratory chain enzymes as a result of selective deficiency of the mitochondrial ATP synthase," *Pediatric Research*, vol. 55, no. 6, pp. 988–994, 2004.
- [20] I. Wittig, H. P. Braun, and H. Schagger, "Blue native PAGE," *Nature Protocols*, vol. 1, no. 1, pp. 418–428, 2006.
- [21] E. Fernandez-Vizarrá and M. Zeviani, "Nuclear gene mutations as the cause of mitochondrial complex III deficiency," *Frontiers in Genetics*, vol. 6, p. 134, 2015.
- [22] S. Haut, M. Brivet, G. Touati et al., "A deletion in the human QP-C gene causes a complex III deficiency resulting in hypoglycaemia and lactic acidosis," *Human Genetics*, vol. 113, no. 2, pp. 118–122, 2003.
- [23] M. Morán, L. Marín-Buera, M. C. Gil-Borlado et al., "Cellular pathophysiological consequences of BCS1L mutations in mitochondrial complex III enzyme deficiency," *Human Mutation*, vol. 31, no. 8, pp. 930–941, 2010.
- [24] C. Dallabona, T. E. Abbink, R. Carrozzo et al., "LYRM7 mutations cause a multifocal cavitating leukoencephalopathy with distinct MRI appearance," *Brain*, vol. 139, Part 3, pp. 782–794, 2016.
- [25] M. Babot, A. Birch, P. Labarbuta, and A. Galkin, "Characterisation of the active/de-active transition of mitochondrial complex I," *Biochimica et Biophysica Acta*, vol. 1837, no. 7, pp. 1083–1092, 2014.
- [26] M. Hüttemann, I. Lee, L. I. Grossman, J. W. Doan, and T. H. Sanderson, "Phosphorylation of mammalian cytochrome c and cytochrome c oxidase in the regulation of cell destiny: respiration, apoptosis, and human disease," *Advances in Experimental Medicine and Biology*, vol. 748, pp. 237–264, 2012.
- [27] G. Mahapatra, A. Varughese, Q. Ji et al., "Phosphorylation of cytochrome c threonine 28 regulates electron transport chain activity in kidney: implications for AMP kinase," *The Journal of Biological Chemistry*, vol. 292, no. 1, pp. 64–79, 2017.
- [28] T. H. Sanderson, G. Mahapatra, P. Pecina et al., "Cytochrome C is tyrosine 97 phosphorylated by neuroprotective insulin treatment," *PloS One*, vol. 8, no. 11, article e78627, 2013.
- [29] R. Acín-Pérez, M. P. Bayona-Bafaluy, P. Fernández-Silva et al., "Respiratory complex III is required to maintain complex I in mammalian mitochondria," *Molecular Cell*, vol. 13, no. 6, pp. 805–815, 2004.
- [30] J. A. Mayr, D. Meierhofer, F. Zimmermann et al., "Loss of complex I due to mitochondrial DNA mutations in renal oncocytoma," *Clinical Cancer Research*, vol. 14, no. 8, pp. 2270–2275, 2008.
- [31] F. A. Zimmermann, J. A. Mayr, R. Feichtinger et al., "Respiratory chain complex I is a mitochondrial tumor suppressor of oncocytic tumors," *Frontiers in Bioscience*, vol. 3, pp. 315–325, 2011.
- [32] H. Schägger, R. de Coo, M. F. Bauer, S. Hofmann, C. Godinot, and U. Brandt, "Significance of respirasomes for the assembly/stability of human respiratory chain complex I," *The Journal of Biological Chemistry*, vol. 279, no. 35, pp. 36349–36353, 2004.
- [33] W. Suthammarak, P. G. Morgan, and M. M. Sedensky, "Mutations in mitochondrial complex III uniquely affect complex I in *Caenorhabditis elegans*," *The Journal of Biological Chemistry*, vol. 285, no. 52, pp. 40724–40731, 2010.
- [34] P. Gaignard, D. Eyer, E. Lebigot et al., "UQCRC2 mutation in a patient with mitochondrial complex III deficiency causing recurrent liver failure, lactic acidosis and hypoglycemia," *Journal of Human Genetics*, vol. 62, no. 7, pp. 729–731, 2017.
- [35] R. Pérez-Pérez, T. Lobo-Jarne, D. Milenkovic et al., "COX7A2L is a mitochondrial complex III binding protein that stabilizes the III2+IV supercomplex without affecting respirasome formation," *Cell Reports*, vol. 16, no. 9, pp. 2387–2398, 2016.
- [36] S. Cogliati, E. Calvo, M. Loureiro et al., "Mechanism of super-assembly of respiratory complexes III and IV," *Nature*, vol. 539, no. 7630, pp. 579–582, 2016.
- [37] T. Hayashi, Y. Asano, Y. Shintani et al., "Higd1a is a positive regulator of cytochrome c oxidase," *Proceedings of the National Academy of Sciences of the United States of America*, vol. 112, no. 5, pp. 1553–1558, 2015.
- [38] F. N. Gellerich, J. A. Mayr, S. Reuter, W. Sperl, and S. Zierz, "The problem of interlab variation in methods for mitochondrial disease diagnosis: enzymatic measurement of respiratory chain complexes," *Mitochondrion*, vol. 4, no. 5–6, pp. 427–439, 2004.
- [39] E. L. Blakely, A. L. Mitchell, N. Fisher et al., "A mitochondrial cytochrome b mutation causing severe respiratory chain enzyme deficiency in humans and yeast," *The FEBS Journal*, vol. 272, no. 14, pp. 3583–3592, 2005.

Review Article

Disrupted Skeletal Muscle Mitochondrial Dynamics, Mitophagy, and Biogenesis during Cancer Cachexia: A Role for Inflammation

Brandon N. VanderVeen, Dennis K. Fix, and James A. Carson

Integrative Muscle Biology Laboratory, Department of Exercise Science, University of South Carolina, Columbia, SC, USA

Correspondence should be addressed to James A. Carson; carsonj@mailbox.sc.edu

Received 31 March 2017; Revised 6 June 2017; Accepted 19 June 2017; Published 13 July 2017

Academic Editor: Moh H. Malek

Copyright © 2017 Brandon N. VanderVeen et al. This is an open access article distributed under the Creative Commons Attribution License, which permits unrestricted use, distribution, and reproduction in any medium, provided the original work is properly cited.

Chronic inflammation is a hallmark of cancer cachexia in both patients and preclinical models. Cachexia is prevalent in roughly 80% of cancer patients and accounts for up to 20% of all cancer-related deaths. Proinflammatory cytokines IL-6, TNF- α , and TGF- β have been widely examined for their regulation of cancer cachexia. An established characteristic of cachectic skeletal muscle is a disrupted capacity for oxidative metabolism, which is thought to contribute to cancer patient fatigue, diminished metabolic function, and muscle mass loss. This review's primary objective is to highlight emerging evidence linking cancer-induced inflammation to the dysfunctional regulation of mitochondrial dynamics, mitophagy, and biogenesis in cachectic muscle. The potential for either muscle inactivity or exercise to alter mitochondrial dysfunction during cancer cachexia will also be discussed.

1. Introduction

Pathological inflammation, a hallmark of numerous chronic diseases, can lead to fatal comorbidities, including cachexia [1–4]. Cachexia is characterized by unintentional body weight loss secondary to an underlying disease [1, 3] and is prevalent in ~60–80% of cancer patients. Cancer patients exhibiting cachexia have increased fatigue, decreased functional independence, reduced life quality, and decreased survival [5–10]. Although no treatments are currently approved for cancer cachexia, improving the mechanistic understanding of skeletal muscle mass loss and more recently skeletal muscle metabolic function is thought to be central to the etiology of cancer cachexia and the successful development of therapeutic interventions.

Skeletal muscle mass and metabolism have established roles for maintaining health in obesity, ageing, and chronic disease [11–13]. Related to health, skeletal muscle serves as an amino acid reservoir for the body and a primary site of insulin-stimulated glucose transport [11, 14]. However,

skeletal muscle relies heavily on lipids as a fuel source during rest and low-intensity activities and contributes to over 20% of whole body fatty acid metabolism [14]. This oxidative metabolism dependence underscores the muscle mitochondria's critical role in metabolic homeostasis [14, 15]. The analysis of muscle oxidative metabolism involves the quantification of mitochondria content, respiratory capacity, and the efficiency of the Krebs cycle and electron transport chain (ETC) [16, 17]. This line of inquiry has significantly advanced our mechanistic understanding of aging, disease, and physical inactivity's effects on muscle metabolism.

Dysfunctional muscle oxidative metabolism occurs with many disease conditions [12, 13, 18–21] and can involve mitochondrial dynamics, mitophagy, and biogenesis regulation [18, 22]. Each of these dysfunctions is being actively investigated for their role in the pathogenesis of cancer cachexia [12, 13, 23]. Skeletal muscle mitochondrial dysfunction has been reported with cachexia in cancer patients and preclinical models [12, 15, 24–27] and is consistent with functional changes involving increased muscle fatigability

and overall weakness [5, 6, 8, 9, 28]. Accelerated catabolism and suppressed anabolism in wasting muscle has been linked to mitochondrial dysfunction [12, 25, 26]. The primary objective of this literature review is to highlight evidence linking cancer-induced inflammation to the regulation of muscle mitochondrial dynamics, mitophagy, and biogenesis. We will stress research areas that warrant further investigation to establish if they are a consequence of cachexia or a cause of the pathology. The examination of inflammatory mediators of cancer cachexia will be delimited to interleukin 6 (IL-6), tumor necrosis factor α (TNF- α), and transforming growth factor β (TGF- β) superfamilies' role. Evidence for these cytokines in the overall regulation of cachexia progression and muscle mass loss has been extensively reviewed elsewhere [29–38] and will only be briefly described here. We will also discuss the potential for either muscle inactivity or exercise to alter the regulation of dysfunctional mitochondrial dynamics, mitophagy, and biogenesis during cancer cachexia.

2. Overview of Inflammation as a Driver of Cancer Cachexia

2.1. Overview. Increased systemic inflammation is an established driver of cachexia development in numerous chronic diseases, including cancer [3]. Several cytokines have been implicated as the mediators of chronic inflammation for cachexia progression in both human and preclinical animal models [1, 29, 39]. Cytokines can regulate intracellular signaling that induces muscle wasting in response to various stimuli. IL-6, TNF- α , and TGF- β are cytokines that have been mechanistically linked to skeletal muscle wasting and disrupted metabolic homeostasis during cancer cachexia [29–38].

2.2. Interleukin-6. The IL-6 cytokine family has been widely investigated in skeletal muscle remodeling due to exercise, aging, and disease [29, 40–43]. IL-6 is a pleiotropic cytokine implicated as a critical regulator of inflammation-induced skeletal muscle and fat wasting during cancer cachexia [35]. Elevated circulating IL-6 can be observed in cachectic cancer patients and preclinical models alike and is strongly correlated to body weight and muscle mass loss [44–46]. IL-6 signals through the ubiquitously expressed glycoprotein 130 (gp130) receptor to activate downstream intracellular signaling pathways [42, 47, 48]. While IL-6 can activate numerous cellular signaling pathways, the phosphorylation of immediate downstream target signal transducer and activator of transcription 3 (STAT3) has been most widely examined with cachexia-induced muscle mass loss [41, 49, 50]. STAT3 activation by IL-6 causes the disruption of skeletal muscle proteostasis through both anabolic and catabolic signaling [51]. STAT3 inhibition can attenuate body weight and muscle mass loss in tumor-bearing mice [52, 53]. This review will discuss the implications for IL-6-induced STAT3 signaling in the regulation of cachexia-induced mitochondrial dysfunction (Figure 1).

2.3. Tumor Necrosis Factor α . TNF- α 's role in muscle wasting during cachexia has been well studied [1, 34, 54–56]. TNF- α ,

released from activated macrophages, can activate skeletal muscle nuclear factor κ B (NF- κ B) transcription factor and promote protein degradation through the transcription of ubiquitin proteasome E3 ligases, MurF1, and Atrogin1 [34, 38]. Muscle MurF1 and Atrogin1 expression are prevalent in cancer patients and preclinical cachexia models and promote skeletal muscle protein degradation [57]. TNF- α can also promote body weight loss through the loss of adipose tissue by stimulating lipolysis and inhibiting lipogenesis [34]. However, TNF- α also promotes anorexia [58, 59]. Cancer-induced TNF- α levels increase corticotrophin-releasing hormone (CRH), which reduces appetite and food intake [33, 34, 60]. However, TNF- α overexpression in mice lacking tumors induced weight loss, which was not different than pair-fed controls [61]. This portion of the review will focus on TNF- α 's induction of NF- κ B to disrupt mitochondrial homeostasis (Figure 1).

2.4. Transforming Growth Factor β . TGF- β cytokine super family consists of 34 proteins that regulate a myriad of cellular functions. Several family members have been found to promote cancer-induced skeletal muscle wasting [30, 62]. TGF- β 1, Activin A, TNF like weak inducer of apoptosis (TWEAK), and myostatin are TGF- β super family members that bind to either type I or type II activin receptors in skeletal muscle and activate Smad (SMA, mothers against decapentaplegic) signaling [1, 30, 56, 63–66]. Smad regulation of skeletal muscle wasting is still an area of active inquiry, but evidence suggests a role for forkhead box O3- (FOXO3-) dependent protein degradation as well as protein synthesis suppression through protein kinase B (Akt) [30, 38]. Activin A administration can induce the cachectic phenotype in nontumor-bearing mice through Smad2/3 activation, which increases atrophy and fibrotic gene transcription [67]. While TGF- β signaling's role in cachexia continues to be elucidated, this review will discuss evidence for the TGF- β superfamily to regulate skeletal muscle mitochondria function (Figure 1).

3. Mitochondrial Dysfunction in Cachectic Muscle and Inflammatory Mediators

3.1. Overview. Cachexia can be defined as a complex metabolic syndrome, and thus skeletal muscle mitochondria have become an intriguing focus for determining the underpinnings of cancer-induced muscle catabolism [3]. To this end, the maintenance of mitochondrial content and capacity for ATP production in cachectic muscle have become active areas of inquiry. While numerous studies have reported mitochondrial content loss with wasting, there remains a need to better define mitochondrial function and the regulators of this process in cachectic muscle. Mitochondrial function is classically defined as the capacity for ATP production through oxidative phosphorylation and beta-oxidation [24, 68, 69]. Disruptions to the ETC decrease mitochondrial respiration and the ability to produce ATP. While relatively few published studies have directly examined muscle mitochondrial respiration with cancer cachexia, cachectic

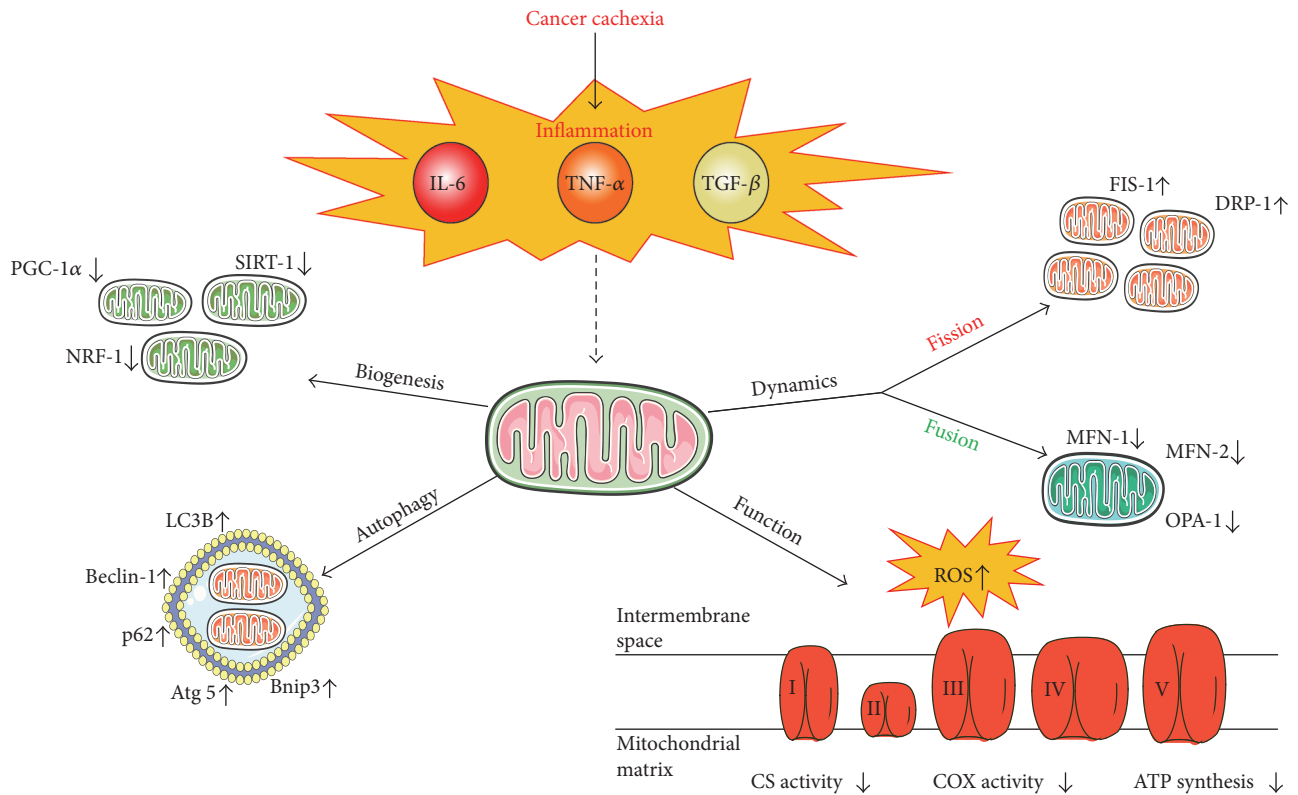


FIGURE 1: Cancer cachexia-induced inflammation regulates mitochondria. Chronic inflammation during cancer cachexia is associated with increased circulatory proinflammatory cytokines IL-6, TNF- α , and TGF- β . Chronic inflammation through these cytokines has been demonstrated to decrease mitochondrial biogenesis through decreased activation of PGC-1 α , NRF-1, and Sirt-1. Increased autophagy is apparent in cachectic muscle through inducing LC3B, Beclin-1, p62, Atg 5, and Bnip3 and dysregulating dynamics shown by increased FIS-1 and Drp-1 and decreased MFN-1, MFN-2, and OPA-1. These factors contribute to decreased mitochondrial function and ATP synthesis. The figure was made with Servier Medical Art (<http://www.servier.com/Powerpoint-image-bank>).

skeletal muscle exhibits decreased cytochrome c oxidase enzymatic activity and oxygen consumption [70, 71].

Inflammatory signaling has been linked to cancer-induced mitochondrial dysfunction in skeletal muscle [12]. Specifically, activation of either NF- κ B, STAT3, or Smad3 signaling has been associated with cancer-induced muscle mitochondria dysfunction in tumor-bearing mice. In vivo and in vitro analysis of Lewis lung carcinoma-driven cachexia demonstrated decreased muscle ATP synthesis rates and decreased mitochondrial electron flow with associative increases in TNF- α [68, 72]. Furthermore, inhibiting NF- κ B signaling improved diaphragm mitochondrial respiration in mice bearing P07 lung-derived tumors [70]. The IL-6 signaling pathway has also been linked to muscle mitochondrial function with cachexia [12]. STAT3 accumulation in isolated liver and heart mitochondria negatively regulates mitochondrial respiration and ATP production through binding to Complex I in the inner mitochondrial membrane and interacting with retinoid-interferon-induced mortality (GRIM) 19 [73]. Reduced enzyme activity in isolated skeletal muscle mitochondria is demonstrated in mice with elevated Smad 3 signaling [71]. Currently, our understanding of muscle mitochondrial respiration during cancer cachexia is extremely limited due to the dearth of published studies and the heterogeneity of the preclinical cancer cachexia

models used in these investigations. However, further mechanistic inquiries into both the drivers of mitochondrial dysfunction and the ramifications of this dysfunction for muscle wasting and functional decline are warranted.

Mitochondrial dysfunction has been tightly associated with excess production of reactive oxygen species (ROS) [72]. While ROS generation is involved in muscle cellular signaling that supports cell homeostasis [72], chronically elevated ROS can initiate DNA damage, protein oxidation, and apoptosis [70, 74, 75]. To this end, substantial evidence points to increased ROS production in cachectic skeletal muscle [76–78]. The role for ROS to promote skeletal muscle dysfunction and atrophy is well established and has been reviewed extensively [79–85]. Although elevated ROS has been identified in wasting skeletal muscle, it has not yet been determined if ROS initiates muscle catabolism in cancer cachexia or is a consequence of the wasting process [82].

3.2. Mitochondrial Dynamics. Understanding skeletal muscle mitochondrial dynamics during cancer cachexia has become an extremely active area of investigation. While initial studies focused on describing changes to mitochondrial dynamics in cachectic muscle, recent research has begun to elucidate the drivers of disrupted mitochondrial dynamics in cachectic muscle and the ramifications this disruption has on muscle

mass loss and metabolic dysfunction [12, 13, 25]. The interconnected muscle mitochondrial network undergoes tightly regulated processes related to fusion and fission, which are coordinated to influence mitochondrial homeostasis [13, 86, 87]. The fusion of mitochondria induces extension of the mitochondrial network thought to increase energy efficiency and increase ATP production [20]. Conversely, the process of fission involves the fragmentation of mitochondria and segregates damaged areas of the mitochondrial network that may be dysfunctional, allowing for their removal [86–90]. Mitochondrial dysfunction can result from the disrupted coordination of fission and fusion processes; several preclinical models of cancer cachexia and cancer patients have demonstrated altered indices of mitochondrial fission and fusion [91–93].

Mitochondrial dynamics' processes have been extensively studied and characterized both in vivo and in vitro and have been previously reviewed [13, 90, 94, 95]. The fusion process is regulated by mitofusin 1 and 2 (MFN-1, MFN-2) and optic atrophy protein 1 (OPA1) [88, 95]. While these proteins are similar in structure, their functions are thought to be nonredundant. MFN-1 regulates GTP tethering whereas MFN-2 regulates the assembly of the fusion complexes [12, 13]. OPA-1 is expressed as several different isoforms and is necessary for the regulation of fusion GTP tethering in conjunction with MFN-1 [87]. The loss of mitochondrial fusion has detrimental effects in skeletal muscle shown by genetic knockout of MFN-1 and 2 resulting in muscle atrophy and reduced mitochondrial DNA (mtDNA) [96].

Circulating IL-6 and muscle STAT3 signaling have been linked to suppressed MFN-1 expression in cachectic muscle. Systemic IL-6 overexpression in *Apc^{Min/+}* suppressed MFN-1 expression, but was rescued by administration of an IL-6 receptor antibody [92]. Additionally, IL-6 administration to cultured myotubes increased STAT3 activation and suppressed MFN-2 in a dose-dependent manner [92]. Similarly, TNF- α was able to decrease myotube MFN-2 expression associated with elevated ROS and reduced ATP production [97].

Mitochondrial fission is necessary for skeletal muscle mitochondria maintenance and quality [13, 86, 89, 90, 98]. Mitochondrial fission machinery is controlled by the GTPase cytosolic dynamin-related protein 1 (DRP-1) which can translocate to the outer mitochondrial membrane and develop active fission sites [13, 86, 87]. DRP-1 can be regulated by phosphorylation and sumoylation by small ubiquitin-related modifiers (SUMOs) [13]. Fission protein 1 (FIS-1) is proposed to be required for mitochondrial division as it serves to recruit DRP-1 to the outer mitochondrial membrane [87]. Accelerated fission results in proapoptotic signals that lead to mitochondria isolation from the network and reduces its ATP efficiency [90]. Interestingly, accelerated mitochondrial fission is associated with AMPK activation, which can stimulate mitochondrial biogenesis in healthy muscle [86, 99]. However, while accelerated fission is often regarded as a sign of mitochondrial dysfunction in inflammatory diseases [12, 77, 89, 92], failure to undergo fission will result in mitochondrial dysfunction and muscle atrophy [86, 89, 92] (Figure 2).

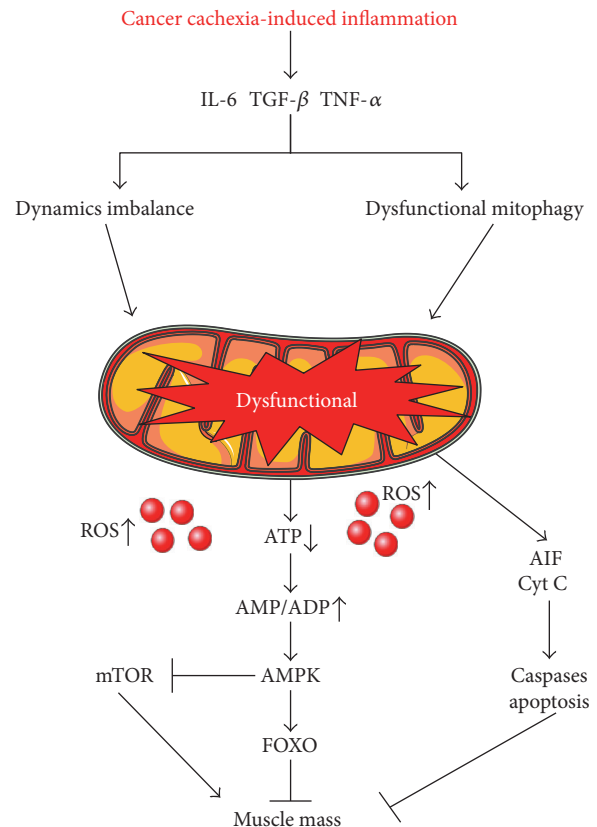


FIGURE 2: Mitochondrial dysfunction in skeletal muscle negatively regulates muscle mass. Elevated IL-6, TNF- α , and TGF- β during cancer cachexia disrupt mitochondrial homeostasis leading to dysfunction mitochondria. Dysfunctional mitochondria release aberrant amounts of reactive oxygen species (ROS) and decrease ATP production. This leads to chronic activation of AMPK to negatively regulate protein synthesis causing decreased muscle mass. The figure was made with Servier Medical Art (<http://www.servier.com/Powerpoint-image-bank>).

Although evidence suggests an important role, the direct effects of inflammation on mitochondrial fission continue to be established. Systemic IL-6 overexpression in *Apc^{Min/+}* mice had elevated FIS-1 protein levels prior to the onset of cachexia [92]. Interestingly, IL-6-induced muscle FIS-1 expression is not selective to muscle phenotype as it occurs equally in both highly oxidative and highly glycolytic fibers [77, 92]. While a direct link between TNF- α and skeletal muscle mitochondrial fission is not well established, the TNF- α induction of ROS provides intriguing rationale. Interestingly, overexpression of FIS-1 in healthy animals has been demonstrated to be proapoptotic and is tightly associated with accelerated production of ROS [86]. However, it is not well understood if elevated ROS production is causal or consequence of disrupted mitochondrial dynamics in cachectic muscle [100].

3.3. Mitophagy. Hyperactivation of cellular degradation pathways has become an established target of chronic inflammatory conditions [101, 102]. Autophagy in cachectic muscle has become widely investigated for the regulation of skeletal muscle mass loss and disrupted metabolism [38, 103, 104].

Autophagy is a highly conserved cellular process that contributes to the lysosomal degradation of proteins and organelles (including mitochondria) that are either dysfunctional, damaged, long lived, or misfolded [88, 105]. The process of autophagy consists of a small portion of the cytoplasm that includes organelles or proteins being sequestered by a phagophore to form an autophagosome. This autophagosome will then fuse with the lysosome to become an autolysosome which then degrades the cellular cargo contained within it. These processes require a family of proteins known as autophagy-related genes (Atgs) which are important in the signaling and regulation of autophagy [106–111]. Autophagy can be both a nonselective process (e.g., starvation) and a highly selective process that degrades specific organelles such as mitochondria which has been termed mitophagy [12, 106, 107]. The selectivity of this process can be determined by specific proteins, p62 and BCL2 interacting protein 3 (Bnip3), which have cargo-binding domains and LC3-interacting domains which are responsible for recruitment and binding of autophagosome proteins [13, 90, 112]. The autophagic removal of damaged and dysfunctional mitochondria, mitophagy, is critical for maintaining a healthy network of mitochondria. Failure of these processes can lead to an accumulation of damaged mitochondria which can negatively regulate metabolism and mass [13, 110, 113].

Increased lysosomal protease activity, indicative of accelerated autophagy flux, has been reported in cachectic muscle from tumor-bearing mice [113, 114]. Interestingly, circulating branched chain amino acids are elevated in cancer patients prior to weight loss, suggesting accelerated autophagy is an early event in cachexia development [115]. Tumor growth is associated with a reduced nutrient availability, and it has been suggested that tumor-derived factors can accelerate mitophagy [116]. Accelerated mitophagy has the potential to contribute to skeletal muscle mitochondrial dysfunction [92, 117, 118]. Skeletal muscle from cancer patients and preclinical models of cancer cachexia (*Apc^{Min/+}*, C26, and LLC) have demonstrated accelerated mitophagy indices [92, 101, 104, 119–121]. Muscle mitophagy can occur through an AMPK, FOXO, and mTORC1 signaling axis, which are established regulators of both muscle metabolism and mass; the cachectic environment also disrupts this signaling axis [110, 121, 122] (Figure 2). Tumor necrosis receptor factor 6 (TRAF6) is a potent inducer of mitophagy, and TRAF6 deletion can prevent cancer-induced muscle mass in tumor-bearing mice [123]. Interestingly, both Activin A and TWEAK have identified roles in the modulation of LC3, potentially indicating disrupted mitophagy [56, 67]. Recently, tumor-derived factors released into circulation were shown to induce mitophagy in skeletal muscle through IL-6-dependent signaling [124]. The autophagy inducing bioactivity of serum collected from gastrointestinal and lung cancer patients was significantly correlated to weight loss, but was normalized with the administration of an IL-6 receptor antibody [124]. Together, current evidence suggests that during cancer cachexia, tumor-secreted IL-6 has an important role in mitophagy regulation. Further, work is warranted to determine if disrupted mitophagy regulation is a viable therapeutic target for cancer-induced muscle wasting or if

mitophagy is being induced in cachectic muscle to correct other metabolic dysfunctions.

3.4. Mitochondrial Biogenesis. Muscle adaptation to increased and decreased use provides a clear demonstration that healthy skeletal muscle fiber's mitochondria content is plastic and reflects the fiber's energy requirements [13, 125–127]. However, chronic inflammation can create an environment that disrupts this regulation to incite the loss of muscle oxidative metabolic capacity [128–131]. Mitochondrial biogenesis is a critical process for maintaining the necessary mitochondria content to meet energy demands [13, 125, 127, 132]. The peroxisome-proliferator gamma-activated receptor (PGC-1) has been extensively examined as a critical regulator of muscle mitochondrial biogenesis. There are several PGC-1 isoforms, and each has significant but independent roles in oxidative metabolism. PGC-1 α regulates muscle protein synthesis through IGF-1 and myostatin signaling cascades [133, 134]. PGC-1 β can regulate myosin heavy-chain isoform expression, and increased expression induces an oxidative muscle phenotype [135]. PGC-1 α can induce nuclear response factors (NRF-1, NRF-2) and mitochondrial transcription factor A (Tfam) transcription, which regulate mitochondrial biogenesis [125–127, 136]. Moreover, PGC-1 α loss results in reduced muscle mitochondrial content and ATP production [137–139].

Increased PGC-1 α expression is protective against muscle atrophy in aging, decreased use, and inflammatory cytokine administration. However, the limited number of investigations in preclinical cancer cachexia models is equivocal [140–143]. While suppressed PGC-1 α expression is consistently reported in cachectic skeletal muscle [77, 92, 144], overexpression was not sufficient to prevent Lewis lung carcinoma- (LLC-) induced muscle wasting [145]. Interestingly, PGC-1 α overexpression could stimulate mitochondrial biogenesis in the cachectic muscle, indicating that the pathways to induce mitochondrial biogenesis were functional in the cachectic environment. Regulators of PGC-1 α activity are also major determinants of muscle metabolic capacity in both healthy and cachectic muscle [146]. AMPK, an energy stress sensor, regulates muscle oxidative metabolism through PGC-1 α -regulated biogenesis and ULK-dependent mitophagy [147–149]. In healthy muscle, activated AMPK can stimulate mitochondrial biogenesis and has been demonstrated as therapeutic in type II diabetes [149, 150]. Muscle AMPK is chronically activated in some preclinical cancer cachexia models, however, fails to induce mitochondrial biogenesis. Interestingly, chronic AMPK activation in cachectic muscle may have a role in the suppression of muscle protein synthesis [151]. Circulating IL-6 has been associated with muscle AMPK activation in the cachectic *Apc^{Min/+}* mouse. IL-6 overexpression in tumor-bearing mice can activate AMPK and reduce PGC-1 α expression, whereas IL-6 receptor antibody administration attenuates cancer-induced AMPK activation [151]. Although in vivo evidence for the direct effects of IL-6 signaling on cachectic muscle AMPK activation is lacking, IL-6 administration to skeletal muscle myotubes can directly activate AMPK [151]. Further research is needed to understand the disrupted feedback caused by the cachectic

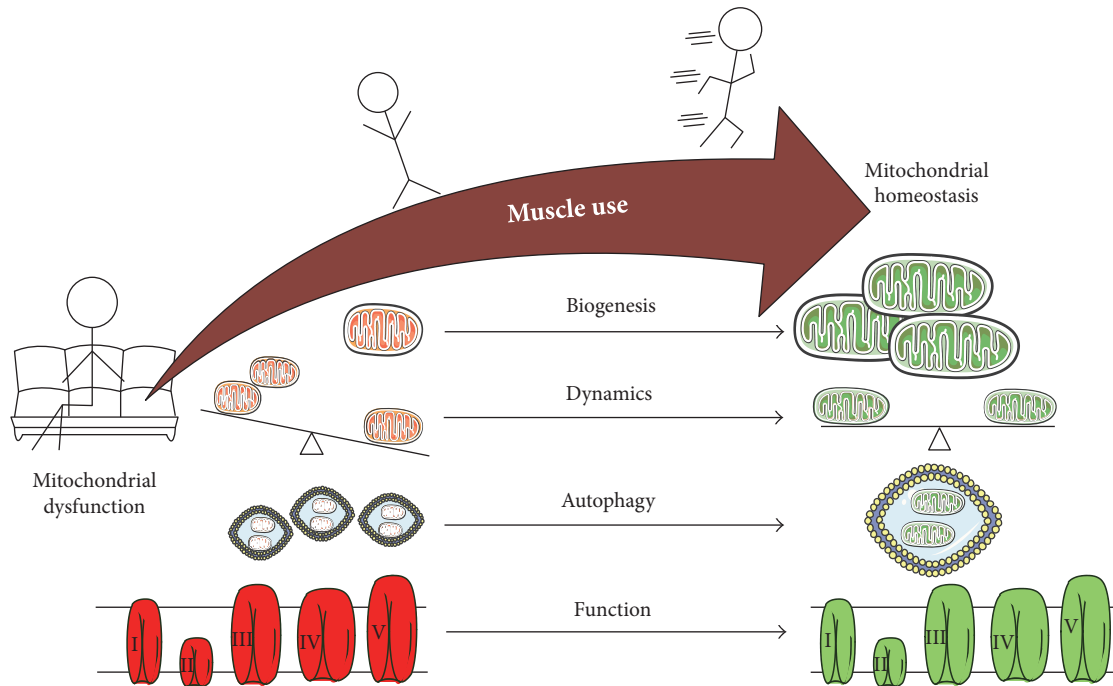


FIGURE 3: Increased muscle use improves skeletal muscle mitochondrial homeostasis in healthy and cachectic conditions. Sedentary behavior or muscle disuse is associated with decreased mitochondrial biogenesis, improper balance of mitochondrial dynamics, dysregulation of autophagy, and mitochondrial dysfunction. Increasing muscle use by reducing sedentary behavior or exercise will increase mitochondrial biogenesis, regulate mitochondrial dynamics, improve autophagic flux, and improve mitochondrial function and ATP efficiency. Overall increased muscle use will lead to skeletal muscle mitochondrial and metabolic homeostasis. The figure was made with Servier Medical Art (<http://www.servier.com/Powerpoint-image-bank>).

environment that uncouples AMPK signaling from mitochondrial biogenesis.

Activin A and myostatin have the potential to also disrupt mitochondrial biogenesis. Ge et al. demonstrated that the lack of Smad3 signaling resulted in decreased NRF and Tfam activation [152]. However, Smad3 activation via the TGF- β super family in cachectic skeletal muscle remains to be determined. Interestingly, both Activin A and TWEAK were able to disrupt mitochondrial biogenesis by reducing PGC1- α [67, 153]. Further research is needed to establish if this mitochondrial biogenesis suppression is a therapeutic target for either preventing muscle mass loss or improving metabolic health during cancer cachexia.

4. Exercise Countermeasures to Cancer-Induced Mitochondrial Dysfunction

The capacity to regenerate from injury and adapt to altered use are defining features of skeletal muscle that also provide optimism for therapeutic interventions for cachectic muscle. Exercise has shown to be beneficial in diabetes, COPD, and CHF and continues to show beneficial results in cancer patients as well [154, 155]. Activity level can dramatically impact skeletal muscle mass and metabolism [88, 156]. Increased muscle activity can also induce a more oxidative muscle phenotype by increasing mitochondria content and function [95, 157–159]. Increased muscle use can positively impact muscle mass, and the extent of this change is

dependent on the exercise type, intensity, duration, and frequency [5, 160]. The metabolic plasticity of muscle is reinforced by the dramatic alterations that occur to skeletal muscle after an acute bout of exercise [88, 156, 157]. Increasing the muscle metabolic demand with exercise can stimulate mitochondrial biogenesis to increase mitochondrial content and function [138, 139, 161]. Cachectic muscle from tumor-bearing mice subjected to an acute bout of low frequency electrical stimulation maintains the capacity to activate genes responsible for mitochondrial biogenesis, PGC-1 α , NRF-1, and Tfam [144]. However, cachectic muscle had deficits in the acute activation of protein expression after a single bout of stimulated concentric contractions, which could be rescued by systemic inhibition of inflammatory signaling [144].

Decreased muscle use, either by unloading or extreme sedentary behavior, can induce a shift to a more glycolytic phenotype, coinciding with decreased mitochondrial content and function and muscle atrophy [155]. Cancer patients commonly suffer from excessive fatigue prior to and during treatments [5, 6, 162]. This fatigue is accompanied by a dramatic decrease in physical activity and the ability to perform activities of daily living (ADLs) [5, 163–165]. Preclinical cancer models also have shown that cachectic mice undergo limited volitional activity [166, 167]. However, minimizing sedentary time and using alternative muscle contraction methods may serve as a first line of action to attenuate cachexia-induced decrements in muscle mitochondria

[168–171] (Figure 3). IL-6 overexpression in tumor-bearing mice was not able to induce muscle mass loss and metabolic changes when they were regularly exercised on a treadmill [172]. It is interesting to speculate if disuse alters the muscle sensitivity to the cachectic environment, causing a more rapid decline in muscle metabolic function and mass. Conversely, research is needed to determine if muscle contraction or exercise serves to desensitize the muscle to the cachectic environment.

Exercise also regulates mitochondrial dynamics, increasing both fission and fusion. This is thought to aid in mitochondrial turnover and improve efficiency (Figure 3). Similarly, autophagy flux increases after an acute bout of exercise. IL-6 overexpression in exercising tumor-bearing mice was resistant to muscle mass loss and metabolic changes [172]. Cachectic muscle in tumor-bearing mice also retains the capacity to respond to repeated bouts of stimulated eccentric contractions. Cachectic muscle in *Apc^{Min/+}* mice undergoing 7 bouts of eccentric contractions increased muscle succinate dehydrogenase activity and decreased AMPK signaling [173]. Exercise training is implicated as a potential therapeutic to either prevent or reverse muscle wasting. It is evident from preclinical studies that cachectic muscle maintains the ability to robustly respond to an acute bout of exercise or contraction. Further work is needed to determine if repeated bouts of exercise can confer the metabolic health benefits of exercise after the development of cancer cachexia [139, 174].

Physical activity and contraction has been established as a potent regulator of mitophagy and may possess the potential to correct or attenuate dysfunction mitophagy processes in cachectic muscle [88, 105, 175–179]. In C26 tumor-implanted mice, voluntary wheel running attenuated cachexia-induced p62 and LC3 II/I accumulation indicating improved mitophagy [179]. Additionally, AMPK activation via AICAR suppressed p62 accumulation through promotion of mitophagy and accelerating the turnover of p62 accumulation in cachectic muscle [179]. While there is growing evidence for mitophagic processes in the regulation of cancer cachexia, additional studies are warranted to establish a direct role for inflammation in the regulation of these processes and to clearly examine mitophagy flux in vivo. Additionally, the role of exercise and/or muscle contraction in the regulation of mitophagy in diseased or chronically inflamed muscle may prove to be a powerful therapeutic for the restoration of mitophagic balance in cachectic muscle. Clearly, further research is warranted to examine the complex interaction between cancer-induced inflammation, muscle contraction, and muscle disuse for maintenance or improvement of cachectic muscle oxidative metabolism.

5. Conclusions

Disrupted mitochondrial homeostasis contributes to the loss of functional capacity in cancer patients and can negatively impact the quality of life and survival. Skeletal muscle mitochondria not only regulate oxidative metabolism but also proteostasis and muscle mass maintenance. The role of mitochondria in skeletal muscle wasting during cancer cachexia

has emerged as novel investigative target in cachexia studies. There is a clear relationship between inflammation and mitochondrial dysfunction related to dynamics, mitophagy, and biogenesis. While the alterations to mitochondrial dynamics during cachexia appear evident, a more mechanistic approach is necessary to understand regulatory mechanisms and functional outcomes. A growing body of research suggests an important therapeutic strategy involving the reduction of muscle disuse and increasing muscle contractile activity for the maintenance of skeletal muscle metabolic health, even in the presence of a cachectic environment. To this end, analysis of functional and metabolic outcomes, muscle strength, and fatigability are necessary to understand the totality of the cachectic condition.

Conflicts of Interest

The authors declare that there is no conflict of interest regarding the publication of this paper.

Acknowledgments

This work was supported by the National Institutes of Health, grant no. R01-CA121249 from the National Cancer Institute (JAC) and grant no. P20 RR-017698 from the National Center for Research (JAC).

References

- [1] J. M. Argiles, S. Busquets, M. Toledo, and F. J. López-Soriano, "The role of cytokines in cancer cachexia," *Current Opinion in Supportive and Palliative Care*, vol. 3, no. 4, pp. 263–268, 2009.
- [2] K. C. Fearon, "Cancer cachexia: developing multimodal therapy for a multidimensional problem," *European Journal of Cancer*, vol. 44, no. 8, pp. 1124–1132, 2008.
- [3] W. J. Evans, J. E. Morley, J. Argilés et al., "Cachexia: a new definition," *Clinical Nutrition*, vol. 27, no. 6, pp. 793–799, 2008.
- [4] M. J. Tisdale, "Cachexia in cancer patients," *Nature Reviews. Cancer*, vol. 2, no. 11, pp. 862–871, 2002.
- [5] S. al-Majid and D. O. McCarthy, "Cancer-induced fatigue and skeletal muscle wasting: the role of exercise," *Biological Research for Nursing*, vol. 2, no. 3, pp. 186–197, 2001.
- [6] P. Stone, J. Hardy, K. Broadley, A. J. Tookman, A. Kurowska, and R. A'Hern, "Fatigue in advanced cancer: a prospective controlled cross-sectional study," *British Journal of Cancer*, vol. 79, no. 9-10, pp. 1479–1486, 1999.
- [7] P. O'Gorman, D. C. McMillan, and C. S. McArdle, "Longitudinal study of weight, appetite, performance status, and inflammation in advanced gastrointestinal cancer," *Nutrition and Cancer*, vol. 35, no. 2, pp. 127–129, 1999.
- [8] S. Haehlingvon and S. D. Anker, "Prevalence, incidence and clinical impact of cachexia: facts and numbers-update 2014," *Journal of Cachexia, Sarcopenia and Muscle*, vol. 5, no. 4, pp. 261–263, 2014.
- [9] J. F. Christensen, L. W. Jones, J. L. Andersen, G. Daugaard, M. Rorth, and P. Hojman, "Muscle dysfunction in cancer patients," *Annals of Oncology*, vol. 25, no. 5, pp. 947–958, 2014.

- [10] M. L. Winningham, L. M. Nail, M. B. Burke et al., "Fatigue and the cancer experience: the state of the knowledge," *Oncology Nursing Forum*, vol. 21, no. 1, pp. 23–36, 1994.
- [11] R. R. Wolfe, "The underappreciated role of muscle in health and disease," *The American Journal of Clinical Nutrition*, vol. 84, no. 3, pp. 475–482, 2006.
- [12] J. A. Carson, J. P. Hardee, and B. N. VanderVeen, "The emerging role of skeletal muscle oxidative metabolism as a biological target and cellular regulator of cancer-induced muscle wasting," *Seminars in Cell & Developmental Biology*, vol. 54, pp. 53–67, 2016.
- [13] V. Romanello and M. Sandri, "Mitochondrial quality control and muscle mass maintenance," *Frontiers in Physiology*, vol. 6, p. 422, 2015.
- [14] C. M. Kummitha, S. C. Kalhan, G. M. Saidel, and N. Lai, "Relating tissue/organ energy expenditure to metabolic fluxes in mouse and human: experimental data integrated with mathematical modeling," *Physiological Reports*, vol. 2, no. 9, 2014.
- [15] J. M. Argiles, N. Campos, J. M. Lopez-Pedrosa, R. Rueda, and L. Rodriguez-Mañas, "Skeletal muscle regulates metabolism via interorgan crosstalk: roles in health and disease," *Journal of the American Medical Directors Association*, vol. 17, no. 9, pp. 789–796, 2016.
- [16] D. F. Wilson, "Energy metabolism in muscle approaching maximal rates of oxygen utilization," *Medicine and Science in Sports and Exercise*, vol. 27, no. 1, pp. 54–59, 1995.
- [17] R. I. Close, "Dynamic properties of mammalian skeletal muscles," *Physiological Reviews*, vol. 52, no. 1, pp. 129–197, 1972.
- [18] P. Deng and C. M. Haynes, "Mitochondrial dysfunction in cancer: potential roles of ATF5 and the mitochondrial UPR," *Seminars in Cancer Biology*, 2017.
- [19] K. Prasai, "Regulation of mitochondrial structure and function by protein import: a current review," *Pathophysiology*, 2017.
- [20] M. Bordi, F. Nazio, and S. Campello, "The close interconnection between mitochondrial dynamics and mitophagy in cancer," *Frontiers in Oncology*, vol. 7, p. 81, 2017.
- [21] M. L. Boland, A. H. Chourasia, and K. F. Macleod, "Mitochondrial dysfunction in cancer," *Frontiers in Oncology*, vol. 3, p. 292, 2013.
- [22] A. Picca, A. M. S. Lezza, C. Leeuwenburgh et al., "Fueling inflamm-aging through mitochondrial dysfunction: mechanisms and molecular targets," *International Journal of Molecular Sciences*, vol. 18, no. 5, 2017.
- [23] R. Thibault, S. Chanséaume, K. Azarnoush et al., "Mitochondrial protein synthesis is increased in oxidative skeletal muscles of rats with cardiac cachexia," *Nutrition Research*, vol. 34, no. 3, pp. 250–257, 2014.
- [24] C. M. Julienne, J. F. Dumas, C. Goupille et al., "Cancer cachexia is associated with a decrease in skeletal muscle mitochondrial oxidative capacities without alteration of ATP production efficiency," *Journal of Cachexia, Sarcopenia and Muscle*, vol. 3, pp. 265–275, 2012.
- [25] J. M. Argiles, F. J. Lopez-Soriano, and S. Busquets, "Muscle wasting in cancer: the role of mitochondria," *Current Opinion in Clinical Nutrition and Metabolic Care*, vol. 18, no. 3, pp. 221–225, 2015.
- [26] R. Vitorino, D. Moreira-Goncalves, and R. Ferreira, "Mitochondrial plasticity in cancer-related muscle wasting: potential approaches for its management," *Current Opinion in Clinical Nutrition and Metabolic Care*, vol. 18, no. 3, pp. 226–233, 2015.
- [27] V. Adams, S. D. Anker, and G. Schuler, "Muscle metabolism and exercise capacity in cachexia," *Current Pharmaceutical Design*, vol. 17, no. 35, pp. 3838–3845, 2011.
- [28] B. M. Roberts, G. S. Frye, B. Ahn, L. F. Ferreira, and A. R. Judge, "Cancer cachexia decreases specific force and accelerates fatigue in limb muscle," *Biochemical and Biophysical Research Communications*, vol. 435, no. 3, pp. 488–492, 2013.
- [29] J. A. Carson and K. A. Baltgalvis, "Interleukin 6 as a key regulator of muscle mass during cachexia," *Exercise and Sport Sciences Reviews*, vol. 38, no. 4, pp. 168–176, 2010.
- [30] J. L. Chen, T. D. Colgan, K. L. Walton, P. Gregorevic, and C. A. Harrison, "The TGF-beta signalling network in muscle development, adaptation and disease," *Advances in Experimental Medicine and Biology*, vol. 900, pp. 97–131, 2016.
- [31] A. Loumaye, M. Barysyde, M. Nachit et al., "Role of Activin A and myostatin in human cancer cachexia," *The Journal of Clinical Endocrinology and Metabolism*, vol. 100, no. 5, pp. 2030–2038, 2015.
- [32] T. C. Mueller, J. Bachmann, O. Prokopchuk, H. Friess, and M. E. Martignoni, "Molecular pathways leading to loss of skeletal muscle mass in cancer cachexia—can findings from animal models be translated to humans?," *BMC Cancer*, vol. 16, p. 75, 2016.
- [33] J. K. Onesti and D. C. Guttridge, "Inflammation based regulation of cancer cachexia," *BioMed Research International*, vol. 2014, Article ID 168407, 7 pages, 2014.
- [34] H. J. Patel and B. M. Patel, "TNF-alpha and cancer cachexia: molecular insights and clinical implications," *Life Sciences*, vol. 170, pp. 56–63, 2017.
- [35] M. Pal, M. A. Febbraio, and M. Whitham, "From cytokine to myokine: the emerging role of interleukin-6 in metabolic regulation," *Immunology and Cell Biology*, vol. 92, no. 4, pp. 331–339, 2014.
- [36] M. B. Reid and Y. P. Li, "Tumor necrosis factor-alpha and muscle wasting: a cellular perspective," *Respiratory Research*, vol. 2, no. 5, pp. 269–272, 2001.
- [37] J. Rodriguez, B. Vernus, I. Chelch et al., "Myostatin and the skeletal muscle atrophy and hypertrophy signaling pathways," *Cellular and Molecular Life Sciences*, vol. 71, no. 22, pp. 4361–4371, 2014.
- [38] M. Sandri, "Signaling in muscle atrophy and hypertrophy," *Physiology (Bethesda)*, vol. 23, pp. 160–170, 2008.
- [39] J. E. Belizario, C. C. Fontes-Oliveira, J. P. Borges, J. A. Kashiabara, and E. Vannier, "Skeletal muscle wasting and renewal: a pivotal role of myokine IL-6," *Spring*, vol. 5, p. 619, 2016.
- [40] T. R. Flint, T. Janowitz, C. M. Connell et al., "Tumor-induced IL-6 reprograms host metabolism to suppress anti-tumor immunity," *Cell Metabolism*, vol. 24, no. 5, pp. 672–684, 2016.
- [41] A. Bonetto, J. K. Kays, V. A. Parker et al., "Differential bone loss in mouse models of colon cancer cachexia," *Frontiers in Physiology*, vol. 7, p. 679, 2016.
- [42] A. A. Narsale and J. A. Carson, "Role of interleukin-6 in cachexia: therapeutic implications," *Current Opinion in Supportive and Palliative Care*, vol. 8, no. 4, pp. 321–327, 2014.

- [43] B. K. Pedersen, "Muscular interleukin-6 and its role as an energy sensor," *Medicine and Science in Sports and Exercise*, vol. 44, no. 3, pp. 392–396, 2012.
- [44] N. Fortunati, R. Manti, N. Birocco et al., "Pro-inflammatory cytokines and oxidative stress/antioxidant parameters characterize the bio-humoral profile of early cachexia in lung cancer patients," *Oncology Reports*, vol. 18, no. 6, pp. 1521–1527, 2007.
- [45] K. A. Baltgalvis, F. G. Berger, M. M. Peña, J. M. Davis, J. P. White, and J. A. Carson, "Muscle wasting and interleukin-6-induced atrogen-1 expression in the cachectic *Apc^{Min/+}* mouse," *Pflügers Archiv*, vol. 457, no. 5, pp. 989–1001, 2009.
- [46] D. N. Seto, S. C. Kandarian, and R. W. Jackman, "A key role for leukemia inhibitory factor in C26 cancer cachexia," *The Journal of Biological Chemistry*, vol. 290, no. 32, pp. 19976–19986, 2015.
- [47] M. J. Puppa, S. Gao, A. A. Narsale, and J. A. Carson, "Skeletal muscle glycoprotein 130's role in Lewis lung carcinoma-induced cachexia," *The FASEB Journal*, vol. 28, no. 2, pp. 998–1009, 2014.
- [48] L. Cron, T. Allen, and M. A. Febbraio, "The role of gp130 receptor cytokines in the regulation of metabolic homeostasis," *The Journal of Experimental Biology*, vol. 219, Part 2, pp. 259–265, 2016.
- [49] A. Bonetto, T. Aydogdu, X. Jin et al., "JAK/STAT3 pathway inhibition blocks skeletal muscle wasting downstream of IL-6 and in experimental cancer cachexia," *American Journal of Physiology. Endocrinology and Metabolism*, vol. 303, no. 3, pp. E410–E421, 2012.
- [50] A. Bonetto, T. Aydogdu, N. Kunzevitzky et al., "STAT3 activation in skeletal muscle links muscle wasting and the acute phase response in cancer cachexia," *PloS One*, vol. 6, no. 7, article e22538, 2011.
- [51] A. Miller, L. McLeod, S. Alhayani et al., "Blockade of the IL-6 trans-signalling/STAT3 axis suppresses cachexia in Kras-induced lung adenocarcinoma," *Oncogene*, vol. 36, no. 21, pp. 3059–3066, 2017.
- [52] J. P. White, J. W. Baynes, S. L. Welle et al., "The regulation of skeletal muscle protein turnover during the progression of cancer cachexia in the *Apc^{min/+}* mouse," *PLoS One*, vol. 6, no. 9, article e24650, 2011.
- [53] A. Bonetto, T. Aydogdu, X. Jin et al., "JAK/STAT3 pathway inhibition blocks skeletal muscle wasting downstream of IL-6 and in experimental cancer cachexia," *American Journal of Physiology Endocrinology and Metabolism*, vol. 303, no. 3, pp. E410–E421, 2012.
- [54] M. B. Reid, J. Lannergren, and H. Westerblad, "Respiratory and limb muscle weakness induced by tumor necrosis factor-alpha: involvement of muscle myofilaments," *American Journal of Respiratory and Critical Care Medicine*, vol. 166, no. 4, pp. 479–484, 2002.
- [55] A. H. Remels, H. R. Gosker, P. Schrauwen et al., "TNF-alpha impairs regulation of muscle oxidative phenotype: implications for cachexia?," *The FASEB Journal*, vol. 24, no. 12, pp. 5052–5062, 2010.
- [56] A. Kumar, S. Bhatnagar, and P. K. Paul, "TWEAK and TRAF6 regulate skeletal muscle atrophy," *Current Opinion in Clinical Nutrition and Metabolic Care*, vol. 15, no. 3, pp. 233–239, 2012.
- [57] M. J. Tisdale, "The ubiquitin-proteasome pathway as a therapeutic target for muscle wasting," *The Journal of Supportive Oncology*, vol. 3, no. 3, pp. 209–217, 2005.
- [58] J. S. Patton, P. M. Peters, J. McCabe et al., "Development of partial tolerance to the gastrointestinal effects of high doses of recombinant tumor necrosis factor-alpha in rodents," *The Journal of Clinical Investigation*, vol. 80, no. 6, pp. 1587–1596, 1987.
- [59] M. C. Stovroff, D. L. Fraker, J. A. Swedenborg, and J. A. Norton, "Cachectin/tumor necrosis factor: a possible mediator of cancer anorexia in the rat," *Cancer Research*, vol. 48, no. 16, pp. 4567–4572, 1988.
- [60] I. L. Bernstein, E. M. Taylor, and K. L. Bentson, "TNF-induced anorexia and learned food aversions are attenuated by area postrema lesions," *The American Journal of Physiology*, vol. 260, 5 Part 2, pp. R906–R910, 1991.
- [61] H. D. Mulligan, S. M. Mahony, J. A. Ross, and M. J. Tisdale, "Weight loss in a murine cachexia model is not associated with the cytokines tumour necrosis factor-alpha or interleukin-6," *Cancer Letters*, vol. 65, no. 3, pp. 239–243, 1992.
- [62] T. Yoshida, A. M. Tabony, S. Galvez et al., "Molecular mechanisms and signaling pathways of angiotensin II-induced muscle wasting: potential therapeutic targets for cardiac cachexia," *The International Journal of Biochemistry & Cell Biology*, vol. 45, no. 10, pp. 2322–2332, 2013.
- [63] M. E. Benny Klimek, T. Aydogdu, M. J. Link, M. Pons, L. G. Koniaris, and T. A. Zimmers, "Acute inhibition of myostatin-family proteins preserves skeletal muscle in mouse models of cancer cachexia," *Biochemical and Biophysical Research Communications*, vol. 391, no. 3, pp. 1548–1554, 2010.
- [64] K. T. Murphy, A. Chee, B. G. Gleeson et al., "Antibody-directed myostatin inhibition enhances muscle mass and function in tumor-bearing mice," *American Journal of Physiology. Regulatory, Integrative and Comparative Physiology*, vol. 301, no. 3, pp. R716–R726, 2011.
- [65] T. A. Zimmers, M. V. Davies, L. G. Koniaris et al., "Induction of cachexia in mice by systemically administered myostatin," *Science*, vol. 296, no. 5572, pp. 1486–1488, 2002.
- [66] A. I. Padrao, D. Moreira-Gonçalves, P. A. Oliveira et al., "Endurance training prevents TWEAK but not myostatin-mediated cardiac remodelling in cancer cachexia," *Archives of Biochemistry and Biophysics*, vol. 567, pp. 13–21, 2015.
- [67] J. L. Chen, K. L. Walton, H. Qian et al., "Differential effects of IL6 and Activin A in the development of cancer-associated cachexia," *Cancer Research*, vol. 76, no. 18, pp. 5372–5382, 2016.
- [68] C. Constantinou, C. C. Fontes de Oliveira, D. Mintzopoulos et al., "Nuclear magnetic resonance in conjunction with functional genomics suggests mitochondrial dysfunction in a murine model of cancer cachexia," *International Journal of Molecular Medicine*, vol. 27, no. 1, pp. 15–24, 2011.
- [69] D. Antunes, A. I. Padrão, E. Maciel et al., "Molecular insights into mitochondrial dysfunction in cancer-related muscle wasting," *Biochimica et Biophysica Acta-Molecular and Cell Biology of Lipids*, vol. 1841, no. 6, pp. 896–905, 2014.
- [70] C. Femoselle, E. García-Arumí, E. Puig-Vilanova et al., "Mitochondrial dysfunction and therapeutic approaches in respiratory and limb muscles of cancer cachectic mice," *Experimental Physiology*, vol. 98, no. 9, pp. 1349–1365, 2013.
- [71] A. I. Padrao, P. Oliveira, R. Vitorino et al., "Bladder cancer-induced skeletal muscle wasting: disclosing the role of mitochondria plasticity," *The International Journal of Biochemistry & Cell Biology*, vol. 45, no. 7, pp. 1399–1409, 2013.

- [72] J. B. McLean, J. S. Moylan, and F. H. Andrade, "Mitochondria dysfunction in lung cancer-induced muscle wasting in C2C12 myotubes," *Frontiers in Physiology*, vol. 5, p. 503, 2014.
- [73] J. Wegrzyn, R. Potla, Y. J. Chwae et al., "Function of mitochondrial Stat3 in cellular respiration," *Science*, vol. 323, no. 5915, pp. 793–797, 2009.
- [74] C. C. Fontes-Oliveira, S. Busquets, M. Toledo et al., "Mitochondrial and sarcoplasmic reticulum abnormalities in cancer cachexia: altered energetic efficiency?," *Biochimica et Biophysica Acta*, vol. 1830, no. 3, pp. 2770–2778, 2013.
- [75] A. A. Tzika, C. C. Fontes-Oliveira, A. A. Shestov et al., "Skeletal muscle mitochondrial uncoupling in a murine cancer cachexia model," *International Journal of Oncology*, vol. 43, no. 3, pp. 886–894, 2013.
- [76] Z. Yu, P. Li, M. Zhang, M. Hannink, J. S. Stamler, and Z. Yan, "Fiber type-specific nitric oxide protects oxidative myofibers against cachectic stimuli," *PLoS One*, vol. 3, no. 5, article e2086, 2008.
- [77] J. P. White, K. A. Baltgalvis, M. J. Puppa, S. Sato, J. W. Baynes, and J. A. Carson, "Muscle oxidative capacity during IL-6-dependent cancer cachexia," *American Journal of Physiology. Regulatory, Integrative and Comparative Physiology*, vol. 300, no. 2, pp. R201–R211, 2011.
- [78] E. Barreiro, B. Puente de la, S. Busquets, F. J. López-Soriano, J. Gea, and J. M. Argilés, "Both oxidative and nitrosative stress are associated with muscle wasting in tumour-bearing rats," *FEBS Letters*, vol. 579, no. 7, pp. 1646–1652, 2005.
- [79] Y. P. Li, Y. Chen, A. S. Li, and M. B. Reid, "Hydrogen peroxide stimulates ubiquitin-conjugating activity and expression of genes for specific E2 and E3 proteins in skeletal muscle myotubes," *American Journal of Physiology. Cell Physiology*, vol. 285, no. 4, pp. C806–C812, 2003.
- [80] F. L. Muller, W. Song, Y. C. Jang et al., "Denervation-induced skeletal muscle atrophy is associated with increased mitochondrial ROS production," *American Journal of Physiology. Regulatory, Integrative and Comparative Physiology*, vol. 293, no. 3, pp. R1159–R1168, 2007.
- [81] D. A. Hood, G. Ugucioni, A. Vainshtein, and D. D'souza, "Mechanisms of exercise-induced mitochondrial biogenesis in skeletal muscle: implications for health and disease," *Comprehensive Physiology*, vol. 1, no. 3, pp. 1119–1134, 2011.
- [82] S. K. Powers, A. J. Smuder, and A. R. Judge, "Oxidative stress and disuse muscle atrophy: cause or consequence?," *Current Opinion in Clinical Nutrition and Metabolic Care*, vol. 15, no. 3, pp. 240–245, 2012.
- [83] S. K. Powers, E. E. Talbert, and P. J. Adhihetty, "Reactive oxygen and nitrogen species as intracellular signals in skeletal muscle," *The Journal of Physiology*, vol. 589, Part 9, pp. 2129–2138, 2011.
- [84] S. K. Powers, M. P. Wiggs, J. A. Duarte, A. M. Zergeroglu, and H. A. Demirel, "Mitochondrial signaling contributes to disuse muscle atrophy," *American Journal of Physiology Endocrinology and Metabolism*, vol. 303, no. 1, pp. E31–E39, 2012.
- [85] L. F. Ferreira and M. B. Reid, "Muscle-derived ROS and thiol regulation in muscle fatigue," *Journal of Applied Physiology*, vol. 104, no. 3, pp. 853–860, 2008.
- [86] V. Romanello, E. Guadagnin, L. Gomes et al., "Mitochondrial fission and remodelling contributes to muscle atrophy," *The EMBO Journal*, vol. 29, no. 10, pp. 1774–1785, 2010.
- [87] S. Iqbal and D. A. Hood, "The role of mitochondrial fusion and fission in skeletal muscle function and dysfunction," *Frontiers in Bioscience (Landmark Edition)*, vol. 20, pp. 157–172, 2015.
- [88] Z. Yan, V. A. Lira, and N. P. Greene, "Exercise training-induced regulation of mitochondrial quality," *Exercise and Sport Sciences Reviews*, vol. 40, no. 3, pp. 159–164, 2012.
- [89] S. Wu, F. Zhou, Z. Zhang, and D. Xing, "Mitochondrial oxidative stress causes mitochondrial fragmentation via differential modulation of mitochondrial fission-fusion proteins," *The FEBS Journal*, vol. 278, no. 6, pp. 941–954, 2011.
- [90] R. J. Youle and A. M. v. d. Blik, "Mitochondrial fission, fusion, and stress," *Science*, vol. 337, no. 6098, pp. 1062–1065, 2012.
- [91] E. Marzetti, M. Lorenzi, F. Landi et al., "Altered mitochondrial quality control signaling in muscle of old gastric cancer patients with cachexia," *Experimental Gerontology*, vol. 87, Part A, pp. 92–99, 2017.
- [92] J. P. White, M. J. Puppa, S. Sato et al., "IL-6 regulation on skeletal muscle mitochondrial remodeling during cancer cachexia in the *Apc^{Min/+}* mouse," *Skeletal Muscle*, vol. 2, p. 14, 2012.
- [93] C. Guido, D. Whitaker-Menezes, Z. Lin et al., "Mitochondrial fission induces glycolytic reprogramming in cancer-associated myofibroblasts, driving stromal lactate production, and early tumor growth," *Oncotarget*, vol. 3, no. 8, pp. 798–810, 2012.
- [94] S. Iqbal, O. Ostojic, K. Singh, A. M. Joseph, and D. A. Hood, "Expression of mitochondrial fission and fusion regulatory proteins in skeletal muscle during chronic use and disuse," *Muscle & Nerve*, vol. 48, no. 6, pp. 963–970, 2013.
- [95] J. C. Drake, R. J. Wilson, and Z. Yan, "Molecular mechanisms for mitochondrial adaptation to exercise training in skeletal muscle," *The FASEB Journal*, vol. 30, no. 1, pp. 13–22, 2016.
- [96] J. Y. Lee, M. Kapur, M. Li et al., "MFN1 deacetylation activates adaptive mitochondrial fusion and protects metabolically challenged mitochondria," *Journal of Cell Science*, vol. 127, Part 22, pp. 4954–4963, 2014.
- [97] Y. Zhang, L. Yang, Y. F. Gao et al., "MicroRNA-106b induces mitochondrial dysfunction and insulin resistance in C2C12 myotubes by targeting mitofusin-2," *Molecular and Cellular Endocrinology*, vol. 381, no. 1–2, pp. 230–240, 2013.
- [98] H. F. Jheng, P. J. Tsai, S. M. Guo et al., "Mitochondrial fission contributes to mitochondrial dysfunction and insulin resistance in skeletal muscle," *Molecular and Cellular Biology*, vol. 32, no. 2, pp. 309–319, 2012.
- [99] K. Marcinko and G. R. Steinberg, "The role of AMPK in controlling metabolism and mitochondrial biogenesis during exercise," *Experimental Physiology*, vol. 99, no. 12, pp. 1581–1585, 2014.
- [100] T. Hennen, C. Richter, and E. Peterhans, "Tumour necrosis factor- α induces superoxide anion generation in mitochondria of L929 cells," *The Biochemical Journal*, vol. 289, Part 2, pp. 587–592, 1993.
- [101] J. M. McClung, A. R. Judge, S. K. Powers, and Z. Yan, "p38 MAPK links oxidative stress to autophagy-related gene expression in cachectic muscle wasting," *American Journal of Physiology. Cell Physiology*, vol. 298, no. 3, pp. C542–C549, 2010.

- [102] E. Puig-Vilanova, D. A. Rodriguez, J. Lloreta et al., "Oxidative stress, redox signaling pathways, and autophagy in cachectic muscles of male patients with advanced COPD and lung cancer," *Free Radical Biology and Medicine*, vol. 79, pp. 91–108, 2015.
- [103] Y. Luo, J. Yoneda, H. Ohmori et al., "Cancer usurps skeletal muscle as an energy repository," *Cancer Research*, vol. 74, no. 1, pp. 330–340, 2014.
- [104] E. E. Talbert, G. A. Metzger, W. A. He, and D. C. Guttridge, "Modeling human cancer cachexia in colon 26 tumor-bearing adult mice," *Journal of Cachexia, Sarcopenia and Muscle*, vol. 5, no. 4, pp. 321–328, 2014.
- [105] V. A. Lira, M. Okutsu, M. Zhang et al., "Autophagy is required for exercise training-induced skeletal muscle adaptation and improvement of physical performance," *FASEB Journal*, vol. 27, no. 10, pp. 4184–4193, 2013.
- [106] E. J. Jokl and G. Blanco, "Disrupted autophagy undermines skeletal muscle adaptation and integrity," *Mammalian Genome*, vol. 27, no. 11–12, pp. 525–537, 2016.
- [107] N. Kimura, T. Kumamoto, Y. Kawamura et al., "Expression of autophagy-associated genes in skeletal muscle: an experimental model of chloroquine-induced myopathy," *Pathobiology*, vol. 74, no. 3, pp. 169–176, 2007.
- [108] A. S. Nichenko, W. M. Southern, M. Atuan et al., "Mitochondrial maintenance via autophagy contributes to functional skeletal muscle regeneration and remodeling," *American Journal of Physiology Cell Physiology*, vol. 311, no. 2, pp. C190–C200, 2016.
- [109] G. G. Rodney, R. Pal, and R. Abo-Zahrah, "Redox regulation of autophagy in skeletal muscle," *Free Radical Biology and Medicine*, vol. 98, pp. 103–112, 2016.
- [110] M. Sandri, "Autophagy in skeletal muscle," *FEBS Letters*, vol. 584, no. 7, pp. 1411–1416, 2010.
- [111] E. Masiero, L. Agatea, C. Mammucari et al., "Autophagy is required to maintain muscle mass," *Cell Metabolism*, vol. 10, no. 6, pp. 507–515, 2009.
- [112] Y. Luo, J. Yoneda, H. Ohmori et al., "Cancer usurps skeletal muscle as an energy repository," *Cancer Research*, vol. 74, no. 1, pp. 330–340, 2014.
- [113] F. Penna, D. Costamagna, F. Pin et al., "Autophagic degradation contributes to muscle wasting in cancer cachexia," *The American Journal of Pathology*, vol. 182, no. 4, pp. 1367–1378, 2013.
- [114] L. Tessitore, P. Costelli, G. Bonetti, and F. M. Baccino, "Cancer cachexia, malnutrition, and tissue protein turnover in experimental animals," *Archives of Biochemistry and Biophysics*, vol. 306, no. 1, pp. 52–58, 1993.
- [115] J. R. Mayers, C. Wu, C. B. Clish et al., "Elevation of circulating branched-chain amino acids is an early event in human pancreatic adenocarcinoma development," *Nature Medicine*, vol. 20, no. 10, pp. 1193–1198, 2014.
- [116] U. E. Martinez-Outschoorn, D. Whitaker-Menezes, S. Pavlides et al., "The autophagic tumor stroma model of cancer or "battery-operated tumor growth": a simple solution to the autophagy paradox," *Cell Cycle*, vol. 9, no. 21, pp. 4297–4306, 2010.
- [117] Z. Aversa, F. Pin, S. Lucia et al., "Autophagy is induced in the skeletal muscle of cachectic cancer patients," *Scientific Reports*, vol. 6, p. 30340, 2016.
- [118] F. Penna, S. Busquets, F. Pin et al., "Combined approach to counteract experimental cancer cachexia: eicosapentaenoic acid and training exercise," *Journal of Cachexia, Sarcopenia and Muscle*, vol. 2, no. 2, pp. 95–104, 2011.
- [119] P. F. Cospser and L. A. Leinwand, "Cancer causes cardiac atrophy and autophagy in a sexually dimorphic manner," *Cancer Research*, vol. 71, no. 5, pp. 1710–1720, 2011.
- [120] H. Ding, G. Zhang, K. W. Sin et al., "Activin A induces skeletal muscle catabolism via p38beta mitogen-activated protein kinase," *Journal of Cachexia, Sarcopenia and Muscle*, vol. 8, no. 2, pp. 202–212, 2017.
- [121] A. M. Fritzen, C. Frøsig, J. Jeppesen et al., "Role of AMPK in regulation of LC3 lipidation as a marker of autophagy in skeletal muscle," *Cellular Signalling*, vol. 28, no. 6, pp. 663–674, 2016.
- [122] A. M. Sanchez, A. Csibi, A. Raibon et al., "AMPK promotes skeletal muscle autophagy through activation of forkhead FoxO3a and interaction with Ulk1," *Journal of Cellular Biochemistry*, vol. 113, no. 2, pp. 695–710, 2012.
- [123] P. K. Paul and A. Kumar, "TRAF6 coordinates the activation of autophagy and ubiquitin-proteasome systems in atrophying skeletal muscle," *Autophagy*, vol. 7, no. 5, pp. 555–556, 2011.
- [124] K. Pettersen, S. Andersen, S. Degen et al., "Cancer cachexia associates with a systemic autophagy-inducing activity mimicked by cancer cell-derived IL-6 trans-signaling," *Scientific Reports*, vol. 7, article 2046, 2017.
- [125] K. Baar, "Involvement of PPARγ co-activator-1, nuclear respiratory factors 1 and 2, and PPARα in the adaptive response to endurance exercise," *Proceedings of the Nutrition Society*, vol. 63, no. 2, pp. 269–273, 2004.
- [126] P. Puigserver and B. M. Spiegelman, "Peroxisome proliferator-activated receptor-γ coactivator 1α (PGC-1α): transcriptional coactivator and metabolic regulator," *Endocrine Reviews*, vol. 24, no. 1, pp. 78–90, 2003.
- [127] Z. Wu, P. Puigserver, U. Andersson et al., "Mechanisms controlling mitochondrial biogenesis and respiration through the thermogenic coactivator PGC-1," *Cell*, vol. 98, no. 1, pp. 115–124, 1999.
- [128] F. W. Booth, G. N. Rueggsegger, R. G. Toedebusch, and Z. Yan, "Endurance exercise and the regulation of skeletal muscle metabolism," *Progress in Molecular Biology and Translational Science*, vol. 135, pp. 129–151, 2015.
- [129] P. Zhang, X. Chen, and M. Fan, "Signaling mechanisms involved in disuse muscle atrophy," *Medical Hypotheses*, vol. 69, no. 2, pp. 310–321, 2007.
- [130] S. V. Brooks and J. A. Faulkner, "Contractile properties of skeletal muscles from young, adult and aged mice," *The Journal of Physiology*, vol. 404, pp. 71–82, 1988.
- [131] J. J. Widrick, J. G. Romatowski, K. M. Norenberg et al., "Functional properties of slow and fast gastrocnemius muscle fibers after a 17-day spaceflight," *Journal of Applied Physiology*, vol. 90, no. 6, pp. 2203–2211, 2001.
- [132] A. Garnier, D. Fortin, J. Zoll et al., "Coordinated changes in mitochondrial function and biogenesis in healthy and diseased human skeletal muscle," *The FASEB Journal*, vol. 19, no. 1, pp. 43–52, 2005.
- [133] J. L. Brown, M. E. Rosa-Caldwell, D. E. Lee et al., "PGC-1α4 gene expression is suppressed by the IL-6-MEK-ERK 1/2 MAPK signalling axis and altered by resistance exercise, obesity and muscle injury," *Acta Physiologica (Oxford, England)*, vol. 220, no. 2, pp. 275–288, 2017.

- [134] J. L. Ruas, J. P. White, R. R. Rao et al., "A PGC-1alpha isoform induced by resistance training regulates skeletal muscle hypertrophy," *Cell*, vol. 151, no. 6, pp. 1319–1331, 2012.
- [135] Z. Arany, N. Lebrasseur, C. Morris et al., "The transcriptional coactivator PGC-1beta drives the formation of oxidative type IIX fibers in skeletal muscle," *Cell Metabolism*, vol. 5, no. 1, pp. 35–46, 2007.
- [136] J. Lin, H. Wu, P. T. Tarr et al., "Transcriptional co-activator PGC-1 alpha drives the formation of slow-twitch muscle fibres," *Nature*, vol. 418, no. 6899, pp. 797–801, 2002.
- [137] A. M. Joseph, H. Pilegaard, A. Litvintsev, L. Leick, and D. A. Hood, "Control of gene expression and mitochondrial biogenesis in the muscular adaptation to endurance exercise," *Essays in Biochemistry*, vol. 42, pp. 13–29, 2006.
- [138] V. A. Lira, C. R. Benton, Z. Yan, and A. Bonen, "PGC-1alpha regulation by exercise training and its influences on muscle function and insulin sensitivity," *American Journal of Physiology Endocrinology and Metabolism*, vol. 299, no. 2, pp. E145–E161, 2010.
- [139] A. Vainshtein, L. D. Tryon, M. Pauly, and D. A. Hood, "Role of PGC-1alpha during acute exercise-induced autophagy and mitophagy in skeletal muscle," *American Journal of Physiology Cell Physiology*, vol. 308, no. 9, pp. C710–9, 2015.
- [140] J. Cannavino, L. Brocca, M. Sandri, R. Bottinelli, and M. A. Pellegrino, "PGC1-alpha over-expression prevents metabolic alterations and soleus muscle atrophy in hindlimb unloaded mice," *The Journal of Physiology*, vol. 592, no. 20, pp. 4575–4589, 2014.
- [141] J. Cannavino, L. Brocca, M. Sandri, B. Grassi, R. Bottinelli, and M. A. Pellegrino, "The role of alterations in mitochondrial dynamics and PGC-1alpha over-expression in fast muscle atrophy following hindlimb unloading," *The Journal of Physiology*, vol. 593, no. 8, pp. 1981–1995, 2015.
- [142] A. Vainshtein, E. M. Desjardins, A. Armani, M. Sandri, and D. A. Hood, "PGC-1alpha modulates denervation-induced mitophagy in skeletal muscle," *Skeletal Muscle*, vol. 5, p. 9, 2015.
- [143] M. Sandri, J. Lin, C. Handschin et al., "PGC-1alpha protects skeletal muscle from atrophy by suppressing FoxO3 action and atrophy-specific gene transcription," *Proceedings of the National Academy of Sciences of the United States of America*, vol. 103, no. 44, pp. 16260–16265, 2006.
- [144] M. J. Puppa, E. A. Murphy, R. Fayad, G. A. Hand, and J. A. Carson, "Cachectic skeletal muscle response to a novel bout of low-frequency stimulation," *Journal of Applied Physiology*, vol. 116, no. 8, pp. 1078–1087, 2014.
- [145] X. Wang, A. M. Pickrell, T. A. Zimmers, and C. T. Moraes, "Increase in muscle mitochondrial biogenesis does not prevent muscle loss but increased tumor size in a mouse model of acute cancer-induced cachexia," *PloS One*, vol. 7, no. 3, article e33426, 2012.
- [146] S. Jager, C. Handschin, J. St-Pierre, and B. M. Spiegelman, "AMP-activated protein kinase (AMPK) action in skeletal muscle via direct phosphorylation of PGC-1alpha," *Proceedings of the National Academy of Sciences of the United States of America*, vol. 104, no. 29, pp. 12017–12022, 2007.
- [147] R. Bergeron, J. M. Ren, K. S. Cadman et al., "Chronic activation of AMP kinase results in NRF-1 activation and mitochondrial biogenesis," *American Journal of Physiology Endocrinology and Metabolism*, vol. 281, no. 6, pp. E1340–6, 2001.
- [148] M. M. Mihaylova and R. J. Shaw, "The AMPK signalling pathway coordinates cell growth, autophagy and metabolism," *Nature Cell Biology*, vol. 13, no. 9, pp. 1016–1023, 2011.
- [149] D. Carling, "AMPK signalling in health and disease," *Current Opinion in Cell Biology*, vol. 45, pp. 31–37, 2017.
- [150] B. Cool, B. Zinker, W. Chiou et al., "Identification and characterization of a small molecule AMPK activator that treats key components of type 2 diabetes and the metabolic syndrome," *Cell Metabolism*, vol. 3, no. 6, pp. 403–416, 2006.
- [151] J. P. White, M. J. Puppa, S. Gao, S. Sato, S. L. Welle, and J. A. Carson, "Muscle mTORC1 suppression by IL-6 during cancer cachexia: a role for AMPK," *American Journal of Physiology Endocrinology and Metabolism*, vol. 304, no. 10, pp. E1042–E1052, 2013.
- [152] X. Ge, A. Vajjala, C. McFarlane, W. Wahli, M. Sharma, and R. Kambadur, "Lack of Smad3 signaling leads to impaired skeletal muscle regeneration," *American Journal of Physiology Endocrinology and Metabolism*, vol. 303, no. 1, pp. E90–102, 2012.
- [153] S. M. Hindi, V. Mishra, S. Bhatnagar et al., "Regulatory circuitry of TWEAK-Fn14 system and PGC-1alpha in skeletal muscle atrophy program," *The FASEB Journal*, vol. 28, no. 3, pp. 1398–1411, 2014.
- [154] A. J. Grande, V. Silva, R. Riera et al., "Exercise for cancer cachexia in adults," *Cochrane Database of Systematic Reviews*, vol. 11, article CD010804, 2014.
- [155] F. W. Booth, C. K. Roberts, and M. J. Laye, "Lack of exercise is a major cause of chronic diseases," *Comprehensive Physiology*, vol. 2, no. 2, pp. 1143–1211, 2012.
- [156] J. O. Holloszy and E. F. Coyle, "Adaptations of skeletal muscle to endurance exercise and their metabolic consequences," *Journal of Applied Physiology: Respiratory, Environmental and Exercise Physiology*, vol. 56, no. 4, pp. 831–838, 1984.
- [157] J. O. Holloszy, "Adaptations of skeletal muscle mitochondria to endurance exercise: a personal perspective," *Exercise and Sport Sciences Reviews*, vol. 32, no. 2, pp. 41–43, 2004.
- [158] O. Holloszy, "Enzymatic adaptations of skeletal muscle to endurance exercise," *Current Problems in Clinical Biochemistry*, vol. 11, pp. 118–121, 1982.
- [159] D. A. Hood, "Invited review: contractile activity-induced mitochondrial biogenesis in skeletal muscle," *Journal of Applied Physiology*, vol. 90, no. 3, pp. 1137–1157, 2001.
- [160] S. al-Majid, D. O. McCarthy, "Resistance exercise training attenuates wasting of the extensor digitorum longus muscle in mice bearing the colon-26 adenocarcinoma," *Biological Research for Nursing*, vol. 2, no. 3, pp. 155–166, 2001.
- [161] D. C. Wright, D. H. Han, P. M. Garcia-Roves, P. C. Geiger, T. E. Jones, and J. O. Holloszy, "Exercise-induced mitochondrial biogenesis begins before the increase in muscle PGC-1alpha expression," *The Journal of Biological Chemistry*, vol. 282, no. 1, pp. 194–199, 2007.
- [162] G. D. Stewart, R. J. Skipworth, and K. C. Fearon, "Cancer cachexia and fatigue," *Clinical Medicine (London, England)*, vol. 6, no. 2, pp. 140–143, 2006.
- [163] E. Ferriolli, R. J. Skipworth, P. Hendry et al., "Physical activity monitoring: a responsive and meaningful patient-centered outcome for surgery, chemotherapy, or radiotherapy?," *Journal of Pain and Symptom Management*, vol. 43, no. 6, pp. 1025–1035, 2012.

- [164] J. Farkas, S. Haehlingvon, K. Kalantar-Zadeh, J. E. Morley, S. D. Anker, and M. Lainscak, "Cachexia as a major public health problem: frequent, costly, and deadly," *Journal of Cachexia, Sarcopenia and Muscle*, vol. 4, pp. 173–178, 2013.
- [165] A. Montazeri, "Quality of life data as prognostic indicators of survival in cancer patients: an overview of the literature from 1982 to 2008," *Health and Quality of Life Outcomes*, vol. 7, p. 102, 2009.
- [166] K. A. Baltgalvis, F. G. Berger, M. M. Peña, J. Mark Davis, J. P. White, and J. A. Carson, "Activity level, apoptosis, and development of cachexia in *Apc^{Min/+}* mice," *Journal of Applied Physiology*, vol. 109, no. 4, pp. 1155–1161, 2010.
- [167] K. T. Murphy, A. Chee, J. Trieu, T. Naim, and G. S. Lynch, "Importance of functional and metabolic impairments in the characterization of the C-26 murine model of cancer cachexia," *Disease Models & Mechanisms*, vol. 5, no. 4, pp. 533–545, 2012.
- [168] F. W. Booth and M. V. Chakravarthy, "Physical activity and dietary intervention for chronic diseases: a quick fix after all?" *Journal of Applied Physiology*, vol. 100, no. 5, pp. 1439–1440, 2006.
- [169] M. Dahele, R. J. Skipworth, L. Wall, A. Voss, T. Preston, and K. C. Fearon, "Objective physical activity and self-reported quality of life in patients receiving palliative chemotherapy," *Journal of Pain and Symptom Management*, vol. 33, no. 6, pp. 676–685, 2007.
- [170] A. Gratas-Delamarche, F. Derbré, S. Vincent, and J. Cillard, "Physical inactivity, insulin resistance, and the oxidative-inflammatory loop," *Free Radical Research*, vol. 48, no. 1, pp. 93–108, 2014.
- [171] J. P. Thyfault and F. W. Booth, "Lack of regular physical exercise or too much inactivity," *Current Opinion in Clinical Nutrition and Metabolic Care*, vol. 14, no. 4, pp. 374–378, 2011.
- [172] M. J. Puppa, J. P. White, K. T. Velázquez et al., "The effect of exercise on IL-6-induced cachexia in the *Apc (Min/+)* mouse," *Journal of Cachexia, Sarcopenia and Muscle*, vol. 3, no. 2, pp. 117–137, 2012.
- [173] J. P. Hardee, J. E. Mangum, S. Gao et al., "Eccentric contraction-induced myofiber growth in tumor-bearing mice," *Journal of Applied Physiology*, vol. 120, no. 1, pp. 29–37, 2016.
- [174] A. Sheldon, F. W. Booth, and C. R. Kirby, "cAMP levels in fast- and slow-twitch skeletal muscle after an acute bout of aerobic exercise," *The American Journal of Physiology*, vol. 264, 6 Part 1, pp. C1500–C1504, 1993.
- [175] A. M. Sanchez, "Autophagy regulation in human skeletal muscle during exercise," *The Journal of Physiology*, vol. 594, no. 18, pp. 5053–5054, 2016.
- [176] A. M. Sanchez, H. Bernardi, G. Py, and R. B. Candau, "Autophagy is essential to support skeletal muscle plasticity in response to endurance exercise," *American Journal of Physiology. Regulatory, Integrative and Comparative Physiology*, vol. 307, no. 8, pp. R956–R969, 2014.
- [177] C. Schwalm, C. Jamart, N. Benoit et al., "Activation of autophagy in human skeletal muscle is dependent on exercise intensity and AMPK activation," *The FASEB Journal*, vol. 29, no. 8, pp. 3515–3526, 2015.
- [178] A. Vainshtein, P. Grumati, M. Sandri, and P. Bonaldo, "Skeletal muscle, autophagy, and physical activity: the menage a trois of metabolic regulation in health and disease," *Journal of Molecular Medicine (Berlin, Germany)*, vol. 92, no. 2, pp. 127–137, 2014.
- [179] E. Pigna, E. Berardi, P. Aulino et al., "Aerobic exercise and pharmacological treatments counteract cachexia by modulating autophagy in colon cancer," *Scientific Reports*, vol. 6, article 26991, 2016.

Research Article

Mitochondrial Respiration in Human Colorectal and Breast Cancer Clinical Material Is Regulated Differently

Andre Koit,¹ Igor Shevchuk,¹ Lyudmila Ounpuu,¹ Aleksandr Klepinin,¹ Vladimir Chekulayev,¹ Natalja Timohhina,¹ Kersti Tepp,¹ Marju Puurand,¹ Laura Truu,¹ Karoliina Heck,² Vahur Valvere,² Rita Guzun,³ and Tuuli Kaambre^{1,4}

¹Laboratory of Bioenergetics, National Institute of Chemical Physics and Biophysics, Tallinn, Estonia

²Oncology and Haematology Clinic at the North Estonia Medical Centre, Tallinn, Estonia

³Laboratory of Fundamental and Applied Bioenergetics, INSERM, University Grenoble Alpes, U1055 Grenoble, France

⁴School of Natural Sciences and Health, Tallinn University, Tallinn, Estonia

Correspondence should be addressed to Tuuli Kaambre; tuuli.kaambre@kbfi.ee

Received 27 January 2017; Revised 10 April 2017; Accepted 19 April 2017; Published 11 July 2017

Academic Editor: Moh H. Malek

Copyright © 2017 Andre Koit et al. This is an open access article distributed under the Creative Commons Attribution License, which permits unrestricted use, distribution, and reproduction in any medium, provided the original work is properly cited.

We conducted quantitative cellular respiration analysis on samples taken from human breast cancer (HBC) and human colorectal cancer (HCC) patients. Respiratory capacity is not lost as a result of tumor formation and even though, functionally, complex I in HCC was found to be suppressed, it was not evident on the protein level. Additionally, metabolic control analysis was used to quantify the role of components of mitochondrial interactosome. The main rate-controlling steps in HBC are complex IV and adenine nucleotide transporter, but in HCC, complexes I and III. Our kinetic measurements confirmed previous studies that respiratory chain complexes I and III in HBC and HCC can be assembled into supercomplexes with a possible partial addition from the complex IV pool. Therefore, the kinetic method can be a useful addition in studying supercomplexes in cell lines or human samples. In addition, when results from culture cells were compared to those from clinical samples, clear differences were present, but we also detected two different types of mitochondria within clinical HBC samples, possibly linked to two-compartment metabolism. Taken together, our data show that mitochondrial respiration and regulation of mitochondrial membrane permeability have substantial differences between these two cancer types when compared to each other to their adjacent healthy tissue or to respective cell cultures.

1. Introduction

The field of cellular bioenergetics is gaining increased attention and studies performed during the last years have shown that targeting cancer cell energy metabolism may be a new and promising area for selective tumor treatment [1]. The literature describing changes in energy metabolism and mitochondrial function during carcinogenesis is, unfortunately, full of contradictions. Majority of previous studies about the bioenergetics of malignant tumors were performed in vitro on different cell models with the conclusion that cancer cells have increased glucose uptake and, due to mitochondrial damage, it is not metabolized via oxidative phosphorylation (OXPHOS) [2–4]. It is clear that for many

tumors, glycolysis is the main energy provider, but in others, OXPHOS is still crucial for survival and progression and produces necessary ATP [1, 5, 6]. Recently, a new concept for tumor metabolism was proposed—metabolic coupling between mitochondria in cancer cells and catabolism in stromal cells—which promotes tumor growth and development of metastases. In other words, tumor cells induce reprogramming in surrounding nontumor cells so that the latter acquire the Warburg phenotype [7] and start producing and exporting the necessary fuels for the anabolic cancer cells (“reverse Warburg”). The cancer cells will then metabolize these fuels via their tricarboxylic acid cycle and OXPHOS [8–10]. Complex interplay between developing cancer cells and host physiology, possibly mediated by “waves” of gene expression

in the tumor [11, 12], can only develop in vivo and therefore in vitro studies cannot give conclusive information about the functional activity and capacity of OXPHOS in human samples. In vitro models ignore many factors arising from the tumor microenvironment (TME), which can and will exert significant effects in vivo. TME consists of nonmalignant cells, soluble growth factors, signaling molecules, and extracellular matrix that support tumor progression [13], but high heterogeneity within cancers cell population on top of it contributes to even further complexity in clinical samples [14]. At the same time, the metabolic profiles of tumor cells that are grown in culture have significant variations primarily due to the culture conditions, such as concentrations of glucose, glutamine, and/or fetal serum. Cells grown in glucose-free medium display relatively high rates of oxygen consumption, but cultivation in high-glucose medium increases their glycolytic capacity together with reduced respiratory flux [15–19].

In addition to intercellular differences, there are also intracellular rearrangements resulting from tumor formation. The functional units within cells are often macromolecular complexes rather than single species [20]. In case of OXPHOS, it has been shown that complexes of the respiratory chain can form assemblies—supercomplexes—that lead to kinetic and possibly homeostatic advantages [21]. Therefore, pure genome or transcriptome data are not sufficient for describing the final in situ modifications and the final outcomes of a pathway or cellular processes are defined by actual activities of their separate proteins—or their assemblies—together with the respective regulatory mechanisms. More specifically, previous studies have shown that in cardiac and yeast cells, a large protein supercomplex is centrally positioned in regulation of mitochondrial respiration and mitochondrial energy fluxes. The supercomplex consists of ATP synthasome, mitochondrial creatine kinase (MtCK) or hexokinase (HK), voltage-dependent anion channel (VDAC), and some regulatory proteins expectedly coordinate the selective permeability of it. This complex is known as mitochondrial interactosome (MI) [22], and it is located in the contact sites of outer and inner mitochondrial membranes. This unit also includes supercomplexes formed by the respiratory chain [23, 24]. Changes in the content of ATP synthasome and respiratory chain supercomplexes in pathological conditions are still poorly studied. Inhibiting key respiratory enzymes or avoiding restructuring of mitochondrial supercomplexes in tumors has potential to disrupt disease progression without affecting normal cells, thus, providing a powerful new approach for developing novel therapeutic targets. Specifically, Rohlenova et al. recently demonstrated that breast cancer cells expressing HER2 oncogene develop specific RC supercomplexes which make complex I in these susceptible to treatment with chemically altered tamoxifen called MitoTam [25]. MitoTam is taken to a phase I clinical study [25], and there are other clinical studies undergoing that target OXPHOS in different cancer types (e.g., trial numbers NCT01957735 and NCT02650804). Therefore, despite the assumed glycolytic nature of human tumors, inhibition of oxidative respiration is proving to be a viable therapeutic strategy and further studies are needed to define differences

between cancer types but also individual patients in regard to such treatment.

We have previously shown on clinical samples that both human breast cancer (HBC) and human colorectal cancer (HCC) are not purely glycolytic, but these tumors have sustained OXPHOS as a substantial provider of ATP [26–28]. Here, we extend our studies by comparing bioenergetics of HBC and HCC using kinetic methods.

2. Materials and Methods

2.1. Chemicals. All chemicals were purchased from Sigma-Aldrich (USA) and were of the highest purity available (>98%).

2.2. Clinical Materials. The tissue samples were provided by the Oncology and Haematology Clinic at the North Estonia Medical Centre (Tallinn). All the samples were analyzed immediately after surgery. Only primary tumors were examined and information from respective pathology reports was provided by the North Estonia Medical Centre for all the analyzed samples. Informed consent was obtained from all the patients and coded identity protection was applied. All investigations were approved by the Tallinn Medical Research Ethics Committee and were in accordance with the Helsinki Declaration and Convention of the Council of Europe on Human Rights and Biomedicine. The entire group consisted of 34 patients with breast cancer and 55 with colorectal cancer.

2.3. Cell Cultures. MDA-MB-231 and MCF-7 cells were grown as adherent monolayers in low glucose (1.0 g/L) Dulbecco's modified Eagle's medium (DMEM) with stable L-glutamine and sodium pyruvate (from Capricorn Scientific GmbH) supplemented with 10% heat-inactivated fetal bovine serum, 10 $\mu\text{g}/\text{mL}$ human recombinant Zn insulin, and antibiotics: penicillin (100 U/mL), streptomycin (100 $\mu\text{g}/\text{mL}$), and gentamicin at a final concentration of 50 $\mu\text{g}/\text{mL}$. Cells were grown at 37°C in a humidified incubator containing 5% CO₂ in air and were subcultured at 2-3-day intervals.

2.4. Mitochondrial Respiration in Saponin-Permeabilized Tissue Samples. Numerous studies have demonstrated that isolated mitochondria behave differently from mitochondria in situ [29–32]. We therefore have investigated respiratory activity of tumor and control tissues in situ using the skinned sample technique [26, 28, 29, 33]. This method allows analysis of the function of mitochondria in cells in their natural environment and leaves links between cytoskeletal structures and mitochondrial outer membranes intact [34–37]. Cytochrome c test was used to confirm integrity of the mitochondrial outer membrane (MOM) [22, 26, 28, 33]; mitochondrial inner membrane quality was checked using a carboxyatractylolide (CAT) test as the last procedure in every experiment [22, 26, 28, 33]. Rates of O₂ consumption were assayed at 25°C using Oxygraph-2k high-resolution respirometer (Oroboros Instruments, Innsbruck, Austria) loaded with pre-equilibrated respiration buffer medium B [26]. Activity of the respiratory chain was measured by substrate-inhibitor

titration as described earlier [26, 38]. The solubility of oxygen at 25°C was taken as 240 nM/mL [39]. The solubility of oxygen is much lower at 37 than at 25°C, but also, the skinned samples from malignant clinical material are more stable at 25°C. All rates of respiration (V) are expressed in nM O_2 /min per mg dry tissue weight for solid tumors and in nM O_2 /min per million cells for cell cultures.

2.5. Metabolic Control Analysis. Metabolic control analysis (MCA) is a method for studying regulatory mechanisms in complex metabolic systems [40–42]. Flux control coefficient (FCC) is defined as the ratio of fractional change in a system variable to fractional change in a biochemical activity that caused the change in the given system [42]. FCC or C_{vi}^J is the extent to which an enzyme in a pathway controls the flux (J); it corresponds to the percentage decrease in flux caused by a 1% decrease in the activity (v_i) of that enzyme [41, 43]:

$$C_{vi}^J = \frac{(dJ/dv_i)}{(J/v_i)} = \frac{d \ln J}{d \ln v_i}. \quad (1)$$

This method shows how the control is shared between the enzymes and the transporters of the pathway and enables to identify the steps that could be modified to achieve successful alteration of the flux or metabolite concentration in the pathway. But it also permits the identification of system components that are crucial in the regulation of energy transfer and regulatory networks [40–42, 44–46].

MCA has previously been applied in our lab to human breast and colorectal cancer skinned samples to determine the FCCs for respiratory chain complexes. The flux was measured as the rate of O_2 consumption in permeabilized tissues derived from HCC patients when all components of the OXPHOS system were titrated with specific irreversible or pseudoirreversible inhibitors to stepwise decrease selected respiratory chain complex activities according to a previously published method [26, 27, 47, 48].

2.6. Western Blot Analysis of the Level of Mitochondrial RC Complexes Expression. Postoperative human tissue samples (70–100 mg) were crushed in liquid nitrogen and homogenized in 20 volumes of RIPA lysis buffer (50 mM Tris-HCl pH 8.0, 150 mM NaCl, 2 mM EDTA, 0.5% sodium deoxycholate, 0.1% SDS, 0.1% Triton X-100, and complete protease inhibitor cocktail (Roche)) by Retsch Mixer Mill at 25 Hz for 2 min. After homogenization, samples were incubated for 30 min on ice and centrifuged at 12,000 rpm for 20 min at 4°C. The proteins in the supernatants were precipitated using acetone/TCA to remove nonprotein contaminants. Briefly, supernatants were mixed with 8 volumes of ice-cold acetone and 1 volume of 100% TCA, kept at –20°C for 1 h and then pelleted at 11500 rpm for 15 min at 4°C. The pellets were washed twice with acetone and resuspended in 1x Laemmli sample buffer.

Proteins were separated by polyacrylamide gel electrophoresis, transferred to a polyvinylidene difluoride (PVDF) membrane, and subjected to immunoblotting with the total OXPHOS antibody cocktail (ab110411). Then, the membranes were incubated with corresponding horseradish

peroxidase-conjugated secondary antibody and visualized using an enhanced chemiluminescence system (ECL; Pierce, Thermo Fisher Scientific). After chemiluminescence reaction, the PVDF membranes were stained with Coomassie brilliant blue R250 to measure the total protein amount. The complexes I–V signal intensities were calculated by ImageJ software and normalized to total protein intensities.

Expression levels of complex I in HCC and normal tissues were additionally estimated using anti-NDUFA9 antibody that corresponds to NADH dehydrogenase 1 α sub-complex 9 (SAB1100073). The samples were incubated and visualized as described above. Levels of NDUFA9 encoding protein were normalized to total protein content.

2.7. Citrate Synthase Activity. Activity of citrate synthase in tissue homogenates was measured as described by Srere [49]. Reactions were performed in 96-well plates containing 100 mM Tris-HCl pH 8.1, 0.3 mM AcCoA, 0.5 mM oxaloacetate, and 0.1 mM DTNB using FLUOstar Omega plate reader spectrophotometer (BMG Labtech).

2.8. Data Analysis. Data in the text, tables, and figures are presented as mean \pm standard error (SEM). Results were analyzed by the Student t -test; p values <0.05 were considered statistically significant.

3. Results and Discussion

3.1. Respiratory Chain Analysis and Presence of Supercomplexes. Suppression of mitochondrial electron transport chain function is widespread in cancer, and this is closely connected to apoptosis resistance [50–54]. However, studies are often conducted on cell cultures and therefore little is known about respiratory chain (RC) function in clinical human breast and colorectal carcinomas in situ. To reveal possible disturbances, we conducted comparative quantitative analysis on the respiration rates for different RC complexes in permeabilized HBC and HCC and their adjacent normal tissue samples. Data for healthy breast tissue has been left out from most of the following calculations due to very low ADP-dependent oxygen consumption in this tissue type as it is not sufficient to assess inhibitory effects of antimycin A or rotenone or compare these results to other studied samples.

Multiple substrate-inhibitor titration protocol was used for measuring respiratory capacities of different respiratory chain segments (Table 1) [30, 55]. All respiration rates corresponding to the activities of different RC complexes are increased in both investigated human cancers when compared to their adjacent normal tissue. The mean value of basal respiration (state 2, V_o) in skinned HCC samples is higher than that in normal tissue and depends on the used respiratory substrates. Specifically, in the presence of glutamate and malate, HCC and its control tissue fibers exhibit lower state 2 respiration rates than in the presence of glutamate, malate, and succinate; similar dependence was observed for the breast cancer samples (Figure 1). One possible reason for this difference can be succinate-dependent proton leak in tumor tissue [56–58]. Addition of 2 mM

MgADP for studying complex I-based state 3 (in the presence of glutamate and malate without succinate) increased mitochondrial respiration rates in all tissue samples and following addition of complex I-specific inhibitor (rotenone) inhibited the respiration back to the initial state 2 levels (Table 1). Similarly, the function of complex II was quantified upon ADP-stimulated respiration in the presence of rotenone and succinate; at these conditions, the complex I activity is inhibited and apparent respiration rate originates from complex II. Complex III in both HBC and HCC was confirmed to be fully functional as an addition of antimycin A inhibited the electron flow from complex III to mitochondrial complex IV (COX) (Table 1). The activation of mitochondrial complex IV (addition of 5 mM ascorbate and 1 mM tetramethyl-p-phenylenediamine) resulted in a remarkable increase in the rate of O_2 consumption in all examined samples, both cancerous and normal, but the increase was nearly two times higher in cancer tissue.

Complex I deficiency is the hallmark of multiple mitochondrial diseases and is generally considered to be an intrinsic property of some cancers [58–63]. Indeed, our experiments confirm that development of HCC results in reduced $V_{\text{Glut}}/V_{\text{Succ}}$ ratio which indicates relative suppression of the complex I-dependent respiration [58]. Similar results have previously been described for gastric and ovarian cancer tissues but also in some cancer cell cultures [58, 63–66]. Deficiency of complex I in some tumors might be an early event causing an increase in mitochondrial biogenesis in an attempt to compensate for the reduction in OXPHOS function [63]. Computer modeling predicts that the mechanisms of this compensation can use multiple pathways like β -oxidation of fatty acids, mitochondrial folate metabolism, and others [67]. Our results showed that this suppression is pronounced on the functional level in HCC (Figure 2(a)), but to identify the changes on the protein expression level, we analyzed the RC complexes with total OXPHOS antibody cocktail (Figure 3). Based on this type of approach, the suppression of RC complex I was found to be absent if the results were normalized to total protein. The suppression of complex I in HCC was additionally studied by Western blot analysis with antibodies against only one complex I subunit—NDUFA9 (see Supplementary Fig 1 available online at <https://doi.org/10.1155/2017/1372640>). This result, however, confirmed the suppression of complex I. As seen from those experiments, analysis of RC, using the semi-quantitative WB method, can be strongly dependent on experimental conditions: against what complex I subunit the antibodies were used and which normalization conditions are applied. Additionally, complex II in colon samples did not indicate possible suppression in that alternative pathway as differences in $V_{\text{Succ}}/V_{\text{COX}}$ ratios were not significant (Figure 2(b)) [68].

In contrast to HCC, mitochondrial respiration in HBC samples is not accompanied with suppression of complex I-dependent respiration (Figures 2(a) and 2(b)). Altogether, the relative complex I deficiency on the functional level in our oxygen consumption measurements is characteristic for HCC but not for HBC tissue.

TABLE 1: Characterization of respiratory parameters of permeabilized tissue samples derived from patients with breast or colorectal cancer.

Parameters	HBC patients, $n = 7$ [26]		HCC patients, $n = 7$ [28]	
	Tumor	Control	Tumor	Control
V_o	0.294 ± 0.024	0.004 ± 0.007	1.06 ± 0.14	0.82 ± 0.15
V_{ADP}	0.71 ± 0.06	0.055 ± 0.004	2.02 ± 0.21	1.39 ± 0.21
V_{rot}	0.34 ± 0.04	0.070 ± 0.015	0.91 ± 0.11	0.85 ± 0.14
V_{Succ}	0.74 ± 0.10	0.076 ± 0.008	2.22 ± 0.26	1.33 ± 0.18
VANM	0.38 ± 0.04	0.071 ± 0.018	1.04 ± 0.09	0.69 ± 0.07
V_{COX}	2.36 ± 0.33	1.23 ± 0.18	6.59 ± 0.71	3.84 ± 0.58

Note: here, each data point is the mean \pm SEM of respiratory values. V_o : basal respiration without ADP or ATP; V_{ADP} : ADP-stimulated respiration (final concentration 2 mM) in the presence of 5 mM glutamate and 2 mM malate (indicating the function of the respiratory chain complex I); V_{rot} : rates of respiration after addition of 50 μM rotenone (an inhibitor of complex I); V_{Succ} : ADP-stimulated respiration in the presence of rotenone and 10 mM succinate (to estimate the function of complex II); VANM: rates of respiration after addition 10 μM antimycin-A (an inhibitor of complex III); V_{COX} : rates of O_2 consumption in the presence of complex IV substrates (5 mM ascorbate jointly with 1 mM tetramethyl-p-phenylenediamine).

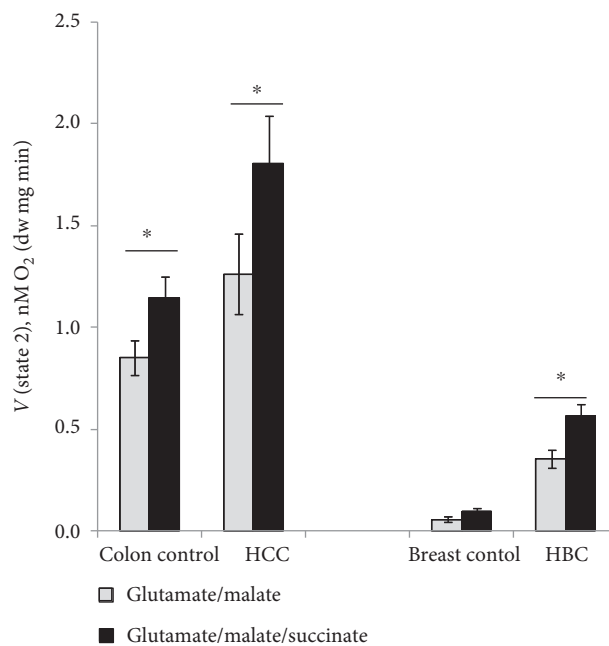


FIGURE 1: Assessment of state 2 respiration rates of the permeabilized HCC, HBC, and normal adjacent tissue samples in the presence of different combinations of respiratory substrates (5 mM glutamate, 2 mM malate, and 10 mM succinate). Bars are SEM, $n = 8$ for colon samples, and $n = 12$ for breast tissue samples, $*p < 0.05$.

Remarkable numbers of studies have shown that RC complexes can form protein assemblies (supercomplexes). These supramolecular structures provide kinetic advantage such as substrate channeling, increased efficiency in electron transport, prevention of destabilization, and degradation of respiratory enzyme complexes [21] and means to regulate

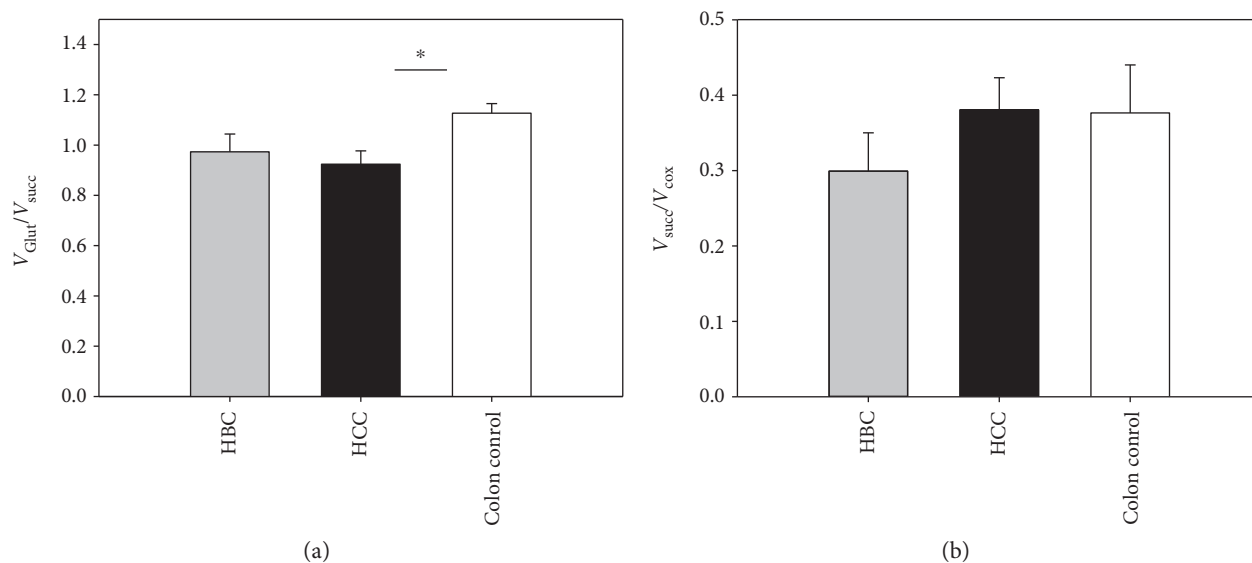


FIGURE 2: (a) Oxygraphic analysis of the functioning of complex I in skinned tissues from patients with HBC or HCC; here, $V_{\text{Glut}}/V_{\text{Succ}}$ is the ratio of ADP-stimulated respiration rate in the presence of 5 mM glutamate and 2 mM malate (activity of complex I) to ADP-stimulated respiration rate in the presence of 50 μM rotenone and 10 mM succinate (activity of complex II). (b) $V_{\text{Succ}}/V_{\text{COX}}$ is the ratio of complex II respiration rate to complex IV respiration rate. Data shown as mean \pm SEM; $n = 7$ for colon [28] and breast tissue samples [26], * $p < 0.05$.

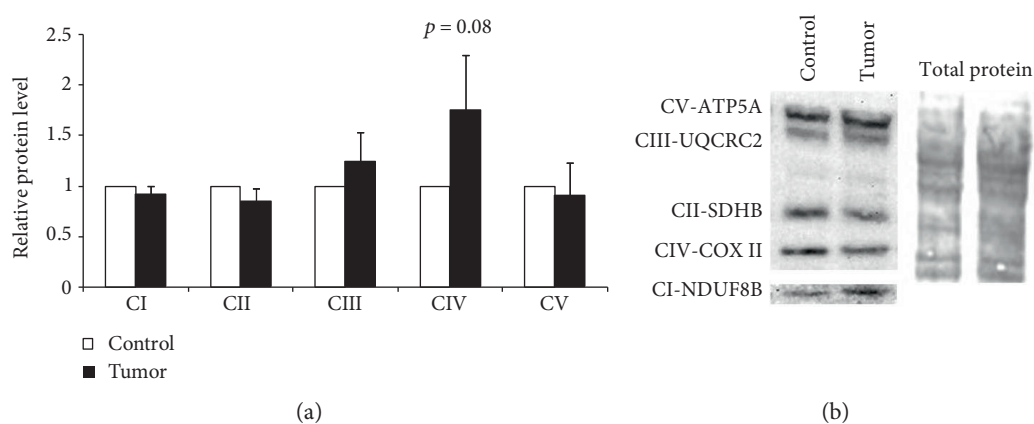


FIGURE 3: Quantitative analysis of the expression levels of the respiratory chain complexes in HCC and normal tissue samples (a) along with a representative Western blot image (b). Protein levels were normalized to total protein staining by Coomassie blue; data shown as mean \pm SEM of 5 independent experiments.

ROS levels in the cell (most of the mitochondrial ROS originates from complexes I and III) [69] and hence, homeostasis. The RC complex I is considered to be the most important component in these assemblies, and it is a member of almost all known respirasomes [70–74]. In previous studies, complexes I, III, and IV were found to be assembled into supercomplexes in different configurations, but complex II was not confirmed to be a component of these RC supercomplexes and was assumed to move freely in the mitochondrial inner membrane [70, 75, 76]. Relative deficiency of the RC complex I on the functional level (as shown above) may be a result of changes in supercomplex composition as a part of malignant transformation.

In addition to RC supercomplexes, along with respirasomes, one more molecular transmembrane protein supercomplex (which is known as ATP synthasome; [77])

was identified as the component of the OXPHOS system. The ATP synthasome complex consists of ATP synthase, inorganic phosphate carrier, and adenine nucleotide translocator (ANT) [48]. The current model of mitochondrial interactosome (MI) considers the ATP synthasome and RC complexes together with voltage-dependent anion channel (VDAC) and mitochondrial creatine kinase (MtCK) as components of intracellular energetic units [22]. Even though MI is proven in striated muscles, the functional role of it, together with MtCK, in malignant samples remains controversial [78], but it indicates that both ATP synthasome and RC complexes can form even more complex functional structures.

In addition to steady-state proteome studies, kinetic testing of metabolic fluxes using MCA can provide preliminary information about supramolecular organization in the

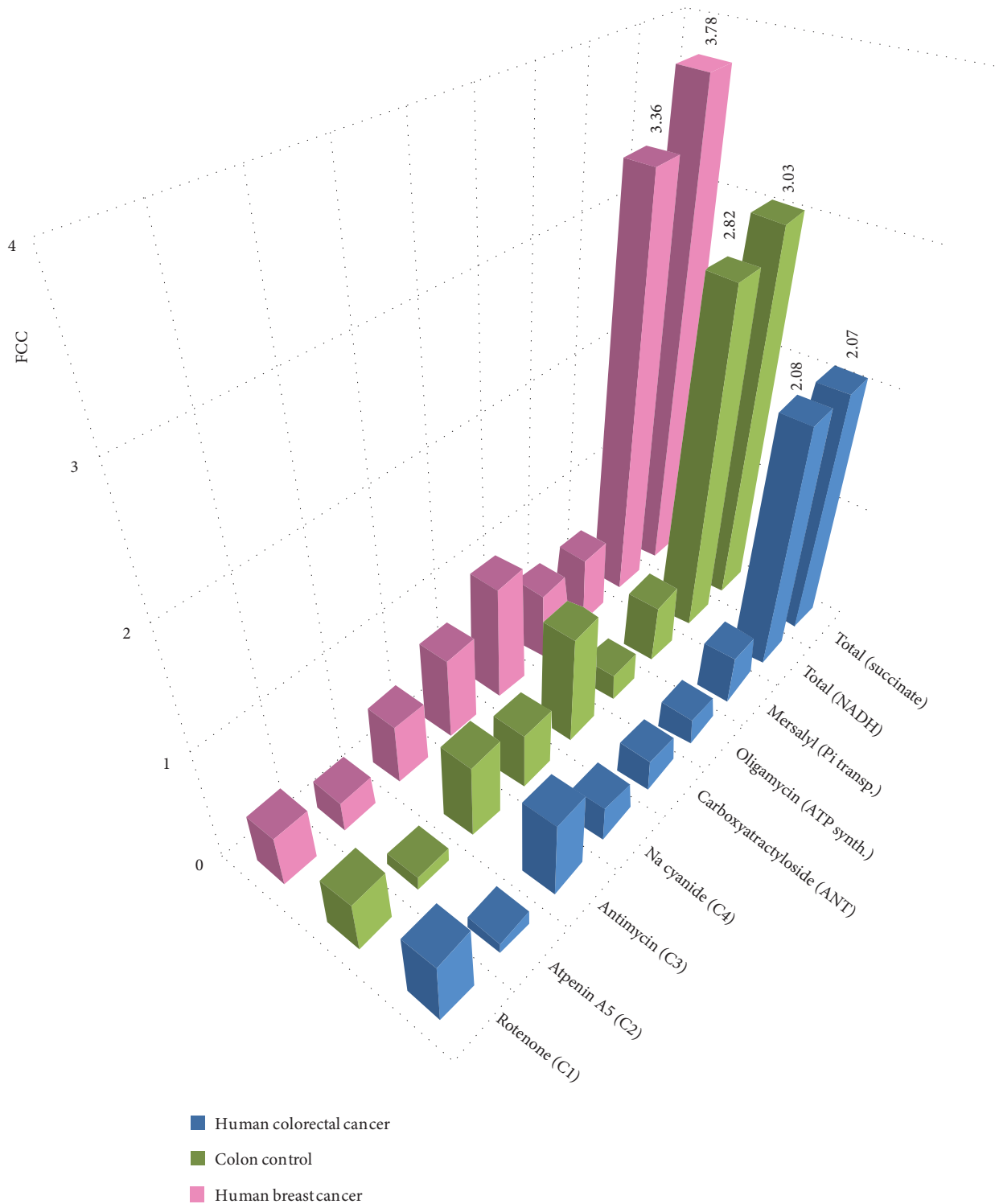


FIGURE 4: FCCs for ATP synthasome and RC complexes as determined by MCA. Two ways of electron transfer were examined: NADH-dependent and succinate-dependent electron transfers, and respective sums of FCCs are calculated as the last bars. Data for HBC is published before in [26], except for complex II with atpenin A5. Isolated mucosal tissue was used for colon control.

energy transfer system and enables to quantify the flux exerted by the different RC and the ATP synthasome complexes [27, 28, 79]. MCA can discriminate between two prevailing models: the former model, based on the assumption that each enzyme can be rate controlling to a different extent,

and a subsequent model, where whole metabolic pathway can behave as a single channel and inhibition of any of its components would give the same flux control [80]. Bianchi et al. proposed that both complexes I and III are highly rate controlling in NADH oxidation, suggesting the existence of

TABLE 2: FCCs for different components in mitochondrial Interactosome and ranges of the concentrations of inhibitors.

MI component	Inhibitor	Range of inhibitor concentration	FCC		
			HCC	Control colon tissue (mucosa)	HBC
Complex I	Rotenone	1–100 nM	0.56	0.45	0.46*
Complex II	Atpenin A5	0.1–6 μ M	0.12	0.13	0.28
Complex III	Antimycin	1–200 nM	0.68	0.66	0.54*
Complex IV	Na cyanide	0.1–40 μ M	0.31	0.50	0.74*
ANT	Carboxyatractyloside	1–200 nM	0.28	0.97	1.02*
ATP synthase	Oligomycin	1–600 nM	0.25	0.24	0.61*
Pi transporter	Mersalyl	1–200 μ M	0.43	0.53	0.60*
Sum 1, 3–7	Total (NADH)		2.08	2.82	3.36
Sum 2–7	Total (succinate)		2.07	3.03	3.78

Note: *from [26].

functional association between these two complexes [80]. To confirm the formation of supercomplexes in HCC- and HBC-skinned samples using MCA, we investigated the flux control coefficients (FCCs) for the complexes involved in aerobic NADH oxidation (I, III, and IV), in succinate oxidation (II, III, and IV), and for components of the ATP synthasome. For this purpose, cancerous and normal tissue samples were titrated with increasing concentrations of specific inhibitors against all of the ATP synthasome and RC complexes. Figure 4 summarizes the data analyzed in three different ways: by a graphical model [40, 41, 81], according to Small [82], and the Gellerich model [44]. The obtained FCC values did not depend on which exact method was used for calculations. The main problem in these calculations is high heterogeneity of the clinical material, which from the one hand originates from cancer molecular subtypes (e.g., Luminal A/B, HER2 or triple negative in HBC; unknown subtypes in HCC) but on the other hand originates from heterogeneity of tumor cells within each tumor [14] or irregular stromal burden. Therefore, the obtained coefficient values do not only depend on which patients were included to the study, but the results may also depend on which particular tumor region was used from each patient sample. This can be considered as an inevitable part in analyzing clinical samples.

Previous work has shown that the main respiratory rate-controlling steps in HBC cells are complex IV (FCC = 0.74) and adenine nucleotide transporter (ANT, FCC = 1.02) [26]. Similar control distribution was not observed within HCC ATP synthasome complex as FCCs for ANT were found to be significantly lower when HCC was compared to the results of healthy colon mucosa (FCC = 0.284 for HCC and FCC = 0.970 for healthy colon). These results show that ANT exerts high flux control in healthy colon tissue (and in HBC), but ANT seems to lose its limiting role in HCC. Ramsay et al. believe that hexokinase-voltage-dependent anion channel-ANT complex, which spans across the outer and inner mitochondrial membranes, is critical in cancer cells as this complex is the link between glycolysis, oxidative phosphorylation, and mitochondrial-mediated apoptosis [83]. Therefore, the difference between HBC and HCC, in regard to ANT-exerted flux control, indicates to distinct difference in energy metabolism between these two tumor types

(Table 2; Figure 4). In addition, HBC is showing equal FCCs for ATP synthase and inorganic phosphate transporter (Pi) in ATP synthasome, but this phenomenon is not characteristic neither for healthy colon mucosa nor for colorectal cancer. These alterations could be related to mitochondrial permeability transition pore (mtPTP) and apoptosis. Bernardi et al. studied the key regulatory features of the mtPTP [84–87], and the same group of authors has pointed to the fact that ANT can modulate the mtPTP, possibly through its effects on the surface potential, but it is not a mandatory component of this channel.

FCCs within the RC system in HBC do not differ significantly and the flux control is distributed almost uniformly throughout the different complexes (Table 2, Figure 4). Such condition is an indication of possible presence of protein supercomplexes (approximately equal values of FCCs for RC complexes I and III—0.46 versus 0.54, resp.). On the other hand, the flux distribution for normal colon tissue, when compared to HCC, showed slight difference for that for complex IV (FCC 0.50 versus 0.31), but flux control coefficients with close values were calculated for complex I (FCC 0.45 versus 0.56) and complex III (FCC 0.66 versus 0.68). Similarity in FCCs for complex I and complex III for both HCC and healthy colon tissue enables to propose that in healthy conditions, complex III is attached to complex I (possibly together with multiple copies of complex IV), but during carcinogenesis, the supercomplex assembly changes and even though complex I and complex III seem to stay linked, the participation of complex IV in this assembly becomes uncertain. Functional assembly of complexes I and III together with their rate-limiting roles will lead to sum of FCCs being greater than 1 [73] (see below).

Role of complex IV is multifaceted as three populations of it have previously been suggested: population assembled with complex I and complex III, population assembled with complex III alone and a non-interacting population [74]. Several data show that the absence of functional supercomplex assembly factor I (SCAF1) may be involved in distribution of complex IV [74, 75, 88]. As outlined in the review article by Enriquez, total cell respiration (glucose, pyruvate, and glutamine as substrates) was significantly higher in cells lacking functional SCAF1

[74]. High total cell respiration was registered also for both cancer types described in this paper, but presence or absence of functional SCAF1 was not investigated.

The sums of the determined FCCs within cancerous and healthy sample groups were calculated to be in the range from 2.07 to 3.78. In theory, sum of FCCs in a linear system is 1 [5, 40, 42–44, 89, 90], but the value of it can increase if the system includes enzyme–enzyme interactions, direct channeling, and/or recycling within multienzyme complexes (i.e., system becomes nonlinear) [79, 80, 91, 92]. The higher sum of FCCs from our tests is not a result of diffusion restrictions because the concentration ranges for all of the inhibitors in various samples were similar and did not depend on the nature of the samples [26, 28, 47, 48].

The organization of RC complexes in the mitochondrial inner membrane has been an object of intense debate and it is not studied systematically in human normal or cancerous tissues. Given the known theoretical framework, our results confirm the plasticity model and agree with the data from Bianchi et al. [80], but the distribution of complex IV remains unclear—both random distribution and association into I-III-IV supercomplex can be possible. Large FCC for complex II is not characteristic neither for HBC, for HCC, nor for healthy colon tissue, and therefore, our kinetic studies confirmed previous findings that this complex is not a part of RC supercomplexes.

The question about the changes in the composition and stoichiometry of protein supercomplexes, which result from carcinogenesis, needs further studies, and in addition, as mitochondria have other additional roles in cellular metabolism, it can be presumed that changes in RC are also affecting cataplerotic processes sprouting from the mitochondria, but such link has not yet been studied yet.

3.2. ADP-Regulated Mitochondrial Respiration in HBC and HCC Fibers. Table 3 summarizes ADP-regulated mitochondrial respiration parameters determined for skinned tissue samples taken from both patient groups. Differences in the rates of maximal ADP-activated respiration (V_{\max}) in colon tissue samples are corresponding to the differences in the content of mitochondria in these cells (the amount of mitochondria in HCC is 50% higher than that in healthy control tissue [28] (supplementary Table 1)). Our previous experiments have shown that HBC tissue, too, contains an increased number of mitochondria in comparison to its adjacent normal tissue [27, 93] (supplementary Table 1). As indicated above, ADP-dependent respiration in healthy human breast tissue is absent. Breast samples contain lot of fat tissue, but low V_{\max} values were evident even if clearly lobular/ductal structures were separated and tested. Low respiratory capacity can also be indicating to lowered metabolic activity in normal ductal/lobular tissue in older women (average age of HBC patients in this study was 63.4 years). In contrast to normal breast tissue, the colon control tissue samples have significantly higher respiration rates (Table 3). Specifically, respiratory capacity is higher in apparent mucosal/submucosal section of the normal colon tissue samples compared to that of the underlying smooth muscle part as we manually

TABLE 3: Apparent K_m ($^{app}K_m$) and maximal rate of respiration (V_{\max}) values for ADP-dependent respiration calculated for HBC, HCC and their adjacent healthy tissue samples.

Tissues	$^{app}K_m, \mu M \pm SEM$	$V_{\max} \pm SEM$
Human breast cancer tissue	114.8 \pm 13.6*	1.09 \pm 0.04*
Healthy adjacent breast control tissue	—	0.02 \pm 0.01*
Human colorectal cancer tissue	93.6 \pm 7.7**	2.41 \pm 0.32
Healthy adjacent colon control tissue	256** \pm 34	0.71 \pm 0.23

Note: * from [26] and ** [38]; V_{\max} values are presented as nM O₂/min/mg dry tissue weight without proton leak rates. These K_m and V_{\max} values for ADP were determined from corresponding titration curves by fitting experimental data to non-linear regression equation according to a Michaelis–Menten model. 35 patients used for analysis of HBC and 35 for HCC.

separated and tested these two layers in a selection of colon tissue samples (Figure 5(b)).

HBC arises from tissue with almost absent ADP-related respiration, but once formed, the mechanism of energy conversion seems to acquire a more complicated form and it can be associated with both increased mitochondrial biogenesis and interplay between cancer and stromal cells [26]. HBC can be classified into four clinically distinct and significant molecular subtypes: luminal-A, luminal-B, HER2 expressing, and triple negative. Clinically, luminal-A is considered the least and triple negative as the most aggressive subtype. Therefore, we expected to see clear differences when respiratory parameters of those two extreme subtypes were measured. Initially, respiration rates were analyzed in Luminal-A type MCF7 and triple negative MDA-MB-231 cell lines. When compared, respiration rates in presence of glutamate or pyruvate clearly showed that oxygen consumption in luminal-A subtype cells is remarkably higher (Figure 5(b)). But in contrast, the exact opposite was registered for the same parameters in clinical samples (Figure 5(a)) as the highest respiratory rates were registered for the most aggressive triple negative subtype. From the one hand, this contradicting result shows that cell cultures are not directly comparable to respective clinical counterparts and can lead to misleading expectations. On the other hand, it proves that the role of OXPHOS becomes increasingly important in clinical samples as aggressiveness of the tumor increases, but it is not evident in the respective culture cells. In the present case, it is not a result of increased glucose availability in the growth medium, which could lead the cells to acquire glycolytic phenotype and explain the difference with clinical samples, because low-glucose media was used.

For HCC, which is without distinct clinical subtypes, we compared disease stage to average V_{\max} value for that stage (Figure 6(a)). Even though increase in V_{\max} in initial stages can be calculated in comparison to control sample, the decrease in V_{\max} for stages IIIC and IVB does not fit this increase in dependence. The disease stage at diagnosis itself is not a valid marker of aggressiveness and therefore such plotting can be debated. Therefore, we gathered initial longitudinal data on patient progression in our HCC cohort and confirmed that 7 out of 32 eligible patients had died (median

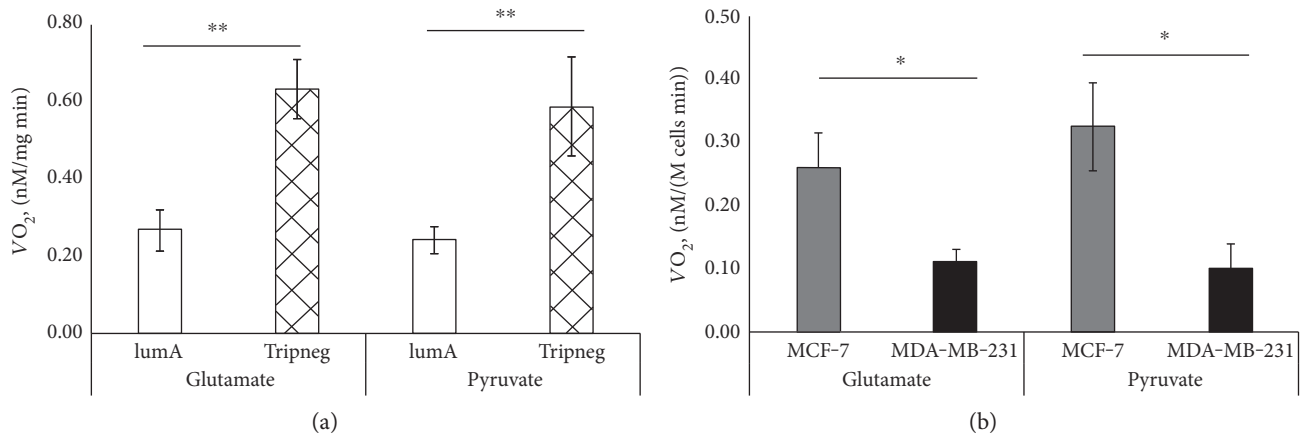


FIGURE 5: (a) Respiration rates for clinical samples of luminal-A and triple negative HBC subtypes in the presence of 5 mM glutamate or 5 mM pyruvate; $n = 13/12$ for luminal-A and $n = 7/8$ for triple negative subtypes, respectively. (b) Respiratory rates for luminal-A type MCF-7 and triple negative MDA-MB-231 cells in the presence of 5 mM glutamate or 5 mM pyruvate; $n = 3$ for each measurement; * $p < 0.05$, ** $p < 0.005$.

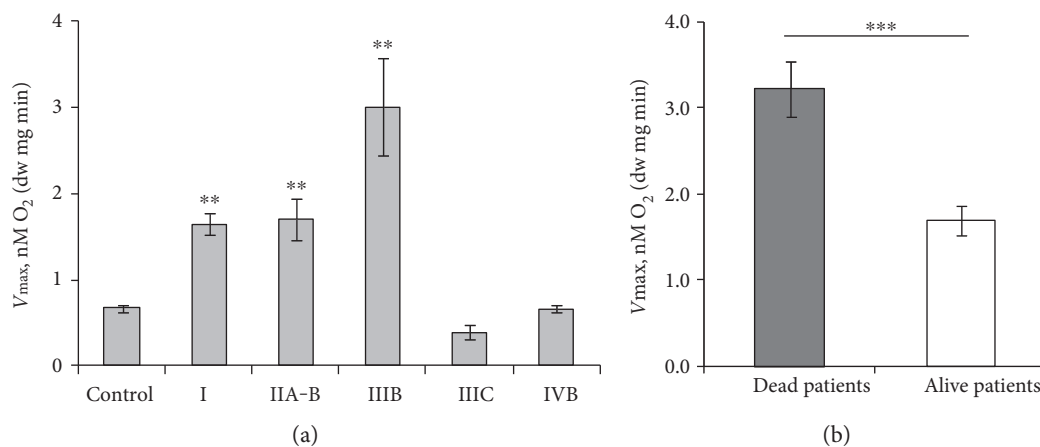


FIGURE 6: (a) Dependence of maximal rate of mitochondrial respiration (V_{max}) compared with the HCC at different stages. Stage I was calculated as the mean of 13 patients, IIA, IIB - 13 patients, IIIB-4 patients, IIIC-3 patients and IVB-1 patient. Control colon tissue is obtained from 34 patients. Maximal respiration rate V_{max} is compared with that in control tissue. Bars are SEM; ** $p < 0.005$. (b) V_{max} in HCC patients based on disease state in follow-up setting. Seven patients out of 32 are confirmed to have succumbed to HCC ($V_{max} = 3.19 \pm 0.34$); 25 patients out of 32 stay in remission ($V_{max} = 1.70 \pm 0.17$), *** $p < 0.001$.

follow-up time 47.3 ± 4.9 months). V_{max} values in patients that succumbed to the disease were significantly higher than that in the currently not progressed group (Figure 6(b)). As was shown for HBC above, higher respiratory capacity was registered for the most aggressive triple negative subgroup. Therefore, it can be argued based on similarity that higher tumor respiratory parameters in the dead HCC patients were indicating to more aggressive disease. In addition, lower than expected respiratory rate in some triple negative tumors can therefore indicate that given patient, when compared to the average in the triple negative subgroup, has less aggressive disease than could be expected. To confirm this in larger cohorts and relate aggressiveness in HCC and HBC to V_{max} value, additional longitudinal studies are necessary.

We next measured apparent Michaelis–Menten constants (K_m) for ADP to characterize the affinity of mitochondria for exogenous ADP (i.e., permeability of mitochondrial outer membrane). Corresponding K_m values for permeabilized tumor and nontumorous tissues were determined from titration experiments using exogenously added ADP. The obtained data were plotted as rates of O_2 consumption versus ADP concentration and apparent K_m values were calculated from these plots by nonlinear regression equation. Healthy colon tissue displayed low affinity for ADP ($K_m = 256 \pm 3 \mu M$), whereas that in HCC is significantly higher ($K_m = 93.6 \pm 7.7 \mu M$) [38]. The K_m (ADP) value for HBC tissue samples ($K_m = 114.8 \pm 13.6 \mu M$) was similar to that for HCC [26].

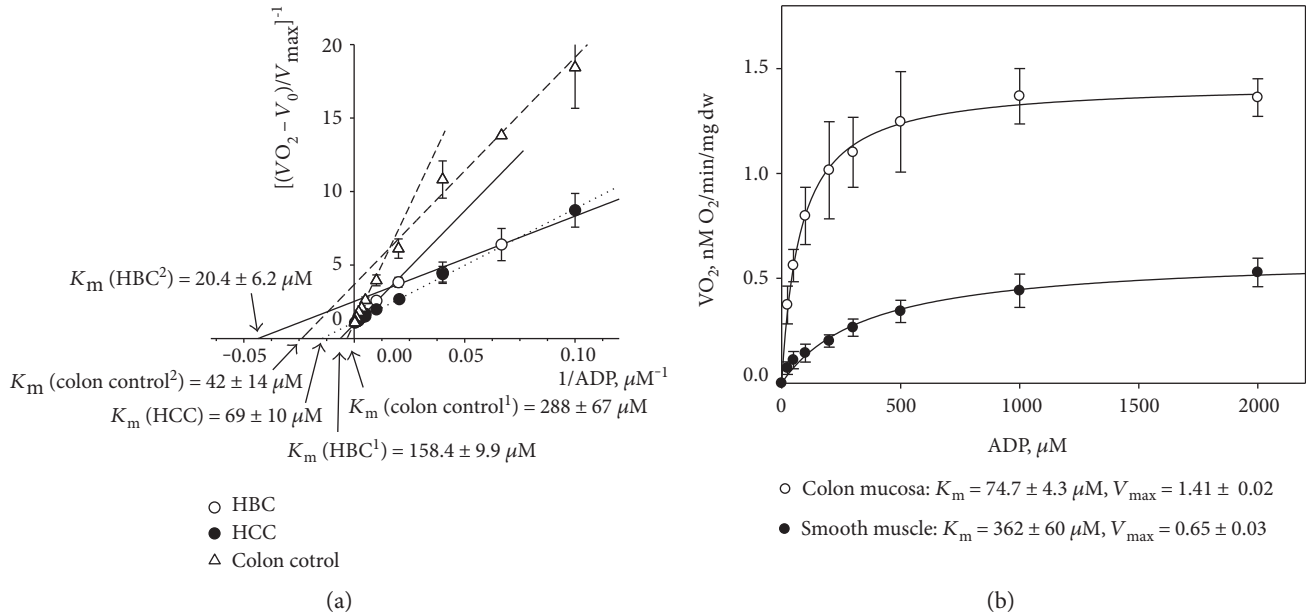


FIGURE 7: (a) Dependences of normalized respiration rate values for HCC (dotted line), HBC (solid line), and healthy colon tissue samples (dashed line); double reciprocal Lineweaver-Burk plots. Samples from 32 patients with breast cancer and 10 patients with colorectal cancer were examined. (b) ADP-dependent respiration in healthy colon mucosa and smooth muscle tissue samples (Michaelis-Menten curve, $n = 8$). Here, V_0 and V_{max} are rates of basal and maximal ADP-activated respiration, respectively.

According to the classical studies by Chance and Williams [94, 95] and the data of many other investigators [29, 30, 37], the apparent K_m value for ADP for isolated mitochondria is low, about $15 \mu M$, but the observed apparent K_m values in our study for permeabilized clinical HBC and HCC samples were 6–8 times higher than this value (Table 3). Our previous studies have shown that sensitivity of the mitochondrial respiration for exogenous ADP for permeabilized NB HL-1 cells is also high as the apparent K_m equaled to $25 \pm 4 \mu M$ and was similar to that of isolated heart mitochondria [34, 96]. The similar low apparent K_m values were also registered for undifferentiated and differentiated neuroblastoma culture cells, where the corresponding K_m for ADP were measured as $20.3 \pm 1.4 \mu M$ and $19.4 \pm 3.2 \mu M$, respectively [97]. The registered difference between culture cells and clinical samples, despite the used preparation method, again indicates to differences present in these two sample groups.

We treated permeabilized samples with incremental concentrations of ADP and the measured O_2 consumption rates (normalized to V_{max}) were analyzed against respective ADP concentration values as double reciprocal Lineweaver-Burk plots (Figures 7(a) and 7(b)) [29]. Figure 7(a) shows the results of the Lineweaver-Burk treatment of the experimental data linked with ADP-regulated mitochondrial respiration in skinned fibers of HCC, healthy colon, and HBC. Corresponding V_{max} and K_m values were calculated from the linearization approach. Saks and colleagues have previously shown that the presence of biphasic respiration regulation on the graph curve indicates the existence of two populations of mitochondria with different affinities for ADP [29]. Our results indicated such differences in colon

control and HBC samples. Specifically, monophasic regulation of mitochondrial respiration is apparent in HCC tissue, but in healthy colon tissue, two populations of mitochondria with very different properties were found (Figure 7(a)). One population of mitochondria is characterized with lower K_m ($42 \pm 14 \mu M$), whereas the apparent K_m (ADP) value for the second mitochondrial population is nearly seven times higher ($288 \pm 67 \mu M$). We thereafter again separated mucosal and smooth muscle parts from the colon samples before additional K_m measurements to characterize their isolated contributions. Apparent K_m value for mucosal part was measured to be $74.7 \pm 4.3 \mu M$ and the same value for colon smooth muscle tissues was found to be $362 \pm 60 \mu M$ (Figure 7(b)). Therefore, results after separation explain the results from the initial experiment where the entire colon wall was analyzed and two separate groups of mitochondria were discovered. Additionally, we could also distinguish two differently regulated types of mitochondria in HBC samples: one with apparent K_m value for MgADP of $20.4 \pm 6.2 \mu M$, but the same for the second mitochondrial population was nearly ten times higher, $158.5 \pm 9.9 \mu M$ (Figure 4(a)). The phenomenon shown in Figure 7(a) can be associated, on the one hand, simply with elevated stromal content (in such case, similar results should have been also registered for HCC), but on the other hand, with possible two-compartment tumor metabolism in HBC, what states that tumor cells function as metabolic parasites and extract energy from supporting host cells such as fibroblasts [98–103]. In such case, the stromal part of the HBC samples can be characterized with glycolytic metabolism representing the low K_m value due to high levels of autophagy, mitophagy, glycolysis, and lipolysis, while cancer cells

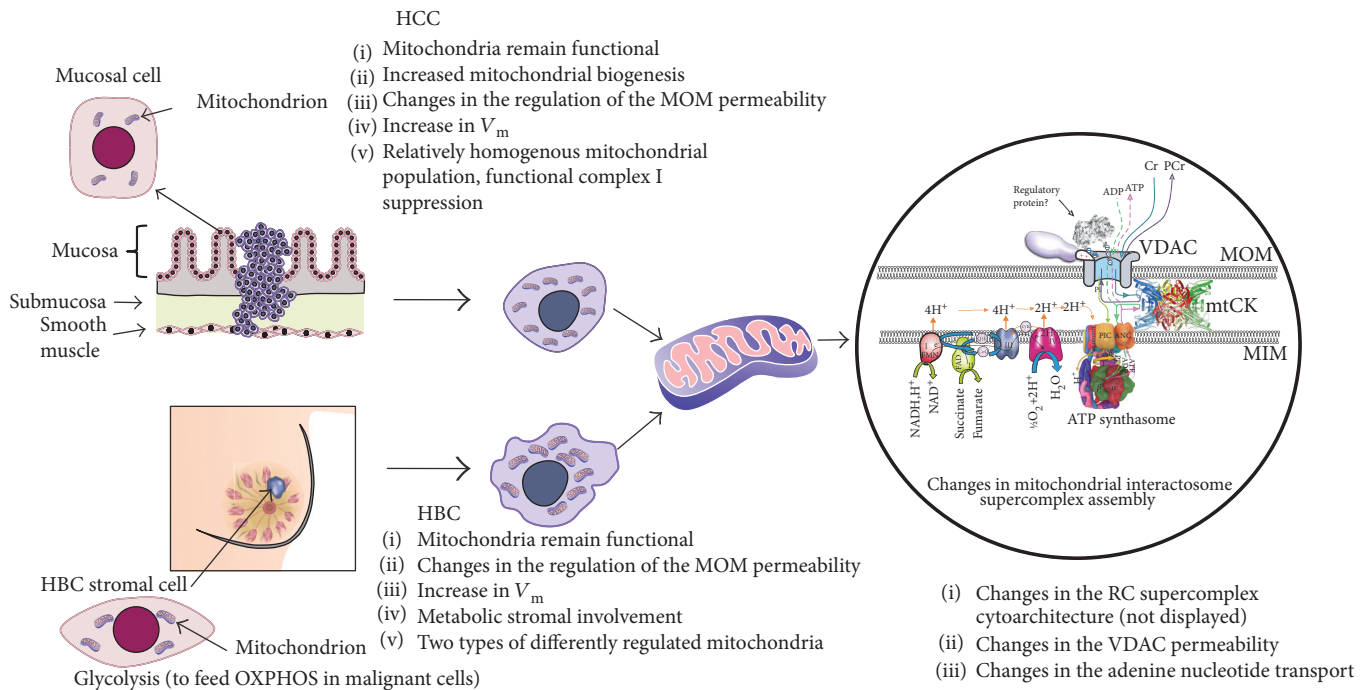


FIGURE 8: Mitochondrial alterations in HCC and HBC tissue cells. Mitochondrial interactosome is a large supercomplex consisting of ATP synthasome, VDAC, mitochondrial kinases like adenylate kinase, hexokinase or mitochondrial creatine kinase (MtCK), and respiratory chain (super)complexes. Here, the octameric MtCK characteristic is shown for the striated muscles and also as the possible component of the MI in the healthy colon [108–110]. The complex of VDAC together with other proteins controls the exchange of adenine nucleotides and regulates energy fluxes between mitochondrial and cytosolic compartments. Changes in the structure and function of MI are the important parts of cancer mitochondrial metabolism.

have high mitochondrial mass, OXPHOS, and β -oxidation activity, which is represented by the mitochondrial population with the high K_m (ADP) values. From the given comparison between HBC and HCC, the two subpopulations of mitochondria are specific only to HBC samples (confirmed in 32 cases out of the total 34) but not to HCC samples, and it indicates that tumor formation leads to distinct changes, which is related to the tissue type the tumor originates from.

Altogether, these results indicate the remarkable differences in the regulation of mitochondrial outer membrane (MOM) permeability between cultured tumor cells and clinical material (including between different tumor types and even between patients). Even further, the results can be contradictory as registered for respiration parameters. It can be estimated, based on the results from our lab, that low K_m value for ADP can be a common characteristic for cancer cells grown in culture, but in *in vivo* tumor samples, the regulation of MOM permeability is more complicated and probably related to interplay between energy transfer pathways and changes in the phosphorylation state of VDAC channels [32, 104–107] and also with modulation of cytoskeleton or membrane potential as a result of tumor formation.

4. Concluding Remarks

To understand the energy metabolism of tumors, it is necessary to detect bioenergetic fingerprints of each individual

tumor type. Our results confirmed that respiratory capacity is preserved in both HBC and HCC as these both demonstrated substantial rates of oxidative phosphorylation, which contradicts with earlier widespread understanding that the metabolism of human breast and colorectal carcinomas is prevalently glycolytic. Studies on cell lines up to now have led to many lifesaving technologies and treatments in humans, but the scientific level might be nearing the end of readily transferrable results between the cell model and human physiology. Our results indicated that apparent glycolytic nature of some breast cancer types could be expected based on cell cultures, but this presumption was in sharp conflict when culture cell results were compared with these from respective clinical samples. In addition, when compared to their healthy adjacent tissue, both clinical cancer types showed increased respiratory capacity. Despite the increased respiratory capacity in HCC, relative deficiency of complex I was registered for it on the functional level Western blot analysis was not sufficient to confirm this deficiency on the protein level as two different antibody approaches gave conflicting results, but this result proves the necessity to measure pathways also on the functional level whenever possible to compare the function to steady-state markers like presence or abundance of certain enzymes. Our experiments indicate that the respiratory chain and ATP synthasome can form macromolecular assemblies (supercomplexes) with reorganized composition and/or stoichiometry while the changes are specific for different tumor types. This is in good agreement with recent studies from other laboratories [25] and

the current work shows that equal results can be obtained using kinetic methods, but additional studies are warranted to include results from protein level studies using the blue native gel electrophoresis (BNGE) technique. Our K_m measurements confirmed that two populations of mitochondria registered in healthy colon tissue can be categorized as different layers of the colon wall, but in HBC, the subgroups can be linked to two-compartment metabolism where tumor acts as a metabolic parasite on normal stromal cells. Mitochondria of HCC are homogenous in terms of regulation of the mitochondrial outer membrane permeability and MCA (Figure 8).

Mitochondria are not only the centers of cellular energy conversion but are also the important part in biosynthetic metabolism and apoptosis. Therefore, direct detection of profound changes in the ATP synthasome components and in the architecture of the respiratory chain complexes, as shown in the current work, can support development of new predictive models or therapies.

Abbreviations

ANT:	Adenine nucleotide translocator
CAT:	Carboxyatractyloside
COX:	Cytochrome c oxidase
FCC:	Flux control coefficient
HBC:	Human breast cancer
HCC:	Human colorectal cancer
HK:	Hexokinase
MCA:	Metabolic control analysis
MI:	Mitochondrial interactosome
MOM:	Mitochondrial outer membrane
MtCK:	Mitochondrial creatine kinase
mtPTP:	Mitochondrial permeability transition pore
OXPHOS:	Oxidative phosphorylation
RC:	Respiratory chain
SCAF1:	Supercomplex assembly factor I
TME:	Tumor microenvironment
VDAC:	Voltage-dependent anion channel.

Additional Points

Highlights. (1) Relative complex I functional deficiency is characteristic for HCC but not for HBC. (2) HBC respiratory capacity severely higher than in adjacent normal breast tissue. (3) Complexes I and III expectedly assembled in both tumorous and normal tissues. (4) K_m for ADP shows distinct differences between cell cultures and clinical samples. (5) Two distinct mitochondrial populations present in HBC but not in HCC.

Conflicts of Interest

The authors declare that they have no conflicts of interest.

Acknowledgments

This work was supported by the institutional research funding IUT23-1 of the Estonian Ministry of Education.

References

- [1] S. Rodriguez-Enriquez, L. Hernández-Esquivel, A. Marín-Hernández et al., "Mitochondrial free fatty acid beta-oxidation supports oxidative phosphorylation and proliferation in cancer cells," *The International Journal of Biochemistry & Cell Biology*, vol. 65, pp. 209–221, 2015.
- [2] L. S. Gomez, P. Zancan, M. C. Marcondes et al., "Resveratrol decreases breast cancer cell viability and glucose metabolism by inhibiting 6-phosphofructo-1-kinase," *Biochimie*, vol. 95, no. 6, pp. 1336–1343, 2013.
- [3] Y. Ma, R. K. Bai, R. Trieu, and L. J. Wong, "Mitochondrial dysfunction in human breast cancer cells and their trans-mitochondrial cybrids," *Biochimica et Biophysica Acta (BBA) - Bioenergetics*, vol. 1797, no. 1, pp. 29–37, 2010.
- [4] R. C. Sun, M. Fadia, J. E. Dahlstrom, C. R. Parish, P. G. Board, and A. C. Blackburn, "Reversal of the glycolytic phenotype by dichloroacetate inhibits metastatic breast cancer cell growth in vitro and in vivo," *Breast Cancer Research and Treatment*, vol. 120, no. 1, pp. 253–260, 2010.
- [5] R. Moreno-Sanchez, A. Marín-Hernández, E. Saavedra, J. P. Pardo, S. J. Ralph, and S. Rodríguez-Enriquez, "Who controls the ATP supply in cancer cells? Biochemistry lessons to understand cancer energy metabolism," *The International Journal of Biochemistry & Cell Biology*, vol. 50, pp. 10–23, 2014.
- [6] S. Rodriguez-Enriquez, J. C. Gallardo-Pérez, A. Marín-Hernández et al., "Oxidative phosphorylation as a target to arrest malignant neoplasias," *Current Medicinal Chemistry*, vol. 18, no. 21, pp. 3156–3167, 2011.
- [7] O. Warburg, "On respiratory impairment in cancer cells," *Science*, vol. 124, no. 3215, pp. 269–270, 1956.
- [8] M. P. Lisanti, U. E. Martinez-Outschoorn, and F. Sotgia, "Oncogenes induce the cancer-associated fibroblast phenotype: metabolic symbiosis and "fibroblast addiction" are new therapeutic targets for drug discovery," *Cell Cycle*, vol. 12, no. 17, pp. 2740–2749, 2013.
- [9] F. Sotgia, D. Whitaker-Menezes, U. E. Martinez-Outschoorn et al., "Mitochondrial metabolism in cancer metastasis: visualizing tumor cell mitochondria and the "reverse Warburg effect" in positive lymph node tissue," *Cell Cycle*, vol. 11, no. 7, pp. 1445–1454, 2012.
- [10] A. K. Witkiewicz, D. Whitaker-Menezes, A. Dasgupta et al., "Using the "reverse Warburg effect" to identify high-risk breast cancer patients: stromal MCT4 predicts poor clinical outcome in triple-negative breast cancers," *Cell Cycle*, vol. 11, no. 6, pp. 1108–1117, 2012.
- [11] K. Smolkova, L. Plecítá-Hlavatá, N. Bellance, G. Benard, R. Rossignol, and P. Ježek, "Waves of gene regulation suppress and then restore oxidative phosphorylation in cancer cells," *The International Journal of Biochemistry & Cell Biology*, vol. 43, no. 7, pp. 950–968, 2011.
- [12] V. L. Payen, P. E. Porporato, B. Baselet, and P. Sonveaux, "Metabolic changes associated with tumor metastasis, part 1: tumor pH, glycolysis and the pentose phosphate pathway," *Cellular and Molecular Life Sciences*, vol. 73, no. 7, pp. 1333–1348, 2016.
- [13] M. A. Swartz, N. Iida, E. W. Roberts et al., "Tumor microenvironment complexity: emerging roles in cancer therapy," *Cancer Research*, vol. 72, no. 10, pp. 2473–2480, 2012.
- [14] N. McGranahan and C. Swanton, "Biological and therapeutic impact of intratumor heterogeneity in cancer evolution," *Cancer Cell*, vol. 27, no. 1, pp. 15–26, 2015.

- [15] R. H. Swerdlow, E. Lezi, D. Aires, and J. Lu, "Glycolysis-respiration relationships in a neuroblastoma cell line," *Biochimica et Biophysica Acta (BBA) - General Subjects*, vol. 1830, no. 4, pp. 2891–2898, 2013.
- [16] C. Jose and R. Rossignol, "Rationale for mitochondria-targeting strategies in cancer bioenergetic therapies," *The International Journal of Biochemistry & Cell Biology*, vol. 45, no. 1, pp. 123–129, 2013.
- [17] E. Gnaiger and R. B. Kemp, "Anaerobic metabolism in aerobic mammalian cells: information from the ratio of calorimetric heat flux and respirometric oxygen flux," *Biochimica et Biophysica Acta (BBA) - Bioenergetics*, vol. 1016, no. 3, pp. 328–332, 1990.
- [18] G. Gstraunthaler, T. Seppi, and W. Pfaller, "Impact of culture conditions, culture media volumes, and glucose content on metabolic properties of renal epithelial cell cultures. Are renal cells in tissue culture hypoxic?" *Cellular Physiology and Biochemistry*, vol. 9, no. 3, pp. 150–172, 1999.
- [19] C. J. Sherr and R. A. DePinho, "Cellular senescence: mitotic clock or culture shock?" *Cell*, vol. 102, no. 4, pp. 407–410, 2000.
- [20] R. Moreno-Sanchez, E. Saavedra, J. C. Gallardo-Pérez, F. D. Rumjanek, and S. Rodríguez-Enríquez, "Understanding the cancer cell phenotype beyond the limitations of current omics analyses," *The FEBS Journal*, vol. 283, no. 1, pp. 54–73, 2016.
- [21] G. Lenaz and M. L. Genova, "Kinetics of integrated electron transfer in the mitochondrial respiratory chain: random collisions vs. solid state electron channeling," *American Journal of Physiology. Cell Physiology*, vol. 292, no. 4, pp. C1221–C1239, 2007.
- [22] N. Timohhina, R. Guzun, K. Tepp et al., "Direct measurement of energy fluxes from mitochondria into cytoplasm in permeabilized cardiac cells in situ: some evidence for mitochondrial interactosome," *Journal of Bioenergetics and Biomembranes*, vol. 41, no. 3, pp. 259–275, 2009.
- [23] G. Lenaz and M. L. Genova, "Structural and functional organization of the mitochondrial respiratory chain: a dynamic super-assembly," *The International Journal of Biochemistry & Cell Biology*, vol. 41, no. 10, pp. 1750–1772, 2009.
- [24] J. Vonck and E. Schafer, "Supramolecular organization of protein complexes in the mitochondrial inner membrane," *Biochimica et Biophysica Acta (BBA) - Molecular Cell Research*, vol. 1793, no. 1, pp. 117–124, 2009.
- [25] K. Rohlenova, K. Sachaphibulkij, J. Stursa et al., "Selective disruption of respiratory supercomplexes as a new strategy to suppress Her2high breast cancer," *Antioxidants & Redox Signaling*, vol. 26, no. 2, pp. 84–103, 2017.
- [26] T. Kaambre, V. Chekulayev, I. Shevchuk et al., "Metabolic control analysis of cellular respiration in situ in intraoperational samples of human breast cancer," *Journal of Bioenergetics and Biomembranes*, vol. 44, no. 5, pp. 539–558, 2012.
- [27] T. Kaambre, V. Chekulayev, I. Shevchuk et al., "Metabolic control analysis of respiration in human cancer tissue," *Frontiers in Physiology*, vol. 4, article 151, pp. 1–6, 2013.
- [28] A. Kaldma, A. Klepinin, V. Chekulayev et al., "An in situ study of bioenergetic properties of human colorectal cancer: the regulation of mitochondrial respiration and distribution of flux control among the components of ATP synthasome," *The International Journal of Biochemistry & Cell Biology*, vol. 55, pp. 171–186, 2014.
- [29] V. A. Saks, V. I. Veksler, A. V. Kuznetsov et al., "Permeabilized cell and skinned fiber techniques in studies of mitochondrial function in vivo," *Molecular and Cellular Biochemistry*, vol. 184, no. 1-2, pp. 81–100, 1998.
- [30] A. V. Kuznetsov, D. Strobl, E. Ruttman, A. Königsrainer, R. Margreiter, and E. Gnaiger, "Evaluation of mitochondrial respiratory function in small biopsies of liver," *Analytical Biochemistry*, vol. 305, no. 2, pp. 186–194, 2002.
- [31] A. V. Kuznetsov, "Structural organization and dynamics of mitochondria in the cells in vivo," in *Molecular System Bioenergetics: Energy for Life*, V. Saks, Ed., pp. 137–162, Wiley-VCH Verlag GmbH & Co KGaA, Weinheim, Germany, 2007.
- [32] M. Varikmaa, R. Bagur, T. Kaambre et al., "Role of mitochondria-cytoskeleton interactions in respiration regulation and mitochondrial organization in striated muscles," *Biochimica et Biophysica Acta (BBA) - Bioenergetics*, vol. 1837, no. 2, pp. 232–245, 2014.
- [33] A. V. Kuznetsov, V. Veksler, F. N. Gellerich, V. Saks, R. Margreiter, and W. S. Kunz, "Analysis of mitochondrial function in situ in permeabilized muscle fibers, tissues and cells," *Nature Protocols*, vol. 3, no. 6, pp. 965–976, 2008.
- [34] C. Monge, N. Beraud, K. Tepp et al., "Comparative analysis of the bioenergetics of adult cardiomyocytes and nonbeating HL-1 cells: respiratory chain activities, glycolytic enzyme profiles, and metabolic fluxes," *Canadian Journal of Physiology and Pharmacology*, vol. 87, no. 4, pp. 318–326, 2009.
- [35] F. Appaix, A. V. Kuznetsov, Y. Usson et al., "Possible role of cytoskeleton in intracellular arrangement and regulation of mitochondria," *Experimental Physiology*, vol. 88, no. 1, pp. 175–190, 2003.
- [36] A. V. Kuznetsov, T. Tiivel, P. Sikk et al., "Striking differences between the kinetics of regulation of respiration by ADP in slow-twitch and fast-twitch muscles in vivo," *European Journal of Biochemistry*, vol. 241, no. 3, pp. 909–915, 1996.
- [37] V. A. Saks, A. V. Kuznetsov, Z. A. Khuchua et al., "Control of cellular respiration in vivo by mitochondrial outer membrane and by creatine kinase. A new speculative hypothesis: possible involvement of mitochondrial-cytoskeleton interactions," *Journal of Molecular and Cellular Cardiology*, vol. 27, no. 1, pp. 625–645, 1995.
- [38] V. Chekulayev, K. Mado, I. Shevchuk et al., "Metabolic remodeling in human colorectal cancer and surrounding tissues: alterations in regulation of mitochondrial respiration and metabolic fluxes," *Biochemistry and Biophysics Reports*, vol. 4, pp. 111–125, 2015.
- [39] E. Gnaiger, "Oxygen solubility in experimental media," *OROBOROS Bioenerg. News*, vol. 6, no. 3, pp. 1–6, 2001.
- [40] H. Kacser and J. A. Burns, "The control of flux," *Symposia of the Society for Experimental Biology*, vol. 27, pp. 65–104, 1973.
- [41] D. Fell, "Understanding the control of metabolism," in *Frontiers in Metabolism 2*, K. Snell, Ed., vol. xiip. 301, Portland Press, London, Miami, 1997.
- [42] D. Fell, "Metabolic control analysis," in *Systems Biology*, L. Alberghina and H. V. Westerhoff, Eds., pp. 69–80, Springer: Verlag, Berlin, 2005.
- [43] R. Moreno-Sanchez, E. Saavedra, S. Rodríguez-Enríquez, and V. Olín-Sandoval, "Metabolic control analysis: a tool for designing strategies to manipulate metabolic pathways," *Journal of Biomedicine & Biotechnology*, vol. 2008, Article ID 597913, 30 pages, 2008.
- [44] F. N. Gellerich, W. S. Kunz, and R. Bohnensack, "Estimation of flux control coefficients from inhibitor titrations by non-

- linear regression," *FEBS Letters*, vol. 274, no. 1-2, pp. 167–170, 1990.
- [45] A. V. Kuznetsov, J. F. Clark, K. Winkler, and W. S. Kunz, "Increase of flux control of cytochrome c oxidase in copper-deficient mottled brindled mice," *The Journal of Biological Chemistry*, vol. 271, no. 1, pp. 283–288, 1996.
- [46] A. V. Kuznetsov, K. Winkler, E. Kirches, H. Lins, H. Feistner, and W. S. Kunz, "Application of inhibitor titrations for the detection of oxidative phosphorylation defects in saponin-skinned muscle fibers of patients with mitochondrial diseases," *Biochimica et Biophysica Acta (BBA) - Molecular Basis of Disease*, vol. 1360, no. 2, pp. 142–150, 1997.
- [47] K. Tepp, I. Shevchuk, V. Chekulayev et al., "High efficiency of energy flux controls within mitochondrial interactosome in cardiac intracellular energetic units," *Biochimica et Biophysica Acta (BBA) - Bioenergetics*, vol. 1807, no. 12, pp. 1549–1561, 2011.
- [48] K. Tepp, N. Timohhina, V. Chekulayev, I. Shevchuk, T. Kaambre, and V. Saks, "Metabolic control analysis of integrated energy metabolism in permeabilized cardiomyocytes - experimental study," *Acta Biochimica Polonica*, vol. 57, no. 4, pp. 421–430, 2010.
- [49] P. A. Srere, "[1] Citrate synthase," *Methods in Enzymology*, vol. 13, pp. 3–11, 1969.
- [50] M. Davoudi, H. Kotarsky, E. Hansson, and V. Fellman, "Complex I function and supercomplex formation are preserved in liver mitochondria despite progressive complex III deficiency," *PloS One*, vol. 9, no. 1, article e86767, 2014.
- [51] M. Castro-Gago, M. O. Blanco-Barca, C. Gómez-Lado, J. Eiris-Puñal, Y. Campos-González, and J. Arenas-Barbero, "Respiratory chain complex I deficiency in an infant with Ohtahara syndrome," *Brain dev*, vol. 31, no. 4, pp. 322–325, 2009.
- [52] J. Finsterer, G. G. Kovacs, H. Rauschka, and U. Ahting, "Adult, isolated respiratory chain complex IV deficiency with minimal manifestations," *Folia Neuropathologica*, vol. 53, no. 2, pp. 153–157, 2015.
- [53] D. Mowat, D. M. Kirby, K. R. Kamath, A. Kan, D. R. Thorburn, and J. Christodoulou, "Respiratory chain complex III [correction of complex] in deficiency with pruritus: a novel vitamin responsive clinical feature," *The Journal of Pediatrics*, vol. 134, no. 3, pp. 352–354, 1999.
- [54] A. Lemarie and S. Grimm, "Mitochondrial respiratory chain complexes: apoptosis sensors mutated in cancer?" *Oncogene*, vol. 30, no. 38, pp. 3985–4003, 2011.
- [55] M. Eimre, K. Paju, S. Pelloux et al., "Distinct organization of energy metabolism in HL-1 cardiac cell line and cardiomyocytes," *Biochimica et Biophysica Acta (BBA) - Bioenergetics*, vol. 1777, no. 6, pp. 514–524, 2008.
- [56] E. Seppet, M. Eimre, N. Peet et al., "Compartmentation of energy metabolism in atrial myocardium of patients undergoing cardiac surgery," *Molecular and Cellular Biochemistry*, vol. 270, no. 1-2, pp. 49–61, 2005.
- [57] N. Parker, A. Vidal-Puig, and M. D. Brand, "Stimulation of mitochondrial proton conductance by hydroxynonenal requires a high membrane potential," *Bioscience Reports*, vol. 28, no. 2, pp. 83–88, 2008.
- [58] M. Puurand, N. Peet, A. Piirsoo et al., "Deficiency of the complex I of the mitochondrial respiratory chain but improved adenylate control over succinate-dependent respiration are human gastric cancer-specific phenomena," *Molecular and Cellular Biochemistry*, vol. 370, no. 1-2, pp. 69–78, 2012.
- [59] R. H. Triepels, L. P. Van Den Heuvel, J. M. Trijbels, and J. A. Smeitink, "Respiratory chain complex I deficiency," *American Journal of Medical Genetics*, vol. 106, no. 1, pp. 37–45, 2001.
- [60] H. Swalwell, D. M. Kirby, E. L. Blakely et al., "Respiratory chain complex I deficiency caused by mitochondrial DNA mutations," *European Journal of Human Genetics*, vol. 19, no. 7, pp. 769–775, 2011.
- [61] E. Ostergaard, R. J. Rodenburg, M. van den Brand et al., "Respiratory chain complex I deficiency due to NDUFA12 mutations as a new cause of Leigh syndrome," *Journal of Medical Genetics*, vol. 48, no. 11, pp. 737–740, 2011.
- [62] D. M. Kirby, M. Crawford, M. A. Cleary, H. H. Dahl, X. Dennett, and D. R. Thorburn, "Respiratory chain complex I deficiency: an underdiagnosed energy generation disorder," *Neurology*, vol. 52, no. 6, pp. 1255–1264, 1999.
- [63] H. Simonnet, J. Demont, K. Pfeiffer et al., "Mitochondrial complex I is deficient in renal oncocytomas," *Carcinogenesis*, vol. 24, no. 9, pp. 1461–1466, 2003.
- [64] M. Gruno, N. Peet, A. Tein et al., "Atrophic gastritis: deficient complex I of the respiratory chain in the mitochondria of corpus mucosal cells," *Journal of Gastroenterology*, vol. 43, no. 10, pp. 780–788, 2008.
- [65] H. Y. Lim, Q. S. Ho, J. Low, M. Choolani, and K. P. Wong, "Respiratory competent mitochondria in human ovarian and peritoneal cancer," *Mitochondrion*, vol. 11, no. 3, pp. 437–443, 2011.
- [66] E. Bonora, A. M. Porcelli, G. Gasparre et al., "Defective oxidative phosphorylation in thyroid oncocyctic carcinoma is associated with pathogenic mitochondrial DNA mutations affecting complexes I and III," *Cancer Research*, vol. 66, no. 12, pp. 6087–6096, 2006.
- [67] Ł. P. Zieliński, A. C. Smith, A. G. Smith, and A. J. Robinson, "Metabolic flexibility of mitochondrial respiratory chain disorders predicted by computer modelling," *Mitochondrion*, vol. 31, pp. 45–55, 2016.
- [68] S. Demine, N. Reddy, P. Renard, M. Raes, and T. Arnould, "Unraveling biochemical pathways affected by mitochondrial dysfunctions using metabolomic approaches," *Metabolites*, vol. 4, no. 3, pp. 831–878, 2014.
- [69] M. L. Genova and G. Lenaz, "The interplay between respiratory supercomplexes and ROS in aging," *Antioxidants & Redox Signaling*, vol. 23, no. 3, pp. 208–238, 2015.
- [70] R. Acin-Perez and J. A. Enriquez, "The function of the respiratory supercomplexes: the plasticity model," *Biochimica et Biophysica Acta (BBA) - Bioenergetics*, vol. 1837, no. 4, pp. 444–450, 2014.
- [71] N. V. Dudkina, M. Kudryashev, H. Stahlberg, and E. J. Boekema, "Interaction of complexes I, III, and IV within the bovine respirasome by single particle cryoelectron tomography," *Proceedings of the National Academy of Sciences of the United States of America*, vol. 108, no. 37, pp. 15196–15200, 2011.
- [72] D. Moreno-Lastres, F. Fontanesi, I. García-Consuegra et al., "Mitochondrial complex I plays an essential role in human respirasome assembly," *Cell Metabolism*, vol. 15, no. 3, pp. 324–335, 2012.
- [73] G. Lenaz, G. Tioli, A. I. Falasca, and M. L. Genova, "Complex I function in mitochondrial supercomplexes," *Biochimica et*

- Biophysica Acta (BBA) - Bioenergetics*, vol. 1857, no. 7, pp. 991–1000, 2016.
- [74] J. A. Enriquez, “Supramolecular organization of respiratory complexes,” *Annual Review of Physiology*, vol. 78, pp. 533–561, 2016.
- [75] E. Lapuente-Brun, R. Moreno-Loshuertos, R. Acín-Pérez et al., “Supercomplex assembly determines electron flux in the mitochondrial electron transport chain,” *Science*, vol. 340, no. 6140, pp. 1567–1570, 2013.
- [76] R. Acín-Pérez, P. Fernández-Silva, M. L. Peleato, A. Pérez-Martos, and J. A. Enriquez, “Respiratory active mitochondrial supercomplexes,” *Molecular Cell*, vol. 32, no. 4, pp. 529–539, 2008.
- [77] P. L. Pedersen, “Voltage dependent anion channels (VDACs): a brief introduction with a focus on the outer mitochondrial compartment’s roles together with hexokinase-2 in the “Warburg effect” in cancer,” *Journal of Bioenergetics and Biomembranes*, vol. 40, no. 3, pp. 123–126, 2008.
- [78] X. L. Qian, Y. Q. Li, F. Gu et al., “Overexpression of ubiquitous mitochondrial creatine kinase (uMtCK) accelerates tumor growth by inhibiting apoptosis of breast cancer cells and is associated with a poor prognosis in breast cancer patients,” *Biochemical and Biophysical Research Communications*, vol. 427, no. 1, pp. 60–66, 2012.
- [79] G. Lenaz and M. L. Genova, “Supramolecular organisation of the mitochondrial respiratory chain: a new challenge for the mechanism and control of oxidative phosphorylation,” *Advances in Experimental Medicine and Biology*, vol. 748, pp. 107–144, 2012.
- [80] C. Bianchi, M. L. Genova, G. P. Castelli, and G. Lenaz, “The mitochondrial respiratory chain is partially organized in a supercomplex assembly: kinetic evidence using flux control analysis,” *The Journal of Biological Chemistry*, vol. 279, no. 35, pp. 36562–36569, 2004.
- [81] A. K. Groen, R. J. Wanders, H. V. Westerhoff, R. Van der Meer, and J. M. Tager, “Quantification of the contribution of various steps to the control of mitochondrial respiration,” *The Journal of Biological Chemistry*, vol. 257, no. 6, pp. 2754–2757, 1982.
- [82] J. R. Small, “Flux control coefficients determined by inhibitor titration: the design and analysis of experiments to minimize errors,” *The Biochemical Journal*, vol. 296, Part 2, pp. 423–433, 1993.
- [83] E. E. Ramsay, P. J. Hogg, and P. J. Dilda, “Mitochondrial metabolism inhibitors for cancer therapy,” *Pharmaceutical Research*, vol. 28, no. 11, pp. 2731–2744, 2011.
- [84] P. Bernardi, “The mitochondrial permeability transition pore: a mystery solved?” *Frontiers in Physiology*, vol. 4, article 95, pp. 1–12, 2013.
- [85] F. Di Lisa, F. Fogolari, and G. Lippe, “From ATP to PTP and back: a dual function for the mitochondrial ATP synthase,” *Circulation Research*, vol. 116, no. 11, pp. 1850–1862, 2015.
- [86] P. Bernardi, A. Rasola, M. Forte, and G. Lippe, “The mitochondrial permeability transition pore: channel formation by F-ATP synthase, integration in signal transduction, and role in pathophysiology,” *Physiological Reviews*, vol. 95, no. 4, pp. 1111–1155, 2015.
- [87] A. Rasola and P. Bernardi, “The mitochondrial permeability transition pore and its adaptive responses in tumor cells,” *Cell Calcium*, vol. 56, no. 6, pp. 437–445, 2014.
- [88] T. Althoff, D. J. Mills, J. L. Popot, and W. Kühlbrandt, “Arrangement of electron transport chain components in bovine mitochondrial supercomplex I1III2IV1,” *The EMBO Journal*, vol. 30, no. 22, pp. 4652–4664, 2011.
- [89] A. Marín-Hernández, S. Y. López-Ramírez, J. C. Gallardo-Pérez, S. Rodríguez-Enríquez, R. Moreno-Sánchez, and E. Saavedra, “Systems biology approaches to cancer energy metabolism,” in *Systems Biology of Metabolic and Signaling Networks*, M. A. Aon, V. Saks and U. Schlattner, Eds., pp. 213–239, Springer, Berlin Heidelberg, 2014.
- [90] B. N. Kholodenko and H. V. Westerhoff, “Metabolic channelling and control of the flux,” *FEBS Letters*, vol. 320, no. 1, pp. 71–74, 1993.
- [91] B. N. Kholodenko, J. M. Rohwer, M. Cascante, and H. V. Westerhoff, “Subtleties in control by metabolic channelling and enzyme organization,” *Molecular and Cellular Biochemistry*, vol. 184, no. 1-2, pp. 311–320, 1998.
- [92] B. N. Kholodenko, O. V. Demin, and H. V. Westerhoff, “‘Channelled’ pathways can be more sensitive to specific regulatory signals,” *FEBS Letters*, vol. 320, no. 1, pp. 75–78, 1993.
- [93] A. Cormio, F. Guerra, G. Cormio et al., “Mitochondrial DNA content and mass increase in progression from normal to hyperplastic to cancer endometrium,” *BMC Research Notes*, vol. 5, no. 1, p. 279, 2012.
- [94] B. Chance and G. R. Williams, “Respiratory enzymes in oxidative phosphorylation. I. Kinetics of oxygen utilization,” *The Journal of Biological Chemistry*, vol. 217, no. 1, pp. 383–393, 1955.
- [95] B. Chance and G. R. Williams, “Respiratory enzymes in oxidative phosphorylation. VI. The effects of adenosine diphosphate on azide-treated mitochondria,” *The Journal of Biological Chemistry*, vol. 221, no. 1, pp. 477–489, 1956.
- [96] T. Anmann, R. Guzun, N. Beraud et al., “Different kinetics of the regulation of respiration in permeabilized cardiomyocytes and in HL-1 cardiac cells. Importance of cell structure/organization for respiration regulation,” *Biochimica et Biophysica Acta (BBA) - Bioenergetics*, vol. 1757, no. 12, pp. 1597–1606, 2006.
- [97] A. Klepinin, V. Chekulayev, N. Timohhina et al., “Comparative analysis of some aspects of mitochondrial metabolism in differentiated and undifferentiated neuroblastoma cells,” *Journal of Bioenergetics and Biomembranes*, vol. 46, no. 1, pp. 17–31, 2014.
- [98] A. F. Salem, D. Whitaker-Menezes, Z. Lin et al., “Two-compartment tumor metabolism: autophagy in the tumor microenvironment and oxidative mitochondrial metabolism (OXPHOS) in cancer cells,” *Cell Cycle*, vol. 11, no. 13, pp. 2545–2556, 2012.
- [99] U. E. Martinez-Outschoorn, M. P. Lisanti, and F. Sotgia, “Catabolic cancer-associated fibroblasts transfer energy and biomass to anabolic cancer cells, fueling tumor growth,” *Seminars in Cancer Biology*, vol. 25, pp. 47–60, 2014.
- [100] U. Martinez-Outschoorn, F. Sotgia, and M. P. Lisanti, “Tumor microenvironment and metabolic synergy in breast cancers: critical importance of mitochondrial fuels and function,” *Seminars in Oncology*, vol. 41, no. 2, pp. 195–216, 2014.
- [101] F. Sotgia, D. Whitaker-Menezes, U. E. Martinez-Outschoorn et al., “Mitochondria ‘fuel’ breast cancer metabolism: fifteen markers of mitochondrial biogenesis label epithelial cancer cells, but are excluded from adjacent stromal cells,” *Cell Cycle*, vol. 11, no. 23, pp. 4390–4401, 2012.

- [102] M. P. Lisanti, F. Sotgia, R. G. Pestell, A. Howell, and U. E. Martinez-Outschoorn, "Stromal glycolysis and MCT4 are hallmarks of DCIS progression to invasive breast cancer," *Cell Cycle*, vol. 12, no. 18, pp. 2935-2936, 2013.
- [103] F. Sotgia, U. E. Martinez-Outschoorn, S. Pavlides, A. Howell, R. G. Pestell, and M. P. Lisanti, "Understanding the Warburg effect and the prognostic value of stromal caveolin-1 as a marker of a lethal tumor microenvironment," *Breast Cancer Research*, vol. 13, no. 4, p. 213, 2011.
- [104] K. Tepp, K. Mado, M. Varikmaa et al., "The role of tubulin in the mitochondrial metabolism and arrangement in muscle cells," *Journal of Bioenergetics and Biomembranes*, vol. 46, no. 5, pp. 421-434, 2014.
- [105] M. Varikmaa, N. Timohhina, K. Tepp et al., "Formation of highly organized intracellular structure and energy metabolism in cardiac muscle cells during postnatal development of rat heart," *Biochimica et Biophysica Acta (BBA) - Bioenergetics*, vol. 1837, no. 8, pp. 1350-1361, 2014.
- [106] K. L. Sheldon, E. N. Maldonado, J. J. Lemasters, T. K. Rostovtseva, and S. M. Bezrukov, "Phosphorylation of voltage-dependent anion channel by serine/threonine kinases governs its interaction with tubulin," *PLoS One*, vol. 6, no. 10, article e25539, 2011.
- [107] T. K. Rostovtseva and S. M. Bezrukov, "VDAC inhibition by tubulin and its physiological implications," *Biochimica et Biophysica Acta (BBA) - Biomembranes*, vol. 1818, no. 6, pp. 1526-1535, 2012.
- [108] M. Gruno, N. Peet, E. Seppet et al., "Oxidative phosphorylation and its coupling to mitochondrial creatine and adenylate kinases in human gastric mucosa," *American Journal of Physiology. Regulatory, Integrative and Comparative Physiology*, vol. 291, no. 4, pp. R936-R946, 2006.
- [109] Y. Ishida, M. Wyss, W. Hemmer, and T. Wallimann, "Identification of creatine kinase isoenzymes in the guinea-pig. Presence of mitochondrial creatine kinase in smooth muscle," *FEBS Letters*, vol. 283, no. 1, pp. 37-43, 1991.
- [110] M. J. Kushmerick, "Energetics studies of muscles of different types," *Basic Research in Cardiology*, vol. 82, Supplement 2, pp. 17-30, 1987.

Research Article

Mitochondria-Targeted Antioxidant SkQ1 Improves Dermal Wound Healing in Genetically Diabetic Mice

Ilya A. Demyanenko,¹ Vlada V. Zakharova,² Olga P. Ilyinskaya,¹ Tamara V. Vasilieva,¹ Artem V. Fedorov,¹ Vasily N. Manskikh,^{2,3} Roman A. Zinovkin,^{1,2,3} Olga Yu Pletjushkina,² Boris V. Chernyak,² Vladimir P. Skulachev,^{2,3} and Ekaterina N. Popova²

¹Faculty of Biology, Lomonosov Moscow State University, Leninskie Gory 1-12, Moscow 119234, Russia

²Belozersky Institute of Physico-Chemical Biology, Lomonosov Moscow State University, Leninskie Gory 1-40, Moscow 119992, Russia

³Institute of Mitoengineering, Lomonosov Moscow State University, Leninskie Gory 1-73, Moscow 119992, Russia

Correspondence should be addressed to Ekaterina N. Popova; k_popova_ch@mail.ru

Received 21 February 2017; Accepted 20 April 2017; Published 6 July 2017

Academic Editor: Maik Hüttemann

Copyright © 2017 Ilya A. Demyanenko et al. This is an open access article distributed under the Creative Commons Attribution License, which permits unrestricted use, distribution, and reproduction in any medium, provided the original work is properly cited.

Oxidative stress is widely recognized as an important factor in the delayed wound healing in diabetes. However, the role of mitochondrial reactive oxygen species in this process is unknown. It was assumed that mitochondrial reactive oxygen species are involved in many wound-healing processes in both diabetic humans and animals. We have applied the mitochondria-targeted antioxidant 10-(6'-plastoquinonyl)decyltriphenylphosphonium (SkQ1) to explore the role of mitochondrial reactive oxygen species in the wound healing of genetically diabetic mice. Healing of full-thickness excisional dermal wounds in diabetic C57BL/KsJ-db⁻/db⁻ mice was significantly enhanced after long-term (12 weeks) administration of SkQ1. SkQ1 accelerated wound closure and stimulated epithelization, granulation tissue formation, and vascularization. On the 7th day after wounding, SkQ1 treatment increased the number of α -smooth muscle actin-positive cells (myofibroblasts), reduced the number of neutrophils, and increased macrophage infiltration. SkQ1 lowered lipid peroxidation level but did not change the level of the circulatory IL-6 and TNF. SkQ1 pretreatment also stimulated cell migration in a scratch-wound assay in vitro under hyperglycemic condition. Thus, a mitochondria-targeted antioxidant normalized both inflammatory and regenerative phases of wound healing in diabetic mice. Our results pointed to nearly all the major steps of wound healing as the target of excessive mitochondrial reactive oxygen species production in type II diabetes.

1. Introduction

Impaired wound healing and chronic wounds are a significant source of complications of diabetes mellitus. Wound healing is a complex sequence of cellular and molecular processes consisting of inflammation, formation of the granulation tissue (including myofibroblast accumulation, extracellular matrix synthesis, and angiogenesis), reepithelialization, and tissue remodeling. The impact of diabetes is widespread and pleiotropic, affecting the majority of cells and mechanisms involved in the repair process. These in particular include prolonged and exacerbated inflammatory stage, inadequate

expression of growth factors at the site of injury, impaired angiogenesis, dysfunction of fibroblasts and epidermal cells, and impaired ability of bone marrow progenitor cells to migrate to the lesion [1].

Oxidative stress is now recognized as a key participant in the development of many diabetic complications. Excessive generation of reactive oxygen species (ROS) in diabetes is largely due to acute rises in serum glucose and accumulation of advanced glycation end products (AGEs) [2]. A delicate balance between the positive role of ROS and their deleterious effects is important for proper wound healing. Oxidative stress in diabetes may be involved in nearly all of the above-

mentioned pathologies related to impaired wound healing [1, 3, 4].

It was hypothesized that the damaging effects of hyperglycemia are activated by mitochondrial ROS (mtROS) overproduction [5, 6]. However, a recently proposed mitochondrial hormesis theory challenged this point of view [7]. Probably, mtROS are also the key players in the development of insulin resistance [8] thus participating in a vicious cycle of diabetes progression.

Plastoquinone derivatives covalently conjugated with lipophilic cations (SkQ) are one of the most intensively studied groups of mitochondria-targeted antioxidants [9]. It was shown that SkQ1 treatment of obese mice kept on a high-fat, high-sucrose diet normalized H_2O_2 and protein carbonyl levels in muscles [10]. At the same time, SkQ1 did not affect weight gain, triacylglycerol, glucose, and insulin level in plasma and did not protect insulin signaling in the skeletal muscle. Interestingly, SkQ1 prevents high-fat diet-induced increases in mitochondrial biogenesis probably mediated by activation of Ca^{2+} /calmodulin-dependent protein kinase CaMKII [10, 11].

In our recent study, we have found that long-term (8 months) oral administration of SkQ1 dramatically improves impaired dermal wound healing in aging mice [12]. In the present study, we have investigated whether SkQ1 could affect wound healing in the mice model of type II diabetes.

2. Materials and Methods

2.1. Animals and Antioxidant Treatment. Male mutant homozygous C57BL/KsJ- db^{-}/db^{-} (*db/db*) mice were obtained from the Center of Biomedical Technologies, RAMS, Moscow. The experimental group of animals ($n = 12$) received 250 nmol/kg of body weight per day of SkQ1 (synthesized at Institute of Mitoengineering, Lomonosov Moscow State University) per os for 12 weeks starting from the 9th week of life. The daily dose of SkQ1 was chosen according to our earlier studies [9]. The control group of *db/db* mice ($n = 9$) and heterozygous C57BL/KsJ- db^{+}/db^{-} (*db/+*) mice ($n = 5$) was treated with a vehicle (20% glycerol). Heterozygous mice had normal phenotype and did not display any diabetic features.

2.2. Ethical Approval. All animal care and experimental procedures complied with Guide for the Care and Use of Laboratory Animals, Eighth edition (2011).

2.3. Blood Glucose, Glycated Hemoglobin, and Body Mass Analysis. During administration of the SkQ1, body mass and blood glucose levels were measured every two-three weeks. In the final week of treatment, the level of glycated hemoglobin (HbA1c) was also analyzed. For all measurements, blood was collected from the tail vein ($5 \mu\text{l}$) after 12 hours of starvation. Blood glucose and glycated hemoglobin were measured with an Accu-Check Perfoma Nano (Roche Diagnostics, France) and Nycocard Reader II (Axis-Shiel, Norway), respectively.

2.4. Wounding Protocol and Wound Closure Analysis. Animals were anesthetized using zoletil (50 mg per 1 kg of

body weight). Hair on the dorsal side of mice was shaved and the skin was cleaned with 70% ethanol. Full-thickness excisional skin wound 0.7 cm in diameter was created surgically in the interscapular area. No dressing was placed on the wounds.

For macroscopic examination, digital photos of the wound area were made once a day. The wound surface area was measured at the photographs using ImageJ software.

2.5. Blood Cytokine Level and Liver TBARS Measurement. At the 7th day of healing, animals were euthanized by decapitation, blood was collected, and the serum concentrations of IL-6 and tumor necrosis factor (TNF) were determined with enzyme-linked immunosorbent assay (ELISA) kits (eBioscience, USA) according to manufacturer's protocols. Liver samples were excised, and thiobarbituric acid reactive substance (TBARS) content was measured by the method of Mihara and Uchiyama [13].

2.6. Histological and Immunohistochemical Studies. After euthanasia, wounds with surrounding tissues were excised and fixed with 10% phosphate-buffered (pH = 7.4) formalin. The samples were transversely cut exactly through the center of the wound, dehydrated, and paraffin-embedded according to the routine protocols. Cross sections ($5 \mu\text{m}$ thick) were stained with hematoxylin and eosin (H&E) and Mallory's trichrome stain. For immunostaining, sections were treated with 3% H_2O_2 for 10 min and then with 10% nonimmune goat serum before incubation with rabbit polyclonal antibodies against α -smooth muscle actin (α -SMA) and CD31 (Abcam, UK) or rat monoclonal antibodies against f4/80 (Serotec, UK). Goat anti-rabbit and anti-rat IgG biotinylated antibodies (Vector, USA) were applied and stained with avidin-peroxidase conjugate and diaminobenzidine (Vector, USA). Before CD31 staining, heat-mediated antigen retrieval with Vector Antigen Unmasking Solution (Vector, USA) at 98°C for 40 min was applied additionally.

Samples were analyzed with a DM 5000B microscope equipped with a DFC 320 digital camera (Leica, Germany).

2.7. Morphometric Analysis. The granulation tissue area and epithelization of wound were analyzed on the H&E-stained sections. Epithelization was calculated as the ratio of the wound surface covered by regenerating epidermis to the total wound surface. Vessel density was calculated as the ratio of the summarized blood vessel area revealed with CD31 immunostaining to the granulation tissue area. Neutrophils were counted on H&E-stained sections and macrophages were detected as f4/80-positive cells after immunostaining. Histomorphometric analysis was performed on digital microphotographs by ImageJ software.

Myofibroblasts areal density was measured after immunostaining as the ratio of α -SMA-positive cytoplasm to the total area of granulation tissue. A method of color subtractive-computer-assisted image analysis [14] was applied.

2.8. In Vitro Studies of Fibroblast Motility. Human subcutaneous fibroblasts HSF (Russian Cell Culture Collection, Institute of Medical Genetics, Russian Academy of Sciences) were grown in Dulbecco's modified Eagle's medium (DMEM)

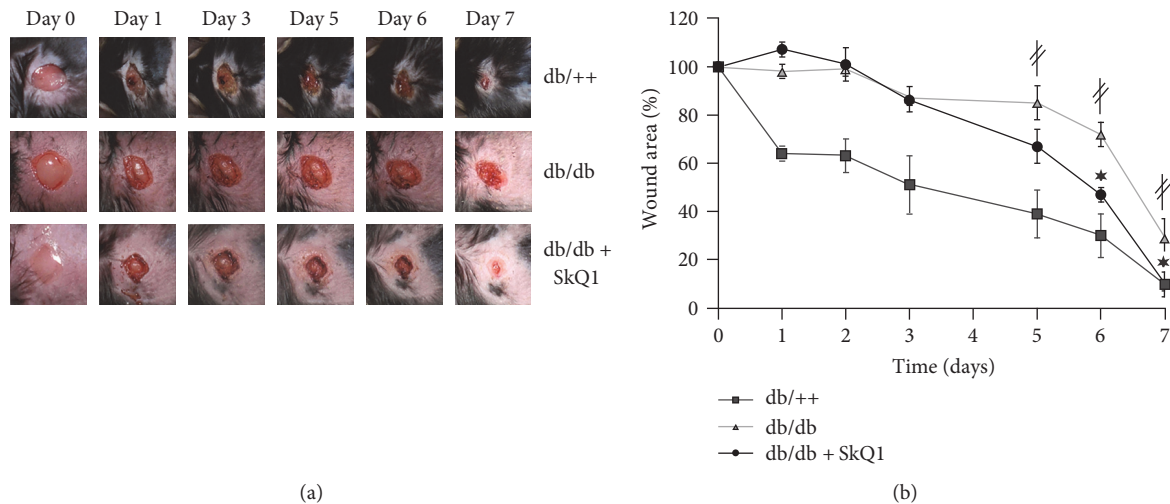


FIGURE 1: SkQ1 accelerates wound closure in diabetic mice. Full-thickness excisional skin wounds were created surgically in the interscapular area on the back of nondiabetic ($db/++$, $n = 5$), diabetic (db/db , $n = 9$), and diabetic mice receiving SkQ1 (250 nmol/kg of body mass per day) during 12 weeks ($n = 12$). (a) Representative images of the wounds, (b) dynamics of the wound closure. Data are presented as mean \pm SEM; * $P < 0.05$ for SkQ1-treated versus untreated diabetic mice. [#] $P < 0.05$ for the untreated diabetic mice versus nondiabetic mice.

(Gibco, USA) supplemented with 10% fetal calf serum (Hyclone, USA) at 37°C in a humidified atmosphere containing 5% CO₂. Cells were incubated with 20 nM SkQ1 for 3 days and transferred to the fresh medium with 25 mM glucose (control), 50 mM glucose (hyperglycemia), or 50 mM mannitol (osmotic control) with 20 nM SkQ1. After 24 hours, the cells were scratched with the rille pipette tip. Cell motility was analyzed in a scratch-wound assay as described earlier [12]. The images were taken with an Axiovert microscope (Carl Zeiss, Germany) equipped with an AxioCam camera (Carl Zeiss), and “wound” areas were analyzed using ImageJ software.

2.9. Statistical Analysis. Statistical analysis was done with STATISTICA 7.0 software. The data were expressed as mean \pm SEM or mean \pm SD (see figure legend). Mann-Whitney U test or Kruskal-Wallis H test (one-way ANOVA on ranks) followed by Dunn’s test for multiple comparisons were conducted, and significance was set at level $P < 0.05$.

3. Results

Comparative analysis of the wound healing in db/db versus $db/+$ mice has shown a dramatic delay in wound area contraction (Figure 1) and granulation tissue formation (Figures 2(a) and 2(b)). However, epithelization of the wounds was not impaired (Figure 2(c)). These observations are in a perfect agreement with the studies pointed to db/db mice as a good experimental model of type II diabetes-impaired wound healing [15, 16]. Oral administration of 250 nmol/kg SkQ1 resulted in a significant reduction of wound area in db/db mice on the 6th and 7th days, so on the 7th day, the wound size was the same as in $db/++$ mice (Figure 1(b)). Administration of SkQ1 also strongly increased the amount of granulation tissue in diabetic animals (Figures 2(a) and 2(b)). Moreover, new-formed connective tissue of SkQ1-treated db/db mice consisted of more

mature and regularly oriented bundles of collagen fibers compared to the granulation tissue of control animals (Figures 2(a) and 2(b) and Figure 3(a)). SkQ1 induced the dramatic increase in content of α -SMA-positive fibroblast-like cells referred to as myofibroblasts (Figures 3(b) and 3(d)). These cells play an important role in the formation and maturation of the granulation tissue due to increased formation of extracellular matrix molecules (including collagen) and growth factors. Furthermore, myofibroblasts can directly participate in mechanical wound closure due to their contractility.

Treatment with SkQ1 significantly stimulated epithelization of the wounds in diabetic animals (Figure 2(c)) though it was not compromised in db/db mice in line with earlier observations [16].

Diabetes mellitus is often accompanied by macro- and microvascular complications leading to local tissue hypoxia and chronic wound formation. Vascularization of the wounds was delayed in db/db mice (Figure 3(c)). Treatment with SkQ1 significantly increased vessel density in granulation tissue (Figures 3(c) and 3(e)). This effect probably contributes to the acceleration of tissue regeneration.

Persistence of neutrophil infiltration and a delay in accumulation of macrophages were observed in the wounds of db/db mice (Figure 4), indicating the delay in the resolution of an inflammatory phase of wound healing. Administration of SkQ1 decreased the number of neutrophils in the granulation tissue of db/db mice to the level observed in their nondiabetic $db/++$ littermates (Figures 4(a) and 4(c)) and significantly increased macrophage content (Figures 4(b) and 4(d)). The effect of SkQ1 on the neutrophil and macrophage infiltration was not related to the changes of inflammatory status in db/db mice. We have detected significant elevation in the level of proinflammatory cytokines TNF and IL-6 in plasma of diabetic mice with strong individual variations of these parameters. Treatment with SkQ1 did not change the level of these cytokines (Figure 5(e)). We suggest that SkQ1 accelerated the resolution of an inflammation

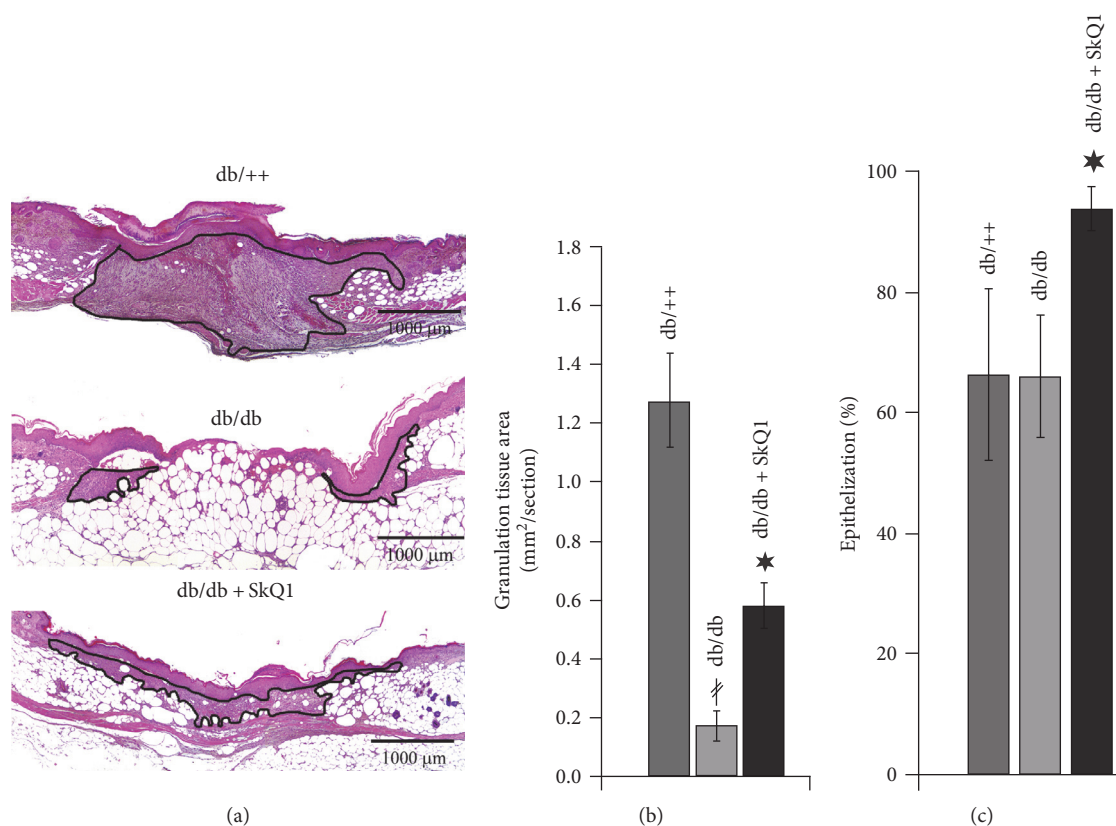


FIGURE 2: SkQ1 promotes granulation tissue formation and epithelization of the wounds in diabetic mice. (a) Representative images of the H&E-stained transverse sections of the wounds at the 7th day of healing. (b) Granulation tissue formation and (c) epithelization of the wounds. Data are presented as mean \pm SEM; * $P < 0.05$ for SkQ1-treated versus untreated diabetic mice. $^{\#}P < 0.05$ for the untreated diabetic mice versus nondiabetic mice.

phase of wound healing by local inhibition of inflammatory activation of endothelial cells and by improvement of immune cells functioning in the regenerating tissues, rather than by a systemic anti-inflammatory effect.

SkQ1 affected neither serum glucose level nor weight gain in diabetic mice (Figures 5(a) and 5(b)). The level of glycated HbA1c reflecting sustained hyperglycemia was also not affected (Figure 5(c)). At the same time, SkQ1 significantly decreased the level of lipid peroxidation end products (measured as TBARS) in the liver of *db/db* mice confirming high antioxidant efficiency of this compound (Figure 5(d)).

We have shown earlier that SkQ1 initiated myofibroblast differentiation and actin cytoskeleton rearrangements in fibroblasts in vitro [17]. These changes were accompanied by the increased migration of fibroblasts into the scratched “wound” made in a cell monolayer [18]. Migration of fibroblasts was strongly inhibited by high-glucose (50 mM) medium and SkQ1 pretreatment prevented this inhibition (Figure 6). These data indicate that fibroblasts could be directly affected by excessive mtROS production caused by hyperglycemia both in vivo and in vitro.

4. Discussion

Our study demonstrated that mitochondria-targeted antioxidant SkQ1 did not affect weight gain and hyperglycemia in

diabetic *db/db* mice but suppressed oxidative stress and improved healing of full-thickness excisional skin wounds. These data are in agreement with the results of earlier studies on SkQ1 [10] and on related mitochondria-targeted antioxidant 10-(6'-ubiquinonyl)decyltriphenylphosphonium (MitoQ) [19] that only slightly inhibited development of hyperglycemia and insulin resistance but strongly protected against various complications in animal models of diabetes. These data indicate that excessive mtROS production is crucial for hyperglycemia-induced damage in various tissues being less important for insulin resistance.

Compromised wound healing in diabetes obviously has complex pleiotropic etiology [1], and our results pointed to the major steps of wound healing as the targets of excessive mtROS. Recruitment of neutrophils to the wound is important for controlling microbial invasion, but neutrophil persistence results in the delayed resolution of an inflammatory phase and impairment of diabetic wound healing [20]. In neutropenic *db/db* mice, wound closure was improved due to accelerated reepithelialization [21]. The similar effect of SkQ1 on acute wound healing or aseptic inflammation was observed earlier in healthy animals [18].

ROS may enhance insulin action [22, 23] and insulin secretion [24, 25]. On the other hand, chronic oxidative stress is a central mechanism for glucose toxicity in pancreatic islet beta cells in diabetes [26], and ROS levels are an

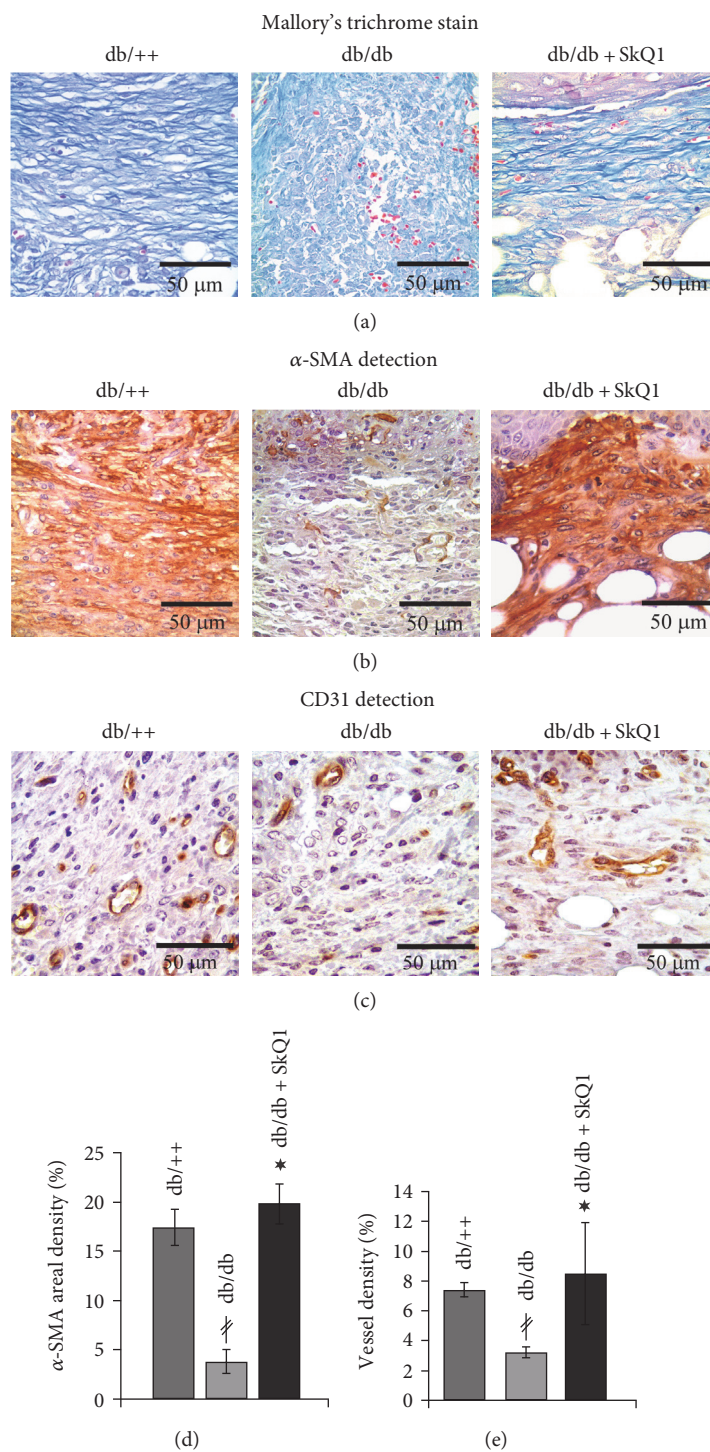


FIGURE 3: Effect of SkQ1 on the maturation of granulation tissue in diabetic mice. Representative images of the (a) Mallory's trichrome-stained and (b) α-SMA- and (c) CD-31-immunostained granulation tissue at the 7th day of wound healing. (d) Percentage of the area containing α-SMA-positive cytoplasm (areal density). (e) Percentage of the area containing microvessels (vessel density). Data are presented as mean ± SEM; * $P < 0.05$ for SkQ1-treated versus untreated diabetic mice. [#] $P < 0.05$ for the untreated diabetic mice versus nondiabetic mice.

important trigger for insulin resistance in numerous settings [8]. Thus, theoretically antioxidant treatment could affect the diabetes progression. However, both in our work and in the previous paper, SkQ1 had antioxidant activities but had no effect on the diabetic features [10]. Noteworthy,

SkQ1 mostly affected cellular content in the wounds thus implying its potential to be used in the form of topical application. In our previous work, we have observed some stimulatory effect of topical SkQ1 application on the wound healing in young rats [18].

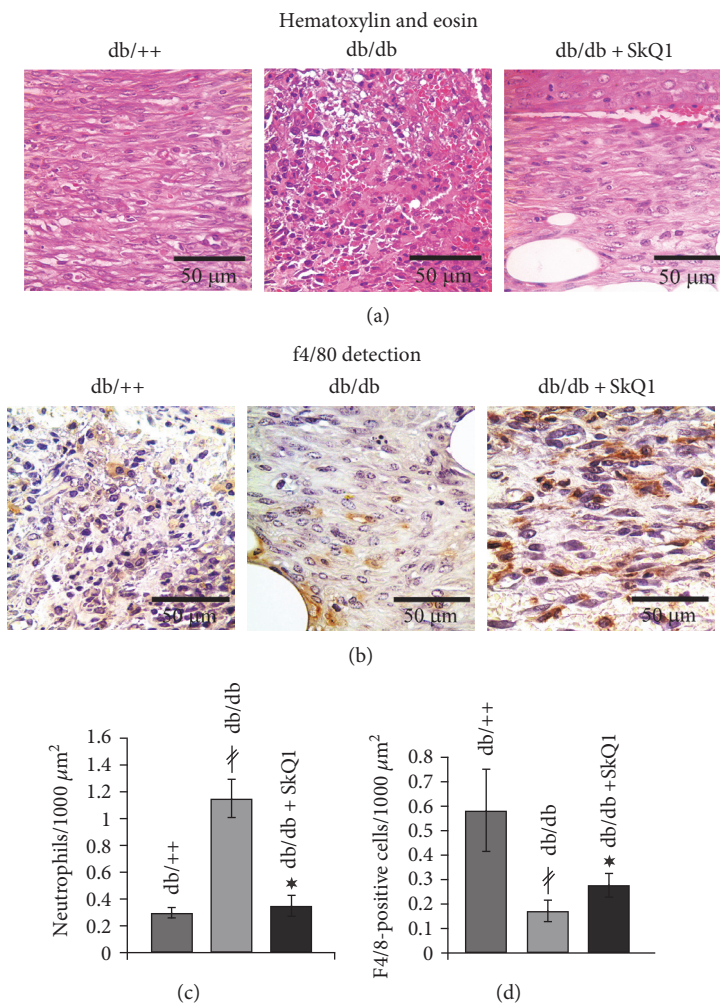


FIGURE 4: Effect of SkQ1 on the leukocyte composition of granulation tissue in diabetic mice. Representative images of the (a) H&E-stained and (b) f4/80-immunostained granulation tissue at the 7th day of wound healing. (c) Neutrophil and (d) macrophage (F4/80-positive cells) infiltration of the granulation tissue. Data are presented as mean \pm SEM; * $P < 0.05$ for SkQ1-treated versus untreated diabetic mice. # $P < 0.05$ for the untreated diabetic mice versus nondiabetic mice.

It was previously shown that SkQ1 attenuates expression of adhesion molecules ICAM1, VCAM, and E-selectin in endothelial cell culture treated with TNF as well in aorta of aging mice [27] via inhibition of NF- κ B signaling. SkQ1 also prevented TNF-induced decomposition of VE-cadherin-containing contacts, following an increase in the permeability of endothelial cell monolayer [12]. SkQ1 also inhibited apoptosis of endothelial cells induced by high doses of TNF [28]. SkQ1 did not influence the elevated level of proinflammatory cytokines in the blood of diabetic (this study) or aged mice [27], so we suggest that its anti-inflammatory action in the skin wounds of diabetic mice may be at least partially mediated by prevention of endothelial cell activation, following excessive neutrophil infiltration.

Treatment with SkQ1 improved the resolution of an inflammatory phase of wound healing, simultaneously decreasing content of neutrophils and increasing content of macrophages (Figure 4). Macrophages are actively involved in the resolution of inflammation by efficient dead cell clearance (efferocytosis) followed by a transition from pro- to

anti-inflammatory prohealing phenotype. A significant delay in macrophage infiltration is typical for diabetic mice [29]. It is followed by increased apoptotic cell burden and a prolonged inflammatory phase [30]. The persistence of the pro-inflammatory macrophages in the diabetic wounds is mediated by the sustained NLRP3 inflammasome activity [31]. NLRP3 inflammasome activation is dependent on the mtROS production [32], and mitochondria-targeted ROS scavenger MitoQ decreases NLRP3-dependent IL-1 beta and IL-18 production in human macrophage-like cell line THP-1 [33]. It seems reasonable to suggest the similar mechanism for SkQ1 during diabetic wound healing. Currently, targeting of the inflammasome is considered a clinically efficacious strategy in restoring insulin action in humans with type 2 diabetes.

Our results indicated that SkQ1 stimulated growth and maturation of granulation tissue in dermal wounds of diabetic mice (Figure 2). Earlier, it was shown that scavenging of mtROS by SkQ1 in the subcutaneous fibroblast culture stimulated metalloprotease-dependent activation of latent

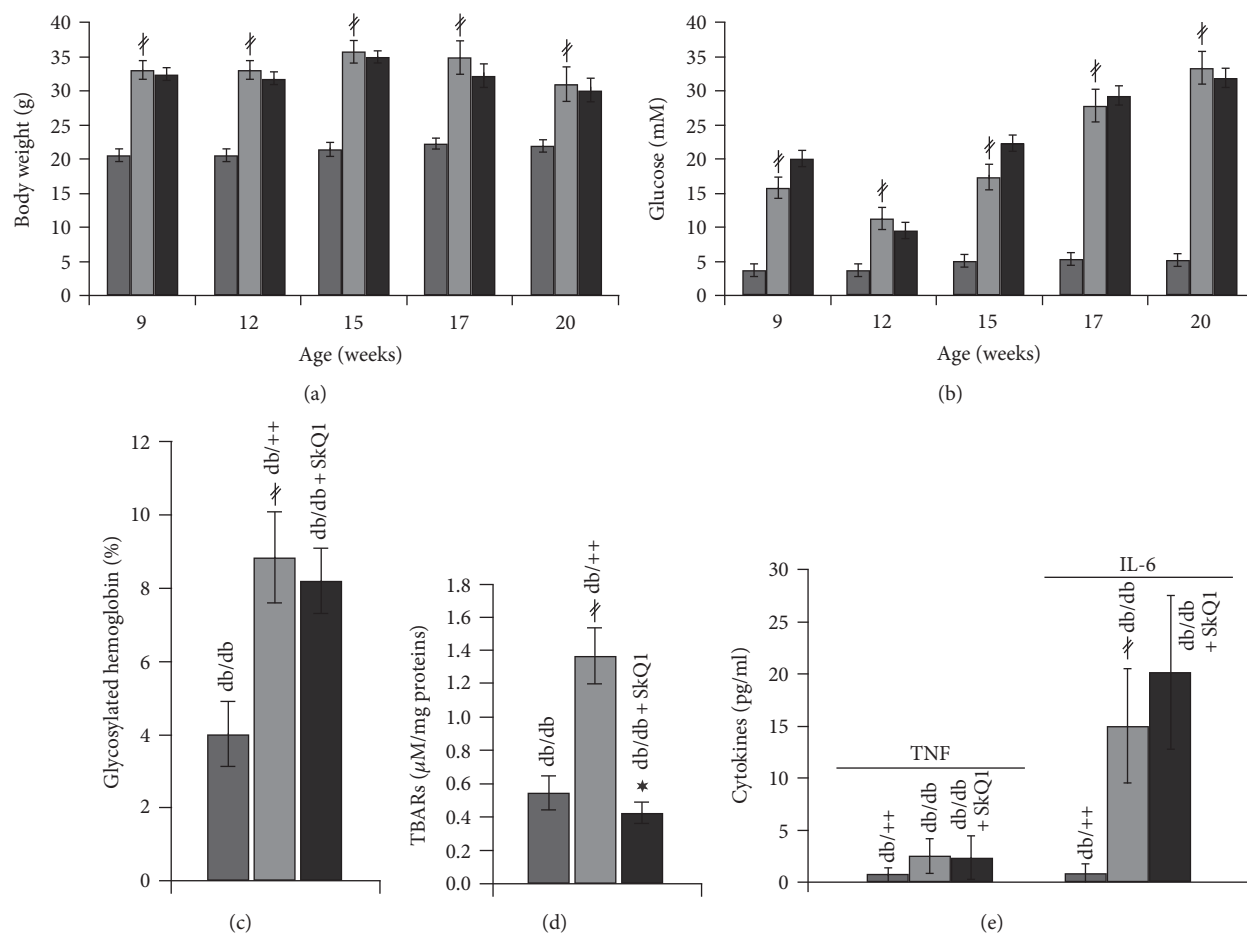


FIGURE 5: Effect of SkQ1 on the metabolic parameters and circulatory cytokine levels of diabetic mice. Dynamics of (a) body mass and (b) blood glucose level during the antioxidant administration. (c) Glycated hemoglobin level at the 11th week of treatment. Data are presented as mean \pm SEM. (d) Liver TBARS level and (e) serum cytokine concentration at the 7th day of wound healing. Data are presented as mean \pm SD. * $P < 0.05$ for SkQ1-treated versus untreated diabetic mice. $^{\#}P < 0.05$ for the untreated diabetic mice versus nondiabetic mice.

TGF β 1 and downstream SMAD-dependent expression of EDA isoform of fibronectin and α -SMA, the major markers of myofibroblasts [17]. The myofibroblasts produce various growth factors (including TGF β 1), collagen, and other ECM components and participate in wound contraction due to their contractility.

We have shown earlier that SkQ1 activated the Rho/ROCK/LIMK pathway leading to stabilization of actin filaments and accelerated fibroblast migration into the “wound” in the cell monolayer in vitro [17, 18]. Hyperglycemia inhibited fibroblast migration in vitro and SkQ1 prevented this effect (Figure 6). It was suggested that inhibition of fibroblast motility resulted from impaired cell polarity, protrusion destabilization, and inhibition of adhesion maturation at least in part due to oxidative stress that stimulated Rac1 activity [34]. Our data indicated that hyperglycemia-induced Rac1 activation could be mediated by mtROS either directly or via stimulation of RhoA that balanced Rac1-dependent cytoskeleton rearrangements. The effect of SkQ1 on fibroblast motility at high glucose could be important for stimulation of their migration to the wound area from the surrounding tissues and for granulation tissue formation.

Another potential source of myofibroblasts is multipotent mesenchymal stromal cells (MSC) from the bone marrow [35]. Diabetes is accompanied by the bone marrow dysfunction due to neuropathy and microangiopathy leading to the niche dysfunction [36]. p66shc protein is known to stimulate mtROS production. Its knockout partially rescued the defective progenitor cell mobilization from the bone marrow in two different mice models of diabetes [37], so the damaging role of mtROS could be suggested [38]. In agreement with this suggestion, we have found earlier that SkQ1 strongly promoted accumulation of MSC progeny fibroblast colony-forming units (CFU-F). CFU-F content was doubled after SkQ1 treatment in the bone marrow of mice [39]. This source of myofibroblasts may also be important for granulation tissue formation in diabetic mice.

Earlier, we have shown that SkQ1 stimulated active TGF β 1 secretion by fibroblasts [17]. TGF β 1 is known for decades as an important regulator of wound healing deficient in diabetic wounds [40]. TGF β 1 also promotes macrophage differentiation into alternatively activated (or M2) macrophages capable of active efferocytosis [41], and this effect could be implicated in the resolution of inflammation in

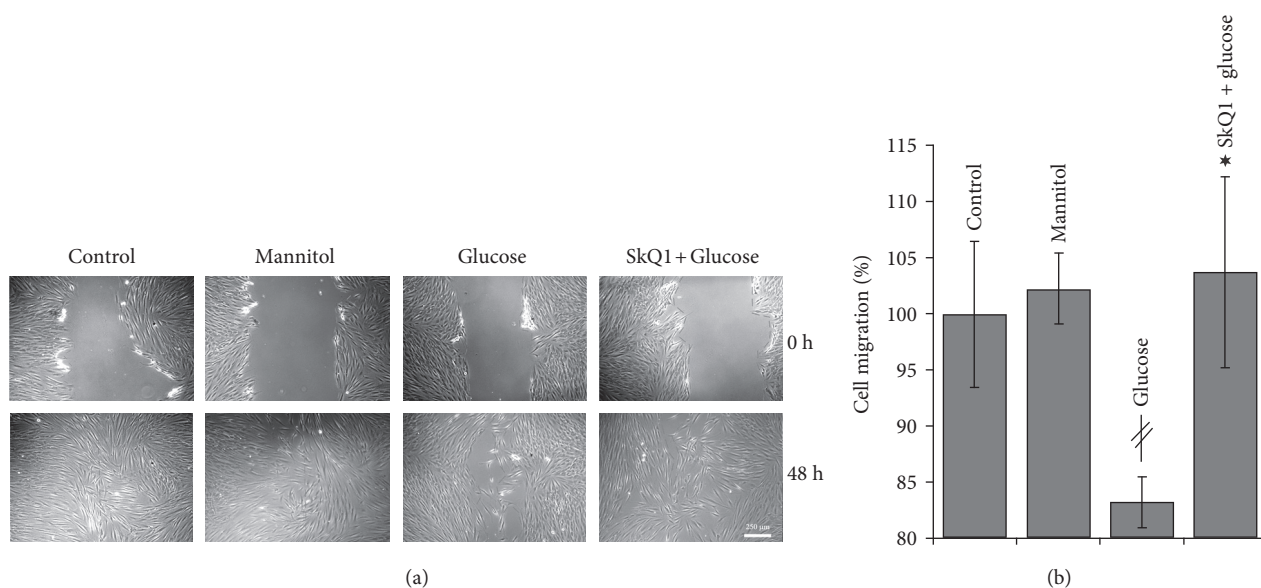


FIGURE 6: Effect of SkQ1 on the cell motility in the scratch-wound assay under high-glucose conditions. Migration of human subcutaneous fibroblasts in a scratch-wound assay (48 h after wounding). (a) Representative images. (b) Percentage of the wound area occupied with migrated cells. “Control”—control medium (25 mM glucose); “mannitol”—control medium (50 mM mannitol); “glucose”—high-glucose medium (50 mM glucose); “SkQ1 + glucose”—high-glucose medium (20 nM SkQ1). Data are presented as mean \pm SEM; * P < 0.05 for the high-glucose versus control medium. * P < 0.05 for SkQ1-treated high-glucose versus high-glucose medium.

addition to the effects of mtROS scavenging on neutrophil infiltration and inflammasome inhibition (see above). Moreover, growth medium conditioned with SkQ1-treated fibroblasts stimulated endothelial cell migration and tubular structure formation in vitro in a matrigel angiogenesis assay [12]. Stimulation was at least partially mediated by TGF β 1 since the inhibitor of its receptor TGF β 1R1 suppressed the effect [12]. Increased secretion of TGF β 1 (and probably some other growth factors) by fibroblasts could be responsible for improvement of angiogenesis in diabetic wounds (Figure 3).

The other target of SkQ1 treatment could be endothelial progenitor cells (EPCs), a key cell type involved in angiogenesis. It was found that the number of circulating EPCs and ex vivo functions of EPCs were impaired in diabetic patients due to oxidative stress [3]. MtROS produced in a p66shc-dependent manner in the bone marrow were shown to determine defective EPC mobilization in diabetic mice [37]. Moreover, transplantation of diabetic EPCs after MnSOD gene therapy restored their ability to mediate angiogenesis and wound repair [42], indicating the key role of mtROS in EPC dysfunction.

We have previously shown that long-term (8 months) administration of SkQ1 prevented age-dependent impairment of dermal wound healing in mice [12]. In the present study, SkQ1 treatment improved the same components of a wound healing process in genetically diabetic mice. These findings are in line with numerous studies demonstrating therapeutic action of mitochondria-targeted antioxidants against various age-related disorders [9, 12, 43, 44] and support the key role of mtROS in pathogenesis of many complications inherent to both aging and diabetes.

5. Conclusions

The mitochondria-targeted antioxidant SkQ1 enhances dermal wound healing in diabetic mice accompanied by improved resolution of inflammation, increased myofibroblast content, and vascularization of granulation tissue. These results imply that nearly all major stages of diabetic wound healing are hindered by excessive mitochondrial reactive oxygen species production.

Conflicts of Interest

The authors declare that there is no duality of interest associated with this manuscript.

Acknowledgments

This work was supported by the grants from the Russian Scientific Foundation (14-50-00029 (experiments in vivo and histological examination) and 14-24-00107 (experiments in vitro)).

References

- [1] R. Gary Sibbald and K. Y. Woo, “The biology of chronic foot ulcers in persons with diabetes,” *Diabetes/Metabolism Research and Reviews*, vol. 24, pp. S25–S30, 2008.
- [2] L. Monnier, E. Mas, C. Ginet et al., “Activation of oxidative stress by acute glucose fluctuations compared with sustained chronic hyperglycemia in patients with type 2 diabetes,” *Journal of the American Medical Association*, vol. 295, pp. 1681–1687, 2006.

- [3] M. J. Callaghan, D. J. Ceradini, and G. C. Gurtner, "Hyperglycemia-induced reactive oxygen species and impaired endothelial progenitor cell function," *Antioxidants & Redox Signaling*, vol. 7, pp. 1476–1482, 2005.
- [4] F. Folli, D. Corradi, P. Fanti et al., "The role of oxidative stress in the pathogenesis of type 2 diabetes mellitus micro- and macrovascular complications: avenues for a mechanistic-based therapeutic approach," *Current Diabetes Reviews*, vol. 7, pp. 313–324, 2011.
- [5] M. Brownlee, "The pathobiology of diabetic complications," *Diabetes*, vol. 54, pp. 1615–1625, 2005.
- [6] F. Giacco and M. Brownlee, "Oxidative stress and diabetic complications," *Circulation Research*, vol. 107, pp. 1058–1070, 2010.
- [7] K. Sharma, "Mitochondrial hormesis and diabetic complications," *Diabetes*, vol. 64, pp. 663–672, 2015.
- [8] N. Houstis, E. D. Rosen, and E. S. Lander, "Reactive oxygen species have a causal role in multiple forms of insulin resistance," *Nature*, vol. 440, pp. 944–948, 2006.
- [9] M. V. Skulachev, Y. N. Antonenko, V. N. Anisimov et al., "Mitochondrial-targeted plastoquinone derivatives. Effect on senescence and acute age-related pathologies," *Current Drug Targets*, vol. 12, pp. 800–826, 2011.
- [10] S. Paglialunga, B. Van Bree, M. Bosma et al., "Targeting of mitochondrial reactive oxygen species production does not avert lipid-induced insulin resistance in muscle tissue from mice," *Diabetologia*, vol. 55, pp. 2759–2768, 2012.
- [11] S. S. Jain, S. Paglialunga, C. Vigna et al., "High-fat diet-induced mitochondrial biogenesis is regulated by mitochondrial-derived reactive oxygen species activation of CaMKII," *Diabetes*, vol. 63, 2014.
- [12] I. A. Demyanenko, E. N. Popova, V. V. Zakharova et al., "Mitochondria-targeted antioxidant SkQ1 improves impaired dermal wound healing in old mice," *Aging (Albany NY)*, vol. 7, pp. 475–485, 2015.
- [13] M. Mihara and M. Uchiyama, "Determination of malonaldehyde precursor in tissues by thiobarbituric acid test," *Analytical Biochemistry*, vol. 86, pp. 271–278, 1978.
- [14] R. A. Underwood, N. S. Gibran, L. A. Muffley, M. L. Usui, and J. E. Olerud, "Color subtractive-computer-assisted image analysis for quantification of cutaneous nerves in a diabetic mouse model," *The Journal of Histochemistry and Cytochemistry*, vol. 49, pp. 1285–1291, 2001.
- [15] J. Michaels, S. S. Churgin, K. M. Blechman et al., "*db/db* mice exhibit severe wound-healing impairments compared with other murine diabetic strains in a silicone-splinted excisional wound model," *Wound Repair and Regeneration*, vol. 15, pp. 665–670, 2007.
- [16] V. I. Tkalčević, S. Čužić, M. J. Parnham, I. Pašalić, and K. Brajša, "Differential evaluation of excisional non-occluded wound healing in *db/db* mice," *Toxicologic Pathology*, vol. 37, pp. 183–192, 2009.
- [17] E. N. Popova, O. Y. Pletjushkina, V. B. Dugina et al., "Scavenging of reactive oxygen species in mitochondria induces myofibroblast differentiation," *Antioxidants & Redox Signaling*, vol. 13, pp. 1297–1307, 2010.
- [18] I. A. Demianenko, T. V. Vasilieva, L. V. Domnina et al., "Novel mitochondria-targeted antioxidants, "Skulachev-ion" derivatives, accelerate dermal wound healing in animals," *Biochemistry (Moscow)*, vol. 75, pp. 274–280, 2010.
- [19] C. Feillet-Coudray, G. Fouret, R. Ebabe Elle et al., "The mitochondrial-targeted antioxidant MitoQ ameliorates metabolic syndrome features in obesogenic diet-fed rats better than apocynin or allopurinol," *Free Radical Research*, vol. 48, pp. 1232–1246, 2014.
- [20] S. A. Eming, T. Krieg, and J. M. Davidson, "Inflammation in wound repair: molecular and cellular mechanisms," *The Journal of Investigative Dermatology*, vol. 127, pp. 514–525, 2007.
- [21] J. V. Dovi, L.-K. He, and L. A. DiPietro, "Accelerated wound closure in neutrophil-depleted mice," *Journal of Leukocyte Biology*, vol. 73, pp. 448–455, 2003.
- [22] K. Mahadev, A. Zilbering, L. Zhu, and B. J. Goldstein, "Insulin-stimulated hydrogen peroxide reversibly inhibits protein-tyrosine phosphatase 1B in vivo and enhances the early insulin action cascade," *The Journal of Biological Chemistry*, vol. 276, pp. 21938–21942, 2001.
- [23] S. Biosciences, "Epigenetic modifications regulate gene expression, Pathways Mag. 2008," March 2017, <http://www.sabiosciences.com/pathwaymagazine/pathways8/epigenetic-modifications-regulate-gene-expression.php>.
- [24] J. P. Gray and E. Heart, "Usurping the mitochondrial supremacy: extramitochondrial sources of reactive oxygen intermediates and their role in beta cell metabolism and insulin secretion," *Toxicology Mechanisms and Methods*, vol. 20, pp. 167–174, 2010.
- [25] C. Leloup, C. Tourrel-Cuzin, C. Magnan et al., "Mitochondrial reactive oxygen species are obligatory signals for glucose-induced insulin secretion," *Diabetes*, vol. 58, pp. 673–681, 2009.
- [26] R. P. Robertson, "Chronic oxidative stress as a central mechanism for glucose toxicity in pancreatic islet beta cells in diabetes," *The Journal of Biological Chemistry*, vol. 279, pp. 42351–42354, 2004.
- [27] R. A. Zinovkin, V. P. Romaschenko, I. I. Galkin et al., "Role of mitochondrial reactive oxygen species in age-related inflammatory activation of endothelium," *Aging (Albany NY)*, vol. 6, pp. 661–674, 2014.
- [28] I. I. Galkin, O. Y. Pletjushkina, R. A. Zinovkin et al., "Mitochondria-targeted antioxidants prevent TNF α -induced endothelial cell damage," *Biochemistry (Moscow)*, vol. 79, pp. 124–130, 2014.
- [29] K. Maruyama, J. Asai, M. Ii, T. Thorne, D. W. Losordo, and P. A. D'Amore, "Decreased macrophage number and activation lead to reduced lymphatic vessel formation and contribute to impaired diabetic wound healing," *The American Journal of Pathology*, vol. 170, pp. 1178–1191, 2007.
- [30] S. Khanna, S. Biswas, Y. Shang et al., "Macrophage dysfunction impairs resolution of inflammation in the wounds of diabetic mice," *PLoS One*, vol. 5, article e9539, 2010.
- [31] R. E. Mirza, M. M. Fang, E. M. Weinheimer-Haus, W. J. Ennis, and T. J. Koh, "Sustained inflammasome activity in macrophages impairs wound healing in type 2 diabetic humans and mice," *Diabetes*, vol. 63, 2014.
- [32] R. Zhou, A. S. Yazdi, P. Menu, and J. Tschopp, "A role for mitochondria in NLRP3 inflammasome activation," *Nature*, vol. 469, pp. 221–225, 2011.
- [33] A. Dashdorj, K. Jyothi, S. Lim et al., "Mitochondria-targeted antioxidant MitoQ ameliorates experimental mouse colitis by suppressing NLRP3 inflammasome-mediated inflammatory cytokines," *BMC Medicine*, vol. 11, p. 178, 2013.

- [34] M. L. Lamers, M. E. S. Almeida, M. Vicente-Manzanares, A. F. Horwitz, and M. F. Santos, "High glucose-mediated oxidative stress impairs cell migration," *PloS One*, vol. 6, article e22865, 2011.
- [35] C. H. Lee, B. Shah, E. K. Moioli, and J. J. Mao, "CTGF directs fibroblast differentiation from human mesenchymal stem/stromal cells and defines connective tissue healing in a rodent injury model," *The Journal of Clinical Investigation*, vol. 120, pp. 3340–3349, 2010.
- [36] F. Ferraro, S. Lymperi, S. Méndez-Ferrer et al., "Diabetes impairs hematopoietic stem cell mobilization by altering niche function," *Science Translational Medicine*, vol. 3, no. 104, article 104ra101, 2011.
- [37] M. Albiero, N. Poncina, M. Tjwa et al., "Diabetes causes bone marrow autonomic neuropathy and impairs stem cell mobilization via dysregulated p66Shc and Sirt1," *Diabetes*, vol. 63, 2014.
- [38] E. R. Galimov, B. V. Chernyak, A. S. Sidorenko, A. V. Tereshkova, and P. M. Chumakov, "Prooxidant properties of p66shc are mediated by mitochondria in human cells," *PloS One*, vol. 9, article e86521, 2014.
- [39] I. N. Shipounova, D. A. Svinareva, T. V. Petrova et al., "Reactive oxygen species produced in mitochondria are involved in age-dependent changes of hematopoietic and mesenchymal progenitor cells in mice. A study with the novel mitochondria-targeted antioxidant SkQ1," *Mechanisms of Ageing and Development*, vol. 131, pp. 415–421, 2010.
- [40] M. S. Bitar and Z. N. Labbad, "Transforming growth factor- β and insulin-like growth factor-I in relation to diabetes-induced impairment of wound healing," *The Journal of Surgical Research*, vol. 61, pp. 113–119, 1996.
- [41] D. Gong, W. Shi, S. Yi, H. Chen, J. Groffen, and N. Heisterkamp, "TGF β signaling plays a critical role in promoting alternative macrophage activation," *BMC Immunology*, vol. 13, p. 31, 2012.
- [42] E. J. Marrotte, D. D. Chen, J. S. Hakim, and A. F. Chen, "Manganese superoxide dismutase expression in endothelial progenitor cells accelerates wound healing in diabetic mice," *The Journal of Clinical Investigation*, vol. 120, pp. 4207–4219, 2010.
- [43] V. P. Skulachev, V. N. Anisimov, Y. N. Antonenko et al., "An attempt to prevent senescence: a mitochondrial approach," *Biochimica et Biophysica Acta - Bioenergetics*, vol. 1787, pp. 437–461, 2009.
- [44] V. N. Anisimov, M. V. Egorov, M. S. Krasilshchikova et al., "Effects of the mitochondria-targeted antioxidant SkQ1 on lifespan of rodents," *Aging (Albany NY)*, vol. 3, pp. 1110–1119, 2011.

Research Article

Oxidative Phosphorylation System in Gastric Carcinomas and Gastritis

René G. Feichtinger,¹ Daniel Neureiter,² Tom Skaria,¹ Silja Wessler,³ Timothy L. Cover,⁴ Johannes A. Mayr,⁵ Franz A. Zimmermann,⁵ Gernot Posselt,³ Wolfgang Sperl,⁵ and Barbara Kofler¹

¹Laura-Bassi Centre of Expertise, Research Program for Receptor Biochemistry and Tumor Metabolism, Department of Pediatrics, Paracelsus Medical University, 5020 Salzburg, Austria

²Institute of Pathology, Paracelsus Medical University, 5020 Salzburg, Austria

³Division of Molecular Biology, Department of Microbiology, Paris-Lodron University, 5020 Salzburg, Austria

⁴Department of Medicine and Department of Pathology, Microbiology, and Immunology, Vanderbilt University School of Medicine and Veterans Affairs Tennessee Valley Healthcare System, Nashville, TN 37232, USA

⁵Department of Pediatrics, Paracelsus Medical University, 5020 Salzburg, Austria

Correspondence should be addressed to René G. Feichtinger; r.feichtinger@salk.at

Received 31 January 2017; Revised 10 April 2017; Accepted 10 May 2017; Published 28 June 2017

Academic Editor: Maik Hüttemann

Copyright © 2017 René G. Feichtinger et al. This is an open access article distributed under the Creative Commons Attribution License, which permits unrestricted use, distribution, and reproduction in any medium, provided the original work is properly cited.

Switching of cellular energy production from oxidative phosphorylation (OXPHOS) by mitochondria to aerobic glycolysis occurs in many types of tumors. However, the significance of this switching for the development of gastric carcinoma and what connection it may have to *Helicobacter pylori* infection of the gut, a primary cause of gastric cancer, are poorly understood. Therefore, we investigated the expression of OXPHOS complexes in two types of human gastric carcinomas (“intestinal” and “diffuse”), bacterial gastritis with and without metaplasia, and chemically induced gastritis by using immunohistochemistry. Furthermore, we analyzed the effect of HP infection on several key mitochondrial proteins. Complex I expression was significantly reduced in intestinal type (but not diffuse) gastric carcinomas compared to adjacent control tissue, and the reduction was independent of HP infection. Significantly, higher complex I and complex II expression was present in large tumors. Furthermore, higher complex II and complex III protein levels were also obvious in grade 3 versus grade 2. No differences of OXPHOS complexes and markers of mitochondrial biogenesis were found between bacterially caused and chemically induced gastritis. Thus, intestinal gastric carcinomas, but not precancerous stages, are frequently characterized by loss of complex I, and this pathophysiology occurs independently of HP infection.

1. Introduction

Histologically, two main types of gastric cancers (GCs) can be distinguished according to the Laurén classification [1, 2]. The intestinal type of GC progresses through a well-characterized process of morphological changes: normal mucosa, chronic gastritis, atrophic gastritis, intestinal metaplasia, and cancer. The relative frequencies are approximately 54% for the intestinal type and 32% for the diffuse type, with the remaining 15% of CGs being indeterminate

[3]. The prognostic relevance of the Laurén classification is still a matter of debate as some studies found no correlation with patient outcome [4]. Intestinal type GC is most prevalent in older men, whereas the diffuse type is more prevalent in young women [5]. Intestinal type was reported to be associated with intestinal metaplasia of the gastric mucosa and presence of *Helicobacter pylori* (HP) [6].

Most human tumors are characterized by a shift from oxidative phosphorylation (OXPHOS) to aerobic glycolysis called the Warburg effect [7–13]. At least two of the five

OXPPOS complexes act as tumor suppressors, namely, complex I in oncogenic tumors and complex II in both pheochromocytomas and paragangliomas [11, 14–17]. In addition, several mutations affecting mitochondrial complex I genes have been described in gastric cancers and other neoplasms, suggesting that mitochondrial energy metabolism may play a critical role in tumor development [18–22]. During the last decade, our understanding of cancer energy metabolism changed fundamentally. It is now known that tumor cells can use glucose and glutamine, the latter is the preferred substrate for OXPPOS. In addition, it is proposed that many cancer types use respiration and glycolysis for energy production [23]. Other models of cancer metabolism like the “reverse Warburg effect” and the “lactate shuttle hypothesis” have emerged reflecting the heterogeneity and flexibility of tumor energy metabolism [24–27].

The most common cause of GC is infection by HP, which is classified as a type 1 (definite) carcinogen for GC by the World Health Organization [28]. The two major virulence factors of HP are vacuolating cytotoxin A (VacA) and cytotoxin-associated gene A (CagA). VacA is excreted into the extracellular space, where it can bind and enter host cells and form channels in the inner mitochondrial membrane, leading to depolarization of mitochondrial membrane potential, disruption of mitochondrial function, and ultimately cell death [29–33]. Infection of AGS (adenocarcinoma gastric cell line) cells with HP leads to mtDNA instability and a decrease in mtDNA copy number [34, 35]. The amount and activity of complex I decreased after infection with HP [36]. VacA can induce the recruitment of dynamin-related protein-1 (DRP-1) to induce mitochondrial network fragmentation [32]. Finally, VacA can induce (acute exposure) or repress (prolonged exposure) autophagy, events which also can potentially influence mitochondrial energy metabolism [37]. Intracellular VacA is significantly associated with the development of progressive atrophic gastritis and intestinal metaplasia [38]. We hypothesized that a large number of gastric carcinomas similar to other solid tumors are characterized by the Warburg effect. Furthermore, we propose that HP infection has an influence on mitochondrial energy metabolism.

The aim of the present study was to elucidate changes in aerobic mitochondrial energy metabolism in GC and gastritis and evaluate the pathophysiological significance of HP infection on expression of subunits of the OXPPOS complexes. Immunohistochemical staining was used, because it is impossible to get a sufficient amount of frozen tissue for functional evaluation of the OXPPOS enzymes especially in diffuse gastric carcinomas and gastritis. Diffuse GCs grow in relatively small cell clusters interspersed by a large number of normal cells. Intestinal gastric carcinomas also are heterogeneous with regard to tissue composition. In addition, heterogeneity is also present within a single intestinal GC. Furthermore, a tumor cell content of over 80% is needed to generate reliable functional data on the OXPPOS enzyme activity. Immunohistochemical staining of homogenous tissue samples correlates well with enzymatic analysis as the OXPPOS system is mainly regulated via protein amount [7, 10, 11]. Therefore, immunohistochemical staining of

heterogeneous samples represents the method of choice since it excellently reflects the *in vivo* situation.

2. Materials and Methods

2.1. Ethics. Human tumors were obtained from the Department of Pathology, Paracelsus Medical University, Salzburg. The study was performed according to the Austrian Gene Technology Act. Experiments were conducted in accordance with the Helsinki Declaration of 1975 (revised 1983) and the guidelines of the Salzburg State Ethics Research Committee (ethical agreement: AZ 209-11-E1/823-2006), being no clinical drug trial or epidemiological investigation. All patients signed an informed consent document concerning the surgical intervention. Furthermore, the study did not extend to examination of individual case records. Patient anonymity was ensured at all times. Patient characteristics are given in Supplementary Table 2 available online at <https://doi.org/10.1155/2017/1320241>.

2.2. Samples. Formalin fixed paraffin-embedded (FFPE) tissue from intestinal ($n = 20$) and diffuse-type ($n = 20$) gastric carcinomas, bacterial gastritis ($n = 5$), bacterial gastritis with metaplasia ($n = 5$), and chemical (C) gastritis ($n = 5$) was obtained by the Institute of Pathology Salzburg. Since it is a matter of debate which classification of gastric carcinomas should be used, we added in addition to the Laurén classification also the WHO classification 2010 in Supplementary Tables 2 and 3. All gastric specimens were routinely stained with H&E to obtain the basic morphology of acute or chronic inflammation, fibrosis, and intestinal metaplasia. The presence of metaplasia was confirmed by a periodic acid-Schiff procedure/Alcian blue stain. Additionally, Giemsa staining was performed to visualize *H. pylori*. Based on these detailed histological evaluation patterns, the human gastric biopsies were categorized as chemical gastropathies caused by NSAIDs (nonsteroidal anti-inflammatory drugs) and/or alkaline reflux (in short chemical gastritis) as well as *H. pylori*-associated chronic gastritis with and without intestinal metaplasia (in short, bacterial gastritis).

2.3. Immunohistochemical Staining and Analysis of FFPE Tissues. For immunohistochemistry, the following antibodies were used: complex I subunit NDUF54 (mouse monoclonal, 1 : 1000; Abcam, Cambridge, UK), complex II subunit 70 kDa Fp (mouse monoclonal, 1 : 2000; MitoSciences, Eugene, Oregon), complex III subunit Core 2 (mouse monoclonal, 1 : 1500; MitoSciences), complex IV subunit I (mouse monoclonal, 1 : 1000; MitoSciences), complex V subunit alpha (mouse monoclonal, 1 : 2000; MitoSciences), porin 31HL (mouse monoclonal, 1 : 3000; MitoSciences), and VacA antibody (rabbit polyclonal, 1 : 1000) [39]. All antibodies were diluted in Dako antibody diluent with background reducing components (Dako, Glostrup, Denmark). Immunohistochemistry was performed as described previously [40]. For antigen retrieval, the sections were immersed for 45 min in 1 mM EDTA, 0.05% Tween-20, pH 8, at 95°C. Tissue sections were incubated for 30 min with the above-mentioned primary antibodies. The staining intensities of the tumor and

control tissues were determined by two examiners on a stereomicroscope. Staining intensities were rated using a scoring system ranging from 0 to 3, with 0 indicating no staining, 1 mild, 2 moderate, and 3 strong staining. The intensities were multiplied by the percentage of positive cells, resulting in score values.

The specificity of the antibodies was previously shown by Western blot analysis: ([9]; Figure 3), ([8], Figure 2); NDUFS4 ([9]; Figure 3), ([8], Figure 2); SDHA ([9]; Figure 3), ([8], Figure 2); UQCRC2 ([9]; Figure 3), ([8], Figure 2); MT-CO1 ([41], Figure 2); ATP5A ([9]; Figure 3), ([42]; Figure 3).

2.4. Immunofluorescence Staining of Gastritis. Cells grown on chamber slides were fixed overnight in neutral-buffered formalin. For antigen retrieval, the sections were immersed for 45 min in 1 mM EDTA, 0.05% Tween-20, pH 8, at 95°C. Tissue sections were incubated for 1 h with the above-mentioned primary antibodies. Slides were incubated with a mixture of donkey anti-mouse AlexaFluor488 (1 : 500; Fisher Scientific) and donkey anti-rabbit AlexaFluor594 (1 : 1000; Fisher Scientific) in PBS-T for 1 h. Nuclei were stained with DAPI for 10 min. Slides were mounted with fluorescence mounting medium (DAKO) and sealed with a nail polish. For immunofluorescence staining, the same antibodies as for immunohistochemical staining were used with the following dilution: porin (rabbit polyclonal; 1 : 400, Abcam), NDUFS4 (1 : 100), SDHA (1 : 400), UQCRC2 (1 : 400), MT-CO1 (1 : 100), ATP5A (1 : 400), TFAM (1 : 100), and VacA (1 : 100).

2.5. Determination of mtDNA Mutations. Three 5 μ m-thick tissue sections were microdissected to separate normal tissue and tumor tissue. The microdissected regions were used for isolation of DNA. mtDNA copy number and mitochondrial common deletions were determined by quantitative PCR as previously described [43].

In addition, the genes of mitochondrially encoded subunits of complex I and tRNAs were sequenced in samples that showed the most severe loss of complexes I and IV. Primer sequences are given in Supplementary Table 1 that were previously published [8]. Sequencing was performed with a GenomeLab™ DTCS Quick Start Kit (Beckman Coulter, Fullerton, CA) on a CEQ™ 2000 DNA Analysis System (Beckman Coulter). The CEQ 8000 Genetic Analysis System (Beckman Coulter) was used for analysis of the sequencing data. These sequences were compared with the complete *Homo sapiens* mitochondrial genome (GenBank accession number: J01415.1).

2.6. Statistical Analysis. Patient characteristics and clinical data were analyzed with the χ^2 test and Student's *t*-test. For multiple comparisons of intestinal and diffuse-type GC and control tissue, one-way ANOVA and Bonferroni correction were used. For analysis of clinical parameters and OXPHOS enzyme expression, *t*-test or ANOVA and Bonferroni post hoc test were used. For analysis of gastritis, the nonparametric Kruskal-Wallis test was used. For comparison of mtDNA

copy number in intestinal GC with and without HP history, a *t*-test was used.

3. Results

3.1. Expression of OXPHOS Complexes and Porin Differs between Intestinal and Diffuse-Type Gastric Carcinomas. To investigate potential alterations of mitochondrial metabolism in GC, we carried out immunohistochemical staining of the mitochondrial outer membrane protein porin (a marker of mitochondrial mass) as well as all five OXPHOS complexes in tumor samples from 40 patients and compared the staining intensities with those of adjacent normal mucosal columnar epithelial tissues (Figures 1–3; Supplementary Figure 1; Supplementary Tables 4 and 5). We observed significantly higher porin expression in diffuse-type GC compared to adjacent normal tissue (Figures 2(a) and 2(d) and Figure 3(a)). We also detected a trend toward higher porin levels in intestinal GC compared to adjacent normal tissue in 15 of 19 cases examined (Figures 1(a) and 1(d) and Figure 3(a)). Comparison of the seven cases with OXPHOS deficiencies (six complex I and complex IV) revealed that porin, the marker for the mitochondrial mass, is higher in the OXPHOS-deficient cases (mean score value 230) compared to OXPHOS competent cases (mean score value 183).

Complex I staining was significantly reduced in 16 of 20 (80%) intestinal type GCs compared to normal adjacent control tissue (Figures 1(b) and 1(e) and Figure 3(b)). Moreover, although we observed complex I-negative cells in all 20 intestinal GCs, connected large foci of complex I-negative tumor cells were evident in 30% of the cases (35–65% of the tumor cells were negative for complex I in the latter tumors). These cases were also used for microdissection to elucidate the underlying genetic causes (see below).

Overall, complex II showed a trend toward reduced levels in intestinal GCs, as a minor reduction of complex II was present in 16 of 20 (80%) cases compared to adjacent control tissue (Supplementary Figure 1). One case with reduced complex I expression had higher complex II expression (case M17), and one case with unchanged complex I expression had a reduced complex II expression (case M16) compared to normal tissue. In 18 of 20 cases (90%), a combined reduction ($n = 15$) or upregulation ($n = 3$) of complexes I and II was evident. Complex V expression was greatly reduced (by about 50%) in only a single case (case M4); no major differences in complex V were detected in any of the other cases (Supplementary Figure 1). Alterations of complex III and IV were quite heterogeneous, as complex III and complex IV were both higher in 8/20, equal in 3/20, or both lower in 9/20 intestinal GCs.

In the diffuse-type GCs, we detected a trend toward lower expression levels of complex I compared to adjacent control tissue (Figure 1(b)). However, complex I deficiency was rare and found only in a subset of carcinoma cells. Complex III, complex IV, and complex V levels were all significantly higher in diffuse-type GCs compared to normal tissue (Figures 3(d), 3(e), and 3(f); Supplementary Figure 2).

The normal epithelium surrounding intestinal and diffuse-type GCs differed significantly with respect to

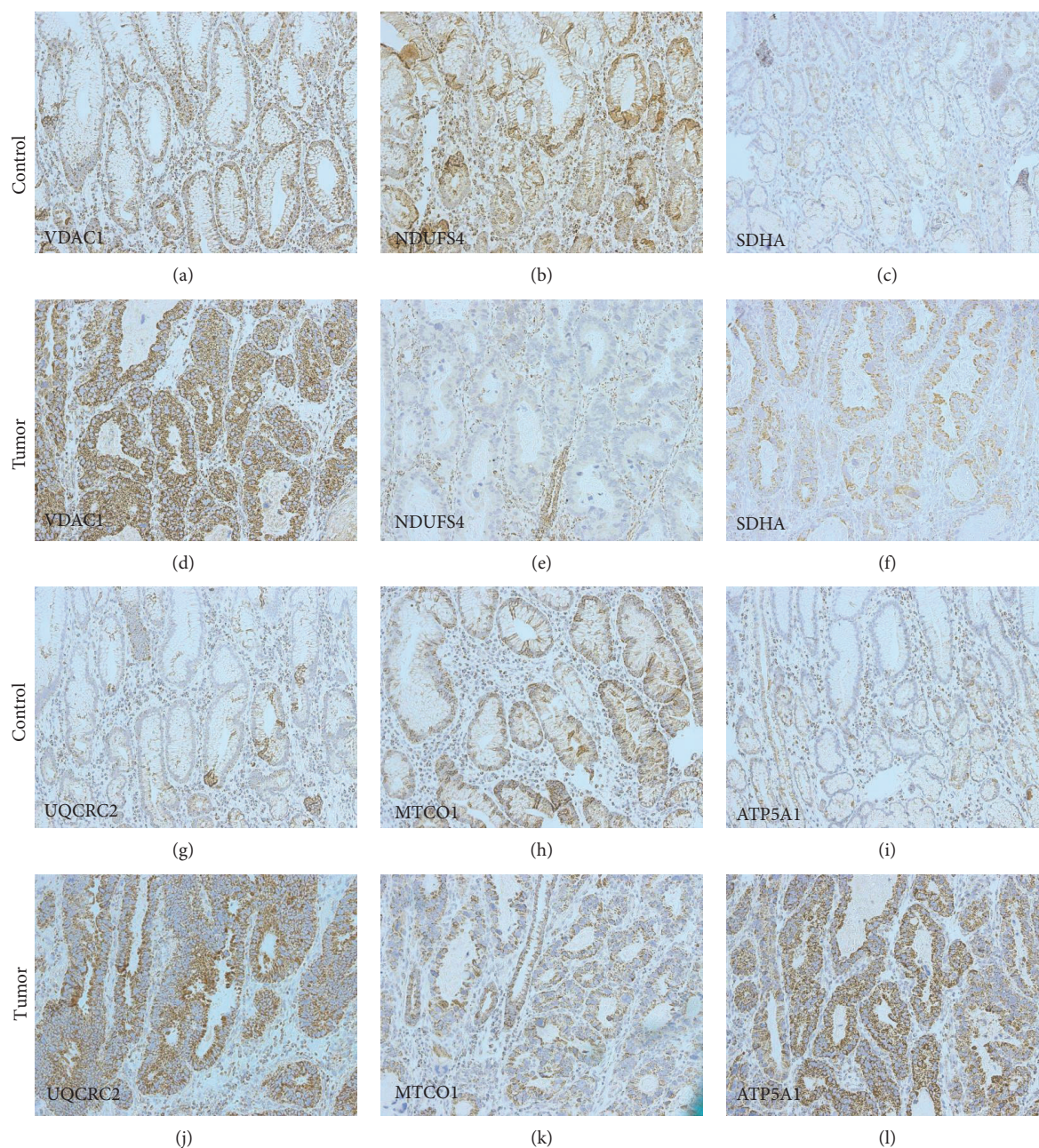


FIGURE 1: Expression of the OXPHOS complexes and porin in intestinal GC (case M5). Immunohistochemical staining of (a–c); (g–i) normal gastric mucosa and (d–f); (j–l) intestinal gastric carcinoma for (a), (d) porin, (b), (e) complex I, (c), (f) complex II, (g), (j) complex III, (h), (k) complex IV, (i), and (l) complex V. Magnification 20x.

complexes II and III expression (Figures 3(c) and 3(d); Supplementary Figure 2). This can be explained by the anatomic localization of the biopsy site, since diffuse-type GCs are not associated with the antrum [44], whereas HP-associated intestinal GCs are often found in the antrum [45]. Regional differences in OXPHOS enzyme expression might be present between the fundus, cardia, and antrum.

Of the 20 intestinal GCs, ten had a former histochemical-proven HP infection and we compared them to the ten cases without it. All gastric specimens were routinely stained with

H&E to obtain the basic morphology of acute or chronic inflammation, fibrosis, and intestinal metaplasia. The presence of metaplasia was confirmed by a periodic acid-Schiff procedure/Alcian blue stain. Gastric specimens were classified as HP-positive or HP-negative based on the results of the Giemsa stain [46]. We detected significantly lower levels of porin (Figure 4(a)) and complex III (Figure 4(d)) in intestinal GC cases with a history of HP infection. Furthermore, the other complexes also showed a trend toward lower levels in the HP-infected cases. mtDNA copy number was significantly higher in tumors with versus tumors without a history

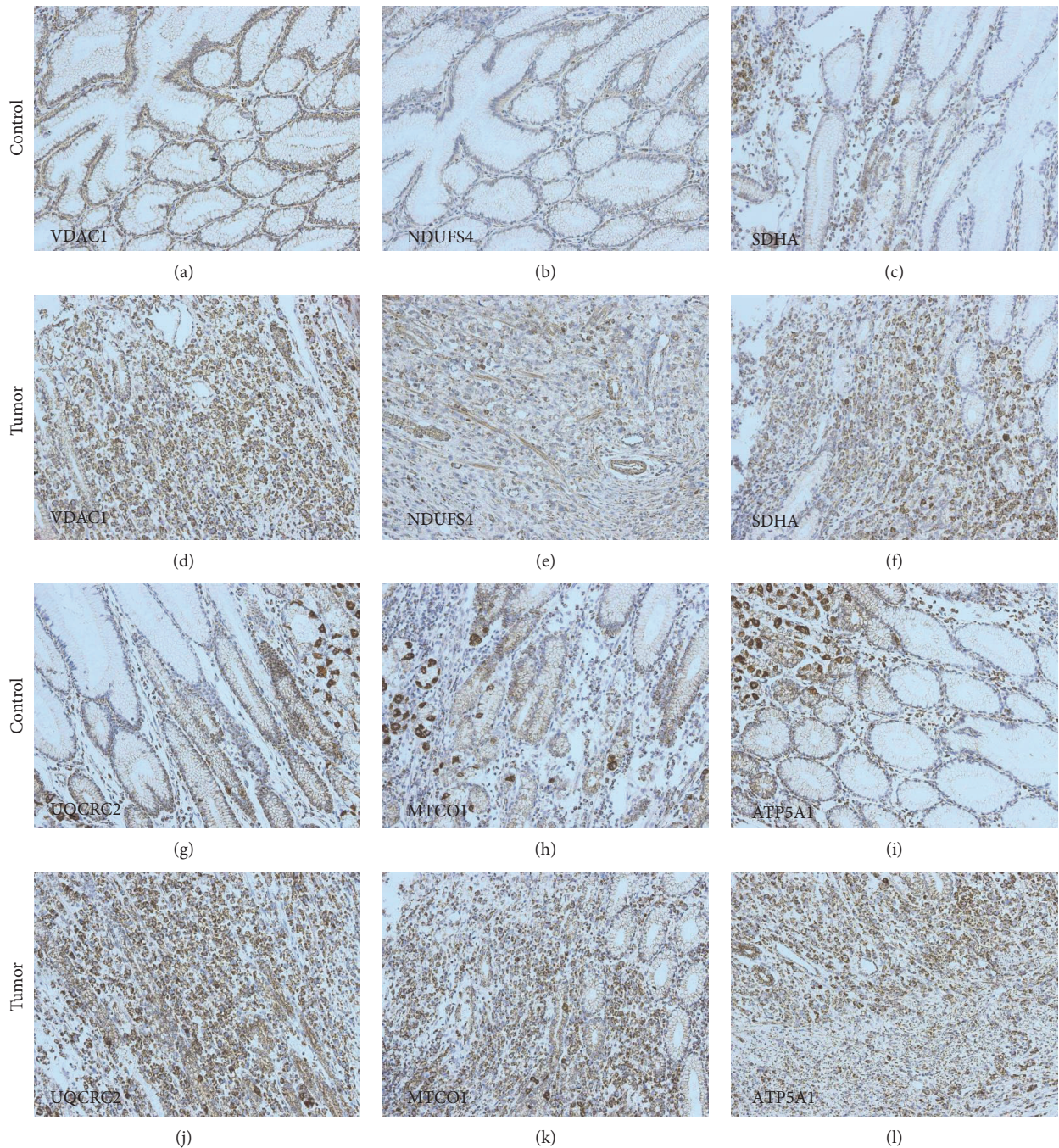


FIGURE 2: Expression of the OXPHOS complexes and porin in diffuse-type GC (case M39). Immunohistochemical staining of (a–c); (g–i) normal gastric mucosa and (d–f); (j–l) diffuse-type gastric carcinoma for (a), (d) porin, (b), (e) complex I, (c), (f) complex II, (g), (j) complex III, (h), (k) complex IV, (i), and (l) complex V. Parietal cells show strong staining for the OXPHOS complexes (g–i). Magnification 20x.

of HP infection. The expression levels of porin and the OXPHOS complexes from normal tissue adjacent to cancerous tissue did not differ between HP-infected and noninfected samples.

3.2. Differences in OXPHOS Complex and Porin Expression Related to Clinical Data. Tumors were categorized in low-size (<5 cm) and high-size (>5 cm) tumors by the mean tumor size (5 cm). A significantly higher complex I ($p = 0.005$) and

complex II ($p = 0.011$) expression was present in high-size tumors. Furthermore, a higher expression of complex II was found in grade 3 versus grade 2 ($p = 0.018$) and T4 versus T1 ($p = 0.013$). Significantly lower complex III protein levels were found in tumors localized in the prepyloric antrum compared to the cardia ($p = 0.049$). Significantly higher complex III expression was also found in UICC (Union Internationale Contre le Cancer) III compared to UICC II tumors (Supplementary Table 3).

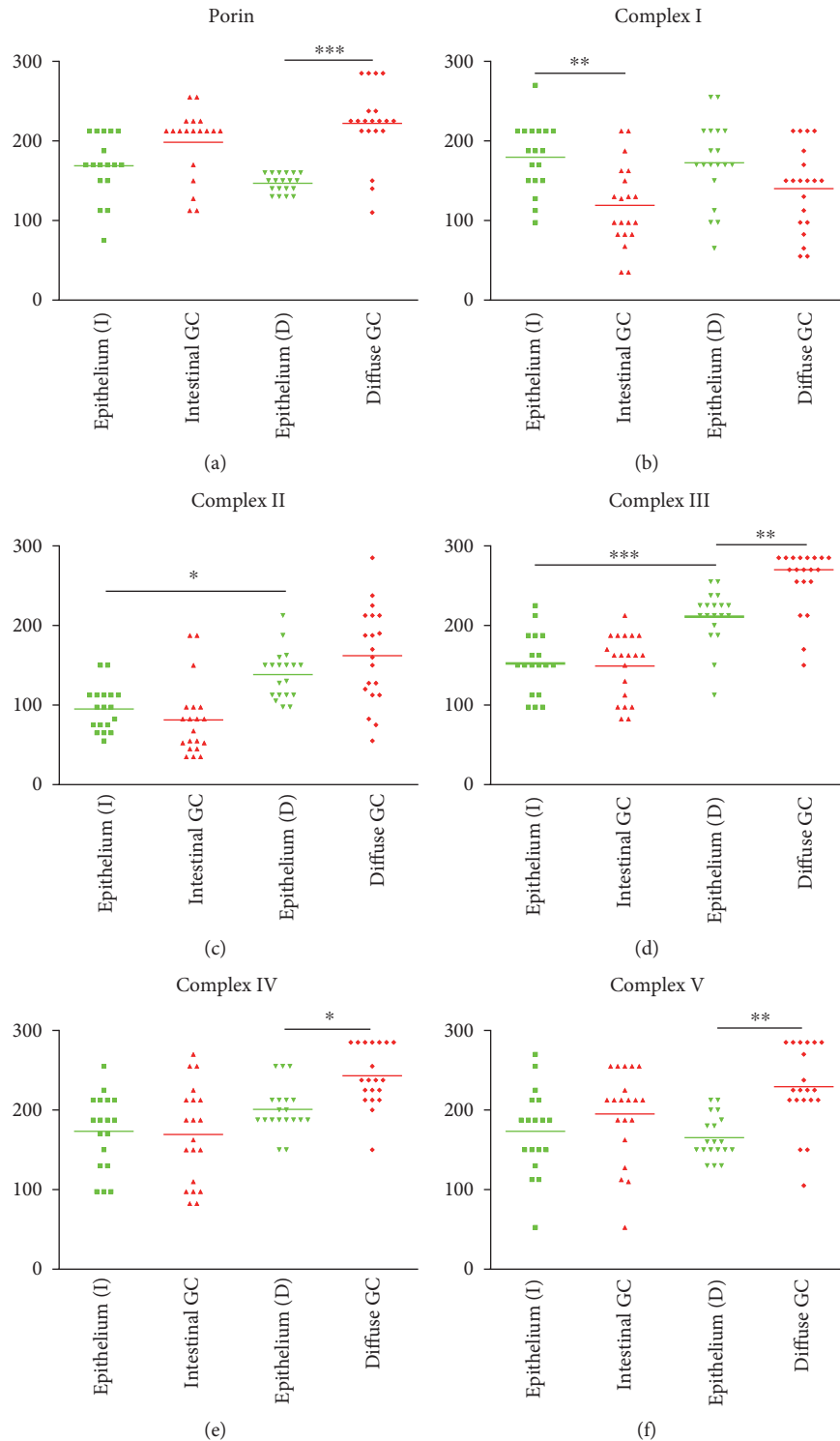


FIGURE 3: Score values of immunohistochemical staining of the OXPHOS complexes and porin in intestinal and diffuse-type GCs. (a) Porin. (b) Complex I. (c) Complex II. (d) Complex III. (e) Complex IV. (f) Complex V. Tumors were compared to corresponding adjacent control tissue. Corresponding epithelium was used for comparison with intestinal carcinoma I and diffuse-type carcinomas (d). For statistical analysis, a one-way ANOVA with a Bonferroni correction to compare multiple groups was used. * $p < 0.05$; ** $p < 0.01$; *** $p < 0.001$.

3.3. mtDNA Mutations Are Rare in Intestinal Carcinomas. To investigate if the complex I-negative foci of intestinal GCs are caused by mtDNA mutation, we obtained complex I-negative tissue by microdissection and sequenced selected

mtDNA regions, including genes encoding subunits of complex I and tRNAs, from six intestinal GC cases. Only one of the six GCs (case M5; histology shown in Figure 1(e)) harbored a somatic pathogenic mutation, a frame shift

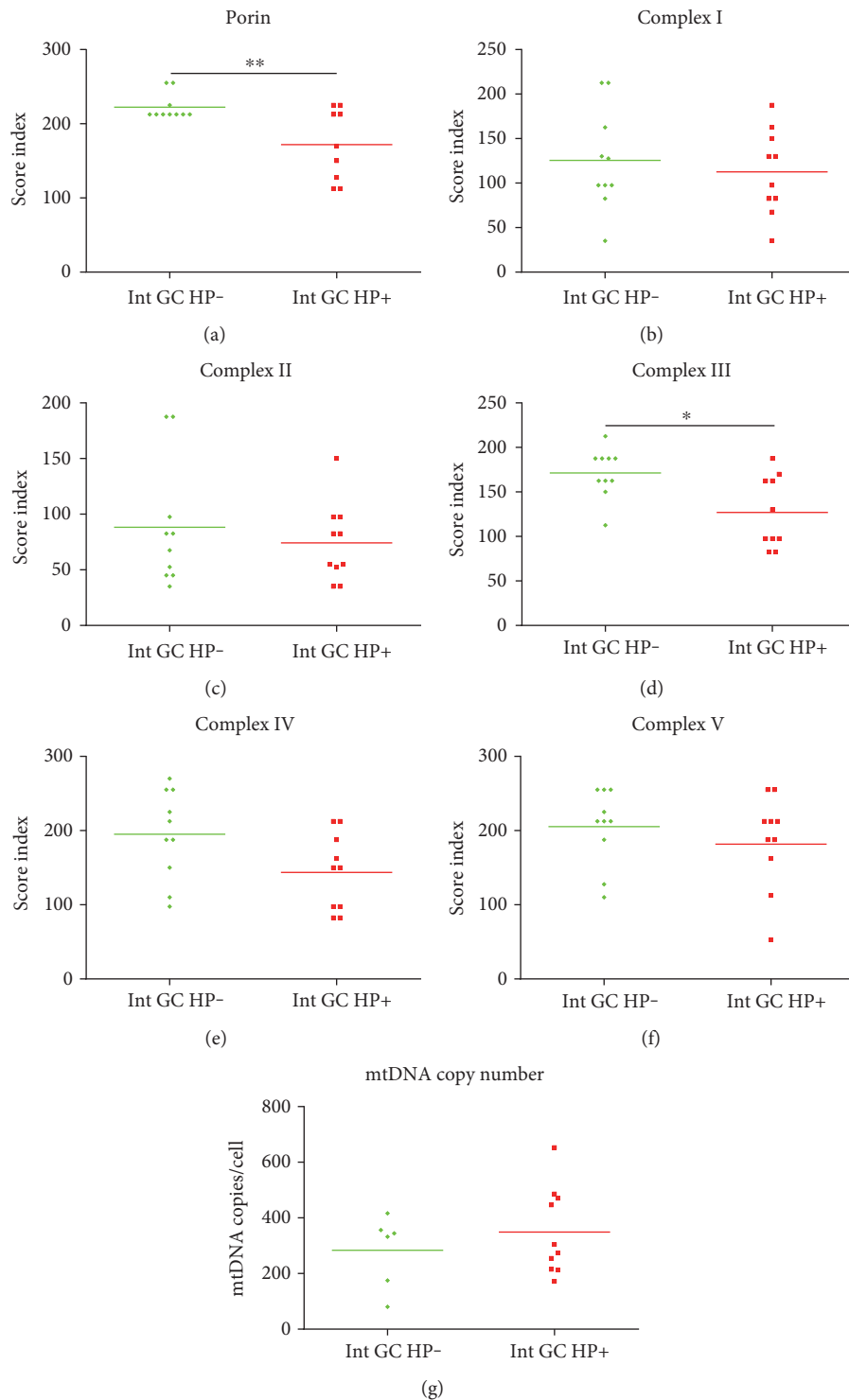


FIGURE 4: Comparison of score values of immunohistochemical staining of the OXPHOS complexes and porin in intestinal GCs with and without HP history. (a) Porin. (b) Complex I. (c) Complex II. (d) Complex III. (e) Complex IV. (f) Complex V. (g) mtDNA copy number. For statistical analysis, a *t*-test was used. * $p < 0.05$; ** $p < 0.01$.

(10952_10953insC) in a poly cytosine stretch of the complex I subunit ND4 (Figure 5). This insertion causes a frameshift and creates a stop codon ~150 bp downstream, which results in a truncated ND4 protein. The same mutation has also been reported in thyroid oncocyomas [40].

3.4. Analysis of Reported Mutations in Nuclear-Encoded Complex I Subunits. The Cancer Genome Project database COSMIC was used to check the frequency of potentially pathogenic nuclear-encoded complex I subunits in diffuse and intestinal gastric carcinomas. The pathogenicity of the

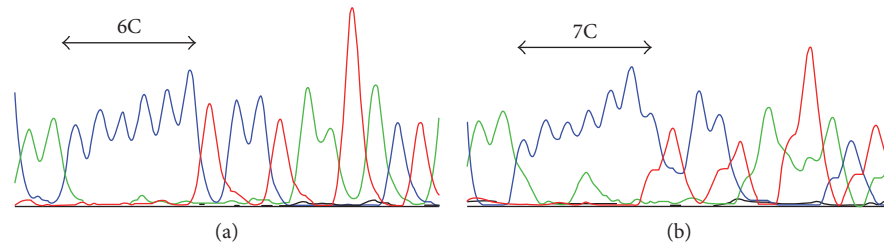


FIGURE 5: Sequence analysis of complex I coding mtDNA genes in an intestinal GC (case M5). (a) Sequence analysis showing the normal sequence for the poly C stretch of the *ND4* gene from normal corresponding tissue. (b) Sequence analysis showing an insertion of cytosine in the poly cytosine stretch of the *ND4* gene in the tumor tissue. The mutation appears to be heteroplasmic, but the tissue of case M5 was heterogeneous and contaminated with nontumor cells. In addition, complex IV was reduced in M5 (Figures 1(h) and 1(k)).

mutations was analyzed with MutationTaster. In total, 8 potentially pathogenic mutations were identified in 85 analyzed intestinal adenocarcinomas. Mutations included 2 frame shift mutations, one stop mutation and five missense mutations. In 9.4% of the adenocarcinomas, mutations were identified. This could only partially explain the high frequency of complex I deficiency as found in our study that was 35%. However, since the tumors often show a partial complex I loss restricted to some areas, it is possible that mutations cannot be detected.

Potentially pathogenic mutations were found in 3.8% (3/78) diffuse carcinomas, including one stop mutation and two missense mutations. The following 37 nuclear complex I genes were checked for mutations: *NDUFA1*, 2, 3, 5, 6–13; *NDUFAB1*; *NDUFB1–11*; *NDUFC1–2*; *NDUFS1–8*; *NDUFV1–3*. In summary, a 2.5-fold higher frequency of nuclear complex I mutations in intestinal carcinomas compared to diffuse carcinomas was found.

3.5. VacA Positivity Does Not Correlate with OXPHOS Alterations. As indicated in the literature, the major HP virulence factor VacA seems to affect mitochondrial biology. To investigate if HP infection, which is a known risk factor for the development of intestinal GC, influences mitochondrial biology in gastric cells, we immunohistochemically analyzed biopsies from type B gastritis with and without metaplasia, type C gastritis, and GC patients for the presence of the major virulence factor VacA by immunohistochemical staining. We also examined the expression of complex I, mitochondrial transcription factor A (TFAM), and porin as markers for mitochondrial biogenesis.

VacA was never detected in type C gastritis. We detected VacA mainly in gastric glands (Figures 6(f) and 6(g)) and the gastric lumen (Figure 6(a)), consistent with its localization in previous studies [38, 47]. Chief cells never showed positivity for VacA, and intracellular VacA was rarely detected in epithelial cells. Interestingly, we observed localization of VacA to human gut parietal cells in biopsies of patients with HP gastritis (Figures 6(b), 6(c), 6(d), 6(f), and 6(g) and Figure 7). HP is able to repopulate the extracellular gut environment after complete elimination of extracellular bacteria with gentamicin [48, 49], suggesting that HP may be

sheltered for long periods within some host cell population, like parietal cells.

Parietal cells are mitochondria-rich whereas chief cells only show weak porin expression (Figures 6(b) and 6(f) and Figures 2(g), 2(h), and 2(i)).

We found no correlation between VacA positivity and TFAM or porin staining intensity in gastritis (Figures 6 and Figure 7). The chemical ($n = 5$), bacterial ($n = 5$), and bacterial gastritis cases with metaplasia ($n = 5$) did not differ in terms of expression of TFAM, porin, and the OXPHOS complexes (Figure 7). In general, expression of all mitochondrial markers was significantly lower in chief cells than in epithelial and parietal cells (Figure 7), as expected.

4. Discussion

About one third (30%) of the 20 intestinal GCs we examined exhibited focal complex I deficiency, with 35–65% of the tumor cells negative for complex I. It was reported that gastric cancers are composed of different tumor cell clones [50, 51]. However, few OXPHOS-deficient tumors might be overseen by immunohistochemical analysis, since it is proposed that mutations just affecting the enzymatic activity and not protein levels exist, but this might be the exception not the rule.

In only one of these six cases, the complex I deficiency could be explained by a pathogenic mtDNA mutation. The relatively low percentage of mitochondrial DNA mutations in our sample cohort (5%) points to a limited significance; Habano et al. also reported potentially pathogenic mitochondrial complex I mutations in 2/34 (6%) of their analyzed intestinal carcinomas [19]. As most of the complex I subunits are encoded by nuclear genes, mutations in the latter are likely responsible for the isolated loss of complex I in most cases of intestinal GC. In summary, a 2.5-fold higher frequency of nuclear complex I mutations in intestinal carcinomas compared to diffused carcinomas was found by analysis of data from the Cancer Genome Project suggesting that indeed nuclear mutations might contribute to the observed complex I loss in a high percentage of intestinal carcinomas. The phenomenon that complex I is most frequently affected has several reasons. First, complex I is the biggest OXPHOS complex composed of 45 (44 + 1) subunits. Therefore, more mutations might be found in complex I since 44 genes encode complex I subunits but only 4 genes encode for

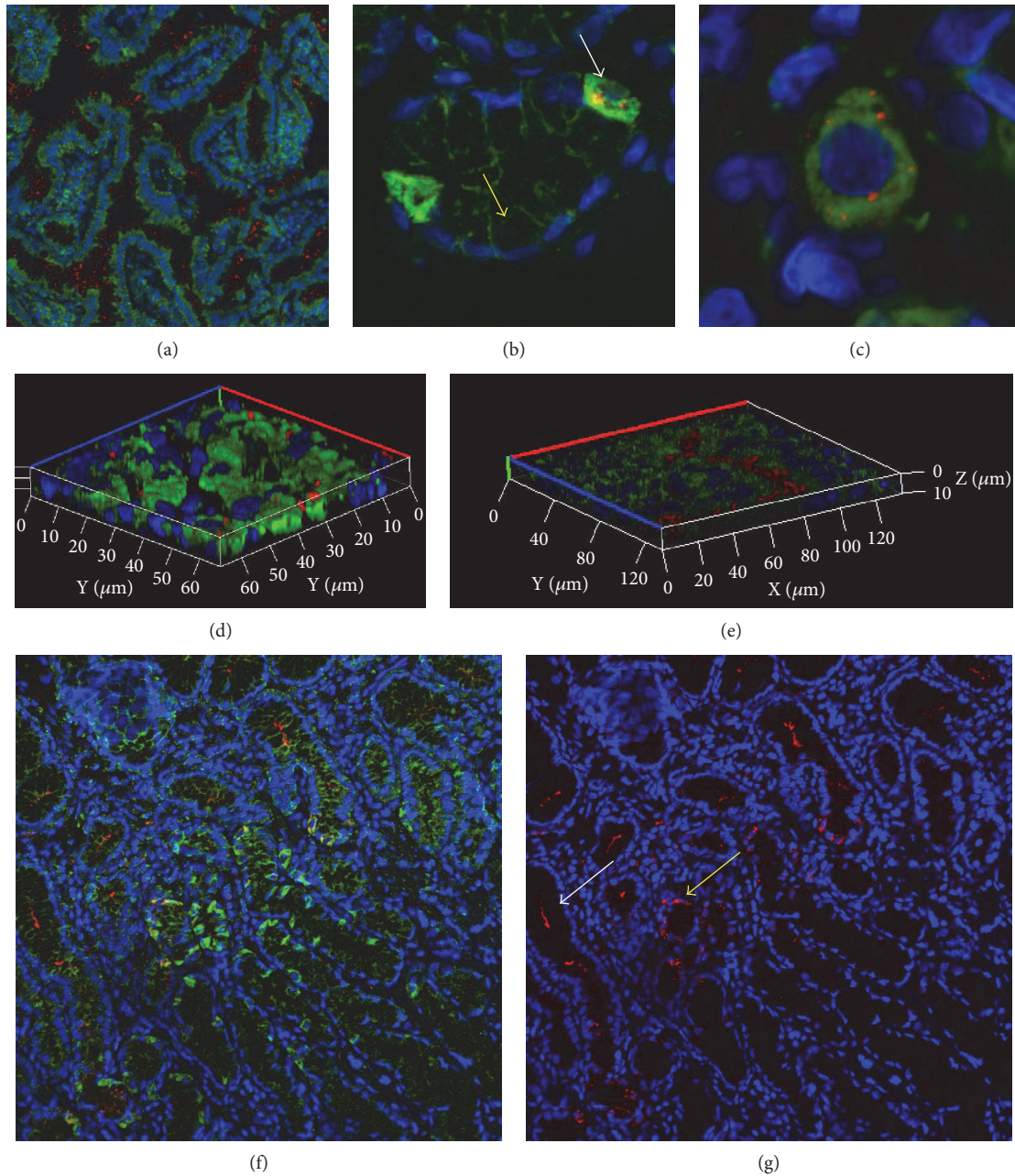


FIGURE 6: Localization of VacA in gastritis. (a) Triple immunofluorescence staining (complex I/VacA/DAPI) of case BGM-4 revealed strong HP colonization of the gastric lumen (10x magnification). (b) Triple immunofluorescence staining (porin/VacA/DAPI) of case BG-3 revealed selective staining of mitochondria-rich parietal cells. No differences in porin expression between the infected and noninfected parietal cells were detected. Parietal cells (white arrow) and mucous-secreting cells (yellow arrow) (63x magnification). (c) Triple immunofluorescence staining (TFAM/VacA/DAPI) of case BG-3 showed intracellular staining of VacA in parietal cells. (d) Z-stack of triple immunofluorescence staining (TFAM/VacA/DAPI) of case BG-1 revealed cytoplasmic localization of VacA (63x magnification). (e) Intraglandular VacA in case BG-1 (TFAM/VacA/DAPI); (20x magnification). (f) Triple immunofluorescence staining (Porin/VacA/DAPI) of case BG-3. (g) Figure f without the green channel to better visualize the intraglandular (white arrow) and intraparietal (yellow arrow) localization of VacA.

complex II subunits. In addition, mitochondrial DNA is specifically prone to damage. Complex II is encoded by nuclear genes. Second, complex I is linked to several other important metabolic pathways and apoptosis. Mitochondrial fatty acid biosynthetic pathway and lipoylation important especially for the pyruvate dehydrogenase are linked to the acyl carrier

protein (ACP; NDUFAB1) [52]. Defects of complex I have pleiotropic effects leading to more global changes and reprogramming of cancer metabolism. Furthermore, the complex I subunit NDUFS1 can be cleaved by caspase 3 and granzyme A to induce apoptosis [53, 54]. Therefore, lack of complex I might represent a growth advantage for tumor cells.

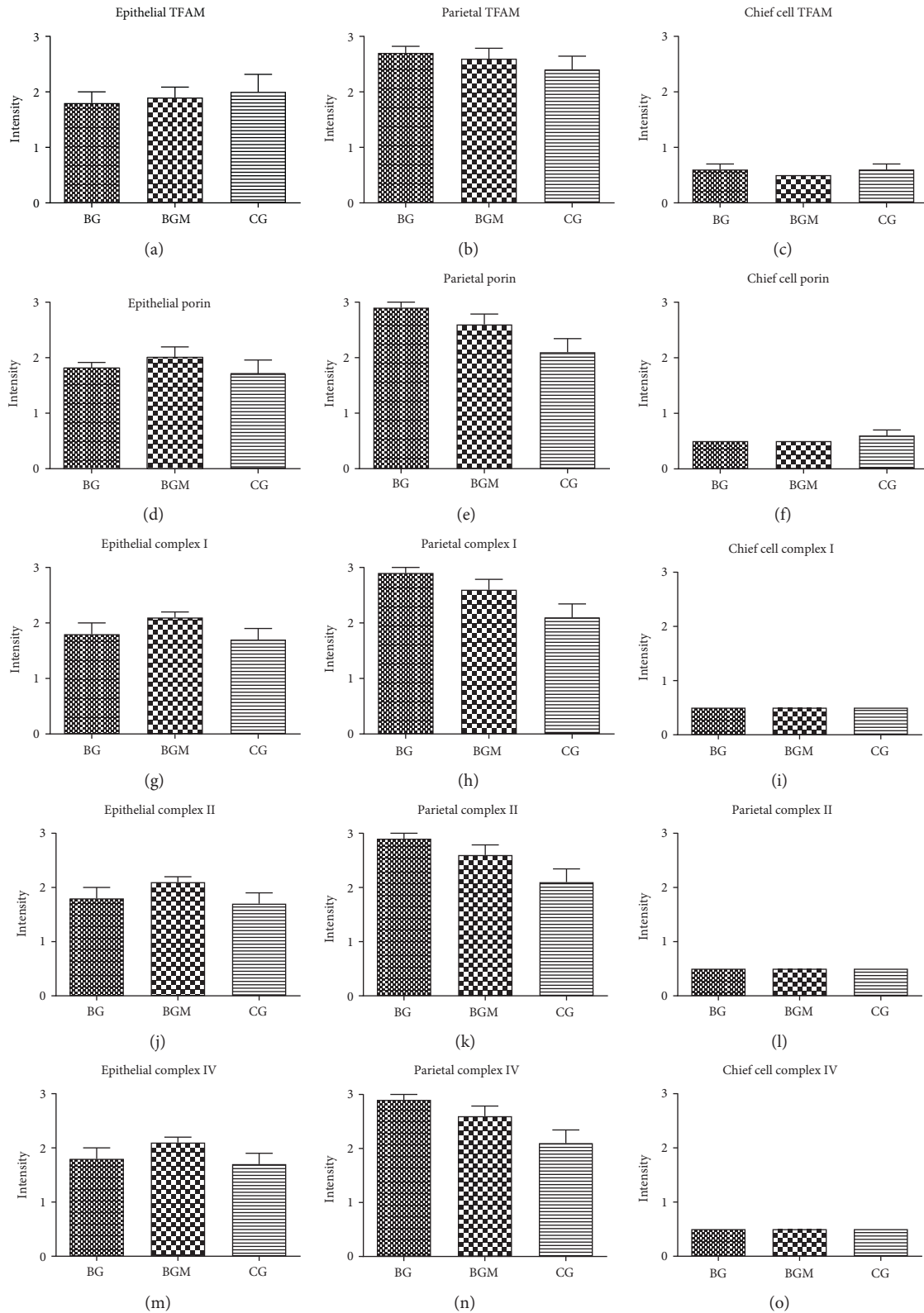


FIGURE 7: No differences of the OXPHOS complex, porin, and TFAM expression between chemical, bacterial, and bacterial gastritis with metaplasia. (a–c) TFAM expression in bacterial gastritis (BG), bacterial gastritis with metaplasia (BGM), and chemical gastritis (CG). (d–f) Porin expression. (g–i) Complex I expression. (j–l) Complex II expression. (m–o) Complex IV expression. (a), (d), (g), (j), and (m) epithelial cells; (b), (e), (h), (k), and (n) parietal cells; (c), (f), (i), (l), and (o) chief cells. For statistical analysis, a nonparametric Kruskal-Wallis test was used. Note that in some figures, no SEM is indicated because the staining intensity was the same for all samples. For all groups $n = 5$.

In the 20 cases of diffuse-type GC that we examined, complex I deficiency was rare. Therefore, complex I deficiency might be of importance for the pathogenesis of intestinal GC only. However, as we found no complex I-negative cells in type B gastritis with or without metaplasia or in type C gastritis, loss of complex I does not appear to be an early event in GC tumor development. Moreover, HP-infected cells (parietal cells, mucous-secreting cells, and metaplasia) showed no signs of OXPHOS dysregulation.

In complex I-deficient tumors, compensatory mechanisms are found which indicate that a partial rescue of mitochondrial respiration can be achieved by an increase of mitochondrial biogenesis, especially complex II [55]. Since complex II is able to feed electrons into the respiratory chain, it is thought that residual respiration can be sustained via complex II in complex I-deficient tumor cells. However, complex II is not able to transport protons across the mitochondrial membrane.

Comparison of the seven cases with OXPHOS deficiencies revealed that porin, the marker for the mitochondrial mass, is higher in the OXPHOS-deficient cases compared to OXPHOS competent cases.

Also other proteins feed electrons into the respiratory chain like the mitochondrial sulfide:quinone oxidoreductase (SQORL), the electron transfer flavoprotein-ubiquinone oxidoreductase (ETFHD), the glycerol-3-phosphate dehydrogenase (GPD2), and the sulfite oxidase (SUOX) that potentially contribute to residual respiration in complex I-negative tumors [56–59]. However, evidence that mitochondrial respiration is crucial for tumor cells comes from therapeutic studies, which, for example, show that inhibition of complex I and glucose restriction is lethal for cancer cells [60].

Karita et al. reported VacA localization in mucous neck, chief, and parietal cells of HP-infected patients [38]. However, to our knowledge, ours is the first study to show VacA positivity exclusively in parietal cells. We detected intracellular localization of this major pathogenicity factor of HP in parietal cells but found no positivity in chief cells. In addition, we noted obvious VacA/HP positivity in the lumen of gastric glands and the gastric lumen. VacA can permeabilize the apical membrane of isolated rat parietal cells, inducing hypochloridia [61]. The selective localization in parietal cells has potential therapeutic implications, because HP might avoid drug therapy by localizing in deep layers of the mucosa [38, 62, 63]. HP can repopulate the extracellular gut environment after complete elimination of extracellular bacteria with gentamicin [49, 64].

Importantly, in our study, intestinal GCs in patients with a history of HP infection had a lower mitochondrial mass compared to cases with no prior HP infection, as indicated by porin expression. Since the OXPHOS complexes showed a trend (complex III significantly reduced) toward lower levels in cases with an HP-positive history, HP might therefore affect mitochondrial function only in intestinal GC cells, since we found no alterations of mitochondrial parameters in any of the gastritis cases. We speculate that some mitochondrial alterations reported in the literature might be associated with induction of apoptosis and not HP infection per se as

previously reported [36]. We suppose that results have to be interpreted with regard to acute or chronic infection. It is highly doubtful that the high MOIs (100–400) which are usually used for cell culture experiments would be reached during infection in vivo [65, 66]. Previous studies supposed that MOIs between 1 and 10 are found in the stomach [65, 66]. Low MOIs (1–10) inhibit apoptosis whereas high MOIs (>75) induce apoptosis in splenocytes [67].

Previous studies reported that infection with low MOI (=10) did not induce mtDNA destabilization [35]. We suggest that studies that used a very high MOI are of limited biological significance, because most of the reported changes in mitochondrial energy metabolism might be attributable to apoptotic changes. Furthermore, based on molecular genetic analysis, mainly, mutations in the highly variable D-loop region of mtDNA were found, alterations unlikely to cause severe mitochondrial dysfunction [34, 68].

However, the biological significance seems to be limited, as we found no associations between infection and parameters of mitochondrial energy metabolism in gastritis. Our data indicate that the alterations of energy metabolism found in a large percentage of GCs might occur independently of bacterial infection.

Although HP can influence mitochondrial physiology in vitro, there are no signs of impact on the OXPHOS system in gastritis and cancer. A high percentage of intestinal gastric carcinomas exhibits complex I deficiency, independent of HP history. Complex I deficiency might have therapeutic implications since tumors with mitochondrial defects and high glycolytic activity can potentially be inhibited in growth via a low-carbohydrate, high-fat (ketogenic) diet.

Evidence suggests that HP can overcome eradication therapy and repopulate the gastric lumen from deep layers of the mucosa. Intracellular *Helicobacter pylori* VacA positivity is found exclusively in parietal cells that might be used as a niche. Testing for HP positivity especially VacA in deep layers might be important for evaluation of the effectiveness of eradication therapy.

In addition, correlations between OXPHOS complex expression and parameters of tumor malignancy were present. A significantly higher complex I and complex II expression was present in large tumors. Tumor size is an independent prognostic factor for a 5-year survival rate in advanced gastric cancer [69, 70]. The mean tumor size in the study by Wang et al. was 4.9 cm who analyzed 430 individuals. In our study, the mean size was 5 cm. Furthermore, a higher expression of complex II was found in grade 3 versus grade 2 and T4 versus T1 gastric carcinomas. The higher complex II levels found in high grade tumors might reflect the degree of OXPHOS deficiency. A highly dysfunctional respiratory chain might lead to a stronger compensatory upregulation of complex II to sustain a residual OXPHOS. Significantly, higher complex III expression was also found in UICC III compared to UICC II tumors. Significantly lower complex III protein levels were found in tumors localized in the prepyloric antrum compared to the cardia ($p = 0.049$). This is consistent with the previous results. Patients with tumors of the antrum show a better survival than individuals with tumors of the antrum [71]. The more malignant tumors

therefore again show a higher OXPHOS enzyme expression. However, it has to be mentioned that the increased expression of OXPHOS complexes might be due to a compensatory effect. Patients with a lack of complex I frequently show an increase of the other respiratory chain complexes. A high expression of complex II does not exclude complex I deficiency; rather, it could be suggestive of a respiratory chain defect. However, in case of our study, no compensatory upregulation of complex II was present in the 35% of the intestinal carcinomas with complex I deficiency. Complex II and complex III were higher in the tumors without complex I deficiency. An increase in complex II might cause an increase in respiration, since complex II can feed electrons into the transport chain. A singular upregulation of complex III should not be sufficient to enhance OXPHOS. In addition, the mitochondrial mass was equal in both groups suggesting no compensatory mechanism. In summary, gastric carcinomas exhibit a high percentage of OXPHOS enzyme defects and an association of a high expression of several OXPHOS enzymes and malignancy.

Disclosure

The authors alone are responsible for the content and writing of the paper.

Conflicts of Interest

The authors declare that there is no conflict of interests regarding the publication of this paper.

Acknowledgments

This research was supported by grants from the “Vereinigung zur Förderung der pädiatrischen Forschung und Fortbildung Salzburg”; Cancer Foundation Salzburg, the Children’s Cancer Foundation Salzburg, the Austrian Research Promotion Agency (822782/THERAPEP), the National Institutes of Health (AI039657 and CA116087) and the Department of Veterans Affairs (2I01BX000627).

References

- [1] Y. C. Chen, W. L. Fang, R. F. Wang et al., “Clinicopathological variation of Lauren classification in gastric cancer,” *Pathology Oncology Research*, vol. 22, no. 1, pp. 197–202, 2016.
- [2] P. Lauren, “The two histological main types of gastric carcinoma: diffuse and so-called intestinal-type carcinoma. An attempt at a histo-clinical classification,” *Acta Pathologica et Microbiologica Scandinavica*, vol. 64, pp. 31–49, 1965.
- [3] W. Polkowski, J. W. van Sandick, G. J. Offerhaus et al., “Prognostic value of Lauren classification and *c-erbB-2* oncogene overexpression in adenocarcinoma of the esophagus and gastroesophageal junction,” *Annals of Surgical Oncology*, vol. 6, no. 3, pp. 290–297, 1999.
- [4] F. Berlth, E. Bollschweiler, U. Drebber, A. H. Hoelscher, and S. Moenig, “Pathohistological classification systems in gastric cancer: diagnostic relevance and prognostic value,” *World Journal of Gastroenterology*, vol. 20, no. 19, pp. 5679–5684, 2014.
- [5] H. Zheng, H. Takahashi, Y. Murai et al., “Pathobiological characteristics of intestinal and diffuse-type gastric carcinoma in Japan: an immunostaining study on the tissue microarray,” *Journal of Clinical Pathology*, vol. 60, no. 3, pp. 273–277, 2007.
- [6] P. Correa and M. B. Piazuelo, “*Helicobacter pylori* infection and gastric adenocarcinoma,” *US Gastroenterology & Hepatology Review*, vol. 7, no. 1, pp. 59–64, 2011.
- [7] R. G. Feichtinger, D. Neureiter, J. A. Mayr et al., “Loss of mitochondria in ganglioneuromas,” *Frontiers in Bioscience (Elite Edition)*, vol. 3, pp. 179–186, 2011.
- [8] R. G. Feichtinger, S. Weis, J. A. Mayr et al., “Alterations of oxidative phosphorylation complexes in astrocytomas,” *Glia*, vol. 62, no. 4, pp. 514–525, 2014.
- [9] R. G. Feichtinger, S. Weis, J. A. Mayr et al., “Alterations of oxidative phosphorylation in meningiomas and peripheral nerve sheath tumors,” *Neuro-Oncology*, vol. 18, no. 2, pp. 184–194, 2016.
- [10] R. G. Feichtinger, F. Zimmermann, J. A. Mayr et al., “Low aerobic mitochondrial energy metabolism in poorly- or undifferentiated neuroblastoma,” *BMC Cancer*, vol. 10, p. 149, 2010.
- [11] J. A. Mayr, D. Meierhofer, F. Zimmermann et al., “Loss of complex I due to mitochondrial DNA mutations in renal oncocytoma,” *Clinical Cancer Research*, vol. 14, no. 8, pp. 2270–2275, 2008.
- [12] O. Warburg, “Über den Stoffwechsel der Carcinomzelle,” *Die Naturwissenschaften*, vol. 50, pp. 1131–1137, 1924.
- [13] O. Warburg, “The Metabolism of Tumors,” in pp. 129–169, Richard R. Smith Inc., New York, 1931.
- [14] D. Astuti, F. Latif, A. Dallol et al., “Gene mutations in the succinate dehydrogenase subunit SDHB cause susceptibility to familial pheochromocytoma and to familial paraganglioma,” *American Journal of Human Genetics*, vol. 69, no. 1, pp. 49–54, 2001.
- [15] D. E. Benn, M. S. Croxson, K. Tucker et al., “Novel succinate dehydrogenase subunit B (SDHB) mutations in familial pheochromocytomas and paragangliomas, but an absence of somatic SDHB mutations in sporadic pheochromocytomas,” *Oncogene*, vol. 22, no. 9, pp. 1358–1364, 2003.
- [16] G. Gasparre, A. M. Porcelli, E. Bonora et al., “Disruptive mitochondrial DNA mutations in complex I subunits are markers of oncogenic phenotype in thyroid tumors,” *Proceedings of the National Academy of Sciences of the United States of America*, vol. 104, no. 21, pp. 9001–9006, 2007.
- [17] F. A. Zimmermann, J. A. Mayr, R. Feichtinger et al., “Respiratory chain complex I is a mitochondrial tumor suppressor of oncogenic tumors,” *Frontiers in Bioscience*, vol. 3, pp. 315–325, 2011.
- [18] N. O. Bianchi, M. S. Bianchi, and S. M. Richard, “Mitochondrial genome instability in human cancers,” *Mutation Research*, vol. 488, no. 1, pp. 9–23, 2001.
- [19] W. Habano, T. Sugai, S. I. Nakamura, N. Uesugi, T. Yoshida, and S. Sasou, “Microsatellite instability and mutation of mitochondrial and nuclear DNA in gastric carcinoma,” *Gastroenterology*, vol. 118, no. 5, pp. 835–841, 2000.
- [20] W. Y. Hung, C. W. Wu, P. H. Yin et al., “Somatic mutations in mitochondrial genome and their potential roles in the progression of human gastric cancer,” *Biochimica et Biophysica Acta*, vol. 1800, no. 3, pp. 264–270, 2010.
- [21] K. Kose, T. Hiyama, S. Tanaka, M. Yoshihara, W. Yasui, and K. Chayama, “Somatic mutations of mitochondrial DNA in

- digestive tract cancers,” *Journal of Gastroenterology and Hepatology*, vol. 20, no. 11, pp. 1679–1684, 2005.
- [22] V. Máximo, P. Soares, R. Seruca, A. S. Rocha, P. Castro, and M. Sobrinho-Simões, “Microsatellite instability, mitochondrial DNA large deletions, and mitochondrial DNA mutations in gastric carcinoma,” *Genes, Chromosomes & Cancer*, vol. 32, no. 2, pp. 136–143, 2001.
- [23] M. M. Alam, S. Lal, F. G. KE, and L. Zhang, “A holistic view of cancer bioenergetics: mitochondrial function and respiration play fundamental roles in the development and progression of diverse tumors,” *Clinical and Translational Medicine*, vol. 5, no. 1, p. 3, 2016.
- [24] G. A. Brooks, “Mammalian fuel utilization during sustained exercise,” *Comparative Biochemistry and Physiology. Part B, Biochemistry & Molecular Biology*, vol. 120, no. 1, pp. 89–107, 1998.
- [25] Y. J. Chen, N. G. Mahieu, X. Huang et al., “Lactate metabolism is associated with mammalian mitochondria,” *Nature Chemical Biology*, vol. 12, no. 11, pp. 937–943, 2016.
- [26] I. Georgescu, R. J. Gooding, R. C. Doiron et al., “Molecular characterization of Gleason patterns 3 and 4 prostate cancer using reverse Warburg effect-associated genes,” *Cancer & Metabolism*, vol. 4, p. 8, 2016.
- [27] S. Pavlides, D. Whitaker-Menezes, R. Castello-Cros et al., “The reverse Warburg effect: aerobic glycolysis in cancer associated fibroblasts and the tumor stroma,” *Cell Cycle*, vol. 8, no. 23, pp. 3984–4001, 2009.
- [28] K. R. Jones, J. M. Whitmire, and D. S. Merrell, “A tale of two toxins: *Helicobacter pylori* CagA and VacA modulate host pathways that impact disease,” *Frontiers in Microbiology*, vol. 1, p. 115, 2010.
- [29] T. L. Cover and S. R. Blanke, “*Helicobacter pylori* VacA, a paradigm for toxin multifunctionality,” *Nature Reviews. Microbiology*, vol. 3, no. 4, pp. 320–332, 2005.
- [30] J. H. Foo, J. G. Culvenor, R. L. Ferrero, T. Kwok, T. Lithgow, and K. Gabriel, “Both the p33 and p55 subunits of the *Helicobacter pylori* VacA toxin are targeted to mammalian mitochondria,” *Journal of Molecular Biology*, vol. 401, no. 5, pp. 792–798, 2010.
- [31] A. Galmiche and J. Rasso, “Targeting of *Helicobacter pylori* VacA to mitochondria,” *Gut Microbes*, vol. 1, no. 6, pp. 392–395, 2010.
- [32] P. Jain, Z. Q. Luo, and S. R. Blanke, “*Helicobacter pylori* vacuolating cytotoxin A (VacA) engages the mitochondrial fission machinery to induce host cell death,” *Proceedings of the National Academy of Sciences of the United States of America*, vol. 108, no. 38, pp. 16032–16037, 2011.
- [33] S. L. Palframan, T. Kwok, and K. Gabriel, “Vacuolating cytotoxin A (VacA), a key toxin for *Helicobacter pylori* pathogenesis,” *Frontiers in Cellular and Infection Microbiology*, vol. 2, p. 92, 2012.
- [34] X. W. Huang, R. H. Luo, Q. Zhao et al., “*Helicobacter pylori* induces mitochondrial DNA mutation and reactive oxygen species level in AGS cells,” *International Journal of Medical Sciences*, vol. 8, no. 1, pp. 56–67, 2011.
- [35] A. M. Machado, C. Figueiredo, E. Touati et al., “*Helicobacter pylori* infection induces genetic instability of nuclear and mitochondrial DNA in gastric cells,” *Clinical Cancer Research*, vol. 15, no. 9, pp. 2995–3002, 2009.
- [36] A. M. Machado, C. Desler, S. Bøggild et al., “*Helicobacter pylori* infection affects mitochondrial function and DNA repair, thus, mediating genetic instability in gastric cells,” *Mechanisms of Ageing and Development*, vol. 134, no. 10, pp. 460–466, 2013.
- [37] L. K. Greenfield and N. L. Jones, “Modulation of autophagy by *Helicobacter pylori* and its role in gastric carcinogenesis,” *Trends in Microbiology*, vol. 21, no. 11, pp. 602–612, 2013.
- [38] M. Karita, S. Teramukai, S. Matsumoto, and H. Shibuta, “Intracellular VacA is a valuable marker to predict whether *Helicobacter pylori* induces progressive atrophic gastritis that is associated with the development of gastric cancer,” *Digestive Diseases and Sciences*, vol. 50, no. 1, pp. 56–64, 2005.
- [39] T. L. Cover and M. J. Blaser, “Purification and characterization of the vacuolating toxin from *Helicobacter pylori*,” *The Journal of Biological Chemistry*, vol. 267, no. 15, pp. 10570–10575, 1992.
- [40] F. A. Zimmermann, J. A. Mayr, D. Neureiter et al., “Lack of complex I is associated with oncocyctic thyroid tumours,” *British Journal of Cancer*, vol. 100, no. 9, pp. 1434–1437, 2009.
- [41] M. S. Reuter, J. O. Sass, T. Leis et al., “HIBCH deficiency in a patient with phenotypic characteristics of mitochondrial disorders,” *American Journal of Medical Genetics. Part a*, vol. 164A, no. 12, pp. 3162–3169, 2014.
- [42] J. Koch, P. Freisinger, R. G. Feichtinger et al., “Mutations in TTC19: expanding the molecular, clinical and biochemical phenotype,” *Orphanet Journal of Rare Diseases*, vol. 10, p. 40, 2015.
- [43] B. Acham-Roschitz, B. Plecko, F. Lindbichler et al., “A novel mutation of the RRM2B gene in an infant with early fatal encephalomyopathy, central hypomyelination, and tubulopathy,” *Molecular Genetics and Metabolism*, vol. 98, no. 3, pp. 300–304, 2009.
- [44] B. J. Dicken, D. L. Bigam, C. Cass, J. R. Mackey, A. A. Joy, and S. M. Hamilton, “Gastric adenocarcinoma: review and considerations for future directions,” *Annals of Surgery*, vol. 241, no. 1, pp. 27–39, 2005.
- [45] R. M. Peek Jr. and M. J. Blaser, “*Helicobacter pylori* and gastrointestinal tract adenocarcinomas,” *Nature Reviews. Cancer*, vol. 2, no. 1, pp. 28–37, 2002.
- [46] O. Rotimi, A. Cairns, S. Gray, P. Moayyedi, and M. F. Dixon, “Histological identification of *Helicobacter pylori*: comparison of staining methods,” *Journal of Clinical Pathology*, vol. 53, no. 10, pp. 756–759, 2000.
- [47] V. Necchi, M. E. Candusso, F. Tava et al., “Intracellular, intercellular, and stromal invasion of gastric mucosa, preneoplastic lesions, and cancer by *Helicobacter pylori*,” *Gastroenterology*, vol. 132, no. 3, pp. 1009–1023, 2007.
- [48] M. R. Amieva, N. R. Salama, L. S. Tompkins, and S. Falkow, “*Helicobacter pylori* enter and survive within multivesicular vacuoles of epithelial cells,” *Cellular Microbiology*, vol. 4, no. 10, pp. 677–690, 2002.
- [49] A. Dubois and T. Boren, “*Helicobacter pylori* is invasive and it may be a facultative intracellular organism,” *Cellular Microbiology*, vol. 9, no. 5, pp. 1108–1116, 2007.
- [50] K. Chen, D. Yang, X. Li et al., “Mutational landscape of gastric adenocarcinoma in Chinese: implications for prognosis and therapy,” *Proceedings of the National Academy of Sciences of the United States of America*, vol. 112, no. 4, pp. 1107–1112, 2015.
- [51] Y. Guo, A. Huang, C. Hu et al., “Complex clonal mosaicism within microdissected intestinal metaplastic glands without

- concurrent gastric cancer,” *Journal of Medical Genetics*, vol. 53, no. 9, pp. 643–646, 2016.
- [52] D. Feng, A. Witkowski, and S. Smith, “Down-regulation of mitochondrial acyl carrier protein in mammalian cells compromises protein lipoylation and respiratory complex I and results in cell death,” *The Journal of Biological Chemistry*, vol. 284, no. 17, pp. 11436–11445, 2009.
- [53] D. Martinvalet, D. M. Dykxhoorn, R. Ferrini, and J. Lieberman, “Granzyme A cleaves a mitochondrial complex I protein to initiate caspase-independent cell death,” *Cell*, vol. 133, no. 4, pp. 681–692, 2008.
- [54] J. E. Ricci, C. Muñoz-Pinedo, P. Fitzgerald et al., “Disruption of mitochondrial function during apoptosis is mediated by caspase cleavage of the p75 subunit of complex I of the electron transport chain,” *Cell*, vol. 117, no. 6, pp. 773–786, 2004.
- [55] M. V. Yusenko, T. Ruppert, and G. Kovacs, “Analysis of differentially expressed mitochondrial proteins in chromophobe renal cell carcinomas and renal oncocytomas by 2-D gel electrophoresis,” *International Journal of Biological Sciences*, vol. 6, no. 3, pp. 213–224, 2010.
- [56] M. Alcazar-Fabra, P. Navas, and G. Brea-Calvo, “Coenzyme Q biosynthesis and its role in the respiratory chain structure,” *Biochimica et Biophysica Acta*, vol. 1857, no. 8, pp. 1073–1078, 2016.
- [57] T. K. Er, C. C. Chen, Y. Y. Liu et al., “Computational analysis of a novel mutation in ETFDH gene highlights its long-range effects on the FAD-binding motif,” *BMC Structural Biology*, vol. 11, p. 43, 2011.
- [58] J. L. Johnson, K. E. Coyne, R. M. Garrett et al., “Isolated sulfite oxidase deficiency: identification of 12 novel SUOX mutations in 10 patients,” *Human Mutation*, vol. 20, no. 1, p. 74, 2002.
- [59] E. Lagoutte, S. Mimoun, M. Andriamihaja, C. Chaumontet, F. Blachier, and F. Bouillaud, “Oxidation of hydrogen sulfide remains a priority in mammalian cells and causes reverse electron transfer in colonocytes,” *Biochimica et Biophysica Acta*, vol. 1797, no. 8, pp. 1500–1511, 2010.
- [60] R. Palorini, T. Simonetto, C. Cirulli, and F. Chiaradonna, “Mitochondrial complex I inhibitors and forced oxidative phosphorylation synergize in inducing cancer cell death,” *International Journal of Cell Biology*, vol. 2013, Article ID 243876, 14 pages, 2013.
- [61] F. Wang, P. Xia, F. Wu et al., “Helicobacter pylori VacA disrupts apical membrane-cytoskeletal interactions in gastric parietal cells,” *The Journal of Biological Chemistry*, vol. 283, no. 39, pp. 26714–26725, 2008.
- [62] M. S. Kim, N. Kim, S. E. Kim et al., “Long-term follow up Helicobacter pylori reinfection rate after second-line treatment: bismuth-containing quadruple therapy versus moxifloxacin-based triple therapy,” *BMC Gastroenterology*, vol. 13, p. 138, 2013.
- [63] P. P. Tagkalidis, S. G. Royce, F. A. Macrae, and P. S. Bhathal, “Selective colonization by Helicobacter pylori of the deep gastric glands and intracellular canaliculi of parietal cells in the setting of chronic proton pump inhibitor use,” *European Journal of Gastroenterology & Hepatology*, vol. 14, no. 4, pp. 453–456, 2002.
- [64] J. P. Gisbert, M. Luna, B. Gómez et al., “Recurrence of Helicobacter pylori infection after several eradication therapies: long-term follow-up of 1000 patients,” *Alimentary Pharmacology & Therapeutics*, vol. 23, no. 6, pp. 713–719, 2006.
- [65] S. Khulusi, M. A. Mendall, P. Patel, J. Levy, S. Badve, and T. C. Northfield, “Helicobacter pylori infection density and gastric inflammation in duodenal ulcer and non-ulcer subjects,” *Gut*, vol. 37, no. 3, pp. 319–324, 1995.
- [66] K. T. Wilson, K. S. Ramanujam, H. L. Mobley, R. F. Musselman, S. P. James, and S. J. Meltzer, “Helicobacter pylori stimulates inducible nitric oxide synthase expression and activity in a murine macrophage cell line,” *Gastroenterology*, vol. 111, no. 6, pp. 1524–1533, 1996.
- [67] F. I. Bussiere, R. Chaturvedi, M. Asim et al., “Low multiplicity of infection of Helicobacter pylori suppresses apoptosis of B lymphocytes,” *Cancer Research*, vol. 66, no. 13, pp. 6834–6842, 2006.
- [68] T. Hiyama, S. Tanaka, H. Shima et al., “Somatic mutation of mitochondrial DNA in Helicobacter pylori-associated chronic gastritis in patients with and without gastric cancer,” *International Journal of Molecular Medicine*, vol. 12, no. 2, pp. 169–174, 2003.
- [69] W. J. Im, M. G. Kim, T. K. Ha, and S. J. Kwon, “Tumor size as a prognostic factor in gastric cancer patient,” *Journal of Gastric Cancer*, vol. 12, no. 3, pp. 164–172, 2012.
- [70] H. M. Wang, C. M. Huang, C. H. Zheng et al., “Tumor size as a prognostic factor in patients with advanced gastric cancer in the lower third of the stomach,” *World Journal of Gastroenterology*, vol. 18, no. 38, pp. 5470–5475, 2012.
- [71] J. Pinto-De-Sousa, L. David, M. Seixas, and A. Pimenta, “Clinicopathologic profiles and prognosis of gastric carcinomas from the cardia, fundus/body and antrum,” *Digestive Surgery*, vol. 18, no. 2, pp. 102–110, 2001.

Review Article

MNRR1, a Biorganellar Regulator of Mitochondria

Lawrence I. Grossman, Neeraja Purandare, Rooshan Arshad, Stephanie Gladysck, Mallika Somayajulu, Maik Hüttemann, and Siddhesh Aras

Center for Molecular Medicine and Genetics, Wayne State University School of Medicine, 540 E. Canfield Ave., Detroit, MI 48201, USA

Correspondence should be addressed to Lawrence I. Grossman; lgrossman@wayne.edu

Received 6 March 2017; Accepted 9 April 2017; Published 8 June 2017

Academic Editor: Ryuichi Morishita

Copyright © 2017 Lawrence I. Grossman et al. This is an open access article distributed under the Creative Commons Attribution License, which permits unrestricted use, distribution, and reproduction in any medium, provided the original work is properly cited.

The central role of energy metabolism in cellular activities is becoming widely recognized. However, there are many gaps in our knowledge of the mechanisms by which mitochondria evaluate their status and call upon the nucleus to make adjustments. Recently, a protein family consisting of twin CX₉C proteins has been shown to play a role in human pathophysiology. We focus here on two family members, the isoforms CHCHD2 (renamed MNRR1) and CHCHD10. The better studied isoform, MNRR1, has the unusual property of functioning in both the mitochondria and the nucleus and of having a different function in each. In the mitochondria, it functions by binding to cytochrome *c* oxidase (COX), which stimulates respiration. Its binding to COX is promoted by tyrosine-99 phosphorylation, carried out by ABL2 kinase (ARG). In the nucleus, MNRR1 binds to a novel promoter element in *COX4I2* and itself, increasing transcription at 4% oxygen. We discuss mutations in both MNRR1 and CHCHD10 found in a number of chronic, mostly neurodegenerative, diseases. Finally, we propose a model of a graded response to hypoxic and oxidative stresses, mediated under different oxygen tensions by CHCHD10, MNRR1, and HIF1, which operate at intermediate and very low oxygen concentrations, respectively.

1. Introduction

The coiled-coil-helix-coiled-coil-helix domain- (CHCHD-) containing proteins are small, nuclear-encoded proteins that are characterized by four cysteine residues organized in twin cysteine motifs, where the cysteines are separated by nine amino acids (twin CX₉C proteins). They were initially thought to localize only to the intermembrane space (IMS) of the mitochondria, into which at least some have been shown to be imported via the Mia40/Erv1 relay system, although some of them have since been found in the nucleus [1–3]. This review will focus on two members of the twin CX₉C protein family, the isoforms CHCHD2/MNRR1 and CHCHD10, that are turning out to have surprisingly far ranging effects on mitochondrial function.

The twin CX₉C family is characterized by the CHCH domain [4], which contains a helix-turn-helix fold, where each helix contains the CX₉C motif [5–7]. The structure of the CHCH domain was resolved by protein-folding studies for Cox17, which is another CHCH protein [5, 6]. These cysteine-containing motifs help to stabilize twin alpha helices by forming disulfide bonds between the cysteine residues [8]. Although each protein in the family contains the above elements, they are unique in other aspects including their size, other structural elements, and their functions (see [9] for review).

The discovery of the Mia40 (CHCHD4)/Erv1 import pathway in the mitochondrial intermembrane space (IMS) heightened interest in the CHCHD-containing protein family [10–13]. Unlike matrix or inner-membrane-bound proteins, proteins that use the Mia40 pathway do not require

a mitochondrial-targeting sequence (MTS) precursor. Import via Mia40 works through a disulfide relay system wherein Mia40 is anchored to the inner mitochondrial membrane, facing into the IMS. In this system, CX₉C proteins are brought into the IMS from the cytosol via the translocase of the outer membrane (TOM) in a reduced, unfolded state. The oxidized cysteine residues of Mia40 then form disulfide bridges with the cysteine residues of the incoming twin CX₉C protein. After further modification to the disulfide bridges, the imported CX₉C protein is released into the IMS and Mia40 is reoxidized by Erv1 [13]. It is interesting to note that some CHCHD-containing proteins are predicted to have an MTS; these include CHCHD1, CHCHD2, and CHCHD10 [9]. Such observations suggest that these proteins can use the translocase of the inner-membrane (TIM)/TOM import as an alternative route or that they may be able to also localize to the mitochondrial matrix (or the inner mitochondrial membrane). A third possibility is that these presequences are not functional since MNRR1/CHCHD2 has been shown to localize to the mitochondria even after the removal of its MTS (Aras and Grossman, unpublished data).

CX₉C proteins were initially well characterized in *Saccharomyces cerevisiae*. The systematic analysis of the full complement of the CX₉C protein family by Longen and others [8] revealed that 13 of the 14 putative family members identified were highly conserved from yeast to mammals. A genome-wide analysis of CX₉C proteins in eukaryotes [14] expanded information on this protein family. Twin CX₉C proteins were found to be conserved across the organisms included in the study, except for three obligate intercellular parasites that contain mitosomes. The evolutionary conservation across organisms containing true mitochondria suggested that these CX₉C proteins are important in mitochondrial function and, indeed, members of this family operate as subunits in complexes I and IV of the electron transport chain (ETC), as cytochrome *c* oxidase (COX) assembly factors, and they participate in mitochondrial protein import, structure, and function. Some of the proteins also cluster into groups of unknown functions [14]. In this review, we will focus on two of these proteins that have very recently been associated with neurodegenerative diseases, MNRR1/CHCHD2 and CHCHD10. CHCHD2 was recently renamed as Mitochondrial Nuclear Retrograde Regulator 1, MNRR1 [3], which will be used from here on.

MNRR1 and CHCHD10 have a common ancestor in yeast, Mix17p (formerly known as Mic17p). Both mammalian proteins are 42% conserved with Mix17p. On a screen of deletion mutants for all twin CX₉C proteins in yeast to identify their role, the deletion of Mix17 decreased oxygen consumption to ~50% of WT [8]. Mix17 was originally characterized by Huh et al. to be located in the nucleus [15]. Gabriel et al. [16] considered the possibility that the presence of the GFP tag used in the Huh study interfered with the localization of the protein and hence characterized the localization of endogenous Mix17. Besides the nucleus, they found that Mix17 is localized to the mitochondrial IMS and is imported via the Mia40 pathway

[16]. Mix17 appeared to be a stress sensitive protein whose levels increase in response to treatment with chemicals that induce DNA replication stress [17]. The same study also characterized changes in protein localization in response to the stress. However, this study used GFP-tagged proteins and hence raises the possibility that stress-induced Mix17 localization changes could not be detected. The alignment of human MNRR1, CHCHD10, and yeast Mix17 (Figure 1) shows a highly conserved region in the hydrophobic central domain of the protein. The identification of several disease-associated mutations in this region and the *in silico* prediction of a membrane-binding function for this domain [18] suggest that this highly conserved region is necessary for the role of both proteins in a key process for mitochondrial function that can be activated in response to different conditions. An example of a protein-specific change is the Tyr residue present only in MNRR1, which lies just outside of this region. The residue contains a predicted site for tyrosine phosphorylation (<http://www.cbs.dtu.dk/services/NetPhos/>) and is discussed in the next section. The known functions and properties of MNRR1 and CHCHD10 are compared in Table 1.

2. MNRR1 Function

Although MNRR1 was originally picked up in a screening study designed to identify new genes that affect oxidative phosphorylation [19], recent evidence shows that MNRR1 is a biorganellar protein found in both the mitochondria and the nucleus. Interestingly, it appears to have a different function in each compartment: in the mitochondria, it binds to COX and in the nucleus it functions in the transcriptional regulation of genes that contain a highly conserved promoter motif termed the oxygen-responsive element (ORE) [3]. Loss and gain of function experiments have shown that MNRR1 also regulates mitochondrial membrane potential, production of reactive oxygen species (ROS) levels, and cellular redox state [3].

2.1. Mitochondrial Function. Regulation of respiration in the mitochondria by MNRR1 has been shown to require its binding to COX [3, 20]. Depletion of MNRR1 results in pleiotropic effects that include an about 50% reduction in cellular oxygen consumption, two-fold-increased ROS levels, 2-fold slower growth [3], and a fragmented mitochondrial phenotype as is associated with stress [21–23]. The binding of MNRR1 to COX is promoted by its phosphorylation at Tyr-99, a reaction that is carried out by ABL2/ARG kinase [20]. ABL2/ARG is a nonreceptor tyrosine kinase that was previously found or predicted to be in the cytosol and nucleus (<http://compartments.jensenlab.org/>) [24] and now also the mitochondria [20], where MNRR1 is currently the only known mitochondrial target.

2.2. Nuclear Function. In the nucleus, MNRR1 is the activator protein in the triad consisting of itself, RBPJ κ , and CXXC5, identified on a yeast one-hybrid screen of proteins that specifically interact with the conserved ORE [25]. We have

```

MNRR1      MPR--GSRSRTRMAPPASRAPQMRAAPRPAPVAQPPAAAPPSAVGSSAAA---P
CHCHD10    MPR--GSRSAASR---PASRP-----AAPSAHPPAHPPSAAAPAPAP---S
Mix17      MARSRGSSRPISRSRPTQTRS-----ASTMAAPVHPQQQQPNAYSHPPAAGAQT
          * * * * *      *      . *      *      . *      * *      *
          * * * * *      *      . *      *      . *      * *      *

MNRR1      RQPGLMAQMATTAAGVAVGSAVGHTLGHAI TGGFSG--GSNAEPARPDITYQEPQG
CHCHD10    GQPGLMAQMATTAAGVAVGSAVGHVMSAL TGA FSG--GS-SEPSQPAVQQAPTPA
Mix17      RQPGMFAQMASTAAGVAVGSTIGHTLGAGITGMFSGSGSDSAPVEQQQNMANTS
          ***. ****.*****.***.*.*** ** * . *

MNRR1      --TQPAQQQQ--PCLYEIKQFLECAQ-NQGDIKLCEGFNEVLKQCRLANGLA
CHCHD10    --APQLQMG-PCAYEIRQFLDCST-TQSDL SLCEGFSEALKQCKYYHGLSSLP
Mix17      GGTQTDQLGR TCEIDARNFTRCLDENNGNFQICDYLLQQLKACQEAARQY
          .      *      *      . . *      *      . .      . *      . . * * *

```

FIGURE 1: Alignment of human CHCHD10, human MNRR1, and yeast Mix17. Identical residues (*) and similar residues (.) are indicated.

TABLE 1: Comparison of various identified functions, effects, and properties of MNRR1 and CHCHD10.

	MNRR1	CHCHD10
Protein length	151	142
CHCH domain	114–144	102–132
Interactions identified using mass spectrometry (BioGRID database)	97 total unique interactors (common interactors for both: C1QBP, NDUFS3, NDUFA8, COX5A, COX6A1, COX6C, ATP5H, ECH1, USMG5)	42 total unique interactors (common interactors for both: C1QBP, NDUFS3, NDUFA8, COX5A, COX6A1, COX6C, ATP5H, ECH1, USMG5)
Expression (Human Protein Atlas)	Expressed in all tissues at medium to high levels	Muscle, heart, liver (high), brain (medium), and low levels for other tissues
Mitochondrial function	Regulation of COX activity, ROS production [3], apoptosis [27]	Regulation of COX activity and ATP production [67], cristae morphology [68, 69]
Nuclear function	Transcriptional activator for <i>COX4I2</i> and itself [3]	Not known to be localized to nucleus
Hypoxia sensitivity	Upregulated at 4% oxygen [25]	Unknown
Posttranslational regulation	Phosphorylated at Y99 by Abl2 kinase which activates mitochondrial function [20]	Unknown
Disease association (altered protein/transcript levels)	Huntington's disease [57], hepatocellular carcinoma [66], nonsmall cell lung carcinoma [28], lissencephaly [60]	Gastric cancer [91]
Mutation in protein associated with disease	Parkinson's disease [47]	Mitochondrial myopathy, amyotrophic lateral sclerosis, Alzheimer's disease, frontotemporal dementia, cerebellar ataxia, spinal muscular atrophy, Charcot-Marie-Tooth disease type 2A, motor neuron disease (specific references and mutations summarized in Table 2)
Functionally characterized mutations	Q112H [20], 300+5G>A [47]	S59L and P34S [68, 69], R15L/G58R [71]

previously shown in reporter assays that MNRR1 activates the promoters for COX subunit 4 isoform 2 (*COX4I2*), as well as itself [3]. Mutation of this element reduces the transactivation potential of the reporter [26]. The current model for the role of MNRR1 in the nucleus is that, under low oxygen tension, it displaces the inhibitory factors from the docking protein RBPJ κ to facilitate transactivation.

Depletion of MNRR1 has also been shown to reduce cellular growth rate [3]. MNRR1 knockdown studies in

cells have shown a reduction in levels of Atg7, a protein required for the fusion of the vacuolar membrane during autophagy and some subunits of mitochondrial complex I [3], consistent with the effect of MNRR1 reduction in other systems [19].

MNRR1 has been identified as a negative regulator of the mitochondrial apoptotic pathway. A study by Liu et al. [27] revealed that MNRR1 binds to the antiapoptotic protein Bcl-xL under normal physiological conditions and inhibits

TABLE 2: Mutations identified in CHCHD10 associated with neurodegenerative disorders and mitochondrial myopathy.

Mutation	Disease	Reference
Pro12→Ser*	ALS	[76]
Arg15→Leu	ALS, motor neuron disease	[72, 75, 79, 81]
His22→Tyr	Behavioural variant FTD	[92]
Pro23→Thr/Ser/Leu	FTLD (T), behavioural variant FTD (S), semantic dementia (L)	[75] (T); [76] (S); [92] (L)
Pro34→Ser	FTD-ALS, ALS	[73, 74, 76]
Ala35→Asp	FTLD, Alzheimer's disease	[75, 93]
G58→Arg (in cis with Arg15→Ser)	Mitochondrial myopathy	[71]
Ser59→Leu	FTD-ALS, cerebellar ataxia	[68, 73]
Gly66→Val	ALS, LOSMoN/SMAJ, motor neuron disease, CMT2A	[79–82]
Pro80→Leu	ALS	[75, 83, 76]
Gln82→X	Atypical FTD with Parkinsonism	[76]
Tyr92→Cys**	ALS	[9]
Pro96→Thr*	ALS	[76, 94]
Gln102→His**	ALS	[9]
Gln108→X*	Atypical FTD and Parkinson's disease	[84]

*Found outside exon 2. **Incorrectly assigned mutations in canonical CHCHD10.

the accumulation of the proapoptotic protein Bax in the mitochondria. However, under stress conditions, mitochondrial levels of MNRR1 are reduced followed by increased Bax and Bak oligomerization, leading to apoptosis. Currently, there is a paucity in the understanding of how the interaction between MNRR1 and Bcl-xL regulates inhibition of Bax activation. The authors hypothesized that, in addition to being a key player in regulating apoptosis in mitochondria, MNRR1 may have an additional role in the cytoplasm or nucleus.

Cell migration is another function that has been linked to MNRR1 [28, 29]. Overexpression of MNRR1 promotes cell migration in a cell culture-based migration assay, whereas reduced motility is observed upon knockdown of the endogenous protein [29]. Interestingly, analysis of the functional domain revealed that neither the CHCH motif alone nor replacement of a predicted Ser-45 phosphorylation site could exert cell migration-stimulating activity. MNRR1 was shown to interact with HABP1, suppressing migration, whereas MNRR1 was proposed to stimulate cell migration by activating Akt phosphorylation, which in turn leads to RhoA activation, increased Jnk phosphorylation, and ultimately focal adhesion and actin polymerization [29]. Thus, the activities of MNRR1 and HABP1 were proposed to balance cell migration.

MNRR1 has been shown to prime pluripotent stem cells to differentiate towards a neuroectodermal lineage [64]. MNRR1 was identified as a new marker whose expression significantly varies between human-embryonic stem cells (hESC) and human-induced pluripotent stem cells (hiPSC). MNRR1 directly interacts with SMAD4 and segregates it to the mitochondria, resulting in decreased levels of SMAD4 in the nucleus, where it acts as a transcription factor for many of genes of the TGF β signaling pathway. This in turn leads to a reduction in TGF β and an increased differentiation toward neuroectodermal lineages. SMAD4 has been known to associate with COX subunit II in the mitochondria to regulate

apoptotic response. hiPSC have a reduced level of MNRR1 and have a higher expression of nuclear SMAD4 and increased TGF β activity, whereas the pluripotent stem cells have a higher MNRR1 expression. These observations suggest that a direct inverse relationship exists between MNRR1 and the activity of the TGF β pathway in pluripotent stem cells.

3. CHCHD10

In the recent years, high-throughput mass spectrometry analysis has revealed several interacting partners for both MNRR1 and CHCHD10. Unsurprisingly, MNRR1 and CHCHD10 have several common interactors, mostly associated with mitochondrial function such as ETC proteins NDUFS3, NDUF8 (complex I), COX5A, COX6A1, COX6C (complex IV), and ATP5H (complex V). Other, less intuitive ones include Enoyl-CoA hydratase 1 (ECH1), which is associated with fatty acid metabolism, and complement C1q binding protein (C1QBP), associated with immune function. Both ECH1 and C1QBP are localized to multiple compartments including mitochondria and may play a role in interorganellar communication in conjunction with MNRR1 and CHCHD10. The interaction of MNRR1 and C1QBP has been studied in the context of nonsmall cell lung carcinoma and the network has been predicted to affect cell proliferation, migration, and respiration in cancer cells [28]. An interesting common interactor is USMG5 (upregulated during skeletal muscle growth), also known as DAPIT (diabetes-associated protein in insulin-sensitive tissues). DAPIT is also involved in maintaining ATP synthase (complex V) subunit levels in mitochondria [30]. Although there are no studies linking MNRR1 with diabetes, a CHCHD10 mutation (G66V) was identified in one family to be associated with adult onset type 2 diabetes [31]. However, as the authors note, additional studies beyond a single family will be needed to confirm an actual disease association.

Both CHCHD10 and MNRR1 have been linked to a number of diseases. For MNRR1, there is a greater number of diseases associated with altered protein levels, whereas in the case of CHCHD10, a number of mutations were associated with disease, particularly neurodegenerative diseases, as well as one case of mitochondrial myopathy (Table 2). This observation, along with the tissue-specific differences in level, may signify that both proteins, though highly similar, are necessary under different conditions. One such condition is the presence of different oxygen levels throughout the body and it is possible that both proteins work together in order to fine-tune mitochondrial function.

4. Hypoxic Regulation by MNRR1

Oxygen is critical to cellular physiology. Once absorbed by the lungs, it diffuses into the blood, bound to hemoglobin in the red cells. Delivery of oxygen to the tissues via the circulating blood is finely regulated depending on their metabolic requirements. The partial pressure of oxygen (pO_2) is widely used to indicate the amount of oxygen in a particular tissue. In a clinical setting, the units for the pO_2 are mm Hg and in an experimental setting, the units are percent O_2 . Under physiological conditions, the pO_2 in human tissues ranges widely between and within mammalian tissues (reviewed in [32]) but is well below those used in standard cell culture experiments. For example, relatively low in vivo oxygen levels were found in the bone marrow of mice, ranging from 11.7 to 31.7 mm Hg (1.5–4.2% O_2) with an average value of 20.4 mm Hg (2.7% O_2) [33]. Intermediate levels of 5% O_2 (37.8 mm Hg) were reported to be optimal for myogenic commitment of muscle stem cells [34], while higher average levels ranging from 29.7 to 61.8 mm Hg (3.9–8.2% O_2) were reported in the mouse brain [35]. In sharp contrast, for the oxygen tension in a standard experimental cell culture setting, the pO_2 is ~20%. Generally, in the experimental cell culture setting, a reduction in the levels of oxygen from the ~20% standard is termed hypoxia. Obviously, ~20% oxygen is hyperoxic in comparison to in vivo oxygen tensions, and great caution should be taken when extrapolating conclusions derived from cell culture work to the in vivo situation.

With a reduction in the available oxygen, a cell activates multiple signaling pathways in an attempt to maintain homeostasis. The most widely studied hypoxic regulators are the HIFs (hypoxia-inducible factors). Two distinct factors, HIF1 α and HIF2 α , have received the most attention. In cell culture models, HIFs are stabilized at an oxygen tension of 1–2% or lower [26, 36–38]. However, a study by Holmquist-Mengelbier et al. has shown HIF2 α stabilization at a moderate level of hypoxia (5% O_2) in a neuroblastoma cell line [39], an effect observed only when the cells are maintained under chronic hypoxia (72 h). HIFs, once stabilized, translocate to the nucleus to bind the hypoxia-responsive elements (RCGTG) in the promoters of genes they will activate. An additional family member, HIF3 α , has come to light in recent years. HIF3 α has multiple spliced variants, with HIF3 α 2 being induced under hypoxia. The most intriguing

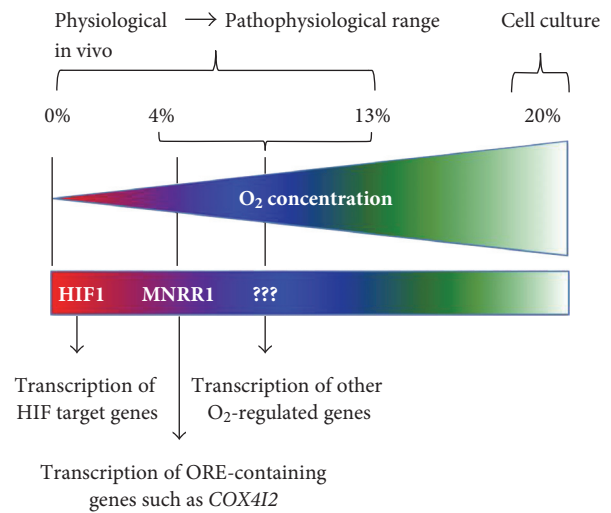


FIGURE 2: Model for transcriptional response to decreasing oxygen levels. The model proposes that, as tissue oxygen levels decrease from the artificial 20% level typically used for tissue culture, different transcriptional programs come into play to try to achieve homeostasis.

part is that HIF3 α functions as an inhibitory factor for HIF signaling [40].

In addition to being a transcription factor under hypoxic conditions, HIF1 α was shown in a breast cancer model to be instrumental in activating γ -secretase by interacting with and repositioning the catalytic subunit [41]. Several groups have shown HIF-independent pathways to play a key role in the regulation of hypoxia-responsive genes. HMG1.2 has been shown to be one such gene in *Caenorhabditis elegans* that binds promoter DNA at low oxygen tensions. In addition, mammalian transcriptional regulators such as c-Myc [42], ATF-4 [43], and NF- κ B [44] have also been shown to function in hypoxia in a HIF-independent manner. Other signaling pathways, such as mTOR [45], are also regulated under hypoxia in a HIF-independent manner. Thus, how does a cell respond to oxygen tensions that are low but not sufficiently so to stabilize HIFs?

We have previously shown MNRR1 to be a biorganellar regulator. In addition to its localization and function in the mitochondria, this protein is also localized to the nucleus, where it binds a conserved 13 bp DNA sequence, the ORE, along with RBPJ κ . MNRR1 activates the ORE by displacing the inhibitory factor CXXC5 that is bound to RBPJ κ . This ORE is also independent of the HIFs and is maximally active in a cell culture system at 4% oxygen, in marked contrast to a reporter with HIF-binding elements that is maximally active at oxygen tensions of $\leq 1\%$ [26]. Although 4% oxygen in an experimental system is hypoxic, considering the oxygen tension in the human body, it could be that MNRR1 is the basal transcriptional factor for genes harboring the ORE in organs that have an oxygen tension of ~4% (Figure 2).

Every cell in the body is exposed to an oxygen tension that may vary from cell to cell or organ to organ. A regulatory system is required to cope with differential oxygen tensions, to induce a transcriptional program that would lead the cell

towards normalcy, that is, to achieve its normal homeostatic state. It is logical to hypothesize that cells induce a distinct regulatory signature at a very specific oxygen tension. We propose, based on the available literature, that MNRR1 under moderate hypoxia, and HIFs under severe hypoxia, carry out these functions. Identification of the factors that play a key role at distinct oxygen tensions, specifically other CHCH domain-containing proteins, and their mechanism of regulation will undoubtedly be of considerable importance in understanding signaling pathways involving the mitochondria of a cell under hypoxic stress.

5. MNRR1 and Disease

MNRR1 has been associated with a number of diseases, most commonly Parkinson's (PD) and Lewy body diseases [46–48]. The association with PD is difficult to pin down, however. First, the associations found are quite rare: although a number of studies have identified nonsynonymous amino acid changes that have a higher frequency in patients with PD than in controls, the absolute population frequency is <<1%. Furthermore, some studies have not found the reported amino acid changes or have not found them at a higher level in patient than in control populations [49–55]. Second, few studies have involved extended families that allow tracking the segregation of putative mutations among affected and unaffected members. Lastly, the disease associations have been based on allele frequencies and lack a mechanistic basis for their pathological action.

Funayama et al. carried out a large study with Japanese populations [47]. They identified a missense mutation in MNRR1 (T61I) in a family by next-generation sequencing, then obtained samples from an additional 340 patients with autosomal dominant (AD) PD, 517 patients with sporadic PD, and 559 controls. Three MNRR1 mutations in four of 341 index cases from independent families with ADPD were detected: T61I, R145Q, and a splice site mutation. Of these, the T61I mutation is notable because it was not present in control populations and because it cosegregated in a Japanese family with ADPD. These studies are important in that they show segregation with Parkinson's disease in a family as assessed by Sanger sequencing.

Lewy body diseases (LBD), a form of dementia that includes PD, were also targeted for a study of MNRR1 sequence variants [48]. More than 1600 patients from the US, Ireland, and Poland had PD, 610 had a non-PD LBD, and altogether 1432 were controls. The T61I variant, however, was not found in this study, and other coding region variants were found a maximum of 3 times among the pooled 2237 patients compared to 0 or 1 time among the various control groups.

The rarity of MNRR1 variants among PD patients in all the studies taken together, along with the presence of most variants also in nonsymptomatic controls, raises the question of whether MNRR1 is indeed a risk factor for PD. It will require mechanistic—including animal—studies to address this question.

MNRR1 has been examined for association with other genetic diseases. One study sought associations with multiple

system atrophy (MSA) and amyotrophic lateral sclerosis (ALS) in Han Chinese patients, based on previous detection of common genetic factors [56]. All four exons of MNRR1 were sequenced after PCR amplification in 89 MSA patients, 424 sporadic ALS patients, and 594 controls. No exonic variant was detected in the MSA patients; four were detected in 6 ALS patients, including P2L and S85R present in PD patients; however, P2L was present at about an equal frequency in controls without neurological disease and S85R was present in 1 patient and 0 controls. Thus, genetic variants of MNRR1 did not appear important in MSA or ALS in this population.

The neurological connection to MNRR1 was further explored in several other conditions, one of which was Huntington's disease (HD). Human pluripotent stem cell (hPSC) lines were generated containing the mutant *huntingtin* (*HTT*) gene to explore early developmental changes in gene expression [57]. Both human-embryonic stem cells (hESCs) and differentiated neural stem cells (NSCs) were examined. One of the three genes whose expression differed significantly from wild-type cells in both hESCs and NSCs was MNRR1, for which also corresponding protein level differences were confirmed. Dysregulation of MNRR1 was previously observed in blood cells from HD patients [58]. In both cell types, MNRR1 increased with differentiation but more so in *HTT* mutant cells. Since *HTT* interacts with both mitochondrial metabolism via an effect on PGC-1 α activation and production [59] and cell migration [29], a role in neuronal differentiation is not surprising although the precise nature of that role has yet to be clarified.

MNRR1 was further connected to neurological development when it was shown to be downregulated in iPS cells derived from patients with lissencephaly, a congenital brain malformation caused by defects in neuronal migration [60]. The iPS cells were generated from two patients; one contained a chromosome 17 microdeletion that includes *LIS1*, a known microcephaly gene [61]. The other contained a missense mutation in *TUBA1A*, another gene associated with cortical migration disorders [62]. Since both genes are associated with iPS cells generated from both patients and MNRR1 has been shown to be relevant to cell migration [29], Shimojima et al. examined the expression of MNRR1 in patient and control iPS cells undergoing neural differentiation [60]. Control cells increased MNRR1 expression at 8 and 16 days whereas cells from both patients started with a lower level of expression and only marginally increased it with time. The association noted above between MNRR1 and huntingtin, of MNRR1 and cell migration [29], and of huntingtin with microtubules [63], suggests that MNRR1 could be involved in neuronal migration. Furthermore, MNRR1 has also been suggested to prime the differentiation potential of human iPS cells to neuroectodermal lineages [64] and to inhibit apoptosis [27], an important component of normal brain development [65]. Taken together, there is ample reason to connect MNRR1 with cortical development but clearly this area is in need of further investigation.

Finally, MNRR1 has been connected to tumorigenesis. One report shows that it is coamplified with the epidermal

growth factor receptor (EGFR) in nonsmall cell lung carcinoma (NSCLC) [28]. Protein levels of MNRR1 and EGFR protein are upregulated in NSCLC tumor-derived xenografts as compared to those of the normal lung. Experiments on proteome changes in NSCLC cells upon MNRR1 knockdown suggest that MNRR1 gene copy number and protein levels are linked with EGFR as a driver in NSCLC. Moreover, the MNRR1 knockdown in NSCLC cells alleviates cell proliferation, migration, and mitochondrial respiration. Examination of protein-protein interactions of MNRR1 revealed two interactome hub proteins, CIQBP/HABP1, a mitochondrial protein, and YBX1, an oncogenic transcription factor. The nature of these linkages will need to be better defined.

MNRR1 has also been connected to liver carcinogenesis (HCC) via the effect of hepatitis C virus nonstructural protein 2 (NS2) on upregulating the expression of MNRR1 [66]. MNRR1 was highly stained in a biopsy of liver cancer but not in the adjacent normal tissue. Furthermore, in examining histological biomarkers for HCC, MNRR1 was found highly expressed in >95% of samples. Whether altering its expression level can alter markers of tumorigenesis awaits further studies. Furthermore, it was revealed that c-AMP response element binding protein (CREBP) plays an important role in the transcriptional activation of MNRR1. Owing to the complexity of MNRR1 function, it is likely to be controlled at many levels. The mechanisms that control the expression of MNRR1 are yet to be clearly understood.

6. CHCHD10 and Disease

The CHCHD10 isoform is a 142 amino acid protein. CHCHD10 was originally picked up in a screen using the guilt by association approach to be highly enriched in the heart and skeletal muscle [67]. This study also confirmed that CHCHD10 is a mitochondrial protein, and a transient knockdown in HeLa cells decreased both COX activity and ATP levels to ~50% of wild-type cells. Within the mitochondria, CHCHD10 localizes to the intermembrane space [68] and interacts with the members of the mitochondrial contact site and cristae organizing system (MICOS) complex, whose stability may also require CHCHD3 and CHCHD6 [69].

CHCHD10 has been linked to a number of neurodegenerative disorders in the past few years. The first study identified and characterized a mutation, S59L, to be associated with a frontotemporal dementia- (FTD-) amyotrophic lateral sclerosis (ALS) phenotype [68]. Since then, several mutations in CHCHD10 have been associated with neurodegenerative disorders such as ALS and one was linked to a mitochondrial myopathy. Table 2 summarizes the mutations identified so far; their clinical implications have been well summarized in a recent review [70]. Although over 10 different mutations have been discovered, few of them have been analyzed in detail and causally associated with the phenotypes seen. Three have been tested thus far in cell culture model systems to elucidate the effects of these mutations, S59L, P34S [68, 69], and R15S/G58R [71]. Bannwarth et al. identified the S59L mutation in a family of French origin. They also determined the effects of this mutation in skin fibroblasts obtained from two patients and found that the

mitochondria were decreased in length, had altered cristae morphology, and showed defects in MICOS assembly and nucleoid formation [68, 69]. The same group also functionally characterized the S59L mutation along with another, P34S. Overexpression of both these CHCHD10 mutants led to altered cristae morphology. The only other CHCHD10 mutation assessed in a cell culture system is the double-mutation R15S in cis with G58R, identified in a family of Puerto Rican origin [71]. The authors investigated its effects in cells overexpressing this mutant protein and found that it led to a loss of mitochondrial networks, forming smaller, more punctate mitochondria. In comparing this double mutant with individual R15S or G58R mutants, they found that the G58R mutant is sufficient to cause the altered phenotype. Hence, they concluded that the R15S mutation may not be pathogenic and the effects seen may be only due to the G58R mutation.

Since the original discovery of mutations in CHCHD10 linked to ALS, many screens were conducted across different populations to detect other harmful mutations in CHCHD10. Despite the seemingly large number of mutations identified, all the variants may not necessarily contribute to disease. There have been cases where the same mutation is found in both the disease patients and in control groups, leading to speculation whether the mutation is pathogenic, a risk factor, or a benign polymorphism. For example, the P34S mutation is associated with ALS and FTD by several studies [72–74], but the same mutation has been identified in healthy control individuals and hence is considered nonpathogenic [75–78]. One shortcoming may be that some of the ALS studies did not consider a sufficient number of control individuals [9, 78]. However, another problem with the interpretation of the data is the age of disease onset, which for neurodegenerative disorders is often relatively late. Therefore, individuals classed as controls may actually be ones where the disease has not manifested yet, leading to a premature classification of the mutation as nonpathogenic. As a result, it seems essential to ensure age-matched control and affected populations as well as to estimate from follow-up studies the proportion of controls who change status after initial data collection. Lastly, there is at least one case where the identified mutation is incorrect due to improper annotation of the gene [9]. The canonical CHCHD10 protein sequence (UniProtKB) has 4 cysteines at positions 102, 112, 122, and 132 which are connected by 2 disulfide linkages to form the CHCH domain. Any mutation in one of these critical cysteines is likely to lead to protein misfolding. One study has identified a mutation of Glu-102 to His whereas, in the canonical protein, position 102 is a cysteine and part of the twin CX₂C motif [16]. The same group also found a mutation at Tyr-92 whereas the original residue in the CHCHD10 sequence is alanine. The template sequence that was analyzed for identifying mutations is a 149-amino acid sequence expressed from a splice variant (ENST00000401675.7) for which the protein status is unreviewed on UniProtKB (B5MBW9).

Despite the presence of such confounding data, some mutations such as G66V have been identified exclusively in

TABLE 3: List of genes containing the oxygen-responsive element (ORE) identified using Geneious (www.geneious.com). ORE sequences for MNRR1/CHCHD2 and COX4I2 in the table were used as reference sequences and searched against the human genome (GRCH38/hg38). Matches of 83.5% or above within 1000 bp 5' to the start of translation were listed.

ORE	Genes containing ORE up to 1000 bp upstream of the gene
MNRR1 (5'-TGTCACGCTCCGGA-3')	LOC105370119, MIR661, MNRR1, ST18, MADCAM1, RBBP8NL
COX4I2 (5'-TTCCACGCTGGGG-3')	ADPRHL1, ADRA2A, C18orf8, C2CD2, CASZ1, CDH4, CNPY4, COX4I2, EEF1DP3, ESYT1, FBP1, KIAA1614, LACTB, LINC00403, MAP2K5, MARCKSL1, MIR36481, NOL9, RNF150, SDHAF1, USP28, WWC1

patient populations. The G66V mutation has been associated with a diverse spectrum of disorders including ALS [79, 80] and motor neuron disease [81, 82]. In one study, it was seen that, even within a single family where all the affected individuals carried the G66V variant, many different phenotypes were displayed ranging from CMT2-type axonal neuropathy to spinal muscular atrophy that presented as an ALS-like disease [31]. Another mutation, P80L, is almost exclusively present in patients with ALS [75, 76, 83]. The P80L mutation recently was seen in one control subject, but the authors state that this subject was 57 years of age at the time of the study and may develop symptoms at a later age. They concluded that the P80L mutation might be a pathogenic one with reduced penetrance [84]. What is suggested by this data is that (1) the association with disease is not always clear and (2) different mutations may have different penetrance in different individuals. Some of these issues will be clarified by the study of CHCHD10 function in the cell both under physiological and pathological conditions.

7. Other Genes That Harbor the ORE in Their Promoters

The oxygen-responsive element (ORE) is a 13 bp sequence originally identified in the promoter of *COX4I2*, one of the subunit isoforms of COX. The transcription of genes from the ORE is regulated by 3 proteins, RBPJ κ , CXXC5, and MNRR1 [25]. Genes containing the ORE are a target for transcriptional activation by MNRR1, which includes MNRR1 itself [3]. A systematic in silico analysis of human genes containing the ORE identified 28 genes containing the ORE derived from *COX4I2* or MNRR1 upstream of the first exon. These are listed in Table 3. Many of the genes in the list are yet to be characterized (*LOC105370119*, *RBBP8NL*, *KIAA1614*, *ADPRHL1*, *NOL9*, *C18ORF8*, *C2CD2*, and *RNF150*), or are microRNA genes (*MIR36481*, and *MIR661*), long noncoding RNA genes (*LINC00403*), or pseudogenes (*EEF1DP3*), and hence cannot be classified into any major category for cell function.

The genes on the list whose function has been characterized to some extent have interesting implications. The target list includes genes that control mitochondrial function such as *SDHAF1* (succinate dehydrogenase assembly factor 1), a complex II assembly factor, and *FBP1* (fructose bisphosphatase 1), an enzyme that regulates gluconeogenesis (Lamont 2006). Other target genes encode proteins such as *MADCAM1* (mucosal vascular addressin cell adhesion molecule 1), *MARCKSL1* (macrophage myristoylated

alanine-rich C kinase substrate-like 1), and *CDH4* (cadherin 4), which are associated with cell adhesion and migration, a process known to be regulated by MNRR1 [29] and *LACTB* (lactamase beta), which forms filaments in the mitochondrial IMS and is part of a network of genes that were validated to have a casual association with obesity traits [85]. Another putative MNRR1 target gene is *USP28* (ubiquitin-specific peptidase 28), which encodes a deubiquitinating enzyme that contributes to DNA damage-induced activation of apoptosis [86], another key pathway with which MNRR1 is associated [27].

Other ORE-harboring genes include some that may affect neuronal and CNS function but require further characterization. *WWC1* plays a role in Hippo/SWH signaling [87] and variants of this protein have been associated with memory performance and lipid binding [88]. *CNPY4* is a transcriptional inhibitor that modulates FGF signaling in the midbrain-hindbrain region in the zebrafish model system [89]. *ADRA2A* is a protein belonging to the GPCR family and is involved in the regulation of neurotransmitter release from adrenergic neurons in the CNS [90].

8. Conclusion

CHCHD10 and MNRR1 are both important proteins that regulate cell growth and metabolism. The functional studies regarding MNRR1's role as biorganellar regulator of oxidative phosphorylation [3], and the characterization of a posttranslational modification [20], provide clues to identify the role of this protein in cellular function and pathways that can be targeted in order to regulate its levels under hypoxic stress conditions. Similar studies are necessary for CHCHD10. Since hypoxia is associated with so large a proportion of diseases, it is not surprising that disease-associated variants are coming to light. One important corollary that can be drawn from the high similarity between the two proteins and the fact that both have a common ancestor is that both proteins would be part of a similar process [14]. It would be tempting to speculate that during the course of evolution, when the ancestral gene was duplicated, both copies underwent distinct changes, giving rise to two separate genes, perhaps in order to respond to different conditions but to regulate one critical process—oxidative phosphorylation—that is vital for cell survival. Hence, basic mechanistic studies in the case of CHCHD10, and further studies for MNRR1, would provide a platform for identifying the effects of both these proteins individually and as part of a system of regulation in response to different

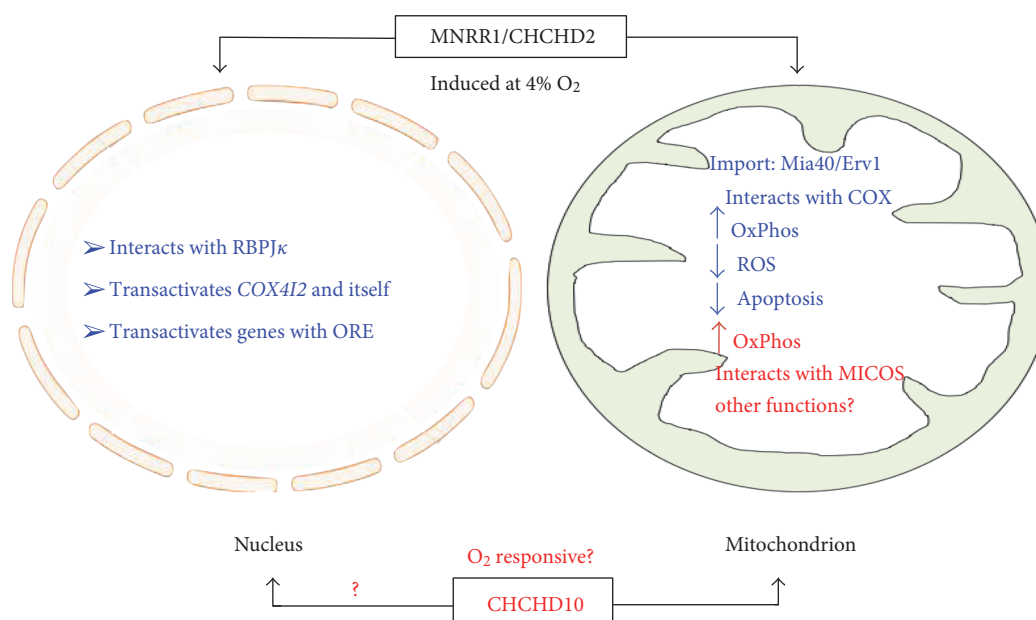


FIGURE 3: Model for MNRR1 function. The model shows the known functions of MNRR1 in both the nucleus and the mitochondria. Whether CHCHD10 functions similarly remains to be determined.

stress conditions including but not limited to hypoxia (Figure 3).

An interesting possibility is that each of the CHCH domain-containing proteins is responsive at distinct experimental oxygen tensions. If true, this would provide a mechanism, together with the HIF system, to adapt and fine-tune cellular responses to the wide range of oxygen concentrations found under physiological and pathological conditions. Furthermore, one can ask whether oxygen tension is the sole regulator for CHCH domain-containing proteins or whether there are other conditions that affect their function, as for example shown for MNRR1 tyrosine phosphorylation. Finally, it will be critical to further identify and characterize the mutations associated with these proteins so that they could be exploited clinically in diagnosis as well as treatment.

Disclosure

Opinions, interpretations, conclusions, and recommendations are those of the authors and are not necessarily endorsed by the Department of Defense.

Conflicts of Interest

The authors declare that they have no conflicts of interest with the contents of this article.

Acknowledgements

This work was supported by the Office of the Assistant Secretary of Defense for Health Affairs through the Peer Reviewed Medical Research Program under Award No. W81XWH-16-1-0516 and the Henry L. Brasza endowment.

References

- [1] H. Liu, Y. Li, Y. Li et al., "Cloning and functional analysis of FLJ20420: a novel transcription factor for the BAG-1 promoter," *PLoS One*, vol. 7, no. 5, article e34832, 2012.
- [2] B. A. Westerman, A. Poutsma, E. A. Steegers, and C. B. Oudejans, "C2360, a nuclear protein expressed in human proliferative cytotrophoblasts, is a representative member of a novel protein family with a conserved coiled coil-helix-coiled coil-helix domain," *Genomics*, vol. 83, no. 6, pp. 1094–1104, 2004.
- [3] S. Aras, M. Bai, I. Lee, R. Springett, M. Hüttemann, and L. I. Grossman, "MNRR1 (formerly CHCHD2) is a bi-organelle regulator of mitochondrial metabolism," *Mitochondrion*, vol. 20, no. 1, pp. 43–51, 2015.
- [4] J. Beers, D. M. Glerum, and A. Tzagoloff, "Purification, characterization, and localization of yeast Cox17p, a mitochondrial copper shuttle," *The Journal of Biological Chemistry*, vol. 272, no. 52, pp. 33191–33196, 1997.
- [5] D. M. Glerum, A. Shtanko, and A. Tzagoloff, "Characterization of Cox17, a yeast gene involved in copper metabolism and assembly of cytochrome oxidase," *The Journal of Biological Chemistry*, vol. 271, no. 24, pp. 14504–14509, 1996.
- [6] C. Abajian, L. A. Yatsunyk, B. E. Ramirez, and A. C. Rosenzweig, "Yeast Cox17 solution structure and copper (I) binding," *The Journal of Biological Chemistry*, vol. 279, no. 51, pp. 53584–53592, 2004.
- [7] F. Arnesano, E. Balatri, L. Banci, I. Bertini, and D. R. Winge, "Folding studies of Cox17 reveal an important interplay of cysteine oxidation and copper binding," *Structure*, vol. 13, no. 5, pp. 713–722, 2005.
- [8] S. Longen, M. Bien, K. Bihlmaier et al., "Systematic analysis of the twin CX₉C protein family," *Journal of Molecular Biology*, vol. 393, no. 2, pp. 356–368, 2009.
- [9] Q. Zhou, Y. Chen, Q. Wei et al., "Mutation screening of the CHCHD10 gene in Chinese patients with amyotrophic lateral

- sclerosis," *Molecular Neurobiology*, vol. 54, no. 5, pp. 3189–3194, 2017.
- [10] A. Chacinska, S. Pfannschmidt, N. Wiedemann et al., "Essential role of Mia40 in import and assembly of mitochondrial intermembrane space proteins," *The EMBO Journal*, vol. 23, no. 19, pp. 3735–3746, 2004.
- [11] M. Naoe, Y. Ohwa, D. Ishikawa et al., "Identification of Tim40 that mediates protein sorting to the mitochondrial intermembrane space," *The Journal of Biological Chemistry*, vol. 279, no. 46, pp. 47815–47821, 2004.
- [12] N. Terziyska, T. Lutz, C. Kozany et al., "Mia40, a novel factor for protein import into the intermembrane space of mitochondria is able to bind metal ions," *FEBS Letters*, vol. 579, no. 1, pp. 179–184, 2005.
- [13] N. Mesecke, N. Terziyska, C. Kozany et al., "A disulfide relay system in the intermembrane space of mitochondria that mediates protein import," *Cell*, vol. 121, no. 7, pp. 1059–1069, 2005.
- [14] G. Cavallaro, "Genome-wide analysis of eukaryotic twin CX₂C proteins," *Molecular BioSystems*, vol. 6, no. 12, pp. 2459–2470, 2010.
- [15] W. K. Huh, J. V. Falvo, L. C. Gerke et al., "Global analysis of protein localization in budding yeast," *Nature*, vol. 425, no. 6959, pp. 686–691, 2003.
- [16] K. Gabriel, D. Milenkovic, A. Chacinska et al., "Novel mitochondrial intermembrane space proteins as substrates of the MIA import pathway," *Journal of Molecular Biology*, vol. 365, no. 3, pp. 612–620, 2007.
- [17] J. M. Tkach, A. Yimit, A. Y. Lee et al., "Dissecting DNA damage response pathways by analysing protein localization and abundance changes during DNA replication stress," *Nature Cell Biology*, vol. 14, no. 9, pp. 966–976, 2012.
- [18] N. Modjtahedi, K. Tokatlidis, P. Dessen, and G. Kroemer, "Mitochondrial proteins containing coiled-coil-helix-coiled-coil-helix (CHCH) domains in health and disease," *Trends in Biochemical Sciences*, vol. 41, no. 3, pp. 245–260, 2016.
- [19] J. M. Baughman, R. Nilsson, V. M. Gohil, D. H. Arlow, Z. Gauhar, and V. K. Mootha, "A computational screen for regulators of oxidative phosphorylation implicates SLIRP in mitochondrial RNA homeostasis," *PLoS Genetics*, vol. 5, no. 8, article e1000590, 2009.
- [20] S. Aras, H. Arrabi, N. Purandare et al., "Abl2 kinase phosphorylates bi-organellar regulator MNRR1 in mitochondria, stimulating respiration," *Biochimica et Biophysica Acta*, vol. 1864, no. 2, pp. 440–448, 2017.
- [21] S. Wu, F. Zhou, Z. Zhang, and D. Xing, "Mitochondrial oxidative stress causes mitochondrial fragmentation via differential modulation of mitochondrial fission-fusion proteins," *The FEBS Journal*, vol. 278, no. 6, pp. 941–954, 2011.
- [22] R. J. Youle and A. M. van der Bliek, "Mitochondrial fission, fusion, and stress," *Science*, vol. 337, no. 6098, pp. 1062–1065, 2012.
- [23] T. MacVicar and T. Langer, "OPA1 processing in cell death and disease - the long and short of it," *Journal of Cell Science*, vol. 129, no. 12, pp. 2297–2306, 2016.
- [24] B. Wang and G. D. Kruh, "Subcellular localization of the Arg protein tyrosine kinase," *Oncogene*, vol. 13, no. 1, pp. 193–197, 1996.
- [25] S. Aras, O. Pak, N. Sommer et al., "Oxygen-dependent expression of cytochrome *c* oxidase subunit 4-2 gene expression is mediated by transcription factors RBPJ, CXXC5 and CHCHD2," *Nucleic Acids Research*, vol. 41, no. 4, pp. 2255–2266, 2013.
- [26] M. Hüttemann, I. Lee, J. Liu, and L. I. Grossman, "Transcription of mammalian cytochrome *c* oxidase subunit IV-2 is controlled by a novel conserved oxygen responsive element," *The FEBS Journal*, vol. 274, no. 21, pp. 5737–5748, 2007.
- [27] Y. Liu, H. V. Clegg, P. L. Leslie et al., "CHCHD2 inhibits apoptosis by interacting with Bcl-xL to regulate Bax activation," *Cell Death and Differentiation*, vol. 22, no. 6, pp. 1035–1046, 2015.
- [28] Y. Wei, R. N. Vellanki, E. Coyaud et al., "CHCHD2 is coamplified with EGFR in NSCLC and regulates mitochondrial function and cell migration," *Molecular Cancer Research*, vol. 13, no. 7, pp. 1119–1129, 2015.
- [29] M. Seo, W. H. Lee, and K. Suk, "Identification of novel cell migration-promoting genes by a functional genetic screen," *The FASEB Journal*, vol. 24, no. 2, pp. 464–478, 2010.
- [30] S. Ohsakaya, M. Fujikawa, T. Hisabori, and M. Yoshida, "Knockdown of DAPIT (diabetes-associated protein in insulin-sensitive tissue) results in loss of ATP synthase in mitochondria," *The Journal of Biological Chemistry*, vol. 286, no. 23, pp. 20292–20296, 2011.
- [31] P. Pasanen, L. Myllykangas, M. Poyhonen et al., "Intrafamilial clinical variability in individuals carrying the CHCHD10 mutation Gly66Val," *Acta Neurologica Scandinavica*, vol. 133, no. 5, pp. 361–366, 2016.
- [32] A. Carreau, B. El Hafny-Rahbi, A. Matejuk, C. Grillon, and C. Kieda, "Why is the partial oxygen pressure of human tissues a crucial parameter? Small molecules and hypoxia," *Journal of Cellular and Molecular Medicine*, vol. 15, no. 6, pp. 1239–1253, 2011.
- [33] J. A. Spencer, F. Ferraro, E. Roussakis et al., "Direct measurement of local oxygen concentration in the bone marrow of live animals," *Nature*, vol. 508, no. 7495, pp. 269–273, 2014.
- [34] Z. Redshaw and P. T. Loughna, "Oxygen concentration modulates the differentiation of muscle stem cells toward myogenic and adipogenic fates," *Differentiation*, vol. 84, no. 2, pp. 193–202, 2012.
- [35] S. Sakadzic, E. Roussakis, M. A. Yaseen et al., "Two-photon high-resolution measurement of partial pressure of oxygen in cerebral vasculature and tissue," *Nature Methods*, vol. 7, no. 9, pp. 755–759, 2010.
- [36] A. Y. Yu, M. G. Frid, L. A. Shimoda, C. M. Wiener, K. Stenmark, and G. L. Semenza, "Temporal, spatial, and oxygen-regulated expression of hypoxia-inducible factor-1 in the lung," *The American Journal of Physiology*, vol. 275, no. 4 Part 1, pp. L818–L826, 1998.
- [37] C. Schroedl, D. S. McClintock, G. R. S. Budinger, and N. S. Chandel, "Hypoxic but not anoxic stabilization of HIF-1 α requires mitochondrial reactive oxygen species," *American Journal of Physiology. Lung Cellular and Molecular Physiology*, vol. 283, no. 5, pp. L922–L931, 2002.
- [38] C. P. Bracken, A. O. Fedele, S. Linke et al., "Cell-specific regulation of hypoxia-inducible factor (HIF)-1 α and HIF-2 α stabilization and transactivation in a graded oxygen environment," *The Journal of Biological Chemistry*, vol. 281, no. 32, pp. 22575–22585, 2006.
- [39] L. Holmquist-Mengelbier, E. Fredlund, T. Lofstedt et al., "Recruitment of HIF-1 α and HIF-2 α to common target genes is differentially regulated in neuroblastoma:

- HIF-2 α promotes an aggressive phenotype,” *Cancer Cell*, vol. 10, no. 5, pp. 413–423, 2006.
- [40] A. Augstein, D. M. Poitz, R. C. Braun-Dullaeus, R. H. Strasser, and A. Schmeisser, “Cell-specific and hypoxia-dependent regulation of human HIF-3 α : inhibition of the expression of HIF target genes in vascular cells,” *Cellular and Molecular Life Sciences*, vol. 68, no. 15, pp. 2627–2642, 2011.
- [41] J. C. Villa, D. Chiu, A. H. Brandes et al., “Nontranscriptional role of HIF-1 α in activation of γ -secretase and notch signaling in breast cancer,” *Cell Reports*, vol. 8, no. 4, pp. 1077–1092, 2014.
- [42] Y. Mizukami, K. Fujiki, E. M. Duerr et al., “Hypoxic regulation of vascular endothelial growth factor through the induction of phosphatidylinositol 3-kinase/Rho/ROCK and c-Myc,” *The Journal of Biological Chemistry*, vol. 281, no. 20, pp. 13957–13963, 2006.
- [43] K. Ameri, C. E. Lewis, M. Raida, H. Sowter, T. Hai, and A. L. Harris, “Anoxic induction of ATF-4 through HIF-1-independent pathways of protein stabilization in human cancer cells,” *Blood*, vol. 103, no. 5, pp. 1876–1882, 2004.
- [44] Y. Mizukami, W. S. Jo, E. M. Duerr et al., “Induction of interleukin-8 preserves the angiogenic response in HIF-1 α -deficient colon cancer cells,” *Nature Medicine*, vol. 11, no. 9, pp. 992–997, 2005.
- [45] A. M. Arsham, J. J. Howell, and M. C. Simon, “A novel hypoxia-inducible factor-independent hypoxic response regulating mammalian target of rapamycin and its targets,” *The Journal of Biological Chemistry*, vol. 278, no. 32, pp. 29655–29660, 2003.
- [46] N. N. Li, L. Wang, E. K. Tan et al., “Genetic analysis of CHCHD2 gene in Chinese Parkinson’s disease,” *American Journal of Medical Genetics. Part B, Neuropsychiatric Genetics*, vol. 171, no. 8, pp. 1148–1152, 2016.
- [47] M. Funayama, K. Ohe, T. Amo et al., “CHCHD2 mutations in autosomal dominant late-onset Parkinson’s disease: a genome-wide linkage and sequencing study,” *Lancet Neurology*, vol. 14, no. 3, pp. 274–282, 2015.
- [48] K. Ogaki, S. Koga, M. G. Heckman et al., “Mitochondrial targeting sequence variants of the CHCHD2 gene are a risk for Lewy body disorders,” *Neurology*, vol. 85, no. 23, pp. 2016–2025, 2015.
- [49] M. Gagliardi, G. Iannello, C. Colica, G. Annesi, and A. Quattrone, “Analysis of CHCHD2 gene in familial Parkinson’s disease from Calabria,” *Neurobiology of Aging*, vol. 50, pp. 169.e5–169.e6, 2017.
- [50] C. Gao, Y. M. Chen, Q. Sun et al., “Mutation analysis of CHCHD2 gene in Chinese Han familial essential tremor patients and familial Parkinson’s disease patients,” *Neurobiology of Aging*, vol. 49, pp. 218.e9–218.e11, 2017.
- [51] C. Tejera-Parrado, S. Jesus, I. Huertas-Fernandez et al., “Genetic analysis of CHCHD2 in a southern Spanish population,” *Neurobiology of Aging*, vol. 50, pp. 169.e1–169.e2, 2017.
- [52] Q. Lu, X. Deng, Z. Song, Y. Guo, Y. Yang, and H. Deng, “Mutation analysis of the CHCHD2 gene in Chinese Han patients with Parkinson’s disease,” *Parkinsonism & Related Disorders*, vol. 29, pp. 143–144, 2016.
- [53] M. Zhang, Z. Xi, S. Fang et al., “Mutation analysis of CHCHD2 in Canadian patients with familial Parkinson’s disease,” *Neurobiology of Aging*, vol. 38, pp. 217.e7–217.e8, 2016.
- [54] Z. Liu, J. Guo, K. Li et al., “Mutation analysis of CHCHD2 gene in Chinese familial Parkinson’s disease,” *Neurobiology of Aging*, vol. 36, no. 11, pp. 3117.e7–3117.e8, 2015.
- [55] T. S. Fan, H. I. Lin, C. H. Lin, and R. M. Wu, “Lack of CHCHD2 mutations in Parkinson’s disease in a Taiwanese population,” *Neurobiology of Aging*, vol. 38, pp. 218.e1–218.e2, 2016.
- [56] X. Yang, R. An, Q. Zhao et al., “Mutational analysis of CHCHD2 in Chinese patients with multiple system atrophy and amyotrophic lateral sclerosis,” *Journal of the Neurological Sciences*, vol. 368, pp. 389–391, 2016.
- [57] M. Feyeux, F. Bourgois-Rocha, A. Redfern et al., “Early transcriptional changes linked to naturally occurring Huntington’s disease mutations in neural derivatives of human embryonic stem cells,” *Human Molecular Genetics*, vol. 21, no. 17, pp. 3883–3895, 2012.
- [58] F. Borovecki, L. Lovrecic, J. Zhou et al., “Genome-wide expression profiling of human blood reveals biomarkers for Huntington’s disease,” *Proceedings of the National Academy of Sciences of the United States of America*, vol. 102, no. 31, pp. 11023–11028, 2005.
- [59] L. Cui, H. Jeong, F. Borovecki, C. N. Parkhurst, N. Tanese, and D. Krainc, “Transcriptional repression of PGC-1 α by mutant huntingtin leads to mitochondrial dysfunction and neurodegeneration,” *Cell*, vol. 127, no. 1, pp. 59–69, 2006.
- [60] K. Shimojima, A. Okumura, M. Hayashi, T. Kondo, H. Inoue, and T. Yamamoto, “CHCHD2 is down-regulated in neuronal cells differentiated from iPS cells derived from patients with lissencephaly,” *Genomics*, vol. 106, no. 4, pp. 196–203, 2015.
- [61] K. Shimojima, A. Okumura, and T. Yamamoto, “A de novo microdeletion involving PAFAH1B (LIS1) related to lissencephaly phenotype,” *Data in Brief*, vol. 4, pp. 488–491, 2015.
- [62] K. Shimojima, A. Narita, Y. Maegaki, A. Saito, T. Furukawa, and T. Yamamoto, “Whole-exome sequencing identifies a de novo TUBA1A mutation in a patient with sporadic malformations of cortical development: a case report,” *BMC Research Notes*, vol. 7, no. 1, p. 465, 2014.
- [63] L. R. Gauthier, B. C. Charrin, M. Borrell-Pages et al., “Huntingtin controls neurotrophic support and survival of neurons by enhancing BDNF vesicular transport along microtubules,” *Cell*, vol. 118, no. 1, pp. 127–138, 2004.
- [64] L. Zhu, A. Gomez-Duran, G. Saretzki et al., “The mitochondrial protein CHCHD2 primes the differentiation potential of human induced pluripotent stem cells to neuroectodermal lineages,” *The Journal of Cell Biology*, vol. 215, no. 2, pp. 187–202, 2016.
- [65] R. R. Buss, W. Sun, and R. W. Oppenheim, “Adaptive roles of programmed cell death during nervous system development,” *Annual Review of Neuroscience*, vol. 29, pp. 1–35, 2006.
- [66] R. Song, B. Yang, X. Gao et al., “Cyclic adenosine monophosphate response element-binding protein transcriptionally regulates CHCHD2 associated with the molecular pathogenesis of hepatocellular carcinoma,” *Molecular Medicine Reports*, vol. 11, no. 6, pp. 4053–4062, 2015.
- [67] R. S. Martherus, W. Sluiter, E. D. Timmer, S. J. VanHerle, H. J. Smeets, and T. A. Ayoubi, “Functional annotation of heart enriched mitochondrial genes GBAS and CHCHD10 through guilt by association,” *Biochemical and Biophysical Research Communications*, vol. 402, no. 2, pp. 203–208, 2010.
- [68] S. Bannwarth, S. Ait-El-Mkadem, A. Chaussenot et al., “A mitochondrial origin for frontotemporal dementia and amyotrophic lateral sclerosis through CHCHD10 involvement,” *Brain*, vol. 137, Part 8, pp. 2329–2345, 2014.
- [69] E. C. Genin, M. Plutino, S. Bannwarth et al., “CHCHD10 mutations promote loss of mitochondrial cristae junctions

- with impaired mitochondrial genome maintenance and inhibition of apoptosis,” *EMBO Molecular Medicine*, vol. 8, no. 1, pp. 58–72, 2016.
- [70] S. Ait-El-Mkadem, A. Chaussonot, S. Bannwarth, C. Rouzier, and V. Paquis-Flucklinger, “CHCHD10-related disorders,” in *GeneReviews(R)*, R. A. Pagon, M. P. Adam, H. H. Ardinger, S. E. Wallace, A. Amemiya, L. J. H. Bean, T. D. Bird, N. Ledbetter, H. C. Mefford, R. J. H. Smith and K. Stephens, Eds., University of Washington, Seattle (WA), 2015.
- [71] S. Ajroud-Driss, F. Fecto, K. Ajroud et al., “Mutation in the novel nuclear-encoded mitochondrial protein CHCHD10 in a family with autosomal dominant mitochondrial myopathy,” *Neurogenetics*, vol. 16, no. 1, pp. 1–9, 2015.
- [72] D. Kurzweily, S. Kruger, S. Biskup, and M. T. Heneka, “A distinct clinical phenotype in a German kindred with motor neuron disease carrying a CHCHD10 mutation,” *Brain*, vol. 138, Part 9, p. e376, 2015.
- [73] A. Chaussonot, I. Le Ber, S. Ait-El-Mkadem et al., “Screening of CHCHD10 in a French cohort confirms the involvement of this gene in frontotemporal dementia with amyotrophic lateral sclerosis patients,” *Neurobiology of Aging*, vol. 35, no. 12, pp. 2884.e1–2884.e4, 2014.
- [74] A. Chio, G. Mora, M. Sabatelli et al., “CHCH10 mutations in an Italian cohort of familial and sporadic amyotrophic lateral sclerosis patients,” *Neurobiology of Aging*, vol. 36, no. 4, pp. 1767.e3–1767.e6, 2015.
- [75] M. Zhang, Z. Xi, L. Zinman et al., “Mutation analysis of CHCHD10 in different neurodegenerative diseases,” *Brain*, vol. 138, Part 9, p. e380, 2015.
- [76] O. Dols-Icardo, I. Nebot, A. Gorostidi et al., “Analysis of the CHCHD10 gene in patients with frontotemporal dementia and amyotrophic lateral sclerosis from Spain,” *Brain*, vol. 138, Part 12, p. e400, 2015.
- [77] C. H. Wong, S. Topp, A. S. Gkazi et al., “The CHCHD10 P34S variant is not associated with ALS in a UK cohort of familial and sporadic patients,” *Neurobiology of Aging*, vol. 36, no. 10, pp. 2908.e17–2908.e18, 2015.
- [78] N. Marroquin, S. Stranz, K. Muller et al., “Screening for CHCHD10 mutations in a large cohort of sporadic ALS patients: no evidence for pathogenicity of the p.P34S variant,” *Brain*, vol. 139, Part 2, p. e8, 2016.
- [79] K. Muller, P. M. Andersen, A. Hubers et al., “Two novel mutations in conserved codons indicate that CHCHD10 is a gene associated with motor neuron disease,” *Brain*, vol. 137, Part 12, p. e309, 2014.
- [80] S. Penttila, M. Jokela, A. M. Saukkonen et al., “CHCHD10 mutations and motor neuron disease: the distribution in Finnish patients,” *Journal of Neurology, Neurosurgery, and Psychiatry*, vol. 88, no. 3, pp. 272–277, 2017.
- [81] J. O. Johnson, S. M. Glynn, J. R. Gibbs et al., “Mutations in the CHCHD10 gene are a common cause of familial amyotrophic lateral sclerosis,” *Brain*, vol. 137, Part 12, p. e311, 2014.
- [82] M. Auranen, E. Ylikallio, M. Shcherbii et al., “CHCHD10 variant p.(Gly66Val) causes axonal Charcot-Marie-Tooth disease,” *Neurology. Genetic*, vol. 1, no. 1, p. e1, 2015.
- [83] D. Ronchi, G. Riboldi, R. Del Bo et al., “CHCHD10 mutations in Italian patients with sporadic amyotrophic lateral sclerosis,” *Brain*, vol. 138, Part 8, p. e372, 2015.
- [84] F. Perrone, H. P. Nguyen, S. Van Mossevelde et al., “Investigating the role of ALS genes CHCHD10 and TUBA4A in Belgian FTD-ALS spectrum patients,” *Neurobiology of Aging*, vol. 51, pp. 177.e9–177.e16, 2017.
- [85] Y. Chen, J. Zhu, P. Y. Lum et al., “Variations in DNA elucidate molecular networks that cause disease,” *Nature*, vol. 452, no. 7186, pp. 429–435, 2008.
- [86] D. Zhang, K. Zaugg, T. W. Mak, and S. J. Elledge, “A role for the deubiquitinating enzyme USP28 in control of the DNA-damage response,” *Cell*, vol. 126, no. 3, pp. 529–542, 2006.
- [87] J. Yu, Y. Zheng, J. Dong, S. Klusza, W. M. Deng, and D. Pan, “KIBRA functions as a tumor suppressor protein that regulates Hippo signaling in conjunction with Merlin and Expanded,” *Developmental Cell*, vol. 18, no. 2, pp. 288–299, 2010.
- [88] K. Duning, D. O. Wennmann, A. Bokemeyer et al., “Common exonic missense variants in the C2 domain of the human KIBRA protein modify lipid binding and cognitive performance,” *Translational Psychiatry*, vol. 3, p. e272, 2013.
- [89] Y. Hirate and H. Okamoto, “Canopy1, a novel regulator of FGF signaling around the midbrain-hindbrain boundary in zebrafish,” *Current Biology*, vol. 16, no. 4, pp. 421–427, 2006.
- [90] J. D. Altman, A. U. Trendelenburg, L. MacMillan et al., “Abnormal regulation of the sympathetic nervous system in α 2A-adrenergic receptor knockout mice,” *Molecular Pharmacology*, vol. 56, no. 1, pp. 154–161, 1999.
- [91] H. Y. Chen, B. H. Zhu, C. H. Zhang et al., “High CpG island methylator phenotype is associated with lymph node metastasis and prognosis in gastric cancer,” *Cancer Science*, vol. 103, no. 1, pp. 73–79, 2012.
- [92] B. Jiao, T. Xiao, L. Hou et al., “High prevalence of CHCHD10 mutation in patients with frontotemporal dementia from China,” *Brain*, vol. 139, Part 4, p. e21, 2016.
- [93] T. Xiao, B. Jiao, W. Zhang et al., “Identification of CHCHD10 mutation in Chinese patients with Alzheimer disease,” *Molecular Neurobiology*, 2016.
- [94] E. Teyssou, L. Chartier, M. Albert et al., “Genetic analysis of CHCHD10 in French familial amyotrophic lateral sclerosis patients,” *Neurobiology of Aging*, vol. 42, pp. 218.e1–218.e3, 2016.

Review Article

Mitochondrial Nucleoid: Shield and Switch of the Mitochondrial Genome

Sung Ryul Lee¹ and Jin Han²

¹*Department of Integrated Biomedical Science, Cardiovascular and Metabolic Disease Center, College of Medicine, Inje University, Busan, Republic of Korea*

²*National Research Laboratory for Mitochondrial Signaling, Department of Physiology, Cardiovascular and Metabolic Disease Center, College of Medicine, Inje University, Busan, Republic of Korea*

Correspondence should be addressed to Jin Han; phyhanj@inje.ac.kr

Received 18 January 2017; Revised 6 March 2017; Accepted 3 April 2017; Published 7 June 2017

Academic Editor: Maik Hüttemann

Copyright © 2017 Sung Ryul Lee and Jin Han. This is an open access article distributed under the Creative Commons Attribution License, which permits unrestricted use, distribution, and reproduction in any medium, provided the original work is properly cited.

Mitochondria preserve very complex and distinctively unique machinery to maintain and express the content of mitochondrial DNA (mtDNA). Similar to chromosomes, mtDNA is packaged into discrete mtDNA-protein complexes referred to as a nucleoid. In addition to its role as a mtDNA shield, over 50 nucleoid-associated proteins play roles in mtDNA maintenance and gene expression through either temporary or permanent association with mtDNA or other nucleoid-associated proteins. The number of mtDNA(s) contained within a single nucleoid is a fundamental question but remains a somewhat controversial issue. Disturbance in nucleoid components and mutations in mtDNA were identified as significant in various diseases, including carcinogenesis. Significant interest in the nucleoid structure and its regulation has been stimulated in relation to mitochondrial diseases, which encompass diseases in multicellular organisms and are associated with accumulation of numerous mutations in mtDNA. In this review, mitochondrial nucleoid structure, nucleoid-associated proteins, and their regulatory roles in mitochondrial metabolism are briefly addressed to provide an overview of the emerging research field involving mitochondrial biology.

1. Introduction

Normal cellular physiology is critically dependent upon energy in eukaryotic cells, making mitochondria indispensable organelles for energy production in the form of adenosine triphosphate (ATP) via the electron-transport chain and oxidative phosphorylation system (OXPHOS). Additionally, numerous biological functions, including ATP transport, heat production, metal homeostasis, and stress signaling and defense responses, involve mitochondria [1–5]. Stationary (or immobilized) mitochondria serve as calcium buffers to avoid harmful intracellular calcium overload. Depending on cellular demand, their composition is highly variable from tissue to tissue to enable fulfillment of specialized functions, with accumulation at regions of high-energy demand [4, 6]. The position of mitochondria within the cell is determined largely by the cytoskeleton, which comprises

a highly dynamic network of actin filaments, microtubules, and intermediate filaments [7, 8]. Mitochondrial movement, which appears to be influenced by intermediate filament proteins, is highly coordinated with changes in organelle shape in order to produce mitochondria with sizes compatible with their movement [9]. Therefore, the correct distribution of mitochondria is achieved by directed movement and docking and anchoring mechanisms [8]. Unlike other subcellular organelles, such as Golgi, lysosomes, and endosomes, mitochondria individually encapsulate their own genome, referred to as mitochondrial DNA (mtDNA). The size range of mtDNAs found in multicellular animals is relatively narrow (~16.5 kb; Figure 1), with some exceptions varying from 14 kb in the nematode to 42 kb in the scallop [10]. However, the mitochondrial genome of higher plants is much larger than that in multicellular animals, ranging from 200 kb to 2400 kb [6, 10]. Many aspects of mtDNA differ

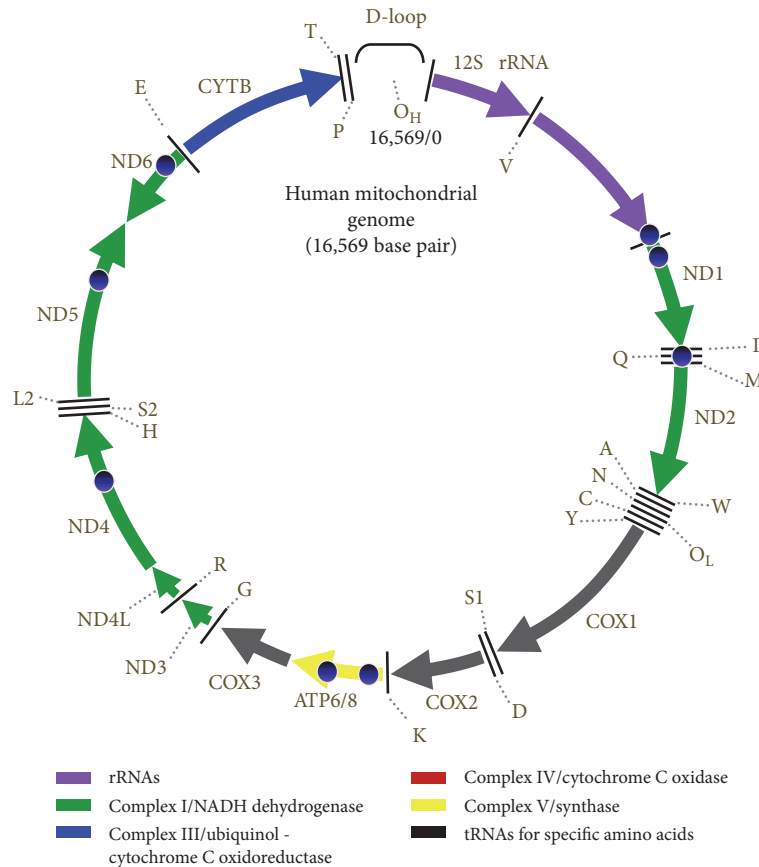


FIGURE 1: Human mtDNA. Human mtDNA is circular, with 16,569 bps that encode seven of the 43 subunits of complex I, one of the 11 subunits of complex III (CYTB), three of the 13 subunits of complex IV (COXI, COXII, and COXIII), and two of the 16 subunits of complex V (ATP synthase 6 and ATP synthase 8). It also encodes two ribosomal RNAs and 22 transfer RNAs. ATP, adenosine triphosphate; COX, cyclooxygenase; CYTB, cytochrome B; mtDNA, mitochondrial DNA.

from those of nuclear DNA, including its non-Mendelian genetics and the polyploid nature of the genome within a single cell [11, 12].

Mitochondria preserve very complex and unique machinery to maintain and express the content of mtDNA. For example, mtDNA replication occurs independent of the cell cycle and irrespective of the replication of genes in the nucleus [13]. Mutations originating from chromosomal DNA cannot completely explain mitochondrial diseases manifested in cardiomyopathies [14, 15], neurodegenerative diseases, aging [16–18], and cancer. Mitochondrial genomes are not naked but rather packaged into chromosome-like organellar nuclei, termed nucleoids, that exhibit a discrete macromolecular assembly that dictates mtDNA-protein interactions related to mitochondrial genetics [19]. In eukaryotic cells, thousands of mtDNA molecules are organized into several hundred nucleoids [1, 13, 19–24], which function as units of mtDNA propagation for mtDNA replication, segregation, and gene expression [25–28]. As an organizing body of mtDNA, nucleoids work as a platform for the subtle and controlled regulation of mitochondrial genomes and their efficient integration into cellular signaling [26, 29]. Naked mtDNA in the mitochondrial matrix would preclude efficient mtDNA maintenance, resulting in increased accumulation of mutations and the inevitable

faulty segregation of mtDNA. Numerous cellular metabolic processes are connected to dynamic regulation associated with mitochondrial nucleoids in order to control the stabilization, maintenance, distribution, and inheritance of the mitochondrial genome [30, 31]. In this review, we addressed the putative mitochondrial nucleoid structure, proteins involved in nucleoid formation, and their regulatory roles in mitochondrial metabolism. Although in-depth mechanistic findings regarding mtDNA nucleoids have been extensively revealed in model organisms, such as *Saccharomyces cerevisiae* [32], this review will be limited to findings from human and mammalian systems.

2. Mitochondrial Structure and Shape

Mitochondrial morphology, suggested as ovoid or rod-shaped, is not static, and mitochondria have no fixed size but vary in appearance of the cristae and structure, which can be branched, curved, or elongated and rod-like and fragmented into multiple smaller mitochondria depending on cell type [33–35]. Even within individual cells, mitochondrial structure varies. For example, mitochondria in skeletal muscle are ovoid structures, with two possible populations: one positioned close to the sarcolemma and the other embedded among the myofibrils [33]. In unstressed or

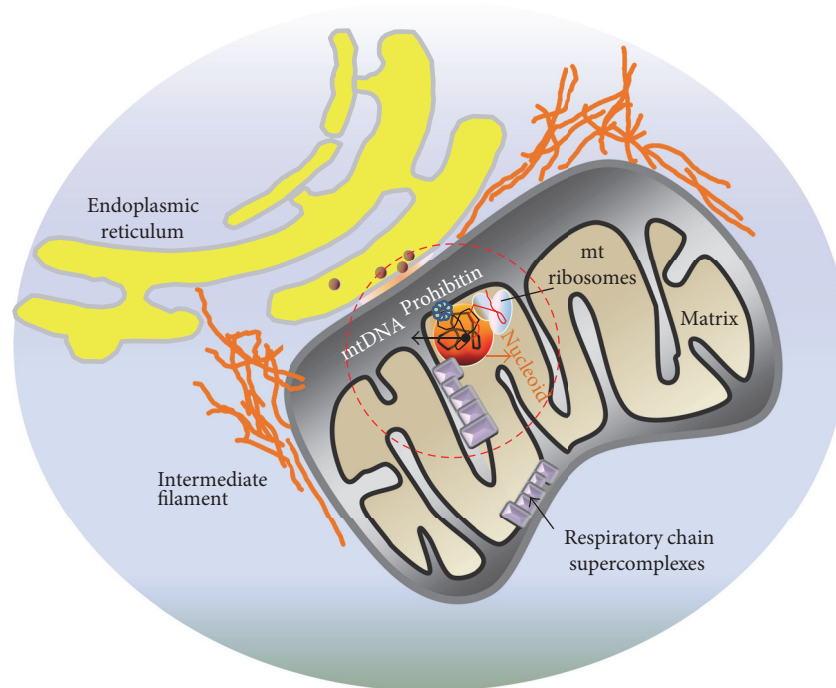


FIGURE 2: Spatial organization (localization) of mitochondrion and mitochondrial nucleoids. The contour length of circular mtDNA (~16.5 kb) is $\sim 5 \mu\text{m}$ [47] and requires tight packaging into nucleoids to fit into the tubules of the mitochondrial network comprised of cylinders $\sim 250 \text{ nm}$ to $\sim 400 \text{ nm}$ in diameter. Nucleoids are organized in higher-ordered assemblies, including respiratory chain supercomplexes [31] and ER-mitochondria complexes (red circle). ER, endoplasmic reticulum; mtDNA, mitochondrial DNA.

intact nondividing cells, mitochondria exist not as a separate, individual mitochondrion, which is routinely seen in isolated mitochondria as a fractional artifact, but rather as a highly connected reticular network. This reticular network of mitochondria is influenced by fission and fusion executed by mitochondria-shaping proteins called mitodynaminins [34]. Fission can be initiated through the response of mitodynaminins to mitochondrial energetics, oxidative stress, hypoxia, or mtDNA damage [34]. When a daughter mitochondrion depolarizes following a fission event and is unable to fuse to the reticular network, this solitary mitochondrion will be removed by mitophagy [36]. Structurally, mitochondria exhibit a double-membrane arrangement, which separates the organelle into four distinct compartments (Figure 2): the outer membrane, the intermembrane space, the inner membrane, and the matrix [33, 37]. The outer membrane separates mitochondria from the cytoplasm and surrounds the inner membrane, which separates the intermembrane space from the protein-dense central matrix. Unlike the outer membrane, the inner membrane constitutes a tight diffusion barrier against all ions and molecules and is differentiated into the inner boundary membrane and the cristae, which is the site of mtDNA replication, transcription, protein biosynthesis, and numerous enzymatic reactions. The two regions are continuous at cristae junctions, with cristae extending into the matrix and acting as the primary sites of mitochondrial energy conversion by ATP synthase located in cristae membranes [37]. Mitochondria do not float freely in the cytosol but are positioned in the cytosol with the aid of intermediate filaments and likely through molecular linkages, networks, and bidirectional signaling between

cellular components and intermediate filaments [7, 8]. Mitochondrial dynamics are responsible for intracellular distribution and reactions based on functional requirements that are maintained through fission, fusion, growth, and structural reorganization, followed by turnover and rearrangements of mitochondrial proteins and DNA [33, 38–40]. Nucleoid foci containing mtDNA are attached to the cytoskeleton [7] and organize the translation machinery on both sides of the mitochondrial membranes [7]. In view of the organization of general mitochondrial functions (Figure 2), many processes are organized in higher-ordered assemblies, including the respiratory chain supercomplexes [41], endoplasmic reticulum-(ER-) mitochondria complexes [42, 43] involved in organelle biogenesis and inheritance, mitochondrial-contact sites and cristae-organizing-system complexes [44] responsible for the organization of mitochondrial ultrastructure and biogenesis, and mitochondrial membrane supercomplexes that mediate protein trafficking [45, 46]. The detailed description of these complexes is under investigation and is beyond the scope of this review.

3. Mitochondrial DNA

Human mtDNA consists of circular, double-stranded 16,569 bp DNA with a contour length of $\sim 5 \mu\text{m}$ [47], thus requiring mtDNA to be highly packaged to fit into a $\sim 100 \text{ nm}$ (in diameter) nucleoid [37]. A mitochondrion contains at least 800 to 1500 proteins of varying relative abundance between tissues [48]; however, mtDNA contains only 37 genes [49, 50] encoding 13 proteins of the mitochondrial respiratory chain, two ribosomal RNAs (12S and 16S),

and 22 transfer RNAs (Figure 1). The remaining protein subunits that comprise the OXPHOS, together with those required for mtDNA maintenance, are encoded by nuclear DNA, synthesized by cytoplasmic ribosomes, and are specifically targeted and sorted into their correct locations within the mitochondrion. Unlike nuclear DNA, mtDNA is characterized by high gene density and the absence of introns [51]. With the exception of a ~1 kb noncoding regulatory fragment (D-loop), mtDNA is entirely transcribed as large polycistrons from both strands [51]. Technically, mtDNA in the nucleoid can be localized in fixed cells in two ways: immunolabeling using an anti-DNA antibody or cell growth for one generation in bromodeoxyuridine (BrdU) to uniformly label the DNA to enable detection using an anti-BrdU antibody [7]. Additionally, mtDNA can be stained with 4',6-diamidino-2-phenylindole, ethidium bromide, or PicoGreen dye [52]. Despite mtDNA being essential for normal physiological functions, the genome is vulnerable to oxidative stress [53]. When isolated rat cardiomyocytes were treated with 50 μ M H₂O₂, the amount of intact 16 kbp mtDNA decreased by 50% over 10 min, resulting in oxidative stress and leading to mitochondrial dysfunction due to the decline in the activities of complexes I, III, and IV, all of which contain mtDNA-encoded subunits [54]. mtDNA constantly undergoes mutation, with clonal expansion or loss of either point mutations or deletions [12], and mutations of mtDNA, both point mutations and deletions, cause a host of tissue-specific [15] and systemic diseases [12, 55]. The polyploid nature of the mitochondrial genome (up to several thousand copies per cell) gives rise to the important features of homoplasmy, heteroplasmy [56–59], and clonal expansion of mtDNA, even in the same mitochondrion, with random mitochondrial segregations capable of occurring in mitochondria within the same cell [11, 12]. Based on the presence of heteroplasmy and clonal segregation, mtDNA status, regardless of harbored mutations, may not be an important factor in the construction and maintenance of nucleoid organization, given that nucleoid-containing mutated mtDNA can segregate in the cell. Although additional study is required to understand the behavior of nucleoid-containing mutated mtDNA and its propagation, why and how mitochondria (or cells) tolerate this aberrant condition remain an interesting question.

4. Mitochondrial Nucleoid Structure and Dynamics

The term nucleoid was first used in 1937 by Piekarski to describe the envelope-lacking structure of the bacterial chromosome as being distinct from that of eukaryotes [60]. Similar DNA-containing structures were later discovered in mitochondria and plastids [61]. Nucleoids do not contain membranes capable of separating the nucleoid compartment from the matrix [27]. The mitochondrial nucleoid is composed of mtDNA and numerous nucleoid-associated proteins (Figure 2) that form a macromolecular structure capable of providing submitochondrial organization of mtDNA [29, 62]. Efficient maintenance of mtDNA in discrete, segregated units located at intervals throughout the

mitochondrial network is concerted through the control of nucleoid structure [32].

The organization of the nucleoid is a very fundamental question in mitochondrial biology. The crucial structural difference between nuclear chromatin and mitochondrial nucleoid is that mtDNA is not associated with histones in the form of nucleosomes [20, 63]. Nucleoids are roughly spherical, with a diameter of ~100 nm and with each containing more than one copy of mtDNA [37]. In view of their size, nucleoids must fit into the ~10 μ m tubules of the mitochondrial tubular network, which can be approximated by infinite cylinders of ~250 nm to ~400 nm diameter [64, 65]. In human cells, the multilayer model of mitochondrial nucleoid organization [66], which describes separation into the inner core region where DNA and proteins (DNA-packaging proteins and proteins involved in replication and transcription) are concentrated and the outer peripheral region containing proteins temporarily recruited to execute special functions in the nucleoid, was suggested based on the tightly bound mtDNA [35, 61]. mtDNA replication and transcription occur in the core region through the activity of mitochondrial transcription factor A (TFAM), mitochondrial RNA polymerase (POLRMT), mitochondrial single-stranded DNA-binding protein (mtSSB), mitochondrial polymerase γ (POLG), and Twinkle helicase, with subsequent RNA processing and translation occurring in the outer region (peripheral region) [22, 61, 67]. In the peripheral region of nucleoids, numerous putative proteins were also identified [61]; however, less is known concerning nucleoid states during mtDNA replication and/or transcription. As shown in Figure 3, mtDNA can be compactly packaged by the binding of mitochondrial transcription factor A (TFAM). The D-loop region of mtDNA, which constitutes a regulatory site for mtDNA replication and transcription, is anchored to the inner mitochondrial membrane (Figures 2 and 3) likely through a multiprotein complex [41, 42, 44] and serves as a central hub for forming nucleoids. As depicted in Figure 4, POLG, ATPase family AAA-domain-containing protein 3 (ATAD3), and the mitochondrial AAA proteases Lon peptidase 1 (LONP1) and mtSSB, including TFAM, are believed to be nucleoid-associated proteins that might interact with the D-loop region of mtDNA [22, 62, 68]. These mtDNA-binding proteins are involved in interactions between mtDNA and the mitochondrial inner membrane, ribosome, and other supercomplexes to facilitate transport of proteins or molecules [45, 69–71]. Mutations in the D-loop region might result in altered binding affinities for the nuclear proteins involved in mtDNA replication and transcription, resulting in severe depletion of mtDNA content due to replication failure and disruption of nucleoid structure [12, 32, 72–75].

5. Nucleoid Structure and Dynamics

Nucleoid structure may vary between tissue types and according to age [76]. Nucleoids are tethered directly or indirectly via the mitochondrial membrane to kinesin and microtubules in the surrounding cytoplasm [7]. Additionally, nucleoids are composed of thin filaments that protrude

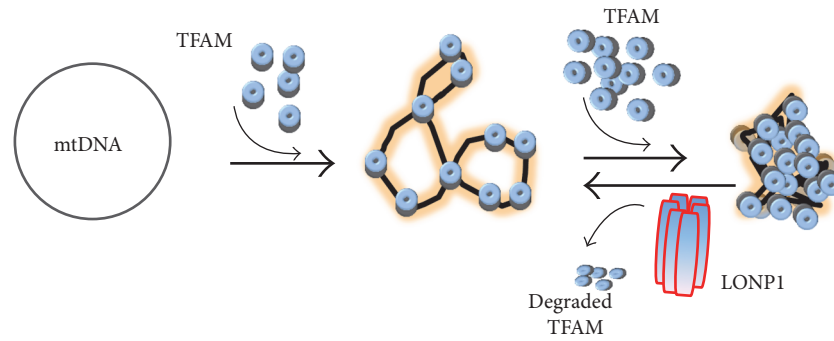


FIGURE 3: mtDNA packaging by TFAM and its degradation by the mitochondrial AAA protease LONP1. Human circular mtDNA is packaged by TFAMs, but their excessive packing of mtDNA may result in shutdown of mtDNA transcription and replication. TFAM can be degraded by the mitochondrial protease LONP1. LONP1, mitochondrial AAA protease; mtDNA, mitochondrial DNA; TFAM, mitochondrial transcription factor A.

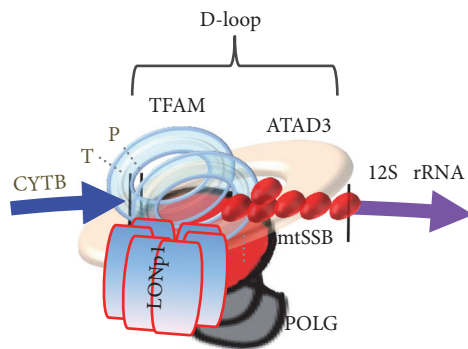


FIGURE 4: Putative nucleoid-associated proteins located in the D-loop region of mtDNA. TFAM, POLG, ATAD3, LONP1, and mtSSB are nucleoid-associated proteins that possibly interact with the D-loop region of mtDNA. These five proteins might exhibit DNA-binding capacity and, therefore, directly associate with mtDNA. ATAD3, ATPase family AAA-domain-containing protein 3; LONP1, mitochondrial AAA protease; mtDNA, mitochondrial DNA; mtSSB mitochondrial single-stranded DNA-binding protein; POLG, mitochondrial polymerase γ ; TFAM, mitochondrial transcription factor A.

outward and serve as anchors to the membrane [21]. Movement of nucleoids located in the protein-dense matrix compartment is limited due to their attachment to the mitochondrial inner membrane (Figure 5), which precludes free diffusion through the matrix compartment [7]. A subset of nucleoids can be observed in close proximity to microtubules, which are used to transport mitochondria over long distances and suggest important roles for the cytoskeleton in nucleoid movement, division, and/or sorting [63]. Nucleoids containing nascent mtDNA localize to mitochondrial tips, with these products of division preferentially distributed within cells as compared with nonreplicative nucleoids [70]. In addition, nucleoids actively engaged in mtDNA synthesis in mammalian cells are spatially and temporally linked to a small subset of ER-mitochondria contacts destined for mitochondrial division [37].

During mtDNA transcription or replication, numerous nucleoid-associated proteins are recruited, indicating that

the mitochondrial nucleoid is dynamic and not a single discrete entity [7, 77]. The kinetics of replication and transcription (monitored by immunolabeling after incorporation of BrdU or bromouridine) suggest that each mtDNA replicates independently of others and that newly made RNA remains (resident half-life: ~ 43 min) long after it has been made [7]. During transcription or replication, nucleoids should be relaxed to facilitate attachment of transcription factors; therefore, the size of such active nucleoids might be larger than that of quiescent nucleoids due to the surrounding shell of proteins associated with the replication and transcription machinery [64]. Unlike a single nucleoid, nucleoid clusters will be formed and mostly contain nucleoids surrounding newly replicated mtDNA; however, the nucleoid population not in replication mode remains outside of these clusters [78]. It was suggested that mitochondrial nucleoids can be reversibly clustered with the aid of TFAM upon mtDNA stress and that this nucleoid clustering might be beneficial for newly replicated mtDNA against intercalators, such as the mtDNA-depletion agent ethidium bromide or anticancer drugs [78].

Within the mitochondrion, nucleoids show an asymmetric intracellular distribution determined by mitochondrial division, fusion, and motility events [70], suggesting that the nucleoid-transmission process is DNA-independent and reliant upon protein-protein interactions [63]. At division sites, mtDNA replication occurs upstream of mitochondrial constriction and assembly of the division machinery. In the absence of mtDNA leading to defects in respiratory activity and energy production, nucleoid integrity is lost due to the absence of protein-DNA and additional protein-protein interactions, and the mitochondrial reticulum is compromised due to the reduced cristal-membrane content [79]. However, nucleoid proteins are capable of binding to their proper sites on the inner mitochondrial membrane and are sorted normally in the absence of mtDNA, given the near-uniform distribution of mtSSB in mtDNA-depleted rho-zero cells [80]. The maintenance or selective degradation of mitochondrial nucleoids free of mtDNA remains unknown.

In mammalian cells, mtDNA exhibits a closed, circular form; however, upon strand breakage or partial deletion, this circular structure is linearized. This linearized and unsealed

distribution within the mitochondrial network upon network-morphological changes remains limited. Apart from nucleoid redistribution in the cell, it remains unclear whether the nucleoid fission/reintegration process is involved in compensating for or selectively segregating nucleoids containing mutated mtDNA.

6. mtDNA Content in the Mitochondrial Nucleoid

In mitochondrial genetics, the number of mtDNA(s) contained within a single nucleoid is a fundamental question that remains somewhat controversial. Strong discrepancies in mtDNA number present in a single nucleoid might be associated with methodological differences, different cell types, or the unveiled complex behaviors of a nucleoid [22, 87]. According to stimulated emission-depletion microscopy or photoactivated light microscopy [22], mammalian cells might contain an average of 1.45 mtDNA molecules per nucleoid (ranging from ~2.4 to ~7.8 per nucleoid). However, a recent study of mitochondrial nucleoids from mouse embryonic fibroblasts reported that a single nucleoid could contain more than two mtDNA molecules based on the characteristics of TFAM-mediated mtDNA packaging indicating a spherical shape [87]. These different points regarding mtDNA-molecule population within a single nucleoid highlight the continued importance of understanding nucleoid ultrastructure, but questions concerning control of individual mtDNA transcription and replication nucleoids remain unsolved. Interestingly, mtDNA does not mix between two different nucleoids, despite their proximity in space and time within the mitochondrial network, but rather, mitochondrial nucleoids are tightly regulated by their genetic content rather than the free exchange of mtDNAs [88]. However, heterologous mtDNAs within maximal diffusible distance of mtDNA transcripts in the same mitochondrion can trans-complement to restore mitochondrial function, a result that provides a basis for future research in mitochondrial therapeutics [32, 83].

7. Mitochondrial Nucleoid-Associating Proteins

In the previous section, the characteristics of mitochondrial nucleoids were briefly addressed (Figures 1–5). Principally, nucleoid-associated proteins can be defined as any protein that either temporarily or permanently associates directly with mtDNA or with other nucleoid proteins and plays roles in mtDNA maintenance [28]. To better understand the biological functions and regulation of mitochondrial nucleoids, identification of proteins involved in nucleoid formation is necessary [89]. Except for conserved TFAM and mtSSB [19, 53], there is no consensus regarding nucleoid composition due to differences in cell types or tissues used for preparations, the various biochemical approaches used for examination based on noncovalent protein-DNA and protein-protein interactions [90], formaldehyde cross-linking [91] or proximity-based biotinylation techniques [43], the low abundance of proteins within mitochondrial nucleoids, and the limited characterization of proteins

related to mtDNA maintenance and gene expression [89]. Additionally, it is difficult to use genetic methods to study these associations, because all of the proteins identified are likely required to maintain mitochondrial function [67].

Nucleoids from most organisms contain ≥ 50 proteins, many of which have not been characterized with respect to nucleoid function [22, 28, 66, 67, 92–94]. Generally, proteins involved in mtDNA packaging or covering exhibit low molecular weight and function as multimers (Table 1). Nucleoid-associated proteins from various organisms can be classified into at least four groups: (1) proteins with known functions in DNA transactions and packaging, (2) proteins participating in protein quality control, (3) bifunctional metabolic enzymes with various activities, and (4) cytoskeletal components [63]. Some examples of these nucleoid-associated proteins are presented in Table 1 and Figure 5. Among those identified as nucleoid-associated proteins, many exhibit identifiable activities unrelated directly to mtDNA maintenance, suggesting that their bifunctionality might involve participation in both mitochondrial metabolism and mtDNA maintenance [32, 89, 95]. Interestingly, mutations in proteins associated with the mitochondrial nucleoid might cause either the loss of mtDNA content from the cell or generation of mtDNA mutations [32, 96].

7.1. Mitochondrial TFAM. TFAM is a nuclear-DNA-encoded 24-kDa protein containing two high-mobility group-(HMG-) box domains and able to bend, wrap, and unwind DNA through modes involving sliding, collisions, and patch formation [29, 89, 90, 97–101]. TFAMs cover mtDNA with a footprint of between 10 bp and 30 bp (Figure 3) and mediate the tight compaction of relaxed mtDNA [62]. In addition to a role as a master transcription factor, TFAM plays an equally important role in promoter selection, initiation of genome replication, and the regulation of mtDNA copy number [98]. TFAM concentration can increase mtDNA content through its preferential binding at the light-strand promoter (LSP) in the D-loop and TFAM-mediated stabilization of mtDNA, perhaps by reducing the rate of DNA turnover [98]. The molecular ratio of TFAM relative to mtDNA is ~900:1 in human mitochondria [102], with this amount of TFAM sufficient to coat 16.6 kbp circular human mtDNA [96]. Theoretically, mtDNA density, TFAM/mtDNA stoichiometry, or TFAM density within a single nucleoid may differ under various physiological (mtDNA transcription or replication) or pathological conditions [64], thereby implying the presence of mechanisms that select only a subset of mtDNA molecules for replication, with others remaining in a silent state [101]. A recent finding suggested that human TFAM plays an important role in the equal distribution and symmetric segregation of mtDNA in cultured cells [66]. For example, enlarged mtDNA nucleoids have been observed in both TFAM-knockdown HeLa cells and TFAM-overexpressing mice [103]. The process of uncoating mtDNA has not been elucidated but likely involves the selective and processive dissociation of TFAM [104]. In view of TFAM turnover [7], LONP1 determines the proteolytic degradation of TFAM and constitutes an additional step in controlling mtDNA content (Figure 3). Apart from regulating

TABLE 1: Mitochondrial nucleoid-associated proteins with known functions.

Nucleoid protein	Location/shape	Function in mtDNA metabolism and/or nucleoid	Reference
Mitochondrial transcription factor A (TFAM)	Core region/homodimerization	(i) Transcription initiation (ii) mtDNA binding, bending, and packaging (iii) mtDNA copy number regulation and segregation	[66, 89, 90]
Mitochondrial single-stranded DNA-binding protein (mtSSB)	Core region	(i) Single-stranded mtDNA binding (ii) Coating of single strands of mtDNA	[66, 89, 90, 122]
ATP-dependent Lon protease (LONP1)	Core region/homo-oligomeric ring	(i) Binding to G-rich single-stranded mtDNA (ii) Interaction with POLG and Twinkle (iii) mtDNA quality control (iv) TFAM degradation	[63, 66, 96, 123]
Twinkle	Core region/hexamer	(i) mtDNA replication	[66]
mtDNA polymerase γ (POLG/POLG2)	Core region	(i) mtDNA replication and repair	[66, 89, 90, 122]
Mitochondrial transcription factor B1/B2 (TFB2M/TFB1M)	Core region	(i) Transcription	[66]
Mitochondrial RNA polymerase (POLRMT)	Core region	(i) Transcription	[66]
Mitochondrial transcription termination factor (mTERF)	Core region	(i) Transcription and replication	[94]
Mitochondrial topoisomerase I (TOP1M)	Core region	(i) Replication	[62]
ATPase AAA-domain-containing protein 3 (ATAD3)	Peripheral region/hexamer	(i) Binding to the D-loop region of mtDNA (ii) Molecular scaffolding for mitochondrial translation via association with both the mitochondrial inner membrane and the ribosome	[62, 66]
Prohibitins 1 and 2 (PHB1 and PHB2)	Peripheral region/oligomeric ring	(iii) Organization and segregation of nucleoids (i) Stabilizing TFAM in mitochondrial nucleoids (ii) Maintenance of mitochondrial morphology (iii) Regulation of mtDNA copy number	[62]
Mitochondrial nucleoid factor 1 (MNF1 or M19)	Peripheral zone	(i) Linking between mtDNA and mitochondrial ATP production (ii) mtDNA translation	[76]
Mitochondrial AAA protein ClpX	Peripheral region (?)	(iii) Assembly of respiratory complexes (i) mtDNA distribution (ii) TFAM quality control	[66]
Leucine-rich pentatricopeptide-repeat motif-containing protein 130 (LRP130)	Peripheral region (?)	(i) Increased mtDNA transcription and RNA stability	[124]

TFAM expression and turnover, posttranslational modification of TFAM by glycosylation, phosphorylation, acetylation, or ubiquitination might constitute alternative control points of TFAM activity, given that these modifications can influence DNA-binding activity, protein-protein interactions, homodimerization, or cooperative-binding characteristics [98]. For example, TFAM can be phosphorylated within its HMG1 domain by cyclic adenosine monophosphate-dependent protein kinase in mitochondria, thereby impairing its ability to bind DNA and activate transcription [104]. By contrast, in the cytosol, TFAM phosphorylation might alter its degradation by the proteasome or its association with mitochondrial protein-translocation machinery [104].

7.2. Mitochondrial Transcription and Replication Machinery.

The minimal proteins required for mtDNA transcription (e.g., POLRMT and mitochondrial transcription factor B (mtTFB)) and replication (POLG and POLG2) are embedded in the core region of nucleoids through their mtDNA-binding capabilities [13, 43, 62]. Due to the high degree of compaction in mtDNA, mitochondrial topoisomerase 1, found in the core region of mitochondrial nucleoids, is required during replication to ease torsional strain resulting from replication progression [62]. Additionally, POLRMT and mtTFB, located in the core region of nucleoids, are necessary for mitochondrial transcription [13, 62].

7.3. *mtSSB*. mtSSB is a 16-kDa protein that forms a tetramer and binds ssDNA with high affinity in a sequence-independent manner, thereby aiding DNA replication, recombination, and repair processes [64, 105]. Similar to TFAM, mtSSB is a major nucleoid-associated protein also involved in mtDNA/nucleoid distribution within the mitochondrial network [106]. Additionally, mtSSB influences mitochondrial biogenesis [105, 106], and its downregulation leads to increases in morphological alterations, such as fragmentation or elongation, of mitochondria [107].

7.4. *Twinkle Helicase*. Twinkle helicase is a nucleoid-associated protein found in the core region [66] and the only known mitochondrial helicase involved in unwinding mtDNA during the replication process, synthesis of the nascent D-loop strand, and completion of mtDNA replication [108, 109]. Decreases in Twinkle helicase concentration result in mtDNA depletion, whereas overexpression leads to increases in mtDNA copy number [109]. Many disease-causing mutations, including autosomal dominant progressive external ophthalmoplegia, have been mapped to the Twinkle helicase gene, with mutation resulting in defects in OXPHOS and the onset of neuromuscular symptoms [109]. Twinkle helicase might also promote nucleoid attachment to membrane structures highly enriched in cholesterol, thereby providing a replication platform at ER-mitochondrial junctions [71].

7.5. *Mitochondrial ATPase AAA-Domain-Containing Proteins (AAA)*. Several ATP-dependent proteases, including LONP1, ATP-dependent Clp protease ATP-binding subunit ClpX-like protein, and m-AAA protease, localize to the mitochondrial matrix [96] and are associated with the peripheral

region of nucleoids [61, 96, 110]. Among these, LONP1 is a quality control enzyme that degrades oxidatively modified and misfolded proteins and also binds to specific regions of the mitochondrial genome, including ssDNA in both the LSP region and RNA produced from the LSP region [98]. Additionally, LONP1 might recognize oxidized TFAM or degrade unbound TFAM; alternatively, LONP1 can also remove TFAM from oxidatively modified DNA, to which TFAM binds with higher efficiency than it does unmodified DNA [98]. Although the triggers for LONP1-mediated TFAM degradation remain unclear, mitochondrial stress might activate LONP1 activity to initiate TFAM degradation and activate transcription in quiescent mtDNAs [98]. Interestingly, LONP1 expression decreases with age or exposure to chronic stress, possibly resulting in accumulation of oxidized proteins and disturbance of the nucleoid dynamics [111].

7.6. *ATAD3*. ATAD3A and the less abundant ATAD3B are protein paralogs that form heterohexamers or homohexamers with ATAD3A and extend from the inner membrane into the outer mitochondrial membrane [66, 112]. ATAD3 was discovered as an important membrane-bound mitochondrial ATPase [112]. Although ATAD3 appeared to be bound to the D-loop of mtDNA in nucleoid [75], subsequent experiments indicated that ATAD3 made direct contact with mtDNA but is among the nucleoid-associated proteins involved in connections between mitochondrial nucleoids and mitochondrial ribosomes [66, 93]. ATAD3 associates with ER-mitochondrial junctions and holds together Twinkle helicase-containing mammalian nucleoids attached to membrane structures highly enriched in cholesterol [71]. Therefore, ATAD3 also plays an important role in nucleoid positioning in human mitochondria, with altered ATAD3 expression disturbing mtDNA maintenance and replication [77].

7.7. *Prohibitin*. Prohibitin proteins (PHB1 and PHB2) are membrane-anchored molecular chaperones and protein stabilizers [67, 103]. In addition to pleiotropic functions, including apoptosis, in mitochondria, PHB1 is required for the organization and stability of mitochondrial nucleoids either through a TFAM-dependent or through a TFAM-independent pathway, in which it regulates nucleoid organization directly or through undefined nucleoid factors [113]. Several reports supported the notion that PHBs are important in mtDNA copy number regulation [103, 113].

7.8. *Other Putative Nucleoid-Associated Proteins*. A group of heat-shock proteins (HSPs) are associated with nucleoids in both yeast and human cells [63]. HSP60 functions both in mitochondrial protein import and as a nucleoid protein required for nucleoid division [63]. The components of detergent-resistant mtDNA nucleoids include adenine nucleotide translocator (ANT), the E2 subunits of two large dehydrogenase complexes, pyruvate dehydrogenase, and branched-chain keto acid dehydrogenase without association with other subunits [67].

8. Links between Mitochondrial Nucleoid Composition and Metabolic Control

Mitochondrial nucleoids undergo remodeling, such as transition of its structure or recruitment of other proteins that influence nucleoid-related activities in response to metabolic cues in yeast [114, 115]. There is less concrete evidence of yeast-like nucleoid remodeling in mammalian systems; however, nucleoid remodeling might be possible according to metabolic demand [5, 32], because access to mtDNA for transcription, translation, and replication is highly coordinated by various factors inside and outside of the nucleoid compartment. Moreover, nucleoid-associated proteins are directly involved in not only mtDNA maintenance and propagation but also metabolic activities not directly linked to mtDNA stability [62]. Additionally, retrograde signaling from the mitochondria to the nucleus can be promoted through interactions between mtDNA and nucleoid-associated factors [2, 7]. It is unclear whether nucleoid-associated proteins can directly regulate mitochondrial gene expression or bioenergetics.

9. Pathological Changes Associated with Mitochondrial Nucleoids

Mitochondrial morphology is coupled to function, as a loss in mitochondrial bioenergetic capacity results in an inability to maintain a highly ordered structure [62]. The shaping, maintenance, and dissociation of nucleoids in a mitochondrion is undertaken by numerous proteins that communicate with one another and the nucleoid in order to determine cellular demands dependent upon physiological conditions. The general principles of nucleoid organization and its pathological implications remain unclear; however, significant interest in the role of nucleoids and their impact on mitochondria-related diseases has focused on their association with the accumulation of numerous mtDNA mutations [27]. Mutations in mtDNA and/or aberrant nucleoid organization might be a causal factor in etiologies of various diseases, including cancers [15, 106]. In addition to mutations or damage to nucleoid-associated proteins, aberrant interactions between or dysfunction of nucleoid-interacting proteins causes pathological conditions due to failed mtDNA maintenance. For example, ANT1 interacts with mtDNA [67], and its mutation causes a genetic disorder leading to multiple mtDNA deletions and autosomal dominant progressive external ophthalmoplegia [116]. Additionally, the subunits of complex I and the E2 subunits of ATP synthase and 2-oxo-acid dehydrogenase have been identified in nucleoids and are involved in mitochondrial diseases and aging [67]. Under physiological or various cellular stress conditions, p53 can maintain nuclear genome stability through the repair of damaged DNA and the integration of cell-death-signaling pathways with DNA-damage checkpoints [117]. Recently, an additional role for p53 as guardian of the mitochondrial genome was suggested [118]. Mitochondria-translocated p53 can interact with TFAM and POLG located in the core region of nucleoids and involved in mtDNA maintenance [119]. It was suggested that

the expression of dynamin-related protein 1 and OPA1 involved in mitochondrial dynamics is regulated by p53 [118]. Interestingly, human mtDNA also contains a putative p53-binding sequence [120], suggesting that p53 functions involve both the nuclear and mitochondrial subcellular compartments and are responsible for maintaining mtDNA integrity through its activities in both regions (Figure 5). It remains unclear whether p53 directly affects the structure and dynamics of mitochondrial nucleoids.

Oxidative damage can disturb the regulation of nucleoid dynamics. For example, oxidized mtDNA is degraded by lysosomes; however, oxidized mitochondrial nucleoids are not degraded via the lysosomal pathway in neutrophils in human lupus, resulting in activation of type I interferon production [121]. Oxidative stress may deteriorate the dynamics of nucleoids due to their resulting structural modifications and the breakdown of redox control, resulting in mitochondrial dysfunction. However, more extensive work is needed to clarify the mechanisms associated with oxidative-stress-mediated disruption and/or dysfunction of mitochondrial nucleoids. The clustering of multiple mtDNA genomes into a single nucleoid complex might promote the progressive age-related accumulation of deletions and point mutations in mtDNA in many somatic tissues and particularly in postmitotic cells. By contrast, oocytes appear to have the ability to select against deleterious mutations in mtDNA, at least in mice [17]. Therefore, the processes by which nucleoids are actively chosen for mtDNA replication and distribution within mitochondrial networks are not clearly understood and remain as highly relevant issues associated with understanding the basis of human metabolic diseases, aging, and neurodegenerative disorders caused by mtDNA mutations, as well as those in nuclear genes, that affect mtDNA maintenance [70].

10. Concluding Remarks and Perspectives

In mitochondrial biology and its role in human diseases, nucleoids remain an unexplored feature. Their role as entities that organize mtDNA by forming complexes with accessory proteins, as well as regulators of gene expression, greatly influences the phenotypic expression of mtDNA defects [17]. In this review, we addressed the newly emerging field of nucleoid research, including investigations of its structure and dynamic regulation. Nucleoid-associated proteins function as building blocks of nucleoids, which are intimately involved in mitochondrial genetics and the fine tuning of metabolic demands (Figure 5). To understand the complex behavior of nucleoids, it will be necessary to examine the specific interactions between different nucleoid-associated proteins and mtDNA to definitively elucidate their roles in nucleoid organization. In addition to posttranslational modifications of nucleoid-associated proteins, oxidative changes that occur in nucleoid-associated proteins and their impact on mtDNA likely influence nucleoid dynamics and function and might be necessary to understand the real functional role of nucleoid and mitochondria. Furthermore, the assembly and dynamic control of nucleoid

structure involving mtDNA also remains unclear and should be the subject of future investigation.

Collectively, mtDNA is preserved in a highly ordered manner by nucleoids. Mitochondrial nucleoids act not as simple shields or parcels for mtDNA but constitute a switch for controlling mitochondrial metabolism in response to cellular demands. New findings associated with mitochondria should be interpreted in conjunction with nucleoid dynamics to fully understand its overall physiological and pathophysiological role.

Conflicts of Interest

The authors declare that there are no conflicts of interest.

Acknowledgments

The authors apologize for the vast number of outstanding publications that could not be cited due to space limitations. This work was supported by the Priority Research Centers Program (2010-0020224) and the Basic Science Research Program (2015R1A2A1A13001900 and 2015R1D1A3A01015596) through the National Research Foundation of Korea (NRF) funded by the Ministry of Education, Science, and Technology.

References

- [1] A. Kaniak-Golik and A. Skoneczna, "Mitochondria-nucleus network for genome stability," *Free Radical Biology & Medicine*, vol. 82, pp. 73–104, 2015.
- [2] F. M. da Cunha, N. Q. Torelli, and A. J. Kowaltowski, "Mitochondrial retrograde signaling: triggers, pathways, and outcomes," *Oxidative Medicine and Cellular Longevity*, vol. 2015, Article ID 482582, 10 pages, 2015.
- [3] M. Guha and N. G. Avadhani, "Mitochondrial retrograde signaling at the crossroads of tumor bioenergetics, genetics and epigenetics," *Mitochondrion*, vol. 13, no. 6, pp. 577–591, 2013.
- [4] H. M. McBride, M. Neuspiel, and S. Wasiak, "Mitochondria: more than just a powerhouse," *Current Biology*, vol. 16, no. 14, pp. R551–RR60, 2006.
- [5] I. Bohovych and O. Khalimonchuk, "Sending out an SOS: mitochondria as a signaling hub," *Frontiers in Cell and Development Biology*, vol. 4, no. 109, pp. 1–15, 2016.
- [6] I. E. Scheffler, *Mitochondria*, John Wiley & Sons, Inc., New Jersey, 2nd edition, 2008.
- [7] F. J. Iborra, H. Kimura, and P. R. Cook, "The functional organization of mitochondrial genomes in human cells," *BMC Biology*, vol. 2, no. 1, p. 9, 2004.
- [8] N. Schwarz and R. E. Leube, "Intermediate filaments as organizers of cellular space: how they affect mitochondrial structure and function," *Cell*, vol. 5, no. 3, p. 30, 2016.
- [9] S. Campello and L. Scorrano, "Mitochondrial shape changes: orchestrating cell pathophysiology," *EMBO Reports*, vol. 11, no. 9, pp. 678–684, 2010.
- [10] I. E. Scheffler, "Biogenesis of mitochondria," in *Mitochondria*, pp. 60–167, John Wiley & Sons, Inc., Hoboken, NJ, USA, 2007.
- [11] M. Schwartz and J. Vissing, "Paternal inheritance of mitochondrial DNA," *The New England Journal of Medicine*, vol. 347, no. 8, pp. 576–580, 2002.
- [12] R. W. Taylor and D. M. Turnbull, "Mitochondrial DNA mutations in human disease," *Nature Reviews. Genetics*, vol. 6, no. 5, pp. 389–402, 2005.
- [13] M. Falkenberg, N.-G. Larsson, and C. M. Gustafsson, "DNA replication and transcription in mammalian mitochondria," *Annual Review of Biochemistry*, vol. 76, pp. 679–699, 2007.
- [14] B. Thornton, B. Cohen, W. Copeland, and B. L. Maria, "Mitochondrial disease: clinical aspects, molecular mechanisms, translational science, and clinical frontiers," *Journal of Child Neurology*, vol. 29, no. 9, pp. 1179–1207, 2014.
- [15] S. Lee, N. Kim, Y. Noh et al., "Mitochondrial DNA, mitochondrial dysfunction, and cardiac manifestations," *Frontiers in Bioscience (Landmark Edition)*, vol. 21, pp. 1410–1426, 2016.
- [16] H. Huang and K. G. Manton, "The role of oxidative damage in mitochondria during aging: a review," *Frontiers in Bioscience*, vol. 9, pp. 1100–1117, 2004.
- [17] D. F. Bogenhagen, "Does mtDNA nucleoid organization impact aging?" *Experimental Gerontology*, vol. 45, no. 7-8, pp. 473–477, 2010.
- [18] C. B. Park and N. G. Larsson, "Mitochondrial DNA mutations in disease and aging," *The Journal of Cell Biology*, vol. 193, no. 5, pp. 809–818, 2011.
- [19] Y. Wang and D. F. Bogenhagen, "Human mitochondrial DNA nucleoids are linked to protein folding machinery and metabolic enzymes at the mitochondrial inner membrane," *Journal of Biological Chemistry*, vol. 281, no. 35, pp. 25791–25802, 2006.
- [20] F. Legros, F. Malka, P. Frachon, A. Lombes, and M. Rojo, "Organization and dynamics of human mitochondrial DNA," *Journal of Cell Science*, vol. 117, no. Part 13, pp. 2653–2662, 2004.
- [21] J. Prachar, "Ultrastructure of mitochondrial nucleoid and its surroundings," *General Physiology and Biophysics*, vol. 35, no. 3, pp. 273–286, 2016.
- [22] D. F. Bogenhagen, "Mitochondrial DNA nucleoid structure," *Biochimica et Biophysica Acta*, vol. 1819, no. 9-10, pp. 914–920, 2012.
- [23] D. Bogenhagen and D. A. Clayton, "The number of mitochondrial deoxyribonucleic acid genomes in mouse L and human HeLa cells. Quantitative isolation of mitochondrial deoxyribonucleic acid," *The Journal of Biological Chemistry*, vol. 249, no. 24, pp. 7991–7995, 1974.
- [24] R. Garesse and C. G. Vallejo, "Animal mitochondrial biogenesis and function: a regulatory cross-talk between two genomes," *Gene*, vol. 263, no. 1-2, pp. 1–16, 2001.
- [25] R. Ban-Ishihara, T. Ishihara, N. Sasaki, K. Mihara, and N. Ishihara, "Dynamics of nucleoid structure regulated by mitochondrial fission contributes to cristae reformation and release of cytochrome c," *Proceedings of the National Academy of Sciences of the United States of America*, vol. 110, no. 29, pp. 11863–11868, 2013.
- [26] G. L. Ciesielski, M. Plotka, M. Manicki et al., "Nucleoid localization of Hsp40 Mdj1 is important for its function in maintenance of mitochondrial DNA," *Biochimica et Biophysica Acta*, vol. 1833, no. 10, pp. 2233–2243, 2013.
- [27] A. A. Kolesnikov, "The mitochondrial genome. The nucleoid," *Biochemistry (Moscow)*, vol. 81, no. 10, pp. 1057–1065, 2016.

- [28] J. N. Spelbrink, "Functional organization of mammalian mitochondrial DNA in nucleoids: history, recent developments, and future challenges," *IUBMB Life*, vol. 62, no. 1, pp. 19–32, 2010.
- [29] I. J. Holt, J. He, C. C. Mao et al., "Mammalian mitochondrial nucleoids: organizing an independently minded genome," *Mitochondrion*, vol. 7, no. 5, pp. 311–321, 2007.
- [30] S. Meeusen and J. Nunnari, "Evidence for a two membrane-spanning autonomous mitochondrial DNA replisome," *The Journal of Cell Biology*, vol. 163, no. 3, pp. 503–510, 2003.
- [31] M. Navratil, B. G. Poe, and E. A. Arriaga, "Quantitation of DNA copy number in individual mitochondrial particles by capillary electrophoresis," *Analytical Chemistry*, vol. 79, no. 20, pp. 7691–7699, 2007.
- [32] R. W. Gilkerson, "Mitochondrial DNA nucleoids determine mitochondrial genetics and dysfunction," *The International Journal of Biochemistry & Cell Biology*, vol. 41, no. 10, pp. 1899–1906, 2009.
- [33] J. G. McCarron, C. Wilson, M. E. Sandison et al., "From structure to function: mitochondrial morphology, motion and shaping in vascular smooth muscle," *Journal of Vascular Research*, vol. 50, no. 5, pp. 357–371, 2013.
- [34] P. Jezek and L. Plecita-Hlavata, "Mitochondrial reticulum network dynamics in relation to oxidative stress, redox regulation, and hypoxia," *The International Journal of Biochemistry & Cell Biology*, vol. 41, no. 10, pp. 1790–1804, 2009.
- [35] A. Dlaskova, H. Engstova, L. Plecita-Hlavata et al., "Distribution of mitochondrial DNA nucleoids inside the linear tubules vs. bulk parts of mitochondrial network as visualized by 4Pi microscopy," *Journal of Bioenergetics and Biomembranes*, vol. 47, no. 3, pp. 255–263, 2015.
- [36] G. Twig, A. Elorza, A. J. Molina et al., "Fission and selective fusion govern mitochondrial segregation and elimination by autophagy," *The EMBO Journal*, vol. 27, no. 2, pp. 433–446, 2008.
- [37] W. Kuhlbrandt, "Structure and function of mitochondrial membrane protein complexes," *BMC Biology*, vol. 13, no. 1, p. 89, 2015.
- [38] J. Bereiter-Hahn, M. Voth, S. Mai, and M. Jendrach, "Structural implications of mitochondrial dynamics," *Biotechnology Journal*, vol. 3, no. 6, pp. 765–780, 2008.
- [39] A. E. Frazier, C. Kiu, D. Stojanovski, N. J. Hoogenraad, and M. T. Ryan, "Mitochondrial morphology and distribution in mammalian cells," *Biological Chemistry*, vol. 387, no. 12, pp. 1551–1558, 2006.
- [40] C. Vasquez-Trincado, I. Garcia-Carvajal, C. Pennanen et al., "Mitochondrial dynamics, mitophagy and cardiovascular disease," *The Journal of Physiology*, vol. 594, no. 3, pp. 509–525, 2015.
- [41] H. Schagger and K. Pfeiffer, "Supercomplexes in the respiratory chains of yeast and mammalian mitochondria," *The EMBO Journal*, vol. 19, no. 8, pp. 1777–1783, 2000.
- [42] B. Kornmann and P. Walter, "ERMES-mediated ER-mitochondria contacts: molecular hubs for the regulation of mitochondrial biology," *Journal of Cell Science*, vol. 123, Part 9, pp. 1389–1393, 2010.
- [43] S. U. Liyanage, E. Coyaud, E. M. Laurent et al., "Characterizing the mitochondrial DNA polymerase gamma interactome by BioID identifies Ruvbl2 localizes to the mitochondria," *Mitochondrion*, vol. 32, pp. 31–35, 2016.
- [44] M. Harner, C. Körner, D. Walther et al., "The mitochondrial contact site complex, a determinant of mitochondrial architecture," *The EMBO Journal*, vol. 30, no. 21, pp. 4356–4370, 2011.
- [45] K. Kehrein, R. Schilling, B. V. Möller-Hergt et al., "Organization of mitochondrial gene expression in two distinct ribosome-containing assemblies," *Cell Reports*, vol. 10, no. 6, pp. 843–853, 2015.
- [46] A. Chacinska, P. Rehling, B. Guiard et al., "Mitochondrial translocation contact sites: separation of dynamic and stabilizing elements in formation of a TOM-TIM-preprotein supercomplex," *The EMBO Journal*, vol. 22, no. 20, pp. 5370–5381, 2003.
- [47] M. M. Nass and S. Nass, "Intramitochondrial fibers with DNA characteristics. I. Fixation and electron staining reactions," *The Journal of Cell Biology*, vol. 19, pp. 593–611, 1963.
- [48] C. Meisinger, A. Sickmann, and N. Pfanner, "The mitochondrial proteome: from inventory to function," *Cell*, vol. 134, no. 1, pp. 22–24, 2008.
- [49] N. D. Bonawitz, D. A. Clayton, and G. S. Shadel, "Initiation and beyond: multiple functions of the human mitochondrial transcription machinery," *Molecular Cell*, vol. 24, no. 6, pp. 813–825, 2006.
- [50] M. G. Claros, J. Perea, Y. Shu, F. A. Samatey, J. L. Popot, and C. Jacq, "Limitations to in vivo import of hydrophobic proteins into yeast mitochondria. The case of a cytoplasmically synthesized apocytochrome b," *European Journal of Biochemistry*, vol. 228, no. 3, pp. 762–771, 1995.
- [51] S. Anderson, A. T. Bankier, B. G. Barrell et al., "Sequence and organization of the human mitochondrial genome," *Nature*, vol. 290, no. 5806, pp. 457–465, 1981.
- [52] J. Magnusson, M. Orth, P. Lestienne, and J. W. Taanman, "Replication of mitochondrial DNA occurs throughout the mitochondria of cultured human cells," *Experimental Cell Research*, vol. 289, no. 1, pp. 133–142, 2003.
- [53] D. Kang and N. Hamasaki, "Mitochondrial transcription factor A in the maintenance of mitochondrial DNA: overview of its multiple roles," *Annals of the New York Academy of Sciences*, vol. 1042, no. 1, pp. 101–108, 2005.
- [54] N. Suematsu, H. Tsutsui, J. Wen et al., "Oxidative stress mediates tumor necrosis factor- α -induced mitochondrial DNA damage and dysfunction in cardiac myocytes," *Circulation*, vol. 107, no. 10, pp. 1418–1423, 2003.
- [55] D. C. Wallace, "Mitochondrial diseases in man and mouse," *Science*, vol. 283, no. 5407, pp. 1482–1488, 1999.
- [56] J. B. Stewart and P. F. Chinnery, "The dynamics of mitochondrial DNA heteroplasmy: implications for human health and disease," *Nature Reviews. Genetics*, vol. 16, no. 9, pp. 530–542, 2015.
- [57] D. M. Krzywanski, D. R. Moellering, J. L. Fetterman, K. J. Dunham-Snary, M. J. Sammy, and S. W. Ballinger, "The mitochondrial paradigm for cardiovascular disease susceptibility and cellular function: a complementary concept to Mendelian genetics," *Laboratory Investigation*, vol. 91, no. 8, pp. 1122–1135, 2011.
- [58] J. Wang, F. Lin, L. L. Guo, X. J. Xiong, and X. Fan, "Cardiovascular disease, mitochondria, and traditional Chinese medicine," *Evidence-Based Complementary and Alternative Medicine*, vol. 2015, Article ID 143145, 7 pages, 2015.
- [59] M. Scheibye-Knudsen, E. F. Fang, D. L. Croteau, D. M. Wilson Iii, and V. A. Bohr, "Protecting the mitochondrial

- powerhouse,” *Trends in Cell Biology*, vol. 25, no. 3, pp. 158–170, 2015.
- [60] C. Robinow and E. Kellenberger, “The bacterial nucleoid revisited,” *Microbiological Reviews*, vol. 58, no. 2, pp. 211–232, 1994.
- [61] L. Ambro, V. Pevala, J. Bauer, and E. Kutejova, “The influence of ATP-dependent proteases on a variety of nucleoid-associated processes,” *Journal of Structural Biology*, vol. 179, no. 2, pp. 181–192, 2012.
- [62] R. Gilkerson, L. Bravo, I. Garcia et al., “The mitochondrial nucleoid: integrating mitochondrial DNA into cellular homeostasis,” *Cold Spring Harbor Perspectives in Biology*, vol. 5, no. 5, article a011080, 2013.
- [63] M. Kucej and R. A. Butow, “Evolutionary tinkering with mitochondrial nucleoids,” *Trends in Cell Biology*, vol. 17, no. 12, pp. 586–592, 2007.
- [64] L. Alan, T. Spacek, and P. Jezek, “Delaunay algorithm and principal component analysis for 3D visualization of mitochondrial DNA nucleoids by Biplane FPALM/dSTORM,” *European Biophysics Journal*, vol. 45, no. 5, pp. 443–461, 2016.
- [65] J. Tauber, A. Dlaskova, J. Santorova et al., “Distribution of mitochondrial nucleoids upon mitochondrial network fragmentation and network reintegration in HEPG2 cells,” *The International Journal of Biochemistry & Cell Biology*, vol. 45, no. 3, pp. 593–603, 2013.
- [66] D. F. Bogenhagen, D. Rousseau, and S. Burke, “The layered structure of human mitochondrial DNA nucleoids,” *The Journal of Biological Chemistry*, vol. 283, no. 6, pp. 3665–3675, 2008.
- [67] D. F. Bogenhagen, Y. Wang, E. L. Shen, and R. Kobayashi, “Protein components of mitochondrial DNA nucleoids in higher eukaryotes,” *Molecular & Cellular Proteomics*, vol. 2, no. 11, pp. 1205–1216, 2003.
- [68] C. Kukat and N.-G. Larsson, “mtDNA makes a U-turn for the mitochondrial nucleoid,” *Trends in Cell Biology*, vol. 23, no. 9, pp. 457–463, 2013.
- [69] H. Li, Y. Ruan, K. Zhang et al., “Mic60/Mitofilin determines MICOS assembly essential for mitochondrial dynamics and mtDNA nucleoid organization,” *Cell Death and Differentiation*, vol. 23, no. 3, pp. 380–392, 2016.
- [70] S. C. Lewis, L. F. Uchiyama, and J. Nunnari, “ER-mitochondria contacts couple mtDNA synthesis with mitochondrial division in human cells,” *Science*, vol. 353, no. 6296, p. aaf5549, 2016.
- [71] J. M. Gerhold, S. Cansiz-Arda, M. Lohmus et al., “Human mitochondrial DNA-protein complexes attach to a cholesterol-rich membrane structure,” *Scientific Reports*, vol. 5, no. 15292, pp. 1–14, 2015.
- [72] V. M. Pastukh, O. M. Gorodnya, M. N. Gillespie, and M. V. Ruchko, “Regulation of mitochondrial genome replication by hypoxia: the role of DNA oxidation in D-loop region,” *Free Radical Biology & Medicine*, vol. 96, pp. 78–88, 2016.
- [73] X. Z. Chen, Y. Fang, Y. H. Shi et al., “Deciphering the spectrum of somatic mutations in the entire mitochondrial DNA genome,” *Genetics and Molecular Research*, vol. 14, no. 2, pp. 4331–4337, 2015.
- [74] M. Di Re, H. Sembongi, J. He et al., “The accessory subunit of mitochondrial DNA polymerase gamma determines the DNA content of mitochondrial nucleoids in human cultured cells,” *Nucleic Acids Research*, vol. 37, no. 17, pp. 5701–5713, 2009.
- [75] J. He, C. C. Mao, A. Reyes et al., “The AAA+ protein ATAD3 has displacement loop binding properties and is involved in mitochondrial nucleoid organization,” *The Journal of Cell Biology*, vol. 176, no. 2, pp. 141–146, 2007.
- [76] M. Sumitani, K. Kasashima, E. Ohta, D. Kang, and H. Endo, “Association of a novel mitochondrial protein M19 with mitochondrial nucleoids,” *Journal of Biochemistry*, vol. 146, no. 5, pp. 725–732, 2009.
- [77] A. Hubstenberger, N. Merle, R. Charton, G. Brandolin, and D. Rousseau, “Topological analysis of ATAD3A insertion in purified human mitochondria,” *Journal of Bioenergetics and Biomembranes*, vol. 42, no. 2, pp. 143–150, 2010.
- [78] L. Alan, T. Spacek, D. Pajuelo Reguera, M. Jaburek, and P. Jezek, “Mitochondrial nucleoid clusters protect newly synthesized mtDNA during doxorubicin- and ethidium bromide-induced mitochondrial stress,” *Toxicology and Applied Pharmacology*, vol. 302, pp. 31–40, 2016.
- [79] R. W. Gilkerson, D. H. Margineantu, R. A. Capaldi, and J. M. Selker, “Mitochondrial DNA depletion causes morphological changes in the mitochondrial reticulum of cultured human cells,” *FEBS Letters*, vol. 474, no. 1, pp. 1–4, 2000.
- [80] N. Garrido, L. Griparic, E. Jokitalo, J. Wartiovaara, A. M. van der Bliek, and J. N. Spelbrink, “Composition and dynamics of human mitochondrial nucleoids,” *Molecular Biology of the Cell*, vol. 14, no. 4, pp. 1583–1596, 2003.
- [81] P. A. Gammage, J. Rorbach, A. I. Vincent, E. J. Rebar, and M. Minczuk, “Mitochondrially targeted ZFNs for selective degradation of pathogenic mitochondrial genomes bearing large-scale deletions or point mutations,” *EMBO Molecular Medicine*, vol. 6, no. 4, pp. 458–466, 2014.
- [82] R. Jajoo, Y. Jung, D. Huh et al., “Accurate concentration control of mitochondria and nucleoids,” *Science*, vol. 351, no. 6269, pp. 169–172, 2016.
- [83] E. A. Schon and R. W. Gilkerson, “Functional complementation of mitochondrial DNAs: mobilizing mitochondrial genetics against dysfunction,” *Biochimica et Biophysica Acta*, vol. 1800, no. 3, pp. 245–249, 2010.
- [84] Y. H. Chan and W. F. Marshall, “How cells know the size of their organelles,” *Science*, vol. 337, no. 6099, pp. 1186–1189, 2012.
- [85] G. Elachouri, S. Vidoni, C. Zanna et al., “OPA1 links human mitochondrial genome maintenance to mtDNA replication and distribution,” *Genome Research*, vol. 21, no. 1, pp. 12–20, 2011.
- [86] T. Landes, I. Leroy, A. Bertholet et al., “OPA1 (dys)functions,” *Seminars in Cell & Developmental Biology*, vol. 21, no. 6, pp. 593–598, 2010.
- [87] C. Kukat, K. M. Davies, C. A. Wurm et al., “Cross-strand binding of TFAM to a single mtDNA molecule forms the mitochondrial nucleoid,” *Proceedings of the National Academy of Sciences of the United States of America*, vol. 112, no. 36, pp. 11288–11293, 2015.
- [88] R. W. Gilkerson, E. A. Schon, E. Hernandez, and M. M. Davidson, “Mitochondrial nucleoids maintain genetic autonomy but allow for functional complementation,” *The Journal of Cell Biology*, vol. 181, no. 7, pp. 1117–1128, 2008.
- [89] F. Hensen, S. Cansiz, J. M. Gerhold, and J. N. Spelbrink, “To be or not to be a nucleoid protein: a comparison of mass-spectrometry based approaches in the identification of

- potential mtDNA-nucleoid associated proteins,” *Biochimie*, vol. 100, pp. 219–226, 2014.
- [90] N. Rajala, F. Hensen, H. J. Wessels, D. Ives, J. Gloerich, and J. N. Spelbrink, “Whole cell formaldehyde cross-linking simplifies purification of mitochondrial nucleoids and associated proteins involved in mitochondrial gene expression,” *PLoS One*, vol. 10, no. 2, article e0116726, 2015.
- [91] D. F. Bogenhagen, “Biochemical isolation of mtDNA nucleoids from animal cells,” *Methods in Molecular Biology*, vol. 554, pp. 3–14, 2009.
- [92] K. Kasashima, M. Sumitani, and H. Endo, “Maintenance of mitochondrial genome distribution by mitochondrial AAA + protein ClpX,” *Experimental Cell Research*, vol. 318, no. 18, pp. 2335–2343, 2012.
- [93] J. He, H. M. Cooper, A. Reyes et al., “Mitochondrial nucleoid interacting proteins support mitochondrial protein synthesis,” *Nucleic Acids Research*, vol. 40, no. 13, pp. 6109–6121, 2012.
- [94] A. P. Rebelo, L. M. Dillon, and C. T. Moraes, “Mitochondrial DNA transcription regulation and nucleoid organization,” *Journal of Inherited Metabolic Disease*, vol. 34, no. 4, pp. 941–951, 2011.
- [95] M. Macierzanka, M. Plotka, D. Pryputniewicz-Drobinska, A. Lewandowska, R. Lightowlers, and J. Marszalek, “Maintenance and stabilization of mtDNA can be facilitated by the DNA-binding activity of Hlvp5p,” *Biochimica et Biophysica Acta*, vol. 1783, no. 1, pp. 107–117, 2008.
- [96] Y. Matsushima and L. S. Kaguni, “Matrix proteases in mitochondrial DNA function,” *Biochimica et Biophysica Acta*, vol. 1819, no. 9–10, pp. 1080–1087, 2012.
- [97] G. Farge, N. Laurens, O. D. Broekmans et al., “Protein sliding and DNA denaturation are essential for DNA organization by human mitochondrial transcription factor A,” *Nature Communications*, vol. 3, article 1013, pp. 1–9, 2012.
- [98] C. T. Campbell, J. E. Kolesar, and B. A. Kaufman, “Mitochondrial transcription factor A regulates mitochondrial transcription initiation, DNA packaging, and genome copy number,” *Biochimica et Biophysica Acta*, vol. 1819, no. 9–10, pp. 921–929, 2012.
- [99] K. Kasashima and H. Endo, “Interaction of human mitochondrial transcription factor A in mitochondria: its involvement in the dynamics of mitochondrial DNA nucleoids,” *Genes to Cells*, vol. 20, no. 12, pp. 1017–1027, 2015.
- [100] H. B. Ngo, G. A. Lovely, R. Phillips, and D. C. Chan, “Distinct structural features of TFAM drive mitochondrial DNA packaging versus transcriptional activation,” *Nature Communications*, vol. 5, no. 3077, pp. 1–23, 2014.
- [101] G. Farge, M. Mehmedovic, M. Baclayon et al., “In vitro-reconstituted nucleoids can block mitochondrial DNA replication and transcription,” *Cell Reports*, vol. 8, no. 1, pp. 66–74, 2014.
- [102] T. I. Alam, T. Kanki, T. Muta et al., “Human mitochondrial DNA is packaged with TFAM,” *Nucleic Acids Research*, vol. 31, no. 6, pp. 1640–1645, 2003.
- [103] K. Kasashima, Y. Nagao, and H. Endo, “Dynamic regulation of mitochondrial genome maintenance in germ cells,” *Reproductive Medicine and Biology*, vol. 13, no. 1, pp. 11–20, 2014.
- [104] B. Lu, J. Lee, X. Nie et al., “Phosphorylation of human TFAM in mitochondria impairs DNA binding and promotes degradation by the AAA+ Lon protease,” *Molecular Cell*, vol. 49, no. 1, pp. 121–132, 2013.
- [105] A. H. Marceau, “Functions of single-strand DNA-binding proteins in DNA replication, recombination, and repair,” *Methods in Molecular Biology*, vol. 922, pp. 1–21, 2012.
- [106] T. Olejar, D. Pajuelo-Reguera, L. Alan, A. Dlaskova, and P. Jezek, “Coupled aggregation of mitochondrial single-strand DNA-binding protein tagged with Eos fluorescent protein visualizes synchronized activity of mitochondrial nucleoids,” *Molecular Medicine Reports*, vol. 12, no. 4, pp. 5185–5190, 2015.
- [107] N. Arakaki, T. Nishihama, A. Kohda et al., “Regulation of mitochondrial morphology and cell survival by Mitogenin I and mitochondrial single-stranded DNA binding protein,” *Biochimica et Biophysica Acta*, vol. 1760, no. 9, pp. 1364–1372, 2006.
- [108] J. A. Korhonen, X. H. Pham, M. Pellegrini, and M. Falkenberg, “Reconstitution of a minimal mtDNA replisome in vitro,” *The EMBO Journal*, vol. 23, no. 12, pp. 2423–2429, 2004.
- [109] D. Milenkovic, S. Matic, I. Kuhl et al., “TWINKLE is an essential mitochondrial helicase required for synthesis of nascent D-loop strands and complete mtDNA replication,” *Human Molecular Genetics*, vol. 22, no. 10, pp. 1983–1993, 2013.
- [110] S. Gumeni and I. P. Trougakos, “Cross talk of proteostasis and mitostasis in cellular homeodynamics, ageing, and disease,” *Oxidative Medicine and Cellular Longevity*, vol. 2016, Article ID 4587691, 24 pages, 2016.
- [111] J. K. Ngo, L. C. Pomatto, and K. J. Davies, “Upregulation of the mitochondrial Lon protease allows adaptation to acute oxidative stress but dysregulation is associated with chronic stress, disease, and aging,” *Redox Biology*, vol. 1, no. 1, pp. 258–264, 2013.
- [112] S. Li and D. Rousseau, “ATAD3, a vital membrane bound mitochondrial ATPase involved in tumor progression,” *Journal of Bioenergetics and Biomembranes*, vol. 44, no. 1, pp. 189–197, 2012.
- [113] K. Kasashima, M. Sumitani, M. Satoh, and H. Endo, “Human prohibitin 1 maintains the organization and stability of the mitochondrial nucleoids,” *Experimental Cell Research*, vol. 314, no. 5, pp. 988–996, 2008.
- [114] M. Kucej, B. Kucejova, R. Subramanian, X. J. Chen, and R. A. Butow, “Mitochondrial nucleoids undergo remodeling in response to metabolic cues,” *Journal of Cell Science*, vol. 121, no. 11, pp. 1861–1868, 2008.
- [115] X. J. Chen, X. Wang, B. A. Kaufman, and R. A. Butow, “Aconitase couples metabolic regulation to mitochondrial DNA maintenance,” *Science*, vol. 307, no. 5710, pp. 714–717, 2005.
- [116] J. Kaukonen, J. K. Juselius, V. Tiranti et al., “Role of adenine nucleotide translocator 1 in mtDNA maintenance,” *Science*, vol. 289, no. 5480, pp. 782–785, 2000.
- [117] S. Sengupta and C. C. Harris, “p53: traffic cop at the crossroads of DNA repair and recombination,” *Nature Reviews. Molecular Cell Biology*, vol. 6, no. 1, pp. 44–55, 2005.
- [118] J. H. Park, J. Zhuang, J. Li, and P. M. Hwang, “p53 as guardian of the mitochondrial genome,” *FEBS Letters*, vol. 590, no. 7, pp. 924–934, 2016.
- [119] Y. Yoshida, H. Izumi, T. Torigoe et al., “P53 physically interacts with mitochondrial transcription factor A and differentially regulates binding to damaged DNA,” *Cancer Research*, vol. 63, no. 13, pp. 3729–3734, 2003.

- [120] K. Heyne, S. Mannebach, E. Wuertz, K. X. Knaup, M. Mahyar-Roemer, and K. Roemer, "Identification of a putative p53 binding sequence within the human mitochondrial genome," *FEBS Letters*, vol. 578, no. 1-2, pp. 198–202, 2004.
- [121] S. Caielli, S. Athale, B. Domic et al., "Oxidized mitochondrial nucleoids released by neutrophils drive type I interferon production in human lupus," *The Journal of Experimental Medicine*, vol. 213, no. 5, pp. 697–713, 2016.
- [122] F. Malka, A. Lombes, and M. Rojo, "Organization, dynamics and transmission of mitochondrial DNA: focus on vertebrate nucleoids," *Biochimica et Biophysica Acta*, vol. 1763, no. 5-6, pp. 463–472, 2006.
- [123] T. Liu, B. Lu, I. Lee, G. Ondrovicova, E. Kutejova, and C. K. Suzuki, "DNA and RNA binding by the mitochondrial Lon protease is regulated by nucleotide and protein substrate," *The Journal of Biological Chemistry*, vol. 279, no. 14, pp. 13902–13910, 2004.
- [124] L. Liu, M. Sanosaka, S. Lei et al., "LRP130 protein remodels mitochondria and stimulates fatty acid oxidation," *The Journal of Biological Chemistry*, vol. 286, no. 48, pp. 41253–41264, 2011.

Research Article

Mitochondrial Uncoupler Prodrug of 2,4-Dinitrophenol, MP201, Prevents Neuronal Damage and Preserves Vision in Experimental Optic Neuritis

Reas S. Khan,¹ Kimberly Dine,¹ John G. Geisler,² and Kenneth S. Shindler¹

¹Scheie Eye Institute and FM Kirby Center for Molecular Ophthalmology, University of Pennsylvania, Philadelphia, PA 19104, USA

²Mitochon Pharmaceuticals, Inc., 970 Cross Lane, Blue Bell, PA, USA

Correspondence should be addressed to Kenneth S. Shindler; kenneth.shindler@uphs.upenn.edu

Received 27 March 2017; Accepted 30 April 2017; Published 7 June 2017

Academic Editor: Moh H. Malek

Copyright © 2017 Reas S. Khan et al. This is an open access article distributed under the Creative Commons Attribution License, which permits unrestricted use, distribution, and reproduction in any medium, provided the original work is properly cited.

The ability of novel mitochondrial uncoupler prodrug of 2,4-dinitrophenol (DNP), MP201, to prevent neuronal damage and preserve visual function in an experimental autoimmune encephalomyelitis (EAE) model of optic neuritis was evaluated. Optic nerve inflammation, demyelination, and axonal loss are prominent features of optic neuritis, an inflammatory optic neuropathy often associated with the central nervous system demyelinating disease multiple sclerosis. Currently, optic neuritis is frequently treated with high-dose corticosteroids, but treatment fails to prevent permanent neuronal damage and associated vision changes that occur as optic neuritis resolves, thus suggesting that additional therapies are required. MP201 administered orally, once per day, attenuated visual dysfunction, preserved retinal ganglion cells (RGCs), and reduced RGC axonal loss and demyelination in the optic nerves of EAE mice, with limited effects on inflammation. The prominent mild mitochondrial uncoupling properties of MP201, with slow elimination of DNP, may contribute to the neuroprotective effect by modulating the entire mitochondria's physiology directly. Results suggest that MP201 is a potential novel treatment for optic neuritis.

1. Introduction

Optic neuritis is an inflammatory demyelinating disease of the optic nerve often associated with multiple sclerosis (MS) [1]. Optic neuritis may lead to complete or partial loss of vision in one or both eyes [2]. In 15%–20% of people who eventually develop MS, optic neuritis is their first symptom [3]. Current therapies used for optic neuritis, intravenous corticosteroids, show no benefit on final visual recovery, with up to 60% of patients failing to return to normal visual function, even though steroids have an effect in hastening acute visual recovery, decreasing inflammation, and reducing pain on eye movement associated with optic neuritis [1, 4].

In addition to inflammation and demyelination, optic neuritis is characterized by significant retinal ganglion cell (RGC) loss in the retina and axonal damage along the optic nerve, features that correspond to permanent visual loss [5, 6] that corticosteroids fail to prevent. Indeed, corticosteroids also show limited effect in preventing RGC

axonal damage [7, 8]. Therefore, new therapies for the treatment of optic neuritis that specifically prevent RGC loss and preserve visual function are needed.

Mitochondrial dysfunction plays an important role in the neurodegeneration of optic neuritis and MS [9, 10]. Excessive reactive oxygen species (ROS) accumulation in the optic nerve is attributed to disease progression. Our studies have demonstrated compounds that modulate mitochondrial activity directly or indirectly attenuate ROS levels and disease progression by improved cellular function, improved biomarkers, and reduction in oxidative stress [11–14].

Mitochondrial uncoupling is the process in which protons (H^+) generated indirectly via glycolysis of glucose and beta-oxidation of lipids, by generating NADH and $FADH_2$ to be used in the electron transport system to generate a membrane potential by pumping protons out of the mitochondrial matrix, do not return through the ATPase channel to generate ATP once the membrane potential has been established [15]. This can happen from a naturally occurring

phenomena coined “proton leak” in which ~25% of the body’s potentially useful energy is dissipated as heat or via small molecule drugs called protonophores, ionophores, or uncouplers [16–18]. Protons leaking across the mitochondrial membrane are proposed as protective mechanism to minimize ROS generation during oxidative phosphorylation to slow aging [19]. Mitochondrial uncoupling also exists in hibernating animals and nonhibernating mammals such as humans [20, 21], but in low quantities [15, 22], in a specialized tissue called brown adipose tissue in which a protein channel called uncoupling protein 1 is highly expressed. In this case, protons travel into the mitochondria to generate heat [23]. There are other related uncoupling proteins (UCPs), which do not generate heat but are related to stress [24, 25]. Neurons express at least three UCP isoforms including the widely expressed UCP2 and the neuron specific UCP4 and UCP5, which play important roles in adaptive responses of neurons to oxidative stress. Mitochondrial uncoupling has been exhibited as a neuroprotective strategy in studies in which activity or overexpression of UCP2 exhibited improved functional recovery in models of epilepsy, ischemic stroke, Alzheimer’s disease, and NMDA-induced retinal excitotoxicity [26–29]. Recent studies also have shown that pharmacological agents that induce mild mitochondrial uncoupling have tremendous therapeutic potential in a range of acute and chronic neurodegenerative conditions [25, 30–36].

MP201 is a prodrug of the mitochondrial uncoupler 2,4-dinitrophenol (DNP) that harnesses the power of the mitochondria by increasing energy expenditure that results in strengthening cellular survival [25], similar to the positive effects seen with fasting and exercise [37]. A recent study showed that mitochondrial uncoupling achieved by overexpression of UCP2 protected RGCs from glutamate excitotoxicity [29]. Thus, we hypothesized that MP201 may have similar neuroprotective properties that suppress RGC loss in optic neuritis and improve visual outcomes. The potential ability of MP201 to suppress optic neuritis and prevent RGC loss was examined in EAE mice.

2. Methods

2.1. Experimental Animals. Six-week old female C57/Bl6 mice were purchased from the Jackson Laboratory (Bar Harbor, ME, USA). Mice were housed at the University of Pennsylvania in accordance with university and National Institutes of Health guidelines. All procedures were approved by the Institutional Animal Care and Use Committee at the University of Pennsylvania.

2.2. Induction and Scoring of EAE. EAE was induced in C57/Bl6 mice according to a previously published protocol [11, 13, 38]. Briefly, 8-week old female mice were anesthetized with isoflurane and were given a total of 200 μ g of myelin oligodendrocyte glycoprotein (MOG) peptide (MOG_{35–55}; Genscript, Piscataway, NJ, USA) emulsified in Complete Freund’s Adjuvant (Difco, Detroit, MI, USA) containing 2.5 mg/ml *Mycobacterium tuberculosis* (Difco), administered via subcutaneous injections at two sites on the

back. Control, sham-immunized mice were injected with an equal volume of phosphate buffered saline (PBS) and Complete Freund’s Adjuvant. All animals received 200 ng pertussis toxin (List Biological, Campbell, CA, USA) in 0.1 ml PBS at 0 h and 48 h postimmunization, administered by intraperitoneal injection. EAE was scored using a previously published 5-point scale: no disease=0; partial tail paralysis=0.5; tail paralysis or waddling gait=1.0; partial tail paralysis and waddling gait=1.5; tail paralysis and waddling gait=2.0; partial limb paralysis=2.5; paralysis of one limb=3.0; paralysis of one limb and partial paralysis of another=3.5; paralysis of two limbs=4.0; moribund state=4.5; and death=5.0 [11, 13, 38].

2.3. MP201 Treatment. MP201 (Mitochon Pharmaceuticals, Inc., Blue Bell, PA, USA) was dissolved in 1% DMSO, 40% polyethylene glycol 400 (PEG400), and 59% water and then diluted in PBS. EAE mice were treated by oral gavage (~300 μ L or 10 ml/kg) once daily with 16 or 80 mg/kg MP201 as indicated, starting from day 15 postimmunization until sacrifice (day 42). MP201 is a prodrug of DNP with ~10x lower exposure to DNP at the same doses. Prior studies have shown that the therapeutic window between 0.5, 1, and 5 mg/kg of DNP is neuroprotective [25]. To dose at equivalent exposures of 1 and 5 mg/kg of DNP with MP201, there is a factor of 10x, plus the extra molecular weight (1.6x) of the prodrug, thus 16 and 80 mpk provide equivalent exposures. Control, non-EAE mice, and sham-treated EAE mice were treated with an equal volume (~300 μ L or 10 ml/kg) of PBS.

2.4. Measurement of Optokinetic Responses (OKR). Optokinetic responses (OKR) were used to assess visual function in control and EAE mice treated with or without MP201. OKR were measured as the highest spatial frequency at which mice track a 100% contrast grating projected at varying spatial frequencies using OptoMetry software and apparatus (Cerebral Mechanics Inc., Medicine Hat, AB, Canada), as in prior studies [11, 38]. Data are reported as cyc/deg.

2.5. Quantification of Retinal Ganglion Cell Survival. RGCs were immunolabeled in flat-mounted retinas and counted as described previously [11, 38]. Briefly, retinas isolated from mice following sacrifice at day 42 were prepared as flattened whole mounts. Retinas were then permeabilized in 0.5% Triton X-100 in PBS by freezing for 15 min at -70° C followed by washing in PBS containing 0.5% Triton X-100. Specimens were then incubated overnight at 4° C with goat-anti-Brn3a antibody (RGC marker) (Santa Cruz Biotechnology, Dallas, TX, USA) diluted 1 : 100 in PBS containing 2% bovine serum albumin and 2% Triton X-100 (blocking buffer). The retinas were washed three times in PBS, incubated for 2 hours at room temperature with Alexa Fluor 488-conjugated anti-goat secondary antibody (Thermo Fisher Scientific, Waltham, MA, USA), diluted 1 : 500 in blocking buffer, washed in PBS 3 to 4 times, and mounted vitreous side up on slides in fluorescent anti-fading solution. RGCs were photographed at 40x magnification in 12 standard fields: 1/6, 3/6, and 5/6 of the retinal radius from the center of the retina in each

quadrant, and counted by a masked investigator using image analysis software (Image-Pro Plus 5.0; Media Cybernetics, Silver Spring, MD).

2.6. Quantification of RGC Axon Staining. Neurofilament staining in optic nerve sections was done to quantify the area of intact RGC axons using a previously published protocol [11, 38]. Briefly, optic nerves were isolated following sacrifice after 42 days, fixed in 4% paraformaldehyde, and embedded in paraffin. 5 μm longitudinal paraffin sections of the optic nerve were deparaffinized, rehydrated, and then permeabilized with 0.5% tween-20 in PBS. Blocking reagent (Vector Laboratories, Burlingame, CA, USA) was used to reduce non-specific binding. Specimens were then incubated in rabbit anti-neurofilament antibody 1:100 (Abcam, Cambridge, MA, USA) at 4°C overnight and then washed three times with PBS and incubated with anti-rabbit secondary antibody (Vectastain Elite ABC Rabbit kit) for 30 min at 37°C. Avidin/Biotin Complex detection was performed using the Vectastain Elite ABC kit and DAB (diaminobenzidine) substrate kit (Vector Laboratories) according to the manufacturer's instructions. Photographs of three fields/nerve (one each at the distal, central, and proximal regions of the longitudinal optic nerve section) at 20x magnification were taken by a blinded investigator. Neurofilament staining was quantified by calculating the optical density using ImageJ software (<http://nih.gov>).

2.7. Quantification of Demyelination in the Optic Nerve. Luxol fast blue (LFB) staining was used to evaluate demyelination in the optic nerves. Optic nerve sections were stained with LFB as in prior studies [11, 38], and the entire length of each optic nerve section was examined by light microscopy by a blinded investigator. Demyelination in optic nerves was quantified on a 0–3 point relative scale: 0 = no demyelination; 1 = scattered foci of demyelination; 2 = prominent foci of demyelination; and 3 = large (confluent) areas of demyelination.

2.8. Quantification of Inflammation in the Optic Nerve. Hematoxylin and Eosin (H&E) staining was used to evaluate inflammation in the optic nerves. Optic nerve sections were stained with H&E as in prior studies [11, 38], and the entire length of each optic nerve section was examined by light microscopy by a blinded investigator. Presence of inflammatory cell infiltration in the optic nerves was assessed according to a 0–4 point scale: 0 = no infiltration; 1 = mild cellular infiltration of the optic nerve or optic nerve sheath; 2 = moderate infiltration; 3 = severe infiltration; and 4 = massive infiltration.

2.9. Statistics. Data are expressed as means \pm SEM. Differences in OKR across time were compared by ANOVA of repeated measures using GraphPad Prism 5.0 (GraphPad Software, San Diego, CA, USA). Differences in RGC numbers, RGC axon staining, inflammation, and demyelination were compared using one-way ANOVA followed by Student-Newman-Keuls test using GraphPad Prism 5.0. Differences were considered statistically significant at $p < 0.05$. For all experiments, each eye was used as an

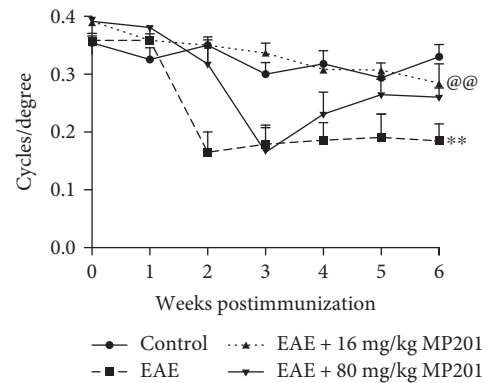


FIGURE 1: MP201 preserves RGC function. Visual function, measured by OKR responses, shows significant (** $p < 0.01$) decreases in eyes of EAE mice ($N = 10$ eyes) compared to control mouse eyes ($N = 10$) by 6 weeks after induction of EAE. Daily oral treatment of 16 mg/kg MP201 ($N = 10$) from days 15 to 42 postimmunization leads to significantly (@@@ $p < 0.01$ versus EAE) improved OKR responses in EAE mice. Mice receiving 80 mg/kg MP201 daily ($N = 10$) show initial vision loss by week 3 that then reverses with improved OKR score in subsequent weeks.

independent data point similar to prior studies [11–14], based on previous studies showing that optic neuritis can occur bilaterally, or unilaterally in either eye, and thus can occur as an independent event.

3. Results

3.1. MP201 Treatment Preserves Visual Function. Eight-week old female C57BL/6J mice were immunized with MOG_{35–55} peptide to induce EAE, or sham-immunized with PBS as controls. Mice were sham-treated with PBS, or treated with 16 or 80 mg/kg MP201, daily by oral gavage beginning after onset of optic neuritis on day 15 postimmunization. OKR was measured every week until sacrifice at day 42. By day 42 postimmunization, OKR responses were significantly decreased in the eyes of PBS-treated EAE mice as compared to both control mice and EAE mice treated with either 16 or 80 mg/kg MP201 (Figure 1). EAE mice that received 80 mg/kg MP201 daily showed an initial vision loss at week 3 that reversed and improved significantly at later time points. EAE mice that received 16 mg/kg MP201 daily showed a significant improvement in OKR scores at all time points compared to PBS-treated EAE mice ($p < 0.01$).

3.2. MP201 Treatment Reduces RGC Loss in the Retina. Previous studies demonstrate that MOG-induced EAE mice develop significant RGC loss 30 to 40 days postimmunization and that this model can be used to evaluate the neuroprotective potential of therapies to prevent RGC loss [11, 13, 38]. To examine potential neuroprotective effects of MP201, PBS- and MP201-treated mice were sacrificed 42 days postimmunization, and RGCs were counted in isolated retinas. RGC numbers in eyes from PBS-treated EAE mice showed a significant decrease ($p < 0.01$) compared to control mice (Figure 2). Daily treatment on days 15–42 postimmunization with either

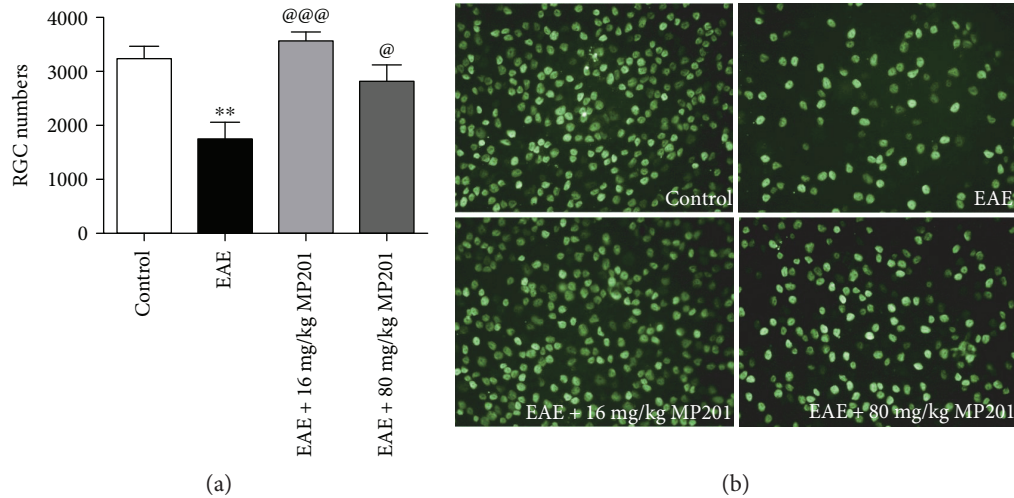


FIGURE 2: MP201 treatment attenuates RGC loss. Neuroprotective effects of MP201 were evaluated by counting RGCs immunolabelled with Brn3a antibody in 12 standardized fields, three from each quadrant of the retina. (a) RGC loss in eyes of EAE mice (** $p < 0.01$ versus control, $N = 10$ eyes) is reduced by 16 mg/kg MP201 treatment from days 15 to 42 (@@@ $p < 0.001$ versus EAE, $N = 10$). 80 mg/kg MP201 also induces a significant (@ $p < 0.05$ versus EAE, $N = 10$) improvement in RGC numbers. (b) Representative images show RGCs in one field of retina from each group (original magnification $\times 20$).

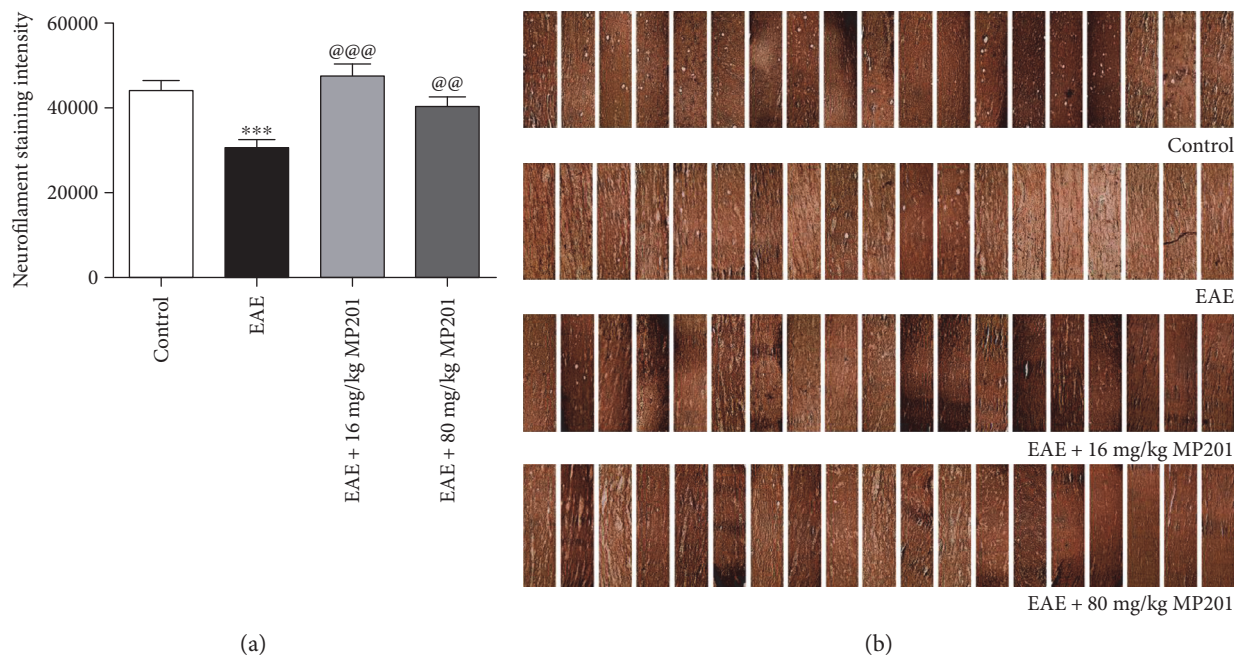


FIGURE 3: MP201 treatment reduces axonal loss in optic neuritis. Neurofilament staining was used to evaluate axonal loss in sections of optic nerves isolated at day 42 postimmunization. (a) The optical density of neurofilament staining calculated from three equal-sized fields from each optic nerve shows a significant decrease (*** $p < 0.001$) in optic nerves ($N = 10$ nerves) from EAE mice compared to optic nerves ($N = 10$) from control mice. Treatment with 16 mg/kg (@@@ $p < 0.001$, $N = 10$) or 80 mg/kg (@@ $p < 0.01$, $N = 10$) MP201 induces a significant increase in neurofilament staining compared to optic nerves from PBS-treated EAE mice. (b) A series of photographs of axon staining from multiple optic nerve sections shows the normal degree of variability of neurofilament staining in optic nerves of control mice and EAE mice treated with 16 mg/kg or 80 mg/kg MP201 and shows more patchy loss of neurofilament staining in optic nerves from PBS-treated EAE mice.

16 mg/kg MP201 ($p < 0.001$) or 80 mg/kg MP201 ($p < 0.05$) led to a significant attenuation of RGC loss compared to PBS-treated EAE mice.

3.3. MP201 Treatment Reduces RGC Axonal Loss in Optic Nerve. Neurofilament staining was used to quantify axon density in PBS- and MP201-treated EAE mice as in prior

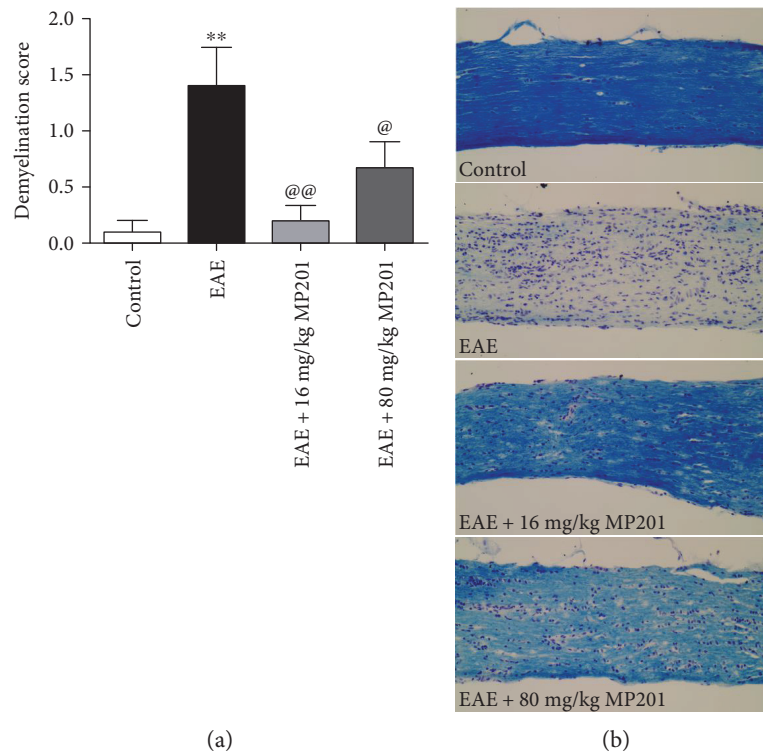


FIGURE 4: MP201 treatment attenuates demyelination in optic nerves during EAE. To examine whether MP201 treatment prevents demyelination, optic nerves were isolated from mice 42 days postimmunization and were stained with LFB. (a) LFB-stained optic nerve longitudinal sections were examined by a blinded investigator, and demyelination was quantified on a 0–3 point scale. Optic nerves ($N = 10$ nerves) from EAE mice had a significantly ($**p < 0.01$) higher demyelination score compared to optic nerves ($N = 10$) from control mice, and treatment with 16 mg/kg (@@ $p < 0.01$ versus EAE, $N = 10$) or 80 mg/kg (@ $p < 0.05$ versus EAE, $N = 10$) MP201 leads to a significant decrease in demyelination scores. (b) A representative image of one optic nerve from a PBS-treated EAE mouse shows less LFB (blue) staining than an optic nerve from a control mouse, as well as optic nerves of EAE mice treated with either 16 mg/kg or 80 mg/kg MP201 (original magnification $\times 20$).

studies [11, 38]. Significant ($p < 0.001$) reduction in axonal staining occurred in optic nerves from PBS-treated EAE mice as compared to optic nerves from control mice (Figure 3), similar to prior studies [11, 38]. Treatment with 16 mg/kg of MP201 showed a significant ($p < 0.001$) attenuation of optic nerve axonal loss compared to PBS-treated EAE mice, and treatment with 80 mg/kg also resulted in a significant ($p < 0.01$) reduction in axonal loss.

3.4. MP201 Treatment Reduces Demyelination in Optic Nerve. Inflammatory demyelination of RGC axons leading to poor nerve conduction is believed to be a prominent pathophysiology of optic neuritis [39]. To examine whether MP201 can block demyelination, optic nerves from control, PBS-treated EAE, and MP201-treated EAE mice were stained with LFB and evaluated for demyelination. PBS-treated EAE mice showed a significant increase in demyelination score compared to control mice ($p < 0.01$) (Figure 4), consistent with previous studies [11, 38]. Daily treatment with 16 mg/kg ($p < 0.01$) and 80 mg/kg ($p < 0.05$) resulted in a significant suppression in the degree of demyelination in EAE optic nerves.

3.5. MP201 Treatment Does Not Affect Optic Nerve Inflammation. Optic nerves of EAE mice treated with PBS

or with MP201 were stained with H&E to evaluate inflammation. Significant ($p < 0.001$) inflammatory cell infiltration was detected in optic nerves from PBS-treated EAE mice as compared to control mouse optic nerves that demonstrated normal histology without inflammation (Figure 5). Optic nerves of EAE mice treated daily with both 16 mg/kg and 80 mg/kg MP201 also showed significant inflammatory cell infiltration compared to control mouse optic nerves, with no statistical difference compared to optic nerves from PBS-treated EAE mice.

4. Discussion

Results indicate that oral administration of MP201 provides significant neuroprotective benefits in an experimental model of optic neuritis. MP201 treatment led to a significant reduction in the loss of RGCs and their axons and attenuated demyelination along optic nerves. In addition to these structural effects, MP201 also helped preserve OKR responses. OKR is an objective means of detecting visual activity in mouse [40]. The optokinetic system plays an essential role in stabilizing the visual image on the retina by producing compensatory eye movement in the direction of visual motion and can be used as a marker of RGC function [41]. Previous studies have shown that OKR responses decrease

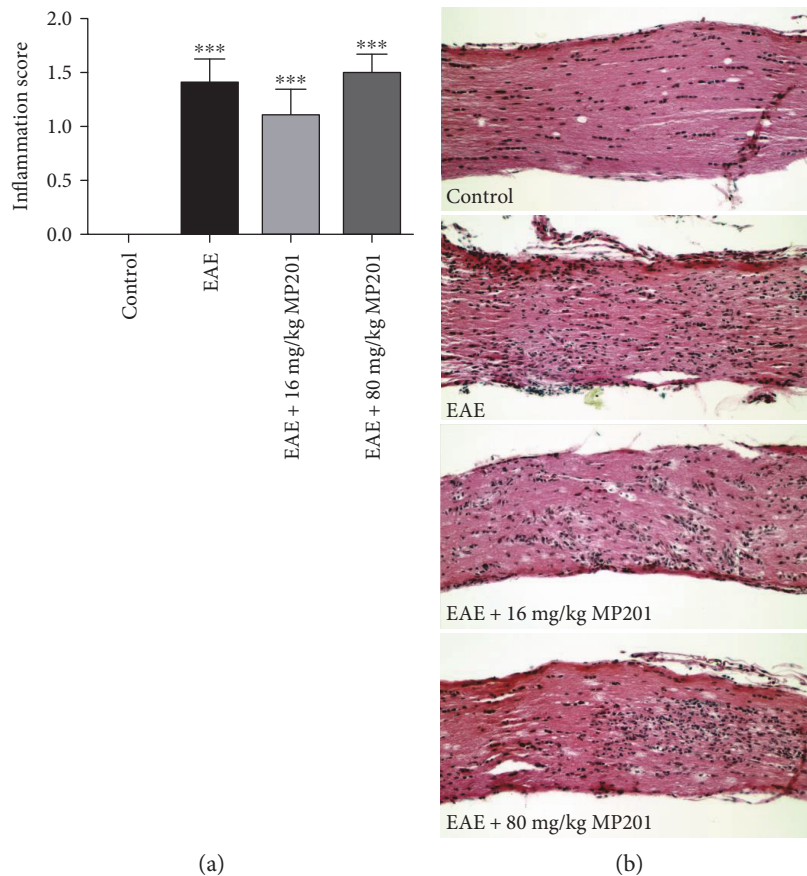


FIGURE 5: MP201 treatment does not suppress inflammation in optic nerves during EAE. To examine whether MP201 treatment prevents inflammation, optic nerves were isolated from mice 42 days postimmunization and stained with H&E to examine levels of cellular infiltration. (a) H&E-stained optic nerve longitudinal sections were examined by a blinded investigator, and inflammation was quantified on a 0–4 point scale. Optic nerves ($N = 10$ nerves) from EAE mice showed significantly ($***p < 0.001$) higher inflammation scores compared to optic nerves ($N = 10$) from control mice, and treatment with 16 mg/kg ($***p < 0.001$ versus control, $N = 10$) or 80 mg/kg ($***p < 0.001$ versus control, $N = 10$) showed no change in inflammation score compared to EAE. (b) A representative image of one optic nerve from a PBS-, 16 mg/kg MP201-, and 80 mg/kg MP201-treated EAE mouse each show increased numbers of cells, representative of inflammatory cell infiltration, as compared to an optic nerve from a control mouse (original magnification $\times 20$).

in EAE mice and some treatments that prevent RGC loss preserve OKR responses [11, 38], consistent with the current results. Thus, MP201 promotes improvement in both structural and functional outcomes in experimental optic neuritis.

Mitochondrial oxidative stress and loss of mitochondrial membrane potential are classically believed to be major mediators of many neurodegenerative diseases [42, 43], and accumulating evidence suggests that oxidative stress plays a major role specifically in the pathogenesis of MS and optic neuritis [44, 45]. Indeed, various treatment strategies that reduce oxidative stress show promising neuroprotective effects in models of optic neuritis and other optic neuropathies. Previous studies have shown that increasing mitochondrial defenses against accumulating superoxide protect RGCs and their axons [46]. In addition, viral-mediated gene delivery of antioxidant genes MnSOD (manganese superoxide dismutase) and catalase are effective in suppressing not only myelin loss in the optic nerve but also mitochondrial vacuolization, optic nerve head swelling, and dissolution of cristae in optic nerve axons [46, 47]. Our previous studies show significant RGC neuroprotective effects mediated by

compounds that activate SIRT1 (Sirtuin 1, silent mating type information regulation 2 homolog) in both EAE- and mouse hepatitis virus-induced optic neuritis [11, 13, 14, 48] and similar neuroprotective effects of SIRT1 overexpression in a traumatic optic nerve injury model [49]. While these studies show SIRT1 activation significantly attenuates RGC damage by reducing oxidative stress via deacetylation of PGC1 α (peroxisome proliferator-activated receptor gamma coactivator 1- α) and subsequent increase in mitochondrial biogenesis, effects on visual function are only transient. Thus, previous studies show that mitochondrial biogenesis and reduction of oxidative stress are important targets for neuroprotective therapies in optic neuritis, but the significant improvement in visual function following MP201 treatment in the current studies suggests that this mitochondrial uncoupling therapy provides stronger neuroprotective effects than other antioxidant treatment strategies.

Mild mitochondrial uncoupling is proposed to be one of the central mechanisms through which oxidant production is controlled in mitochondria [50, 51]. Overexpression of UCPs in neuronal cells results in better preservation of cellular ATP

levels and lower oxidative stress with normal mitochondrial morphology *in vitro* [52, 53]. UCPs promote neuroprotective effects by diminishing oxidative stress in models of Parkinson disease [54], focal cerebral ischemia [30] seizures [26, 55], and brain trauma [30, 56], and UCP2 itself exerts protective effects in EAE [57]. In addition to UCPs, pharmacological agents that induce mitochondrial uncoupling are effective therapeutic tools for preventing neurodegeneration in a wide range of neurodegenerative diseases [30–33]. The compound used in present study, MP201, is a prodrug of DNP, the most widely studied and consistently effective mitochondrial uncoupling agent in experimental models of neurodegeneration [25, 32, 58, 59]. MP201 has a linker on the hydroxyl group that caps the oxygen, but once it crosses into portal vein, enzymes cleave the linker and the oxygen group gets protonated to the active form of DNP [60]. DNP can prevent calcium accumulation and related ROS generation to promote neuroprotective effects [32, 36, 61] and stimulates cAMP (cyclic adenosine monophosphate) production, tau expression (nonphosphorylated), and neurite outgrowth in cultured neuronal cells at low concentrations [62]. Low doses of DNP ameliorate learning and memory deficits in a mouse model of Alzheimer's disease [25] and protect neurons against dysfunction and degeneration in experimental models of ischemic stroke [58], traumatic brain injury [32], Huntington disease [36], and peripheral nerve injury [59]. DNP at low doses appears to provide a benefit in models of known and unknown genetic causes, including epilepsy [25]. Collectively, data suggest that DNP may be a broad spectrum treatment for a host of indications associated with mitochondrial dysfunction, without necessarily mitochondrial mutations. Interestingly, a recent study shows that enhanced mitochondrial uncoupling by overexpression of UCP2 decreases apoptosis in RGCs and protects against the toxic effects of glutamate agonists by regulating ROS production [29]. Overall, previous studies support the concept that the mitochondrial uncoupling property of DNP likely contributes to its neuroprotective actions. Therefore, preservation of RGCs and improved visual function mediated by MP201 in the current studies may be related to its mitochondrial uncoupling properties after conversion to DNP.

DNP was used as a medication in the 1930's for weight loss, but a host of adverse side effects prompted a ban on its use as a prescription drug [63–65]. For our present study, we used MP201, a prodrug of DNP that may reduce the risk of overdose and abuse of DNP, and we used MP201 doses that generate DNP at doses ~10 to 50 times lower than the dose used in the past for weight loss [25], suggesting that this hormetic-like therapy may be much better tolerated than past treatment with DNP directly. Other potential beneficial features of MP201 are its ability to suppress the C_{max} of DNP 10-fold, triple its elimination time, and apparent ability to improve its pharmacology, perhaps due to its trickle-like systemic delivery [60]. The potential safety of DNP at lower doses distributed over time is supported by recent studies showing no evidence of toxic effects during chronic administration of controlled-release of DNP [66]. Previous literature supports this idea, as chronic low dose treatment of DNP in

drinking water (mimicking controlled release) increased longevity with low levels of oxidative proteins and DNA damage in mice [67]. One eye-related potential side effect of DNP is cataracts, which were reported in some patients treated with high doses of DNP [68], but the result was not replicated in follow-up experiments [69]. Given that the significant neuroprotective effects found in the current studies were induced by essentially a sustained release prodrug formulation of DNP requiring much lower doses than those found to be toxic in the past, this novel prodrug therapy warrants further investigation as a potential neuroprotective therapy.

Interestingly, the higher dose of MP201, 80 mg/kg, examined here did not lead to improved neuroprotective effects as compared to the lower dose, 16 mg/kg. This may suggest that effects of MP201 reach a homeostatic or hormetic level at low doses that lessens at higher doses. This is consistent with previous studies that found low sustained levels of DNP administration ameliorate neurological disease processes and improve functional outcomes, without reducing body weight as seen at much higher doses [25, 58, 61, 70].

5. Conclusion

The current data demonstrate potential neuroprotective effects of MP201, a prodrug of the mitochondrial uncoupling agent DNP, in experimental optic neuritis. MP201 represents a promising new potential therapy for use in optic neuritis and other optic neuropathies which warrants further investigation.

Abbreviations

DNP: 2,4-Dinitrophenol
RGC: Retinal ganglion cells
EAE: Experimental autoimmune encephalomyelitis
ROS: Reactive oxygen species
UCPs: Uncoupling proteins
MOG: Myelin oligodendrocyte glycoprotein
OKR: Optokinetic responses
H&E: Hematoxylin and Eosin
LFB: Luxol fast blue.

Conflicts of Interest

The MP201 therapy used in these studies was provided to the Shindler Laboratory at no cost by Mitochon Pharmaceuticals, Inc. Coauthors Reas S. Khan, Kimberly Dine, and Kenneth S. Shindler have no conflicts of interest with the material presented in this manuscript and specifically no financial interests in MP201 or Mitochon. Coauthor John G. Geisler is a full time employee of Mitochon and contributed knowledge about the composition of the MP201 therapy and its effects in other disease models, but he played no role in the design, conduct, or analysis of the studies described in this manuscript.

Acknowledgments

This work was supported by the National Institutes of Health grant EY019014; Research to Prevent Blindness Physician Scientist Award; and the F. M. Kirby Foundation. The authors thank Mitochon Pharmaceuticals, Inc. for providing MP201 for the studies reported in this manuscript.

References

- [1] R. W. Beck, P. A. Cleary, M. M. Anderson et al., "A randomized, controlled trial of corticosteroids in the treatment of acute optic neuritis," *The New England Journal of Medicine*, vol. 326, pp. 581–588, 1992.
- [2] R. W. Beck, R. L. Gal, and M. T. Bhatti, "Visual function more than 10 years after optic neuritis: experience of the optic neuritis treatment trial," *American Journal of Ophthalmology*, vol. 137, pp. 77–83, 2004.
- [3] C. Arnold, "Evolving management of optic neuritis and multiple sclerosis," *American Journal of Ophthalmology*, vol. 139, pp. 1101–1108, 2005.
- [4] D. W. Paty and D. K. Li, "Interferon beta-1b is effective in relapsing-remitting multiple sclerosis. II. MRI analysis results of a multicenter, randomized, double-blind, placebo-controlled trial," *Neurology*, vol. 43, pp. 662–667, 1993.
- [5] S. A. Trip, P. G. Schlottmann, S. J. Jones et al., "Retinal nerve fiber layer axonal loss and visual dysfunction in optic neuritis," *Annals of Neurology*, vol. 58, pp. 383–391, 2005.
- [6] F. Costello, S. Coupland, W. Hodge et al., "Quantifying axonal loss after optic neuritis with optical coherence tomography," *Annals of Neurology*, vol. 59, pp. 963–969, 2006.
- [7] R. W. Beck and R. L. Gal, "Treatment of acute optic neuritis: a summary of findings from the optic neuritis treatment trial," *Archives of Ophthalmology*, vol. 126, pp. 994–995, 2008.
- [8] Optic Neuritis Study Group, "Multiple sclerosis risk after optic neuritis: final optic neuritis treatment trial follow-up," *Archives of Neurology*, vol. 65, pp. 727–732, 2008.
- [9] K. Su, D. Bourdette, and M. Forte, "Mitochondrial dysfunction and neurodegeneration in multiple sclerosis," *Frontiers in Physiology*, vol. 4, p. 169, 2013.
- [10] M. E. Witte, D. J. Mahad, H. Lassmann, and J. van Horssen, "Mitochondrial dysfunction contributes to neurodegeneration in multiple sclerosis," *Trends in Molecular Medicine*, vol. 20, no. 3, pp. 179–187, 2014.
- [11] R. S. Khan, K. Dine, E. Luna, C. Ahlem, and K. S. Shindler, "HE3286 reduces axonal loss and preserves retinal ganglion cell function in experimental optic neuritis," *Investigative Ophthalmology & Visual Science*, vol. 55, no. 9, pp. 5744–5751, 2014.
- [12] R. S. Khan, K. Dine, J. Das Sarma, and K. S. Shindler, "SIRT1 activating compounds reduce oxidative stress mediated neuronal loss in viral induced CNS demyelinating disease," *Acta Neuropathologica Communications*, vol. 2, pp. 2–3, 2014.
- [13] Z. Fonseca-Kelly, M. Nassrallah, and J. Uribe, "Resveratrol neuroprotection in a chronic mouse model of multiple sclerosis," *Frontiers in Neurology*, vol. 3, p. 84, 2012.
- [14] K. S. Shindler, E. Ventura, M. Dutt, P. Elliott, D. C. Fitzgerald, and A. Rostami, "Oral resveratrol reduces neuronal damage in a model of multiple sclerosis," *Journal of Neuro-Ophthalmology*, vol. 30, no. 4, pp. 328–339, 2010.
- [15] J. G. Geisler, "Targeting energy expenditure via fuel switching and beyond," *Diabetologia*, vol. 54, no. 2, pp. 237–244, 2011.
- [16] V. P. Skulachev, A. A. Sharaf, and E. A. Liberman, "Proton conductors in respiratory chain and artificial membranes," *Nature*, vol. 216, no. 5116, pp. 718–719, 1967.
- [17] S. S. Korshunov, V. P. Skulachev, and A. A. Starkov, "High protonic potential actuates a mechanism of production of reactive oxygen species in mitochondria," *FEBS Letters*, vol. 416, no. 1, pp. 15–18, 1997.
- [18] R. K. Porter, "Mitochondrial proton leak: a role for uncoupling proteins 2 and 3," *Biochimica et Biophysica Acta*, vol. 1504, pp. 120–127, 2001.
- [19] S. A. Mookerjee, A. S. Divakaruni, M. Jastroch, and M. D. Brand, "Mitochondrial uncoupling and lifespan," *Mechanisms of Ageing and Development*, vol. 131, no. 7–8, pp. 463–472, 2010.
- [20] C. R. Christensen, P. B. Clark, and K. A. Morton, "Reversal of hypermetabolic brown adipose tissue in F-18 FDG PET imaging," *Clinical Nuclear Medicine*, vol. 31, no. 4, pp. 193–196, 2006.
- [21] K. A. Virtanen, M. E. Lidell, J. Orava et al., "Functional brown adipose tissue in healthy adults," *The New England Journal of Medicine*, vol. 360, no. 15, pp. 1518–1525, 2009.
- [22] A. M. Cypess, S. Lehman, G. Williams et al., "Identification and importance of brown adipose tissue in adult humans," *The New England Journal of Medicine*, vol. 360, no. 15, pp. 1509–1517, 2009.
- [23] V. Golozoubova, E. Hohtola, A. Matthias, A. Jacobsson, B. Cannon, and J. Nedergaard, "Only UCP1 can mediate adaptive nonshivering thermogenesis in the cold," *The FASEB Journal*, vol. 15, no. 11, pp. 2048–2050, 2001.
- [24] J. Nedergaard, A. Matthias, V. Golozoubova, A. Jacobsson, and B. Cannon, "UCP1: the original uncoupling protein—and perhaps the only one? New perspectives on UCP1, UCP2, and UCP3 in the light of bioenergetics of the UCP1-ablated mice," *Journal of Bioenergetics and Biomembranes*, vol. 31, no. 5, pp. 475–491, 1999.
- [25] J. G. Geisler and K. Marosi, J. Halpern and M. P. Mattson, "DNP, mitochondrial uncoupling, and neuroprotection: a little dab'll do ya," *Alzheimers Dement*, vol. 16, pp. S1552–S1560, 2016.
- [26] S. Diano, R. T. Matthews, P. Patrylo et al., "Uncoupling protein 2 prevents neuronal death including that occurring during seizures: a mechanism for preconditioning," *Endocrinology*, vol. 144, no. 11, pp. 5014–5021, 2003.
- [27] T. Deierborg and T. Wieloch, S. Diano, "Overexpression of UCP2 protects neurons following global ischemia in the mouse," *Journal of Cerebral Blood Flow and Metabolism*, vol. 28, no. 6, pp. 1186–1195, 2008.
- [28] Z. Wu, Y. Zhao, and B. Zhao, "Superoxide anion, uncoupling proteins and Alzheimer's disease," *Journal of Clinical Biochemistry and Nutrition*, vol. 46, pp. 187–194, 2010.
- [29] C. J. Barnstable, R. Reddy, H. Li, and T. L. Horvath, "Mitochondrial uncoupling protein 2 (UCP2) regulates retinal ganglion cell number and survival," *Journal of Molecular Neuroscience*, vol. 58, pp. 461–469, 2016.
- [30] G. Mattiasson, M. Shamloo, G. Gido et al., "Uncoupling protein-2 prevents neuronal death and diminishes brain dysfunction after stroke and brain trauma," *Nature Medicine*, vol. 9, pp. 1062–1068, 2003.
- [31] M. Calvo-Rodríguez, L. Núñez, and C. Villalobos, "Non-steroidal anti-inflammatory drugs (NSAIDs) and neuroprotection

- in the elderly: a view from the mitochondria,” *Neural Regeneration Research*, vol. 10, no. 9, pp. 1371–1372, 2015.
- [32] J. D. Pandya, J. R. Pauly, and V. N. Nukala, “Post-injury administration of mitochondrial uncouplers increases tissue sparing and improves behavioral outcome following traumatic brain injury in rodents,” *Journal of Neurotrauma*, vol. 24, pp. 798–811, 2007.
- [33] F. G. De Felice, S. T. Ferreira, “Novel neuroprotective, neurotogenic and anti-amyloidogenic properties of 2,4-dinitrophenol: the gentle face of Janus,” *IUBMB Life*, vol. 58, no. 4, pp. 185–189, 2006.
- [34] D. Liu, M. Pitta, J. H. Lee et al., “The KATP channel activator diazoxide ameliorates amyloid- β and tau pathologies and improves memory in the 3xTgAD mouse model of Alzheimer’s disease,” *Journal of Alzheimer’s Disease*, vol. 22, pp. 443–457, 2010.
- [35] R. Alemzadeh, M. D. Karlstad, K. Tushaus, and M. Buchholz, “Diazoxide enhances basal metabolic rate and fat oxidation in obese Zucker rats,” *Metabolism*, vol. 57, pp. 1597–1607, 2008.
- [36] B. Wu, M. Jiang, Q. Peng et al., “2,4 DNP improves motor function, preserves medium spiny neuronal identity, and reduces oxidative stress in a mouse model of Huntington’s disease,” *Experimental Neurology*, vol. 28, pp. 83–90, 2017.
- [37] M. P. Mattson, “Energy intake and exercise as determinants of brain health and vulnerability to injury and disease,” *Cell Metabolism*, vol. 16, pp. 706–722, 2012.
- [38] R. S. Khan, K. Dine, and B. Bauman, “Intranasal delivery of a novel amnion cell secretome prevents neuronal damage and preserves function in a mouse multiple sclerosis model,” *Scientific Reports*, vol. 7, p. 41768, 2017.
- [39] E. Voss, P. Raab, C. Trebst, and M. Stangel, “Clinical approach to optic neuritis: pitfalls, red flags and differential diagnosis,” *Therapeutic Advances in Neurological Disorders*, vol. 4, no. 2, pp. 123–134, 2011.
- [40] H. Cahill and J. Nathans, “The optokinetic reflex as tool for quantitative analyses of nervous system function in mice: application to genetic and drug-induced variation,” *PLoS One*, vol. 3, no. 4, article e2055, 2008.
- [41] V. Lee, M. Dutt, and K. S. Shindler, “Histologic correlation of retinal ganglion cell loss to optical coherence tomography and optokinetic response in murine model of optic nerve crush,” *Investigative Ophthalmology & Visual Science*, vol. 52, p. 639, 2010.
- [42] A. Federico, E. Cardaioli, P. Da Pozzo et al., “Mitochondria, oxidative stress and neurodegeneration,” *Journal of the Neurological Sciences*, vol. 15, no. 322, pp. 1–2, 2012.
- [43] M. T. Lin and M. F. Beal, “Mitochondrial dysfunction and oxidative stress in neurodegenerative diseases,” *Nature*, vol. 443, no. 7113, pp. 787–795, 2006.
- [44] C. J. Lieven, M. J. Hoegger, C. R. Schlieve, and L. A. Levin, “Retinal ganglion cell axotomy induces an increase in intracellular superoxide anion,” *Investigative Ophthalmology & Visual Science*, vol. 47, pp. 1477–1485, 2006.
- [45] F. Lu, M. Selak, J. O’Connor et al., “Oxidative damage to mitochondrial DNA and activity of mitochondrial enzymes in chronic active lesions of multiple sclerosis,” *Journal of the Neurological Sciences*, vol. 177, pp. 95–103, 2000.
- [46] X. Qi, A. S. Lewin, L. Sun, W. W. Hauswirth, and J. Guy, “Suppression of mitochondrial oxidative stress provides long-term neuroprotection in experimental optic neuritis,” *Investigative Ophthalmology & Visual Science*, vol. 48, no. 2, pp. 681–691, 2007.
- [47] J. Guy, X. Qi, and W. W. Hauswirth, “Adeno-associated viral-mediated catalase expression suppresses optic neuritis in experimental allergic encephalomyelitis,” *Proceedings of the National Academy of Sciences*, vol. 95, no. 23, pp. 13847–13852, 1998.
- [48] R. S. Khan, Z. Fonseca-Kelly, C. Callinan, L. Zuo, M. M. Sachdeva, and K. S. Shindler, “SIRT1 activating compounds reduce oxidative stress and prevent cell death in neuronal cells,” *Frontiers in Cellular Neuroscience*, vol. 6, no. 63, pp. 1–13, 2012.
- [49] L. Zuo, R. S. Khan, and V. Lee, “SIRT1 promotes RGC survival and delays loss of function following optic nerve crush,” *Investigative Ophthalmology & Visual Science*, vol. 54, no. 7, pp. 5097–5102, 2013.
- [50] V. P. Skulachev, “Role of uncoupled oxidations in maintenance of safety low levels of oxygen and its one-electron reductants,” *Quarterly Reviews of Biophysics*, vol. 29, no. 2, pp. 169–202, 1996.
- [51] R. S. Balaban, S. Nemoto, and T. Finkel, “Mitochondria, oxidants, and aging,” *Cell*, vol. 20, no. 4, pp. 483–495, 2005.
- [52] A. C. Chu, P. W. Ho, K. H. Kwok et al., “Mitochondrial UCP4 attenuates MPP+ - and dopamine-induced oxidative stress, mitochondrial depolarization, and ATP deficiency in neurons and is interlinked with UCP2 expression,” *Free Radical Biology & Medicine*, vol. 46, pp. 810–820, 2009.
- [53] K. H. Kwok, P. W. Ho, A. C. Chu et al., “Mitochondrial UCP5 is neuroprotective by preserving mitochondrial membrane potential, ATP levels, and reducing oxidative stress in MPP+ and dopamine toxicity,” *Free Radical Biology & Medicine*, vol. 49, pp. 1023–1035, 2010.
- [54] Z. B. Andrews, B. Horvath, and C. J. Barnstable, “Uncoupling protein-2 is critical for nigral dopamine cell survival in a mouse model of Parkinson’s disease,” *The Journal of Neuroscience*, vol. 25, pp. 184–191, 2005.
- [55] P. G. Sullivan, C. Dube, K. Dorenbos, O. Steward, and T. Z. Baram, “Mitochondrial uncoupling protein-2 protects the immature brain from excitotoxic neuronal death,” *Annals of Neurology*, vol. 53, pp. 711–717, 2003.
- [56] L. Qi, X. Cui, W. Dong et al., “Ghrelin protects rats against traumatic brain injury and hemorrhagic shock through upregulation of UCP2,” *Annals of Surgery*, vol. 260, no. 1, pp. 169–178, 2014.
- [57] S. Vogler, J. Pahnke, S. Rousset et al., “Uncoupling protein has protective function during experimental autoimmune encephalomyelitis,” *The American Journal of Pathology*, vol. 168, no. 5, pp. 1570–1575, 2006.
- [58] A. S. Korde, L. C. Pettigrew, S. D. Craddock, and W. F. Maragos, “The mitochondrial uncoupler 2,4-dinitrophenol attenuates tissue damage and improves mitochondrial homeostasis following transient focal cerebral ischemia,” *Journal of Neurochemistry*, vol. 94, no. 6, pp. 1676–1684, 2005.
- [59] R. F. da Costa, A. M. Martinez, and S. T. Ferreira, “2,4-Dinitrophenol blocks neurodegeneration and preserves sciatic nerve function after trauma,” *Journal of Neurotrauma*, vol. 27, no. 5, pp. 829–841, 2010.
- [60] J. G. Geisler, *The Disease Modifying Effects of a Mitochondrial Specific Protonophore, MP101, a Broad Spectrum Treatment for Insidious Neuromuscular, Neurodegenerative & Developmental Diseases by Modulating Mitochondrial Physiology*, World CNS Summit, Boston, MA, USA, 2017.

- [61] D. Liu, Y. Zhang, R. Gharavi et al., "The mitochondrial uncoupler DNP triggers brain cell mTOR signaling network reprogramming and CREB pathway up-regulation," *Journal of Neurochemistry*, vol. 134, pp. 677–692, 2015.
- [62] A. P. Wasilewska-Sampaio, M. S. Silveira, and O. Holub, "Neuritogenesis and neuronal differentiation promoted by 2,4-dinitrophenol, a novel anti-amyloidogenic compound," *The FASEB Journal*, vol. 19, pp. 1627–1636, 2005.
- [63] M. L. Tainter, A. B. Stockton, and W. C. Cutting, "Dinitrophenol in the treatment of obesity: final report," *Jama*, vol. 105, pp. 332–337, 1935.
- [64] J. Parascandola, "Dinitrophenol and bioenergetics: an historical perspective," *Molecular and Cellular Biochemistry*, vol. 5, pp. 69–77, 1974.
- [65] M. O. Harris and J. J. Cocoran, "Toxicological profile for dinitrophenols," in *Agency for Toxic Substances and Disease Registry (ATSDR)*, pp. 1–262, U.S. Department of Health and Human Services, Public Health Service, Atlanta, GA, 1995.
- [66] R. J. Perry, D. Zhang, X. M. Zhang, J. L. Boyer, and G. I. Shulman, "Controlled release mitochondrial protonophore reverses diabetes and steatohepatitis in rats," *Science*, vol. 347, pp. 1253–1262, 2015.
- [67] W. C. Cutting, H. G. Mehrtens, and M. L. Tainter, "Actions and uses of dinitrophenol. Promising metabolic applications," *Jama*, vol. 101, pp. 193–195, 1933.
- [68] W. D. Horner, "A study of dinitrophenol and its relation to cataract formation," *Transactions of the American Ophthalmological Society*, vol. 39, pp. 405–437, 1941.
- [69] P. J. Gehring and J. F. Buerge, "The distribution of 2,4-dinitrophenol relative to its cataractogenic activity in ducklings and rabbits," *Toxicology and Applied Pharmacology*, vol. 15, pp. 574–592, 1969.
- [70] C. C. Caldeira da Silva, F. M. Cerqueira, L. F. Barbosa, M. H. Medeiros, and A. J. Kowaltowski, "Mild mitochondrial uncoupling in mice affects energy metabolism, redox balance and longevity," *Aging Cell*, vol. 7, no. 4, pp. 552–560, 2008.

Review Article

Impact of Aging and Exercise on Mitochondrial Quality Control in Skeletal Muscle

Yuho Kim,^{1,2} Matthew Triolo,^{1,2} and David A. Hood^{1,2}

¹Muscle Health Research Centre, York University, Toronto, ON, Canada M3J 1P3

²School of Kinesiology and Health Science, York University, Toronto, ON, Canada M3J 1P3

Correspondence should be addressed to David A. Hood; dhood@yorku.ca

Received 31 March 2017; Accepted 3 May 2017; Published 1 June 2017

Academic Editor: Moh H. Malek

Copyright © 2017 Yuho Kim et al. This is an open access article distributed under the Creative Commons Attribution License, which permits unrestricted use, distribution, and reproduction in any medium, provided the original work is properly cited.

Mitochondria are characterized by its pivotal roles in managing energy production, reactive oxygen species, and calcium, whose aging-related structural and functional deteriorations are observed in aging muscle. Although it is still unclear how aging alters mitochondrial quality and quantity in skeletal muscle, dysregulation of mitochondrial biogenesis and dynamic controls has been suggested as key players for that. In this paper, we summarize current understandings on how aging regulates muscle mitochondrial biogenesis, while focusing on transcriptional regulations including PGC-1 α , AMPK, p53, mtDNA, and Tfam. Further, we review current findings on the muscle mitochondrial dynamic systems in aging muscle: fusion/fission, autophagy/mitophagy, and protein import. Next, we also discuss how endurance and resistance exercises impact on the mitochondrial quality controls in aging muscle, suggesting possible effective exercise strategies to improve/maintain mitochondrial health.

1. Introduction

Skeletal muscle accounts for approximately 40% of total body mass, and it plays an indispensable role in locomotion and metabolism. Skeletal muscle undergoes a gradual loss of fat-free mass, size, and function in the aging process, called *sarcopenia* [1]. The etiology of sarcopenia is complex and involves the interplay of various factors such as oxidative stress, physical inactivity, imbalanced protein homeostasis, apoptosis, inflammation, malnutrition, and/or mitochondrial dysregulation [2–5]. Mitochondria play an essential role in the aging-related muscle deterioration because of their importance in the production of energy and reactive oxygen species (ROS) [6], apoptotic signaling, and calcium (Ca²⁺) handling [7]. Thus, the natural aging process, along with coincident inactivity, progressively impairs mitochondrial integrity which might be a leading factor for sarcopenia.

The underlying mechanisms of aging-associated mitochondrial dysregulation in skeletal muscle remain incompletely understood. Morphologically, aging muscles appear to have either fragmented, round-shaped mitochondrial

networks [8] or unusually enlarged mitochondrial fragments [9, 10]. For example, subsarcolemmal (SS) and intermyofibrillar (IMF) mitochondrial fractions in the skeletal muscle of old rats tend to be thinner and smaller, respectively [8]. In contrast, other findings have shown that aging muscle mitochondria appear as an elongated, “giant” network [9, 10]. To better understand these inconsistent findings in the mitochondrial structure of aging muscle, it becomes important to investigate the mechanisms involved in mitochondrial turnover, the balance between organelle biogenesis, dynamics, and degradation, which may also help delineate the underlying causes of aging-related dysregulation of mitochondria in skeletal muscle.

Exercise and physical activity have been suggested as effective tools for either improving the quality of aging muscle or delaying the onset of sarcopenia, yet the underlying mechanisms in the exercise-inducible adaptations are still obscure. A growing number of studies have sought to define mitochondrial adaptations in aging skeletal muscle following various exercise regimens. While mitochondrial biogenesis has been relatively well investigated, research interests

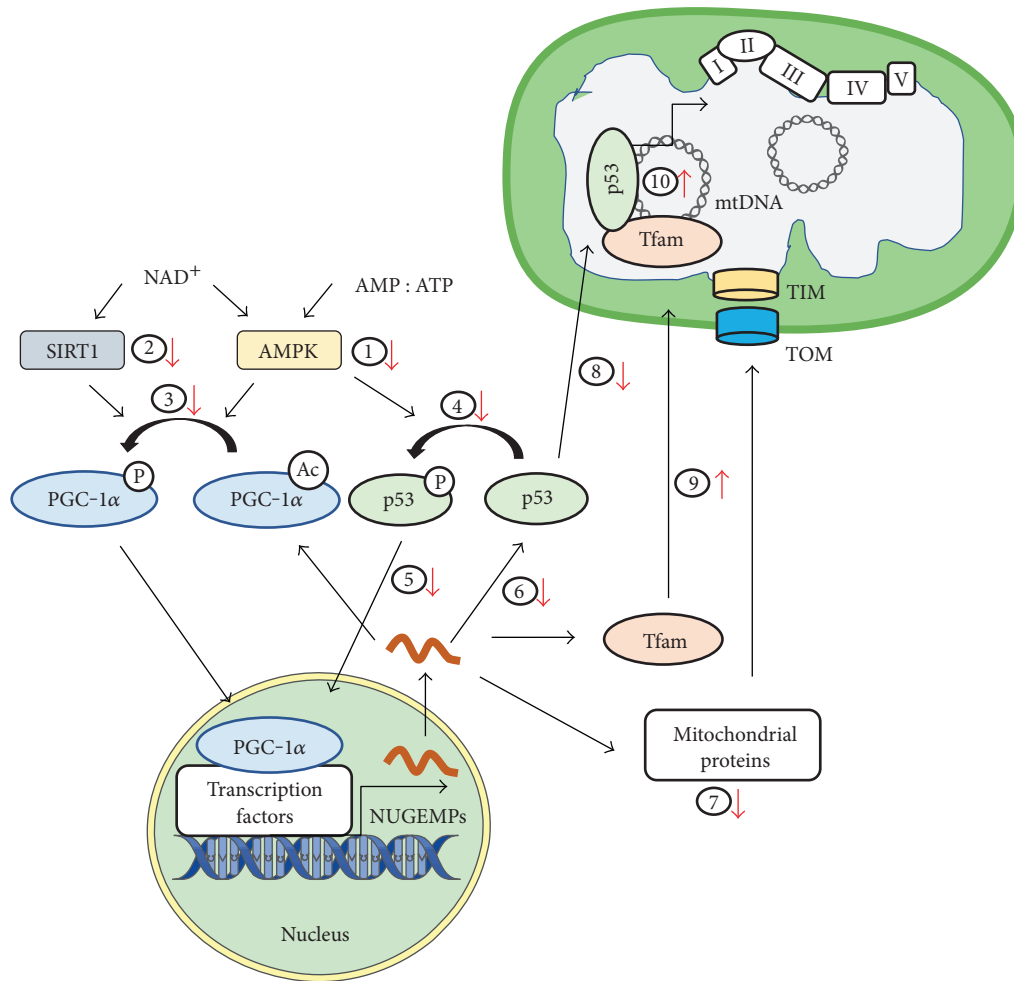


FIGURE 1: Aging is associated with reductions in mitochondrial biogenesis. Initial signaling through (1) AMPK and (2) SIRT1 is reduced with aging, thereby reducing (3) PGC-1 α coactivation and (4) p53 activation of (5) NUGEMP expression, leading to a decrease in (6) PGC-1 α protein and (7) mitochondrial targeted proteins. However, aging is associated with increased (8) TFAM and (9) p53 which has the capacity to enhance (10) mtDNA replication. Depending on age, this mtDNA may contain elevated mutations and may not promote efficient biogenesis in skeletal muscle.

have more recently been directed to other mitochondrial dynamic mechanisms (fusion/fission; autophagy/mitophagy) in aging muscle.

This review summarizes current findings on the aging-related mitochondrial adaptations in skeletal muscle, with a specific focus on mitochondrial biogenesis and dynamic controls. In addition, this paper also outlines current research findings on the effects of exercise on mitochondrial quality control in aging skeletal muscle.

2. Mitochondrial Biogenesis and Aging

The synthesis of new mitochondria, termed mitochondrial biogenesis, promotes the expansion of an existing mitochondrial network. This process is constantly ongoing within skeletal muscle in order to maintain mitochondrial content and function in response to various stimuli including exercise, as well as other cellular stressors. Aging is known to be a leading factor for the reductions in mitochondrial components and capacity [11–13]. Furthermore, aged skeletal muscle

has a reduced ability to synthesize mitochondria in response to biogenesis-inducing factors [14, 15]. Thus, an understanding of the regulation of mitochondrial biogenesis in healthy skeletal muscle, and the changes associated with advanced aging, is important in developing an intervention to prevent the progression of sarcopenia (Figure 1).

2.1. PGC-1 α as a Regulator of Mitochondrial Biogenesis. Mitochondrial biogenesis requires the coordination of the nuclear and mitochondrial genomes, as 99% of approximately 1150 mitochondrial proteins are nuclear-encoded [16], whereas only 13 proteins, along with 2 rRNAs and 22 tRNAs, are mitochondrially encoded [17, 18]. Peroxisome proliferator-activated receptor (PPAR) gamma coactivator 1 α (PGC-1 α) is a master regulator of this process [19, 20], and it plays a significant role in muscular phenotypic changes and aerobic performance. Studies utilizing overexpression [19, 21, 22] and deletion [23–25] of PGC-1 α have shown that it is critical in determining the oxidative phenotype and mitochondrial content in skeletal muscle. Functionally,

PGC-1 α coactivates various transcription factors, such as nuclear respiratory factors 1 and 2 (NRF-1/2), PPAR γ , and estrogen-related receptors (ERR), all of which are important in activating the expression of nuclear genes encoding mitochondrial proteins (NUGEMPs) [26–29]. A critical PGC-1 α -regulated NUGEMP is a mitochondrial DNA-specific transcription factor, transcription factor A of the mitochondria (Tfam), which serves to coordinate the nuclear and mitochondrial genomes in the regulation of mitochondrial biogenesis [30]. Furthermore, PGC-1 α coactivates its own gene expression by positive feedback, thus inadvertently acting to increase its protein content as well [31, 32].

Various splice variants of PGC-1 α have been identified within skeletal muscle. For example, the full-length isoforms, PGC-1 α 1–3, are associated with mitochondrial biogenesis and oxidative phosphorylation [33], and the truncated variants, NT-PGC-1 α , are produced by alternative 3' splicing of PGC-1 α mRNA at exon1a. These truncated variants are expressed in a similar ratio to that of PGC-1 α in skeletal muscle [34]. In contrast, a truncated splice variant of PGC-1 α , termed NT-PGC-1 α -b or PGC-1 α 4, is involved in muscle hypertrophy [35, 36]. Although several studies have indicated that these truncated variants are upregulated by cold exposure in brown adipose tissue [37] and are differentially regulated by various exercise intensities in skeletal muscle [38], the underlying mechanisms of actions of these variants within skeletal muscle are not well understood, and even less studied in the context of aging. A variety of studies have indicated that PGC-1 α is responsive to stimuli such as Ca²⁺ [31, 39–41], ROS [42], nitric oxide [43], thyroid hormone [44, 45], and increased energy imbalances such as nutrient deprivation [25, 46, 47] and exercise [44, 48]. Thus, alterations in signaling from these sources can lead to changes in mitochondrial content within skeletal muscle, which are also linked with aging-associated alterations in PGC-1 α expression.

Considering the importance of PGC-1 α in maintaining skeletal muscle mitochondrial content through organelle biogenesis, aging-associated modifications in the expression and/or activation of PGC-1 α are a timely and highly relevant research area. Although contradictory findings were observed in human studies [11, 49, 50], aging is associated with a decline in PGC-1 α expression in the skeletal muscle of rodents [51]. The age-related reductions in PGC-1 α have the potential to reduce the transcriptional drive for mitochondrial biogenesis, partially explaining the decreased skeletal muscle mitochondrial content associated with age. Further, knockdown of PGC-1 α expression in mice intensifies the decline in mitochondrial gene expression and function in aging skeletal muscle [52].

PGC-1 α is also important for preventing or delaying the onset of muscle atrophy by suppressing atrophy-related gene expression, through the inhibition of Forkhead box O3a (FoxO3a), a potent transcriptional inducer of muscle atrophy. For example, PGC-1 α overexpression in adult rodents suppressed FoxO3a activity, promoted muscle mass maintenance [53], and similarly prevented starvation-associated protein degradation and atrophy in myotubes [54]. Together, this may explain the contribution of age-related PGC-1 α

deficits to the phenotypic loss of muscle size, which thus suggests the therapeutic potential of this protein in the prevention of sarcopenia.

2.2. AMPK and NAD⁺. Various regulatory networks converge to activate PGC-1 α and promote mitochondrial biogenesis. In response to a reduced cellular energy status, energy-sensing networks associated with AMP-activated protein kinase (AMPK) and silent mating type information regulation 2 homolog 1 (SIRT1) are activated via AMP and nicotinamide adenine dinucleotide (NAD⁺), respectively. These proteins converge at PGC-1 α to promote organelle biogenesis [55, 56]. AMPK is an energy-sensitive kinase that is activated by low energy status, as signified by an increase in the AMP:ATP ratio [57–59], and it also phosphorylates PGC-1 α on threonine-177 and serine-538 [44, 60–62]. SIRT1 is an NAD⁺-dependent deacetylase that acts on PGC-1 α in response to an increase in NAD⁺, which is also indicative of a reduction in cellular energy [32, 46, 63, 64]. AMPK and SIRT1 are functionally interdependent, as AMPK can increase NAD⁺ and subsequently activate SIRT1 within muscle, and vice versa [55, 57, 65]. Moreover, AMPK may function as a switch between PGC-1 α -dependent and PGC-1 α -independent mitochondrial biogenesis pathways which are promoted by SIRT1 [66]. Nevertheless, the phosphorylation and subsequent deacetylation of PGC-1 α by AMPK and SIRT1 activate PGC-1 α and promote mitochondrial biogenesis. Using exercise, caloric restriction, and/or pharmacological activation models, it has been shown that both AMPK and SIRT1 promote an oxidative phenotype within skeletal muscle, along with increased mitochondrial content [44, 46, 56, 58, 64, 65, 67–71].

Most reports on aged skeletal muscle show blunted AMPK activation in response to exercise and AICAR treatment [14, 70], with no apparent change in AMPK expression [72]. These findings may partially explain the age-associated declines in mitochondrial biogenesis since diminished AMPK activation may downregulate PGC-1 α . It may further indicate a mechanism whereby reductions in AMPK activity in aging muscle may reduce its ability to increase NAD⁺ levels and activate SIRT1. This evidence suggests that targeting AMPK activation within skeletal muscle may promote mitochondrial biogenesis and thus healthier skeletal muscle with age.

Reductions in NAD⁺ are evident within aged skeletal muscle due to an increase in its breakdown, without reductions in SIRT1 protein [66, 73, 74], suggesting that this signaling pattern toward mitochondrial biogenesis may be hindered with aging. Using a knockdown model for cell-specific nicotinamide mononucleotide (NMN) adenylyltransferase (NMNAT) which regulates NAD⁺ levels within skeletal muscle, it was found that reductions in nuclear NAD⁺ are partially responsible for the deficits in oxidative phosphorylation (OXPHOS) and mitochondrial biogenesis [66], which may help to explain the reductions in mitochondrial content with age. In the same study, aging mice treated with the NAD⁺ precursor, NMN, restored skeletal muscle NAD⁺, as well as increased mitochondrial function and OXPHOS gene expression [66]. In addition, nicotinamide

ribose treatment was also shown to increase NAD⁺ and to prevent age-related muscle stem cell senescence, along with an improvement in mitochondrial and muscle health with age [75]. These data support the idea that age-related deficits in NAD⁺ are partially responsible for the age-associated reduction in mitochondrial biogenesis and suggest a possible target for the replenishment in aging muscle.

2.3. Mitochondrial DNA. A unique characteristic of the mitochondrion is that it possesses its own mitochondrial DNA (mtDNA), a circular molecule of approximately 16.6 kb in size. mtDNA exists as a result of the mitochondrial evolutionary upbring as a prokaryote, maintaining a symbiotic relationship with eukaryotic cells [76, 77]. Within each organelle, there are multiple maternally inherited copies of mtDNA, which are heteroplasmic due to the variant nature of mtDNA copies within the cell [78].

Mitochondrial gene transcription is initiated by the nuclear-encoded mitochondrial RNA polymerase (POLRMT) [79], with the aid of mitochondrial transcription factors B1 and B2 (TFB1/2) and Tfam [80, 81]. Since the synthesis of new mitochondria depends upon the coordination of the nuclear and mitochondrial genomes, the integrity of mtDNA and the machinery involved in its replication and gene transcription are crucial in maintaining a healthy pool of mitochondria and efficient biogenesis.

Within the skeletal muscle of humans, primates, and rodents, aging has long been associated with an accumulation of large-scale mtDNA deletions and mutations, which ultimately contribute to sarcopenia and age-related myopathies [3, 82–88]. This is likely because mtDNA is more readily exposed to damaging free radical species due to its close proximity to the electron transport chain (ETC), along with the lack of protective proteins that nuclear DNA possess [89]. Further, replicative damage to mtDNA leads to elevated ROS production [90, 91], which is seen in aged skeletal muscle [83], suggesting that aging is likely to lead to an impairment in mtDNA replication. Taken together, mtDNA damage likely ultimately reduces the quality and quantity of mitochondrial biogenesis in aging muscle.

Aging skeletal muscle has also been associated with declines in mtDNA copy number. For example, aged rats (27 months old) were shown to have 20–40% less mtDNA in skeletal muscle compared to young rats (6 months old), corresponding to reductions in mitochondrial transcripts in less oxidative muscle fibers [92]. However, it is unclear whether aging-related reductions in mtDNA copy number occur in humans, since inconsistent results have been reported, whereby no changes [93] and even increase in mtDNA have been observed [94]. Furthermore, elimination of mtDNA in cells altered nuclear gene expression and reduced mitochondrial proliferation [95], indicating that mtDNA is required for organelle biogenesis and nuclear coordination. These findings provide the opportunity to formulate two potential theoretical frameworks. If mtDNA reductions are evident in aged skeletal muscle, it may limit the potential for mitochondrial biogenesis, as alluded to above. On the other hand, if mtDNA is accumulating within aged skeletal muscle, it could be indicative of a compensatory

mechanism in response to reduced respiratory chain function. This elevated level of mtDNA could contain mutations, thus resulting in further overall respiratory chain defects.

2.4. Transcription Factor p53. As a tumor suppressor, the transcription factor p53 promotes the expression of various genes involved in cellular defense systems such as apoptosis and cell cycle arrest in response to DNA damage [96, 97]. More recently, p53 has been identified as a regulator of mitochondrial integrity, content, and function as well as organelle biogenesis [98–103]. In particular, p53 can be colocalized within cytoplasm, nucleus, and mitochondria, whereby it facilitates both nuclear and mitochondrial gene expression [101, 104–106]. Mitochondrial p53 interacts with and stabilizes mtDNA [102], and mtDNA expression is dependent, in part, on the presence of p53 in skeletal muscle [107]. Indeed, the value of p53 to the mitochondrial genome became more evident following a study showing that an exercise-induced upregulation of p53 lessens mtDNA damage in the skeletal muscle of a mtDNA mutator mouse model of aging, compared to the mutator mouse model with skeletal muscle-specific knockdown of p53 [108].

Reductions in muscle mitochondrial content and complex assembly in p53 knockout (KO) mice further implicate p53 as an important factor for the maintenance of mitochondrial aerobic capacity [100, 109]. Within the nuclear genome, p53 supports mitochondrial biogenesis by upregulating the expression of genes indicative of oxidative phenotypes, such as Tfam and NRF-1, as well as the ETC assembly protein synthesis of cytochrome c oxidase (COX) 2 [23, 103, 105, 107, 110]. Moreover, PGC-1 α has a p53 binding site in its promoter region [61, 111] so that p53 could potentially increase PGC-1 α transcription, inducing downstream NUGEMP expression [112], further suggesting a role for p53 in the regulation of mitochondrial biogenesis. Within the mitochondrial genome, p53 induces the transcription of 16S rRNA and COX subunit I [101, 105]. Thus, the reductions in mitochondrial content in p53-KO animals are likely due to decreased p53-induced gene expression important to mitochondrial biogenesis.

Aging is associated with increases in skeletal muscle p53 protein, suggesting that p53 may promote a proapoptotic environment in aged muscle [113–116]. This increase is clearly insufficient to maintain mitochondrial content at levels similar to those observed in the muscle of young animals. p53 receives a regulatory input from AMPK, whereby AMPK phosphorylates and activates p53 [117–119]. Thus, the age-related deficiency in AMPK activation in rodent skeletal muscle (see above) potentially suppresses p53 activation and signaling for mitochondrial biogenesis. Contrary to AMPK, SIRT1 normally deacetylates and inactivates p53, whereby it is liberated from its stimulating effect on biogenesis [120, 121]. However, aging is associated with reductions in SIRT1 activity, which may promote the proapoptotic functions of p53 rather than biogenesis. Importantly, the aging-related reductions in PGC-1 α may also reduce p53 because of its coactivity with PGC-1 α [112]. It was recently revealed that aging is also correlated with reduced s-nitrosylation of p53, a modification that enhances p53 binding to the PGC-

1α promoter and promotes its associated antioxidant response [122], further suggesting a reduced ability of p53 to promote biogenesis through its cooperative action with PGC- 1α . However, more research is necessary to characterize the role of p53 in aged skeletal muscle and to determine if there is a therapeutic potential in targeting p53.

2.5. Mitochondrial Transcription Factor A (Tfam). Regulation of mtDNA transcription and replication is mediated by factors such as POLRMT, mitochondrial TFB1M/TFB2M, and Tfam [80, 123], all of which are nuclear gene products. The transcription of Tfam, TFB1M, and TFB2M is activated by NRF-1 and NRF-2, which are, in turn, coactivated by PGC- 1α , thus connecting the nuclear and mitochondrial genomes in mitochondrial biogenesis [30, 124].

Tfam is crucial for the regulation of mtDNA, and whole-body loss of its function is associated with embryonic lethality, whereas partial loss leads to reductions in mtDNA content and tissue-wide respiratory deficits [125, 126]. Categorically, Tfam has the high-mobility group box domains, which have the ability to induce a U-turn-like conformation of mtDNA [127–129]. Once this is completed, TFB2M and POLRMT are recruited to the H and L promoters of mtDNA allowing for gene transcription. Furthermore, Tfam packages and compacts mtDNA into nucleoid-like structures [130, 131], protecting this genome against ROS-induced mutations.

Tfam levels are positively correlated with mtDNA content [132, 133]. Within developing skeletal muscle, the increase in Tfam mRNA is associated with elevations in mitochondrial content and localization [134]. Mitochondrial biogenesis is associated with an elevated abundance in Tfam transcripts, as well as its mitochondrial localization [135–140], whereas muscle-specific depletion of Tfam serves to reduce mtDNA abundance [141]. Together, these data indicate an essential role for Tfam in promoting mtDNA replication, transcription, and its subsequent effects on elevating the synthesis of mitochondria.

Several studies suggest that Tfam is elevated in aged skeletal muscle, although reductions in mitochondrial content are evident. This was shown to be the case in the skeletal muscle of both aged rats [88] and humans [142]. In humans, these increases were correlated with increases in NRF-1 mRNA and protein bound to nuclear DNA [142]. Altogether, these data suggest that aging may lead to a compensatory increase in Tfam, probably to maintain or increase mitochondrial content and respiratory function. Nevertheless, it may also further promote the production of mutated mtDNA, leading to mitochondrial dysfunction.

3. Mitochondrial Dynamics and Aging

In addition to organelle biogenesis discussed in the previous sections, mitochondrial quality is finely adjusted by reshaping mitochondrial structures that are primarily controlled by fusion/fission, as well as autophagy/mitophagy. The following sections summarize our current understanding in these mitochondrial regulatory systems in skeletal muscle in the context of aging, as well as the mechanisms by which

proteins are imported into the mitochondria, allowing for the expansion of the mitochondrial reticulum.

3.1. Fusion and Fission. Mitochondria are dynamic organelles that are continuously undergoing the processes of fusion and fission. Mitochondrial fusion is the expansion of the mitochondrial network that is accomplished by mitofusin 1 (Mfn1) and mitofusin 2 (Mfn2) in the outer mitochondrial membrane [143], as well as by optic atrophy 1 (OPA1) in the inner mitochondrial membrane [144]. These mitochondrial fusion proteins contain GTPase functional domains, which, when activated, lead to an expanded, elongated mitochondrial network. Mitochondrial fission is the process that opposes fusion, whereby the mitochondrial network can be divided, resulting in small, fragmented, and globular mitochondria. Fission is also governed by GTPase proteins such as dynamin-related protein (Drp1) and fission 1 protein (Fis1) [145, 146]. Healthy mitochondrial dynamics are regulated through the maintenance of a balance between these opposing processes, which is fundamental for sustaining mitochondrial quality and function in skeletal muscle. However, aging muscle appears to have an imbalance between the fusion and fission processes, thus disposing mitochondria toward undergoing either fusion or fission.

Several studies have revealed that aging skeletal muscle mitochondria may preferentially undergo fission, resulting in smaller and fragmented mitochondrial structures [8, 147]. For example, in a study comparing young (5 months) and old (35 months) Fisher 344 Brown Norway (BN) rats, aging skeletal muscles were observed to have elevated protein levels of Fis1 and Drp1, as well as downregulated Mfn2 levels, compared to their young counterparts [8]. Notably, a remarkable reduction in Mfn2 protein levels was also found in the skeletal muscle of old mice, and the age-related decline was shown to be progressive throughout aging [148]. This Mfn2 deficiency in aging muscle is also linked to mitochondrial dysfunction, along with diminished oxidative capacity [148], and this can contribute to muscle atrophy and weakness. Thus, the absence of Mfn2 may play a significant role in contributing to mitochondrial fragmentation and associated sarcopenia in aging muscle.

Contradictory results have been also reported that skeletal muscle may be more dependent on mitochondrial fusion in response to aging. Using a two-dimensional microscopic analysis, Leduc-Gaudet et al. showed more elongated SS mitochondria in the skeletal muscle of old mice, as well as more branched IMF mitochondria, as compared to those of young mice [9]. In this study, although no significant difference in fusion and fission proteins was found, the ratio of Mfn2 to Drp1 appeared to increase, indicating an elevation in the fusion index in the aging muscle [9]. It may be that mitochondrial fusion is more active than fission in the early-aging skeletal muscle of mice (~15 months old), as indicated by significantly increased Mfn1 and Mfn2 protein levels in the skeletal muscle, as well as decreased Fis1 protein levels [149]. In addition, other studies have revealed that both fusion and fission proteins are not changed [150] or are all upregulated [151] in the skeletal muscle of old animals. These inconsistent results in the process of mitochondrial dynamics

may be due to differences in age, species, and/or muscle types of animals. Taken together, it is still unclear how aged skeletal muscle regulates fusion and fission to meet the aging-related alterations in mitochondrial structure and capacity.

3.2. Autophagy/Mitophagy. Autophagy is a “self-eating” system by which damaged organelles and cellular byproducts are degraded in the lysosome to help maintain cellular homeostasis. Autophagic substrates are nonselectively encapsulated by a double-membrane structure, an autophagosome, wherein they are conjugated and ubiquitinated by both the lipidated, active form of microtubule-associated protein 1A/1B-light chain 3 II (LC3-II) and p62. The autophagosome is then fused with a lysosome, whereupon an autolysosome is formed. The engulfed substrates are subsequently degraded by a variety of pH-dependent lysosomal proteases. Mitophagy is a mitochondria-specific form of autophagy. Damaged and/or dysfunctional mitochondria, characterized by a loss of mitochondrial membrane potential, recruit PTEN-induced kinase 1 (PINK1), which in turn activates parkin and leads to the ubiquitination of the outer membrane proteins. This mitochondria-ubiquitinated complex is encapsulated by autophagosome and then is degraded in the lysosome. Mitophagy has been identified to be crucial in maintaining healthy mitochondria in various tissues and disease states through the deletion of malfunctioning mitochondrial segments within the network.

The literature is replete with statements that the autophagy system is dysregulated with age [152–154], including within aged skeletal muscle [155, 156]; however, variations and contradictory findings are present in the literature [149, 155–157]. For instance, an increased accumulation of the autophagy markers p62 and LC3-II was observed in both slow (soleus) and fast (tibialis anterior) skeletal muscles of aged Fisher 344 BN rats [155], which may be indicative of diminished autophagic degradation in aging muscle, because LC3-II is degraded during autophagy. Others have shown that basal autophagic regulation in skeletal muscle may be not altered with aging [150, 158]. For example, muscle protein abundance of key autophagy markers such as Beclin-1, ULK1, and p62, as well as the protein ratio of LC3-II to LC3-I, is not different between young and older subjects [150, 158]. Meanwhile, the LC3 ratio (II to I) was observed to be lower in the skeletal muscle of middle-aged animals [159], suggesting that autophagy may be differentially regulated with age. Importantly, many of these observations are based on data in which autophagy (or mitophagy) flux has been not assessed. Colchicine, an inhibitor of autophagosome transport, is an effective chemical for estimating “autophagic flux.” Using colchicine, Baehr et al. provided some information to suggest that autophagy flux is impaired in the skeletal muscle of old animals [155]. However, much more research is required to clarify the contradictory findings in the literatures.

Recent studies have also sought to understand the effects of aging on mitophagy in skeletal muscle [160], even though the number of studies is limited. In *Drosophila*, Rana et al. have suggested the necessity of parkin not only for prolonging lifespan but also for sustaining mitochondrial quality and function in aging flight muscles [160]. They further

suggest a notable link between parkin and mitochondrial fusion, as parkin overexpression appears to downregulate aging-related increases in Mfn abundance, thus accelerating the degradation of polyubiquitinated proteins and relieving mitochondrial proteotoxicity [160]. In contrast, a recent study by Sebastian et al. showed that the aging-associated Mfn2 deficiency may contribute to a decrease in mitophagic flux, as suggested by an increased accumulation of LC3-II and parkin on the mitochondria [148]. This aging-associated decline in muscle mitophagy seems to be compensated by increasing other signaling pathways including hypoxia-inducible factor 1-alpha (HIF1 α) and BCL2/adenovirus E1B 19 kDa protein-interacting protein 3 (BNIP3) in a ROS-dependent manner [148].

AMPK is a key player in autophagy and mitophagy during starvation and aging [149, 161], and its activation in skeletal muscle appears to be diminished by aging [14, 149]. Bujak et al. showed that AMPK is important in maintaining mitochondrial integrity and mitophagic capacity in aging skeletal muscle [161]. In response to muscle-specific AMPK deletion, both SS and IMF mitochondrial sizes were shown to be increased in comparison to those of age-matched wild-type mice, along with a significant decline in mtDNA copy numbers [161]. In this animal model, remarkable accumulations of p62 and parkin proteins were also observed, thus indicating a link between AMPK and mitophagy in aging muscle [161]. In addition, Fritzen et al. also revealed data that following AMPK knockdown, the ratio of LC3-II to LC3-I was increased in the skeletal muscle of old mice as compared to that of age-matched animals [157]. AMPK has also been observed to regulate transcription factor EB (TFEB), a master regulator of lysosomal biogenesis. In mouse liver, AMPK is activated in response to starvation, which leads to the upregulation of autophagy and lysosomal genes via the interaction between TFEB and its coactivator, arginine methyltransferase 1 (CARM1) [162]. Whether this occurs in skeletal muscle is not known and further investigation is warranted.

Autophagy that is achieved via the direct transport of substrates into the lysosome is termed chaperone-mediated autophagy (CMA). This process requires carrier proteins such as heat shock cognate 70 (HSC70) to deliver the substrates to lysosomal-associated membrane protein 2A (LAMP2A), whereupon the substrates are translocated into the lysosomal lumen for degradation. In the context of the lysosomal system itself, aging may downregulate lysosomal activities, as LAMP2A [163] and HSC70 protein levels [164] are all reduced in the liver of old rats. To our knowledge, very few studies have been done to understand CMA in aging muscle, and a single study showed that HSC70 protein abundance appears to be elevated in the skeletal muscle of old (30 months) mice than in young (12 months) animals [165]. Moreover, the skeletal muscle of old Fisher 344 BN rats appeared to be characterized by lipofuscin accumulation within the lysosomal lumen [166], suggesting that defects in lysosomal function exist in aging muscle. It was also reported that LAMP2 mRNA levels are decreased in the aging plantaris of Fisher 344 BN rats as compared to those in young animals [167], which is supported by data revealing that the

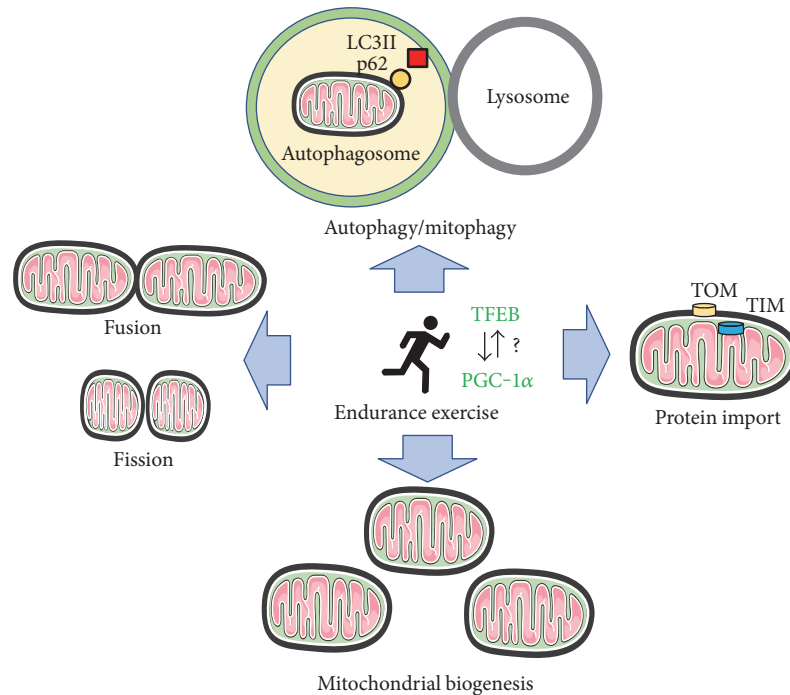


FIGURE 2: Exercise and mitochondrial dynamics in aging muscle. Endurance exercise training increases mitochondrial biogenesis in aging muscle, although its extent may be lessened compared to young muscle. In addition, chronic exercise leads to a global upregulation of protein markers for mitochondrial dynamic controls: fusion/fission, autophagy/mitophagy, and protein import. Since the lysosomal system has been suggested as a key player for governing mitochondrial quality control, the role of TFEB, a master regulator of lysosomal biogenesis, appears to be important and its relationship with PGC-1 α may be also considerable for the exercise-inducible upregulation of mitochondrial turnovers. However, more studies are needed to clarify the effects of endurance training exercise on the mitochondrial turnover systems in aging muscle.

activity of the lysosomal protease cathepsin L was also lower in aging skeletal muscle, regardless of muscle type [155]. Thus, dysregulation of the lysosomal system may play a limiting role in aging muscle autophagic regulation. However, more detailed studies are needed to clarify the underlying mechanisms of CMA and other lysosomal activities in aging skeletal muscle.

3.3. Protein Import. Mitochondrial biogenesis is dependent on protein components encoded by both mitochondrial and nuclear DNA (mtDNA and nDNA, resp.). Only thirteen proteins are encoded by mtDNA, while the remainder (~1100) are dependent on the transcription of nDNA. Proteins that are encoded by nDNA are transported from the cytosol to the mitochondrial membrane import machineries, named the translocases of the outer/inner membrane (TOM/TIM). Through these complexes, the proteins are moved into mitochondrial matrix by the mitochondrial heat shock protein 70 (mHSP70) and are subsequently posttranslationally modified by mitochondrial processing peptidase (MPP). This important machinery contributes importantly to the management of mitochondrial quality and the correct stoichiometry of ETC components in skeletal muscle mitochondria.

Although it was shown that TOM proteins (e.g., TOM22) are not changed in the aging skeletal muscle of humans [147] and rodents [149], studies using mitochondrial fractions have suggested that the aging process may lead to the upregulation of TOM protein levels in skeletal muscle [168]. For

example, key protein markers for TOM complex such as TOM40 and TOM22 were increased in the muscle mitochondrial fraction of old rats, as compared to those in young animals [168]. Moreover, it was also shown that TOM22 levels are increased in the skeletal muscle of functionally inactive old subjects [147]. Taken together, it seems likely that the mitochondrial protein import system is activated in order to compensate for age-related mitochondrial dysfunctions in skeletal muscle.

4. Exercise, Mitochondrial Adaptations, and Aging

Exercise has been relatively well accepted as an effective strategy for delaying either the onset or the progression of sarcopenia; however, its effects on mitochondrial biogenesis and turnover have been less studied in aging skeletal muscle. In the following sections, we outline studies focusing on the effects of exercise on mitochondrial quality control in aging skeletal muscle (Figure 2).

4.1. Exercise and Mitochondrial Biogenesis. As compared to young, healthy skeletal muscle, fewer studies have been accomplished to delineate the effects of exercise on mitochondrial quality controls in aging skeletal muscle. Endurance exercise training or chronic contractile activity (CCA) successfully leads to mitochondrial adaptations in aging skeletal muscle, to a lesser extent than which is

observed in young muscle [51, 151, 169]. Following endurance training, aging skeletal muscle does exhibit increases in the gene and protein abundances of PGC-1 α , accompanied by increases in mtDNA, mitochondrial mass, ETC components, and mitochondrial transcriptional regulators such as Tfam [151, 169]. These training-inducible mitochondrial adaptations are regulated by various signaling pathways. Several studies have reported that endurance training activates AMPK, p38 mitogen-activated protein kinase (MAPK), and SIRT1 in the skeletal muscle of old rodents and humans, all of which are activators of PGC-1 α and thus of mitochondrial biogenesis [151, 169]. Nonetheless, some findings have suggested that the decline in mitochondrial markers was not prevented in the skeletal muscles of animals at advanced age (i.e., 34~36-month-old Fisher 344 BN rats) in response to endurance training [14, 170]. Also, it was reported that mitochondrial biogenesis following 12 weeks of cycling exercise training was attained in the skeletal muscle of old women without an increase in PGC-1 α protein [171], suggesting possible alternative signaling pathways to lead to exercise-induced mitochondrial biogenesis in aging muscle, as compared to young muscle [172].

Research trials employing lifelong physical activity also suggest an important role of chronic muscle activity in the maintenance and improvement in mitochondrial integrity and aerobic performance that are attenuated with aging [173, 174]. Higher mitochondrial volume density following lifelong exercise is observed, and it is highly correlated with aerobic capacity (VO_{2max}) in the skeletal muscle of healthy individuals over 60 years old [175].

Resistance exercise for aging individuals has been well defined as an effective regimen for lessening aging-associated muscle atrophy and weakness [176, 177]. However, only few studies have sought to investigate the underlying mechanism by which resistance exercise alters mitochondrial abundance and function in aging skeletal muscle. Acute resistance exercise with leg extensions was shown to significantly increase the mRNA levels of both total PGC-1 α and PGC-1 $\alpha 4$, as well as Tfam, in the muscle of aged men [178]. While Flack et al. [179] observed no changes in mitochondrial markers in the skeletal muscle of individuals over 60 years old following 12 weeks of resistance exercise, other studies have shown that 6 months of resistance training partially reversed the aging-related dysregulation of genes for mitochondrial function [176]. Furthermore, a mixed type of chronic exercise (voluntary resistance wheel exercise training) was found to have a significant effect on increasing muscle aerobic capacity in aging muscle, as well as muscle mass and size [158], indicating the therapeutic potential of using a mixed training type to prevent the atrophy and reduction in mitochondria that is associated with age.

4.2. Exercise and Mitochondrial Turnover

4.2.1. Fusion/Fission and Exercise. Recent studies have sought to understand the effects of exercise on mitochondrial dynamics in aging skeletal muscle. While mixed results have been found in young skeletal muscle [180, 181], several studies have shown parallel changes in both fusion and fission

proteins in aging skeletal muscle following chronic physical activity or endurance exercise training [151, 182, 183]. For example, 6 weeks of treadmill exercise upregulated both Fis1 and Mfn1 protein abundances in the skeletal muscle of old animals [151]. Furthermore, lifelong physically active older women demonstrated elevated levels of both Mfn2 and Drp1 mRNA in their skeletal muscle as compared to age-matched inactive women [184]. Hence, chronic muscle activity seems to control mitochondrial dynamics in aging skeletal muscle through the coregulation of both fusion and fission processes.

4.2.2. Autophagy/Mitophagy and Exercise. Although contradictory findings have been observed [185, 186], acute aerobic exercise is likely to increase the autophagic responses in skeletal muscle [187]. For example, a bout of treadmill exercise elevated muscle and mitochondrial autophagic flux in young skeletal muscle, wherein LC3-II and p62 fluxes were upregulated immediately after exercise, as well as during recovery [187]. Interestingly, this acute exercise-related increase in muscle autophagic and mitophagic flux appeared to be diminished in the absence of PGC-1 α , which suggests the importance of PGC-1 α on the exercise-inducible muscle remodeling [187]. This is also supported by a study by Vainshtein et al. [188], wherein denervation-induced upregulation of the mitophagy system was lessened in the skeletal muscle of PGC-1 α -KO mice. Future work will be required to determine whether PGC-1 α plays a key role inactivity-dependent changes in autophagy/mitophagy in aging skeletal muscle.

Several studies have sought to understand endurance training effects on the cellular systems in aging muscle. For instance, it has been claimed that endurance exercise training may upregulate the autophagy process in the skeletal muscle of old animals [158, 189, 190]. However, these interpretations have been derived from measurements of the ratio of LC3-II to LC3-I without changes in p62 protein accumulation [158], which is a limitation as they did not measure autophagy flux. Nonetheless, in response to endurance training, these aging muscles were shown to have increased expression of autophagic markers such as autophagy-related protein 7 (ATG7) and Beclin-1 that are all significant players in the formation of the autophagosome. The CMA protein LAMP2A also followed the same pattern [185]. Further, physically active elderly individuals have increased mRNA levels of autophagy markers such as Beclin-1, ATG7, and p62 [173, 184], and they also had increased mitophagy markers including BNIP3 and parkin in the muscle [173, 184]. Indeed, in a recent study (in Press), we observed that muscle autophagy may be concomitantly altered along with mitochondrial adaptations over the course of chronic muscle activity. In addition, lysosomal proteins appear to adapt prior to mitochondrial changes. Therefore, it is possible that endurance exercise training or chronic muscle activity may lead to a mitochondrial remodeling in the skeletal muscle of aged individuals, but more studies are warranted to clearly understand endurance exercise training effects on the autophagy/mitophagy systems.

Autophagic responses following resistance exercise are shown to be different from the endurance exercise-induced changes discussed above. For example, it has been reported that in response to a bout of resistance exercise, the protein ratio of LC3-II to LC3-I was decreased in the muscle of old individuals compared to that in the young group [191, 192], while p62 protein accumulated [178]. As in the acute responses, resistance training appears to accelerate autophagic degradation (flux) in aging skeletal muscle. For example, 6 weeks of ladder climbing exercise training was shown to downregulate the ratio of LC3-II to LC3-I and p62 protein abundance in the muscle of old rats [193]. In this study, other autophagy protein markers including Beclin-1, ATG7, and cathepsin L were all upregulated in the aging muscle [193], collectively suggesting that resistance exercise may accelerate autophagy with age.

4.2.3. Protein Import and Exercise. As in other aging studies, there have been few studies examining the effects of exercise or chronic activity on the mitochondrial protein import system in aging muscle. Using a CCA model, Ljubicic and Hood [14] observed an attenuated change in protein import systems (TIM17, TIM23, and mtHSP70) in aging skeletal muscle following 7 days of CCA, whereas the same markers were significantly elevated by CCA in young muscle. In addition, Joseph and colleagues have shown that the increase in protein import with CCA is correspondingly reduced in aged muscle [168]. Thus, while the import process is not affected with age basally, the adaptive potential in response to exercise appears to be reduced.

5. Conclusion

Mitochondrial quality control in aging skeletal muscle is regulated via mitochondrial biogenesis and mitochondrial turnover; however, the regulation of these processes seems to be less sensitive to the effects of exercise compared to that in young, healthy muscle. Regulation of mitochondrial quality in skeletal muscle can be also accomplished by other cellular systems including ubiquitin proteasomal degradation, lysosomal regulation, and apoptosis. In particular, the lysosomal system has been recently suggested as a key player for regulating autophagy/mitophagy, as well as mitochondrial energy balance [194]. Indeed, a key component of lysosomal biogenesis, the transcription factor TFEB, appears to determine exercise capacity [194], and we have suggested a coordinated function between TFEB and PGC-1 α during both denervation- [188] and CCA- (in Press) induced skeletal muscle remodeling, suggesting an importance of maintaining a balance between mitochondrial biogenesis and lysosomal system for the muscle quality control. Therefore, it will be interesting for future studies to examine aging-related alterations in the lysosomal system in skeletal muscle, as well as to study how endurance and/or resistance exercise regulates lysosomal capacity in aging muscle. These findings will suggest a possible pharmaceutical target for improving aging-related mitochondrial dysregulation in skeletal muscle.

It is evident that maintaining healthy mitochondrial quality is essential for defeating aging-related muscle

dysfunction and weakness. To better understand the regulation of mitochondrial quality control in aging muscle, more studies are warranted to reveal the underlying mechanisms behind the effects of exercise on the mitochondrial biogenesis and turnover. Hopefully, the results will suggest the most effective exercise strategies for attaining optimal mitochondrial quality in aging skeletal muscle.

Abbreviations

AICAR:	5-Aminoimidazole-4-carboxamide ribonucleotide
AMP:	Adenosine monophosphate
AMPK:	AMP-activated protein kinase
ATG7:	Autophagy-related protein 7
ATP:	Adenosine triphosphate
BNIP3:	BCL2/adenovirus E1B 19 kDa protein-interacting protein 3
CARM1:	Coactivator-associated arginine methyltransferase 1
CCA:	Chronic contractile activity
CMA:	Chaperone-mediated autophagy
COX:	Cytochrome c oxidase
DNA:	Deoxyribonucleic acid
Drp1:	Dynamin-related protein 1
ERR:	Estrogen-related receptor
ETC:	Electron transport chain
Fis1:	Fission 1 protein
Fisher 344 BN rats:	Fisher 344 Brown Norway rats
FoxO3a:	Forkhead box O3a
GTP:	Guanosine triphosphate
HIF1 α :	Hypoxia-inducible factor 1-alpha
HSC70:	Heat shock cognate 70
IMF:	Intermyofibrillar
KO:	Knockout
LAMP2A:	Lysosomal-associated membrane protein 2A
LC3-I or -II:	Microtubule-associated protein 1A/1B-light chain 3 I or II
MAPK:	Mitogen-activated protein kinase
Mfn1/2:	Mitofusins 1 and 2
mHSP70:	Mitochondrial heat shock protein 70
MPP:	Mitochondrial processing peptidase
mtDNA:	Mitochondrial DNA
TFB1/2:	Transcription factors B1 and B2
NAD ⁺ :	Nicotinamide adenine dinucleotide
nDNA:	Nuclear DNA
NMN:	Nicotinamide mononucleotide
NMNAT:	NMN adenylyltransferase
NRF-1/2:	Nuclear respiratory factors 1 and 2
NUGEMP:	Nuclear genes encoding mitochondrial proteins
OPA1:	Optic atrophy 1
OXPPOS:	Oxidative phosphorylation
p53:	Tumor protein 53
p62:	Ubiquitin-binding protein p62
PGC-1 α :	PPAR-coactivator 1 alpha
PINK-1:	PTEN-induced kinase 1
POLRMT:	Mitochondrial RNA polymerase

PPAR:	Peroxisome proliferator-activated receptor
ROS:	Reactive oxygen species
rRNA:	Ribosomal ribonucleic acid
SIRT1:	Silent mating type information regulation 2 homolog 1
SS:	Subsarcolemmal
Tfam:	Transcription factor A of the mitochondria
TFEB:	Transcription factor EB
TIM:	Translocase of the inner mitochondrial membrane
TOM:	Translocase of the outer mitochondrial membrane
tRNA:	Transfer RNA.

Conflicts of Interest

No potential conflict of interests was disclosed. David A. Hood is also the holder of a Canada Research Chair in Cell Physiology.

Acknowledgments

This work was supported by funding from the Natural Sciences and Engineering Research Council of Canada (NSERC) to David A. Hood.

References

- [1] I. H. Rosenberg, "Sarcopenia: origins and clinical relevance," *The Journal of Nutrition*, vol. 127, no. 5, Supplement, pp. 990S-991S, 1997.
- [2] D. Heber, S. Ingles, J. M. Ashley, M. H. Maxwell, R. F. Lyons, and R. M. Elashoff, "Clinical detection of sarcopenic obesity by bioelectrical impedance analysis," *The American Journal of Clinical Nutrition*, vol. 64, no. 3, Supplement, pp. 472S-477S, 1996.
- [3] A. Hiona, A. Sanz, G. C. Kujoth et al., "Mitochondrial DNA mutations induce mitochondrial dysfunction, apoptosis and sarcopenia in skeletal muscle of mitochondrial DNA mutator mice," *PLoS One*, vol. 5, no. 7, article e11468, 2010.
- [4] G. C. Kujoth, A. Hiona, T. D. Pugh et al., "Mitochondrial DNA mutations, oxidative stress, and apoptosis in mammalian aging," *Science*, vol. 309, no. 5733, pp. 481-484, 2005.
- [5] L. A. Schaap, S. M. Pluijm, D. J. Deeg, and M. Visser, "Inflammatory markers and loss of muscle mass (sarcopenia) and strength," *The American Journal of Medicine*, vol. 119, no. 6, p. 526, 2006.
- [6] L. A. Esposito, S. Melov, A. Panov, B. A. Cottrell, and D. C. Wallace, "Mitochondrial disease in mouse results in increased oxidative stress," *Proceedings of the National Academy of Sciences of the United States of America*, vol. 96, no. 9, pp. 4820-4825, 1999.
- [7] E. Rapizzi, P. Pinton, G. Szabadkai et al., "Recombinant expression of the voltage-dependent anion channel enhances the transfer of Ca²⁺ microdomains to mitochondria," *The Journal of Cell Biology*, vol. 159, no. 4, pp. 613-624, 2002.
- [8] S. Iqbal, O. Ostojic, K. Singh, A. M. Joseph, and D. A. Hood, "Expression of mitochondrial fission and fusion regulatory proteins in skeletal muscle during chronic use and disuse," *Muscle & Nerve*, vol. 48, no. 6, pp. 963-970, 2013.
- [9] J. P. Leduc-Gaudet, M. Picard, F. St-Jean Pelletier et al., "Mitochondrial morphology is altered in atrophied skeletal muscle of aged mice," *Oncotarget*, vol. 6, no. 20, pp. 17923-17937, 2015.
- [10] M. Navratil, A. Terman, and E. A. Arriaga, "Giant mitochondria do not fuse and exchange their contents with normal mitochondria," *Experimental Cell Research*, vol. 314, no. 1, pp. 164-172, 2008.
- [11] J. M. Zahn, R. Sonu, H. Vogel et al., "Transcriptional profiling of aging in human muscle reveals a common aging signature," *PLoS Genetics*, vol. 2, no. 7, article e115, 2006.
- [12] E. Bua, J. Johnson, A. Herbst et al., "Mitochondrial DNA-deletion mutations accumulate intracellularly to detrimental levels in aged human skeletal muscle fibers," *American Journal of Human Genetics*, vol. 79, no. 3, pp. 469-480, 2006.
- [13] C. N. Lyons, O. Mathieu-Costello, and C. D. Moyes, "Regulation of skeletal muscle mitochondrial content during aging," *The Journals of Gerontology. Series A, Biological Sciences and Medical Sciences*, vol. 61, no. 1, pp. 3-13, 2006.
- [14] V. Ljubicic and D. A. Hood, "Diminished contraction-induced intracellular signaling towards mitochondrial biogenesis in aged skeletal muscle," *Aging Cell*, vol. 8, no. 4, pp. 394-404, 2009.
- [15] V. Ljubicic, A. M. Joseph, P. J. Adhihetty et al., "Molecular basis for an attenuated mitochondrial adaptive plasticity in aged skeletal muscle," *Aging (Albany, NY)*, vol. 1, no. 9, pp. 818-830, 2009.
- [16] S. E. Calvo, K. R. Clauser, and V. K. Mootha, "MitoCarta2.0: an updated inventory of mammalian mitochondrial proteins," *Nucleic Acids Research*, vol. 44, no. D1, pp. D1251-D1257, 2016.
- [17] J. W. Taanman, "The mitochondrial genome: structure, transcription, translation and replication," *Biochimica et Biophysica Acta*, vol. 1410, no. 2, pp. 103-123, 1999.
- [18] K. Boengler, G. Heusch, and R. Schulz, "Nuclear-encoded mitochondrial proteins and their role in cardioprotection," *Biochimica et Biophysica Acta*, vol. 1813, no. 7, pp. 1286-1294, 2011.
- [19] J. Lin, H. Wu, P. T. Tarr et al., "Transcriptional co-activator PGC-1 alpha drives the formation of slow-twitch muscle fibres," *Nature*, vol. 418, no. 6899, pp. 797-801, 2002.
- [20] P. Puigserver, Z. Wu, C. W. Park, R. Graves, M. Wright, and B. M. Spiegelman, "A cold-inducible coactivator of nuclear receptors linked to adaptive thermogenesis," *Cell*, vol. 92, no. 6, pp. 829-839, 1998.
- [21] O. H. Mortensen, L. Frandsen, P. Schjerling, E. Nishimura, and N. Grunnet, "PGC-1alpha and PGC-1beta have both similar and distinct effects on myofiber switching toward an oxidative phenotype," *American Journal of Physiology. Endocrinology and Metabolism*, vol. 291, no. 4, pp. E807-E816, 2006.
- [22] V. K. Mootha, C. M. Lindgren, K. F. Eriksson et al., "PGC-1alpha-responsive genes involved in oxidative phosphorylation are coordinately downregulated in human diabetes," *Nature Genetics*, vol. 34, no. 3, pp. 267-273, 2003.
- [23] T. C. Leone, J. J. Lehman, B. N. Finck et al., "PGC-1alpha deficiency causes multi-system energy metabolic derangements: muscle dysfunction, abnormal weight control and hepatic steatosis," *PLoS Biology*, vol. 3, no. 4, article e101, 2005.

- [24] C. Zechner, L. Lai, J. F. Zechner et al., "Total skeletal muscle PGC-1 deficiency uncouples mitochondrial derangements from fiber type determination and insulin sensitivity," *Cell Metabolism*, vol. 12, no. 6, pp. 633–642, 2010.
- [25] L. W. Finley, J. Lee, and A. Souza, "Skeletal muscle transcriptional coactivator PGC-1 α mediates mitochondrial, but not metabolic, changes during calorie restriction," *Proceedings of the National Academy of Sciences of the United States of America*, vol. 109, no. 8, pp. 2931–2936, 2012.
- [26] R. B. Vega, J. M. Huss, and D. P. Kelly, "The coactivator PGC-1 cooperates with peroxisome proliferator-activated receptor α in transcriptional control of nuclear genes encoding mitochondrial fatty acid oxidation enzymes," *Molecular and Cellular Biology*, vol. 20, no. 5, pp. 1868–1876, 2000.
- [27] S. N. Schreiber, D. Knutti, K. Brogli, T. Uhlmann, and A. Kralli, "The transcriptional coactivator PGC-1 regulates the expression and activity of the orphan nuclear receptor estrogen-related receptor α (ERR α)," *The Journal of Biological Chemistry*, vol. 278, no. 11, pp. 9013–9018, 2003.
- [28] S. N. Schreiber, R. Emter, M. B. Hock et al., "The estrogen-related receptor α (ERR α) functions in PPAR γ coactivator 1 α (PGC-1 α)-induced mitochondrial biogenesis," *Proceedings of the National Academy of Sciences of the United States of America*, vol. 101, no. 17, pp. 6472–6477, 2004.
- [29] P. Puigserver, G. Adelmant, Z. Wu et al., "Activation of PPAR γ coactivator-1 through transcription factor docking," *Science*, vol. 286, no. 5443, pp. 1368–1371, 1999.
- [30] J. V. Virbasius and R. C. Scarpulla, "Activation of the human mitochondrial transcription factor A gene by nuclear respiratory factors: a potential regulatory link between nuclear and mitochondrial gene expression in organelle biogenesis," *Proceedings of the National Academy of Sciences of the United States of America*, vol. 91, no. 4, pp. 1309–1313, 1994.
- [31] C. Handschin, J. Rhee, J. Lin, P. T. Tarr, and B. M. Spiegelman, "An autoregulatory loop controls peroxisome proliferator-activated receptor γ coactivator 1 α expression in muscle," *Proceedings of the National Academy of Sciences of the United States of America*, vol. 100, no. 12, pp. 7111–7116, 2003.
- [32] R. Amat, A. Planavila, S. L. Chen, R. Iglesias, M. Giralt, and F. Villarroya, "SIRT1 controls the transcription of the peroxisome proliferator-activated receptor- γ coactivator-1 α (PGC-1 α) gene in skeletal muscle through the PGC-1 α autoregulatory loop and interaction with MyoD," *The Journal of Biological Chemistry*, vol. 284, no. 33, pp. 21872–21880, 2009.
- [33] D. P. Millay and E. N. Olson, "Making muscle or mitochondria by selective splicing of PGC-1 α ," *Cell Metabolism*, vol. 17, no. 1, pp. 3–4, 2013.
- [34] Y. Zhang, P. Huypens, A. W. Adamson et al., "Alternative mRNA splicing produces a novel biologically active short isoform of PGC-1 α ," *The Journal of Biological Chemistry*, vol. 284, no. 47, pp. 32813–32826, 2009.
- [35] J. L. Ruas, J. P. White, R. R. Rao et al., "A PGC-1 α isoform induced by resistance training regulates skeletal muscle hypertrophy," *Cell*, vol. 151, no. 6, pp. 1319–1331, 2012.
- [36] M. Silvennoinen, J. P. Ahtiainen, J. J. Hulmi et al., "PGC-1 isoforms and their target genes are expressed differently in human skeletal muscle following resistance and endurance exercise," *Physiological Reports*, vol. 3, no. 10, 2015.
- [37] J. S. Chang, V. Fernand, Y. B. Zhang et al., "NT-PGC-1 α protein is sufficient to link β (3)-adrenergic receptor activation to transcriptional and physiological components of adaptive thermogenesis," *Journal of Biological Chemistry*, vol. 287, no. 12, pp. 9100–9111, 2012.
- [38] X. Wen, J. Wu, J. S. Chang et al., "Effect of exercise intensity on isoform-specific expressions of NT-PGC-1 α mRNA in mouse skeletal muscle," *BioMed Research International*, vol. 2014, Article ID 402175, 11 pages, 2014.
- [39] D. C. Wright, P. C. Geiger, D. H. Han, T. E. Jones, and J. O. Holloszy, "Calcium induces increases in peroxisome proliferator-activated receptor γ coactivator-1 α and mitochondrial biogenesis by a pathway leading to p38 mitogen-activated protein kinase activation," *The Journal of Biological Chemistry*, vol. 282, no. 26, pp. 18793–18799, 2007.
- [40] D. Freyssenet, M. Di Carlo, and D. A. Hood, "Calcium-dependent regulation of cytochrome c gene expression in skeletal muscle cells. Identification of a protein kinase c-dependent pathway," *The Journal of Biological Chemistry*, vol. 274, no. 14, pp. 9305–9311, 1999.
- [41] D. Freyssenet, I. Irrcher, M. K. Connor, M. Di Carlo, and D. A. Hood, "Calcium-regulated changes in mitochondrial phenotype in skeletal muscle cells," *American Journal of Physiology. Cell Physiology*, vol. 286, no. 5, pp. C1053–C1061, 2004.
- [42] I. Irrcher, V. Ljubcic, and D. A. Hood, "Interactions between ROS and AMP kinase activity in the regulation of PGC-1 α transcription in skeletal muscle cells," *American Journal of Physiology. Cell Physiology*, vol. 296, no. 1, pp. C116–C123, 2009.
- [43] E. Nisoli, S. Falcone, C. Tonello et al., "Mitochondrial biogenesis by NO yields functionally active mitochondria in mammals," *Proceedings of the National Academy of Sciences of the United States of America*, vol. 101, no. 47, pp. 16507–16512, 2004.
- [44] I. Irrcher, P. J. Adhietty, T. Sheehan, A. M. Joseph, and D. A. Hood, "PPAR γ coactivator-1 α expression during thyroid hormone- and contractile activity-induced mitochondrial adaptations," *American Journal of Physiology. Cell Physiology*, vol. 284, no. 6, pp. C1669–C1677, 2003.
- [45] Y. Zhang, K. Ma, S. Song, M. B. Elam, G. A. Cook, and E. A. Park, "Peroxisomal proliferator-activated receptor- γ coactivator-1 α (PGC-1 α) enhances the thyroid hormone induction of carnitine palmitoyltransferase I (CPT-I α)," *The Journal of Biological Chemistry*, vol. 279, no. 52, pp. 53963–53971, 2004.
- [46] Z. Gerhart-Hines, J. T. Rodgers, O. Bare et al., "Metabolic control of muscle mitochondrial function and fatty acid oxidation through SIRT1/PGC-1 α ," *The EMBO Journal*, vol. 26, no. 7, pp. 1913–1923, 2007.
- [47] A. E. Civitarese, S. Carling, L. K. Heilbronn et al., "Calorie restriction increases muscle mitochondrial biogenesis in healthy humans," *PLoS Medicine*, vol. 4, no. 3, article e76, 2007.
- [48] K. Baar, A. R. Wendt, T. E. Jones et al., "Adaptations of skeletal muscle to exercise: rapid increase in the transcriptional coactivator PGC-1," *The FASEB Journal*, vol. 16, no. 14, pp. 1879–1886, 2002.
- [49] B. Chabi, V. Ljubcic, K. J. Menzies, J. H. Huang, A. Saleem, and D. A. Hood, "Mitochondrial function and apoptotic susceptibility in aging skeletal muscle," *Aging Cell*, vol. 7, no. 1, pp. 2–12, 2008.

- [50] C. Ling, P. Poulsen, E. Carlsson et al., "Multiple environmental and genetic factors influence skeletal muscle PGC-1alpha and PGC-1beta gene expression in twins," *The Journal of Clinical Investigation*, vol. 114, no. 10, pp. 1518–1526, 2004.
- [51] A. R. Konopka, M. K. Suer, C. A. Wolff, and M. P. Harber, "Markers of human skeletal muscle mitochondrial biogenesis and quality control: effects of age and aerobic exercise training," *The Journals of Gerontology. Series a, Biological Sciences and Medical Sciences*, vol. 69, no. 4, pp. 371–378, 2014.
- [52] S. Sczelecki, A. Besse-Patin, A. Abboud et al., "Loss of Pgc-1alpha expression in aging mouse muscle potentiates glucose intolerance and systemic inflammation," *American Journal of Physiology. Endocrinology and Metabolism*, vol. 306, no. 2, pp. E157–E167, 2014.
- [53] M. Sandri, J. Lin, C. Handschin et al., "PGC-1alpha protects skeletal muscle from atrophy by suppressing FoxO3 action and atrophy-specific gene transcription," *Proceedings of the National Academy of Sciences of the United States of America*, vol. 103, no. 44, pp. 16260–16265, 2006.
- [54] J. J. Brault, J. G. Jespersen, and A. L. Goldberg, "Peroxisome proliferator-activated receptor gamma coactivator 1alpha or 1beta overexpression inhibits muscle protein degradation, induction of ubiquitin ligases, and disuse atrophy," *The Journal of Biological Chemistry*, vol. 285, no. 25, pp. 19460–19471, 2010.
- [55] C. Canto, L. Q. Jiang, A. S. Deshmukh et al., "Interdependence of AMPK and SIRT1 for metabolic adaptation to fasting and exercise in skeletal muscle," *Cell Metabolism*, vol. 11, no. 3, pp. 213–219, 2010.
- [56] C. Canto, Z. Gerhart-Hines, J. N. Feige et al., "AMPK regulates energy expenditure by modulating NAD⁺ metabolism and SIRT1 activity," *Nature*, vol. 458, no. 7241, pp. 1056–1060, 2009.
- [57] R. Rafaeloff-Phail, L. Ding, L. Conner et al., "Biochemical regulation of mammalian AMP-activated protein kinase activity by NAD and NADH," *The Journal of Biological Chemistry*, vol. 279, no. 51, pp. 52934–52939, 2004.
- [58] P. de Lange, P. Farina, M. Moreno et al., "Sequential changes in the signal transduction responses of skeletal muscle following food deprivation," *The FASEB Journal*, vol. 20, no. 14, pp. 2579–2581, 2006.
- [59] D. Carling, "The AMP-activated protein kinase cascade—a unifying system for energy control," *Trends in Biochemical Sciences*, vol. 29, no. 1, pp. 18–24, 2004.
- [60] S. Jager, C. Handschin, J. St-Pierre, and B. M. Spiegelman, "AMP-activated protein kinase (AMPK) action in skeletal muscle via direct phosphorylation of PGC-1alpha," *Proceedings of the National Academy of Sciences of the United States of America*, vol. 104, no. 29, pp. 12017–12022, 2007.
- [61] I. Irrcher, V. Ljubicic, A. F. Kirwan, and D. A. Hood, "AMP-activated protein kinase-regulated activation of the PGC-1alpha promoter in skeletal muscle cells," *PloS One*, vol. 3, no. 10, article e3614, 2008.
- [62] H. Zong, J. M. Ren, L. H. Young et al., "AMP kinase is required for mitochondrial biogenesis in skeletal muscle in response to chronic energy deprivation," *Proceedings of the National Academy of Sciences of the United States of America*, vol. 99, no. 25, pp. 15983–15987, 2002.
- [63] B. J. Gurd, "Deacetylation of PGC-1alpha by SIRT1: importance for skeletal muscle function and exercise-induced mitochondrial biogenesis," *Applied Physiology, Nutrition, and Metabolism*, vol. 36, no. 5, pp. 589–597, 2011.
- [64] J. A. Baur, K. J. Pearson, N. L. Price et al., "Resveratrol improves health and survival of mice on a high-calorie diet," *Nature*, vol. 444, no. 7117, pp. 337–342, 2006.
- [65] N. L. Price, A. P. Gomes, A. J. Ling et al., "SIRT1 is required for AMPK activation and the beneficial effects of resveratrol on mitochondrial function," *Cell Metabolism*, vol. 15, no. 5, pp. 675–690, 2012.
- [66] A. P. Gomes, N. L. Price, A. J. Ling et al., "Declining NAD(+) induces a pseudohypoxic state disrupting nuclear-mitochondrial communication during aging," *Cell*, vol. 155, no. 7, pp. 1624–1638, 2013.
- [67] M. Lagouge, C. Argmann, Z. Gerhart-Hines et al., "Resveratrol improves mitochondrial function and protects against metabolic disease by activating SIRT1 and PGC-1alpha," *Cell*, vol. 127, no. 6, pp. 1109–1122, 2006.
- [68] M. Suwa, H. Nakano, and S. Kumagai, "Effects of chronic AICAR treatment on fiber composition, enzyme activity, UCP3, and PGC-1 in rat muscles," *Journal of Applied Physiology (Bethesda, Md.:1985)*, vol. 95, no. 3, pp. 960–968, 2003.
- [69] M. Fulco, Y. Cen, P. Zhao et al., "Glucose restriction inhibits skeletal myoblast differentiation by activating SIRT1 through AMPK-mediated regulation of Nampt," *Developmental Cell*, vol. 14, no. 5, pp. 661–673, 2008.
- [70] R. M. Reznick, H. Zong, J. Li et al., "Aging-associated reductions in AMP-activated protein kinase activity and mitochondrial biogenesis," *Cell Metabolism*, vol. 5, no. 2, pp. 151–156, 2007.
- [71] R. Bergeron, J. M. Ren, K. S. Cadman et al., "Chronic activation of AMP kinase results in NRF-1 activation and mitochondrial biogenesis," *American Journal of Physiology. Endocrinology and Metabolism*, vol. 281, no. 6, pp. E1340–E1346, 2001.
- [72] W. Qiang, K. Weiqiang, Z. Qing, Z. Pengju, and L. Yi, "Aging impairs insulin-stimulated glucose uptake in rat skeletal muscle via suppressing AMPKalpha," *Experimental & Molecular Medicine*, vol. 39, no. 4, pp. 535–543, 2007.
- [73] T. D. Pugh, M. W. Conklin, T. D. Evans et al., "A shift in energy metabolism anticipates the onset of sarcopenia in rhesus monkeys," *Aging Cell*, vol. 12, no. 4, pp. 672–681, 2013.
- [74] J. Camacho-Pereira, M. G. Tarrago, C. C. Chini et al., "CD38 dictates age-related NAD decline and mitochondrial dysfunction through an SIRT3-dependent mechanism," *Cell Metabolism*, vol. 23, no. 6, pp. 1127–1139, 2016.
- [75] H. Zhang, D. Ryu, Y. Wu et al., "NAD(+) repletion improves mitochondrial and stem cell function and enhances life span in mice," *Science*, vol. 352, no. 6292, pp. 1436–1443, 2016.
- [76] T. Gabaldon and M. A. Huynen, "From endosymbiont to host-controlled organelle: the hijacking of mitochondrial protein synthesis and metabolism," *PLoS Computational Biology*, vol. 3, no. 11, article e219, 2007.
- [77] S. E. Calvo and V. K. Mootha, "The mitochondrial proteome and human disease," *Annual Review of Genomics and Human Genetics*, vol. 11, pp. 25–44, 2010.
- [78] J. B. Stewart and P. F. Chinnery, "The dynamics of mitochondrial DNA heteroplasmy: implications for human health and disease," *Nature Reviews. Genetics*, vol. 16, no. 9, pp. 530–542, 2015.
- [79] V. Tiranti, A. Savoia, F. Forti et al., "Identification of the gene encoding the human mitochondrial RNA polymerase (h-mtRPOL) by cyberscreening of the expressed sequence tags

- database," *Human Molecular Genetics*, vol. 6, no. 4, pp. 615–625, 1997.
- [80] M. Falkenberg, M. Gaspari, A. Rantanen, A. Trifunovic, N. G. Larsson, and C. M. Gustafsson, "Mitochondrial transcription factors B1 and B2 activate transcription of human mtDNA," *Nature Genetics*, vol. 31, no. 3, pp. 289–294, 2002.
- [81] V. McCulloch, B. L. Seidel-Rogol, and G. S. Shadel, "A human mitochondrial transcription factor is related to RNA adenine methyltransferases and binds S-adenosylmethionine," *Molecular and Cellular Biology*, vol. 22, no. 4, pp. 1116–1125, 2002.
- [82] C. M. Lee, S. S. Chung, J. M. Kaczowski, R. Weindruch, and J. M. Aiken, "Multiple mitochondrial DNA deletions associated with age in skeletal muscle of rhesus monkeys," *Journal of Gerontology*, vol. 48, no. 6, pp. B201–B205, 1993.
- [83] Y. Wang, Y. Michikawa, C. Mallidis et al., "Muscle-specific mutations accumulate with aging in critical human mtDNA control sites for replication," *Proceedings of the National Academy of Sciences of the United States of America*, vol. 98, no. 7, pp. 4022–4027, 2001.
- [84] M. Khaidakov, R. H. Heflich, M. G. Manjanatha, M. B. Myers, and A. Aidoo, "Accumulation of point mutations in mitochondrial DNA of aging mice," *Mutation Research*, vol. 526, no. 1–2, pp. 1–7, 2003.
- [85] A. Herbst, J. W. Pak, D. McKenzie, E. Bua, M. Bassiouni, and J. M. Aiken, "Accumulation of mitochondrial DNA deletion mutations in aged muscle fibers: evidence for a causal role in muscle fiber loss," *The Journals of Gerontology. Series a, Biological Sciences and Medical Sciences*, vol. 62, no. 3, pp. 235–245, 2007.
- [86] J. Wanagat, Z. Cao, P. Pathare, and J. M. Aiken, "Mitochondrial DNA deletion mutations colocalize with segmental electron transport system abnormalities, muscle fiber atrophy, fiber splitting, and oxidative damage in sarcopenia," *The FASEB Journal*, vol. 15, no. 2, pp. 322–332, 2001.
- [87] J. M. Cooper, V. M. Mann, and A. H. Schapira, "Analyses of mitochondrial respiratory chain function and mitochondrial DNA deletion in human skeletal muscle: effect of ageing," *Journal of the Neurological Sciences*, vol. 113, no. 1, pp. 91–98, 1992.
- [88] V. Pesce, A. Cormio, F. Fracasso, A. M. Lezza, P. Cantatore, and M. N. Gadaleta, "Age-related changes of mitochondrial DNA content and mitochondrial genotypic and phenotypic alterations in rat hind-limb skeletal muscles," *The Journals of Gerontology. Series a, Biological Sciences and Medical Sciences*, vol. 60, no. 6, pp. 715–723, 2005.
- [89] M. Pinto and C. T. Moraes, "Mechanisms linking mtDNA damage and aging," *Free Radical Biology & Medicine*, vol. 85, pp. 250–258, 2015.
- [90] M. Lagouge and N. G. Larsson, "The role of mitochondrial DNA mutations and free radicals in disease and ageing," *Journal of Internal Medicine*, vol. 273, no. 6, pp. 529–543, 2013.
- [91] K. E. Conley, D. J. Marcinek, and J. Villarin, "Mitochondrial dysfunction and age," *Current Opinion in Clinical Nutrition and Metabolic Care*, vol. 10, no. 6, pp. 688–692, 2007.
- [92] R. Barazzoni, K. R. Short, and K. S. Nair, "Effects of aging on mitochondrial DNA copy number and cytochrome c oxidase gene expression in rat skeletal muscle, liver, and heart," *The Journal of Biological Chemistry*, vol. 275, no. 5, pp. 3343–3347, 2000.
- [93] F. J. Miller, F. L. Rosenfeldt, C. Zhang, A. W. Linnane, and P. Nagley, "Precise determination of mitochondrial DNA copy number in human skeletal and cardiac muscle by a PCR-based assay: lack of change of copy number with age," *Nucleic Acids Research*, vol. 31, no. 11, article e61, 2003.
- [94] V. Pesce, A. Cormio, F. Fracasso et al., "Age-related mitochondrial genotypic and phenotypic alterations in human skeletal muscle," *Free Radical Biology & Medicine*, vol. 30, no. 11, pp. 1223–1233, 2001.
- [95] K. Li, P. D. Neuffer, and R. S. Williams, "Nuclear responses to depletion of mitochondrial DNA in human cells," *The American Journal of Physiology*, vol. 269, no. 5, Part 1, pp. C1265–C1270, 1995.
- [96] N. D. Marchenko, A. Zaika, and U. M. Moll, "Death signal-induced localization of p53 protein to mitochondria. A potential role in apoptotic signaling," *The Journal of Biological Chemistry*, vol. 275, no. 21, pp. 16202–16212, 2000.
- [97] Y. Yoshida, H. Izumi, T. Torigoe et al., "p53 physically interacts with mitochondrial transcription factor A and differentially regulates binding to damaged DNA," *Cancer Research*, vol. 63, no. 13, pp. 3729–3734, 2003.
- [98] A. Saleem, H. N. Carter, S. Iqbal, and D. A. Hood, "Role of p53 within the regulatory network controlling muscle mitochondrial biogenesis," *Exercise and Sport Sciences Reviews*, vol. 39, no. 4, pp. 199–205, 2011.
- [99] J. D. Bartlett, G. L. Close, B. Drust, and J. P. Morton, "The emerging role of p53 in exercise metabolism," *Sports Medicine*, vol. 44, no. 3, pp. 303–309, 2014.
- [100] A. Saleem, P. J. Adhietty, and D. A. Hood, "Role of p53 in mitochondrial biogenesis and apoptosis in skeletal muscle," *Physiological Genomics*, vol. 37, no. 1, pp. 58–66, 2009.
- [101] R. J. Donahue, M. Razmara, J. B. Hoek, and T. B. Knudsen, "Direct influence of the p53 tumor suppressor on mitochondrial biogenesis and function," *The FASEB Journal*, vol. 15, no. 3, pp. 635–644, 2001.
- [102] J. H. Park, J. Zhuang, J. Li, and P. M. Hwang, "p53 as guardian of the mitochondrial genome," *FEBS Letters*, vol. 590, no. 7, pp. 924–934, 2016.
- [103] S. Matoba, J. G. Kang, W. D. Patino et al., "p53 regulates mitochondrial respiration," *Science*, vol. 312, no. 5780, pp. 1650–1653, 2006.
- [104] K. Heyne, S. Mannebach, E. Wuertz, K. X. Knaup, M. Mahyar-Roemer, and K. Roemer, "Identification of a putative p53 binding sequence within the human mitochondrial genome," *FEBS Letters*, vol. 578, no. 1–2, pp. 198–202, 2004.
- [105] A. Saleem and D. A. Hood, "Acute exercise induces tumour suppressor protein p53 translocation to the mitochondria and promotes a p53-Tfam-mitochondrial DNA complex in skeletal muscle," *The Journal of Physiology*, vol. 591, no. 14, pp. 3625–3636, 2013.
- [106] S. H. Liang and M. F. Clarke, "Regulation of p53 localization," *European Journal of Biochemistry*, vol. 268, no. 10, pp. 2779–2783, 2001.
- [107] J. Y. Park, P. Y. Wang, T. Matsumoto et al., "p53 improves aerobic exercise capacity and augments skeletal muscle mitochondrial DNA content," *Circulation Research*, vol. 105, no. 7, pp. 705–712, 2009.
- [108] A. Safdar, K. Khrapko, J. M. Flynn et al., "Exercise-induced mitochondrial p53 repairs mtDNA mutations in mutator mice," *Skeletal Muscle*, vol. 6, p. 7, 2016.

- [109] A. Saleem, S. Iqbal, Y. Zhang, and D. A. Hood, "Effect of p53 on mitochondrial morphology, import, and assembly in skeletal muscle," *American Journal of Physiology. Cell Physiology*, vol. 308, no. 4, pp. C319–C329, 2015.
- [110] A. Saleem, H. N. Carter, and D. A. Hood, "p53 is necessary for the adaptive changes in cellular milieu subsequent to an acute bout of endurance exercise," *American Journal of Physiology. Cell Physiology*, vol. 306, no. 3, pp. C241–C249, 2014.
- [111] K. Aquilano, S. Baldelli, B. Pagliei, S. M. Cannata, G. Rotilio, and M. R. Ciriolo, "p53 orchestrates the PGC-1 α -mediated antioxidant response upon mild redox and metabolic imbalance," *Antioxidants & Redox Signaling*, vol. 18, no. 4, pp. 386–399, 2013.
- [112] N. Sen, Y. K. Satija, and S. Das, "PGC-1 α , a key modulator of p53, promotes cell survival upon metabolic stress," *Molecular Cell*, vol. 44, no. 4, pp. 621–634, 2011.
- [113] M. M. Ziaaldini, E. Koltai, Z. Csente et al., "Exercise training increases anabolic and attenuates catabolic and apoptotic processes in aged skeletal muscle of male rats," *Experimental Gerontology*, vol. 67, pp. 9–14, 2015.
- [114] J. Tamilselvan, G. Jayaraman, K. Sivarajan, and C. Panneerselvam, "Age-dependent upregulation of p53 and cytochrome c release and susceptibility to apoptosis in skeletal muscle fiber of aged rats: role of carnitine and lipoic acid," *Free Radical Biology & Medicine*, vol. 43, no. 12, pp. 1656–1669, 2007.
- [115] L. Chung and Y. C. Ng, "Age-related alterations in expression of apoptosis regulatory proteins and heat shock proteins in rat skeletal muscle," *Biochimica et Biophysica Acta*, vol. 1762, no. 1, pp. 103–109, 2006.
- [116] M. G. Edwards, R. M. Anderson, M. Yuan, C. M. Kendzierski, R. Weindruch, and T. A. Prolla, "Gene expression profiling of aging reveals activation of a p53-mediated transcriptional program," *BMC Genomics*, vol. 8, no. 1, p. 80, 2007.
- [117] N. J. MacLaine and T. R. Hupp, "The regulation of p53 by phosphorylation: a model for how distinct signals integrate into the p53 pathway," *Aging (Albany, NY)*, vol. 1, no. 5, pp. 490–502, 2009.
- [118] G. He, Y. W. Zhang, J. H. Lee et al., "AMP-activated protein kinase induces p53 by phosphorylating MDMX and inhibiting its activity," *Molecular and Cellular Biology*, vol. 34, no. 2, pp. 148–157, 2014.
- [119] R. G. Jones, D. R. Plas, S. Kubek et al., "AMP-activated protein kinase induces a p53-dependent metabolic checkpoint," *Molecular Cell*, vol. 18, no. 3, pp. 283–293, 2005.
- [120] A. Philp and S. Schenk, "Unraveling the complexities of SIRT1-mediated mitochondrial regulation in skeletal muscle," *Exercise and Sport Sciences Reviews*, vol. 41, no. 3, pp. 174–181, 2013.
- [121] H. Vaziri, S. K. Dessain, E. Ng Eaton et al., "hSIR2(SIRT1) functions as an NAD-dependent p53 deacetylase," *Cell*, vol. 107, no. 2, pp. 149–159, 2001.
- [122] S. Baldelli and M. R. Ciriolo, "Altered S-nitrosylation of p53 is responsible for impaired antioxidant response in skeletal muscle during aging," *Aging (Albany, NY)*, vol. 8, no. 12, pp. 3450–3467, 2016.
- [123] E. Yakubovskaya, K. E. Guja, E. T. Eng et al., "Organization of the human mitochondrial transcription initiation complex," *Nucleic Acids Research*, vol. 42, no. 6, pp. 4100–4112, 2014.
- [124] N. Gleyzer, K. Vercauteren, and R. C. Scarpulla, "Control of mitochondrial transcription specificity factors (TFB1M and TFB2M) by nuclear respiratory factors (NRF-1 and NRF-2) and PGC-1 family coactivators," *Molecular and Cellular Biology*, vol. 25, no. 4, pp. 1354–1366, 2005.
- [125] N. G. Larsson, J. Wang, H. Wilhelmsson et al., "Mitochondrial transcription factor A is necessary for mtDNA maintenance and embryogenesis in mice," *Nature Genetics*, vol. 18, no. 3, pp. 231–236, 1998.
- [126] Y. Shi, A. Dierckx, P. H. Wanrooij et al., "Mammalian transcription factor A is a core component of the mitochondrial transcription machinery," *Proceedings of the National Academy of Sciences of the United States of America*, vol. 109, no. 41, pp. 16510–16515, 2012.
- [127] H. B. Ngo, J. T. Kaiser, and D. C. Chan, "The mitochondrial transcription and packaging factor Tfam imposes a U-turn on mitochondrial DNA," *Nature Structural & Molecular Biology*, vol. 18, no. 11, pp. 1290–1296, 2011.
- [128] A. Rubio-Cosials, J. F. Sidow, N. Jimenez-Menendez et al., "Human mitochondrial transcription factor A induces a U-turn structure in the light strand promoter," *Nature Structural & Molecular Biology*, vol. 18, no. 11, pp. 1281–1289, 2011.
- [129] R. P. Fisher, T. Lisowsky, M. A. Parisi, and D. A. Clayton, "DNA wrapping and bending by a mitochondrial high mobility group-like transcriptional activator protein," *The Journal of Biological Chemistry*, vol. 267, no. 5, pp. 3358–3367, 1992.
- [130] D. F. Bogenhagen, "Mitochondrial DNA nucleoid structure," *Biochimica et Biophysica Acta*, vol. 1819, no. 9–10, pp. 914–920, 2012.
- [131] H. B. Ngo, G. A. Lovely, R. Phillips, and D. C. Chan, "Distinct structural features of TFAM drive mitochondrial DNA packaging versus transcriptional activation," *Nature Communications*, vol. 5, p. 3077, 2014.
- [132] N. G. Larsson, A. Oldfors, E. Holme, and D. A. Clayton, "Low levels of mitochondrial transcription factor A in mitochondrial DNA depletion," *Biochemical and Biophysical Research Communications*, vol. 200, no. 3, pp. 1374–1381, 1994.
- [133] M. I. Ekstrand, M. Falkenberg, A. Rantanen et al., "Mitochondrial transcription factor A regulates mtDNA copy number in mammals," *Human Molecular Genetics*, vol. 13, no. 9, pp. 935–944, 2004.
- [134] M. Collu-Marchese, M. Shuen, M. Pauly, A. Saleem, and D. A. Hood, "The regulation of mitochondrial transcription factor A (Tfam) expression during skeletal muscle cell differentiation," *Bioscience Reports*, vol. 35, no. 3, 2015.
- [135] H. N. Carter and D. A. Hood, "Contractile activity-induced mitochondrial biogenesis and mTORC1," *American Journal of Physiology. Cell Physiology*, vol. 303, no. 5, pp. C540–C547, 2012.
- [136] J. W. Gordon, A. A. Rungi, H. Inagaki, and D. A. Hood, "Effects of contractile activity on mitochondrial transcription factor A expression in skeletal muscle," *Journal of Applied Physiology (Bethesda, Md.:1985)*, vol. 90, no. 1, pp. 389–396, 2001.
- [137] R. Y. Lai, V. Ljubcic, D. D'Souza, and D. A. Hood, "Effect of chronic contractile activity on mRNA stability in skeletal muscle," *American Journal of Physiology. Cell Physiology*, vol. 299, no. 1, pp. C155–C163, 2010.
- [138] H. Pilegaard, B. Saltin, and P. D. Neuffer, "Exercise induces transient transcriptional activation of the PGC-1 α gene

- in human skeletal muscle,” *The Journal of Physiology*, vol. 546, Part 3, pp. 851–858, 2003.
- [139] G. Ugucioni and D. A. Hood, “The importance of PGC-1 α in contractile activity-induced mitochondrial adaptations,” *American Journal of Physiology. Endocrinology and Metabolism*, vol. 300, no. 2, pp. E361–E371, 2011.
- [140] H. C. Lee, P. H. Yin, C. Y. Lu, C. W. Chi, and Y. H. Wei, “Increase of mitochondria and mitochondrial DNA in response to oxidative stress in human cells,” *The Biochemical Journal*, vol. 348, Part 2, pp. 425–432, 2000.
- [141] A. Wredenberg, R. Wibom, H. Wilhelmsson et al., “Increased mitochondrial mass in mitochondrial myopathy mice,” *Proceedings of the National Academy of Sciences of the United States of America*, vol. 99, no. 23, pp. 15066–15071, 2002.
- [142] A. M. Lezza, V. Pesce, A. Cormio et al., “Increased expression of mitochondrial transcription factor A and nuclear respiratory factor-1 in skeletal muscle from aged human subjects,” *FEBS Letters*, vol. 501, no. 1, pp. 74–78, 2001.
- [143] H. Chen, M. Vermulst, Y. E. Wang et al., “Mitochondrial fusion is required for mtDNA stability in skeletal muscle and tolerance of mtDNA mutations,” *Cell*, vol. 141, no. 2, pp. 280–289, 2010.
- [144] S. Cipolat, O. Martins de Brito, B. Dal Zilio, and L. Scorrano, “OPA1 requires mitofusin 1 to promote mitochondrial fusion,” *Proceedings of the National Academy of Sciences of the United States of America*, vol. 101, no. 45, pp. 15927–15932, 2004.
- [145] O. C. Loson, Z. Song, H. Chen, and D. C. Chan, “Fis1, Mff, MiD49, and MiD51 mediate Drp1 recruitment in mitochondrial fission,” *Molecular Biology of the Cell*, vol. 24, no. 5, pp. 659–667, 2013.
- [146] S. Mai, M. Klinkenberg, G. Auburger, J. Bereiter-Hahn, and M. Jendrach, “Decreased expression of Drp1 and Fis1 mediates mitochondrial elongation in senescent cells and enhances resistance to oxidative stress through PINK1,” *Journal of Cell Science*, vol. 123, Part 6, pp. 917–926, 2010.
- [147] A. M. Joseph, P. J. Adhihetty, T. W. Buford et al., “The impact of aging on mitochondrial function and biogenesis pathways in skeletal muscle of sedentary high- and low-functioning elderly individuals,” *Aging Cell*, vol. 11, no. 5, pp. 801–809, 2012.
- [148] D. Sebastian, E. Sorianoello, J. Segales et al., “Mfn2 deficiency links age-related sarcopenia and impaired autophagy to activation of an adaptive mitophagy pathway,” *The EMBO Journal*, vol. 35, no. 15, pp. 1677–1693, 2016.
- [149] A. M. Joseph, P. J. Adhihetty, N. R. Wawrzyniak et al., “Dysregulation of mitochondrial quality control processes contribute to sarcopenia in a mouse model of premature aging,” *PLoS One*, vol. 8, no. 7, article e69327, 2013.
- [150] G. Distefano, R. A. Standley, J. J. Dube et al., “Chronological age does not influence ex-vivo mitochondrial respiration and quality control in skeletal muscle,” *The Journals of Gerontology. Series A, Biological Sciences and Medical Sciences*, vol. 72, no. 4, pp. 535–542, 2017.
- [151] E. Koltai, N. Hart, A. W. Taylor et al., “Age-associated declines in mitochondrial biogenesis and protein quality control factors are minimized by exercise training,” *American Journal of Physiology. Regulatory, Integrative and Comparative Physiology*, vol. 303, no. 2, pp. R127–R134, 2012.
- [152] H. Tai, Z. Wang, H. Gong et al., “Autophagy impairment with lysosomal and mitochondrial dysfunction is an important characteristic of oxidative stress-induced senescence,” *Autophagy*, vol. 13, no. 1, pp. 99–113, 2017.
- [153] A. M. Cuervo and J. F. Dice, “Age-related decline in chaperone-mediated autophagy,” *The Journal of Biological Chemistry*, vol. 275, no. 40, pp. 31505–31513, 2000.
- [154] A. Terman, H. Dalen, J. W. Eaton, J. Neuzil, and U. T. Brunk, “Mitochondrial recycling and aging of cardiac myocytes: the role of autophagocytosis,” *Experimental Gerontology*, vol. 38, no. 8, pp. 863–876, 2003.
- [155] L. M. Baehr, D. W. West, G. Marcotte et al., “Age-related deficits in skeletal muscle recovery following disuse are associated with neuromuscular junction instability and ER stress, not impaired protein synthesis,” *Aging (Albany, NY)*, vol. 8, no. 1, pp. 127–146, 2016.
- [156] K. Sakuma, M. Kinoshita, Y. Ito, M. Aizawa, W. Aoi, and A. Yamaguchi, “p62/SQSTM1 but not LC3 is accumulated in sarcopenic muscle of mice,” *Journal of Cachexia, Sarcopenia and Muscle*, vol. 7, no. 2, pp. 204–212, 2016.
- [157] A. M. Fritzen, C. Frosig, J. Jeppesen et al., “Role of AMPK in regulation of LC3 lipidation as a marker of autophagy in skeletal muscle,” *Cellular Signalling*, vol. 28, no. 6, pp. 663–674, 2016.
- [158] Z. White, J. Terrill, R. B. White et al., “Voluntary resistance wheel exercise from mid-life prevents sarcopenia and increases markers of mitochondrial function and autophagy in muscles of old male and female C57BL/6J mice,” *Skeletal Muscle*, vol. 6, no. 1, p. 45, 2016.
- [159] D. W. Russ, J. Krause, A. Wills, and R. Arreguin, ““SR stress” in mixed hindlimb muscles of aging male rats,” *Biogerontology*, vol. 13, no. 5, pp. 547–555, 2012.
- [160] A. Rana, M. Rera, and D. W. Walker, “Parkin overexpression during aging reduces proteotoxicity, alters mitochondrial dynamics, and extends lifespan,” *Proceedings of the National Academy of Sciences of the United States of America*, vol. 110, no. 21, pp. 8638–8643, 2013.
- [161] A. L. Bujak, J. D. Crane, J. S. Lally et al., “AMPK activation of muscle autophagy prevents fasting-induced hypoglycemia and myopathy during aging,” *Cell Metabolism*, vol. 21, no. 6, pp. 883–890, 2015.
- [162] H. J. Shin, H. Kim, S. Oh et al., “AMPK-SKP2-CARM1 signalling cascade in transcriptional regulation of autophagy,” *Nature*, vol. 534, no. 7608, pp. 553–557, 2016.
- [163] R. Kiffin, S. Kaushik, M. Zeng et al., “Altered dynamics of the lysosomal receptor for chaperone-mediated autophagy with age,” *Journal of Cell Science*, vol. 120, Part 5, pp. 782–791, 2007.
- [164] M. A. Bonelli, S. Desenzani, G. Cavallini et al., “Low-level caloric restriction rescues proteasome activity and Hsc70 level in liver of aged rats,” *Biogerontology*, vol. 9, no. 1, pp. 1–10, 2008.
- [165] A. Vasilaki, F. McArdle, L. M. Iwanejko, and A. McArdle, “Adaptive responses of mouse skeletal muscle to contractile activity: the effect of age,” *Mechanisms of Ageing and Development*, vol. 127, no. 11, pp. 830–839, 2006.
- [166] M. F. O’Leary, A. Vainshtein, S. Iqbal, O. Ostojic, and D. A. Hood, “Adaptive plasticity of autophagic proteins to denervation in aging skeletal muscle,” *American Journal of Physiology. Cell Physiology*, vol. 304, no. 5, pp. C422–C430, 2013.
- [167] S. E. Wohlgemuth, A. Y. Seo, E. Marzetti, H. A. Lees, and C. Leeuwenburgh, “Skeletal muscle autophagy and apoptosis during aging: effects of calorie restriction and life-long

- exercise," *Experimental Gerontology*, vol. 45, no. 2, pp. 138–148, 2010.
- [168] A. M. Joseph, V. Ljubicic, P. J. Adhietty, and D. A. Hood, "Biogenesis of the mitochondrial Tom40 channel in skeletal muscle from aged animals and its adaptability to chronic contractile activity," *American Journal of Physiology. Cell Physiology*, vol. 298, no. 6, pp. C1308–C1314, 2010.
- [169] C. Kang, E. Chung, G. Diffie, and L. L. Ji, "Exercise training attenuates aging-associated mitochondrial dysfunction in rat skeletal muscle: role of PGC-1alpha," *Experimental Gerontology*, vol. 48, no. 11, pp. 1343–1350, 2013.
- [170] A. C. Betik, M. M. Thomas, K. J. Wright, C. D. Riel, and R. T. Hepple, "Exercise training from late middle age until senescence does not attenuate the declines in skeletal muscle aerobic function," *American Journal of Physiology. Regulatory, Integrative and Comparative Physiology*, vol. 297, no. 3, pp. R744–R755, 2009.
- [171] A. R. Konopka, M. D. Douglass, L. A. Kaminsky et al., "Molecular adaptations to aerobic exercise training in skeletal muscle of older women," *The Journals of Gerontology. Series a, Biological Sciences and Medical Sciences*, vol. 65, no. 11, pp. 1201–1207, 2010.
- [172] G. C. Rowe, R. El-Khoury, I. S. Patten, P. Rustin, and Z. Arany, "PGC-1alpha is dispensable for exercise-induced mitochondrial biogenesis in skeletal muscle," *PLoS One*, vol. 7, no. 7, article e41817, 2012.
- [173] S. Zampieri, L. Pietrangelo, S. Loeffler et al., "Lifelong physical exercise delays age-associated skeletal muscle decline," *The Journals of Gerontology. Series a, Biological Sciences and Medical Sciences*, vol. 70, no. 2, pp. 163–173, 2015.
- [174] R. Garcia-Valles, M. C. Gomez-Cabrera, L. Rodriguez-Manas et al., "Life-long spontaneous exercise does not prolong lifespan but improves health span in mice," *Longevity & Healthspan*, vol. 2, no. 1, p. 14, 2013.
- [175] N. T. Broskey, C. Greggio, A. Boss et al., "Skeletal muscle mitochondria in the elderly: effects of physical fitness and exercise training," *The Journal of Clinical Endocrinology and Metabolism*, vol. 99, no. 5, pp. 1852–1861, 2014.
- [176] S. Melov, M. A. Tarnopolsky, K. Beckman, K. Felkey, and A. Hubbard, "Resistance exercise reverses aging in human skeletal muscle," *PLoS One*, vol. 2, no. 5, article e465, 2007.
- [177] K. E. Yarasheski, J. Pak-Loduca, D. L. Hasten, K. A. Obert, M. B. Brown, and D. R. Sinacore, "Resistance exercise training increases mixed muscle protein synthesis rate in frail women and men ≥ 76 yr old," *The American Journal of Physiology*, vol. 277, no. 1, Part 1, pp. E118–E125, 1999.
- [178] D. I. Ogborn, B. R. McKay, J. D. Crane et al., "Effects of age and unaccustomed resistance exercise on mitochondrial transcript and protein abundance in skeletal muscle of men," *American Journal of Physiology. Regulatory, Integrative and Comparative Physiology*, vol. 308, no. 8, pp. R734–R741, 2015.
- [179] K. D. Flack, B. M. Davy, M. DeBerardinis et al., "Resistance exercise training and in vitro skeletal muscle oxidative capacity in older adults," *Physiological Reports*, vol. 4, no. 13, 2016.
- [180] N. P. Greene, D. E. Lee, J. L. Brown et al., "Mitochondrial quality control, promoted by PGC-1alpha, is dysregulated by Western diet-induced obesity and partially restored by moderate physical activity in mice," *Physiological Reports*, vol. 3, no. 7, 2015.
- [181] J. S. Ju, S. I. Jeon, J. Y. Park et al., "Autophagy plays a role in skeletal muscle mitochondrial biogenesis in an endurance exercise-trained condition," *The Journal of Physiological Sciences*, vol. 66, no. 5, pp. 417–430, 2016.
- [182] Z. Bori, Z. Zhao, E. Koltai et al., "The effects of aging, physical training, and a single bout of exercise on mitochondrial protein expression in human skeletal muscle," *Experimental Gerontology*, vol. 47, no. 6, pp. 417–424, 2012.
- [183] S. Lee, M. Kim, W. Lim, T. Kim, and C. Kang, "Strenuous exercise induces mitochondrial damage in skeletal muscle of old mice," *Biochemical and Biophysical Research Communications*, vol. 461, no. 2, pp. 354–360, 2015.
- [184] M. J. Drummond, O. Addison, L. Bruncker et al., "Downregulation of E3 ubiquitin ligases and mitophagy-related genes in skeletal muscle of physically inactive, frail older women: a cross-sectional comparison," *The Journals of Gerontology. Series a, Biological Sciences and Medical Sciences*, vol. 69, no. 8, pp. 1040–1048, 2014.
- [185] Y. A. Kim, Y. S. Kim, and W. Song, "Autophagic response to a single bout of moderate exercise in murine skeletal muscle," *Journal of Physiology and Biochemistry*, vol. 68, no. 2, pp. 229–235, 2012.
- [186] C. Schwalm, C. Jamart, N. Benoit et al., "Activation of autophagy in human skeletal muscle is dependent on exercise intensity and AMPK activation," *The FASEB Journal*, vol. 29, no. 8, pp. 3515–3526, 2015.
- [187] A. Vainshtein, L. D. Tryon, M. Pauly, and D. A. Hood, "Role of PGC-1alpha during acute exercise-induced autophagy and mitophagy in skeletal muscle," *American Journal of Physiology. Cell Physiology*, vol. 308, no. 9, pp. C710–C719, 2015.
- [188] A. Vainshtein, E. M. A. Desjardins, A. Armani, M. Sandri, and D. A. Hood, "PGC-1 alpha modulates denervation-induced mitophagy in skeletal muscle," *Skeletal Muscle*, vol. 5, no. 1, p. 9, 2015.
- [189] S. M. Garvey, D. W. Russ, M. B. Skelding, J. E. Dugle, and N. K. Edens, "Molecular and metabolomic effects of voluntary running wheel activity on skeletal muscle in late middle-aged rats," *Physiological Reports*, vol. 3, no. 2, 2015.
- [190] Y. A. Kim, Y. S. Kim, S. L. Oh, H. J. Kim, and W. Song, "Autophagic response to exercise training in skeletal muscle with age," *Journal of Physiology and Biochemistry*, vol. 69, no. 4, pp. 697–705, 2013.
- [191] C. S. Fry, M. J. Drummond, E. L. Glynn et al., "Skeletal muscle autophagy and protein breakdown following resistance exercise are similar in younger and older adults," *The Journals of Gerontology. Series a, Biological Sciences and Medical Sciences*, vol. 68, no. 5, pp. 599–607, 2013.
- [192] J. M. Dickinson, P. T. Reidy, D. M. Gundermann et al., "The impact of postexercise essential amino acid ingestion on the ubiquitin proteasome and autophagosomal-lysosomal systems in skeletal muscle of older men," *Journal of Applied Physiology (Bethesda, Md.:1985)*, vol. 122, no. 3, pp. 620–630, 2017.
- [193] L. Luo, A. M. Lu, Y. Wang et al., "Chronic resistance training activates autophagy and reduces apoptosis of muscle cells by modulating IGF-1 and its receptors, Akt/mTOR and Akt/FOXO3a signaling in aged rats," *Experimental Gerontology*, vol. 48, no. 4, pp. 427–436, 2013.
- [194] G. Mansueto, A. Armani, C. Viscomi et al., "Transcription factor EB controls metabolic flexibility during exercise," *Cell Metabolism*, vol. 25, no. 1, pp. 182–196, 2017.

Review Article

Evidence of Mitochondrial Dysfunction in Autism: Biochemical Links, Genetic-Based Associations, and Non-Energy-Related Mechanisms

Keren K. Griffiths and Richard J. Levy

Department of Anesthesiology, Columbia University Medical Center, New York, NY, USA

Correspondence should be addressed to Richard J. Levy; rl2740@cumc.columbia.edu

Received 24 March 2017; Accepted 30 April 2017; Published 29 May 2017

Academic Editor: Moh H. Malek

Copyright © 2017 Keren K. Griffiths and Richard J. Levy. This is an open access article distributed under the Creative Commons Attribution License, which permits unrestricted use, distribution, and reproduction in any medium, provided the original work is properly cited.

Autism spectrum disorder (ASD), the fastest growing developmental disability in the United States, represents a group of neurodevelopmental disorders characterized by impaired social interaction and communication as well as restricted and repetitive behavior. The underlying cause of autism is unknown and therapy is currently limited to targeting behavioral abnormalities. Emerging studies suggest a link between mitochondrial dysfunction and ASD. Here, we review the evidence demonstrating this potential connection. We focus specifically on biochemical links, genetic-based associations, non-energy related mechanisms, and novel therapeutic strategies.

1. Introduction

Autism spectrum disorder (ASD) describes a group of neurodevelopmental disorders characterized by impaired social interaction and communication as well as restricted and repetitive behavior [1]. The diagnostic criteria have recently been modified in the Diagnostic and Statistical Manual of Mental Disorders (DSM V) and require each of the following for diagnosis: persistent deficits in social and emotional reciprocity, impairments in nonverbal communication, and abnormalities in establishing relationships with peers [1]. Secondarily, to be diagnosed with autism, patients must display at least two of the following: stereotypical and repetitive motor or verbal behavior, excessive or repetitive adherence to routines and patterns of behavior, highly restricted and overly fixated interests, or exaggerated or hyporeactive responses to sensory input [1]. Finally, symptoms must manifest early in childhood and impair day-to-day functioning [1].

ASD is the fastest growing developmental disability in the United States and approximately 1 in 68 children carry the diagnosis [2, 3]. Males are affected 4 to 5 times more commonly than females and the prevalence has increased 10 to 17% each year over the last several years [2, 3]. There is

currently no cure for autism and medical therapy is limited to targeting behavioral symptoms [4]. Although the underlying cause of autism is unknown, the most promising hypotheses suggest genetic predisposition, epigenetic modifications, nutritional influences, and exposure to environmental toxins at critical periods during development [5, 6]. A growing body of clinical, genetic, and biochemical evidence now suggests that ASD, or at least a subset of ASDs, may also be linked to impaired mitochondrial function [7].

Mitochondria are organelles primarily responsible for aerobic energy production in vertebrate eukaryotic cells [8]. In addition, they also play an important role in calcium homeostasis and signaling, regulation of apoptosis, and reactive oxygen species (ROS) formation [9]. Because the central nervous system (CNS) accounts for 20% of the body's metabolic demand and developing neurons depend on oxidative phosphorylation for critical developmental processes, the immature brain is uniquely vulnerable to defects in bioenergetic capacity [8, 10, 11]. Thus, it is not surprising that emerging studies suggest that mitochondrial impairments may contribute to or cause a variety of neurodevelopmental disorders [10]. Here, we review the evidence demonstrating a potential connection between mitochondrial dysfunction

and autism. We focus specifically on biochemical links, genetic-based associations, non-energy related mechanisms, and novel therapeutic strategies.

2. The Biochemical Link between Mitochondrial Dysfunction and Autism

In 1985, Coleman and Blass observed elevated levels of lactate in the plasma of four patients with autism, suggesting a defect in oxidative phosphorylation [12]. However, it was not until 1998 that the concept of autism as a mitochondrial disease was first proposed [13]. This hypothesis was based on finding lactic acidosis, elevated urine levels of Krebs cycle metabolites, plasma carnitine deficiency, and decreased brain glucose utilization and adenosine triphosphate (ATP) levels in autistic patients [13]. Over the last 30 years, numerous reports have corroborated the notion of bioenergetic deficiency in children with ASD by detecting a variety of abnormal biomarkers in the brain, plasma, cerebral spinal fluid (CSF), urine, fibroblasts, skeletal muscle, and buccal mucosa [7, 11, 14]. In this section, we present the evidence of a potential biochemical link between impaired mitochondrial function and ASD.

2.1. Indirect and Direct Evidence from Non-CNS Tissue. Defects in oxidative phosphorylation are known to result in lactic acidemia, abnormal lactate: pyruvate ratios, accumulation of alanine, and increased acyl-carnitine levels in the plasma and urine [7]. A number of investigators have identified such indirect evidence of mitochondrial dysfunction in a variety of peripheral tissues and samples obtained from autistic children [14]. For example, in a study of 60 autistic patients aged 2 to 40 years of age, 8.3% of them demonstrated biochemical markers of abnormal aerobic respiration [7]. These included elevated plasma lactate and alanine levels and the presence of organic acids in the urine such as 3-methyl-glutaconic acid, citric acid cycle intermediates, and dicarboxylic acids [7]. In other work, 20% of children with ASD had elevated plasma lactate levels along with increase lactate: pyruvate ratios [15]. Further evidence included reduced total and free serum carnitine levels, decreased pyruvate, and increased alanine and ammonia in a cohort of patients with a diagnosis of ASD [16]. In a retrospective review of the medical records from 25 children with autism, 76% had elevated blood lactate, 53% had increase pyruvate levels, 20% demonstrated an increase lactate: pyruvate ratio in fibroblasts, and 42% displayed abnormal urine organic acid analysis [17].

As far as direct evidence of abnormal electron transport chain (ETC) function in peripheral tissues, Graf et al. reported pathologically increased complex I activity in mitochondria isolated from a skeletal muscle biopsy of a patient with autism [18]. On the other hand, defects in complex I, III, IV, and V were identified in skeletal muscle mitochondria obtained from a cohort of autistic children who also exhibited hypotonia, epilepsy, and developmental delay [19]. In other work, two children diagnosed with autism and a chromosome 15q11-q13 inverted duplication demonstrated decreased skeletal muscle complex III activity [20]. Further

evidence of impaired ETC activity was described in another case series of patients with ASD [21]. These patients exhibited impairments in skeletal muscle complexes I, II, II + III, and IV [21]. In the retrospective chart review of 25 autistic children described above, quadriceps muscle, skin fibroblasts, and liver biopsy samples revealed a complex I defect in 64% of patients, a complex II impairment in 8%, a complex III defect in 20% of patients, and depressed complex IV function in 4% of children [17]. In other work, Shoffner and colleagues found deficits in skeletal muscle mitochondria complexes I, I + III, I + III + IV, and V in 28 children co-diagnosed with ASD and mitochondrial disease [22]. In addition, impaired activity of complex I, complex III, and/or complex IV was also described in leukocytes or buccal mucosa obtained from autistic patients in a study published in 2010 [23, 24]. Since then, a number of other publications have corroborated these findings in children with ASD [25–28]. Although, a few studies have demonstrated increased activity of certain ETC complexes, the majority have identified depressed function in autism [14]. As a whole, complex I appears to most frequently affected, followed in descending order by complex IV, complex III, complex V, and complex II [14].

2.2. Direct Evidence from Brain Tissue. In work that evaluated postmortem brain samples, investigators found decreased steady-state levels of complexes III and V in the cerebellum, complex I in the frontal cortex, and complexes II, III and V in the temporal cortex in the autistic developing brain versus that of age-matched controls [29]. In addition, markers of oxidative stress were significantly increased in the cerebellum and temporal cortex of children with ASD [29]. Of note, no differences in ETC complex protein expression were detected between groups in the parietal and occipital cortices and no changes were observed in adults with autism. The results suggested mitochondrial impairment in the brains of autistic children who were between the ages of 4 and 10 years, defining a potential window of vulnerability [29].

In follow up work, the investigators demonstrated more than 30% reduction in the activities of complexes I and V, and pyruvate dehydrogenase in the frontal cortex of the post-mortem autistic brain [30]. Such defects in complexes I or V activity were identified in 43% of autistic specimens while complex III impairment was found in 29% of autistic brains [30]. Furthermore, 29% of autistic brain samples displayed a combination of abnormal activities involving multiple complexes while 14% demonstrated deficits in all ETC complexes [30]. The authors also identified increased mitochondrial gene copy number [30]. Taken together, the findings provided direct evidence for mitochondrial dysfunction in the developing autistic brain.

In corroborative work, Brodmann area 21 within the lateral temporal lobe of the ASD brain was assessed in post-mortem samples [31]. This region of the brain is responsible for auditory processing, language, and social perception and has been implicated in the manifestation of the autistic phenotype [31]. Similar to the prior studies, the researchers identified decreased protein levels of complexes I, III, IV, and V in the autistic brain and impaired complex I and IV activities [31]. They also found reduced levels of superoxide

dismutase (SOD) and enhanced oxidative DNA damage [31]. Also, consistent with prior work, much of the mitochondrial abnormalities were identified in younger children (under 10 years of age) indicating vulnerability in the developing autistic brain [31].

These findings were confirmed in yet another postmortem analysis [32]. In this work, investigators reported reduced protein expression of various subunits of complex I, III, IV and V in the motor cortex, thalamus, and cingulate gyrus of the autistic brain compared to controls [32]. Specifically, ATP5A1 (complex V), ATP5G3 (complex V), and NDUFA5 (complex I) were consistently decreased in all brain regions examined. In other work, protein expression of 84 genes important for mitochondrial homeostasis was also evaluated in the postmortem ASD brain [33]. Researchers found decreased expression of many different genes such as *MTX2* (import receptor for mitochondrial pre-proteins), *NEFL* (regulates mitochondrial morphology, fusion, and motility) and *SLC25A27* (mitochondrial uncoupling protein 4) [33]. These gene products are responsible for a wide range of mitochondrial functions and the findings suggest a possible mechanistic role for impaired mitochondria in autism beyond oxidative phosphorylation.

Neuroradiographic imaging has been helpful in identifying metabolic abnormalities in the brain in patients with autism [34]. For example, proton magnetic resonance spectroscopy (^1H -MRS), a non-invasive imaging modality, permits in vivo quantification of specific markers of brain metabolism such as creatine, phosphocreatine, choline, myo-inositol, lactate and N-acetyl aspartate (NAA) [34]. In addition, phosphorous-31 magnetic resonance spectroscopy (^{31}P -MRS), a different, but related technique, enables non-invasive measurement of high-energy phosphates such as adenosine triphosphate (ATP), adenosine diphosphate (ADP), phosphocreatine, and inorganic phosphate within the brain [35]. Such neuroradiographic assessments have identified consistent decreases in brain levels of NAA, creatine, phosphocreatine, choline and myo-inositol in children affected by ASD compared to healthy controls [34, 36–42]. Variable levels of these metabolic markers have been described in different brain regions in adults with ASD [34, 43]. Results from non-invasive measurement of lactate have been less consistent and likely relate to challenges in detecting lactate by these techniques [34, 41]. It should also be noted that interpretation of MRS data has limitations and may be complicated by inconsistencies in methodology and variability in the phenotype of subjects examined [34]. As a whole, however, the data from non-invasive imaging suggests metabolic dysfunction in the autistic brain.

3. The Genetic Link between Mitochondrial Dysfunction and Autism

Each mitochondrion has multiple copies of the mitochondrial genome (mtDNA) within its matrix [44]. mtDNA encodes for 13 essential subunits of the ETC enzymes (complexes I, III, IV, and V), 22 transfer RNAs (tRNAs), and 2 types of ribosomal RNA (rRNA) [44, 45]. The remaining ETC complex subunits are encoded by nuclear deoxyribonucleic acid (nDNA)

[44, 45]. In addition, mitochondria contain a variety of non-ETC enzymes, membrane proteins, and other molecular components that are necessary for maintaining homeostasis and mitochondrial function [44, 45]. These proteins and enzymes are also encoded by nDNA [44, 45]. Therefore, genetic mutations in either mtDNA or nDNA have the potential to cause mitochondrial dysfunction [44]. It is estimated that 1 in 2000 children born in the United States will develop a genetic-based mitochondrial disease [46]. Of these, 15% result from a mutation in mtDNA while 85% manifest from mutations in nDNA [9].

Defects in mitochondrial function are classified as primary or secondary in nature [7, 9]. Primary mitochondrial defects arise as a direct consequence of gene mutations that impair aerobic ATP synthesis, while secondary mitochondrial dysfunction is characterized by deficits in oxidative phosphorylation that result indirectly from other genetic or metabolic derangements [7, 9]. Because of the high prevalence of ASD, it would be expected that a proportion of patients with an inherited mitochondrial cytopathy also carry a diagnosis of autism [7]. If there was no link between mitochondrial disease and autism, it would be expected that ~1 in 2000 children with ASD would also carry a diagnosis of mitochondrial cytopathy [7]. However, the co-existence of mitochondrial disease in cohorts with ASD is higher than the general population, suggesting a role for mitochondrial dysfunction in autism (Figure 1) [7]. In this section, we review the mitochondrial disease-related genetic abnormalities that have been identified in autistic children.

3.1. Mitochondrial DNA Abnormalities. Defects in mtDNA have been demonstrated in children in which ASD and mitochondrial disease co-exist [7, 14]. Although many of these mtDNA mutations and mitochondrial diseases are well known and have been thoroughly classified, some are poorly understood and have yet to be characterized. For example, mutations of mtDNA were identified in a unique cohort of children that suffered from hypotonia, epilepsy, autism, and developmental delay (HEADD) [19]. Although this group of patients could not be placed into a previously described category of mitochondrial disease, they displayed autistic features and ~50% harbored large-scale mtDNA deletions [19]. A limitation of such observations, in general, is that conclusions regarding cause and effect cannot be made. Thus, with many of these reports, only an association between mtDNA mutation and autism can be inferred. However, some studies suggest a functional contribution of mitochondrial disease to the autistic phenotype [22]. For example, in a retrospective analysis of 28 patients co-diagnosed with ASD and mitochondrial disease, autistic regression occurred with fever in 71% of those who regressed versus regression without fever in 29% [22].

One of the best described mitochondrial diseases, mitochondrial encephalomyopathy, lactic acidosis, and stroke-like episodes (MELAS), is also known to co-exist with autism. MELAS results commonly from the A3243G mtDNA mutation and this genetic defect has been shown to be associated with autism [21, 47]. In 1999, Sue et al. published a report of three children with the MELAS A3243G mutation and

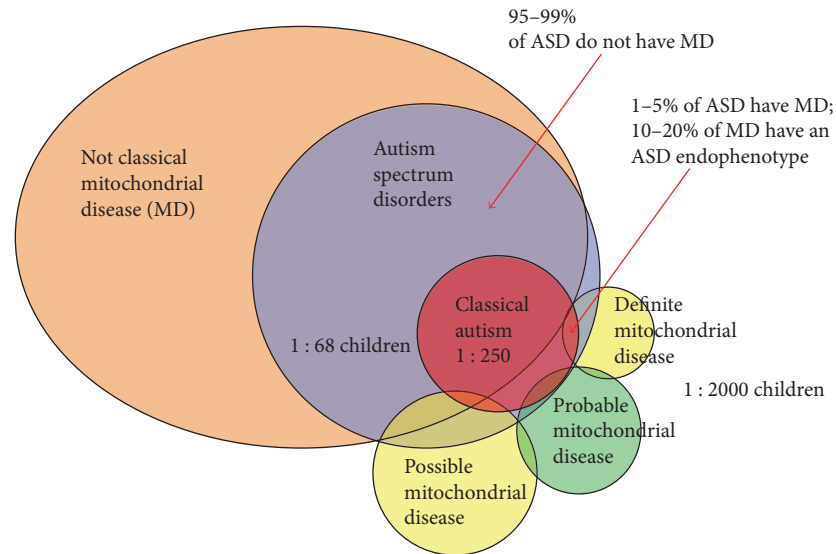


FIGURE 1: Relationship between mitochondrial disease, ASD, and autism. Mitochondrial disease in most children with ASD is of the non-classical variety. Up to 5% of children with autism have classical mitochondrial disease while 10–20% of patients with classic mitochondrial disease demonstrate ASD features. The co-existence of ASD with mitochondrial disease is higher than the prevalence of either ASD or mitochondrial disease in the general population, suggesting a link between mitochondrial dysfunction and autism. Reprinted from [9].

infantile encephalopathy [47]. One of these children went on to develop autistic features later in life [14]. Subsequently, Pons et al. analyzed 5 autistic children who had a family history of mitochondrial disease [21]. Two of these patients harbored the A3243G mutation while, in two others, the A3243G mutation was identified in maternal samples [21]. The fifth child in this study was found to have mtDNA depletion syndrome [21].

Another early report connecting a mtDNA mutation with ASD was published in 2000 [18]. In this work, Graf et al. reported on two siblings who carried a point mutation (G8362A) in the mitochondrial tRNA for lysine [18]. The 6 year-old sister was diagnosed with Leigh syndrome after developing ataxia and myoclonus at 15 months of age [18]. She was dysarthric, had a moderate intellectual disability, and demonstrated a complex IV defect in her skeletal muscle [18]. Her younger brother was diagnosed with ASD following a regression of developmental milestones between 1.5 to 2 years of age [18]. He carried the same mtDNA mutation as his sister, yet at a lower level of heteroplasmy [18]. By 3.5 years of age, he was hyperactive, lacked verbal communication, and exhibited self-injurious behavior [18]. Unlike his sister, his skeletal muscle biopsy demonstrated hyperactivity of complex I [18].

In another study, the records of 25 patients with a primary diagnosis of ASD were reviewed [17]. Twenty-one of these children met criteria for definitive mitochondrial disease and four met criteria for probable mitochondrial disease [17]. Whole mitochondrial genome sequencing was performed in 11 patients and 16 underwent selected mitochondrial mutation analysis [17]. They identified mtDNA mutations in 7 of these cases [17]. Three mutations occurred in highly conserved regions of the mitochondrial genome,

known to encode for the mitochondrial tRNA^{leu} and the ND1 and ND4 subunits of complex I [17]. These mutations were interpreted as likely having functional sequelae given prior characterization of the tRNA^{leu} mutation, that the patient with the ND1 variant demonstrated reduced muscle complex I activity and an increased fibroblast lactate: pyruvate ratio, and that a missense mutation of ND4 had previously been reported in a patient with Leigh syndrome [17, 48, 49]. The four remaining mutations were of unclear functional significance [17].

In 2010, Giulivi and colleagues analyzed mtDNA from the leukocytes of 10 children, aged 2 to 5 years, who were diagnosed with ASD [23]. This was a subanalysis of the Childhood Autism Risk from Genes and Environment (CHARGE) study [23]. Five children with autism had an increased mtDNA copy number compared to controls and 2 of the 10 autistic children had mutations in the cytochrome b gene segment which was associated with over replication [23]. In another subset of patients from the CHARGE study, Napoli and colleagues compared 67 autistic children with 46 controls [50]. The investigators assessed for mtDNA mutations of *CYTB*, the gene that encodes cytochrome b and *ND4*, the gene that encodes the ND4 subunit of complex I [50]. They found that children with autism had a significantly higher incidence of mutation of these two genes compared to controls [50]. Fifteen percent of patients with ASD harbored an *ND4* deletion while 21% had a mutation of *CYTB* compared to 7% and 9% of healthy children, respectively [50].

Recently, whole exome sequencing from 903 ASD proband-mother-sibling trios demonstrated that autistic children were 53% more likely to have heteroplasmic mutations in non-polymorphic sites (regions more likely to produce deleterious effects in oxidative phosphorylation) than unaffected

siblings [51]. Autistic individuals also had 1.5 times as many non-synonymous mutations and 2.2 times as many predicted pathogenic mutations than non-autistic siblings [51]. These findings were in contrast to an earlier report in which whole mitochondrial genome sequencing of ~400 autistic children failed to identify evidence of an association between mitochondrial mutations and autism using the proband's father as a control [52].

3.2. Nuclear DNA Gene Defects. As discussed above, defects in nuclear expression of mitochondrial proteins can impair oxidative phosphorylation and mitochondrial homeostasis. In fact, the majority of inherited mitochondrial diseases occur due to mutations in nDNA [9]. Thus, if mitochondrial disease and dysfunction cause autism, there should be evidence of an association between nDNA mutations and ASD. In 2003, Filipek et al. reported two cases of children diagnosed with autism who also had chromosome 15q11-q13 inverted duplication [20]. Both children exhibited mitochondrial dysfunction with decreased complex III activity and marked mitochondrial hyperproliferation in skeletal muscle [20]. Although the mechanism of a 15q11-q13 defect is unknown, it is possible that the gene product is involved in complex III regulation [20].

In work that investigated a link between potential candidate genes in the 2q24-q33 region and autism, Ramos and colleagues identified two single nucleotide polymorphisms (SNPs) (rs2056202 and rs2292813) in the *SLC25A12* gene [53]. The *SLC25A12* gene is associated with neurite development, encodes the calcium-dependent mitochondrial aspartate/glutamate carrier (AGC1) that is known to be functionally important in metabolically active neurons, and has been shown to be upregulated in the autistic prefrontal cortex [14, 54]. Ramos and colleagues found that 48% of autistic patients harbored these SNPs in the *SLC25A12* gene [53]. Although these findings have been corroborated by other investigators, it should be noted that some studies have demonstrated discrepant results [55–58].

Candidate genes for mitochondrial proteins that may contribute to the autistic phenotype have also been explored in other regions of nDNA. For example, Marui et al. evaluated the 7q32 region and studied a cohort of 235 Japanese patients [59]. The investigators identified two SNPs (rs12666974 and rs23779262) in the *NDUFA5* gene which were associated with ASD. *NDUFA5* encodes NADH-ubiquinone oxidoreductase 1 alpha subcomplex 5, an accessory subunit of complex I of the ETC [60]. Thus, such mutations could have consequences for complex I activity. In other research, a 1 Mb deletion was identified in the 5q14.3 region in a 12 year-old child with autism, mitochondrial disease, cognitive impairment, and dysmorphic features [24]. Buccal mucosa obtained from the patient demonstrated severely decreased complex IV activity and mildly reduced complex I activity [24]. The authors suggested that the gene product likely regulates expression or assembly of subunits of complexes I and IV [24].

In a recent meta-analysis, Rossingol and Frye attempted to determine the prevalence of genetic abnormalities in autistic children with mitochondrial disease [11]. They identified 18 publications that described a total of 112 children

diagnosed with both ASD and mitochondrial disease [11]. Symptoms and signs attributable to classic mitochondrial disease in these children were similar to the general population with mitochondrial disease, however, were significantly higher than the general autistic population [11]. This indicated that the cohort in which ASD and mitochondrial disease co-exist represented a distinct subgroup of children [11]. Importantly, they found that only 21% of patients in this cohort had mutations in mtDNA or nDNA or chromosomal abnormalities [11]. Thus, the majority was not directly associated with known genetic abnormalities, suggesting a role for secondary mitochondrial dysfunction [11]. So, although genetic mutations have been described in children with autism and mitochondrial disease, the role of such abnormalities in the ASD phenotype, whether causative or associative, is not fully known.

4. Limitations of the Presented Studies

Although the literature suggests potential biochemical and genetic links between impaired mitochondrial function and ASD, there are limitations that should be noted. First, it is not possible to determine if mitochondrial dysfunction causes ASD or results from autism or other associated processes. A major confounding factor is the presence of comorbidities in this patient population [61]. Epilepsy, cerebral palsy, and non-mitochondrial genetic syndromes, for example, can secondarily affect mitochondrial function [61]. Thus, interpretation of mitochondrial-based research in autistic subjects can be challenging in the context of such comorbid states. Next, studies of patients with ASD are prone to selection bias and many of the investigations fail to report the lack of an association between mitochondrial impairment and autism [61]. In addition, small sample sizes limit interpretation and the generalizability of many of these studies [61].

When considering measures of metabolism, biological tissue and sample preservation and handling are critical factors necessary for proper data interpretation [61]. For example, false positive values can result from imperfect technique and methodology [61]. Unfortunately, many of the published studies did not adequately detail exactly how samples were handled or processed [61]. Another limitation is the use of lymphocytes, fibroblasts, skeletal muscle, or buccal mucosa as surrogates for brain tissue in order to detect mitochondrial defects [61]. Defects in such peripheral samples do not necessarily indicate CNS disease. In addition, analyzing lymphocytes may be specifically problematic given that children with ASD can have altered immunological function and mitochondria within inflammatory cells may be indirectly affected [61]. However, despite these limitations, there is general agreement in the research community that the evidence suggests an association between mitochondrial disease and autism [61].

5. Alternative Mechanisms of ASD Pathogenesis

In addition to producing aerobic energy, mitochondria also regulate calcium signaling, mediate apoptosis, and generate ROS [9]. Such processes are important for normal brain

development. Thus, mitochondrial dysfunction has the potential to affect the immature brain via non-energetic pathways. It has been hypothesized that ASD may manifest from oxidative stress, immune dysfunction, or defects in calcium homeostasis [7, 14, 62]. Therefore, in this section we will summarize the evidence that supports these alternative mitochondria-related mechanisms of ASD.

5.1. Oxidative Stress and Abnormal Redox Regulation. The mitochondrion is a major source of ROS produced within the cell [63–65]. Superoxide, the principal free radical formed within mitochondria, is generated by complexes I and III as a by-product of oxidative phosphorylation [66, 67]. Low levels of ROS are known to be required for physiological signaling and homeostasis and play a critical role in processes such as the regulation of vascular tone, erythropoietin production, and programmed cell death [66]. However, when generated pathologically, ROS can irreversibly damage DNA, cellular proteins, and membrane lipids [66]. Such oxidative stress has been implicated in a variety of neurodegenerative disease states [68].

To counterbalance ROS toxicity and to provide cytoprotection, cells are equipped with a variety of antioxidants such as glutathione (GSH), SOD, glutathione peroxidase, catalase, ascorbic acid, α -tocopherol, and β -carotene [66]. In addition, mitochondria contain their own antioxidant enzymes such as manganese-dependent superoxide dismutase (MnSOD) in the mitochondrial matrix and copper-zinc superoxide dismutase (CuZnSOD) in the intermembrane space [69, 70]. Thus, endogenous antioxidants are important to enable the cell to strike a balance between superoxide formation and aerobic energy production in order to prevent oxidative stress and cellular damage. Excess ROS formation and oxidant injury can result from impaired ETC activity, defects in antioxidant content and function, or their combination [71]. Furthermore, free radicals can target and alter respiratory chain integrity, leading to further superoxide production [71, 72]. Thus, mitochondrial dysfunction can cause oxidative stress and result from it as well.

A number of studies have found that individuals with ASD display hallmarks of increased oxidative stress or abnormalities in redox regulation, supporting the notion of a mechanistic role for ROS in the manifestation of the autistic phenotype [7, 14, 62]. Such evidence of increased oxidative damage to DNA, proteins and lipids has been identified in blood, urine, and post-mortem brain samples from autistic individuals [62]. For example, markers of impaired capacity for methylation and enhanced oxidative stress, such as lower S-adenosylmethionine-to-S-adenosylhomocysteine ratios and lower redox ratios of reduced glutathione-to-oxidized glutathione (GSH/GSSG), have been found in the plasma of children with ASD [73, 74]. With regard to biomarkers in urine, elevated levels of the lipid peroxidation biomarker, 8-isoprostane- $F_{2\alpha}$, have been detected in autistic children [75]. Further investigation corroborating these results found increased urinary levels of isoprostane $F_{2\alpha}$ -VI, 2,3-dinor-thromboxane B_2 (a marker of platelet activation), and 6-keto-prostaglandin $F_{1\alpha}$ (a marker of endothelial activation) in 26 children with ASD [76]. In another study, plasma

levels of malondialdehyde (a marker of fatty acid peroxidation) were found to be significantly increased in children with ASD and were associated with a concomitant decline in levels of α -tocopherol and GSH [77]. Decreased levels of other antioxidant enzymes, such as erythrocyte SOD, erythrocyte and plasma glutathione peroxidase, serum transferrin, and serum ceruloplasmin have also been described in autism [78, 79]. Importantly, a correlation between such reduced levels and loss of language skills has been established in children with ASD [79].

Post-mortem analyses have more directly demonstrated abnormalities in enzymes involved in redox homeostasis and have identified evidence of oxidative damage to proteins, lipids, and DNA within the autistic brain [31, 62, 78, 80]. For instance, decreased MnSOD activity and increased 8-hydroxy-2'-deoxyguanosine, a marker of oxidatively modified DNA, were identified in Brodmann area 21 within the temporal lobe of autistic subjects [31]. Gu et al. found decreased activity of glutathione peroxidase, glutathione-S-transferase, and glutamate cysteine ligase in the ASD cerebellum [80]. In addition, investigators have demonstrated decreased levels of reduced GSH, increased levels of GSSG, and lower GSH/GSSG ratios in the cerebellum, temporal lobe, and Brodmann area 22 of individuals with ASD [81, 82]. Evidence of lipid peroxidation has been reported in different language areas of the brain, the cerebellum, hippocampus, and temporal cortex of autistic patients while increased levels of 3-nitrotyrosine, a marker of protein oxidation, have been identified in the cerebellum, orbitofrontal cortex, Wernicke's area, cerebellar vermis, pons, and Brodmann area 22 [29, 83–87].

Thus, autism appears to be associated with a pro-oxidant state. Although mitochondrial dysfunction could certainly cause oxidative stress, the etiology of ASD-related oxidant injury and mechanisms of reduced anti-oxidant defense systems remains unclear. Furthermore, it is unknown if brain-specific oxidative stress is important for the manifestation of symptoms in autism or if generalized redox imbalance is a contributor to the disease phenotype. These are obvious questions for future investigation.

5.2. Immune Dysfunction and Inflammation. The inflammatory response and resolution of inflammation are necessary processes for maintaining cellular and tissue homeostasis [88]. In contrast, however, an impaired immune system along with pathological or persistent inflammation can result in disease. In the brain, unchecked neuroinflammation and failure of its resolution can lead to neuropathology and neurodegeneration [88]. Evidence of both inflammation and immune system dysregulation has been identified in the autistic brain and in CSF obtained from subjects with ASD, suggesting a mechanistic role [62].

In 1977, Stubbs and Crawford evaluated the host cellular immune system in 12 children diagnosed with autism [89]. They reported decreased response to phytohemagglutinin in lymphocytes obtain from affected children, suggesting impaired defense mechanisms in autism [89]. More recent work has demonstrated decreases in circulating CD4+ T cells, natural killer cell activity, and Th1/Th2 helper cell

ratios in subjects with ASD as well as abnormal accumulation of T lymphocytes in tissues such as the gastrointestinal tract [90–93]. On the other hand, elevated levels of pro-inflammatory cytokines have been identified in postmortem brain tissue, CSF, plasma, and even amniotic fluid of ASD patients [94–101]. Importantly, multiple postmortem studies and one in vivo evaluation that employed positron emission tomography (PET) imaging demonstrated marked neuroinflammation in multiple brain regions in individuals with ASD as evidenced by increased activation of microglia and astroglia [99, 102, 103].

Mitochondria are known to play a role in innate and adaptive immune responses, inflammation, and signaling in response to infection [14, 104]. However, it is unknown how mitochondrial dysfunction affects the immune system or the inflammatory response in autism. Furthermore, it is unknown if such mitochondrial impairments cause autism-associated neuroinflammation and if such inflammation within the developing brain contributes to the ASD phenotype. These are questions that will need to be answered with future investigation.

5.3. Abnormal Calcium Homeostasis. Calcium is a ubiquitous second messenger, involved in a variety of cell signaling pathways [105–107]. Because of its central importance to cellular viability, calcium has the potential to adversely affect a wide range of cellular processes when its homeostasis is disrupted. Since calcium is not metabolized, activation and termination of intracellular calcium signaling relies on tight regulation of local calcium concentrations [105–107]. Mitochondria are known to play a vital role in calcium handling within the cell [108]. For example, in response to elevations in cytosolic calcium, mitochondria serve as high-capacity sinks and increase calcium uptake in order to buffer cytosolic levels [108, 109]. This process is carried out by a number of mitochondrial calcium transporters [109].

Oxidative phosphorylation is sensitive to calcium and accumulation within mitochondria is known to stimulate aerobic ATP production by the ETC [108, 109]. Mitochondrial calcium overload, however, can collapse the electrochemical proton gradient, leading to bioenergetic failure and necrotic cell death [108]. Calcium is also known to play a role in mitochondria-mediated apoptotic cell death by inducing opening of the permeability transition pore and increasing ROS following binding to cardiolipin on the inner mitochondrial membrane [105, 110]. Thus, defects in calcium homeostasis can result in mitochondrial dysfunction, oxidative stress, and cytotoxicity.

Neurotransmitter-mediated calcium signaling is important for the recruitment and accumulation of mitochondria to postsynaptic regions, a process that is critical for neuronal calcium buffering and synapse strength [111]. Calcium signaling is important for neurotransmitter release from presynaptic neurons as well as signaling in postsynaptic neurons in response to neurotransmitters such glutamate and γ -aminobutyric acid (GABA) [111, 112]. Glutamate receptors are ligand-gated calcium channels while GABA receptors trigger calcium influx via voltage-gated calcium channels [112]. Calcium transients evoked by GABA, principally an excitatory

neurotransmitter during neurodevelopment, are necessary for the critical processes of brain development [112]. Thus, aberrant calcium homeostasis could interfere with proliferation, migration, dendritic arborization, Purkinje cell development, synapse formation and maintenance, and cell death [111, 112]. Furthermore, defects in calcium signaling could be further compounded by mitochondrial dysfunction and can result in decreased neurotransmitter signaling, especially in neurons that have high firing rates of firing [112, 113]. This could explain the relative increase in excitatory-to-inhibitory neuron ratio observed in patients with ASD [114].

Finally, calcium is impacted by ATP-mediated neuronal purinergic signaling [111]. Perisynaptic ATP binds to astrocyte receptors, leading to calcium release from mitochondria, depolarization of the mitochondrial membrane potential, and generation of ROS [111]. In addition, extracellular ATP binds to microglial purinergic receptors, resulting in an increase in intracellular calcium, activation of microglia, neuroinflammation, and cell death [9, 111]. Thus, aberrancies in calcium signaling could account for oxidative stress and neuroinflammation observed in ASD.

Abnormalities in the expression of a number of genes involved in calcium signaling or homeostasis have been associated with autism [14, 112, 115]. These include *ATP13A4*, *ATP2B2*, *CACNA1C*, *CACNA1F*, *CNCNA1H*, *KCNMA1*, *IL1RAPL1*, *NCS1*, *CAPS2*, and *SLC25A12* [14, 112, 115]. The calcium-dependent mitochondrial aspartate/glutamate carrier, *AGC1*, and the gene that encodes it (*SLC25A12*) are of particular interest because they link defects in calcium regulation with mitochondrial dysfunction [115]. For example, expression of *SLC25A12* was found to be decreased in the motor cortex and cingulate gyrus and increased in the prefrontal cortex of autistic individuals [54]. Other work identified elevated neocortical calcium levels as the cause of increased *AGC1* activity in the ASD brain [116]. Importantly, the authors also identified an association between abnormal calcium signaling in autism with pathologically increased cytochrome oxidase activity and oxidative stress [116]. Thus, increased *AGC1* transport activity may result in mitochondrial dysfunction and ROS formation. Because defects in calcium homeostasis can cause or result from disturbances in mitochondrial function, it is possible that impaired calcium signaling plays a role in the connection between mitochondrial dysfunction and autism.

6. Treatment of ASD

There is currently no cure for autism because the underlying cause of ASD is unknown. Therefore, medical management has been limited to therapies that address the behavioral symptoms [1]. Intensive behavioral intervention, implemented early in life, remains the widely accepted standard of care for children with autism [117, 118]. However, the accumulating evidence of metabolic abnormalities associated with ASD provides insight into potential mechanisms of disease and has elucidated novel candidate targets for therapeutic intervention [117, 119]. Here we review the different experimental approaches that target mitochondrial dysfunction and oxidative stress in autism and have been trialed in an

effort to restore mitochondrial homeostasis and improve the clinical manifestations of ASD.

6.1. Targeting Mitochondrial Dysfunction and Oxidative Stress. Dietary supplements, like those typically used for the treatment of mitochondrial diseases, have been used to treat children with ASD [117, 119]. Such supplements include L-carnitine, coenzyme Q10, ubiquinol, B vitamin-containing multivitamins, ascorbic acid, α -tocopherol, and N-acetyl-L-cysteine [117, 119]. Treatment with L-carnitine, an essential nutrient important for the fatty acid transport across the mitochondrial membrane, was shown to improve core and associated ASD symptoms in a number of controlled trials [119–121]. In one of these investigations, serum carnitine levels were found to correlate with cognitive and behavioral scores [121].

In other work, supplementation with antioxidants such as N-acetyl-L-cysteine (a precursor to glutathione), coenzyme Q10, ubiquinol, ascorbic acid, α -tocopherol, methylcobalamin, and carnosine also improved behavioral symptoms associated with autism [122–129]. In a randomized double-blind placebo controlled trial, a formulation of multivitamins combined with mineral supplements (containing multiple mitochondrial cofactors, vitamins, and antioxidants) improved plasma or erythrocyte levels of methylation, glutathione, oxidative stress, sulfation, ATP, nicotinamide adenine dinucleotide (NADH), and nicotinamide adenine dinucleotide phosphate (NADPH) and improved overall behavior, hyperactivity, tantrums, and receptive language in children and adults with ASD [126, 127]. Trials involving other antioxidants such as the phytochemical sulforaphane and the flavonoid luteolin also improved ASD symptoms, however no metrics of oxidative stress were examined [130, 131].

6.2. Other Metabolic Targets. Folic acid is important for redox metabolism, methylation, and mitochondrial homeostasis [132, 133]. Disruption of folate receptor α activity occurs in autism due to autoantibodies and mitochondrial dysfunction and results in CNS folate deficiency [134]. Severe reductions in cerebral folate levels can lead to neurodevelopmental regression and the autism phenotype [119]. Importantly, targeted treatment with folinic acid has been shown to partially or completely improve communication, social interaction, attention, and stereotypical ASD behavior in patients with autoantibodies to folate receptor α [135–137]. Thus, targeting various causes and effects of mitochondrial dysfunction in autism may rescue behavior and minimize the clinical manifestations of ASD.

7. Conclusion

The literature reviewed here suggests a link between abnormalities in mitochondrial homeostasis and ASD and provides biochemical and genetic evidence to support a role for mitochondrial dysfunction in the pathogenesis of the autism phenotype. Mechanistically, the connection may involve defects in bioenergetic capacity as well as non-energy related pathways. However, it is not clear if mitochondrial impairments cause ASD or if they are merely associated with the

disease process. Positive patient behavioral responses to conventional mitochondrial disease therapies are promising, however, further investigation is necessary. Future work should focus on determining how mitochondrial dysfunction causes the autistic phenotype as well as how defects in mitochondrial homeostasis predispose individuals to ASD via interaction with environmental toxins, dietary factors, and epigenetic modifications during critical periods of development. Establishing a causative relationship between mitochondrial dysfunction and ASD and elucidating the exact mechanisms will permit the development of more precisely targeted therapies in the future. Ultimately, with improved knowledge and innovation, we may one day be able to prevent or cure autism.

Conflicts of Interest

The authors declare that there is no conflict of interest regarding the publication of this article.

Acknowledgments

This paper is supported by NIH/NIGMS R01GM103842-01 (Richard J. Levy) and NIH/NIEHS P30 ES009089 (Richard J. Levy).

References

- [1] Association, A.P., *Diagnostic and Statistical Manual of Mental Disorders: DSM-5*, pp. 50–59, American Psychiatric Association, Washington, DC, 2013.
- [2] Autism and Developmental Disabilities Monitoring Network Surveillance Year 2008 Principal Investigators; Centers for Disease Control and Prevention, “Prevalence of autism spectrum disorders—autism and developmental Disabilities monitoring network, 14 sites, United States, 2008,” *Morbidity and Mortality Weekly Report. Surveillance Summaries (Washington, D.C.: 2002)*, vol. 61, no. 3, pp. 1–19, 2012.
- [3] S. J. Blumberg, M. D. Bramlett, M. D. Kogan, L. A. Schieve, J. R. Jones, and M. C. Lu, “Changes in prevalence of parent-reported autism spectrum disorder in school-aged U.S. children: 2007 to 2011-2012,” *National Health Statistics Reports*, vol. 65, no. 65, pp. 1–11, 2013.
- [4] L. K. Wink, M. H. Plawecki, C. A. Erickson, K. A. Stigler, and C. J. McDougle, “Emerging drugs for the treatment of symptoms associated with autism spectrum disorders,” *Expert Opinion on Emerging Drugs*, vol. 15, no. 3, pp. 481–494, 2010.
- [5] S. A. Currenti, “Understanding and determining the etiology of autism,” *Cellular and Molecular Neurobiology*, vol. 30, no. 2, pp. 161–171, 2010.
- [6] D. H. Geschwind and P. Levitt, “Autism spectrum disorders: developmental disconnection syndromes,” *Current Opinion in Neurobiology*, vol. 17, no. 1, pp. 103–111, 2007.
- [7] R. H. Haas, “Autism and mitochondrial disease,” *Developmental Disabilities Research Reviews*, vol. 16, no. 2, pp. 144–153, 2010.
- [8] D. Voet, J. G. Voet, and C. W. Pratt, *Fundamentals of Biochemistry*, p. 931, Wiley, New York, 1999.
- [9] R. K. Naviaux, “Mitochondria and autism Spectrum disorders,” in *The Neuroscience of Autism Spectrum Disorders*, pp. 179–193, Academic Press, Elsevier, Waltham, MA, 2013.

- [10] D. Valenti, L. de Bari, B. De Filippis, A. Henrion-Caude, and R. A. Vacca, "Mitochondrial dysfunction as a central actor in intellectual disability-related diseases: an overview of down syndrome, autism, fragile X and Rett syndrome," *Neuroscience and Biobehavioral Reviews*, vol. 46, Part 2, pp. 202–217, 2014.
- [11] D. A. Rossignol and R. E. Frye, "Mitochondrial dysfunction in autism spectrum disorders: a systematic review and meta-analysis," *Molecular Psychiatry*, vol. 17, no. 3, pp. 290–314, 2012.
- [12] M. Coleman and J. P. Blass, "Autism and lactic acidosis," *Journal of Autism and Developmental Disorders*, vol. 15, no. 1, pp. 1–8, 1985.
- [13] J. Lombard, "Autism: a mitochondrial disorder?" *Medical Hypotheses*, vol. 50, no. 6, pp. 497–500, 1998.
- [14] A. Legido, R. Jethva, and M. J. Goldenthal, "Mitochondrial dysfunction in autism," *Seminars in Pediatric Neurology*, vol. 20, no. 3, pp. 163–175, 2013.
- [15] G. Oliveira, L. Diogo, M. Grazina et al., "Mitochondrial dysfunction in autism spectrum disorders: a population-based study," *Developmental Medicine and Child Neurology*, vol. 47, no. 3, pp. 185–189, 2005.
- [16] P. A. Filipek, J. Juranek, M. T. Nguyen, C. Cummings, and J. J. Gargus, "Relative carnitine deficiency in autism," *Journal of Autism and Developmental Disorders*, vol. 34, no. 6, pp. 615–623, 2004.
- [17] J. R. Weissman, R. I. Kelley, M. L. Bauman et al., "Mitochondrial disease in autism spectrum disorder patients: a cohort analysis," *PloS One*, vol. 3, no. 11, article e3815, 2008.
- [18] W. D. Graf, J. Marin-Garcia, H. G. Gao et al., "Autism associated with the mitochondrial DNA G8363A transfer RNA(Lys) mutation," *Journal of Child Neurology*, vol. 15, no. 6, pp. 357–361, 2000.
- [19] J. J. Fillano, M. J. Goldenthal, C. H. Rhodes, and J. Marin-García, "Mitochondrial dysfunction in patients with hypotonia, epilepsy, autism, and developmental delay: HEADD syndrome," *Journal of Child Neurology*, vol. 17, no. 6, pp. 435–439, 2002.
- [20] P. A. Filipek, J. Juranek, M. Smith et al., "Mitochondrial dysfunction in autistic patients with 15q inverted duplication," *Annals of Neurology*, vol. 53, no. 6, pp. 801–804, 2003.
- [21] R. Pons, A. L. Andreu, N. Checcarelli et al., "Mitochondrial DNA abnormalities and autistic spectrum disorders," *The Journal of Pediatrics*, vol. 144, no. 1, pp. 81–85, 2004.
- [22] J. Shoffner, L. Hyams, G. N. Langley et al., "Fever plus mitochondrial disease could be risk factors for autistic regression," *Journal of Child Neurology*, vol. 25, no. 4, pp. 429–434, 2010.
- [23] C. Giulivi, Y. F. Zhang, A. Omanska-Klusek et al., "Mitochondrial dysfunction in autism," *Jama*, vol. 304, no. 21, pp. 2389–2396, 2010.
- [24] H. Ezugha, M. Goldenthal, I. Valencia, C. E. Anderson, A. Legido, and H. Marks, "5q14.3 deletion manifesting as mitochondrial disease and autism: case report," *Journal of Child Neurology*, vol. 25, no. 10, pp. 1232–1235, 2010.
- [25] J. Guevara-Campos, L. González-Guevara, P. Briones et al., "Autism associated to a deficiency of complexes III and IV of the mitochondrial respiratory chain," *Investigacion Clinica*, vol. 51, no. 3, pp. 423–431, 2010.
- [26] J. Guevara-Campos, L. González-Guevara, and O. Cauli, "Autism and intellectual disability associated with mitochondrial disease and hyperlactacidemia," *International Journal of Molecular Sciences*, vol. 16, no. 2, pp. 3870–3884, 2015.
- [27] J. Guevara-Campos, L. González-Guevara, C. Puig-Alcaraz, and O. Cauli, "Autism spectrum disorders associated to a deficiency of the enzymes of the mitochondrial respiratory chain," *Metabolic Brain Disease*, vol. 28, no. 4, pp. 605–612, 2013.
- [28] M. J. Goldenthal, S. Damle, S. Sheth et al., "Mitochondrial enzyme dysfunction in autism spectrum disorders; a novel biomarker revealed from buccal swab analysis," *Biomarkers in Medicine*, vol. 9, no. 10, pp. 957–965, 2015.
- [29] A. Chauhan, F. Gu, M. M. Essa et al., "Brain region-specific deficit in mitochondrial electron transport chain complexes in children with autism," *Journal of Neurochemistry*, vol. 117, no. 2, pp. 209–220, 2011.
- [30] F. Gu, V. Chauhan, K. Kaur et al., "Alterations in mitochondrial DNA copy number and the activities of electron transport chain complexes and pyruvate dehydrogenase in the frontal cortex with subjects with autism," *Translational Psychiatry*, vol. 3, no. 2, article e299, 2013.
- [31] G. Tang, P. Gutierrez Rios, S. H. Kuo et al., "Mitochondrial abnormalities in temporal lobe of autistic brain," *Neurobiology of Disease*, vol. 54, pp. 349–361, 2013.
- [32] A. Anitha, K. Nakamura, I. Thanseem et al., "Downregulation of the expression of mitochondrial electron transport complex genes in autism brains," *Brain Pathology (Zurich, Switzerland)*, vol. 23, no. 3, pp. 294–302, 2013.
- [33] A. Anitha, K. Nakamura, I. Thanseem et al., "Brain region-specific altered expression and association of mitochondria-related genes in autism," *Molecular Autism*, vol. 3, no. 1, p. 2, 2012.
- [34] T. C. Ford and D. P. Crewther, "A comprehensive review of the (1)H-MRS metabolite Spectrum in autism Spectrum disorder," *Frontiers in Molecular Neuroscience*, vol. 9, p. 14, 2016.
- [35] N. J. Minshew, G. Goldstein, S. M. Dombrowski, K. Panchalingam, and J. W. Pettegrew, "A preliminary 31P MRS study of autism: evidence for undersynthesis and increased degradation of brain membranes," *Biological Psychiatry*, vol. 33, no. 11–12, pp. 762–773, 1993.
- [36] N. M. Corrigan, D. W. Shaw, A. M. Estes et al., "Atypical developmental patterns of brain chemistry in children with autism spectrum disorder," *JAMA Psychiatry*, vol. 70, no. 9, pp. 964–974, 2013.
- [37] S. D. Friedman, D. W. Shaw, A. A. Artru et al., "Regional brain chemical alterations in young children with autism spectrum disorder," *Neurology*, vol. 60, no. 1, pp. 100–107, 2003.
- [38] J. G. Levitt, J. O'Neill, R. E. Blanton et al., "Proton magnetic resonance spectroscopic imaging of the brain in childhood autism," *Biological Psychiatry*, vol. 54, no. 12, pp. 1355–1366, 2003.
- [39] A. Y. Hardan, N. J. Minshew, N. M. Melhem et al., "An MRI and proton spectroscopy study of the thalamus in children with autism," *Psychiatry Research*, vol. 163, no. 2, pp. 97–105, 2008.
- [40] T. J. DeVito, D. J. Drost, R. W. Neufeld et al., "Evidence for cortical dysfunction in autism: a proton magnetic resonance spectroscopic imaging study," *Biological Psychiatry*, vol. 61, no. 4, pp. 465–473, 2007.
- [41] D. C. Chugani, B. S. Sundram, M. Behen, M. L. Lee, and G. J. Moore, "Evidence of altered energy metabolism in autistic children," *Progress in Neuro-Psychopharmacology & Biological Psychiatry*, vol. 23, no. 4, pp. 635–641, 1999.

- [42] A. Goji, H. Ito, K. Mori et al., "Assessment of anterior cingulate cortex (ACC) and left cerebellar metabolism in Asperger's syndrome with proton magnetic resonance spectroscopy (MRS)," *PLoS One*, vol. 12, no. 1, article e0169288, 2017.
- [43] Y. Aoki, K. Kasai, and H. Yamasue, "Age-related change in brain metabolite abnormalities in autism: a meta-analysis of proton magnetic resonance spectroscopy studies," *Translational Psychiatry*, vol. 2, no. 1, article e69, 2012.
- [44] R. W. Taylor and D. M. Turnbull, "Mitochondrial DNA mutations in human disease," *Nature Reviews. Genetics*, vol. 6, no. 5, pp. 389–402, 2005.
- [45] D. C. Wallace and D. Chalkia, "Mitochondrial DNA genetics and the heteroplasmy conundrum in evolution and disease," *Cold Spring Harbor Perspectives in Biology*, vol. 5, no. 11, p. a021220, 2013.
- [46] R. K. Naviaux, "Developing a systematic approach to the diagnosis and classification of mitochondrial disease," *Mitochondrion*, vol. 4, no. 5-6, pp. 351–361, 2004.
- [47] C. M. Sue, C. Bruno, A. L. Andreu et al., "Infantile encephalopathy associated with the MELAS A3243G mutation," *The Journal of Pediatrics*, vol. 134, no. 6, pp. 696–700, 1999.
- [48] L. Levinger, R. Giegé, and C. Florentz, "Pathology-related substitutions in human mitochondrial tRNA(Ile) reduce precursor 3' end processing efficiency in vitro," *Nucleic Acids Research*, vol. 31, no. 7, pp. 1904–1912, 2003.
- [49] A. Vanniarajan, G. P. Rajshanker, M. B. Joshi, A. G. Reddy, L. Singh, and K. Thangaraj, "Novel mitochondrial mutation in the ND4 gene associated with Leigh syndrome," *Acta Neurologica Scandinavica*, vol. 114, no. 5, pp. 350–353, 2006.
- [50] E. Napoli, S. Wong, and C. Giulivi, "Evidence of reactive oxygen species-mediated damage to mitochondrial DNA in children with typical autism," *Molecular Autism*, vol. 4, no. 1, p. 2, 2013.
- [51] Y. Wang, M. Picard, and Z. Gu, "Genetic evidence for elevated pathogenicity of mitochondrial DNA Heteroplasmy in autism Spectrum disorder," *PLoS Genetics*, vol. 12, no. 10, article e1006391, 2016.
- [52] A. Hadjixenofontos, M. A. Schmidt, P. L. Whitehead et al., "Evaluating mitochondrial DNA variation in autism spectrum disorders," *Annals of Human Genetics*, vol. 77, no. 1, pp. 9–21, 2013.
- [53] N. Ramoz, J. G. Reichert, C. J. Smith et al., "Linkage and association of the mitochondrial aspartate/glutamate carrier SLC25A12 gene with autism," *The American Journal of Psychiatry*, vol. 161, no. 4, pp. 662–669, 2004.
- [54] A. M. Lepagnol-Bestel, G. Maussion, B. Boda et al., "SLC25A12 expression is associated with neurite outgrowth and is upregulated in the prefrontal cortex of autistic subjects," *Molecular Psychiatry*, vol. 13, no. 4, pp. 385–397, 2008.
- [55] R. Segurado, J. Conroy, E. Meally, M. Fitzgerald, M. Gill, and L. Gallagher, "Confirmation of association between autism and the mitochondrial aspartate/glutamate carrier SLC25A12 gene on chromosome 2q31," *The American Journal of Psychiatry*, vol. 162, no. 11, pp. 2182–2184, 2005.
- [56] J. M. Silverman, J. D. Buxbaum, N. Ramoz et al., "Autism-related routines and rituals associated with a mitochondrial aspartate/glutamate carrier SLC25A12 polymorphism," *American Journal of Medical Genetics. Part B, Neuropsychiatric Genetics*, vol. 147, no. 3, pp. 408–410, 2008.
- [57] C. Correia, A. M. Coutinho, L. Diogo et al., "Brief report: high frequency of biochemical markers for mitochondrial dysfunction in autism: no association with the mitochondrial aspartate/glutamate carrier SLC25A12 gene," *Journal of Autism and Developmental Disorders*, vol. 36, no. 8, pp. 1137–1140, 2006.
- [58] W. H. Chien, Y. Y. Wu, S. S. Gau et al., "Association study of the SLC25A12 gene and autism in Han Chinese in Taiwan," *Progress in Neuro-Psychopharmacology & Biological Psychiatry*, vol. 34, no. 1, pp. 189–192, 2010.
- [59] T. Marui, I. Funatogawa, S. Koishi et al., "The NADH-ubiquinone oxidoreductase 1 alpha subcomplex 5 (NDUFA5) gene variants are associated with autism," *Acta Psychiatrica Scandinavica*, vol. 123, no. 2, pp. 118–124, 2011.
- [60] K. Tensing, I. Pata, I. Wittig, M. Wehnert, and A. Metspalu, "Genomic organization of the human complex I 13-kDa subunit gene NDUFA5," *Cytogenetics and Cell Genetics*, vol. 84, no. 1-2, pp. 125–127, 1999.
- [61] R. E. Frye and D. A. Rossignol, "Mitochondrial dysfunction can connect the diverse medical symptoms associated with autism spectrum disorders," *Pediatric Research*, vol. 69, no. 5 Part 2, pp. 41R–47R, 2011.
- [62] D. A. Rossignol and R. E. Frye, "Evidence linking oxidative stress, mitochondrial dysfunction, and inflammation in the brain of individuals with autism," *Frontiers in Physiology*, vol. 5, p. 150, 2014.
- [63] J. F. Turrens, "Mitochondrial formation of reactive oxygen species," *The Journal of Physiology*, vol. 552, no. Part 2, pp. 335–344, 2003.
- [64] R. S. Balaban, S. Nemoto, and T. Finkel, "Mitochondria, oxidants, and aging," *Cell*, vol. 120, no. 4, pp. 483–495, 2005.
- [65] V. Adam-Vizi and C. Chinopoulos, "Bioenergetics and the formation of mitochondrial reactive oxygen species," *Trends in Pharmacological Sciences*, vol. 27, no. 12, pp. 639–645, 2006.
- [66] W. Dröge, "Free radicals in the physiological control of cell function," *Physiological Reviews*, vol. 82, no. 1, pp. 47–95, 2002.
- [67] M. P. Murphy, "How mitochondria produce reactive oxygen species," *Biochemical Journal*, vol. 417, no. 1, pp. 1–13, 2009.
- [68] X. Chen, C. Guo, and J. Kong, "Oxidative stress in neurodegenerative diseases," *Neural Regeneration Research*, vol. 7, no. 5, pp. 376–385, 2012.
- [69] R. A. Weisiger and I. Fridovich, "Mitochondrial superoxide simutase. Site of synthesis and intramitochondrial localization," *The Journal of Biological Chemistry*, vol. 248, no. 13, pp. 4793–4796, 1973.
- [70] V. C. Culotta, M. Yang, and T. V. O'Halloran, "Activation of superoxide dismutases: putting the metal to the pedal," *Biochimica et Biophysica Acta*, vol. 1763, no. 7, pp. 747–758, 2006.
- [71] D. B. Zorov, M. Juhaszova, and S. J. Sollott, "Mitochondrial reactive oxygen species (ROS) and ROS-induced ROS release," *Physiological Reviews*, vol. 94, no. 3, pp. 909–950, 2014.
- [72] C. Guo, L. Sun, X. Chen, and D. Zhang, "Oxidative stress, mitochondrial damage and neurodegenerative diseases," *Neural Regeneration Research*, vol. 8, no. 21, pp. 2003–2014, 2013.
- [73] S. Melnyk, G. J. Fuchs, E. Schulz et al., "Metabolic imbalance associated with methylation dysregulation and oxidative damage in children with autism," *Journal of Autism and Developmental Disorders*, vol. 42, no. 3, pp. 367–377, 2012.

- [74] S. J. James, P. Cutler, S. Melnyk et al., "Metabolic biomarkers of increased oxidative stress and impaired methylation capacity in children with autism," *The American Journal of Clinical Nutrition*, vol. 80, no. 6, pp. 1611–1617, 2004.
- [75] X. Ming, T. P. Stein, M. Brimacombe, W. G. Johnson, G. H. Lambert, and G. C. Wagner, "Increased excretion of a lipid peroxidation biomarker in autism," *Prostaglandins, Leukotrienes, and Essential Fatty Acids*, vol. 73, no. 5, pp. 379–384, 2005.
- [76] Y. Yao, W. J. Walsh, M. G. WR, and D. Praticò, "Altered vascular phenotype in autism: correlation with oxidative stress," *Archives of Neurology*, vol. 63, no. 8, pp. 1161–1164, 2006.
- [77] Y. Al-Gadani, A. El-Ansary, O. Attas, and L. Al-Ayadhi, "Metabolic biomarkers related to oxidative stress and antioxidant status in Saudi autistic children," *Clinical Biochemistry*, vol. 42, no. 10–11, pp. 1032–1040, 2009.
- [78] O. Yorbik, A. Sayal, C. Akay, D. I. Akbiyik, and T. Sohmen, "Investigation of antioxidant enzymes in children with autistic disorder," *Prostaglandins, Leukotrienes, and Essential Fatty Acids*, vol. 67, no. 5, pp. 341–343, 2002.
- [79] A. Chauhan and V. Chauhan, "Oxidative stress in autism," *Pathophysiology*, vol. 13, no. 3, pp. 171–181, 2006.
- [80] F. Gu, V. Chauhan, and A. Chauhan, "Impaired synthesis and antioxidant defense of glutathione in the cerebellum of autistic subjects: alterations in the activities and protein expression of glutathione-related enzymes," *Free Radical Biology & Medicine*, vol. 65, pp. 488–496, 2013.
- [81] A. Chauhan, T. Audhya, and V. Chauhan, "Brain region-specific glutathione redox imbalance in autism," *Neurochemical Research*, vol. 37, no. 8, pp. 1681–1689, 2012.
- [82] S. Rose, S. Melnyk, T. A. Trusty et al., "Intracellular and extracellular redox status and free radical generation in primary immune cells from children with autism," *Autism Research and Treatment*, vol. 2012, Article ID 986519, p. 10, 2012.
- [83] E. Lopez-Hurtado and J. J. Prieto, "A microscopic study of language-related cortex in autism," *American Journal of Biochemistry and Biotechnology*, vol. 4, no. 2, pp. 130–145, 2008.
- [84] T. A. Evans, S. L. Siedlak, L. Lu et al., "The autistic phenotype exhibits a remarkably localized modification of brain protein by products of free radical-induced lipid oxidation," *American Journal of Biochemistry and Biotechnology*, vol. 4, no. 2, pp. 61–72, 2008.
- [85] E. M. Sajdel-Sulkowska, B. Lipinski, H. Windom, T. Audhya, and W. McGinnis, "Oxidative stress in autism: elevated cerebellar 3-nitrotyrosine levels," *American Journal of Biochemistry and Biotechnology*, vol. 4, no. 2, pp. 73–84, 2008.
- [86] E. M. Sajdel-Sulkowska, M. Xu, W. McGinnis, and N. Koibuchi, "Brain region-specific changes in oxidative stress and neurotrophin levels in autism spectrum disorders (ASD)," *Cerebellum (London, England)*, vol. 10, no. 1, pp. 43–48, 2011.
- [87] S. Rose, S. Melnyk, O. Pavliv et al., "Evidence of oxidative damage and inflammation associated with low glutathione redox status in the autism brain," *Translational Psychiatry*, vol. 2, no. 7, article e134, 2012.
- [88] W. W. Chen, X. Zhang, and W. J. Huang, "Role of neuroinflammation in neurodegenerative diseases (review)," *Molecular Medicine Reports*, vol. 13, no. 4, pp. 3391–3396, 2016.
- [89] E. G. Stubbs and M. L. Crawford, "Depressed lymphocyte responsiveness in autistic children," *Journal of Autism and Childhood Schizophrenia*, vol. 7, no. 1, pp. 49–55, 1977.
- [90] R. P. Warren, A. Foster, and N. C. Margaretten, "Reduced natural killer cell activity in autism," *Journal of the American Academy of Child and Adolescent Psychiatry*, vol. 26, no. 3, pp. 333–335, 1987.
- [91] R. P. Warren, N. C. Margaretten, N. C. Pace, and A. Foster, "Immune abnormalities in patients with autism," *Journal of Autism and Developmental Disorders*, vol. 16, no. 2, pp. 189–197, 1986.
- [92] C. Onore, M. Careaga, and P. Ashwood, "The role of immune dysfunction in the pathophysiology of autism," *Brain, Behavior, and Immunity*, vol. 26, no. 3, pp. 383–392, 2012.
- [93] G. Bjorklund, K. Saad, S. Chirumbolo et al., "Immune dysfunction and neuroinflammation in autism spectrum disorder," *Acta Neurobiologiae Experimentalis*, vol. 76, no. 4, pp. 257–268, 2016.
- [94] M. Malik, A. M. Sheikh, G. Wen, W. Spivack, W. T. Brown, and X. Li, "Expression of inflammatory cytokines, Bcl2 and cathepsin D are altered in lymphoblasts of autistic subjects," *Immunobiology*, vol. 216, no. 1–2, pp. 80–85, 2011.
- [95] M. W. Abdallah, N. Larsen, J. Grove et al., "Amniotic fluid inflammatory cytokines: potential markers of immunologic dysfunction in autism spectrum disorders," *The World Journal of Biological Psychiatry*, vol. 14, no. 7, pp. 528–538, 2013.
- [96] M. G. Chez, T. Dowling, P. B. Patel, P. Khanna, and M. Kominsky, "Elevation of tumor necrosis factor-alpha in cerebrospinal fluid of autistic children," *Pediatric Neurology*, vol. 36, no. 6, pp. 361–365, 2007.
- [97] X. Li, A. Chauhan, A. M. Sheikh et al., "Elevated immune response in the brain of autistic patients," *Journal of Neuroimmunology*, vol. 207, no. 1–2, pp. 111–116, 2009.
- [98] H. Wei, H. Zou, A. M. Sheikh et al., "IL-6 is increased in the cerebellum of autistic brain and alters neural cell adhesion, migration and synaptic formation," *Journal of Neuroinflammation*, vol. 8, no. 1, p. 52, 2011.
- [99] D. L. Vargas, C. Nascimbene, C. Krishnan, A. W. Zimmerman, and C. A. Pardo, "Neuroglial activation and neuroinflammation in the brain of patients with autism," *Annals of Neurology*, vol. 57, no. 1, pp. 67–81, 2005.
- [100] L. Y. Al-ayadhi and G. A. Mostafa, "Increased serum osteopontin levels in autistic children: relation to the disease severity," *Brain, Behavior, and Immunity*, vol. 25, no. 7, pp. 1393–1398, 2011.
- [101] L. Y. Al-Ayadhi and G. A. Mostafa, "Elevated serum levels of macrophage-derived chemokine and thymus and activation-regulated chemokine in autistic children," *Journal of Neuroinflammation*, vol. 10, no. 1, p. 72, 2013.
- [102] K. Suzuki, G. Sugihara, Y. Ouchi et al., "Microglial activation in young adults with autism spectrum disorder," *JAMA Psychiatry*, vol. 70, no. 1, pp. 49–58, 2013.
- [103] J. T. Morgan, G. Chana, C. A. Pardo et al., "Microglial activation and increased microglial density observed in the dorsolateral prefrontal cortex in autism," *Biological Psychiatry*, vol. 68, no. 4, pp. 368–376, 2010.
- [104] M. Monlun, C. Hyernard, P. Blanco, L. Lartigue, and B. Faustin, "Mitochondria as molecular platforms integrating multiple innate immune Signalings," *Journal of Molecular Biology*, vol. 429, no. 1, pp. 1–13, 2017.
- [105] M. Brini, T. Cali, D. Ottolini, and E. Carafoli, "Intracellular calcium homeostasis and signaling," *Metal Ions in Life Sciences*, vol. 12, pp. 119–168, 2013.

- [106] D. E. Clapham, "Calcium signaling," *Cell*, vol. 80, no. 2, pp. 259–268, 1995.
- [107] T. Pozzan, R. Rizzuto, P. Volpe, and J. Meldolesi, "Molecular and cellular physiology of intracellular calcium stores," *Physiological Reviews*, vol. 74, no. 3, pp. 595–636, 1994.
- [108] F. Celsi, P. Pizzo, M. Brini et al., "Mitochondria, calcium and cell death: a deadly triad in neurodegeneration," *Biochimica et Biophysica Acta*, vol. 1787, no. 5, pp. 335–344, 2009.
- [109] M. V. Ivannikov and G. T. Macleod, "Mitochondrial free Ca^{2+} levels and their effects on energy metabolism in drosophila motor nerve terminals," *Biophysical Journal*, vol. 104, no. 11, pp. 2353–2361, 2013.
- [110] S. Orrenius, B. Zhivotovsky, and P. Nicotera, "Regulation of cell death: the calcium-apoptosis link," *Nature Reviews. Molecular Cell Biology*, vol. 4, no. 7, pp. 552–565, 2003.
- [111] D. Lindberg, D. Shan, J. Ayers-Ringler et al., "Purinergic signaling and energy homeostasis in psychiatric disorders," *Current Molecular Medicine*, vol. 15, no. 3, pp. 275–295, 2015.
- [112] J. F. Krey and R. E. Dolmetsch, "Molecular mechanisms of autism: a possible role for Ca^{2+} signaling," *Current Opinion in Neurobiology*, vol. 17, no. 1, pp. 112–119, 2007.
- [113] M. P. Anderson, B. S. Hooker, and M. R. Herbert, "Bridging from cells to cognition in autism pathophysiology: biological pathways to defective brain function and plasticity," *American Journal of Biochemistry and Biotechnology*, vol. 4, no. 2, pp. 167–176, 2008.
- [114] J. L. Rubenstein and M. M. Merzenich, "Model of autism: increased ratio of excitation/inhibition in key neural systems," *Genes, Brain, and Behavior*, vol. 2, no. 5, pp. 255–267, 2003.
- [115] V. Napolioni, A. M. Persico, V. Porcelli, and L. Palmieri, "The mitochondrial aspartate/glutamate carrier AGC1 and calcium homeostasis: physiological links and abnormalities in autism," *Molecular Neurobiology*, vol. 44, no. 1, pp. 83–92, 2011.
- [116] L. Palmieri, V. Papaleo, V. Porcelli et al., "Altered calcium homeostasis in autism-spectrum disorders: evidence from biochemical and genetic studies of the mitochondrial aspartate/glutamate carrier AGC1," *Molecular Psychiatry*, vol. 15, no. 1, pp. 38–52, 2010.
- [117] R. E. Frye and D. A. Rossignol, "Treatments for biomedical abnormalities associated with autism spectrum disorder," *Frontiers in Pediatrics*, vol. 2, p. 66, 2014.
- [118] B. Reichow, E. E. Barton, B. A. Boyd, and K. Hume, "Early intensive behavioral intervention (EIBI) for young children with autism spectrum disorders (ASD)," *The Cochrane Database of Systematic Reviews*, vol. 10, no. CD009260, 2012.
- [119] R. E. Frye and D. A. Rossignol, "Identification and treatment of pathophysiological comorbidities of autism Spectrum disorder to achieve optimal outcomes," *Clinical Medicine Insights. Pediatrics*, vol. 10, pp. 43–56, 2016.
- [120] D. A. Geier, J. K. Kern, G. Davis et al., "A prospective double-blind, randomized clinical trial of levocarnitine to treat autism spectrum disorders," *Medical Science Monitor*, vol. 17, no. 6, pp. PI15–PI23, 2011.
- [121] S. F. Fahmy, M. H. El-hamamsy, O. K. Zaki, and O. A. Badary, "L-carnitine supplementation improves the behavioral symptoms in autistic children," *Research in Autism Spectrum Disorders*, vol. 7, no. 1, pp. 159–166, 2013.
- [122] A. Y. Hardan, L. K. Fung, R. A. Libove et al., "A randomized controlled pilot trial of oral N-acetylcysteine in children with autism," *Biological Psychiatry*, vol. 71, no. 11, pp. 956–961, 2012.
- [123] A. Ghanizadeh and E. Moghimi-Sarani, "A randomized double blind placebo controlled clinical trial of N-acetylcysteine added to risperidone for treating autistic disorders," *BMC Psychiatry*, vol. 13, no. 1, p. 196, 2013.
- [124] M. G. Chez, C. P. Buchanan, M. C. Aimonovitch et al., "Double-blind, placebo-controlled study of L-carnosine supplementation in children with autistic spectrum disorders," *Journal of Child Neurology*, vol. 17, no. 11, pp. 833–837, 2002.
- [125] M. C. Dolske, J. Spollen, S. McKay, E. Lancashire, and L. Tolbert, "A preliminary trial of ascorbic acid as supplemental therapy for autism," *Progress in Neuro-Psychopharmacology & Biological Psychiatry*, vol. 17, no. 5, pp. 765–774, 1993.
- [126] J. B. Adams, T. Audhya, S. McDonough-Means et al., "Effect of a vitamin/mineral supplement on children and adults with autism," *BMC Pediatrics*, vol. 11, no. 1, p. 111, 2011.
- [127] J. B. Adams and C. Holloway, "Pilot study of a moderate dose multivitamin/mineral supplement for children with autistic spectrum disorder," *Journal of Alternative and Complementary Medicine (New York, N.Y.)*, vol. 10, no. 6, pp. 1033–1039, 2004.
- [128] R. E. Frye, S. Melnyk, G. Fuchs et al., "Effectiveness of methylcobalamin and folic acid treatment on adaptive behavior in children with autistic disorder is related to glutathione redox status," *Autism Res Treat*, vol. 2013, Article ID 609705, p. 9, 2013.
- [129] S. J. James, S. Melnyk, G. Fuchs et al., "Efficacy of methylcobalamin and folic acid treatment on glutathione redox status in children with autism," *The American Journal of Clinical Nutrition*, vol. 89, no. 1, pp. 425–430, 2009.
- [130] K. Singh, S. L. Connors, E. A. Macklin et al., "Sulforaphane treatment of autism spectrum disorder (ASD)," *Proceedings of the National Academy of Sciences of the United States of America*, vol. 111, no. 43, pp. 15550–15555, 2014.
- [131] A. Taliou, E. Zintzaras, L. Lykouras, and K. Francis, "An open-label pilot study of a formulation containing the anti-inflammatory flavonoid luteolin and its effects on behavior in children with autism spectrum disorders," *Clinical Therapeutics*, vol. 35, no. 5, pp. 592–602, 2013.
- [132] R. Obeid, A. McCaddon, and W. Herrmann, "The role of hyperhomocysteinemia and B-vitamin deficiency in neurological and psychiatric diseases," *Clinical Chemistry and Laboratory Medicine*, vol. 45, no. 12, pp. 1590–1606, 2007.
- [133] A. Desai, J. M. Sequeira, and E. V. Quadros, "The metabolic basis for developmental disorders due to defective folate transport," *Biochimie*, vol. 126, pp. 31–42, 2016.
- [134] R. E. Frye, J. M. Sequeira, E. V. Quadros, S. J. James, and D. A. Rossignol, "Cerebral folate receptor autoantibodies in autism spectrum disorder," *Molecular Psychiatry*, vol. 18, no. 3, pp. 369–381, 2013.
- [135] P. Moretti, T. Sahoo, K. Hyland et al., "Cerebral folate deficiency with developmental delay, autism, and response to folic acid," *Neurology*, vol. 64, no. 6, pp. 1088–1090, 2005.
- [136] V. T. Ramaekers, N. Blau, J. M. Sequeira, M. C. Nassogne, and E. V. Quadros, "Folate receptor autoimmunity and cerebral folate deficiency in low-functioning autism with neurological deficits," *Neuropediatrics*, vol. 38, no. 6, pp. 276–281, 2007.
- [137] V. T. Ramaekers, S. P. Rothenberg, J. M. Sequeira et al., "Autoantibodies to folate receptors in the cerebral folate deficiency syndrome," *The New England Journal of Medicine*, vol. 352, no. 19, pp. 1985–1991, 2005.

Review Article

Mitophagy Transcriptome: Mechanistic Insights into Polyphenol-Mediated Mitophagy

Sijie Tan and Esther Wong

School of Biological Sciences, Nanyang Technological University, Singapore

Correspondence should be addressed to Esther Wong; estherwong@ntu.edu.sg

Received 19 March 2017; Accepted 26 April 2017; Published 25 May 2017

Academic Editor: Moh H. Malek

Copyright © 2017 Sijie Tan and Esther Wong. This is an open access article distributed under the Creative Commons Attribution License, which permits unrestricted use, distribution, and reproduction in any medium, provided the original work is properly cited.

Mitochondria are important bioenergetic and signalling hubs critical for myriad cellular functions and homeostasis. Dysfunction in mitochondria is a central theme in aging and diseases. Mitophagy, a process whereby damaged mitochondria are selectively removed by autophagy, plays a key homeostatic role in mitochondrial quality control. Upregulation of mitophagy has shown to mitigate superfluous mitochondrial accumulation and toxicity to safeguard mitochondrial fitness. Hence, mitophagy is a viable target to promote longevity and prevent age-related pathologies. Current challenge in modulating mitophagy for cellular protection involves identification of physiological ways to activate the pathway. Till date, mitochondrial stress and toxins remain the most potent inducers of mitophagy. Polyphenols have recently been demonstrated to protect mitochondrial health by facilitating mitophagy, thus suggesting the exciting prospect of augmenting mitophagy through dietary intake. In this review, we will first discuss the different surveillance mechanisms responsible for the removal of damaged mitochondrial components, followed by highlighting the transcriptional regulatory mechanisms of mitophagy. Finally, we will review the functional connection between polyphenols and mitophagy and provide insight into the underlying mechanisms that potentially govern polyphenol-induced mitophagy.

1. Introduction

Mitochondria are energy-generating organelles that synthesize adenosine triphosphate (ATP) to support various cellular activities. Numerous recent studies further advocate an expanded role of the organelle in regulating plethora signalling pathways for cellular survival and homeostasis [1–3]. Mitochondria are also the principal sites of reactive oxygen species (ROS) production inside the cells. Cytosolic ROS need to be tightly regulated to prevent cellular redox imbalance that contributes to the cumulative oxidative damage of macromolecules observed in aging and diseases [4]. Mitochondrial health is a key determinant to the level of ROS produced by the mitochondria. Compromised mitochondrial fitness diminishes cellular bioenergetics, disrupts signalling events, and heightens ROS production [5]. The pivotal roles of mitochondria in various cellular processes highlight the importance of maintaining healthy mitochondrial populations to ensure cellular functions and survival.

Mitophagy plays an instrumental role in influencing mitochondrial health and quality control by eliminating damaged mitochondria in the lysosomes [6–8]. Defects in mitophagy result in accumulation of dysfunctional mitochondria seen in aging and age-related disorders [9–11]. Conversely, upregulation of mitophagy successfully ameliorates mitochondrial dysfunction and cell toxicity in diseases like diabetes mellitus (DM) and Parkinson's disease [12, 13]. Most significantly, enhanced mitophagy activity extends lifespan and healthspan in *Caenorhabditis elegans* (*C. elegans*) and mouse models [14–17]. Currently, mitophagy activity is mainly known to be induced by mitochondrial stress while knowledge of physiological ways to regulate mitophagy lacks behind. A few recent studies indicate that the master transcriptional factors that regulate the expression of autophagy and lysosomal genes can be specifically induced by mitochondrial stress to orchestrate expansion of autophagy-lysosomal fitness to perform mitophagy [18–22]. These transcription factors include forkhead transcription factor (FOXO) and

transcription factor EB (TFEB) [18–23], which serve as potential therapeutic targets for modulating mitophagy.

Modulation of dietary intake via the consumption of polyphenol-enriched functional food has been widely researched as a health-promoting measure associated with longevity [24]. Multiple lines of evidence suggest that the beneficial effects of polyphenols, in part, can be attributed to its ability to upregulate mitophagy [25, 26]. Notably, recent studies support a role of polyphenols in influencing the transcriptional regulation of autophagy via the FOXO and TFEB signalling axes to upregulate mitophagy [27–30]. These studies demonstrate that polyphenols modulate mitophagy transcriptome as part of its protective mechanisms to counteract mitochondrial stress [31–33], further strengthening the attractiveness of polyphenols as a therapy for mitochondrial-related pathologies and aging.

In this review, we look at the different surveillance mechanisms involved in the removal of damaged mitochondrial contents, with specific focus on the transcriptional regulation of mitophagy in response to mitochondrial stress. We will also review the functional connection between polyphenols and mitophagy. Based on these reported findings, we propose a mechanistic model by which the intracellular environment senses the administration of polyphenols, to transcriptionally upregulate autophagy and mitophagy genes expression to enhance mitophagy for cellular protection.

2. Mitochondrial Quality Control: Different Types of Mitophagy

Besides generating ATP via oxidative phosphorylation to fuel all energy-consuming processes, mitochondria also participate in myriad cellular processes such as ion homeostasis, oxygen sensing, apoptosis, and specification of cell fate in adult and cancer stem cells [2, 3, 34, 35]. Mitochondria are also the prime sites of endogenous ROS production. Mitochondrial health determines the levels of mitochondrial ROS produced. While low amounts of ROS generated by redox competent mitochondria serve important signalling functions, excessive ROS production by dysfunctional mitochondria causes oxidative stress and damage [3, 4]. Safeguarding mitochondrial functions and integrity is, thus, of utmost importance to cell survival.

Mitochondrial homeostasis is complex, and its regulation includes several aspects: mitochondrial dynamics, biogenesis, and the timely removal of worn-out portions [36–41]. Mitochondria undergo continuous fission and fusion events that allow the organelle to alter its shape and size. Such plasticity permits quick adaptation of mitochondrial functions in response to intracellular and extracellular cues [2]. Mitochondrial fission and fusion are also involved in mitochondrial biogenesis and clearance, and the interplay of these processes ensures constant mitochondrial renewal [2]. Deregulation of these processes underlies mitochondrial-related disorders, highlighting the therapeutic prospect of treating human diseases by manipulating mitochondrial biology [42].

Recent insights into mitochondrial quality control via organelle turnover revolutionized our understanding of

how a cell vigorously protects itself from dysfunctional mitochondria through multiple defense mechanisms [6–8]. Cells can eliminate different types of damaged mitochondrial contents to cope with varying degrees of mitochondrial stress. During mild mitochondrial stress, such as when mitochondrial proteostasis is perturbed by deranged expression, impaired import, misfolding, or aggregation of mitochondrial proteins, mitochondrial unfolded protein response (UPR^{mt}) serves as the first line of mitochondrial quality control [36–38]. UPR^{mt} resolves proteotoxicity in mitochondria by activating a transcriptional response to promote folding, limit import, reduce translation, and enhance degradation of deleterious mitochondrial proteins [36–38]. Mild oxidative stress that inhibits the respiratory chain without causing mitochondrial membrane depolarization leads to the selective incorporation of oxidized mitochondrial proteins into mitochondrial-derived vesicles (MDVs). These MDVs are then delivered to the lysosomes for degradation [43]. This form of mitochondrial component self-eating is independent of autophagy. Instead, the MDVs are engulfed by multivesicular bodies that will subsequently fuse with the lysosomes [8].

In the event of severe oxidative stress leading to global mitochondrial damage due to mitochondrial depolarization, sequestration of individual damaged mitochondria into autophagosomes is activated for targeted disposal via the autophagy-lysosomal pathway [6–8]. This form of selective removal of dysfunctional mitochondria by autophagy is known as mitophagy (*mitochondria + autophagy*), which eliminates damaged mitochondria while preserving the integrity of the remaining healthy mitochondria [44]. Hence, mitophagy represents an important quality control pathway to monitor mitochondrial health and homeostasis [6–8]. Besides degradation of damaged mitochondria in cell autonomous manner, recent studies have reported the discovery of a transcellular mitophagy phenomenon in the mice optic nerve head [45, 46]. Unlike classical mitophagy, damaged mitochondria in the retinal ganglion cells are delivered to the neighbouring astrocytes for degradation by mitophagy (Figure 1). The transcellular mitochondrial transfer is facilitated by the release of mitochondria-filled axonal vesicles from the retinal ganglion cells into the extracellular spaces for uptake by the astrocytes. Distinct membrane-enclosed evulsions containing mitochondria were seen in astrocytes proximal to the ganglion axonal projections [45]. Whether this type of mitophagy occurs in other neuronal cell types remains to be elucidated [46]. Nonetheless, the varied sophisticated measures put in place by the cell to maintain mitochondrial quality control highlight the significance of timely and accurate destruction of toxic mitochondrial portions. Mitophagy is currently the best characterized form of mitochondrial quality control. Research into the discovery and understanding of the components and mechanisms of UPR^{mt} and MDVs, although intriguing, are still in its infancy. Hence, in this review, we will focus on mitophagy with regard to polyphenol modulation of mitochondrial quality control.

Mitophagy declines with age, and the impairment in mitochondrial clearance is associated with several human pathologies. This includes age-associated disorders such as

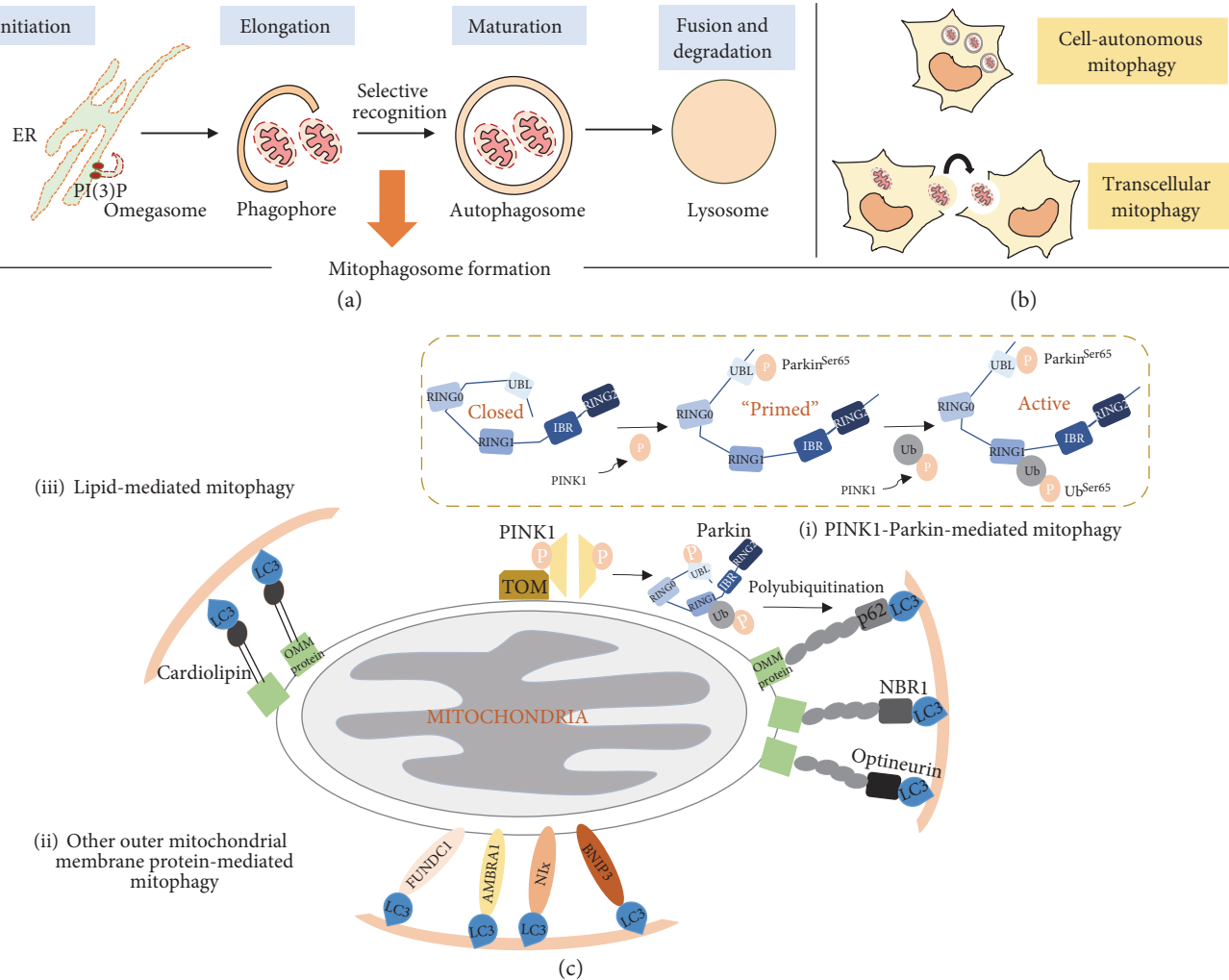


FIGURE 1: Different mechanisms of mitophagy. (a) Autophagy cascade showing initiation of autophagosome membrane formation from endoplasmic reticulum (omegasome), elongation of the early autophagosome membrane (phagophore), engulfment of mitochondria into the matured autophagosome to form mitophagosome, and final fusion with lysosome for degradation. (b) Mitophagy can occur intracellularly (autonomous) or via a transcellular process where damaged mitochondria are exported to neighbouring cell for degradation by mitophagy. (c) (i) The most well-studied mitophagy pathway is mediated by PINK1 and Parkin. Under mitochondrial stress, PINK1 is stabilized on the outer mitochondrial membrane (OMM) where it associates with the TOM complex. Subsequently, PINK1 undergoes dimerization and autophosphorylation to promote recruitment of Parkin to the OMM for its activation. Under physiological conditions, Parkin adopts a closed conformation and is kept inactive due to the association between its UBL and RING1 domain. Mitochondrial membrane depolarization causes PINK1 to phosphorylate Parkin at Ser65 which perturbs the UBL-RING1 association. PINK1 mediates a second phosphorylation event on the ubiquitin (Ub) molecule at Ser65 to fully activate the E3 ligase activity of Parkin through phosphorylated Ub^{Ser65} binding. Activated Parkin ubiquitinates OMM proteins via K27 or K63-linked polyubiquitination to serve as recognition tags to recruit cargo adaptor proteins like p62, NBR1, and optineurin for selective targeting of mitochondria into the autophagosome. OMM proteins can also directly bind phosphorylated Ub^{Ser65} to recruit cargo adaptors. (ii) OMM proteins such as BNIP3, NIX, FUNDC1, and AMBRA1 also possess the LIR motif and can interact directly with LC3 to facilitate selective targeting of the mitochondria to the autophagosome. (iii) Lipid moieties on the OMM can alternatively bind LC3 independent of cargo adaptor proteins. For example, phospholipid cardiolipin has shown to translocate from the inner mitochondrial membrane to the OMM to recruit LC3.

cancer, metabolic syndrome, and neurodegeneration [9, 47–49]. On the other hand, upregulation of mitophagy mitigates disease progression and protects against diseases. This has been demonstrated in DM. Accumulation of advanced glycation end products (AGEs) due to chronic hyperglycaemia induces glycoxidative stress in DM, leading to massive mitochondrial dysfunction. Mitophagy is important in protecting cells from mitochondrial toxicity in DM condition [12].

Indeed, mitophagy induction in diabetic platelets protects it against oxidative stress-induced mitochondrial damage and apoptosis, thereby reducing thrombotic injuries in DM [50]. Mitophagy therefore displays therapeutic potential for treating human diseases. Elucidation of the mechanisms governing mitophagy holds a promise for the development of novel pharmacological interventions to delay aging and to prevent age-related pathologies. Current challenges in

modulating mitophagy for cellular protection include delineating the different variants of mitophagy and identification of more physiological ways to activate mitophagy or individual mitophagy variants. Ironically, mitochondrial toxins such as CCCP, a strong mitochondrial uncoupler, remain the most effective inducer of mitophagy but with accompanying grave mitochondrial damage. There is a clear need to search for drugs or natural compounds that activate mitophagy without incurring such undesirable side effects. Here, we will review the current understandings on natural polyphenolic modulators of mitophagy and their associated benefits and mechanisms.

2.1. Formation of Mitophagosome: When Mitochondria Meet Autophagy. Autophagy is a catabolic process where unwanted or damaged intracellular constituents are engulfed in autophagosomes for delivery to lysosomes for degradation (Figure 1). The degradation pathway consists of four stages: (1) initiation, (2) elongation of the autophagosomal membrane, (3) maturation of the autophagosome, and (4) fusion of the autophagosome with the lysosome [51]. A set of conserved proteins encoded by the autophagy-related (*atg*) genes control the different stages of the autophagy cascade. In yeast, more than 30 *atg* genes have been characterized thus far and the mammalian orthologs have also been subsequently identified [52]. The strong evolutionary conservation of the *atg* genes across lower and higher eukaryotes highlights the critical role of autophagy in the maintenance of cellular homeostasis and survival.

Under physiological conditions, basal autophagy is important for constitutive turnover of proteins and organelles for quality control critical to sustain cellular activities. The functional importance of basal autophagy is highlighted in several studies. For example, brain-specific ablation of the autophagy pathway via *Atg5* and *Atg7* knockouts in mice caused an accumulation of ubiquitinated protein inclusions accompanied by neurodegenerative deficits [53, 54]. Liver-specific inhibition of autophagy led to the development of multiple liver tumors [55], and systemic inhibition of autophagy in mice resulted in neonatal lethality [56]. These studies highlight the importance of basal autophagy as a protective mechanism to prevent accumulation of damaged or redundant cellular constituents and, consequently, the development of diseases in healthy organisms.

In addition to basal autophagy, autophagy can be upregulated as an adaptive response to cope with cellular stress as seen in the case for mitophagy. Stress-inducible autophagy is now increasingly recognized for its selectivity, wherein specific substrates damaged by a particular stressor are targeted for lysosomal degradation while the remaining cellular milieu is preserved [57]. In mitophagy, the selective recognition and precise loading of dysfunctional mitochondria into the autophagosomes to form mitophagosomes underlies the targeted removal of damaged mitochondria (Figure 1). The selectivity of mitophagosomes is facilitated by specialized autophagy receptors known as cargo adaptor proteins. These adaptors contain a microtubule light chain 3- (LC3-) interacting region (LIR) motif that binds LC3 in the autophagosomal membrane, thereby linking the substrate

to the autophagosome. Till date, several cargo adaptors have been identified for mitophagy and this underscores the different mechanisms of mitophagosome formation which we briefly discuss below.

Prior to mitophagy induction, mitochondria undergo fission (or fragmentation) to sieve out the damaged mitochondria from the healthy mitochondrial network for efficient targeting of the former for degradation [58]. The mitochondrial dynamics is regulated by members of the guanosine-5'-triphosphate (GTP)ase family: (1) dynamin-1-like protein (Drp1), which is a fission-promoting protein and (2) mitofusins 1 and 2, which are fusion-promoting proteins. Drp1 mediates fission by forming a multimeric complex around the mitochondria tubule to induce membrane scission and mitochondria excision [59]. Conversely, mitofusins mediate fusion via dimerization with the adjacent mitofusins on the neighbouring mitochondria to promote membrane tethering between mitochondria [60]. Induction of mitophagy promotes ubiquitination and degradation of mitofusins to favour mitochondrial fragmentation for efficient autophagy targeting [61].

2.2. Different Facets of Mitophagosome Formation

2.2.1. PINK1-Parkin-Mediated Mitophagy. The most well-studied mitophagy pathway is mediated by PTEN-induced putative kinase 1 (PINK1) and E3 ligase Parkin (Figure 1(c), (i)). Under physiological conditions, PINK1 is kept inactive in the mitochondrial matrix via cleavage by mitochondrial processing peptidase (MPP) and presenilin-associated rhomboid-like (PARL) protease [62–64]. On the other hand, mitochondrial stress induced by membrane depolarization stabilizes and activates PINK1 on the outer mitochondrial membrane, where it promotes recruitment and activation of Parkin [65, 66].

PINK1-mediated activation of Parkin is orchestrated by an interplay between phosphorylation and ubiquitination. Under physiological conditions, Parkin adopts a closed conformation and is kept inactive due to the association between the N-terminal ubiquitin-like (UBL) and the RING1 domain (Figure 1(c), (i)). Mitochondrial membrane depolarization induces Parkin phosphorylation at Ser65 by PINK1, promoting a conformational change and partially relieving the autoinhibition on Parkin [67, 68]. A second phosphorylation event, which involves phosphorylation of the ubiquitin molecule also at Ser65 by PINK1, is an important event for full activation of Parkin. The phosphorylated ubiquitin binds to the UBL domain of Parkin to fully activate the E3 ligase activity [69, 70]. Activated Parkin polyubiquitinates the outer mitochondrial membrane proteins, where the ubiquitination serves as recognition tag for cargo adaptor proteins to initiate mitophagy. In addition, the PINK1-Parkin complex can also directly interact with Beclin-1 in the class III phosphoinositide 3-kinase (PI3K) complex, or indirectly with the PI3K complex via AMBRA1, to initiate autophagosome membrane biogenesis around the damaged organelle [71, 72].

2.2.2. Other Mitochondrial Membrane Proteins and Lipid-Mediated Mitophagy. Apart from the PINK1-Parkin

mechanism, mitophagy can alternatively be initiated by other proteins and lipids on the outer mitochondrial membrane (Figure 1(c), (ii, iii)). BCL2/adenovirus E1B 19 kDa protein-interacting protein 3 (BNIP3), NIP3-like protein X (NIX), and FUN14 domain containing 1 (FUNDC1) are outer mitochondrial membrane proteins that harbour the LIR motif. The outer mitochondrial membrane can, therefore, also directly interact with the autophagosome during mitophagy. Additionally, AMBRA1 participates in both Parkin-dependent and independent mitophagy [73]. In Parkin-independent mitophagy, AMBRA1 binds LC3 directly through its LIR motif. Lipid moieties on mitochondrial proteins similarly can interact with the autophagosome. For example, the inner mitochondrial membrane phospholipid cardiolipin translocates to the outer mitochondrial membrane under mitochondrial stress to interact with LC3 [74, 75]. Ceramide, a sphingolipid on the mitochondrial membrane, has also been shown to interact with LC3 [76].

3. Transcriptional Regulation of Mitophagy

Studies have begun to show that transcriptional mechanisms play a pivotal role in modulating autophagy. These transcription factors are often activated in response to lowered nutrient or energy status in order to upregulate expression of autophagy and lysosomal genes to expedite the recycling and generation of amino acids, lipids, and ATP from degraded cellular components. FOXO and more recently, TFEB, are transcription factors that have been intensively studied and established to upregulate autophagy and lysosomal biogenesis under starvation conditions [19, 23, 77, 78]. Activation of FOXO and TFEB transcriptional activities has been linked to beneficial autophagy associated with lifespan extensions in model organisms [79, 80]. Transcriptional upregulation of autophagic flux induced by starvation also enhances protein-organelle quality control where mitochondria may be degraded as part of the autophagic cargoes. It remains unclear whether selection factors are involved in mitochondrial degradation by starvation-induced autophagy [8]. Importantly, recent studies have revealed that FOXO and TFEB specifically respond to mitochondrial stress to induce mitophagy by upregulating autophagy and several mitophagy genes. Many lines of emerging evidence suggest that stress-induced transcriptional upregulation of mitophagy has its own unique signalling signature (discussed below) (Figure 2(a)). Thus, targeting these mitophagy-specific transcriptional signalling pathways serves as an avenue for preferentially inducing mitophagy. The global effects of transcriptional regulation may offer an overarching advantage over interventions aimed at augmenting the formation of specific types of mitophagosomes (Figure 1). Furthermore, these transcription regulators also coregulate mitochondrial biogenesis in addition to mitochondrial turnover, hence allowing coordinated enhancement of mitochondrial proliferation and degradation to better triage mitochondrial homeostasis [19, 40, 41].

3.1. FOXO3a Signalling. FOXO is a family of transcription factors characterized by a conserved DNA-binding domain

termed the “forkhead box.” In human, the FOXO family contains four members, namely, FOXO1, FOXO3/3a, FOXO4, and FOXO6 [27]. All 4 FOXO members are expressed in skeletal muscle cells and are implicated in transcriptional activation of genes involved in protein degradation (proteasome and autophagy), glycolysis, lipophagy (selective autophagic degradation of lipid droplets), and mitochondrial respiration for skeletal muscle homeostasis [81]. FOXO is activated by AMP-activated protein kinase (AMPK) and nicotinamide adenine dinucleotide- (NAD⁺-) dependent deacetylase sirtuin-1 (SIRT1) signalling pathways to upregulate autophagy in response to nutrient and energy cues. Low ATP levels activate AMPK to directly induce FOXO nuclear localization and autophagy upregulation [82, 83]. In contrast, a low nutrient supply increases the level of NAD⁺ leading to SIRT1 activation. Activated SIRT1 thereafter deacetylates FOXO to promote its nuclear translocation and transcription activity [84]. Amongst the 4 members, FOXO3 is most frequently associated with autophagy induction. FOXO3 controls the expression of genes involved in autophagosome biogenesis [81, 85–87].

Two recent studies delineate a role of FOXO3a in modulating mitophagy. In the first study, mitochondrial proteotoxic stress activates UPR^{mt} and elevates sirtuin-3 (SIRT3) expression (Figure 2(a)). SIRT3 is another member of the sirtuin family that is localized to the mitochondria and plays predominant roles in mitochondrial processes. A study found that increased SIRT3 levels lead to FOXO3a deacetylation and activation [88]. Active FOXO3a induces the transcription of genes involved in mitophagy, including *lc3*, *atg9*, and *bnip3l/nix* [88]. Notably, the study observed that only the fragmented mitochondria were engulfed by autophagosomes whereas the remaining mitochondrial network was unaffected [88]. This observation is consistent with the notion of mitophagy, where only the damaged mitochondria are targeted for autophagic clearance. It was also observed that Parkin expression levels remained unchanged, suggesting that SIRT3-FOXO3a-mediated mitophagy is independent of Parkin [88]. It appears that the Parkin-independent mitophagy induced by SIRT3-FOXO3a is a peculiar response to mitochondrial UPR. In contrast, another study reported that SIRT3-FOXO3a signalling upregulated Parkin expression to mediate enhanced mitophagy to protect against diabetic cardiomyopathy in mice [89]. This shows that SIRT3-FOXO3a activation can induce different mitophagy mechanisms, possibly determined by the type of mitochondrial stress.

3.2. TFEB Signalling. TFEB is the first member of the microphthalmia family of basic helix-loop-helix-leucine-zipper (bHLH-Zip) transcription factors (MiTF) identified to be a master regulator of autophagy-lysosomal genes [90]. TFEB binds to the coordinated lysosomal expression and regulation (CLEAR) motif, a 10-base E-box-like palindromic sequence found in the promoters of autophagy and lysosomal genes, to activate their transcription [91]. Thus far, TFEB is mainly activated by cellular stressors such as starvation and ROS production [20, 92]. ROS regulation of TFEB activity serves as an important route for cells to detect mitochondrial

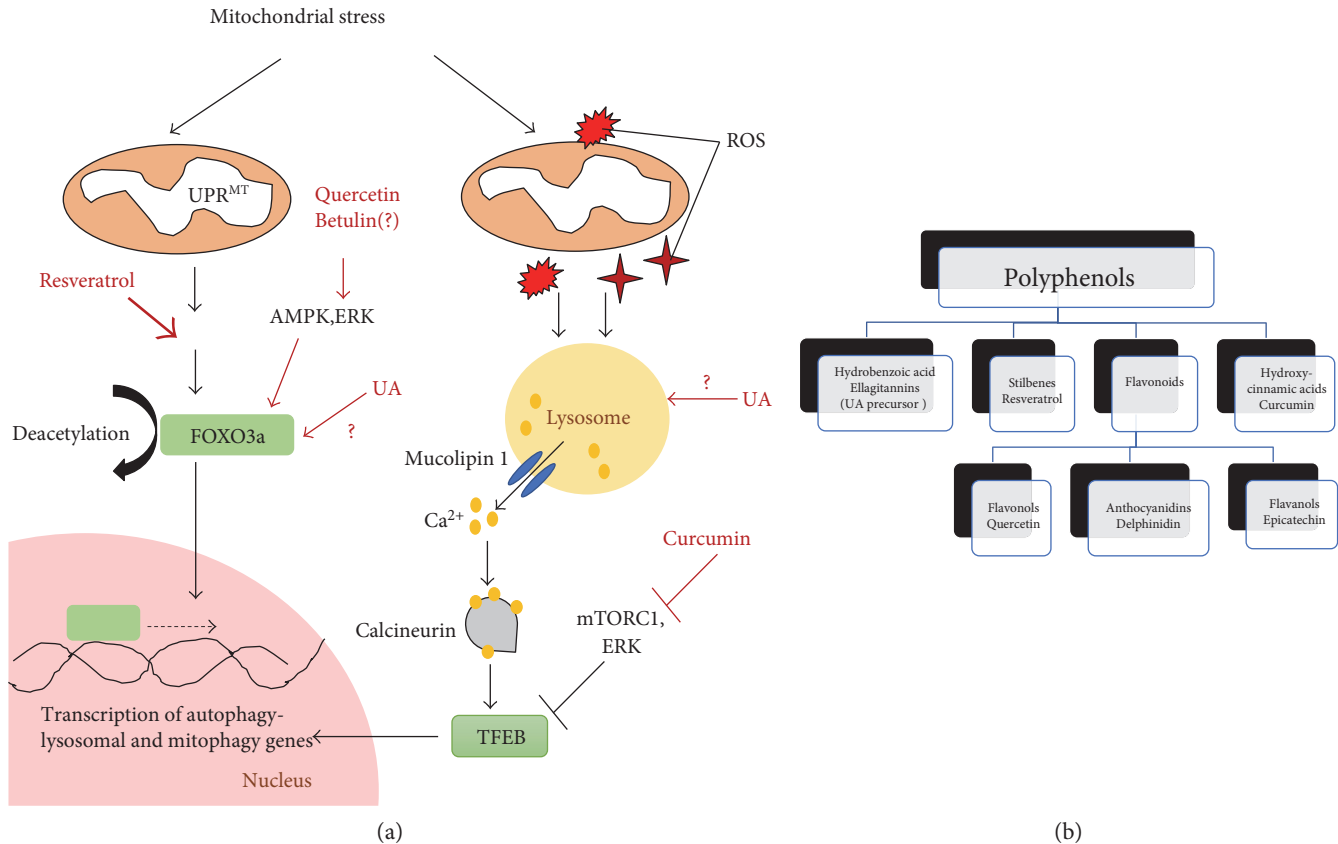


FIGURE 2: Regulation of FOXO3a and TFEB transcriptional control of mitophagy by polyphenols. (a) Mitochondrial stress activates mitochondrial unfolded protein responses (UPR^{MT}) to upregulate expression of SIRT3. SIRT3 deacetylates transcription factor FOXO3a to promote its nuclear translocation. Resveratrol, betulin, and quercetin potentially influence FOXO3a activation via SIRT3 dependent or independent pathways. Mitochondrial stress also generates reactive oxygen species (ROS) to activate the lysosomal Ca^{2+} signalling and calcineurin to dephosphorylate TFEB and promote its nuclear translocation. Curcumin activates TFEB via mTORC1 inhibition. Urolithin A (UA) may modulate mitophagy transcriptome via regulating FOXO3a or TFEB activity. Once in the nucleus, FOXO3a and TFEB initiate transcription of autophagy-lysosomal and mitophagy genes to facilitate mitochondrial clearance. (b) Classification of polyphenols.

malfunction in order to upregulate transcription of autophagy-lysosomal genes to enhance mitophagy and suppress oxidative stress [20].

In TFEB-induced autophagy, the lysosome acts as a signalling hub that senses changes in amino acid levels in the lysosomal lumen or intracellular ROS levels to regulate TFEB activity. Lysosome regulates TFEB phosphorylation and activation status through 3 signalling cascades: (1) mammalian target of rapamycin complex 1 (mTORC1), (2) extracellular signal-regulated kinase 2 (ERK2), and (3) lysosomal Ca^{2+} -activated calcineurin [93–95]. For nutrient regulation of TFEB, high level of amino acids in the lysosomal lumen induces conformational changes in vacuolar-type H^+ -ATPase proton pump (v -ATPase) to stabilize Ragulator complex at the lysosomal surface to recruit and activate mTORC1. Active lysosomal mTORC1 in turn recruits and phosphorylates TFEB at Ser142 and Ser211 to sequester TFEB in the cytosol and render it inactive [93–95]. In addition to mTORC1, Ragulator also promotes translocation of ERK2 towards the lysosome vicinity under amino acid-rich conditions to promote TFEB Ser142 phosphorylation [96]. This mechanism provides another regulatory route to inhibit TFEB activity. Conversely, under amino acid deprivation,

Ragulator and mTORC1 are not recruited to the lysosomal surface, which relieves TFEB suppression. Nutrient regulation of TFEB activity is also governed by dephosphorylation of TFEB. Recently, it has been shown that the lysosome responds to starvation by facilitating Ca^{2+} release from the lysosomal lumen through the lysosomal Ca^{2+} channel mucolipin 1 (Figure 2(a)). The localized lysosomal Ca^{2+} release activates calcineurin, a phosphatase that dephosphorylates TFEB to promote TFEB nuclear shuffling and transcription activity [97].

Besides being an effector of the lysosomal nutrient sensing pathway to adapt cell metabolism, TFEB also responds to other cellular stressors to orchestrate plethora homeostatic responses [92]. A recent example is TFEB activation by mitochondrial stress to upregulate autophagy-lysosomal transcriptome for specific removal of dysfunctional mitochondria (Figure 2(a)). The first evidence demonstrating TFEB as a transcriptional regulator of mitophagy came from the observation that mitochondrial depolarizing agents, oligomycin and antimycin A, induced TFEB dephosphorylation and nuclear translocation [98]. Unlike starvation, mTORC1 inactivation is dispensable in TFEB activation by mitochondrial stress, which instead is dependent on

Parkin activity [98]. E3 ligase Parkin promotes TFEB-induced mitophagy by degrading Parkin interacting substrate (PARIS), a transcriptional repressor of proliferator-activated receptor- γ coactivator-1 α (PGC-1 α) [99]. PGC-1 α has recently shown to regulate TFEB expression in addition to mitochondrial biogenesis and energy metabolism. Parkin therefore relieves PARIS inhibition on PGC-1 α to drive PGC-1 α -mediated TFEB expression for mitophagy [99]. Perturbation of Parkin activity in Q311X Parkin mutant and sporadic Parkinson's disease mouse models led to an increase in PARIS levels that coincided with disrupted PGC-1 α -TFEB signalling [13]. Disruption of Parkin intricate control of PARIS level resulted in mitochondrial impairment and degeneration of dopaminergic neuronal cells in these mouse models, which were successfully reversed via upregulation of PGC-1 α -TFEB signalling [13]. In turn, TFEB reciprocally regulates PGC-1 α expression to enhance compensatory mitochondrial biogenesis to replenish the mitochondrial pool removed by mitophagy [18]. Therefore, TFEB not only senses the need for increasing autophagy-lysosomal activity in order to degrade damaged mitochondria, but also coordinates the replacement of mitochondria through PGC-1 α -mediated synthesis of new mitochondria. TFEB hence acts as an integrative node linking mitochondrial quality control by mitophagy to mitochondrial biogenesis to maintain mitochondrial homeostasis.

The question of how the lysosome senses mitochondrial dysfunction to activate TFEB signalling independent of mTORC1 remained elusive until the recent identification of a ROS-lysosome-TFEB signalling mechanism [20]. In this study, ROS production caused by CCCP-induced mitochondrial stress increases Ca²⁺ efflux from lysosome via mucolipin 1 (Figure 2(a)). Addition of reducing or antioxidant reagents prevented activation of mucolipin 1, demonstrating that ROS induces lysosomal Ca²⁺ release. The localized Ca²⁺ surge in the cytosol activates calcineurin-dependent dephosphorylation of TFEB to release TFEB for nuclear shuffling and upregulates autophagosome and lysosome biogenesis to increase the cellular capacity for mitophagy. This study hence demonstrates that ROS may function as protective signalling molecules to upregulate adaptive cellular responses to combat oxidative stress.

4. Polyphenols and Mitophagy

Traditionally characterized as secondary metabolites for protection against ROS insults in plants [100], polyphenols are now intensively studied for their health-promoting properties [25]. Indeed, polyphenol-enriched diet can protect against neurodegeneration to favour healthy aging [25]. Mitochondria are a major cellular target of polyphenols. Many polyphenols demonstrate positive effects on mitochondrial biogenesis, integrity, and respiratory capacity [101]. For example, resveratrol has been shown to ameliorate mitochondrial bioenergetics and biogenic impairments in neuronal progenitor cells of the Down syndrome mice model. Resveratrol mitigates by activating mitochondrial biogenesis via PGC-1 α -SIRT1-AMPK signalling and restoring mitochondrial oxidative phosphorylation capabilities [102].

Low doses of resveratrol also protect against respiration dysfunction induced by mitochondrial mutations in patient-derived fibroblast cells [103]. In another example, rosmarinic acid was reported to attenuate insulin resistance in rat skeletal muscle via enhancing mitochondrial proliferation through increasing mitochondrial synthesis factors such as PGC-1 α , SIRT1, and transcription factor A mitochondria (TFAM) [104]. Epicatechin, another polyphenol highly enriched in cocoa, was similarly shown to increase the expression of key mitochondrial respiratory and biogenesis factors, including PGC-1 α , TFAM, and SIRT1, to improve mitochondrial respiratory function in skeletal muscle and myocardial cells [105–113]. Alma, a plant found in traditional Indian medicine, protects against oxidative stress in skeletal muscle cells by upregulating mitochondrial biogenesis and respiration via AMPK activation [114].

While many studies have looked at the influence of polyphenols on mitochondrial synthesis and functions, few have explored the effects of these natural compounds on mitophagy. Although polyphenols have been reported to induce autophagy [25], degradation of mitochondria in these cases is often a consequence of global autophagy upregulation for energy production rather than due to selective mitochondrial clearance. It is only recently that evidence supporting a role of polyphenols in specific transcriptional regulation of mitophagy has been reported. Based on these findings, we propose a mechanistic model on how the general classes of polyphenols (Figure 2(b)) could transcriptionally induce mitophagy to protect against mitochondrial stress.

4.1. Polyphenols Enhance FOXO3a Activation to Mediate Mitophagy. Recently, stilbenes (resveratrol) and flavonols (quercetin) have been shown to alter mitophagy transcriptome via FOXO3a signalling to potentiate Parkin-PINK1 mitophagy in cardiac and hepatic cells. These natural compounds upregulate mitophagy, in part, by enhancing the gene expressions of Parkin and PINK1 under myocardial infarction and liver injury (see below).

Resveratrol, a trans-3,4',5-trihydroxystilbene enriched in grapes and berries, along with its modified form Longevinex, was shown to induce mitophagy to attenuate myocardial infarction in rats subjected to ischemic reperfusion (I/R) injury [27]. In the study, resveratrol and its mimetic induced the acetylation of SIRT3 to activate the downstream effector FOXO3a. Enhanced PINK1 and Parkin localization to the mitochondria were observed in the injured cardiac cells [27]. It is unknown whether FOXO3a activation exerts a direct effect on the transcriptional upregulation of these mitophagy factors. However, PINK1 has been shown to be a downstream target of FOXO3a [115], thus suggesting the possibility that resveratrol and Longevinex may induce PINK1 expression via FOXO3a activation to subsequently facilitate Parkin recruitment to the mitochondria in the infarction area. Enhanced mitochondrial fission was also observed in the infarction area, which was postulated to mediate efficient mitophagy of the fragmented mitochondria [27]. Indeed, the interdependence between mitochondrial fission and Parkin-mediated mitophagy to maintain

mitochondria quality has been reported in the hearts of mice undergoing cardiac ischemia [116]. Disruption of mitochondrial fission through Drp1 ablation results in failure to separate the damaged mitochondria from the healthy network leading to perturbed mitophagy and mitochondrial homeostasis [116]. Taken together, resveratrol and Longevinex potentiate mitophagy in cardiac cells by promoting efficient PINK1-Parkin-mediated mitophagy via influencing two factors: (1) enhancing mitochondrial fragmentation and (2) potentially inducing expression of PINK1 in a FOXO3a-dependent manner.

Similar to resveratrol, quercetin was also reported to activate FOXO3a-mediated mitophagy. Quercetin is a flavonoid found enriched in many fruits, vegetables, and grains and has earlier been shown to alleviate mitochondrial oxidative stress via its antioxidant properties in ethanol-induced dyslipidemia [117]. In a recent study, the phenolic compound was shown to protect against mitochondrial damage in ethanol-induced liver injury through activation of mitophagy [28]. Ethanol feeding led to mitochondrial impairment in the mouse liver, characterized by degenerative changes in mitochondrial ultrastructure and membrane potential and fluidity. In addition, repression of Parkin expression and accumulation of partially sequestered mitochondria by the autophagosome were also observed, suggesting inefficient mitophagy during ethanol exposure. Administration of quercetin attenuated the pathological mitochondrial changes and restored mitophagy by activating FOXO3a, unlike resveratrol, in an AMPK- and ERK2-dependent pathway. This was accompanied by reversion of Parkin transcriptional inhibition, enhanced lysosome biogenesis, and fusion with mitophagosomes [28]. Another polyphenol, betulin, was also reported to alleviate ethanol-induced alcoholic liver injury via the SIRT1-AMPK signalling pathway to enhance lipophagy [118]. Whether betulin can concomitantly upregulate mitophagy to attenuate mitochondrial oxidative stress under alcohol-induced hepatotoxicity remains to be elucidated. Its potential to activate AMPK, however, suggests that betulin may similarly be able to activate FOXO3a-dependent mitophagy for hepatic protection.

The role of AMPK signalling as an interface for mitophagy was also observed in anthocyanin delphinidin-3-glucoside- (D3G-) mediated cytoprotection against oxidized low-density lipoprotein (oxLDL) toxicity during vascular endothelial cell injury [106]. D3G-mediated AMPK activation increases NAD⁺ levels to enhance SIRT1 activity which in turn upregulate mitophagy to prevent mitochondria dysfunction in oxLDL injured endothelial cells [119]. The mechanisms underlying D3G-driven SIRT1-mediated mitophagy currently remain unclear. It is possible that FOXO3a may underscore the link between SIRT1 activation and enhanced mitophagy for D3G effects. Alternatively, SIRT1 may directly mediate deacetylation and activation of key autophagic proteins such as Atg5, Atg7, and Atg8 to induce autophagy for mitochondrial removal [120].

4.2. Polyphenols and TFEB Signalling in Mitophagy. Since TFEB is regulated by mTORC1 activity, polyphenols that inhibit mTORC1 may be a viable activator of TFEB.

However, it remains mostly unknown whether polyphenols that inhibit mTORC1 also influence TFEB signalling and mitophagy. Curcumin, a diferuloylmethane and component of the turmeric plant, is currently the only polyphenol reported to regulate TFEB activity by inhibiting the AKT-mTORC1 signalling pathway [30]. A curcumin analog C1 that possesses better cellular uptake and a longer half-life has been shown to induce TFEB signalling in vitro and in vivo via distinct TFEB activation mechanisms. Unlike curcumin, TFEB activation by C1 is independent of mTORC1 and dephosphorylation events. Instead, C1 binds directly to TFEB at the N-terminal to alter the conformation of TFEB in order to expose its nuclear localization signal to facilitate nuclear translocation [121]. However, whether mitophagy activation is a downstream effector of curcumin-induced TFEB activation has yet to be addressed and warrants future investigation.

Melanoidin extract from aged vinegar and pomegranate extract (PE) have recently been shown to mediate mitophagy in injury-induced hepatocytes and cardiomyocytes by increasing Beclin-1 levels [29]. Beclin-1 is a component of the class III PI3K complex important for autophagosome membrane biogenesis [122] and is recently shown to influence mitophagy in cardiac I/R injury via novel regulation of mTORC1 [123]. A role of Beclin-1 in regulating autophagic mitochondrial clearance is further affirmed by another study showing that calpain-2-mediated degradation of Beclin-1 impaired mitophagy in rat hepatocytes [124]. Taken together, the Beclin-1-mTORC1 signalling axis potentially represents a novel signalling route to activate mitophagy and may underscore melanoid-mediated mitophagy. However, it remains unclear if TFEB participates in Beclin-1-mTORC1-regulated mitophagy.

Urolithin A (UA), another metabolite derived from PE, has recently shown to induce mitophagy in *C. elegans* and rodents [15]. UA is one of the hydrolysed end products of ellagitannins found highly enriched in PE. UA supplementation prolongs lifespan in *C. elegans* and consistently increases healthspan in aged worms and mice by preventing age-related muscle deterioration. In *C. elegans*, exposure to UA increased the expression of autophagy (*bec-1*, *sqs-1*, and *vps-34*) and mitophagy (*pink1*, *dct-1*, and *skn-1*) genes that contributed to mitophagy induction. A reduced expression of mitochondrial fusion factors was also observed that aligned with an increase in mitochondrial fragmentation observed in UA-treated cells and tissues. This alteration in mitochondrial dynamics potentially favours autophagic targeting of the fragmented mitochondria to enhance mitophagy flux. The mechanism underlying UA-induced transcriptional upregulation of mitophagy was not explored in the study. It will be interesting to explore if UA potentiates mitophagy via influencing FOXO3 and TFEB, the two major transcriptional activators of mitophagy.

4.3. The Hormetic Effect: Polyphenols as Pro-Oxidants to Activate Lysosomal Ca²⁺ Signalling for Mitophagy? ROS are widely accepted to be damaging molecules. However, emerging evidence suggests ROS also serve important functional roles by acting as signalling molecules to regulate important

physiological processes [125, 126]. In the concept of “hormesis,” low doses of ROS stress may be protective by activating stress response pathways that promote longevity [127, 128]. Hormesis describes the upregulation of pre-emptive adaptive responses to enhance the readiness of the cells to counteract the onset of more aggressive cellular stress thereby increasing cell resilience [129]. Mitophagy is also subjected to ROS regulation via mitochondrial ROS-mediated lysosome Ca^{2+} signalling pathway. Low level mitochondrial ROS therefore may facilitate mitochondrial hormesis by priming mitophagy on standby to attenuate oxidative stress through efficient removal of dysfunctional mitochondria to protect mitochondrial and cellular redox homeostasis.

Interestingly, polyphenols also elicit hormetic effects via its pro-oxidant properties when administered at regulated doses. The pro-oxidant effects often involve interactions of polyphenols with transition metal ions [130]. An example is curcumin which exhibits a pro-oxidant property at very low doses ($\leq 1 \mu\text{M}$) in the presence of Cu(II) but operates primarily as an autophagy inducer when present in the range of 5–10 μM , wherein it mediates the protective effects of autophagy [131]. How do pro-oxidant effects mediated by polyphenols benefit cells? It is tempting to postulate that a plausible mechanism underlying hormetic effects of polyphenol pro-oxidant properties is the induction of mitophagy via ROS-lysosomal Ca^{2+} signalling. In this model, we propose that low levels of ROS generated by polyphenols when administered in an acute or nonlethal dose may stimulate lysosome- Ca^{2+} signalling to activate TFEB to increase transcription of autophagy-lysosomal and mitophagy genes (Figure 2(a)). Under physiological conditions, expression of these genes may increase autophagy-lysosomal fitness to prime the mitochondria for efficient transit to mitophagy in the event of mitochondrial stress.

5. Concluding Thoughts

In recent years, transcriptional modulation of autophagy has become a focus of attention owing to the identification of TFEB. TFEB activation has also been recently shown to regulate mitophagy. The identification of ROS-lysosome- Ca^{2+} signalling to activate TFEB presents an exciting interface for crosstalk between mitochondria and the lysosome to modulate mitochondria quality control. Interestingly, impairment in the activity of one organelle affects the other. For example, in Pompe disease, a lysosomal storage disorder, the impaired lysosome function is associated with perturbed mitochondrial membrane potential and Ca^{2+} homeostasis [132]. Mitochondrial dysfunction similarly leads to accumulation of damaged lysosomes in mouse fibroblast cells deficient in mitophagy factors [133]. For the latter, accumulation of ROS is the cause for lysosomal impairment, which further highlights the importance of lysosome as a ROS sensing hub to upregulate mitophagy (via TFEB) to remove damaged mitochondria and restore lysosome integrity.

Most studies thus far have only examined the role of polyphenols in general autophagy modulation. Very few polyphenols have been identified to specifically regulate mitophagy, and even lesser is known about polyphenols that

regulate mitophagy via transcriptional control. Nonetheless, the identification of several phenolic compounds that could influence mitochondrial clearance via FOXO3a and TFEB signalling highlights the potential of dietary intake as an avenue for mitophagy upregulation in humans. It will be exciting to explore the prospect of augmenting mitophagy through polyphenol consumption as a therapeutic approach towards mitochondria-related diseases.

Conflicts of Interest

The authors declare no conflicts of interest regarding the publication of this article.

Acknowledgments

Work in our laboratory is supported by grants from MOE Tier 2 M4020161.080 (ARC 25/13), MOE Tier 1 M4011565.080 (RG139/15), and SUG M4080753.080.

References

- [1] D. D. Newmeyer and S. Ferguson-Miller, “Mitochondria: releasing power for life and unleashing the machineries of death,” *Cell*, vol. 112, no. 4, pp. 481–490, 2003.
- [2] A. Y. Seo, A. M. Joseph, D. Dutta, J. C. Hwang, J. P. Aris, and C. Leeuwenburgh, “New insights into the role of mitochondria in aging: mitochondrial dynamics and more,” *Journal of Cell Science*, vol. 123, Part 15, pp. 2533–2542, 2010.
- [3] D. K. Woo and G. S. Shadel, “Mitochondrial stress signals. Revise an old aging theory,” *Cell*, vol. 144, no. 1, pp. 11–12, 2011.
- [4] D. F. Dai, Y. A. Chiao, D. J. Marcinek, H. H. Szeto, and P. S. Rabinovitch, “Mitochondrial oxidative stress in aging and healthspan,” *Longevity & Healthspan*, vol. 3, no. 1, p. 6, 2014.
- [5] A. Bratic and N. G. Larsson, “The role of mitochondria in aging,” *The Journal of Clinical Investigation*, vol. 123, no. 3, pp. 951–957, 2013.
- [6] C. F. Bento, M. Renna, G. Ghislat et al., “Mammalian autophagy: how does it work?” *Annual Review of Biochemistry*, vol. 85, pp. 685–713, 2016.
- [7] L. Liu, K. Sakakibara, Q. Chen, and K. Okamoto, “Receptor-mediated mitophagy in yeast and mammalian systems,” *Cell Research*, vol. 24, no. 7, pp. 787–795, 2014.
- [8] J. J. Lemasters, “Variants of mitochondrial autophagy: types 1 and 2 mitophagy and micromitophagy (type 3),” *Redox Biology*, vol. 2, pp. 749–754, 2014.
- [9] E. M. Fivenson, S. Lautrup, N. Sun et al., “Mitophagy in neurodegeneration and aging,” *Neurochemistry International*, 2017, In press.
- [10] N. Sun, R. J. Youle, and T. Finkel, “The mitochondrial basis of aging,” *Molecular Cell*, vol. 61, no. 5, pp. 654–666, 2016.
- [11] C. Correia-Meio, F. D. Marques, R. Anderson et al., “Mitochondria are required for pro-ageing features of the senescent phenotype,” *The EMBO Journal*, vol. 35, no. 7, pp. 724–742, 2016.
- [12] M. C. Lo, C. I. Lu, M. H. Chen, C. D. Chen, H. M. Lee, and S. H. Kao, “Glycooxidative stress-induced mitophagy modulates mitochondrial fates,” *Annals of the New York Academy of Sciences*, vol. 1201, no. 1, pp. 1–7, 2010.

- [13] A. Siddiqui, D. Bhaumik, S. J. Chinta et al., "Mitochondrial quality control via the PGC1alpha-TFEB signaling pathway is compromised by Parkin Q311X mutation but independently restored by rapamycin," *The Journal of Neuroscience*, vol. 35, no. 37, pp. 12833–12844, 2015.
- [14] A. Schiavi, S. Maglioni, K. Palikaras et al., "Iron-starvation-induced mitophagy mediates lifespan extension upon mitochondrial stress in *C. elegans*," *Current Biology*, vol. 25, no. 14, pp. 1810–1822, 2015.
- [15] D. Ryu, D. Ryu, L. Mouchiroud et al., "Urolithin A induces mitophagy and prolongs lifespan in *C. elegans* and increases muscle function in rodents," *Nature Medicine*, vol. 22, no. 8, pp. 879–888, 2016.
- [16] K. F. Mills, K. F. Mills, S. Yoshida et al., "Long-term administration of nicotinamide mononucleotide mitigates age-associated physiological decline in mice," *Cell Metabolism*, vol. 24, no. 6, pp. 795–806, 2016.
- [17] M. S. Bonkowski and D. A. Sinclair, "Slowing ageing by design: the rise of NAD+ and sirtuin-activating compounds," *Nature Reviews. Molecular Cell Biology*, vol. 17, no. 11, pp. 679–690, 2016.
- [18] D. Ivankovic, D. Ivankovic, K. Y. Chau, A. H. Schapira, and M. E. Gegg, "Mitochondrial and lysosomal biogenesis are activated following PINK1/parkin-mediated mitophagy," *Journal of Neurochemistry*, vol. 136, no. 2, pp. 388–402, 2016.
- [19] N. Raben and R. Puertollano, "TFEB and TFE3: linking lysosomes to cellular adaptation to stress," *Annual Review of Cell and Developmental Biology*, vol. 32, pp. 255–278, 2016.
- [20] X. Zhang, X. Zhang, X. Cheng et al., "MCOLN1 is a ROS sensor in lysosomes that regulates autophagy," *Nature Communications*, vol. 7, p. 12109, 2016.
- [21] E. F. Fang, M. Scheibye-Knudsen, K. F. Chua, M. P. Mattson, D. L. Croteau, and V. A. Bohr, "Nuclear DNA damage signaling to mitochondria in ageing," *Nature Reviews. Molecular Cell Biology*, vol. 17, no. 5, pp. 308–321, 2016.
- [22] E. F. Fang, E. F. Fang, H. Kassahun et al., "NAD+ replenishment improves lifespan and healthspan in ataxia telangiectasia models via mitophagy and DNA repair," *Cell Metabolism*, vol. 24, no. 4, pp. 566–581, 2016.
- [23] L. R. Lapierre, L. R. Lapierre, C. Kumsta, M. Sandri, A. Ballabio, and M. Hansen, "Transcriptional and epigenetic regulation of autophagy in aging," *Autophagy*, vol. 11, no. 6, pp. 867–880, 2015.
- [24] K. Pallauf, N. Duckstein, and G. Rimbach, "A literature review of flavonoids and lifespan in model organisms," *The Proceedings of the Nutrition Society*, vol. 76, no. 2, pp. 145–162, 2016.
- [25] K. Pallauf and G. Rimbach, "Autophagy, polyphenols and healthy ageing," *Ageing Research Reviews*, vol. 12, no. 1, pp. 237–252, 2013.
- [26] G. Testa, G. Testa, F. Biasi, G. Poli, and E. Chiarotto, "Calorie restriction and dietary restriction mimetics: a strategy for improving healthy aging and longevity," *Current Pharmaceutical Design*, vol. 20, no. 18, pp. 2950–2977, 2014.
- [27] S. Das, S. Das, G. Mitrovsky, H. R. Vasanthi, and D. K. Das, "Antiaging properties of a grape-derived antioxidant are regulated by mitochondrial balance of fusion and fission leading to mitophagy triggered by a signaling network of Sirt1-Sirt3-Foxo3-PINK1-PARKIN," *Oxidative Medicine and Cellular Longevity*, vol. 2014, Article ID 345105, p. 13, 2014.
- [28] X. Yu, X. Yu, Y. Xu et al., "Quercetin attenuates chronic ethanol-induced hepatic mitochondrial damage through enhanced mitophagy," *Nutrients*, vol. 8, no. 1, p. 27, 2016.
- [29] L. Yang, X. Wang, and X. Yang, "Possible antioxidant mechanism of melanoidins extract from Shanxi aged vinegar in mitophagy-dependent and mitophagy-independent pathways," *Journal of Agricultural and Food Chemistry*, vol. 62, no. 34, pp. 8616–8622, 2014.
- [30] J. Zhang, J. Zhang, J. Wang et al., "Curcumin targets the TFEB-lysosome pathway for induction of autophagy," *Oncotarget*, vol. 7, no. 46, pp. 75659–75671, 2016.
- [31] U. Cagin and J. A. Enriquez, "The complex crosstalk between mitochondria and the nucleus: what goes in between?" *The International Journal of Biochemistry & Cell Biology*, vol. 63, pp. 10–15, 2015.
- [32] C. Cherry, B. Thompson, N. Saptarshi, J. Wu, and J. Hoh, "2016: a "Mitochondria" odyssey," *Trends in Molecular Medicine*, vol. 22, no. 5, pp. 391–403, 2016.
- [33] P. M. Quiros, A. Mottis, and J. Auwerx, "Mitonuclear communication in homeostasis and stress," *Nature Reviews. Molecular Cell Biology*, vol. 17, no. 4, pp. 213–226, 2016.
- [34] D. H. Margineantu and D. M. Hockenbery, "Mitochondrial functions in stem cells," *Current Opinion in Genetics & Development*, vol. 38, pp. 110–117, 2016.
- [35] J. A. Menendez and J. Joven, "Energy metabolism and metabolic sensors in stem cells: the metabostem crossroads of aging and cancer," *Advances in Experimental Medicine and Biology*, vol. 824, pp. 117–140, 2014.
- [36] C. M. Haynes and D. Ron, "The mitochondrial UPR - protecting organelle protein homeostasis," *Journal of Cell Science*, vol. 123, Part 22, pp. 3849–3855, 2010.
- [37] V. Jovaisaite, L. Mouchiroud, and J. Auwerx, "The mitochondrial unfolded protein response, a conserved stress response pathway with implications in health and disease," *The Journal of Experimental Biology*, vol. 217, Part 1, pp. 137–143, 2014.
- [38] M. W. Pellegrino, A. M. Nargund, and C. M. Haynes, "Signaling the mitochondrial unfolded protein response," *Biochimica et Biophysica Acta*, vol. 1833, no. 2, pp. 410–416, 2013.
- [39] K. Palikaras, E. Lionaki, and N. Tavernarakis, "Coordination of mitophagy and mitochondrial biogenesis during ageing in *C. elegans*," *Nature*, vol. 521, no. 7553, pp. 525–528, 2015.
- [40] K. Palikaras, E. Lionaki, and N. Tavernarakis, "Coupling mitogenesis and mitophagy for longevity," *Autophagy*, vol. 11, no. 8, pp. 1428–1430, 2015.
- [41] K. Palikaras and N. Tavernarakis, "Mitochondrial homeostasis: the interplay between mitophagy and mitochondrial biogenesis," *Experimental Gerontology*, vol. 56, pp. 182–188, 2014.
- [42] H. B. Suliman and C. A. Piantadosi, "Mitochondrial quality control as a therapeutic target," *Pharmacological Reviews*, vol. 68, no. 1, pp. 20–48, 2016.
- [43] G. Juhasz, "A mitochondrial-derived vesicle HOPS to endolysosomes using Syntaxin-17," *The Journal of Cell Biology*, vol. 214, no. 3, pp. 241–243, 2016.
- [44] G. Ashrafi and T. L. Schwarz, "The pathways of mitophagy for quality control and clearance of mitochondria," *Cell Death and Differentiation*, vol. 20, no. 1, pp. 31–42, 2013.
- [45] C. H. Davis, K. Y. Kim, E. A. Bushong et al., "Transcellular degradation of axonal mitochondria," *Proceedings of the*

- National Academy of Sciences of the United States of America*, vol. 111, no. 26, pp. 9633–9638, 2014.
- [46] C. H. Davis and N. Marsh-Armstrong, “Discovery and implications of transcellular mitophagy,” *Autophagy*, vol. 10, no. 12, pp. 2383–2384, 2014.
- [47] K. Palikaras, E. Lionaki, and N. Tavernarakis, “Mitophagy: in sickness and in health,” *Molecular & Cellular Oncology*, vol. 3, no. 1, article e1056332, 2016.
- [48] E. Lionaki, E. Lionaki, M. Markaki, K. Palikaras, and N. Tavernarakis, “Mitochondria, autophagy and age-associated neurodegenerative diseases: new insights into a complex interplay,” *Biochimica et Biophysica Acta*, vol. 1847, no. 11, pp. 1412–1423, 2015.
- [49] I. G. Onyango, S. M. Khan, and J. P. Bennett Jr., “Mitochondria in the pathophysiology of Alzheimer’s and Parkinson’s diseases,” *Frontiers in Bioscience (Landmark edition)*, vol. 22, pp. 854–872, 2017.
- [50] S. H. Lee, S. H. Lee, J. Du et al., “Inducing mitophagy in diabetic platelets protects against severe oxidative stress,” *EMBO Molecular Medicine*, vol. 8, no. 7, pp. 779–795, 2016.
- [51] Y. Feng, Y. Feng, D. He, Z. Yao, and D. J. Klionsky, “The machinery of macroautophagy,” *Cell Research*, vol. 24, no. 1, pp. 24–41, 2014.
- [52] N. Mizushima, T. Yoshimori, and Y. Ohsumi, “The role of Atg proteins in autophagosome formation,” *Annual Review of Cell and Developmental Biology*, vol. 27, pp. 107–132, 2011.
- [53] T. Hara, T. Hara, K. Nakamura et al., “Suppression of basal autophagy in neural cells causes neurodegenerative disease in mice,” *Nature*, vol. 441, no. 7095, pp. 885–889, 2006.
- [54] M. Komatsu, M. Komatsu, S. Waguri et al., “Loss of autophagy in the central nervous system causes neurodegeneration in mice,” *Nature*, vol. 441, no. 7095, pp. 880–884, 2006.
- [55] A. Takamura, A. Takamura, M. Komatsu et al., “Autophagy-deficient mice develop multiple liver tumors,” *Genes & Development*, vol. 25, no. 8, pp. 795–800, 2011.
- [56] A. Kuma, A. Kuma, M. Hatano, M. Matsui, and A. Yamamoto, “The role of autophagy during the early neonatal starvation period,” *Nature*, vol. 432, no. 7020, pp. 1032–1036, 2004.
- [57] A. Stolz, A. Ernst, and I. Dikic, “Cargo recognition and trafficking in selective autophagy,” *Nature Cell Biology*, vol. 16, no. 6, pp. 495–501, 2014.
- [58] H. M. Ni, J. A. Williams, and W. X. Ding, “Mitochondrial dynamics and mitochondrial quality control,” *Redox Biology*, vol. 4, pp. 6–13, 2015.
- [59] E. Smirnova, E. Smirnova, L. Griparic, D. L. Shurland, and A. M. Van Der Bliek, “Dynamin-related protein Drp1 is required for mitochondrial division in mammalian cells,” *Molecular Biology of the Cell*, vol. 12, no. 8, pp. 2245–2256, 2001.
- [60] H. Chen, S. A. Detmer, A. J. Ewald, E. E. Griffin, S. E. Fraser, and D. C. Chan, “Mitofusins Mfn1 and Mfn2 coordinately regulate mitochondrial fusion and are essential for embryonic development,” *The Journal of Cell Biology*, vol. 160, no. 2, pp. 189–200, 2003.
- [61] M. E. Gegg, J. M. Cooper, K. Y. Chau, M. Rojo, A. H. Schapira, and J. W. Taanman, “Mitofusin 1 and mitofusin 2 are ubiquitinated in a PINK1/parkin-dependent manner upon induction of mitophagy,” *Human Molecular Genetics*, vol. 19, no. 24, pp. 4861–4870, 2010.
- [62] E. Deas, H. Plun-Favreau, S. Gandhi et al., “PINK1 cleavage at position A103 by the mitochondrial protease PARL,” *Human Molecular Genetics*, vol. 20, no. 5, pp. 867–879, 2011.
- [63] A. W. Greene, K. Grenier, M. A. Aguieta et al., “Mitochondrial processing peptidase regulates PINK1 processing, import and Parkin recruitment,” *EMBO Reports*, vol. 13, no. 4, pp. 378–385, 2012.
- [64] C. Meissner, H. Lorenz, A. Weihofen, D. J. Selkoe, and M. K. Lemberg, “The mitochondrial intramembrane protease PARL cleaves human Pink1 to regulate Pink1 trafficking,” *Journal of Neurochemistry*, vol. 117, no. 5, pp. 856–867, 2011.
- [65] S. M. Jin, M. Lazarou, C. Wang, L. A. Kane, D. P. Narendra, and R. J. Youle, “Mitochondrial membrane potential regulates PINK1 import and proteolytic destabilization by PARL,” *The Journal of Cell Biology*, vol. 191, no. 5, pp. 933–942, 2010.
- [66] M. Lazarou, S. M. Jin, L. A. Kane, and R. J. Youle, “Role of PINK1 binding to the TOM complex and alternate intracellular membranes in recruitment and activation of the E3 ligase Parkin,” *Developmental Cell*, vol. 22, no. 2, pp. 320–333, 2012.
- [67] T. R. Caulfield, F. C. Fiesel, E. L. Moussaud-Lamodière, D. F. Dourado, S. C. Flores, and W. Springer, “Phosphorylation by PINK1 releases the UBL domain and initializes the conformational opening of the E3 ubiquitin ligase Parkin,” *PLoS Computational Biology*, vol. 10, no. 11, article e1003935, 2014.
- [68] A. Kazlauskaitė, V. Kelly, C. Johnson et al., “Phosphorylation of Parkin at Serine65 is essential for activation: elaboration of a Miro1 substrate-based assay of Parkin E3 ligase activity,” *Open Biology*, vol. 4, no. 3, p. 130213, 2014.
- [69] A. Kazlauskaitė, C. Kondapalli, R. Gourlay et al., “Parkin is activated by PINK1-dependent phosphorylation of ubiquitin at Ser65,” *The Biochemical Journal*, vol. 460, no. 1, pp. 127–139, 2014.
- [70] A. Kazlauskaitė, R. J. Martínez-Torres, S. Wilkie et al., “Binding to serine 65-phosphorylated ubiquitin primes Parkin for optimal PINK1-dependent phosphorylation and activation,” *EMBO Reports*, vol. 16, no. 8, pp. 939–954, 2015.
- [71] S. Michiorri, V. Gelmetti, E. Giarda et al., “The Parkinson-associated protein PINK1 interacts with Beclin1 and promotes autophagy,” *Cell Death and Differentiation*, vol. 17, no. 6, pp. 962–974, 2010.
- [72] C. Van Humbeecq, T. Cornelissen, H. Hofkens et al., “Parkin interacts with Ambra1 to induce mitophagy,” *The Journal of Neuroscience*, vol. 31, no. 28, pp. 10249–10261, 2011.
- [73] F. Strappazon, F. Nazio, M. Corrado et al., “AMBRA1 is able to induce mitophagy via LC3 binding, regardless of PARKIN and p62/SQSTM1,” *Cell Death and Differentiation*, vol. 22, no. 3, pp. 419–432, 2015.
- [74] C. T. Chu, J. Ji, R. K. Dagda et al., “Cardiolipin externalization to the outer mitochondrial membrane acts as an elimination signal for mitophagy in neuronal cells,” *Nature Cell Biology*, vol. 15, no. 10, pp. 1197–1205, 2013.
- [75] V. E. Kagan, V. E. Kagan, J. Jiang et al., “NDPK-D (NM23-H4)-mediated externalization of cardiolipin enables elimination of depolarized mitochondria by mitophagy,” *Cell Death and Differentiation*, vol. 23, no. 7, pp. 1140–1151, 2016.
- [76] R. D. Sentelle, C. E. Senkal, W. Jiang et al., “Ceramide targets autophagosomes to mitochondria and induces lethal mitophagy,” *Nature Chemical Biology*, vol. 8, no. 10, pp. 831–838, 2012.

- [77] J. Fullgrabe, D. J. Klionsky, and B. Joseph, "The return of the nucleus: transcriptional and epigenetic control of autophagy," *Nature Reviews. Molecular Cell Biology*, vol. 15, no. 1, pp. 65–74, 2014.
- [78] A. E. Webb and A. Brunet, "FOXO transcription factors: key regulators of cellular quality control," *Trends in Biochemical Sciences*, vol. 39, no. 4, pp. 159–169, 2014.
- [79] L. R. Lapierre, C. D. De Magalhaes Filho, M. Q. PR et al., "The TFEB orthologue HLH-30 regulates autophagy and modulates longevity in *Caenorhabditis elegans*," *Nature Communications*, vol. 4, article 2267, pp. 1–8, 2013.
- [80] C. T. Murphy, C. T. Murphy, M. C. SA et al., "Genes that act downstream of DAF-16 to influence the lifespan of *Caenorhabditis elegans*," *Nature*, vol. 424, no. 6946, pp. 277–283, 2003.
- [81] A. M. Sanchez, R. B. Candau, and H. Bernardi, "FoxO transcription factors: their roles in the maintenance of skeletal muscle homeostasis," *Cellular and Molecular Life Sciences*, vol. 71, no. 9, pp. 1657–1671, 2014.
- [82] E. L. Greer, P. R. Oskoui, M. R. Banko et al., "The energy sensor AMP-activated protein kinase directly regulates the mammalian FOXO3 transcription factor," *The Journal of Biological Chemistry*, vol. 282, no. 41, pp. 30107–30119, 2007.
- [83] E. L. Greer, D. Dowlatshahi, M. R. Banko et al., "An AMPK-FOXO pathway mediates longevity induced by a novel method of dietary restriction in *C. elegans*," *Current Biology*, vol. 17, no. 19, pp. 1646–1656, 2007.
- [84] A. Brunet, L. B. Sweeney, J. F. Sturgill et al., "Stress-dependent regulation of FOXO transcription factors by the SIRT1 deacetylase," *Science*, vol. 303, no. 5666, pp. 2011–2015, 2004.
- [85] C. Mammucari, C. Mammucari, G. Milan et al., "FoxO3 controls autophagy in skeletal muscle in vivo," *Cell Metabolism*, vol. 6, no. 6, pp. 458–471, 2007.
- [86] C. Mammucari, S. Schiaffino, and M. Sandri, "Downstream of Akt: FoxO3 and mTOR in the regulation of autophagy in skeletal muscle," *Autophagy*, vol. 4, no. 4, pp. 524–526, 2008.
- [87] J. Zhao, J. J. Brault, A. Schild et al., "FoxO3 coordinately activates protein degradation by the autophagic/lysosomal and proteasomal pathways in atrophying muscle cells," *Cell Metabolism*, vol. 6, no. 6, pp. 472–483, 2007.
- [88] L. Papa and D. Germain, "SirT3 regulates the mitochondrial unfolded protein response," *Molecular and Cellular Biology*, vol. 34, no. 4, pp. 699–710, 2014.
- [89] W. Yu, B. Gao, N. Li et al., "Sirt3 deficiency exacerbates diabetic cardiac dysfunction: role of Foxo3A-Parkin-mediated mitophagy," *Biochimica et Biophysica Acta*, 2016, In press.
- [90] M. Sardiello, M. Sardiello, M. Palmieri et al., "A gene network regulating lysosomal biogenesis and function," *Science*, vol. 325, no. 5939, pp. 473–477, 2009.
- [91] M. Palmieri, M. Palmieri, S. Impey et al., "Characterization of the CLEAR network reveals an integrated control of cellular clearance pathways," *Human Molecular Genetics*, vol. 20, no. 19, pp. 3852–3866, 2011.
- [92] M. Sardiello, "Transcription factor EB: from master coordinator of lysosomal pathways to candidate therapeutic target in degenerative storage diseases," *Annals of the New York Academy of Sciences*, vol. 1371, no. 1, pp. 3–14, 2016.
- [93] Y. Sancak, L. Bar-Peled, R. Zoncu, A. L. Markhard, S. Nada, and D. M. Sabatini, "Ragulator-Rag complex targets mTORC1 to the lysosomal surface and is necessary for its activation by amino acids," *Cell*, vol. 141, no. 2, pp. 290–303, 2010.
- [94] R. Zoncu, L. Bar-Peled, A. Efeyan, S. Wang, Y. Sancak, and D. M. Sabatini, "mTORC1 senses lysosomal amino acids through an inside-out mechanism that requires the vacuolar H(+)-ATPase," *Science*, vol. 334, no. 6056, pp. 678–683, 2011.
- [95] A. Rocznik-Ferguson, C. S. Petit, F. Froehlich et al., "The transcription factor TFEB links mTORC1 signaling to transcriptional control of lysosome homeostasis," *Science Signaling*, vol. 5, no. 228, p. ra42, 2012.
- [96] C. Settembre, C. Di Malta, V. A. Polito et al., "TFEB links autophagy to lysosomal biogenesis," *Science*, vol. 332, no. 6036, pp. 1429–1433, 2011.
- [97] D. L. Medina, S. Di Paola, I. Peluso et al., "Lysosomal calcium signalling regulates autophagy through calcineurin and TFEB," *Nature Cell Biology*, vol. 17, no. 3, pp. 288–299, 2015.
- [98] C. L. Nezich, C. Wang, A. I. Fogel, and R. J. Youle, "MiT/TFE transcription factors are activated during mitophagy downstream of Parkin and Atg5," *The Journal of Cell Biology*, vol. 210, no. 3, pp. 435–450, 2015.
- [99] Y. Lee, D. A. Stevens, S. U. Kang et al., "PINK1 primes Parkin-mediated ubiquitination of PARIS in dopaminergic neuronal survival," *Cell Reports*, vol. 18, no. 4, pp. 918–932, 2017.
- [100] J. B. Harborne, "Role of secondary metabolites in chemical defence mechanisms in plants," *Ciba Foundation Symposium*, vol. 154, pp. 126–139, 1990.
- [101] C. Sandoval-Acuna, J. Ferreira, and H. Speisky, "Polyphenols and mitochondria: an update on their increasingly emerging ROS-scavenging independent actions," *Archives of Biochemistry and Biophysics*, vol. 559, pp. 75–90, 2014.
- [102] D. Valenti, L. de Bari, D. de Rasmio et al., "The polyphenols resveratrol and epigallocatechin-3-gallate restore the severe impairment of mitochondria in hippocampal progenitor cells from a Down syndrome mouse model," *Biochimica et Biophysica Acta*, vol. 1862, no. 6, pp. 1093–1104, 2016.
- [103] Y. Mizuguchi, H. Hatakeyama, K. Sueoka, M. Tanaka, and Y. I. Goto, "Low dose resveratrol ameliorates mitochondrial respiratory dysfunction and enhances cellular reprogramming," *Mitochondrion*, 2017.
- [104] G. Jayanthi, V. Roshana Devi, K. Ilango, and S. P. Subramanian, "Rosmarinic acid mediates mitochondrial biogenesis in insulin resistant skeletal muscle through activation of AMPK," *Journal of Cellular Biochemistry*, vol. 118, no. 7, pp. 1839–1848, 2017.
- [105] M. Huttemann, I. Lee, and M. H. Malek, "(–)-Epicatechin maintains endurance training adaptation in mice after 14 days of detraining," *The FASEB Journal*, vol. 26, no. 4, pp. 1413–1422, 2012.
- [106] M. Huttemann, I. Lee, G. A. Perkins, S. L. Britton, L. G. Koch, and M. H. Malek, "(–)-Epicatechin is associated with increased angiogenic and mitochondrial signalling in the hindlimb of rats selectively bred for innate low running capacity," *Clinical Science (London, England)*, vol. 124, no. 11, pp. 663–674, 2013.
- [107] I. Lee, M. Huttemann, A. Kruger, A. Bollig-Fischer, and M. H. Malek, "(–)-Epicatechin combined with 8 weeks of treadmill exercise is associated with increased angiogenic and mitochondrial signaling in mice," *Frontiers in Pharmacology*, vol. 6, article 43, pp. 1–10, 2015.

- [108] A. Moreno-Ulloa, A. Cid, I. Rubio-Gayosso, G. Ceballos, F. Villarreal, and I. Ramirez-Sanchez, "Effects of (-)-epicatechin and derivatives on nitric oxide mediated induction of mitochondrial proteins," *Bioorganic & Medicinal Chemistry Letters*, vol. 23, no. 15, pp. 4441–4446, 2013.
- [109] A. Moreno-Ulloa, L. Nogueira, A. Rodriguez et al., "Recovery of indicators of mitochondrial biogenesis, oxidative stress, and aging with (-)-epicatechin in senile mice," *The Journals of Gerontology. Series a, Biological Sciences and Medical Sciences*, vol. 70, no. 11, pp. 1370–1378, 2015.
- [110] L. Nogueira, I. Ramirez-Sanchez, G. A. Perkins et al., "(-)-Epicatechin enhances fatigue resistance and oxidative capacity in mouse muscle," *The Journal of Physiology*, vol. 589, Part 18, pp. 4615–4631, 2011.
- [111] I. Ramirez-Sanchez, L. Nogueira, A. Moreno et al., "Stimulatory effects of the flavanol (-)-epicatechin on cardiac angiogenesis: additive effects with exercise," *Journal of Cardiovascular Pharmacology*, vol. 60, no. 5, pp. 429–438, 2012.
- [112] I. Ramirez-Sanchez, A. Rodriguez, A. Moreno-Ulloa, G. Ceballos, and F. Villarreal, "(-)-Epicatechin-induced recovery of mitochondria from simulated diabetes: potential role of endothelial nitric oxide synthase," *Diabetes & Vascular Disease Research*, vol. 13, no. 3, pp. 201–210, 2016.
- [113] K. G. Yamazaki, A. Y. Andreyev, P. Ortiz-Vilchis et al., "Intravenous (-)-epicatechin reduces myocardial ischemic injury by protecting mitochondrial function," *International Journal of Cardiology*, vol. 175, no. 2, pp. 297–306, 2014.
- [114] H. Yamamoto, K. Morino, L. Mengistu et al., "Amla enhances mitochondrial spare respiratory capacity by increasing mitochondrial biogenesis and antioxidant systems in a murine skeletal muscle cell line," *Oxidative Medicine and Cellular Longevity*, vol. 2016, Article ID 1735841, p. 11, 2016.
- [115] Y. Mei, Y. Zhang, K. Yamamoto, W. Xie, T. W. Mak, and H. You, "FOXO3a-dependent regulation of Pink1 (Park6) mediates survival signaling in response to cytokine deprivation," *Proceedings of the National Academy of Sciences of the United States of America*, vol. 106, no. 13, pp. 5153–5158, 2009.
- [116] M. Song, G. Gong, Y. Burelle et al., "Interdependence of Parkin-mediated mitophagy and mitochondrial fission in adult mouse hearts," *Circulation Research*, vol. 117, no. 4, pp. 346–351, 2015.
- [117] Y. Tang, C. Gao, M. Xing et al., "Quercetin prevents ethanol-induced dyslipidemia and mitochondrial oxidative damage," *Food and Chemical Toxicology*, vol. 50, no. 5, pp. 1194–1200, 2012.
- [118] T. Bai, Y. Yang, Y. L. Yao et al., "Betulin alleviated ethanol-induced alcoholic liver injury via SIRT1/AMPK signaling pathway," *Pharmacological Research*, vol. 105, pp. 1–12, 2016.
- [119] X. Jin, M. Chen, L. Yi et al., "Delphinidin-3-glucoside protects human umbilical vein endothelial cells against oxidized low-density lipoprotein-induced injury by autophagy upregulation via the AMPK/SIRT1 signaling pathway," *Molecular Nutrition & Food Research*, vol. 58, no. 10, pp. 1941–1951, 2014.
- [120] I. H. Lee, L. Cao, R. Mostoslavsky et al., "A role for the NAD-dependent deacetylase Sirt1 in the regulation of autophagy," *Proceedings of the National Academy of Sciences of the United States of America*, vol. 105, no. 9, pp. 3374–3379, 2008.
- [121] J. X. Song, Y. R. Sun, I. Peluso et al., "A novel curcumin analog binds to and activates TFEB in vitro and in vivo independent of MTOR inhibition," *Autophagy*, vol. 12, no. 8, pp. 1372–1389, 2016.
- [122] M. Wirth, J. Joachim, and S. A. Tooze, "Autophagosome formation—the role of ULK1 and Beclin1-PI3KC3 complexes in setting the stage," *Seminars in Cancer Biology*, vol. 23, no. 5, pp. 301–309, 2013.
- [123] X. Ma, H. Liu, J. T. Murphy et al., "Regulation of the transcription factor EB-PGC1alpha axis by beclin-1 controls mitochondrial quality and cardiomyocyte death under stress," *Molecular and Cellular Biology*, vol. 35, no. 6, pp. 956–976, 2015.
- [124] J. S. Kim, T. Nitta, D. Mohuczy et al., "Impaired autophagy: a mechanism of mitochondrial dysfunction in anoxic rat hepatocytes," *Hepatology*, vol. 47, no. 5, pp. 1725–1736, 2008.
- [125] T. Finkel, "Signal transduction by mitochondrial oxidants," *The Journal of Biological Chemistry*, vol. 287, no. 7, pp. 4434–4440, 2012.
- [126] T. Finkel, "Signal transduction by reactive oxygen species," *The Journal of Cell Biology*, vol. 194, no. 1, pp. 7–15, 2011.
- [127] Y. Wang and S. Hekimi, "Mitochondrial dysfunction and longevity in animals: untangling the knot," *Science*, vol. 350, no. 6265, pp. 1204–1207, 2015.
- [128] G. S. Shadel and T. L. Horvath, "Mitochondrial ROS signaling in organismal homeostasis," *Cell*, vol. 163, no. 3, pp. 560–569, 2015.
- [129] J. Yun and T. Finkel, "Mito-hormesis," *Cell Metabolism*, vol. 19, no. 5, pp. 757–766, 2014.
- [130] B. Halliwell, "Are polyphenols antioxidants or pro-oxidants? What do we learn from cell culture and in vivo studies?" *Archives of Biochemistry and Biophysics*, vol. 476, no. 2, pp. 107–112, 2008.
- [131] F. Pietrocola, G. Mariño, D. Lissa et al., "Pro-autophagic polyphenols reduce the acetylation of cytoplasmic proteins," *Cell Cycle*, vol. 11, no. 20, pp. 3851–3860, 2012.
- [132] J. A. Lim, L. Li, O. Kakhlon, R. Myerowitz, and N. Raben, "Defects in calcium homeostasis and mitochondria can be reversed in Pompe disease," *Autophagy*, vol. 11, no. 2, pp. 385–402, 2015.
- [133] J. Demers-Lamarche, G. Guillebaud, M. Tlili et al., "Loss of mitochondrial function impairs lysosomes," *The Journal of Biological Chemistry*, vol. 291, no. 19, pp. 10263–10276, 2016.

Review Article

Tissue- and Condition-Specific Isoforms of Mammalian Cytochrome *c* Oxidase Subunits: From Function to Human Disease

Christopher A. Sinkler,¹ Hasini Kalpage,¹ Joseph Shay,¹ Icksoo Lee,² Moh H. Malek,³ Lawrence I. Grossman,¹ and Maik Hüttemann¹

¹Center for Molecular Medicine and Genetics, Wayne State University School of Medicine, Detroit, MI 48201, USA

²College of Medicine, Dankook University, Cheonan-si, Chungcheongnam-do 31116, Republic of Korea

³Department of Health Care Sciences, Eugene Applebaum College of Pharmacy and Health Sciences, Wayne State University, Detroit, MI 48201, USA

Correspondence should be addressed to Maik Hüttemann; mhuttema@med.wayne.edu

Received 2 February 2017; Accepted 29 March 2017; Published 16 May 2017

Academic Editor: Ryuichi Morishita

Copyright © 2017 Christopher A. Sinkler et al. This is an open access article distributed under the Creative Commons Attribution License, which permits unrestricted use, distribution, and reproduction in any medium, provided the original work is properly cited.

Cytochrome *c* oxidase (COX) is the terminal enzyme of the electron transport chain and catalyzes the transfer of electrons from cytochrome *c* to oxygen. COX consists of 14 subunits, three and eleven encoded, respectively, by the mitochondrial and nuclear DNA. Tissue- and condition-specific isoforms have only been reported for COX but not for the other oxidative phosphorylation complexes, suggesting a fundamental requirement to fine-tune and regulate the essentially irreversible reaction catalyzed by COX. This article briefly discusses the assembly of COX in mammals and then reviews the functions of the six nuclear-encoded COX subunits that are expressed as isoforms in specialized tissues including those of the liver, heart and skeletal muscle, lung, and testes: COX IV-1, COX IV-2, NDUFA4, NDUFA4L2, COX VIaL, COX VIaH, COX VIb-1, COX VIb-2, COX VIIaH, COX VIIaL, COX VIIaR, COX VIIH/L, and COX VIII-3. We propose a model in which the isoforms mediate the interconnected regulation of COX by (1) adjusting basal enzyme activity to mitochondrial capacity of a given tissue; (2) allosteric regulation to adjust energy production to need; (3) altering proton pumping efficiency under certain conditions, contributing to thermogenesis; (4) providing a platform for tissue-specific signaling; (5) stabilizing the COX dimer; and (6) modulating supercomplex formation.

1. Introduction

Mammalian mitochondria are remarkable cellular organelles, possessing a unique, conserved genome distinct from the nuclear genome, as well as providing the means for energy generation theorized as a principle requirement for the advent of multicellular organisms [1]. The evolution of the electron transport chain (ETC) together with ATP synthase—a series of large multisubunit protein complexes responsible for oxidative phosphorylation (OxPhos)—was pivotal in this development, increasing the amount of adenosine triphosphate (ATP) generated from the oxidation of glucose by ~15-fold compared to fermentative processes [2]. The ETC consists of three proton pumps, NADH

dehydrogenase (complex I), *bc*₁-complex (complex III), and cytochrome *c* oxidase (COX; complex IV). In addition, the ETC contains succinate dehydrogenase (complex II), which feeds electrons from succinate into the ETC but does not pump protons, and the small electron carriers cytochrome *c* and ubiquinone.

In addition to their essential function in aerobic energy metabolism, mitochondria have been found to have vital functions in apoptosis [3–7], aging [8–10], and numerous diseases ranging from cancer [11] to diseases involving ischemia/reperfusion injury [12] to inflammation [13, 14] and sepsis [15–17]. Within the context of the cell itself, mitochondria perform multiple functions beyond the scope of oxidative phosphorylation, including calcium modulation

and sequestration [18–20] as well as production of reactive oxygen species (ROS). ROS have been implicated in numerous pathways as an essential signal [14, 21–23] and further as an important regulator of mitochondrial proteins, including COX biogenesis and assembly [24]. Cellular production of ROS can be directly modulated by uncoupling the electron transport function from OxPhos or by attenuating mitochondrial electron flow through the addition of respiratory inhibitors [25, 26]. It is important to note that despite directly interacting with dioxygen, COX itself is not known to generate ROS—this function is specifically linked to the NADH dehydrogenase and *bc*₁ complexes of the ETC [27–29]. Given the inherently dangerous nature of ROS and their ability to modify nonspecific targets, defense mechanisms exist to attenuate their destructive potential. Superoxide dismutase and catalase exist to degrade ROS products into less reactive forms, while glutathione, thioredoxin, and other thiols exist to act as buffering agents [30–32]. Together, these systems represent a vital component of a balanced system that must be tightly regulated.

Mitochondria themselves are thought to have evolved from symbiosis (known as the serial endosymbiotic theory, or SET) between early eukaryotic cells and aerobic bacteria in an event that occurred over a billion years ago [33, 34]. Often referred to as bacteria-size organelles (2–4 μ m), mitochondria vary not only in their number per cell but in their localization, size, shape, and features, adapting their function to the needs of the cell at hand. For example, while it has been estimated that hepatocytes in mammals contain roughly 800 mitochondria per cell, mammalian oocytes are estimated to contain over 100,000 [35]. Nearly 200,000 copies of the mitochondrial genome can be found per oocyte on average, with content affecting fertilization capacity [36].

Mitochondria possess two membranes: the inner mitochondrial membrane (IMM) that forms the cristae and the outer mitochondrial membrane (OMM). Central to the organelle are also the aqueous compartments, the mitochondrial matrix, and the intermembrane space. Tight regulation of ion flow between these distinct pockets is essential for the ETC's core functions. In animals, the mitochondrial genome is comparatively small, averaging about 16,500 base pairs and equaling 16,569 base pairs in humans [37]. It is devoid of introns, with the exception in select lower animals such as sea anemones [38]. In comparison, the mitochondrial genome of plants has evolved in a remarkably opposite direction, amassing much larger sizes in the range of 15 kbp to 2.4 Mbp and containing numerous processing elements, including introns [39]. It is apparent that despite divergent evolutionary tracks, mitochondria are essential to support increased energy demand under certain conditions such as exercise, and controlled regulation is critically needed for multicellular life to exist.

The ETC utilizes electrons derived from food molecules that enter the chain at complexes I and II. Both complexes transfer the electrons to ubiquinone from their substrates NADH and FADH₂, respectively. These electrons are subsequently transferred to complex III, where they are used to reduce two molecules of cytochrome *c*. Cytochrome *c* will

then shuttle these electrons to COX, which terminates the chain by transferring the electrons to dioxygen, generating water. COX is similar to complexes I and III in that electron transport is coupled to the pumping of protons from the mitochondrial matrix to the intermembrane space, contributing to the formation of the electrochemical gradient, of which the mitochondrial membrane potential ($\Delta\Psi_m$) constitutes the major part in animals. This force drives ATP synthase in its synthesis of ATP from ADP and inorganic phosphate [40]. Acting as a rotary motor, ATP synthase uses the combined proton motive force generated from the other complexes to generate rotational and eventually chemical energy by changing conformation to combine a phosphate molecule with ADP to form ATP [41].

Until recently, characterization of the ETC has largely been based around a random-collision model, where individual components and substrates interact as a function of concentration and chance [42, 43]. There has been a growing trend towards studying the ETC as a solid-state system, a phenomenon known as supercomplexes. With the exception of succinate dehydrogenase (complex II) and ATP synthase, the remaining components of the ETC have been shown to associate with one another with varying stoichiometries of complexes I, III, and IV [44–47]. Evidence for the formation and stabilization of supercomplexes has largely been based around the isolation of complexes using two-dimensional blue native gel electrophoresis (2D-BN-PAGE) [48, 49]. Recently, new factors have been identified to be important for the formation and modulation of supercomplexes, including isozymes and assembly factors of COX [50–52].

2. Composition of Cytochrome *c* Oxidase

COX is the terminal enzyme of the mitochondrial respiratory chain. Mammalian COX from bovine heart was crystallized as a 13-subunit, homodimeric enzyme [53]. However, it contains at least one more less tightly bound subunit in stoichiometric amounts, NDUFA4 [54], which was initially thought to be a subunit of complex I. COX is one of only four mitochondrial complexes that are encoded by both the nuclear and mitochondrial genomes and that are all components of the OxPhos process (i.e., complexes I, III, IV, and V but not complex II, which is encoded entirely by nuclear DNA). Bigenomic enzymes are unique in that their regulation requires tight coordination between the nuclear and mitochondrial genomes. For the sake of clarity and consistency, in this review, the nomenclature assigned to each of the subunits by Kadenbach et al. will be used [55]. Of these subunits, the three largest subunits (COX I, II, and III) are encoded by the mitochondrial DNA; the remaining 11 subunits (COX IV, Va, Vb, VIa, VIb, VIc, VIIa, VIIb, VIIc, VIII, and NDUFA4) are encoded by the nuclear genome and play critical roles in energy metabolism and regulation. With the exception of subunits Va and Vb, which are bound to the matrix side, and subunit VIb, which faces solely the intermembrane space, each of the remaining subunits contains a hydrophobic transmembrane region. Through the contribution of four electrons transferred via cytochrome *c* and four

protons channeled from the mitochondrial matrix, it is capable of reducing dioxygen to water.

Of the mitochondrial-encoded subunits, subunits I and II carry out the catalytic reaction. They are the largest and third largest subunits of the holoenzyme, respectively. Subunits I and III are highly hydrophobic in nature and contain multiple transmembrane domains, which suggests a rationale for being encoded in the mitochondria, thereof avoiding complicated protein import from the cytosol and possible aggregation. In contrast, the relatively smaller and more hydrophilic nature of the nuclear-encoded subunits allows for posttranslational localization to the mitochondria. Catalytic subunits I and II contain prosthetic metal groups. Subunit I contains both a low-spin heme *a* redox center and a high-spin Cu_B-heme *a*₃ binuclear center, while subunit II contains a Cu_A redox center formed by two copper ions. Of these redox sites, the Cu_A site is responsible for the initial step of the catalytic cycle by accepting the electrons transferred from cytochrome *c*, which then reduces the heme *a* site in COX I. These electrons are then subsequently transferred to the Cu_B-heme *a*₃ site, where molecular oxygen binds and is reduced to water [56]. Molecular inhibitors such as CO, NO, cyanide, or azide bind to the Cu_B-heme *a*₃ center, preventing the binding of oxygen and stopping the enzyme's catalytic action.

The movement of protons is accomplished through two proton uptake pathways, known as the D and K channels [57–59], named after the conserved residues located at the matrix side and the opening of the proton channels. These two channels deliver protons required for the water formation reaction as well as the pumping of protons. The D and K channels are well understood and demarcate the lower half of the proton network from the matrix up to the heme groups located near the middle of the membrane including the oxygen binding site. However, the proton exit pathways and the precise proton pumping mechanism remain unknown despite a wealth of proposed models [58, 60–62]. A third channel, referred to as the H channel, was proposed based on the bovine COX structure and mutational analyses [63–65]. However, mutational studies with the corresponding amino acids in bacterial COX from *Paracoccus denitrificans* questioned the presence of this pathway at least in the bacterial enzyme [66].

3. Allosteric and Posttranslational Regulation of Cytochrome *c* Oxidase

As expected of an enzyme with critical functions in membrane potential homeostasis and control of electron flux, COX is tightly controlled through multiple regulatory processes including allosteric regulation and posttranslational modifications. Although it is not a focus of the current article, a few select examples will be briefly discussed.

In the presence of ADP, the binding affinity for cytochrome *c* to COX is increased by fivefold as compared to that of ATP, indicating that enzyme activity is modulated allosterically by the ATP/ADP ratio [67–69]. Unsurprisingly, COX is also regulated through phosphorylation of serine/threonine and tyrosine residues [70]. To date, detection of

in vivo phosphorylation sites through mass spectrometry has yielded 18 different targets [71], though the specific functions of most remain unknown. One such modification that has been characterized is the inhibitory phosphorylation of tyrosine 304 of COX I, in a cAMP-dependent manner [72]. This modification was later shown to be also stimulated by TNF α in the liver through an inflammatory cascade, resulting in diminished COX function and ATP levels [14]. This phosphorylation was then proposed to be an underlying mechanism of disease conditions as seen in acute inflammation or sepsis, in which oxygen utilization is impaired despite oxygen availability, a phenomenon called cytopathic hypoxia. Serine 441 on the same subunit was suggested to act as a functional toggle for the allosteric inhibition of COX by ATP through phosphorylation, but subsequent mass spectrometry analysis was unable to detect this modification [73]. Furthermore, on subunit IV-1, serine 58 was suggested through targeted mutational analysis as capable of performing this function, and protein kinase A (PKA) was proposed to phosphorylate this site and enable ATP to inhibit the enzyme allosterically [74]. However, experimental evidence that this site can be phosphorylated, for example, through mass spectrometry, still has to be provided. It should also be noted that this cAMP-dependent phosphorylation takes place on the matrix side of COX and is distinct from the indirect cAMP-dependent phosphorylation on tyrosine 304 [72], which occurs in the mitochondrial intermembrane space and cannot be mediated by PKA since it does not target tyrosine residues. See [4, 71] for comprehensive reviews of this literature.

As a side glance, COX can also be externally regulated through application of near-infrared light (IRL). COX contains two copper centers that are involved in enzyme catalysis and have been shown to function as the photoacceptors for IRL [75, 76] because Cu²⁺ broadly absorbs IRL in the range of 700–1000 nm as can be seen in the COX spectrum [77]. IRL was proposed to activate COX leading to health benefits in several studies including improving cognitive function in humans, increasing cell survival in cultured neurons in vitro after poisoning of COX with inhibitor potassium cyanide, and improving wound healing, just to name a few [78–82]. Modulation of COX activity in conditions of mitochondrial dysfunction seems to be an interesting area worth exploring for clinical applications, in particular because of the noninvasive nature of the treatment.

4. Synthesis and Assembly of Cytochrome *c* Oxidase

The assembly of COX is a complex, tightly-regulated process with a large number of auxiliary components. To date, over 30 gene products have been identified that are solely involved in the biogenesis of the holoenzyme [83]. These products include a variety of participants, ranging from translocases, translational activators, and molecular chaperones to metallochaperones and enzymes involved in the biosynthesis of heme A [84]. The earliest points of translation and assembly have best been studied in the yeast *Saccharomyces cerevisiae*, where the translational activators Mss51 and Pet309 are

TABLE 1: Nuclear-encoded cytochrome *c* oxidase subunit isoform mutations¹.

Gene ID	Type of mutation	Disease phenotypes reported
<i>COX4I2</i>	Human homozygous missense mutation in 4 patients	Exocrine pancreatic insufficiency; dyserythropoietic anemia; calvarial hyperostosis [163]
<i>COX4I2</i>	Mouse homozygous knockout	Reduced airway activity; airway hyporeactivity; lung pathologies [151]
<i>COX6A1</i>	5 bp deletion in a splicing element of intron 2 in two consanguineous families	Charcot-Marie-Tooth disease [204]
<i>COX6B1</i>	Identical homozygous missense mutation in two patients	Infantile encephalomyopathy [181]
<i>COX6B1</i>	Homozygous missense mutation in one patient	Hydrocephalus and cardiomyopathy [182]
<i>COX7B</i>	One patient heterozygous for a 1 bp deletion leading to a frameshift in exon 3; one patient heterozygous for a splice site mutation; one patient with a missense mutation in exon 2	X-linked microphthalmia with linear skin lesions [205]
<i>NDUFA4</i>	Homozygous splice site mutation in four siblings	Leigh syndrome-like [167]
<i>COX8</i>	Homozygous splice site mutation causing frame shift in one patient	Leigh syndrome leukodystrophy and severe epilepsy [202]

¹Note that additional *heterozygous* mutations have been identified in individual patients with COX deficiency in *COX4I2*, *COX5a*, and *COX6a2* but have not been functionally confirmed as disease causing [164].

responsible for the early regulation of COX I transcription and translation [85–90]. In mammals, however, mitochondrial mRNAs contain minimal 5'-UTR regions for translational activators to bind to, indicating that regulation of COX I translation may be controlled through an alternative pathway [91]. The gene *TACO1* has been hypothesized to fulfill this role, as patients with mutations in the gene suffer from a progressive form of Leigh syndrome alongside reduced translation of COX I [92]. In mice, a *TACO1* missense mutation was linked with reduced COX I translation, deficit in total COX levels, and late-onset mitochondrial dysfunction contributing to visual deficit and motor impairment [93]. In general, much of what is known of mammalian COX assembly is gleaned from investigation of mitochondrial diseases and the enzymatic deficiencies presented [94–96]. The majority of reported COX-associated disease has been attributed to mutations in assembly factors and early chaperones [97]. However, the nuclear-encoded subunits, particularly those with tissue- or condition-specific isoform expression, have also emerged as disease-causing or likely disease-causing candidate genes in COX deficiencies (see Table 1). The fact that mutations in the nuclear-encoded subunits of COX are very rare highlights the subunits' importance for COX function, regulation, and stability.

Assembly of COX is a highly regulated process which integrates cytosolic and matrix protein synthesis of nuclear- and mitochondrial-encoded subunits (Figure 1). Even the first step, synthesis of COX subunit I, is controlled, via interaction of COX I mRNA containing ribosomes with COX assembly factors to synchronize with the influx of nuclear-encoded subunits [98]. COX assembly begins with the translocation of COX I to the membrane, followed closely by the association of subunits IV and Va [99]. The twin-CX₅C intermembrane protein *CMC1* stabilizes COX I, in tandem with the COA3-COX14 early intermediate, prior to the incorporation of any other COX subunits. *CMC1*-knockout cells showed a 30% reduced basal respiratory rate, accumulation of COX assembly intermediates, and very low to undetectable

levels of COX in I + III₂ + IV_n supercomplexes [100]. Translation of COX I mRNA is completed through integration of the critical heme A moiety. Biosynthesis and insertion of heme A into COX I require the assembly factors COX10 and COX15, which are involved in maturation of the protoheme through several stages, as shown from multiple studies of yeast mitochondria [101–103]. These assembly factors have been implicated in COX assembly in mammals primarily through studies linking their defect to mitochondrial disease, specifically Leigh syndrome and cardiomyopathies [104–108]. The assembly protein SURF1 has been a subject of investigation for its known role in early COX biogenesis, as complexes lacking the protein stall in assembly with partial holoenzyme products containing only subunits I, IV, and Va in humans [109]. Mutations in the *SURF1* gene in humans cause Leigh Syndrome [110], a severe neurodegenerative condition with early lethality due to COX deficiency. In stark contrast, mice that are null for *Surf1* live longer than control mice despite lower COX activity [111]. The knockout of SURF1 has also been linked to increased oxidative stress and induction of the mitochondrial unfolded protein response [112, 113]. Furthermore, despite increased reactive oxygen species (ROS) production, *Surf1*-knockout mice have shown increases in glucose metabolism, memory, and blood flow in the brain [114]. Analysis of mouse fibroblasts with a homozygous *Surf1* knockout showed only marginal differences in assembly products compared to that of wild-type mouse fibroblasts, indicating that SURF1 may vary in its importance in assembly in a species-specific manner [115, 116]. Since *Surf1* knockout in mice results in a much milder phenotype to that seen in patients with point mutations, an alternative interpretation would be that the mutant protein products may still interact and bind to COX assembly intermediates. This could result in assembly pausing and accumulation of dysfunctional COX intermediates, further enhancing mitochondrial dysfunction. Indirect evidence of such a scenario was seen in three cell lines from Leigh syndrome patients, which showed a higher running band in a Western blot with a

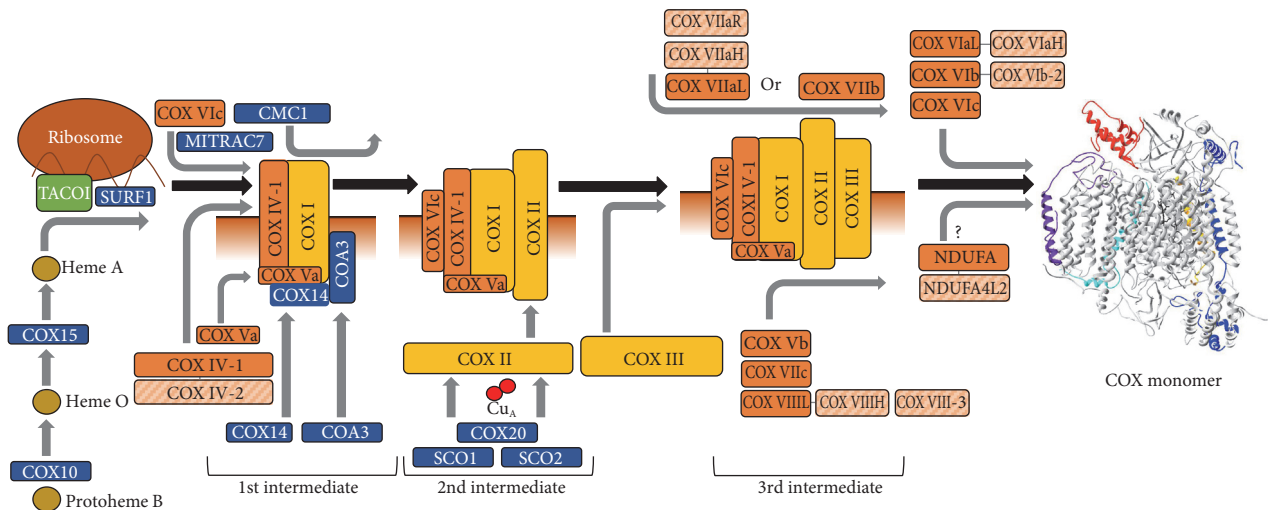


FIGURE 1: The early assembly of cytochrome *c* oxidase. Assembly of COX begins with translation of mitochondrial RNA with mitochondrial ribosomes and proceeds in a series of intermediates. The inner mitochondrial membrane is shown in conjunction with the partially assembled enzyme intermediates, with the bottom region denoting the matrix side. TACO1, which is involved in RNA binding, is shown in green, assembly factors are in blue, and mitochondrial-encoded subunits (COX I, COX II, and COX III) are in yellow. Nuclear subunits are indicated in orange, with isoforms grouped and denoted with a striped pattern in light orange.

COX subunit IV antibody [117]. Since denaturing conditions were used in this experiment, it is conceivable that COX subunit IV forms a covalent intermediate with SURF1 (or another protein acting in concert with SURF1), but mutation or truncation of SURF1 prevents the release of COX subunit IV. Such COX subunit IV-SURF1 intermediates would not be possible in the knockout, possibly explaining the mild phenotype. Future work should further characterize the COX subunit IV containing covalent intermediates with the potential of revealing the molecular mechanism of SURF1's chaperone function.

The human analog of the yeast protein COA3, known as CCDC56 or hCOA3, has been shown to stabilize subunit I in the process of assembly and is critical for proper COX function [118]. Another study identified the mitochondrial chaperone MITRAC7 in the early assembly of COX [119]. The authors concluded that it associates with a COX I/COX IV/COX VIc intermediate to stabilize it before progressing to the next stage of assembly (Figure 1). Knockouts of MITRAC7 show increased COX I turnover and reduced biogenesis, whereas overexpression leads to accumulation of the early intermediate and concurrent reduction in complete COX assembly.

Assembly continues with association of the mitochondrial-encoded COX subunit II into a transient intermediate [120]. Continued assembly requires incorporation of copper into the catalytic core before the mature holoenzyme can be established. This is accomplished through action of the metallochaperones SCO1 and SCO2; both have independent functions in incorporating copper into the Cu_A site of COX II [121–123]. The COX assembly factor COX20, also known as FAM36A, is an integral part of this process—COX20 stabilizes COX II in the process of copper insertion, and its absence results in inefficient incorporation into assembly intermediates [124]. Mutation of this

gene results in ataxia and muscle hypotonia as a consequence of COX deficiency [125]. After insertion of heme *a* and copper, the COX I/COX II/COX IV/COX Va intermediate associates with COX3 and subsequently incorporates the remaining nuclear subunits in a relatively swift manner. Very little is known about the exact order of incorporation, though hypotheses may be drawn from the physical relationship of the individual subunits. It has been shown that the immature enzyme incorporates subunits Vb, VIc, and VIIa or VIIb, VIIc, and VIII, before subsequent incorporation of VIa, VIb, and whichever of VIIa or VIIb that remains [94, 126]. In addition, the time point of the incorporation of NDUFA4 remains unknown. After full assembly of the 14 subunits into a monomer, the holoenzyme stabilizes as a functional dimer [53, 127].

Although many of the unique interactions surrounding COX assembly are still unclear, the molecular mechanisms responsible for degradation or replacement of the individual subunits remain even more obscure. Regulation of COX subunit transcription at the mRNA level has been explored in the context of temperature fluctuations in goldfish. It was concluded that individual subunits are universally controlled at the transcription level, but degradation rates may differ and be responsible for differential transcript levels in cold acclimation [128]. Recently, the mitochondrial ATPase lactation elevated 1 (LACE1) was investigated for its role in degradation of COX, based on sequence homology with the yeast ATPase Afg1, which serves a similar role [129, 130]. It was found that LACE1 directly interacts with subunits IV and Va and is responsible for proteolysis of excess subunits IV, Va, and VIa [131].

The hypothesis that the function of COX may be controlled by tissue-specific isoform expression was first proposed by the Kadenbach group [132] and later confirmed by many others. Small differences in molecular weights of

subunits harvested from multiple mammalian species and tissues led to the suggestion that there may be different isoforms present. Given the distinct energy demand and response to external regulators such as hormones and second messengers in highly specialized organs such as the heart, kidney, liver, skeletal muscle, lung, testes, and brain, it is not surprising that divergent isoforms have evolved to accommodate these conditions. It is surprising, however, that in mammals, only COX and its partner cytochrome *c* have tissue-specific and developmentally regulated isoforms, whereas none have been reported for the other OxPhos complexes. An explanation for the requirement of a fine-tuned regulation in COX may be as follows: it was suggested that the reaction catalyzed by COX and cytochrome *c* is the rate-limiting step of the ETC in intact cells and tissues under physiological conditions [133–137]. The free energy released in this reaction ($\Delta G^\circ = 100 \text{ kJ/mol}$) is about twice as high compared to that in complexes I and III [138]. This makes it an essentially irreversible reaction, which may explain why the terminal step of the ETC is a particularly important target for regulation. Thus, one central purpose of this article is to highlight the regulatory features of tissue-specific isoform expression of COX subunits in mammalian systems. The intent is to present this topic from two perspectives: the regulatory elements that control expression on a genetic level for the induction of isoforms triggered by certain conditions such as hypoxia and the effect of isoform expression and regulatory function within the context of the COX holoenzyme itself. Investigating the nature of these features within their given tissue context including tissue-specific energy requirements will allow elucidation of potential hypotheses for their existence, summarized in Figure 3, and connect tissue-specific isoform expression with varying properties of COX.

5. Isoforms of Cytochrome *c* Oxidase Subunits

Given the critical role of COX in regulating oxygen consumption and ATP production, it is of no surprise that isoform expression is regulated through multiple mechanisms. It can be broadly sorted into two overlapping categories: hypoxia-induced and development-induced. The first category comprises isoforms that are differentially expressed through oxygen tension, including subunit IV-2 and the newly identified subunit NDUFA4. These subunits carry a ubiquitously expressed isoform alongside an isoform preferentially induced under hypoxic conditions and expressed only in certain tissues. It is important to note that in addition to regulation via oxygen, COX subunit IV-2 is also developmentally induced as discussed below. The second class of COX isoform pairs can be described as development-specific isoforms, including isoforms of subunits VIa, VIb, VIIa, and VIII. A subset of these, subunits VIa, VIIa, and VIII, contain a “liver-type” (L) and “heart-type” (H) isoform. During maturation, in particular after birth, the liver-type isoforms are switched to heart-type in the heart and skeletal muscle. Finally, subunit VIb has a somatic- and testes-specific isoform. Note that roman numbers are used to refer to the protein whereas standard numerals and italics

are used to refer to the gene with all capital letters referring to the human gene.

5.1. Oxygen-Regulated Isoforms

5.1.1. Subunit IV. The largest of the nuclear-encoded subunits, COX subunit IV, is located adjacent to the catalytic subunits, containing numerous contact sites with subunits I and II [53] (Figure 2). This pivotal location allows the subunit to play a major role in regulation of overall COX activity. As discussed below, COX IV has been shown to contain a conserved ATP binding pocket on the matrix side, allowing for allosteric inhibition of COX activity at high ATP/ADP ratios [74, 139, 140]. In *S. cerevisiae*, the corresponding COX subunit (subunit V in yeast nomenclature) is expressed as two isoforms, COX Va and COX Vb, which are expressed in varying amounts dependent on the oxygen concentration. COX Va is preferentially expressed in normoxic conditions, while COX Vb is induced under hypoxia, allowing for control of enzyme function dependent on oxygen concentration [141–143]. The hypoxic isoform Vb has a higher turnover rate and intramolecular electron transfer rate than isoform Va contained in yeast COX [144]. It was proposed that mammalian COX IV serves a similar purpose to that of yeast COX V, with differential expression of two isoforms in response to local oxygen conditions [140, 145].

The principal isoform, mammalian COX IV-1, is ubiquitously expressed in all tissues in vertebrates. It has been shown to be a required component for COX biogenesis, coordinating the assembly of the holoenzyme alongside the mitochondrial-encoded subunit I [126]. This subunit has been shown to be responsible for modulating COX activity through allosteric regulation—ATP and ADP are capable of binding to COX through subunit IV, resulting in fine-tuned control of respiration [67, 69, 139]. This ATP-mediated inhibitory effect was proposed to require phosphorylation of the subunit by PKA [146, 147].

Analogous to yeast COX, there is a second isoform of COX subunit IV in animals, which is expressed differentially in response to changes in oxygen concentration. Interestingly, the COX IV-1/IV-2 isoform pair found in mammals today arose by a gene duplication event about 320 million years ago [140], earlier in evolution compared to that of the origin of the other isoform pairs and at a time when atmospheric oxygen concentrations fluctuated dramatically [148], suggesting a possible adaptation to varying oxygen levels. The second isoform, named COX isoform IV-2 (*COX4-2* or *COX4I2* for the gene), was first discovered in tuna fish and found to share 56% sequence homology with *COX4-1* at the protein level [149]. Following these studies, *COX4-2* was identified and characterized as a component of COX expressed in mammals including humans [140]. The precursor peptides of *COX4-1* and *COX4-2* are similar in length with 169 and 171 amino acids, respectively. The two isoforms share only 44% nucleotide homology averaged across mammalian species, while *COX4-2* itself shows high sequence homology of 78% between the species analyzed [140]. Quantitative PCR performed on rat tissues revealed that *COX4-2* is primarily lung-specific, showing similar

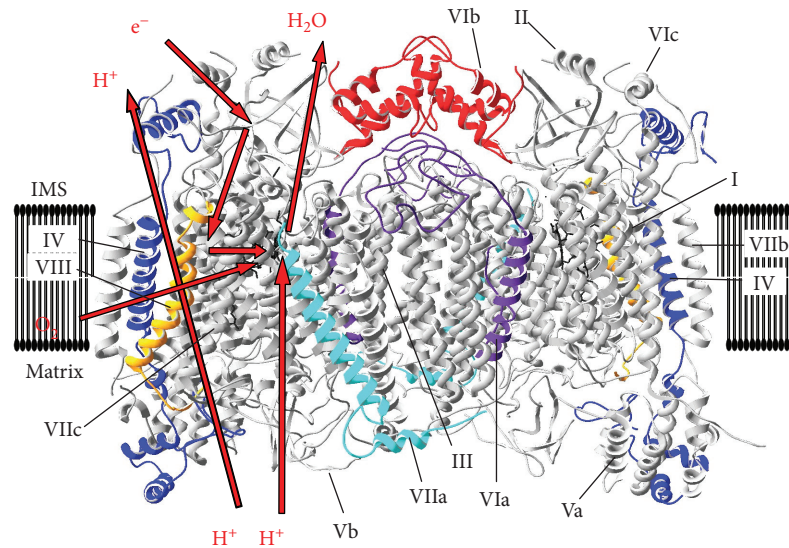


FIGURE 2: Structure of cytochrome *c* oxidase. Crystallographic data of cow heart COX [53] were processed with the program Swiss-PDBViewer 4.1. COX subunits that have isoforms are highlighted in color: IV, blue; VIa, purple; VIb, red; VIIa, cyan; and VIII, yellow. Left monomer: electron flow from cytochrome *c* to Cu_A, heme *a*, heme *a*₃/Cu_B and molecular oxygen and concomitant proton pumping are schematically shown. Note that COX subunit NDUFA4, which is less tightly bound to COX and lost during purification, is not shown.

expression levels compared to the ubiquitous *COX4-1* isoform, followed by expression in the placenta [150] and minor expression in the heart (~8%) and brain (~4%) [140]. Similar results have been found in mice, showing virtually no expression in liver or pancreatic tissue [151]. *COX4-2* is also developmentally regulated and strongly induced after birth in human lung [140], as discussed for other COX isoforms in the next section.

One interesting feature of COX IV-2 is that it contains three unique cysteine residues, one within the transmembrane region and two on the matrix side, near the proposed ATP binding site for allosteric regulation [140]. The ubiquitous COX IV-1 contains no cysteine residues. This suggests that *COX4-2* may incorporate redox signaling as part of its function, given that the twin cysteines on the matrix side are close enough to potentially form a disulfide bond. In addition, the internal cysteine residue may interact with other proteins or be modified posttranslationally in response to redox changes within the membrane.

The biochemical and physiological effects of incorporating COX IV-2 in the COX holoenzyme have begun to be characterized, providing necessary insight into the functional features of this isoform. Isolated COX from cow lung, containing COX IV-2, was shown to have about twofold increased activity compared to liver COX, which does not contain COX IV-2 [151]. In order to study the effects of COX IV-2 in vivo, a mouse model containing a knockout of *Cox4-2*, created by deletion of exons 2 and 3, was established [151]. It was demonstrated that COX activity was similarly modulated by knocking out *Cox4-2*, as lung COX from the wild-type mice showed twofold increased activity compared to that from the knockouts. In addition, ATP levels were reduced by 29% in the knockout mice versus the controls, suggesting that COX

activity modulates cellular energy levels by acting as a bottleneck for ETC flux. The physiological consequences of *Cox4-2* expression, or lack thereof, have been demonstrated with varying levels of severity. The knockout mouse model was studied through a detailed functional screen with a focus on lung function, and it was discovered that lack of *Cox4-2* has significant ramifications. *Cox4-2*-knockout mice showed reduced airway responsiveness, with 60% reduced P_{enh} and 58% reduced airway resistance when challenged with methacholine [151]. This finding in the knockouts of decreased ability for the airways to constrict—a process that requires energy—may be explained by decreased energy levels found in the lungs of the knockout mice. Furthermore, the mice showed a consistent, chronically deteriorating lung pathology and presented with lung inflammation, fibrosis, the recruitment of macrophages, and the development of Charcot-Leyden crystals, which are hypothesized to be formed from the products of eosinophil breakdown [152, 153].

Given the profound effect of isoform expression on the activity of COX, it is likely that expression of *COX4-2* presents an intricate and complex story of transcriptional regulation. We showed previously that *COX4-2* is regulated by a novel oxygen responsive element (ORE) located in the proximal promoter of the gene. Using reporter gene analyses, expression of *COX4-2* was shown to be maximal at 4% O₂ with an about threefold induction compared to normoxia [154]. The highly conserved 13 bp ORE was later shown via a yeast one-hybrid screen to interact with transcription factors MNRR1, RBPJ, and CXXC5 in a complex manner to regulate the expression of *COX4-2* [155]. Of the three factors, the protein MNRR1 (mitochondria nuclear retrograde regulator 1), also known as CHCHD2, has some novel features. It has been found to function as a biorganellar signaling

molecule to communicate between the mitochondria and the nucleus. It directly binds to and modulates COX activity when localized to the mitochondria, and it has been shown to be present in the nucleus, where it functions as a transcriptional regulator of *COX4-2* [156]. In this model, RBPJ and MNRR1 work in tandem to activate transcription of *COX4-2*, while CXXC5 functions as a repressor, allowing up- or downregulation of gene expression depending on signals or stresses, such as a change in the oxygen concentration. Interestingly, analysis of HEK293 cells exposed to 4% oxygen showed a significant increase in MNRR1 protein levels, supporting the idea that *MMNR1* and *COX4-2* share regulatory features under hypoxic stress [155]. In fact, the *MNRR1* promoter contains its own ORE and its expression is thus under autoregulatory transcriptional control. Oxygen regulation of *COX4-2* is a unique phenomenon for mammals, as nonmammalian species including several fish and reptiles do not show any changes in transcription levels in response to oxygen concentration [157].

COX4-2 was also proposed to be regulated through the HIF-1 at very low oxygen concentrations [158]. Here, 1% oxygen was sufficient to induce and stabilize HIF-1 and in turn upregulate expression of a *COX4-2* reporter gene. In addition, the mitochondrial protease LON was induced, which is proposed to be required for the degradation of COX IV-1 and insertion of COX IV-2. It is not fully clear whether or not 1% oxygen is physiologically relevant in regard to the lung, given the much higher exposure to oxygen taking place in this organ, but it may well be encountered during pathological conditions such as chronic obstructive pulmonary disease. However, the role of HIF-1 in regulating *COX4-2* remains controversial, since a recent study, using HIF-1 wild-type and knockout mouse embryonic fibroblasts, concluded that the oxygen-dependent regulation of *COX4-2* is not mediated by HIF-1 [159].

In addition to expression in the lung, *COX4-2* has also been detected at lower levels and studied in other tissues and tissue models. Under toxic conditions applying complex II inhibitor 3-nitropropionic acid [160] or anoxic conditions [161], *COX4-2* was shown to be upregulated in cortical astrocytes about threefold, confirming that the gene responds to stress and oxygen concentration. However, it remains to be shown what the basal ratio of the two isoforms is in COX of astrocytes and, consequently, if an induction of *COX4-2* can result in a significant change in the composition of the COX protein pool towards an enzyme pool containing more COX IV-2. In addition, *COX4-2* expression was found to be negatively correlated with cancer aggressiveness in gliomas, while those expressing only *COX4-1* were found to be more aggressive and capable of cell growth [162]. Finally, mutation of *COX4-2* in humans has also been linked to pancreatic pathology, as an E138K mutation was identified as the driver of exocrine pancreatic insufficiency, dyserythropoietic anemia, and calvarial hyperostosis in a clinical investigation of four patients [163]. As *COX4-2* is predominantly expressed in the lung and has not otherwise been reported as a pancreatic gene, this data may suggest that deficiency of certain organs or cell types where *COX4-2* is expressed may result in diseases of other organs, potentially during development.

Alternatively, *COX4-2* may be expressed in a minor pancreatic cell type. Another heterozygous missense mutation was reported in a patient with COX deficiency but not functionally confirmed [164].

5.1.2. *NDUFA4*. The latest subunit to become a recognized stoichiometric component of COX is NADH dehydrogenase (ubiquinone) 1 alpha subcomplex 4, also known as *NDUFA4*. This nuclear-encoded transmembrane protein was originally described as one of the 45 subunits of complex I [165]. However, recent advances in gene expression analysis have shown that expression patterns of *NDUFA4* diverge from those of other nuclear-encoded complex I subunits, potentially highlighting its role in other complexes [166]. In support of this concept, Balsa and colleagues recently presented data showing that the subunit is instead a functional and stoichiometric component of COX [54]. This was done by using the mild detergent digitonin to solubilize the mitochondrial membrane, allowing isolation of intact COX while preserving protein-protein interactions with high integrity. As a component of complex IV, *NDUFA4* could prove to be a useful target in discerning the genetic nature underlying diseases caused by mitochondrial energy deficit, such as Leigh syndrome and similar COX deficits. Pitceathly and colleagues recently provided this link by examining a consanguineous family afflicted with isolated COX deficiency [167]. It was found that rather than mutations in traditionally associated COX subunits, the family was affected by homozygous donor splice site mutations in *NDUFA4*, resulting in protein loss-of-function, with the further suggestion that families suffering from unexplained COX deficiency should be screened for *NDUFA4* mutations.

There is an isoform of *NDUFA4* known as *NDUFA4L2*, whose functions have only been studied in the context of NADH dehydrogenase up to this point. Under hypoxic conditions, *NDUFA4L2* transcription has been found to be upregulated through HIF-1 α stabilization, where it was the only gene categorized as a component of complex I to be responsive [168]. Expression of *NDUFA4L2* was found to reduce oxygen consumption by 42% under hypoxic conditions in HeLa cells, compared to 27% reduction when *NDUFA4L2* expression was silenced by 80%. Transient overexpression under normoxic conditions was found to have a similar effect, reducing oxygen consumption by 20%. Silencing of *NDUFA4L2* was also found to increase ROS production as measured by H₂-DCFDA and MitoSOX, as well as to increase the mitochondrial membrane potential. Interestingly, under hypoxic conditions, complex I activity was reduced by 20% in *NDUFA4L2* knockdowns while complex IV activity was not affected. Given that *NDUFA4* was only recently established as a component of complex IV, this may indicate that *NDUFA4* and its alternative isoform instead play a role in supercomplex formation or association and may attenuate complex I activity through some unknown interaction in hypoxic conditions. A further study on both the ubiquitous and the hypoxia-induced isoforms is necessary to establish the specifics of this potentially critical regulatory relationship.

Although the specific functions of *NDUFA4L2* remain elusive, its clinical significance has recently been underscored in a number of studies relating to several types of cancer. *NDUFA4L2* expression has been shown to be highly induced in clear-cell renal cell carcinoma, whereas normal kidney shows no significant expression [169]. In addition, expression levels were positively correlated with stage, with increasing expression in later-stage renal cancer. Cell culture models knocking down *NDUFA4L2* showed impaired proliferation and colony-forming capacity. Additionally, metabolic pathways were shifted away from the pentose phosphate pathway, with downregulation of key enzymes involved and upregulation of TCA cycle pathway members, indicating a shift towards glycolytic growth. A separate study associated an increase in *NDUFA4L2* expression with poor prognosis in patients with colorectal cancer [170]. Overexpression of *NDUFA4L2* was found in 84% of colorectal cancer tissue samples, compared to about 25% of adjacent normal tissue. Kaplan-Meier statistical analyses for overall survival and tumor-free survival both showed reduced survival rates in patients with *NDUFA4L2* overexpression versus those with low or undetectable expression. Similarly, using human hepatocellular carcinoma cell lines, *NDUFA4L2* was found to be dramatically overexpressed when exposed to hypoxia, as a result of HIF-1 α induction [171]. A comparison of 100 cases of human hepatocellular carcinoma revealed that 71% showed overexpression of *NDUFA4L2* and had a lower 5-year overall survival rate as compared to controls. Knock-down of *NDUFA4L2* suppressed proliferation of tumors in a mouse model and increased ROS production as measured by H₂-DCFDA fluorescence. Notably, suppression of HIF-1 α through the pharmacological inhibitor digoxin resulted in suppressed tumor proliferation without affecting mouse bodyweight, indicating that targeting HIF-1 α may be a valuable therapeutic tool in cells overexpressing *NDUFA4L2*.

5.2. Developmentally Switched Tissue-Specific Isoforms. COX subunits VIa, VIIa, and VIII have multiple tissue-specific isoforms expressed in mammals. During heart and skeletal muscle development, there is an isoform class switch from the liver (nonmuscle form) to the muscle isoform. The liver-type isoforms are thought to be ubiquitously expressed, while the heart-type subunits (VIaH, VIIaH, and VIIIH) are expressed in the heart and skeletal muscle [172]. In rats, an increase in COX VIaH and VIIIH and a concurrent decrease in liver-type isoforms were observed shortly after birth [173, 174]. All these isoforms are products of separate genes located on different chromosomes rather than products of alternative splicing of the same gene.

5.2.1. Subunit VIa. The gene duplication event that gave rise to nowadays mammalian subunit VIa isoform pair occurred about 240 million years ago [175]. The protein looks somewhat like an S-shaped hook, connects the COX monomers in the membrane region of the enzyme [53], and therefore stabilizes the COX dimer (Figure 2).

The liver isoform of subunit VIa was indirectly concluded to modulate proton pumping efficiency of COX (i.e., the proton to electron stoichiometry). COX purified from cow

kidney tissue, a tissue that similarly to that of the liver expresses the liver-type isoforms and reconstituted into vesicles, showed a 50% reduction in the proton to electron stoichiometry in the presence of the fatty acid palmitate whereas other fatty acids showed no effect [176]. The authors proposed that such an uncoupling mechanism could contribute to thermogenesis in warm-blooded animals.

The heart enzyme, containing COX VIaH, did not show a change of the proton to electron stoichiometry in the presence of palmitate. However, this isoform binds to allosteric regulator ADP on the matrix side of the enzyme, increasing enzyme activity, an effect that could be prevented in the presence of a COX VIaH-specific antibody [177]. In the presence of very high ATP/ADP ratios, COX VIaH mediates a 50% decrease in the proton to electron stoichiometry [178]. Similar to the effect of palmitate on COX VIaL, the authors proposed that ATP-mediated uncoupling contributes to thermogenesis during periods of physical inactivity with high ATP/ADP ratios in muscle, such as during sleep.

In 2002, the first COX subunit isoform-knockout model was introduced, in which the gene encoding isoform VIaH was deleted in mice [179]. A surprising finding was that despite reduced COX activity, myocardial ATP levels were similar to those of controls under basal conditions. However, since the mice developed cardiomyopathy over time, it is clear that COX VIaH is required for proper COX function and likely more so under increased performance conditions, such as strenuous exercise, which have not been studied yet.

5.2.2. Subunit VIb. COX subunit VIb occurs as a somatic (COX VIb1) and testes-specific isoform (COX VIb2). This subunit is unique among the nuclear-encoded subunits of COX in that it is solely located on the mitochondrial intermembrane space side of the holoenzyme, connecting the COX monomers [53] (Figure 2). This subunit can be separated from the core enzyme through treatment with the detergent dodecylmaltoside, resulting in twofold increased enzyme activity [180]. These kinetic alterations suggest that subunit VIb downregulates COX activity and that removal of this subunit may monomerize the holoenzyme. Accordingly, it has been proposed that COX VIb may be responsible for the cooperative activity of the two COX monomers once assembled into the dimer. Mutations in COX VIb1 have been implicated in disease phenotypes associated with COX deficiency. A missense mutation in a conserved arginine residue, R19H, resulted in severe infantile encephalomyopathy [181]. A second study found that alteration of the same residue to a cysteine, R19C, resulted in encephalomyopathy, hydrocephalus, and hypertrophic cardiomyopathy [182].

More recently, a second isoform of the subunit, COX VIb2, was discovered in human, mouse, rat, and bull [183]. Interestingly, the *COX6b2* gene was found to be exclusively expressed in the testis; in mouse and rat, it is the only transcript present, while in humans and bulls, both isoforms are present. In rodents, a testis-specific isoform of cytochrome *c* is also present [184]. This suggests that there may be unique energy demands of spermatozoa that are addressed through isoform expression of ETC components. Given the

function of COX VIb1 to downregulate COX activity, equipping the enzyme with a subunit isoform in sperm may provide a unique target for cell signaling during sperm activation, to activate OxPhos when energy is needed for movement.

5.2.3. Subunit VIIa. Subunit VIIa (Figure 2) has three isoforms. Similar to subunit VIa, there is a liver-type and heart-/skeletal muscle-type isoform (note that nomenclature of the heart-/muscle-type isoform genes for subunits 6a and 7a is reversed, i.e., *COX6a1* and *COX7a2* are the liver-type genes and *COX6a2* and *COX7a1* are the heart-type genes).

The expression of *COX7a1* was determined by Northern blot to be present strongest in adult mouse heart and skeletal muscle, with minor hybridization present in adult kidney and lung tissue [173]. For *COX7a2*, expression was detected in all adult and fetal tissues, which included those of the heart and skeletal muscle. The fact that the liver-type mRNAs are present but not (humans) or not highly (rodents) translated in the heart and skeletal muscle can be explained by posttranscriptional regulation. In tissues that express the liver-type isoform proteins, translation is assisted by the presence of auxiliary proteins, which bind to the 3'-untranslated regions of the mRNAs [185, 186].

Similar to the knockout approach of the heart-type isoform of subunit VIa, we later generated a whole-body mouse knockout of *Cox7a1* [187]. The knockouts were normal in appearance with morphologically normal mitochondria. However, their heart mitochondria showed a 15% reduction in COX levels, a 32% reduction in COX activity, and a 29% reduced respiratory control ratio, which is a measure of mitochondrial coupling. The heart size was increased significantly and the heart weight was 15–20% higher compared to that of controls. In addition, as demonstrated by echocardiography, the hearts of the knockout mice showed reduced systolic and diastolic function.

Analysis of the skeletal muscle in the *Cox7aH* knockouts also revealed dysfunction with over 60% reduced resting COX-specific activity and ATP levels in both glycolytic and oxidative skeletal muscle types [188]. Knockout mice had no difference in quadriceps muscle mass, but soleus, a highly aerobic muscle, was significantly smaller. Incremental treadmill exercise tests showed that the wild-type mice were able to run about 38% longer than their *Cox7aH*-knockout counterparts. This was correlated with a 47% decrease in distance and a 47% decrease in workload as compared to that of the wild-type mice. The capillary indices present in the wild-type quadriceps muscle were also found to be significantly higher, in addition to a significant difference in the fiber cross-sectional area and perimeter between the two groups of mice, suggesting that mitochondrial dysfunction in turn causes deterioration of the vascular system feeding them.

Surprisingly, *Cox7aH* was among the most highly upregulated genes in brown fat of mice after cold exposure, but *Cox7aH*-knockout mice exposed to cold were similar in skin temperature, UCP1 production, and other physiological parameters as the controls, demonstrating that nonshivering thermogenesis is not dependent on *Cox7aH* [189].

The pronounced upregulation after cold exposure thus remains puzzling.

A third isoform of subunit VIIa has been under investigation recently for its potential role in supercomplex formation and regulation. The gene *COX7aR*, also known as *COX7a2L* or *SIG81*, was first identified from a silica-induced gene library [190]. Similar to the ubiquitous liver isoform, *COX7AR* is expressed in all tissue types, with higher expression levels in those of the kidney and liver. Functional studies remained elusive until recently, when it was proposed that *COX7AR* was a critical component of supercomplex formation and should be renamed to supercomplex assembly factor I, or SCAFI [191]. Respiratory complexes were screened for proteins that appeared solely in supercomplexes versus free complexes. In the same study, a mutation in the *Cox7aR* gene was discovered in a screen of immortalized mouse fibroblasts resulting in a truncation of the protein from 113 to 111 amino acids, which conferred a defect in supercomplex formation. The authors showed that when *Cox7aR* is silenced or otherwise defective, COX does not participate in supercomplex formation. These results suggest that modulation of COX isoforms may play a critical role in the formation and dispersion of supercomplexes (Figure 3), allowing tight modulation of the electron transport chain through substrate channeling and availability. However, the effect of the truncation remains controversial since two other studies showed that truncated *COX VIIaR* found in C57BL/6 mice is phenotypically identical to that in nontruncated littermates and as part of supercomplexes [192, 193]. These studies concluded that mice bearing the shortened form of the subunit have normal biogenesis, no related respiratory defects, and normal levels of complex IV-associated supercomplexes, although differences in levels of different supercomplex subtypes were observed. In support of the hypothesis that *COX VIIaR* is required for supercomplex assembly, however, another recent publication showed that the long form of *COX7AR* was required for interaction of complexes III and IV [194]. Here, it was shown that the individual supercomplexes employ different isoforms to achieve different stoichiometries. Association of complexes III and IV requires *COX7AR*, while complex IV dimers instead utilize *COX VIIaL*. Another study recently showed that *COX VIIaR* binds primarily to free complex III and secondarily to *COX*, where it participates in assembly of the complex III₂ + IV supercomplex [195]. Recently, the structure of the I + III₂ + IV supercomplex from pig heart was solved at 4 Å resolution [196], in which *COX* interacts with both complexes I and III. The position of subunit VIIa appears to be a key in bridging *COX* with complexes I and III. *COX VIIa* is close to NDUFB8 of complex I and subunits UQCRC1, UQCRC11, and UQCRB of complex III. However, the resolution of the data set does not allow unambiguous assignment of *COX VIIaH* or *COX VIIa2R* (Dr. Yang personal communication), leaving this an open question. There are some discrepancies in the above studies regarding supercomplex composition. Likely, other regulatory mechanisms are in place that contribute to the regulation and stabilization of supercomplexes such as posttranslational modifications, which may explain some of the discrepancies between the

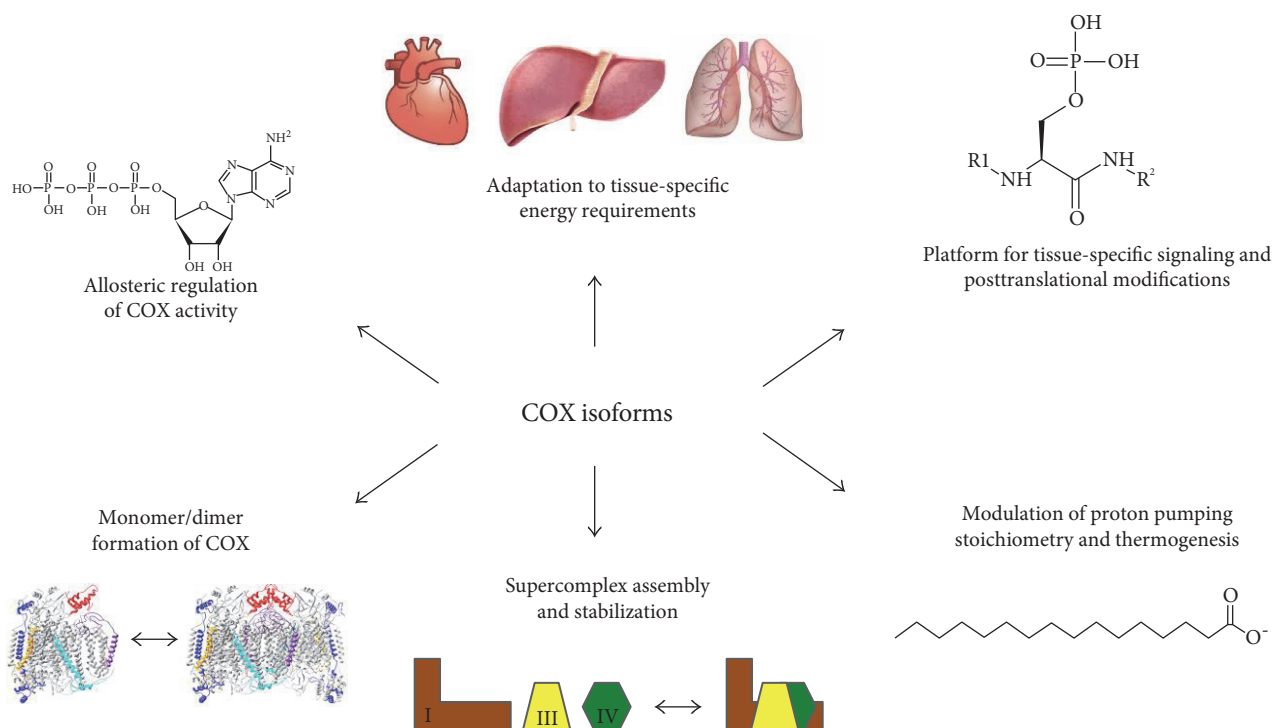


FIGURE 3: Proposed functions of cytochrome *c* oxidase subunit isoforms. Top left, going clockwise: several COX subunits were proposed to bind to allosteric effector molecules such as ADP and/or ATP, with the most conclusive evidence pointing to COX subunit IV isoforms binding to ADP and ATP at the matrix side, adjusting enzyme activity to energetic demand. COX isoforms also inversely adjust basal enzyme activity to mitochondrial capacity of a tissue, with the activity of COX following the order heart-type < liver-type < lung-type. Due to sequence differences, isoforms may be targeted by signaling molecules such as kinases in a tissue-specific manner. COX subunit VIaL but not VIaH was proposed to bind to the fatty acid palmitate, reducing the stoichiometry of pumped protons per transferred electron, and a similar effect was mediated by VIaH at very high ATP/ADP ratios, which was proposed to contribute to thermogenesis. Finally, COX subunits are key players both in stabilizing the COX dimer (subunits Vb, VIa, and VIb) as seen in the crystal structure of dimeric COX and in supercomplex formation (subunits VIIa, VIIc, and VIII). In both cases, two of the three subunits mediating the contacts have isoforms.

above studies. In addition, small but potentially important experimental differences such as precise detergent concentrations and gel running conditions, including temperature and voltage, may affect supercomplex separation and stability.

Finally, a recent study showed that *COX7aR* is a gene that is stress-induced and that its expression also correlates with cancer aggressiveness where it contributes to cancer proliferation and invasion [197]. This suggests that cancer metabolism may be modulated at the level of mitochondrial supercomplexes.

5.2.4. Subunit VIII. The smallest nuclear-encoded subunit is COX VIII (Figure 2), which has three known isoforms in rodents and two in humans. Gene structures and sequence similarities indicate that all three are a result of gene duplications [183]. The primarily expressed liver-type isoform, COX VIII_L (also known as COX VIII₂), is expressed ubiquitously in humans [198, 199]. While rodents and most other mammals have a heart-type isoform, COX VIII_H (also known as COX VIII₁), with an expression pattern similar to that of COX VIaH and VIIaH in the heart and skeletal muscle, the gene became a pseudogene in the stem of the catarrhines and is thus no longer active in humans [200]. Interestingly,

COX VIII_H was also found to be expressed in brown adipose tissue of rats [201].

One important function of COX subunit VIII is to stabilize the supercomplex consisting of complexes I + III₂ + IV, where it is involved in contacts with subunits NDUFB3, NDUFB7, and NDUFB8 of complex I [196].

The important role of subunit VIII for COX function and stability was further suggested by a recently published clinical study [202]. Here, a female patient with Leigh syndrome-like symptoms who died at age 12 was identified with a homozygous G to C transversion in intron 1 of the ubiquitous *COX8* gene. This mutation disrupts the regular AG acceptor splice site at the end of intron 1, resulting in aberrant splicing, leading to a 49 nucleotide deletion and frameshift of exon 2 and thus a nonfunctional protein. As a consequence, only 10% COX activity was retained in the skeletal muscle and fibroblasts of the patient, which could be restored by expression of wild-type *COX8*.

The presence of a third isoform of COX VIII (also known as COX VIII_C or COX VIII₃) was shown in several mammalian species (human, lemur, mouse, and rat) [183]. Phylogenetic analysis based on nucleotide sequence showed high levels of divergence within *COX8-3*, and the protein also

had higher amino acid replacement rates compared to the other two isoforms. Of a small number of tissues analyzed to date, *COX8-3* was detected at the highest levels in tissues of the testes followed by those of the pancreas and placenta [202]. Its functional role is currently unknown.

6. Conclusions

In this review, we highlight the variation in COX subunit expression in mammals and how tissue-specific and environment-specific conditions necessitate the tight regulation of enzyme activity through differential expression (Figure 3). While decades of research have shaped a thorough understanding of the function and importance of COX, the specific function of many of the nuclear-encoded subunits, as well as their isoforms, remains unclear. Of the 11 nuclear-encoded subunits of COX, six possess tissue- and condition-specific isoforms. We propose that one reason for tissue-specific isoform expression is related to the different capacities of tissues for mitochondria. For example, heart-/skeletal muscle-type COX isoforms of subunits VIa, VIIa, and VIII are expressed in tissues with a high aerobic capacity. Heart and skeletal muscle tissues contain a high density of mitochondria, whereas other tissues including those of the liver and brain, which express the liver-type isoforms, have other specialized functions, which are not compatible with a high mitochondrial load. Because tissues such as those of the liver and brain still fully depend on aerobic energy production, they are equipped with an enzyme containing the liver-type isoforms, which has a higher basal activity [203]. Lung tissue has even fewer mitochondria than that of the liver and expresses the liver-type isoforms of subunits VIa, VIIa, and VIII, together with a lung-specific isoform COX IV-2, leading to yet another increase in basal activity [154]. Therefore, basal activity increases from heart-type over liver-type to lung-type COX, suggesting that one important role of tissue-specific isoforms is to compensate for lack of room for mitochondria in tissues such as those of the liver and lung compared to those of the heart and skeletal muscle. Of the COX isoforms, some additional functional protein data is primarily only available for the isoforms of subunits IV, VIa, VIb, and VIIa—data on the direct enzymatic effects of isoforms of subunits VIII and NDUFA4 has not yet been published. We propose that another functional role of isoforms may be to serve as a platform for tissue-specific signaling and/or allosteric regulation, since amino acid sequence differences between the isoforms may, for example, affect kinase recognition or allosteric effector molecules such as ATP and ADP (Figure 3). In addition, of the three subunits that constitute the primary contact interface with complexes I and III in the supercomplex, that is, VIIaL, VIIc, and VIII, two of these—VIIaL and VIII—are expressed in a tissue-specific manner. This raises the exciting possibility that changes in supercomplex composition, stability, and functionality, including altered metabolic flux, can take place in a tissue-specific manner, adding another layer of regulation to a fundamental bioenergetic process that is most crucial for multicellular organisms. Finally, the emergence of clinical data pointing to individual COX subunits as drivers of

critical biological functions and causes of human disease, as well as of individual subunits being potential biomarkers and participants in processes such as oncogenesis, highlights the necessity of continued diligence in their study.

Disclosure

Opinions, interpretations, conclusions, and recommendations are those of the authors and are not necessarily endorsed by the Department of Defense or the National Institutes of Health.

Conflicts of Interest

The authors declare that they have no conflicts of interest with the contents of this article.

Acknowledgments

This work was supported by the U.S. National Institutes of Health Grants R01 NS091242 and T32 HL120822 and by the Office of the Assistant Secretary of Defense for Health Affairs through the Peer Reviewed Medical Research Program under Award no. W81XWH-16-1-0175 and Award no. W81XWH-16-1-0516.

References

- [1] N. Lane and W. Martin, "The energetics of genome complexity," *Nature*, vol. 467, no. 7318, pp. 929–934, 2010.
- [2] B. Alberts, A. Johnson, J. Lewis, M. Raff, K. Roberts, and P. Walter, *The Molecular Biology of the Cell*, Garland Science, New York, 2002.
- [3] G. Kroemer, B. Dallaporta, and M. Resche-Rigon, "The mitochondrial death/life regulator in apoptosis and necrosis," *Annual Review of Physiology*, vol. 60, no. 1, pp. 619–642, 1998.
- [4] M. Hüttemann, I. Lee, L. I. Grossman, J. W. Doan, and T. H. Sanderson, "Phosphorylation of mammalian cytochrome c and cytochrome c oxidase in the regulation of cell destiny: respiration, apoptosis, and human disease," *Advances in Experimental Medicine and Biology*, vol. 748, pp. 237–264, 2012.
- [5] A. Krippner, A. Matsuno-Yagi, R. A. Gottlieb, and B. M. Babor, "Loss of function of cytochrome c in Jurkat cells undergoing fas-mediated apoptosis," *The Journal of Biological Chemistry*, vol. 271, no. 35, pp. 21629–21636, 1996.
- [6] X. Wang, "The expanding role of mitochondria in apoptosis," *Genes & Development*, vol. 15, no. 22, pp. 2922–2933, 2001.
- [7] X. Liu, C. N. Kim, J. Yang, R. Jemmerson, and X. Wang, "Induction of apoptotic program in cell-free extracts: requirement for dATP and cytochrome c," *Cell*, vol. 86, no. 1, pp. 147–157, 1996.
- [8] D. C. Chan, "Mitochondria: dynamic organelles in disease, aging, and development," *Cell*, vol. 125, no. 7, pp. 1241–1252, 2006.
- [9] C. Mammucari and R. Rizzuto, "Signaling pathways in mitochondrial dysfunction and aging," *Mechanisms of Ageing and Development*, vol. 131, no. 7-8, pp. 536–543, 2010.
- [10] N. Sun, R. J. Youle, and T. Finkel, "The mitochondrial basis of aging," *Molecular Cell*, vol. 61, no. 5, pp. 654–666, 2016.

- [11] P. S. Ward and C. B. Thompson, "Metabolic reprogramming: a cancer hallmark even warburg did not anticipate," *Cancer Cell*, vol. 21, no. 3, pp. 297–308, 2012.
- [12] T. H. Sanderson, C. A. Reynolds, R. Kumar, K. Przyklenk, and M. Hüttemann, "Molecular mechanisms of ischemia-reperfusion injury in brain: pivotal role of the mitochondrial membrane potential in reactive oxygen species generation," *Molecular Neurobiology*, vol. 47, no. 1, pp. 9–23, 2013.
- [13] D. W. Kamp, E. Shacter, and S. A. Weitzman, "Chronic inflammation and cancer: the role of the mitochondria," *Oncology (Williston Park)*, vol. 25, no. 5, pp. 400–410, 2011.
- [14] L. Samavati, I. Lee, I. Mathes, F. Lottspeich, and M. Hüttemann, "Tumor necrosis factor α inhibits oxidative phosphorylation through tyrosine phosphorylation at subunit I of cytochrome *c* oxidase," *The Journal of Biological Chemistry*, vol. 283, no. 30, pp. 21134–21144, 2008.
- [15] A. J. Ruggieri, R. J. Levy, and C. S. Deutschman, "Mitochondrial dysfunction and resuscitation in sepsis," *Critical Care Clinics*, vol. 26, no. 3, pp. 567–575, 2010.
- [16] J. C. Duvigneau, C. Piskernik, S. Haindl et al., "A novel endotoxin-induced pathway: upregulation of heme oxygenase 1, accumulation of free iron, and free iron-mediated mitochondrial dysfunction," *Laboratory Investigation*, vol. 88, no. 1, pp. 70–77, 2008.
- [17] D. Brealey, M. Brand, I. Hargreaves et al., "Association between mitochondrial dysfunction and severity and outcome of septic shock," *Lancet*, vol. 360, no. 9328, pp. 219–223, 2002.
- [18] G. J. Wang, J. G. Jackson, and S. A. Thayer, "Altered distribution of mitochondria impairs calcium homeostasis in rat hippocampal neurons in culture," *Journal of Neurochemistry*, vol. 87, no. 1, pp. 85–94, 2003.
- [19] Y. Gouriou, N. Demareux, P. Bijlenga, and U. De Marchi, "Mitochondrial calcium handling during ischemia-induced cell death in neurons," *Biochimie*, vol. 93, no. 12, pp. 2060–2067, 2011.
- [20] D. G. Nicholls, "Mitochondria and calcium signaling," *Cell Calcium*, vol. 38, no. 3–4, pp. 311–317, 2005.
- [21] P. Jezek and L. Hlavata, "Mitochondria in homeostasis of reactive oxygen species in cell, tissues, and organism," *The International Journal of Biochemistry & Cell Biology*, vol. 37, no. 12, pp. 2478–2503, 2005.
- [22] Y. S. Yoon, J. H. Lee, S. C. Hwang, K. S. Choi, and G. Yoon, "TGF β 1 induces prolonged mitochondrial ROS generation through decreased complex IV activity with senescent arrest in Mv1Lu cells," *Oncogene*, vol. 24, no. 11, pp. 1895–1903, 2005.
- [23] D. M. Muntean, A. Sturza, M. D. Danila, C. Borza, O. M. Duicu, and C. Mornos, "The role of mitochondrial reactive oxygen species in cardiovascular injury and protective strategies," *Oxidative Medicine and Cellular Longevity*, vol. 2016, Article ID 8254942, p. 19, 2016.
- [24] M. Bourens, F. Fontanesi, I. C. Soto, J. Liu, and A. Barrientos, "Redox and reactive oxygen species regulation of mitochondrial cytochrome C oxidase biogenesis," *Antioxidants & Redox Signaling*, vol. 19, no. 16, pp. 1940–1952, 2013.
- [25] K. S. Echtay, D. Roussel, J. St-Pierre et al., "Superoxide activates mitochondrial uncoupling proteins," *Nature*, vol. 415, no. 6867, pp. 96–99, 2002.
- [26] J. St-Pierre, J. A. Buckingham, S. J. Roebuck, and M. D. Brand, "Topology of superoxide production from different sites in the mitochondrial electron transport chain," *The Journal of Biological Chemistry*, vol. 277, no. 47, pp. 44784–44790, 2002.
- [27] M. Rigoulet, E. D. Yoboue, and A. Devin, "Mitochondrial ROS generation and its regulation: mechanisms involved in H₂O₂ signaling," *Antioxidants & Redox Signaling*, vol. 14, no. 3, pp. 459–468, 2011.
- [28] D. E. Handy and J. Loscalzo, "Redox regulation of mitochondrial function," *Antioxidants & Redox Signaling*, vol. 16, no. 11, pp. 1323–1367, 2012.
- [29] W. J. Koopman, L. G. Nijtmans, C. E. Dieteren et al., "Mammalian mitochondrial complex I: biogenesis, regulation, and reactive oxygen species generation," *Antioxidants & Redox Signaling*, vol. 12, no. 12, pp. 1431–1470, 2010.
- [30] R. J. Mailloux and W. G. Willmore, "S-Glutathionylation reactions in mitochondrial function and disease," *Frontiers in Cell and Developmental Biology*, vol. 2, pp. 1–17, 2014.
- [31] R. J. Mailloux, S. L. McBride, and M. E. Harper, "Unearthing the secrets of mitochondrial ROS and glutathione in bioenergetics," *Trends in Biochemical Sciences*, vol. 38, no. 12, pp. 592–602, 2013.
- [32] J. Lu and A. Holmgren, "The thioredoxin antioxidant system," *Free Radical Biology & Medicine*, vol. 66, pp. 75–87, 2014.
- [33] L. Sagan, "On the origin of mitosing cells. 1967," *Journal of NIH Research*, vol. 5, no. 3, pp. 65–72, 1993.
- [34] F. J. Taylor, "An overview of the status of evolutionary cell symbiosis theories," *Annals of the New York Academy of Sciences*, vol. 503, pp. 1–16, 1987.
- [35] I. E. Scheffler, *Mitochondria*, John Wiley & Sons, New York, 1999.
- [36] P. Reynier, P. May-Panloup, M. F. Chretien et al., "Mitochondrial DNA content affects the fertilizability of human oocytes," *Molecular Human Reproduction*, vol. 7, no. 5, pp. 425–429, 2001.
- [37] B. F. Lang, M. W. Gray, and G. Burger, "Mitochondrial genome evolution and the origin of eukaryotes," *Annual Review of Genetics*, vol. 33, no. 1, pp. 351–397, 1999.
- [38] C. T. Beagley, R. Okimoto, and D. R. Wolstenholme, "The mitochondrial genome of the sea anemone *Metridium senile* (Cnidaria): introns, a paucity of tRNA genes, and a near-standard genetic code," *Genetics*, vol. 148, no. 3, pp. 1091–1108, 1998.
- [39] B. L. Ward, R. S. Anderson, and A. J. Bendich, "The mitochondrial genome is large and variable in a family of plants (Cucurbitaceae)," *Cell*, vol. 25, no. 3, pp. 793–803, 1981.
- [40] D. G. Nicholls and S. J. Ferguson, *Bioenergetics 3*, Academic Press, Elsevier Science Ltd., London, UK, 2001.
- [41] D. Stock, A. G. Leslie, and J. E. Walker, "Molecular architecture of the rotary motor in ATP synthase," *Science*, vol. 286, no. 5445, pp. 1700–1705, 1999.
- [42] C. R. Hackenbrock, B. Chazotte, and S. S. Gupte, "The random collision model and a critical assessment of diffusion and collision in mitochondrial electron transport," *Journal of Bioenergetics and Biomembranes*, vol. 18, no. 5, pp. 331–368, 1986.
- [43] S. Gupte, E. S. Wu, L. Hoehchli et al., "Relationship between lateral diffusion, collision frequency, and electron transfer of mitochondrial inner membrane oxidation-reduction components," *Proceedings of the National Academy of Sciences of the United States of America*, vol. 81, no. 9, pp. 2606–2610, 1984.

- [44] H. Schagger and K. Pfeiffer, "The ratio of oxidative phosphorylation complexes I-V in bovine heart mitochondria and the composition of respiratory chain supercomplexes," *The Journal of Biological Chemistry*, vol. 276, no. 41, pp. 37861–37867, 2001.
- [45] H. Schagger and K. Pfeiffer, "Supercomplexes in the respiratory chains of yeast and mammalian mitochondria," *The EMBO Journal*, vol. 19, no. 8, pp. 1777–1783, 2000.
- [46] C. M. Cruciat, S. Brunner, F. Baumann, W. Neupert, and R. A. Stuart, "The cytochrome bc1 and cytochrome c oxidase complexes associate to form a single supracomplex in yeast mitochondria," *The Journal of Biological Chemistry*, vol. 275, no. 24, pp. 18093–18098, 2000.
- [47] H. Seelert, D. N. Dani, S. Dante et al., "From protons to OXPHOS supercomplexes and Alzheimer's disease: structure-dynamics-function relationships of energy-transducing membranes," *Biochimica et Biophysica Acta*, vol. 1787, no. 6, pp. 657–671, 2009.
- [48] I. Wittig, R. Carrozzo, F. M. Santorelli, and H. Schagger, "Supercomplexes and subcomplexes of mitochondrial oxidative phosphorylation," *Biochimica et Biophysica Acta*, vol. 1757, no. 9-10, pp. 1066–1072, 2006.
- [49] H. Schagger and G. von Jagow, "Blue native electrophoresis for isolation of membrane protein complexes in enzymatically active form," *Analytical Biochemistry*, vol. 199, no. 2, pp. 223–231, 1991.
- [50] V. Strecker, Z. Kadeer, J. Heidler et al., "Supercomplex-associated Cox26 protein binds to cytochrome c oxidase," *Biochimica et Biophysica Acta*, vol. 1863, no. 7 Part A, pp. 1643–1652, 2016.
- [51] N. Kovarova, A. Cizkova Vrbacka, P. Pecina et al., "Adaptation of respiratory chain biogenesis to cytochrome c oxidase deficiency caused by SURF1 gene mutations," *Biochimica et Biophysica Acta*, vol. 1822, no. 7, pp. 1114–1124, 2012.
- [52] S. Saddar, M. K. Dienhart, and R. A. Stuart, "The F1F0-ATP synthase complex influences the assembly state of the cytochrome bc1-cytochrome oxidase supercomplex and its association with the TIM23 machinery," *The Journal of Biological Chemistry*, vol. 283, no. 11, pp. 6677–6686, 2008.
- [53] T. Tsukihara, H. Aoyama, E. Yamashita et al., "The whole structure of the 13-subunit oxidized cytochrome c oxidase at 2.8 Å," *Science*, vol. 272, no. 5265, pp. 1136–1144, 1996.
- [54] E. Balsa, R. Marco, E. Perales-Clemente et al., "NDUFA4 is a subunit of complex IV of the mammalian electron transport chain," *Cell Metabolism*, vol. 16, no. 3, pp. 378–386, 2012.
- [55] B. Kadenbach, J. Jarausch, R. Hartmann, and P. Merle, "Separation of mammalian cytochrome c oxidase into 13 polypeptides by a sodium dodecyl sulfate-gel electrophoretic procedure," *Analytical Biochemistry*, vol. 129, no. 2, pp. 517–521, 1983.
- [56] G. T. Babcock and M. Wikstrom, "Oxygen activation and the conservation of energy in cell respiration," *Nature*, vol. 356, no. 6367, pp. 301–309, 1992.
- [57] P. Hellwig, J. Behr, C. Ostermeier et al., "Involvement of glutamic acid 278 in the redox reaction of the cytochrome c oxidase from *Paracoccus denitrificans* investigated by FTIR spectroscopy," *Biochemistry*, vol. 37, no. 20, pp. 7390–7399, 1998.
- [58] H. Michel, "The mechanism of proton pumping by cytochrome c oxidase," *Proceedings of the National Academy of Sciences of the United States of America*, vol. 95, no. 22, pp. 12819–12824, 1998.
- [59] S. Yoshikawa, K. Muramoto, and K. Shinzawa-Itoh, "The O(2) reduction and proton pumping gate mechanism of bovine heart cytochrome c oxidase," *Biochimica et Biophysica Acta*, vol. 1807, no. 10, pp. 1279–1286, 2011.
- [60] E. Fadda, C. H. Yu, and R. Pomes, "Electrostatic control of proton pumping in cytochrome c oxidase," *Biochimica et Biophysica Acta*, vol. 1777, no. 3, pp. 277–284, 2008.
- [61] V. Sharma, G. Enkavi, I. Vattulainen, T. Rog, and M. Wikstrom, "Proton-coupled electron transfer and the role of water molecules in proton pumping by cytochrome c oxidase," *Proceedings of the National Academy of Sciences of the United States of America*, vol. 112, no. 7, pp. 2040–2045, 2015.
- [62] N. Yano, K. Muramoto, A. Shimada et al., "The Mg²⁺-containing water cluster of mammalian cytochrome c oxidase collects four pumping proton equivalents in each catalytic cycle," *The Journal of Biological Chemistry*, vol. 291, no. 46, pp. 23882–23894, 2016.
- [63] S. Yoshikawa, "A cytochrome c oxidase proton pumping mechanism that excludes the O₂ reduction site," *FEBS Letters*, vol. 555, no. 1, pp. 8–12, 2003.
- [64] T. Tsukihara, K. Shimokata, Y. Katayama et al., "The low-spin heme of cytochrome c oxidase as the driving element of the proton-pumping process," vol. 100, no. 26, pp. 15304–15309, 2003.
- [65] K. Shimokata, Y. Katayama, H. Murayama et al., "The proton pumping pathway of bovine heart cytochrome c oxidase," *Proceedings of the National Academy of Sciences of the United States of America*, vol. 104, no. 10, pp. 4200–4205, 2007.
- [66] J. Salje, B. Ludwig, and O. M. Richter, "Is a third proton-conducting pathway operative in bacterial cytochrome c oxidase?" *Biochemical Society Transactions*, vol. 33, no. Part 4, pp. 829–831, 2005.
- [67] J. Napiwotzki, K. Shinzawa-Itoh, S. Yoshikawa, and B. Kadenbach, "ATP and ADP bind to cytochrome c oxidase and regulate its activity," *Biological Chemistry*, vol. 378, no. 9, pp. 1013–1021, 1997.
- [68] B. Kadenbach, V. Frank, T. Rieger, and J. Napiwotzki, "Regulation of respiration and energy transduction in cytochrome c oxidase isozymes by allosteric effectors," *Molecular and Cellular Biochemistry*, vol. 174, no. 1-2, pp. 131–135, 1997.
- [69] J. Napiwotzki and B. Kadenbach, "Extramitochondrial ATP/ADP-ratios regulate cytochrome c oxidase activity via binding to the cytosolic domain of subunit IV," *Biological Chemistry*, vol. 379, no. 3, pp. 335–339, 1998.
- [70] S. Helling, M. Hüttemann, R. Ramzan et al., "Multiple phosphorylations of cytochrome c oxidase and their functions," *Proteomics*, vol. 12, no. 7, pp. 950–959, 2012.
- [71] R. Covian and R. S. Balaban, "Cardiac mitochondrial matrix and respiratory complex protein phosphorylation," *American Journal of Physiology. Heart and Circulatory Physiology*, vol. 303, no. 8, pp. H940–H966, 2012.
- [72] I. Lee, A. R. Salomon, S. Ficarro et al., "cAMP-dependent tyrosine phosphorylation of subunit I inhibits cytochrome c oxidase activity," *The Journal of Biological Chemistry*, vol. 280, no. 7, pp. 6094–6100, 2005.
- [73] I. Lee, E. Bender, S. Arnold, and B. Kadenbach, "New control of mitochondrial membrane potential and ROS formation—a

- hypothesis," *Biological Chemistry*, vol. 382, no. 12, pp. 1629–1636, 2001.
- [74] R. Acin-Perez, D. L. Gatti, Y. Bai, and G. Manfredi, "Protein phosphorylation and prevention of cytochrome oxidase inhibition by ATP: coupled mechanisms of energy metabolism regulation," *Cell Metabolism*, vol. 13, no. 6, pp. 712–719, 2011.
- [75] T. I. Karu and N. I. Afanas'eva, "Cytochrome c oxidase as the primary photoacceptor upon laser exposure of cultured cells to visible and near IR-range light," *Doklady Akademii Nauk*, vol. 342, no. 5, pp. 693–695, 1995.
- [76] M. G. Mason, P. Nicholls, and C. E. Cooper, "Re-evaluation of the near infrared spectra of mitochondrial cytochrome c oxidase: implications for non invasive in vivo monitoring of tissues," *Biochimica et Biophysica Acta*, vol. 1837, no. 11, pp. 1882–1891, 2014.
- [77] D. C. Wharton and A. Tzagoloff, "Studies on the electron transfer system. Lvii. The near infrared absorption band of cytochrome oxidase," *The Journal of Biological Chemistry*, vol. 239, no. 6, pp. 2036–2041, 1964.
- [78] W. Yu, J. O. Naim, M. McGowan, K. Ippolito, and R. J. Lanzafame, "Photomodulation of oxidative metabolism and electron chain enzymes in rat liver mitochondria," *Photochemistry and Photobiology*, vol. 66, no. 6, pp. 866–871, 1997.
- [79] M. T. Wong-Riley, H. L. Liang, J. T. Eells et al., "Photobiomodulation directly benefits primary neurons functionally inactivated by toxins: role of cytochrome c oxidase," *The Journal of Biological Chemistry*, vol. 280, no. 6, pp. 4761–4771, 2005.
- [80] M. T. Wong-Riley, X. Bai, E. Buchmann, and H. T. Whelan, "Light-emitting diode treatment reverses the effect of TTX on cytochrome oxidase in neurons," *Neuroreport*, vol. 12, no. 14, pp. 3033–3037, 2001.
- [81] N. J. Blanco, W. T. Maddox, and F. Gonzalez-Lima, "Improving executive function using transcranial infrared laser stimulation," *Journal of Neuropsychology*, vol. 11, no. 1, pp. 14–25, 2015.
- [82] J. T. Eells, M. T. Wong-Riley, J. VerHoeve et al., "Mitochondrial signal transduction in accelerated wound and retinal healing by near-infrared light therapy," *Mitochondrion*, vol. 4, no. 5-6, pp. 559–567, 2004.
- [83] A. Barrientos, M. H. Barros, I. Valnot, A. Rotig, P. Rustin, and A. Tzagoloff, "Cytochrome oxidase in health and disease," *Gene*, vol. 286, no. 1, pp. 53–63, 2002.
- [84] L. Stiburek and J. Zeman, "Assembly factors and ATP-dependent proteases in cytochrome c oxidase biogenesis," *Biochimica et Biophysica Acta*, vol. 1797, no. 6-7, pp. 1149–1158, 2010.
- [85] M. Siep, K. van Oosterum, H. Neufeglise, H. van der Spek, and L. A. Grivell, "Mss51p, a putative translational activator of cytochrome c oxidase subunit-1 (COX1) mRNA, is required for synthesis of Cox1p in *Saccharomyces cerevisiae*," *Current Genetics*, vol. 37, no. 4, pp. 213–220, 2000.
- [86] E. Decoster, M. Simon, D. Hatat, and G. Faye, "The MSS51 gene product is required for the translation of the COX1 mRNA in yeast mitochondria," *Molecular & General Genetics*, vol. 224, no. 1, pp. 111–118, 1990.
- [87] G. M. Manthey and J. E. McEwen, "The product of the nuclear gene PET309 is required for translation of mature mRNA and stability or production of intron-containing RNAs derived from the mitochondrial COX1 locus of *Saccharomyces cerevisiae*," *The EMBO Journal*, vol. 14, no. 16, pp. 4031–4043, 1995.
- [88] A. Zamudio-Ochoa, Y. Camacho-Villasana, A. E. Garcia-Guerrero, and X. Perez-Martinez, "The Pet309 pentatricopeptide repeat motifs mediate efficient binding to the mitochondrial COX1 transcript in yeast," *RNA Biology*, vol. 11, no. 7, pp. 953–967, 2014.
- [89] X. Perez-Martinez, C. A. Butler, M. Shingu-Vazquez, and T. D. Fox, "Dual functions of Mss51 couple synthesis of Cox1 to assembly of cytochrome c oxidase in *Saccharomyces cerevisiae* mitochondria," *Molecular Biology of the Cell*, vol. 20, no. 20, pp. 4371–4380, 2009.
- [90] I. C. Soto and A. Barrientos, "Mitochondrial cytochrome c oxidase biogenesis is regulated by the redox state of a heme-binding translational activator," *Antioxidants & Redox Signaling*, vol. 24, no. 6, pp. 281–298, 2016.
- [91] R. J. Temperley, M. Wydro, R. N. Lightowers, and Z. M. Chrzanowska-Lightowers, "Human mitochondrial mRNAs—like members of all families, similar but different," *Biochimica et Biophysica Acta*, vol. 1797, no. 6-7, pp. 1081–1085, 2010.
- [92] W. Weraarpachai, H. Antonicka, F. Sasarman et al., "Mutation in TACO1, encoding a translational activator of COX I, results in cytochrome c oxidase deficiency and late-onset Leigh syndrome," *Nature Genetics*, vol. 41, no. 7, pp. 833–837, 2009.
- [93] T. R. Richman, H. Spahr, J. A. Ermer et al., "Loss of the RNA-binding protein TACO1 causes late-onset mitochondrial dysfunction in mice," *Nature Communications*, vol. 7, pp. 1–14, 2016.
- [94] E. Fernandez-Vizarra, V. Tiranti, and M. Zeviani, "Assembly of the oxidative phosphorylation system in humans: what we have learned by studying its defects," *Biochimica et Biophysica Acta*, vol. 1793, no. 1, pp. 200–211, 2009.
- [95] F. Diaz, H. Kotarsky, V. Fellman, and C. T. Moraes, "Mitochondrial disorders caused by mutations in respiratory chain assembly factors," *Seminars in Fetal & Neonatal Medicine*, vol. 16, no. 4, pp. 197–204, 2011.
- [96] R. B. Vega, J. L. Horton, and D. P. Kelly, "Maintaining ancient organelles: mitochondrial biogenesis and maturation," *Circulation Research*, vol. 116, no. 11, pp. 1820–1834, 2015.
- [97] M. Rak, P. Benit, D. Chretien et al., "Mitochondrial cytochrome c oxidase deficiency," *Clinical Science (London, England)*, vol. 130, no. 6, pp. 393–407, 2016.
- [98] R. Richter-Dennerlein, S. Oeljeklaus, I. Lorenzi et al., "Mitochondrial protein synthesis adapts to influx of nuclear-encoded protein," *Cell*, vol. 167, no. 2, pp. 471–483.e410, 2016.
- [99] L. Stiburek, K. Vesela, H. Hansikova et al., "Tissue-specific cytochrome c oxidase assembly defects due to mutations in SCO2 and SURF1," *The Biochemical Journal*, vol. 392, no. Part 3, pp. 625–632, 2005.
- [100] M. Bourens and A. Barrientos, "A CMC1-knockout reveals translation-independent control of human mitochondrial complex IV biogenesis," *EMBO Reports*, vol. 18, no. 3, pp. 477–494, 2017.
- [101] M. H. Barros, C. G. Carlson, D. M. Glerum, and A. Tzagoloff, "Involvement of mitochondrial ferredoxin and Cox15p in hydroxylation of heme O," *FEBS Letters*, vol. 492, no. 1-2, pp. 133–138, 2001.
- [102] M. H. Barros, F. G. Nobrega, and A. Tzagoloff, "Mitochondrial ferredoxin is required for heme A synthesis in

- Saccharomyces cerevisiae*,” *The Journal of Biological Chemistry*, vol. 277, no. 12, pp. 9997–10002, 2002.
- [103] M. H. Barros and A. Tzagoloff, “Regulation of the heme A biosynthetic pathway in *Saccharomyces cerevisiae*,” *FEBS Letters*, vol. 516, no. 1–3, pp. 119–123, 2002.
- [104] H. Antonicka, S. C. Leary, G. H. Guercin et al., “Mutations in COX10 result in a defect in mitochondrial heme A biosynthesis and account for multiple, early-onset clinical phenotypes associated with isolated COX deficiency,” *Human Molecular Genetics*, vol. 12, no. 20, pp. 2693–2702, 2003.
- [105] M. Bugiani, V. Tiranti, L. Farina, G. Uziel, and M. Zeviani, “Novel mutations in COX15 in a long surviving Leigh syndrome patient with cytochrome c oxidase deficiency,” *Journal of Medical Genetics*, vol. 42, no. 5, p. e28, 2005.
- [106] M. J. Coenen, L. P. van den Heuvel, C. Ugalde et al., “Cytochrome c oxidase biogenesis in a patient with a mutation in COX10 gene,” *Annals of Neurology*, vol. 56, no. 4, pp. 560–564, 2004.
- [107] M. Miryounesi, M. Fardaei, S. M. Tabei, and S. Ghafouri-Fard, “Leigh syndrome associated with a novel mutation in the COX15 gene,” *Journal of Pediatric Endocrinology & Metabolism*, vol. 29, no. 6, pp. 741–744, 2016.
- [108] B. Bareth, S. Dennerlein, D. U. Mick, M. Nikolov, H. Urlaub, and P. Rehling, “The heme a synthase Cox15 associates with cytochrome c oxidase assembly intermediates during Cox1 maturation,” *Molecular and Cellular Biology*, vol. 33, no. 20, pp. 4128–4137, 2013.
- [109] L. Stiburek, K. Vesela, H. Hansikova, H. Hulkova, and J. Zeman, “Loss of function of Sco1 and its interaction with cytochrome c oxidase,” *American Journal of Physiology. Cell Physiology*, vol. 296, no. 5, pp. C1218–C1226, 2009.
- [110] Z. Zhu, J. Yao, T. Johns et al., “SURF1, encoding a factor involved in the biogenesis of cytochrome c oxidase, is mutated in Leigh syndrome,” *Nature Genetics*, vol. 20, no. 4, pp. 337–343, 1998.
- [111] C. Dell’agnello, S. Leo, A. Agostino et al., “Increased longevity and refractoriness to Ca(2+)-dependent neurodegeneration in Surf1 knockout mice,” *Human Molecular Genetics*, vol. 16, no. 4, pp. 431–444, 2007.
- [112] G. Pharaoh, D. Pulliam, S. Hill, K. Sataranatarajan, and H. Van Remmen, “Ablation of the mitochondrial complex IV assembly protein Surf1 leads to increased expression of the UPR(MT) and increased resistance to oxidative stress in primary cultures of fibroblasts,” *Redox Biology*, vol. 8, pp. 430–438, 2016.
- [113] D. A. Pulliam, S. S. Deepa, Y. Liu et al., “Complex IV-deficient Surf1(-/-) mice initiate mitochondrial stress responses,” *The Biochemical Journal*, vol. 462, no. 2, pp. 359–371, 2014.
- [114] A. L. Lin, D. A. Pulliam, S. S. Deepa et al., “Decreased in vitro mitochondrial function is associated with enhanced brain metabolism, blood flow, and memory in Surf1-deficient mice,” *Journal of Cerebral Blood Flow and Metabolism*, vol. 33, no. 10, pp. 1605–1611, 2013.
- [115] N. Kovarova, P. Pecina, H. Nuskova et al., “Data on cytochrome c oxidase assembly in mice and human fibroblasts or tissues induced by SURF1 defect,” *Data in Brief*, vol. 7, pp. 1004–1009, 2016.
- [116] N. Kovarova, P. Pecina, H. Nuskova et al., “Tissue- and species-specific differences in cytochrome c oxidase assembly induced by SURF1 defects,” *Biochimica et Biophysica Acta*, vol. 1862, no. 4, pp. 705–715, 2016.
- [117] S. Possekkel, C. Marsac, and B. Kadenbach, “Biochemical analysis of fibroblasts from patients with cytochrome c oxidase-associated Leigh syndrome,” *Biochimica et Biophysica Acta*, vol. 1316, no. 3, pp. 153–159, 1996.
- [118] P. Clemente, S. Peralta, A. Cruz-Bermudez et al., “hCOA3 stabilizes cytochrome c oxidase 1 (COX1) and promotes cytochrome c oxidase assembly in human mitochondria,” *The Journal of Biological Chemistry*, vol. 288, no. 12, pp. 8321–8331, 2013.
- [119] S. Dennerlein, S. Oeljeklaus, D. Jans et al., “MITRAC7 acts as a COX1-specific chaperone and reveals a checkpoint during cytochrome c oxidase assembly,” *Cell Reports*, vol. 12, no. 10, pp. 1644–1655, 2015.
- [120] S. L. Williams, I. Valnot, P. Rustin, and J. W. Taanman, “Cytochrome c oxidase subassemblies in fibroblast cultures from patients carrying mutations in COX10, SCO1, or SURF1,” *The Journal of Biological Chemistry*, vol. 279, no. 9, pp. 7462–7469, 2004.
- [121] M. Jaksch, I. Ogilvie, J. Yao et al., “Mutations in SCO2 are associated with a distinct form of hypertrophic cardiomyopathy and cytochrome c oxidase deficiency,” *Human Molecular Genetics*, vol. 9, no. 5, pp. 795–801, 2000.
- [122] M. Jaksch, C. Paret, R. Stucka et al., “Cytochrome c oxidase deficiency due to mutations in SCO2, encoding a mitochondrial copper-binding protein, is rescued by copper in human myoblasts,” vol. 10, no. 26, pp. 3025–3035, 2001.
- [123] S. C. Leary, B. A. Kaufman, G. Pellicchia et al., “Human SCO1 and SCO2 have independent, cooperative functions in copper delivery to cytochrome c oxidase,” *Human Molecular Genetics*, vol. 13, no. 17, pp. 1839–1848, 2004.
- [124] M. Bourens, A. Boulet, S. C. Leary, and A. Barrientos, “Human COX20 cooperates with SCO1 and SCO2 to mature COX2 and promote the assembly of cytochrome c oxidase,” *Human Molecular Genetics*, vol. 23, no. 11, pp. 2901–2913, 2014.
- [125] R. Szklarczyk, B. F. Wanschers, L. G. Nijtmans et al., “A mutation in the FAM36A gene, the human ortholog of COX20, impairs cytochrome c oxidase assembly and is associated with ataxia and muscle hypotonia,” *Human Molecular Genetics*, vol. 22, no. 4, pp. 656–667, 2013.
- [126] L. G. Nijtmans, J. W. Taanman, A. O. Muijsers, D. Speijer, and C. Van den Bogert, “Assembly of cytochrome-c oxidase in cultured human cells,” *European Journal of Biochemistry*, vol. 254, no. 2, pp. 389–394, 1998.
- [127] J. W. Taanman and S. L. Williams, “Assembly of cytochrome c oxidase: what can we learn from patients with cytochrome c oxidase deficiency?” *Biochemical Society Transactions*, vol. 29, no. Part 4, pp. 446–451, 2001.
- [128] K. Bremer and C. D. Moyes, “mRNA degradation: an underestimated factor in steady-state transcript levels of cytochrome c oxidase subunits?” *The Journal of Experimental Biology*, vol. 217, Part 12, pp. 2212–2220, 2014.
- [129] Y. J. Lee and R. B. Wickner, “AFG1, a new member of the SEC18-NSF, PAS1, CDC48-VCP, TBP family of ATPases,” *Yeast*, vol. 8, no. 9, pp. 787–790, 1992.
- [130] O. Khalimonchuk, A. Bird, and D. R. Winge, “Evidence for a pro-oxidant intermediate in the assembly of cytochrome oxidase,” *The Journal of Biological Chemistry*, vol. 282, no. 24, pp. 17442–17449, 2007.

- [131] J. Cesnekova, M. Rodinova, H. Hansikova, J. Houstek, J. Zeman, and L. Stiburek, "The mammalian homologue of yeast Afg1 ATPase (lactation elevated 1) mediates degradation of nuclear-encoded complex IV subunits," *The Biochemical Journal*, vol. 473, no. 6, pp. 797–804, 2016.
- [132] B. Kadenbach and P. Merle, "On the function of multiple subunits of cytochrome c oxidase from higher eukaryotes," *FEBS Letters*, vol. 135, no. 1, pp. 1–11, 1981.
- [133] G. Villani and G. Attardi, "In vivo control of respiration by cytochrome c oxidase in wild-type and mitochondrial DNA mutation-carrying human cells," *Proceedings of the National Academy of Sciences of the United States of America*, vol. 94, no. 4, pp. 1166–1171, 1997.
- [134] W. S. Kunz, A. Kudin, S. Vielhaber, C. E. Elger, G. Attardi, and G. Villani, "Flux control of cytochrome c oxidase in human skeletal muscle," *The Journal of Biological Chemistry*, vol. 275, no. 36, pp. 27741–27745, 2000.
- [135] R. Acin-Perez, M. P. Bayona-Bafaluy, M. Bueno et al., "An intragenic suppressor in the cytochrome c oxidase I gene of mouse mitochondrial DNA," *Human Molecular Genetics*, vol. 12, no. 3, pp. 329–339, 2003.
- [136] C. Piccoli, R. Scrima, D. Boffoli, and N. Capitanio, "Control by cytochrome c oxidase of the cellular oxidative phosphorylation system depends on the mitochondrial energy state," *The Biochemical Journal*, vol. 396, no. 3, pp. 573–583, 2006.
- [137] M. E. Dalmonte, E. Forte, M. L. Genova, A. Giuffre, P. Sarti, and G. Lenaz, "Control of respiration by cytochrome c oxidase in intact cells: role of the membrane potential," *The Journal of Biological Chemistry*, vol. 284, no. 47, pp. 32331–32335, 2009.
- [138] P. C. Hinkle, M. A. Kumar, A. Resetar, and D. L. Harris, "Mechanistic stoichiometry of mitochondrial oxidative phosphorylation," *Biochemistry*, vol. 30, no. 14, pp. 3576–3582, 1991.
- [139] S. Arnold and B. Kadenbach, "Cell respiration is controlled by ATP, an allosteric inhibitor of cytochrome-c oxidase," *European Journal of Biochemistry*, vol. 249, no. 1, pp. 350–354, 1997.
- [140] M. Hüttemann, B. Kadenbach, and L. I. Grossman, "Mammalian subunit IV isoforms of cytochrome c oxidase," *Gene*, vol. 267, no. 1, pp. 111–123, 2001.
- [141] P. A. Burke and R. O. Poyton, "Structure/function of oxygen-regulated isoforms in cytochrome c oxidase," *The Journal of Experimental Biology*, vol. 201, Part 8, pp. 1163–1175, 1998.
- [142] M. R. Hodge, G. Kim, K. Singh, and M. G. Cumsy, "Inverse regulation of the yeast COX5 genes by oxygen and heme," *Molecular and Cellular Biology*, vol. 9, no. 5, pp. 1958–1964, 1989.
- [143] M. R. Hodge, K. Singh, and M. G. Cumsy, "Upstream activation and repression elements control transcription of the yeast COX5b gene," *Molecular and Cellular Biology*, vol. 10, no. 10, pp. 5510–5520, 1990.
- [144] L. A. Allen, X. J. Zhao, W. Caughey, and R. O. Poyton, "Isoforms of yeast cytochrome c oxidase subunit V affect the binuclear reaction center and alter the kinetics of interaction with the isoforms of yeast cytochrome c," *The Journal of Biological Chemistry*, vol. 270, no. 1, pp. 110–118, 1995.
- [145] R. Dodia, B. Meunier, C. W. Kay, and P. R. Rich, "Comparisons of subunit 5A and 5B isoenzymes of yeast cytochrome c oxidase," *The Biochemical Journal*, vol. 464, no. 3, pp. 335–342, 2014.
- [146] E. Bender and B. Kadenbach, "The allosteric ATP-inhibition of cytochrome c oxidase activity is reversibly switched on by cAMP-dependent phosphorylation," *FEBS Letters*, vol. 466, no. 1, pp. 130–134, 2000.
- [147] I. Lee, E. Bender, and B. Kadenbach, "Control of mitochondrial membrane potential and ROS formation by reversible phosphorylation of cytochrome c oxidase," *Molecular and Cellular Biochemistry*, vol. 234–235, no. 1–2, pp. 63–70, 2002.
- [148] R. Dudley, "Atmospheric oxygen, giant Paleozoic insects and the evolution of aerial locomotor performance," *The Journal of Experimental Biology*, vol. 201, no. Part 8, pp. 1043–1050, 1998.
- [149] M. Hüttemann, "New isoforms of cytochrome c oxidase subunit IV in tuna fish," *Biochimica et Biophysica Acta*, vol. 1492, no. 1, pp. 242–246, 2000.
- [150] C. Wu, C. Orozco, J. Boyer et al., "BioGPS: an extensible and customizable portal for querying and organizing gene annotation resources," *Genome Biology*, vol. 10, no. 11, p. R130, 2009.
- [151] M. Hüttemann, I. Lee, X. Gao et al., "Cytochrome c oxidase subunit 4 isoform 2-knockout mice show reduced enzyme activity, airway hyporeactivity, and lung pathology," *The FASEB Journal*, vol. 26, no. 9, pp. 3916–3930, 2012.
- [152] P. F. Weller, D. S. Bach, and K. F. Austen, "Biochemical characterization of human eosinophil Charcot-Leyden crystal protein (lysophospholipase)," *The Journal of Biological Chemistry*, vol. 259, no. 24, pp. 15100–15105, 1984.
- [153] S. J. Ackerman, L. Liu, M. A. Kwatia et al., "Charcot-Leyden crystal protein (galectin-10) is not a dual function galectin with lysophospholipase activity but binds a lysophospholipase inhibitor in a novel structural fashion," *The Journal of Biological Chemistry*, vol. 277, no. 17, pp. 14859–14868, 2002.
- [154] M. Hüttemann, I. Lee, J. Liu, and L. I. Grossman, "Transcription of mammalian cytochrome c oxidase subunit IV-2 is controlled by a novel conserved oxygen responsive element," *The FEBS Journal*, vol. 274, no. 21, pp. 5737–5748, 2007.
- [155] S. Aras, O. Pak, N. Sommer et al., "Oxygen-dependent expression of cytochrome c oxidase subunit 4-2 gene expression is mediated by transcription factors RBPJ, CXXC5 and CHCHD2," *Nucleic Acids Research*, vol. 41, no. 4, pp. 2255–2266, 2013.
- [156] S. Aras, M. Bai, I. Lee, R. Springett, M. Hüttemann, and L. I. Grossman, "MNRR1 (formerly CHCHD2) is a bi-organellar regulator of mitochondrial metabolism," *Mitochondrion*, vol. 20C, pp. 43–51, 2015.
- [157] K. M. Kocha, K. Reilly, D. S. Porplycia, J. McDonald, T. Snider, and C. D. Moyes, "Evolution of the oxygen sensitivity of cytochrome c oxidase subunit 4," *American Journal of Physiology. Regulatory, Integrative and Comparative Physiology*, vol. 308, no. 4, pp. R305–R320, 2015.
- [158] R. Fukuda, H. Zhang, J. W. Kim, L. Shimoda, C. V. Dang, and G. L. Semenza, "HIF-1 regulates cytochrome oxidase subunits to optimize efficiency of respiration in hypoxic cells," *Cell*, vol. 129, no. 1, pp. 111–122, 2007.
- [159] H. J. Hwang, S. G. Lynn, A. Vengellur et al., "Hypoxia inducible factors modulate mitochondrial oxygen consumption and transcriptional regulation of nuclear-encoded electron

- transport chain genes," *Biochemistry*, vol. 54, no. 24, pp. 3739–3748, 2015.
- [160] S. Singh, M. Misiak, C. Beyer, and S. Arnold, "Cytochrome c oxidase isoform IV-2 is involved in 3-nitropropionic acid-induced toxicity in striatal astrocytes," *Glia*, vol. 57, no. 14, pp. 1480–1491, 2009.
- [161] S. Horvat, C. Beyer, and S. Arnold, "Effect of hypoxia on the transcription pattern of subunit isoforms and the kinetics of cytochrome c oxidase in cortical astrocytes and cerebellar neurons," *Journal of Neurochemistry*, vol. 99, no. 3, pp. 937–951, 2006.
- [162] C. R. Oliva, T. Markert, G. Y. Gillespie, and C. E. Griguer, "Nuclear-encoded cytochrome c oxidase subunit 4 regulates BMI1 expression and determines proliferative capacity of high-grade gliomas," *Oncotarget*, vol. 6, no. 6, pp. 4330–4344, 2015.
- [163] E. Shteyer, A. Saada, A. Shaag et al., "Exocrine pancreatic insufficiency, dyserythropoietic anemia, and calvarial hyperostosis are caused by a mutation in the COX4I2 gene," *American Journal of Human Genetics*, vol. 84, no. 3, pp. 412–417, 2009.
- [164] A. Vondrackova, K. Vesela, H. Hansikova et al., "High-resolution melting analysis of 15 genes in 60 patients with cytochrome-c oxidase deficiency," *Journal of Human Genetics*, vol. 57, no. 7, pp. 442–448, 2012.
- [165] J. Carroll, I. M. Fearnley, J. M. Skehel, R. J. Shannon, J. Hirst, and J. E. Walker, "Bovine complex I is a complex of 45 different subunits," *The Journal of Biological Chemistry*, vol. 281, no. 43, pp. 32724–32727, 2006.
- [166] Y. Garbian, O. Ovadia, S. Dadon, and D. Mishmar, "Gene expression patterns of oxidative phosphorylation complex I subunits are organized in clusters," *PloS One*, vol. 5, no. 4, article e9985, 2010.
- [167] R. D. Pitceathly, S. Rahman, Y. Wedatilake et al., "NDUFA4 mutations underlie dysfunction of a cytochrome c oxidase subunit linked to human neurological disease," *Cell Reports*, vol. 3, no. 6, pp. 1795–1805, 2013.
- [168] D. Tello, E. Balsa, B. Acosta-Iborra et al., "Induction of the mitochondrial NDUFA4L2 protein by HIF-1 α decreases oxygen consumption by inhibiting complex I activity," *Cell Metabolism*, vol. 14, no. 6, pp. 768–779, 2011.
- [169] D. R. Minton, L. Fu, N. P. Mongan, M. M. Shevchuk, D. M. Nanus, and L. J. Gudas, "Role of NADH dehydrogenase (ubiquinone) 1 α subcomplex 4-like 2 in clear cell renal cell carcinoma," *Clinical Cancer Research*, vol. 22, no. 11, pp. 2791–2801, 2016.
- [170] Y. Lv, S. L. Nie, J. M. Zhou et al., "Overexpression of NDUFA4L2 is associated with poor prognosis in patients with colorectal cancer," *ANZ Journal of Surgery*, pp. 1–5, 2016, Epub ahead of print.
- [171] R. K. Lai, I. M. Xu, D. K. Chiu et al., "NDUFA4L2 fine-tunes oxidative stress in hepatocellular carcinoma," *Clinical Cancer Research*, vol. 22, no. 12, pp. 3105–3117, 2016.
- [172] L. Kuhn-Nentwig and B. Kadenbach, "Isolation and properties of cytochrome c oxidase from rat liver and quantification of immunological differences between isozymes from various rat tissues with subunit-specific antisera," *European Journal of Biochemistry*, vol. 149, no. 1, pp. 147–158, 1985.
- [173] S. A. Jaradat, M. S. Ko, and L. I. Grossman, "Tissue-specific expression and mapping of the Cox7ah gene in mouse," *Genomics*, vol. 49, no. 3, pp. 363–370, 1998.
- [174] L. I. Grossman and M. I. Lomax, "Nuclear genes for cytochrome c oxidase," *Biochimica et Biophysica Acta*, vol. 1352, no. 2, pp. 174–192, 1997.
- [175] T. R. Schmidt, S. A. Jaradat, M. Goodman, M. I. Lomax, and L. I. Grossman, "Molecular evolution of cytochrome c oxidase: rate variation among subunit VIa isoforms," *Molecular Biology and Evolution*, vol. 14, no. 6, pp. 595–601, 1997.
- [176] I. Lee and B. Kadenbach, "Palmitate decreases proton pumping of liver-type cytochrome c oxidase," *European Journal of Biochemistry*, vol. 268, no. 24, pp. 6329–6334, 2001.
- [177] G. Anthony, A. Reimann, and B. Kadenbach, "Tissue-specific regulation of bovine heart cytochrome-c oxidase activity by ADP via interaction with subunit VIa," *Proceedings of the National Academy of Sciences of the United States of America*, vol. 90, no. 5, pp. 1652–1656, 1993.
- [178] V. Frank and B. Kadenbach, "Regulation of the H⁺/e⁻ stoichiometry of cytochrome c oxidase from bovine heart by intramitochondrial ATP/ADP ratios," *FEBS Letters*, vol. 382, no. 1-2, pp. 121–124, 1996.
- [179] N. B. Radford, B. Wan, A. Richman et al., "Cardiac dysfunction in mice lacking cytochrome-c oxidase subunit VIaH," *American Journal of Physiology. Heart and Circulatory Physiology*, vol. 282, no. 2, pp. H726–H733, 2002.
- [180] A. Weishaupt and B. Kadenbach, "Selective removal of subunit VIb increases the activity of cytochrome c oxidase," *Biochemistry*, vol. 31, no. 46, pp. 11477–11481, 1992.
- [181] V. Massa, E. Fernandez-Vizarra, S. Alshahwan et al., "Severe infantile encephalomyopathy caused by a mutation in COX6B1, a nucleus-encoded subunit of cytochrome c oxidase," *American Journal of Human Genetics*, vol. 82, no. 6, pp. 1281–1289, 2008.
- [182] U. N. Abdulhag, D. Soiferman, O. Schueler-Furman et al., "Mitochondrial complex IV deficiency, caused by mutated COX6B1, is associated with encephalomyopathy, hydrocephalus and cardiomyopathy," *European Journal of Human Genetics*, vol. 23, no. 2, pp. 159–164, 2015.
- [183] M. Hüttemann, T. R. Schmidt, and L. I. Grossman, "A third isoform of cytochrome c oxidase subunit VIII is present in mammals," *Gene*, vol. 312, pp. 95–102, 2003.
- [184] B. Hennig, "Change of cytochrome c structure during development of the mouse," *European Journal of Biochemistry*, vol. 55, no. 1, pp. 167–183, 1975.
- [185] T. Preiss, Z. M. Chrzanowska-Lightowlers, and R. N. Lightowlers, "The tissue-specific RNA-binding protein COLBP is differentially regulated during myogenesis," *Biochimica et Biophysica Acta*, vol. 1221, no. 3, article 8167150, pp. 286–289, 1994.
- [186] T. Preiss, A. E. Sang, Z. M. Chrzanowska-Lightowlers, and R. N. Lightowlers, "The mRNA-binding protein COLBP is glutamate dehydrogenase," *FEBS Letters*, vol. 367, no. 3, pp. 291–296, 1995.
- [187] M. Hüttemann, S. Klewer, I. Lee et al., "Mice deleted for heart-type cytochrome c oxidase subunit 7a1 develop dilated cardiomyopathy," *Mitochondrion*, vol. 12, no. 2, pp. 294–304, 2012.
- [188] I. Lee, M. Hüttemann, J. Liu, L. I. Grossman, and M. H. Malek, "Deletion of heart-type cytochrome c oxidase subunit 7a1 impairs skeletal muscle angiogenesis and oxidative

- phosphorylation,” *The Journal of Physiology*, vol. 590, no. 20, pp. 5231–5243, 2012.
- [189] S. F. Maurer, T. Fromme, L. I. Grossman, M. Hüttemann, and M. Klingenspor, “The brown and brite adipocyte marker Cox7a1 is not required for non-shivering thermogenesis in mice,” *Scientific Reports*, vol. 5, pp. 1–14, 2015.
- [190] F. Segade, B. Hurlle, E. Claudio, S. Ramos, and P. S. Lazo, “Identification of an additional member of the cytochrome c oxidase subunit VIIa family of proteins,” *The Journal of Biological Chemistry*, vol. 271, no. 21, pp. 12343–12349, 1996.
- [191] E. Lapuente-Brun, R. Moreno-Loshuertos, R. Acin-Perez et al., “Supercomplex assembly determines electron flux in the mitochondrial electron transport chain,” *Science*, vol. 340, no. 6140, pp. 1567–1570, 2013.
- [192] A. Mourier, S. Matic, B. Ruzzenente, N. G. Larsson, and D. Milenkovic, “The respiratory chain supercomplex organization is independent of COX7a2l isoforms,” *Cell Metabolism*, vol. 20, no. 6, pp. 1069–1075, 2014.
- [193] E. G. Williams, Y. Wu, P. Jha et al., “Systems proteomics of liver mitochondria function,” *Science*, vol. 352, no. 6291, p. aad0189, 2016.
- [194] S. Cogliati, E. Calvo, M. Loureiro et al., “Mechanism of superassembly of respiratory complexes III and IV,” *Nature*, vol. 539, no. 7630, pp. 579–582, 2016.
- [195] R. Perez-Perez, T. Lobo-Jarne, D. Milenkovic et al., “COX7A2L is a mitochondrial complex III binding protein that stabilizes the III2+IV supercomplex without affecting respirasome formation,” *Cell Reports*, vol. 16, no. 9, pp. 2387–2398, 2016.
- [196] M. Wu, J. Gu, R. Guo, Y. Huang, and M. Yang, “Structure of mammalian respiratory supercomplex I1III2IV1,” *Cell*, vol. 167, no. 6, pp. 1598–1609.e1510, 2016.
- [197] K. Zhang, G. Wang, X. Zhang et al., “COX7AR is a stress-inducible mitochondrial COX subunit that promotes breast cancer malignancy,” *Scientific Reports*, vol. 6, pp. 1–12, 2016.
- [198] P. Merle and B. Kadenbach, “The subunit composition of mammalian cytochrome c oxidase,” *European Journal of Biochemistry*, vol. 105, no. 3, pp. 499–507, 1980.
- [199] R. Rizzuto, H. Nakase, B. Darras et al., “A gene specifying subunit VIII of human cytochrome c oxidase is localized to chromosome 11 and is expressed in both muscle and non-muscle tissues,” *The Journal of Biological Chemistry*, vol. 264, no. 18, pp. 10595–10600, 1989.
- [200] A. Goldberg, D. E. Wildman, T. R. Schmidt et al., “Adaptive evolution of cytochrome c oxidase subunit VIII in anthropoid primates,” *Proceedings of the National Academy of Sciences of the United States of America*, vol. 100, no. 10, pp. 5873–5878, 2003.
- [201] B. Kadenbach, A. Stroh, A. Becker, C. Eckerskorn, and F. Lottspeich, “Tissue- and species-specific expression of cytochrome c oxidase isozymes in vertebrates,” *Biochimica et Biophysica Acta*, vol. 1015, no. 2, pp. 368–372, 1990.
- [202] K. Hallmann, A. P. Kudin, G. Zsurka et al., “Loss of the smallest subunit of cytochrome c oxidase, COX8A, causes Leigh-like syndrome and epilepsy,” *Brain*, vol. 139, no. Part 2, pp. 338–345, 2016.
- [203] C. Vijayasarathy, I. Biunno, N. Lenka et al., “Variations in the subunit content and catalytic activity of the cytochrome c oxidase complex from different tissues and different cardiac compartments,” *Biochimica et Biophysica Acta*, vol. 1371, no. 1, pp. 71–82, 1998.
- [204] G. Tamiya, S. Makino, M. Hayashi et al., “A mutation of COX6A1 causes a recessive axonal or mixed form of Charcot-Marie-Tooth disease,” *American Journal of Human Genetics*, vol. 95, no. 3, pp. 294–300, 2014.
- [205] A. Indrieri, V. A. van Rahden, V. Tiranti et al., “Mutations in COX7B cause microphthalmia with linear skin lesions, an unconventional mitochondrial disease,” *American Journal of Human Genetics*, vol. 91, no. 5, pp. 942–949, 2012.

Research Article

The Stimulated Glycolytic Pathway Is Able to Maintain ATP Levels and Kinetic Patterns of Bovine Epididymal Sperm Subjected to Mitochondrial Uncoupling

João D. A. Losano,¹ Juan Fernando Padín,^{2,3} Iago Méndez-López,² Daniel S. R. Angrimani,¹ Antonio G. García,² Valquiria H. Barnabe,¹ and Marcilio Nichi^{1,4}

¹Department of Animal Reproduction, Faculty of Veterinary Medicine, University of São Paulo, São Paulo, SP, Brazil

²Department of Pharmacology, Faculty of Medicine, Autonomous University of Madrid, Madrid, Spain

³Department of Medical Science, Faculty of Medicine Ciudad Real, University of Castilla-La Mancha, Ciudad Real, Spain

⁴School of Veterinary Medicine and Animal Science, Avenue Orlando Marques de Paiva, No. 87, 05508-270 São Paulo, SP, Brazil

Correspondence should be addressed to Marcilio Nichi; mnichi@usp.br

Received 3 February 2017; Accepted 8 March 2017; Published 9 May 2017

Academic Editor: Moh H. Malek

Copyright © 2017 João D. A. Losano et al. This is an open access article distributed under the Creative Commons Attribution License, which permits unrestricted use, distribution, and reproduction in any medium, provided the original work is properly cited.

Studies have reported the importance of mitochondria in sperm functionality. However, for some species, the glycolytic pathway appears to be as important as oxidative phosphorylation in ATP synthesis and sperm kinetics. These mechanisms have not been fully elucidated for bovine spermatozoa. Therefore, the aim of this study was to evaluate the role of mitochondria and the glycolytic pathway in ATP synthesis, sperm movement patterns, and oxidative homeostasis of epididymal spermatozoa in bovine specimens. We observed that mitochondrial uncoupling with protonophores significantly reduced ATP levels. However, these levels were reestablished after stimulation of the glycolytic pathway. We verified the same pattern of results for sperm kinetic variables and the production of reactive oxygen species (ROS). Thus, we suggest that, after its appropriate stimulation, the glycolytic pathway is capable of maintaining ATP levels, sperm kinetic patterns, and oxidative balance of bovine epididymal spermatozoa submitted to mitochondrial uncoupling.

1. Introduction

Studies have shown the importance of mitochondria in sperm functionality, as they are considered the main source of ATP for cellular homeostasis and motility [1, 2]. However, the role of mitochondria in sperm metabolism has been a matter of debate. Mukai and Okuno [3] verified that ATP levels and flagellar beating remained constant when the mitochondria of mouse sperm was uncoupled concurrently with glycolysis stimulation. However, by inhibiting glycolysis and stimulating oxidative phosphorylation, authors observed that flagellar beating and ATP levels were quickly reduced. These results indicate that glycolysis plays an important role in murine sperm energy production.

In a similar study, Nascimento et al. [4] performed inhibitory and stimulatory treatments for both oxidative

phosphorylation and glycolysis in human sperm. Authors concluded that oxidative phosphorylation, despite contributing to ATP production, is not sufficient to sustain sperm motility, confirming that the glycolytic pathway is the primary energy source for human sperm. Additionally, ATP produced by oxidative phosphorylation in the sperm midpiece is not efficiently released into the distal portions of the tail, indicating that glycolysis plays a key role in the flagellar beat of such sperm regions [5–7].

Davila et al. [8] demonstrated that equine spermatozoa require oxidative phosphorylation as glycolytic pathway to maintain motility. Complementary in ram, Losano et al. [9] demonstrated that mitochondrial depolarization did not affect total motility; however, sperm kinetic patterns were altered. On the other hand, they found that glycolytic pathway inhibition impaired total motility and sperm move-

ment patterns. For both species, glycolytic pathway seems to be as important as oxidative phosphorylation for sperm physiology. However, the role of these pathways on bovine sperm functionality has not been fully elucidated. This information is extremely important for the understanding of bull sperm physiology. In addition, studies evaluating the energy metabolism of bovine sperm may contribute to the understanding of possible causes for the reduction in sperm quality and fertilization failures related to these metabolic pathways and then improve existent biotechnology's, such as artificial insemination which can impact in higher fertility rates.

Sperm collected directly from the epididymis seem to be the ideal cellular model to study energy metabolism. This is due to the many glycolysis, citric acid cycle, and oxidative phosphorylation stimulants contained in the seminal plasma derived from the accessory glands [10–12]. The fact that epididymal spermatozoa have not been stimulated with these substances provides a better *in vitro* manipulation of these cells, allowing the stimulation and inhibition of these pathways to evaluate the role of each metabolic pathway on sperm functionality.

Therefore, the aim of this study was to evaluate the role of mitochondria and glycolysis in ATP production, generation of reactive oxygen species (ROS), and kinetic patterns of epididymal bovine sperm by means of mitochondrial uncoupling and glycolytic pathway stimulation.

2. Material and Methods

The present experiment was conducted according to ethical guidelines for animal experiments and approved by the Bioethics Committee of the School of Veterinary Medicine and Animal Science at the University of São Paulo (protocol number 7978040914).

In this study, we submitted bovine epididymal spermatozoa to treatment with the oxidative phosphorylation uncoupler carbonyl cyanide 4-(trifluoromethoxy)phenylhydrazine (FCCP) to significantly reduce mitochondrial ATP synthesis and stimulated the glycolytic pathway by glucose addition. However, in order to verify the optimal concentrations of the uncoupler, FCCP, we performed a dose-response curve in experiment 1. Thus, the selected concentrations were used in the subsequent experiments. The aim of these experiments was to evaluate the contribution of mitochondria to ATP synthesis (experiment 2), patterns of sperm kinetics (experiment 3), and oxidative homeostasis (experiment 4) of bovine epididymal sperm and verify if stimulation of the glycolytic pathway would be able to maintain these sperm parameters that are probably suppressed by mitochondrial uncoupling.

2.1. Sample Collection. Epididymal sperm samples were collected and then dissecting the epididymis cauda with a scalpel blade, according to previous protocol [13]. To limit blood contamination, dissection was performed carefully. The flowing epididymal fluid was collected with an automatic pipette. Then, samples were used in each respective experiment proposed.

2.2. Experiment 1—Concentration-Response Curve of Mitochondrial Uncoupler, FCCP. To evaluate the effect of mitochondrial uncoupling by FCCP, spermatozoa from 3 bovine epididymides ($n = 3$) were collected and diluted to a concentration of 100 million spermatozoa per mL in modified TALP. Despite a minimum number of epididymides used, we evaluated the mitochondria of each spermatozoon singly, as experimental unit. Thus, we used 15 to 26 cells per FCCP concentration. Thereafter, the spermatozoa were incubated in a perfusion chamber with mitochondrial fluorophore tetramethylrhodamine-ethyl-ester perchlorate at 500 nM (ThermoFisher® Scientific, 0.5 μ L of TMRE in 1 mL of medium) for 5 minutes at 37°C. For the spermatozoa to remain attached during perfusion with FCCP, coverslips of the perfusion chamber were treated with polylysine.

After incubation, the amount of TMRE fluorescence captured by each sperm mitochondrion was recorded by the software LAS AF Lite (Leica® Microsystems, Germany) at an emission of 500 nm and excitation of 600 nm by a fluorescence microscope (Leica Microsystems, Germany). Thirty seconds of mitochondrial basal fluorescence was recorded, and then perfusions were performed with increasing FCCP concentrations (Tocris Bioscience®, MN, USA; 0.3, 1, 3, 10, 30, 60, and 100 μ M) by means of an electrovalve controller. Stimulation performed with FCCP at 30 seconds was recorded, and the percentage of mitochondrial depolarization was calculated based on the difference between the basal fluorescence and the amount of fluorescence retained in the mitochondria of each spermatozoon after 30 seconds of FCCP stimulation.

The lower FCCP concentrations of the dose-response curve (0.3, 1, and 3 μ M) and the concentration insufficient for the promotion of mitochondrial depolarization (0.1 μ M, concentration under the curve) were selected to be used in the subsequent experiments. We selected these concentrations in order to significantly reduce the mitochondrial ATP synthesis without promoting disruption in this organelle.

2.3. Experiment 2—Effect of Mitochondrial Uncoupling and Glycolysis Stimulation on ATP Levels. In this experiment, spermatozoa from 6 bovine epididymides ($n = 6$) were collected and diluted to a concentration of 100 million spermatozoa per mL in modified TALP medium. Each sample was divided into ten aliquots, which were submitted to a 5 \times 2 factorial design wherein one of the factors was the addition of glucose (5 mM) and the other factor was the treatment with increasing concentrations of FCCP (0.1, 0.3, 1, and 3 μ M). After a 15-minute incubation, the treatments were subjected to measurements of ATP levels by means of a luminescence technique. For this procedure, 50 μ L aliquots in duplicate from each treatment containing 100000 spermatozoa were added to 50 μ L of CellTiter-Glo® Luminescent Cell Viability Assay kit (Promega®, USA) and incubated for 30 minutes at 37°C according to the manufacturer's recommendations. Immediately after this procedure, ATP levels were measured in a luminescence apparatus (ThermoFisher Scientific, MA, USA) in duplicate. The results obtained, expressed in arbitrary light units (AUL), were interpolated

on a standard curve containing different concentrations of ATP (10, 100, 1000, 5000, and 10000 nM) and were then expressed in nM ATP.

2.4. Experiment 3—Effect of Mitochondrial Uncoupling and Glycolysis Stimulation on Sperm Kinetic Patterns. To evaluate the effect of mitochondrial uncoupling and glycolysis stimulation on sperm kinetic patterns, spermatozoa from 7 bovine epididymides ($n = 7$) were collected and diluted to a concentration of 100 million spermatozoa per mL in modified TALP medium. Each sample was divided into ten aliquots, which were submitted to a 5×2 factorial design wherein one of the factors was the addition of glucose (5 mM) and the other was the treatment with increasing concentrations of FCCP (0.1, 0.3, 1, and $3 \mu\text{M}$). After 5 minutes of incubation, the sperm samples were subjected to computerized analysis of sperm kinetics (ISASPBOS, Proiser®, Valencia, Spain). The following variables were considered: motility (%), progressive motility (%), VAP (average path velocity, $\mu\text{m/s}$), VSL (straight-line velocity, $\mu\text{m/s}$), VCL (curvilinear velocity, $\mu\text{m/s}$), ALH (amplitude of lateral head displacement, μm), BCF (beat cross-frequency, Hz), STR (straightness, %), and LIN (linearity, %). In addition to these parameters, the sperm were also divided into four groups based on velocity: rapid (VAP > $50 \mu\text{m/s}$; %), medium ($30 \mu\text{m/s} < \text{VAP} < 50 \mu\text{m/s}$; %), slow (VAP < $30 \mu\text{m/s}$ or VSL < $15 \mu\text{m/s}$; %), and static (%) [14].

2.5. Experiment 4—Effect of Mitochondrial Uncoupling and Glycolysis Stimulation on Reactive Oxygen Species Production. To evaluate the effect of mitochondrial uncoupling and glycolysis stimulation on reactive oxygen species production, spermatozoa from 6 bovine epididymides ($n = 6$) were collected and diluted to a concentration of 100 million spermatozoa per mL in modified TALP. Each sample was divided into ten aliquots, which were submitted to a 4×2 factorial design wherein one of the factors was the addition of glucose (5 mM) and the other was the treatment with increasing concentrations of FCCP (0.1, 0.3, 1, and $3 \mu\text{M}$). These treatments were incubated for 30 minutes at 37°C and subjected to the detection of reactive oxygen species. To perform this technique, 100000 sperm were incubated in modified TALP solution containing $10 \mu\text{M}$ (final concentration) of the fluorescent probe CM-H2DCFDA for 30 minutes (triplicate samples). After incubation was performed, the ROS were detected using a fluorometer (Fluostar microplate reader Omega, Labtec-BMG, Germany) at excitation 492–495 nm and emission 517–527 nm. The fluorescence intensity results obtained were interpolated on a standard curve containing different concentrations of hydrogen peroxide (H_2O_2 : 3, 10, 30, 60, 100, 200, and $300 \mu\text{M}$) and were then expressed in μL of O_2 generated. Data were normalized relative to the control group (untreated samples).

2.6. Statistical Analysis. The concentration-response curve for FCCP (experiment 1) was performed by nonlinear regression using the software GraphPad Prism 6. Data relating to the measurement of ATP levels and computerized analysis

of sperm kinetics (experiments 2 and 3, resp.) were analyzed using the SAS System for Windows (SAS Institute Inc., Cary, NC, USA). Thus, the interaction between FCCP and glucose factors was determined by PROC GLM. Differences between treatments were assessed using parametric (Student's t -test for each factor separately or LSD test for the combination of factors) and nonparametric tests (Wilcoxon) in accordance with the normality of the residuals (Gaussian distribution) and homogeneity of the variances. To analyze the effect of FCCP in the presence or absence of glucose in the ROS production, data normalized to the control group were compared by ANOVA variance analysis (LSD test) using the SAS System for Windows program (SAS Institute Inc., Cary, NC, USA). The level of significance to reject the H_0 (null hypothesis) was 5%; that is, the significance level was 0.05. Significant differences between classificatory variables (treatments) and a specific response variable were considered.

3. Results

3.1. Experiment 1—Concentration-Response Curve of Mitochondrial Uncoupler FCCP. By using a nonlinear regression, we found that the concentration-response curve is square root = 0.7 and $\text{EC}_{50} = 4.67 \times 10^{-5} \mu\text{M}$. We observed a high percentage of depolarization with FCCP concentrations of $30 \mu\text{M}$, $60 \mu\text{M}$, and $100 \mu\text{M}$ (Figure 1). Thus, in order to select points where there is a reduction in ATP without promoting disruption in the organelle, we selected $3 \mu\text{M}$, $1 \mu\text{M}$, $0.3 \mu\text{M}$, and $0.1 \mu\text{M}$ for the concentrations used in the subsequent experiments (concentration under the curve—Figure 1).

3.2. Experiment 2—Effect of Mitochondrial Uncoupling and Glycolysis Stimulation on ATP Levels. There were significant effects of FCCP, glucose, and FCCP-by-glucose interaction in the ATP ($P < 0.0001$; Table 1) analysis. Then, it was possible to compare the effects of the addition of glucose in the FCCP sample (Figure 2). We observed a lower ATP production in the FCCP group at concentrations of $0.3 \mu\text{M}$ ($180.3 \pm 31.9 \text{ nM}$), $1 \mu\text{M}$ ($220.2 \pm 40.4 \text{ nM}$), and $3 \mu\text{M}$ ($272.3 \pm 70.4 \text{ nM}$) than at $0 \mu\text{M}$ (control— $448.6 \pm 63.7 \text{ nM}$) and $0.1 \mu\text{M}$ ($422.4 \pm 41.5 \text{ nM}$ —Figure 2). However, in the group treated with FCCP supplemented with glucose, the concentrations were similar between the groups treated with $0.1 \mu\text{M}$ ($610.8 \pm 57.8 \text{ nM}$), $0.3 \mu\text{M}$ ($606.2 \pm 64.2 \text{ nM}$), $1 \mu\text{M}$ ($670.9 \pm 61.9 \text{ nM}$), and $3 \mu\text{M}$ ($696.1 \pm 68.5 \text{ nM}$) FCCP and the group treated with glucose without FCCP ($577.2 \pm 70.4 \text{ nM}$) (Figure 2).

3.3. Experiment 3—Effect of Mitochondrial Uncoupling and Glycolysis Stimulation on Sperm Kinetics Patterns. There were significant effects of FCCP, glucose, and FCCP-by-glucose interaction ($P < 0.05$) on all CASA parameters (Table 1).

We observed a decrease in the total motility between samples without FCCP (control) and with glucose (Figure 3(a)); however, it was possible to note an increase in motility in the groups treated with $0.3 \mu\text{M}$, $0.1 \mu\text{M}$, $1 \mu\text{M}$, and $3 \mu\text{M}$ FCCP supplemented with glucose (Figure 3(a)).

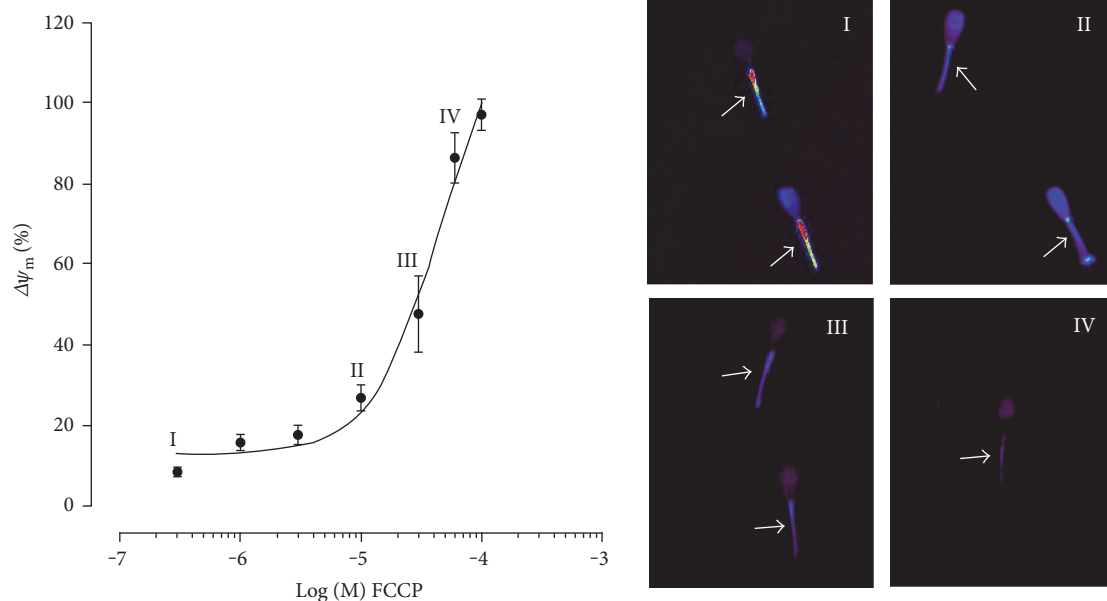


FIGURE 1: Dose-response curve of FCCP concentrations (0.3, 1, 3, 10, 30, 60, and 100 μM) in sperm of bovine epididymal samples. Superscript numerals indicate the FCCP concentration used and their respective images. Mitochondrial depolarization of bovine spermatozoa at FCCP concentration of 0 μM (I), 10 μM (II), 30 μM (III), and 60 μM (IV). Arrows indicate mitochondria labeled with the TMRE fluorescent probe at different percentages of mitochondrial depolarization. 400x magnification.

TABLE 1: Probability values for the FCCP (0, 0.1, 0.3, 1, and 3 μM), glucose, and their interaction on computer-assisted sperm analysis (CASA).

	FCCP	Glucose	FCCP \times glucose
Total sperm motility (%)	<0.0001	0.0003	<0.0001
Sperm progressive motility (%)	<0.0001	0.0005	<0.0001
Percentage of rapid sperm (%)	0.0006	0.0077	<0.0001
Percentage of medium sperm (%)	0.0087	0.0033	<0.0001
Percentage of slow sperm (%)	0.3993	0.0361	0.0045
Amplitude of lateral head displacement (ALH— μm)	0.0009	0.0119	0.0095
Average path velocity (VAP— $\mu\text{m/s}$)	<0.0001	0.0002	<0.0001
Straight line velocity (VSL— $\mu\text{m/s}$)	<0.0001	0.0002	<0.0001
Curvilinear velocity (VCL— $\mu\text{m/s}$)	0.0002	0.0038	0.0002
Beat cross-frequency (BCF—Hz)	<0.0001	0.0020	<0.0001
Sperm straightness (STR—%)	0.0002	0.0020	<0.0001
Sperm linearity (LIN—%)	<0.0001	0.0003	<0.0001
Wobble (WOB—%)	<0.0001	0.0003	<0.001

This same effect was detected for progressive motility (Figure 3(b)), VAP, VSL, VCL, and rapid sperm velocity (see Supplementary Material available online at <https://doi.org/10.1155/2017/1682393>).

Next, we examined the effects of the addition of glucose in the FCCP samples (Figure 3 and Supplementary Material). In the BCF analysis, we observed an increase in the groups with 1 μM and 3 μM of FCCP supplemented with glucose but a decrease in the glucose group (Supplementary Material). Furthermore, we observed an increase in the slow sperm velocity in the samples supplemented with glucose in the groups treated with 1 μM and 3 μM of FCCP and glucose

alone but a decrease in the group treated with 0.3 μM FCCP (Supplementary Material).

With FCCP treatment, the control and 0.1 μM groups had higher values of total sperm motility, VAP, and VSL than the 0.3 μM group, which was superior to the 1 μM and 3 μM samples (Figure 3 and Supplementary Material). However, in the ALH, BCF, straightness, linearity, and wobble analyses, the control, 0.1 μM , and 3 μM groups had higher rates than the 1 μM and 3 μM groups (Supplementary Material). In the VCL and percentage of medium sperm velocity, we observed that the 3 μM and 1 μM groups had lower values than the 0.3 μM group,

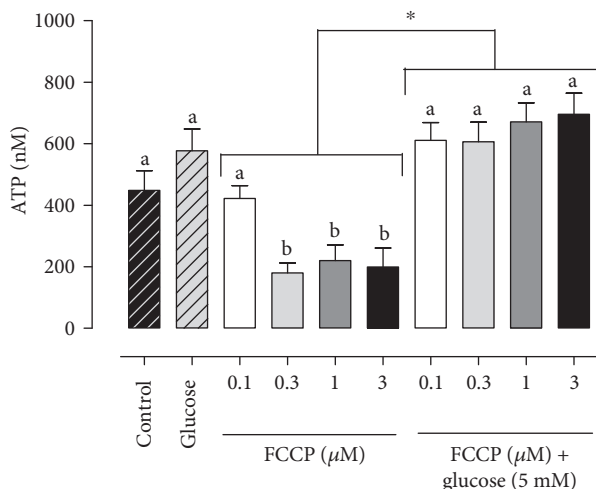


FIGURE 2: ATP production by bovine epididymal sperm treated with FCCP in different concentrations (0 μM , 0.1 μM , 0.3 μM , 1 μM , and 3 μM) in absence or presence of glucose 5 mM. a-b superscripts indicate differences between concentrations ($P < 0.05$). * indicates differences after the glucose supplementation ($P < 0.05$).

which was similar to the 0.1 μM group but lower than the control (Supplementary Material). In progressive motility (PM), the control group had the highest rates (Figure 3). However, we observed lower rates of PM in the 3 μM and 1 μM groups than in the 0.3 μM group, which was inferior to the 0.1 μM group (Figure 3). In the medium sperm velocity, the control group was superior to the 1 μM and 3 μM groups (Supplementary Material). On the other hand, in the slow sperm velocity, the control and 1 μM groups had lower rates than the 0.1 μM and 0.3 μM groups (Supplementary Material).

When we compared the results between the concentrations of FCCP supplemented with glucose, we highlighted the higher values of progressive motility, straightness, and rapid sperm velocity in the groups treated with 3 μM and 0.3 μM of FCCP, which were superior to the glucose group (Figure 3 and Supplementary Material). In the total motility analysis, the 3 μM group was superior to the glucose group (Figure 3). However, in the VCL, the 0.3 μM group had higher values than the 1 μM group (Supplementary Material). The glucose group was lower than the 0.3 μM , 1 μM and 3 μM groups in the BCF parameter (Supplementary Material). However, in the slow sperm velocity, the 1 μM group was higher than the 0.3 μM group (Supplementary Material). The remaining CASA variables did not show any difference between the groups (Supplementary Material).

3.4. Experiment 4—Effect of Mitochondrial Uncoupling and Glycolysis Stimulation on Reactive Oxygen Species Production. In the production of the reactive oxygen species, we highlight in Figure 4 the higher ROS generated by sperm treated with 3 μM of FCCP supplemented with glucose ($332.9 \pm 34.58 \mu\text{L}$) than that with FCCP concentrations of 0.1 μM ($213.2 \pm 38.77 \mu\text{L}$), 1 μM ($191.44 \pm 50.39 \mu\text{L}$), and 3 μM ($170.06 \pm 49.34 \mu\text{L}$).

4. Discussion

The aim of this study was to evaluate the role of mitochondria and the glycolytic pathway in the maintenance of ATP levels, the parameters of sperm movement, and the production of reactive oxygen species in epididymal bovine sperm. To perform this experiment, we submitted bovine sperm to mitochondrial uncoupling with FCCP to significantly reduce the synthesis of ATP by the mitochondria and evaluate the effect of this reduction in sperm functionality. Furthermore, we promoted stimulation of the glycolytic pathway by glucose addition concurrently with the mitochondrial uncoupling to assess whether glycolysis would be able to maintain the ATP levels, sperm kinetic patterns, and oxidative homeostasis possibly harmed by mitochondrial depolarization.

The mitochondrial uncoupler FCCP is a lipophilic molecule with protonophore properties; in other words, it is capable of interacting with the inner mitochondrial membrane to allow pumped protons to return to the mitochondrial matrix, dissipating the proton gradient and influencing the mitochondrial chemiosmosis [15, 16]. Indeed, in our experiment, we confirmed the depolarizing effect of the uncoupler FCCP. In experiment 2, we observed a significant reduction in ATP levels in the groups treated with 0.3, 1, and 3 μM of FCCP compared to the control group. ATP production in the mitochondria occurs by means of the coupling of two reactions: the transport of electrons throughout the respiratory chain and the proton gradient. This latest gradient is capable of storing energy, called proton motive force, which drives the synthesis of ATP through ADP and inorganic phosphate [17]. FCCP has a protonophore effect that will dissipate the proton gradient, thereby reducing ATP synthesis, as noted in our results. On the other hand, the groups that were treated with these same FCCP concentrations but were supplemented with glucose had higher levels of ATP, similar to the control group. From these results, we can suggest that the glycolytic pathway, after being stimulated, is able to maintain ATP levels in bovine epididymal sperm. In fact, our results were consistent with a previous study in boars, which demonstrated that sperm mitochondria account for only 5% of energy production, while the glycolytic pathway contributes to 95% [18]. Additionally, species such as mice may use ATP from glycolysis and mitochondrial respiration depending on their biological conditions without changing sperm functionality or sperm ATP levels [19].

In experiment 3, we observed a very similar pattern of results as in experiment 2. The motility and spermatic movement patterns were affected by mitochondrial uncoupling. However, stimulation of the glycolytic pathway maintained sperm kinetic patterns, even with cells undergoing mitochondrial uncoupling. These results suggest that for bovine sperm, there is a close relationship between motility and ATP levels. However, this relationship is still a matter of controversy. In accordance with our study, Mukai and Okuno [3] verified that ATP levels and flagellar beating remained constant when mouse sperm mitochondria were uncoupled concurrently with the supplementation of substrates for glycolysis.

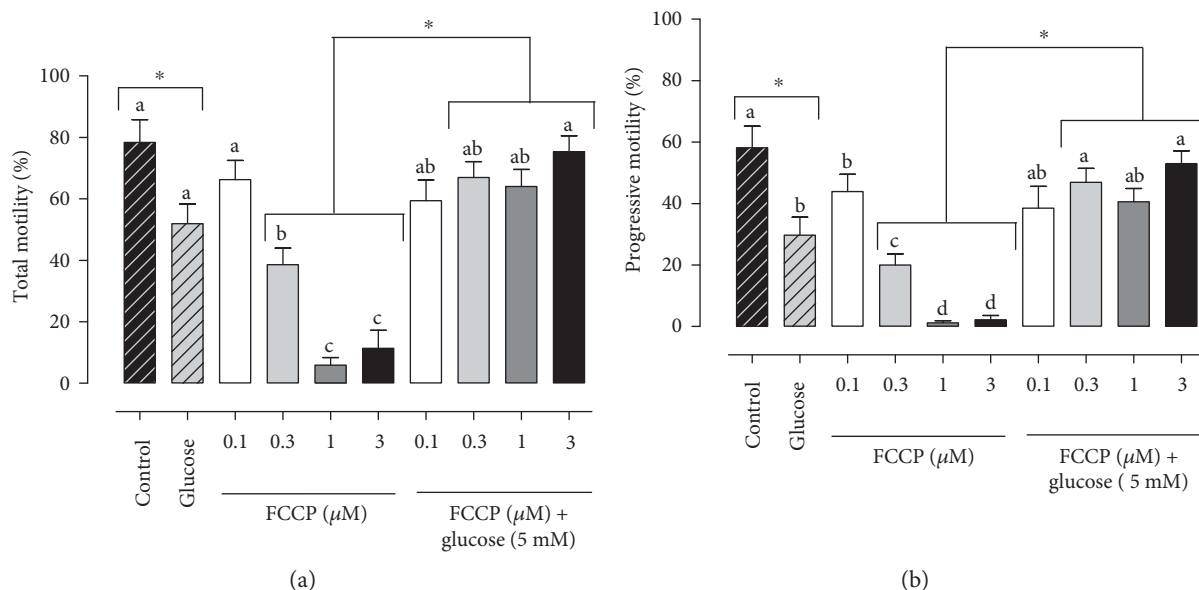


FIGURE 3: Total (a) and progressive (b) motility in bovine epididymal sperm treated with FCCP in different concentrations ($0 \mu\text{M}$, $0.1 \mu\text{M}$, $0.3 \mu\text{M}$, $1 \mu\text{M}$, and $3 \mu\text{M}$) in absence or presence of glucose 5 mM . a–d superscripts indicate differences between concentrations ($P < 0.05$). * indicates differences after the glucose supplementation ($P < 0.05$).

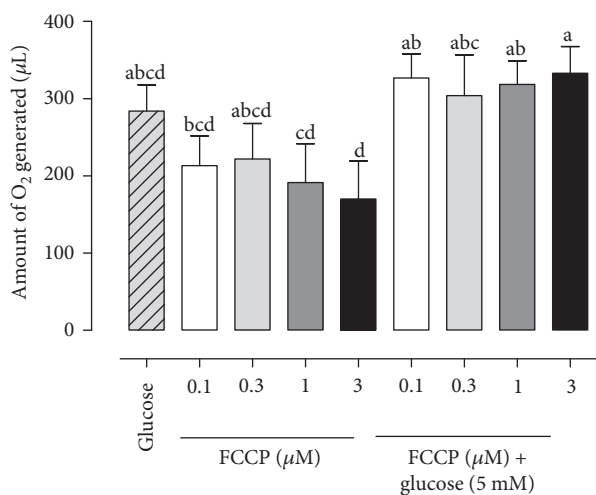


FIGURE 4: Amount of O_2 generated by bovine epididymal sperm treated with FCCCP in different concentrations ($0 \mu\text{M}$, $0.1 \mu\text{M}$, $0.3 \mu\text{M}$, $1 \mu\text{M}$, and $3 \mu\text{M}$) in absence or presence of glucose 5 mM . a–d superscripts indicate differences between concentrations ($P < 0.05$).

Additionally, Krzyzosiak et al. [20] also observed that bovine sperm are capable of maintaining similar motility patterns in both aerobic and anaerobic conditions, assuming that glycolysis is capable of maintaining sperm motility. On the other hand, Ramió-Lluch et al. [21] demonstrated that the inhibition of ATP synthase impairs sperm motility, while intracellular ATP levels remain unchanged. Therefore, the author suggested an unknown essential mitochondrial mechanism responsible for motility maintenance that does not rely only on the maintenance of ATP levels. The variations in the results of the different experiments seem to be related to the

species involved and the biological conditions to which such cells have been subjected [22, 23]. Therefore, there is a need for further studies to elucidate these mechanisms.

Regarding experiment 4, we observed that the groups treated with FCCP at 1 and $3 \mu\text{M}$ in the absence of glucose had a lower production of reactive oxygen species (ROS). The reactive oxygen species produced by sperm play a key role in many physiological processes such as hyperactivation [24], capacitation [25], and the interaction between the sperm and oocyte [26]. The fact that the groups treated with FCCP and glucose did not differ from the control group suggests that glycolysis stimulation is able to maintain the physiological ROS production and, ultimately, oxidative balance. Moreover, the ability of FCCP in the absence of glucose to reduce ROS production reveals a possible therapeutic potential for preventing the release of excessive reactive oxygen species. This ability to prevent ROS production may be due to the increase of the electron transport rates accompanied by a reduction in mitochondrial intermediate states which is able to donate electrons to oxygen [27]. Furthermore, studies have demonstrated that the reduction in ATP synthesis by mitochondria is accompanied by a reduction in ROS production [28]. In fact, studies have shown this ability of mitochondrial uncouplers in somatic cells [29, 30].

Therefore, knowledge of the role of each metabolic pathway on sperm functionality may target therapies using substrates to stimulate these pathways in reproduction biotechnologies. Furthermore, the data of mitochondrial uncoupling FCCP reduces the reactive oxygen species production and suggests that this molecule can be used to prevent seminal oxidative stress during procedures that induce this stress, such as cryopreservation. Thus, such procedure can improve reproductive indexes by means of assisted reproduction techniques in cattle, especially

intrauterine artificial insemination. Nevertheless, this therapeutic effect should be further studied in spermatozoa.

5. Conclusion

In conclusion, after its stimulation, the glycolytic pathway is capable of maintaining ATP levels, sperm kinetic patterns, and oxidative balance of bovine epididymal spermatozoa submitted to mitochondrial uncoupling.

Abbreviations

ALH: Amplitude of lateral head displacement
 ATP: Adenosine triphosphate
 BCF: Beat cross-frequency
 CASA: Computer-assisted sperm analysis
 FCCP: Carbonyl cyanide 4-(trifluoromethoxy) phenylhydrazone
 LIN: Sperm linearity
 LSD: Least significant difference
 ROS: Reactive oxygen species
 STR: Sperm straightness
 TALP: Tyrode albumin lactate pyruvate
 VAP: Average path velocity
 VCL: Curvilinear velocity
 VSL: Straight line velocity
 WOB: Wobble.

Conflicts of Interest

The authors declare that they have no competing interests.

Acknowledgments

This research was financially supported by Instituto de Farmacología Teófilo Hernando. Also, the authors thank The Brazilian National Council for Scientific and Technological Development (CNPq, Project no. 460764/2014-4) for the financial assistance and Francisco J. Blasco (Integrated Semen Analysis System, Proiser R+D Systems, Valencia, Spain) for the computerized analysis of the motility.

References

- [1] A. J. Travis, J. A. Foster, N. A. Rosenbaum et al., "Targeting of a germ cell-specific type 1 hexokinase lacking a porin-binding domain to the mitochondria as well as to the head and fibrous sheath of murine spermatozoa," *Molecular Biology of the Cell*, vol. 9, no. 2, pp. 263–276, 1998.
- [2] J. C. S. John, "The transmission of mitochondrial DNA following assisted reproductive techniques," *Theriogenology*, vol. 57, no. 1, pp. 109–123, 2002.
- [3] C. Mukai and M. Okuno, "Glycolysis plays a major role for adenosine triphosphate supplementation in mouse sperm flagellar movement," *Biology of Reproduction*, vol. 71, no. 2, pp. 540–547, 2004.
- [4] J. M. Nascimento, L. Z. Shi, J. Tam et al., "Comparison of glycolysis and oxidative phosphorylation as energy sources for mammalian sperm motility, using the combination of fluorescence imaging, laser tweezers, and real-time automated tracking and trapping," *Journal of Cellular Physiology*, vol. 217, no. 3, pp. 745–751, 2008.
- [5] A. C. Nevo and R. Rikmenspoel, "Diffusion of ATP in sperm flagella," *Journal of Theoretical Biology*, vol. 26, no. 1, pp. 11–18, 1970.
- [6] R. M. Turner, "Tales from the tail: what do we really know about sperm motility?" *Journal of Andrology*, vol. 24, no. 6, pp. 790–803, 2003.
- [7] S. du Plessis, A. Agarwal, G. Mohanty, and M. van der Linde, "Oxidative phosphorylation versus glycolysis: what fuel do spermatozoa use?" *Asian Journal of Andrology*, vol. 17, no. 2, pp. 230–235, 2015.
- [8] M. P. Davila, P. M. Munoz, J. M. Bolanos et al., "Mitochondrial ATP is required for the maintenance of membrane integrity in stallion spermatozoa, whereas motility requires both glycolysis and oxidative phosphorylation," *Reproduction*, vol. 152, no. 6, pp. 683–694, 2016.
- [9] J. D. A. Losano, D. S. R. Angrimani, A. Dalmazzo et al., "Effect of mitochondrial uncoupling and glycolysis inhibition on ram sperm functionality," *Reproduction in Domestic Animals*, vol. 52, no. 2, pp. 289–297, 2017.
- [10] D. L. Garner and E. S. E. Hafez, "Spermatozoa and seminal plasma," in *Reproduction in Farm Animals*, pp. 96–109, Lippincott Williams & Wilkins, Philadelphia, Pennsylvania, 2000.
- [11] A. Zöpfigen, F. Priem, F. Sudhoff et al., "Relationship between semen quality and the seminal plasma components carnitine, alpha-glucosidase, fructose, citrate and granulocyte elastase in infertile men compared with a normal population," *Human Reproduction*, vol. 15, no. 4, pp. 840–845, 2000.
- [12] G. Aguiar, M. Van Tilburg, A. Catunda et al., "Sperm parameters and biochemical components of goat seminal plasma in the rainy and dry seasons in the Brazilian Northeast: the season's influence on the cooling of semen," *Arquivo Brasileiro de Medicina Veterinária e Zootecnia*, vol. 65, no. 1, pp. 6–12, 2013.
- [13] M. Nichi, T. Rijsselaere, J. Losano et al., "Evaluation of epididymis storage temperature and cryopreservation conditions for improved mitochondrial membrane potential, membrane integrity, sperm motility and in vitro fertilization in bovine epididymal sperm," *Reproduction in Domestic Animals*, vol. 52, no. 2, pp. 257–263, 2016.
- [14] I. G. F. Goovaerts, G. G. Hoflack, A. Van Soom et al., "Evaluation of epididymal semen quality using the Hamilton–Thorne analyser indicates variation between the two caudae epididymides of the same bull," *Theriogenology*, vol. 66, no. 2, pp. 323–330, 2006.
- [15] H. Terada, "Uncouplers of oxidative phosphorylation," *Environmental Health Perspectives*, vol. 87, p. 213, 1990.
- [16] G. Bagkos, K. Koufopoulos, and C. Piperi, "A new model for mitochondrial membrane potential production and storage," *Medical Hypotheses*, vol. 83, no. 2, pp. 175–181, 2014.
- [17] B. B. Lowell and G. I. Shulman, "Mitochondrial dysfunction and type 2 diabetes," *Science*, vol. 307, no. 5708, pp. 384–387, 2005.
- [18] S. Marin, K. Chiang, S. Bassilian et al., "Metabolic strategy of boar spermatozoa revealed by a metabolomic characterization," *FEBS Letters*, vol. 554, no. 3, pp. 342–346, 2003.
- [19] V. Pasupuleti, *Role of Glycolysis and Respiration in Sperm Metabolism and Motility*, Kent State University, Ohio, Kent State University, 2007.
- [20] J. Krzyzosiak, P. Molan, and R. Vishwanath, "Measurements of bovine sperm velocities under true anaerobic and aerobic conditions," *Animal Reproduction Science*, vol. 55, no. 3–4, pp. 163–173, 1999.

- [21] L. Ramió-Lluch, M. Yeste, J. M. Fernández-Novell et al., "Oligomycin A-induced inhibition of mitochondrial ATP-synthase activity suppresses boar sperm motility and in vitro capacitation achievement without modifying overall sperm energy levels," *Reproduction, Fertility and Development*, vol. 26, no. 6, pp. 883–897, 2014.
- [22] B. T. Storey, "Mammalian sperm metabolism: oxygen and sugar, friend and foe," *International Journal of Developmental Biology*, vol. 52, no. 5-6, pp. 427–437, 2004.
- [23] A. Amaral, B. Lourenço, M. Marques, and J. Ramalho-Santos, "Mitochondria functionality and sperm quality," *Reproduction*, vol. 146, no. 5, pp. R163–R174, 2013.
- [24] E. de Lamirande and C. Cagnon, "Human sperm hyperactivation and capacitation as parts of an oxidative process," *Free Radical Biology and Medicine*, vol. 14, no. 2, pp. 157–166, 1993.
- [25] R. J. Aitken, A. L. Ryan, M. A. Baker, and E. A. McLaughlin, "Redox activity associated with the maturation and capacitation of mammalian spermatozoa," *Free Radical Biology and Medicine*, vol. 36, no. 8, pp. 994–1010, 2004.
- [26] R. J. Aitken, M. Paterson, H. Fisher, D. W. Buckingham, and M. van Duin, "Redox regulation of tyrosine phosphorylation in human spermatozoa and its role in the control of human sperm function," *Journal of Cell Science*, vol. 108, Part 5, pp. 2017–2025, 1995.
- [27] M. F. Cunha, C. Caldeira da Silva, M. F. Cerqueira, and J. A. Kowaltowski, "Mild mitochondrial uncoupling as a therapeutic strategy," *Current Drug Targets*, vol. 12, no. 6, pp. 783–789, 2011.
- [28] P. Newsholme, E. Haber, S. Hirabara et al., "Diabetes associated cell stress and dysfunction: role of mitochondrial and non-mitochondrial ROS production and activity," *The Journal of Physiology*, vol. 583, Part 1, pp. 9–24, 2007.
- [29] A. M. Vincent, J. A. Olzmann, M. Brownlee, W. I. Sivitz, and J. W. Russell, "Uncoupling proteins prevent glucose-induced neuronal oxidative stress and programmed cell death," *Diabetes*, vol. 53, no. 3, pp. 726–734, 2004.
- [30] R. J. Mailloux and M. E. Harper, "Uncoupling proteins and the control of mitochondrial reactive oxygen species production," *Free Radical Biology and Medicine*, vol. 51, no. 6, pp. 1106–1115, 2011.